NUCLEAR PHYSICS

JOURNAL DEVOTED TO THE EXPERIMENTAL AND
THEORETICAL STUDY OF THE FUNDAMENTAL
CONSTITUENTS OF MATTER AND THEIR INTERACTIONS

EDITOR: L. ROSENFELD - COPENHAGEN
ASSOCIATE EDITOR: O. NATHAN - COPENHAGEN

VOLUME XXIII

N·H
P C

NORTH-HOLLAND PUBLISHING COMPANY - AMSTERDAM

NUCLEAR PHYSICS

EDITORIAL BOARD

AUSTRALIA & NEW ZEALAND: H. Messel (Sydney), M. L. Oliphant (Canberra)
AUSTRIA: B. Karlik (Vienna), H. Thirring (Vienna)
BELGIUM: M. de Hemptinne (Louvain), J. Verhaeghe (Ghent)
CANADA: G. Volkoff (Vancouver)
DENMARK: C. Møller (Copenhagen), S. Rozental (Copenhagen), G. E. Brown (Copenhagen)
FINLAND: L. Simons (Helsinki)
FRANCE: A. Berthelot (Saclay), S. Gorodetzky (Strasbourg)
GERMANY (DEM. REP.): G. Hertz (Leipzig)
GERMANY (FED. REP.): W. Gentner (Freiburg i. B.), J. H. D. Jensen (Heidelberg)
GREAT BRITAIN: W. E. Burcham (Birmingham), T. H. R. Skyrme (Harwell)
HUNGARY: L. Janossy (Budapest)
INDIA: H. Bhabha (Bombay), R. Ramanna (Trombay)
IRISH REPUBLIC: J. McConnell (Maynooth)
ISRAEL: G. Racah (Jerusalem)
ITALY: E. Amaldi (Rome)
JAPAN: S. Kikuchi (Tokai), S. Tomonaga (Tokyo)
MEXICO: M. Moshinsky (Mexico)
NETHERLANDS: H. Brinkman (Groningen), S. R. de Groot (Leiden)
NORWAY: E. Hylleraas (Oslo), A. Lundby (Oslo), H. Wergeland (Trondheim)
POLAND: L. Infeld (Warsaw), J. Werle (Warsaw)
PORTUGAL: J. M. Araújo (Porto), J. R. de Almeida Santos (Coimbra)
SOUTH AMERICA: G. Beck (Saõ Paulo), J. Leite Lopes (Rio de Janeiro)
SPAIN: J. M. Otero (Madrid), C. Sanchez del Rio (Madrid)
SWEDEN: O. Klein (Stockholm), K. Siegbahn (Uppsala), I. Waller (Uppsala)
SWITZERLAND: P. Huber (Basel), P. Scherrer (Zürich)
U.A.R. & ARAB COUNTRIES: F. El Bedewi (Cairo), M. G. Nooh (Cairo)
U.S.A.: H. H. Barschall (Madison, Wisconsin), S. Devons (New York), V. F. Weisskopf (Cambridge, Mass.)
U.S.S.R.: M. A. Markov (Moscow), I. S. Shapiro (Moscow), D. V. Skobeltzyn (Moscow)
YUGOSLAVIA: I. Supek (Zagreb)

NUCLEAR PHYSICS

JOURNAL DEVOTED TO THE EXPERIMENTAL AND
THEORETICAL STUDY OF THE FUNDAMENTAL
CONSTITUENTS OF MATTER AND THEIR INTERACTIONS

EDITOR: L. ROSENFELD - COPENHAGEN

VOLUME XXIII
FEBRUARY 1961—MARCH 1961

NORTH-HOLLAND PUBLISHING COMPANY-AMSTERDAM

PRINTED IN THE NETHERLANDS

10.C Nuclear Physics 23 (1961) 1—4; © North-Holland Publishing Co., Amsterdam

Not to be reproduced by photoprint or microfilm without written permission from the publisher

PROFESSOR H. W. B. SKINNER, F.R.S.
(1900—1960)

R. E. PEIERLS

Department of Mathematical Physics, University of Birmingham, England

Received 4 November 1960

Herbert Wakefield Banks Skinner was born on 7th October, 1900. He was educated at Rugby and Trinity College, Cambridge, where he remained for research at the Cavendish Laboratory from 1922—1927. He joined the staff of the H. H. Wills Physical Laboratory of the University of Bristol in 1927 and remained at Bristol until 1939, with the exception of the year 1932—1933, which he spent at M.I.T. on a Rockefeller Fellowship. On the outbreak of war he joined the radar team at Dundee which transferred to Swanage and later to Malvern. In 1944 he moved to Berkeley to help in the development of the electromagnetic isotope separation plant in the atomic energy project.

At the end of 1945 he returned to England as one of the first senior staff members of the new Atomic Energy Research Establishment at Harwell, where he directed the 'general physics division' until his appointment to the Lyon Jones professorship in physics in the University of Liverpool, as a successor to Sir James Chadwick.

Skinner's early work in the Cavendish Laboratory followed the current interest in β-ray spectra and radiation, and the early papers show him as a skilled experimenter with a taste for accuracy and clarity.

His spectroscopic work led him to take a particular interest in the borderland between short-wave ultraviolet and soft X-rays, a field not yet adequately explored at the time because of the experimental difficulties. It is probable that the challenge of just these difficulties was for him one of the attractions to this subject.

This was during his Bristol period where the contact with N. G. Mott and H. Jones, who were then developing the now generally accepted ideas of the electron theory of metals led to a powerful combination of an experimental and theoretical study.

This showed in particular that the energy spectra of the electron bands in metals, which were fundamental to the theory, could show up in the X-ray spectra and that Skinner's techniques for handling the soft X-ray region were capable of revealing an impressive amount of detail of these electron bands.

This possibility of seeing the dynamical details of the electron motion rather than only the integral features which are shown up in the magnetic and electric properties played a great part in establishing our knowledge of metals on sound and realistic foundations.

The papers of the Bristol period represent Skinner's main direct contribution to pure physics and this work rightly earned him a name as an experimenter of outstanding skill, judgment and reasoning power. But an assessment of his role in physics based only on his own publications would ignore the great contribution of later years surviving in the record only through the publications of others.

His war work on radar and on atomic energy was, of necessity, applied physics. It required for its execution the best and most experienced of the modern physicists, and Skinner's contribution was very much that of a physicist. Yet it was, in purpose and motivation, more engineering than physics. Skinner was outstandingly successful in adapting himself to this situation, and on his return to Harwell he became one of the key figures in building up an institution which combined strength in its practical outlook and its handling of large-scale equipment with a strong position in fundamental physics.

His own general physics division became a good model of this duality. Its cyclotron was a sound piece of engineering which ever since its construction has been working smoothly with as little trouble as the smaller laboratory instruments of earlier generations of physicists, allowing the research workers to concentrate on their results and techniques without concerning themselves with the problems of machine operational performance. In spite of its unfashionable energy range the machine is even today making important contributions to fundamental nuclear problems.

His influence at Harwell far transcended his own division and even after his move to Liverpool, his advice, his enthusiasm and his pungent criticism continued to be available for many of the projects arising at the Atomic Energy Establishment.

He was clearly the right man to take over the work started by Chadwick in building up the high energy research at Liverpool and to look after the completion of the cyclotron then in construction. He increased the team at Liverpool by attracting more outstanding physicists and by training others, and the group of people he had brought together become one of the important centres for work in the several 100 MeV range, in particular for pion physics, in spite of the fact that they had entered this field rather later than many groups elsewhere. This is not the occasion to write at length of his personal qualities but no account of Skinner's work could omit some mention of the part he played in amongst his colleagues in his University, in his subject and in his country. In all discussions to form policy he was liable to express strong views, and he would stand up for what he judged to be right regardless of whether his views were fashionable or conformed with conventions. He would listen to argument but was not impressed by authority.

His outspoken comments could irritate his seniors but his judgment and his integrity were always respected and his counsel was in great demand. The number of committees and discussions in which he was asked to take part was such that only a man of his sense of duty could agree to serve, and only a man of his energy and capacity for work could combine them with the work of running his own department. In the last few years, these outside commitments involved many contacts with CERN, the progress of which was close to his heart, and work on the development of a National Bubble Chamber, by a combined effort of several groups of physicists in Britain.

In looking after his collaborators no trouble was ever too much and anyone in difficulty or with problems would find Skinner's house open and could count on a patient hearing, active interest and ready help.

The suddenness of his unexpected death in Geneva deepened the sense of loss felt by all his colleagues and by all those who had come to rely on his judgment and help and who were inspired by the example he had set in standing up for what he believed to be right.

List of Publications

1) Absolute energies of groups in magnetic β-ray spectra (with C. D. Ellis), Proc. Roy. Soc. A **105** (1924) 60
2) A reinvestigation of the β-ray spectra of a B and RaC (with C. D. Ellis), Proc. Roy. Soc. A **105** (1924) 165
3) Interpretation of β-ray spectra (with C. D. Ellis), Proc. Roy. Soc. A **105** (1924) 185
4) Relative absorbing power of levels for radiation of varying wave-length, Proc. Camb. Phil. Soc. **23** (1927) 508
5) The Zeeman effect in strong magnetic fields (with P. Kapitza), Proc. Roy. Soc. A **109** (1925) 224
6) On the excitation of polarised light by electron impact (I), Proc. Roy. Soc. A **112** (1926) 642
7) On the polarisation of mercury lines emitted from a discharge tube in a magnetic field, Proc. Camb. Phil. Soc. **23** (1927) 508
8) A case of double reflexion (with E. T. S. Appleyard), Proc. Camb. Phil. Soc. **23** (1927) 951
9) On the excitation of polarised light by electron impact (II) Mercury (with E. T. S. Appleyard), Proc. Roy. Soc. A **117** (1927) 223
10) Variation of intensities in the helium spectrum with velocity of the exciting electrons (with J. H. Lees), Nature (June 1st, 1929)
11) Design of the electron collector for retarding voltage analysis (with S. H. Piper), Phil. Mag. **8** (1929) 313

12) Bemerkung zu dem Experiment von Herrn Rupp usw, Naturwiss. **18** (1930) 1098
13) The technique of copper pyrex tube seals (with J. H. Burrow), J. Sci. Inst. **7** (1930) 290
14) Excitation potentials of metallic lethium, Nature (July 18th, 1931)
15) Notes on the excitation processes in helium (with J. H. Lees), Proc. Roy. Soc. A **137**
16) The excitation potentials of light metals (II) Beryllium, Proc. Roy. Soc. A **140** (1933) 277
17) Theory of the form of X-ray emission bands of metals (with N. F. Mott and H. Jones), Phys. Rev. **45** (1934) 380
18) Characteristics soft X-rays from metals in the extreme ultraviolet (with H. M. O'Bryan), Phys. Rev. **45** (1934) 572
19) Finestructure of L_{23} absorption edge of Mg metal (with J. E. Johnston), Nature **137** (1936) 826
20) Fine structure of soft X-ray absorption edges (with J. E. Johnston), Proc. Roy. Soc. **906** (1937) 420
21) Soft X-rays bands from dilute alloys (with J. E. Johnston), Proc. Camb. Phil. Soc. **34** (1938) 129
22) Direct proof of the effect of temperature in the conduction electrons of a metal, Nature **142** (1938) 432
23) The soft X-ray spectroscopy of the solid state, Rep. Progr. Phys. (Phys. Soc.) **5** (1939) 257
24) The soft X-ray spectroscopy of solids (I), Phil. Trans. A **209** (1940) 95
25) The soft X-ray spectroscopy of solids (II) (with H. M. O'Bryan), Proc. Roy. Soc. **176** (1940) 229
26) Patent on cell for common T. R. working at cm wave-lengths (This is probably a master-patent for common T. R. for cm wave-lengths). (1944)
27) Atomic energy in post-war Britain, Bulletin of the Atomic Scientists **9** (1953) 156
28) Notes on soft X-ray spectra, particularly of the Fe group of elements (with T. G. Bullen and J. E. Johnston), Phil. Mag. **45** (1954) 1070
29) The ABC of nuclear weapons, The New Scientist **5** (1959) 473

1.D.4

Nuclear Physics **23** (1961) 5—22; © *North-Holland Publishing Co., Amsterdam*

Not to be reproduced by photoprint or microfilm without written permission from the publisher

POSITIVE-PARITY STATES IN MASS-13 NUCLEI

D. KURATH and R. D. LAWSON

Argonne National Laboratory, Argonne, Illinois †

Received 4 October 1960

Abstract: The strength of coupling between the positive-parity nucleon and the C^{12} core is investigated. Strong coupling, as implied by using the Nilsson model to generate wave functions, contradicts experiment. A reasonable picture arises from weak coupling with a strength consistent with that derivable from summing the two-body interaction integrals between the positive-parity nucleon and the core.

1. Introduction

The generator formalism has been successful in obtaining intermediate-coupling functions for the low-lying normal-parity states in the 1p-shell. In this procedure ¹), the two-body interaction is replaced by a quadrupole deformation of the effective potential for the individual nucleons. Since such a procedure circumvents a large part of the labor required to obtain wave functions from the interaction picture, it is of interest to see if the method can be applied to the states of nonnormal parity. Such states were investigated for those mass-13 nuclei for which a relatively large amount of experimental data exists.

The straightforward generalization of the generating procedure is to use the Nilsson picture ²) and promote the odd nucleon from level No. 4 (where it is for normal-parity states) to one of the low positive-parity levels of the (2s—1d) region. Since there are three levels, with angular momentum projections $K = \frac{1}{2}, \frac{3}{2}$, and $\frac{5}{2}$, the bands would be mixed for angular momentum $I > \frac{1}{2}$. However, there is one feature which all three levels have in common, namely, that they give strongly inhibited E1 transitions to the low-lying normal-parity states. In the limit of very large deformation this is understandable as a consequence of a selection rule for the asymptotic quantum number n_z which has been found responsible for inhibiting E1 transitions in the heavy elements ³). The experimental results do not support such strong E1 inhibitions, so the strong-coupling approach is not appropriate.

The model to which one is led starts from a deformed core for C^{12} to which the positive-parity nucleon is weakly coupled. The calculation is carried out by keeping only the two low states of $C^{12}(I_0 = 0, 2)$ which arise from the generating procedure, and varying the strength of coupling between the core and the

---

† Work performed under the auspices of the U. S. Atomic Energy Commission.

positive-parity nucleon. With fairly weak coupling one obtains a picture which is in much better agreement with experiment than the previous results.

Finally a check is made on the coupling strength by taking a two-body interaction between the positive-parity nucleon and the core nucleons and integrating over the core coordinates. This leads to an effective quadrupole coupling strength consistent with what is found empirically.

2. Formalism and Strong-Coupling Approximation

Since most of the formalism is common to both weak and strong coupling, it is presented in this section. The low-lying negative-parity states in C^{13} or N^{13} can be generated from the Hill-Wheeler integral:

$$\psi^{I'}_{M'(K')}(x) = (2I'+1)N^{I'}_{K'}\int \mathrm{d}R'\, D^{I'}_{M'K'}(R')X_{K'}(R'x). \tag{1}$$

Here $X_{K'}$ is a normalized nine-nucleon determinant constructed by filling the Nilsson levels through level number 3 and putting the remaining nucleon in level 4. The coordinate system $(R'x)$ is oriented with respect to the laboratory system x, and functions of angular momentum I′ are related by the rotation matrix $D^{I'}_{M'K'}(R')$. The function $X_{K'}$ can be expanded in a representation of angular momentum eigenfunctions, namely,

$$X_{K'}(R'x) = \sum_{I',s'} C^{I's'}_{K'}\Phi^{I's'}_{K'}(R'x), \tag{2}$$

where s' encompasses any additional labels necessary to specify states of the same I'. Then the normalization constant $N^{I'}_{K'}$ of eq. (1) is defined by

$$|N^{I'}_{K'}|^2 \sum_{s'} |C^{I's'}_{K'}|^2 = 1. \tag{3}$$

In a similar way, one can generate low-lying positive-parity wave functions by replacing the $X_{K'}$ of eq. (1) by a new X_K in which the ninth particle is now placed in either level 5, 6 or 7 of the Nilsson diagram of fig. 1. This assumes that the C^{12} core, for which the second and third levels are full, remains intact — an assumption which seems justified since level 4 is fairly well isolated from 2 and 3. The possibility that appreciable components of the low-lying positive-parity levels arise from putting a particle in levels 8, 9 and 11 has also been neglected on energetic grounds.

If we let Q_μ^λ denote the operator giving rise to the emission of multipole radiation of order λ, with z component μ, then the reduced transition probability for a transition between a positive-parity state of spin I and a negative-parity state of spin I' is simply shown to be

$$\begin{aligned}\frac{1}{2I+1}\sum_{M'M\mu}\left|\langle\psi^{I'}_{M'(K')}(x)|Q_\mu{}^\lambda(x)|\psi^{I}_{M(K)}(x)\rangle\right|^2 &= B(Q\lambda; I\rightarrow I') \\ &= \left(\frac{2I+1}{2I'+1}\right)(N^I_K)^2(N^{I'}_{K'})^2\left|\sum_{s'\mu} C^{*I's'}_{K'}(\lambda I\mu K|I'K+\mu)\int \mathrm{d}y\Phi^{*I's'}_{K+\mu}(y)Q_\mu{}^\lambda(y)X_K(y)\right|^2,\end{aligned} \tag{4}$$

where the bracket is a Clebsch-Gordan coefficient.

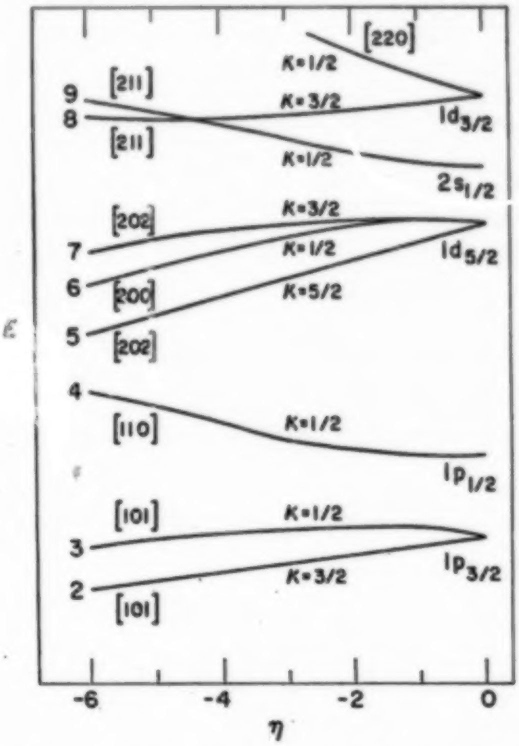

Fig. 1. Nilsson diagram of energy levels for the 1p and (2s−1d) shells with oblate deformation. Nilsson's label is at the left, and a value of η near $\eta = -6$ seems appropriate for C^{12}. The notation $[Nn_z\Lambda]$, where N is the principal quantum number and n_z and Λ are asymptotic quantum numbers, is also given at the left.

Because $X_{K'}$ and the negative-parity states generated from it lie entirely within the 1p-shell, the integral in eq. (4) has contributions only for that part of $[Q_\mu{}^\lambda X_K]$ which returns the nucleon from the positive-parity level to the 1p-shell. Furthermore since levels 2 and 3 are full in X_K, the nucleon can be returned only to level 4, which then produces the generator for the normal-parity states. The effect of the single-particle operator $Q_\mu{}^\lambda$ on the single-particle positive-parity state $\phi_{K\nu}$, which produces a contribution to the right side of eq. (4), is then

$$Q_\mu{}^\lambda\phi_{K\nu}\rightarrow g_{\lambda\mu}(K\nu\rightarrow \tfrac{1}{2}4)\phi_{\frac{1}{2}(4)}+g_{\lambda\mu}(K\nu\rightarrow -\tfrac{1}{2}4)\phi_{-\frac{1}{2}(4)}, \tag{5}$$

where

$$g_{\lambda\mu}(K\nu \to \pm\tfrac{1}{2}4) = \int \phi^{*}_{\pm\frac{1}{2},4} Q_{\mu}{}^{\lambda} \phi_{K\nu}$$

is now the single-particle matrix element for $Q_{\mu}{}^{\lambda}$. Therefore one can carry out the summations in eq. (4) to obtain

$$\begin{aligned} B(Q\lambda; I \to I') = {} & \left(\frac{2I+1}{2I'+1}\right) [N^{I}_{K}/N^{I'}_{\frac{1}{2}}]^{2} \\ & \times [(I\lambda K\tfrac{1}{2}-K|I'\tfrac{1}{2}) g_{\lambda(\frac{1}{2}-K)}(K\nu \to \tfrac{1}{2}4) \\ & + (-1)^{I'+\frac{1}{2}} (I\lambda K-K-\tfrac{1}{2}|I'-\tfrac{1}{2}) g_{\lambda(-\frac{1}{2}-K)}(K\nu \to -\tfrac{1}{2}4)]^{2}. \qquad (4') \end{aligned}$$

For transitions between states of this particular nature, there is a simple relationship between the expression for the reduced transition probability in eq. (4′) and that obtained from the usual Bohr-Mottelson wave function where one does not carry out the Hill-Wheeler integration. Starting from

$$\psi^{I}_{M(K)} = \sqrt{I+\tfrac{1}{2}}[D^{I}_{MK}(R')X_{K}(R'x) + (i)^{-2I} D^{I}_{M-K}(R')[R_1 X_K](R'x)], \qquad (6)$$

where $[R_1 X_K]$ is the function obtained by reversing coordinate axes 2 and 3, one finds that the expressions for reduced transition probability are related by

$$B(Q\lambda; I \to I') = \left(\frac{2I+1}{2I'+1}\right) [N^{I}_{K}/N^{I'}_{\frac{1}{2}}]^{2} \tilde{B}(Q\lambda; I \to I'). \qquad (7)$$

Here $\tilde{B}$ is the usual result one finds in the Bohr-Mottelson approximation. The existence of such a simple relationship is the result of being able to select one single-nucleon function as providing the possibility of transition, and would not be the case, for example, for transitions within the 1p-shell. For the transitions between low-lying opposite-parity states which were investigated, the range of the proportionality coefficient in eq. (7) is found to lie between about 0.5 and 3.0 so that B and $\tilde{B}$ have quite similar magnitudes.

Since there are three levels with $K = \frac{1}{2}, \frac{3}{2}$ and $\frac{5}{2}$ available for the positive-parity state, any calculation would have to include the effects of mixing rotational bands for $I > \frac{1}{2}$. However, all three levels have a common feature, namely, that in the asymptotic limit of large deformation the single-particle matrix elements [eq. (5)] for E1 transition to level 4 vanish. Such a selection rule is understandable in terms of the asymptotic quantum numbers [4]) n_z, the number of energy quanta for oscillations along the nuclear symmetry axis, and Λ, the projection of orbital angular momentum on the nuclear symmetry axis. The designations $[Nn_z\Lambda]$ at the left in fig. 1 include the principal quantum number N also. The E1 operator can only change Λ by 0 or 1, a selection rule that allows only levels 4 and 6 to be connected. The further rule that for $\Delta\Lambda = 0$, ΔN and

Δn_z must be both $+1$ or both -1 makes all E1 transitions from level 4 to levels 5, 6 and 7 asymptotically forbidden †.

Even away from the strong-deformation limit, the calculated E1 transitions are still strongly inhibited by something like a factor of 10^{-4} to 10^{-5} from the usual single-particle estimate. The calculated lifetimes are at least 100 times as long as the observed E1 lifetimes in C^{13} and N^{13}. Since there is little one can do within this model to change the estimated lifetimes, the strong-coupling picture can be ruled out on this basis.

3. Weak-Coupling Approximation

In this section we treat the nonnormal-parity states of mass-13 nuclei as consisting of a C^{12} core to which a positive-parity nucleon is weakly coupled. This is an idea which has been suggested often, probably first by Lane [5]), and we recast it in the language of the generating procedure from a rotational model. Actually the strength of the coupling between core and particle can be made large in the calculation, but weak coupling is found to be appropriate to experiment.

The picture from which we start is that of a deformed C^{12} core, represented by the generator state which leads to [1]) the $I_0 = 0, 2, 4$ band for C^{12}. In addition there is a positive-parity nucleon which in zero order is not coupled to the core, and therefore effectively sees a spherical core with an outer shell of lower density since it does not know the orientation of the nuclear symmetry axis. The zero-order functions are

$$\Phi^I_M(I_0, j) = \sqrt{2I_0+1}\times \sum_m (I_0\, jM-mm|IM) D^{I_0}_{(M-m)0}(R) X_0(Rx)\phi^j_m(x_n), \tag{8}$$

where (Rx) is the C^{12} coordinate system and the last nucleon is in the laboratory system x_n. Alternatively we can transform ϕ^j_m to the coordinate system of the C^{12} nucleus to obtain

$$\Phi^I_M(I_0, j) = \sqrt{2I_0+1}\times \sum_k (I_0\, j0k|Ik) D^I_{Mk}(R) X_0(Rx)\phi^j_k(Rx_n). \tag{8'}$$

For the zero-order energies the C^{12} rotor has spacings $E_{I_0} = I_0(I_0+1)A$, and we take the energy of the $I_0 = 2^+$ state from experiment at 4.43 MeV, so that $A = 0.74$ MeV. This puts the $I_0 = 4$ state up so high that it will give a negligible contribution to the low positive-parity states, and it is not included in the calculation. For the single-particle energies there is experimental information in O^{17} and F^{17} for which the ground state is $1d_{\frac{5}{2}}$ with the $1d_{\frac{3}{2}}$ level some 5 MeV higher. The $2s_{\frac{1}{2}}$ level lies at 0.87 MeV in O^{17} and at 0.50 MeV in F^{17}. If the outer radii are about equal, the difference that a positive-parity nucleon sees when it looks at the C^{12} core rather than the O^{16} core is that the former has an outer shell of lower density. This will tend to lower the states of smaller orbital angular momentum in going from O^{16} to C^{12}, as is seen experimentally. A quantitative estimate is difficult to obtain, so we have arbitrarily lowered the $2s_{\frac{1}{2}}$ state by about 1 MeV so that it lies 300 keV below the $1d_{\frac{5}{2}}$ state. These energy differences then account for the level spacing at the left in fig. 2.

---

† There is also asymptotic forbiddenness for the spin-dependent part of the M2 operator among these levels. Hence such M2 transitions in C^{13} are forbidden asymptotically.

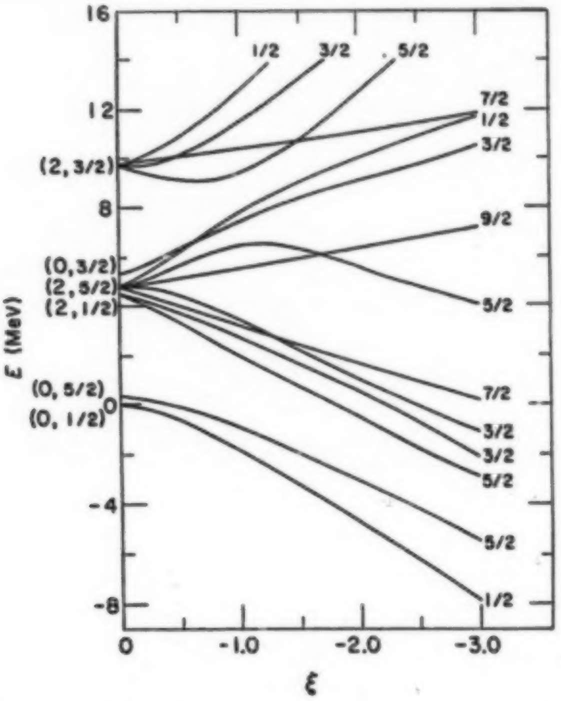

Fig. 2. Energy level spectrum for positive-parity states as a function of the strength ξ of coupling between the core and the positive-parity nucleon.

The coupling between the positive-parity nucleon and the oblate quadrupole deformed core can be written in the nuclear coordinate system as was done by Nilsson [2])

$$H_{\text{cplg}} = +k(r_n)\beta_0 Y_0^2(Rx_n). \tag{9}$$

The combined Hamiltonian of the C^{12} rotor † plus the single-particle energies plus H_{cplg} is then diagonalized as a function of the coupling parameter

$$\xi = -\frac{1}{4\sqrt{5\pi}}\beta_0 \int R_{nl}(r)R_{n'l'}(r)k(r)r^2\mathrm{d}r. \tag{10}$$

Both β_0 and $k(r)$ are positive quantities and the integral with the radial functions of the positive-parity states is assumed to be the same for all the states. The energy spectrum as a function of ξ is given in fig. 2. To the extent that such a quadrupole term as eq. (9) correctly represents the interaction of the core with the positive-parity nucleon, this spectrum should agree with observation. Comparison with the experimental data of fig. 3 shows that this is apparently true over a wide range of ξ values, and in fact, by shifting the $2s_{\frac{1}{2}}$ state downward one could also have done it in the strong-coupling approximation. However, there would not have been any justification of the type given above in the weak-coupling case, for making such a shift.

---

† Notice that the entire energy of the rotor is included here, whereas in the strong-coupling representation one must go to rotation-particle-coupling band mixing to include all the rotor energy. The band-mixing comes from the $(\mathbf{I}\cdot\mathbf{j})A$ term in the rotor energy $I_0^2A = (\mathbf{I}-\mathbf{j})^2A$.

For a particular eigenvalue ε, the wave functions which result from the diagonalization are linear combinations of the $\Phi^I_M(I_0, j)$ of eq. (8′) i.e.,

$$\Phi^I_M(\varepsilon) = \sum_{I_0, j} a_\varepsilon^{\,I}(I_0, j)\Phi^I_M(I_0, j). \tag{11}$$

The coefficients $a_\varepsilon^{\,I}(I_0, j)$ are given in table 1 for the lowest and next to lowest eigenstate of $I = \frac{1}{2}^+, \frac{3}{2}^+$ and $\frac{5}{2}^+$ as a function of ξ. For wave functions which do not contain the extra Euler angles of the nuclear orientation, integrate over dR to generate wave functions in the laboratory system and obtain

TABLE 1

dmixture coefficients in the wave functions of the lowest and next to lowest positive-parity states for $I = \frac{1}{2}^+, \frac{3}{2}^+$ and $\frac{5}{2}^+$ as a function of the coupling parameter ξ

	$a^{\frac{1}{2}}(I_0, j)$			$a^{\frac{3}{2}}(I_0, j)$				$a^{\frac{5}{2}}(I_0, j)$			
ξ \ I_0, j	0, $\frac{1}{2}$	2, $\frac{5}{2}$	2, $\frac{3}{2}$	2, $\frac{1}{2}$	2, $\frac{5}{2}$	0, $\frac{3}{2}$	2, $\frac{3}{2}$	0, $\frac{5}{2}$	2, $\frac{1}{2}$	2, $\frac{5}{2}$	2, $\frac{3}{2}$
0	1	0	0	1	0	0	0	1	0	0	0
	0	1	0	0	1	0	0	0	1	0	0
−0.5	0.961	−0.252	0.112	0.884	0.269	−0.367	0.106	0.966	−0.163	0.193	−0.043
	0.234	0.961	0.149	0.033	0.721	0.665	0.193	−0.023	0.707	0.706	−0.039
−1.0	0.921	−0.348	0.174	0.862	0.274	−0.391	0.171	0.925	−0.207	0.311	−0.069
	0.271	0.895	0.353	0.058	0.618	0.709	0.335	−0.080	0.710	0.696	−0.062
−2.0	0.880	−0.411	0.238	0.798	0.443	−0.093	0.397	0.859	−0.156	0.475	−0.113
	0.200	0.776	0.597	−0.282	0.383	0.815	0.330	−0.216	0.751	0.618	−0.087

$$\psi^I_M(\varepsilon) = N_\varepsilon^{\,I}\int \mathrm{d}R\, \Phi^I_M(\varepsilon), \tag{12}$$

where

$$[N_\varepsilon^{\,I}]^2 \sum_{I_0, j}\left[\frac{a_\varepsilon^{\,I}(I_0, j)}{\sqrt{2I_0+1}N^{I_0}}\right]^2 = 1, \tag{13}$$

and N^{I_0} is defined by eq. (3). With these wave functions, the reduced transition probability for a transition of multipolarity λ between a low normal-parity state and one of the positive-parity levels is given by

$$B(Q\lambda; I \rightarrow I') = \frac{1}{(2I+1)(2I'+1)} \left| \frac{N_\epsilon^{\,I}}{N_{\frac{1}{2}}^{\,I'}} \sum_{I_0, j, k} a_\epsilon^{\,I}(I_0, j)\sqrt{2I_0+1}\,(I_0 j 0 k | I k) G_\lambda \right|^2, \tag{14}$$

where

$$G_\lambda = (I \lambda k \tfrac{1}{2}-k | I' \tfrac{1}{2}) g_{\lambda, \frac{1}{2}-k}(jk \rightarrow \tfrac{1}{2}4)$$
$$+(-1)^{I'+\frac{1}{2}} (I \lambda k -k-\tfrac{1}{2} | I'-\tfrac{1}{2}) g_{\lambda(-\frac{1}{2}-k)}(jk \rightarrow -\tfrac{1}{2}4)$$

and the $g_{\lambda\mu}$ are defined after eq. (5). From that definition it is apparent that the $g_{\lambda\mu}$ depend on the deformation of the C^{12} core through the dependence of $\phi_{\pm\frac{1}{2}, 4}$ on the Nilsson parameter η.

Just as in the strong-coupling case, there is a relation between the expression for the reduced transition probability given in eq. (14) and $\bar{B}$, the expression one obtains by using the wave functions in their "Bohr-Mottelson" form, eq. (11); this relation is

$$B(Q\lambda; I \rightarrow I') = \left(\frac{2}{2I'+1}\right) \left[\frac{N_\epsilon^{\,I}}{N_{\frac{1}{2}}^{\,I'}}\right]^2 \bar{B}(Q\lambda; I \rightarrow I'). \tag{15}$$

The little that is known experimentally about γ transitions in N^{13} is consistent with information in the C^{13} mirror nucleus, so we discuss mostly C^{13}. The transitions between levels of opposite parity in C^{13} are either E1 or M2 transitions. For the E1 transitions the operator including centre-of-mass correction is

$$Q_0^{\,1}(\mathrm{E1}) = e \sum_i \tau_p^{\,i}(z^i - Z_{\mathrm{CM}}),$$

which reduces to

$$Q_0^{\,1}(\mathrm{E1}) \rightarrow -\tfrac{1}{2}e\left(1-\frac{1}{A}\right)\tau_z z \tag{16}$$

for the single-nuclear operator appearing in the integrals for g_{10} of eq. (5). Similarly, when centre-of-mass corrections are neglected, the M2 operator for neutrons reduces to

$$Q_0^{\,2}(\mathrm{M2}) = \sqrt{10}\mu_{\mathrm{N}}\left(\frac{e\hbar}{2mc}\right) r \sum_\nu (1 1 \nu -\nu | 2 0) Y_\nu^{\,1} \sigma_{-\nu}^1, \tag{17}$$

where σ^1 is the Pauli spin vector. For protons there would also be an orbital contribution, but there is no M2 transition observed in N^{13}. In both of these matrix elements there will be radial integrals which are matrix elements of r. These are evaluated with harmonic oscillator functions, so the reduced transition probabilities for E1 and M2 transitions all include the factor $(1/\alpha)$ where α is the parameter appearing in the harmonic oscillator functions as $\exp\left[-\tfrac{1}{2}\alpha r^2\right]$.

When α is expressed in units of 10^{25} cm^{-2}, μ_N in nuclear magnetons and energy in MeV, the width for gamma transition (in electron volts) is given by

$$\Gamma(\mathrm{E1}) = 2.50\ \mathrm{E}^3 B(\mathrm{E1}; I \rightarrow I'), \quad \Gamma(\mathrm{M2}) = 2.13\times 10^{-7} \mathrm{E}^5 B(\mathrm{M2}; I \rightarrow I'). \quad (18)$$

The widths for E1 and M2 transitions in C^{13} are summarized in table 2 for several values of ξ. They are also given for the two values of the Nilsson parameter η that correspond to the most likely values for the C^{12} core. Since branching ratios are independent of the parameter α, widths are listed as the product $\alpha\Gamma$. An estimate of α can be obtained by starting with the electron scattering data in C^{12} which led to an expectation value of $\langle r^2 \rangle = 5.8\times 10^{-26}$ cm^2. For harmonic oscillator functions, this gives $\alpha \approx 4\times 10^{25}$ cm^{-2}. In C^{13} the positive-parity neutron probably has a greater value of $\langle r^2 \rangle$ if it is weakly bound, so $\alpha = 2\times 10^{25}$ cm^{-2} is a reasonable guess for a lower limit to α. The widths are calculated by use of eq. (14) for $B(Q\lambda; I \rightarrow I')$, and table 2 also lists the proportionality factor f between B and the Bohr-Mottelson expression for $\tilde{B}$, namely,

TABLE 2

Widths Γ_γ for various E1 and M2 transitions in C^{13}, as obtained by the generator procedure. Values are listed as a nction of the coupling parameter ξ for two values of the core-deformation parameter η. The parameter α is the armonic-oscillator range parameter in units of 10^{25} cm^{-2}, and the quantity $\alpha\Gamma$ is listed. A likely value for α is 2. The quantity f is the factor by which the "Bohr-Mottelson" width must be multiplied to get Γ.

	ξ	$\frac{5}{2}^+ \xrightarrow{\mathrm{E1}} \frac{3}{2}^-$		$\frac{5}{2}^+ \xrightarrow{\mathrm{M2}} \frac{1}{2}^-$		$\frac{3}{2}^- \xrightarrow{\mathrm{E1}} \frac{1}{2}^+$		$\frac{1}{2}^+ \xrightarrow{\mathrm{E1}} \frac{1}{2}^-$	
		f	$\alpha\Gamma$(eV)	f	$\alpha\Gamma$(eV)	f	$\alpha\Gamma$(eV)	f	$\alpha\Gamma$(eV)
$\eta = -6$	0	0.717	3.866×10^{-4}	1.197	6.192×10^{-4}	0.717	5.386×10^{-3}	1.197	1.831
	$-\frac{1}{2}$	0.718	1.568×10^{-4}	1.197	4.059×10^{-4}	0.717	1.699×10^{-3}	1.197	0.669
	-1	0.778	0.830×10^{-4}	1.297	3.225×10^{-4}	0.780	0.616×10^{-3}	1.303	0.529
	-2	0.834	0.327×10^{-4}	1.392	2.296×10^{-4}	0.815	0.060×10^{-3}	1.359	0.348
$\eta = -4$	0	0.479	1.861×10^{-4}	1.219	7.548×10^{-4}	0.479	2.593×10^{-3}	1.219	2.232
	$-\frac{1}{2}$	0.479	0.648×10^{-4}	1.219	5.387×10^{-4}	0.479	0.650×10^{-3}	1.219	1.045
	-1	0.529	0.300×10^{-4}	1.348	4.633×10^{-4}	0.533	0.152×10^{-3}	1.355	0.912
	-2	0.581	0.094×10^{-4}	1.476	3.633×10^{-4}	0.563	0.028×10^{-3}	1.433	0.695

$$f = \left[\frac{2}{2I'+1}\right] [N_\epsilon^I / N_{\frac{1}{2}}^{I'}]^2. \quad (19)$$

Before we can make a comparison with experiment, two more transitions between states of like parity must be calculated. One is the M1 transition from the $\frac{3}{2}^-$ state to the $\frac{1}{2}^-$ ground state while the other is the E2 transition from the $\frac{5}{2}^+$ state to the $\frac{1}{2}^+$ state. The M1 calculation has been done for N^{13} by Lane [5]) who finds that $\Gamma_{\mathrm{M1}} \approx 0.75$ eV for a value of spin-orbit coupling appropriate to this region. A similar calculation for C^{13} gives values for Γ_{M1} about 20 % lower than in C^{13}, so one obtains $\Gamma_{M1} \approx 0.60$ eV in C^{13}.

The E2 transition from $\frac{5}{2}^+$ to $\frac{1}{2}^+$ is most easily estimated by keeping the wave functions in the Bohr-Mottelson form, eq. (11). Aside from a small recoil correction, the E2 transition probability in C^{13} is simply related to that in C^{12}. The reduced matrix element is just

$$\langle \tfrac{1}{2}^+ \varepsilon \| Q^2 \| \tfrac{5}{2}^+ \varepsilon' \rangle = P(\tfrac{5}{2}^+ \to \tfrac{1}{2}^+) \int X_0{}^*(C^{12}) Q_0{}^2 X_0(C^{12}), \tag{20}$$

in which

$$P(\tfrac{5}{2}^+ \to \tfrac{1}{2}^+ +) = \sum_{I_0, I'_0, j} \sqrt{6(2I_0+1)}\,(I_0 2 0 0 | I'_0 0)\, W(j I_0 \tfrac{5}{2} 2; \tfrac{1}{2} I'_0)\, a_\varepsilon^{\frac{1}{2}}(I_0, j)\, a_{\varepsilon'}^{\frac{1}{2}}(I'_0, j), \tag{20'}$$

where W is a Racah coefficient, and the integral is the same one which occurs in the reduced matrix element for E2 transitions in C^{12}. Therefore we can relate the reduced transition probability to that for the transition from $I_0 = 2$ to $I'_0 = 0$ in C^{12} by the expression

$$B(\mathrm{E2}; \tfrac{5}{2}^+ \to \tfrac{1}{2}^+) = (\tfrac{5}{3}) P^2(\tfrac{5}{2}^+ \to \tfrac{1}{2}^+) B(\mathrm{E2}; 2^+ \to 0^+). \tag{21}$$

Notice that for the zero-order functions the factor P goes to zero since only $I_0 = 0 = I'_0$ occurs in the sum. For other values of ξ the factor is readily evaluated by use of the coefficients in table 1, and one finds that the ratio of reduced transition probabilities varies about linearly from 0 to 0.1 as ξ goes from 0 to 1. It soon falls again and does not get larger than 0.11. If we take the reduced transition probability for the C^{12} case from experiment and insert the energy factor, we find $\Gamma(\mathrm{E2}; \frac{5}{2}^+ \to \frac{1}{2}^+)$ is about $(1.0 \text{ to } 1.5) \times 10^{-7}$ eV in the range of ξ from 0 to -2†. From a comparison with the other widths involving the $\frac{5}{2}^+$ state, it would seem to have a relative strength of $\leqq 0.1$ % for the range of ξ in table 2. If one calculates via the generating procedure one can again make the comparison with C^{12} transitions; but strictly speaking one would need to know all the transition strengths in the C^{12} band. By assuming these are simply related by Clebsch-Gordan coefficients, one obtains answers within 30 % of the Bohr-Mottelson estimate given above.

The experimental results about the gamma transitions are mainly concerned with the branching ratios for decay from the $\frac{5}{2}^+$ and $\frac{3}{2}^-$ states as indicated in fig. 3. In addition there are some limits on the total gamma lifetimes obtained from experiments using the Doppler shift, but these limits are easily satisfied by the calculations. Breit-Wigner analyses of (p, γ) resonances in N^{13} give estimates for two E1 widths, namely, that the $\frac{3}{2}^- \to \frac{1}{2}^+$ transition [6]) has $\Gamma_\gamma = 0.04$ eV and that the $\frac{1}{2}^+ \to \frac{1}{2}^-$ transition [7]) has $\Gamma_\gamma = 0.67$ eV.

From table 2 one sees that in the range of ξ from 0 to -0.5 the percentages for M2 and E1 decay of the $\frac{5}{2}^{+}$ state are given in reasonable agreement with the observations listed in fig. 3. Including the E2 contribution one obtains, for example, 72 % M2, 28 % E1, and 0.05 % E2 with a total $\Gamma_\gamma = 2.8\times10^{-4}$ eV at $\xi = -0.5$, $\eta = -6$.

---

† The effect of recoil which is proportional to (z/A^2) increases this estimate by about 50 %.

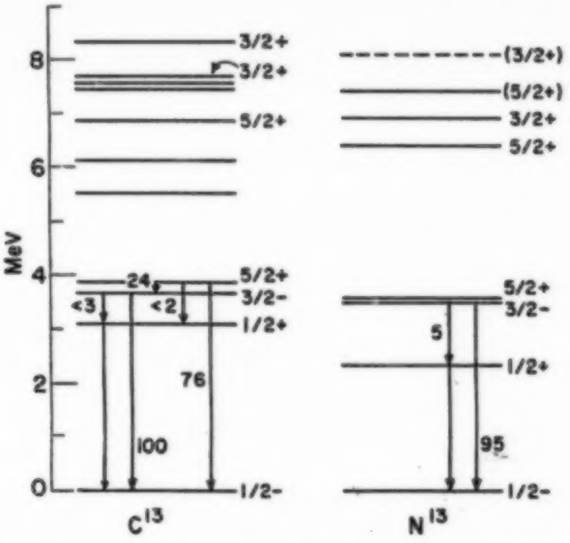

Fig. 3. Experimental data on the low levels of C^{13} and N^{13} (from F. Ajzenberg-Selove and T. Lauritsen 6)).

The decay of the $\frac{3}{2}^{-}$ state involves a competition between the M1 decay to the $\frac{1}{2}^{-}$ ground state and an E1 decay to the $\frac{1}{2}^{+}$ excited state. If one combines the branching ratio measurement in N^{13} with the determination of the E1 width, $\Gamma_\gamma(\mathrm{E1}) = 0.04$ eV, one obtains an M1 width, $\Gamma_\gamma(\mathrm{M1}) = 0.76$ eV. This is in excellent agreement with the calculation of Lane 5) cited previously. The predictions for the E1 width can be gotten from table 2 since the only difference between the C^{13} and N^{13} calculations is the energy factor. For $\eta = -6$ one obtains values between $\Gamma_\gamma(\mathrm{E1}) = 0.02$ eV for $\xi = 0$ and $\Gamma_\gamma(\mathrm{E1}) = 0.006$ eV for $\xi = -0.5$. Therefore it appears that the calculated E1 width is smaller than experiment[†] by a factor between two and seven, although it is a considerable improvement over the strong coupling result which is low by a factor of about 100.

Finally the calculated width for the E1 transition from $\frac{1}{2}^{+}$ to $\frac{1}{2}^{-}$ in N^{13}, adjusted for the different energy from the C^{13} case listed in table 2, lies between $\Gamma_\gamma(\mathrm{E1}) = 0.41$ eV for $\xi = 0$ and $\Gamma_\gamma(\mathrm{E1}) = 0.15$ eV for $\xi = -0.5$, $\eta = -6$. These values are again somewhat lower than the quoted 8) experimental result 7) $\Gamma_\gamma(\mathrm{E1}) = 0.67$ eV.

The spectrum in fig. 2 shows two low $\frac{3}{2}^{+}$ levels which can be identified with the levels at 7.64 MeV and 8.33 MeV in C^{13}. These levels are both excited in elastic scattering of neutrons on C^{12}, so that they must have a sizeable amount of C^{12} ground state in their parentage †. The probable mirror levels in N^{13} at 6.91 MeV and 8.08 MeV prefer to decay by proton emission to the first excited state of C^{12}, $I_0 = 2^+$, so they must also have a large fraction of this state in their parentage. By consulting table 1, one can see that both of these properties are satisfied for $\xi \neq 0$, and that by $\xi = -0.5$ the $I_0 = 0$ components are of magnitude comparable to that of the $I_0 = 2$ components. Thus there is qualitative agreement with what is observed.

[†] A similar measurement has been made recently by D. H. Wilkinson (private communication) for C^{13} who finds a branching ratio of $7\pm1\times10^{-3}$. This is consistent with the N^{13} measurement and greater than calculated by the same sort of factor as in N^{13}.

The general conclusion from comparison with experiment is that ξ should be small in order that the E1 transition probabilities are large enough to be of observed magnitudes. The evidence that ξ should not be zero comes from the E2 transition, $\frac{5}{2}^+ \rightarrow \frac{1}{2}^+$ which would be forbidden in the zero-order approximation, and from the presence of $I_0 = 0$ parentage in more than one of the $\frac{3}{2}^+$ states. The most likely value for ξ is somewhere between $\xi = 0$ and $\xi = -0.5$.

4. Core-Particle Coupling with Two-Body Interactions

In the previous section a comparison of calculation and experiment was made to obtain an idea of the magnitude of the parameter ξ which represents the strength of coupling between the C^{12} core and the positive-parity nucleon. Instead of this calculation wherein a single-particle quadrupole term provides the coupling, one could treat the problem with a conventional shell-model calculation, wherein the coupling is provided by the two-body interaction. By limiting oneself to the same zero-order representation as in the original problem one can see whether corresponding matrix elements have comparable values in the two calculations. One can thereby check the consistency of the two approaches and furthermore obtain an estimate of ξ from the interaction picture.

It is reasonable to suppose that the single-particle quadrupole-coupling term represents only the effect of the spatial part of the interaction, so any spin-dependence is omitted. If one makes the usual multipole expansion of the spatial interaction one obtains

$$V(|\mathbf{r}_1-\mathbf{r}_2|) = \sum_L f_L(r_1, r_2) P_L(\cos\theta_{12}). \tag{22}$$

Only the Legendre polynomials $L = 0, 2$ occur in the direct interaction integrals involving one 1p nucleon and one (2s, 1d) nucleon. If the $L = 0$ part contributes equally to all diagonal matrix elements it will not affect the wave functions or relative spacing one obtains from diagonalization. Numerical evaluation shows that the $L = 0$ contributions are all within a few hundred kilovolts of each other, so they can be lumped into the zero-order energies as an additive constant.

---

† A. M. Lane discusses this point in a treatment of what would be the $\xi = 0$ limit in an unpublished report (1955).

So far we have neglected the antisymmetrization between the positive-parity nucleon and the 1p-shell nucleons of the core. This plays no role in the original calculation where the coupling is done with a single-particle operator, but in the interaction calculation it will lead to exchange integrals. These will involve the multipoles $L = 1, 3$ in the interaction expansion, eq. (22), and affect the estimate of ξ.

The zero-order functions for the interaction calculations are simply related to the functions in eq. (8) by

$$U^I_M(I_0, j^+) = \sqrt{2I_0+1}\,N_0^{I_0}\int \mathrm{d}R\,\Phi^I_M(I_0, j^+) \\ = \sum_m (I_0 j^+ M-m m|IM)\,\psi^{I_0}_{M-m}\,\phi^{j^+}_m(x_n), \quad (23)$$

where j^+ refers to the positive-parity nucleon. The matrix elements of the interaction which couple the positive-parity nucleon n with the core are given in this representation as

$$\langle IM(I_0 j^+)|\sum_{q<n} V_{qn}|IM(\tilde{I}_0 \tilde{j}^+)\rangle.$$

A general expression can be obtained for these matrix elements which allows one to compare them with those of the original procedure. A complete comparison of these matrix elements with the corresponding ones from the previous calculation would be a long and tedious operation, so we restrict ourselves to the cases $I_0 = 0$ and $\tilde{I}_0 = 2$. This simplifies the expressions and in addition it is just these off-diagonal matrix elements which are dominant for the two low states $I = \frac{1}{2}^+$ and $\frac{5}{2}^+$ that are involved in the observed gamma transitions. The expression for the pertinent matrix elements is

$$\langle IM(0j^+)|\sum_{q<n} V_{qn}|IM(2\tilde{j}^+)\rangle = D-E, \quad (24)$$

where naturally $I = j^+$ and D and E are the direct and exchange integrals defined by

$$D = 8\sqrt{5}\,S^{(2)}(-1)^{\tilde{j}^+-j^+}(j^+2\tfrac{1}{2}0|\tilde{j}^+\tfrac{1}{2})\sum_{j,s,\bar{j}}\langle js, j|\}0\rangle\langle js, \bar{j}|\}2\rangle(j2\tfrac{1}{2}0|\bar{j}\tfrac{1}{2}), \quad (25)$$

$$E = 4\sqrt{5}\sum_{k\,\mathrm{odd}} S^{(k)}\sqrt{2\tilde{j}^++1}\sum_{j,s,\bar{j}}\langle js, j|\}0\rangle\langle js, \bar{j}|\}2\rangle \\ \times(-1)^{j^+-\bar{j}}\sqrt{2\bar{j}+1}\,W(j\tilde{j}^+\bar{j}j^+; k2)(j\tilde{j}^+\tfrac{1}{2}-\tfrac{1}{2}|k0)(\bar{j}j^+\tfrac{1}{2}-\tfrac{1}{2}|k0). \quad (26)$$

In these equations $\langle js, j|\}0\rangle$ is the fractional parentage coefficient for splitting off a single p-shell nucleon of spin j from the ground state of C^{12} and $\langle js\bar{j}|\}2\rangle$

is the analogous coefficient for taking out a p-particle with spin $\tilde{j}$ from the first excited state. The label s, which is summed over, defines a representation for the mass 11 states. These expressions contain the radial integrals involving the expansion coefficients of eq. (22). For k even, one has

$$(2k+1)S^{(k)} = \iint R^{1p}(r_1)R^{nl^+}(r_2)R^{1p}(r_1)R^{\tilde{n}\tilde{l}^+}(r_2)f_k(r_1, r_2)r_1^2r_2^2\mathrm{d}r_1\mathrm{d}r_2. \quad (27)$$

For k odd, one has

$$(2k+1)S^{(k)} = \iint R^{1p}(r_1)R^{nl^+}(r_2)R^{\tilde{n}\tilde{l}^+}(r_1)R^{1p}(r_2)f_k(r_1, r_2)r_1^2r_2^2\mathrm{d}r_1\mathrm{d}r_2. \quad (28)$$

The dependence of the direct integral D on the total angular momenta of the positive-parity states is seen to be quite simple. In fact, it is the same as the dependence exhibited by the corresponding matrix elements of the quadrupole coupling term, eq. (9). By equating corresponding matrix elements, one can therefore obtain an expression for the coupling parameter ξ of eq. (10), namely,

$$\xi = \left[\frac{2CS^{(2)}}{\sqrt{10}}\right]\left[1-\frac{E}{D}\right], \quad (29)$$

where

$$C = -2\sqrt{10}\sum_{js\tilde{j}} \langle js, j|\}0\rangle\langle js, \tilde{j}|\}2\rangle(j2\tfrac{1}{2}0|\tilde{j}\tfrac{1}{2})$$

is a factor which is unity in the jj-limit, but becomes about 1.5 in the range of intermediate coupling appropriate to C^{12}. The only remaining dependence on j^+ and $\tilde{j}^+$ is contained in the ratio (E/D), and if this could be reduced to a dependence on only the orbital angular momenta l^+ and $\tilde{l}^+$, the consistency of the corresponding matrix elements in the two approaches would be established.

In order to make numerical estimates one needs the radial integrals of eqs. (27) and (28). These have been evaluated on the assumption of a Gaussian dependence for the interaction and harmonic oscillator wave functions. The parameters have been taken from a previous calculation in the 1p-shell [9]), the same oscillator parameters being assumed for the 1p and positive-parity nucleons. The relative values of the radial integrals $S^{(k)}(nl^+, \tilde{n}\tilde{l}^+)$, labelled by the positive-parity nucleons involved, are $S^{(3)}$(1d, 1d) : $S^{(2)}$(1d, 1d) : $S^{(1)}$(1d, 1d): $S^{(1)}$(1d, 2s) : $S^{(2)}$(1d, 2s) equal to 0.89 : 1.77 : 2.77 : 0.80 : 1. The values of (E/D) then still depend on the degree of intermediate coupling in C^{12} through the coefficients of fractional parentage. By means of the generating procedure [1]) this can be expressed in terms of the Nilsson parameter, η. Table 3 lists the values of $[1-(E/D)]$ for the $I = \frac{1}{2}$ and $I = \frac{5}{2}$ cases as a function of η. It is apparent from table 3 that while for $\eta = 0$ there is a factor of two between the extreme values of $[1-(E/D)]$, because in this limit the exchange integral sometimes even differs in sign from the direct integral, by the time $\eta = -6$ the spread in values is less than 20 % of the average value.

Since eq. (29) shows that ξ is proportional to the integral $S^{(2)}(nl^+, \tilde{n}\tilde{l}^+)$ and the numerical evaluation gives $S^{(2)}(\text{1d, 1d}) = 1.77\, S^{(2)}(\text{1d, 2s})$, there will be different values of ξ for these two cases. One sees from eq. (10) that this merely implies that the corresponding radial integrals for these two cases are different, instead of being the same as was assumed in section 3 so this result is not inconsistent with the model. Putting numbers into eq. (29) for $\eta = -6$ leads to the value

$$\xi(\text{1d, 2s}) \approx -0.6.$$

TABLE 3

Values of $[1-(E/D)]$, where E and D are the exchange and direct integrals, respectively, for various pairs of positive-parity states $(j^+, \bar{j}^+)$. The quantity is given as a function of the Nilsson parameter η between the jj limit ($\eta = 0$) and the LS limit ($\eta = -\infty$). The value appropriate to experiment is $\eta \approx -5$

η \ $(j^+, \bar{j}^+)$	$\frac{1}{2}, \frac{5}{2}$	$\frac{1}{2}, \frac{3}{2}$	$\frac{5}{2}, \frac{1}{2}$	$\frac{5}{2}, \frac{3}{2}$	$\frac{5}{2}, \frac{5}{2}$
0	0.60	1.10	1.00	1.19	0.87
-2	0.64	1.03	0.95	1.03	0.86
-4	0.72	0.92	0.88	0.80	0.82
-6	0.76	0.86	0.84	0.72	0.77
$-\infty$	0.80	0.80	0.80	0.69	0.69

Not too much significance should be attached to the numerical value because of its dependence on the radial integrals. It may be possible to change the number by as much as a factor of 2 by variations in the potential parameters and the radial wave functions.

Nevertheless there is a strong indication from the interaction picture that the coupling parameter ξ is small. Furthermore the off-diagonal matrix elements† which are dominant for small ξ have comparable relative values in the interaction case and the quadrupole coupling case. Therefore the two approaches would lead to about the same wave functions for the lowest $I = \frac{1}{2}^+$ and $I = \frac{5}{2}^+$ states in which the $I_0 = 0$ component is dominant. Hence the predictions of gamma transition probabilities would also agree.

There are indications that the similarity of matrix elements in the two approaches extends beyond the particular ones investigated here. For example, the direct integrals with $I_0 = 2 = \bar{I}_0$ have the same dependence on j^+ and $\bar{j}^+$ in the interaction approach as in the quadrupole coupling case, so it is likely that there is a near congruence between the two approaches. There is also the question of having space-exchange in the interaction. This would certainly modify the estimate of ξ. When one of the simple matrix elements was evaluated. the resulting value of ξ was about 0.8 of the value with no space exchange, However, the object of the interaction calculation was only to obtain a magnitude estimate of ξ rather than to make a detailed comparison of matrix elements for various interactions.

---

† It should be noted that the exchange integral E also contributes to the diagonal elements. For $I_0 = 0$ these contributions were found to be all about the same. If they are about alike for $I_0 = 2$, any difference between the cases for $I_0 = 0$ and $I_0 = 2$ can be lumped with the zero-order splitting of the rotor energy.

5. Summary and Conclusions

The properties of the positive-parity states in mass 13 nuclei have been investigated using a model in which there is a quadrupole coupling of variable strength between the positive-parity particle and the C^{12} core. A theoretical estimate based on the effect of the $L = 2$ component of two-body interactions favors weak coupling. However, this calculation is not sufficiently reliable to give more than a rough estimate of the coupling strength so one must see whether comparison with experiment is more definitive.

The relative spacing of the positive-parity levels in C^{13} is not a sensitive indication of the coupling strength ξ, since the calculation agrees with the present experimental evidence over a wide range of ξ. Therefore one must turn to the transition probabilities for evidence.

The strong coupling model seems inadequate chiefly because it predicts strongly reduced E1 transition probabilities. The observed transitions seem to be 100 to 1000 times more likely than predicted. The small calculated values are a manifestation of the selection rule which in the asymptotic limit of large deformation forbids E1 transitions between such states as come into the calculation. Even when the deformation is of the magnitude expected for C^{12} there still remains a large effect of this selection rule so that the E1 transitions are very weak.

The E1 transitions calculated with weak coupling have the same magnitude as the observed transitions, but they still appear to be somewhat weak. However, this may be due to the fact that we have not adequately taken into account the rather small binding energy of the states involved. (Excluding the ground state of C^{13} all the levels considered are bound by less than 2 MeV.) Instead of the oscillator potential one should take some finite well which would give the nuclear wave function a longer tail. This could mean that we have underestimated the square of the matrix element of r by something like a factor of two. However, such an effect would be of little help if one retained strong coupling because the large degree of forbiddenness is not caused by a lack of overlap of radial functions. It is rather the result of the fact that the nucleon distributions have different shapes in the two states — namely, prolate for the positive-parity state and oblate for the negative-parity state. Therefore, the experimental results on E1 transitions are evidence for weak coupling.

The recent measurement [10]) of the E2 branch in the decay of the $\frac{5}{2}^+$ state in C^{13} presents a serious problem for the theory. The measured strength of this branch is (0.9 ± 0.2) %, which is much greater than the calculated 0.05 % obtained in weak coupling. The reason for the latter small value is the relatively small amount of $I_0=2$ state from C^{12} in the parentage of the C^{13} functions. It might appear that this is an argument for strong coupling since those wave functions have very strong $I_0 = 2$ components of parentage. However, the strong coupling estimate also gives a weak E2 branch, primarily because the initial and final states come from bands of different K. The E2 strength is proportional to the strength of the $K = \frac{1}{2}$ component in the $I = \frac{5}{2}^+$ wave function. This amount of $K = \frac{1}{2}$ function is about 5 % in intensity for band mixing with the Nilsson levels as in fig. 1.

In order to obtain the relative order of the $\frac{5}{2}^+$ and $\frac{1}{2}^+$ levels in the C^{13} spectrum it is necessary to lower the position of the jj-limit of the $2s_{\frac{1}{2}}$ state in fig. 1. Even then the intensity of the $K = \frac{1}{2}$ component after band-mixing does not exceed 10 %, and the resultant E2 strength in strong coupling is about the same as one calculates with weak coupling. Therefore it does not seem that either calculation can explain the observed strength.

It is possible that some of the difficulty lies in the calculation of the M2 transition from the same $\frac{5}{2}^+$ state to the $\frac{1}{2}^-$ ground-state. This was calculated without including centre-of-mass corrections, and resulted in a value about that of a single particle transition. If the corrections were to reduce the calculated value for M2, our estimate of the relative strength of the E2 transition would go up, and since the E1 strength varies rapidly with ξ one might also be able to obtain the proper relative strength of the E1 branch without too much trouble. However, it is extremely unlikely that this would provide anything like the factor of 10 to 20 by which one must increase the calculated relative strengths of E2 to M2 in order to suit experiment. It would be of great interest to obtain an experimental value for the total transition probability from the $\frac{5}{2}^+$ state to check the calculated value of $\Gamma = 2.8\times10^{-4}$ eV.

The general conclusion from our investigation is that the evidence favors weak quadrupole coupling between the positive-parity nucleon and the C^{12} core. The wave functions of the lowest $\frac{1}{2}^+$ state and the lowest $\frac{5}{2}^+$ state have a parentage which consists predominately of the C^{12} ground state. The calculation of the $L = 2$ components in the interaction is consistent with this picture.

One might wonder whether such a picture is not contradictory to the fact that the positive-parity states in C^{13} and N^{13} lies quite low relative to the negative-parity ground state. There are two factors which give a qualitative idea that there need not be any contradiction. In the first place, one must remember that only the $L = 2$ components of the interaction are needed to obtain the positive-parity wave functions above. The $L = 0$ components actually contribute the major part of the binding energy between particle and core, and these integrals have the same order of magnitude whether only 1p radial functions are involved or whether a (2s, 1d) radial function and a 1p function occur. In the second place, the core consists mainly of the C^{12} ground state which has especially strong binding.

For the negative-parity states since the situation is far from the *jj*-limit, it is not meaningful to make the same separation into core and core-particle contributions. The reason is that the single-nucleon function which is added to the C^{12} core has strong components in common with some of the functions within the core. Therefore the Pauli principle will have a large effect. All one can say is that the system will have a binding energy per nucleon that is appreciably smaller than it is in the C^{12} ground state.

Therefore our general picture can be consistent with the observed binding energies. It would require calculation to see whether the effects mentioned above can give quantitative agreement. A necessary ingredient for the arguments above is the especially stable C^{12} core. If this were not present, the effects of the Pauli principle would not be important. For example, the B^{11}, C^{11} nuclei have no such stable core, so one should not expect low-lying positive-parity states there. On the other hand, Be^9 does have such a core, and there is evidence [11]) that a weak-coupling picture accounts for the low positive-parity state there.

The authors would like to thank Professor D. H. Wilkinson for stimulating this investigation by communicating some experimental results.

References

1) D. Kurath and L. Pičman, Nuclear Physics **10** (1959) 313
2) S. G. Nilsson, Mat. Fys. Medd. Dan. Vid. Selsk. **29**, No. 16 (1955)
3) D. Strominger and J. O. Rasmussen, Nuclear Physics **3** (1957) 197
4) G. Alaga, Phys. Rev. **100** (1955) 432; Nuclear Physics **4** (1957) 625
5) A. M. Lane, Proc. Phys. Soc. (London) A **68** (1955) 197
6) Woodbury, Tollestrup and Day, Phys. Rev. **93** (1954) 1311
7) J. D. Seagrave, Ph. D. Thesis, California Institute of Technology (1951)
8) F. Ajzenberg-Selove and T. Lauritsen, Nuclear Physics **11** (1959) 1
9) D. Kurath, Phys. Rev. **101** (1956) 216
10) Pixley, Kane and Wilkinson, Phys. Rev. Lett. **5** (1960) 226 (abstract)
11) F. R. Paolini, Ph. D. Thesis, Massachusetts Institute of Technology (1960)

8.A

Nuclear Physics **23** (1961) 23—31; © *North-Holland Publishing Co., Amsterdam*

Not to be reproduced by photoprint or microfilm without written permission from the publisher

CONSERVATION OF μ^+-MESON POLARIZATION IN EMULSION WITH AID OF MAGNETIC FIELD

A. O. WAISSENBERG and V. A. SMIRNITSKY

Experimental and Theoretical Physics Institute, Academy of Sciences of the U.S.S.R., Moscow

Received 15 July 1960

Abstract: The space asymmetry coefficient in $\pi^+ \rightarrow \mu^+ \rightarrow e^+$ decay is measured as a function of external magnetic field in the 0-17 kG range. It is shown that this dependence can be explained by the Paschen-Bach effect for muonium and the assumption that there is additional polarization owing to charge-exchange at the end of the μ-meson path, or to exchange collisions after the μ-meson has stopped. The minimum value of the asymmetry coefficient for NIKFI-R emulsions is equal to -0.09 ± 0.01 (without a magnetic field); the maximum value is equal to 0.29 ± 0.01 (in a strong field). The 10 % difference between the coefficients -0.29 ± 0.01 and -0.33 predicted by the V−A theory is far outside the limits of experimental errors.

Among 340 000 $\pi^+ \rightarrow \mu^+ \rightarrow e^+$-decays scanned we have not detected a single decay into 3 electrons corresponding to the schemes $\mu \rightarrow 3e$ or $\mu \rightarrow e+\nu+\bar{\nu}+\gamma$ with the internal conversion of a γ-ray into an e^+-e^- pair.

1. Introduction

The discovery of non-conservation of parity in $\pi \rightarrow \mu \rightarrow e$ decays led to an experimental study of muonium, a new hydrogen-like atom which is a stable system composed of a μ^+-meson and an electron. This system can be formed when the velocity of a slowing μ^+-meson becomes comparable with the velocities of atomic electrons of the medium. While slowing down, the μ^+-meson, just like a retarding proton, captures and loses a number of electrons in succession ("charge-exchange") and finally attains thermal velocities either in a free or bound state. As a result of the ionization process the μ^+-meson sufficiently slowed down can no longer capture or lose electrons and now its interaction with electrons may consist in the electron exchange with electrons of the medium. The initial formation of muonium and subsequent charge-exchanges and electron exchanges with the unpolarized electrons of the medium may explain μ^+-meson depolarization observed experimentally in various substances. To check these assumptions experimentally we investigated the effect of a permanent magnetic field on the μ^+-meson polarization value. This phenomenon was also studied in refs. [1–4]). Since the assumed depolarization mechanism is the interaction of the μ^+-meson and electron magnetic moments in the ground state of muonium (hyperfine splitting), a strong magnetic field decoupling the two magnetic moments (Paschen-Bach effect) should decrease the depolarization and, consequently, preserve space asymmetry in the angular distribution of positrons from $\mu^+ \rightarrow e^+$-decay. It can be shown [5]) that an increase in polarization P due to the magnetic field is given by

$$P = 3a = \xi(0.5+0.5x^2/1+x^2) \tag{1}$$

where $x = H/H_0$ is the ratio of the applied magnetic field to the mean internal field $H_0 = 1580$ gauss produced by the magnetic moment of μ^+-meson in the electron orbit in muonium, and ξ is the asymmetry parameter which determines the degree of longitudinal polarization of μ^+-mesons in $\pi^+ \rightarrow \mu^+$-decays and equal to the tripled coefficient of space asymmetry a in $\pi \rightarrow \mu \rightarrow e$-decays [6]).

It follows from this formula firstly that there is practically no depolarization $P \rightarrow \xi$ in fields of the order of a 10kOe ($x^2 \gg 1$), and secondly that in weak magnetic fields ($x^2 \approx 0$) the polarization must be equal to half its maximum value ξ.

The aim of the present work is to investigate the dependence of the asymmetry coefficient in $\pi^+ \rightarrow \mu^+ \rightarrow e^+$ decays observed in NIKFI-R emulsions as the external magnetic field varied in the 0—20 kOe range. We have measured the asymmetry coefficients in NIKFI-R emulsions carefully shielded from the field ($H = 0$) and in fields of 54, 110, 206, 420, 680, 1300, 1900, 2500, 3500, 5100, 6300, 14000 and 17000 Oe. To shield off the magnetic field in the experimental area of the synchrocyclotron, the emulsion stack was protected by a double magnetic shield of soft steel, the vertical component of the magnetic field in the centre of the shielded volume being less than 10^{-2} Oe. Small fields of the order of 54—420 Oe were produced by an ironless solenoid, with inner diameter 16 cm, placed in a double cylindrical magnetic shield. To produce fields of 1900 to 6300 Oe we used a solenoid with inner diameter of 14 cm surrounded by a powerful iron magnetic shield. The resultant field in the emulsion volume was uniform up to 1 %. Exposures in fields of 14 and 17 kOe were performed in a special electromagnet and we are thankful to I. I. Gurevich for making it available to us.

2. Exposure and Scanning

The 10×10 or 10×15 cm^2 emulsion stacks of 50—100 NIKFI-R emulsion pellicles 400μm thick, shielded during the exposure in the field $H = 0$ or placed in the appropriate magnetic field parallel to the emulsion plane, were exposed to a π^+-meson beam from the synchrocyclotron of the Joint Institute for Nuclear Research. The absorbers placed after the collimator were chosen in such a way as to make π^+-mesons slow down in the central part of the emulsion stack.

In the presence of the magnetic field the usual formula of angular correlation $dN \propto (1+a\cos\vartheta)d\cos\vartheta$ used in the analysis of the data is conveniently replaced by another formula

$$dN \propto (1+a\cos\gamma\cos\beta)d\cos\gamma\, d\cos\beta,$$

where γ and β are the angles of muon and electron emission with respect to the direction of the magnetic fied. The asymmetry coefficient was therefore measured in the following way. A scale with two perpendicularly crossing lines was placed in the field of vision of a microscope. The scale was oriented so as to make the magnetic field direction a bisector of the right angle formed by the scale lines. The scanners recorded those $\pi^+ \rightarrow \mu^+ \rightarrow e^+$ events, within a given emulsion pellicle, in which the projections of γ and β angles on the emulsion plane were within $0 \pm 45°$ (the first square of the scale) or within $180 \pm 45°$ (the third square) and the peak of $\mu^+ \rightarrow e^+$ decay was removed from the surface of the emulsion or glass by no less than 50 μm. With these selection criteria 99442 $\pi^+ \rightarrow \mu^+ \rightarrow e^+$ events were recorded in different magnetic fields. Out of these there are 20 events in which no positron from the $\mu \rightarrow e$ decay was observed. If N_B is the number of decays with the projections of γ and β angles lying in one square of the scale (the first or the third square) and N_H is the number of decays with the projections of these angles lying in the opposite squares, then the asymmetry coefficient a is equal to

$$a = \mathrm{K}\frac{N_B - N_H}{N_B + N_H} \pm \frac{K}{\sqrt{N_B + N_H}}.$$

The coefficient $K = 1.57$ provided all μ^+-meson tracks are assumed, in the first approximation, valid within several per cent, to lie in the emulsion plane and all the electron tracks distributed isotropically over the vertical angle.

Table 1 lists the measured values of N_H and N_B and the calculated asymmetry

TABLE 1

Measured values and calculated coefficients. The value of a for $H = 0$ is obtained in two runs of measurements. In the first run all the angular distribution was measured, in the second run measurements were similar to those for $H = 0$. The given value is the weighted mean of both runs of measurements

Magnetic field (Oe)	N_B	N_H	$N = N_B + N_H$	$-a$
$<10^{-2}$	7363	8270	15633	0.093 ± 0.013
54	3005	3477	6482	0.117 ± 0.020
110	3133	3592	6725	0.110 ± 0.020
206	2897	3247	6144	0.093 ± 0.020
420	2778	3317	6095	0.142 ± 0.020
680	3921	4718	8639	0.149 ± 0.017
1300	4052	4830	8882	0.142 ± 0.017
1900	2214	2692	4906	0.155 ± 0.022
2500	3246	4200	7446	0.206 ± 0.020
3500	2854	3589	6443	0.185 ± 0.020
5100	2619	3339	5958	0.196 ± 0.020
6300	2384	3319	5703	0.265 ± 0.021
14000	1333	1848	3181	0.262 ± 0.028
17000	2977	4228	7205	0.282 ± 0.018

coefficients for the magnetic employed fields, a 3 % correction being introduced into the value $K = 1.57$ which takes into account the distribution of μ^+-meson and positron tracks over vertical angles [2]). To make sure that there are no systematic errors in the asymmetry coefficients thus measured we conducted a control series of measurements which consisted in calculating the number of electrons emitted not "forward" or "backward" but "to the left" or "to the right", i.e., the number of electrons emitted in the β angle interval equal to 90±45° and 270±45° (the second and the third squares of the scale). These measurements yielded $N_{\text{left}} = 4213$, $N_{\text{right}} = 4196$, hence

$$\frac{N_{\text{left}}-N_{\text{right}}}{N_{\text{left}}-N_{\text{right}}} = \frac{17}{8409} \approx 2\times 10^{-3},$$

which shows that there are no systematic errors.

3. Discussion of the Results

The data obtained on the asymmetry coefficients in different fields are given in table 1 and fig. 1 in which the quantity $x^2/1+x^2$ is marked off on the absciss

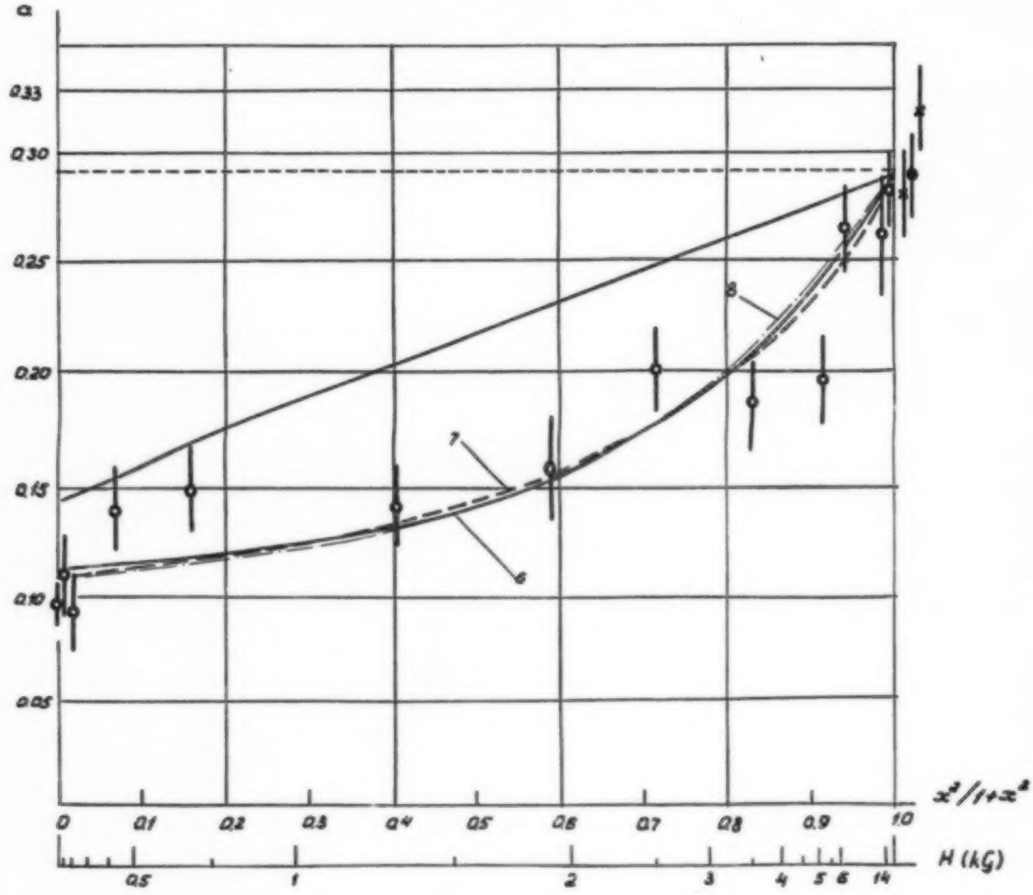

Fig. 1. The asymmetry coefficient a versus the field strength H.

axis and the asymmetry coefficient measured on the ordinate axis. Since the values of the asymmetry coefficient in the zero field and very strong fields are of particular importance in analyzing the data obtained, we shall first of all consider these values. Our value is $a = -0.093 \pm 0.13$ which coincides with the value $a = -0.092 \pm 0.018$ obtained in ref. 1) with the same NIKFI-P emulsion.

Our value of a at the maximum field of 17000 Oe is equal to $a = -0.282 \pm 0.018$ Table 2 lists our and all other known values in strong fields. To avoid complicating fig. 1, the values of coefficient a are taken from table 2 (H = 20, 25 and 27 kOe) and plotted outside the line $x^2/1+x^2 = 1$.

TABLE 2

Values of a

Authors	H (kOe)	$-a$	Notes
Our data	17	0.282 ± 0.18	
Lych *et al.* 7)	25	0.290 ± 0.013	black circle in fig. 1
Ali-Zade *et al.* 8)	20	0.28 ± 0.020	crosses in fig. 1
	27	0.320 ± 0.020	

Averaging these groups of consistent data we obtain $a = -0.292 \pm 0.009$. It follows from (1) that the value of a in strong magnetic fields ($H \gg H_0$) yields directly $\xi = 3a$. Thus, $\xi = 0.88 \pm 0.03$. The value of $\frac{1}{3}\xi$ is plotted in fig. 1 by a dotted line.

A straight line in the same figure reflects the dependence on $x^2/1+x^2$ which follows from formula (1). It can be seen that the experimental data obtained show no agreement at all with this dependence and, generally, with the assumption of the linear increase of the coefficient a. This points to the existence of a depolarization mechanism in addition to the one described by eq. (1). A charge-exchange of electron exchange between the muonium formed and the medium may be this mechanism as was mentioned above. Since the electrons of the medium are not polarized, each such exchange causes further "dilution" of the remaining polarization so that several exchanges are suffiecent to decrease drastically or even destroy the polarization of μ^+-mesons in weak fields. Sens *et al.* 9) derived the following depolarization formula which is a simple generalized version of eq. (1) for the case when all exchanges n take a longer time than the hyperfine splitting period, but an essentially shorter time than the μ^+-meson lifetime:

$$P = \xi \left[\frac{1+2x^2}{2(1+x^2)} \right]^n . \tag{3}$$

For $n = 1$ this formula becomes identical to eq. (1) and for $x^2 \to \infty$ $P \to \xi$ in a way similar to eq. (1).

Under the assumption that all exchanges occur within the entire lifetime of μ^+-mesons, Perelomov [10]) obtained the following formula for polarization:

$$P = \xi\left(1-\frac{1}{2\Delta^2}\right)\left(\frac{1}{1+W/\Delta^2}\right), \tag{4}$$

where $\Delta^2 = 1+x^2$ while W is the number of exchange collisions during the μ^+-meson lifetime. Like the preceding formula this formula becomes identical to (1) at $W = 0$ and the polarization is completely restored in strong fields ($P \to \xi$ at $x^2 \to \infty$).

Finally, Ferrell, Lee and Pal [11]) considered a different mechanism of additional polarization. They assumed that the latter is caused not by exchange but by charge-exchange, i.e., that the slowed down, yet sufficiently fast μ^+-meson captures and loses its electron several (n) times. Each capture is on the average τ long (τ is the mean lifetime of muonium in units of $\hbar/\Delta E = 3.6\times10^{-11}$). The formula which they obtained,

$$P = \xi\left(1-0.5\,\frac{1}{1+\tau^{-2}+x^2}\right)^n, \tag{5}$$

also displays limiting processes similar to those indicated before.

In analyzing our data one has to take into account the fact that some μ^+-mesons stop in gelatine in which depolarization is either small or absent and some in AgBr crystals, responsible for the greater part of depolarization [10]). The ratio f of the number of stoppings in gelatine to that in AgBr is equal under these assumptions to $f = 0.093+0.01/0.292\pm0.09 = 0.32$ and we obtain the following dependence for our data:

$$P = 3a = \xi\left[f+(1-f)\left(1-0.5\,\frac{1}{1+\tau^{-2}+x^2}\right)^n\right]. \tag{6}$$

A similar analysis can also be performed for the dependence of the asymmetry coefficient on the field described by eqs. (3) and (4) derived under the assumption of additional depolarization owing to electron exchange. The collision itself is characterized in this case by only the parameter W (7) or n (8); a second parameter which we can obtain in this case is the quantity $K = \rho(1-f)$, where $(1-f)$ is the relative number of stoppings in AgBr, and ρ is the probability of muonium production in these stoppings.

The corresponding eqs. (3) and (4) have the form

$$P = \xi\left[(1-K)+K\left(1-\frac{1}{2\Delta^2}\right)\left(\frac{1}{1+W/\Delta^2}\right)\right], \tag{7}$$

$$P = \xi\left[(1-K)+K\left\{\frac{1+2x^2}{2(1+x^2)}\right\}^n\right]. \tag{8}$$

Our data were compared with eqs. (6), (7) and (8) by the least squares method. We have looked for the values of parameters τ and n (eq. 6) or K and W (eq. 7), or K and n (eq. 8) which minimize the function

$$\chi^2 = \sum_{i=1}^{14} \frac{N_i}{1.57^2} (\Delta a_i)^2.$$

The data obtained are represented in table 3 and fig. 1. The first column of the table indicates the formula used in the analysis, the second the estimated values of the corresponding parameters, the third the value χ^2 which corresponds to these parameters, the fourth the quantity $P(\chi^2 > \chi_{\min})$.

TABLE 3
Parameter values

Formula	Parameters	χ^2 (min)	P (%)
(6)	$\tau = 1.3,\ n = 7$	21	7.0
(7)	$W = 3.3,\ K = 0.7$	18	15
(8)	$n = 6,\ K = 0.65$	18	15

Fig. 1 shows the curves described by eqs. (6), (7) and (8) for the parameter values indicated in table 3.

It can be seen that agreement is fairly good in all three cases. Thus the assumption of several charge-exchanges at the end of the path or of several exchanges after the stopping, is sufficient to account for the measured dependence of the asymmetry coefficient on the field. The difference between the quantities $\chi^2_{\min}$ is too small to decide in favour of one of the three possibilities.

4. Conclusions

The above data on the dependence of the asymmetry coefficient on the external field strength lead us to the following conclusions:

1) The asymmetry coefficient changes from $a = -0.09 \pm 0.01$ without a field to $a = -0.29 \pm 0.01$ in fields of 17 to 27 kilogauss.

2) The measured dependence of the asymmetry coefficient on the field in the 0—17 kG range is inconsistent with the assumption of the linear dependence of this coefficient on the value $x^2/1+x^2$ which follows from eq. (1) for the polarization induced by the Paschen-Bach effect in muonium.

3) Our data are in sufficiently good agreement with μ^+-meson depolarization through muonium production under the assumptions either that muonium undergoes several electron exchanges with the medium after the slow-down or that several charge-exchanges of muonium occur at the end of the μ^+-meson path. Our data do not make it possible to distinguish between these two mech-

anisms of additional "dilution" of the initial polarization. From the electronic measurements [10]) it follows that the depolarization time is less than 10^{-6} sec. This gives grounds for preferring eq. (8) to eq. (7) though both are in equally good agreement with our data. The mechanism proposed by Ferrell *et al.* [9]) (eq. (6)) also accounts for very fast depolarization. Being universal, this mechanism has considerable advantage over the exhange mechanism. More universal. the charge-exchange of muonium occurs in all substances quite unlike electron exchange.

4) The asymmetry coefficient $a = -0.29 \pm 0.01$ observed in the strongest magnetic fields is 10 % less than the value of $a = -\frac{1}{3}$ predicted by the V—A interaction theory [15]). This difference is beyond the limits of measurement errors and cannot be explained by systematic experimental errors. Rather this difference is to be attributed either to an additional 10 % depolarization in emulsion which is unrestored by the magnetic field and the mechanism of which is not clear, or to the fact that the assumption of V—A-intearction is not sufficient for describing the asymmetry in $\mu \rightarrow$ e-decay.

5) In the course of our present and previous works [2]) we have scanned about 340000 $\pi^+ \rightarrow \mu^+ \rightarrow e^+$ decays. Special care was taken in detecting the decays of a μ^+-meson into three electrons, i.e., $\mu \rightarrow 3e$ or $\mu \rightarrow e+\nu+\bar{\nu}+\gamma$ with the internal conversion of γ-quantum into an electron pair (several decays of the latter type were observed in refs. [13, 14]). The efficiency of detecting these decays should be rather close to unity. Not a single authentic event of such decays was detected; some likely events of the second type are explained by the accidental overlapping of slow electron tracks.

The authors are thankful to A. I. Alikhanov for his interest in the work, D. M. Samoilovich who kindly permitted to use his laboratory facilities for developing the emulsion stacks, Ya. B. Zeldovich and A. M. Perelomov for calculating the depolarization due to exchange, L. P. Panova for estimating parameters on the R.V.M. computer, and the members of the scanning team.

References

1) I. I. Gurevich, V. M. Katukova, A. P. Mishakova, B. A. Nikolsky and L. B. Surkova, JETP **34** (1958) 280
2) A. O. Waissenberg, I. B. Rabin and V. A. Smirnitsky, JETP **36** (1959) 1680
3) J. Orear, G. Harris and E. Bierman, Phys. Rev. **107** (1957) 323
4) W. Barkas, P. S. Giles, H. H. Heckman, F. W. Inman and F. M. Smith, Phys. Rev. **107** (1957) 911
5) R. A. Ferrell and F. Chaos, Phys. Rev. **107** (1957) 1322
6) T. Kinoshita and A. Sirlin, Phys. Rev. **108** (1957) 844
7) G. Lynch and J. Orear, preprint;
G. Lynch, J. Orear and S. Rosendorf, Phys. Rev. Letters **1** (1958) 471 No. 12
8) S. A. Ali-zade, P. P. Gurevich, Yu. P. Dobretsov, B. A. Nikolsky and L. B. Surkova, JETP **36** (1959) 1327

9) Sens, Swanson, Telegdi and Yovanovitch, Phys. Rev. **107** (1957) 1465
10) Perelomov, JETP (in the press)
11) R. A. Ferrell, J. Lee and Pal (preprint)
12) R. A. Swanson, Phys. Rev. **112** (1958) 580
13) P. P. Gurevich, B. A. Nikolsky and L. V. Surkova, JETP **37** (1959) 318
14) J. Lee and N. R. Samios, Phys. Rev. Letters **3** (1959) 55
15) R. Feynman and M. Gell-Mann, Phys. Rev. **109** (1958) 193—198

2.H

Nuclear Physics **23** (1961) 32—39; © *North-Holland Publishing Co., Amsterdam*

Not to be reproduced by photoprint or microfilm without written permission from the publisher

COULOMB EXCITATION OF Au^{197} AND W^{186} BY PROTONS OF ENERGY UP TO 12.6 MeV

A. V. COHEN and J. A. COOKSON

Atomic Weapons Research Establishment, Aldermaston, Berkshire

Received 17 November 1960

Abstract: The excitation function for inelastic scattering of protons of energies between 6.7 and 12.6 MeV from Au^{197}, exciting the 279 keV level and the 548 keV level, has been determined. Results are compared with the predictions of semi-classical theory, and reasons for possible discrepancies are discussed. The (2+) nature of the 730 keV level in W^{186} has been confirmed.

1. Introduction

The Tandem Electrostatic Generator [1]) produces protons and deuterons of energy up to 12.6 MeV. A double-focussing magnetic particle spectrometer [2]) deflects protons of this energy through 180° with an energy resolving power of 850, a solid angle of 0.007 steradians and a low background. With this apparatus, the inelastically scattered protons associated with the Coulomb excitation of Au^{197} have been observed. Elbek and Bockelman [3]) studied the process at 6 MeV proton energy with results in good agreement with the semiclassical Coulomb excitation theory as reviewed by Alder *et al.* [4]); the present work extends observations to 12.6 MeV, where the classical distance of closest approach is only $1.12\times 1.2(A_1^{\frac{1}{3}}+A_2^{\frac{1}{3}})\times 10^{-13}$ cm.

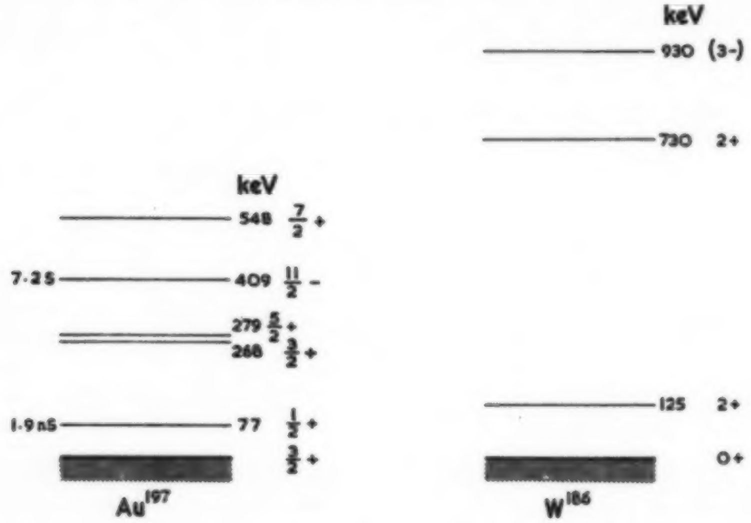

Fig. 1. Level schemes for Au^{197} and W^{186}.

Inelastic proton scattering from W^{186} has also been examined. Gamma rays from a (2+) level at 125 keV excitation have been observed at lower bombarding energies by many workers [4]) while gamma rays from another (2+) level at 730 keV have been observed by Barloutaud *et al.* [5]), McGowan and Stelson [6]) and Alkhazov *et al.* [7]), the first two using protons of 4—5 MeV, and the Russian workers using alpha particles of 8.3—14.5 MeV. This 730 keV level did not appear with the expected intensity when W^{186} was bombarded with oxygen ions up to 35 MeV (D. Eccleshall, private communication), and it was decided to examine protons inelastically scattered so as to excite this level. Another level, believed to be (3−), is said [8]) to exist at 930 keV, and an upper limit has been placed on the excitation of this.

Fig. 1 shows the level schemes of Au^{197} and W^{186}, as summarised by Strominger *et al.* [9]) and Dzelepov and Peker [8]) respectively.

2. Experimental Method

The vertical proton beam, accelerated to energies up to 12.6 MeV in the Tandem Electrostatic Generator, and stabilised to about ±1 keV, was deflected magnetically into a horizontal direction, and focussed by magnetic quadrupoles on to thin foil targets, being collimated by a 0.24 cm diameter stop, 38 cm before the target. The beam was collected in a Faraday cup 10 cm after the target, and measured by a current integrator; beams of 0.5 μA were available up to 12 MeV, while the beam was 0.05 μA at 12.6 MeV.

The target, at the axis of the magnetic particle spectrometer, was situated inside a target chamber, which was connected to the spectrometer vacuum box by a sliding seal, thus enabling reaction product spectra to be viewed at any angle to the incident proton beam from −10° to +130°.

Particles passing through an adjustable slit at the focus of the spectrometer were detected in a 2 mm thick CsI crystal mounted on a Du Mont 6292 photomultiplier, and then counted by a discriminator and scaler. Peaks associated with a given level in the target nucleus were explored by noting the protons counted per unit beam as a function of magnet current, the detector slit being set to accept only part of a group. The proton resonance frequency at a standard field position measured the $H\rho$ of the peak maximum.

The elastic yield was measured by the corresponding peak height. To measure with reasonable statistical accuracy the much lower inelastic peak yields, the mean of three points straddling the peak was taken, and related to the peak value by an analysis of the elastic peak forms. This procedure was adopted since the peak area is not a true measure of yield; the peak width may be altered by variation of beam distribution upon the target during the time taken to traverse the peak (30 minutes at 11 MeV and 3 hours at 12.6 MeV). In this way the strength of an inelastic peak could be related to that of the elastic peak at the same energy, with an error of ±10 %.

With this apparatus, and the target thicknesses used, cross-sections of order 40 μb/sr could be detected.

3. Results

3.1. Au^{197}

Targets of 200 μg/cm^2 self-supporting gold leaf were set at 0° to the incident beam, to observe at backward angles, where the ratio of Coulomb to elastic scattering was likely to be enhanced. One of the main sources of energy spread was then that due to target thickness (8 keV at 12 MeV). Fig. 2 shows an exploratory spectrum observed at 130° to an incident beam of 10.62 MeV protons. Peaks observed in this and other runs were identified by the variation of their $H\rho$ with energy and angle, and included:

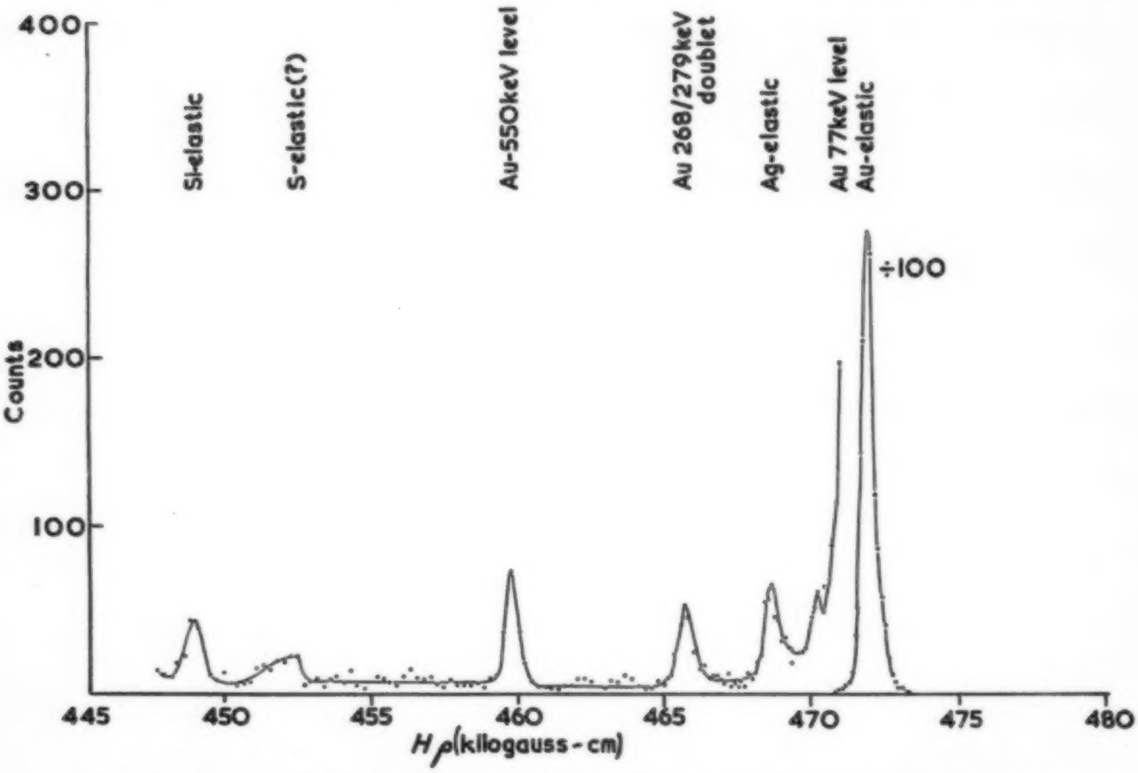

Fig. 2. Spectrum obtained with 200 μg/cm^2 gold target at 130° to a 10.62 MeV proton beam.

a) the gold elastic peak;

b) inelastic peaks from the 77 keV level, the unresolved doublet at 268 keV and 279 keV, and the 548 keV level, all in Au^{197};

c) elastic peaks due to impurities and contaminants (silver, silicon and perhaps sulphur);

d) a weak elastic peak from an element of mass 63±2 which developed during the run, thought to be due to sputtering of copper or zinc.

The uniform background in the region above 150 keV excitation was about 3×10^{-4} of the elastic peak. As might be expected, there was no sign of a group corresponding to the $(\frac{11}{2}-)$ metastable level at 409 keV, while the group belonging to the 77 keV level was not always visible, since fluctuations in beam focussing often caused it to be swamped by the tail of the elastic group. The cross section for production of this level was estimated to be 50 ± 30 μb/sr at 130° to an incident beam of 10.62 MeV protons. Previous workers 3,10) quote B(E2) values, the mean of which leads one to expect a cross-section about 100 ± 40 μb/sr; agreement may be considered reasonable.

Systematic studies were therefore confined to the gold elastic peak, the unresolved doublet, and the 548 keV level at 130° for eleven beam energies: the group (d) interfered with some of the doublet measurements. The doublet separation (1 in 550 at 6 MeV, 1 in 1150 at 12.6 MeV) was just below the effective resolving power, and at 6 MeV the 279 keV level is known to be excited about 4 times more strongly than is the 268 keV level 4) while for Coulomb excitation this ratio will not be expected to alter appreciably in the relevant energy range. The counting rate near the peak therefore contained little contribution ($\leq 10\,\%$) from the lower component of the doublet; the results will therefore be referred to as those from the 279 keV level.

Fig. 3a shows the excitation function for the elastic peak. At 7.5 MeV the cross-section has been shown to agree with that predicted by the Rutherford scattering process 11). A $1/E^2$ curve was therefore normalised to fit the points at the lower energies; significant departures from this curve occur only above 10 MeV. Thus target thicknesses were estimated to within $\pm 10\,\%$, and the inelastic cross-sections (determined relative to elastic yields within $\pm 10\,\%$) absolutely determined to $\pm 14\,\%$.

Excitation functions for the 548 keV level and the 279 keV level are shown in figs. 3b and 3c respectively (the $\pm 10\,\%$ error due to target thickness estimates not being shown) together with the observations of Elbek and Bockelman. The curves drawn represent the predictions of semiclassical Coulomb excitation theory using B(E2) values of 0.42 and 0.33 ($e^2 \times 10^{-48}$ cm^4) respectively, as derived from observations at lower energies 12). The agreement within 10 % at lower energies of the 279 keV level results with the curve strengthens the view that no more than ≈ 10 % of the recorded yield was due to the weaker component of the doublet.

The significance of the results is discussed in section 4.

3.2. W^{186}

Targets consisted of 100 μg/cm^2 layers of separated W^{186} oxide (supplied by the Atomic Energy Research Establishment, Harwell) deposited on a 20 μg/cm^2 carbon backing. The angular variation of the tungsten-elastic group at 10 MeV proton energy showed only 10 % deviations from a $\operatorname{cosec}^4 \frac{1}{2}\theta$ dependence, so the elastic yields could again be normalised to the Rutherford cross-section, and inelastic cross-sections determined, with an estimated uncertainty of ±17 %.

The 125 keV level in W^{186} was observed at 130°, and the 730 keV level at both 120° and 130° with incident proton energies of 9.0 and 10.0 MeV. Yields

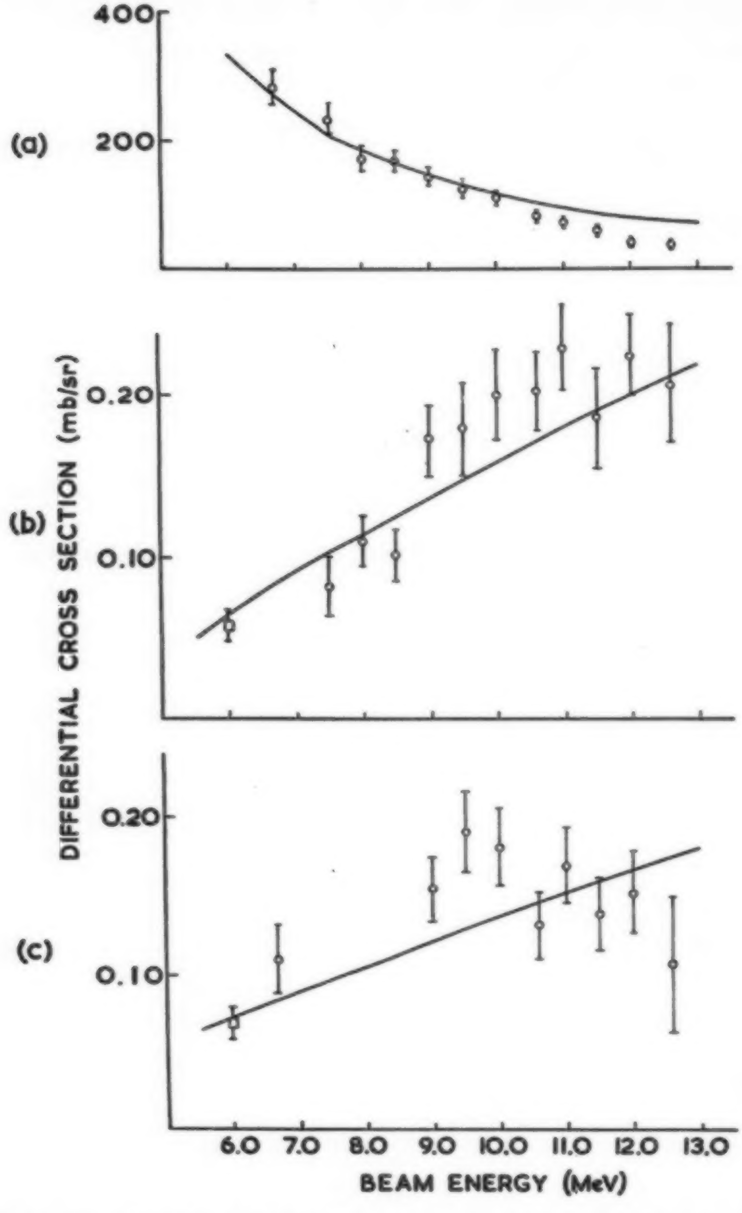

Fig. 3. Excitation curves for gold at 130°. Circles represent results of present experiment; squares the results of Elbek and Bockelman [8]). a) Elastically scattered protons. The line represents the Rutherford cross-section. b) Inelastic scattering from the 548 keV level in Au^{197}. c) Inelastic scattering from the 279 keV level in Au^{197}.

were consistent with an elastic quadrupole excitation, and the values of $B(E2)$ were calculated. That of the 125 keV level is $4.0 \pm 0.8 (e^2 \times 10^{-48} \text{ cm}^4)$, compared with the accepted value of 4.2 units [4]). The ratio of $B(E2)$ for the 730 keV level to that of the 125 keV level is 0.057 ± 0.004, agreeing with 0.049 ± 0.010 as given by McGowan and Stelson [6]). Taking the value of 4.2 units for the 125 keV level as better established than the present result, one may deduce a value $0.24 \pm 0.03 (e^2 \times 10^{-48} \text{ cm}^4)$ for the $B(E2)$ value of the 730 keV level. This agrees well with the figure 0.20 ± 0.05 units obtained by Alkhazov *et al.* [7]).

No significant group due to a level near 930 keV was observed; the yield at 10 MeV and 130° to the incident proton direction was less than 50 μb/sr. Peker [13]) has suggested that this level is (3−); if this is correct, our failure to see a level would imply $B(E3) \leqq 0.5 (e^3 \times 10^{-72} \text{ cm}^6)$.

4. Discussion

In the following discussion, all B-values, whether for excitation or decay, are reduced to the value for excitation: $B(\lambda; I_i \rightarrow I_f)$ in the notation of Alder *et al.* [4]).

4.1. Au^{197}

The ground state of Au^{197} is $(\frac{3}{2}+)$ while the 77 keV level is $(\frac{1}{2}+)$ and has a half-life of 1.9 ns [14]). Decay and excitation both by M1 and E2 is thus possible, but calculations comparing the half-life with the excitation show that, as might be expected, M1 excitation is negligible. Our observed yield, if significant, corresponds to $B(E2) = 0.10 \pm 0.06 (e^2 \times 10^{-48} \text{ cm}^4)$ comparing reasonably with the results 0.18 ± 0.06 units [10]) and 0.22 units [3]). A mean of 0.17 units corresponds to 3 % E2 decay, with $B(M1) = 0.024 (e\hbar/2Mc)^2$. The L-conversion of this gamma ray appears to correspond to 40 % E2 decay transitions (Mihelich and de Shalit [15])) but these workers emphasize the uncertainties of interpreting conversion coefficients in this energy region. Our conclusion, that the percentage of E2 transitions is much lower, seems to be on a firmer basis.

For the 548 keV and 279 keV levels, (figs. 3b and 3c) predictions are shown of cross-sections using semi-classical theory and values of $B(E2)$ established at lower energies, together with the present results, subject to a ±10 % normalisation error not shown. Bearing this in mind, the semi-classical theory appears to describe the excitation of the 548 keV level quite well, even at the highest energies. Agreement is much worse for the 279 keV level; the observed yield may be significantly higher than theoretical predictions at the lower energies, and the yield would appear to drop off at the highest energies. It is quite difficult to explain this. Possible mechanisms are:

a) *Effect of* M1 *excitation.* The 548 keV level must be excited by E2, while the 279 keV level may be excited either by M1 or E2. The proportion of M1 decay radiation is 0.89 ± 0.03 [16]), whence the proportion of M1 excitation, and of interference between M1 and E2 in the excitation process [17]) can then be shown to be less than 10^{-5}.

b) *Quantum Effects*. Semi-classical theory assumes $\eta = Z_1 Z_2 e^2/\hbar v = \infty$. The actual values of η range from 5.11 at 6 MeV to 3.53 at 12.6 MeV, so the effects of using quantum theory might be significant. This has been investigated [18]) for $\xi = 0$ (the ξ range in this experiment is 0.03 to 0.23) and the effect in the present experiment should be no more than ± 2 %.

c) *Onset of Compound Nucleus Formation*. The distance of closest approach to the gold nucleus for a 12.6 MeV proton deflected inelastically through 130°, is 1.11 r_0 for the 279 keV level, and 1.13 r_0 for the 548 keV level, where $r_0 = 1.2$ $(A_1^{\frac{1}{3}}+A_2^{\frac{1}{3}})\times 10^{-13}$ cm. Semi-classical calculations imply point projectiles; in practice, orbits partially penetrating the nucleus will almost certainly contribute to the (p, p′) process to a lesser degree than is predicted by semi-classical theory. The observed cross-section is therefore expected progressively to fall below the semi-classical value as the proton energy approaches that of the Coulomb barrier. This does not explain the observed difference in behaviour of the two levels.

d) *Interference between Coulomb scattering and Direct Interaction Inelastic scattering*.

This is a more likely mechanism. Direct interaction inelastic scattering at backward angles is difficult to estimate theoretically, and depends on the nature of individual levels. Measurements in typical cases, where the incident proton energy exceeds that of the barrier, vary from 1 mbarn/steradian in Fe^{56} to 40 μb/sr per level in Au and Pt [19, 20]). Thus interference terms between this process and Coulomb excitation might be large enough to explain the observed phenomenon: the difference between the two levels might then be ascribed to specific level properties.

e) *Second Order Coulomb Processes*. Dr. A. C. Douglas has pointed out (private communication) that these, and more particularly interference between first and second order processes, might be important but are difficult to estimate; the effect might be enhanced for the 279 keV level which has a close neighbour.

Processes d) and e) might in principle be tested by examining the angular dependence of the effect; this has not been done because of the difficulties of observing against the much higher background at forward angles.

4.2. W^{186}

In the region 9—10 MeV proton energy, Coulomb excitation seems the likely mechanism for inelastic scattering. The observed cross-sections for the formation of the 730 keV level give rise to a B(E2) value in agreement both with that derived from proton experiments at lower energies (which confirms the view that Coulomb excitation is the dominant process) and with that derived from alpha-particle experiments (Alkhazov *et al.* [7])). Such agreement can only arise if the excitation is indeed E2. M1 or M2 excitation could not produce the observed cross-sections with a reasonable transition probability, while E1 or E3 excitation would give rise to a discrepancy of at least 2 between the present measurements and those of the Russians. Thus the (2+) character of the level is confirmed.

5. Conclusions

Excitation functions for the reaction $Au^{197}(p, p')$, in which the residual nucleus is left in the 279 keV and 548 keV states, have been determined in the energy range 6.7 to 12.6 MeV, and compared with the predictions of semi-classical theory. Two mechanisms might account for an observed discrepancy between theory and experiment: direct interaction inelastic scattering or second order Coulomb processes.

Measurements of the reaction $W^{186}(p, p')$ confirm the assignment (2+) to the 730 keV level, but are not sensitive enough to detect the reported 930 keV level.

We are indebted to Dr. K. W. Allen for his advice and encouragement throughout the course of this work. Thanks are also due to Professor D. H. Wilkinson and Dr. A. Winther for very helpful discussions of the mechanism of Coulomb excitation. We would like also to acknowledge the technical assistance of Mr. J. L. Wankling and Mr. A. J. Cole.

References

1) K. W. Allen, F. A. Julian, W. D. Allen, A. E. Pyrah and J. Blears, Nature **188** (1959) 303
2) A. V. Cohen, J. A. Cookson and J. L. Wankling, Nuclear Instruments and Methods (1961) (in the press)
3) B. Elbek and C. K. Bockelman, Phys. Rev. **105** (1957) 657
4) K. Alder, A. Bohr, T. Huus, B. Mottelson and A. Winther, Rev. Mod. Phys. **28** (1956) 432
5) R. Barloutaud, A. Lévêque, P. Lehmann and J. Quidort, J. de Phys. et Rad. **19** (1958) 60
6) F. K. McGowan and P. H. Stelson, Bull. Am. Phys. Soc. **3** (1958) 228
7) D. G. Alkhazov, A. P. Grinberg, G. M. Gusinskii, K. I. Erokhina and I. Kh. Lemberg, JETP (USSR) **35** (1958) 1325
8) B. S. Dzelepov and L. K. Peker, Decay Schemes of Radioactive Nuclei (Publishing House of the Academy of Sciences of the USSR Moscow, 1958)
9) D. Strominger, J. M. Hollander and G. T. Seaborg, Rev. Mod. Phys. **30** (1958) 585
10) E. M. Bernstein and H. W. Lewis, Phys. Rev. **100** (1955) 1345
11) W. F. Waldorf and N. S. Wall, Phys. Rev. **107** (1957) 1602
12) P. H. Stelson and F. K. McGowan, Phys. Rev. **99** (1955) 112
13) L. K. Peker, Bull. Acad. of Sciences of the USSR (Physics Series) **22**, (1958) 213
14) A. W. Sunyar, Phys. Rev. **98** (1955) 653
15) J. W. Mihelich and A. de Shalit, Phys. Rev. **91** (1953) 78
16) J. V. Kane and S. Frankel, Bull. Am. Phys. Soc. **1** (1956) 171
17) L. C. Biedenharn and R. M. Thaler, Phys. Rev. **104** (1956) 1643
18) J. Bang, Mat. Fys. Medd. Dan. Vid. Selsk **32**, No. 5 (1960)
19) G. Schranck, P. C. Gugelot and I. E. Dayton, Phys. Rev. **96** (1954) 1156
20) P. C. Gugelot, Phys. Rev. **93** (1954) 425

2.E:2.G

Nuclear Physics **23** (1961) 40—52; © *North-Holland Publishing Co., Amsterdam*

Not to be reproduced by photoprint or microfilm without written permission from the publisher

THE OPTICAL MODEL AND DEUTERON STRIPPING

JAMES E. YOUNG

University of California, Los Alamos Scientific Laboratory, Los Alamos, New Mexico †

Received 4 November 1960

Abstract: A development is given which stresses the underlying similarity between the deuteron stripping theory on the one hand and direct interaction theory of inelastic nucleon scattering on the other. The assumption here is that both formulations are given in distorted Born approximation. Some implications for the form of the stripping theory, e.g., construction of the distorting potentials are discussed. The entire theory, as given, for the transition matrix element is first-order in the two-body scattering operators. Probable corrections to this description, such as those arising from multiple scattering, are discussed.

1. Introduction

An overwhelmingly great amount of attention is currently given to direct interaction theories. Yet, despite this effort, there is a certain inability to translate the many, and seemingly different results, into a single unified scheme. Such is certainly the fact in the case of deuteron stripping reactions. Since the original work of Butler [1]), the area and methodology have grown with almost complete disregard for connecting and transitional formulations. Of course, this is not the first time for such a charge. So to give it meaning, we shall have to be specific.

It is currently the fashion to discuss the direct interaction processes in distorted Born approximation. For the stripping process, which interests us specifically, the description involves the channel distortions through certain optical potentials. Further, transitions between initial and final distorted states occur through some "residual potential" in the generic treatment [2]). The optical potentials ought to be viewed as those arising from the Watson [3]) multiple scattering theory. However, cognizance of this fact is scarcely ever taken. This contention is supportable, since indeed the optical potentials of the stripping problem are not in general those for elastic scattering in the respective channels. Such a situation has already been noticed in the problem of inelastic neutron scattering. Rodberg [4]) has been able to show that there are A^{-1}-corrections to the usual optical potential of elastic scattering. This in an important result for it brings the kind of consistency to the direct reaction picture otherwise not possible.

---

† Work performed under the auspices of the U. S. Atomic Energy Commission.

We are prepared at this point to observe a further connection between the theory of direct-interaction, inelastic scattering and that for deuteron stripping. The demonstration of this connection is indeed the subject and purpose of this note. Our result is that the optical potentials of the two theories cited are modified in almost the same way. The presence of rearrangement in the stripping process makes it necessary to discuss an additional optical potential, say, that for the deuteron in addition to the neutron potential in the case of (d,n). The implications for this additional potential will be detailed in a later section.

Characteristically in the direct-interaction, distorted wave theories for inelastic scattering, transitions are induced by some t, a two-body scattering operator or the sum of such operators. This is to be viewed as the elimination of v, the potential effective for transitions, in favor of t. In the distorted-wave formulation of stripping, it is again t and not v which induces transitions. Unfortunately, many writers in the field, while appreciating the differences between t and v, nevertheless continue to fail to emphasise them. This would be of no consequence if one were assured that the non-locality of t was unimportant. For then, the t-matrix could be replaced by an equivalent Yukawa with no serious harm. It is not clear that the non-locality of t can be ignored. In particular, there begins to be an accumulation of evidence [5]) that the direct interactions involving light ($A \leqq 20$) nuclei may only be properly treated using t. Indeed, such an observation, together with another, the impulse approximation (t in the medium equals t for free scattering), seems to describe direct interactions even at low energies (≈ 5 MeV) and appears to provide a basis of describing the stated interactions upon very *light* nuclei.

We view the present work, which emphasizes the essential unity of deuteron stripping and direct-interaction, inelastic scattering theories, as a synthesis of the work of many authors. In particular, the stripping formulations of Thomas [6]) and Tobocman [7]), on the one hand, and the scattering descriptions of Watson and Rodberg on the other, find their natural amalgamation here.

The distorted Born expression we shall derive for the transition amplitude has existed in one or another form for quite some time. Nonetheless, it is interesting to sketch some aspects of its evolution insofar as concerns the stripping reaction. Originally, it was thought that the fairly small (relative to cross sections for compound processes) observed probability for the subject process could be maintained by restricting the matrix element to the channel region of configuration space. The point of view was accomplished by the ingenious and consistent use of surface potentials, so-called, to derive the *desired* form of the matrix element. The procedure here is largely due to Tobocman and Ui [8]). It was alternately possible to obtain the matrix element upon introduction of the assumption that the S-matrix for the over-all process, S_{nd}, was of the factorable form $S_{\text{n}}S_{\text{d}}$. Imposition of the conservation of current viewed on the "surface-at-infinity" then led to appropriate matrix element. The point of view here has been described, in effect, by Thomas and Tobocman.

As the redoubtable benefit of hindsight is our present legacy, we know now that the distorted-wave matrix element can be given for the whole of configuration space. When we properly incorporate shell model wave functions into the description, the matrix element drops off toward the interior of the nucleus due to the decreased mean free path for absorption; also exterior to the nucleus, the matrix element falls off because of the influence of the bound particle. These features are just those associated with earlier cut off models. For very light nuclei where the shell model may be of dubious utility, one or another form of the cluster model wave function is often useful. We stress this point because the appropriate basis set for evaluating the propagators of the theory is that in A particles (the reaction per se involves $A+2$ particles). This fact has implications for the fractional parentage representations [9]) of nuclear states. The Thomas model for (n, d) clearly recognizes the utility of such representations. The resulting complete set of nuclear states, i.e., "core" states in A particles, are those which that author uses to generate the widths and to evaluate the matrix elements of the theory. In many cases, e.g., the triton [10]), in particular for very light nuclei, the cluster model wave function of nuclear states is the logical extension of the fractional parentage representation. In view of this aspect, the cluster model may serve as a useful adjunct for discussing direct interaction processes upon light nuclei. Again, this interpretation may be seen in the work of Thomas and provides one of the alternatives for expanding the nucleus of $(A+1)$ constituents as an optical particle plus A-particle core.

Apart from aspects which are better discussed in connection with the logical development of our analysis, our discursive survey is complete. In the next section, we review those aspects of Watson's multiple scattering theory which are relevant for our purposes. Here, as well, we find it in the interest of coherence to present some notions concerning the fractional parentage representation of nuclear states. This is contrasted with the corresponding cluster model representation of the Thomas description. Section 3 is given to the calculation of the transition matrix element and the development of certain approximations. Finally, the recapitulation of our results and the conclusions are stated briefly in section 4.

2. Some Useful Preliminaries

In order to make the present treatment self-contained, certain developments of other authors are reproduced here. The first of these has to do with multiple scattering as formulated by Watson.

It is convenient to obtain the (d, n) cross section from that for Y(n, d)X by the usual methods of reciprocity. Consequently, our discussions are hereafter restricted to the corresponding pickup process. We first want to discuss the neutron distortion by the nucleus Y in its ground state. If the actual reaction situation does not leave Y in its ground state, the necessary modifications are easily made. The stationary state of interaction is written as

$$\Psi_{\mathrm{n}}^{(+)}(\xi_{A+1}, \mathbf{r}_{\mathrm{n}}) = \lambda_0(\mathbf{r}_{\mathrm{n}}) g_0(\xi_{A+1}) + \frac{1}{a_{0\mathrm{n}}^{(+)}} \sum_{j=1}^{A+1} v_{\mathrm{n}j} \Psi_{\mathrm{n}}^{(+)}(\xi_{A+1}, \mathbf{r}_{\mathrm{n}}), \tag{1}$$

with $a_{0\mathrm{n}}^{(+)} = E_{\mathrm{n}} - H_{\mathrm{n}}^0 + i\varepsilon$.

The notation above is self-evident, however, we amplify it by giving the explicit decomposition of the total Hamiltonian H,

$$(H - E_{\mathrm{n}}) \Psi_{\mathrm{n}}^{(+)} = 0,$$

in terms of the Hamiltonians H_{n}^0 and H_{d}^0 for non-interacting system. In particular, we observe that the following is true:

$$\begin{aligned} H &= T_{\mathrm{n}} + H_{\mathrm{Y}} + \sum_{j=1}^{A+1} v_{\mathrm{n}j} = H_{\mathrm{n}}^0 + \sum v_{\mathrm{n}j} \\ &= T_{\mathrm{n}} + H_{\mathrm{X}} + \sum_{j=1}^{A} v_{\mathrm{p}j} + T_{\mathrm{p}} + \sum_{j=1}^{A} v_{\mathrm{n}j} + v_{\mathrm{np}} = H_{\mathrm{d}}^0 + \sum_{j=1}^{A} (v_{\mathrm{p}j} + v_{\mathrm{n}j}). \end{aligned} \tag{2}$$

The subscripts n, p and d have been reserved for the designations — neutron, proton, and deuteron.

Eq. (1) does not really interest us as it stands. It is actually our aim to construct the stationary state from the chosen configuration so-called, i.e., the distorted-wave state. This state is imagined to satisfy the equation

$$\eta_0^{(+)}(\mathbf{r}_{\mathrm{n}}) g_0(\xi_{A+1}) = \lambda_0(\mathbf{r}_{\mathrm{n}}) g_0(\xi_{A+1}) + \frac{1}{a_{0\mathrm{n}}^{(+)}} U_0 \eta_0(\mathbf{r}_{\mathrm{n}}) g_0(\xi_{A+1}). \tag{3}$$

Alternately, we indicate that this state is constructed from the plane wave state by introducing the Møller wave matrix Ω_{c}, whereupon

$$\begin{aligned} \eta_0^{(+)}(\mathbf{r}_{\mathrm{n}}) g_0(\xi_{A+1}) &= \Omega_{\mathrm{c}}^{(+)} \lambda_0(\mathbf{r}_{\mathrm{n}}) g_0(\xi_{A+1}), \\ \Omega_{\mathrm{c}}^{(+)} &= 1 + \frac{1}{a_{0\mathrm{n}}^{(+)}} U_0 \Omega_{\mathrm{c}}^{(+)} = 1 + \frac{1}{a_{0\mathrm{n}}^{(+)} - U_0} U_0 \equiv 1 + \frac{1}{e_{0\mathrm{n}}^{(+)}} U_0. \end{aligned} \tag{4}$$

At this point, the auxiliary potential is unspecified, for we have not said how to choose it. Now the stationary state is generated, as noted earlier, by introducing the operator F_{n} and the corresponding operator statement

$$\Psi_{\mathrm{n}}^{(+)}(\xi_{A+1}, \mathbf{r}_{\mathrm{n}}) = F_{\mathrm{n}} \eta_0^{(+)}(\mathbf{r}_{\mathrm{n}}) g_0(\xi_{A+1}). \tag{5}$$

A trivial algebraic manipulation of eq. (1) allows us to rewrite that relation as

$$\Psi_{\mathrm{n}}^{(+)}(\xi_{A+1}, \mathbf{r}_{\mathrm{n}}) = \eta_0^{(+)}(\mathbf{r}_{\mathrm{n}}) g_0(\xi_{A+1}) + \frac{1}{e_{0\mathrm{n}}^{(+)}} \Big(\sum^{A+1} v_{\mathrm{n}j} - U_0\Big) \Psi_{\mathrm{n}}^{(+)}(\xi_{A+1}, \mathbf{r}_{\mathrm{n}}),$$

and thus to establish that

$$F_{\mathrm{n}} = 1 + \frac{1}{a_{0\mathrm{n}}^{(+)} - U_0} P \sum^{A+1} v_{\mathrm{n}j} F_{\mathrm{n}}, \quad P \sum v_{\mathrm{n}j} = \left(\sum v_{\mathrm{n}j} - U_0\right). \tag{6}$$

It is useful to introduce the wave function $\Psi_{\mathrm{n}j}^{(+)}$ having correlations for all pairs of particles except the jth pair, i.e., particles "n" and "j". Such a function satisfies the equation

$$\Psi_{\mathrm{n}j}^{(+)} = \eta_0{}^{(+)} g_0 + \frac{1}{e_{0\mathrm{n}}^{(+)}} P \sum_{i \neq j} v_{\mathrm{n}i} \Psi_{\mathrm{n}}{}^{(+)},$$

and in terms of it, the stationary state is expressed as

$$\Psi_{\mathrm{n}}{}^{(+)} = \Psi_{\mathrm{n}j}^{(+)} + \frac{1}{e_{0\mathrm{n}}^{(+)}} P v_{\mathrm{n}j} \Psi_{\mathrm{n}}{}^{(+)}.$$

The final introduction of operator statements

$$v_{\mathrm{n}j} \Psi_{\mathrm{n}} = t_{\mathrm{n}j} \Psi_{\mathrm{n}j}, \quad \Psi_{\mathrm{n}j} = F_{\mathrm{n}j} \eta_0{}^{(+)} g_0 \tag{7}$$

produces the equations

$$F_{\mathrm{n}} = 1 + \frac{1}{e_{0\mathrm{n}}^{(+)}} P \sum_{j=1}^{A+1} t_{\mathrm{n}j} F_{\mathrm{n}j}, \quad F_{\mathrm{n}j} = 1 + \frac{1}{e_{0\mathrm{n}}^{(+)}} P \sum_{i \neq j} t_{\mathrm{n}i} F_{\mathrm{n}i}. \tag{8}$$

and

$$t_{\mathrm{n}j} = v_{\mathrm{n}j} + v_{\mathrm{n}j} \frac{1}{e_{0\mathrm{n}}^{(+)}} P t_{\mathrm{n}j}. \tag{9}$$

Eq. (3)—(9) are the Watson equations when augmented with that author's prescription for choosing P. The two choices made are $P = P_{\mathrm{ND}}$, $P_{\mathrm{ND}} = 1 - |g_0(\xi_{A+1})\rangle\langle g_0(\xi_{A+1})|$, which projects off the nuclear ground state and $P = P_0$, an operator which forbids the recurrence of a nuclear state after any subsequent scatterings. Although we do not know how to write a representation for P_0, it is far the more useful operator, as it leads to the definition,

$$U_0 = \langle g_0(\xi_{A+1})| \sum t_{\mathrm{n}j} F'_{\mathrm{n}j} |g_0(\xi_{A+1})\rangle, \tag{10}$$

of the optical potential U_0. In applying this statement, recall that U_0 acts only on the distorted state. The prime on the sum denotes the omissions of the *last* scattering in F_{n}, i.e., the first scattering in $F_{\mathrm{n}j}$ cannot occur from the same particle which terminally generates the fully correlated stationary state $\Psi_{\mathrm{n}}{}^{(+)}$.

The above considerations provide the essential details of the Watson theory insofar as we require it. Next we turn to an examination of the propagator $e_{0\mathrm{n}}^{(+)}$ which we describe as being in a basis of $(A+2)$ particles. The meaning of such a statement derives from the expansion

$$(a_{0n}^{(+)}-U_0)^{-1} = |\tilde{\eta}_\mu{}^{(+)}(\mathbf{r}_n)g_\mu(\xi_{A+1})\rangle \frac{1}{(E_n-\varepsilon_\mu)-T_n-U_0+i\varepsilon} \cdot \langle \eta_\mu{}^{(+)}(\mathbf{r}_n)g_\mu(\xi_{A+1})|. \tag{11}$$

In this result, $\tilde{\eta}_\mu{}^{(+)}$ is the time-reversed state, namely, that with ingoing scattered waves; ε_μ is the energy of the nuclear eigenstate μ. We have previously stated that it is convenient to expand the wave function for the nucleus Y, upon which the neutron impinges, as a core plus extra particle. Eventually, the core will be the nucleus X, and the extra particle a proton. The stated procedure as we shall detail it is properly the next topic, fractional parentage representations [11]), which interests us.

It is our aim to re-express the propagator of eq. (11) in terms of a *nuclear* basis of A particles. While this may not seem immediately useful, the results of the next section will require such a representation. Our notation follows that given by Jahn [12]). Let us write the generic nuclear, (LS)-state, suppressing the energy quantum number, as

$$\Psi(l^n[\lambda]TSLM_TM_SM_L) = \sum_{\lambda' T' S' L'} \langle l^n[\lambda]TSL|l^{n-1}[\lambda']T'S'L'\rangle \cdot \Phi(l^{n-1}[\lambda']T'S'L'; l; TSLM_TM_SM_L). \tag{12}$$

The generic nuclear state is imagined to be described by a l^n configuration, the orbital symmetry of which is given by the partition $[\lambda]$. We observe that the given state is expanded in the terms of functions Φ. These functions are those arising when the parent state, configuration l^{n-1}, symmetry $[\lambda']$, is vector coupled to the one-particle state. The expansion coefficients which arise are the so-called coefficients of fractional parentage (c.f.p.). We do not bother to enumerate any further the remaining quantum labels in eq. (12) as they conform to standard notation.

The vector coupling noted factors into those separate couplings for each of the spaces — spin, charge, and orbit. Given that the one-particle state is

$$|\tfrac{1}{2}t\,\tfrac{1}{2}slm_l\rangle = \chi_{\frac{1}{2}}{}^t\chi_{\frac{1}{2}}{}^s Y_{lm_l}(\Omega_r)r^{-1}W_l(k_Nr), \tag{13}$$

with N measuring the excitation, e.g., the radial nodes, we obtain the following result:

$$\Phi(l^{n-1}[\lambda']T'S'L'; l; TSLM_TM_SM_L) = \sum \left[\begin{matrix} T' & \frac{1}{2} \\ M'_T & t \end{matrix}\middle|\begin{matrix} T \\ M_T \end{matrix}\right] \left[\begin{matrix} S' & \frac{1}{2} \\ M'_S & s \end{matrix}\middle|\begin{matrix} S \\ M_S \end{matrix}\right] \left[\begin{matrix} L' & l \\ M'_L & m_l \end{matrix}\middle|\begin{matrix} L \\ M_L \end{matrix}\right] |\tfrac{1}{2}t\,\tfrac{1}{2}slm_l\rangle \cdot |l^{n-1}[\lambda']T'M'_TS'M'_SL'M'_L\rangle. \tag{14}$$

The sums in the given equation are, as usual, over the various projections.

Note that a slightly unconventional representation has been used for the vector-coupling coefficients.

For completeness, we mention that when the charge-spin part of the wave function, (12), is chosen to have the adjoint symmetry $[\tilde{\lambda}]$, the c.f.p. factorize. In particular, Jahn shows that the decomposition into charge-spin and orbital c.f.p. is given by

$$\begin{aligned}&\langle l^n[\lambda]TSL|l^{n-1}[\lambda']T'S'L'\rangle\\ &\quad=\sqrt{\frac{n_{\lambda'}}{n_\lambda}}\,\langle l^n[\lambda]L|l^{n-1}[\lambda']L'\rangle\langle\gamma^n[\tilde{\lambda}]TS|\gamma^{n-1}[\tilde{\lambda}']T'S'\rangle,\end{aligned}\tag{15}$$

the quantities n_λ, $n_{\lambda'}$ being the dimensions of the representations in λ, λ'.

The actual nuclear state $g_\mu(\xi_{A+1})$ carries an additional quantum number M which represents the $(2J+1)$- and $(2T+1)$-fold degeneracy of the state, whose spin and i-spin are J and T. This is the only degeneracy at the energy ε_μ which we consider. It follows that the representation of $g_\mu(\xi_{A+1})\equiv g_{\mu,M}$ which concerns us is that in the so-called intermediate coupling. According to this scheme, we would write

$$g_{\mu M}=\sum a^{JT}_{LS[\lambda]}\,{}^{2T+1,\,2S+1}L_J^{[\lambda]},\tag{16}$$

where

$${}^{2T+1,\,2S+1}L_J^{[\lambda]}=\sum_{M_S M_L}\left[\begin{matrix}L & S\\ M_L & M_S\end{matrix}\middle|\begin{matrix}J\\ M_J\end{matrix}\right]\Psi(l^n[\lambda]TSLM_T M_S M_L).\tag{17}$$

The admixture coefficients in (16) are fixed by the experimentally observed properties of the relevant nuclear states.

Eq. (12)—(17) represent then the expansion of a nuclear state in terms of core plus extra particle. Quite often it is economical to represent the totality of such statements by the single expression

$$g_\mu(\xi_{A+1})=\sum C^\mu_{\nu\beta}\varphi_\nu(\zeta_A)f_\beta(\mathbf{r}).\tag{18}$$

Now, in the work of Thomas we encounter an expression such as (18) where the charge state for the extra particle is specified. In the case of Y(n, d), the nucleus Y is represented as the sum of X and a proton. The representation which Thomas utilizes takes the form

$$\begin{aligned}g_{\mu M_J}(\xi_{A+1})=\sum_{lS'\nu}\gamma(lS'\nu)\sum_{\substack{m_l m'_S\\ m_j p}}&\left[\begin{matrix}l & S'\\ m_l & m'_S\end{matrix}\middle|\begin{matrix}J\\ M_J\end{matrix}\right]\left[\begin{matrix}j & \frac{1}{2}\\ m_j & p\end{matrix}\middle|\begin{matrix}S'\\ m'_S\end{matrix}\right]\\ &\cdot\varphi^{m_j}_{\nu j}(\zeta_A)|\tfrac{1}{2}\,\tfrac{1}{2}\,\tfrac{1}{2}plm_l\rangle.\end{aligned}\tag{19}$$

We have employed the single particle wave function of (13) and the expansion coefficient is the so-called reduced-width amplitude. From the development given in the previous equations, it is possible to understand Thomas' expansion as a fractional parentage representation. Should the shell model fail to be applicable, we interpret (19) in terms of the cluster model representation of the nucleus Y. This is indeed the situation which confronts us in case of the reaction $He^3(n, d)D$, for example. Here the He^3 nucleus is expanded as a *physical* deuteron plus a proton. Without commenting extensively on the difference between the cluster model expansions and those of the type (16), which have largely to do with completeness of sets, we summarize the present considerations. Decompositions of a nuclear state into a core plus extra particle, on the basis of models currently extant, is symbolized by the statement (18).

Being given the decompositions, just discussed, on to an A-particle nuclear basis, we seek to modify the propagator of (11). The relations given in (2) are helpful in this connection, and we write

$$(a_{0\mathrm{n}}^{(+)}-U_0)^{-1} = |\tilde{\eta}_\mu{}^{(+)}(\mathbf{r}_\mathrm{n})g_\mu(\xi_{A+1})\rangle \frac{1}{E_\mathrm{n}-T_\mathrm{p}-(\sum^{A} v_{\mathrm{p}j}-V_\mathrm{p})-V_\mathrm{p}-H_\mathrm{x}-T_\mathrm{n}-U_0+i\varepsilon} \cdot \langle \eta_\mu{}^{(+)}(\mathbf{r}_\mathrm{n})g_\mu(\xi_{A+1})|.$$

The potential V_p is chosen to be diagonal in the quantum labels of the extra particle, i.e., the proton. On the average, it is supposed that this potential represents the binding, albeit to a centre-of-force. Following this supposition, we then set the residual potential to zero in the propagator. Upon introducing the expansion of (18), the following result is obtained:

$$(a_{0\mathrm{n}}^{(+)}-U_0)^{-1} \approx \tilde{\eta}_\mu{}^{(+)}(\mathbf{r}_\mathrm{n})C^{\mu}_{\nu\beta}\psi_\nu(\zeta_A)f_\beta(\mathbf{r}_\mathrm{p})\rangle \cdot \frac{1}{(E_\mathrm{n}-\mathscr{E}_\nu)-T_\mathrm{n}-T_\mathrm{p}-U_0-V_\mathrm{p}+i\varepsilon} \langle \eta_\mu{}^{(+)}(\mathbf{r}_\mathrm{n})C^{\mu}_{\nu\beta}\psi_\nu(\zeta_A)f_\beta(\mathbf{r}_\mathrm{p})|. \tag{20}$$

Representations of this specific nature are certainly implied for the developments of the next section. And indeed, expansions such as (20) with $\mu = 0$, the two-particle excited states, have implications for a broader class of problems than we can profitably discuss here.

Having completed our discussion of the relevant preliminaries, we turn now to the construction of the stripping (in actual fact, pickup) transition matrix element. This is the main task of this paper and the details appear in the following section.

3. Distorted Born Amplitude

We shall derive, without specific attention to rigor, the distorted Born matrix element. The rate of transition into final plane wave states

$$D(\mathbf{r}_\mathrm{p}\mathbf{r}_\mathrm{n})\psi_\nu(\zeta_A), \quad D(\mathbf{r}_\mathrm{p}\mathbf{r}_\mathrm{n}) = \phi_\mathrm{d}(\mathbf{r}_\mathrm{pn})e^{i\mathbf{k}\cdot\mathbf{R}_\mathrm{pn}},$$

is determined by

$$\begin{aligned} T_{\mathrm{dn}} &= \langle D(\mathbf{r}_{\mathrm{p}}\mathbf{r}_{\mathrm{n}})\psi_{\nu}(\zeta_A)|\Psi_{\mathrm{n}}{}^{(+)}(\xi_{A+1}, \mathbf{r}_{\mathrm{n}})\rangle \\ &= \left\langle D(\mathbf{r}_{\mathrm{p}}\mathbf{r}_{\mathrm{n}})\chi_{\nu}(\zeta_A)\left|\frac{1}{a_{0\mathrm{n}}^{(+)}}\left(v_{\mathrm{np}}+\sum_{1}^{A}{}' v_{\mathrm{n}j}\right)\Psi_{\mathrm{n}}{}^{(+)}(\xi_{A+1}, \mathbf{r}_{\mathrm{n}})\right.\right\rangle. \end{aligned} \tag{21}$$

We have used the integral equation of (1) to obtain this result. It is useful to separate the n—p force from the remaining interactions of the neutron with the target. This has been done in the expression above. Now let us introduce the distorted-wave state for final particles according to

$$\begin{aligned} \Delta^{(+)}(\mathbf{r}_{\mathrm{p}}\mathbf{r}_{\mathrm{n}})\psi_{\nu}(\zeta_A) &= D(\mathbf{r}_{\mathrm{p}}\mathbf{r}_{\mathrm{n}})\psi_{\nu}(\zeta_A) \\ &\quad + \frac{1}{a_{0\mathrm{d}}^{(+)}}({}'U_0(\mathbf{r}_{\mathrm{n}}, \zeta_A)+V_{\mathrm{p}}(\mathbf{r}_{\mathrm{p}}, \zeta_A))\Delta^{(+)}(\mathbf{r}_{\mathrm{p}}\mathbf{r}_{\mathrm{n}})\psi_{\nu}(\zeta_A). \end{aligned} \tag{22}$$

The potentials appearing in this equation are, as yet, undefined. However, we proceed to eliminate the plane wave in (21) by means of this expression. We find as a result, the following statement:

$$\begin{aligned} T_{\mathrm{dn}} &= \left\langle \Delta^{(-)}(\mathbf{r}_{\mathrm{p}}\mathbf{r}_{\mathrm{n}})\psi_{\nu}(\zeta_A)\left|\frac{1}{a_{0\mathrm{n}}^{(+)}}\left(v_{\mathrm{np}}+\sum_{1}^{A}{}' v_{\mathrm{n}j}\right)\Psi_{\mathrm{n}}{}^{(+)}(\xi_{A+1}, \mathbf{r}_{\mathrm{n}})\right.\right\rangle \\ &\quad - \left\langle \frac{1}{a_{0\mathrm{d}}^{(-)}-V_{\mathrm{p}}-{}'U_0{}^*}(V_{\mathrm{p}}+{}'U_0{}^*)\left|\Psi_{\mathrm{n}}{}^{(+)}(\xi_{A+1}, \mathbf{r}_{\mathrm{n}})-\lambda_0(\mathbf{r}_{\mathrm{n}})g_0(\xi_{A+1})\right.\right\rangle. \end{aligned} \tag{23}$$

It is to be observed that the time-reversed distorted state appears in this relation.

Next, we rewrite the first matrix element as

$$\begin{aligned} &\langle \Delta^{(-)}(\mathbf{r}_{\mathrm{p}}\mathbf{r}_{\mathrm{n}})\psi_{\nu}(\zeta_A)|\,\frac{1}{a_{0\mathrm{n}}^{(+)}-U_0}\left(1-U_0\frac{1}{a_{0\mathrm{n}}^{(+)}}\right)W\left(1+\frac{1}{a_{0\mathrm{n}}^{(+)}-U_0}(W-U_0)\right)|\eta_0{}^{(+)}(\mathbf{r}_{\mathrm{n}})g_0(\xi_{A+1})\rangle \\ &\qquad \approx \langle \Delta^{(-)}(\mathbf{r}_{\mathrm{p}}\mathbf{r}_{\mathrm{n}})|\,\frac{1}{a_{0\mathrm{n}}^{(+)}-U_0}W\left(1+\frac{1}{a_{0\mathrm{n}}^{(+)}-U_0}[W-U_0]\right)|\eta_0{}^{(+)}(\mathbf{r}_{\mathrm{n}})g_0(\xi_{A+1})\rangle. \end{aligned}$$

The substance of this first approximation is to neglect all orders of the two-body scattering operators higher than the first. In the preceding expressions, we have introduced the definition

$$W = \sum{}' v_{\mathrm{n}j}+v_{\mathrm{np}}.$$

To proceed further, we introduce an additional relation, namely,

$$U_0(\mathbf{r}_{\mathrm{n}}, \xi_{A+1}) = {}'U_0(\mathbf{r}_{\mathrm{n}}, \zeta_A)+V_{\mathrm{np}}(\mathbf{r}_{\mathrm{n}}\mathbf{r}_{\mathrm{p}}). \tag{24}$$

This defines one of the potentials which was introduced in (22). The potential V_{np} will shortly be taken equal to v_{np}, the two-nucleon potential. However, for the moment, this equality is not imposed. What we do wish to establish is that

V_{np}, by assumption, is not diagonal in nuclear states μ. Further, the auxiliary potential, $'U_0$, is assumed to be diagonal in nuclear states v. As it is implicit in (18) that we are dealing with two complete sets of orthonormal functions, it follows that $'U_0$ is also diagonal in μ.

If now we are to maintain $\eta_0{}^{(+)}(\mathbf{r}_{\mathrm{n}})g_0(\xi_{A+1})$ as a distorted-wave state, for the entrance channel, the defining relation (3) must be modified. In lowest order of approximation, this is achieved by replacing U_0 by $'U_0$ in the equation noted.

If at this point we imagine that $V_{\mathrm{np}} \approx v_{\mathrm{np}}$ holds, then to the same order,

$$(a_{0\mathrm{n}}^{(+)} - U_0) = (a_{0\mathrm{d}}^{(+)} - V_{\mathrm{p}} - {}'U_0) \tag{25}$$

obtains. This relation means that the energy-shell matrix element, the δ-function for energy conservation being suppressed, is given by

$$\langle \varDelta^{(-)}(\mathbf{r}_{\mathrm{p}}\mathbf{r}_{\mathrm{n}})\psi_{\nu}(\zeta_A)|Q|\eta_0{}^{(+)}(\mathbf{r}_{\mathrm{n}})g_0(\xi_{A+1})\rangle .$$

The operator Q, which induces transitions, is defined as

$$Q = W + W\frac{1}{a_{0\mathrm{n}}^{(+)} - U_0}W - W\frac{1}{a_{0\mathrm{n}}^{(+)} - U_0}U_0 . \tag{26}$$

We wish to argue here in a specific way in order to simplify Q. There is a region of mass number and energy for which heavy-particle stripping 13), so-called, and multiple scattering within the target are comparatively unimportant processes. Our interest and, indeed, the considerations which follow are restricted to just such a regime.

The first assumption or restriction can be interpreted as meaning that neutron capture by the core, through $\sum' v_{\mathrm{n}j}$, into a compound state which subsequently decays by boiling off a deuteron is energetically not very probable. However, this is not the way one is given to thinking about heavy-particle stripping. It is generally imagined that a neutron from the core replaces the incoming neutron; an event brought about by the exchange part of the two-body force. The exchanged neutron then picks up a proton on its way out of the nucleus. It is a common feature of both processes described that the associated amplitudes are of at least second order and are proportional to $\sum' v_{\mathrm{n}j}$. One thing which suppresses the relative importance of these processes is the "long times" which characterize them. Since the same situation is encountered for the multiple scattering, one statement (to follow shortly) will make the nomenclature precise.

As for the multiple scattering, this occurs through $'U_0$ and leaves the core unexcited. In reality then, the physical situation is that of multiple reflection. The neutron, having a fairly long mean free path against absorption at the energies in question, spends a long time within the nucleus by being reflected at the nuclear boundaries. As such, it is in a quasi-stationary state. When the neutron finally scatters out of the nucleus, picking up a proton, the resulting beam of deuterons so formed is incoherent with that from *direct* processes. This is, of course, what we mean by "long times" being involved. Furthermore, we insist that the *number* of such "compound-state" deuterons be small. This may indeed be a fairly difficult criterion to meet in actual practice. Recall that the mean free path in nuclear matter for $4 \leqq E_\mathrm{n} \leqq 14$ MeV is about 6–9 fm 14). If, for example, we work with nuclei such that $A \leqq 20$, the radii involved are certainly smaller than this value. In contrast to this, the boiling off of deuterons described in the previous paragraph can be controlled by diminishing the excitation energies involved. This is accomplished through judicious choices of target, i.e., mass number, and bombarding energies.

Our approximations to the transition operator Q, then, consist of writing $W \approx V_\mathrm{np}$ and neglect of the last term in (26) when it is expressed as a perturbation series in $'U_0$. The result of all this gives the expression

$$\begin{aligned} Q \equiv t_\mathrm{np} &= v_\mathrm{np} + v_\mathrm{np} \frac{1}{a_{0\mathrm{n}}^{(+)} - 'U_0 - v_\mathrm{np}} v_\mathrm{np} \\ &= v_\mathrm{np} + v_\mathrm{np} \frac{1}{a_{0\mathrm{n}}^{(+)} - 'U_0} t_\mathrm{np}. \end{aligned} \tag{27}$$

We must, finally, evaluate the second matrix element in (23). Because of the approximate equality postulated in (25), it is possible to write the matrix element in question as

$$-\langle D(\mathbf{r}_\mathrm{p}\mathbf{r}_\mathrm{n})\varphi_\nu(\zeta_A)|(V_\mathrm{p} + 'U_0)\left[\frac{1}{a_{0\mathrm{n}}^{(+)} - U_0}\right]|\Psi_\mathrm{n}^{(+)}(\xi_{A+1}, \mathbf{r}_\mathrm{n}) - \lambda_0(\mathbf{r}_\mathrm{n})g_0(\xi_{A+1})\rangle.$$

Simple algebraic rearrangements of the type previously discussed permit us to rewrite this as the sum of *energy-shell* matrix elements. This result, which we quote, is

$$\begin{aligned} &-\langle D(\mathbf{r}_\mathrm{p}\mathbf{r}_\mathrm{n})\varphi_\nu(\zeta_A)|(V_\mathrm{p} + 'U_0)\left[1 + \frac{1}{a_{0\mathrm{n}}^{(+)} - U_0}(U_0 - W)\right]|\Psi_\mathrm{n}^{(+)}(\xi_{A+1}, \mathbf{r}_\mathrm{n})\rangle \\ &+\langle D(\mathbf{r}_\mathrm{p}\mathbf{r}_\mathrm{n})\varphi_\nu(\zeta_A)|(V_\mathrm{p} + 'U_0)\left[1 + \frac{1}{a_{0\mathrm{n}}^{(+)} - U_0}U_0\right]|\lambda_0(\mathbf{r}_\mathrm{n})g_0(\xi_{A+1})\rangle \\ \approx &-\langle D(\mathbf{r}_\mathrm{p}\mathbf{r}_\mathrm{n})\varphi_\nu(\zeta_A)|(V_\mathrm{p} + 'U_0)|\Psi_\mathrm{n}^{(+)}(\xi_{A+1}, \mathbf{r}_\mathrm{n}) - \eta_0^{(+)}(\mathbf{r}_\mathrm{n})g_0(\xi_{A+1})\rangle, \end{aligned}$$

if

$$\textstyle\sum' v_{\mathrm{n}j} \approx 'U_0 \text{ (operating on } \Psi_\mathrm{n}^{(+)}).$$

Then, if we can choose the A-particle potential $'U_0$ in such a way as to reproduce the average scattering, the matrix element under discussion vanishes. For, the lowest order of approximation permitted in our analysis is that which replaces the stationary state by the chosen configuration. Our summarizing result for the (pickup) matrix element is

$$T_\mathrm{dn} = \langle \Delta^{(-)}(\mathbf{r}_\mathrm{p}\mathbf{r}_\mathrm{n})\chi_\nu(\zeta_A)|t_\mathrm{np}|\eta_0^{(+)}(\mathbf{r}_\mathrm{n})g_0(\xi_{A+1})\rangle. \tag{28}$$

At least one feature, relative to (28), is worthy of mention here. There is another, but we shall defer its discussion to the next section. It has been possible to obtain the stripping (pickup) matrix element without specifying the potential V_p. We have considered it to be Hermitean but that is all. The potential is part of that which makes up the deuteron distortion in final states. We interpret the arbitrariness of the specification as support of the statement that: the potential (U_0+V_p) by which the deuteron distortion is achieved is *not necessarily* that which reproduces elastic scattering. It is possible to enumerate two additional instances in which this is also true (undoubtedly there are many others). In the case of the reaction (d, np), we have found [15]) an optical potential for the deuteron which is made up in equal parts of the proton and neutron optical potentials. Francis and Watson [16]), however, found a deuteron optical potential which was that one nucleon alone. In his discussion of (d, p), Tobocman [17]) finds that the deuteron optical potential which he requires has a slightly larger radius and absorption than that associated with a proton.

4. Conclusions and Summary

The matrix element of (28) has been shown to arise also in the case of the reactions (d, np) [15] †) and (p, 2p) [18]). This is undoubtedly not accidental but rather, in fact, due to the common basis of the several theories. We make this observation because the common feature is the appearance of some two-body *t*-matrix evaluated between distorted-wave states. In our view, this aspect is an important one for it implies the use of an additional approximation, the impulse approximation. It would seem quite reliable to replace the given *t*-matrix by that for free scattering in the distorted wave theories. We have cited some work in the introductory section of this paper which seems to support such a view.

The optical potentials of the theory are not those for elastic scattering as our arguments have indicated. That for the neutron-Y (target nucleus, for pickup) interaction certainly is generated by A and not $(A+1)$ particles. It doesnot seem possible to make equally definite statements concerning the deuteron potential. We have, however, discussed the various forms extant for this potential.

It next seems clear that the wave functions of shell model and cluster model representation are suited, if not demanded, for evaluation of the transition amplitude expressions. It is probably also true that the initial antisymmetrization of the target nucleus Y in $A+1$ particles has implications beyond that of heavy-particle stripping for the generic stripping reaction. We consider this to be an open question having aspects beyond the scope of the present investigation.

---

† Eq. (43) of this reference gives the result $T_{\mathrm{ba}} = \langle \psi_\mathrm{b}^{(-)}|V_{\mathrm{np}}|\psi_\mathrm{a}^{(+)}\rangle$ which is equal to $\langle \psi_\mathrm{b}^{(-)}|t_{\mathrm{np}}|\chi_\mathrm{a}^{(+)}\rangle$ using results such as (7).

The general validity of (28) is quite hard to assess, at least in terms of the simple methods employed. We do know, apart from obvious, superficial inspection, that it is a result which is first-order in the two-body scattering operators of the theory. We have been able to indicate that even in this order of approximation, certain other corrections arise. In particular, that arising out of multiple scattering has not been dealt with by us. Finally, it is clear that expressions such as (28) do seem to form the basis of the direct-interaction theories. Evaluations which then proceed to ignore the implications carried by such representations are, in our opinion, likely to encounter very many difficulties.

References

1) S. T. Butler, Proc. Roy. Soc. A **208** (1951) 559
2) The literature on this subject is extensive; see, for example, G. R. Satchler, Nuclear Physics **18** (1960) 110
3) K. M. Watson, Phys. Rev. **105** (1957) 1388
4) L. S. Rodberg, Ann. Phys. **9** (1960) 373
5) J. E. Young and P. R. Stein, Reactions in the $A = 4$ system (III) T(p, n) (to be published)
6) R. G. Thomas, Phys. Rev. **100** (1955) 25
7) W. Tobocman, Nucl. Phys. Lab. of Case Inst. of Techn., Technical Report No. 29 (1956)
8) H. Ui, Prog. Theor. Phys. **16** (1956) 299
9) A. M. Lane and D. H. Wilkinson, Phys. Rev. **97** (1955) 1199
10) J. E. Young and P. R. Stein, Cluster model wave functions for the three-body ground state (I) (to be published)
11) J. P. Elliott and A. M. Lane, Handbuch der Physik (Springer-Verlag, Berlin, 1957) Vol. 39, p. 398
12) H. A. Jahn, Proc. Roy. Soc. A **205** (1951) 192
13) L. Madansky and G. E. Owen, Phys. Rev. **99** (1955) 1608;
K. Hasegawa and Y. Ichikawa, Prog. Theor. Phys. **24** (1959) 569;
V. G. Neudachin, Soviet Physics (JETP) **8** (1959) 815
14) See, for example, J. S. Nodvik, in Proc. Intern. Conf. on the Nuclear Optical Model, Florida State University, Tallahassee, Florida (1959);
K. B. Mather and P. Swan, Nuclear scattering (Cambridge University Press) (see, in particular, pp. 395–401);
F. Bjorklund and S. Fernbach, Phys. Rev. **109** (1958) 1295
15) J. E. Young, Phys. Rev. **116** (1959) 1201
16) N. C. Francis and K. M. Watson, Phys. Rev. **93** (1954) 313
17) W. Tobocman, in Proc. Intern. Conf. on the Nuclear Optical Model, Florida State University, Tallahassee, Florida (1959)
18) K. F. Riley, H. G. Pugh and T. J. Gooding Nuclear Physics **18** (1960) 65

8.C

Nuclear Physics **23** (1961) 53—61; © *North-Holland Publishing Co., Amsterdam*

Not to be reproduced by photoprint or microfilm without written permission from the publisher

FERMIONS AND THE INTRINSIC PAULI PRINCIPLE

WOJCIECH KRÓLIKOWSKI

Institute of Theoretical Physics, University of Warsaw

and

Institute for Nuclear Research, Polish Academy of Sciences, Warsaw

Received 20 September 1960

Abstract: An approach to the problem of classification of elementary fermions proposed previously by the author is summed up. A possible extension of the formalism is pointed out. Then, some, so far undiscovered fermions ("hyperbaryons") are allowed, whereas in the primary formalism only the presently known ones appear (namely leptons ν, ν', e^-, μ^-, and baryons p, n, Λ, Σ^+, Σ^0, Σ^-, Ξ^0, Ξ^-, provided there are two types of neutrinos ν and ν').

1. Introduction

The aim of this paper is to sum up and extend an approach [1]) to the problem of elementary particles, which has as its starting point the experimental fact of absence of the multiple charges for leptons, baryons and mesons.

The experimental absence of multiple charges and also of higher spins is striking enough to be one of the most important qualitative questions of particle theory. A possible way to answer this question would be to look for some reasons of instability of particles with higher charges and spins. In this paper, however, another point of view is represented, namely that the lack of multiple charges and higher spins is a consequence of a fundamental principle, which plays in elementary particle physics a similar role to that of the Pauli principle in atomic and nuclear physics. We might call it the "intrinsic Pauli principle", because it would be related to intrinsic quantities. What is presented in this paper is just a formal realization of the intrinsic Pauli principle in the domain of charge properties of fermions. On the present stage spin properties will be treated phenomenologically.

It may be useful to say some words in advance about the relation between the present approach and the known compound theories e.g. Goldhaber's compound model. The compound theories would like to consider elementary particles as bound states of some primary particles. The present approach takes over some algebraic features of the compound theories, but avoids their mechanical picture. The following analogy may be here profitable. The intrinsic angular momentum or spin has some algebraic properties of the orbital angular momentum, but it is free from the mechanical picture of the latter. In a similar way, elementary particles have, according to the proposed approach, some formal properties of bound states, but the mechanical picture of bound states is avoided.

2. Formalism

In the formal scheme of field theory the state vector is acted on by field operators and the latter by some "universal operators" like coordinates x_μ, derivatives ∂_μ, spin matrices (e.g. Dirac matrices γ_μ) and isospin matrices (e.g. matrices τ_i): universal operators → field operators → state vector.

The appearance of some universal operators induces in the formal scheme some indices of field operators and, therefore, some degrees of freedom of particles. In this way, for instance, the operators $\tau_i = (\tau_{iBA})$ induce the isospinor index $A = 1, 2$ corresponding to a charge degree of freedom of the nucleon: $+e$ or 0 respectively. Here,

$$\tau_3 = \begin{pmatrix} 1 & 0 \\ 0 & -1 \end{pmatrix}.$$

Now, we will show that there are some simple universl operators, which induce the strangeness degree of freedom of the baryons and, moreover, do it in such a way that one gets exactly the presently known types of baryons. To this end let us take into account some operators ξ_α and their hermitian conjugates ξ_α^* satisfying the anticommutation relations,

$$\{\xi_\alpha, \xi_\beta^*\} = \delta_{\alpha\beta}, \quad \{\xi_\alpha, \xi_\beta\} = 0, \tag{1}$$

where $\alpha = 1, 2$ is by definition an isospinor index corresponding to charges 0 or $-e$ respectively. These operators have formal properties of annihilation and creation operators for the index α at the baryon field, and the index α is a statistical object obeying the Fermi-Dirac statistics and, therefore, the Pauli principle.

3. Baryons

Going on, let us denote by $B(x)$ a spinor field in the ordinary space and besides an abstract vector in a linear space induced by the existence of operators τ_i and ξ_α. In this abstract space the field $B(x)$ can be represented as follows

$$B(x) = \begin{pmatrix} B_A(x) \\ B_{A\alpha}(x) \\ B_{A\alpha_1\alpha_2}(x) \end{pmatrix}.$$

This representation could be called the "intrinsic Fock representation" for the field $B(x)$. The components with more than two α indices do not exist because of the Pauli principle.

Now, we can easily write down various observables connected with the field $B(x)$. For instance, the total isospin and total charge of the field $B(x)$ have the forms

$$\mathbf{T}^B = \int \mathrm{d}_3 x B^*(x)(\tfrac{1}{2}\boldsymbol{\tau}+\tfrac{1}{2}\xi_\alpha{}^* \tau_{\alpha\beta}\xi_\beta)B(x), \tag{3}$$

and

$$Q^B = \int \mathrm{d}_3 x B^*(x)[\tfrac{1}{2}(\tau_3+1)+\tfrac{1}{2}\xi_\alpha{}^*(\tau_3-1)_{\alpha\beta}\xi_\beta]B(x) = T_3{}^B+\tfrac{1}{2}N^B-\tfrac{1}{2}S^B, \tag{4}$$

where

$$N^B = \int \mathrm{d}_3 x B^*(x)B(x) \tag{5}$$

is the total number of B particles and

$$S^B = \int \mathrm{d}_3 x B^*(x)\xi_\alpha{}^*\xi_\alpha B(x) \tag{6}$$

can be identified with the total strangeness (with opposite sign). Then (4) is just the Gell-Mann-Nishijima formula.

The components of $B(x)$ in the representation (2) do not correspond to definite values of the total isospin. Thus, we change the representation by Clebsch-Gordan addition of individual isospins corresponding to A and α indices. In this way we obtain a new representation:

$$B(x) = \left(\begin{array}{cc} \multicolumn{2}{c}{\text{isodoublet}} \\ \multicolumn{2}{c}{(S^B = 0, Q^B = +e, 0)} \\ \text{isosinglet} & \text{isotriplet} \\ (S^B = 1, Q^B = 0) & (S^B = 1, Q^B = +e, 0, -e) \\ \multicolumn{2}{c}{\text{isodoublet}} \\ \multicolumn{2}{c}{(S^B = 2, Q^B = 0, -e)} \end{array}\right),$$

where S^B and Q^B denote the strangeness (with opposite sign) and charge of a single particle of the given fields. Thus we can identify

$$B(x) = \left(\begin{array}{cc} & p(x), n(x) \\ \Lambda(x) & \Sigma^+(x), \Sigma^0(x), \Sigma^-(x) \\ & \Xi^0(x), \Xi^-(x) \end{array}\right),$$

where

$$\left.\begin{matrix} p \\ n \end{matrix}\right\} = B_A, \quad \Lambda = \frac{1}{\sqrt{2}}(B_{12}-B_{21}), \quad \Sigma^+ = B_{11}, \quad \Sigma^0 = \frac{1}{\sqrt{2}}(B_{12}+B_{21}),$$

$$\Sigma^- = B_{22}, \quad \left.\begin{matrix} \Xi^0 \\ \Xi^- \end{matrix}\right\} = \frac{1}{\sqrt{2}}(B_{A12}-B_{A21}).$$

The quartet $S^B = 2$ is here impossible because of the Pauli principle (it would lead to symmetric combinations in α indices).

4. Leptons

Turning now to the leptons it seems natural to assume that the lepton field does not contain the index A, which was previously connected with nucleon features of the baryons. Thus, let us denote by $L(x)$ a spinor field in the ordinary space and besides an abstract vector in linear space induced by the existence of operators ξ_α (not taking into account operators τ_i). Then we get

$$L(x) = \begin{pmatrix} L_0(x) \\ L_\alpha(x) \\ L_{\alpha_1\alpha_2}(x) \end{pmatrix}, \tag{10}$$

$$\mathbf{T}^L = \int d_3x L^*(x) \tfrac{1}{2}\xi_\alpha{}^* \boldsymbol{\tau}_{\alpha\beta}\xi_\beta L(x), \tag{11}$$

$$Q^L = \int d_3x L^*(x) \tfrac{1}{2}\xi_\alpha{}^*(\tau_3 - 1)_{\alpha\beta}\xi_\beta L(x) = T_3{}^L - \tfrac{1}{2}S^L, \tag{12}$$

where

$$S^L = \int d_3x L^*(x)\xi_\alpha{}^*\xi_\alpha L(x) \tag{13}$$

may be called the total strangeness of the field $L(x)$.

By addition of individual isospins we obtain

$$L(x) = \begin{pmatrix} \text{isosinglet} \\ (S^L = 0,\, Q^L = 0) \\ \text{isodoublet} \\ (S^L = 1,\, Q^L = 0,\, -e) \\ \text{isosinglet} \\ (S^L = 2,\, Q^L = -e) \end{pmatrix}. \tag{14}$$

Here we can identify tentatively

$$L(x) = \begin{pmatrix} \nu(x) \\ \nu'(x),\, e^-(x) \\ \mu^-(x) \end{pmatrix}, \tag{15}$$

where

$$\nu = L_0, \quad \left.\begin{matrix} \nu' \\ e^- \end{matrix}\right\} = L_\alpha, \quad \mu^- = \frac{1}{\sqrt{2}}(L_{12} - L_{21}). \tag{16}$$

The triplet $S^L = 2$ is here impossible. We can see that we get two different kinds of neutrinos.

In this way we have constructed a formalism, in which only the presently known baryons and leptons appear (provided there are two neutrinos).

5. Undiscovered Fermions

If one wants to allow some additional (presently undiscovered) fermions, one must do two things: either to enlarge the number of dimensions of the isospace (see ref. [2]) and other references given there) or to admit beside the L and B fields also a spinor field with two A isospinor indices. In the latter case, denoting the new field by $H(x)$ we have

$$H(x) = \begin{pmatrix} H_{A_1A_2}(x) \\ H_{A_1A_2\alpha}(x) \\ H_{A_1A_2\alpha_1\alpha_2}(x) \end{pmatrix}. \tag{17}$$

Assuming Fermi-Dirac statistics also for the A indices, we obtain

$$\mathbf{T}^H = \int \mathrm{d}_3 x H^*(x) \tfrac{1}{2}\xi_\alpha^* \boldsymbol{\tau}_{\alpha\beta}\xi_\beta H(x) \tag{18}$$

and

$$Q^H = \int \mathrm{d}_3 x H^*(x)[\tfrac{1}{2}+\tfrac{1}{2}+\tfrac{1}{2}\xi_\alpha^*(\tau_3-1)_{\alpha\beta}\xi_\beta]H(x) = T_3{}^H + 2\cdot\tfrac{1}{2}N^H - \tfrac{1}{2}S^H, \tag{19}$$

where

$$N^H = \int \mathrm{d}_3 x H^*(x)H(x) \quad \text{and} \quad S^H = \int \mathrm{d}_3 x H^*(x)\xi_\alpha^*\xi_\alpha H(x). \tag{20}$$

By addition of individual isospins we obtain

$$H(x) = \begin{pmatrix} \text{isosinglet} \\ (S^H = 0, Q^H = +e) \\ \text{isodoublet} \\ (S^H = 1, Q^H = +e, 0) \\ \text{isosinglet} \\ (S^H = 2, Q^H = 0) \end{pmatrix}. \tag{21}$$

Let us remark that the fields $L(x)$, $B(x)$ and $H(x)$ exhaust all possibilities for fermion fields constructed by means of A and α indices obeying the Fermi-Dirac statistics. A general formula for the total isospin and total charge of the unified fermion field

$$F(x) = \begin{pmatrix} L(x) \\ B(x) \\ H(x) \end{pmatrix} \tag{22}$$

would be as follows

$$\mathbf{T}^F = \int \mathrm{d}_3 x F^*(x)(\tfrac{1}{2}X_A^* \boldsymbol{\tau}_{AB} X_B + \tfrac{1}{2}\xi_\alpha^* \boldsymbol{\tau}_{\alpha\beta}\xi_\beta)F(x) \tag{23}$$

and

$$Q^F = \int \mathrm{d}_3 x F^*(x)[\tfrac{1}{2} X_A{}^*(\tau_3+1)_{AB} X_B + \tfrac{1}{2}\xi_\alpha{}^*(\tau_3-1)_{\alpha\beta}\xi_\beta] F(x) = T_3{}^F + \tfrac{1}{2} G^F - \tfrac{1}{2} S^F, \quad (24)$$

where

$$G^F = \int \mathrm{d}_3 x F^*(x) X_A{}^* X_A F(x) \quad \text{and} \quad S^F = \int \mathrm{d}_3 x F^*(x) \xi_\alpha{}^* \xi_\alpha F(x). \quad (25)$$

Here X_A and $X_A{}^*$ are annihilation and creation operators of the index A:

$$\{X_A, X_B{}^*\} = \delta_{AB}, \quad \{X_A, X_B\} = 0. \quad (26)$$

If only L or B or H fermions are present in the system, we have respectively

$$G^F = \begin{cases} 0\, N^L \\ 1\, N^B \\ 2\, N^H \end{cases} \text{for} \begin{cases} L \text{ particles,} \\ B \text{ particles,} \\ H \text{ particles.} \end{cases} \quad (27)$$

We can see that G^F is a quantity of a kind similar to the strangeness S^F. It is a generalized baryonic number.

The proposed extension of the previous formalism would be very natural, but it would lead to four undiscovered fermions (cf. ref. [2])) belonging to a new family H ("hyperbaryons"), which would have unknown interaction properties. Speculations on these interactions may be attractive but are certainly premature. In any rate, these hypothetical hyperbaryons would be created (in collisions of known particles) only in particle-antiparticle pairs due to the conservation of G^F number.

6. Remark on Strong Interactions

From the point of view of the presented formalism only those interactions schemes are admissible, which can be expressed in terms of the formalism. In the case of strong interactions some additional criterion might be eventually provided by looking for only such forms of interaction, which would not be possible for leptons.

Simple, admissible baryon-pion interactions are the following:

$$\bar{B}\gamma_5 \boldsymbol{\tau} B \cdot \boldsymbol{\pi} = (\bar{N}\gamma_5 \boldsymbol{\tau} N + \bar{Y}\gamma_5 \boldsymbol{\tau} Y + \bar{Z}\gamma_5 \boldsymbol{\tau} Z + \bar{\Xi}\gamma_5 \boldsymbol{\tau} \Xi) \cdot \boldsymbol{\pi}, \quad (28)$$

where

$$N_A = B_A = \begin{cases} \mathrm{p} \\ \mathrm{n} \end{cases}, \quad Y_A = B_{A1} = \begin{cases} \Sigma^+ \\ \frac{1}{\sqrt{2}}(\Sigma^0 - \Lambda) \end{cases},$$

$$Z_A = B_{A2} = \begin{cases} \frac{1}{\sqrt{2}}(\Sigma^0 + \Lambda) \\ \Sigma^- \end{cases}, \quad \Xi_A = \frac{1}{\sqrt{2}}(B_{A12} - B_{A21}) = \begin{cases} \Xi^0 \\ \Xi^- \end{cases} \quad (29)$$

and

$$\bar{B}\gamma_5(\tau+\xi_\alpha{}^*\tau_{\alpha\beta}\xi_\beta)B\cdot\pi=\left(\bar{N}\gamma_5\tau N+\frac{2}{i}\bar{\Sigma}\gamma_5 x\Sigma+\bar{\Xi}\gamma_5\tau\Xi\right)\cdot\pi, \qquad (30)$$

where

$$\Sigma_1=-\frac{1}{\sqrt{2}}(\Sigma^+-\Sigma^-),\quad \Sigma_2=-\frac{i}{\sqrt{2}}(\Sigma^++\Sigma^-),\quad \Sigma_3=\Sigma_0. \qquad (31)$$

We can see that the first interaction is the globally-symmetric Gell-Mann interaction. The second interaction represents the coupling in a sense "proportional" to the isospin of baryons. This interaction would be excluded by our additional criterion, because the interaction $\bar{L}\xi_\alpha\tau_{\alpha\beta}\xi_\beta L\pi$ did not appear in the experiment.

A simple baryon-kaon interaction is

$$\begin{aligned}&\bar{B}\gamma_5\xi_\alpha{}^*BK_\alpha{}^G+\text{h.c.}\\ &\qquad=(\bar{Y}\gamma_5N-\bar{\Xi}\gamma_5Z)K_1{}^G+(\bar{Z}\gamma_5N+\bar{\Xi}\gamma_5Y)K_2{}^G+\text{h.c.}, \qquad (32)\\ &\qquad=-\frac{1}{\sqrt{2}}[K^*(\bar{\Lambda}\gamma_5N+\bar{\Sigma}\gamma_5\tau N)+(\bar{\Xi}\gamma_5\Lambda+\bar{\Xi}\gamma_5\tau\Sigma)K^G]+\text{h.c.},\end{aligned}$$

where

$$K=\begin{pmatrix}K^+\\ K^0\end{pmatrix},\quad K^G=i\tau_2K^*=\begin{pmatrix}\bar{K}^0\\ -K^-\end{pmatrix}. \qquad (33)$$

This interaction would be excluded by the additional criterium, because the interaction $\bar{L}\gamma_5\xi_\alpha{}^*LK_\alpha{}^G$+h.c. has not been experimentally observed.

The interaction

$$\bar{B}\xi_\alpha{}^*\tau_iBK_\alpha{}^G\pi_i+\text{h.c.}=[(\bar{Y}\tau N-\bar{\Xi}\tau Z)K_1{}^G+(\bar{Z}\tau N+\Xi\tau Y)]\cdot\pi+\text{h.c.}, \qquad (34)$$

on the contrary, is admissible also by the additional criterion.

7. Remark on Weak Interactions

The presented formalism could be also used to look for a definite form of the universal Fermi interaction. For instance a simple form is the following:

$$j_\mu{}^*j_\mu, \qquad (35)$$

where

$$j_\mu=\bar{L}\gamma_\mu(1+\gamma_5)\xi_-L+\bar{B}\gamma_\mu(1+\gamma_5)(\tau_-+\xi_-)B \qquad (36)$$

and

$$\xi_-=\xi_2,\quad \tau_-=\tau_+{}^*=\tfrac{1}{2}(\tau_1+i\tau_2)=\begin{pmatrix}0&1\\0&0\end{pmatrix}. \qquad (37)$$

Writing (36) explicitly we have

$$\begin{aligned} j_\mu = {} & \bar{\nu}\gamma_\mu(1+\gamma_5)e^- + \bar{\nu}'\gamma_\mu(1+\gamma_5)\mu^- \\ & + \bar{p}\gamma_\mu(1+\gamma_5)n + \bar{Y}^+\gamma_\mu(1+\gamma_5)Y^0 + \bar{Z}^0\gamma_\mu(1+\gamma_5)Z^- + \bar{\Xi}^0\gamma_\mu(1+\gamma_5)\Xi^- \\ & + \bar{p}\gamma_\mu(1+\gamma_5)Z^0 + \bar{n}\gamma_\mu(1+\gamma_5)Z^- + \bar{Y}^+\gamma_\mu(1+\gamma_5)\Xi^0 + \bar{Y}^0\gamma_\mu(1+\gamma_5)\Xi^-. \end{aligned} \tag{38}$$

Using this interaction we diminish the rate for the leptonic decay of $\Lambda(\Lambda \to p + e^- + \bar{\nu})$ by factor $\frac{1}{2}$ in comparison with the original Feynman-Gell-Mann value. It is due to the factor $1/\sqrt{2}$ in the field operator $Z^0 = (\Sigma^0 + \Lambda)/\sqrt{2}$.

Let us remark that the part of (38) containing ν, ν', e^-, μ^- and p, n, Λ only is invariant under simultaneous interchanges

$$\begin{matrix} \nu \leftrightarrow p \\ \nu' \leftrightarrow p \end{matrix}, \quad e^- \leftrightarrow n, \quad \mu^- \leftrightarrow \frac{1}{\sqrt{2}}\Lambda,$$

which is a modification of the symmetry considered by Gamba, Marshak and Okubo.

The lepton weak current in (38) changes the strangeness and charge according to the rule $\Delta S = -\Delta Q$. The same rule is valid also for the strangeness changing part of the baryon weak current in (38).

Instead of (36) one might use the form

$$j_\mu = \bar{L}\gamma_\mu(1+\gamma_5)(\xi_\alpha{}^*\tau_{-\alpha\beta}\xi_\beta + \xi_-)L + \bar{B}\gamma_\mu(1+\gamma_5)(\tau_- + \xi_\alpha{}^*\tau_{-\alpha\beta}\xi_\beta + \xi_-)B. \tag{39}$$

Writing (39) explicitly, one gets

$$\begin{aligned} j_\mu = {} & \bar{\nu}'\gamma_\mu(1+\gamma_5)e^- \\ & + \bar{\nu}\gamma_\mu(1+\gamma_5)e^- + \bar{\nu}'\gamma_\mu(1+\gamma_5)\mu^- \\ & + \bar{p}\gamma_\mu(1+\gamma_5)n + \sqrt{2}[\bar{\Sigma}^+\gamma_\mu(1+\gamma_5)\Sigma^0 + \bar{\Sigma}^0\gamma_\mu(1+\gamma_5)\Sigma^-] + \bar{\Xi}^0\gamma_\mu(1+\gamma_5)\Xi^- \\ & + \bar{p}\gamma_\mu(1+\gamma_5)Z^0 + \bar{n}\gamma_\mu(1+\gamma_5)Z^- + \bar{Y}^+\gamma_\mu(1+\gamma_5)\Xi^0 + \bar{Y}^0\gamma_\mu(1+\gamma_5)\Xi^-. \end{aligned} \tag{40}$$

The extra term $\bar{\nu}'e^-$ in (40) diminishes by a factor $\frac{1}{2}$ the relative coupling constant for μ capture in comparison with the coupling constant for μ decay and β decay, what is in contradiction with experiment.

It may be interesting to remark that one can write

$$Q^L = -\int d_3x L^*(x)\xi_-{}^*\xi_- L(x), \tag{41}$$

and

$$Q^B = \int d_3x B^*(x)(\tau_+{}^*\tau_+ - \xi_-{}^*\xi_-)B(x). \tag{42}$$

So, the universal Fermi interaction given by (35) and (36) is in a sense a factorization of the electromagnetic interaction.

This paper has been completed during the author's stay at the informal meeting on theories of elementary particles physics held at the University of Rochester in August 1—20 of 1960. The author is greatly indebted to Professor R. E. Marshak for his hospitality at the Department of Physics and Astronomy of the University of Rochester.

References

1) W. Królikowski, Nuclear Physics **8** (1958) 461; **11** (1959) 687; **17** (1960) 421
2) W. Królikowski, Bull. Acad. Polon. Sci. **6** (1958) 523

8.A

Nuclear Physics **23** (1961) 62—74; ©*North-Holland Publishing Co., Amsterdam*

Not to be reproduced by photoprint or microfilm without written permission from the publisher

INVESTIGATION OF THE PARAMAGNETISM OF μ-MESIC ATOMS

L. B. EGOROV, G. V. ZHURAVLEV, A. E. IGNATENKO, LI SYUANG-MING
M. G. PETRASHKU and D. CHULTEM
Joint Institute for Nulear Research, Dubna, USSR

Received 25 July 1960

Abstract: The nature of the paramagnetism of various mesic atoms is investigated by measuring the asymmetry of ($\mu-$e)-decay electrons. The results of the experiments indicate that paramagnetism of mesic atoms in dielectrics and diamagnetic and weakly paramagnetic normal metals is due to the magnetic moment of the μ-meson. In paramagnetic transition metals, lanthanides and actinides it is due to the magnetic moments of the electron shell and the meson. It is demonstrated that polarized mesons can be used as a means for investigating the magnetic properties of atoms and hydrides of the transition metals, actinides and lanthanides with zero nuclear spins.

1. Introduction

A study of the fine and hyperfine structure effects in atomic systems and of related quantum electrodynamic effects is of great interest. Many relevant investigations have been concerned with a study of the phenomena in ordinary atoms and in postitronium. However, it should be of considerable interest to investigate them in such atomic systems as muonium and μ-mesic atoms. This is rendered possible by the fact that the μ-meson beams from accelerators are polarized. Unfortunately the beam intensities presently available are such that investigations of muonium and mesic atoms are possible only if they are produced in condensed matter. As is well known complications may be introduced by the medium.

Results of investigation of the hyperfine structure in μ-mesic atoms due to spin coupling between the meson and nucleus have been reported in ref. [1]). In the present work attention is mainly directed to the hyperfine structure caused by meson-electron coupling. Attempts to directly observe this effect during the formation of muonium in condensed matter have not yielded positive results [2]). Likewise, no success was encountered in an attempt to detect the phenomenon in mesic atoms with $Z \leqq 6$ [2]). One naturally inquires whether the phenomenon might exist in μ-mesic atoms with $Z \geqq 6$. There should be some advantage in employing mesic atoms with $Z \geqq 6$ for this purpose. In fact, data on the properties of the magnetic moments of ions of paramagnetic substances indicate that it may be possible to choose such mesic atoms and such substances for which the influence of the medium should be negligible. In this case a study of hyperfine structure effects in a "pure form" should be possible. The practical significance of such effects is manifold. Some of the reasons are presented below.

(a) Considerable depolarization of polarized μ^--mesons in matter occurs as a result of interactions which are the cause of the fine and hyperfine structure in the mesic atoms [1]). The question now arises whether it may not be possible to remove or restore the meson polarization in mesic atoms. Evidently, depolarization due to the hyperfine structure caused by spin coupling between the meson and nucleus can be avoided by employing substances with zero nuclear spin. It would seem that depolarization due to the fine structure or hyperfine structure caused by spin coupling between the meson and electon shell could be excluded by employing a magnetic field of sufficient strength. However removal of depolarization by magnetic neutralization encounters insurmountable experimental difficulties. Moreover, kinematic depolarization during $(\pi-\mu)$-decay in flight also cannot be avoided. The fact that the depolarization time ($\approx 10^{-12}$ sec) is smaller than the meson lifetime τ by several orders of magnitude suggests that statical methods of nuclear polarization may be used to restore the polarization of mesons in mesic atoms with zero nuclear spins. Two methods are of interest for our purposes. These consist in superimposing magnetic fields on the sample at sufficiently low temperatures. The first method is based on the action of an external magnetic field on the nuclear magnetic moment and the second on the action of the internal atomic magnetic field caused by noncompensated electron moments.

The coefficient for nuclear polarization by direct action of the external field can be expressed [3]) as

$$f = \tfrac{1}{3}\frac{I+1}{I}\frac{\mu_N H}{kT}, \tag{1}$$

where I is the nuclear spin, μ_N the nuclear magnetic moment, k Boltzmann's constant, H the impressed magnetic field and T the absolute temperature.

When internal atomic magnetic fields are employed the nuclear polarization is defined by the expressions [3])

$$f \approx \begin{cases} \tfrac{1}{3} f_e \dfrac{I+1}{I}\dfrac{J_e}{2J_e+1}\dfrac{\Delta W}{kT}, & J_e \geqq 1, \quad \text{(2a)} \\ \tfrac{1}{3} f_e \dfrac{I+1}{2I+1}\dfrac{\Delta W}{kT}, & J_e \leqq 1. \quad \text{(2b)} \end{cases}$$

Here, f_e is the electron polarization, J_e their angular momentum and ΔW the hyperfine multiplet splitting energy.

From expressions (1) and (2) it follows that the larger μ_N and ΔW are and the smaller I is, the easier it should be to attain a given polarization.

Since the μ-meson spin is $\frac{1}{2}$ and the magnetic moment is greater than the nuclear magneton by an order of magnitude, it should be possible to obtain a given meson polarization in mesic atoms by employing temperatures which are higher by an order of magnitude or by employing smaller magnetic fields than in the case of nuclei. It is possible that a noticeable restoration of meson polarization may be attained even at helium temperatures. Everything depends on the magnitude of J_e and ΔW in the mesic atoms. Thus in order to select the most suitable polarization method in each given case the nature of mesic atom paramagnetism in various media should be investigated. This problem reduces to that of determining what happens to the electron shell of the initial atoms during mesic atom formation and how the paramagnetism of isolated mesic atoms changes in the medium.

It should be noted that insurmountable difficulties may be encountered by employing the external field method because the meson spin relaxation time is large compared with τ. These difficulties will not arise if atomic internal fields are used. Indeed, the electron moments in the sample atoms may be polarized prior to meson irradiation. The meson spin flip time in the field of the mesic atom shell will then be determined [1]) by the "interaction time" $t' \approx \hbar/\Delta W \approx 10^{-10}$ sec which is smaller than τ by many orders of magnitude.

(b) As is generally known, one of the most effective methods available at present for investigating the electron configuration of paramagnetic atoms consists in studying the asymmetry of emitted polarized nuclei. Evidently this method can be applied only to elements possessing nonzero nuclear spins. Asymmetry studies of decay electrons from polarized μ-mesons in mesic atoms, affords the opportunity for investigating the electron structure of paramagnetic atoms with zero nuclear spins.

(c) The μ^--meson spin can be directly determined by measuring the gyromagnetic ratio for mesic atoms possessing only electron spin paramagnetism due to a single unpaired electron and a zero nuclear spin.

(d) Investigation of mesic atom paramagnetism is necessary for elucidation of the μ^-- meson depolarization processes.

2. Basic Theoretical Premises

The formation of mesic atoms involves violation of the state of the electron shell of the initial atom. The point here is that during cascade transitions excitation and ionization of atoms may occur. After formation of the mesic atoms the shell electrons are found to be in the field of a nucleus with a new effective charge $Z-1$. This circumstance may also lead to ionization of the shell. For free mesic atoms the lifetime t_0 of the excited state of the shell depends only on the electron configuration and degree of excitation. The lifetime t_0 strongly depends on the nature of the binding between atoms of the medium if the mesic atoms are produced in a medium. If the mesic atom is in a metal the electron shell returns to the ground state during a very short time (less than 10^{-12} sec) as compared with t' and τ. On the other hand, in ionic crystals or dielectrics $t_0 > t'$ and τ. Thus at the moment of decay of the mesic atom the state of the electron shell will depend on the type of the compound containing the investigated atom and on the aggregate state of the substance.

It should be noted that if the atom is in a molecule, the reorganization of the electron shell and emission of X-rays from the mesic atoms should respectively lead to destruction of the chemical bonds and ejection of the mesic atom as a free atom. In view of these so-called mesic atom electron and kinetic activation effects, the paramagnetic moment of the mesic atom should be directly related to the values of quantum numbers J, L and S of the atom.

If an isolated mesic atom with zero nuclear spin has an electron shell moment, the paramagnetic moment will consist of three parts:

1) the μ-meson magnetic moment

$$\mu_\mu = \frac{\sqrt{3}M_B}{207}, \tag{3}$$

2) electron orbital magnetic moment

$$\mu_L = M_B\sqrt{L(L+1)}, \tag{4}$$

3) electron spin magnetic moment

$$\mu_S = 2M_B\sqrt{S(S+1)}. \tag{5}$$

When formation of mesic atoms occurs in a medium their paramagnetism will be subject to the action of neighboring atoms and as a result some of the moments will be compensated. Everything depends on the shells whose electrons create the magnetic moment. By analogy with the properties of the magnetic moments of paramagnetic ions it may be expected that if the mesic atoms are produced from lanthanide or actinide atoms in which the magnetic moment is caused by low lying atomic electrons not easily affected by external factors, the mesic atom paramagnetism will be due to the μ_L, μ_S and μ_μ moments. For atoms of the transition elements in which the magnetic moment is produced by shallow electrons which are easily affected by external factors, the mesic atoms in a medium will possess only spin moments μ_S and μ_μ (the orbital moments of such atoms as a rule are compensated). Finally, mesic atoms of diagmagnetic or weakly paramagnetic normal metals may possess in a medium only μ_μ moments.

In substances with uncompensated moments, the electon shell can influence the μ^--meson polarization only when the mesic atom is at the ground state. This can easily be verified by comparing the time the meson is at lower levels t, with the time of meson spin flip in the field of the shell t'. It turns out that the inequality $t' \ll t$ as mentioned in section 1, is fulfilled only for the 1s level.

It should be noted that in substances with $J_e \neq 0$ the mesic atoms will be produced in two hyperfine structure states with $F = J_e \pm \frac{1}{2}$. In a first approximation the hyperfine structure interaction energy ΔW will be of the same order of magnitude as that in muonium

$$\Delta W = -\frac{32\mu_\mu p_{\mathrm{eff}}}{3a_{e\mu}^3}.$$

Here μ_μ is the μ-mesic atom magnetic moment, p_{eff} the effective magnetic moment of the electron shell, $a_{e\mu}$ the Bohr radius of the hydrogen atom. The hyperfine splitting in the ground state of the mesic atom is much larger than $\hbar/\tau$. Thus states with $F = J_e + \frac{1}{2}$ and $F = J_e - \frac{1}{2}$ in isolated mesic atoms yield a noncoherent mixture. Each state will be characterized by its own values of the gyromagnetic ratio g and magnetic moment μ. The expressions for g and μ have the following form [4]):

$$g_+ = \frac{1}{J_e+\frac{1}{2}}(\mu_\mu + p_{\mathrm{eff}}), \tag{6}$$

$$g_- = -\frac{1}{J_e+\frac{1}{2}}\left(\mu_\mu - \frac{J_e+1}{J_e}p_{\mathrm{eff}}\right), \tag{7}$$

$$\mu_+ = \mu_\mu + p_{\mathrm{eff}}, \tag{8}$$

$$\mu_- = -\frac{2J_e-1}{2J_e+1}\left(\mu_\mu - \frac{J_e+1}{J_e}p_{\mathrm{eff}}\right). \tag{9}$$

If measurement of decay electron asymmetry is used to study the paramagnetism of mesic atoms, the experimental precession curve will be the superposition of precession curves of mesons decaying from both hyperfine structure states. Evidently, the larger the value of J_e, the more difficult it should be to interpret the curve. Indeed let P_0 denote the degree of polarization of the μ-meson beam. According to refs. [4, 6–8]) the degree of polarization P of a meson in the K-shell averaged over the two hyperfine structure states will be

$$P = \tfrac{1}{6}P_0 \cdot \tfrac{1}{3}\left[1 + \frac{2}{(2J_e+1)^2}\right]. \tag{10}$$

From this formula it follows that the magnitude of the polarization depends on the total moment of the electron shell J_e. Thus, for example, for $J_e = \frac{1}{2}$ the polarization will decrease by two times. For mesic atoms with $J_e \gg 1$ it decreases three times. Obviously the foregoing refers to isolated mesic atoms. The presence of a medium may complicate the picture by causing, for example, the appearance of meson transitions between hyperfine structure levels.

3. Experimental

When choosing a substance for the investigations it should be kept in mind that those consisting of one type of atoms or continaing hydrogen are of practical interest. The reason of this is that substances with various types of atoms complicate the interpretation of the experiments because the probabilities for mesic atom formation in the various components are unknown. It may be expected that hydrogen in hydrogeneous substances will not play an appreciable role in mesic atom production.

In the present experiments the following substances were chosen:

1) dielectrics (paraffin, polythene, water, sulphur);
2) diamagnetic and weakly paramagnetic normal metals (graphite, magnesium, zinc, cadmium and lead);
3) paramagnetic transition metals (chromium, molybdenum, palladium and tungsten).

The results of investigations with H_2O, Mg, Zn, Cd, and Pb have been published [12]). In the present work the remaining substances have been employed. Chromium, molybdenum and palladium were used in the metallic form. Graphite, polythene and paraffin were in carbon containing substances. The reasons for choosing these substances are as follows. As is well known, the problem concerning the direction of the μ^--meson spin is still unsolved [9]). One of the methods suggested for solving this problem [10]) consists in studying the asymmetry of decay electrons from B^{12} in the reaction $\mu^- + C^{12} \rightarrow B^{12} + \nu$. No asymmetry was detected in the corresponding experiments [9]). The explanation of this is probably that the B^{12} in the samples (hexane, penthane) become depolarized.

According to ref. [10]) depolarization of B^{12} nuclei may occur (1) because of the hyperfine structure due to spin coupling between the nucleus and electron shell of the B^{12} atoms, and/or (2) because of the small relaxation time of the B^{12} nuclear spin in the substances employed compared to the lifetime of B^{12}.

In order to verify the existence of a depolarization mechanism of B^{12} nuclei due to the hyperfine structure we worked with samples containing carbon atoms in different compounds. It was expected that in such media the carbon mesic atoms would possess an electron configuration similar to that of the boron atom shell [10]).

The paramagnetism of carbon, chromium, molybdenum, tungsten and palladium mesic atoms in the media mentioned above was studied by the precession method [5]). One can draw conclusions regarding the nature of the paramagnetism by this method by measuring the asymmetry of (μ—e)-decay electrons in any of the two following two ways. Firstly, the electronic circuit is tuned on to record the precession frequency of the free meson spin. It can be seen from formulas (6) and (7) that in a given magnetic field *H*, the spin precession frequency of mesic atoms possessing an electron moment and meson moment will exceed the spin precession frequency of mesic atoms whose paramagnetism is due exclusively to the meson spin. Thanks to the large difference in the frequencies, conclusions regarding the nature of the paramagnetism can be drawn by measuring the number of $(\mu-e)$-decay electron $N_{\max}$ and $N_{\min}$ at two field strengths corresponding to those satisfying the formula

$$t_1+\Delta t = \tfrac{1}{2}T = \frac{\pi mc}{eH}, \tag{11}$$

where t_1 is the delay time, Δt is the "gate" width and T the precession period of a "free" muon. Indeed, for mesic atoms possessing electron moments, the ratio $\xi = N_{\max}/N_{\min}$ will be equal to unity. Mesic atoms whose paramagnetism is due only to the meson spin will have a value of ξ which differs from unity. A straightforward experimental check of the existence of electron paramagnetism would consist in measuring ξ in hydrides of paramagnetic metals at hydrogen concentrations for which the paramagnetism of the compound approaches zero such at in $PdH_{0.6}$. As a matter of fact, the palladium atoms in a $PdH_{0.6}$ solution do not possess a magnetic moment. On the other hand hydrogen will not participate in the formation of the mesic atoms.

A second method for investigating the nature of the paramagnetism would be to measure the asymmetry of $(\mu-e)$-decay electron when the electronics is biased to record the mesic atom spin precession frequency computed in accordance with formulas (6) and (7). However, this type of experiment is more difficult to realize. From formula (10) it can be seen that in this case the quantity ξ will differ much less from unity if the mesic atoms have an electron moment. Moreover, the existence of two hyperfine structure states and also the presence of meson transitions between them (e.g. from $F = 1$ and $F = 0$) complicate interpretation of the experiments. In the present work paramagnetism was investigated by the first method.

The experimental arrangement used was the same as that employed in our previous experiments [11, 12]). The experimental conditions, excluding the electronics, were also the same. A block diagram of the apparatus is shown in fig. 1. Negative μ-mesons stopped in target 6 were recorded by $(1+2-3)$ anticoincidence circuit 8. After amplification in 10 and shaping in 12 the pulses from circuit 8 were delayed by a time t_1. The delayed pulses actuated trigger 16 which simultaneously opened two identical gating circuits 18 and 21 during a time Δt. Muon decay electrons and also the background from spurious radiations were recorded by the $(3+4-2)$ anticoincidence circuit 9. The pulses from circuit 9 were amplified in 11, shaped in 13 and then divided into two pulses. These pulses entered "gate" 18 with a delay $t_2 > t_1+\Delta t$ and gating circuit 21 with no delay. By using two identical gating circuits and introducing the delay t_2 it was possible to record the decay electron counting rate and the background rate in scalar 23 and simultaneously record the background counting rate alone in scalar 20. The difference between these two counting rates yields that due to decay electrons. Pulses from trigger 16 were fed through a separate exit to scalar 17 which recorded the gate opening rate. This scalar served as a monitor.

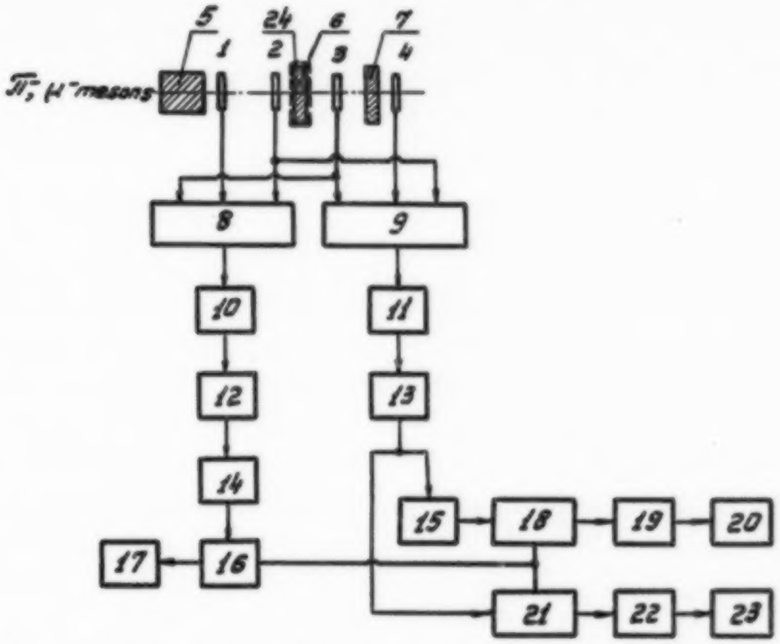

Fig. 1. Block diagram of the experimental arrangement. 1, 2, 3, 4: scintillation counters. 5: copper absorber. 6: target. 7: paraffin absorber. 8, 9: anticoincidence circuit. 10, 11: amplifiers. 12, 13: shaping circuits. 14: delay line t_1. 15: delay line t_2. 16: trigger circuit. 18, 21: gate circuits. 19, 22: discriminators. 17, 20, 23: scalers. 24: magnetic coil.

TABLE 1

Values of ξ

Substance	$\xi = N_{\max}/N_{\min}$
graphite	1.10 ± 0.02
paraffin	1.09 ± 0.02
polythene	1.10 ± 0.02
palladium hydride	1.09 ± 0.02
palladium	1.00 ± 0.02
chromium	1.00 ± 0.02
molybdenum	0.99 ± 0.02
tungsten	0.99 ± 0.02

In each experiment the ratio $t_1/\Delta t$ was approximately equal to 0.2. The angles between the direction of the meson beam and the axes of the electron detector and target were respectively 90° and 45°. The size of the target was 15×15 cm^2; the target thickness was 4—6 g/cm^2. In experiments with graphite, polythene and paraffin the thicknes of paraffin filter 7 between counters 3 and

4 was 4 g/cm^2. In the chromium, molybdenum, tungsten and palladium experiments paraffin filter 7 was replaced by a 4 g/cm^2 aluminium filter. By employing the aluminium filter it was possible to reduce the counting efficiency for γ-rays with energies below 10 MeV emitted from the target as a result of absorption of μ^--mesons [13]) to less than 10^{-3}.

The values of $\xi = N_{\max}/N_{\min}$ thus obtained are given in the second column in table 1. In these values, corrections were included to take into account the delay time, gate width, meson decay and solid angle of the electron detector. The errors are standard statistical deviations.

4. Discussion of the Results

It can be seen from the table that within the experimental errors the values of ξ for graphite, polythene, paraffin and palladium hydride $PdH_{0.6}$ are the same. The values of ξ for chromium, molybdenum, tungsten and palladium also turned out to be the same. However, the absolute values of ξ in these two cases are different. It should be noted that within the experimental errors the value of a_0 for graphite (a_0 is the asymmetry coefficient in the angular distribution $1+a\cos\theta$ integrated over the electron energies) derived from ξ is the same as the value of a_0 obtained in refs. [1, 11, 12]) by measuring a large number of points on the precession curve. The fact that ξ differs from unity in graphite, paraffin and polythene and that they are equal to each other indicates that in such media the paramagnetism of carbon mesic atoms is due exclusively to the magnetic moment of the meson. Indeed, consider first the case of mesic atoms being formed in metals. In a first approximation metals, including graphite, can be considered as a set of ions immersed in an electron gas. If the metal is diamagnetic or a weakly paramagnetic normal metal, its ions will have no magnetic moment. Therefore due to the fact that $t_0 \ll t'$ it is probable that during mesic atom formation in such metals the electron state of the ions ultimately will not be violated and ionization of the atoms will only involve emission of collectivized conductivity electrons. From the fact that the values of a_0 for metals of this group such as Mg, Zn, Cd and Pb are the same according to the results of ref. [12]) and also that they equal the value of a_0 for graphite, it may be concluded that no electron paramagnetism arises during the formation of mesic atoms in diamagnetic or weakly paramagnetic normal metals. The situation will be different for mesic atoms formed in dielectrics for which $t_0 \gg t'$. In carbon mesic atoms in paraffin and polythene, oxygen mesic atoms in water and also sulphur mesic atoms there are two reasons why the electron moment may be absent. This may happen if the mesic atoms are negative ions possessing the electron configuration of the initial atoms. Secondly, it may happen that mesic atom formation is due to a disturbance of the electron shell of the initial atoms. According to (ref· [6] the electron moment will vanish if it is completely compensated under the action of the neighbouring atoms. A choice between these two possibilities can be made only on basis of further investigations. The results of these experiments should permit one to decide whether there really exists a mechanism of depolarization of B^{12} nuclei resulting from the hyperfine structure due to spin coupling between the nucleus and electron shell of boron atoms produced in the $\mu^- + C^{12} \rightarrow B^{12} + \nu$ reaction. As a matter of fact it would appear that carbon mesic atoms in graphite should have the electron configuration of the boron atoms [10]). However, the experiments indicate that there is no magnetic moment. Evidently no electron paramagnetism can arise in boron atoms produced in the $\mu^- + C^{12} \rightarrow B^{12} + \nu$ reaction in graphite. Therefore in graphite there should be no depolarization mechanism of B^{12} nuclei caused by the hyperfine structure. For reasons mentioned above this mechanism may be effective during the formation of boron mesic atoms in dielectrics.

Some information on the probabilities of mesic atom formation in the various components of hydrogeneous media can be obtained by comparing the values of ξ for graphite, polythene and paraffin. In fact within the experimental errors the polarizations of these substances are equal and the precession frequencies of the mesic atom spins are identical to the "free" meson spin frequency. This signifies that in such media the mesons are not "trapped" by the hydrogen atoms. There are two possible explanations of this circumstance. First of all the μ-mesons may chiefly "settle" directly onto the carbon atoms. This explanation is not inconsistent with the Fermi-Teller "Z law". Secondly, there is the possibility that when mesons are stopped in such media the probability for mesic atom formation may not be proportional to Z. The residual meson polarizations in such media will then be equal only if capture of mesons from hydrogen by carbon atoms occurs during a time which is smaller than the time required for transition of the meson in a mesic proton to those orbits in which depolarization occurs. In other words, due to the large density of carbon atoms in such media, capture occurs only from orbits of mesic protons with $n \geqq 3$ (refs. [6, 7])). Indeed, if, for example, the probability for capture into mesic atomic orbits were proportional to the density of the atoms in the medium and capture occurred from the 1s level in hydrogen, the degree of polarization would equal

$$P_{\mathrm{CH}_2} = \tfrac{1}{3}P_{\mathrm{C}} + \tfrac{2}{3}P_{\mathrm{H}}P_{\mathrm{C}} = \tfrac{1}{3}P_{\mathrm{C}},$$

where

$$P_{\mathrm{H}} = \tfrac{1}{6}P_0 \cdot \tfrac{1}{3}\left[1 + \frac{2}{(2I+1)^2}\right] = \tfrac{1}{12}P_0$$

is the degree of polarization of the meson in the mesic hydrogen K orbit, $P_{\mathrm{C}} = \tfrac{1}{6}P_0$ the degree of polarization in the carbon mesic atom orbit and P_0 the degree of polarization of the μ-meson beam. The results of the present experiments, however, indicate that in hydrogeneous media the meson "settle" onto carbon in such a way that their polarization remains unchanged.

The results of experiments with palladium and $PdH_{0.6}$ yield direct proof that the paramagnetism of palladium mesic atoms is due to the magnetic moments of the electron shell and the meson. As a matter of fact, ions of the transition metal palladium possess a magnetic moment which is produced by electrons of the inner magnetoactive 4d shells. Measurements of ξ for graphite, paraffin and polythene indicate that in $PdH_{0.6}$ hydrogen does not effect meson depolarization.

Special mention should be made of the fact that, as experiments with Pd and $PdH_{0,6}$ show, polarized μ^--mesons can be used as a means for investigating the magnetic properties of atoms and hydrides of the transition metals, lanthanides and actinides with zero nuclear spins. Unfortunately, it is not possible to perform a control experiment which would directly confirm the presence of electron paramagnetism in the case of Cr, Mo and W. The reason of this is that hydrides are not formed when hydrogen is dissolved in these metals.

The values of ξ for these transition metals may equal unity and be equal to each other in either of the following cases: 1) complete depolarization of mesons occurs in such metals, or 2) the mesic atom paramagnetism is due to the magnetic moments of the electron shell and μ^--meson.

Consider now the problem of μ^--meson depolarization in various mesic atoms. Measurements [12]) of the degree of depolarization of μ^--mesons in mesic atoms of metals belonging to the zero nuclear spin diamagnetic group of metals show that within the experimental errors the polarization in all cases was the same and was $\approx 17\ \%$. The degree of polarization of mesons for graphite, polythene and paraffin deduced on basis of measured values of ξ are also the same, their absolute value being the same as that for the abovementioned metals. The absolute value of the measured polarization and the fact that for $Z \geqq 6$ it is independent of Z are in good agreement with the theoretical calculations [6, 7]) which take into account only spin-orbit interaction. It is difficult to imagine that in respect to μ^--meson depolarization the metals Cr and Mo should significantly differ from the substances indicated above. In fact, it has been shown in ref. [14]) that during slowing down and capture into the upper layers of mesic atoms, the mesons practically do not depolarize. As is well known the probability for mesic atom formation is equal to one. The elements Cr and Mo also consist of atoms of which 80 to 90 % have zero nuclear spins. The nuclei of these atoms do not possess any properties which can induce complete depolarization of the mesons. Therefore it is very improbable that in mesic atoms with such values of Z there exist depolarization mechanisms which differ from the spin-orbit mechanism. The only difference between Cr and Mo and the substances mentioned above is that the former have unfilled inner electron shells. Thus experiments with Pd and $PdH_{0.6}$ indicate with a high degree of probability that in the case of Cr and Mo whose ions possess a nonzero magnetic moment due to the electrons of the inner magnetoactive 3d and 4d shells respectively, it is the hyperfine structure that is involved.

The results of the tungsten experiments deserve special attention inasmuch as in contrast to Pd, Cr and Mo, tungsten has mesic atoms with deformed nuclei. It has been shown in ref. [15]) that interaction between the meson and quadrupole deformation of the nucleus may lead to considerable depolarization of the μ^--mesons. We may now compare the measured values of $\xi_{\text{meas.}}$ with those predicted theoretically, $\xi_{\text{theor.}}$. If the hypothesis that the observed meson depolarization and quadrupole deformation of the nucleus are related phenomena is correct, then according to theoretical predictions [15]), the following relation should hold for the values ot a_0 for carbon and tungsten: $|a_0|_W = 0.4(a_0)_C$. In this case the precession frequency of a tungsten mesic atom spin in a magnetic field should be the same as that of the "free" meson spin. By employing the normal error distribution law it can be shown that the case $\xi_{\text{theor.}} = \xi_{\text{meas.}}$ can be rejected since $\xi_{\text{meas.}} < \xi_{\text{theor.}}$ with a probability of 70 %. This means that the experimentally observed "complete" depolarization of mesons cannot be explained by invoking only interaction between the meson and quadrupole deformation of the nucleus. Another explanation is required for this purpose. The experiments with Pd, Cr and Mo show that it is highly probable that in the case of W a hyperfine structure due to spin coupling between the meson and electrons of the inner unfilled 5d shell is also involved.

It should be mentioned here that despite the small effective magnetic moment of tungsten with respect, say, to chromium atoms, it is noticeable in the present experiments as a result of the high sensitivity of the investigation technique. In fact, the μ-meson magnetic moment is larger than the nuclear magneton by an order of magnitude, whereas the meson spin flip time in the field of a mesic atom shell ($\approx 10^{-10}$ sec) is smaller than its lifetime by many orders of magnitude. Evidently, to make these conclusions more definite it would be desirable to make straightforward observations on the precession curves of the Cr, Mo and W mesic atom spin curves.

The results of the present work and of other investigations [1, 11, 12]) permit one to draw the following conclusions regarding the μ^--meson depolarization process: 1) interaction between the magnetic moments of the meson and electron shell affects meson polarization only in mesic atoms of the transition elements, lanthanides and actinides; 2) the degree of μ^--meson polarization may decrease by a factor of 6 as a result of spin-orbit interaction. This result is in good agreement with the theoretical calculations carried out in refs. [6, 7]).

The authors consider it a pleasant duty to express their appreciation to Prof. V. P. Dzhelepov for continued interest in this work. The authors are also thankful to S. S. Gerstein, D. F. Zaretsky and V. M. Novikov for discussion of the results.

References

1) L. B. Egorov, A. E. Ignatenko and D. Chultem, JETP **37** (1959) 1517
2) V. W. Hughes, D. Lurio, D. P. Malone, L. Lederman and M. Weinrich, Bull. Am. Phys. Soc. **3** (1958) 51;
D. McColm, V. W. Hughes, D. P. Malone, L. Lederman and A. Lurio, Bull. Am. Phys. Soc. **3** (1958) 229;
D. McColm, K. Ziock, V. W. Hughes, S. Penman and R. Prepost, Bull. Am. Phys. Soc. **5** (1960) 75;
R. A. Swanson, Phys. Rev. **112** (1958) 580;
J. M. Cassels, T. W. O. 'Keeffe, M. Righby, A. M. Wetherell and J. R. Wormald, Proc. Phys. Soc. A **70** (1957) 543
3) M. E. Rose, Nucleonics **3** (1948) 23
4) H. Uberall, Phys. Rev. **114** (1959) 1640
5) R. Garwin, L. Lederman and M. Weinrich, Phys. Rev. **105** (1957) 1415
6) V. A. Djarbsahyan, JETP **36** (1959) 277
7) I. M. Shmushkevich, JETP **36** (1959) 646
8) I. S. Shapiro and L. D. Blokhintsev, JETP **37** (1959) 760;
E. I. Dolinsky, Thesis, Nuclear Research Institute of the Moscow State University (1959)
9) A. I. Alikhanov, Report at the High Energy Physics Conference in Kiev (July 1959) pp. 10–11
10) J. D. Jackson, S. B. Treiman and H. W. Wyld, Phys. Rev. **107** (1957) 327
11) A. E. Ignatenko, L. B. Egorov, B. Khalupa and D. Chultem, JETP **35** (1958) 894
12) A. E. Ignatenko, L. B. Egorov, B. Khalupa and D. Chultem, JETP **35** (1958) 1131
13) D. D. Vovanovitch, Phys. Rev. **117** (1960) 1580
14) G. F. Ford and C. J. Mullin, Phys. Rev. **108** (1958) 477
15) D. F. Zaretsky and V. M. Novikov, JETP **37** (1959) 1824

8.B

Nuclear Physics **23** (1961) 75—89; © *North-Holland Publishing Co., Amsterdam*

Not to be reproduced by photoprint or microfilm without written permission from the publisher

PROCESSES OF DEPOLARIZATION OF NEGATIVE MUONS

A. E. IGNATENKO

Joint Institute for Nuclear Research, Dubna, USSR

Received 4 August 1960

Abstract: The processes of depolarization of negative muons in different substances are investigated by measuring the asymmetry of electrons of the ($\mu-e$)-decay with scintillation counters. It is found that the most intense depolarization of muons occurs after their slowing-down in the formation of mesic atoms. It is shown that there are the following causes of the depolarization of muons in the mesic atom: a) spin-orbit interaction leading to a fine structure of the energy levels; b) interaction of the magnetic moment of muons and nucleus responsible for a hyperfine structure of mesic atoms; c) interaction between the muon and the quadrupole deformation of the nucleus and d) the interaction between the magnetic moment of the muon and that of the electron shell. The principal features of each process of depolarization are analyzed.

1. Introduction

Muons hold a place of their own among the elementary particles known at present. Similar to electrons and positons in many phenomena, they differ essentially in masses and lifetimes. From the field viewpoint this difference could be a consequence of the difference in the interactions of muons and electrons with other elementary particles. Yet the latter difference has not yet been detected. Of immense interest in this connection would be the investigation of the interaction of muons with other particles, the interaction between fermion pairs (proton, neutron; muon, neutrino), for example. Detection of non-conservation of parity in weak interactions has opened up a number of possibilities for investigating this type of interaction experimentally. Thus in a number of papers it has been suggested that the asymmetry of the products of reactions accompanying the nuclear absorption of polarized muons should be studied. The interaction of a muon with nuclei depends largely on the stage of the muon. This state in turn depends on the processes of the polarized muons in a substance before the capture of the latter by the nucleus. Therefore investigation of the depolarization of muons in different substances is of immense interest.

2. Theory

The depolarization of negative muons in a substance can be divided into two stages: the depolarization occurring in the slowing-down of negative muons and that occurring in the formation of mesic atoms. From refs. [1-4]) it follows that there is no depolarization due to the scattering of muons by unpolarized electrons and in the Coulomb nuclear field. Nor can there be any depolarization of the slowed-down muons as a result of the interaction of their magnetic moment with the magnetic fields in a substance, as is shown in refs. [5–7]). The depolarization will be the most essential after the slowing-down in the formation of mesic atoms. The causes of depolarization are as follows: 1) spin-orbit interaction leading to a fine structure of the energy levels of the mesic atom, 2) interaction of the magnetic moments of the muon and the nucleus responsible for a hyperfine structure of mesic atoms, 3) interaction of the muon with the quadrupole deformation of the nucleus and 4) interaction of the magnetic moment of the muon with the magnetic field of the electron shell. We will consider these mechanisms one by one in the following.

2.1. MECHANISM OF SPIN-ORBIT INTERACTION

In the cascade of transitions to the ground state, the mesic atom passes through a large number of intermediate states. For the lower levels the inequality holds

$$\Delta_{nl} \gg \Gamma_{nl}, \tag{1}$$

where Δ_{nl} is the distance between the levels of the fine structure with the quantum numbers n and l but different $j = l \pm \frac{1}{2}$, while Γ_{nl} is the width of the respective level, equal to the sum of the radiation width and the Auger transition width. Physically, the inequality (1) means that the duration of the muons at the given level is much longer than the time of the reorientation of the muon spin in the magnetic field created by the muon orbital motion. The mean value of the degree of polarization of muons in the K-orbit of mesic atoms was calculated in refs. [8–10]). The idea behind the calculations can be summed up as follows. A muon with spin-projection S_z^0 on the z-axis is considered. This muon at the moment $t = 0$ is captured by the Coulomb field of the nucleus into the shell characterized by n and l. Since only the spin state of the muon is determined at the initial moment, the state of the muon in the shell (n, l) at $t = 0$ is described by the set of $(2l+1)$ wave functions

$$\Phi_0(0) = h_{nl}(r) Y_{ll_z^0}(\mathbf{r}/r) \chi_{sS_z^0}, \tag{2}$$

where $R_{nl} Y_{ll_z^0}$ is the normalized wave function of the mesic atom without taking account of the spin, with l_z^0 the projection of the orbital moment. All values $l_z^0 = -l, -l+1, \ldots +l$ have the same degree of probability $P_{l_z^0} = 1/(2l+1)$. If the spin is taken into account the state of the muon in the mesic atom is characterized, apart from n and l, by its total moment $j = l \pm \frac{1}{2}$ and the projection of the total moment j_z on the z-axis. Consequently the wave function of the stationary state will be of the form

$$\psi_{nljj_z}(t) = R_{nlj}(r) \Omega_{jlj_z}(\mathbf{r}/r) \mathrm{e}^{-\frac{i}{\hbar} E_{nlj} t}, \tag{3}$$

where

$$\Omega_{jlj_z} = \sum_{l_z S_z} C^{jj_z}_{ll_z SS_z} Y(\mathbf{r}/r)\chi_{SS_z}$$

is the spherical spinor, $C^{jj_z}_{ll_z SS_z}$ is the Clebsch-Gordan coefficient, and E_{nlj} is the binding energy of the muon in the subsehell (nlj) of the mesic atom. It is to be noted that the initial wave function (2) is not a function of the type (3) taken at the moment $t = 0$, but is the following superposition of two stationary solutions with the given n, l and $j = l \pm \frac{1}{2}$:

$$\Phi(0) = \sum_j C^{jj_z^0}_{ll_z^0 SS_z^0} \varphi_{nljj_z^0}(0), \quad j_z^0 = l_z^0 + S_z^0.$$

Obviously, the wave function of the muon which at $t = 0$ had the form (2) will at the moment $t > 0$ have the form

$$\Phi(t) = \sum_j C^{jj_z^0}_{ll_z^0 SS_z^0} \varphi_{nljj_z^0}(t). \tag{4}$$

If the condition (1) is fulfilled the states with $j = l + \frac{1}{2}$ and $j = l - \frac{1}{2}$ can be considered independently. Then from (4) it is not difficult to obtain the expression for the probability P_j of the muon being in the state (n, l) with the given j

$$P_j = \frac{1}{2l+1} \sum_{l_z^0} (C^{jj_z^0}_{ll_z^0 SS_z^0})^2 = \frac{2j+1}{2(2l+1)}. \tag{5}$$

On the other hand, the average value of the operator σ_z for the muon in the state with the given n, l and j, equal to the degree of its polarization in the state, can be expressed by the relations

$$\langle \sigma_2 \rangle_{nlj} = \frac{[\frac{3}{4} + j(j+1) - l(l+1)]^2}{3j(j+1)} = \begin{cases} \dfrac{2l+3}{3(2l+1)} (2S_z^0) & \text{at} \quad j = l + \frac{1}{2}, \\ \dfrac{2l-1}{3(2l+1)} (2S_z^0) & \text{at} \quad j = l - \frac{1}{2}. \end{cases} \tag{6}$$

Since the muons are probably, initially captured into the states with sufficiently large l 11), we can obtain from (4) and (5)

$$P_j \approx \tfrac{1}{2} \quad \text{and} \quad \langle \sigma_z \rangle_{nlj} \approx \tfrac{1}{3}(2S_z^0). \tag{7}$$

Physically, this means 8) that the mesons, captured to the highly excited levels of the mesic atom, get, with approximately equal probability, into the states $j = l + \frac{1}{2}$ and $j = l - \frac{1}{2}$, conserving about one-third of their initial polarization in the process. Under the assumption that the transitions of muons to the ground states of the mesic atom occur due to the dipole radiative and Auger transitions, it was shown in ref. 8) that starting from the state $(n, l, j = l + \frac{1}{2})$, muons reach the K shell, preserving a polarization equal to one-third of the initial figure, while starting from the state $(n, l, j = l - \frac{1}{2})$ they reach it totally depolarized.

Thus, whereas at the initial moment the totally polarized muon is captured into the shell (n, l), the degree of muon polarization in the K-orbit of the mesic atom will amount to: 17 %, according to refs. [8, 9]) and 50 %, according to ref. [10]). It will be emphasized that the knowledge of the probability of the incidence of mesons at the initial moment on different shells (n, l) and the knowledge of the meson transition paths from the excited to the ground states is of great importance. Yet there is no sufficiently reliable information on this point.

2.2. MECHANISM OF HYPERFINE STRUCTURE CONDITIONED BY THE SPIN BINDING OF MUON AND NUCLEUS

This mechanism will affect the polarization of the muon in the ground and excited states of the mesic atom. This becomes clear if we compare the duration t' of the meson at the lower levels with the time t of the reorientation of the muon spin in the field of the nucleus. According to the estimates in refs. [10, 12–15]) the value of t proves to be much less than t'.

Let us describe the essence of the matter for a particular case when the spin of the nucleus $I = \frac{1}{2}$ and the polarized meson with the projection of spin on the z-axis equal to $\frac{1}{2}$ goes into the K orbit of the mesic atom at the initial moment. Owing to the interaction of the hyperfine structure, the mesic atom in the case under consideration can be in states with the total spin $F = 1$ and $F = 0$. If the nucleus is not polarized, the sum of the projections on the z-axis of the spins of the nucleus and meson assumes, with equal probability, the values $I_z + S_z = 1$ and $I_z + S_z = 0$. In the first case the spin state of the system (muon+nucleus) is assigned at $t = 0$ by the function $\Phi_1(0) = \chi_{\frac{1}{2}}\chi_{\frac{1}{2}}$, and in the second by $\Phi_0(0) = \chi_{\frac{1}{2}}\chi_{-\frac{1}{2}}$ (where the first spinor refers to that of the muon and the second to that of the nucleus). Obviously, at the moment $t > 0$ the wave functions will have the respective forms:

$$\Phi_1(t) = \chi_{\frac{1}{2}}\chi_{\frac{1}{2}} e^{-\frac{i}{\hbar}E_1 t},$$

and

$$\Phi_0(t) = \tfrac{1}{2}\left\{(\chi_{\frac{1}{2}}\chi_{-\frac{1}{2}} + \chi_{-\frac{1}{2}}\chi_{\frac{1}{2}}) e^{-\frac{i}{\hbar}E_1 t} + (\chi_{\frac{1}{2}}\chi_{-\frac{1}{2}} - \chi_{-\frac{1}{2}}\chi_{\frac{1}{2}}) e^{-\frac{i}{\hbar}E_0 t}\right\},$$

where E_1 and E_0 are the mesic atom binding energies in states with $F = 1$ and $F = 0$.

Thus the wave function is the eigenfunction of the mesic atom (with allowances for the hyperfine structure) for the states $F = 1$ and $F_z = 1$ in the case of the initial condition $\Phi_1(0)$ and the superposition of the states with $F = 1$, $F_z = 0$ and $F = 0$ in the case of the initial condition $\Phi_0(0)$. The states with $F = 1$ and $F = 0$ are incoherent [12]). Taking into account the fact that in the states $F = 1$, $F_z = 0$ and $F = 0$ the muon is completely depolarized and in the states $F = 1$ and $F_z = 1$ it conserves polarization, we come to the conclusion that the muons in the K orbit of the mesic atom conserve only 50 % of their initial polarization. In the general case when the spin of the nucleus $I \gg \frac{1}{2}$, the probability for the muon and the nucleus to form the system with total spin $F = I \pm \frac{1}{2}$ and projection M_F [14]) is equal to

$$N_+(M_F) = \frac{I+M_F+\frac{1}{2}}{(2I+1)^2}, \quad N_-(M_F) = \frac{I-M_F+\frac{1}{2}}{(2I+1)^2}.$$

The normalization is chosen so that

$$N_+ = \sum_{M_F} N_+(M_F) = \frac{I+1}{2I+1}, \quad N_- = \sum_{M_F} N_-(M_F) = \frac{I}{2I+1}, \quad N_+ + N_- = 1,$$

where the sign $\pm$ corresponds to $F = I \pm \frac{1}{2}$.

The polarization of the muon in these states

$$\langle \sigma_{z\mu} \rangle_+ = \frac{2I+3}{3(2I+1)}, \quad \langle \sigma_{z\mu} \rangle_- = \frac{2I-1}{3(2I+1)},$$

or, after averaging,

$$\langle \sigma_{z\mu} \rangle = N_+ \langle \sigma_{z\mu} \rangle_+ + N_- \langle \sigma_{z\mu} \rangle_- = \frac{1}{3}\left[1 + \frac{2}{(2I+1)^2}\right]. \tag{8}$$

This formula shows that the polarization of muons depends on the spin of the nucleus: for example, for the nuclei with $I = \frac{1}{2}$, the polarization should decrease to one half; and for the nuclei with $I \gg 1$, to one-third. Detailed consideration was given to the depolarization in the excited states of mesic atoms in ref. [10]) for the case $I = \frac{1}{2}$. Thus, the total decrease of polarization due to the hyperfine structure interaction in the ground and excited states must be equal to one-third. It is noteworthy that each state of the hyperfine structure will be characterized by its value of g gyromagnetic ratios [14])

$$g_+ = \frac{1}{I+\frac{1}{2}} (\mu_\mu + \mu_N), \tag{9}$$

$$g_- = -\frac{1}{I+\frac{1}{2}} \left(\mu_\mu - \frac{I+1}{I} \mu_N\right), \tag{10}$$

where μ_μ and μ_N are the magnetic moments of the meson and the nucleus respectively. Obviously, the above applies to the case of isolated mesic atoms. A medium can complicate the picture, bringing about the muon-transitions between the hyperfine levels, for example. Thus in metals two types of transitions are possible, either accompanied by the conversion on conductivity electrons or magnetic dipole radiation [16]), while in liquid hydrogen a μ-meson may jump from one proton to another with the concurrent transition to the lower state of the hyperfine structure [17]).

2.3. MECHANISM OF DEPOLARIZATION DUE TO THE INTERACTION OF MUON WITH THE DEFORMATION OF NUCLEUS

This mechanism was analyzed in ref. [18]) for even nuclei. The diagonalization of the Hamiltonian of the meson-nucleus system $H = H_0+H_R+H_q$ (where H_0 is the muon Hamiltonian in the monopole field of the nucleus, H_R is the nuclear rotational energy operator and H_q is the operator of quadrupole interaction between muon and nucleus) shows that quadrupole interaction essentially changes the eigenfunctions of the system corresponding to the muon only in two 2p-states [19]). In this approximation, the polarization P of muon in 1S-state can be written in the form

$$P = A_q W_{\frac{1}{2}} \langle \sigma_{2p_{\frac{1}{2}}} \rangle_0 + B_q W_{\frac{3}{2}} \langle \sigma_{2p_{\frac{3}{2}}} \rangle_0,$$

where $W_{\frac{1}{2}}$ and $W_{\frac{3}{2}}$ are the probabilities of the muon's passing through $2p_{\frac{1}{2}}$ and $2p_{\frac{3}{2}}$-states, $\langle \sigma_{2p_{\frac{1}{2}}} \rangle$ and $\langle \sigma_{2p_{\frac{3}{2}}} \rangle$ are the polarizations of the muon in these states without quadrupole interaction, and A_q and B_q are the factors taking into account the depolarization caused by the above-mentioned defect. In the cascade transition of the muon into the 1S-state there is a certain probability that the nucleus will remain in the excited first rotational level [19]) the lifetime of which ($\approx 10^{-9}$ sec) is sufficient for the reorientation of the muon spin in the 1S-state due to the hyperfine splitting of the 1S-state. The factor determining the depolarization D_q caused by this effect is equal to $D_q \approx 1-\frac{2}{3}W_e$, where W_e is the probability of excitation of the first rotational level of the nucleus.

In considering [18]) the muon transitions from the upper levels to the 1S-state through the states described by the eigenfunction of the Hamiltonian H it was found that $P \approx \frac{1}{6}B_q D_q$. The values B_q and D_q obtained and the values of the quantities determining them, the splitting E_{fs} of the fine structure of the 2p-level, the energy E_R of the first rotary level of the nucleus and $E_q = \langle 2p|H_q|2p\rangle$, are given in table 1.

As is clear from table 1, the interaction of the muon with the deformation of the nucleus may lead to considerable muon depolarization.

TABLE 1

Values of B_q and D_q

Element	E_{fs}(keV)	E_R(keV)	E_q(keV)	B_q	D_q
Gd^{156}	91.5	79	52	0.63	0.61
W^{184}	137	112	43	0.64	0.64
Th^{232}	216	52	83	0.38	0.6
U^{238}	226	44	91	0.38	0.59

2.4. MECHANISM OF HYPERFINE STRUCTURE DUE TO THE SPIN CONNECTION OF THE MUON AND THE ELECTRON SHELL

The formation of the mesic atoms involves the destruction of the state of the electron shell of the initial atom, since excitation and ionization of atoms are possible in the muon cascade transitions. After the formation of mesic atoms the shell electrons are found in the field of the nucleus with a new effective charge $z-1$. This can also lead to the ionization of the shell. The lifetime t_0 of the excited state of a shell for free mesic atoms depends only on the electron configuration and degree of excitation.

In the formation of mesic atoms in a medium the time t_0 strongly depends on the nature of the binding of the atoms of the medium. If the mesic atom is in a metal the electron shell returns to the ground state within a very short period (less than 10^{-12} sec) as compared with the lifetime of the muon τ. In ionic crystals or dielectrics, on the other hand, the lifetime $t_0 > \tau$. Consequently at the moment of the mesic atom decay the electron shell state will depend on the type of binding which includes the atom under study and the aggregate state of the substance. The electron shell can influence the polarization of muons only in the ground state [23]). This can easily be seen if the duration t' of the muon in the lower levels is compared with the time t of the reorientation of the muon spin in the field of the shell. Taking into account the fact that in the first approximation the energy of the hyperfine structure interaction in mesic atoms will be of the same order as in muonium,

$$\Delta W = -\frac{32\mu_\mu p_{\text{eff}}}{3a_{e\mu}{}^3},$$

(here μ_μ is the magnetic moment of the muon p_{eff} is the effective magnetic moment of the electron shell and $a_{e\mu}$ is the Bohr radius) it is easy to see that the inequality $t \ll t'$ holds only for the 1S-level.

If the isolated mesic atom with zero nuclear spin has an electron shell moment, the paramagnetic moment will be composed of three parts:

1) magnetic moment of the muon $\mu_\mu = \sqrt{3}M_B/207$;
2) electron orbital moment $\mu_L = M_B\sqrt{L(L+1)}$;
3) electron spin moment $\mu_S = 2M_B\sqrt{S(S+1)}$.

During the formation of mesic atoms in a medium their paramagnetism will be influenced by the neighbouring atoms with the resulting compensation of some moments. Everything depends on which shells give rise to the magnetic moment. By analogy with the properties of the ion magnetic moments of paramagnetic substances, it can be expected that if the mesic atoms are formed out of the atoms of lanthanides or aktinides in which the magnetic moment is due to the deeply seated electrons which are least of all subject to external influences, the paramagnetism of these mesic atoms in the medium will be caused by the moments μ_L, μ_S and μ_μ. In the case of the atoms of the transitional elements in which the magnetic moment of the atoms is due to the valence electrons which are most of all subject to external influences, the mesic atoms in the medium can possess only spin moments μ_S and μ_μ. Finally the mesic atoms of diamagnetic or weakly paramagnetic normal metals can, in the medium, possess only the moments μ_μ.

It is noteworthy that in substances with $p_{\mathrm{eff}} \neq 0$, the mesic atoms of the hyperfine structure with $F = J_e \pm \frac{1}{2}$ will be formed in two states. The hyperfine splitting in the ground state of the mesic atom is much larger than $\hbar/\tau$. Therefore the states with $F = J_e + \frac{1}{2}$ and $F = J_e - \frac{1}{2}$ for the isolated mesic atom form an incoherent mixture. An analysis similar to one for the mechanism of subsection 2.2 shows that the degree of polarization P of a muon in the K orbit averaged over two states of hyperfine structure will be equal

$$P = \tfrac{1}{3}P_0 \left[1 + \frac{2}{(2J_e+1)^2}\right], \tag{12}$$

where J_e is the angular moment of the electron shell and P_0 is the degree of the muon polarization at the initial moment of its entering the K shell.

3. Experiment

The intensities of muon accelerator fluxes being what they are, an experimental check of the predictions of the theory is possible only for the formation of mesic atoms in a condensed substance. A medium can complicate the picture. In selecting a substance for investigation, it is necessary to bear in mind that substances composed of the atoms of one kind are of practical interest, or alternatively, hydrogeneous substances. The fact is that using a substance composed of atoms of different kinds will multiply the difficulties of interpreting the experiments since the relative probabilities of formation of mesic atoms in different components are unknown. There is a hope that hydrogen in hydrogeneous substances will play no essential role in the formation of mesic atoms. It is important to select substances in a way as to ensure the possibility of bringing out the principal features of each mechanism of depolarization. This can be attained by using the following substances as study objects:

1) dielectrics (liquid hydrogen, paraffin, polythene, water, sulphur and phosphorus);

2) diamagnetic and weakly paramagnetic normal metals (graphite, magnesium, aluminium, zinc, cadmium and lead);

3) paramagnetic transitional metals (chromium, molybdenum, palladium and tungsten).

Indeed, in the formation of mesic atoms in those substances of groups 1) and 2) which are from 85 to 95 % atoms with zero nuclear spins, it can be expected that the muons will be depolarized only due to mechanism a). If mesic atoms are formed in the metals of group 3) containing internal d-electrons in atoms with zero nuclear spins, the depolarization of muons will occur due to the mechanisms of subsections 2.1 and 2.4, and in the mesic atoms of deformed nuclei (tungsten) also due to mechanism c). Finally, in using the substances of groups 1) and 2) the atoms of which have non-zero spins the principal mechanism of the depolarization will be that of subsections 2.1 and 2.2.

The polarization of the muons in these substances was studied in refs. [20-23]) by measuring the anisotropy in the angular distribution of the decay electrons $1+a\cos\theta$ by the precession method [24]). The anisotropy was measured in the following manner. For all substances of group 1) in which the mechanism of subsect. 2.1 must be the principal mechanism of depolarization, the electron system was tuned for detecting the frequency of the spin precession of free mesons. In experiments with the substances of group 1) (and group 2)) with non-zero nuclear spins, the electron system was tuned for detecting the frequency of the mesic atom spin precession calculated by eqs. (9) and (10). The case with the existence of the mechanism of subsect. 2.4 in the substances of group 3) is more complicated. The solution can be obtained by measuring the asymmetry of the (μ—e)-decay electrons in the following two methods. Under the first method the electron system is tuned for detecting the frequency of the spin precession of a free meson. As follows from eqs. (9) and (10), in the given magnetic field H the frequency of the spin precession of the mesic atoms possessing an electron moment and a meson moment will be by several orders higher than that of the spin of a free muon. Owing to a large difference in the frequencies, the character of paramagnetism of mesic atoms can be assessed by measuring the number of the electrons $N_{\max}$ and $N_{\min}$ at two values of the strength of the magnetic field (in which the target is) corresponding to those calculated by the formula

$$t_1+\Delta t = \tfrac{1}{2}T = \frac{\pi mc}{eH},$$

where t_1 is the delay time, Δt is the width of "gate" and T is the precession period. Indeed, for the mesic atoms possessing an electron moment the ratio $\xi = N_{\max}/N_{\min}$ is equal to unity; for the mesic atom in which paramagnetism is due solely to the muon spin the value ξ will be different from unity. As a test experiment directly confirming the existence of electron paramagnetism under this method of investigation, the quantities ξ could be measured in the hydrides of paramagnetic metals at the concentration of hydrogen for which the paramagnetism of the compound decreases to zero, $PdH_{0,6}$ for example. Indeed, the atoms of palladium in the solution $PdH_{0,6}$ are devoid of magnetic moments and no hydrogen will take part in the formation of mesic atoms. The second method of investigating the nature of paramagnetism consists in measuring the asymmetry of electrons when the electron system is tuned for detecting the frequency of the spin precession of mesic atoms calculated by eqs. (9) and (10).

These experiments are more difficult, however. Indeed, the quantity ξ in this case will differ from unity much less, as was observed in experiment with the mesic atoms having electron moments and is clear from eq. (12). Besides, the existence of the two states of hyperfine structures as well as the meson transitions among them (from $F = 1$ to $F = 0$, for example) will complicate the interpretation of the experiment. In ref. [23]) paramagnetism was investigated by the first method.

The values of a_0, coefficients of asymmetry for the entire integral spectrum obtained for the above substances in refs. [20–23]), as well as the value of $\xi = N_{max}/N_{min}$ are given in table 2. Corrections were introduced into the indicated quantities a_0 and ξ to take account of the delay time, the width of the "gate", the muon decay and the solid angle on the electron detector. The errors indicated are standard statistical deviations.

TABLE 2

Experimental values

Group	No.	Substance	Nuclear spin	$-a_0$	$\xi = N_{max}/N_{min}$
Dielectrics	1	Liquid hydrogen	$\frac{1}{2}$	0.005 ± 0.005	
	2	Polythene	0		1.10 ± 0.02
	3	Paraffin	0		1.09 ± 0.02
	4	Water	0	0.043 ± 0.005	
	5	Sulphur	0	0.042 ± 0.006	
	6	Phosphorus (red)	$\frac{1}{2}$	0.025 ± 0.005	
Diamagnetic and weakly paramagnetic normal metals	7	Graphite	0	0.045 ± 0.005	1.10 ± 0.02
	8	Magnesium	0	0.058 ± 0.008	
	9	Zinc	0	0.056 ± 0.011	
	10	Cadmium	0	0.055 ± 0.012	
	11	Lead	0	0.054 ± 0.013	
	12	Palladium hydride $PdH_{0,6}$	0		1.09 ± 0.02
	13	Aluminium	$\frac{5}{2}$	0.007 ± 0.007	
Paramanetic transitional metals	14	Chromium	0		1.00 ± 0.02
	15	Molybdenum	0		0.99 ± 0.02
	16	Palladium	0		1.00 ± 0.02
	17	Tungsten	0		0.99 ± 0.02

4. Comparison of Theory with Experiment

Given the quantities a_0 and ξ, it is possible to determine the degree of polarization of μ^--mesons, for example, by comparing with the asymmetry observed in the decay of the μ^+-mesons under the assumption that μ-decay is invariant with respect to the joint transformation of inversion of spacial coordinates and charge conjugation. If this requirement is fulfilled it is easy to show that the following relation holds:

$$\frac{a_-}{P_-} = \frac{a_+}{P_+}, \tag{13}$$

where P_+ and P_- are the degrees of polarization, a_+ and a_- are the asymmetry coefficients integrated over the energy of positon (negaton) angular distribution $1+a_\pm \cos \theta$ for μ^+ and μ^--mesons respectively. From eq. (13) it follows that the degrees of polarization may be compared by comparing the quantities a_0 and ξ. As follows from table 2, the quantities a_0 and ξ for graphite, paraffin, polythene, water, magnesium, sulphur, zinc, cadmium and lead prove to be equal within statistical errors. The degree of polarization obtained from the quantities a_0 and ξ reaches a magnitude of the order of 17 %. The independence of the quantities a_0 and ξ of z for $z \geqq 6$ as well as their absolute values are in good agreement with the theoretical calculations of refs. [8-9]) taking account of only the mechanism of subsect. 2.1 and are not in agreement with similar calculations of ref.[10]). These facts as well as the coincidence of the frequencies of the spin precession of these mesic atoms and the "free" muon show that there is no depolarization by the mechanism of subsect. 2.4. To see this, let us first consider the case when mesic atoms are formed in metal. Metals including graphite can be regarded in the first approximation as aggregates of ions in an electron gas. If a metal belongs to group 2), its ions have no magnetic moments. Therefore it is probable that in the mesic atom formation resulting from the lifetime t_0 of the excited state of the electron shell being far smaller than the time of the reorientation t' of the muon spin in the magnetic field, the electron state of the ion is not destroyed in the last analysis, while the ionization of atoms is accompanied merely by the emission of collectivized conductivity electrons. The equality of the quantities ξ for these metals and palladium hydride $PdH_{0,6}$ is evidence that no electron paramagnetism arises in the above-mentioned metals of group 2).

The case is different for the formation of mesic atoms in dielectrics in which $t_0 \gg t'$. There may be no depolarization mechanism (subsect. 2.4) in the mesic atoms of carbon in paraffin and polythene of hydrogen in water, and of sulphur for two reasons. First, this may happen when mesic atoms are negative ions with the electron configuration of the initial atoms. Second, it is possible that the formation of mesic atoms involves the destruction of the electronic shell of the initial atoms. Then, according to ref. [9]) there will be no electronic moment if the latter is fully compensated by the actions of the neighbouring atoms. Only further investigations can decide which of the two assumptions is true.

The results of experiments with palladium and palladium hydride show directly that the muon depolarization in palladium occurs due to the mechanisms of subsects. 2.1 and 2.4. Indeed, the ions of this transitional metal have a magnetic moment caused by the electrons of the internal magneto-active H_d-shells. In the compound $PdH_{0,6}$ hydrogen has no effect on depolarization, as is shown by the equality of the quantities ξ measured for graphite, polythene and paraffin.

The fact that the quantities ξ for the transitional metals chromium and molybdenum of group 3) coincide and are equal to unity can be observed in two cases:

1) the depolarization of mesons in these substances is total; 2) the paramagnetism of mesic atoms is due to the magnetic moments of the electron shell and the muon.

For these metals it is unfortunately impossible to carry out a test experiment, directly confirming electronic paramagnetism, similar to the experiment with palladium. The cause is that no hydrides are formed in the solution of hydrogen in these metals. It can hardly be supposed that chromium and molybdenum would essentially differ from the above-mentioned substances of groups 1) and 2) in any respect as regards the depolarization of muons. Indeed, the probability of formation of mesic atoms is known to equal unity. The elements Cr and Mo are also from 80 to 90 % atoms with zero nuclear spins. The nuclei of these atoms possess no properties which could entail total muon depolarization. Consequently it is improbable that there might be other depolarization mechanisms apart from mechanism a) in the mesic atoms with such z. The only point of difference of Cr and Mo from the above substances is that the atoms of the former have half-filled inner shells. Therefore, the results of experiments with Pd and $\mathrm{PdH}_{0,6}$ show with high probability that in the case of Cr and Mo whose ions have a non-zero magnetic moment due to the electrons of the 3d- and 4d-shells, respectively, we are also dealing with depolarization mechanism (subsect. 2.4).

The results of experiments with tungsten deserve special notice, since unlike Pd, Cr and Mo, tungsten has mesic atoms with deformed nuclei. If the assumption on the connection between the "depolarization" of muons observed and the quadrupole deformation of the nucleus is correct, then according to theoretical predictions [18]) the following relation $(a_0)_n \approx 0.4\ (a_0)_c$ should exist between the quantities a_0 for carbon and tungsten. In this case the precession frequency in the magnetic field of the spin of tungsten mesic atoms should coincide with that of the spin of a "free" muon. Using the normal law of the distribution of errors it can be shown that the case $\xi_{\mathrm{theor}} = \xi_{\mathrm{meas}}$ is outruled, since $\xi_{\mathrm{meas}} < \xi_{\mathrm{theor}}$ with a 70 % probability. This fact shows that the "total" muon depolarization observed in experiment can hardly be explained by only the interaction of the muon with the deformation of the nucleus. The results of experiment for Pd, Cr and Mo are evidence that, in the case of tungsten, we are probably dealing with mechanism 2.4, apart from depolarization mechanisms 2.1 and 2.2. It will be noted that though the atoms of tungsten have a very small effective magnetic moment, as compared with chromium atoms, for example, this magnetic moment can be observed in these experiments give a sufficiently sensitive method of investigation. Indeed, muons have a magnetic moment which is an order larger than the nucleon magneton, while the time of spin reversal of the muon in the field of the mesic atom shell ($\approx 10^{-10}$ sec) is by many orders smaller than its lifetime. Obviously, to make the above-mentioned conclusions more definite it is also necessary to observe directly the curves of spin precession of the mesic atoms Cr, Mo and W.

Let us now turn to the results of experiments for the substances, the atoms of which have non-zero nuclear spins.

The precession of mesic atoms with mesic nuclei(meson-nucleus system) in the state $F = 1$ [22]) was actually observed in experiments with phosphorus. This fact directly indicates that in such mesic atoms there is mechanism 2.2), apart from depolarization mechanism 2.1).

In experiments with liquid hydrogen [20]) and aluminium [22]) no dependence of the counting speed of electrons on the magnetic coil current was found. Since the precession curve observed in the experiments with aluminium is a result of the superposition of the muon precession curves in the hyperfine structure states $F = 3$ and $F = 2$, it proved impossible to interpret the curve obtained. Let us compare the quantities a_0 measured and those predicted theoretically.

On the strength of what has been said at the beginning of this section it can be expected that there is no influence of the electron shell of atoms on the meson depolarization in such substances as liquid hydrogen, phosphorus and aluminium. If there is no mechanism 2.4 the following relations should exist between the quantities a_0 for carbon, phosphorus, aluminium and hydrogen according to the theoretical predictions of refs. [13–15]):

$$a_H = a_P = \tfrac{1}{2}a_C \quad \text{and} \quad a_{Al} = \tfrac{1}{3}a_C,$$

and according to the prediction of ref. [10]), $a_H = a_P = \frac{1}{3}a_C$.

Using the normal law of error distribution it can be shown that the case $a_H = a_P$ is outruled, since $a_H < a_P$ with 99 % probability. The case $a_{Al} = \frac{1}{3}a_C$ does not contradict experiment; but according to experimental data, the probability that $a_{Al} > \frac{1}{2}a_C$ is equal to 5 % and the probability that $a_{Al} < \frac{1}{5}a_C$ is equal to 39 %. The ratios a_C/a_P were analyzed by the x^2 criterion. The limits of this ratio having a probability of 1 % (the figures without brackets) and 5 % (figures in brackets) are as follows:

1.2 (1.4)—(13.0)3.7 for the case $a_P = \frac{1}{2}a_C$,
0.6(0.7)—(1.5) 1.8 for the case $a_P = a_C$.

As is clear, the experimental value of $a_C/a_P = 1.8$ is in good agreement with the one theoretically expected in the case of $a_P = \frac{1}{2}a_C$, and lies outside the 1 % limits for the case $a_P = a_C$.

Using the fact that the relation $a_P = a_C$ contradicts experiment and the relations $a_P = \frac{1}{2}a_C$ and $a_{Al} = \frac{1}{3}a_C$ do not, it can be claimed that the results of measurements do not contradict the theoretical predictions of refs. [13–15]) but do contradict the results of ref. [10]). This fact shows that in using red phosphorus powder as a target the probability of the transition of the meson from the upper level of the hyperfine structure to the lower one is small [16]). Since the experimental value of a_C/a_P lies outside the 1 % limits for the case $a_P = \frac{1}{3}a_C$, it can be believed that the interaction of the hyperfine structure for μ^--mesons lying in the lower excited states of mesic atoms is probably inessential as compared with the interaction in the K-orbit. Finally, the fact that $a_\mu < a_P$ with 99 % probability tends to indicate the impossibility of explaining the total depolarization of μ^--mesons in liquid hydrogen observed in experiment by the action of mechanisms a) and b) alone; an additional mechanism has to be called into play. The mechanism of total depolarization was explained in ref. [17]) which showed that the scattering of a neutral hydrogen mesic atom on a proton $(\mu^-\text{H})+\text{H} \rightarrow (\mu^-\text{H})+\text{H}$ is predominating in this process. In this process the scattering occurs with a large effective cross section of the transition of μ-meson to another proton with the simultaneous transition of the mesic atom of hydrogen to the lower state of the hyperfine structure. Owing to the fact that the probability of these jumps in liquid hydrogen (10^9 sec^{-1}) exceeds the probability of the meson decay (0.5×10^6 sec^{-1}) of the mesic proton by three powers of 10, the mesic protons will completely pass into the ground state of the hyperfine structure within the lifetime of the μ-mesons, with resulting total depolarization.

The author is indebted to Ya. B. Zeldovich, S. S. Gershtein, I. S. Shapiro, E. I. Dolinsky, L. D. Blokhintsev and D. F. Zaretsky for numerous discussions and valuable suggestions.

Note added in proof: The influence of the hyperfine structure on muon polarization in mesic atoms was also considered theoretically by Elihu Lubkin [25]). The authors are indebted to E. Lubkin for a preprint of this work.

References

1) D. Fournet Davis, A. Engler, C. J. Goebel, T. F. Hoang, M. F. Kaplon and J. Klarman, Nuovo Cim. **6** (1957) 310
2) A. M. Bincer, Phys. Rev. **107** (1957) 1434
3) G. W. Ford, C. J. Mullin, Phys. Rev. **108** (1958) 477
4) I. I. Goldman, JETP **34** (1958) 1017
5) V. W. Hughes, Phys. Rev. **108** (1958) 1106
6) G. Lynch, J. Orear, and S. Rosendorf, Phys. Rev. Lett. **1** (1958) 471
7) S. A. Ali-Zade, I. I. Gurevich, Yu. P. Dobretsov, B. A. Nikolsky and L. V. Surkova, JETP **36** (1959) 2327
8) I. M. Shmushkevich, JETP **36** (1959) 645
9) V. A. Djarbashyan, JETP **35** (1958) 307
10) M. E. Rose, Depolarization processes for negative μ-mesons. Preprint Oak Ridge Nat. Lab. (1958)
11) M. B. Stearns and M. Stearns, Phys. Rev. **105** (1957) 1573

12) J. Bernstein, T. D. Lee, C. N. Yang and M. Promakaft, Phys. Rev. **111** (1958) 313
13) I. M. Shmushkevich, JETP **36** (1959) 953
14) H. Uberall, Phys. Rev. **114** (1959) 1640
15) I. S. Shapiro, L. D. Blokhintsev, JETP **37** (1959) 760;
E. I. Dolinsky, Thesis, Nuclear Physics Research Institute of Moscow State University (1959)
16) H. Primakoff, Rev. Mod. Phys. **31** (1959) 802
17) S. S. Gershtein, JETP **34** (1959) 463
18) D. F. Zaretsky and N. M. Novikov, JETP **37** (1959) 1824
19) L. Wilets, Mat. Fys. Medd. Dan. Vid. Selsk. **29**, No. **3** (1959)
20) A. E. Ignatenko, L. B. Egorov, B. Khaluma and D. Chultem, JETP **35** (1958) 894
21) E. A. Ignatenko, L. B. Egorov, B. Khalupa and D. Chultem, JETP **35** (1958) 1131
22) L. B. Egorov, A. E. Ignatenko and D. Chultem, JETP **37** (1959) 1517
23) L. B. Egorov, G. V. Zhuravlev, A. E. Ignatenko, Li Suan-ming, M. G. Petrashku and D. Chultem, Nuclear Physics **23** (1961) 62
24) R. Garwin, L. Lederman and M. Weinrich, Phys. Rev. **105** (1957) 1415
25) E. Lubkin, Phys. Rev. **119** (1960) 815

1.E.3

Nuclear Physics **23** (1961) 90—106; © *North-Holland Publishing Co., Amsterdam*

Not to be reproduced by photoprint or microfilm without written permission from the publisher

HYPERFINE STRUCTURE AND NUCLEAR MOMENTS OF PROTACTINIUM-233

RICHARD MARRUS, WILLIAM A. NIERENBERG and JOSEPH WINOCUR

Lawrence Radiation Laboratory and Department of Physics, University of California, Berkeley, California

Received 31 October 1960

Abstract: By means of the atomic-beam magnetic resonance method using radioactive detection, the hyperfine structure of ${}_{91}\mathrm{Pa}^{233}$ ($T_{\frac{1}{2}} = 27.4$ days) has been investigated. Three low-lying states are found to be present in the beam, characterized by electronic angular momenta $J = \frac{11}{2}$, $\frac{9}{2}$ and $\frac{7}{2}$, and g values $g_J = -0.8141(4)$, $-0.8062(15)$ and $-0.7923(15)$ respectively. From these results it is inferred that the ground-state configuration of protactinium is almost certainly $(5f)^2(6d)^1(7s)^2$. The nuclear spin is measured and found to be $I = \frac{3}{2}$ and the magnetic dipole and electric quadrupole hyperfine structure coupling constants are measured to be $A = \pm 595(30)$ MHz and $B = \mp 2400(300)$MHz respectively. From a direct measurement, the nuclear moment is found to be $\mu_I = +3.4(0.8)$ n.m. From the hyperfine-structure constants and detailed calculations involving the electronic wave functions, the quadrupole moment is inferred to be $Q = -3.0$ barns.

1. Introduction

The subject of the ground-state electronic configurations of the elements after actinium in the periodic table is of great interest, since they constitute a series with transition-type electronic structure in the same sense as the elements after lanthanum. To date, measurements by either optical spectroscopy or atomic beams have established the ground configuration of all elements from ${}_{90}$Th to ${}_{96}$Cm with the exception of ${}_{91}$Pa [1]). The measurements reported here complete our knowledge for all elements in this range, and effectively verify the large body of chemical evidence supporting the hypothesis of an actinide transition series [2]). Table 1 gives the ground-state configuration for each ele-

TABLE 1

Ground-state configurations for the actinide transition-series elements

Element	Ground configuration	Ground-state J
${}_{90}$Th	$(6d)^2(7s)^2$	2
${}_{91}$Pa	$(5f)^2(6d)^1(7s)^2$	$\frac{11}{2}$
${}_{92}$U	$(5f)^3(6d)^1(7s)^2$	3
${}_{93}$Np	$(5f)^4(6d)^1(7s)^2$	$\frac{11}{2}$
${}_{94}$Pu	$(5f)^6(7s)^2$	0
${}_{95}$Am	$(5f)^7(7s)^2$	$\frac{7}{2}$
${}_{96}$Cm	$(5f)^7(6d)^1(7s)^2$	2

ment and the observed value of total angular momentum J characterizing the ground state.

From the point of view of nuclear physics, interest in Pa^{233} centres about the fact that the ground-state rotational band is characterized 3) by $K = \frac{1}{2}$. Calculations based on the Nilsson model indicate also that the deformation δ is positive, and therefore the charge distribution about the nuclear symmetry axis is prolate. If these considerations are correct, then the measured quadrupole moment should be negative.

The beta decay scheme of Pa^{233} indicates 4) that $I = \frac{3}{2}$. In addition, there is evidence that the level scheme of Pa^{231} is similar to that of Pa^{233}, hence these states are described by the same orbitals. Optical spectroscopic measurements on Pa^{231} indicate 5) that $I = \frac{3}{2}$.

2. Beam Production

Production of Pa^{233} is via the reaction $\mathrm{Th}^{232}+\mathrm{n} \rightarrow \mathrm{Th}^{233}[T_{\frac{1}{2}} = 23.5\ \mathrm{min}] \rightarrow \mathrm{Pa}^{233}+\mathrm{e}^-$. Two grams of thorium metal were bombarded for 10 days at a flux of 2×10^{14} neutrons/cm$^2\cdot$sec to yield about 50 curies of Pa. This quantity provided about one week of running time.

The initial attempt to form a Pa beam was by heating irradiated thorium in a small tantalum oven and boiling out the Pa. However, this procedure yielded a molecular rather than an atomic beam. Carbon and lanthanum were then added to the oven in order to reduce the Pa. This reduction failed, apparently because of interference from the Th. The Th was removed by an ion-exchange method, and the separated Pa was oxidized and placed in a small tantalum oven with an excess of carbon. Removal of the Th ensures the success of the reduction, and at a temperature of 3000° C a beam of Pa atoms is formed. Incidentally, it is found that ovens made from a 90 % tantalum-10 % tungsten alloy give the best service at these high temperatures.

Collection of the protactinium beam is successfully accomplished by condensation on freshly flamed, uncooled platinum discs. The radioactivity deposited is measured by placing the foil in a methane proportional counter.

3. Experimental Data And Observations

At low magnetic fields, i.e., at fields at which the nuclear spin I and the electronic angular momentum J are tightly coupled to a total angular momentum F, resonances are observed at frequencies given by

$$\nu = \frac{1}{2F(F+1)}\left[(g_J+g_I)F(F+1)+(g_J-g_I)\{J(J+1)-I(I+1)\}\right]\frac{\mu_0 H}{h}, \quad (1)$$

where g_J is the spectroscopic splitting factor of the electronic system, g_I is the nuclear g factor, H is the applied magnetic field, and (μ_0/h) is the Bohr magneton divided by Planck's constant. For Pa^{233}, g_I turns out to be about $g_J/700$, and although its effect at low field may be neglected, the influence on the intermediate-field data is measurable.

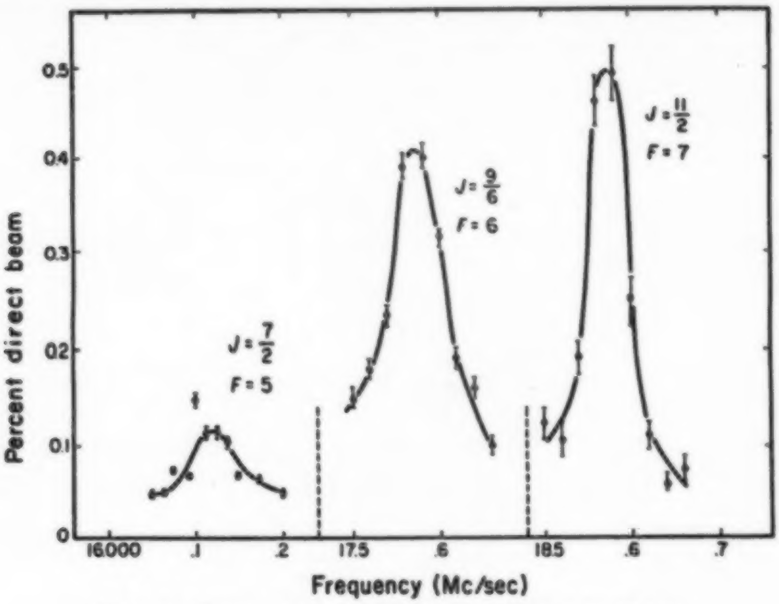

Fig. 1. Three of the observed transitions in Pa^{233}.

TABLE 2

Pa^{233} low-field data

J	H (gauss)	ν (MHz) g_J			
		$F = 7$	$F = 6$	$F = 5$	$F = 4$
$\frac{11}{2}$	2.819(30)	2.512(35) 0.810(11)			
	5.567(30)		5.582(50) 0.813(7)	6.535(50) 0.812(6)	
	10.865(30)	9.700(50) 0.8117(40)	10.912(35) 0.8144(28)	12.812(35) 0.8152(22)	16.112(50) 0.8150(25)
	20.755(30)	18.590(25) 0.8144(11)	20.812(50) 0.8132(20)	24.450(60) 0.8145(20)	30.800(60) 0.8155(16)
$\frac{9}{2}$	2.819(30)		2.400(35) 0.811(11)		
	10.865(30)		9.162(50) 0.8033(43)	10.412(35) 0.8055(27)	12.560(60) 0.8058(40)
	20.755(30)		17.575(30) 0.8067(15)	19.912(50) 0.8065(20)	24.000(50) 0.8060(17)
$\frac{7}{2}$	10.865(30)			8.425(50) 0.7914(48)	
	20.755(30)			16.115(30) 0.7924(15)	

Since none of the parameters entering into (1) was known prior to this experiment, a search was made at a low field to detect all observable resonances. The resonances were then observed at several fields up to a maximum of 20.8 gauss (fig. 1). In all, eight transitions were observed. They are most plausibly fitted to the assumption that three electronic states are present in the beam, characterized by $J = \frac{7}{2}, \frac{9}{2}$ and $\frac{11}{2}$ and that the nuclear spin is $I = \frac{3}{2}$. From the observed resonances intensities it is inferred that the ordering of the electronic energy levels is probably inverted. All data taken at low magnetic field are given in table 2, along with the mean values of g_J.

4. Hyperfine-Structure Measurements

In order to obtain information about the magnetic-dipole and electric-quadrupole hyperfine-structure coupling constants A and B, the transitions in the three highest F states arising from $J = \frac{11}{2}$ and $I = \frac{3}{2}$ were followed up in field (see fig. 2 for a hyperfine-structure diagram of the system). The data obtained were fitted to the Hamiltonian

$$\mathscr{H} = A\,\mathbf{I}\cdot\mathbf{J} + B\,\frac{1}{2IJ(2I-1)(2J-1)}\,[3(\mathbf{I}\cdot\mathbf{J})^2 + \tfrac{3}{2}(\mathbf{I}\cdot\mathbf{J}) - I(I+1)J(J+1)]$$
$$- g_J\mu_0 J_z H - g_I\mu_0 I_z H \qquad (2)$$

by means of an IBM 704 routine designed to give the best values of A, B and g_J for a fixed value of g_I. In table 3 we give the best values of g_J, A and B determined from the routine for different values of g_I, and the value of χ^2, which is a measure of goodness of fit. In table 4, we give the fit to the data for the best set of parameters, $g_J = -0.8141(4)$, $A = \pm 595(30)$ MHz, $B = \mp 2400(300)$ MHz and $g_I = +12.5(3.0)\times 10^{-4}$. The errors quoted for A and B and g_I are about

TABLE 3

Pa^{233} data analysis

$g_I \times 10^4$	g_J	A (MHz)	B (MHz)	χ^2
5.66	−0.81391	566	−2086	3.85
7.65	−0.81396	574	−2172	2.56
9.71	−0.81401	582	−2267	1.68
11.84	−0.81406	592	−2370	1.26
12.39	−0.81408	595	−2396	1.227
12.94	−0.81409	597	−2423	1.231
14.06	−0.81412	603	−2483	1.34
16.38	−0.81418	614	−2608	1.99
18.83	−0.81424	628	−2750	3.31
21.40	−0.81431	643	−2911	5.41

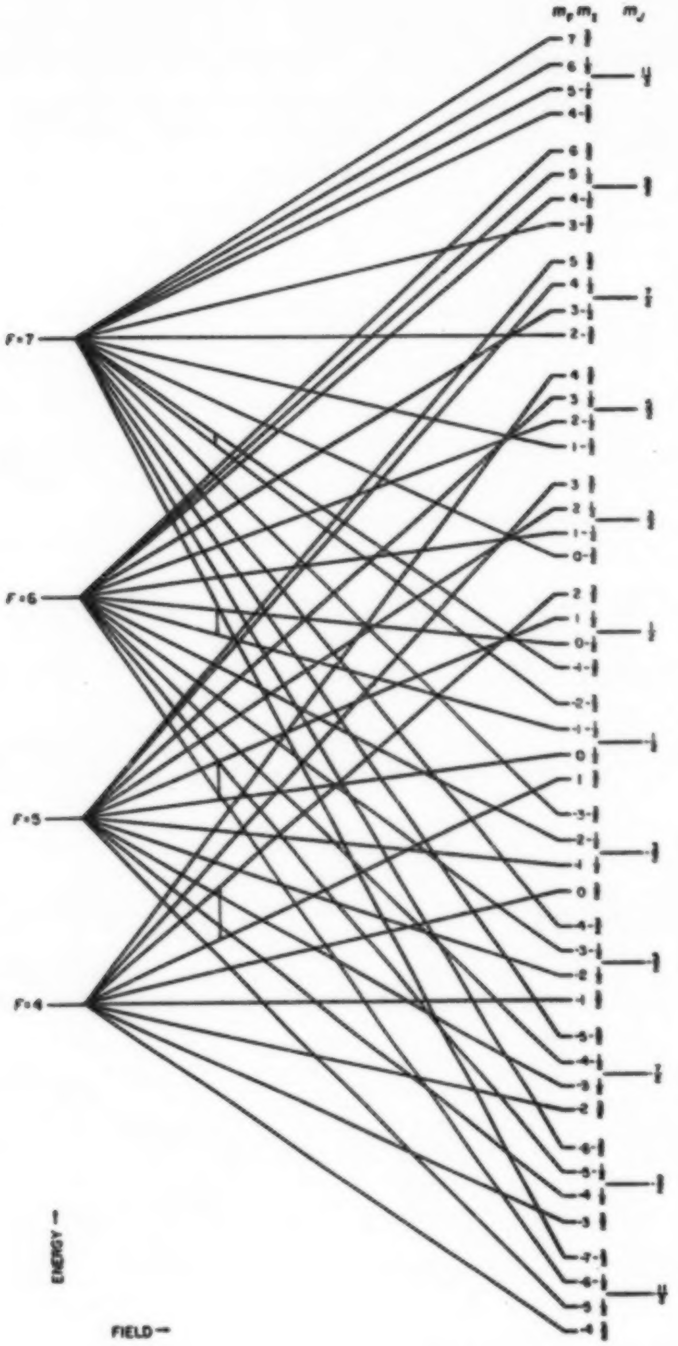
m_F m_I
m_J
F=7
F=6
F=5
F=4
ENERGY →
FIELD →

Fig. 2. Schematic diagram of hyperfine-structure levels of Pa^{233} in a magnetic field.

three times the rms error for the data. The error in g_J is chosen to be 1 part in 2000, to alllow for the possibility of systematic errors present in the apparatus which are proportional to the magnetic field.

TABLE 4

Pa^{233} hfs data

Data No.	H (gauss)	$\nu_{\text{obs.}}$ (MHz)	$\nu_{\text{obs.}} - \nu_{\text{calc.}}$	Transition
1	20.754(18)	18.590(12)	+0.008	(7, −1↔7, −2)
2	55.192(21)	49.470(50)	+0.017	
3	105.804(24)	94.910(75)	−0.002	
4	156.142(29)	140.230(40)	−0.010	
5	225.371(42)	202.770(40)	−0.009	
6	318.227(58)	287.010(40)	−0.042	
7	450.668(74)	408.120(30)	+0.031	
8	149.713(30)	150.330(40)	+0.018	(6,0 ↔ 6, −1)
9	207.147(39)	208.025(40)	+0.014	
10	308.464(58)	309.840(30)	−0.010	
11	99.548(25)	147.800(25)	−0.003	(4,2 ↔ 4,1)
12	144.665(30)	214.980(50)	+0.011	
13	207.147(39)	308.160(50)	−0.006	
14	258.908(48)	385.460(63)	−0.018	

5. Electronic Structure

On the basis of available chemical evidence, it has been postulated [6]) that the ground-state configuration of $_{91}$Pa is either $(5f)^2\ (6d)^1 (7s)^2$ or $(5f)^1\ (6d)^2\ (7s)^2$. No plausible fit to the data can be made with $(5f)^1\ (6d)^2\ (7s)^2$ as the ground state. In contrast, if it is assumed that the ground-state configuration of Pa is $(5f)^2\ (6d)^1\ (7s)^2$, the data are very well fitted by the same model as has given agreement with the observed g_J and J values in other actinide elements containing both 5f and 6d electrons. This model assumes that the electrons in each shell couple independently to the Hund's Rule ground state, and that there is pure J_1—J_2 coupling between the shells. The Hund's Rule state for the configuration $(5f)^2$ is $^3H_4$ with $g_J = -0.800$, and for $(6d)^1$ it is $^2D_{\frac{3}{2}}$, also with $g_J = -0.800$. In the limit of pure $J_1 - J_2$ coupling between shells, four levels are predicted, characterized by $J = \frac{11}{2}, \frac{9}{2}, \frac{7}{2}$ and $\frac{5}{2}$, with $g_J = -0.800$ for all of them. On the other hand, the calculated values of the g factors for pure $L-S$ coupling among all electrons are $g_J(^4K_{\frac{11}{2}}) = -0.769$, $g_J(^4I_{\frac{9}{2}}) = -0.727$ and $g_J(^4H_{\frac{7}{2}}) = -0.702$.

The observed g values deviate from those predicted according to the simple model described above because of the spin-orbit interactions of the 5f and 6d electrons and because of the breakdown of J of each of the shells due to the electrostatic interaction between them. The problem of determining the exact ground state would involve the diagonalization of the matrix of the spin-orbit energy plus electrostatic energy for all terms giving rise to a state with $J = \frac{11}{2}$. Such a calculation would involve the determination of several hundred integrals of the electrostatic energy.

We have attempted an alternative approach based on the J_1—J_2 scheme as a starting approximation. In performing this calculation it is easiest to determine the energy in the L—S scheme and then to transform the energy matrix into the J_1—J_2 scheme.

The L—S matrix elements of the electrostatic energy have the form

$$\left\langle (l_1)^2 L_1 S_1; l_2; LS \left| \frac{e^2}{r_{12}} \right| (l_1)^2 L'_1 S'_1; l_2; LS \right\rangle, \tag{3}$$

where the subscripts 1 and 2 refer to the configurations $(5f)^2$ and $(6d)^1$ respectively. Thus $l_1 = 3$ and $l_2 = 2$. The matrix element may be written as the sum over the Slater radial integrals $F^k(5f, 6d)$ and $G^k(5f, 6d)$,

$$\left\langle LS \left| \frac{e^2}{r_{12}} \right| LS \right\rangle = \sum_{k=2,4} f^k F^k + \sum_{k=1,3,5} g^k G^k. \tag{4}$$

The interaction among the $(5f)^2$ electrons is independent of L and S and merely adds a constant term to eq. (3).

A general expression for the coefficients f^k and g^k has been derived by Judd [7]) for the case of a d electron interacting with n equivalent f electrons. For $n = 2$ these expressions become

$$f^k = (2l_1+1)(2l_2+1)\delta(S_1, S'_1)[(2L_1+1)(2L'_1+1)]^{\frac{1}{2}}$$
$$\times \begin{pmatrix} l_1 & k & l_1 \\ 0 & 0 & 0 \end{pmatrix} \begin{pmatrix} l_2 & k & l_2 \\ 0 & 0 & 0 \end{pmatrix} [1+(-1)^{L_1+L'_1}] (-1)^{k+l_1+L} \begin{Bmatrix} k & l_1 & l_1 \\ l_1 & L'_1 & L_1 \end{Bmatrix} \begin{Bmatrix} L_1 & k & L'_1 \\ l_2 & L & l_2 \end{Bmatrix}, \tag{5a}$$

$$g^k = 2(2l_1+1)(2l_2+1) \begin{pmatrix} l_2 & k & l_1 \\ 0 & 0 & 0 \end{pmatrix}^2 (-)^{S_1+S'_1}$$
$$\times [(2S_1+1)(2S'_1+1)(2L_1+1)(2L'_1+1)]^{\frac{1}{2}} \begin{Bmatrix} \frac{1}{2} & \frac{1}{2} & S'_1 \\ & & \\ \frac{1}{2} & S & S_1 \end{Bmatrix} \begin{Bmatrix} l_1 & l_1 & L'_1 \\ l_1 & k & l_2 \\ l_1 & l_2 & L \end{Bmatrix}. \tag{5b}$$

In this calculation we concern ourselves only with the ^{3}H ground term of the configuration f^2. Therefore, $L'_1 = L^1 = 5$ and $S_1 = S'_1 = 1$, only. Tables of the 3-j and 6-j symbol as well as the definition of the 9-j symbol are all found in Edmonds [8]). The coefficients f^k and g^k for all quartet terms are given in table 5. Coefficients for the doublet terms can be obtained from this table by leaving f^k unchanged and multiplying g^k by $-\frac{1}{2}$.

No experimental or theoretical values of the radial integrals are available for protactinium. However, Racah [9]) has calculated the values of the radial integrals which give best agreement with the observed optical spectrum of Th(III). Another set of radial integrals has been obtained by us from the relativistic wave functions of Cohen for the normal uranium atom [10]). Since there is no preference for either set of integrals, we have calculated the electrostatic energy from both and give the results in table 6. It is encouraging to note the similarity between the level ordering predicted from the two sets.

TABLE 5

Calculations of f^k and g^k for Pa

	f^2	f^4	g^1	g^3	g^5
^4K	2/21	− 4/693	−4/7	− 2/21	−10/2541
^4I	−11/105	8/231	−6/35	−44/315	−205/7623
^4H	− 1/9	− 8/99	6/35	−38/945	−1975/22869
^4G	0	26/297	−1/15	−88/945	−575/3267
^4F	52/315	−26/693	3/245	316/6615	−41605/160083

TABLE 6

Term energies in cm^{-1}

Term	From Th	From U
^4K	−7976	−10645
^4I	−6219	−9267
^2H	−4091	−6412
^4G	−2460	−3612
^4H	−2266	−3682
^2I	788	214
^4F	1196	2432
^2G	3287	4461
^2F	3460	6265
^2K	6702	10120

We now proceed to obtain the electrostatic energy in the J_1—J_2 coupling scheme. The LS—J_1J_2 transformation coefficient is given by [8])

$$\langle (L_1L_2)L,\ (S_1S_2)S,\ J|(L_1S_1)J_1,\ (L_2S_2)J_2,\ J\rangle$$
$$= [(2L+1)(2S+1)(2J_1+1)(2J_2+1)]^{\frac{1}{2}} \begin{Bmatrix} L_1 & L_2 & L \\ S_1 & S_2 & S \\ J_1 & J_2 & J \end{Bmatrix}. \qquad (6)$$

The smallest argument appearing in the 9-j symbol is $S_2 = \frac{1}{2}$. Therefore, the formula for the 9-j symbol can be simplified to an expression involving the sum of only two 6-j symbols.

The ^3H ground term of $(5f)^2$ is split by the spin-orbit interaction into the levels $J_1 = 4$, 5 and 6; the 6d ^2D term is split into $J_2 = \frac{3}{2}$ and $\frac{5}{2}$. The electrostatic interaction between these two systems gives rise to the following states in the J_1J_2J scheme: $4(\frac{3}{2})J$, $4(\frac{5}{2})J$, $5(\frac{3}{2})J$, $5(\frac{5}{2})J$, $6(\frac{3}{2})J$ and $6(\frac{5}{2})J$. Neither the electronic g-factor operator nor the hyperfine structure interaction operator couples the last three states with the $4(\frac{3}{2})J$ ground state. Since they do not produce any first-order effects, these states are neglected. Using formula (6), we find for the electrostatic energy in the J_1—J_2 scheme:

$$\underline{J = \tfrac{11}{2}}$$

$$\begin{array}{cc} & \begin{array}{ccc} 4(\frac{3}{2}) & 5(\frac{3}{2}) & 4(\frac{5}{2}) \end{array} \\ \begin{array}{c} 4(\frac{3}{2}) \\ 5(\frac{3}{2}) \\ 4(\frac{5}{2}) \end{array} & \begin{pmatrix} -6455 & 1507 & -2489 \\ 1507 & -4513 & -1915 \\ -2489 & -1915 & -3287 \end{pmatrix} \end{array} \text{cm}^{-1}, \qquad \begin{array}{c} \begin{array}{ccc} 4(\frac{3}{2}) & 5(\frac{3}{2}) & 4(\frac{5}{2}) \end{array} \\ \begin{pmatrix} -8768 & 1867 & -3052 \\ 1867 & -6889 & -2681 \\ -3052 & -2681 & -5159 \end{pmatrix} \end{array} \text{cm}^{-1},$$

$$\underline{J = \tfrac{9}{2}}$$

$$\begin{array}{cc} \begin{array}{c} 4(\frac{3}{2}) \\ 5(\frac{3}{2}) \\ 4(\frac{5}{2}) \end{array} & \begin{pmatrix} -5290 & 865 & -1174 \\ 865 & -1011 & 296 \\ -1174 & 296 & -3699 \end{pmatrix} \end{array} \text{cm}^{-1}, \qquad \begin{pmatrix} -7689 & 1249 & -1634 \\ 1249 & -1733 & 369 \\ -1634 & 369 & -5633 \end{pmatrix} \text{cm}^{-1},$$

$$\underline{J = \tfrac{7}{2}}$$

$$\begin{array}{cc} \begin{array}{c} 4(\frac{3}{2}) \\ 5(\frac{3}{2}) \\ 4(\frac{5}{2}) \end{array} & \begin{pmatrix} 264 & 1213 & -1574 \\ 1213 & 646 & -1044 \\ -1574 & -1044 & -1284 \end{pmatrix} \end{array} \text{cm}^{-1}, \qquad \begin{pmatrix} 104 & 1955 & -2413 \\ 1955 & 1515 & -1620 \\ -2413 & -1620 & -2038 \end{pmatrix} \text{cm}^{-1}.$$

The matrices in the first column are calculated from Racah's values of the radial integrals; the matrices in the second column are calculated from the uranium radial integrals.

To complete the energy matrix, the spin-orbit energy must be added. This is

$$S = \begin{array}{cc} & \begin{array}{ccc} 4(\frac{3}{2}) & 5(\frac{3}{2}) & 4(\frac{5}{2}) \end{array} \\ \begin{array}{c} 4(\frac{3}{2}) \\ 5(\frac{3}{2}) \\ 4(\frac{5}{2}) \end{array} & \begin{pmatrix} 0 & & \\ & (\frac{5}{2})a_{5f} & \\ & & (\frac{5}{2})a_{5f} \end{pmatrix} \end{array}. \tag{7}$$

The matrix of the total energy may be written in the form

$$W = S + \lambda E, \tag{8}$$

where W is the sum of the spin-orbit matrix S plus the electrostatic matrix E multiplied by a parameter λ. The justification for introducing λ rests on the expectation that the ratios of the F and G integrals are approximately correct even though their strength may not be.

A more accurate representation of the $J = 4$ state of the f^2 configuration can be obtained if we allow for the admixture by the spin-orbit interaction of terms different from ^{3}H. The allowed terms of (f)^2 that can give rise to a state $J_1 = 4$ are ^{1}G and ^{3}F. The matrix of the total energy has been calculated, and is of the form

$$\begin{array}{c} \\ {}^3\mathrm{H} \\ {}^1\mathrm{G} \\ {}^3\mathrm{F} \end{array}\begin{array}{c} \begin{array}{ccc} {}^3\mathrm{H} & {}^1\mathrm{G} & {}^3\mathrm{F} \end{array} \\ \begin{pmatrix} -3a_{5f} & -(\frac{10}{3})^{\frac{1}{2}}a_{5f} & \\ -(\frac{10}{3})^{\frac{1}{2}}a_{5f} & G & (\frac{11}{3})^{\frac{1}{2}}a_{5f} \\ & (\frac{11}{3})^{\frac{1}{2}}a_{5f} & F+\frac{3}{2}a_{5f} \end{pmatrix} \end{array}. \tag{9}$$

Where F and G, the electrostatic energies of the ^{3}F and ^{1}G term with respect to the ^{3}H terms, are given in Condon and Shortley [11]). We have used the values for the ratios F^4/F^2 and F^6/F^2 from the uranium wave functions [12]), and obtained in this way $G = 20.3F_2$ and $F = 12.3F_2$. It has been found that $F_2 = 153$ cm^{-1} gives the best fit with the observed g_J of americium [12]). We have found by extrapolation that, for Pa, the value of F_2 ought to be about 137 cm^{-1}. For a_{5f} we have used the value of 1300 cm^{-1} obtained by Judd in fitting the energy levels of U (I) [7]). For these values of the parameters we obtain, for the ground state of f^2,

$$|J = 4) = -0.939|^3\mathrm{H}_4)-0.323|^1\mathrm{G}_4)+0.095|^3\mathrm{F}_4). \tag{10}$$

The electronic g factor g_J is defined by

$$g_J m_J = \langle Jm_J|\sum_i (-l_z+g_s s_z)_i|Jm_J\rangle. \tag{11}$$

Here $g_s = -2.0023$ is the electron spin g factor; l_z and s_z are the z components of the orbital and spin angular momenta. The g_J matrix in the J_1—J_2 scheme can be obtained by a transformation of the diagonal g_J matrix in the L—S scheme using the transformation coefficients determined from formula (6). It can also be calculated directly by considering the angular momenta as tensors of rank one, and using tensor methods. We here omit the details of this calculation and state the result

$$\begin{array}{l}
\underline{g_J = \tfrac{11}{2}}: \begin{array}{c} \\ 4(\frac{3}{2}) \\ 5(\frac{3}{2}) \\ 4(\frac{5}{2}) \end{array}\begin{array}{c} \begin{array}{ccc} 4(\frac{3}{2}) & 5(\frac{3}{2}) & 4(\frac{5}{2}) \end{array} \\ \begin{pmatrix} 0.8185 & 0.0388 & -0.0572 \\ 0.0388 & 1.0023 & 0 \\ -0.0572 & 0 & 0.9363 \end{pmatrix} \end{array} (-1), \\[2ex]
\underline{g_J = \tfrac{9}{2}}: \begin{array}{c} 4(\frac{3}{2}) \\ 5(\frac{3}{2}) \\ 4(\frac{5}{2}) \end{array}\begin{pmatrix} 0.8211 & 0.0586 & -0.0904 \\ 0.0586 & 1.0405 & 0 \\ -0.0909 & 0 & 0.9089 \end{pmatrix} (-1), \\[2ex]
\underline{g_J = \tfrac{7}{2}}: \begin{array}{c} 4(\frac{3}{2}) \\ 5(\frac{3}{2}) \\ 4(\frac{5}{2}) \end{array}\begin{pmatrix} 0.8260 & 0.0714 & -0.1266 \\ 0.0714 & 1.1114 & 0 \\ -0.1266 & 0 & 0.8568 \end{pmatrix} (-1).
\end{array} \tag{11}$$

The eigenvalues and eigenvectors of the energy matrices W were calculated on an IBM 704 computer. The g_J matrices were then transformed with the same unitary matrix which brings the energy matrix into diagonal form. The elements occurring along the diagonal of the g_J matrix are characteristic g factors.

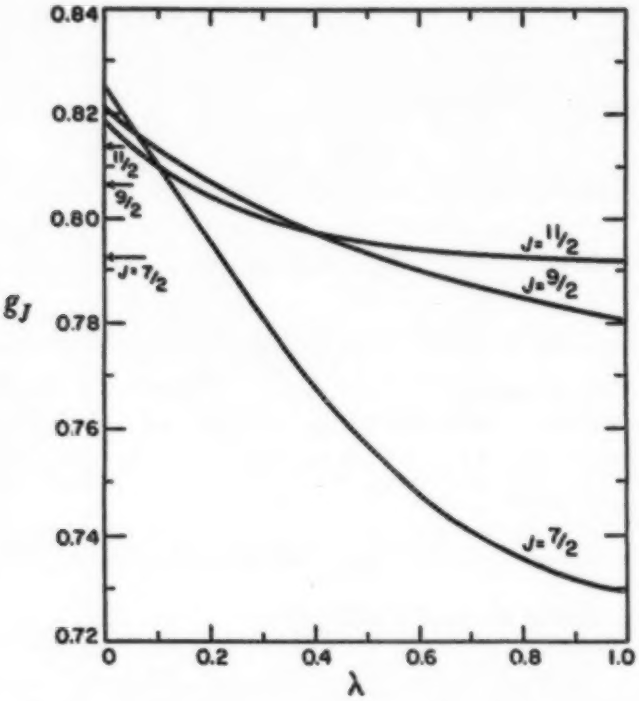

Fig. 3. Calculated g_J factors of the levels $J = \frac{11}{2}$, $\frac{9}{2}$ and $\frac{7}{2}$ of Pa as a function of the strength of the electrostatic interaction.

Fig. 3 shows how g_J varies with λ for the lowest three J states. The observed g_J values are indicated by the arrows. There is no single value of λ for which the observed and calculated g factors are in satisfactory agreement. Thus it appears necessary to go higher order and to include those states not directly coupled to the ground state by the g_J and hyperfine operators. Since these states have larger g_J values than the ground state, it is expected that including them will improve the agreement with the experimental values.

6. Hyperfine Structure

The evaluation of the nuclear moments from the measured hyperfine structure depends on the choice of the angular part of the wave function. In the preceding section, we showed that first-order calculations employing the J_1—J_2 coupling model were inadequate to explain the observed electronic g factors. However, there is much less need for an accurate wave function for the hyperfine-structure calculations, since uncertainties introduced in the values of

$\langle 1/r^3\rangle$ are expected to be larger in any case. Therefore, the wave function we use admits the same states as in the calculation of the g values, with the $J_1 = 4$ state of the $(\mathrm{f})^2$ configuration assumed to be an admixture of ${}^3\mathrm{H}$ and ${}^1\mathrm{G}$ only (eq. (10)).

The ground state is the eigenvector of the W matrix for an appropriate value of λ. Judd [7]) has found that the observed spectrum of U(I) can be fitted if the radial integrals of Racah are multiplied by $\lambda = \frac{1}{2}$. Using this value for protactinium, we obtain, for the ground-state wave function,

$$|J = \tfrac{11}{2}\rangle = -0.976|4(\tfrac{3}{2})\tfrac{11}{2}\rangle + 0.124|5(\tfrac{3}{2})\tfrac{11}{2}\rangle - 0.178|4(\tfrac{5}{2})\tfrac{11}{2}\rangle. \tag{12}$$

On the basis of this wave function, we now proceed with the calculation of the nuclear moments. The magnetic dipole moment (μ_I) can be obtained from the magnetic dipole hyperfine structure according to the relation

$$A = -(1/IJ)\mu_I\langle \bar{H}\rangle_{J,\, m_J = J}, \tag{13}$$

where $\bar{H}$ is the magnetic field at the nucleus due to the orbital electrons. The quantum mechanical expression for this field is

$$\bar{H} = -2\mu_0 \sum_i \left(\frac{1}{r^3}\right)_i \left\{\mathbf{l} - \mathbf{s} + \tfrac{3}{2}\,\frac{(\mathbf{s}\cdot\mathbf{r})\mathbf{r} + \mathbf{r}(\mathbf{s}\cdot\mathbf{r})}{r^2}\right\}_i, \tag{14}$$

where $\mathbf{l}$ and $\mathbf{s}$ are the orbital and spin angular momenta of the individual electrons, and $\mathbf{r}$ is the radius vector. The sum is over-all electrons. Trees has noted that this operator can be written in a form which better exhibits its spherical tensor character [13]),

$$\bar{H} = -2\mu_0 \sum_i \left(\frac{1}{r^3}\right)_i \{\mathbf{l}_i - \sqrt{10}\,\mathbf{X}_i\}, \tag{15}$$

where $\mathbf{X}$ is a spherical tensor of rank one formed from the tensor composition of the spin $(\mathbf{s})$ with the spherical harmonic of rank two $(C^{(2)})$.

$$\mathbf{X}_1{}^m = \sum_{m_1} s_1^{m_1} C^{(2)}_{m-m_1}(1m_1;\, 2m-m_1|121m). \tag{16}$$

$(1m_1;\, 2m-m_1|121m)$ is the Clebsch-Gordan coefficient arising in the coupling of an angular momentum of one unit with another of two units to form a resultant of one unit.

When this form of the operator is used, the theorems concerning the evaluation of matrix elements of spherical tensor operators may be applied. The matrix elements arising from the wave function (12) have the form $\langle J'_1 J'_2 J m_J = J|\bar{H}|J_1 J_2 J m_J = J\rangle$. For the wave function (12) the appropriate matrix elements are

$$
\begin{aligned}
&\langle{}^3\mathrm{H}_4\,{}^2\mathrm{D}_{\frac{3}{2}}\,\tfrac{11}{2}\,|\bar{H}|\,{}^3\mathrm{H}_4\,{}^2\mathrm{D}_{\frac{3}{2}}\,\tfrac{11}{2}\rangle = -\tfrac{8}{5}\mu_0\left[\tfrac{296}{45}\left\langle\frac{1}{r^3}\right\rangle_{5\mathrm{f}} + 3\left\langle\frac{1}{r^3}\right\rangle_{6\mathrm{d}}\right],\\
&\langle{}^1\mathrm{G}_4\,{}^2\mathrm{D}_{\frac{3}{2}}\,\tfrac{11}{2}\,|\bar{H}|\,{}^1\mathrm{G}_4\,{}^2\mathrm{D}_{\frac{3}{2}}\,\tfrac{11}{2}\rangle = -\tfrac{8}{5}\mu_0\left[5\left\langle\frac{1}{r^3}\right\rangle_{5\mathrm{f}} + 3\left\langle\frac{1}{r^3}\right\rangle_{6\mathrm{d}}\right],\\
&\langle{}^3\mathrm{H}_5\,{}^2\mathrm{D}_{\frac{3}{2}}\,\tfrac{11}{2}\,|\bar{H}|\,{}^3\mathrm{H}_5\,{}^2\mathrm{D}_{\frac{3}{2}}\,\tfrac{11}{2}\rangle = -\tfrac{8}{65}\mu_0\left[\tfrac{3472}{45}\left\langle\frac{1}{r^3}\right\rangle_{5\mathrm{f}} + 19\left\langle\frac{1}{r^3}\right\rangle_{6\mathrm{d}}\right],\\
&\langle{}^3\mathrm{H}_4\,{}^2\mathrm{D}_{\frac{5}{2}}\,\tfrac{11}{2}\,|\bar{H}|\,{}^3\mathrm{H}_4\,{}^2\mathrm{D}_{\frac{5}{2}}\rangle\,\tfrac{11}{2} = -\tfrac{8}{65}\mu_0\left[\tfrac{3478}{45}\left\langle\frac{1}{r^3}\right\rangle_{5\mathrm{f}} + 21\left\langle\frac{1}{r^3}\right\rangle_{6\mathrm{d}}\right],\\
&\langle{}^3\mathrm{H}_4\,{}^2\mathrm{D}_{\frac{3}{2}}\,\tfrac{11}{2}\,|\bar{H}|\,{}^3\mathrm{H}_4\,{}^2\mathrm{D}_{\frac{5}{2}}\,\rangle\,\tfrac{11}{2} = \tfrac{4}{65}\sqrt{26}\,\mu_0\left\langle\frac{1}{r^3}\right\rangle_{6\mathrm{d}},\\
&\langle{}^3\mathrm{H}_5\,{}^2\mathrm{D}_{\frac{3}{2}}\,\tfrac{11}{2}\,|\bar{H}|\,{}^3\mathrm{H}_4\,{}^2\mathrm{D}_{\frac{3}{2}}\,\tfrac{11}{2}\rangle = -\tfrac{14}{25}\sqrt{\tfrac{11}{26}}\,\mu_0\left\langle\frac{1}{r^3}\right\rangle_{5\mathrm{f}}.
\end{aligned}
\tag{17}
$$

The values of $\langle 1/r^3\rangle$ were obtained from the relativistic wave functions for uranium,

$$
\left\langle\frac{1}{r^3}\right\rangle = \frac{2}{(l+1)\alpha a_0}\int r^{-2}FG\,\mathrm{d}r = \begin{cases}3.9/a_0^3 & \text{for 5f electrons,}\\ 2.0/a_0^3 & \text{for 6d electrons.}\end{cases}
\tag{18}
$$

Thus, the value for the field is -3.0×10^6 gauss, and, from eq. (13), $A = 227\,\mu_\mathrm{N}$ (n.m.) MHz. Using the experimental value $A = 595$ MHz, we obtain $\mu_\mathrm{N} = 2.1$ n.m. We have neglected in this calculation the effect on the magnetic hyperfine structure of excitation of core electrons to excited s states. Although this effect can be substantial, we take the agreement of the calculated moment with the value obtained from direct measurement as evidence for the essential correctness of our assumptions concerning the electronic structure.

Calculation of the quadrupole interaction proceeds from the formula

$$
B = -e^2Q\sum_i\left(\frac{1}{r^3}\right)_i\langle 3\cos^2\theta_i - 1\rangle_{J,m_J=J}.
\tag{19}
$$

The evaluation of the sum is easily accomplished by using spherical tensor methods. An alternative approach is to expand the wave function (12) into the single-particle quantum numbers, and to evaluate B directly. However, the spherical tensor method has the property of exhibiting the addition of two quadrupole interactions B_1 and B_2 arising from systems with two angular momenta J_1 and J_2 coupled together to a resultant J. Thus,

$$B=\frac{[3C_1(C_1-1)-4J_1(J_1+1)J(J+1)]}{J_1(2J_1-1)(2J+2)(2J+3)}\,B_1 \\ +\frac{[3C_2(C_2-1)-4J_2(J_2+1)J(J+1)]}{J_2(2J_2-1)(2J+2)(2J+3)}\,B_2, \tag{20}$$

where

$$C_1=J(J+1)+J_1(J_1+1)-J_2(J_2+1),\quad C_2=J(J+1)+J_2(J_2+1)-J_1(J_1+1).$$

Applying this formula to the diagonal matrix elements arising from the wave function (12) we obtain, for the matrix elements of

$$q=\sum_i\left(\frac{1}{r^3}\right)_i\langle 3\cos^2\theta_i-1\rangle_{J,\,m_J=J},$$

the following expressions:

$$\begin{aligned}
\langle {}^3\mathrm{H}_4\,{}^2\mathrm{D}_{\frac{3}{2}}\tfrac{11}{2}|q|{}^3\mathrm{H}_4\,{}^2\mathrm{D}_{\frac{3}{2}}\tfrac{11}{2}\rangle &= -\tfrac{4}{5}\left[\tfrac{364}{495}\left\langle\frac{1}{r^3}\right\rangle_{5f}+\tfrac{1}{2}\left\langle\frac{1}{r^3}\right\rangle_{6d}\right],\\
\langle {}^1\mathrm{G}_4\,{}^2\mathrm{D}_{\frac{3}{2}}\tfrac{11}{2}|q|{}^1\mathrm{G}_4\,{}^2\mathrm{D}_{\frac{3}{2}}\tfrac{11}{2}\rangle &= -\tfrac{4}{5}\left[\tfrac{2}{11}\left\langle\frac{1}{r^3}\right\rangle_{5f}+\tfrac{1}{2}\left\langle\frac{1}{r^3}\right\rangle_{6d}\right],\\
\langle {}^3\mathrm{H}_5\,{}^2\mathrm{D}_{\frac{3}{2}}\tfrac{11}{2}|q|{}^3\mathrm{H}_5\,{}^2\mathrm{D}_{\frac{3}{2}}\tfrac{11}{2}\rangle &= -\tfrac{28}{65}\left[\tfrac{6}{5}\left\langle\frac{1}{r^3}\right\rangle_{5f}-\tfrac{1}{2}\left\langle\frac{1}{r^3}\right\rangle_{6d}\right],\\
\langle {}^3\mathrm{H}_4\,{}^2\mathrm{D}_{\frac{5}{2}}\tfrac{11}{2}|q|{}^3\mathrm{H}_4\,{}^2\mathrm{D}_{\frac{5}{2}}\tfrac{11}{2}\rangle &= -\tfrac{4}{5}\left[\tfrac{259}{495}\left\langle\frac{1}{r^3}\right\rangle_{5f}+\tfrac{17}{91}\left\langle\frac{1}{r^3}\right\rangle_{6d}\right],\\
\langle {}^3\mathrm{H}_4\,{}^2\mathrm{D}_{\frac{3}{2}}\tfrac{11}{2}|q|{}^3\mathrm{H}_4\,{}^2\mathrm{D}_{\frac{5}{2}}\tfrac{11}{2}\rangle &= -\tfrac{24}{35}\sqrt{\tfrac{2}{13}}\left\langle\frac{1}{r^3}\right\rangle_{6d},\\
\langle {}^3\mathrm{H}_5\,{}^2\mathrm{D}_{\frac{3}{2}}\tfrac{11}{2}|q|{}^3\mathrm{H}_4\,{}^2\mathrm{D}_{\frac{3}{2}}\tfrac{11}{2}\rangle &= \tfrac{52}{825}\sqrt{\tfrac{22}{13}}\left\langle\frac{1}{r^3}\right\rangle_{5f}.
\end{aligned} \tag{21}$$

The values of $1/r^3$ are taken from the wave functions for uranium:

$$\frac{1}{r^3}=\int(F^2+G^2)\frac{1}{r^3}\,\mathrm{d}r=\begin{cases}3.99/a_0^3 & \text{for 5f electrons,}\\ 2.39/a_0^3 & \text{for 6d electrons.}\end{cases} \tag{22}$$

The value for the quadrupole interaction is thus found to be

$$B=802\,Q(\text{barns})\text{MHz}. \tag{23}$$

The sign of B is determined experimentally to be opposite that of A. Since the A value predicted from the calculated magnetic field and the experimentally measured positive moment is positive, we take for B the negative sign and

$$Q=-2400/802=-3.0\text{ barns}. \tag{24}$$

7. Second-Order Electronic Perturbation

So far we have assumed that J is a good quantum number. This assumption is valid so long as the second-order contribution to the energy,

$$W_F = |\langle J\pm 1\, IFm_f| -\boldsymbol{\mu}_I \cdot \mathbf{H} - e^2 \frac{r_\mathrm{n}^{\,2}}{r_\mathrm{e}^{\,3}} [C^{(2)}_{(\mathrm{n})} C^{(2)}_{(\mathrm{e})}] + \mathscr{H}_{\mathrm{mag}} | IJFm_f\rangle|^2/(E_J - E_{J\pm 1}), \tag{25}$$

is negligible in comparison with the first-order energy. If it is not, then the second-order field-dependent energy terms, which cannot be distinguished experimentally from the first-order terms, affect the computed value of g_I, and — to a smaller extent — A, B and g_J. We will show, however, that for Pa, the effect of this perturbation is negligible.

The second-order dipole and quadrupole interactions calculated by means of the tensor method are, for $J = \frac{11}{2}$ and $I = \frac{3}{2}$,

$$\langle (J-1\, IFm_f| -\boldsymbol{\mu}_I \cdot \mathbf{H} | JIFm_f\rangle = \frac{32\mu_0\mu_I}{165\sqrt{15}} [(F+8)(7-F)(F+4)(F-3)]^{\frac{1}{2}}$$

$$\left[-\tfrac{37}{15}\left\langle\frac{1}{r^3}\right\rangle_{5\mathrm{f}} + 3\left\langle\frac{1}{r^3}\right\rangle_{6\mathrm{d}}\right],$$

and

$$\left\langle (J-1)IFm_f \left| -e^2 \frac{r_\mathrm{n}^{\,2}}{r_\mathrm{e}^{\,3}} [C^{(2)}_{(\mathrm{n})} C^{(2)}_{(\mathrm{e})}] \right| JIFm_f \right\rangle = \frac{2e^2 Q}{495\sqrt{15}} [F(F+1)-33]$$

$$[(F+8)(7-F)(F+4)(F-3)]^{\frac{1}{2}} \left[\tfrac{91}{165}\left\langle\frac{1}{r^3}\right\rangle_{5\mathrm{f}} - \left\langle\frac{1}{r^3}\right\rangle_{6\mathrm{d}}\right].$$

The matrix elements of the magnetic field interaction,

$$\mathscr{H}_{\mathrm{mag}} = \sum_i -(l_z + g_s s_z)_i \frac{\mu_0 H_z}{h}, \text{ may be written}$$

$$\langle J-1IFm_f|\mathscr{H}_{\mathrm{mag}}|JIFm_f\rangle = f(F, m_f)\langle J-1||\sum_i (-l_z+g_s s_z)_i||J\rangle \mu_0 H_z/h,$$

where

$$f(F, m_f) = \frac{m_f}{4\sqrt{165}F(F+1)} [(F+8)(F+4)(7-F)(F-3)]^{\frac{1}{2}}.$$

There are no matrix elements of the hyperfine structure that are off-diagonal in F.

It is not sufficient to calculate the matrix element in pure J—J coupling, because it vanishes in lowest order,

$$\langle 4(\tfrac{3}{2})\tfrac{9}{2}||\sum_i (-l_z+g_s s_z)_i||4(\tfrac{3}{2})\tfrac{11}{2}\rangle = -\frac{12}{\sqrt{11}}(g_{J_2} - g_{J_1}) = 0.$$

We must therefore evaluate matrix elements between the ground state and states that are admixed by the electrostatic interaction. These are

$$\langle {}^3\mathrm{H}_4\,{}^2\mathrm{D}_{\frac{3}{2}}\,\tfrac{9}{2}||\sum_i\,(-l_s+g_s s_s)_i||{}^3\mathrm{H}_5\,{}^2\mathrm{D}_{\frac{3}{2}}\,\tfrac{11}{2}\rangle = 36\sqrt{26}(g_s+1)/55,$$

$$\langle {}^3\mathrm{H}_4\,{}^2\mathrm{D}_{\frac{3}{2}}\,\tfrac{9}{2}||\sum_i\,(-l_s+g_s s_s)_i||{}^3\mathrm{H}_4\,{}^2\mathrm{D}_{\frac{3}{2}}\,\tfrac{11}{2}\rangle = \tfrac{6}{5}\sqrt{\tfrac{26}{11}}\,(g_s+1),$$

$$\langle {}^3\mathrm{H}_5\,{}^2\mathrm{D}_{\frac{3}{2}}\,\tfrac{9}{2}||\sum_i\,(-l_s+g_s s_s)_i||{}^3\mathrm{H}_4\,{}^2\mathrm{D}_{\frac{3}{2}}\,\tfrac{11}{2}\rangle = -\tfrac{6}{55}(g_s+1),$$

$$\langle {}^3\mathrm{H}_4\,{}^2\mathrm{D}_{\frac{5}{2}}\,\tfrac{9}{2}||\sum_i\,(-l_s+g_s s_s)_i||{}^3\mathrm{H}_4\,{}^2\mathrm{D}_{\frac{3}{2}}\,\tfrac{11}{2}\rangle = -(\tfrac{2}{5})\sqrt{\tfrac{14}{11}}\,(g_s+1).$$

The electronic wave function of the $J = \frac{11}{2}$ state is given by eq. (12). For the $J = \frac{9}{2}$ state, it is (for $\lambda = \frac{1}{2}$)

$$|J = \tfrac{9}{2}\rangle = 0.990|4(\tfrac{3}{2})\tfrac{9}{2}\rangle - 0.081|5(\tfrac{3}{2})\tfrac{9}{2}\rangle + 0.115|4(\tfrac{5}{2})\tfrac{9}{2}\rangle.$$

The coefficients $f(F, m_f)$ for observed transitions are

$$f(7, m_f) = 0, \quad f(6, 0) \leftrightarrow f(6, -1) = \tfrac{1}{12}\tfrac{1}{77}^{\frac{1}{2}}, \quad f(4, 2) \leftrightarrow f(4, 1) = \tfrac{1}{20}\tfrac{6}{55}^{\frac{1}{2}}.$$

The separation of the $J = \frac{9}{2}$, $J = \frac{11}{2}$ levels is calculated to be 700 cm^{-1}. Using this value for the separation, and the above matrix elements, we find that the second-order perturbation at a magnetic field of 500 gauss is less than 100 cps for any state F, and may therefore be neglected.

8. Nuclear Structure

Mottelson and Nilsson [3]) have noted that the similarity of the lowest levels of Pa^{231} and Pa^{233} suggests that the spin of Pa^{233} is $\frac{3}{2}$, and that the odd proton belongs to the orbital $\frac{1}{2}-(530)$. The irregularities in the spacing of the levels of the ground-state rotational multiplet suggest that they are characterized by $K = \frac{1}{2}$, and a fit to the spacings has been obtained by assuming for the moment of inertia $\hbar^2/2\mathscr{I} = 6$ keV, and for the decoupling parameter $d = -1.3$.

An expression for the nuclear dipole moment μ_N, in terms of the coefficients $a_{l\Lambda}$ of the eigenvectors of the odd nucleon, has been given by Nilsson. For $K = \frac{1}{2}$, it is

$$\mu_I = \frac{1}{I+1}\,\{(g_s-g_l)[\tfrac{1}{4}\sum_l\,(a_{l0}^2-a_{l1}^2)+(-1)^{I-\frac{1}{2}+l}\tfrac{1}{2}(I+\tfrac{1}{2})\sum_l a_{l0}^2]$$
$$+(g_l-g_R)[\tfrac{1}{4}+(-1)^{I-\frac{1}{2}}\,\tfrac{1}{2}(I+\tfrac{1}{2})d]+g_R I(I+1)\}.$$

For an odd proton, $g_s = 5.58$ and $g_l = 1.0$. The g factor of the core g_R is taken as $Z/A = 0.4$ for a uniformly charged nucleus. The nuclear moment, μ_I, was calculated from the revised wave functions of Mottelson and Nilsson.

The results for $d = -1.3$ are:

δ	0	0.1	0.2	0.3
μ_I(n.m.)	2.09	2.32	2.63	2.77

Here δ is a parameter that characterizes the eccentricity of the nuclear potential. The value of δ may be estimated from the measured nuclear Q. The intrinsic quadrupole moment Q_0, is approximately

$$Q_0 = \tfrac{4}{5} Z R_0^2 \delta (1 + \tfrac{1}{2}\delta).$$

Here $R_0 \approx 1.2 \times 10^{-13} A^{\frac{1}{3}}$ cm is the mean charge radius of the nucleus. The relation between Q and Q_0 is

$$Q = \frac{3K^2 - I(I+1)}{(I+1)(2I+3)} Q_0.$$

For $K = \frac{1}{2}$ and $I = \frac{3}{2}$, we have $Q_0 = -5Q$. The measured $Q = -3.0$ barns; therefore Q_0 is $+15$ barns, and δ is 0.3. The predicted value of the nuclear moment corresponding to $\delta = 0.3$ is $\mu_I = 2.77$ n.m. For a nuclear spin $I = \frac{3}{2}$, the measured Q can be negative only for $K = \frac{1}{2}$. Thus the observed sign and magnitude of Q are in agreement with the configuration assignment $\frac{1}{2}-(530)$ for the odd proton.

The authors are very greatful to Dr. Bryan Judd for his advice and assistance with the calculation of the electronic structure.

References

1) J. C. Hubbs, R. Marrus and J. Winocur, Phys. Rev. **114** (1959) 586;
R. Marrus, W. A. Nierenberg and J. Winocur, UCRL-9207 (to be published);
J. C. Hubbs, W. A. Nierenberg, R. Marrus and J. L. Worcester, Phys. Rev. **109** (1958) 390;
J. C. Hubbs and R. Marrus, Phys. Rev. **110** (1958) 287;
Kiess, Humphrey and Laun, in National Bureau of Standards Report NBS-A 1747 (1944)
2) G. T. Seaborg, The Transuranium Elements (Yale University Press, New Haven 1958)
3) B. R. Mottelson and S. G. Nilsson, Mat. Fys. Skr. Dan. Vid. Selsk. **1**, No. 8 (1958)
4) O. P. Hok and P. Kramer, Physica **21** (1955) 676
5) H. Schüler and H. Gollnow, Naturwiss. **22** (1934) 511
6) E. K. Hyde and G. T. Seaborg, UCRL-3312 (unpublished)
7) Brian Judd, Lawrence Radiation Laboratory, private communication.
8) A. R. Edmonds, Angular Momentum in Quantum Mechanics (Princeton University Press, 1957)
9) G. Racah, Physica **16** (1950) 651
10) S. Cohen, Relativistic Self-consistent Calculation for the Normal Uranium Atom, UCRL-8633 (Feb. 1959)
11) E. U. Condon and G. H. Shortley, The Theory of Atomic Spectra (Cambridge University Press, 1957)
12) R. Marrus, W. A. Nierenberg, and J. Winocur, UCRL-9207 (to be published)
13) R. E. Trees, Phys. Rev. **92** (1953) 308

3.A

Nuclear Physics **23** (1961) 107—115; © *North-Holland Publishing Co., Amsterdam*

Not to be reproduced by photoprint or microfilm without written permission from the publisher

INVESTIGATION OF γ-RAYS FROM Mg^{24}, Mg^{25}, Mg^{26} ISOTOPES BOMBARDED WITH Po α-PARTICLES

E. CSONGOR

Institute of Experimental Physics, Debrecen, Hungary †

Received 24 October 1960

Abstract: Electromagnetically separated Mg^{24}, Mg^{25}, Mg^{26} isotopes were bombarded with Po α-particles. In the case of Mg^{25} and Mg^{26} the excitation function of γ-radiation from the nuclear processes was measured with a thin target. In the case of the Mg^{25} target, resonances were found at α-energies of 3.58, 4.33, 4.47, 4.61, 4.80, 4.99 and 5.09 MeV; in the case of Mg^{26} target, at α-energies of 4.56 and 5.01 MeV. From these data seven highly excited states of the Si^{29} compound nucleus and two of the Si^{30} nucleus were determined. The origin of γ-radiation was cleared up by the observed spectra of γ-rays. A method for a micro-electro-chemical deposition of Mg has been elaborated by the author.

1. Introduction

Bothe and Becker observed gamma-radiation in nuclear reactions for the first time [1]). They bombarded several light elements with Po α-particles, and they demonstrated the presence of γ-radiation among other targets in Mg too. Subsequently Webster [2]) and Savel [3]), then Pollard and Alburger [4]), as well as Alburger [5]) determined the energies of γ-radiation; Slätis [6]) as well as Szalay and Csongor [7]) investigated the excitation function of γ-radiation. Breen and Hertz [8]), as well as Nemilov and Piszarevszkij [9]) measured the spectrum of this γ-radiation.

All the above measurements were carried out on natural Mg targets. In Nature, Mg is a mixture of 3 stable isotopes: Mg^{24} (78.6 %), Mg^{25}(10.11 %) and Mg^{26}(11.29 %). In the case of bombardment with α-particles, there is a possibility both for proton- and neutron-emission, as well as for elastic and inelastic scattering, which — since there are three isotopes — mean 9 such reactions that may be accompanied by γ-radiation. Similarly the β-decays of Al^{28} and Al^{29} radioactive nuclei (remaining after the proton-emission) may be associated with γ-radiation. So, in principle, γ-radiation may arise in the case of 11 different reactions, when natural Mg is bombarded with α-particles.

Previous measurements reveal that: 1) the excitation function has not been defined with sufficient accuracy to allow any conclusion to be drawn regarding the excited states of the compound nucleus; 2) the data on the energy and spectral composition of γ-radiation are contradictory; 3) the origin of γ-radiation is not cleared up, mainly due to the fact that the previous investigations have been made with a natural Mg target.

---

† The research work was carried out at the Institute of Nuclear Research, Debrecen, by the courtesy of the Institute.

To clear up these unsettled problems, a) the excitation functions of γ-radiation and b) the spectra of γ-rays were individually measured on electromagnetically separated MgO isotopes.

2. Experimental Apparatus and Target Preparation

For the observation of γ-particles, a NaJ(Tl) crystal scintillation counter and spectrometer were used. The block-scheme of the apparatus is shown in fig. 1.

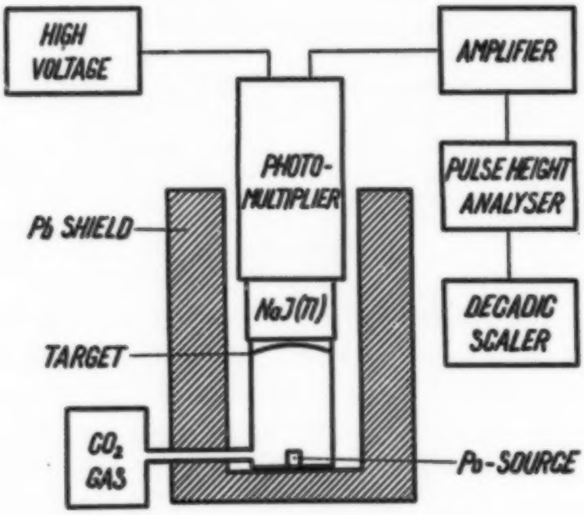

Fig. 1. Block-scheme of the apparatus.

The NaJ(Tl) crystal 30 mm high and 40 mm in diameter was fitted to an RCA 5819-type photo-multiplier. After preamplification, the output signal was further amplified by a wide-band amplifier, and then the signals selected by the analyzer were counted by a decadic scaler. The spectrum was taken by a single-channel differential discriminator of 2 % relative channel-width.

The electromagnetically separated isotopes in the form of MgO were procured from Harwell [10]). Because of the small quantity of substance (5 mg), no attempts were made to prepare the target by the usual method of vacuum evaporation [11–13]), which is by no means an easy task in the case of MgO [14]).

For the preparation of the thin target, a micro-electro-chemical method was finally elaborated by the author [15]). At first MgO was transformed to $MgCl_2$ by adding HCl. After drying, $MgCl_2$ was solved in abs. waterfree pyridine, then the metal ion was electrodeposited from this organic solvent directly on to the spherical stainless-steel target backing. The anode was Pt, bent in ring shape.

The two electrodes were separated by a porous glass partition (Schott G2 filter) and the Cl_2 arising upon the anode was stripped off by bubbling argon gas stream. The electrolysis occurred at 0.2 mA/cm^2 current density.

The thickness of the prepared target was 0.18 mg/cm^2, that is 1.2 mm air-equivalent.

For the α-source, a Po preparation of 40 mC was used which had been volatilized on to a Pt-Ir disk of 3 mm in diameter, according to the method of A. Szalay [16]).

3. Survey of the Excitation Functions and Excited States of Si^{29}, Si^{30} Nuclei

The Po α-source was placed at the geometrical centre of the MgO target (fig. 1). The thin target and the use of small solid angle assured homogeneity in energy of α-particles.

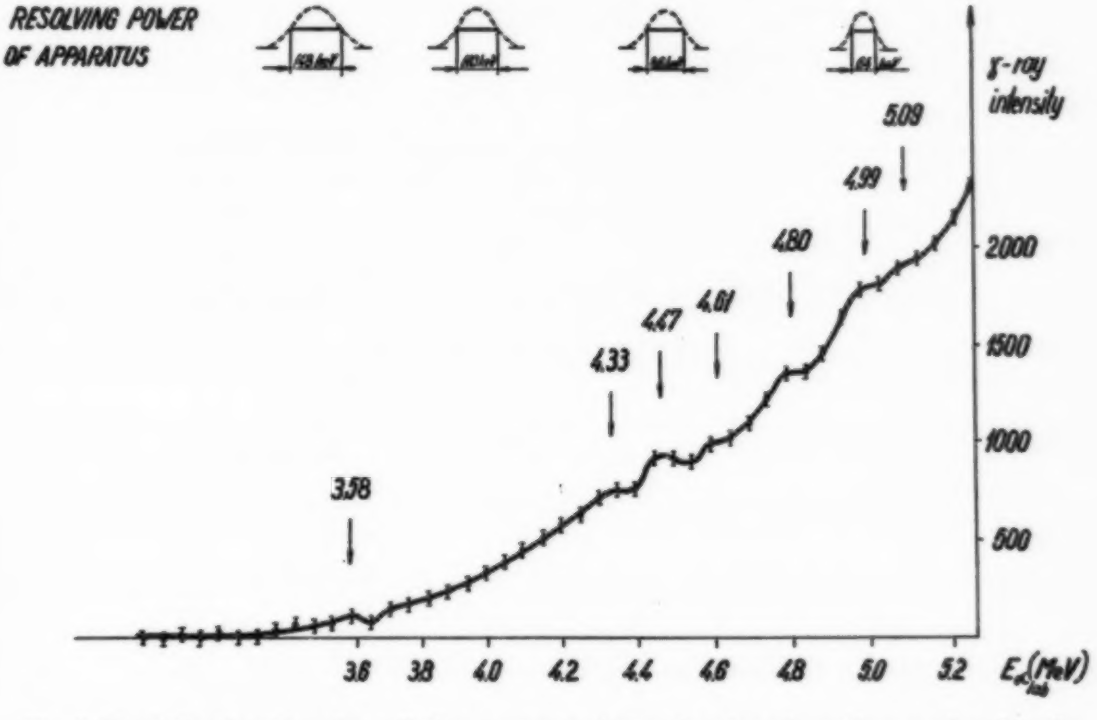

Fig. 2. Excitation function of γ-radiation accompanying nuclear transformations produced by Po α-particles upon a thin Mg^{25} target (0.18 mg MgO per cm^2). Abscissa: energy of bombarding α-particles; ordinate: intensity of γ-radiation in arbitrary units.

The α-particles were slowed down to the level required by regulating the pressure of CO_2 stopping gas, and the yield of γ-rays was measured at the respective α-energies, by an integral discriminator. The adjustment of discriminator voltage made the elimination of the 0.8 MeV γ-radiation of Po possible.

Consequently, in the course of measurements, all the γ-quanta belonging to the respective α-energies and possessing more than 1 MeV energy were counted.

The excitation functions obtained in the bombardment of Mg^{25} and Mg^{26} isotopes are shown in figs. 2 and 3. In the case of the Mg^{24} isotope, it was not possible to take the excitation function because of the small yield of γ-radiation.

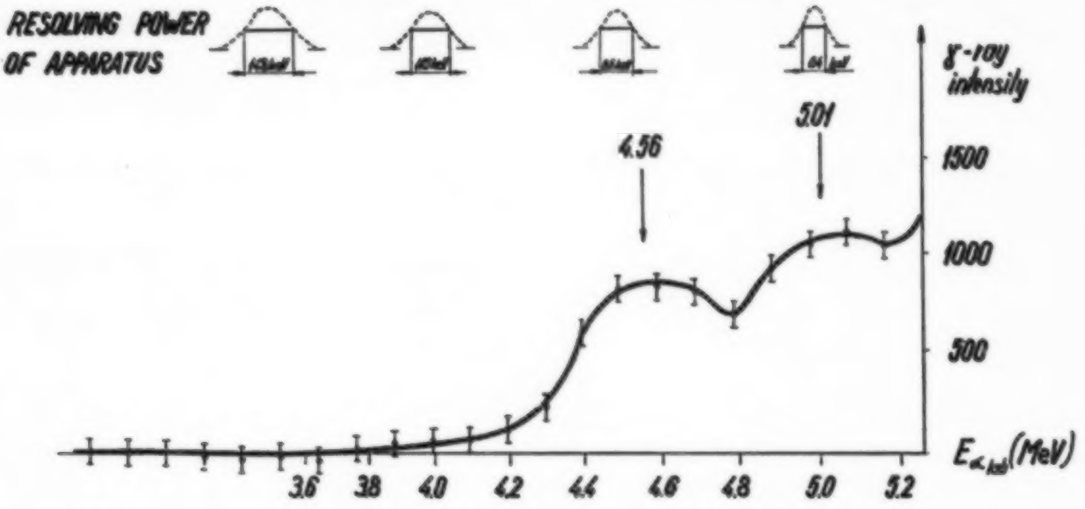

Fig. 3. Excitation function of γ-radiation accompanying nuclear transformations produced by Po α-particles upon a thin Mg^{26} target (0.18 MgO per cm^2). Coordinates: same as in fig. 2.

Both excitation functions revealed marked resonances, and from these resonance energies the highly excited states of Si^{29} and Si^{30} compound nuclei could be determined. The data are included in table 1.

Table 1

The excited states of Si^{29} and Si^{30} nuclei observed in these investigations (on the basis of accumulated data [17]) the binding energy of the α-particle in the compound nucleus was calculated $E_b = 11.141$ MeV for the Si^{29} nucleus, and $E_b = 10.633$ MeV for Si^{30}).

Compound nucleus	Bombarding energy E_{lab} (MeV)	Excited state E_e (MeV)
Si^{29}	3.58 ± 0.07	14.23 ± 0.06
	4.33 ± 0.05	14.87 ± 0.04
	4.47 ± 0.04	14.99 ± 0.04
	4.61 ± 0.04	15.11 ± 0.03
	4.80 ± 0.04	15.28 ± 0.03
	4.99 ± 0.03	15.44 ± 0.03
	5.09 ± 0.03	15.53 ± 0.03
Si^{30}	4.56 ± 0.05	14.59 ± 0.04
	5.01 ± 0.03	14.98 ± 0.03

In the two investigated excitation functions also the absolute cross-section for the (α, γ) process was estimated and the values

$$\sigma_{\mathrm{Mg}^{25}(\alpha,\gamma)} \approx 120\ \mathrm{mbarn} \pm 40\ \%,$$
$$\sigma_{\mathrm{Mg}^{26}(\alpha,\gamma)} \approx 50\ \mathrm{mbarn} \pm 40\ \%,$$

were obtained at maximum α-energy of 5.3 MeV, which is in good agreement with the σ_c value computed theoretically by Shapiro 18)).

On comparing the shape of excitation functions, it is remarkable that while the resonances observed in the case of the Si^{30} nucleus were only two in number which were broad ($\Gamma_1 \approx 350$ keV, $\Gamma_2 \approx 300$ keV), the Si^{29} nucleus had seven narrow resonances, even narrower than the resolving power of the apparatus, which are shown in the upper part of figs. 2 and 3[†].

In the case of the Mg^{24} target, the small yield of γ-radiation is noticeable (see spectra). The binding energy of the last neutron is very high in the Si^{29} compound nucleus, owing to the fact that the Si^{28} nucleus is semimagic and owing to the state of Z (even) $= N$ (even), where neutron emission, when a Po-source is used, is out of the question for energetic reasons. The analysis of the spectrum of γ-rays shows that inelastic scattering is improbable. According to measurements of Kaufmann and collaborators 19)), the elastic scattering of α-particles is the most probable process in this energy range. Thus it stands to reason that the yield of γ-radiation should be small in the case of the Mg^{24} target, because this appears as a concomitant only to the proton emission process of small probability.

4. The Spectra of γ-Rays and Origin of γ-Radiation

Figs. 4, 5 and 6 show the energy spectra of γ-particles in the range of 1—4.5 MeV for the Mg^{24}, Mg^{25} and Mg^{26} targets. The spectra reveal that γ-radiation is more complex and consists of more components than was reported by previous authors 8,9)).

The origin of γ-radiation may be regarded as cleared up if the observed γ-energies can be ascribed to some nuclear reaction, in other words, if the observed γ-ray energies can be fitted into the energy-level scheme of a nucleus.

For this purpose, the energies detected in the spectra were compared with all the possible transitions 20)) of the heretofore known excited states of residual nuclei in the possible nuclear reactions.

[†] *Note added in proof:* Litherland and McCallum 21)) resolved the broad resonances of the Si^{30} nucleus into 3, resp. 2 narrow levels, which our apparatus was not able to resolve.

The detected γ-energies and the conclusions regarding their origin are included in table 2.

TABLE 2
Results from γ-ray spectra

Target	Observed γ-energy (MeV)	Origin of radiation	
		residual nucleus	transition between excited states of the residual nucleus
Mg^{24}	1.0	Al^{27}	$2 \to 0$
	1.36		$3 \to 1$
	1.72		$4 \to 2$
	2.15		$3 \to 0$
	2.65		$4 \to 0$
Mg^{25}	1.78	Si^{28}	$1 \to 0$
	2.85		$2 \to 1$
	3.3		$3 \to 1$
	3.45		$4 \to 1$
	3.65		$2 \to 0$
	4.0		$3 \to 0$
	1.37	Al^{28}	$4 \to 0$
	2.13		$6 \to 0$
	2.21		$7 \to 0$
	2.30		$8 \to 0$
	2.49		$9 \to 0$
	2.58		$10 \to 0$
	2.67		$11 \to 0$
	3.0		$12 \to 0$
Mg^{26}	1.25	Si^{29}	$1 \to 0$
	1.45		$3 \to 0$
	1.75		$4 \to 1$
	2.0		$2 \to 0$
	2.45		$3 \to 0$
	3.0		$4 \to 0$

The transitions corresponding to the observed γ-energies are marked with arrows in the energy-level schemes of figs. 4, 5 and 6. In so far as the respective targets are concerned, the following conclusions may be drawn regarding the origin of γ-radiation:

a) Considering that on bombarding the Mg^{24} target, neutron emission is excluded for reasons of energetics ($Q = -7.2$ MeV) when a Po α-source is used, and as the energy of 1.36 MeV characteristic of inelastic α-scattering does not appear with pronounced intensity in the spectrum, it is obvious that the observed γ-radiation may be assigned to the excited states of the residual

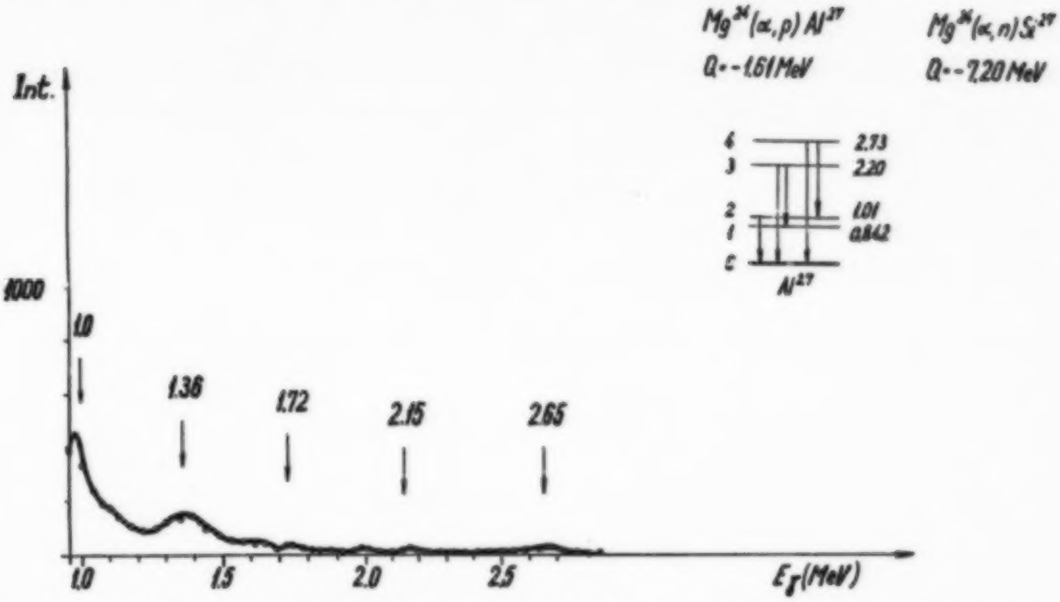

Fig. 4. The spectrum of the γ-radiation (part above 1 MeV) accompanying nuclear transformations produced by Po α-particles on a Mg^{24} target. (Abscissa: γ-energy in MeV; ordinate: intensity of γ-radiation. Also shown is the energy level scheme of the residual nucleus. Arrows indicate observed transitions.

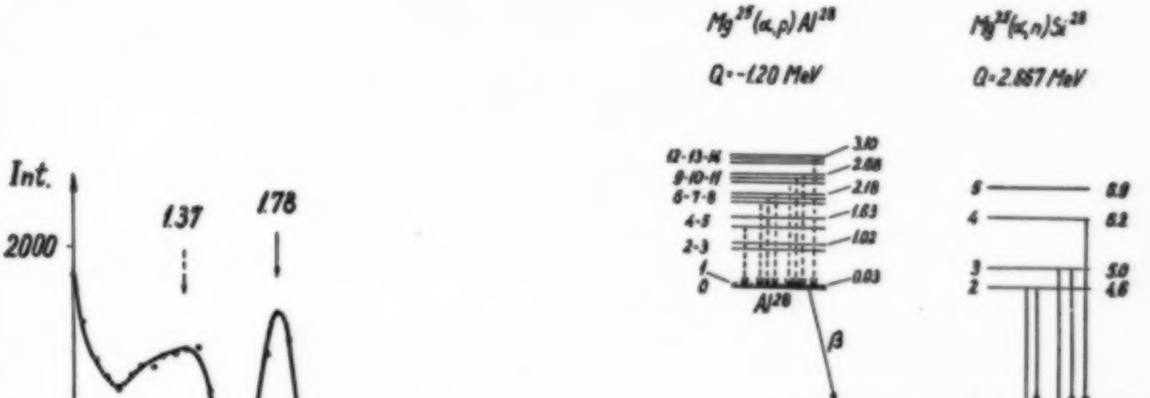

Fig. 5. The spectrum of the γ-radiation (part above 1 MeV) accompanying nuclear transformations produced by Po α-particles on a Mg^{25} target. Coordinates: same as in fig. 4. Also shown are the energy level schemes of the residual nuclei. Arrows indicate observed transitions.

nucleus from the $Mg^{24}(\alpha, p)Al^{27}$ reaction. The observed energies can be very well fitted into the level scheme (fig. 4).

b) The spectrum obtained when the Mg^{25} target is used (fig. 5) derives from the superposition of two spectra; the peaks appearing with a low intensity may be assigned to the excited states of the residual nucleus of the $Mg^{25}(\alpha, p)Al^{28}$ reaction, which has a smaller yield ($Q = -1.20$ MeV); the peaks of the spectrum appearing with higher intensity belong to the excited states of the residual nucleus in the $Mg^{25}(\alpha, n)Si^{28}$ reaction ($Q = 2.667$ MeV).

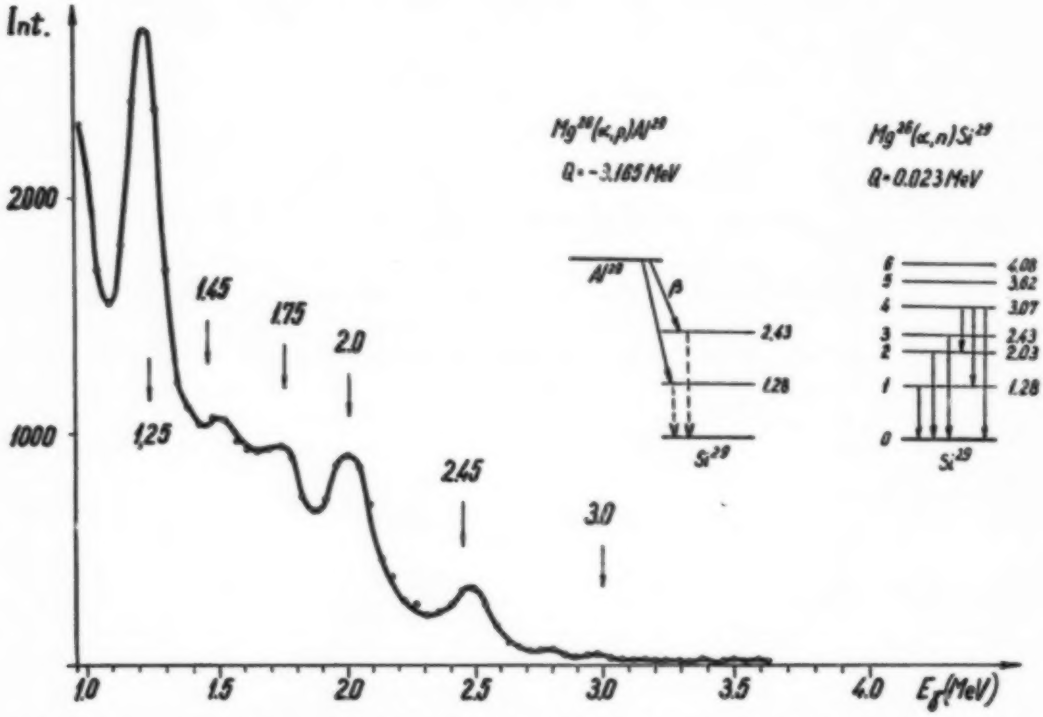

Fig. 6. The spectrum of the γ-radiation (part above 1 MeV) accompanying nuclear transformations produced by Po α-particles on a Mg^{26} target. Coordinates: same as in fig. 4. Also shown the energy-level schemes of the residual nuclei. Arrows indicate observed transitions.

Considering that the high energy component of γ-radiation could only be observed when the Mg^{25} target is bombarded, and as this can — for reasons of energetics — be assigned only to reactions with neutron emission, the fact is supported by direct experimental evidence that the high energy component of γ-radiation observed by previous authors can be exclusively assigned to the $Mg^{25}(\alpha, n)Si^{28}$ reaction.

c) The lines of the spectrum taken with the Mg^{26} target (fig. 6) belong to the excited states of the Si^{29} nucleus. First of all the neutron emission is accompanied by the γ-rays ($Q = 0.023$ MeV), though proton emission also occurs, but because of the high threshold energy, with less probability ($Q = -3.165$ MeV). On the one hand, however, an excited state of the Al^{29} residual nucleus is not known; and on the other hand, the Al^{29} nucleus transforms into the Si^{29} nucleus by β-decay. With this β-decay two γ-lines are concomitant (see fig. 6), and these get superposed upon the γ-spectrum, which accompanies the neutron emission.

The author is greatly indebted to Professor A. Szalay for having prepared the Po source and made it possible to carry out the necessary measurements at the Institute of Nuclear Research. Acknowledgement is due also to Mr. G. Máthé who designed and constructed the scintillation counter.

References

1) W. Bothe und H. Becker, Z. Phys. **66** (1930) 289
2) H. C. Webster, Proc. Roy. Soc. A **136** (1932) 428
3) P. Savel, Ann. de Phys. **4** (1935) 88
4) E. Pollard and D. E. Alburger, Phys. Rev. **72** (1947) 1196
5) D. E. Alburger, Phys. Rev. **73** (1948) 1014
6) H. Slätis, Arkiv. för Mat. Astr. o. Fys. **35 A** (1948) No. 31, 1
7) A. Szalay and E. Csongor, Phys. Rev. **74** (1948) 1063
8) R. J. Breen and M. R. Hertz, Phys. Rev., **98** (1955) 599
9) Ju. A. Nemilov and A. N. Piszarevszkij, JETP (USSR) **32** (1957) 139, resp. Soviet Physics JETP **5** (1957) 117
10) Atomic Energy Research Establishment (Electromagnetic Separation Group) Harwell
11) F. P. Mooring, L. J. Koester, E. Goldberg, D. Saxon and S. G. Kaufmann, Phys. Rev. **84** (1951) 703
12) H. G. Graetzer and A. B. Robbins, Phys. Rev. **105** (1957) 1570
13) L. N. Russel, E. W. Taylor and J. N. Cooper, Rev. Sci. Instr., **23** (1952) 764
14) C. P. Browne, Nuclear Physics **12** (1959) 662
15) E. Csongor, Magyar Fizikai Folyóirat **7** (1959) 517 (in Hungarian)
16) A. Szalay, Z. f. Phys. **112** (1939) 29
17) S. B. Dzelepow, L. K. Peker, Decay schemes of radioactive nuclei, (Academy of Sciences of the USSR Press, Moscow, 1958)
18) M. M. Shapiro, Phys. Rev. **90** (1953) 171
19) S. G. Kaufmann, E. Goldberg, L. J. Koester and F. P. Mooring, Phys. Rev. **88** (1952) 673
20) P. M. Endt and C. M. Braams, Rev. Mod. Phys. **29** (1957) 683
21) Litherland and McCallum, Can. Journ. of Phys. **38** (1960) 927

2.G

Nuclear Physics **23** (1961) 116—121; © *North-Holland Publishing Co., Amsterdam*

Not to be reproduced by photoprint or microfilm without written permission from the publisher

MEASUREMENTS OF NEUTRON SPECTRA FROM FISSION

T. W. BONNER

Rice University, Houston, Texas †

Received 31 October 1960

Abstract: The neutron spectra from the fission of U^{235}, U^{233}, and Pu^{239} by thermal neutrons have been measured by means of the sphere moderated neutron spectrometer. The spectra fit a Maxwellian distribution of the form $N(E) = \sqrt{E}e^{-E/\theta}$. The value of the energy parameter θ was found to be 1.332 ± 0.030 MeV in the case of $U^{235}+n$; the energies of the prompt neutrons from the fission of U^{233} and Pu^{239} were respectively 1.8 % and 4.0 % greater than that of U^{235}. Experiments on the spontaneous fission of Pu^{240} and Cf^{252} give values of θ of 1.189 and 1.367 MeV. The most probable energy of the leakage neutrons from Jezebel was found to be 15 % lower than that of $Pu^{239}+n$. The variation of the energy of fission neutrons with $\bar{\nu}$ is compared to evaporation theory.

1. Introduction

The neutron spectra from the fission of U^{235} has been studied extensively by several techniques including the cloud chamber, nuclear emulsions, recoil proton counters, and time of flight [1]. The measurements by Cranberg, Frye, Nereson, and Rosen [1] show that the spectrum from $U^{235}+n$ can be fit with a Maxwellian distribution $N(E) = \sqrt{E}e^{-E/\theta}$ with an energy parameter of $\theta = 1.29$ MeV. The spectra from the fission of U^{233} and Pu^{239} by thermal neutrons and from the spontaneous fission of Cf^{252} have been studied [1] and these neutrons were observed to have somewhat higher energies than from $U^{235}+n$. Application of evaporation theory by Terrell [2] and by Kovalev and Stavinsky [3] show that the energies of the neutrons increase with excitation of the fragments; the values of the average number of neutrons per fission ($\bar{\nu}$) also increase with excitation; the variation of the energy parameter θ with $\bar{\nu}$ has been calculated from the evaporation model. The purpose of the present experiment was to obtain accurate information about the change in the energy of the neutron spectra from a number of fissionable isotopes.

2. Experimental Method

The sphere moderated neutron spectrometer which was used in this experiment has been previously described [4]. This spectrometer has excellent energy resolution for continuous distributions of neutrons with energies in the range of 0 to 4 MeV. The application 5) of the spectrometer to (p, n) reactions in medium weight nuclei not only shows high accuracy in energy determinations but also enough sensitivity to distinguish between an evaporation spectra of the form $N(E) = E\mathrm{e}^{-E/T}$ and a Maxwellian spectra, $N(E) = \sqrt{E}\mathrm{e}^{-E/\theta}$.

---

† Experimental work was carried out in the summers of 1959 and 1960 at the University of California's Los Alamos Scientific Laboratory, Atomic Energy Division of Phillips Petroleum Company, and Lawrence Radiation Laboratory of the University of California (Livermore), and was supported by the U. S. Atomic Energy Commission.

The neutron spectra from the fission of U^{235}, U^{233}, and Pu^{239} were measured at the M.T.R. reactor in Idaho. The sphere-counter was placed 2.8 m above the top shield of the reactor. The samples to be observed were foils of U^{235}, U^{233}, and Pu^{239} with a thickness from 0.025 to 0.050 cm and an area of about 20 cm^2. The foils were placed in a beam of predominately thermal neutrons, which was of sufficient flux to produce 5×10^7 fission neutrons per second. The samples were placed 35 cm from the centre of the counter. The counting rates were determined for each sample with polyethylene spheres of 30, 20, 13, 7.6 and 5.1 cm diameters. Background counts were made with a cadmium shutter covering the port in the reactor so that effects due to all but thermal neutrons were eliminated. The experiment was carried out by successively measuring the number of counts in ten minute intervals with each of the sphere-counters. Each data point was obtained with 20000 to 100000 counts and each configuration was repeated six times. The variation in the counting rate on successive runs for each counter was about 1 % and the average deviation from the mean was ≈ 0.5 %. A small correction has been made to subtract the counts due to delayed neutrons whose relative abundance as compared to prompt neutrons amounts to 0.64 %, 0.26 %, and 0.22 % respectively or U^{235}, U^{233} and Pu^{239}. The average energy of the delayed neutrons used in this calculation was 0.45 MeV.

TABLE 1

Experimental results on the prompt neutron spectra from fission

Counters used	Experimental values of θ in MeV						Sensitivity of counters a)
	$\mathrm{U}^{235}+\mathrm{n}$	$\mathrm{U}^{233}+\mathrm{n}$	$\mathrm{Pu}^{239}+\mathrm{n}$	Pu^{240}	Jezebel	Cf^{252}	
13/5.1	1.290	1.367	1.355		1.142	1.363	2.8
20/5.1	1.332	1.354	1.380		1.171	1.364	5.1
20/7.6	1.400	1.392	1.433	1.125	1.195	1.419	4.2
30/5.1	1.306	1.345	1.366		1.179	1.342	7.8
30/7.6	1.344	1.366	1.399	1.158	1.193	1.372	6.9
30/13	1.319	1.334	1.374	1.238	1.195	1.332	5.2
Best value of θ	1.332	1.356	1.385	1.189	1.184	1.367	
Most probable neutron energy	0.666	0.678	0.693	0.595	0.592	0.684	

a) Per cent change of counter ratios for a change of θ of 0.1 MeV for $\theta = 1.30$ MeV.

The ratio of the number of counts in any two counters is sufficient to fix a single parameter in a continuous spectrum. The experimental ratios of counts were compared to calculated ratios which were based on the counter calibration curves and the assumed spectrum of the form $N(E) = \sqrt{E}\, e^{-E/\theta}$. The experimental values of the temperature parameter θ for the counter ratios 13/5.1, 20/5.1, 20/7.6, 30/5.1, 30/7.6, and 30/13 are given in table 1 for each of the fission sources. The energy sensitivity of each of the counter ratios is given in the last column of the table. This sensitivity is the per cent change in the particular ratio that is obtained for a change of the energy parameter by 0.1 MeV. The ratio with the greatest energy sensitivity is the 30/5.1; if this ratio is measured to an accuracy of 1 %, the value of the energy parameter θ is obtained to an accuracy of 1 % or 0.013 MeV for the fission spectra. Other ratios that are not quite so sensitive are also included in table 1. The ratios are arranged in order of increasing counter size so that a trend in the values of θ indicates a deviation from the assumed spectra. The spectra from U^{235}, U^{233}, and Pu^{239} show no definite trend with increasing counter size, indicating that the assumed shape of the spectra is correct within the experimental errors of this experiment and the counter calibration. The best value of θ for the U^{235} spectrum was obtained by averaging the data given in table 1; ratios with less sensitivity were included to average out small errors in calibration. The value of $\theta = 1.332$ MeV is estimated to have an absolute error of ± 0.030 MeV. This result agrees within the combined estimated errors with the value of 1.29 ± 0.03 MeV obtained by Cranberg, Frye, Nereson and Rosen [1]). The best values of θ for the spectra of U^{233} and Pu^{239} were obtained by using only the most sensitive ratios: 20/5.1, 30/5.1, 30/7.6, and 30/13. The prompt neutron spectra of U^{233} and Pu^{239} were found to be respectively 1.8 % and 4.0 % greater than that of U^{235}. The probable error in these two values is ± 0.3 %. The energy parameters of all the neutrons, including the delayed neutrons, are 1.317, 1.350, and 1.380 MeV respectively for U^{235}, U^{233}, and Pu^{239}.

In another experiment at Los Alamos the neutron spectra from Jezebel, a critical assembly of Pu^{239}, was measured. In this experiment the techniques were essentially the same as those described above. The sphere-counter was positioned 40 cm from the centre of Jezebel and the whole apparatus suspended 4 m above the ground by a metal tower which was placed outside of the Laboratory building. The assembly was operated so that approximately 5×10^7 neutrons per second escaped. The constancy of the neutron flux was monitored by long counters that were placed 2.5 m away. The ratios of the counting rates obtained with 30, 20, 13, 7.6, and 5.1 cm counters were used to calculate the energy parameter θ. The results are shown in table 1. There is a small trend in θ with counter size which indicates a small deviation from the Maxwellian shape that would be expected from neutrons which have been inelastically scattered. The inelastically scattered neutrons are expected to be of the evaporation type:

$N(E) = Ee^{-E/T}$ and would be expected to be of lower energy than the primary fission neutrons. The best value of θ is 1.185 MeV which is 15 % lower than that obtained for the primary spectrum. The most probable neutron energy is 0.595 MeV which is considerably larger than that reported [6]) for a critical assembly of U^{235}. A higher value of the most probable energy is expected in the case of Pu^{239} since the ratio of the cross section for fission to inelastic scattering is greater than for U^{235}.

A second experiment was carried out at Los Alamos with a source of Pu^{240} which fissions spontaneously. The source of Pu^{240} was approximately 30 kg of Pu^{239} with Pu^{240} impurity. The material was in the form of 28 thin metal discs, approximately 22 cm in diameter and 1.4 mm thick which were fastened to a light aluminium frame. The discs were arranged end to end so that they formed two rings which were mounted on the upper and lower side of a thin aluminium plate whose plane intersected the counter. The flat face of each disc was towards the counter. With this arrangement of material there was little neutron multiplication or inelastic scattering. The fraction of the neutrons which made a nonelastic scattering in getting out of a disc is approximately 1.5 %, and the neutron multiplication is about 4 %. Because of the smaller neutron flux of 2×10^6 n/sec from this source, data were not obtained with the 5.1 cm counter which gives the lowest counting rate. Due to the weak source and a limited amount of time to carry out the experiment, the counting rates are not as accurate as those previously described. As a consequence there is a greater spread in the calculated energy parameter θ than in the other data. The energy of the neutrons produced by the small amount of nonelastic scattering in the Pu^{239} of the discs is essentially the same as that obtained from Jezebel. Because of the small number of these neutrons and the similarity of this spectra with that of Pu^{240} no corrections have been applied for their presence. The best value of θ was found to be 1.189 MeV and the probable error amounts to ±0.030 MeV when compared to the U^{235} source.

The experiment which measured the neutron spectrum from Cf^{252} was carried out at the Lawrence Radiation Laboratory in Livermore in 1960. The Cf^{252} which had a source strength of 6×10^5 neutrons per sec was mounted at the top of a metal tower, 7.2 m above the floor of a large hanger. The distance to the walls was greater than that to the floor. With this weak source the experimental procedure was somewhat different from that previously described. Eight runs were obtained with each counter with a total of 15000 counts or more in a run. The distance from the Cf^{252} source was 40 cm when using the 30, 20, and 13 cm counters and this was reduced to 15 cm when using the 7.6 and 5.1 cm counters. The smaller distance with the small counters increased their counting rate and reducted the relative effect of the background in the counters. The background in the various counters varied from 1 to 2 % of that obtained with the source in position, and was subtracted from the data. Since the Cf^{252} source was essentially a point source, data obtained at the 15 cm distance could be accurately converted to the 40 cm distance by applying the inverse square law. Data with the 13 cm counter were obtained at both distances and the computed value at 40 cm differed by only 0.2 % from that obtained directly.

The calculated values of the energy parameters θ are given in table 1. The best value of θ was found to be 1.367 MeV with a probable error of ± 0.030 MeV. The comparison to the other spectra was not as accurate as that obtained with U^{233} and Pu^{239} sources because a different $Li^6I(Eu)$ scintillator was used in the counter.

3. Discussion of Results

The experimental results show a considerable change of the energy parameter θ with the source of fission neutrons. The ratio of the neutron energies obtained from U^{235}, U^{233}, and Pu^{239} are in good agreement with the results of Grundl and Neuer [1]), and Kovalev *et al.* [1]), which were obtained with threshold detectors. The experimental values of θ are shown as a function of the average number of neutrons per fission in fig. 1. The experimental data indicate a rapid change in θ with $\bar{\nu}$ in the region of Pu^{240}, U^{235}, and U^{233} and a slower increase for larger values of $\bar{\nu}$. The variation of the energy parameter θ is compared to the theoretical results of Terrell [2]), and Kovalev and Stavinsky [3]) in fig. 1. The theoretical data which were based on a value of $\theta = 1.29$ for $U^{235}+n$, have been

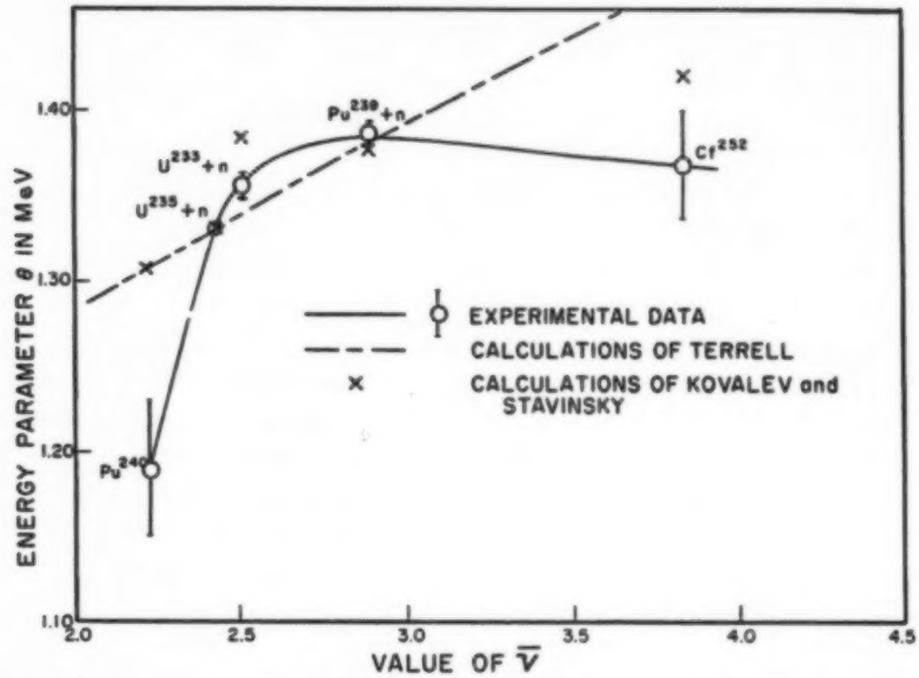

Fig. 1. The variation of the energy parameter θ with the average number of neutrons per fission $\bar{\nu}$. The estimated limits of error relative to $U^{235}+n$ are indicated on the experimental points.

renormalized to the value of $\theta = 1.33$. The value of θ for Cf^{252} attributed to Kovalev and Stavinsky is that obtained from their published curve drawn through the points of the spontaneously fissionable elements Pu^{242}, Pu^{240}, Pu^{238} and Cm^{244}.

The experimental data deviate considerably from the simple relation given by Terrell; this result is not unexpected since he made no allowance for variations in the excitation energy change per emitted neutron or the value of the level density parameter a, both of which vary with Z and A. The experimental data agree somewhat better with that calculated by Kovalev and Stavinsky in the case of Cf^{252}. More accurate measurements on other fissionable materials are needed in order to understand the variation of the neutron spectra with $\bar{\nu}$; shell structure effects are probably important and will cause deviation from a smoothly varying function.

I am much indebted to Dr. D. M. Barton at Los Alamos, to Dr. J. E. Evans, F. B. Simpson, and L. G. Miller at Phillips Petroleum Company, and to Dr. H. Mark at Livermore for their invaluable assistance in carrying out these experiments.

References

1) B. E. Watt, Phys. Rev. **87** (1952) 1037;
Bonner, Ferrell and Rinehart, Phys. Rev. **87** (1952) 1032;
Hjalmar, Slatis and Thompson, Arkiv Fysik **10** (1956) 357;
Smith, Fields and Roberts, Phys. Rev. **108** (1957) 411;
Cranberg, Frye, Nereson and Rosen, Phys. Rev. **103** (1956) 669;
Kovalev, Andreev, Nikolaev, and Guseinov, JETP Phys. (USSR) **33** (1957) 1069;
Grundl and Neuer, Bull. Am. Phys. Soc. **1** (1956) 95
2) J. Terrell, Phys. Rev. **113** (1959) 527 (this paper gives many references to earlier publications)
3) V. P. Kovalev and V. S. Stavinsky, Atomnaya Energiya **5** (1958) 649
4) Bramblett, Ewing and Bonner, Nuclear Instruments and Methods (1960)
5) R. L. Bramblett and T. W. Bonner, Nuclear Physics **20** (1960) 395
6) L. Rosen, Proc. First Intern. Conf. Peaceful Uses Atom. En. **4** (1955) 97

2.A.1 *Nuclear Physics* **23** (1961) 122—130; © *North-Holland Publishing Co., Amsterdam*
Not to be reproduced by photoprint or microfilm without written permission from the publisher

CROSS SECTION FOR THE $Be^9(n,\alpha)He^6$ REACTION

R. BASS [†], T. W. BONNER and H. P. HAENNI
Rice University, Houston, Texas [††]

Received 21 November 1960

Abstract: The cross section for the reaction $Be^9(n,\alpha)He^6$ has been measured for neutron energies from 3.9 to 8.6 MeV by counting the induced He^6 activity. The cross section falls smoothly from 93 mb at 4.0 MeV to 39 mb at 6.5 MeV and 32.5 mb at 8.5 MeV.

1. Introduction

The reaction $Be^9(n,\alpha)He^6$ was studied for two reasons: it was hoped to learn more about the mechanism of interaction of fast neutrons with Be^9 and the level scheme of Be^{10}; also this reaction is of practical interest in connection with the use of beryllium as a neutron moderator. It is the only neutron absorbing process energetically possible at neutron energies below about 10 MeV. Since the final nucleus, He^6, is a β^--emitter of convenient half-life (0.8 sec) and β-energy (3.5 MeV), the cross section can be measured with a pulsed neutron source, counting the induced He^6-activity during the intervals between neutron bursts [1-4]). In this way Stelson and Campbell [3]) have measured the $Be^9(n,\alpha)He^6$ cross section for neutron energies from 0.7 to 4.4 MeV. Their absolute values are appreciably higher than those of earlier workers [1, 2]) but were expected to be more accurate. It seemed worthwhile, however, to check the existent data by independent measurements and to extend them to higher neutron energies using the $D(d,n)He^3$ reaction as a neutron source in connection with the Rice University 6 MeV Van de Graaff accelerator.

2. Relative Cross Section Measurements

The experimental arrangement was similar to that used by Stelson and Campbell [3]) and is shown in fig. 1. The analyzed deuteron beam was deflected electrostatically on and off a tantalum slit at time intervals of approximately 1/10 sec. The deflection voltage varied depending on the beam energy between 1.5 and 8 kV. When the deuteron beam was passing through the slit it entered a deuterium gas target through a thin nickel window of either 0.70 or 1.25

[†] On leave from Institut für Kernphysik der Universität Frankfurt, Frankfurt am Main, Germany.

[††] Work supported in part by the U. S. Atomic Energy Commission.

mg/cm^2 thickness. The gas was contained in a thin walled platinum chamber of 4.2 cm length. A system of electrically insulated tantalum diaphragms (not shown in fig. 1) served to define the deuteron beam diameter and to repell secondary electrons and thereby to ensure proper integration of the beam current entering the gas target. Bursts of neutrons produced by the reaction $D(d, n)He^3$ and emerging from the gas target at zero degrees with respect to the deuteron beam were incident on beryllium disc of 2 mm thickness and 1 cm diameter which was placed at a distance of approximately 5 cm from the gas target. A lead absorber of 3 mm thickness was interposed between the gas target and the beryllium disc in order to stop electrons from β-emitters produced by the deuteron beam in the nickel window. The beryllium disc was in contact with a CsI(Tl) scintillator of 0.32 cm thickness and 1.27 cm diameter which was covered by 2.4 mg/cm^2 aluminium foil and two layers of scotch tape; it was mounted on a lucite lightpipe of 1.27 cm length and a RCA 6342 photomultiplier. Following neutron irradiation of the beryllium disc, electrons from the β-decay of He^6 were detected in the CsI crystal after losing approximately 100 keV in the tape and aluminium foil. The photomultiplier tube was gated by applying an inverse voltage to its focusing electrode synchronously with the beam deflection voltage so that electrons were counted only during the intervals between neutron bursts [5]). The output pulses from the photomultiplier were amplified and fed into a multichannel pulse height analyzer.

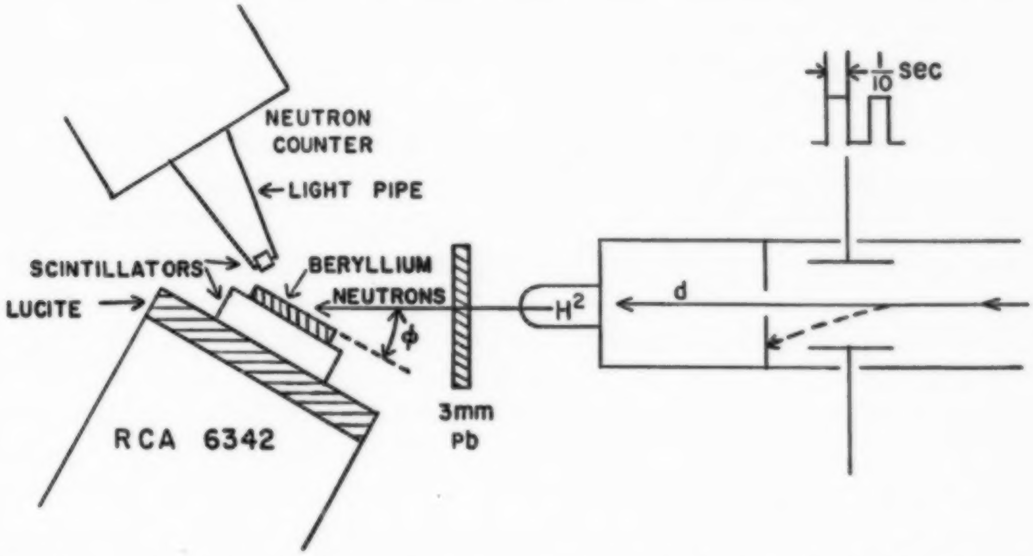

Fig. 1. Experimental arrangement for measurements of the cross section for the reaction $Be^9(n, \alpha)He^6$.

A CsI crystal was chosen for β-counting in preference to an organic scintillator because of its smaller sensitivity for a possible fast neutron background and because of its higher stopping power and heavier constituents, giving the advantage of having less neutron scattering and moderating material near the beryllium sample. On the other hand scattering of electrons out of a scintillator consisting of atoms with comparatively high atomic number was expected to strongly degrade the observed β-spectrum. This was not a serious disadvantage in the relative cross section measurements where a constant, but unknown, fraction of the β-spectrum was counted. In the absolute cross section measurements, however, the total number of electrons had to be obtained by extrapolating the observed β-spectrum and a plastic scintillator was therefore used for the absolute measurements. The lucite lightpipe was interposed between scintillator and photomultiplier in order to prevent electrons from the β-decay of Al^{28}, which was produced by the reaction $Si^{28}(n, p)Al^{28}$ in the glass envelope of the photomultiplier tube, from reaching the scintillator.

The neutron flux was determined by either of two methods. One of them made use of a small (3 mm thick and 3 mm in diameter) plastic scintillator which was mounted on a lucite lightpipe and DuMont 6292 photomultiplier tube and placed near the beryllium sample as shown in fig. 1. Alternatively the number of neutrons incident on the beryllium sample could be calculated from the deuterium pressure in the gas target chamber and the integrated beam charge, using published data of the cross section of the $D(d, n)He^3$ reaction [6]) and taking into account the loss of neutrons (approximately 6 %) due to scattering in the lead absorber. The two methods were checked against each other at various neutron energies and geometries and the agreement was always better than ±10 % on an absolute scale. Relative values of the neutron flux obtained by both methods are believed to be accurate within ±5 %.

The main source of background consisted of activities which were produced by either deuterons or neutrons in materials other than the beryllium disc. Background runs were taken with the beryllium disc removed both before and after each run at approximately the same beam current and the average number of background counts from these two runs was subtracted from the counts obtained with the beryllium sample in place. Fig. 2 shows typical pulse height spectra with and without the beryllium disc at a deuteron bombarding energy of 2.07 MeV corresponding to a neutron energy of 5.31 MeV. These curves show a peak at channel number 55 due to a γ-ray as well as the continuous distribution of the beta particles. The bias at 80, above which the counts were included, is indicated by a vertical line; the bias was chosen such as to keep the relative magnitude of the background low while at the same time using as large as possible a portion of the spectrum. The ratio of background counts to corrected counts varied depending on the bombarding energy, elapsed running time, and bias used. Under actual experimental conditions it was about 5 % at the lowest bombarding energies and increased to about 50 % at the highest bombarding energies.

A second kind of background arose from disintegrations in the beryllium disc by fast background neutrons which were produced by the deuteron beam in the nickel foil and carbon deposits on the nickel foil and the beam defining apertures. This background was determined by evacuating the gas target chamber and then taking runs with and without the beryllium disc in place. It was found to be negligible (less than 1 %) at neutron energies below 6 MeV but increased to about 12 % at a neutron energy of 8 MeV.

Two sets of final data were taken at different times (referred to as first and second run, respectively, in fig. 4), each of which was again subdivided into two sections covering approximate neutron energy regions of 3.9 to 5.9 MeV and 5.2 to 8.6 MeV, respectively. In each case the gas target pressure and the solid angle subtended by the beryllium disc were adjusted such as to obtain as nearly as practical an energy resolution of 200 keV. In practice the spread in neutron energy at the beryllium disc varied between 150 keV and 250 keV. The relative number of beta disintegrations was measured with an estimated accuracy of ±5 %, the uncertainties being due to counting statistics, background fluctuations, and bias shifts. This figure depends somewhat on the

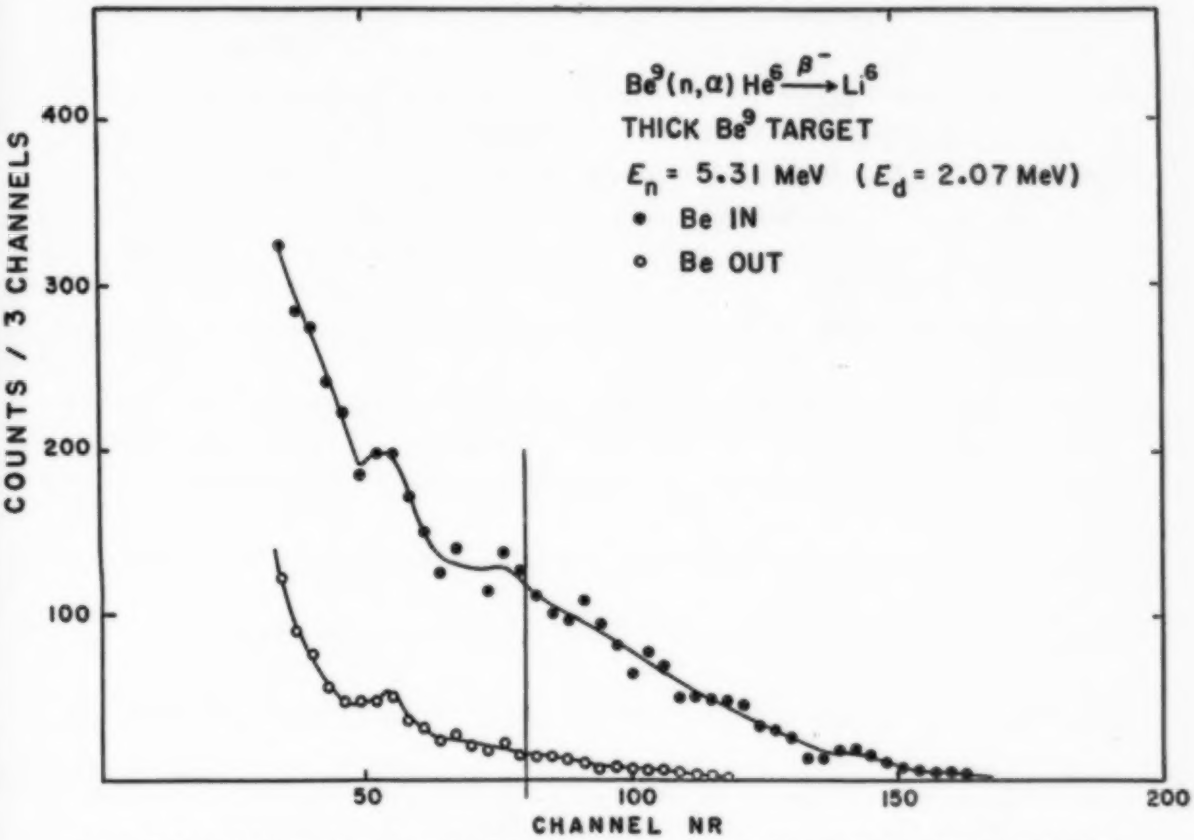

Fig. 2. Pulse height spectrum from the β-decay of He^6 measured with a thick beryllium target and a CsI(Tl) crystal as β-counter at a neutron bombarding energy of 5.31 MeV. The closed circles represent (uncorrected) counts obtained with the beryllium sample in place while the open circles represent background counts obtained with the beryllium sample removed.

relative magnitude of the background and should be understood as an average value. The relative cross section data are believed to be accurate to ±10 %.

3. Absolute Cross Section Measurements

For measurements of the absolute cross section, the CsI(Tl) scintillator was replaced by a plastic scintillator of 2.54 cm diameter and 1.59 cm thickness in order to reduce degradation of the beta spectrum due to electron scattering as discussed in the previous section. In this case the scintillator was covered by a 2.4 mg/cm^2 aluminium foil only. Three beryllium foils with thicknesses of 16.9, 38.6 and 88.6 mg/cm^2, respectively, were used as targets. It was expected that self-absorption of electrons would be negligible (1 %) in the thinnest of these foils, but that improved counting statistics and background ratios could be obtained by taking data with all three foils and extrapolating to zero target thickness. In practice the number of counts was found to be proportional to the total mass of each foil within experimental accuracy; thus it appears that self-absorption was not importnt even for the thickest of the three foils (88.6 mg/cm^2).

In order to avoid attenuation of the incident neutron beam due to scattering in the beryllium foil itself, the scintillator was arranged in such a way that its front face, and thus the plane of the beryllium foil, formed an angle $\phi > 0°$ with the direction of motion of the incident neutrons as shown in fig. 1; in two earlier measurements, where ϕ was equal to zero, a correction for neutron scattering in the beryllium foil was calculated and applied to the data (see table 1). A further correction had to be applied for the effect of neutrons scattered in the scintillator and lightpipe (table 1). This was calculated on the basis of a crude model: single scattering only was considered and both the scattering cross sections and the energy loss of the scattered neutrons were assumed to be isotropic in the laboratory system. The angular distributions were roughly taken into account by using 'effective' values for the scattering cross sections and the mean energy loss depending on the average scattering angle. The 'effective cross sections' were estimated from published data [7,8]). The magnitude of this correction did not exceed 6 % (table 1).

Fig. 3 shows beta spectra obtained with the three thin beryllium foils after background subtraction. The energy scale was calibrated with internal conversion electrons of 0.97 MeV from a Bi^{207} source. All counts in the spectra were included for electrons with energies greater than 0.55 MeV as indicated by a solid vertical line in fig. 3. Below this cutoff energy the shape of the spectra could not be determined due to the sharply rising background; in this region the shape of the spectra has been estimated, somewhat arbitrarily, as shown by the dotted curves. Integration of the areas gives for the ratio of the number of counts above cutoff to the total number of beta disintegrations detected in the scintillator values of 76 %, 78 %, and 80 % for targets I, II, and III, respectively. The uncertainty of these numbers is estimated to be ±5 % in each case. Since the electrons were counted in 2π-geometry and the pulsing period was short compared to the half-life of He^6, the number of He^6 disintegrations in the beryllium foils was obtained from the number of counts in the scintillator multiplied by twice the ratio of running time to counting time.

The absolute cross section measurements are summarized in table 1. The numbers in the first column are given in chronological order. In one of the measurements (No. 4) a tritium gas target was used to obtain neutrons from the reaction $T(p, n)He^3$. It was hoped to take advantage of the lower background of activities produced in this case; however, due to instrumental difficulties counting statistics were comparatively poor so that no improvement in accuracy could be achieved. Measurement No. 5 is considered the most accurate one (±14 %) since in this case good counting statistics and stable background conditions were obtained; stability of the background is important for the cutoff energy of 0.55 MeV since it was comparable in magnitude to the

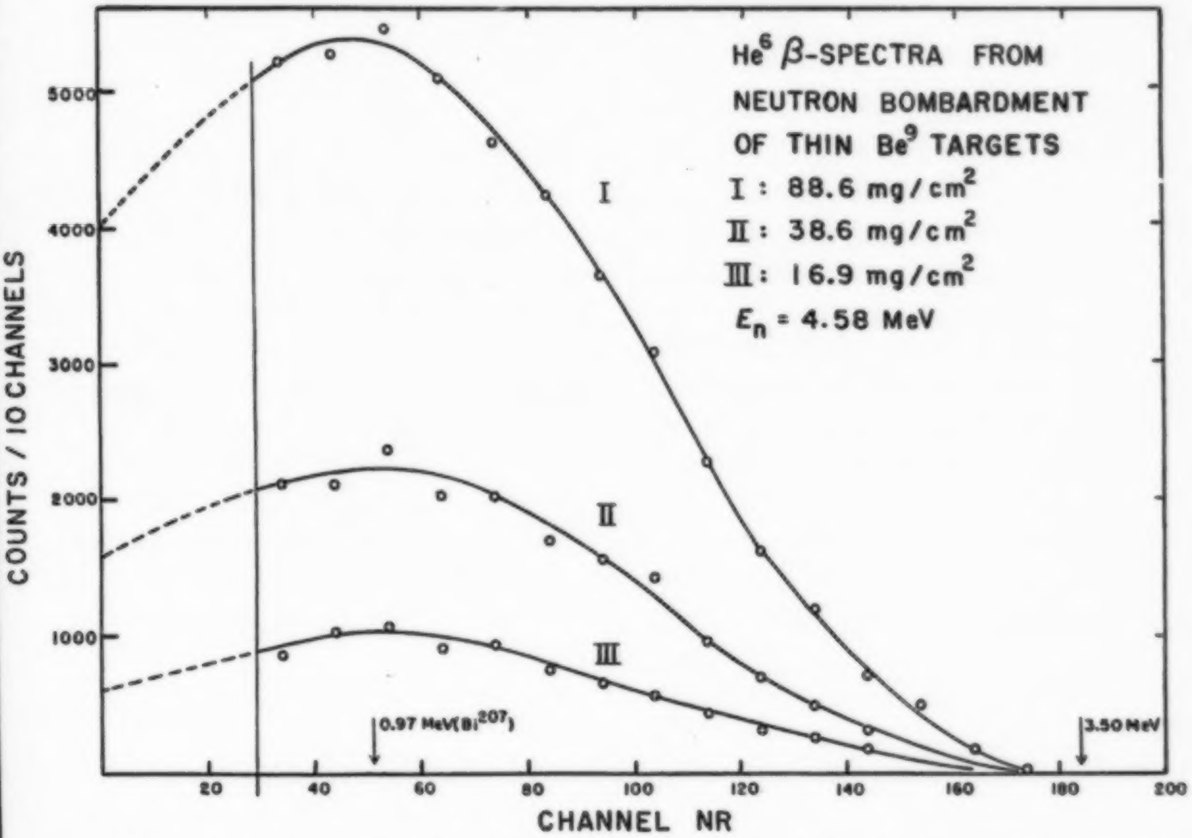

Fig. 3. Pulse height spectra from the β-decay of He^6 measured with three thin beryllium targets and a plastic scintillator as β-counter at a neutron bombarding energy of 4.58 MeV. The background has been subtracted.

Table 1

Summary of information on the measurements of the absolute cross section for the reaction $Be^9(n, \alpha)He^6$

	Source reaction	Neutron energy (MeV)	Neutron energy spread (MeV)	Angle ϕ (fig. 1)	Cross section (uncorrected) (mb)	Correction for neutrons in-scattered by scintillator and lightpipe	Correction for neutrons scattered by Be foil	Cross section (corrected) (mb)
1	D(d, n)	5.82	0.15	0°	45	−2 %	+20 %	53±10
2	D(d, n)	4.79	0.20	0°	56	−2 %	+20 %	66±12
3	D(d, n)	4.58	0.20	30°	75	−4.5 %		72±12
4	T(p, n)	4.06	0.08	30°	97	−4.5 %		93±15
5	D(d, n)	4.58	0.20	45°	79	−6 %		74±10

true counting rate from the thinnest beryllium foil. The error due to counting statistics and background fluctuations was, in this case, within ±1 %; because of the uncertainty in the extrapolation of the beta spectrum below 0.55 MeV (±5 %) the total number of electrons could only be determined to about ±6 % for each foil. Further errors arose from uncertainties in the scattering correction and other geometrical factors (±2 %) and from the neutron flux measurements with the small plastic scintillator (±6 %). The latter is based on published values from the neutron-proton scattering cross section [7]), the mass and composition of the scintillator (Pilot B) and its pulse heigth *versus* energy characteristics which were measured over the relevant energy range. As an additional check the neutron flux was also calculated from gas target data and integrated beam charge, with an estimated accuracy of ±10 %; actual agreement between measured and calculated values of the neutron flux was for all absolute cross section measurements within ±3 %.

4. Results and Discussion

The results are shown in fig. 4. The cross section is seen to decrease from 93 mb at 4.0 MeV to 39 mb at 6.5 MeV, and 32.5 mb at 8.5 MeV. There is no pronounced resonance structure, although the existence of broad resonances near 5 MeV and 8 MeV seems possible. Any narrow resonances having a width much less than 200 keV would, of course, not have been seen in the present experiment. As indicated in fig. 4, the data confirm within experimental accuracy the results of Stelson and Campbell [3]) for neutron energies from 3.9 to 4.4 MeV.

It is interesting to compare the cross section for the $Be^9(n, \alpha)He^6$ reaction with that for competing reactions. In the energy region of interest the following reactions (other than elastic scattering) are energetically possible:

$$Be^9+n \rightarrow Be^{10}+\gamma, \tag{1}$$

$$Be^9+n \rightarrow 2He^4+2n-1.57 \text{ MeV}, \tag{2}$$

$$Be^9+n \rightarrow He^6+\alpha-0.63 \text{ MeV}. \tag{3}$$

Reaction (1) has a very small cross section and shall not be discussed further. Reaction (2) has been studied by a number of observers, most recently by Marion, Levin and Canberg 9)). It can proceed by various mechanisms, namely a) by inelastic scattering of the primary neutron and subsequent decay of the resulting excited state of Be^9 into a neutron and Be^8 or into a neutron and two α particles, b) by direct three- or four-body breakup of the compound system, or c) by the (n, α) reaction going to the first excited state of He^6 at 1.71 MeV and subsequent breakup of this state into two neutrons and an α particle.

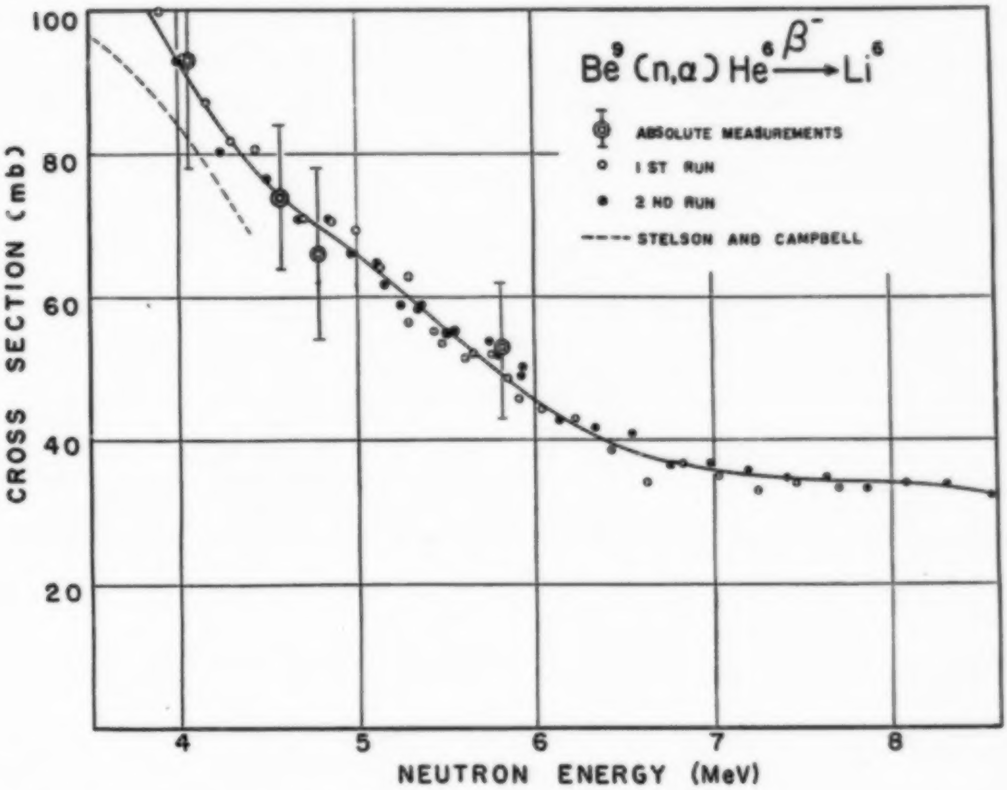

Fig. 4. The cross section for the reaction Be^9(n, α)He^6 as a function of neutron energy. The double circles with error bars are the absolute measurements which are summarized in table 1; single open and closed circles are relative measurements obtained in two separate runs. The energy resolution is approximately 200 keV. The dotted curve gives the results of Stelson and Campbell.

The total nonelastic cross section, comprising contributions from both reactions (2) and (3), remains nearly constant in the neutron energy range from 4.07 to 7.0 MeV with values of 620 mb and 600 mb respectively 10)). The results of Cranberg and Levin show a sharp rise in the (n, 2n) cross section in the region above 2.8 MeV which is attributed to inelastic scattering of the neutrons leaving Be^9 excited to the state at 2.43 MeV which subsequently decays with neutron emission. The threshold for this reaction is 2.70 MeV. The decrease in the cross section for Be^9(n, α)He^6 in the region of 3 to 6 MeV probably is associated with an increase in the formation of He^6 in its first excited state at 1.71 MeV which should be expected to increase rapidly just above 3 MeV; the excited He^6 nucleus then decays by the emission of two neutrons and an α particle. The decrease in the (n, α_0) reaction is probably not due to competition with the inelastic scattering to the 2.43 MeV level in Be^9 since such a decrease would be expected to come at about 2.8 or 2.9 MeV where the (n, 2n) reaction is increasing at the maximum rate. The cross section for reactions going to the 1.71 MeV level in He^6 may be several times larger than that for reactions going to the ground state at neutron energies above 4 MeV. Allen *et al.* [11]) found that in the reaction $Li^7(t, \alpha)He^6$ the cross section leading to the excited state of He^6 at 1.71 MeV was about five times as great as to the ground state. The excitation energy of the compound nucleus (Be^{10}) is about 2 MeV greater in the (t, α) reaction than in the reaction $Be^9(n, \alpha)He^6$ with 8.5 MeV neutrons, but similar results might be expected.

References

1) Allen, Burcham and Wilkinson, Proc. Roy. Soc. A **192** (1947) 114
2) Sattar, Morgan and Hudspeth, Phys. Rev. **100** (1955) 960, and private communication
3) P. H. Stelson and E. C. Campbell, Phys. Rev. **106** (1957) 1252
4) M. E. Battat and F. L. Ribe, Phys. Rev. **89** (1953) 80
5) B. J. Farmer and C. M. Class, Nuclear Physics **15** (1960) 626
6) Jarmie, Seagrave and Argo, Los Alamos Scientific Laboratory Report LA-2014 (1956)
7) D. J. Hughes and J. A. Harvey, Brookhaven National Laboratory Report BNL-325
8) D. J. Hughes and R. S. Carter, Brookhaven National Laboratory Report BNL-400
9) Marion, Levin and Cranberg, Phys. Rev. **114** (1959) 1584; also unpublished results of Cranberg and Levin
10) Beyster, Henkel, Nobles and Kester, Phys. Rev. **98** (1955) 1222;
Beyster, Walt and Salmi, Phys. Rev. **104** (1956) 1319
11) Allen, Almquist, Dewan and Pepper, Phys. Rev. **96** (1954) 684

1.E.1:
3.A:4.E

Nuclear Physics **23** (1961) 131—138;© *North-Holland Publishing Co., Amsterdam*
Not to be reproduced by photoprint or microfilm without written permission from the publisher

PROMETHIUM-148

J. S. ELDRIDGE and W. S. LYON
Oak Ridge National Laboratory[†], *Oak Ridge, Tennessee*

Received 3 November 1960

Abstract: Promethium-148 has been produced by two methods: (1) (n, γ) reaction on Pm-147, (2) (p, n) reaction on enriched Nd-148. In both instances two activities were observed: 5.4d Pm-148 and 41.8d Pm-148. The decay of these isomers has been followed by use of ion-chambers, betacounters, and gamma scintillation spectrometers. Gamma rays of 0.550, 0.910 and 1.460 MeV were found to be associated with the 5.4d isomer with abundances of 0.25, 0.13 and 0.20 respectively. A negaton of 2.5 MeV is associated with the 5.4d isomer with an abundance of approximately 55 %. Gamma rays of 0.085, 0.180, 0.210, 0.290, 0.410, 0.550, 0.630, 0.730, 0.910, 1.01 and 1.46 MeV were found to be associated with the 41.8d isomer with relative abundances of 2, 6, 2, 14, 21, 100, 83, 38, 21, 21 and 2 respectively.

1. Introduction

In addition to the 5.3d Pm-148 first reported by Kurbatov and Pool 1) and subsequently studied by several investigators, a 42d Pm activity has been given a "probable "mass assignment of 148 in the Table of Isotopes 2). Bhattacherjee, Sahai and Baba 3) have recently produced both acitivities by the (p, n) reaction on enriched Nd-148. They reported half-lives of 4.2±0.2d and 45.8±2.9d for the two isomers and proposed decay schemes for them. The present investigation was begun in order to fix the mass assignment for the 42d activity and to further elucidate the properties of Pm-148.

2. Experimental

Promethium-148 was produced by irradiating $Pm_2^{147}O_3$ in the Oak Ridge Research Reactor in quantities up to 0.5 mg in intervals of 2 days to three weeks at fluxes of 6×10^{12} n/cm$^2\cdot$sec. After discharge from the reactor, a portion of the target material was subjected to ion-exchange chromatography with the result that no detectable radioactivity other than promethium was observed. The decay of the target material was followed by the use of ion chambers, beta proportional counters, and scintillation spectrometers.

A second portion of Pm-148 was produced by bombarding 10 mg of electromagnetically enriched[††] $Nd_2^{148}O_3$ with protons for 2 hours at 75 μA in the

---

[†] Operated for the U. S. Atomic Energy Commission by Union Carbide Nuclear Corporation.

[††] Mass Analysis: Nd^{142}—1.6 %, Nd^{143}—0.87 %, Nd^{144}—5.49 %, Nd^{145}—1.05 %, Nd^{146}—3.3 %, Nd^{148}—84.5 %, Nd^{150}—3.1 %.

O.R.N.L. 218 cm cyclotron. The beam energy was adjusted so that the (p, n) reaction predominated. The promethium produced in the target was separated by ion-exchange chromatography. The radiations from the activities produced in both irradiations were studied using the same instruments and techniques.

Gamma ray energies and intensities were determined using a 7.6 cm × 7.6 cm NaI(Tl) spectrometer and 20-channel pulse-height analyzer. The resolution of the spectrometer for 0.662 MeV Cs-137 gamma rays was 7.6 %. Techniques similar to those described by Heath[4]) were used for analyzing the spectra.

Beta energies were determined by absorption techniques using a beta proportional counter, and in some experiments, by use of β—γ coincidence measurements in which coincident events were observed as a function of aluminium absorber thickness placed before the beta detector. Some γ—γ coincidence measurements were made using two 7.6 cm × 7.6 cm NaI(Tl) spectrometers and single-channel analyzers. In all spectrometric determinations, sufficient beryllium absorber was present to stop beta particles.

3. Results

Half-lives: The reactor-produced material showed the presence of two components in addition to the Pm-147 target activity. These two components had half-lives of 5.4 ± 0.1 days and 41.8 ± 0.2 days based on decay measurements made on several instruments. The decay was followed for 250 days. The cyclotron-produced material showed the same two components; but a contaminant having gamma rays of approximately 0.48, 0.63 and 0.70 MeV was also observed. This contaminant is probably 300d Pm-144[5]). Decay data from observations with γ-sensitive instruments showed a higher ratio of the 42d isomer to the 5.4d isomer than did data from observations with β^- sensitive detectors. This can be accounted for by the strong beta group of 2.5 MeV in the 5.4d isomer which goes directly to the ground state of Sm-148.

Gamma rays and intensities: Fig. 1a shows the gamma-ray spectrum associated with the 42d isomer. Fig. 1b shows the spectrum of the same isomer on an expanded scale to indicate more detail in the low energy region. Fig. 2 shows the gamma-ray spectrum associated with the 5.4d isomer. This is a net spectrum obtained by subtracting the contribution due to the 42d isomer from the gross spectrum. By use of techniques similar to those described by Heath[4]), the gamma energies and intensities associated with the major transitions in the 5.4d isomer were determined and are shown in table 1. The gamma/beta branching was obtained by determining the absolute disintegration rate of a sample of the 5.4d isomer using $4\pi\beta-\gamma$ coincidence and $4\pi\beta$ determinations on the cyclotron-produced material. Appropriate corrections were made for the presence of longer-lived components in these samples. Gamma energies and relative intensities only were measured for the 42d isomer. These results are shown in table 2.

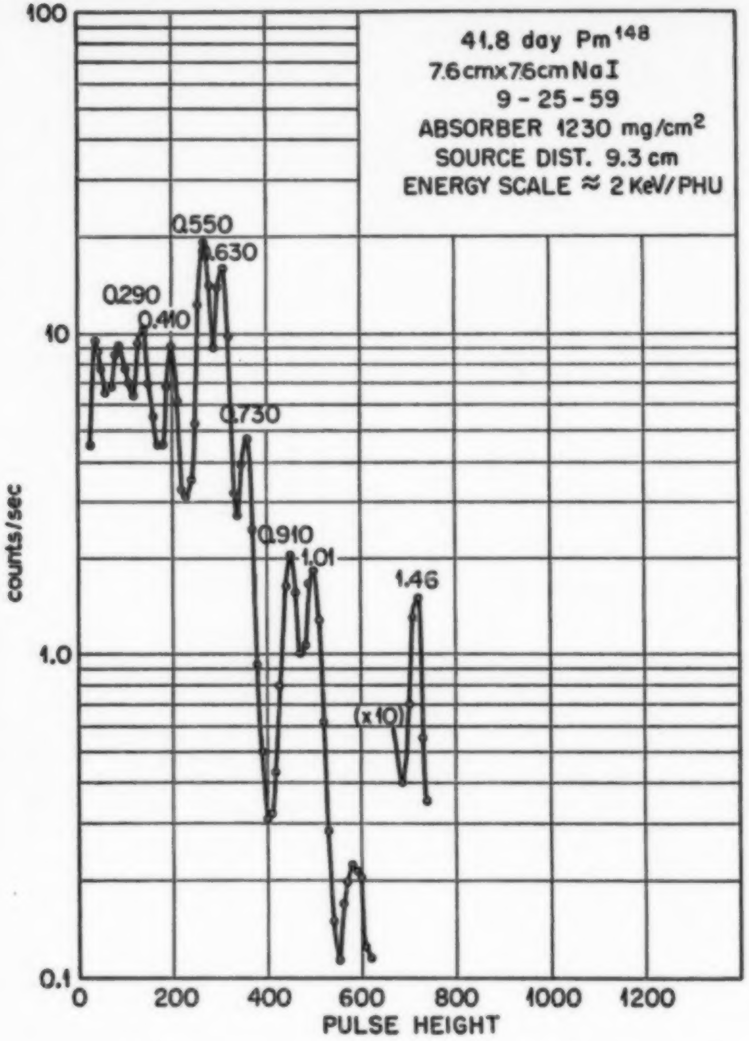

Fig. 1a. Gamma ray spectrum of the 42d isomer.

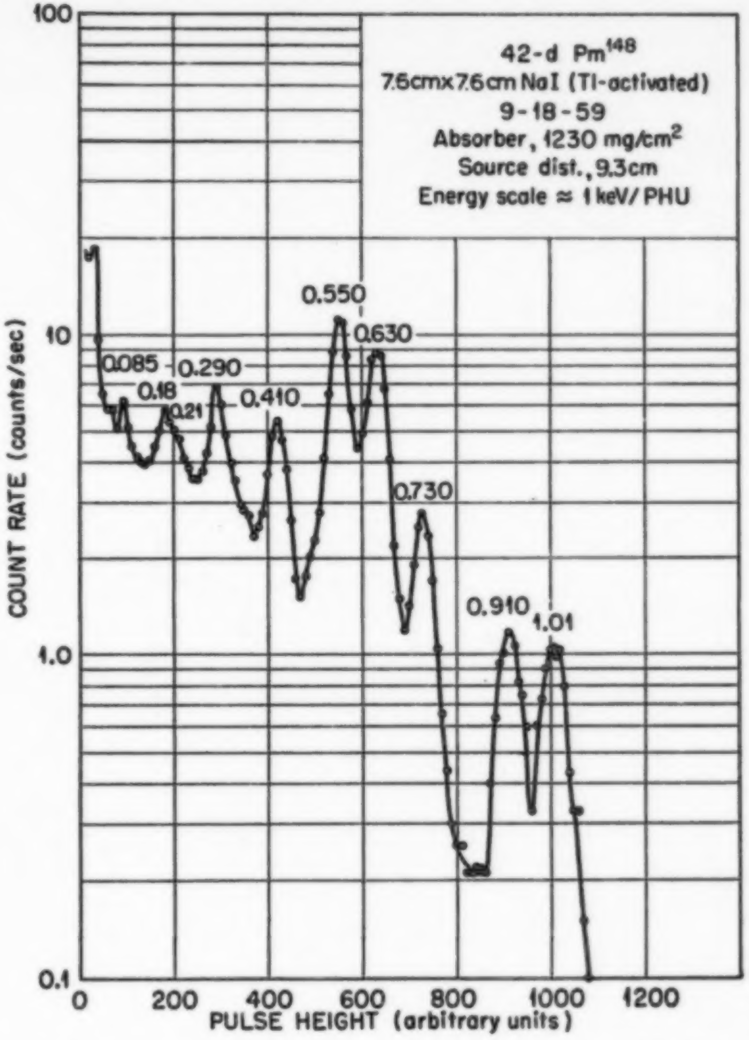

Fig. 1b. Gamma ray spectrum of the 42d isomer (expanded scale).

Beta energy determinations: Precise measurements of beta energies were difficult because of the complexities of the decay schemes. Beta-gamma coincidence measurements were made in an effort to determine the energy of the beta groups in coincidence with each of the various gamma rays. However, this task was made difficult by the presence of several gamma rays with closely

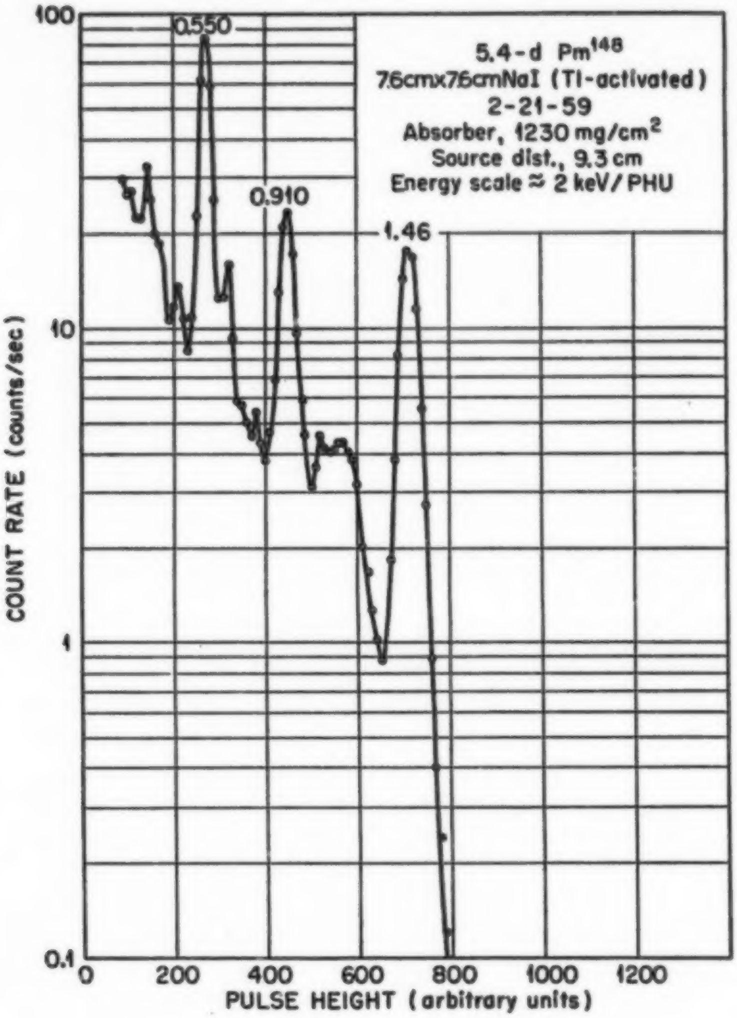

Fig. 2. Gamma ray spectrum of the 5.4d isomer.

TABLE 1

Gamma ray energies and intensities of 5.4d Pm-148

Energy (MeV)	Relative intensity	γ/β
0.550	100	0.25
0.910	50	0.13
1.460	79	0.20

similar energies, and the fact that in the case of the short-lived isomer, beta and gamma rays from the longer-lived component were present. A further difficulty was poor counting statistics caused by the low abundance of some of the transitions.

TABLE 2

Gamma ray energies and intensities of 41.8d Pm-148

Energy (MeV)	Relative intensity
0.085	2
0.180	6
0.210	2
0.290	14
0.410	21
0.550	100
0.630	83
0.730	38
0.910	21
1.010	21
1.460	2

In the coincidence measurements, the source was placed between an end window beta-proportional counter and a 7.6 cm × 7.6 cm NaI(Tl) gamma-ray spectrometer equipped with a single-channel analyzer. The γ-ray spectrometer was adjusted to accept γ-rays of a given energy, and the β—γ coincidences measured as a function of aluminium absorber thickness placed before the β detector. In this way, the half-thickness and hence the approximate energy of the β particles in coincidence with each measured γ ray were obtained. With these measurements, it was found that there was a 1.0 MeV β in coincidence with the 0.55, 0.91 and 1.46 MeV γ rays when both isomers were present. In addition, $\approx$ 0.5 and $\approx$ 1.5 MeV particles were found to be associated with the 0.55 MeV γ with both isomers present. With only the 42d isomer present, beta groups of 0.6—0.7 MeV and 0.2—0.4 MeV were found to be in coincidence with the 0.55, 0.63, 0.73, 0.91 and 1.0 MeV gamma rays. In addition, a 0.6 MeV beta group was found to be in coincidence with the 0.41 MeV gamma ray.

Gross beta absorption measurements were made with both the 5.4 and 41.8d isomers present. The maximum beta energy found was 2.52 MeV (81 % of beta disintegrations at that time). The absorption data indicated an additional beta of apparent energy 0.5 MeV. With only the 41.8d isomer present gross absorption measurements as above indicated a 2.30 MeV beta group, a group of apparent energy 0.9 MeV, and other beta groups of apparent energy 0.2—0.4 MeV. On the basis of other work (fig. 4) the apparent beta group of 0.9 MeV is believed to be the unresolved mixture of 1.78, 1.15 and 0.74 MeV beta groups.

Gamma-gamma coincidence determinations gave results similar to those of Bhattacherjee [3]).

The 1.2 MeV γ of the 42d isomer reported by Bhattacherjee [3]) was not seen in spectra made at 9.3 cm to the extent they reported. An experiment was performed to determine the amount of coincident summing giving rise to this gamma ray. The spectrum was determined at 3.0 cm and compared to that at 9.3 cm. The ratio of the 1.18 MeV peak relative to other gammas at 3.0 cm was very much greater than that at 9.3 cm. The "sum" peak was calculated for coincident summing of 0.55 and 0.63 MeV γ's and found to account for approximately 80 % of the observed 1.18 MeV peak with poor counting statistics. We conclude that there are few, if any, 1.18 MeV γ rays in the decay of this isomer.

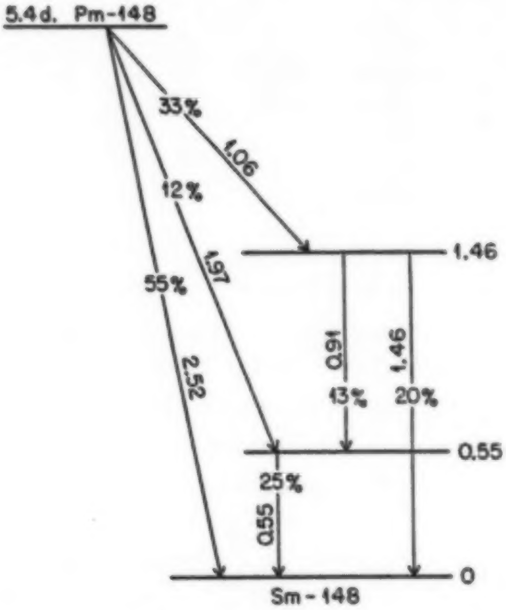

Fig. 3. Proposed decay scheme for the 5.4d isomer.

A similar experiment showed the absence of the 1.76 MeV gamma listed as "uncertain" by Bhattacherjee [3]). Gamma spectrometric measurements made by Bhattacherjee [3]) were at a source-crystal distance of 2.5 cm.

Discussion: Previous workers [3,6,7]) have reported the existence of a 42 d promethium isotope, but it had been produced only by the high energy fission of uranium or by proton bombardment of neodymium. This 42d activity has been produced along with the previously assigned 5.3d Pm-148 from two independent reactions: $\mathrm{Pm}^{147}(\mathrm{n}, \gamma)\mathrm{Pm}^{148}$ and $\mathrm{Nd}^{148}(\mathrm{p}, \mathrm{n})\mathrm{Pm}^{148}$. These experiments settle the mass assignment for this 42d isomer.

The observed 2.52 MeV beta group associated with the 5.4d isomer was seen to be present to a considerable fraction of the decays for this isomer. The 1.9 MeV beta group reported by Bhattacherjee [3]) could not be resolved by us in the presence of the large amount of 2.52 MeV betas. The presence of a 1.0 MeV beta group in coincidence with the 0.55, 0.91 and 1.46 MeV γ rays was found in the beta-gamma coincidence determinations. By use of the γ/β branchings from table 1 and the information concerning the beta transitions as discussed above, the decay scheme for the 5.4d isomer is proposed in fig. 3. The sum of the 2.52 and 1.96 MeV beta branchings is 67 % in the proposed decay scheme. This is in fair agreement with the observed 81 % of hard betas in the gross absorption determination of beta energies when both isomers were present.

Bhattacherjee 3) reported the sum of the 0.56 and 0.90 MeV gamma intensities to be equal to that of the 1.46 MeV gamma in the 5.4d isomer. He has revised his intensity values for the 0.56, 0.90 and 1.46 MeV gamma rays to be 75, 60 and 100 respectively, because the original determinations were made by comparing all gamma intensities with that of the 0.64 MeV gamma in the 42d isomer which was later found to contain a long-lived contaminant 8).

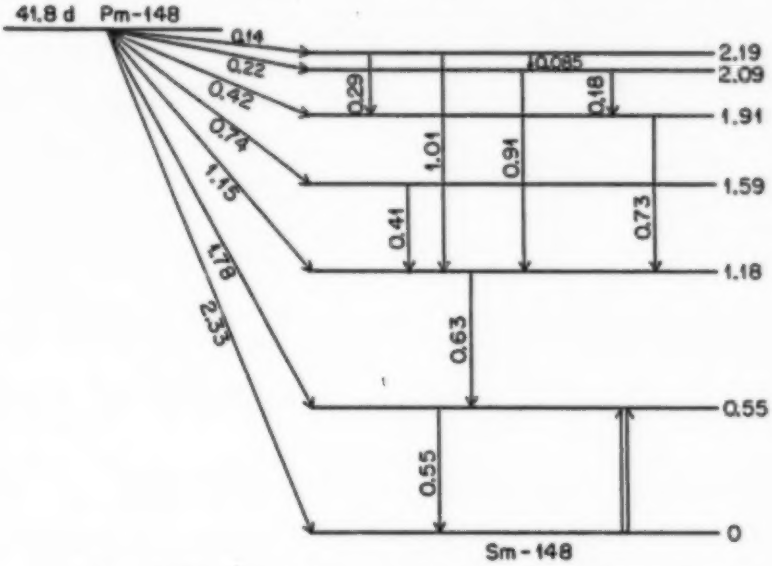

Fig. 4. Proposed decay scheme for the 42d isomer.

No accurate estimation of the abundance of 2.3 MeV betas in the 42d component could be made in the present investigation. However, qualitative results indicate a relatively low (5—10 %) branching for it. Folger and Stevenson 6) assigned a branching of approximately 5—10 % to the 2.3 MeV beta group and Fischer 7) assigned a value of 7.4 % to this branching. Bhattacherjee 3) estimated this transition probability to be 20 %. He reported the 0.56 and 0.63 MeV gammas to have the same relative intensities with no beta groups terminating at the 0.56 MeV level in the 42d isomer. The relative intensities of the 0.55 and 0.63 MeV gammas in the present investigation are 100 and 83 respectively. This would indicate that there is a possibility of a beta group of ≈ 1.8 MeV feeding the 0.55 MeV level. This would account for the "non-linearity of the high energy component in the Kurie plots" as stated by Bhattacherjee 3).

The differences observed in the decay of the 42d isomer have been incorporated in the tentative decay scheme proposed by Bhattacherjee [3]) and shown in fig. 4. The changes we have made in fig. 4 are the addition of the 1780 keV group feeding the 550 keV level and in the removal of the uncertain level at 1760 keV.

References

1) J. D. Kurbatov and M. L. Pool, Phys. Rev. **63** (1943) 463
2) K. Strominger, J. M. Hollander and G. T. Seaborg, Revs. Mod. Phys. **30** (1958) 585
3) S. K. Bhattacherjee, B. Sahai and C. V. K. Baba, Nuclear Physics **12** (1959) 356
4) R. L. Heath, U.S.A.E.C. Report IDO-16408 (July, 1957) (unpublished)
5) S. Ofer, Phys. Rev. **113** (1959) 895
6) R. L. Folger, P. C. Stevenson and G. T. Seaborg, U.S.A.E.C. Report UCRL-1195, revised (May, 1951) (unpublished)
7) V. K. Fischer, U.S.A.E.C. Report UCRL-1629 (Jan. 1952) (unpublished); Phys. Rev. **87** (1952) 859
8) S. K. Bhattacherjee, private communication

8.C

Nuclear Physics **23** (1961) 139—143; © *North-Holland Publishing Co., Amsterdam*

Not to be reproduced by photoprint or microfilm without written permission from the publisher

ON THE "NEW TAMM-DANCOFF" APPROXIMATION TREATMENT OF THE SUPERCONDUCTIVITY HAMILTONIAN

KAZUO YAMAZAKI †

Max-Planck-Institut für Physik und Astrophysik, München, Germany

Received 15 August 1960

Abstract: We apply the "new Tamm-Dancoff" approximation method in the same form as used in Heisenberg's theory of elementary particles to Bardeen's reduced Hamiltonian for the theory of superconductivity. In the limit of infinite volume we obtain exactly the same energy gap as found by Bardeen and Bogoliubov.

In Heisenberg's nonlinear spinor theory of elementary particles [1]), we always use the so called "new Tamm-Dancoff" (abbreviated in the following as N. T. D.) approximation because this is as yet the only available approximation method in this theory. On the other hand the validity of this approximation is very difficult to examine, and until now the only support to this approximation is the case of the anharmonic oscillator treated by Heisenberg [2]). But in such a simple one-dimensional model even a rather rough approximation method can give a rather good numerical value and thus the above example of the anharmonic oscillator is not a strong support for this approximation in quantum field theory. Thus in Heisenberg's theory of elementary particles the approximation method is a weak point for the theory and the numerical values obtained by this approximation are always subject to some doubt.

On the other hand, in the theory of superconductivity the original Bardeen-Cooper-Schrieffer [3]) Hamiltonian can be treated in a very good approximation by the simple Hartree-Fock self-consistent method combined with the so called Bogoliubov [4]) canonical transformation. And here we have an explicit approximate solution, which is rather exact. Recently [5]) Bogoliubov was able to show that in the case of infinite volume the lowest energy eigenvalue is the exact one for this Hamiltonian.

Even though the coupling constant in this model is very small, the interaction can be very strong near the Fermi-surface. Thus the energy gap found by these authors cannot be obtained by perturbation theory, because the energy gap has the form $\exp(-1/JN)$ (J is the coupling constant). And there exists also a curious situation if we use the Bethe-Salpeter approximation [6]). If we use the simple ladder approximation then the so obtained Bethe-Salpeter equation can be exactly solved and this solution shows no energy gap. If we further approximate and use perturbation theory for this Bethe-Salpeter equation, then we get the correct energy gap as found by Bardeen and Bogoliubov. Thus the problem is a good test of the approximation method.

---

† On leave of absence from the Research Institute for Fundamental Physics, Kyoto University, Kyoto, Japan.

In this note we apply the N. T. D. approximation in the same form as used in Heisenberg's theory, to this Hamiltonian, and we derive in the limit of infinite volume the same energy gap as obtained by Bardeen and Bogoliubov. This is a rather nice support for the N. T. D. approximation to Heisenberg's theory because both theories have a similar structure, i.e. a nonlinear (quartic) spinor interaction. The analogy, especially that between the existence of the energy gap (in the theory of superconductivity) and the mass of the nucleon (in the theory of elementary particles) in connection with the breakdown of gauge and γ_5 invariance respectively was stressed by Nambu [7]). If the analogy has any physical sense this means that the vacuum is no longer isobaric spin invariant and it is really infinitely degenerate and may offer some clue to the understanding of the infinite isobaric spin degeneracy of the vacuum in Heisenberg's theory.

Let us start our discussion with the "reduced" Hamiltonian of Bardeen *et al.* [3])

$$\begin{aligned} H &= H_0+H_1, \\ H_0 &= \sum_k \mathscr{E}_k(a^*_{k\uparrow}a_{k\uparrow}+a^*_{-k\downarrow}a_{-k\downarrow}), \quad H_1 = -\frac{1}{\Omega}\sum_{k,k'} J_{kk'}a^*_{k\uparrow}a^*_{-k\downarrow}a_{-k'\downarrow}a_{k'\uparrow}. \end{aligned} \tag{1}$$

Here $\mathscr{E}_k$ means kinetic energy minus chemical potential. The commutation relations are as usual:

$$\{a_{k\uparrow}, a^*_{k'\uparrow}\}_+ = \{a_{-k\downarrow}, a^*_{-k'\downarrow}\}_+ = \delta_{kk'}, \tag{2}$$

and other anticommutators are all zero.

We first remark that there exist three conserved quantities for this system, namely the total momentum, the z-component of the total spin and the particle number,

$$\begin{aligned} \mathbf{p} &= \sum_k \mathbf{k}(a^*_{k\uparrow}a_{k\uparrow}-a^*_{-k\downarrow}a_{-k\downarrow}), \\ S_z &= \tfrac{1}{2}\sum_k (a^*_{k\uparrow}a_{k\uparrow}-a^*_{-k\downarrow}a_{-k\downarrow}), \\ N &= \sum_k (a^*_{k\uparrow}a_{k\uparrow}+a^*_{-k\downarrow}a_{-k\downarrow}). \end{aligned} \tag{3}$$

They all commute with the total Hamiltonian H. Hence the exact eigenstate of H can be the simultaneous eigenstate of these operators. Let $|0\rangle$ and $|\pm k\rangle$ be the exact vacuum and one-particle eigenstates of the total Hamiltonian with the eigenvalues E_0 and $E_0+E_{\pm k}$, total momentum 0 and $\pm\mathbf{k}$, Z-component of total spin 0 and $\pm\frac{1}{2}$ respectively †; we have

$$\begin{aligned} H|0\rangle &= E_0|0\rangle, & \mathbf{p}|0\rangle &= 0, & S_z|0\rangle &= 0, \\ H|k\rangle &= (E_0+E_{+k})|k\rangle, & \mathbf{p}|k\rangle &= +\mathbf{k}|k\rangle, & S_z|k\rangle &= +\tfrac{1}{2}|k\rangle, \\ H|-k\rangle &= (E_0+E_{-k})|-k\rangle, & \mathbf{p}|-k\rangle &= -\mathbf{k}|-k\rangle, & S_z|-k\rangle &= -\tfrac{1}{2}|-k\rangle. \end{aligned} \tag{4}$$

We get

$$E_{+k}\langle k|a^*_{k\uparrow}|0\rangle = \langle k|[H, a^*_{k\uparrow}]|0\rangle,$$

and because of

$$[H_0, a^*_{k\uparrow}] = \mathscr{E}_k a^*_{k\uparrow}, \quad [H_1, a^*_{k\uparrow}] = -\frac{1}{\Omega}\sum_{k'} J_{kk'} a^*_{k'\uparrow}\, a^*_{-k'\downarrow}\, a_{-k\downarrow},$$

we have

$$(E_{+k}-\mathscr{E}_k)\langle k|a^*_{k\uparrow}|0\rangle = -\frac{1}{\Omega}\langle k|\sum_{k'} J_{kk'} a^*_{k'\uparrow}\, a^*_{-k'\downarrow}\, a_{-k\downarrow}|0\rangle. \tag{5a}$$

Similarly we have

$$(E_{+k}+\mathscr{E}_k)\langle k|a_{-k\downarrow}|0\rangle = -\frac{1}{\Omega}\langle k|\sum_{k'} J_{kk'} a^*_{k\uparrow}\, a_{-k'\downarrow}\, a_{k'\uparrow}|0\rangle, \tag{5b}$$

$$(E_{-k}-\mathscr{E}_k)\langle -k|a^*_{-k\downarrow}|0\rangle = +\frac{1}{\Omega}\langle -k|\sum_{k'} J_{kk'} a^*_{k'\uparrow}\, a^*_{-k'\downarrow}\, a_{k\uparrow}|0\rangle, \tag{5c}$$

$$(E_{-k}+\mathscr{E}_k)\langle -k|a_{k\uparrow}|0\rangle = +\frac{1}{\Omega}\langle -k|\sum_{k'} J_{kk'} a^*_{-k\downarrow}\, a_{-k'\downarrow}\, a_{k'\uparrow}|0\rangle. \tag{5d}$$

These are still exact equations.

From the conservation of momentum and spin it can easily be shown that

$$\begin{aligned} &\langle k|a_{k\uparrow}|0\rangle = \langle k|a^*_{-k\downarrow}|0\rangle = \langle -k|a_{-k\downarrow}|0\rangle = \langle -k|a^*_{k\uparrow}|0\rangle = 0, \\ &\langle 0|a^*_{k'\uparrow}\, a_{-k\downarrow}|0\rangle = \langle 0|a^*_{-k'\downarrow}\, a_{k\uparrow}|0\rangle = 0. \end{aligned} \tag{6}$$

We now solve eq. (5) by the N. T. D. approximation, namely

$$\begin{aligned} \langle k|a^*_{k'\uparrow}\, a^*_{-k'\downarrow}\, a_{-k\downarrow}|0\rangle = \langle k|:a^*_{k'\uparrow}\, a^*_{-k'\downarrow}\, a_{-k\downarrow}:|0\rangle + \langle a^*_{k'\uparrow}\, a^*_{-k'\downarrow}\rangle_0 \langle k|a_{-k\downarrow}|0\rangle \\ + \langle a^*_{-k'\downarrow}\, a_{-k\downarrow}\rangle_0 \langle k|a^*_{k'\uparrow}|0\rangle - \langle a^*_{k'\uparrow}\, a_{-k\downarrow}\rangle_0 \langle k|a^*_{-k'\downarrow}|0\rangle, \end{aligned} \tag{7}$$

where $\langle AB\rangle_0 = \langle 0|AB|0\rangle$. The fourth term on the right hand side of (7) vanishes by virtue of eq. (6). Eq. (7) is the definition of $:a^*_{k'\uparrow}\, a^*_{-k'\downarrow}\, a_{-k\downarrow}:$, and the N. T. D. approximation consists in dropping this term. Thus

$$\frac{1}{\Omega}\sum_{k'} J_{kk'}\langle k|a^*_{k'\uparrow}\, a^*_{-k'\downarrow}\, a_{-k\downarrow}|0\rangle = C_k e^{i\varphi}\langle k|a_{-k\downarrow}|0\rangle + \Delta_{-k}\langle k|a^*_{k\uparrow}|0\rangle, \tag{8a}$$

---

† We do not assume that the vacuum and one particle states are the eigenstate of the operator N, because these states may be degenerate with respect to the particle number, as remarked above.

where we have put

$$\begin{aligned} C_k e^{i\varphi} &\equiv \frac{1}{\Omega}\sum_{k'} J_{kk'}\langle a^*_{k'\uparrow}\, a^*_{-k'\downarrow}\rangle_0 \quad (C_k \text{ real}),\\ \Delta_{+k} &\equiv \frac{1}{\Omega} J_{kk}\langle a^*_{k\uparrow}\, a_{k\uparrow}\rangle_0, \quad \Delta_{-k} \equiv \frac{1}{\Omega} J_{kk}\langle a^*_{-k\downarrow}\, a_{-k\downarrow}\rangle_0, \end{aligned} \tag{9}$$

and have also used momentum conservation. It should be noted that C_k is independent of the volume, whereas $\Delta_{\pm k}$ is inversely proportional to the volume so that the latter vanish in the limit of infinite volume. From (5a) and (8a) we get

$$(E_{+k}-\mathscr{E}_k)\langle k|a^*_{k\uparrow}|0\rangle \quad = -C_k e^{i\varphi}\langle k|a_{-k\downarrow}|0\rangle. \tag{10a}$$

Similarly from (5b), (5c) and (5d) we get

$$(E_{+k}+\mathscr{E}_k)\langle k|a_{-k\downarrow}|0\rangle \quad = -C_k e^{-i\varphi}\langle k|a^*_{k\uparrow}|0\rangle, \tag{10b}$$

$$(E_{-k}-\mathscr{E}_k)\langle -k|a^*_{-k\downarrow}|0\rangle = +C_k e^{i\varphi}\langle -k|a_{k\uparrow}|0\rangle, \tag{10c}$$

$$(E_{-k}+\mathscr{E}_k)\langle -k|a_{k\uparrow}|0\rangle = +C_k e^{-i\varphi}\langle -k|a^*_{-k\downarrow}|0\rangle. \tag{10d}$$

From these we first see that

$$E_{+k} = E_{-k} \equiv E_k, \tag{11}$$

as it should be from the symmetry of original Hamiltonian with respect to the momentum and spin directions.

Let us now put

$$\begin{aligned} \langle k|a^*_{k\uparrow}|0\rangle \quad &\equiv u_{+k}, \quad & \langle k|a_{-k\downarrow}|0\rangle \quad &\equiv v_{+k}e^{-i\varphi}\\ \langle -k|a^*_{-k\downarrow}|0\rangle &\equiv u_{-k}, \quad & \langle -k|a_{k\uparrow}|0\rangle &\equiv v_{-k}e^{-i\varphi}. \end{aligned} \quad (u, v \text{ real}) \tag{12}$$

From (10), (11) and (12) we can easily see that $u_{+k} = u_{-k} \equiv u_k$, $v_{+k} = -v_{-k} \equiv v_k$ or $u_{+k} = -u_{-k}$, $v_{+k} = +v_{-k}$ and both are substantially equivalent. We take the first set. Thus finally (10) becomes

$$(E_k-\mathscr{E}_k)u_k = -C_k v_k, \quad (E_k+\mathscr{E}_k)v_k = -C_k u_k. \tag{13}$$

On the other hand, we find that eq. (9) now reads

$$\begin{aligned} C_k &= \frac{1}{\Omega}\sum_{k'} J_{kk'}\langle 0|a^*_{k'\uparrow}\, a^*_{-k'\downarrow}|0\rangle e^{-i\varphi}\\ &= \frac{1}{\Omega}\sum_{k'} J_{kk'}\{\langle 0|a^*_{k'\uparrow}|k'\rangle\langle k'|a^*_{-k'\downarrow}|0\rangle + \langle 0|a^*_{k'\uparrow}|-k'\rangle\langle -k'|a^*_{-k'\downarrow}|0\rangle\}e^{-i\varphi}\\ &= -\frac{1}{\Omega}\sum_{k'} J_{kk'}u_{k'}v_{k'}, \end{aligned} \tag{14}$$

where we have used the approximation in which the contributions only through $|k\rangle$ and $|-k\rangle$ are retained, and have also used the eqs. (6) and (12). This approximation is also used in the N. T. D. treatment of the anharmonic oscillator by Heisenberg, and the corresponding procedure is used in the elementary particle theory, where the propagator is approximated by the one-nucleon propagator. Thus our approximation is exactly the same one as used in those cases.

Next from the anticommutation relation (2) we find

$$\begin{aligned} 1 &= \langle 0|a^*_{k\uparrow}\,a_{k\uparrow}+a_{k\uparrow}\,a^*_{k\uparrow}|0\rangle \\ &= \langle 0|a^*_{k\uparrow}|-k\rangle\langle -k|a_{k\uparrow}|0\rangle+\langle 0|a_{k\uparrow}|k\rangle\langle k|a^*_{k\uparrow}|0\rangle \\ &= v_k{}^2+u_k{}^2, \end{aligned} \tag{15}$$

where the argument is the same as that used above in deriving (14). It is now quite easy to solve (13), (14) and (15) explicitly. The solutions are

$$\begin{aligned} &E_k=\sqrt{\mathcal{E}_k{}^2+C_k{}^2}, \quad C_k=\frac{1}{2\Omega}\sum_{k'}J_{kk'}\frac{C_{k'}}{\sqrt{\mathcal{E}^2_{k'}+C^2_{k'}}} \\ &u_k{}^2=\tfrac{1}{2}\left(1+\frac{\mathcal{E}_k}{\sqrt{\mathcal{E}_k{}^2+C_k{}^2}}\right), \quad v_k{}^2=\tfrac{1}{2}\left(1-\frac{\mathcal{E}_k}{\sqrt{\mathcal{E}_k{}^2+C_k{}^2}}\right). \end{aligned} \tag{16}$$

Eqs. (16) are exactly the same as those obtained by Bardeen and Bogoliubov and the energy gap is given by the non trivial solution $C_k(\neq 0)$.

Our conclusion is that in the limit of infinite volume we also obtain the superconducting state, starting from Bardeen's reduced Hamiltonian by applying the N. T. D. approximation, and the results agree exactly with those obtained by Bardeen and Bogoliubov.

The author would like to express his sincere thanks to Professor W. Heisenberg for suggesting this problem and for his constant encouragement, and to Mr. K. Sekine for his useful comments.

References

1) H. P. Dürr *et al.*, Zs. Naturf. **14a** (1959) 441
2) W. Heisenberg, Nachr. d. Gött. Akad. d. Wiss. (1953) p. 111
3) J. Bardeen, L. N. Cooper and J. R. Schrieffer, Phys. Rev. **108** (1957) 1175
4) N. N. Bogoliubov, V. V. Tolmachev and D. V. Schirkov, A New Method in the Theory of Superconductivity (Consultants Bureau, New York, 1959)
5) N. N. Bogoliubov, Report at the Utrecht Conference on the Many Body problem, June 1960
6) R. Prange, preprint (1959);
W. Wild, Zs. f. Phys. **158** (1960) 322
7) Y. Nambu, Phys. Rev. Letters **4** (1960) 380;
Y. Nambu and J. Lasinio, Phys. Rev., to be published

2.I

Nuclear Physics **23** (1961) 144—152; © *North-Holland Publishing Co., Amsterdam*

Not to be reproduced by photoprint or microfilm without written permission from the publisher

ANGULAR DISTRIBUTIONS OF FAST PHOTONEUTRONS

FRANCA TAGLIABUE and J. GOLDEMBERG

Departamento de Física, Faculdade de Filosofia, Ciências e Letras, Universidade de São Paulo, São Paulo, Brazil

Received 20 September 1960

Abstract: The angular distribution of photoneutrons from thirteen elements has been measured with the $Si^{28}(n, p)Al^{28}$ threshold detector which is primarily sensitive to neutrons with more than 6 MeV. The angular distributions observed do not, within the errors, show a definite maximum at 90° as expected by dipole absorption of the photons, except for Bi, Pb and Au. For Bi and Pb the experimental results are consistent with calculations made using Wilkinson's model.

1. Introduction

It is well known that the energy spectrum of photoneutrons in the low energy region (up to $\approx$ 4 MeV) can be fitted by a curve calculated from the evaporation theory. However, a group of high energy neutrons is observed; it is called the fast component group and refers to neutrons of energy $\gtrsim$ 4 or 5 MeV. According to the evaporation theory [1]) neutrons are "boiled off" from an excited nucleus; as a result, their angular distribution is expected to be isotropic. On the other hand assuming that the photonuclear process is a "direct photoelectric effect", Courant [2]) predicts an anisotropic angular distribution with a maximum at 90° for the neutrons or protons. The angular distribution of the emitted particles should then furnish clues to the mechanism of the photonuclear process.

There are several investigations on the angular distributions of photoneutrons. An extensive bibliography is given by De Sabbata [3]).

The different experiments are difficult to compare and one finds some discrepancies among the authors. Poss [4]) used a 20-MeV bremsstrahlung beam and measured the ratio of fast neutrons (> 4 MeV) emitted at 90° and 0° from Pb, Bi and W and found $N_{90°}/N_{0°} = 2.0 \pm 0.5$; no significant differences for the different targets were noticed within the limits of error. Price and Kerst [5]), with a 19.7-MeV bremsstrahlung beam, found no asymmetry for Fe and Pb, measuring the total neutron flux with a rhodium detector. Demos *et al.* [6]), with a X-ray spectrum of maximum energy 16 MeV, detected the neutrons from Pb with the P^{31} (n, p) Si^{31} threshold detector (effective threshold $\approx$ 3 MeV) and obtained $N_{90°}/N_{0°} = 0.34 \pm 0.07$. Price [7]) measured the angular distribution of photoneutrons from 22-MeV bremsstrahlung in Pb, Bi, Au, Pr, Ag, Nb, Cu and

V. The $Al^{27}(n, p)Mg^{27}$ and $Si^{28}(n, p)Al^{28}$ reactions have been used as threshold detectors. (These reactions are primarily sensitive to neutrons with more than 4 MeV and 6 MeV respectively). The angular distributions observed have a maximum at 90° to the γ-ray beam. He obtained values of $N_{90°}/N_{0°}$ between 0 and 1 (increasing with atomic number). Ferrero *et al.* [8]) did the same experiment in Bi with almost the same maximum bremsstrahlung energy; they obtained $N_{90°}/N_{0°} = 0.9 \pm 0.1$.

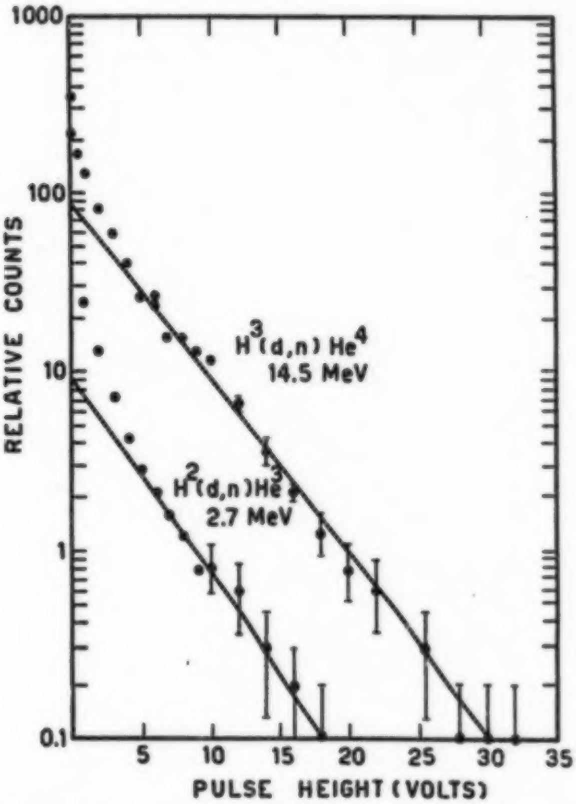

Fig. 1. Integral pulse height spectra for two monochromatic neutron sources obtained with the Hornyak detector.

Geller *et al.* [9]) measured some angular distributions with a 22-MeV bremsstrahlung beam and a zinc sulphide-lucite scintillation detector described by Hornyak [10]). Their results do not show any significant anisotropy. They used the detector with a bias high enough to cut off the gamma-ray pulses. Dixon [11]) used the same technique as Geller but with 70-MeV bremsstrahlung and studied the angular distributions of photoneutrons from Pb, Cu, Sn, Fe, Al, C and Be. He fitted his data to the curve $A + B \sin^2\theta$ and obtained an anisotropy decreasing with the atomic number, in *disagreement* with Price. In all the cases, except for C and Be he obtained isotropy within experimental errors. The isotropy found by both can be understood because both of them used a bias which was too low. Johansson [12]) with the same detector claims to select neu-

TABLE 1

Angular distributions of fast photoneutrons

Element	E_{max} (MeV)	Neutron energy interval (MeV)	B/A	Detector	Ref.
D	22	>6	6.5	$Si^{28}(n, p)Al^{28}$	a)
Be	65	>10	1.7	Hornyak button	b)
	65	>5	1.7	Hornyak button	b)
	65	>2.5	1.7	Hornyak button	b)
	70	total	1.2 ±0.4	Hornyak button	c)
	18	total	1.26±0.11	ZnS-parafin plastic button	d)
C	30	5—7	1.5	nuclear emulsions	e)
	30	3—5	1.5	nuclear emulsions	e)
	30	1.5—3	1.2	nuclear emulsions	e)
	23	total	1.35±0.88	ZnS-parafin plastic button	d)
	70	total	1.6 ±0.8	Hornyak button	c)
Al	65	>10	1.2	Hornyak button	b)
	65	>5	1.1	Hornyak button	b)
	65	>2.5	0.4	Hornyak button	b)
	70	total	0.36±0.29	Hornyak button	c)
V	22	>4	−0.08±0.09	$Al^{27}(n,p)Mg^{27}$	f)
Mn	22	>6	≈0	$Si^{28}(n, p)Al^{28}$	a)
Fe	19.7	total	≈8	Rhodium	g)
	70	total	0.09±0.25	Hornyak button	d)
Cu	22	>6	0.13±0.31	$Si^{28}(n, p)Al^{28}$	a)
	22	>4	0.35±0.05	$Al^{27}(n, p)Mg^{27}$	f)
	22	total	<0.12	Hornyak button	b)
	70	total	0.23±0.17	Hornyak button	d)
Zn	22	>6	0.31±0.17	$Si^{28}(n, p)Al^{28}$	a)
As	22	>6	0.52±0.21	$Si^{28}(n, p)Al^{28}$	a)
Nb	22	>4	0.15±0.07	$Al^{27}(n, p)Mg^{27}$	f)
Ag	22	>6	0.11±0.05	$Si^{28}(n, p)Al^{28}$	a)
	22	>4	0.35±0.07	$Al^{27}(n, p)Mg^{27}$	f)
	22	total	<0.12	Hornyak button	b)
Sn	70	total	0.12±0.17	Hornyak button	d)
I	22	>6	0.06±0.08	$Si^{28}(n, p)Al^{28}$	a)
La	22	>6	0.67±0.48	$Si^{28}(n, p)Al^{28}$	a)
Pr	22	>6	0.34±0.16	$Si^{28}(n, p)Al^{28}$	a)
	22	>4	0.16±0.13	$Al^{27}(n, p)Mg^{27}$	f)
Ta	65	>10	0.7	Hornyak button	c)
	65	>5	0.8	Hornyak button	c)
W	20	>4	2.0 ±0.5	$Al^{27}(n, p)Mg^{27}$	f)
Au	22	>6	0.66±0.14	$Si^{28}(n, p)Al^{28}$	a)
	22	>4	0.53±0.09	$Al^{27}(n, p)Mg^{27}$	f)
Pb	65	>10	0.82	Hornyak button	c)
	22	>6	1.0 ±0.45	$Si^{28}(n, p)Al^{28}$	a)
	65	>5	0.96	Hornyak button	c)
	23	≧4	≈0	Nuclear emulsions	j)
	20	>4	2.0 ±0.05	$Al^{27}(n, p)Mg^{27}$	i)
	22	>4	0.84±0.06	$Al^{27}(n, p)Mg^{27}$	f)
	16	>3	0.34±0.07	$P^{31}(n, p)Si^{31}$	k)
	19.7	total	≈0	Rhodium	g)

TABLE 1 (continued)

Element	$E_{\max}$ (MeV)	Neutron energy interval (MeV)	B/A	Detector	Ref.
Pb	22	total	<0.12	Hornyak button	[h]
	70	total	−0.08±0.08	Hornyak button	[d]
Bi	18.9	>7	21	Nuclear emulsion	[m]
	20	>6	0.9 ±0.1	Si^{28}(n, p)Al^{28} [*]	[n]
	22	>6	5.6	Si^{28}(n, p)Al^{28} [*]	[f]
	22	>6	1.1 ±0.15	Si^{28}(n, p)Al^{28} [*]	[a]
	30	>6	1.0 ±0.1	Si^{28}(n, p)Al^{28} [*]	[n]
	20	>4	2.0 ±0.5	Al^{27}(n, p)Mg^{27} [*]	[i]
	22	>4	0.99±0.10	Al^{27}(n, p)Mg^{27} [*]	[f]
	30	>4	0.67±0.1	Al^{27}(n, p)Mg^{27} [*]	[n]
	18.9	>4	2.0	Nuclear emulsions	[m]
	18.9	>1.5	0.4	Nuclear emulsions	[m]
U	22	>6	0.41±0.21	Si^{28}(n, p)Al^{28}	[a]

[*] There is evidence of electric quadrupole absorption in these data
[a] Present paper
[b] S. A. E. Johansson, Phys. Rev. **97** (1955) 434
[c] W. R. Dixon, Can. J. Phys. **33** (1955) 785
[d] B. P. Fabricand, B. A. Allison and J. Halpern, Phys. Rev. **103** (1956) 1755
[e] V. Emma, C. Milone and A. Rubbino, Phys. Rev. **118** (1960) 1297
[f] G. A. Price, Phys. Rev. **93** (1954) 1279
[g] G. A. Price and D. W. Kerst, Phys. Rev. **77** (1950) 806
[h] K. Geller, J. H. Halpern and P. F. Yergin, Phys. Rev. **95** (1954) 659L
[i] H. L. Poss, Phys. Rev. **79** (1950) 539L
[j] M. E. Toms and W. E. Stephens, Phys. Rev. **108** (1957) 77
[k] P. T. Demos, J. D. Fox, I. Halpern and J. Koch, Phys. Rev. **86** (1952) 605L
[m] G. N. Zatsepina, L. E. Lazareva and A. N. Pospelov, JEPT **5** (1957) 21
[n] F. Ferrero, O. A. Hanson, R. Malvano and C. Tribuno, Nuovo Cim. **4** (1956) 418

trons above 5 and 10 MeV and obtains increasing anisotropy when he moves to higher energies. Dixon and Johansson used a bremsstrahlung spectrum with maximum energy ≈ 70 MeV, far above the "giant resonance" region. On the other hand the efficiency of the Hornyak crystal as a function of discriminator setting drops exponentially as can be seen in fig. 1; thus it is difficult to calibrate the discriminator setting using *end points*. Any kind of extrapolation would be arbitrary since it depends on the counting rate intensity for a "zero" bias.

Toms and Stephens [13], in a more recent investigation, used emulsions to observe the energy and angular distribution of photoneutrons ejected from lead by 23-MeV bremsstrahlung. The angular distribution of neutrons having 4-MeV was nearly isotropic.

Zatsepina *et al.* [14] using the same technique for Bi, found that the anisotropy becomes larger for higher thresholds.

As can be seen in table 1, one can neither find a systematics of angular distributions in the literature, nor compare the results of the various authors because of the diversity of experimental conditions. There are of course Price's data, but most of them where obtained, using the $Al^{27}(n, p)Mg^{27}$ reaction with an effective threshold of $\approx$ 4 MeV. A systematic study using the $Si^{28}(n, p)Al^{28}$ reaction as a detector (with effective threshold $\approx$ 6 MeV) would enable us to see how angular distributions change with threshold. Price [7]), himself, measured the angular distribution for Bi with this detector but the value of $N_{90°}/N_{0°}$ is too large, in disagreement with Ferrero *et al.* [8]).

The angular distributions to be expected for a simple electric dipole transition from a state with angular momentum l to one with $l+1$ or $l-1$ was shown by Courant [2]), to be of the form $A+B\sin^2\theta$, where B/A is a function only of l,

$$\frac{B}{A} = \begin{cases} \frac{1}{2}\left(1+\frac{2}{l}\right) & \text{for} \quad l \rightarrow l+1, \\ \frac{1}{2}\left(\frac{l-1}{l+1}\right) & \text{for} \quad l \rightarrow l-1. \end{cases}$$

The value to be expected for each element will depend on the relative contribution of the various transitions to the fast neutrons group. Wilkinson [15]) predicts the same angular distributions but shows that the transitions of the type $l \rightarrow l+1$ are predominant.

2. Experimental Method

A collimated beam of bremsstrahlung (1.9 cm diameter) from the 22-MeV Betatron of the University of São Paulo bombarded 2.5 cm × 2.0 cm cylindrical

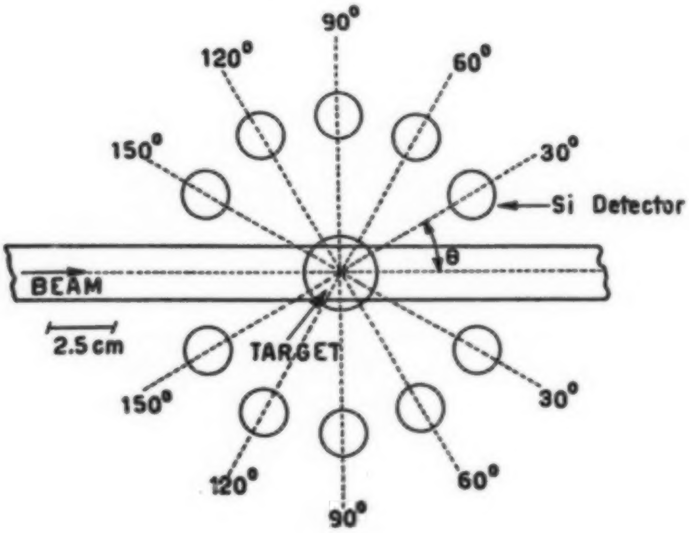

Fig. 2. Experimental setup for observation of angular distributions of fast photoneutrons with the $Si^{28}(n, p)Al^{28}$ threshold detector.

samples with axis perpendicular to the beam. The outgoing neutrons were detected by means of the $\mathrm{Si}^{28}(\mathrm{n, p})\mathrm{Al}^{28}$ reaction. The detector consisted of 25 g of silicon powder poured in two cilindrical containers and placed symmetrically at angles to the beam as shown in fig. 2. The threshold of the (n, p) reactions is ≈ 4 MeV but it is mostly sensitive to neutrons of more than 6 MeV. The measured cross section 16, 17) of the $\mathrm{Si}^{28}(\mathrm{n, p})\mathrm{Al}^{28}$ reaction is shown in fig. 3.

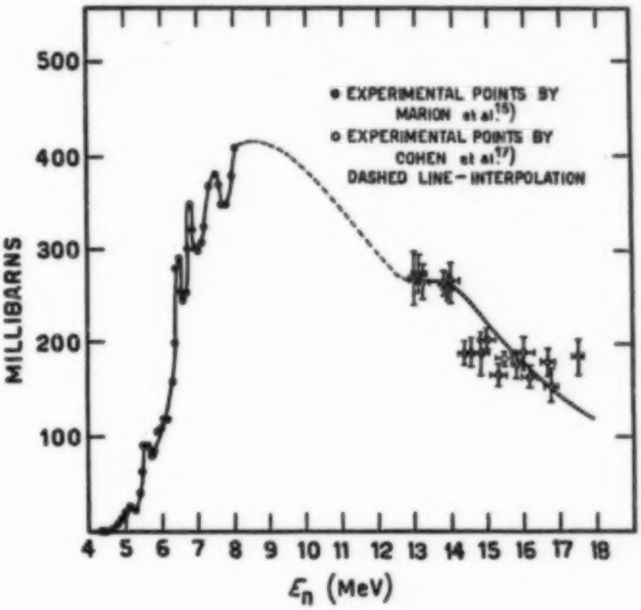

Fig. 3. $\mathrm{Si}^{28}(\mathrm{n, p})\mathrm{Al}^{28}$ cross section.

It was found to be convenient to use silicon in powder form and to pour the powder into the jacket of a Geiger counter, adapted for counting liquids. The procedure of a run was to expose a sample to the X-rays for 5 min with the silicon detectors at the desired angle; 30 sec were allowed to move the Si detector to the Geiger counter. The dose given to the sample in each run was monitored by a parallel plate ionization chamber in connection with an *RC*-integrator circuit. The time constant of the integrator was made equal to the mean life of Al^{28} for the emission of a β^- (2.4 min). The induced radioactivity in Al^{28} was small and it was necessary to reduce the background. A shield with 5 cm of iron and 10 cm of lead and an anticoincidence ring of counters was used. In these conditions the background was of ≈ 5 counts per min.

3. Results

Angular distributions of the high-energy photoneutrons produced by the 22-MeV bremsstrahlung on the elements: D, Mn, Cu, Zn, As, Ag, I, La, Pr, Au, Pb, Bi, U, as observed with the $\mathrm{Si}^{28}(\mathrm{n, p})\mathrm{Al}^{28}$ detector, are shown in fig. 4.

Each point represents the average of at least five runs. Vertical lines indicate statistical errors. The solid curves are a least squares fit of the data to a function of the form $A + B\sin^2\theta$. The values of B/A are plotted against the neutron number N in fig. 5, where we reproduce also Price's points [7]. Good agreement between both experiments can be observed; this is an indication that angular distributions of fast photoneutrons do not depend strongly on the threshold of the detector. Fig. 6 presents the fast neutron yields at 22-MeV of 14 elements. In our experiment the vertical scale was arbitrary. We normalized it using the photoneutron spectrum from lead measured by Toms and Stephens [14]; only 5.5 % of the total neutron yield was detected by our detector. Using the total yield for the emission of neutrons in lead [18] we obtained 1.4×10^6 neutrons per mole-roentgen for the fast neutron group.

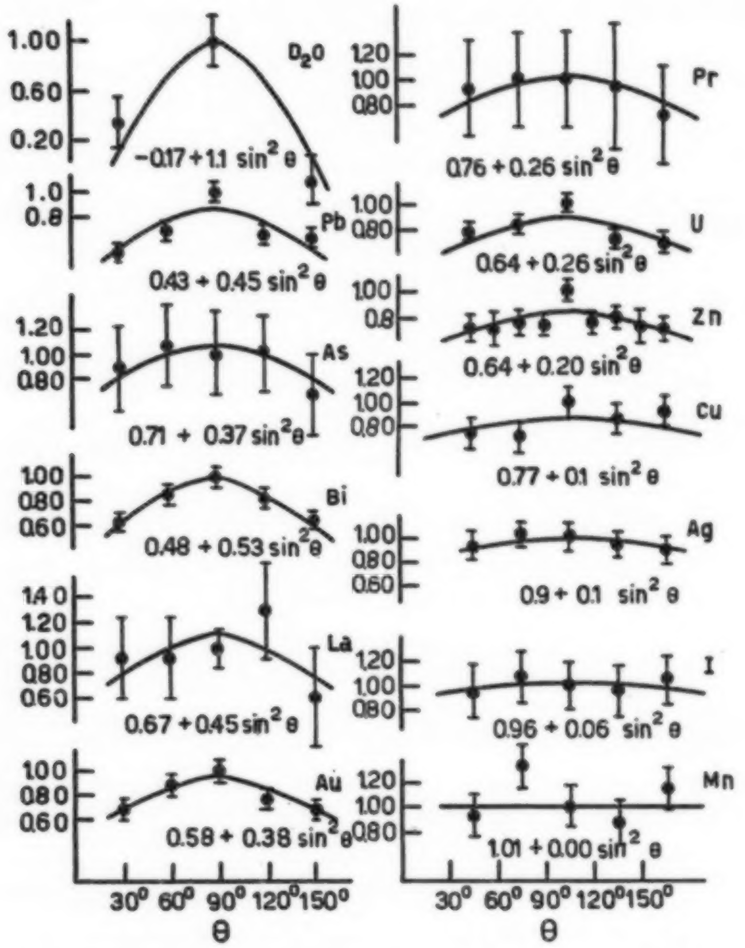

Fig. 4. Angular distributions of fast photoneutrons as observed with the Si^{28}(n, p)Al^{28} detector. Data normalized at 90° in each case.

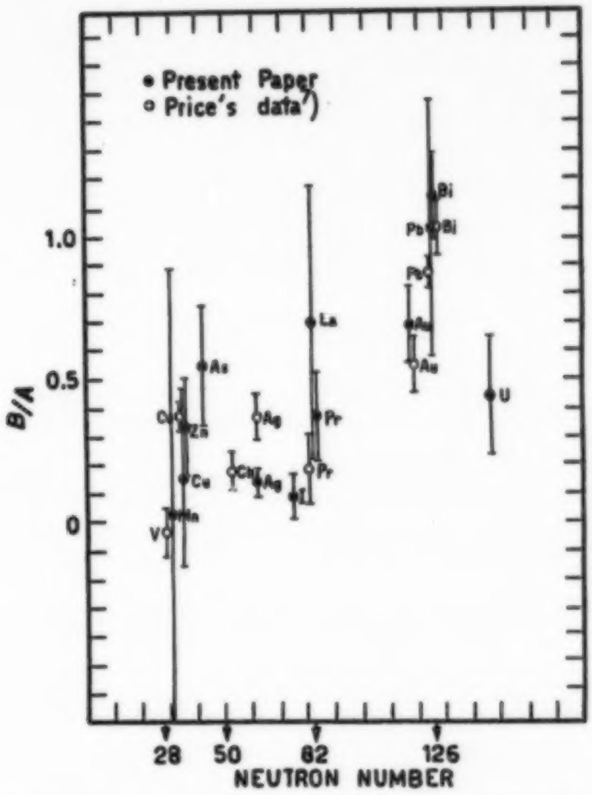

Fig. 5. Experimental anisotropy B/A of fast photoneutrons as observed with the $Si^{28}(n, p)Al^{28}$ detector, when the angular distributions are fitted to the function $A + B \sin^2\theta$. Some points are slightly shifted.

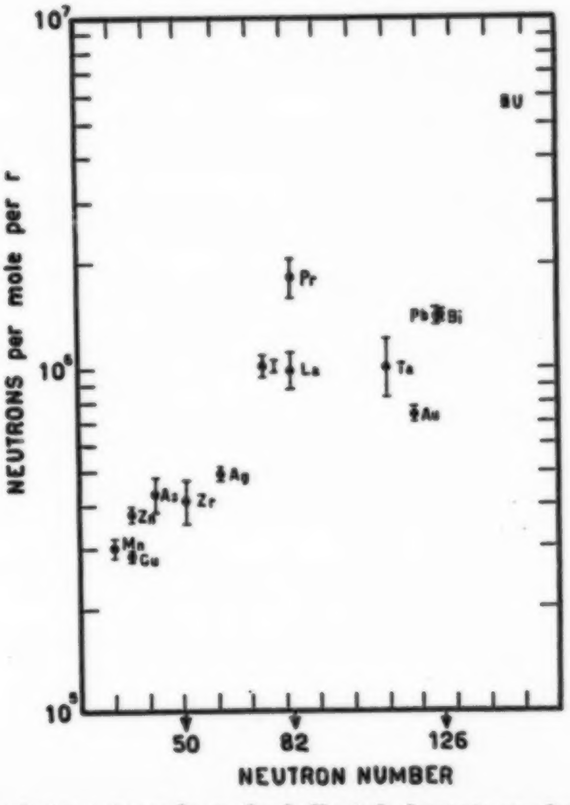

Fig. 6. Yield of fast photoneutrons from the indicated elements as observed by $Si^{28}(n, p)Al^{28}$ detector with a 22-MeV bremsstrahlung beam. Uranium presents a specially high yield.

4. Discussion

Because of the low fraction of fast neutrons in the (γ, n) reactions the points are affected by large errors.

The angular distribution for Bi is consistent with the one obtained by Ferrero *et al.* [8]) using the same detector and bremsstrahlung X-rays of 20 MeV.

Within the experimental errors only Bi, Au and Pb present a definite anisotropy; all the other elements seem to show isotropy or weak anisotropy.

In the extreme Wilkinson model (only $l \rightarrow l+1$ transitions) one expects a minimum B/A of 0.5.

Detailed calculations using this model were done for two cases: lead [15]) and Bismuth [8]). For Bi one gets $1+0.90 \sin^2\theta$ and for Pb, $1+0.7 \sin^2\theta$, which are consistent with the experimental data.

The case of uranium which presents a high yield and low anisotropy seems to be special due to fission.

We wish to acknowledge G. Moscati, E. Lerner and I. C. Nascimento for help during the experiment. We are grateful to Dr. E. W. Hamburger for the Van der Graaff irradiations used in the study of the Hornyak crystal and to Dr. L. C. Gomes for useful discussions.

References

1) V. F. Weisskopf, Phys. Rev. **52** (1935) 295;
   V. F. Weisskopf and D. H. Ewing, Phys. Rev. **57** (1940) 472
2) E. D. Courant, Phys. Rev. **82** (1951) 703
3) V. De Sabbata, Nuovo Cim. Suppl. **11** (1959) 225
4) H. L. Poss, Phys. Rev. **79** (1950) 539L
5) G. A. Price and D. W. Kerst, Phys. Rev. **77** (1950) 806
6) P. T. Demos, J. D. Fox, I. Halpern and J. Koch, Phys. Rev. **86** (1952) 605L
7) G. A. Price, Phys. Rev. **93** (1954) 1279
8) F. Ferrero, A. O. Hanson, R. Malvano and C. Tribuno, Nuovo Cim. **4** (1956) 418
9) K. Geller, J. Halpern and P. F. Yergin, Phys. Rev. **95** (1954) 659L
10) W. F. Hornyak, Rev. Sci. Instr. **23** (1952) 264
11) W. R. Dixon, Can. J. Phys. **33** (1955) 785
12) S. A. E. Johansson, Phys. Rev. **97** (1955) 434
13) M. E. Toms and W. E. Stephens, Phys. Rev. **108** (1957) 77
14) G. N. Zatsepina, L. E. Lazareva and A. N. Pospelov, JETP **5** (1957) 21
15) D. H. Wilkinson, Physica **22** (1956) 1039
16) J. B. Marion, R. M. Brugger and R. A. Chapman, Phys. Rev. **101** (1956) 247
17) A. V. Cohen and P. H. White, Nuclear Physics **1** (1956) 73
18) R. Montalbetti, L. Katz and J. Goldemberg, Phys. Rev. **91** (1953) 659

1.B

Nuclear Physics **23** (1961) 153—157; © *North-Holland Publishing Co., Amsterdam*

Not to be reproduced by photoprint or microfilm without written permission from the publisher

ON THE HARD CORE IN NUCLEAR FORCES

J. K. PERRING and R. J. N. PHILLIPS
Atomic Energy Research Establishment, Harwell, England

Received 14 November 1960

Abstract: It has been argued that static hard-core potentials cannot match observed $^1S_0$ scattering in certain respects. Counter-examples are presented.

1. Introduction

The use of a hard core in potential models of the two-nucleon interaction$^{1-6,\,12}$) has recently been questioned $^{6,\,7}$). There is some evidence that the $^1S_0$ "shape parameter" is positive $^{6,\,8}$), while general arguments $^{7,\,10}$) and specific examples $^{6,\,11}$) have suggested that a hard core of the size needed to fit high-energy data must make it negative. It has also been argued that the $^1S_0$ phase shift would be made too small at 40 MeV ^{9}).

The present note sets out to prove the contrary, by examples. In support, we observe that standard theorems on the construction of a potential from a phase shift can be applied, with a simple modification, to the hard core case.

2. Examples

We consider potential models of the form

$$\left.\begin{aligned} V(r) &= V_{\mathrm{OP}}(r)+V_{\mathrm{A}}(r), \quad \text{for} \quad r > r_{\mathrm{c}}, \\ &= \infty, \quad\quad\quad\quad\quad\quad\; \text{for} \quad r < r_{\mathrm{c}}, \end{aligned}\right\} \tag{1}$$

where r is the internucleon distance. $V_{\mathrm{OP}}(r)$ is the singlet even-parity part of the one-pion exchange potential, believed to be correct asymptotically (see e.g. ref. ^{12}); we take the pion mass = 140 MeV/c^2, and pseudovector coupling constant $f^2/4\pi = 0.08$). $V_{\mathrm{A}}(r)$ is an adjustable term containing two parameters, which we take to have one of the following forms.

$$V_{\mathrm{A}}(r) = -V_0 \mathrm{e}^{-\alpha r}/(\alpha r), \tag{2a}$$

$$V_{\mathrm{A}}(r) = -V_0 \mathrm{e}^{-\alpha r}/(\alpha r)^2, \tag{2b}$$

$$V_{\mathrm{A}}(r) = -V_0 \mathrm{e}^{-\alpha r}/(\alpha r)^3, \tag{2c}$$

$$V_{\mathrm{A}}(r) = -V_0 (2\mathrm{e}^{-\alpha(r-r_{\mathrm{c}})} - \mathrm{e}^{-2\alpha(r-r_{\mathrm{c}})}). \tag{2d}$$

Type (a) is the Yukawa potential: (b) and (c) are modifications suggested by meson theory [12]). For variety, (d) is the Morse potential, chosen to have zero slope at the core edge.

In each case the three parameters V_0, α and r_c are chosen to fit the $^1S_0$ scattering length a, effective range r_0 and 310 MeV phase shift. We then study the shape parameter P, defined by the low-energy expansion

$$k \cot \delta_0 = -\frac{1}{a} + \tfrac{1}{2} r_0 k^2 - P r_0^3 k^4 + \dots, \tag{3}$$

where δ_0 is the $^1S_0$ phase shift and k is the relative momentum, (with $\hbar = c = 1$). We also study δ_0 at higher energies.

The spirit of this work is to fit data well enough to prove our point, without striving for extreme precision. Thus, although the data in question are from p—p scattering, we ignore Coulomb effects for convenience. Only a is seriously affected, and we allow for this fairly well by fitting the n—p value instead (final adjustments would presumably require a small change in V_0 but this would be unimportant for the rest of the problem). r_0 is not closely determined at present; our fits cover a reasonable range. The 310 MeV phase shift has not been precisely matched, because we chose to vary r_c by relatively large steps.

Table 1 records V_0, α and r_c for each case; the units are MeV and fermis

TABLE 1

Case	V_0 in MeV	α in f^{-1}	r_c in f
a1	4839	2.8	0.5
a2	2656	2.4	0.5
b1	4446	2.2	0.5
b2	1942	1.8	0.5
c	1078	1.4	0.5
d1	244	3.0	0.4
d2	211	2.8	0.4

TABLE 2

Low-energy parameters

Experiment [6, 8, 9])	α in f	r_0 in f	P
	−23.7	2.65−2.80	≈0.05
a1	−23.9	2.68	0.03
a2	−23.6	2.80	0.01
b1	−23.8	2.65	0.04
b2	−23.8	2.77	0.02
c	−23.7	2.68	0.03
d1	−23.9	2.69	0.03
d2	−23.8	2.77	0.02

TABLE 3

High-energy $^1S_0$ phase shifts, in degrees

Energy in MeV	39.4	68.3	98	142	210	310
Experiment	45—47 9)	33.5 13) ±1.5 30.5 10)	23.5 13) ±1.2 22.2 10)	11.8 12) ±0.7	5.9 14) 6.3 10)	−8.9 15) ±1.9
a1	44.2	33.9	25.6	15.7	3.5	−10.6
a2	42.1	31.4	22.8	12.7	0.4	−13.7
b1	45.0	35.0	27.0	17.3	5.4	−8.5
b2	42.8	32.4	24.2	14.3	2.3	−12.6
c	44.8	35.0	27.1	17.6	5.9	−7.7
d1	44.2	34.2	26.4	17.1	5.9	−6.6
d2	42.0	32.8	24.8	15.4	4.2	−8.3

($f = 10^{-13}$ cm). There are two examples for each potential (a), (b) and (d), and one for (c). Tables 2 and 3 contain the corresponding low-energy parameters and high-energy phase shifts, with experimental values for comparison.

Our calculations used a Ferranti MERCURY computer. The low-energy parameters were extracted by finding $k \cot \delta_0$ at $\frac{1}{2}$ MeV intervals from $\frac{1}{2}$ to 3 MeV, extrapolating from finite to zero integration step size, and applying finite difference formulae.

3. Conclusions

These examples evidently disprove the main objection to hard cores, since all have positive shape parameters.

As to the 40 MeV phase shift, the values are mostly just below the "experimental" range 45°—47°. However, the latter comes from an analysis 9) in which the $^1D_2$ phase shift was held at the one-pion-exchange value ($\approx 1.0°$): a reasonable increase † would allow smaller values of δ_0.

At some higher energies the $^1S_0$ phase shifts do not agree very closely with experiment. However, it seems reasonable to believe that these differences — and any small discrepancies at 40 MeV — are due to the shape of $V_A(r)$ rather than to the hard core.

Thus there seems to be no clear objection at present to a hard core. Moreover, a modification of the Jost-Kohn theorem 16) can be stated (see Appendix). If an S phase shift is given, which $\to -kr_c$ as $k \to \infty$, then a static hard core potential of core radius r_c can be constructed to fit it, subject to certain conditions. Since an experimental phase shift is always limited to a finite energy range, a potential may be found to fit it with *any* core radius. On the other hand, there is no assurance that such a potential would have an acceptable range, or shape, or asymptotic form.

---

† E.g. in the $^1D_2$ state, our potentials would give phase shifts from 1.27° to 1.45°.

It is interesting that cases (a) to (c) have core radii larger than usual. This seems to come from including $V_{OP}(r)$, the only qualitative difference between the Gammel-Thaler potential [2]) (with $r_c = 0.40\,f$) and our case (a). Other potentials with the one-pion contribution are those of Bryan [3]) and Hamada [4]): the former has $r_c = 0.40\,f$ but gives an insufficiently negative δ_0 at 310 MeV: the latter has $r_c = 0.48\,f$, which supports our reasoning.

Finally, we have sought to show that there is no inconsistency between the observed $^1S_0$ scattering and the hard core static potential model. But whether this is the most useful model, and whether it is proper to ignore relativistic effects [17]), are questions that remain.

Appendix

Jost and Kohn [16]), and others, have shown that under certain circumstances a static central potential can be constructed from a single phase shift, given as a function of energy. This phase shift → 0 as $k \to \infty$.

Now the reduced Schrödinger equation for S-wave scattering by an ordinary potential $V_1(r)$ differs only by a change of origin from that for the hard-core potential $V_2(r) = V_1(r-r_c)$, with core radius r_c. The phase shifts differ by kr_c. (Similar results for higher partial waves are complicated by the centrifugal term).

Thus the problem of constructing a hard-core potential from an S phase shift which $\to -kr_c$ as $k \to \infty$ reduces to the previous problem, which has been solved. Algebraic difficulties can in principle foil the construction, but it seems likely that in the physical case there is enough freedom in choosing the phase shift to avoid them.

These remarks were stimulated by discussions with Professor Peierls and Dr. J. S. Bell, to whom we are grateful.

References

1) R. Jastrow, Phys. Rev. **81** (1951) 165
2) J. L. Gammel and R. M. Thaler, Phys. Rev. **107** (1957) 291, 1337
3) R. A. Bryan, Nuovo Cimento **16** (1960) 895
4) T. Hamada, University of Sydney preprint (1960)
5) T. Hamada, J. Iwadare, S. Otsuki, R. Tamagaki and W. Watari, Progr. Theor. Phys. **22** (1959) 566
6) J. L. Gammel and R. M. Thaler, Progress in Elementary Particle and Cosmic Ray Physics, Vol. 5, p. 97 (1960)
7) H. P. Noyes, Proc. Int. Conf. on Nuclear Forces and Few-Nucleon Problem (Pergamon Press, London, 1960) p. 39
8) L. Heller, Phys. Rev. (in press)
9) M. H. MacGregor, M. J. Moravcsik and H. P. Noyes, University of California report, UCRL 5582-T (1959)
10) J. L. Gammel, private communication

11) R. Preston and M. Preston, Can. J. Phys. **36** (1958) 579
12) R. J. N. Phillips, Reports on Progress in Physics, Vol. 22, p. 562 (1959)
13) J. K. Perring, (to be published)
14) M. H. MacGregor and M. J. Moravcsik, Phys. Rev. Letters, **4** 524 (1960)
15) M. H. MacGregor, M. J. Moravcsik and H. P. Stapp, Phys. Rev. **116** 1248 (1959)
16) R. Jost and W. Kohn, Phys. Rev. **87**, 977; **88** (1952) 382: Dan. Mat-fys. Medd. **27**, No. 2 (1953)
17) M. Gourdin, Ann. Phys. (Paris), Ser. 13, **4** (1959) 595
18) H. P. Noyes, University of California report, UCRL 6108-T (1960)

8.B

Nuclear Physics **23** (1961) 158—163; *©North-Holland Publishing Co., Amsterdam*

Not to be reproduced by photoprint or microfilm without written permission from the publisher

TWO PION ANNIHILATION OF A N—$\overline{\text{N}}$ PAIR

R. P. SAXENA

Department of Physics, Muslim University, Aligarh, India

Received 20 September 1960

Abstract: The problem of double pion annihilation of a nucleon-antinucleon pair is investigated with the help of New-Tamm-Dancoff techniques. It is shown that the empirical selection rules given earlier by Bethe and Hamilton follow automatically from the present formalism. Further, the annihilation cross sections for various specific processes are calculated and a limited effort is made to compare these results with those of the experiments.

1. Introduction

During the past few years a good deal of work has been done on the problem of "multiple production of pions in N—$\overline{\text{N}}$ annihilation" using various statistical models [1]). The results of some of these models seem to be in reasonable agreement with experiments. However, most of the experimental data available on multiple pion annihilation is for $n > 2$, n being the pion multiplicity. On account of the various competing processes (multiple pion production, K—$\overline{\text{K}}$ production, etc.), which are expected to have larger cross sections, it becomes difficult to observe double pion annihilation events. On the other hand, the difficulties involved in a field theoretic calculation of multiple production processes increases like $n!$. Thus it was thought worthwhile to investigate the problem of "double pion annihilation" (the easiest one to be sutdied theoretically) with the help of the New-Tamm-Dancoff formalism for the N—$\overline{\text{N}}$ interaction developed recently by Mitra and Saxena [2]). It will be shown that the empirical selection rules given by Bethe and Hamilton [3]) follow automatically from the present formalism.

2. Derivation of the Two Pion Annihilation Cross-Section

The notation and formalism of ref. [2]) has been used throughout this paper. For the purpose of deriving the double pion annihilation cross-section we have, first to obtain a connection between the New-Tamm-Dancoff amplitudes for the states (0, 0; 2) and (1, 1; 0). The Feynman diagrams for the double pion annihilation process are shown in fig. 1. The two meson amplitude

$$\langle a_{k_1\alpha} a_{k_2\beta} \rangle \tag{1}$$

can now be connected to the one-nucleon one-antinucleon amplitude with the help of standard New-Tamm-Dancoff techniques [4]). The algebra involved is quite cumbersome but straightforward [5]). The final connecting equation runs as

$$\begin{aligned}(\varepsilon-\omega_{k_1}-\omega_{k_2})\langle a_{k_1\alpha}a_{k_2\beta}\rangle = (G^2/8\pi^3)\int \mathrm{d}_3\mathbf{t}\sum_{W}\sum_{W'}\sum_{u}(4\omega_{k_1}\omega_{k_2})^{-\frac{1}{2}}\\ \times\Bigg[\frac{W^*(\mathbf{t}-\mathbf{k}_1-\mathbf{k}_2)\gamma\tau_\beta W'(\mathbf{t}-\mathbf{k}_1)W'^*(\mathbf{t}-\mathbf{k}_1)\gamma\tau_\alpha u(\mathbf{t})}{\varepsilon-\mathbf{E}_{\mathbf{t}-\mathbf{k}_1}-\mathbf{E}_{\mathbf{t}-\mathbf{k}_1-\mathbf{k}_2}-\omega_{k_2}}\\ -\frac{W'^*(\mathbf{t}-\mathbf{k}_2)\gamma\tau_\beta u(\mathbf{t})W^*(\mathbf{t}-\mathbf{k}_1-\mathbf{k}_2)\gamma\tau_\alpha W'(\mathbf{t}-\mathbf{k}_2)}{\varepsilon-E_t-E_{\mathbf{t}-\mathbf{k}_2}-\omega_{k_2}}\\ +(\mathbf{k}_1\rightleftarrows\mathbf{k}_2,\ \alpha\rightleftarrows\beta)\Bigg]\langle b_{tu}b^*_{\mathbf{t}-\mathbf{k}_1-\mathbf{k}_2,W}\rangle.\end{aligned}\tag{2}$$

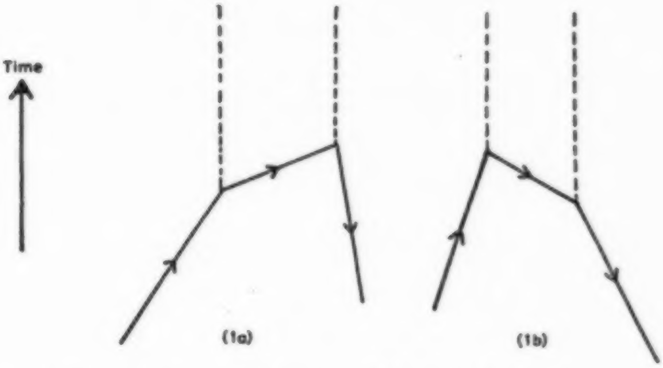

Fig. 1. Feynman diagrams for two pion annihilation of a nucleon-antinucleon pair.

We now put

$$\langle a_{k_1\alpha}a_{k_2\beta}\rangle \equiv \phi_{\alpha\beta}(\mathbf{k}_1,\mathbf{k}_2),\tag{3}$$

use the definition given by MS for the wave-matrix for a N—N̄ pair

$$\psi_{\rho\sigma}(\mathbf{t},\mathbf{t}-\mathbf{k}_1-\mathbf{k}_2)=\sum_{W}\sum_{u}(E_t E_{\mathbf{t}-\mathbf{k}_1-\mathbf{k}_2}/M^2)^{\frac{1}{2}}\times u_\rho(\mathbf{t})W_\sigma{}^*(\mathbf{t}-\mathbf{k}_1-\mathbf{k}_2)\langle b_{tu}b^*_{\mathbf{t}-\mathbf{k}_1-\mathbf{k}_2,W}\rangle\tag{4}$$

and simultaneously make a transformation to the C.M. system with the help of

$$\mathbf{k}_1=-\mathbf{k}_2=\mathbf{k},\quad \phi_{\alpha\beta}(\mathbf{k},-\mathbf{k})\equiv\phi_{\alpha\beta}(\mathbf{k}),\quad\text{and}\quad \psi(\mathbf{t},-\mathbf{t})=\psi(\mathbf{t}).\tag{5}$$

Then, eq. (2) transforms to the form

$$\begin{aligned}(\varepsilon-2\omega_k)\phi_{\alpha\beta}(\mathbf{k}) = (G^2/8\pi^3)\int \mathrm{d}_3\mathbf{t}(M^2/2E_t\omega_k)\\ \times[(\tau_\beta\tau_\alpha)\,\mathrm{Tr}\,\{\Lambda_-(\mathbf{t}-\mathbf{k})\psi(\mathbf{t})\}H_1(\mathbf{t},\mathbf{k})+(\tau_\alpha\tau_\beta)\,\mathrm{Tr}\,\{\Lambda_-(\mathbf{t}+\mathbf{k})\psi(\mathbf{t})\}H_2(\mathbf{t},\mathbf{k})],\end{aligned}\tag{6}$$

where

$$H_1(\mathbf{t},\mathbf{k}) = (E_{\mathbf{t}-\mathbf{k}})^{-1}[(\varepsilon-E_t-\omega_k-E_{\mathbf{t}-\mathbf{k}})^{-1}+(\varepsilon-E_t-\omega_k-E_{\mathbf{t}+\mathbf{k}})^{-1}],\tag{7}$$

$$H_2(\mathbf{t},\mathbf{k}) = H_1(\mathbf{t},-\mathbf{k}),\tag{8}$$

and

$$\Lambda_-(\mathbf{q}) = (\tfrac{1}{2}M)(M+\beta E_q-\beta\gamma_5(\sigma\cdot\mathbf{q})). \tag{9}$$

Eq. (6) is the required connection between a two-meson and one-nucleon one-antinucleon state.

To evaluate the trace in (6) we define the large component of $\psi(\mathbf{t})$ as

$$\psi(\mathbf{t}) = \left(1+\frac{\gamma_5(\sigma\cdot\mathbf{t})}{E_t+M}\right)\psi_{+-}(\mathbf{t})\left(1-\frac{\gamma_5(\sigma\cdot\mathbf{t})}{E_t-M}\right), \tag{10}$$

where

$$\psi_{+-}(\mathbf{t}) = \psi(t)I^m_{Jls}(\hat{t}). \tag{11}$$

The functions I are the conventional angular momentum eigenfunctions [6])

$$I^m_{Jls}(\hat{t}) = \sum_{ls} C_{ls}(J, m; m_l, m_s)Y_l^{m_l}(\hat{t})\chi_s^{m_s}, \tag{12}$$

where Y is a spherical harmonic and C is Clebsch-Gordon coefficient and $\chi_s^{m_s}$ is as given in [2])

$$\chi_s^{m_s} = (AI+B\sigma_1+C\sigma_2+D\sigma_3), \tag{13}$$

A, B, C and D being numerical constants depending upon the spin state under consideration, I is a unit matrix and σ's are the Pauli matrices. It is now easy to see that the matrix dependence inside the trace in (6) is of the form

$$\Lambda_-(\mathbf{q})\left(1+\frac{\gamma_5(\sigma\cdot\mathbf{t})}{E_t+M}\right)(AI+B\sigma_1+C\sigma_2+D\sigma_3)\left(1-\frac{\gamma_5(\sigma\cdot\mathbf{t})}{E_t-M}\right), \tag{14}$$

where $\mathbf{q}$ is either $\mathbf{t}-\mathbf{k}$ or $\mathbf{t}+\mathbf{k}$. The trace of the above expression is

$$-\frac{4A(\mathbf{t}\cdot\mathbf{q})}{t^2}+\frac{4iE_t}{Mt^2}\{B(\mathbf{q}\times\mathbf{t})_1+C(\mathbf{q}\times\mathbf{t})_2+D(\mathbf{q}\times\mathbf{t})_3\}. \tag{15}$$

As an illustration we shall discuss the case $J=1$ in some detail. Now a π—π system of $J=1$ can be connected to both the $^3S_1$ and $^1P_1$ states of the N—$\overline{\text{N}}$ system for antisymmetric isobaric spin states and to the $^3P_1$ state for symmetric isobaric spin states. We consider the former. For $J=1$, the π—π wave-function is

$$\phi_{\alpha\beta}(\mathbf{k}) = \phi_{\alpha\beta}(k)Y_1^0(\hat{k}). \tag{16}$$

The total $J=1$ state of the N—$\overline{\text{N}}$ system is

$$\psi_{+-}(\mathbf{t}) = \psi(t)\left[\frac{1}{\sqrt{2}}Y_0^0(\hat{t})\tfrac{1}{2}(1+\sigma_3)+\frac{1}{\sqrt{2}}Y_1^0(\hat{t})\tfrac{1}{2}(1-\sigma_3)\right], \tag{17}$$

where the numerical values of A, B, C and D listed in MS have been substituted. Substituting (16) and (17) in (6) and making use of eqs. (10) to (15) we get, after a trivial integration over $\hat{t}$,

$$(\varepsilon-2\omega_k)\phi_{\alpha\beta}(k) = (G^2/2\pi^2)\int_0^\infty t^2\mathrm{d}t(E_t\omega_k)^{-1}$$
$$\times\left[(\tau_\beta\tau_\alpha)\left(X_0-\frac{k}{t}X_1\right)+(\tau_\alpha\tau_\beta)\left(Z_0-\frac{k}{t}Z_1\right)\right]\psi(t), \tag{18}$$

where

$$X_n = \int\frac{\mathrm{d}\Omega_t}{4\pi}P_n(\hat{t}\cdot\hat{k})H_1(\mathbf{t},\mathbf{k}) \tag{19}$$

and

$$Z_n = \int\frac{\mathrm{d}\Omega_t}{4\pi}P_n(\hat{t}\cdot\hat{k})H_2(\mathbf{t},\mathbf{k}). \tag{20}$$

In eq. (18) the functions X_2 and Z_2 are not present. On the other hand they would have been present if the $^1\mathrm{P}_1$ state of the N—$\bar{\text{N}}$ system had given a non vanishing contribution to the $J = 1$ state of the π—π system. This result is encouraging since it provides a justification for the empirical selection rule given by Bethe and Hamilton, that in the triplet antisymmetric isobaric spin state of N—$\bar{\text{N}}$ system, the contribution to the double pion annihilation will come only through $^3\mathrm{S}_1$ state (the singlet antisymmetric isobaric spin state will not contribute at all.) In a similar way it can be shown that for singlet symmetric isobaric spin state the only non vanishing contributions to the $J = 0$ and $J = 2$, π—π states would respectively come from the $^3\mathrm{P}_0$ and $^3\mathrm{P}_2$ states of the N—$\bar{\text{N}}$ system. The results are given below:

$$(\varepsilon-2\omega_k)\phi_{\alpha\beta}(k) = (G^2/2\pi^2)\int_0^\infty\frac{t^2\mathrm{d}t}{E_t\omega_k}\times U(k,t)\psi(t), \tag{21}$$

where

$$U(k,t) = [(\tau_\beta\tau_\alpha)X_2+(\tau_\alpha\tau_\beta)Z_2] \quad \text{for} \quad J = 0,$$
$$U(k,t) = \left[(\tau_\beta\tau_\alpha)\left(X_0-\frac{k}{t}X_1\right)+(\tau_\alpha\tau_\beta)\left(Z_0-\frac{k}{t}Z_1\right)\right] \quad \text{for} \quad J = 1, \tag{22}$$

and

$$U(k,t) = \left[(\tau_\beta\tau_\alpha)\left(X_2-\frac{k}{t}X_3\right)+(\tau_\alpha\tau_\beta)\left(Z_2-\frac{k}{t}Z_3\right)\right] \quad \text{for} \quad J = 2.$$

Defining the reduced transition amplitude (in which a multiplicative δ-function is left out) for a transition from an N—$\bar{\text{N}}$ system to a π—π system as [7])

$$T_{\mathrm{N}\bar{\mathrm{N}}\to\pi\pi}(t,k;\alpha,\beta) = (\psi^*(t)\phi_{\alpha\beta}(k)), \tag{23}$$

the differential cross section for two pion annihilation may immediately be written down with the help of the standard Møller formula

$$\left(\frac{\mathrm{d}\sigma}{\mathrm{d}\Omega}\right)_{\mathrm{N\bar{N}}\to\pi\pi}=\tfrac{1}{2}k^2|T_{\mathrm{N\bar{N}}\to\pi\pi}(t,k;\alpha,\beta)|^2\frac{\mathrm{d}t}{\mathrm{d}E_i}\frac{\mathrm{d}k}{\mathrm{d}E_f}, \tag{24}$$

where $E_i = 2E_t$ and $E_f = 2\omega_k$ are the initial and final state energies. Integrating over the angles, the total cross section for double pion annihilation in an eigenstate of total isobaric spin and angular momentum can be written as

$$\sigma^{T,J}_{\mathrm{N\bar{N}}\to\pi\pi} = (kE_t\omega_k/8t)\int \mathrm{d}\Omega|\psi^*(t)(\varepsilon-2\omega_k)^{-1}(G^2/2\pi^2)\times\int_0^\infty \frac{t^2\mathrm{d}t}{E_t\omega_k}U(k,t)\psi(t)|^2. \tag{25}$$

Using the various statistical weight factors we can first write the above cross sections for an eigenstate of T alone and then with the help of eigenstates of total isobaric spin for the π—π system, it would then be possible to write the cross-sections for individual processes. The various relations are listed below

$$\sigma_{\mathrm{p\bar{p}}\to\pi^+\pi^-} = \tfrac{1}{3}\overset{(0)}{\sigma}_{\mathrm{N\bar{N}}\to\pi\pi}+\tfrac{1}{2}\overset{(1)}{\sigma}_{\mathrm{N\bar{N}}\to\pi\pi} = \sigma_{\mathrm{n\bar{n}}\to\pi^+\pi^-}, \quad \sigma_{\mathrm{p\bar{p}}\to\pi^0\pi^0} = \tfrac{1}{6}\overset{(0)}{\sigma}_{\mathrm{N\bar{N}}\to\pi\pi} = \sigma_{\mathrm{n\bar{n}}\to\pi^0\pi^0},$$
$$\sigma_{\mathrm{n\bar{p}}\to\pi^0\pi^-} = \overset{(1)}{\sigma}_{\mathrm{N\bar{N}}\to\pi\pi} = \sigma_{\mathrm{p\bar{n}}\to\pi^0\pi^+}. \tag{26}$$

As the transition amplitude (23) can, with the help of (21) be written down completely in terms of $\psi(t)$, the solution for which has been given in MS, the above cross-sections can very easily be computed numerically. Table 1 below gives the values of the above cross-sections.

TABLE 1

Values of cross-sections

t	k	$\sigma_{\mathrm{p\bar{p}}\to\pi^+\pi^-}$ (mb)	$\sigma_{\mathrm{p\bar{p}}\to\pi^0\pi^0}$ (mb)	$\sigma_{\mathrm{n\bar{p}}\to\pi^0\pi^-}$ (mb)
0.00	0.98	7.00	1.17	9.32
0.05	0.99	8.02	1.40	10.44
0.08	0.992	8.86	1.53	11.59
0.10	0.994	10.87	2.12	13.26
0.12	0.996	13.05	2.52	16.02
0.15	1.00	15.52	3.03	18.91

3. Discussion

The fact that the empirical selection rules of Bethe and Hamilton automatically follow from the present formalism is a satisfying feature of the present investigation. Recently, Desai[8]) working with the Chew and Ball's model[9]) has also obtained essentially the same selection rules.

Since there is no reliable experimental data available for the above cross-sections, a direct comparison is not possible. However, in certain recent California[8]) events of $\mathrm{p\bar{p}}$ annihilation, the percentage of zero prong events (which are essentially $\mathrm{p\bar{p}}\to\pi^0\pi^0$ events) is about 2.5 ± 1.2 percent at an average energy of 80 MeV in the laboratory system (equivalent to our $t \approx 0.12$). The total annihilation cross-section at this energy is about 200 mb, which makes the cross-section for zero prong events to be of the order of a few milibarns. Our $p\bar{p} \to \pi^0\pi^0$ cross-section at $t = 0.12$ is also of the same order. Since we have neglected in our crude estimates, processes like $p\bar{p} \to 3\pi^0$ etc., it is hoped that the increased accuracy of π^0 counting would make the present situation better.

The author expresses his gratitude to Dr. A. N. Mitra for suggesting this problem and for his continued guidance throughout the course of this work.

References

1) E. C. G. Sudarshan, Phys. Rev. **103** (1956) 777
2) A. N. Mitra and R. P. Saxena, Proc. Roy. Soc. (1960) to be published (hereafter referred to as MS)
3) H. A. Bethe and J. Hamilton, Nuovo Cim. **4** (1956) 1
4) R. H. Dalitz and F. J. Dyson, Phys. Rev. **99** (1955) 302
5) R. P. Saxena, Ph. D. thesis, Muslim University, Aligarh (1959) unpublished
6) V. F. Weisskopf and J. M. Blatt, Theoretical nuclear physics (Wiley, New York, 1952)
7) H. A. Bethe and de Hoffmann, Mesons and fields (1955) Vol. II, p. 273;
M. Ross, Phys. Rev. **103** (1956) 760
8) B. R. Desai, UCRL preprint No. 9024 (1960)
9) G. F. Chew and J. S. Ball, Phys. Rev. **109** (1958) 1385

2.A.1:
2.E

Nuclear Physics **23** (1961) 164—168; ©*North-Holland Publishing Co., Amsterdam*

Not to be reproduced by photoprint or microfilm without written permission from the publisher

FONCTION D'EXCITATION DE ^{141}Pr (p, n) ^{141}Nd JUSQU'À 11.1 MeV

J. OLKOWSKY, M. LE PAPE ET I. GRATOT
Section de Physique Nucléaire à Moyenne Énergie, C.E.N. Saclay, France

Reçu le 24 Octobre 1960

Abstract: The absolute (p, n) cross section of ^{141}Pr was measured by the activation method at proton energies up to 11.1 MeV. The energy dependence agrees with that predicted by the optical model.

1. Introduction

Nous avons étudié la réaction ^{141}Pr (p, n) ^{141}Nd pour plusieurs raisons. 1°) Il y a très peu de mesures de sections efficaces (p, n) dans la région des terres rares et aucune fonction d'excitation. Le tableau 1 rassemble les seules valeurs publiées à notre connaissance dans ce domaine. Pr est un élément monoisotopique ($A = 141$).

Tableau 1
Valeurs connues des sections efficaces

Cible	E_p (MeV)	σ(p, n) (mb)	Référence
^{140}Ce	6.7	54	[1])
^{142}Ce	6.7	57	[1])
^{142}Ce	12	110	[2])
^{141}Pr	6.7	16	[1])
^{148}Nd	6.7	36	[1])

2°) En général [2,3,4]), on considère qu'on peut assimiler avec une bonne approximation la section efficace totale de réaction à la section efficace de la réaction (p, n) dans la zone d'énergie comprise entre le seuil de la réaction (p, n) (ici 2.5 MeV) [5]) et l'énergie de liaison du dernier nucléon (ici $B_n \approx 9$ MeV)

Dans le modèle optique, on peut obtenir la section efficace totale de réaction, par le potentiel imaginaire qui décrit l'absorption correspondant à la formation d'un noyau composé.

Pour une énergie de protons $\geqq 15$ MeV on peut utiliser une méthode directe, dite de transmission, pour obtenir la section efficace de réaction et en déduire le potentiel imaginaire; mais à des énergies inférieures à 15 MeV environ, cette méthode n'est plus applicable [6]). Les valeurs du potentiel imaginaire sont alors déduites de l'analyse des diffusions élastiques, mais il n'est pas sûr a priori que ces valeurs soient correctes [7]).

On peut encore, d'une façon beaucoup plus simple pour les calculs, obtenir la section efficace totale en supposant une interaction forte entre le nucléon et le noyau (noyau noir). Shapiro [3]) a fait de tels calculs en prenant un puits carré de potentiel réel de profondeur arbitraire (20 MeV).

Pour qu'on puisse assimiler σ(p, n) $\approx$ σ_t dans la zone d'énergie indiquée, il faut s'assurer que la réaction (p, n) ne procède pas par interaction directe mais par l'intermédiaire d'un noyau composé, et que les autres réactions, énergétiquement possibles, sont négligeables. Un certain nombre d'expériences permettent de répondre à ces questions.

a) Albert *et al.* [8]) ont étudié la distribution angulaire et le spectre énergétique des neutrons émis dans les réactions (p, n) pour V, Mn, Co, Nb, Rh, In, avec des protons de 7.5, 8 et 8.8 MeV. Les distributions angulaires sont isotropes à 10 % près et, sur les éléments les plus lourds ($Z \geqq Z_{\mathrm{Nb}}$), le spectre des neutrons est maxwellien. Ceci montre que, dans la zone d'énergie considérée, et pour des noyaux aussi lourds que les terres rares, la réaction (p, n) se produit par la formation d'un noyau composé.

b) Les réactions énergétiquement possibles pour $E_p \leqq 11$ MeV sur Pr sont: (p, γ), (p, d), (p, α), et la diffusion inélastique (p, p'). La section efficace de la réaction (p, γ) varie peu avec la cible et avec l'énergie des particules incidentes et se situe vers $\sigma_{10\ \mathrm{MeV}}$(p, γ) $\approx$ 1 mb [9]).

Nous avons mesuré (p, d) sur ^{142}Nd. Le résultat est $\sigma_{10\ \mathrm{MeV}}$(p, d) $\approx$ 150 μb [10]). Pour une énergie donnée, σ(p, α) est toujours inférieur à σ(p, d) [11]). Donc, nous pouvons négliger toutes ces réactions. La diffusion inélastique totale (p, p') est plus difficile à évaluer. Vers 30 MeV, σ(p, p') représente environ 15 % de $\sigma_{\text{réaction}}$ [11]). A basse énergie, $E_p \leqq 5.5$ MeV, et pour $A \leqq 120$, Albert [13]) a comparé les sections efficaces totales, en négligeant la diffusion inélastique. Les calculs sont faits dans le modèle optique de Bjorklund et Fernbach (avec les paramètres $a = 0.65 f$, $r_0 = 1.25 f$, $b = 0.98 f$, où l'on a $f = 10^{-13}$ cm). L'accord est satisfaisant.

2. Méthodes expérimentales

2.1. CIBLES

Le praséodyme a été utilisé sous forme d'oxyde à l'état très pur (Johnson Mattey). Cet oxyde est déposé par évaporation sous vide sur de l'aluminium de 10 μm †. Le dépôt est évalué à 600 μg/cm^2 par pesée. Nous préparons à l'aide de ce dépôt un empilement de cibles, séparées entre elles par 20 μm d'aluminium.

2.2. IRRADIATIONS

Nous utilisons le faisceau sorti de protons du Cyclotron de Saclay, l'énergie maximum étant 11.1 MeV. Pour réduire l'énergie du faisceau, nous plaçons entre les cibles des écrans d'aluminium [14]). Pour tenir compte de l'absorption dans le dépôt de praséodyme, nous utilisons, comme relation énergie-parcours, celle de l'élément le plus voisin (Ag) dans la table [14]). Il s'agit là d'une correction très faible. Toutes les irradiations sont courtes (quelques minutes) avec des faisceaux dont l'intensité était de l'ordre de 0.2 μA.

---

† Nous remercions Madame Bourrasse-Marcay pour la préparation des cibles.

2.3. MONITORAGE

Pour connaître le nombre de protons qui ont frappé l'empilement, nous utilisons la fonction d'excitation ^{63}Cu(p, n)^{63}Zn qui est bien connue [15,16]). Une feuille pesée de Cu naturel de 2mg/cm^2 environ recouvre tout l'empilement. A 11.1 MeV nous avons utilisé la valeur σ(p, n) = 500 mb. De la mesure absolue de l'activité de la feuille de Cu nous déduisons le nombre total de protons qui ont frappé la cible pendant l'irradiation.

2.4. MESURES ABSOLUES

Dans cette expérience, il a fallu mesurer de façon absolue a) l'activité β^+ de ^{63}Zn, et b) l'activité X_K (38 keV) de ^{141}Nd. Pour la première mesure, nous utilisons un compteur proportionnel 4π; pour la seconde, un spectromètre à scintillations à NaI (Harshaw) étalonné de façon absolue entre 30 keV et 1 MeV à l'aide de radioéléments émetteurs β et γ de schémas connus; le nombre de désintégrations est obtenu à l'aide d'un compteur proportionnel 4π. Cet étalonnage absolu fera l'objet d'une publication ultérieure. Disons toutefois que l'étalonnage absolu et direct du spectromètre évite de multiples corrections difficiles à évaluer.

2.5. MESURES

Aucun traitement chimique ici n'est nécessaire, car la raie X_K de ^{141}Nd sort parfaitement du fond Compton des activités parasites dues à l'activation de l'aluminium et de l'oxygène. Après l'irradiation, l'activité X_K (38 keV) de chaque feuille est suivie dans le temps. La décroissance X_K ne présente qu'une seule période: celle de ^{141}Nd(2.5 h).

2.6. SCHÉMAS

a) ^{63}Zn : 93 % β^+; 7 % EC table des isotopes [17]).

b) ^{141}Nd : 2 % β^+; 98 % EC; nous avons utilisé le schéma présenté par H. L. Polack *et al.* [18]).

2.7. RÉSULTATS

La fig. 1 présente les valeurs obtenues. La reproductivité des résultats est meilleure que 10 %. Tous les points de la courbe subissent les mêmes erreurs (évaluation par pesée du dépôt de Pr, monitorage, schéma de ^{141}Nd, calibration absolue du spectromètre γ). Les erreurs statistiques sont ici complètement négligeables, l'activité étant importante, c'est à dire que la forme de la courbe est exacte à une translation près. Les erreurs possibles (sauf celles concernant le schéma de ^{141}Nd) pourraient atteindre, selon nos évaluations, ±10 %. La découverte récente [19]) d'un état isomère de vie courte de ^{141}Nd n'influe pas sur les valeurs.

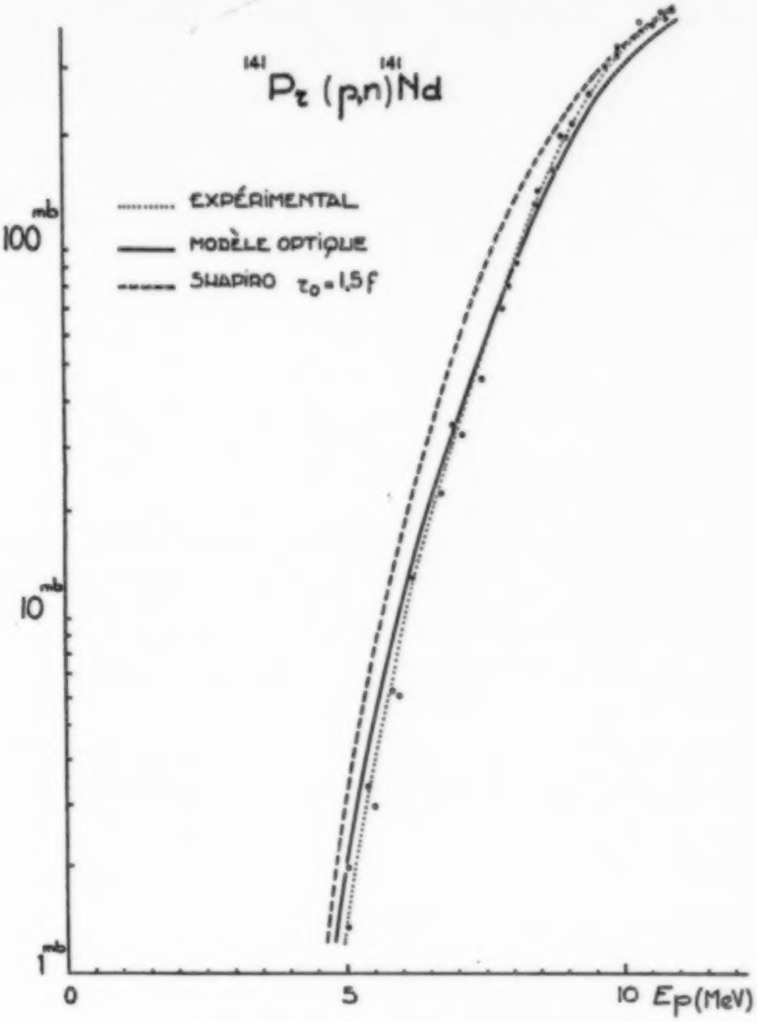

Fig. 1. La section efficace de ^{141}Pr(p, n)^{141}Nd.

3. Comparaison avec la Théorie

Les calculs de $\sigma_{\text{réaction}}$ ont été effectués dans le cadre du modèle optique. Nous avons utilisé le potentiel de F. B. Bjorklund et S. Fernbach 20)

$$U = V\rho(r) + iWq(r) + \frac{A\hbar^2}{4m^2c^2}\frac{V}{r}\frac{\mathrm{d}\rho}{\mathrm{d}r}\,\sigma\cdot 1 + V_c,$$

avec

$$\rho(r) = [1+\exp(r-R_0/a)]^{-1}, \quad q(r) = \exp[-(r-R_0)^2/b^2], \quad R_0 = r_0A^{\frac{1}{3}}.$$

Le potentiel coulombien utilisé est celui d'une sphère de rayon R_0 uniformément chargée. Le potentiel spin-orbite est celui de Thomas, multiplié par un facteur $A\,(E_p)$; les variations de V, W, A, en fonction de l'énergie des particules incidentes, ont été tirées du rapport de F. Bjorklund et S. Fernbach 21)), avec $a = 0.65\,f$, $r_0 = 1.25\,f$, $b = 1f$ (f étant 10^{-13} cm).

Nous avons pris les valeurs suivantes pour le potentiel imaginaire (avec $V = 45$ MeV) †:

E_p (MeV)	5	6	7	8	9	10	11
W (MeV)	8.25	8.7	9.2	9.6	9.7	9.8	10

Nous avons reporté sur la fig. 1 les résultats de $\sigma_{\text{réaction}}$ obtenus avec le modèle optique et aussi ceux de Shapiro 3) avec le modèle du noyau noir, le meilleur accord étant obtenu avec $r_0 = 1.5\,f$.

4. Conclusion

Les paramètres utilisés dans le modèle optique pour interpréter les résultats des diffusions élastiques permettent également d'interpréter les résultats pour les sections efficaces de réaction.

Nous remercions M. Guillou qui a effectué les calculs à la machine Ferranti de Saclay et M. Beurtey qui nous a indiqué la programmation du modèle optique.

Remarque: Des calculs ont montré que la section efficace de réaction donnait plus d'information sur la forme que sur la profondeur du potential imaginaire (à paraître dans Nuclear Physics).

† Les valeurs $W = 8.25$ MeV et $V = 45$ pour $E_p = 5$ MeV ont été utilisées comme étant les meilleures par R. D. Albert 13) pour obtenir les sections efficaces de réaction sur des noyaux de masses comprises entre $A \approx 60$ et $A \approx 120$ avec $E_p \leqq 5.5$ MeV. Le potentiel utilisé suppose une symétrie sphérique au noyau cible. ^{141}Pr a un nombre magique de neutrons égalant 82 et son moment quadrupolaire est très faible (−0.05) 22).

Bibliographie

1) J. P. Blaser, F. Boehm, P. Marmier et P. Scherrer, Helv. Phys. Acta **24** (1951) 441
2) H. G. Blosser et T. H. Handley, Phys. Rev. **100** (1955) 1340
3) M. M. Shapiro, Phys. Rev. **90** (1953) 171
4) R. Nakasima et H. Watanabe, Progr. Theor. Phys. Japan **21** (1959) 462
5) A. H. Wapstra, Physica, **21** (1955) 367
6) R. M. Eisberg, C.I.P.N. Paris (Juillet 1958) p. 36
7) A. E. Glassgold, C.I.P.N. Paris (Juillet 1958) p. 23
8) Albert, Anderson, Wong, McClure et Walker, Wash. 1026, p. 59
9) A. M. Lane et J. E. Lynn, Nuclear Physics, **11** (1959) 646
10) J. Olkowsky, I. Gratot, M. Le Pape et L. Cohen, J. Phys. Radium **11** (1960) 405
11) B. L. Cohen et A. G. Rubin, Phys. Rev. **114** (1959) 1143
12) T. J. Gooding, Nuclear Physics **12** (1959) 241
13) R. D. Albert, Phys. Rev. **115** (1959) 925
14) Aron et Hoffman, A.E.C.U. 663
15) S. N. Ghoshal, Phys. Rev. **80** (1950) 939
16) H. A. Howe, Phys. Rev. **109** (1958) 2083
17) D. Strominger, J. M. Hollander et G. T. Seaborg, Rev. Mod. Phys. **30** (1958) 634
18) H. L. Polack, W. Shoo, B. L. Shram, R. K. Gengis et R. Lieshout, Nuclear Physics **5** (1958) 271
19) R. A. James et C. D. Birgham, Phys. Rev. Letters **4** (1960) 103
20) F. Bjorklund et S. Fernbach, Phys. Rev. **109** (1958) 1295
21) F. Bjorklund et S. Fernbach, UCRL 5028 (1958)
22) M. G. Mayer et J. H. Jensen, Elementary theory of nuclear shell structure (Wiley, New York 1955) p. 79

4.E

Nuclear Physics **23** (1961) 169—172; ©*North-Holland Publishing Co., Amsterdam*

Not to be reproduced by photoprint or microfilm without written permission from the publisher

ASYMMETRY IN DOUBLE MOTT SCATTERING AND ABSOLUTE VALUES OF BETA-ELECTRON LONGITUDINAL POLARIZATION

P. E. SPIVAK, L. A. MIKAELYAN, I. YE. KUTIKOV and V. F. APALIN

I. V. Kurchatov Atomic Energy Institute, Moscow, USSR

Received 5 September 1960

Abstract: Asymmetry values of double unpolarized electron scattering on gold are measured. Absolute values of the longitudinal polarization of β-electrons of P^{32}, In^{114}, Au^{198}, Ho^{166}, Lu^{177} and Sm^{153} are obtained on the basis of the data of this investigation and measurements performed by the present authors before.

Differences in the magnitude of longitudinal polarization up to 12 % [1, 2]) were detected by relative measurements of the longitudinal polarization of β-electrons emitted in the decay of P^{32}, Sm^{153}, Lu^{177}, Ho^{166}, In^{114} and Au^{198}. This showed that there are deviations from the predicted value of polarization equal for electrons to $-v/c$. The range of these deviations was obtained from the absolute measurements of the polarization of electrons of Sm^{153} [2]). Longitudinal electron polarization was converted into transverse polarization in crossed magnetic and electric fields and was determined by the asymmetry of scattering on gold from the relation

$$\langle\sigma\rangle = \frac{1+I_L/I_R}{1-I_L/I_R}\,\frac{1}{S},$$

where $\langle\sigma\rangle$ is the degree of polarization, I_R and I_L are the intensities of right and left scattering, and S is a function of the angle, energy and charge. Taking account of the values of S calculated by N. Sherman [3]) we found that the value of polarization differed from the value $-v/c$ up to 12 to 15 % in the case of Ho^{166} and In^{114}.

As was noted before [1, 2]), it is necessary to have reliable values of the function S to be able to pass a final judgement on the magnitude of polarization deviations from the quantity $-v/c$. Relevant experimental data available at present are insufficiently accurate in most cases and there are no such data at all for the angles and energies of interest to us.

For this reason we had to measure the quantity S through double scattering of unpolarized electrons on gold. Following below is a short description of the set-up and results for 245 and 290 keV and the scattering angles $\theta_1 = \theta_2 = 120°$. At present we are performing measurements in the range 50 to 250 keV and between scattering angles 90° and 150°. A more detailed description of the investigation will be published at a later date.

The geometry of the experiment is shown in fig. 1. A beam of accelerated electrons (2) entered, after passing a system of diaphragms, a chamber where the first scatterer (1) was installed. The second scatterer (4) was installed in a separate chamber at a distance of ≈ 1 m from the first one. Secondary scattered electrons were detected with end-window Geiger counters (3) installed at a distance of some 20 cm from the second scatterer. To decrease the scattering off the walls of the instrument, chamber of large linear dimension (about 400 mm) were chosen and their inner surface was coated with graphite-faced plexiglass. A careful study of the scattering effect of electrons off the walls of the first chamber showed that under the conditions of the experiment the relative number of these electrons hitting the second scatterer amounted to $(0.4 \pm 0.2)\%$. The effect of scattering in the second chamber does not exceed 0.25 %.

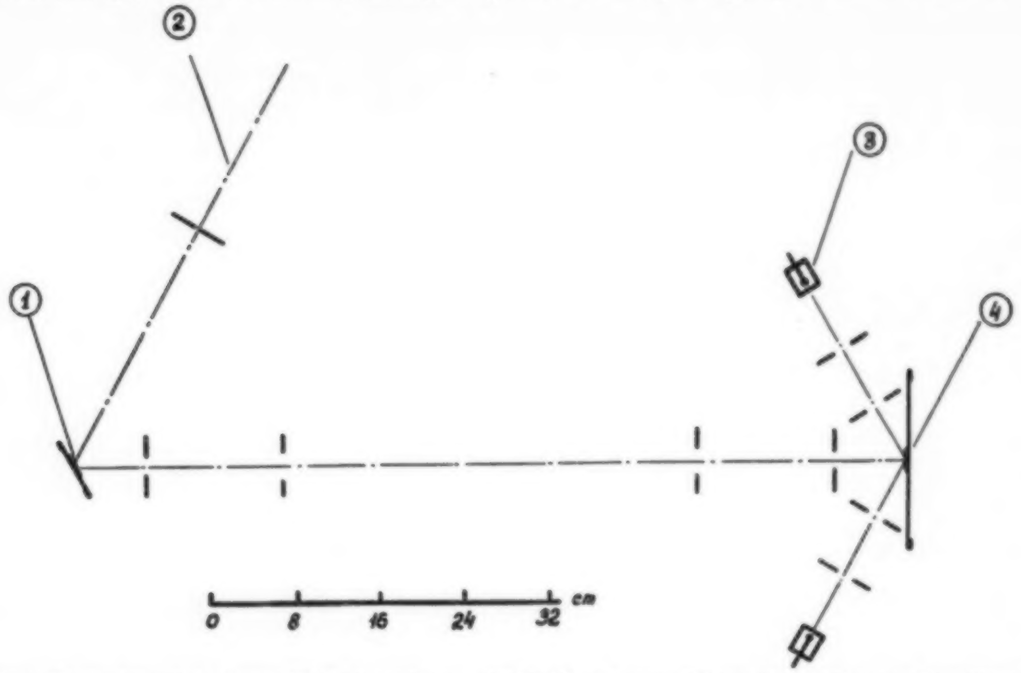

Fig. 1. Experimental set-up: (1) first scatterer, (2) incident beam, (3) counters, (4) second scatterer

Measurements of the energy spectrum of electrons showed that the second scatterer was hit by electrons with the straggling of energies at a semi-height of the line equal to ±1.5 %. The apparatus asymmetry was excluded by replacing the first scatterer of gold with a scatterer of aluminium ≈ 1.4 mg/cm² thick. Since electrons scattered by aluminium also possess a certain degree of polarization the quantity measured in experiment differs from S^2_{Au} and is equal to $S^2_{\mathrm{Au}}(1-S_{\mathrm{Al}}/S_{\mathrm{Au}})$. According to N. Sherman $S_{\mathrm{Al}}/S_{\mathrm{Au}} = 0.1$.

The effect of multiple scattering in scatterers was determined through measurements with first and second scatterers of different thickness. Altogether 4 first and 4 second scatteres were used with thickness ranging from 70 to 300 mkg/cm^2. The statistical accuracy of each measurement of the quantity S^2 amounted to ±3 %. The rate of counting usually amounted to 500 to 1500 pulses per min and the relative background effect did not exceed 5 %. The following corrections were introduced into the experimental values:

a) scattering off the walls of the first chamber (0.4±0.2) %;
b) scattering off the scatterer mounts: from 2 to 4 % depending on the thickness of a scatterer; and
c) the finiteness of observation angles: 0.5 %.

The resulting values are represented in table 1.

TABLE 1

Corrected values of S (S/S_T denotes the ratio of experimentally measured values to those obtained on the basis of N. Sherman's tables)

Energy of electrons	245 keV	290 keV
S^2	0.168±4 %	0.161±4 %
S	0.411±2 %	0.401±2 %
S/S_T	0.960±2 %	0.941±2 %

The results obtained show that the absolute values of longitudinal polarization represented in (2) should be increased by 5 %.

In the present investigation we were also able to find experimentally the magnitude of electron depolarization on the way from the source to the scatterer in the crossed field system used in ref. [2]). The measurements were performed in the following sequence. First the scattering asymmetry was found for a certain pair of scatterers. Then a crossed field system was placed between the scatterers, and measurements of asymmetry were repeated, the strength of the fields being selected so that the spin rotational angle amounted to 180°. The electron energy in these measurements was 175 keV for which the 180° spin rotation is still possible under our conditions.

The measurements showed that depolarization on the way from the source to the scatterer in the crossed field system decreases the magnitude of asymmetry by (2±2) % in accordance with an estimate made before [2]).

Table 2 represents the absolute values of the electron longitudinal polarization at 300 keV with allowances for the results of the present investigation. The

TABLE 2

Values of the electron longitudinal polarization (in v/c units)

Isotope	P^{32}	Sm^{153}	Lu^{177}	Ho^{166}	In^{114}	Au^{198}
Polarization	1.02	0.97	0.92	0.91	0.93	0.94
Error of relative measurements (%)	1.5		1.5	1.5	2.5	2.0

errors listed are those of relative measurements. The error of absolute measurements amounts to 3.3 %.

Thus the investigation has shown that deviations in the degree of longitudinal polarization from the quantity $-v/c$ are not exceptional phenomena as was assumed before. These deviations in the cases we investigated reached 8 or 9 %. The deviation detected should probably be ascribed to the effect of the nuclear structure.

References

1) L. A. Mikaelyan and P. E. Spivak, JETP **37** (1959) 1168
2) P. E. Spivak and L. Mikaelyan, JETP (in the press); Nuclear Physics (in the press)
3) N. Sherman, Phys. Rev. **103** (1956) 1601

10.A Nuclear Physics 23 (1961) 173—176; © North-Holland Publishing Co., Amsterdam

NEWS ITEMS

THE INSTITUTE OF PHYSICS AND THE PHYSICAL SOCIETY AWARDS

(16 November 1960)

The Council of The Institute of Physics and The Physical Society which recently amalgamated has made the following Awards:

The Duddell Medal to Dr. J. B. Adams, the Director-General of C.E.R.N. (the European Organization for Nuclear Research), for his leadership of that team.

The Charles Vernon Boys Prize to Professor A.W. Merrison of the University of Liverpool for his distinguished research in experimental physics.

The Charles Chree Medal and Prize to Dr. S. E. Forbush of The Carnegie Institution of Washington for his distinguished work on the cosmic radiation.

RUTHERFORD JUBILEE INTERNATIONAL CONFERENCE AT MANCHESTER

(4—8 September 1961)

To commemorate the discoveries of Rutherford at Manchester and in particular the fiftieth anniversary of the Rutherford scattering law, an international conference on nuclear physics is to be held here from September 4th to September 8th, 1961. This conference, which is to deal primarily with low and medium energy phenomena, is sponsored by the International Union of Pure and Applied Physics. The Royal Society, The Institute of Physics and the Physical Society, and the University of Manchester.

A programme has been provisionally set up and this is arranged below according to the various sessions that are planned. Several explanatory remarks are added to indicate the scope of each session as envisaged by the Organising Committee.

PROVISIONAL PROGRAMME

Session I. *High Energy Investigations of Nuclei*

This session is meant to deal with those topics of high-energy physics that are relevant to the study of nuclear properties. Among those to be considered are: (a) the nucleon-nucleon interaction (b) the scattering of electrons by nucleons and nuclei and (c) the interactions of hyperons with nuclei.

Session II. *Collective Motion in Nuclei*

It is intended to concentrate on the collective aspects of nuclei as they relate to the superconducting ground state and to collective oscillations.

Session III. *The Nuclear Ground State*

The properties of the ground-state of the nucleus are to be discussed with special consideration to be given to (a) the nuclear surface, (b) the momentum distribution in the nucleus, and (c) the many-body problem (Brueckner theory).

Session IV. *Rutherford Commemorative Session*

This session will be devoted to the experiences of Rutherford at Manchester and will include personal reminiscences by several eminent colleagues and students of Rutherford during his period in Manchester, together with an assessment of his contributions to physics.

Session V. *Direct Interactions*

The emphasis in this session will be on the mechanism of direct interactions as revealed by theory and experiment.

Session VI. *Special Topics*

Two invited papers are to be presented at this session: (a) limitations and needs in instrumentation for nuclear physics, (b) nuclear aspects of astrophysics. It is proposed that these two contributions, which refer to aspects lying on the border-line of nuclear physics, be of larger duration than others at this conference and that the invited speakers entirely concentrate on their own ideas without necessarily fitting into those of others.

Session VII. *Weak Interactions*

This session is meant to deal with those aspects of weak interactions that are relevant to the study of nuclei and will cover the topics of (a) β-decay and (b) muon-capture by nuclei.

Session VIII. *Open Session*

It is not intended to assign a programme for this session until the time of the conference, at which time the session will be available for a discussion of any new developments of outstanding general interest that may occur in the intervening period. Alternatively, it may be used for splinter sessions of specialists for discussion of specific problems.

REMARKS

Each session will have invited speakers who will select from the subjects those aspects in which they, themselves, are particularly interested and which are of current interest. Delegates to the conference are invited to address communications to the conference — more information concerning the format of these contributions will be given in the near future. The speakers, if they wish, may make use of these contributions in their talks. There will be three invited papers per session, each one of which will be of thirty minutes duration, thus leaving half the time of each session for discussion.

It is expected that the communications will be in the hands of the Organising Committee roughly six weeks before the conference, and it is hoped that they will be made available in some form to all the delegates before the conference, so as to allow for a richer discussion and easy contact outside the sessions. It is further planned that some of the contributions together with a verbatim account of the proceedings will appear in printed form some time shortly after the Conference.

We are also trying to arrange a short conference on nuclear instrumentation immediately following the main conference.

More detailed information concerning the invited speakers, the topics to be covered in individual sessions, the registration and accommodation of delegates the submission of communications, planned social activities, and other points will be included in a future notice which will be mailed in January 1961.

Those wishing to attend this conference are requested to ask for further information from the Conference Secretary, Dr. L. J. B. Goldfarb, Rutherford Jubilee International Conference, Physics Department, The University of Manchester, England.

ORGANISING COMMITTEE

Chairman: Professor B. H. Flowers.
General Secretaries: Dr. L. J. B. Goldfarb, Dr. J. E. Bowcock.
Members: Dr. J. B. Birks, Dr. H. J. J. Braddick, Dr. J. Calvert, Dr. A. Herzenberg, Dr. A. A. Jaffe, Dr. F. Mandl, Dr. J. Newton.

Cooperation between IAEA and ENEA

In September 1960 an agreement was concluded for collaboration between the International Atomic Energy Agency and the European Nuclear Energy Agency. This formalization of a collaboration agreement had been preceded by a long period of close cooperation on the informal working-level. Although the two organizations have virtually identical aims their methods necessarily differ: ENEA serves a realatively homogeneous group of countries, whereas IAEA's distinctive feature is its broad and heterogeneous membership. The emphasis of the latter's work is thus concentrated on aiding the world-wide exchange of knowledge and technological know-how, on channelling technical assistance and on supplying source and fissile materials and equipment rather than on the construction of joint large industrial installations or pilot plants in which ENEA had been so successful.

It is particulary stressed that there is need for harmony between regional and world-wide health and safety regulations and practices in which field both organizations have taken important initiatives: the development of regulations to govern international transport of radioactive materials, the implementation of the scientific recommendations of disposal practices for radioactive wastes into the sea and the work now in progress on simple and practical directives on maximum possible radiation exposure levels in the atomic industry. The two organizations have already collaborated fully in all these fields. Mutual access will be provided to the technical facilities available — in the case of ENEA joint enterprises, in the case of IAEA international laboratories.

Karelsruhe Photonuclear Conference

(18—22 August 1960)

The Karlsruhe conference on photonuclear reactions was sponsored by the Kernforschungszentrum, Karlsruhe, and the Heidelberg Akademie der Wissenschaften, under the chairmanship of Professors P. Brix, Darmstadt, and J. H. D. Jensen, Heidelberg. The conference followed the pleasant custom of last year's Gordon conference in having morning and evening meetings, with the afternoon free. The latter could be used to advantage, since the conference site was beautifully chosen, at a sport school with a view over the Rhein plain.

Speakers and subjects of talks were: R. Malvano, Recent results on photonuclear reactions of light nuclei; G. E. Brown, Recent developments in the theory of photonuclear reactions; W. C. Barber, Comparison of electron-induced and gamma-induced reactions; J. H. Smith and M. Danos, Photonuclear reactions above the giant resonance; H. W. Koch, New experimental techniques; G. Dearnaley, The n—p and surface barrier detectors. P. T. Demos chaired a panel discussion on "What can we learn from the study of photonuclear reactions?", and A. Kerman presented a summary of the conference.

Contributions submitted to the Conference were available in a bound volume to all participants upon arrival, enhancing the value of discussions, since one had all of the data at hand. In this and in other matters, the secretary, Dr. K. H. Lindenberger, did a thoroughly efficient job.

This was the first photonuclear conference to be held in Europe. In view of its success there was a general feeling that successive conferences should be held alternately in the U.S. and in Europe.

G. E. Brown

1.C

Nuclear Physics **23** (1961) 177—199; © *North-Holland Publishing Co., Amsterdam*

Not to be reproduced by photoprint or microfilm without written permission from the publisher

GROUP THEORY OF HARMONIC OSCILLATORS

(II). The Integrals of Motion for the Quadrupole-Quadrupole Interaction

V. BARGMANN[†]
Palmer Physical Laboratory, Princeton University, Princeton, N.J.
and
M. MOSHINSKY[††]
Instituto de Física, Universidad de México, e Instituto Nacional de la Investigación Científica, México, D.F.

Received 8 August 1960

Abstract: In the present paper we obtain $3N$ integrals of motion associated with a system of N particles moving in a common harmonic oscillator potential and having a quadrupole-quadrupole interaction. We obtain also the eigenvalues of these $3N$ integrals of motion by applying the corresponding operators to the reduced canonical wave function defined in a previous paper. The reduced canonical wave function is constructed explicitly and it is shown to give a basis for all the irreducible representations of the three dimensional unitary unimodular group. One of the integrals of motion obtained is essentially the quadrupole moment projected along the direction of the angular momentum and its eigenvalues are discussed in detail.

1. Introduction

In the previous paper of this series [1] (to be referred to in what follows as (I)), we discussed the problem of a system of N particles in a common harmonic oscillator potential with a quadrupole-quadrupole interaction. The eigenvalues for the hamiltonian of this problem were obtained and shown to be a superposition of rotational bands. Because of the interest this problem has for the collective model of the nucleus [2,3], one would like to give its complete quantum mechanical description. This implies first obtaining $3N$ integrals of motion of the problem and then determining the corresponding eigenfunctions.

In this paper we shall obtain $3N$ integrals of motion and show what are the corresponding eigenvalues. We shall make full use of the fact that the integrals of motion commute with the transfer operators defined in (I), so we can obtain the eigenvalues by applying the integral of motion operators only to the canonical wave function ((I), eq. (54)).

Using the notation of (I), we denote our hamiltonian by

$$\mathscr{H} = H-(\mathbf{Q}^2/\mathscr{J}). \tag{1}$$

[†] Present address: Physics Dept. Brandeis University, Waltham, Mass.

[††] Alfred P. Sloan Research Fellow.

February (1961)

where H is the hamiltonian for N three dimensional oscillators, $\mathbf{Q}^2$ is the quadrupole-quadrupole interaction, and $\mathscr{J}$ a proportionality constant that could be interpreted as a moment of inertia. In terms of the creation and annihilation operators η_{ir}, ξ_{js} defined in (I) eq. (2), we have

$$H = \sum_{r=1}^{N} \sum_{i=1}^{3} \eta_{ir}\xi_{ir} = \sum_{r=1}^{N} \boldsymbol{\eta}_r \cdot \boldsymbol{\xi}_r, \tag{2}$$

$$\mathbf{Q}^2 = \sum_{i,j=1}^{3} Q_{ij}Q_{ij}, \tag{3}$$

with

$$Q_{ij} = \tfrac{1}{2}\sum_{r=1}^{N} (\eta_{ir}\xi_{jr}+\eta_{jr}\xi_{ir}) - \tfrac{1}{3}\sum_{r=1}^{N} (\boldsymbol{\eta}_r \cdot \boldsymbol{\xi}_r)\delta_{ij}. \tag{4}$$

The quadrupole-quadrupole interaction Q_{ij} is equivalent to the Q_τ of eq. (I) (66c), but here it is given as a second rank tensor in cartesian components, instead of the spherical components of the previous definition.

It was shown in (I) eq. (67) that the quadrupole-quadrupole interaction could be expressed as

$$\mathbf{Q}^2 = G - \tfrac{1}{3}H^2 - (N-3)H - \tfrac{1}{2}\boldsymbol{\lambda}^2, \tag{5}$$

with H given by (2), G being the Casimir operator for the N dimensional unitary group U_N,

$$G = \sum_{r,s=1}^{N} (\boldsymbol{\eta}_r \cdot \boldsymbol{\xi}_s)(\boldsymbol{\eta}_s \cdot \boldsymbol{\xi}_r), \tag{6}$$

and $\boldsymbol{\lambda}$ the total angular momentum

$$\boldsymbol{\lambda} = -i\sum_{r=1}^{N} (\boldsymbol{\eta}_r \times \boldsymbol{\xi}_r). \tag{7}$$

The equation (5) could be checked directly using the definitions (3)—(7).

Once we write $\mathbf{Q}^2$ in the form (5), we obtain the following obvious integrals of motion:

1) The hamiltonians H_r associated with each particle,

$$H_r = \boldsymbol{\eta}_r \cdot \boldsymbol{\xi}_r, \quad r = 1, 2, \ldots, N, \tag{8}$$

clearly commute with H, $\boldsymbol{\lambda}$, and also with the Casimir operator, as we have the same number of creation and annihilation operators for each r in G. Therefore H_r commutes with $\mathscr{H}$.

2) The angular momentum $\boldsymbol{\lambda}$ commutes with H_r and G as these are scalar operators. This means that we could take $\boldsymbol{\lambda}^2$ and λ_z as integrals of motion.

3) The Casimir operator G commutes with $\mathscr{H}$ and the previous integrals of motion.

We have then $N+3$ commuting integrals of motion H_r $(r=1,\dots,N)$, G, $\boldsymbol{\lambda}^2$, λ_z, so that $2N-3$ remain to be found. To find them we first remark that H_r, G are obviously invariant under the 3 dimensional unitary group $\mathscr{U}_3$ affecting the coordinate indices, i.e. they remain invariant under the transformation

$$\eta_{is} = \sum_{i'=1}^{3} \mathscr{U}_{ii'}\eta'_{i's}, \quad \xi_{is} = \sum_{i'=1}^{3} \mathscr{U}^{*}_{ii'}\xi'_{i's}, \tag{9}$$

where $||\mathscr{U}_{ii'}||$ is a 3×3 unitary matrix independent of the particle index s. This suggests that for the other integrals of motion, we should look into the expressions formed from η_{ir}, ξ_{js} that are invariant under $\mathscr{U}_3$. Once we obtain these invariant operators, we shall check directly that they commute between themselves and with the previous integrals of motion. As in our first paper, we would like to remark that while the concepts of group theory underlie all of the present developments, the discussion in this paper will be carried out entirely in terms of elementary algebraic procedures.

2. The Integrals of Motion

To obtain the invariants under $\mathscr{U}_3$ that can be constructed from η_{ir}, ξ_{js}, we start by defining the operator

$$\mathscr{C}^{(p)}_{ij} = \sum_{r=1}^{p} \eta_{ir}\xi_{jr}, \quad p = 1, 2, \dots, N. \tag{10}$$

If we considered an arbitrary polynomial function $P(\eta_{ir})$ of the creation operators for the first p particles, we could easily see that under an infinitesimal unitary transformation of the η_{ir}, the new polynomial $P(\eta'_{ir})$ will differ from $P(\eta_{ir})$ just by a linear combination of the operators $\mathscr{C}^{(p)}_{ij}$ $(i, j = 1, 2, 3)$ acting on $P(\eta_{ir})$. We can interpret then $\mathscr{C}^{(p)}_{ij}$ as the operators associated with the infinitesimal unitary transformations of the group $\mathscr{U}_3$ acting on states of p particles

We would like to obtain operators commuting with $\mathscr{C}^{(p)}_{ij}$ and this suggests that we consider the invariants that can be formed from the matrix $||\mathscr{C}^{(p)}_{ij}||$, as being invariant under a general unitary transformation $\mathscr{U}_3$, they will also be invariant under infinitesimal unitary transformations. One of the invariants of $\mathscr{C}^{(p)}_{ij}$ is the trace, and from (10), we have

$$\operatorname{tr} ||\mathscr{C}^{(p)}_{ij}|| = \sum_{r=1}^{p} H_r \equiv H^{(p)}, \tag{11}$$

so that the trace will only give the obvious integrals of motion discussed in the previous section. It is convenient therefore to deal with a matrix of trace zero, and so we introduce $\mathscr{D}^{(p)}$ by the definition

$$\mathscr{D}^{(p)} = ||\mathscr{D}^{(p)}_{ij}|| = ||\mathscr{C}^{(p)}_{ij} - \tfrac{1}{3}H^{(p)}\delta_{ij}||. \tag{12}$$

In group theoretical language, the trace zero in the matrix emphasizes that we are not interested in the full three dimensional unitary group $\mathscr{U}_3$, but only in its unimodular subgroup $S\mathscr{U}_3$.

The invariants of the 3×3 matrix $\mathscr{D}^{(p)}$ are the coefficients of the powers of x in the expression

$$\det(\mathscr{D}_{ij}^{(p)}-x\delta_{ij}) = -x^3+\tfrac{1}{2}x\Gamma^{(p)}+\tfrac{1}{6}\Delta^{(p)}. \tag{13}$$

As the $\mathscr{D}_{ij}^{(p)}$ are non-commuting operators, the coefficients of the powers of x have been symmetrized and making use of the fact that $\operatorname{tr}\mathscr{D}^{(p)} = 0$, we obtain

$$\Gamma^{(p)} = \sum_{i,j=1}^{3} \mathscr{D}_{ij}^{(p)}\mathscr{D}_{ji}^{(p)}, \tag{14}$$

$$\Delta^{(p)} = \sum_{i,j,k}\ \sum_{i',j',k'} \varepsilon_{ijk}\varepsilon_{i'j'k'}\mathscr{D}_{ii'}^{(p)}\mathscr{D}_{jj'}^{(p)}\mathscr{D}_{kk'}^{(p)}, \tag{15}$$

where ε_{ijk} is the completely antisymmetric tensor in three dimensions.

From the definition (10, 12) of $\mathscr{D}_{ij}^{(p)}$, and using the commutation relations between η_{ir} and ξ_{js} given in (I), eq. (3), we can rewrite $\Gamma^{(p)}$, $\Delta^{(p)}$ in the form

$$\Gamma^{(p)} = \sum_{r,s,=1}^{p} (\eta_r\cdot\xi_s)(\eta_s\cdot\xi_r)-\tfrac{1}{3}[H^{(p)}]^2-(p-3)H^{(p)}, \tag{16}$$

$$\begin{aligned}\Delta^{(p)} = &\sum_{r,s,t=1}^{p} [(\eta_r\times\eta_s)\cdot\eta_t][(\xi_r\times\xi_s)\cdot\xi_t]\\ &+[H^{(p)}+3]\Gamma^{(p)}-2H^{(p)}[H^{(p)}+2]-\tfrac{2}{9}[H^{(p)}]^3.\end{aligned} \tag{17}$$

The discussion of the previous paragraphs suggests then that $\Gamma^{(p)}$, $\Delta^{(p)}$ commute with $\mathscr{C}_{ij}^{(p)}$ and this is checked directly in Appendix 1 of this paper. Now let us consider $\mathscr{C}_{ij}^{(q)}$ with $q \geqq p$. As $\mathscr{C}_{ij}^{(q)}$ can be written as

$$\mathscr{C}_{ij}^{(q)} = \mathscr{C}_{ij}^{(p)}+\sum_{r=p+1}^{q}\eta_{ir}\xi_{jr}, \tag{18}$$

we see that the second part on the right hand side commutes with $\Gamma^{(p)}$, $\Delta^{(p)}$ as it contains only operators for particles $r = p+1, \ldots, q$. Therefore we have

$$[\Gamma^{(p)}, \mathscr{C}_{ij}^{(q)}] = [\Delta^{(p)}, \mathscr{C}_{ij}^{(q)}] = 0,\ q \geqq p. \tag{19}$$

But from eqs. (12), (14), (15) we see that $\Gamma^{(q)}$, $\Delta^{(q)}$ are respectively second and third order homogeneous polynomials in $\mathscr{C}_{ij}^{(q)}$ so that clearly

$$[\Gamma^{(p)}, \Gamma^{(q)}] = [\Gamma^{(p)}, \Delta^{(q)}] = [\Delta^{(p)}, \Gamma^{(q)}] = [\Delta^{(p)}, \Delta^{(q)}] = 0, \tag{20}$$

where we do not even need to restrict ourselves to $q \geqq p$. Furthermore, from the form (16, 17) of $\Gamma^{(p)}$, $\Delta^{(p)}$ we see that for each particle index r there are as many creation as annihilation operators and therefore,

$$[H_r, \Gamma^{(p)}] = [H_r, \Delta^{(p)}] = 0,\quad r, p = 1, \ldots, N. \tag{21}$$

Finally, the operators (16, 17) are scalars so they commute also with the total angular momentum $\boldsymbol{\lambda}$. We have then $2N$ new integrals of motion which combined with $N+3$ given in the previous section, seem to give us more than the $3N$ integrals of motion we are looking for.

This excess in the number of integrals of motion is, of course, due to the fact that not all of them are independent. In the first place, from (6) and (16) we see that

$$G = \Gamma^{(N)} + \tfrac{1}{3}\Big(\sum_{r=1}^{N} H_r\Big)^2 + (N-3)\Big(\sum_{r=1}^{N} H_r\Big). \tag{22a}$$

Furthermore, from (8) and (16) we have that

$$\Gamma^{(1)} = \tfrac{2}{3}H_1(H_1+3). \tag{22b}$$

Finally, the first term in (17) is clearly zero for $p = 1, 2$, so that $\Delta^{(1)}, \Delta^{(2)}$ as well as $\Gamma^{(1)}, G$ are not independent integrals of motion. We are left then with $3N-1$ integrals of motion so we are still missing one. Denoting by Ω the missing integral of motion, we would have the $3N$ integrals of motion

$$H_1, \ldots, H_N, \Gamma^{(2)}, \ldots, \Gamma^{(N)}, \Delta^3, \ldots, \Delta^{(N)}, \boldsymbol{\lambda}^2, \lambda_z, \Omega. \tag{23}$$

To obtain Ω, as well as to justify from another standpoint the appearance of $\boldsymbol{\lambda}^2$ as an integral of motion, let us consider the three dimensional orthogonal subgroup $\mathscr{R}_3$ of $\mathscr{U}_3$. Under a unitary transformation $\mathscr{U}$ of $\mathscr{U}_3$, an arbitrary 3×3 matrix $\mathscr{D}$ transforms into a new matrix $\mathscr{D}'$ by the relation

$$\tilde{\mathscr{U}}^* \mathscr{D} \mathscr{U} = \mathscr{D}', \tag{24}$$

where $\sim$ stands for transposed and * for conjugate. The invariants of the matrix $\mathscr{D}$ are the coefficients of the powers of x in an equation similar to (13). If instead of an arbitrary unitary transformation $\mathscr{U}$, we restrict ourselves to the subgroup of orthogonal matrices $\mathscr{R}$, then the relation (24) becomes

$$\tilde{\mathscr{R}} \mathscr{D} \mathscr{R} = \mathscr{D}'. \tag{25}$$

Transposing both sides and combining the transposed equation with (25) we obtain

$$\tilde{\mathscr{R}}(\mathscr{D} \pm \tilde{\mathscr{D}})\mathscr{R} = (\mathscr{D}' \pm \tilde{\mathscr{D}}'), \tag{26}$$

which states the well known fact that under an orthogonal transformation, the symmetric and antisymmetric parts of a matrix transform independently.

Looking now back on the procedure discussed in this section we see clearly that $\mathscr{C}_{ij}^{(N)}$, and therefore also the corresponding $\mathscr{D}_{ij}^{(N)}$ commute with all the integrals of motion (23), except with $\boldsymbol{\lambda}^2$, λ_z and the still unknown Ω. To have functions that commute with $\boldsymbol{\lambda}$, we would need invariants under the three dimensional orthogonal group only. From (26) it is clear therefore that we need to consider invariants associated with the symmetric and antisymmetric part of $\mathscr{D}_{ij}^{(N)}$ which from (4), (7) and (12), are

$$\tfrac{1}{2}[\mathscr{D}_{ij}^{(N)}+\mathscr{D}_{ji}^{(N)}] = Q_{ij}, \tag{27}$$

$$\tfrac{1}{2}[\mathscr{D}_{ij}^{(N)}-\mathscr{D}_{ji}^{(N)}] \equiv \Lambda_{ij} = \frac{i}{2}\sum_{k=1}^{3} \varepsilon_{ijk}\lambda_k. \tag{28}$$

Again the invariants will be given by the coefficients of powers of x in

$$\det(\Lambda_{ij}-x\delta_{ij}), \quad \det(Q_{ij}-x\delta_{ij}). \tag{29}$$

As $||\Lambda_{ij}||$ is antisymmetric and of trace zero, the only invariant not identically zero is

$$\sum_{i,j=1}^{3} \Lambda_{ij}\Lambda_{ji} = \tfrac{1}{2}\boldsymbol{\lambda}^2. \tag{30}$$

As for the symmetric part we have two invariants, one of which $\sum_{i,j}Q_{ij}Q_{ji}$ is nothing else but $\mathbf{Q}^2$, as Q_{ij} is symmetric and, because of (5) and (22a), is not an independent integral of motion. The other invariant is

$$\Phi = \sum_{ijk}\sum_{i'j'k'} \varepsilon_{ijk}\varepsilon_{i'j'k'}Q_{ii'}Q_{jj'}Q_{kk'}. \tag{31}$$

Instead of Φ we shall choose an invariant closely related to it, but which is of much greater interest from a physical standpoint. Let us notice first that

$$\mathscr{D}_{ij}^{(N)} = Q_{ij}+\Lambda_{ij}, \tag{32}$$

so from (15) we can write †

$$\begin{aligned}\Delta^{(N)} = \sum_{ijk}\sum_{i'j'k'} \varepsilon_{ijk}\varepsilon_{i'j'k'}[&Q_{ii'}Q_{jj'}Q_{kk'}\\ &+3\Lambda_{ii'}Q_{jj'}Q_{kk'}+3Q_{ii'}\Lambda_{jj'}\Lambda_{kk'}+\Lambda_{ii'}\Lambda_{jj'}\Lambda_{kk'}].\end{aligned} \tag{33}$$

Because of the antisymmetric nature of $\Lambda_{ii'}$ we see that the second and fourth term in (33) vanish and so we obtain

$$\Phi = \Delta^{(N)}+6\Omega, \tag{34}$$

where Ω is defined as

$$\Omega = -\tfrac{1}{2}\sum_{ijk}\sum_{i'j'k'} \varepsilon_{ijk}\varepsilon_{i'j'k'}Q_{ii'}\Lambda_{jj'}\Lambda_{kk'} \equiv \sum_{i,j=1}^{3} Q_{ij}\lambda_i\lambda_j \tag{35}$$

We can clearly use Ω instead of Φ as an integral of motion and it has a great deal more of a physical significance, as it will be essentially the projection of the quadrupole moment along the direction of the total angular momentum.

From the way $\boldsymbol{\lambda}^2$, Ω were constructed, they clearly commute with all the other integrals of motion and with $\boldsymbol{\lambda}$. We can then denote the last three integrals of motion in (23) as $\boldsymbol{\lambda}^2$, λ_z, Ω were the last one is given by (35).

---

† Because of the ε_{ijk} we can change the order of Λ's and Q's without changing the expression (33).

Once we have obtained 3N integrals of motion, the next problem is to find their eigenvalues, and this will be achieved by applying them to the canonical wave function of (I), eq. (54). In the next section we discuss the eigenvalues of $\Gamma^{(p)}$, $\Delta^{(p)}$ for which we only need the general form ((I), eq. (54)) of the canonical wave functions. We leave the discussion of the eigenvalues of $\boldsymbol{\lambda}^2$ and Ω to section 5 as for these we will need the explicit expression of the canonical wave function derived in section 4.

The completeness of this set of integrals of motion will be taken up when we discuss the explicit procedure for deriving the eigenfunctions, which will be attempted in the next paper of this series.

3. The Eigenvalues of H, Γ, Δ

We showed in (I) eq. (7) that the most general wave function for a system of N particles moving in a common harmonic oscillator potential, could be expressed as a polynomial P of the components of the creation operators η_r ($r = 1, 2, \ldots, N$) acting on the ground state, i.e.

$$\psi = P(\eta_1, \ldots, \eta_N)\,|0\rangle. \tag{36}$$

If ψ is an eigenfunction of the hamiltonians H_r, $r = 1, \ldots, N$, then, as shown in (I), eq. (30) P is a homogeneous polynomial of order h_r in the components of η_r. The non-negative integers h_r are the eigenvalues of H_r, and their sum gives the degree of the homogeneous polynomial P which corresponds to the total energy E of the state.

To discuss the eigenvalues of the remaining integrals of motion, let us start with those integrals of motion that depend on the complete set of N particles and not only on a sub-set of p particles, i.e. let us consider

$$\Gamma, \Delta, \boldsymbol{\lambda}^2, \lambda_z, \Omega, \tag{37}$$

where in this section we shall indicate $\Gamma^{(N)}$, $\Delta^{(N)}$ simply by Γ, Δ.

The integrals of motion (37) are homogeneous polynomials formed from the operators $\mathscr{C}_{ij}^{(N)}$, $i, j = 1, 2, 3$. Because of the definition (10), we see that these operators are obviously invariant under the N dimensional unitary group of transformations U_N affecting the particle indices, i.e. they remain invariant under the transformation

$$\eta_{is} = \sum_{s'=1}^{N} U_{ss'}\eta'_{is'}, \quad \xi_{is} = \sum_{s'=1}^{N} U^{*}_{ss'}\xi'_{is'}, \tag{38}$$

where U is a $N \times N$ unitary matrix independent of the vector index i. We expect therefore that the operators $\mathscr{C}_{ij}^{(N)}$ will commute with the operators C_{rs} associated with the infinitesimal unitary transformations in the N dimensional space of the particle indices. By a reasoning entirely similar to the one outlined in the first paragraph of section 2, we expect the operators C_{rs} to be

$$C_{rs} = \boldsymbol{\eta}_r \cdot \boldsymbol{\xi}_s, \tag{39}$$

and so we have

$$[C_{rs}, \mathscr{C}_{ij}^{(N)}] = 0. \tag{40}$$

The validity of the commutation relation (40) can also be checked straightforwardly by using the commutation relations between η_{ir}, ξ_{js} given in (I) eq. (3).

If we denote by ψ an eigenfunction of the integrals of motion (37), i.e.

$$\Gamma\psi = \gamma\psi, \quad \Delta\psi = \delta\psi, \quad \boldsymbol{\lambda}^2\psi = \lambda(\lambda+1)\psi, \quad \lambda_z\psi = \mu\psi, \quad \Omega\psi = \omega\psi, \tag{41}$$

where γ, δ, $\lambda(\lambda+1)$, μ, ω are the corresponding eigenvalues, then from (40) these eigenvalues also hold for the wave function $(C_{rs}\psi)$. Applying the transfer operators C_{rs} $(r \leqq s = 1, \ldots, N)$ to ψ as many times as necessary, we showed in section 4 of (I) that we could transform ψ into a canonical wave function ψ_{C} of the form

$$\psi_{\mathrm{C}} = [(\boldsymbol{\eta}_1 \times \boldsymbol{\eta}_2) \cdot \boldsymbol{\eta}_3]^{h'_3} \psi_{\mathrm{RC}}, \tag{42}$$

where ψ_{RC} denotes the reduced canonical wave function given by

$$\psi_{\mathrm{RC}} = P(\boldsymbol{\eta}_1, \boldsymbol{\eta}_2)|0\rangle. \tag{43}$$

The polynomial P is now a homogeneous polynomial of the components of the creation operators $\boldsymbol{\eta}_1$, $\boldsymbol{\eta}_2$ only. Denoting by k_1, k_2 the orders of $\boldsymbol{\eta}_1$, $\boldsymbol{\eta}_2$ respectively in P, we have from eqs. (55), (57) of (I) that

$$k_1 = h'_1 - h'_3 = \tfrac{1}{2}\rho + f, \quad k_2 = h'_2 - h'_3 = \tfrac{1}{2}\rho - f. \tag{44a}$$

As the total degree of the polynomial is the energy E, we have

$$E = \rho + 3h'_3, \quad \text{or} \quad \rho = E, E-3, \ldots, \begin{matrix} 2 \\ 1. \\ 0 \end{matrix} \tag{44b}$$

Furthermore, $2f \leqq \rho$ and f is integer or half integer according to whether ρ is even or odd, so combining this with the fact that $k_1 \geqq k_2$ (to be proved in Appendix 2), we obtain

$$f = \tfrac{1}{2}\rho, \tfrac{1}{2}\rho - 1, \ldots, \begin{matrix} \frac{1}{2} \\ 0. \end{matrix} \tag{44c}$$

To obtain the eigenvalues of the operators (41), we need only to apply the operators to the canonical wave functions ψ_{C} of (42). But we can go even further. We first notice that as the triple scalar product in (42) depends only on the first three particles, we can, by using the commutation relation (3) of (I), write its commutator with $\mathscr{C}_{ij}^{(N)}$ as

$$[\mathscr{C}_{ij}^{(N)}, \{(\eta_1 \times \eta_2) \cdot \eta_3\}] = [\sum_{u=1}^{3} (\eta_{iu} \xi_{ju}), \sum_{k,l,m=1}^{3} (\varepsilon_{klm} \eta_{k1} \eta_{l2} \eta_{m3})]$$

$$= \tfrac{1}{6} \sum_{k,l,m=1}^{3} \varepsilon_{klm} [\sum_{u=1}^{3} (\eta_{iu} \xi_{ju}); \sum_{r,s,t=1}^{3} (\varepsilon_{rst} \eta_{kr} \eta_{ls} \eta_{mt})] = \delta_{ij} \{(\eta_1 \times \eta_2) \cdot \eta_3\}. \tag{45}$$

From (45) and the definition (12) of $\mathscr{D}_{ij}^{(N)}$, we conclude therefore that

$$[\mathscr{D}_{ij}^{(N)}, \{(\eta_1 \times \eta_2) \cdot \eta_3\}^{N/3} P(\eta_1, \eta_2)] = \{(\eta_1 \times \eta_2) \cdot \eta_3\}^{N/3} [\mathscr{D}_{ij}^{(N)}, P(\eta_1, \eta_2)]. \tag{46}$$

As all the operators in (41) are functions of $\mathscr{D}_{ij}^{(N)}$, we see from (46) that to obtain their eigenvalues, we have only to apply them to the reduced canonical wave function (43). For the operator Γ this was already done in (I), so that from eq. (59) of (I) and (22a), we have

$$\gamma = \tfrac{1}{6}\rho(\rho+6) + 2f(f+1). \tag{47}$$

To obtain the eigenvalues of Δ, we apply the expression (17) for this operator to (43). The fist term of (16) clearly gives zero when applied to a two particle wave function. The eigenvalue of the Γ appearing in (17) is given by (47), while the operator $(\sum_{r=1}^{N} H_r)$ in (17), when applied to the reduced canonical wave function (43), gives the eigenvalue ρ, so that the δ of (41) becomes

$$\delta = (\rho+3)[\tfrac{1}{6}\rho(\rho+6) + 2f(f+1)] - 2\rho(\rho+2) - \tfrac{2}{9}\rho^3. \tag{48}$$

The operators Γ, Δ are invariants formed from the operators associated with the infinitesimal transformations of the three dimensional unitary unimodular group $S\mathscr{U}_3$. We expect therefore that γ, δ characterize the irreducible representations of $S\mathscr{U}_3$. From (47) and (48) we see that γ, δ are determined by the two quantum numbers introduced in (I), the energy ρ and pseudo spin f of the reduced two particle states. Instead of γ, δ we could use the much simpler ρ, f (ρ and $2f$ are integers) to characterize the irreducible representations of $S\mathscr{U}_3$. This would be similar to what one does, for example, with the rotation group, where one characterizes the representation by the integer or semiinteger j, and not by the eigenvalue of the Casimir operator for the rotation group $j(j+1)$.

The eigenvalues of $\boldsymbol{\lambda}^2$ are of course $\lambda(\lambda+1)$, with λ integer, and the eigenvalues of λ_z are trivial, but a problem that remains is the determination of the values of λ compatible with a given ρ and f. In (I) this determination was done [†], so to say, empirically by using the tables of Brody [5]) for the transformation brackets for harmonic oscillator functions defined by Moshinsky [6]). The problem will be solved in a closed form in the next section when we obtain the reduced canonical wave function explicitly. As the mathematical problem is to find the irreducible representations of $\mathscr{R}_3$, associated with a definite irreducible representation of $S\mathscr{U}_3$, other procedures than those given in the next section have appeared in the literature [3, 7]).

[†] A correction must be mode in table 2 of (I). fn this table, the value $\lambda = 1$ associated with $\rho = 10$, $f = 1$ should be deleted. Also the value $\lambda = 4$ associated with $\rho = 9$, $f = \frac{3}{2}$ appears only once instead of twice.

To obtain the eigenvalues of Ω, we need to apply the operator (35) to the explicit form of the reduced canonical wave function ψ_{RC}, and this will be done in section 5. We will show there that the reduced canonical wave function is completely specified up to a normalization constant if it is an eigenfunction of $\Gamma, \Delta, \boldsymbol{\lambda}^2, \lambda_z, \Omega$. We could consider then that the eigenvalues ω, λ, μ of $\Omega, \boldsymbol{\lambda}^2, \lambda_z$ characterize the rows of a basis for an irreducible representation (ρ, f) of $S\mathscr{U}_3$.

So far, we have discussed the eigenvalues of the operators (37) involving the full set of N particles. For the operators $\Gamma^{(p)}, \Delta^{(p)}$ with $1 \leqq p < N$, we could carry out an entirely similar analysis as for Γ, Δ and we obtain the same relations (47), 48) between $\gamma^{(p)}, \delta^{(p)}$ and $\rho^{(p)}, f^{(p)}$. We have now though, that $\rho^{(p)}$ is restricted by the energy $E^{(p)} = \sum_{r=1}^{p} h_r$ of the first p particles instead of the total energy E of (44b).

4. The Reduced Canonical Wave Function

In the previous section we showed that the eigenvalues of the integrals of motion can be obtained by applying the corresponding operator to the reduced canonical wave function (43). It is important therefore, to obtain the explicit form of this wave function which was shown in eq. (27a), (55) of (I) to satisfy

$$\boldsymbol{\lambda}^2 \psi_{\mathrm{RC}} = \lambda(\lambda+1)\psi_{\mathrm{RC}}, \quad \lambda_z \psi_{\mathrm{RC}} = \mu \psi_{\mathrm{RC}}, \tag{49a}$$

$$C_{11}\psi_{\mathrm{RC}} = k_1 \psi_{\mathrm{RC}}, \quad C_{22}\psi_{\mathrm{RC}} = k_2 \psi_{\mathrm{RC}}, \quad C_{12}\psi_{\mathrm{RC}} = 0, \tag{49b}$$

with C_{rs} being the operators (39). From the discussion of the previous section we see that (49) automatically guarantees that ψ_{RC} is an eigenfunction of Δ and Γ, and therefore it is an eigenfunction of all the integrals of motion (37) except Ω.

As the eigenvalue μ of ψ_{RC} can be changed with the help of the operators

$$\lambda_\pm = (\lambda_x \pm i\lambda_y), \tag{50}$$

we can restrict ourselves to the reduced canonical wave function with $\mu = \lambda$, and in this case, instead of (49a), we have

$$\lambda_+ \psi_{\mathrm{RC}} = 0, \quad \lambda_z \psi_{\mathrm{RC}} = \lambda \psi_{\mathrm{RC}}. \tag{49c}$$

The operator ξ_{is} appearing in (49) can be replaced by the operator $(\partial/\partial\eta_{is})$ as in eq. (9b) of (I), and from (49b, c) we see that the polynomial $P(\eta_1, \eta_2)$ of (43) satisfies the following first order linear homogeneous partial differential equations

$$C_{11}P = \left(\eta_+ \frac{\partial}{\partial\eta_+} + \eta_0 \frac{\partial}{\partial\eta_0} + \eta_- \frac{\partial}{\partial\eta_-}\right) P = k_1 P, \tag{51a}$$

$$C_{22}P = \left(\eta'_+ \frac{\partial}{\partial\eta'_+} + \eta'_0 \frac{\partial}{\partial\eta'_0} + \eta'_- \frac{\partial}{\partial\eta'_-}\right) P = k_2 P, \tag{51b}$$

$$C_{12}P = \left(\eta_+ \frac{\partial}{\partial\eta'_+} + \eta_0 \frac{\partial}{\partial\eta'_0} + \eta_- \frac{\partial}{\partial\eta'_-}\right) P = 0, \tag{51c}$$

$$\lambda_z P \ = \left[\left(\eta_+ \frac{\partial}{\partial\eta_+} - \eta_- \frac{\partial}{\partial\eta_-}\right) + \left(\eta'_+ \frac{\partial}{\partial\eta'_+} - \eta'_- \frac{\partial}{\partial\eta'_-}\right)\right] P = \lambda P, \tag{51d}$$

$$\lambda_+ P \ = \left[\left(2\eta_0 \frac{\partial}{\partial\eta_-} - \eta_+ \frac{\partial}{\partial\eta_0}\right) + \left(2\eta'_0 \frac{\partial}{\partial\eta'_-} - \eta'_+ \frac{\partial}{\partial\eta'_0}\right)\right] P = 0 \tag{51e}$$

where in this and the following sections and in appendix 2, we denote vectors $\boldsymbol{\eta}_1$, $\boldsymbol{\eta}_2$ simply as $\boldsymbol{\eta}$, $\boldsymbol{\eta}'$ respectively, and set †

$$(\eta_{11} \pm i\eta_{21}) = \eta_\pm, \quad \eta_{31} = \eta_0, \quad (\eta_{12} \pm i\eta_{22}) = \eta'_\pm, \quad \eta_{32} = \eta'_0, \tag{52}$$

so that P is a polynomial in

$$P(\eta_+, \eta_0, \eta_-; \eta'_+, \eta'_0, \eta'_-). \tag{53}$$

The determination of the most general polynomial that satisfies (51), is carried out in appendix 2. Here we would like only to make the following remarks:

1) As the equations are linear homogeneous and of first order, the product of two solutions of the equations will again be a solution, but with an eigenvalue that will be the sum of the eigenvalues. As a corollary, the power of any solution will also be a solution with the original eigenvalue multiplied by the power.

2) Any linear combination of solutions with the same k_1, k_2, λ is again a solution with the same eigenvalues.

We can now check in an elementary way that the following polynomials are solutions of (51)

$$\eta_+, \tag{54a}$$

$$v_+ = (\boldsymbol{\eta} \times \boldsymbol{\eta}')_+ = i(\eta_0 \eta'_+ - \eta'_0 \eta_+), \tag{54b}$$

$$w_+ = [(\boldsymbol{\eta} \times \boldsymbol{\eta}') \times \boldsymbol{\eta}]_+ = \eta'_+(\boldsymbol{\eta}^2) - (\boldsymbol{\eta} \cdot \boldsymbol{\eta}')\eta_+, \tag{54c}$$

$$s = (\boldsymbol{\eta} \cdot \boldsymbol{\eta}) = \eta_+ \eta_- + \eta_0^2, \tag{54d}$$

$$t = [(\boldsymbol{\eta} \times \boldsymbol{\eta}') \cdot (\boldsymbol{\eta} \times \boldsymbol{\eta}')] = (\boldsymbol{\eta}^2)(\boldsymbol{\eta}'^2) - (\boldsymbol{\eta} \cdot \boldsymbol{\eta}')^2. \tag{54e}$$

---

† Note that $\eta_\pm$ is not the same as $\eta_{\pm 1}$ of (I).

The corresponding eigenvalues are given in table 1.

TABLE 1

Eigenvalues of the operators of eqs. (54)

	η_+	v_+	s	t	w_+
k_1	1	1	2	2	2
k_2	0	1	0	2	1
λ	1	1	0	0	1

Any product of powers of the five polynomials (54) is again a solution of (51). Since.

$$w_+{}^2 = -(v_+{}^2s+\eta_+{}^2t), \tag{55}$$

the exponents of w_+ may be restricted to 0 and 1. We obtain two types of solutions which we call even or odd if the exponent of w_+ is 0 or 1 respectively. They are generated by

$$\begin{array}{cc} \text{(Even)} & \text{(Odd)} \\ \eta_+{}^l v_+{}^m s^n t^q, & w_+\eta_+{}^l v_+{}^m s^n t^q, \end{array} \tag{56}$$

where l, m, n, q are any non-negative integers. From the remark 1) and table 1 we conclude that the eigenvalues are

$$\begin{array}{ll} \text{(Even)} & \text{(Odd)} \\ k_1 = l+m+2n+2q, & k_1 = l+m+2n+2q+2, \\ k_2 = m+2q, & k_2 = m+2q+1, \\ \lambda = l+m, & \lambda = l+m+1. \end{array} \tag{57}$$

It is seen that the solutions are even or odd if $k_1-\lambda$ is even or odd. In terms of k_1, k_2, λ and q we find

$$\begin{array}{ll} \text{(Even)} & \text{(Odd)} \\ l = \lambda-k_2+2q, & l = \lambda-k_2+2q, \\ m = k_2-2q, & m = k_2-2q-1, \\ n = \frac{1}{2}(k_1-\lambda)-q, & n = \frac{1}{2}(k_1-\lambda-1)-q. \end{array} \tag{58}$$

In general, q is not uniquely determined by k_1, k_2, λ but since l, m, n, q are non-negative integers, it is restricted by the following inequalities:

$$\begin{array}{ll} \text{(Even)} & \text{(Odd)} \\ 0 \leqq 2q \leqq k_2, & 0 \leqq 2q \leqq k_2-1, \\ k_2-\lambda \leqq 2q \leqq k_1-\lambda, & k_2-\lambda \leqq 2q \leqq k_1-1-\lambda. \end{array} \tag{59}$$

The corresponding polynomials (56) will then be designated as

$$P_{k_1k_2\lambda q} = \begin{cases} \eta_+{}^{\lambda-k_2+2q} v_+{}^{k_2-2q} s^{\frac{1}{2}(k_1-\lambda)-q} t^q, & k_1-\lambda \quad \text{even}, \\ w_+\eta_+{}^{\lambda-k_2+2q} v_+{}^{k_2-1-2q} s^{\frac{1}{2}(k_1-\lambda-1)-q} t^q, & k_1-\lambda \quad \text{odd}. \end{cases} \tag{60}$$

It will be explicitly shown in appendix 2 that any solution of (51), for given k_1, k_2, λ, has necessarily the form

$$\sum_q \alpha_q P_{k_1k_2\lambda q}(\eta, \eta'), \tag{61}$$

where α_q are arbitrary constants, and q assumes the values compatible with the inequalities (59).

The inequalities (59) show which λ are compatible with given values of $\rho = k_1+k_2$ and $f = \frac{1}{2}(k_1-k_2)$, and determine the number τ of integers q which are compatible with a given triplet ρ, f, λ, and thus, we obtain the degeneracy τ of the reduced canonical state. The table 2 of the previous paper may be obtained from (59).

5. The Operator Ω

As we have seen before, Ω commutes with the other operators in (37). If P is a solution of the equations (51), then ΩP is also a solution with the same values k_1, k_2, λ. In general, we shall have

$$\Omega P_{k_1k_2\lambda q} = \sum_{q'} \beta_{q'q} P_{k_1k_2\lambda q'}, \tag{62}$$

where the sum extends over the values q' compatible with k_1, k_2, λ. If, in parcular, the triplet k_1, k_2, λ has multiplicity $\tau = 1$, so that q is uniquely determined, the sum in (62) reduces to one term and $P_{k_1k_2\lambda q}$ is an eigenfunction of Ω.

Since Ω is applied to the two particle function (60), the expression (35) for Ω may be restricted to $N=2$ so that using the commutation relation (3) of (I) we may write, in the notation of the previous section,

$$\Omega = (\eta \cdot \boldsymbol{\lambda})(\xi \cdot \boldsymbol{\lambda}) + (\eta' \cdot \boldsymbol{\lambda})(\xi' \cdot \boldsymbol{\lambda}) - \tfrac{1}{3}(\eta \cdot \xi + \eta' \cdot \xi' + \tfrac{3}{2})\boldsymbol{\lambda}^2. \tag{63}$$

where

$$\boldsymbol{\lambda} = -i(\eta \times \xi + \eta' \times \xi'). \tag{64}$$

From (49), $P_{k_1k_2\lambda q}$ is an eigenfunction of the last term in (63) with eigenvalue

$$-\tfrac{1}{3}(k_1+k_2+\tfrac{3}{2})\lambda(\lambda+1) \tag{65}$$

and we need be concerned only with the first two terms in (63). The application of these terms of (63) to the polynomial $P_{k_1k_2\lambda q}$ is a straightforward though rather lengthy computation, and we shall only quote the final results. The coefficient $\beta_{q'q}$ turns out to be zero unless $q' = q \pm 1$, q, and for these values of q' it becomes

$$(k_1-\lambda \text{ even})$$

$$\beta_{q-1,q} = -2q(\lambda-k_2+2q)(\lambda-k_2+2q-1), \tag{66a}$$

$$\beta_{q+1,q} = (k_2-2q)(k_2-2q-1)(k_1-\lambda-2q), \tag{66b}$$

$$\beta_{qq} = (k_2-2q)^2(k_1+1)+(k_2-2q)(\lambda-k_2+2q)(\lambda+4q+1) \\ +(k_2-2q)+k_2\lambda-\tfrac{1}{3}(k_1+k_2+\tfrac{3}{2})\lambda(\lambda+1); \tag{66c}$$

$$(k_1-\lambda \text{ odd})$$

$$\beta_{q-1,q} = -2q(\lambda-k_2+2q)(\lambda-k_2+2q-1), \tag{67a}$$

$$\beta_{q+1,q} = (k_2-2q-1)(k_2-2q-2)(k_1-\lambda-2q-1), \tag{67b}$$

$$\beta_{q,q} = (k_2-2q-1)[(2k_1+2\lambda+3)+(k_2-2q-1)(k_1-1)+(\lambda-k_2+2q)(\lambda+4q)] \\ +(k_1+1)+(k_2-1)(\lambda-1)-\tfrac{1}{3}(k_1+k_2+\tfrac{3}{2})\lambda(\lambda+1). \tag{67c}$$

We stress an important property of the matrix elements $\beta_{q'q}$. Let, for given k_1, k_2, λ, q_1 be the minimal and q_2 the maximal allowable q value. Then it is seen from the explicit formulae for the β's, that

$$\beta_{q-1,q} = 0 \quad \text{for} \quad q = q_1, \qquad \beta_{q+1,q} = 0 \quad \text{for} \quad q = q_2, \tag{68}$$

so that the sum in (62) ranges over the values q determined by $q_1 \leqq q \leqq q_2$, as it should. Furthermore, it follows from (66a) and (67a) that, in the allowed range,

$$\beta_{q,q+1} \neq 0. \tag{69}$$

The eigenvalues of Ω are, in principle, determined as follows. From (62), an eigenfunction may be obtained in the form

$$P = \sum_q \alpha_q P_{k_1k_2\lambda q}. \tag{70}$$

The equation

$$\Omega P = \omega P \tag{71}$$

is then equivalent to the linear equations

$$\sum_{q=q_1}^{q_2} \beta_{q'q}\alpha_q = \omega\alpha_{q'}, \quad q_2-q_1 = \tau-1. \tag{72}$$

By its construction, Ω is a hermitian operator †; hence there exist τ linearly independent eigenfunctions. The secular equation obtained from (72) gives the eigenvalues ω of the operator Ω. When $\tau = 1$, we have, of course, just one value of q possible and $\omega = \beta_{qq}$. For reasonably low energies, the degeneracies τ

---

† Note incidentally, that the matrix elements $\beta_{q'q}$ in (66) and (67), do not have hermitian symmetry, because the functions (60), to which they refer, are neither orthogonal nor normalized.

are strongly limited. In fact, a simple analysis of the inequalities (59) shows that

$$\begin{aligned} k_1+k_2 &\geqq 6(\tau-1) && \text{if } k_1-\lambda \text{ even,} \\ k_1+k_2 &\geqq 6(\tau-1)+3 && \text{if } k_1-\lambda \text{ odd.} \end{aligned} \tag{73}$$

For example, k_1+k_2 must be at least equal to 12 to permit the degeneracy $\tau = 3$ that appears once in table 2 of (I).

An important consequence of the equation (72) is that no eigenvalue ω is degenerate. To prove this assertion we first show that if $\alpha_{q_1} = 0$ in (72), then all α_q vanish. Writing (72) explicitly, we have from (66, 67) that

$$\begin{aligned} &\beta_{q_1 q_1}\alpha_{q_1}+\beta_{q_1, q_1+1}\alpha_{q_1+1} && = \omega\alpha_{q_1} \\ &\beta_{q_1+1, q_1}\alpha_{q_1}+\beta_{q_1+1, q_1+1}\alpha_{q_1+1}+\beta_{q_1+1, q_1+2}\alpha_{q_1+2} && = \omega\alpha_{q_1+1} \\ &\cdots\cdots\cdots\cdots\cdots\cdots\cdots\cdots\cdots\cdots\cdots\cdots\cdots\cdots\cdots\cdots\cdots\cdots \\ &\beta_{q_2-1, q_2-2}\alpha_{q_2-2}+\beta_{q_2-1, q_2-1}\alpha_{q_2-1}+\beta_{q_2-1, q_2}\alpha_{q_2} && = \omega\alpha_{q_2-1}, \\ &\beta_{q_2, q_2-1}\alpha_{q_2-1}+\beta_{q_2, q_2}\alpha_{q_2} = \omega\alpha_{q_2}. \end{aligned} \tag{74}$$

If $\alpha_{q_1} = 0$ in (74) we obtain, from the first equation and (69), that $\alpha_{q_1+1} = 0$. Inserting α_{q_1}, α_{q_1+1} in the second equation, we get from (69) $\alpha_{q_1+2} = 0$ and so on. The equation before the last, yields $\alpha_{q_2} = 0$ q.e.d. Let us have next a non vanishing polynomial P of the form (70) that satisfies (71). Since $P \neq 0$, we must have $\alpha_{q_1} \neq 0$. Let

$$P' = \sum_q \alpha'_q P_{k_1 k_2 \lambda q} \tag{75}$$

be a second solution of (71), and set

$$P'' \equiv \sum \alpha''_q P_{k_1 k_2 \lambda q} = P' - \kappa P, \qquad \kappa = \alpha'_{q_1}/\alpha_{q_1}. \tag{76}$$

Then P'' also satisfies (71), but, by construction $\alpha''_{q_1} = 0$, hence all α''_q vanish, and $P'' \equiv 0$. Thus $P' = \kappa P$, i.e. there exists at most, one linearly independent eigenfunction for a given eigenvalue ω of Ω.

This result shows that the operator Ω removes the degeneracy in the reduced canonical function. If, for given k_1, k_2, λ, the eigenfunctions

$$P^{\omega}_{k_1 k_2 \lambda} = \sum_q \alpha_q(\omega) P_{k_1 k_2 \lambda q} \tag{77}$$

of Ω are introduced, then the four numbers k_1, k_2, λ, ω determine them uniquely.

As stated in section 3, Ω is essentially the quadrupole moment of the state projected along the direction of its angular momentum. The lowest states for a system of particles moving in a common harmonic oscillator potential with a quadrupole-quadrupole interaction, have a greatly enhanced quadrupole moment. This can be seen from the fact that the lowest rotational band for a given total energy E of the system of particles, is given by ¹)

$$E = \rho = 2f, \tag{78}$$

which implies that the reduced canonical wave function has

$$k_1 = E, \quad k_2 = 0. \tag{79}$$

From (59) we see that q is then restricted by

$$\begin{array}{cc} \text{(Even)} & \text{(Odd)} \\ 0 \leqq 2q \leqq 0, & 0 \leqq 2q \leqq -1, \\ -\lambda \leqq 2q \leqq E-\lambda, & -\lambda \leqq 2q \leqq E-1-\lambda, \end{array} \tag{80}$$

so all the reduced canonical wave functions are of the even type with $q = 0$, i.e. non degenerate. From (66c) the eigenvalue ω of the operator Ω, becomes then

$$\omega = -\tfrac{1}{3}(E+\tfrac{3}{2})\lambda(\lambda+1), \tag{81}$$

where $\lambda = E, E-2, E-4, \ldots \genfrac{}{}{0pt}{}{1}{0}$.

The quadrupole moment is now correlated with the total energy of the system of N particles and not, as in the usual shell model calculations, only with the energy of the last unpaired particle, or of the particles outside closed shells.

6. Summary and Conclusion

In the present paper we have obtained $3N$ integrals of motion for a system of N particles in a common harmonic oscillator potential with a quadrupole-quadrupole interaction. We have also obtained the eigenvalues associated with these integrals of motion. To derive these eigenvalues we had to determine the explicit form of the reduced canonical wave function.

With the help of the integrals of motion and of the reduced canonical wave function, we plan to discuss in the next paper of this series, the explicit construction of the eigenfunctions for the quadrupole-quadrupole interaction.

Appendix

A.1. COMMUTATION RELATIONS

We shall check in this appendix that $\Gamma^{(p)}$, $\Delta^{(p)}$, commute with $\mathscr{C}_{ij}^{(p)}$. As the hamiltonian $H^{(p)}$ of (11) commutes with $\mathscr{C}_{ij}^{(p)}$, $\Gamma^{(p)}$, $\Delta^{(p)}$ given by (10), (14) and (15) respectively, we need only to prove that $\mathscr{D}_{ij}^{(p)}$ of (12) commutes with $\Gamma^{(p)}$ and $\Delta^{(p)}$.

From the commutation relations (3) of (I) we have

$$[\mathscr{D}_{ij}^{(p)}, \mathscr{D}_{i'j'}^{(p)}] = \mathscr{D}_{ij'}^{(p)}\delta_{i'j} - \mathscr{D}_{i'j}^{(p)}\delta_{ij'}, \tag{1.1}$$

so that from the definition (14) of $\Gamma^{(p)}$ we obtain immediately

$$[\Gamma^{(p)}, \mathscr{D}_{ij}^{(p)}] = 0. \tag{1.2}$$

To prove that $\mathscr{D}_{ij}^{(p)}$ commutes with $\Delta^{(p)}$, we make use of (1.1), of the identity

$$\varepsilon_{ijk}\varepsilon_{i'j'k'} = \det\begin{pmatrix} \delta_{ii'} & \delta_{ij'} & \delta_{ik'} \\ \delta_{ji'} & \delta_{jj'} & \delta_{jk'} \\ \delta_{ki'} & \delta_{kj'} & \delta_{kk'} \end{pmatrix}, \tag{1.3}$$

and of the fact that $\operatorname{tr}\|\mathscr{D}^{(p)}\| = 0$, to transform (15) into

$$\Delta^{(p)} = 2\sum_{i,j,k=1}^{3}(\mathscr{D}_{ij}^{(p)}\mathscr{D}_{jk}^{(p)}\mathscr{D}_{ki}^{(p)}) - 3\sum_{j,k}(\mathscr{D}_{jk}^{(p)}\mathscr{D}_{kj}^{(p)}). \tag{1.4}$$

The second term in (1.4) is $\Gamma^{(p)}$ so it commutes with $\mathscr{D}_{i'j'}^{(p)}$ and so does also the first term in (1.4) as seen immediately with the help of (1.1). We have therefore,

$$[\Delta^{(p)}, \mathscr{D}_{ij}^{(p)}] = 0. \tag{1.5}$$

A.2. THE REDUCED CANONICAL WAVE FUNCTION

A.2.1. *Preliminary remarks.*

Our problem is to construct all polynomials P (see eq. (53)) which satisfy the equations (51a) to (51e) for given values k_1, k_2, λ. These five equations will be referred to as a, b, c, d, e[†].

In our construction we shall use not only polynomials, but also rational functions, say f. Let A be one of the operators C_{rs}, λ_z, λ_+. If $f = f_1 f_2$, then

$$Af = f_1(Af_2) + (Af_1)f_2, \quad \text{or} \quad (Af/f) = (Af_1/f_1) + (Af_2/f_2). \tag{2.1}$$

For $g = (f_1/f_2)$,

$$(Ag/A) = (Af_1/f_1) - (Af_2/f_2). \tag{2.2}$$

If $f = F(\varphi_1, \ldots, \varphi_s)$, where φ_i are functions of η, η', then

$$Af = \sum_{i=1}^{s}(A\varphi_i)(\partial F/\partial\varphi_i). \tag{2.3}$$

The operator C_{12}. The quantity $C_{12}f$ obviously vanishes for any function of η only. It also vanishes if f is a component of the vector product $\mathbf{v} = \eta\times\eta'$, and it will be useful to employ these. In analogy with (52) we set

$$\zeta_+ = \eta_0\eta'_+ - \eta'_0\eta_+, \quad \zeta_- = \eta_0\eta'_- - \eta'_0\eta_-, \quad \zeta_0 = \tfrac{1}{2}(\eta_+\eta'_- - \eta_-\eta'_+). \tag{2.4}$$

In terms of the rectangular components v_k of v,

$$v_1 + iv_2 = i\zeta_+, \quad v_1 - iv_2 = -i\zeta_-, \quad v_3 = i\zeta_0. \tag{2.4a}$$

Clearly, $2\eta_0\zeta_0 + \eta_-\zeta_+ - \eta_+\zeta_- = 0$, so that

$$\zeta_0 = \frac{1}{2\eta_0}(\eta_+\zeta_- - \eta_-\zeta_+). \tag{2.5}$$

[†] For the notation see section 4.

For later use, we note that

$$C_{12}\zeta_+ = C_{12}\zeta_- = 0, \quad C_{12}\eta'_0 = \eta_0. \tag{2.6}$$

The functions s, w_+ and t. With the help of the variables introduced here, we find

$$\boldsymbol{\eta}\cdot\boldsymbol{\eta}' = \eta_0\eta'_0 + \tfrac{1}{2}(\eta_+\eta'_- + \eta_-\eta'_+), \quad s = \boldsymbol{\eta}\cdot\boldsymbol{\eta} = \eta_0^2 + \eta_+\eta_-, \tag{2.7}$$

$$w_+ = [(\boldsymbol{\eta}\times\boldsymbol{\eta}')\times\boldsymbol{\eta}]_+ = (w_1 + iw_2) = (\boldsymbol{\eta}\cdot\boldsymbol{\eta})\eta'_+ - (\boldsymbol{\eta}\cdot\boldsymbol{\eta}')\eta_+ = \eta_0\zeta_+ - \eta_+\zeta_0, \tag{2.8}$$

or

$$w_+ = \tfrac{1}{2}\eta_0\zeta_+\left(2 + \frac{\eta_+\eta_-}{\eta_0^2} - \frac{\eta_+^2\zeta_-}{\eta_0^2\zeta_+}\right), \tag{2.8a}$$

where (2.5) has been used. Finally,

$$t = (\boldsymbol{\eta}\times\boldsymbol{\eta}')^2 = \zeta_+\zeta_- - \zeta_0^2, \tag{2.9}$$

or

$$t = \left(\frac{\eta_0\zeta_+}{\eta_+}\right)^2\left[\frac{\eta_+^2}{\eta_0^2}\frac{\zeta_-}{\zeta_+} - \frac{1}{4}\left(\frac{\eta_+^2}{\eta_0^2}\frac{\zeta_-}{\zeta_+} - \frac{\eta_+\eta_-}{\eta_0^2}\right)^2\right], \tag{2.9a}$$

using again (2.5).

Let $P(\neq 0)$ be a polynomial solution of (51a) to (51e). We consider the five equations in succession.

A.2.2. The equations $C_{11}P = k_1P$, $C_{22}P = k_2P$. According to (51a) and (51b), P is homogeneous of order k_1, k_2 in the variables $\boldsymbol{\eta}$ and $\boldsymbol{\eta}'$ respectively. We may write, therefore,

$$P = \eta_0^{k_1}\eta_0'^{k_2}f, \tag{2.10}$$

where f is a polynomial of order $\leqq k_1$ in $(\eta_\pm/\eta_0)$ and of order $\leqq k_2$ in $(\eta'_\pm/\eta'_0)$. Let

$$a_+ = (\eta_+/\eta_0), \quad a_- = (\eta_-/\eta_0). \tag{2.11}$$

In view of our previous remarks we introduce, in addition,

$$\alpha_+ = \frac{\eta'_+}{\eta'_0} - \frac{\eta_+}{\eta_0} = \frac{\zeta_+}{\eta_0\eta'_0}, \quad \alpha_- = \frac{\eta'_-}{\eta'_0} - \frac{\eta_-}{\eta_0} = \frac{\zeta_-}{\eta_0\eta'_0}. \tag{2.12}$$

Thus

$$P = uf(a_+, a_-, \alpha_+, \alpha_-), \quad u = \eta_0^{k_1}\eta_0'^{k_2}. \tag{2.13}$$

In α_+, α_-, the polynomial f has degree $\leqq k_2$.

A.2.3. The equation $C_{12}P = 0$. By (2.1)

$$C_{12}P = (C_{12}u)f + u(C_{12}f). \tag{2.14}$$

Since $C_{12}\eta_0 = C_{12}a_+ = C_{12}a_- = 0$, we find from (2.6),

$$\frac{C_{12}u}{u} = k_2\frac{C_{12}\eta'_0}{\eta'_0} = k_2\frac{\eta_0}{\eta'_0}, \quad \frac{C_{12}\alpha_+}{\alpha_+} = \frac{C_{12}\alpha_-}{\alpha_-} = -\frac{C_{12}\eta'_0}{\eta'_0} = -\frac{\eta_0}{\eta'_0},$$

Inserting this in (2.14) and using (2.3), we obtain

$$\alpha_+\frac{\partial f}{\partial\alpha_+} + \alpha_-\frac{\partial f}{\partial\alpha_-} = k_2 f, \tag{2.15}$$

i.e., f is homogeneous in α_+, α_- of order k_2. We may factor out $\alpha_+^{k_2}$, so that

$$f = \alpha_+^{k_2} f_1(a_+, a_-, \gamma), \quad \gamma = \frac{\alpha_-}{\alpha_+} = \frac{\zeta_-}{\zeta_+}, \tag{2.16}$$

where f_1 is a polynomial in a_+, a_-, γ, of degree $\leqq k_2$ in γ. From (2.13)

$$P = u_1 f_1(a_+, a_-, \gamma), \quad u_1 = \alpha_+^{k_2}u = \eta_0^{k_1-k_2}\zeta_+^{k_2}. \tag{2.17}$$

A.2.4. The equation $\lambda_z P = \lambda P$. We have now

$$\lambda_z P = (\lambda_z u_1)f_1 + u_1(\lambda_z f_1). \tag{2.18}$$

The following relations hold

$$\lambda_z\eta_0 = 0, \quad \frac{\lambda_z\eta_+}{\eta_+} = \frac{\lambda_z\zeta_+}{\zeta_+} = 1, \quad \frac{\lambda_z\eta_-}{\eta_-} = \frac{\lambda_z\zeta_-}{\zeta_-} = -1.$$

Hence

$$\frac{\lambda_z u_1}{u_1} = k_2, \quad \frac{\lambda_z a_+}{a_+} = -\frac{\lambda_z a_-}{a_-} = 1, \quad \frac{\lambda_z\gamma}{\gamma} = \frac{\lambda_z\zeta_-}{\zeta_-} - \frac{\lambda_z\zeta_+}{\zeta_+} = -2.$$

Inserting this in (2.18) and using (2.3), we find that the equation $\lambda_z P = \lambda P$ leads to

$$a_+\frac{\partial f_1}{\partial a_+} - a_-\frac{\partial f_1}{\partial a_-} - 2\gamma\frac{\partial f_1}{\partial\gamma} = (\lambda - k_2)f_1. \tag{2.19}$$

Let

$$f_1 = \sum_{l,m,n} C_{lmn}a_+^l a_-^m\gamma^n, \quad n \leqq k_2.$$

By (2.19), $C_{lmn} = 0$ unless $l-m-2n = \lambda-k_2$, or $l = m+2n+\lambda-k_2$. Thus

$$f_1 = a_+^{\lambda-k_2}\sum_{m,n} C'_{mn}(a_+a_-)^m(a_+^2\gamma)^n \equiv a_+^{\lambda-k_2}g, \quad n \leqq k_2. \tag{2.20}$$

The functions s and w_+ are closely related to the expressions a_+a_- and $a_+^2\gamma$, which appear in the preceding equations. In fact, from (2.7) and (2.8a),

$$s = \eta_0^2\left(1+\frac{\eta_+\eta_-}{\eta_0^2}\right) = \eta_0^2(1+a_+a_-), \tag{2.21}$$

$$w_+ = \eta_0\zeta_+[1+\tfrac{1}{2}(a_+a_- - a_+^2\gamma)]. \tag{2.21a}$$

We introduce, therefore, the variables

$$x = 1+a_+a_-, \quad y = 1+\tfrac{1}{2}(a_+a_- - a_+^2\gamma) \tag{2.22}$$

so that

$$a_+a_- = x-1, \quad a_+^2\gamma = 1+x-2y \tag{2.22a}$$

It follows from (2.20) that g is a polynomial in x, y (of degree $\leqq k_2$ in y), and from (2.17) that

$$P = u_2g(x, y), \quad u_2 = u_1a_+^{\lambda-k_2} = u_1(\eta_+/\eta_0)^{\lambda-k_2} = \eta_0^{k_1-\lambda}\eta_+^{\lambda-k_2}\zeta_+^{k_2}. \tag{2.23}$$

In terms of x and y we now have

$$s = \eta_0^2x, \quad w_+ = \eta_0\zeta_+y \tag{2.24}$$

and, furthermore, from (2.9a) and (2.22a),

$$t = \left(\frac{\eta_0\zeta_+}{\eta_+}\right)^2[a_+^2\gamma - \tfrac{1}{4}(a_+^2\gamma - a_+a_-)^2] = \left(\frac{\eta_0\zeta_+}{\eta_+}\right)^2(x-y^2). \tag{2.24a}$$

A.2.5. The equation $\lambda_+P = 0$. The remaining equation $\lambda_+P = 0$ will now lead to the final form of P. We note first that

$$\lambda_+\eta_+ = \lambda_+\zeta_+ = 0, \quad \lambda_+\eta_0 = -\eta_+ = -a_+\eta_0. \tag{2.25}$$

Hence, from (2.23),

$$\frac{\lambda_+u_2}{u_2} = (k_1-\lambda)\frac{\lambda_+\eta_0}{\eta_0} = -(k_1-\lambda)a_+. \tag{2.25a}$$

The expressions λ_+x and λ_+y are easily obtained from (2.24), for $\lambda_+s = 0$ (s is a scalar) and also $\lambda_+w_+ = 0$ as follows from the definition (2.8) and the first two equations (2.25). Hence

$$\frac{\lambda_+x}{x} = -\frac{2\lambda_+\eta_0}{\eta_0} = 2a_+, \quad \frac{\lambda_+y}{y} = -\frac{\lambda_+\eta_0}{\eta_0} = a_+. \tag{2.26}$$

Inserting (2.25a) and (2.26) in (2.23) we see that $\lambda_+P = 0$ implies

$$2x\frac{\partial g}{\partial x}+y\frac{\partial g}{\partial y} = (k_1-\lambda)g. \tag{2.27}$$

Let

$$g = \sum_{m,n} d_{mn} x^m y^n, \quad n \leqq k_2.$$

It follows from (2.27) that $d_{mn} = 0$ unless

$$2m+n = k_1-\lambda. \tag{2.28}$$

This shows, firstly, that

$$k_1-\lambda \geqq 0 \tag{2.28a}$$

and secondly that n is even or odd according to whether $k_1-\lambda$ is even or odd. We consider these two cases separately.

A.2.6. $k_1-\lambda$ even. Let

$$k_1-\lambda = 2\sigma. \tag{2.29}$$

Then $n = 2(\sigma-m)$, and g is a homogeneous polynomial in x and y^2 of order σ. We may equally well express g as a homogeneous polynomial in x and $x-y^2$ of order σ, so that

$$g = \sum_q C_q (x-y^2)^q x^{\sigma-q}, \tag{2.30}$$

and the inequalities

$$2q \leqq k_2, \quad q \leqq \sigma \tag{2.30a}$$

hold. From (2.23) we now obtain the final form of P. Replacing x and y by s and t,

$$x = \frac{s}{\eta_0{}^2}, \quad x-y^2 = \frac{\eta_+{}^2 t}{\eta_0{}^2 \zeta_+{}^2}, \tag{2.30b}$$

we find from (2.30) and (2.23)

$$P = \sum_q C_q \eta_+{}^{\lambda-k_2+2q} \zeta_+{}^{k_2-2q} s^{\frac{1}{2}(k_1-\lambda)-q} t^q. \tag{2.31}$$

This last equation furnishes an additional inequality for q. Let q_1 be the minimal value of q for which $C_q \neq 0$. Expressing ζ_+, s, t, as polynomials in η_0, η_+, η_-, η'_0, η'_+, η'_-, we find that $\zeta_+(0)$, $s(0)$, $t(0)$, are different from zero (where $\zeta_+(0)$, etc. denotes the value of the corresponding polynomials for $\eta_+ = 0$). Hence, the power $\eta_+{}^{\lambda-k_2+2q_1}$ actually occurs in P, and since P is assumed a polynomial, in η, η',

$$\lambda-k_2+2q \geqq 0. \tag{2.31b}$$

Summarizing: If $k_1-\lambda$ is even, P is necessarily a linear combination of the solutions

$$\eta_+{}^{\lambda-k_2+2q} \zeta_+{}^{k_2-2q} s^{\frac{1}{2}(k_1-\lambda)-q} t^q, \tag{2.32}$$

where

$$0 \leqq 2q \leqq k_2, \quad k_2-\lambda \leqq 2q \leqq k_1-\lambda. \tag{2.32a}$$

These inequalities merely state that all exponents in (2.32) are non-negative integers. The expression (2.32) essentially coincides with (60), since $v_+ = i\zeta_+$.

A.2.7. $k_1-\lambda$ odd. Let

$$k_1-\lambda = 1+2\sigma. \tag{2.33}$$

Then from (2.28), $n = 1+2(\sigma-m)$, so that

$$g = yg_1 \tag{2.33a}$$

where g_1, as before, is a homogeneous polynomial in x and y^2 of order σ and may be written in the form (2.30). Since $n \leqq k_2$, the range of q is now restricted by the inequalities

$$1+2q \leqq k_2, \quad q \leqq \sigma = \tfrac{1}{2}(k_1-1-\lambda). \tag{2.33b}$$

From (2.23) and (2.33a) we again obtain the final form of P by using the variables s and t (see (2.30b)) and in addition, $y = (w_+/\eta_0\zeta_+)$. It follows that

$$P = \sum_q C_q w_+ {\eta_+}^{\lambda-k_2+2q} {\zeta_+}^{k_2-1-2q} s^{\frac{1}{2}(k_1-1-\lambda)-q} t^q. \tag{2.34}$$

As before, we find the additional inequality $\lambda-k_2+2q \geqq 0$ (see (2.31b)).

Summarizing: If $k_1-\lambda$ is odd, P is necessarily a linear combination of the solutions

$$w_+ {\eta_+}^{\lambda-k_2+2q} {\zeta_+}^{k_2-1-2q} s^{\frac{1}{2}(k_1-1-\lambda)-q} t^q, \tag{2.34a}$$

where

$$0 \leqq 2q \leqq k_2-1, \quad k_2-\lambda \leqq 2q \leqq k_1-1-\lambda. \tag{2.34b}$$

Again these inequalities merely express the fact that no negative powers occur in (2.34a).

A.2.8. *Additional remark.* The inequalities (2.32a) and (2.34b) imply, in particular, that $k_1 \geqq k_2$. This, however, is a direct consequence of the equations (51a), (51b), (51c). In fact, consider the three operators

$$F_1 = \tfrac{1}{2}(C_{12}+C_{21}), \quad F_2 = -\tfrac{1}{2}i\,(C_{12}-C_{21}), \quad F_3 = \tfrac{1}{2}(C_{11}-C_{22}),$$

which were shown in eq. (21) of (I) to satisfy the commutation rules of angular momentum. The equations (51a), (51b), (51c) imply that

$$F_3P = \tfrac{1}{2}(k_1-k_2)P, \quad (F_1+iF_2)P = C_{12}P = 0.$$

As is well known, we may conclude from these last equations, that P belongs to the highest eigenvalue of F_3 for a sequence corresponding to the same fixed eigenvalue $j(j+1)$ of $F_1^2+F_2^2+F_3^2$ so that $\frac{1}{2}(k_1-k_2)=j\geqq 0$.

References

1) V. Bargmann and M. Moshinsky, Nuclear Physics **18** (1960) 697
2) J. P. Elliot, Proc. Roy. Soc. A **245** (1958) 128, 562
3) S. A. Moszkowski, Phys. Rev. **110** (1958) 403
4) G. Racah, Group theory and spectroscopy (Mimeographed notes, Institute of Advanced Study, 1951)
5) T. A. Brody, Rev. Mexicana de Física **8** (1959) 139
6) M. Moshinsky, Nuclear Physics **13** (1959) 104
7) G. Racah, Rev. Mod. Phys. **21** (1949) 494;
M. Kretzschmar, Zeit. f. Physik **157** (1960) 433;
A. Pais, private communication

1.D.1

Nuclear Physics **23** (1961) 200—244; © *North-Holland Publishing Co., Amsterdam*
Not to be reproduced by photoprint or microfilm without written permission from the publisher

SHELL-MODEL ANALYSIS OF CALCIUM ISOTOPES

HENRI E. MITLER
Physics Department, Brandeis University, Waltham, Massachusetts †

Received 26 September 1960

Abstract: An intermediate shell model calculation is made for Ca 42 and Ca 43. The effective two-body (static) internucleon potential, acting among the neutrons outside the Ca 40 core, is phenomenologically obtained by fitting the known energy levels of 42 and 43. The fit to eight levels is fair, the rms deviation being 124 keV. The potential is found to differ strongly from that expected from nucleon-nucleon scattering experiments: it is *long*-, rather than short-ranged, has a weak repulsive (rather than attractive) triplet odd part, and a strong, attractive (rather than weak, repulsive) tensor part. The fit to the energy levels is nevertheless better than what has been obtained heretofore. A comparison of the calculated electromagnetic transition probabilities indicates a considerable amount of surface-particle coupling, indicating a strong admixture of one of the core states. A theorem is derived which facilitates computation of tensor force matrix elements in *j—j* coupling.

1. Introduction

The shell model has had remarkable success in predicting many of the static and dynamic characteristics of nuclei, particularly near closed shells, and in the region of light and of very heavy nuclei [1]).

In some intermediate regions of the periodic table, however, success has not been so striking, even when near closed shells, where one would expect collective effects to play a very minor role.

A nucleus in point is calcium. Calcium 40 is a doubly magic nucleus, with the 1s, 1p, and 2s-1d shells being filled in both neutrons and protons (where we assume a harmonic well for the nucleons [2])). Its first excited state lies quite high, at 3.35 MeV, so that we expect this nucleus to be rather rigid and difficult to perturb. Additional nucleons must fill the next subshell, i.e. $f_{\frac{7}{2}}$ [3]) †.

Several analyses of these isotopes have been made [4, 23]), with various degrees of success. Perhaps the most notable one is that made by Levinson and Ford (hereafter referred to as LF I, II, or III), of the nuclei Ca 42 and Ca 43, using configuration interaction. They made the assumption that the nucleon-nucleon interaction in nuclear matter will have the same exchange character as in free space. This is particularly plausible for valence nucleons of high angular momenta, which are going to spend much of their time in the low-density part of the nuclear surface.

---

† This work is based on a thesis submitted to Princeton University, in partial fulfillment of the requirements for the degree of Doctor of Philosophy; it was supported by the U. S. Atomic Energy Commission and the National Science Foundation.

† The notation used in this paper is given in Appendix N. Appendices A—H may be obtained from the author.

The low-energy p—p scattering data are well fitted by the Serber (singlet) force

$$\tfrac{1}{2}(1+P_x), \tag{1}$$

where P_x is the space-exchange operator [5]). Assuming, then, a singlet force, they were able to derive a theorem enabling them to carry out the energy-level calculations for the case of two nucleons outside the core in a much simplified form. Moreover, it permitted them to use the empirical values of the two-particle nucleus (Ca 42) to solve for (some of) the matrix elements. Using these matrix elements, they were able to predict the 3-particle energies exactly, as well as the magnetic moment of Ca 43. Moreover, assuming a Gaussian shape for the internucleon interaction, they were able to infer a consistent range and strength for it from the matrix elements. Taking the range of the 1f wave function as $r_n = 2.9\ f$, they found, for the range of their potential, $r_0 = 3.4\ f$ (here, $f = 10^{-13}$ cm). The strength of the potential was 14.4 MeV. This is about twice the range, but half the strength, of a Gaussian interaction constructed to give the singlet effective range and scattering length found from low-energy scattering.

The initial impetus for this work was an attempt to use the potential they had found, and calculate the energy levels of Ca 42 and Ca 43 in the usual way, with j—j coupling, but not making the approximations made by them: First, they calculated the matrix elements "empirically": by using their theorem to obtain, empirically, the matrix elements $V_J \equiv \langle f^2\colon J|V|f^2\colon J\rangle$ for $J = 0, 2, 4, 6$, they were able to find the Slater parameters F^k ($k = 0, 2, 4, 6$), which are simply related to the V_J. They then interpolated and extrapolated linearly, to find (approximate) values for F^k ($k = 1, 3, 5, 7, 8$). Finally, they used these values of the Slater parameters to find all other matrix elements (which are known linear functions of F^k). Secondly, they did not compute the p-state matrix elements at all, which was likely to affect their Ca 43 calculations in particular.

2. Energy Levels of Calcium

2.1. CALCIUM 41

The most exact measurements of the energy levels of the various calcium isotopes has been made by Braams *et al.* at M.I.T. Of these measurements, however, LF had only his Ca 41 results available [6]). The principal excited levels of interest are at 1.947(4), 2.014(5), 2.469(5), 2.677(6), 3.405(7), and 3.950(7) MeV. The assignments were taken from the work of Holt and Marsham [7]): the first and third excited levels were measured by them to be $p_{\frac{3}{2}}$ and $p_{\frac{1}{2}}$, respectively. These bracket the 2.014 MeV level, which, according to Klinkenberg's scheme [3]), ought therefore to be the $f_{\frac{5}{2}}$ level. However, the stripping onto that level has an intensity down by an order of magnitude from that predicted by the Butler theory. Moreover, the (theoretical) $l = 2$ curve fits the angular distribution better than does the $l = 3$ curve [8]). To date, the single-particle $f_{\frac{5}{2}}$ level has not been found in Ca 41 (below 5.7 MeV). Throughout most of the calculations, therefore, the f doublet splitting $\Delta f = f_{\frac{5}{2}} - f_{\frac{7}{2}}$ has been used as a free parameter †.

Near the end of the calculation, a preprint was received of work done at Rice Institute [9]). Class *et al.* made an analysis of Ca 40 (p, p) reactions, obtaining therefrom a set of levels of Sc 41, and their reduced widths γ^2. The ratio of these to the Wigner limit $\gamma_W^2 = 3\hbar^2/2MR$, when plotted against the excitation energy of Sc 41, shows marked peaks, which are interpreted as indicating these levels have a large single-particle component; for most of the levels, $\gamma^2/\gamma_W^2 < 0.01$. These complex excited states are expected to be due to the excitation of nucleons from the Ca 40 core. The $l = 3$ peak at 6.41 MeV, they interpret as "the" $f_{\frac{5}{2}}$ level, and the $l = 4$ peak at 5.49 MeV, is interpreted as $g_{\frac{9}{2}}$. The 5.97 MeV level is assumed to correspond to the 5.72 MeV level in Ca 41. Again, the 4.02 MeV peak probably corresponds to the 3.95 MeV level in Ca 41. Following this simple pattern, we assumed that to the 5.4 and 6.4 MeV levels in Sc 41 correspond levels at roughly 5.3 and 6.3 MeV, respectively, in Ca 41.

Assuming that the spin-orbit (doublet) separations go as $(2l+1)A^{-\frac{2}{3}}$, and a reasonable value for ω (the oscillator frequency), on the other hand, LF put the $g_{\frac{9}{2}}$ level 2.89 MeV above the ground state.

2.2. CALCIUM 42

The levels used by FL were those measured by Schiffer [10]): at 1.51(3), 1.95(7), 2.29(5), 2.59(7), 3.02(5) and 3.75(7). The ground and first excited states were measured to have spin-parity 0+, 2+ respectively [10, 11]). One would, in general, expect the levels of an even-even nucleus to occur in the order 0+, 2+, 4+, 6+, . . . [12]).

Indeed, it was experimentally found [13]) that the second excited state was 4+. It was therefore assumed that the third excited level was 6+.

Now, Braams measured the position of these levels at 1.523(4), 1.836(4), 2.422(5), 2.750(5), 3.250(6). Keeping the same assignments, these shifts make relatively little difference in their calculations. However, Way [14]) pointed out that the 4+ assignment to the 1.84 MeV level was peculiar, as systematics indicate that it ought to be 0+. Ti 50 has two $f_{\frac{7}{2}}$ protons outside a doubly-magic core, and has levels [15]) at 0, 1.59, 2.76, and 3.27 MeV, 0+, 2+, 4+ and 6+

---

† Many theoretical estimates have been made for the doublet splitting [25]). These range from 2 to 9 MeV, and the question is still unresolved, theoretically. (Using Brueckner's approach, Sawicki obtains 6.5 MeV, which is probably very close, as will be seen later.)

respectively. Similarly, Fe 54 with two $\mathrm{f}_{\frac{7}{2}}$ proton holes, has the same levels at 0, 1.41, 2.54, 3.16 MeV, and Cr 52 at 0, 1.43, 2.37, and 3.16 MeV. These suggest that the 4+ and 6+ levels in Ca 42 are the 2.42 and 3.25 MeV levels, respectively.

Still another line of reasoning is the following: if we assume that the amount of configuration interaction is approximately the same in the (predominantly $\mathrm{f}_{\frac{7}{2}}^2$) 0+, 2+, 4+, and 6+ levels, then even away from the collective region (where $E_J \propto J(J+1)$), we might expect E_J to be a smooth function of J [16]). Thus, in the long-range limit, the $\mathrm{f}_{\frac{7}{2}}^2(J)$ matrix elements for a pure singlet force, have the energy dependence $E_J \propto \text{const.} + J(J+1)$.

Making all the possible spin-parity assignments listed above, a plot of E_J vs. J indicates that no reasonable curve will go through the point at 1.84 MeV, suggesting that it is not the 4+ level. However, it does not differentiate well enough between levels 3 and 4 to enable us to give the 4+ assignment unambiguously to either. Similarly, either level 4 or 5 could be 6+.

Similar analyses have been made, based on the j—j coupling shell model [17]). The differences between the Ca 42 and Ca 44 spectra, however, which should be nonexistent in pure j—j, indicates that the Uretsky analysis will not serve to determine the Ca 43 levels and assignments. Moreover, there is not enough data available to enable us to use the more general centre-of-gravity theorem of Lawson and Uretsky [18]).

Finally, this question was cleared up towards the end of these calculations, when a preprint arrived from Morinaga [19]), who repeated the γ—γ angular correlation experiment. He finds, contrary to Cappeller, the 1.84 MeV level to be 0+ unambiguously, the 2.42 level to be probably 2+, and the 2.75 MeV level as a probable 0+ or 4+.

2.3. CALCIUM 43

Again, LF used the levels and assignments given by Lindqvist and Mitchell[20]): 0, 0.369, 0.627 and 0.81 MeV, with assignments $\frac{7}{2}$, $\frac{5}{2}$, $\frac{3}{2}$ and $\frac{9}{2}$, respectively. Later work [21]) gives the levels 0, 0.374, 0.593, 0.992, 1.395, 1.678 MeV, with spin-parity assignments $\frac{7}{2}-$, $\frac{5}{2}-$, $\frac{3}{2}-$, $(\ldots)+$, $(\ldots)+$, and several close levels at $\approx$ 1.95 MeV. Thus, the fifth excited level is the lowest candidate for the $\frac{9}{2}-$ assignment, which is the only significant deviation from the previous scheme. As Lindqvist points out, the simplest explanation for the even parity of levels 3 and 4 is that a neutron is excited up from a lower shell into $\mathrm{f}_{\frac{7}{2}}$, giving us an $\mathrm{f}_{\frac{7}{2}}^4 l_j^{-1}$ configuration. The holes would then presumably determine the spin and parity of the excited states if the neutrons form themselves into a seniority zero group. We would then expect the lowest even-parity state to be $\mathrm{d}_{\frac{3}{2}}$, since this is the highest level below $\mathrm{f}_{\frac{7}{2}}$, followed by either $\mathrm{d}_{\frac{5}{2}}$ or $\mathrm{s}_{\frac{1}{2}}$. The $l = 2$ assignments given these levels then strongly suggest levels 3 and 4 to be $\mathrm{d}_{\frac{3}{2}}$ and $\mathrm{d}_{\frac{5}{2}}$, respectively.

Ca 42 (d, p) Ca 43 stripping ^{22}) gives very small cross-sections to the $\frac{5}{2}-$ and $\frac{3}{2}-$ levels. More relevant are the relative reduced widths S computed therefrom, as shown in table 1 of French and Raz's analysis ^{23}) of Bockelman's stripping results. These are quite small (<0.05), and therefore of essentially multiparticle character, most likely $f_{\frac{7}{2}}^3$.

The experimental differential scattering cross-section for level 3 is very similar to that for level 2 in Ca 41; neither is well fitted by either $l=2$ or $l=3$ Butler curves, but there is a preference for $l = 2$, since it is known that Coulomb corrections tend to push the maximum to larger angles, whereas the nuclear corrections are generally small ^{24}). Interpreting it as the $f_{\frac{7}{2}}^4 d_{\frac{3}{2}}^{-1}$ level, as we have done above, therefore leads us to interpret the 2.01 MeV level in Ca 41 as $f_{\frac{7}{2}}^2 d_{\frac{3}{2}}^{-1}$. Level 3 in Ca^{43} is lower than 2.01 MeV because it is depressed further by the greater configuration interaction from the richer spectrum of Ca 43.

The Ca 43 levels are obtainable from the matrix elements of Ca 42, and in pure j—j coupling, directly from the levels of Ca 42 (LF's "projection"). With the 2+, 4+, and 6+ levels at 1.523, 2.422 and 3.250 MeV, we find the projected Ca 43 levels as 0. 463, 0.717, 1.631 and 1.851 MeV above the $\frac{7}{2}-$ ground state, with spins $\frac{5}{2}-$, $\frac{3}{2}-$, $\frac{9}{2}-$ and $\frac{11}{2}-$. Thus it is possible that level 5 could be the $\frac{9}{2}-$ and one of the levels at 1.904 or 1.932 MeV, $\frac{11}{2}-$. Sheline (ref. ^{16}), p. 486) points out that one would expect an intense M1 gamma ray from the $\frac{9}{2}-$ level after the β^+ decay of Sc 43. Such a γ is not observed. This is quite reasonable, however, if the $\frac{9}{2}-$ level is, as is suggested here, the 1.68 MeV level (or higher!). Even for electron capture, the energy difference between the Sc 43 ground state and the 1.68 MeV level is only $2.202-1.678 = 0.524$ MeV.

2.4. BINDING AND INTERACTION ENERGIES

We find ^{26}) that

$$\begin{aligned} \text{Ca } 40+\text{n} &= \text{Ca } 41+\ \ 8.364 \text{ MeV}, \\ \text{Ca } 41+\text{n} &= \text{Ca } 42+11.480 \text{ MeV}, \\ \text{Ca } 42+\text{n} &= \text{Ca } 43+\ \ 7.923 \text{ MeV}. \end{aligned}$$

These values for the binding energy of the last neutron are very close to those given by Braams ^{27}). The binding energy may reasonably be attributed to interaction with the core (the "core bond") plus interaction with the other loose neutrons (the "particle bond"). Thus in Ca 42, if we assume each core bond to be 8.364 MeV, this leaves 3.116 MeV for the particle bond. (Braams' values give 3.110 MeV, which is the value used in these calculations.) Calculating similarly for three particles, we have just 2.675 MeV for the particle bond. On the other hand, there is no good a priori reason for attributing any specific value to the core bonds. Indeed, LF calculated 3.57 MeV for the Ca 43 particle bond, a reasonable enough value which was adopted for this work. This implies that the core bond is 8.07 MeV per particle, which is consistent with Kurath's^{12})

A^{-1} dependence for the core bonds. This is not quite consistent, on the other hand, with the assumption of 8.364 MeV for the core bonds in Ca 42, but the effect on the splittings is probably not very great. This is inferred from the near constancy of the calculated Ca 42 and Ca 43 splittings as a function of the two-particle bond, ranging from 2.7 to 3.11 MeV (see table 5).

In view of these uncertainties, it is now felt that it would perhaps be better to make no assumptions as to the distribution of binding energy between core and particles, in any future calculation.

3. Calculations with Central Forces

Empirical evidence [28] indicates that nucleon-nucleon forces for identical nucleons have a large central singlet component, very small central triplet, and an appreciable triplet tensor component. Thus for n—n, we have central singlet even, central triplet odd, and tensor triplet odd contributions, of which the largest is the first. In keeping with the LF calculation, the calculations were begun assuming a pure singlet potential of Gaussian radial dependence:

$$V = -P_s V_0 e^{-r^2/r_0^2}, \tag{2}$$

where P_s is the singlet projection operator.

The general expression for the angular part of the integral is given by eq. (A2) in French and Raz's paper [23]. For the radial integrals, perhaps the best-known general method is that due to Talmi [29]. For harmonic-oscillator wave functions and potentials, however, the simpler formula due to Konopinski [30] is more useful. We make the (usual) approximation that the Ca 40 well looks the same to particles in any level, so that we take the range of the wave functions to be the same,

$$\nu_l = \nu_{l'} = \nu \equiv \frac{2}{r_n^2}. \tag{3}$$

That is, we ignore the $\mathbf{l} \cdot \mathbf{s}$ splitting (which clearly increases the radius for the $l-\frac{1}{2}$ level, and decreases it for the $l+\frac{1}{2}$ level). The matrix elements are then

$$\langle V \rangle = \sum_k N_k[k]\mathscr{F}_k, \tag{4}$$

where $[k]N_k$ are the angular integrals, and $\mathscr{F}_k$ is equal to F_k for nodeless functions, and to linear combinations of F_k's for higher n's. These linear combinations are listed in Appendix A. The angular integrals $[k]N_k$ are given in Appendix B. The radial integrals are in Appendix C, and most of the matrix elements (used in this calculation) for singlet and Wigner forces are given in Appendix D. $1f_{\frac{7}{2}}$, $2p_{\frac{3}{2}}$, $1f_{\frac{5}{2}}$, $2p_{\frac{1}{2}}$ and $1g_{\frac{9}{2}}$ are the single-particle configurations taken into account.

3.1. MATRIX DIAGONALIZATION

In every case except one, we are only interested in the lowest eigenvalue, so that a complete diagonalization is unnecessary. Instead, we note that for an operator H, with eigenvalues and eigenvectors $Hu_n = \lambda_n u_n$, we may expand any wave function in terms of the (presumably complete) basis $\{u_n\}$:

$$\psi = \sum_n a_n u_n. \tag{5}$$

Then $H\psi = \sum_n a_n \lambda_n u_n$, and if we apply H k times, we have

$$H^k \psi = \sum_n a_n \lambda_n{}^k u_n. \tag{6}$$

Clearly, if there is a finite number of eigenvalues (as there must be for any finite matrix) and H is non-degenerate, there is one of maximum modulus, say the m^{th},

$$|\lambda_m| > \lambda_i \quad \text{for all } i \neq m. \tag{7}$$

Then, as k increases, the ratio of the m^{th} term in (6) to the other terms increases without bound. Thus

$$\lim_{k\to\infty} H(H^k\psi) = \lambda_m(H^k\psi). \tag{8}$$

Thus, if the lowest eigenvalue is larger in magnitude than the highest, we can find it by this procedure, merely by continual multiplication by H. Now it may turn out that this is not the case, or that even if it is, the convergence is slow because the next largest eigenvalue is close to the largest. Then we note that

$$(H-\mu 1)\psi = \sum_n a_n(\lambda_n-\mu)u_n. \tag{9}$$

Convergence will be fastest when $(\lambda_m-\mu)/(\lambda_n-\mu)$ is largest, for all $n \neq m$. This will be roughly obtained when the denominator is zero, on the average, i.e. $\overline{\lambda_n-\mu} = 0$. Since $\bar{\mu} = \mu$, $\mu = \bar{\lambda}_n = \text{Tr}\, H-\lambda_m \approx \text{Tr}\, H-H_{mm}$. Again, we will surely speed convergence by taking a good approximation ψ for u_m in the first place. Hence, we use perturbation theory to obtain our first approximation to u_m,

$$u_m{}^0 = \sum_j{}' \frac{H_{mj}}{E_{mm}-E_{jj}}\,\delta_j+\delta_m, \tag{10}$$

where δ_j is a column vector with unity in the j^{th} place, zeros elsewhere. Calling the first guess u_0, and

$$(H-\mu 1)u_j \equiv u_{j+1},$$

we find that the series $(u_j, u_j)/(u_{j-1}, u_j)$ converges much more quickly than $\eta_j \equiv (u_j, \delta_m)/(u_{j-1}, \delta_m)$.

As a check on the LF calculation, we calculated the Slater parameters for the various matrix elements, for the range $\rho = 0.847$ ($\lambda = 1.18$) and strength $V_0 = -14.4$ MeV, used by LF, so as to be able to compare them with those calculated by them using the empirical method.

The latter were found by using table 1 (p. 15) and the values of V_J given in eq. (7) (p. 16) of LF III. The two calculations give different values for F^k. The V_J calculated from either set were about the same, but the inconsistency must have shown up more strongly in the other matrix elements, particularly the off-diagonal ones. This is reflected in the eigenvalue calculation: we find $E_0 = -2.8562$ MeV (rather than the expected -3.2); the wave function is $81.4\ \% \ |f_{7/2}^2(0)\rangle$, $10.5\ \% \ |f_{5/2}^2(0)\rangle$, $5.0\ \% \ |g_{9/2}^2(0)\rangle$, and the p-states contribute $3.1\ \%$. The calculation for $J = 2$ is much simpler if we exclude the p-states; whereupon we find $E_0 = -2.738$ MeV, $E_2 = -1.850$ MeV. Thus we have a $2+ - 0+$ splitting of 0.888 MeV, rather than the 1.51 which should result. Assuming they had made no arithmetic error, we concluded that the singlet force is inadequate to give us the desired splittings; however, if we avoided making any approximations in the calculations of the Slater parameters, it was

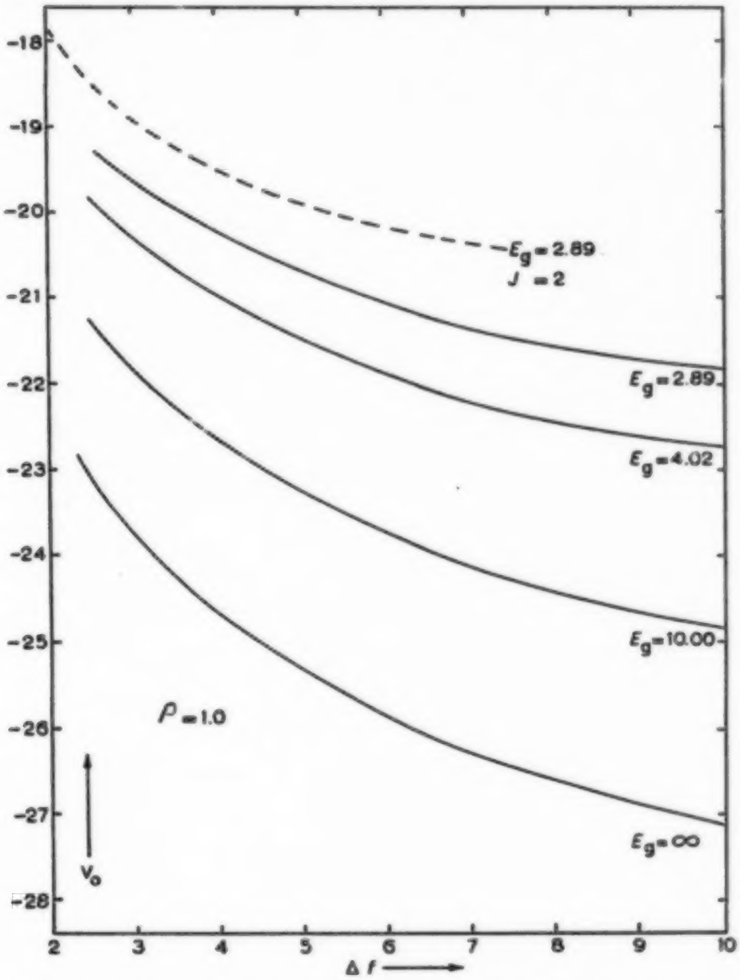

Fig. 1. Strength of singlet potential required to give $E_0 = -3.11$ MeV as a function of Δf and E_g. The dashed curve results from solution of the $J = 2$ secular equation.

still conceivable that a singlet force might work, proviced we find the correct range and strength.

The calculation was set up in the following way: the p-states were ignored as having negligible influence on the Ca 42 levels. The $g_{\frac{9}{2}}-f_{\frac{7}{2}}$ splitting was labeled E_g. Considering V_0, ρ, and Δf as unknowns, the secular equation for $J = 0$ permits us to solve for any of these in terms of the other two. If we include E_g as a parameter, then the $J = 0$ and $J = 2$ equations together permit one to solve for two of the unknowns ρ, V_0, E_g, Δf in terms of the other two. This is done, of course, by inserting the (experimentally known) values of E_0 and E_2 in the respective secular equations. The $J = 0$ secular equation is a 3×3 determinant.

From LF's work, we expect a simplification due to the force being singlet. Indeed, expanding the resulting cubic in V_0, we find that the cubic term vanishes, and we are left with a quadratic in V_0. We solve for V_0 as a function of Δf, for several values of E_g and ρ. The solutions for $\rho = 1.0$ are shown in fig. 1. Then we do the same for $J = 2$, and observe the intersections of the curves, so that there is a unique V_0 and E_g for each ρ and Δf. The $J = 2$ secular equation is a 4×4 determinant. Expanding the determinant, the equation again simplifies, to a cubic.

A simpler procedure, however, can be used: We note that E_g occurs only once in each of the $J = 0$, $J = 2$ secular equations. Thus, these equations are linear in E_g, and they are relatively easy to solve for E_g. Inserting E_g from one of the equations (as a function of ρ, V_0, etc.) in the other, we obtain an equation for V_0 directly. The solutions obtained are given in table 1. Entries left blank

TABLE 1

Simultaneous solutions for the $J = 0$ and $J = 2$ secular equations for singlet forces

ρ	Δf(MeV)	$-V_0$(MeV)	E_g (MeV)
0.6	2		
	4		
0.8	2		
	7		
1.0	2		
	4		
	7		
1.2	2		
	3	17.18	−0.2027
	4	17.62	−0.1886
	7	18.41	−0.1603
1.4	2	19.00	−0.3936
	4	20.04	−0.3842
	7	15.49	−0.8566
1.6	2	21.91	−0.5000
1.7	2	23.59	−0.5339

indicate that no solution exists. Thus, even when the curves *do* cross the E_g obtained is non-physical. Several calculations with $E_0 = -2.9$ and -2.7 MeV carried out as described later, still gave negative E_g.

Thus, it was found that a singlet force is inadequate to give the ground and first excited states of Ca 42.

The next step was to try a mixture of singlet and triplet potentials. Now

$$P_W = P_s + P_t, \tag{11}$$

so that, if we admix a fraction α of Wigner force,

$$V_0[P_s+\alpha P_W] = V_0[P_s+\alpha P_s+\alpha P_t] = V_0(1+\alpha)\left[P_s+\frac{\alpha}{1+\alpha}P_t\right]. \tag{12}$$

TABLE 2

Simultaneous solutions for the $J = 0$ and $J = 2$ secular equations, for mixed exchange forces

ρ	Δf (MeV)	α	$-V_0$ (MeV)	E_g (MeV)
0.6	2.014	−0.2		
		0		
		0.2		
	4	−0.36	26.51	−0.601
		−0.20	21.62	−0.411
		0	17.62	−0.188
		0.20	15.11	0.063
		0.40	13.58	0.425
1.0	2.014	0		
		0.4		
	3	0		
		0.2	9.70	−0.514
		0.4	8.07	−0.489
		0.6	6.98	−0.439
	4	−0.2	19.36	−0.14
		0		
		0.2		
1.2	2.014	0.4	13.0	0.3543
		0.5	12.8	0.8127
		0.7	12.6	1.790
	3	0.4	11.8	0.2595
		0.5	13.0	0.717
		0.6	13.0	1.333
1.6	2.014	0	21.6	−0.489
		0.4	21.7	−0.029
		0.8	20.6	0.721
	4	−0.2		−0.58
		0	23.6	−0.48
		0.2	19.30	−0.389
		0.4	16.43	−0.338
		0.6	14.39	−0.257
		0.8	12.92	−0.188
		1.6	9.05	−0.012

where P_s is the singlet projection operator, P_t the triplet projection operator, and P_W = Wigner projection operator.
This is equivalent to admixing the fraction $\alpha/1+\alpha$ of triplet mixture, and making the potential deeper by the factor $(1+\alpha)$. This is convenient to do, as we have a relatively simple expression for thematrix element of the Wigner force between identical particles,

$$\begin{aligned} N_k &\equiv \langle (l'_1 s'_1) j'_1 (l'_2 s'_2) j'_2 jm | P_k(\cos\theta) | (l_1 s_1) j_1 (l_2 s_2) j_2 jm \rangle \\ &= \frac{(-1)^{j_2+j'_2+j}}{[k]} [j_1]^{\frac{1}{2}} [j_2]^{\frac{1}{2}} [j'_1]^{\frac{1}{2}} [j'_2]^{\frac{1}{2}} C_{j_1 j'_1 k} C_{j_2 j'_2 k} W(j_1 j_2 j'_1 j'_2; jk) \varepsilon(l_1 l'_1 k) \varepsilon(l_2 l'_2 k). \end{aligned} \tag{13}$$

The Clebsch-Gordan coefficients $C^{jj'k}_{\frac{1}{2}-\frac{1}{2}}$ of interest have been conveniently tabulated [31]). All the computed N_k's are given in Appendix B, the matrix elements in D. We tabulate the results of this wider search in table 2. From these results, it appears that the only value of Δf which can give us the first two levels of Ca 42 using a central force only, and with reasonable value of E_g, is $\Delta f = 2.014$ MeV, with $0.8 < \alpha < 1.0$ and $1.1 < \rho < 1.3$. It was decided at this point that, in order to continue this search including the p-states, and calculate the Ca 43 energy levels as well, an electronic calculating machine's speed and patience was required.

3.2. FRACTIONAL PARENTAGE COEFFICIENTS

An n-particle configuration can be considered as arising from an $(n-1)$-particle configuration, angular-momentum coupled to an n^{th} particle. When the n- and $(n-1)$-particle wave functions are properly antisymmetrized, the total wave function is expressible as a linear combination of the parent configurations,

$$\psi_A(JT; n) = \sum_{J'T'} F^{JT}_{J'T'} | \psi_A(J', T'; n-1) \psi(j, t; 1) : J, T \rangle, \tag{14}$$

where the subscript A means the wave function is antisymmetrized in the number of particles shown by the last number in the argument of ψ. The coefficients F are the fractional parentage coefficients, first introduced by Bacher and Goudsmit [32]). When $n = 3$ and the particles are identical, only two kinds appear,

$$F^{j}_{j'j'} \equiv \langle j_a j_c (j'') j_b | \} j_a j_b (j') j_c j \rangle \tag{15}$$

and

$$\hat{F}^{j}_{j'j''} \equiv \langle j_c j_b (j'') j_a | \} j_a j_b (j') j_c j \rangle. \tag{16}$$

If nucleons 1 and 2 are *equivalent* [i.e. $(n_a l_a j_a) = (n_b l_b j_b) \neq (n_c l_c j_c)$], then we find that

$$\begin{aligned} \psi_A(j_a j_a j_c, J'T'JJ_z TT_b) &= \frac{1}{\sqrt{3}} \varphi | (j_a j_a J'T')_A j_c : JT \rangle + (-1)^{j_c+\frac{1}{2}+J+T} \sqrt{\tfrac{2}{3}} \\ &\times \sum_{J'', T''} (-1)^{J''+T''} U(j_a j_b J j_c : J'J'') U(\tfrac{1}{2}\tfrac{1}{2}T\tfrac{1}{2} : T'T'') \varphi | (j_c j_c J''T'')_A j_a JT \rangle, \end{aligned} \tag{17}$$

where the arguments are in standard order, i.e. the *first* angular momentum is that of particle *one*, and so on. The U's are Jahn's normalized Racah coefficients. The coefficients of the φ's are the fractional parentage coefficients (fpc's). If the three nucleons are identical, $T_\zeta = \frac{3}{2}$, and for the lowest energy levels, $T = \frac{3}{2}$. Therefore $T' = T'' = 1$. Since $J'+T'$ and $J''+T''$ are now odd, J' and J'' are even. Moreover, $U(\frac{1}{2}\frac{1}{2}\frac{3}{2}\frac{1}{2}; 11)=1$. When all three particles are equivalent, the derivation follows in the same way, but the normalization is different,

$$j_a = j_b = j_c = j$$

$$\rightarrow |j^3J\rangle = \frac{1}{A}\sum_{J''}^{e}\,[\delta_{J'J''}+(-1)^{j+J}2U(jjJj:J'J'')]\varphi|j^2(J'')j:J\rangle, \tag{18}$$

where the e appearing on the sum symbol means J'' is to be summed over even (integral) values only. A is found, then, by requiring that $\langle j^3J|j^3J\rangle = 1$. Expanding, we find

$$A^2 = \sum_{J''}^{e}\,[\delta_{J'J''}-4(-1)^{j+J}\delta_{J'J''}U(jjJj:J'J'')+4U(jjJj:J'J'')^2].$$

Now,

$$2\sum_{e}^{e} U(aacd:ef)U(aacd:eg) = \delta_{fg}+(-1)^{f+g-2a-c-d}U(acda:fg). \tag{19}$$

Identifying *abcdef* with $jjjJJ''J'$, we therefore have, since J' is an integer,

$$\begin{aligned}2\sum_{J''}^{e} U(jjjJ:J''J')U(jjjJ:J''J') &= 1+(-1)^{2J'-2j-j-J}\,U(jjJj:J'J'),\\ &= 1+(-1)^{j+J}U(jjJj:J'J').\end{aligned}$$

It follows that

$$A^2 = 3[1-2(-1)^{j+J}U(jjJj:J'J')]. \tag{20}$$

This formula has been derived in equivalent ways [33]). Note that there is a degeneracy here, i.e. any even J' (satisfying $0 \leqq J' < 2j$ and $|J'-j| \leqq J \leqq J'+$ $+j$, of course) gives the same wave function. On the other hand, those cases prohibited by the Pauli principle must give $A = 0$, indicating that the wave function vanishes. The sign of A is not given, so that these formulas only give the fractional parentage coefficients up to a phase. They are all listed in Appendix F. When all three particles are inequivalent (but identical), we obtain (instead of (17)), an expression involving the recoupling given by $\hat{F}^{J}_{J'J''}$.

3.3. THREE-PARTICLE MATRIX ELEMENTS; PROJECTION

Thus, in general, abbreviating the Kronecker symbols $\delta_{j_aj_b} \equiv \delta_{ab}$ and $\delta_{ab}\delta_{bc} = \delta_{abc}$, we have the properly coupled and antisymmetrized three-particle wave function:

$$\begin{aligned}\psi_A|j_aj_b(J)_Aj_c:J_0\rangle &= 3^{-\frac{1}{2}}(1-\delta_{abc})|j_aj_b(J)j_c:J_0\rangle\\ &\quad+\sum_{J'} F^{J_0}_{JJ'}|j_aj_c(J')j_b:J_0\rangle+(1-\delta_{ab})\sum_{J'}\hat{F}^{J_0}_{JJ'}|j_cj_b(J')j_a:J_0\rangle,\end{aligned} \tag{21}$$

where, as always, the entries are in standard order.

We wish to compute, in general, the matrix elements of the interaction among three particles,

$$H^{(3)} \equiv \sum_{i>j}^{3} H_{ij}.$$

In general,

$$\langle H^{(n)} \rangle = \tfrac{1}{2}n(n-1)\langle \mathrm{H}_{ij} \rangle \tag{22}$$

so that

$$\begin{aligned}\langle H_3 \rangle \equiv \langle j_a' j'_b(J_1) j'_c : J_0 | H^{(3)} | j_a j_b(J_2) j_c : J_0 \rangle \\ = 3\langle j'_a j'_b(J_1) j'_c : J_0 | H^{(2)} | j_a j_b(J_2) j_c : J_0 \rangle,\end{aligned} \tag{23}$$

and it is easy to find $\langle H_3 \rangle$ by using the expansion (21). We easily find the expression for the three-particle matrix elements in pure j—j coupling, from the result. Thus $j_a = j_b = j_c = j$ leads to only one surviving term,

$$\langle j^3 : J_0 | H | j^3 : J_0 \rangle = 3 \sum_{J'}^{6} |F^{J_0}_{J_1 J'}|^2 \, \langle j^2 : J' | H | j^2 : J' \rangle. \tag{24}$$

Since there is only one term in this "matrix", it is automatically diagonal, and is just the energy level (corresponding to $J = J_0$) for three particles, in terms of the two-particle levels. This is, then, the "projection" formula referred to above.

3.4. RESULTS OF PRELIMINARY MACHINE CALCULATIONS

The Ca 43 matrices were calculated for $J = \frac{3}{2}, \frac{5}{2}, \frac{7}{2}, \frac{9}{2}$ and $\frac{11}{2}$. The matrices were limited to 25×25, which was sufficiently large to include most of the 3-particle configurations arising from the given two-particle configurations.

The first calculation that was made was an attempt to duplicate the FL calculation. A singlet (even) potential was used, where the strength V of the interaction is calculated so as to give a particle bond of 3.11 MeV for Ca 42. As in LF III, we take $E_g = 2.89$ MeV, $\Delta f = 2.014$ MeV. Their range was $\lambda = 1.18$, corresponding to $\rho = 0.847$; this was approximated by 0.850. The eigenvalues and principal diagonal elements are shown in table 3a and the normalized eigenvectors, together with those found by Kennedy in a similar calculation with a Rosenfeld interaction [4]), in table 3b. The energy levels predicted for Ca 42 and Ca 43 are shown in fig. 2. As is seen, the overlaps are excellent,

TABLE 3a

Calcium 42 : lowest eigenvalues $E(J)$ and diagonal elements $f_{\frac{7}{2}}^2(J)$

$\Delta f = 2.014$, $\rho = 0.850$, $\alpha = 0$, $V = -15.41143$, $E(\frac{3}{2}) = 2.890$ MeV	
$E(0) = -3.1100$ -1.98610	$E(4) = -1.4629$ -0.74106
$E(2) = -2.0692$ -1.34114	$E(6) = -1.3900$ -0.39828

TABLE 3b

Eigenvectors corresponding to eigenvalues shown in table 3a. The notation has been further simplified here by dropping the ket symbol and the resultant angular momentum J (which appears in the first column)

J	Configuration	Mixture amplitude		Overlap
		This calculation	Kennedy	
0	77	0.895	0.89	0.9998
	33	0.161	0.17	
	55	0.338	0.34	
	11	0.099	0.11	
	99	−0.237	−0.22	
2	77	0.906	0.93	0.9702
	37	0.157	0.22	
	57	−0.225	−0.19	
	55	0.261	0.17	
	99	−0.180		
	35	0.043	0.05	
	33	0.043	0.05	
	13		−0.07	
	15		0.09	
4	77	0.813	0.95	0.9509
	37	0.247	0.11	
	57	−0.360	−0.24	
	17	−0.254	−0.13	
	35	0.209	0.09	
	55	0.169	0.10	
	99	−0.111		
6	77	0.706	0.91	0.9364
	57	−0.706	−0.42	
	99	−0.064		

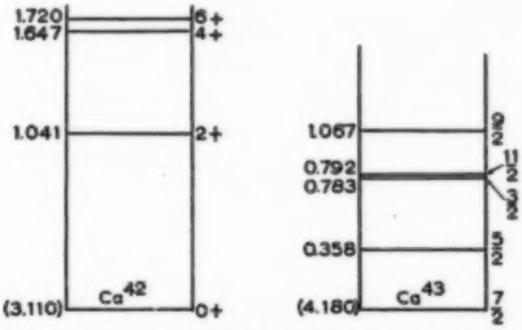

Fig. 2. Energy levels of Ca^{42} and Ca^{43} as given in tables 3a and 3b.

particularly for the ground and lowest excited state. This seems to argue that the mixture amplitudes, at any rate, are insensitive to the force shape and mixture (and are, possibly, model-independent).

TABLE 4

Eigenvectors and eigenvalues of calcium 43 matrices

$E(\frac{3}{2}) = -3.3975$			$E(\frac{5}{2}) = -3.8223$		$E(\frac{7}{2}) = -4.1803$		$E(\frac{9}{2}) = -3.1129$		$E(\frac{11}{2}) = -3.3888$	
Configuration	Kennedy's amplitudes	Present amplitudes	K	L	K	L	K	L	K	L
777	0.948	0.882	0.937	0.923	0.933	0.902	0.934	0.873	0.916	0.859
77(0)5	0.0	0.0	−0.040	0.035	0.0	0.0	0.0	0.0	0.0	0.0
77(2)5	−0.074	0.063	0.026	0.101	−0.028	−0.113	−0.037	−0.114	0.0	0.0
77(4)5	0.019	−0.056 *	0.080	0.078	−0.040	−0.087	−0.246	−0.333	−0.193	−0.305
77(6)5	0.0	0.0	0.0	0.0	−0.073	−0.091	0.092	0.112	−0.261	−0.291
77(0)3	−0.030	0.088	0.0	0.0	0.0	0.0	0.0	0.0	0.0	0.0
77(2)3	−0.209	−0.290	0.160	−0.117	−0.035	0.066 *	0.0	0.0	0.0	0.0
77(4)3	0.0	0.0	0.175	−0.135	−0.027	−0.027	0.005	0.045	−0.028	0.058 *
77(6)3	0.0	0.0	0.0	0.0	0.0	0.0	0.091	0.017	0.141	−0.114
77(2)1	0.099	−0.184	−0.042	−0.070	0.0	0.0	0.0	0.0	0.0	0.0
77(4)1	0.0	0.0 *	0.0	0.0	−0.025	−0.043	0.146	0.191	0.0	0.0
77(6)1	0.0	0.0	0.0	0.0	0.0	0.0	0.0	0.0	−0.035	−0.035
55(0)7	0.0	0.0	0.0	0.0	−0.287	0.273	0.0	0.0	0.0	0.0
55(2)7	0.129	0.153	0.181	0.233	0.061	−0.084 *	0.083	0.114	−0.120	0.166 *
55(4)7	−0.085	−0.131	0.019	0.031	0.031	0.052	−0.085	−0.123	0.058	−0.070
35(2)7	0.033	0.013	0.052	0.035	0.015	0.016 *	0.024	0.011	−0.048	0.050 *
35(4)7	−0.077	−0.161	0.023	0.042	0.031	−0.057	−0.085	−0.123	0.049	−0.074
33(0)7	0.0	0.0	0.0	0.0	−0.142	0.124 *	0.0	0.0	0.0	0.0
33(2)7	0.036	0.038	0.048	0.053	0.017	−0.012	0.026	0.014	−0.040	0.027 *
11(0)7	0.0	0.0	0.0	0.0	−0.089	0.070 *	0.0	0.0	0.0	0.0 *
99(0)7		0.0		0.0		−0.188		0.0		0.0
99(2)7		−0.109		−0.180		0.067		−0.093		−0.155
99(4)7		0.093		−0.025		0.052		0.093		0.031
99(6)7		0.0		0.005		0.017		−0.032		0.033
99(8)7		0.0		0.0		0.0		0.005		−0.009
13(1)7	0.0		0.001		0.0		−0.001		0.0	
13(2)7	−0.053		−0.080		−0.026		−0.034		0.058	
15(2)7	0.067		0.097		0.027		0.055		−0.067	
15(3)7	−0.002		0.003		0.0		−0.008		−0.005	
35(1)7	0.0		−0.005		−0.001		−0.006		0.0	
35(3)7	0.001		0.002		0.001		0.001		−0.009	
(K/L) ≡ overlap = 0.9631			(K/L) = 0.9657		(K/L) = 0.9695		(K/L) = 0.9725		(K/L) = 0.9717	

Note: The letters K and L stand for "Kennedy" and "Levinson", respectively; the latter, because the present calculation was made using his prescription.

The Ca 43 eigenvectors resulting from the above calculations are given in table 4, again together with Kennedy's. For the first vector (corresponding to $j = \frac{3}{2}$), we list the configurations. The first 25 are those considered in this work. The last 6 are those considered by Kennedy, but not by us; finally, configurations 21—25, which include the g-states, were not included by Kennedy.

Presumably because of a different set of phases in Kennedy's fpc's and those derived here, sets of mixture amplitudes differ in sign; these are bracketed and starred. (Of course, the eigenvalues are unaffected by these phase differences.) Again, the overlaps are seen to be very good. On the other hand, though it might be thought that with such good overlaps the spectra would be similar, this is not the case, as is seen from the energy levels calculated by Kennedy: for Ca 42, an interaction energy of 2.40 MeV, and the 2+, 4+, 6+ levels 1.50, 1.86 and 1.99 MeV above the ground state 0+; for Ca 43, an interaction energy of 1.80 MeV, with the $\frac{5}{2}-$, $\frac{11}{2}-$, $\frac{3}{2}-$ and $-\frac{9}{2}$ states 0.80, 0.98, 1.03 and 1.10 MeV above the ground state $\frac{7}{2}-$.

Now, every additional configuration which is included will depress the ground state. Since we did not include all possible configurations, it was thought not unreasonable that we should fit to an interaction energy somewhat smaller than 3.11 MeV in magnitude. Calculations with $E_0 = 2.9$ and 2.7 MeV were carried out, using still the same parameters, but there was no significant difference in the splittings (see table 5). A systematic search was then made for a set of parameters which would give us the desired results. It was found that the simplest criterion was to insist that $E_g \geqq 2$ MeV. Over most of parameter space, the calculated E_g is negative (when there is a solution at all). For $\Delta f =$ $= 2.014$ MeV, it was thus found that if a solution exists, it must lie in the area $1.26 \leqq \rho \leqq 1.37$, $1.1 \leqq \alpha \leqq 1.7$. The behavior is generally similar to that found by the hand calculations (where the p-states were ignored). The remarkable thing, however, is that for any set of parameters in this area, the calculated energy levels are almost constant, at 1.52, 2.14 and 2.26 MeV for the 2+, 4+, 6+ levels in Ca 42, and 0.60, 1.01, 1.31 and 1.67 MeV for the $\frac{5}{2}-$, $\frac{3}{2}-$, $\frac{11}{2}-$ and $\frac{9}{2}-$ levels in Ca 43. These hardly change for different Δf values.

TABLE 5

Ca 42 and Ca 43 spectra as a function of the 2-particle bond

E_0	E_2-E_0	E_4-E_0	E_6-E_0	$E_{\frac{7}{2}}$	$E_{\frac{5}{2}}-E_{\frac{7}{2}}$	$E_{\frac{3}{2}}-E_{\frac{7}{2}}$	$E_{\frac{11}{2}}-E_{\frac{7}{2}}$	$E_{\frac{9}{2}}-E_{\frac{7}{2}}$
2.7	0.904	1.472	1.553	3.675	0.301	0.693	0.706	0.947
2.9	0.971	1.559	1.635	3.923	0.328	0.737	0.748	1.006
3.11	1.041	1.647	1.720	4.180	0.358	0.783	0.792	1.067

Thus the fits are highly unsatisfactory. This could be attributed to:

a) neglect of higher configurations;

b) inadequacy of the shell model;

c) neglect of core configurations, or equivalently, of surface-particle (collective) interactions;

d) poor choice of an interparticle force.

Higher configurations, we can confidently expect, contribute little. We must ignore the second possibility, within the spirit of this work! Moreover, Talmi's success in calculating the binding energies of nuclei in the f shell à la $j-j$ coupling shell model argues for its validity, as do all the other successes of the shell model. Finally, since we had already decided to neglect the core, there is no choice left but to generalize the forces we use. The most plausible generalization seems to be to include non-central forces, and of these, the tensor force was chosen as likeliest to play a rôle.

4. Tensor Forces

The matrix elements of the tensor operator

$$S_{12} \equiv \frac{(\boldsymbol{\sigma}_1 \cdot \mathbf{r}_{12})(\boldsymbol{\sigma}_2 \cdot \mathbf{r}_{12})}{r_{12}^2} - \tfrac{1}{3}(\boldsymbol{\sigma}_1 \cdot \boldsymbol{\sigma}_2)$$

(where $\mathbf{r}_{12} \equiv \mathbf{r}_1 - \mathbf{r}_2$) have been explicitly calculated by several authors [34]). We shall use a method developed by Hope and Longdon [35-37]) to evaluate the matrix elements of the Hamiltonian

$$H^T = T_{12} J(r_{12}) S_{12}, \tag{24}$$

where T_{12} is the i-spin operator.

The calculation made by Hope and Longdon was for LS coupled wave functions. Since we work in a $j-j$ coupled representation, we may use their result simply by transforming the wave functions, using the LS-jj coupling coefficients:

$$\langle j_a j_b J m | H^T | j_c j_d J m \rangle$$
$$= \sum_{L,L'} \begin{bmatrix} l_a & \frac{1}{2} & j_a \\ l_b & \frac{1}{2} & j_b \\ L & 1 & J \end{bmatrix} \begin{bmatrix} l_c & \frac{1}{2} & j_c \\ l_d & \frac{1}{2} & j_d \\ L' & 1 & J \end{bmatrix} \langle (l_a l_b) L (S=1) J m | H^T || (l_c l_d) L' (S'=1) J m \rangle. \tag{25}$$

The straightforward calculations using this expression are very tedious, but can, fortunately, be simplified: we sum over L, L' first. To make the notation less cumbersome, call $l_a \equiv a$, $j_a \equiv a'$, etc. Then defining

$$F(xy; rs) \equiv F(abcd; xy; krs\, 2)$$
$$\equiv \sqrt{[x][y]}\, \sqrt{C(axc)C(byd)C(krx)C(ksy)}\, W(rsxy; 2k)$$

and

$$G(x, y) \equiv \sum_{L, L'} (-1)^{L} \begin{bmatrix} a & \frac{1}{2} & a' \\ b & \frac{1}{2} & b' \\ L & 1 & J \end{bmatrix} \begin{bmatrix} c & \frac{1}{2} & c' \\ d & \frac{1}{2} & d' \\ L' & 1 & J \end{bmatrix} \begin{bmatrix} a & b & L \\ c & d & L' \\ x & y & 2 \end{bmatrix} W(L1L'1 : j2),$$

we can write

$$\langle a'b'Jm|H^{T}|c'd'Jm\rangle = 2\sqrt{5}(-1)^{1-J} \sum_{k} \left\{ \frac{A_1^{\,k}}{\sqrt{6}} \sum_{x} F(xk; 20) G(x, k) \right.$$
$$\left. + \frac{A_2^{\,k}}{\sqrt{6}} \sum_{x} F(kx; 02) G(k, x) - B^{k} \sum_{x, y} F(xy, 11) G(x, y) \right\}.$$

Note that, if L and L' have the same parity, and $a = b$, $c = d$, then $G(x, y) = G(y, x)$. Now we find an expression for $G(x, y)$. We write the $LS-jj$ coefficients in Wigner's notation and then expand these in terms of their definition in terms of terms of $6-j$ coefficients,

$$G(x, y) = 3\sqrt{[x][y][a'][b'][c'][d']} \sum_{\substack{L, L' \\ \lambda, \mu, \nu}} (-1)^{L'} [\lambda][\mu][L][L'] \times \begin{Bmatrix} L & 1 & J \\ 1 & L' & 2 \end{Bmatrix} \begin{Bmatrix} a & c & x \\ y & 2 & \lambda \end{Bmatrix}$$
$$\times \begin{Bmatrix} \frac{1}{2} & \frac{1}{2} & 1 \\ b & \mu & b' \end{Bmatrix} \begin{Bmatrix} a' & b' & J \\ \mu & a & \frac{1}{2} \end{Bmatrix} \begin{Bmatrix} \frac{1}{2} & \frac{1}{2} & 1 \\ d & \nu & d' \end{Bmatrix} \begin{Bmatrix} c' & d' & J \\ \nu & c & \frac{1}{2} \end{Bmatrix} \begin{Bmatrix} b & d & y \\ c & \lambda & L' \end{Bmatrix} \begin{Bmatrix} L & L' & 2 \\ \lambda & a & b \end{Bmatrix} \begin{Bmatrix} a & b & L \\ 1 & J & \mu \end{Bmatrix} \begin{Bmatrix} c & d & L' \\ 1 & J & \nu \end{Bmatrix}.$$

We can sum the terms in L, obtaining

$$\begin{Bmatrix} J & a & \mu \\ L' & \lambda & b \\ 1 & 2 & 1 \end{Bmatrix}.$$

We cannot yet sum over L', so we expand the product

$$\begin{Bmatrix} b & d & y \\ c & \lambda & L' \end{Bmatrix} \begin{Bmatrix} c & d & L' \\ 1 & j & \nu \end{Bmatrix} = \sum_{\theta} (-1)^{b+c+d+1+J+L'+y+\lambda+\nu+\theta} [\theta] \begin{Bmatrix} \lambda & y & c \\ \nu & J & \theta \end{Bmatrix} \begin{Bmatrix} y & d & b \\ 1 & \theta & \nu \end{Bmatrix} \begin{Bmatrix} \lambda & b & L' \\ 1 & J & \theta \end{Bmatrix}$$

This leaves us with a single $6-j$ involving L', and we can now sum,

$$\sum_{L'} [L'] \begin{Bmatrix} J & a & \mu \\ L' & \lambda & b \\ 1 & 2 & 1 \end{Bmatrix} \begin{Bmatrix} \lambda & b & L' \\ 1 & J & \theta \end{Bmatrix} = (-1)^{2\theta} \begin{Bmatrix} \mu & a & J \\ \lambda & \theta & 2 \end{Bmatrix} \begin{Bmatrix} 1 & 2 & 1 \\ \theta & b & \mu \end{Bmatrix}.$$

This leaves an expression which we can sum over λ. Finally, we can sum that over θ, and find

$$G(x, y) = 3\sqrt{[x][y][a'][b'][c'][d']} (-1)^{b-a-d+a'+c'-x} \sum_{\mu\nu} (-1)^{\nu} [\mu][\nu]$$
$$\times W(\tfrac{1}{2}1b'\mu : \tfrac{1}{2}b) W(a'ab'\mu : \tfrac{1}{2}J) W(\tfrac{1}{2}1d'\nu : \tfrac{1}{2}d) W(c'cd'\nu : \tfrac{1}{2}J)$$
$$\times W(\mu a\nu c : Jx) \begin{Bmatrix} 1 & \mu & b \\ 1 & \nu & d \\ 2 & x & y \end{Bmatrix}. \tag{26}$$

Note that in this form, there are never more than four terms to compute: $\mu = b' \pm \frac{1}{2}, \nu = d' \pm \frac{1}{2}$.

4.1. THE RADIAL INTEGRALS.

The Konopinski method is inconvenient to use for the "singulated Gaussian" $J(r)/r^2$. We therefore use Talmi's procedure 26). As has been mentioned elsewhere (e.g. by Thieberger 26)), there is an inconsistency in Talmi's definition of I_p. If

$$\psi_{nlm} = \frac{R_{nl}(r)}{r} Y_l^m(\omega),$$

then for the nodeless wave functions, as in Thieberger,

$$R_l(r, \nu) = N_l r^{l+1} e^{-\nu r^2}. \tag{27}$$

Defining $I_l(\nu) \equiv \int_0^\infty R_l^2(\nu, r) V(r) dr$, the radial integral

$$R^k(l_1 l_2, l'_1 l'_2) \equiv \int_0^\infty \int_0^\infty R_{l_1} R_{l_2} R_{l'_1} R_{l'_2} V_k dr_1 dr_2 \tag{28}$$

is given in terms of $I_l(\frac{1}{2}\nu)$:

$$R^k = \sum_{l=0}^{m} T_l^k I_l(\tfrac{1}{2}\nu),$$

where $m \equiv \frac{1}{2}(l_1 + l_2 + l'_1 + l'_2)$, and the T_l^k are coefficients given by Talmi, Thieberger, etc. From the definition (28), we have

$$R^k(l_1 l_2 l'_1 l'_2) = R^k(l'_1 l'_2 l_1 l_2) = R^k(l_2 l_1 l'_2 l'_1),$$

$$R^k(l_1 l_2 l_1 l_2) \equiv F^k(l_1 l_2), \qquad R^k(l_1 l_2 l_2 l_1) \equiv G^k(l_1 l_2).$$

With the LF definition $\lambda \equiv r_0/r_n$, where $r_n^{-2} \equiv \nu$, we see that $\nu r_0^2 = \lambda^2$. Therefore, defining $\eta^2 \equiv \lambda^2/(1+\lambda^2)$, we have, for the singulated Gaussian potential

$$V_{sg}(r) = V_0 \frac{e^{-r^2/r_0^2}}{r^2/r_0^2}, \qquad I_p(\tfrac{1}{2}\nu) = \frac{2V_0 \lambda^2}{[p]} \eta^{2p+1}.$$

Now

$$A_1^k = \frac{N_{l_1} N_{l'_1}}{N_{l_1+1} N_{l'_1+1}} \langle l_1+1, l_2 | J_k | l'_1+1, l'_2 \rangle.$$

Hence, with the potential $V = r_0^{-2} V_{sg}$, which we are using, we can write

$$A_1^k(l_1 l_2 l'_1 l'_2) = \tfrac{1}{4}\sqrt{(2l_1+3)(2l'_2+3)}\,\hat{R}^k(l_1+1, l_2; l'_1+1, l'_2), \tag{29}$$

where

$$\hat{R}^k = \sum_{p=0}^{m} T_p^k \hat{I}_p(\tfrac{1}{2}\nu),$$

with

$$\hat{I}_p = \frac{2V_0}{[p]}\eta^{2p+1}.$$

Note that a similar manipulation enables us to write, equally validly,

$$A_1{}^k = \frac{1}{4\nu}\sqrt{(2l_1+3)(2l_1+5)}R^k(l_1+2, l_2; l'_1, l'_2).$$

The choice we make is one of convenience, i.e. which of these expressions is closest to diagonal form. It follows, in the same way, that

$$A_2{}^k = \tfrac{1}{4}\sqrt{(2l_2+3)(2l'_2+3)}\hat{R}^k(l_1, l_2+1; l'_1, l'_2+1)$$

and

$$\begin{aligned} B^k &= \tfrac{1}{4}\sqrt{(2l_1+3)(2l'_2+3)}\hat{R}^k(l_1+1, l_2; l'_1, l'_2+1) \\ &= \tfrac{1}{4}\sqrt{(2l_1+3)(2l_2+3)}\hat{R}^k(l_1+1, l_2; l'_1, l'_2). \end{aligned}$$

If $l_1 = l_2 = l$ and $l'_1 = l'_2 = l'$, then

$$A_1{}^k = A_2{}^k = \tfrac{1}{4}\sqrt{(2l+3)(2l'+3)}\hat{R}^k(l+1, l; l'+1, l'). \tag{30}$$

Thieberger [29]) does not list all the $T_p{}^k$'s we need, i.e. for the fg matrix elements. But for $l_1 l_2 l'_1 l'_2 = 3, 3, 4, 4$ we have, from (30),

$$A^k = \tfrac{3}{4}\sqrt{11}\,\hat{R}^k(4, 3, 5, 4).$$

We extend the Thieberger table for $R^k(4, 3, 5, 4)$. This is tabulated along with $G^k(0f0g)$ and $G^k(0g0h)$, which are also needed, in Appendix G. (Incidentally, note well that the F^k given by Thieberger are $[k]$ times the corresponding quantities as derived by Konopinski's procedure.)

The range $\lambda = 1$ was arbitrarily chosen, as convenient to work with, and not unreasonable. The matrix elements are listed in Appendix E. Some of the 9-*j* coefficients used in these calculations, and not found listed elsewhere in the literature, are in Appendix H.

At this point, it becomes interesting to see how well we can do in fitting the energy levels *without* configuration interaction, having all this variety of forces to choose from.

4.2. *J–J* COUPLING CALCULATIONS

In $j-j$ coupling, we have reasonable projections from the Ca 42 energy levels, corresponding to the configurations $f_{\frac{7}{2}}{}^2(J)$, to those of Ca 43 ($f_{\frac{7}{2}}{}^3$) only if we take the 4+ level at 2.42 MeV and 6+ at 3.25 MeV (see table 4). Let us then assume these to be the correct levels, rather than 1.84 and 2.42 MeV.

If we include only the $f_{\frac{7}{2}}{}^2(J)$ configurations, with $\rho = 1$ for singlet and tensor forces, we find a "best" fit to the proposed level splittings at $V_{cs} = -38.7$ MeV,

$V_t = 4.7$ MeV. The energy levels are at 1.436, 2.606 and 3.152 MeV above the ground state. The interaction energy, however, is 3.841 MeV, which is off by a considerable amount. The rms error for the splittings above is 140 keV, while for all four levels, it is 386 keV.

We can do much better if we include a (central) triplet interaction V_{ct}. We then find a best fit at

$V_{cs} = -40.0$ MeV, $V_{ct} = 11.8$ MeV (i.e. $V_0 = -51.8$ MeV, $\alpha = -0.228$),
$V_t = 6.2$ MeV

The level splittings are now 1.455, 2.550, 3.202, and the interaction energy, 3.091 MeV. The rms deviation in splittings is now 88 keV, and in all four levels, 77 keV. However, this puts the $\frac{5}{2}$— and $\frac{3}{2}$-levels at 298 and 959 keV, respectively (and gives an interaction energy of 5.987, which is to be expected).

We may compare this work with a similar calculation done by DuttaRoy [4]). He takes, for the (principally $f_{\frac{7}{2}}^2$) 4+ and 6+ levels, the 2.42 and 3.25 MeV levels, for essentially the same reason as that given above: if the 4+ level were at 2.75 MeV, for example, the projected $\frac{5}{2}$- and $\frac{3}{2}$-levels would be at 286 and 1245 keV, respectively, which is very far from the experimentally observed splittings, so that configuration mixing would have to be very great to account for these levels. For the radial (harmonic oscillator) wave function, he takes a range $b\sqrt{2} = 2.9$ fermi, where $b^2 \equiv \hbar/m\omega$. He, too, takes a Gaussian interaction, and considers ranges of $r_0 = 1.4f$, $2.6f$, $2.9f$ and $3.2f$, (i.e. $\lambda = 0.483$, 0.897, 1.000, 1.103). For each of these ranges, he fits the best singlet, singlet-plus-triplet, and singlet-plus-(triplet odd) tensor force, as found by varying the parameters and calculating the sum of the squares of the deviations of the 0—2, 0—4 and 0—6 splittings from the proposed levels. For the Serber force above, he finds the lowest rms deviation δ at $V_0 = 33.282$ MeV, $r_0 = 3.2f$; the levels are at 0, 1.402, 2.577, and 3.178 MeV, with a resulting $\delta = 121$ keV. With a triplet (odd-state central) force as well, the best value is at $r_0 = 2.9\,f$, $V_0 = 35.714$ MeV, $\alpha = -0.501$, i.e. $V = 71.57$; and the levels are at 0.0, 1.598, 2.420, 3.219 MeV, yielding $\delta = 47$ MeV. Finally, he used the Serber exchange force at $r_0 = 2.6\,f$. Then between the two values, $2.6\,f$ and $4.0\,f$ for the range of the *tensor* force, the latter was found to be somewhat better, giving, at $V_0 = 50.44$ MeV and a repulsive tensor force of 5.09 MeV, the levels 0.0, 1.429, 2.575, 3.171 MeV, with $\delta = 113$ keV. Thus the results are rather similar to those found in this work.

4.3. CONFIGURATION MIXING

Next, we consider the influence of the $f_{\frac{5}{2}}$ level. Its most noticeable effect is to pull the 6+ level down quite low, to below the 4+ level. We permit Δf, the range of the central forces, and the relative singlet-triplet strengths to vary. It was found easiest to fit 4+ to 2.42 MeV (rather than 2.75). The best fit was found at

$$V_{cs} = -29.05 \text{ MeV}, \quad V_{ct} = +15.95 \text{ MeV}, \quad V_t = -6.35 \text{ MeV},$$

with

$$\rho_c = 1.016, \quad \Delta_f = 5.9 \text{ MeV}.$$

(ρ_c is the inverse range of the central force, ρ_t is always taken as 1 in this work). This is a Rosenfeld force, of strength 45 MeV, since, according to eq. (12)

$$V = V_0[P_s+\alpha P_W] = V_{cs}+V_{ct}, \quad V_0 = V_{cs}-V_{ct}, \quad \alpha = V_{ct}/V_0, \tag{31}$$

so that here

$$V_0 = -45.00 \text{ MeV}, \quad \alpha = -0.356.$$

The resulting splittings are 1.819, 2.388 and 3.105 MeV, with an interaction energy of 3.083 MeV. The rms deviation from (3.110), 1.523, 2.422, 3.250 MeV is $\delta = 167$ keV. When the Ca 43 matrices for $J = \frac{3}{2}, \frac{5}{2}, \frac{7}{2}$ were computed and the lowest eigenvalue found for each, however, the $\frac{5}{2}$ level was computed to be at 1.103 MeV (above $\frac{7}{2}$) and the $\frac{3}{2}$ level at 1.686 MeV. (The interaction energy was relatively reasonable, at 2.668 MeV).

4.3. COLLECTIVE EFFECTS

It was also attempted to fit the levels by admixing some weak collective interaction [38]). A phonon may be emitted by a particle, absorbed by the surface, then reemitted by the latter and absorbed by another particle. This second-order process, therefore, leads to a particle-particle interaction which can be shown [39]) to be of the form

$$V_{12} = -\left(\pm \frac{k^2}{C}\right)\left(\frac{5}{4\pi}\right) P_2(\cos\theta_{12}).$$

Some sample calculations involving f-states only indicated that the level splittings were changed in the wrong directions, and so it was decided to assume zero surface-particle coupling.

4.4. FINAL MACHINE CALCULATIONS

The program was modified so that instead of finding the V_0 necessary to give $E_0 = -3.11$ MeV, etc., it merely computed the Ca 42 matrices and eigenvalues from the parameters given it: $\Delta f, V, \alpha, \rho, V_t$. With these five parameters, we try to fit the five levels: 0 and 2 in Ca 42, $\frac{3}{2}$, $\frac{5}{2}$ and $\frac{7}{2}$ in Ca 43. Each parameter was made to vary, and new parameters then calculated by the machine by a least-squares procedure, which would minimize the deviations of the calculated levels from the empirical ones †.

---

† For this calculation, the more important tensor matrix elements involving p-states had to be calculated.

This procedure was found to converge. The program was run for $\Delta f = 2, 3, 4$, 6.3 and 8.4 MeV. The 6.3 MeV choice was made in view of the then just-received preprint of Class *et al.* [9]). The larger Δf was, the faster was the convergence, and to a set giving smaller rms deviations from the empirical values. To test the uniqueness of the solution, parameters very far from those already known to be correct were inserted as starting values for the $\Delta f = 6.3$ MeV case. Just one pass gave the new parameters rather close to the correct ones.

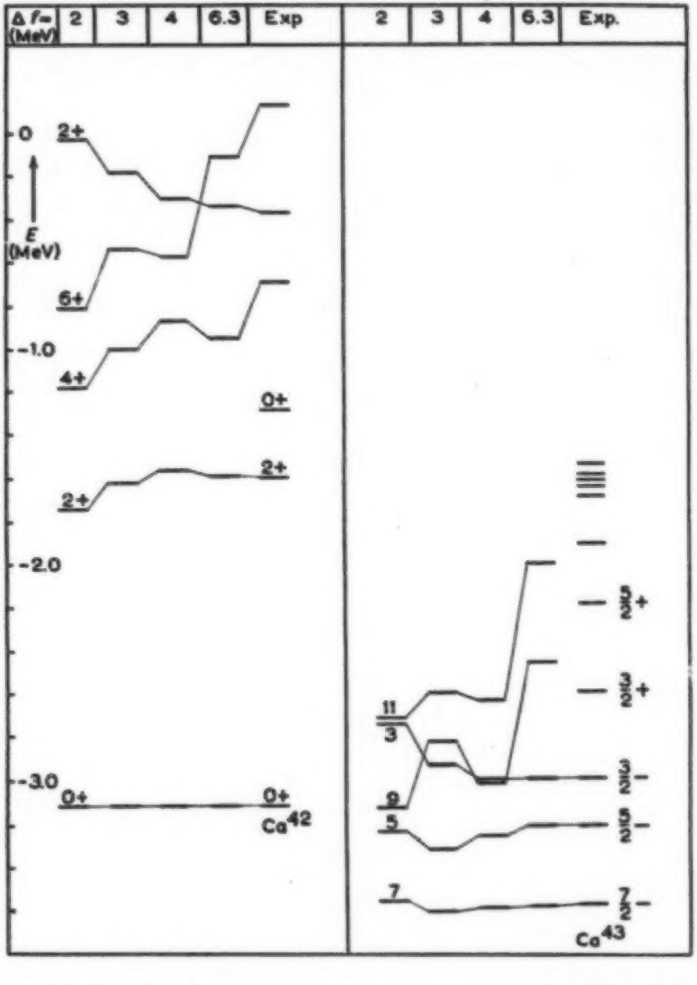

Fig. 3. Calculated Ca^{43} and Ca^{42} energy levels for several values of the f-doublet splitting.

In table 6, we list the best parameters for each Δf, with the rms deviation (from the five prescribed levels), and the energy levels (including a hand calculation of the *second* 2+ level). These levels are plotted in fig. 3, together with the experimentally-found levels, except for the 8.4 MeV results, which were found to be almost identical to those at 6.3 MeV.

From fig. 3, we see that it is tempting to take the third excited state in Ca 42

TABLE 6

Best force parameters and resulting energy levels for various f doublet splittings. All quantities except α and ρ are in MeV

Δf	2	3	4	6.3	8.4
E_g	2.89	2.89	2.89	5.3	5.3
V	−18.000	−16.563	−15.013	−18.884	−18.710
α	− 0.200	− 0.216	− 0.232	− 0.195	− 0.195
ρ	0.820	0.742	0.676	0.760	0.736
V_t	−10.000	−15.830	−20.282	−14.988	−15.137
$-E_0$	3.0904	3.1064	3.0987	3.1077	3.1209
E_2-E_0	1.3825	1.4940	1.5153	1.5222	1.5185
E_4-E_0	1.9350	2.1146	2.2449	2.1715	2.1958
E_6-E_0	2.2987	2.5739	2.5381	3.0068	3.0424
E'_2-E_0	3.08	2.9341	2.8098	2.78	
E'_0-E_0				4.020	
$-E_{\frac{7}{2}}$	3.5480	3.6028	3.5769	3.5653	3.5846
$E_{\frac{5}{2}}-E_{\frac{7}{2}}$	0.3247	0.2931	0.3370	0.3747	0.3752
$E_{\frac{3}{2}}-E_{\frac{7}{2}}$	0.8171	0.6796	0.5929	0.5928	0.5878
$E_{\frac{9}{2}}-E_{\frac{7}{2}}$	0.4412	0.7868	0.5797	1.1271	1.1646
$E_{\frac{11}{2}}-E_{\frac{7}{2}}$	0.8404	1.0150	0.9592	1.5856	1.6563
δ_{rms}	0.1210	0.0565	0.0179	0.0024	0.0087

as the 4+ level, and the following one at 2.75 MeV as the second 2+ level. On the other hand, with the force mixtures we are getting, it is impossible to obtain a 6+ level of more than ≈ 3 MeV excitation: a much more strongly repulsive force would be necessary.

As has usually been found in previous such calculations, the $\frac{9}{2}$- and $\frac{11}{2}$-levels are predicted to be quite low, for $\Delta f \leqq 4$ MeV. When we go to 6 MeV, however, there is a great jump. Unfortunately, it is insufficient to put them as high as they belong, but it is heartening to know that they *can* be made to go high.

If we accept the Class-Davis-Johnson results as valid and applicable to Ca 41, particularly in view of the insensitivity of the energy levels to changes in Δf *above* 6.3 MeV, then the force mixture is, according to table 6,

$$V = -18.884\,\text{MeV}, \quad \alpha = -0.195\,\text{MeV}$$

$$(\text{i.e., } V_{cs} = -15.20\,\text{MeV}, \quad V_{ct} = +3.68\,\text{MeV}),$$

$$\rho_c = 0.760, \quad \rho_t = 1.000, \quad V_t = -14.988\,\text{MeV}.$$

Note, incidentally, that the large value of Δf means we will be close to $j-j$ coupling — this explains the considerable success of Talmi[4,34]), who assumed pure $j-j$ coupling. The wave functions, matrices, etc., are in Appendix J.

A rough estimate of the "strength" of this interaction is $V_c \equiv (1+2\alpha)V =$

$= -11.52$ MeV, and normalizing it for the range,

$$V_c/\rho^2 = 19.94 \text{ MeV}.$$

It is interesting to compare this force mixture with those of Levinson-Ford and French-Raz:

Present work	$18.9(P_s - 0.195\, P_W)$,	$\rho = 0.760$;	$V_t = -15$;
L & F	$14.4(P_s + 0.0\, P_W)$,	$\rho = 0.847$;	
F & R	$12.0(P_s + 0.500\, P_W)$,	$\rho = 1.000$.	

4.4. DISCUSSION OF RESULTS

There are several things which strike us about this phenomenologica linteraction:

First, it is quite complicated, requiring a more complex potential than is usually needed to explain a nuclear spectrum.

Secondly, we should imagine that it would rather resemble the (free) two-particle potential. The empirically inferred potential [40]) has a strong attractive singlet (even), a weak attractive triplet (odd) central, and a weak repulsive tensor (triplet odd) part. The potential we found has, on the contrary, a weak *repulsive* triplet and a strong *attractive* tensor part.

Third, the singlet potential (empirical), in particular, has a quite short range. Now, the effective internucleon potential (in nuclear matter) is just the reaction matrix, and the latter is asymptotically the same as the actual potential. Since the latter is short-ranged, so ought the pseudopotential to be, whereas ours is exceptionally long-ranged. The significance (if any) of this very long range of the effective Gaussian interaction is obscure; but presumably it is a mathematical fiction. We suggest that rather than the Gaussian interaction, one which is closer to the actual (hard core) potential, such as the "soft-core" Gaussian $V_0(r/r_0)^2 e^{-(r/r_0)^2}$ considered by LF(I), be used. It should not be substantially more difficult to handle than the Gaussian, using the technique indicated in eqs. (27)—(30).

As for the strong attractive tensor force, it is a complete mystery. It is certainly contrary to the weak repulsive tensor force found by Gammel and Thaler, yet is consistently called for in this model. It can only be suggested that, if this problem were done more realistically, i.e. using core configurations and hard-core Gaussian interactions, that the phenomenological potential will be more like the expected form.

On the other hand, the spectra, though far from being really good fits, are nevertheless better than anything found heretofore. In Ca 42, it is tempting to identify the 2.75 MeV level with the second $J = 2$ level, which is $p_{\frac{3}{2}} f_{\frac{7}{2}}$. The 2.42 MeV level would then be 4+, and the 3.25 MeV level, 6+. In Ca 43, the $\frac{9}{2}$-level is calculated to be 1.13 MeV above the ground state; but this, though low (since from Lindqvist's work, the $\frac{9}{2}$-level is probably at 1.678 MeV or above), is still higher than this level has been placed heretofore (at 0.81 MeV, by LF). Of course with the $\frac{9}{2}$-level so high, the difficulty with the unobserved β-decay from K 43 to this level, pointed out by Sheline [41]), disappears.

As French and Raz showed, we ought to have the amplitudes

$$|\mathrm{K}(\mathrm{f}_{\frac{7}{2}}{}^{2}(0)\mathrm{p}_{\frac{3}{2}})| \approx 0.208, \quad |\mathrm{K}(\mathrm{f}_{\frac{7}{2}}{}^{2}(0)\mathrm{f}_{\frac{5}{2}})| < \sqrt{0.03} \approx 0.17.$$

The calculated amplitudes, on the other hand, are 0.060 and -0.071, respectively. Thus the small stripping cross-section to the first excited state of Ca 43 is obtained, all right. On the other hand, a stripping cross-section $(0.208/0.060)^2 \approx 12$ times too small is predicted to the $\mathrm{p}_{\frac{3}{2}}$ level. Even if we remark that this level is only 55 % sp in nature, the cross-section is 6.6 times too small.

Finally, we note that it is essential to take as many configurations as possible into account. We will illustrate this with one specific case.

One of the early machine calculations, for

$$\rho = 1.32, \quad \alpha = 0.6, \quad \Delta f = 2.014 \text{ MeV},$$

gave

$$E_{\mathrm{g}} = 2.343 \text{ MeV}, \quad V = -14.16403 \text{ MeV},$$

i.e.

$$V_{\mathrm{cs}} = -22.66 \text{ MeV}, \quad V_{\mathrm{ct}} = -8.50 \text{ MeV}.$$

The principal diagonal and off-diagonal matrix elements for $J = \frac{3}{2}, \frac{5}{2}, \frac{7}{2}$ were easily calculated from the Ca 42 matrices computed by the machine, and are shown below together with the actual energy denominators and the configurations. The resulting energy shifts ΔE were calculated by second-order perturbation theory, and of course vary, depending on how many configurations are included. Finally, the correct shifts, as calculated by the machine with all 25 configurations and *no* approximations, are given. The levels are plotted in fig. 4. It is seen that perturbation theory usually gives a fair approximation to the exact shifts, the main discrepancy coming from a neglect of various configurations, rather than from the approximate nature of the calculation. Indeed, LF did not include the p-state configurations in their Ca 43 calculations, and this might have led to an inaccurate value for the splittings, as witness the 0.2465 MeV depression of the $J = \frac{3}{2}$ level in the above

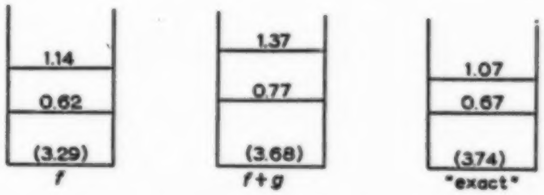

Fig. 4. Energy levels resulting from taking various amounts of configuration interaction in Ca^{43}.

TABLE 7

Matrix elements

	$\frac{7}{2}^3$	$\frac{5}{2}^2(2)\frac{7}{2}$	$\frac{5}{2}^2(4)\frac{7}{2}$	$\frac{7}{2}^2(2)\frac{5}{2}$	$\frac{7}{2}^2(4)\frac{5}{2}$	$\frac{9}{2}^2(2)\frac{7}{2}$	$\frac{9}{2}^2(4)\frac{7}{2}$	$\frac{7}{2}^2(0)\frac{3}{2}$	$\frac{7}{2}^2(2)\frac{3}{2}$
$J=\frac{3}{2}$		−0.3260	0.2952	−0.0269	0.1469	0.7097	−0.6870	0.1347	0.5729
	−2.0975	−1.5895	−0.8959	−1.4224	−1.2198	−1.0103	−0.5709	−2.8159	−2.6279
	4.5360								
	5.2296								
	2.6891								
	2.8917								
	5.7732								
	6.2126								
	1.2286								
	1.4166								

configurations	ΔE(MeV)
f	0.0478
f and g	0.2110
f+g+ some p	0.4575
correct	0.5835

	$\frac{7}{2}^3$	$\frac{5}{2}^2(2)\frac{7}{2}$	$\frac{9}{2}^2(2)\frac{7}{2}$	$\frac{7}{2}^2(0)\frac{5}{2}$	$\frac{7}{2}^2(2)\frac{5}{2}$	$\frac{7}{2}^2(4)\frac{5}{2}$	$\frac{5}{2}^2(4)\frac{7}{2}$
$J=\frac{5}{2}$		−0.5505	1.1984	−0.2334	−0.3340	−0.0499	−0.0820
	−2.5259	−1.1545	−1.3482	−3.1384	−2.1307	−1.3808	−0.7501
	5.3994						
	5.8637						
	1.4015						
	2.4092						
	3.1591						
	5.8038						

configurations	ΔE(MeV)
f states only	0.1433
f and g	0.3882
correct	0.5509

	$\frac{7}{2}^3$	$\frac{5}{2}^2(0)\frac{7}{2}$	$\frac{9}{2}^2(0)\frac{7}{2}$	$\frac{7}{2}^2(2)\frac{5}{2}$	$\frac{7}{2}^2(4)\frac{5}{2}$	$\frac{7}{2}^2(6)\frac{5}{2}$	$\frac{5}{2}^2(2)\frac{7}{2}$	$\frac{5}{2}^2(4)\frac{7}{2}$	$\frac{9}{2}^2(2)\frac{7}{2}$	$\frac{9}{2}^2(4)\frac{7}{2}$
$J=\frac{7}{2}$		−0.9172	1.3720	0.3674	0.2407	0.1343	0.2624	0.1665	−0.5713	−0.3875
	−2.8810	−4.1505	−1.6937	−2.7577	−1.0570	−1.1753	−1.8768	−1.2247	−1.0103	−0.5709
	2.7585									
	5.8733									
	2.1373									
	3.8380									
	3.7197									
	5.0322									
	5.6843									
	6.5567									
	6.9961									

configurations	ΔE (MeV)
f states only	0.4067
f and g	0.7984
correct	0.8675

calculation, just from the $\frac{7}{2}^2(0)\frac{3}{2}$ and $\frac{7}{2}^2(2)\frac{3}{2}$ configurations. This is of the same order of magnitude as the actual splittings. The differences are not greater only because the p and the g states happen to be working against each other, in this case.

We list the relevant matrix elements in table 7; the first line gives the configurations, the second, the first row of the matrix, i.e. the most important off-diagonal matrix elements, and the third line gives the diagonal elements, before the spin-orbit terms are added. The column at the left gives the energy denominators (i.e. *after* the spin-orbit terms are added). Finally, the column at the right gives the depressions of the energy, resulting from the use of various amounts of configuration interaction, as indicated, and the correct depression. These are all for $\Delta j = 2.014$ MeV.

5. Magnetic Moments

Now that we have the wave functions for the various states in the Ca 42 and Ca 43, we may, in principle, calculate all the properties of these nuclei. Let us begin with the magnetic moment of Ca 43. The single-particle magnetic moment operator is

$$\boldsymbol{\mu} = (g_L \mathbf{L} + g_S \mathbf{S})\mu_0,$$

where μ_0 is the nuclear magneton and g_L, g_S are the magnetogyric ratios. Now in a $j-j$ coupling representation, we find in general

$$\langle jm|\mu_z|j'm'\rangle = m\delta_{ll'}\delta_{mm'}\delta_{jj'}\{g_L + (-1)^{j+l-\frac{1}{2}}(g_S - g_L)/[l]\}$$
$$+ (g_L - g_S)\,\frac{\delta_{ll'}\delta_{mm'}\delta_{j'j\pm1}}{[l]}\,\sqrt{(l+\tfrac{1}{2})^2 - m^2}$$

in units of nuclear magnetons. Thus the magnetic moment contributed by a single particle is

$$\mu \equiv \langle jm|\mu_z|jm\rangle_{m=j} = j\{g_L + (-1)^{j+l-\frac{1}{2}}(g_S - g_L)/[l]\} \equiv jg_j.$$

The Schmidt theory assumes that the total magnetic moment of the nucleus is contributed by the odd particle, and uses

$$g_L = 1, \quad g_S = 5.585 \text{ (odd } Z\text{)}, \text{ or } g_L = 0, \quad g_S = -3.826 \text{ (odd } N\text{)}.$$

When we have configuration interaction, a state consists of a linear combination of orbitals α($j-j$ coupled, in our case), with mixture amplitudes K_α:

$$\psi = \sum_\alpha K_\alpha|\alpha\rangle.$$

Thus the expectation value of μ_z in such a state is a linear combination of terms:

$$\langle\mu_z\rangle = \sum_{\alpha\beta} K_\alpha K_\beta \langle\beta|\mu_z|\alpha\rangle.$$

Some of the matrix elements $\langle\beta|\mu_z|\alpha\rangle$ are given in LF I, eqs. (20) to (22). The rest will be given shortly.

The first calculations of this kind (i.e. taking configuration interaction into account) were carried out by Blin-Stoyle for spin $\frac{1}{2}$ nuclei, but done in a general way first by Arima and Horie [42]). The latter obtained, for the magnetic moment deviation from the Schmidt line (i.e. from the pure $j-j$ coupling value) for our configuration,

$$\delta\mu = (p-1)\,\frac{(l+1)(l+2)}{(2l+1)(2l+3)}\,(g_S - g_L)\left(\frac{V_S I}{\Delta E}\right)$$

in n.m., where p is the number of nucleons in the $j = l+\frac{1}{2}$ shell, V_S is the strength of the singlet part of the internucleon force, I is a radial integral, and ΔE is a perturbation-theoretic energy denominator, which is essentially the doublet splitting. They made a rough calculation which indicated that

$$V_S I \approx -25/A \text{ MeV}.$$

Finally, they chose $\Delta E = 3$ MeV for the f doublet splitting. Thus, to find the magnetic moment of Ca 43, we take $p = 3$, $l = 3$, $g_L = 0$, $g_S = -3.3263$ n.m.,

$$V_{SI} = -25/43 = -0.581 \text{ MeV}.$$

Hence $\delta\mu = 0.470$ n.m. In $j-j$ coupling, $\mu_0 = -1.913$ n.m. Hence

$$\mu_{\text{calc}} = \mu_0+\delta\mu = -1.442 \text{ n.m.},$$

which is a good approximation to the experimental value, $\mu = -1.315$ n.m. On the other hand, had they used $\Delta E = 6.3$ MeV, they would have found

$$\delta\mu = 0.470\times 3/6.3 = 0.224,$$

hence

$$\mu_{\text{calc}} = -1.689 \text{ n.m.}$$

We shall now do the problem exactly. We have the mixture amplitudes K_α, and need only know the three-particle matrix elements. Abbreviating j_α by α, and so on, where practicable, we have

$$\langle\alpha\beta(j_{\alpha\beta})\gamma(3)JJ|\mu_z(3)|\delta\varepsilon(j_{\delta\varepsilon})\theta(3)JJ\rangle$$
$$= \begin{bmatrix} J & 1 & J \\ J & 0 & J \end{bmatrix} \delta_{j_{\alpha\beta}}\delta_{j_{\delta\varepsilon}} U(j_{\delta\varepsilon}0J1: J\gamma)\langle\gamma||\mu||\theta\rangle[\delta_{\alpha\delta}\delta_{\beta\varepsilon}-\delta_{\alpha\varepsilon}\delta_{\beta\varepsilon}],$$

where the last parentheses follow from the antisymmetry of the wave function in particles 1 and 2. From the expansion of the three-particle wave function in terms of its parents, we may write down the general expression for

$$\langle j'_a j'_b(J_1)j'_c JJ|\mu_z|j_a j_b(J_2)j_c JJ\rangle.$$

Following LF, we denote the configurations as:

$$\alpha_1\text{: a} = \text{b} = \text{c}; \quad \alpha_2\text{: a} = \text{b} \neq \text{c}; \quad \alpha_3\text{: a} \neq \text{b} \neq \text{c} \neq \text{a}.$$

We then find, calling $[j_1 j_2] \equiv J(J+1)+j_1(j_1+1)-j_2(j_2+1)$,

$$\mu(\alpha_1, \alpha_3) \equiv 0$$
$$\mu(\alpha_1, \alpha_2) \equiv \langle j_a{}^3(J)|\mu_z|j_a{}^2(j)j_b J, M = J\rangle = (g_L-g_S)\delta_{l_a l_b}\delta_{j_a j_b\pm 1}$$
$$\times \frac{\langle j_a{}^2(j)j_a J|\}j_a{}^3 J\rangle}{2(J+1)(2l_a+1)}\sqrt{3(J+j-l_a+\tfrac{1}{2})(J+j+l_a+\tfrac{3}{2})(J-j+l_a+\tfrac{1}{2})(j-J+l_a+\tfrac{1}{2})}.$$

This differs from eq. (23) of LF I by the factor $(-\delta_{j_a j_b \pm 1})$.

$$\mu(\alpha_2, \alpha_3) \equiv \langle j_a j_b (J_1) j_c J | \mu_z | j_a j_b (J_2) j_c J, M = J \rangle$$

$$= \frac{1}{2(J+1)} \{\delta_{J_1 J_2}[j_c J_2] g_{j_c} + 3g_{j_b} \sum_{J'} F'^{J}_{J_1 J'} F^{J}_{J_2 J'} [j_b J'] + 3g_{j_a} \sum_{J'} \hat{F}'^{J}_{J_1 J'} \hat{F}^{J}_{J_2 J'} [j_a J']\}.$$

With the $J = \frac{7}{2}$ vector found for the $\Delta f = 6.3$ MeV, $E_g = 5.3$ MeV calculation, we have

$$\mu = 0.4954\, g_S = -1.8956 \text{ n.m.}$$

Finally, we make a small correction for the motion of the core about the centre of mass. As shown in LF III,

$$\mu = g_{\text{core}} \langle I_{\text{core}} \rangle + g_J \langle I_J \rangle,$$

where I_c and I_J are the total angular momenta about the centre of mass of the system. Clearly $I_c + I_J = J$, and we have

$$\mu = g_c \langle I_c \rangle + g_J \langle J - I_c \rangle = g_J \langle J \rangle + (g_c - g_J) \langle I_c \rangle.$$

$g_J \langle J \rangle$ is the part computed when one assumes the total angular momentum is associated with the particle structure, and the remainder is the correction term due to motion of the core about the centre of mass. We take, roughly,

$$g_c \approx Z/A = 20/43 = 0.4651,$$

and

$$g_J = g_{\frac{7}{2}} = g_S/[l] = -3.8263/7 = -0.5466$$

(since $g_l = 0$ for neutrons). $\langle I_c \rangle \approx 3\hbar/A$, since, being in the $f_{\frac{7}{2}}$ state mostly, this is an orbital angular momentum of 3 units, carried in effect by one particle (the core). Thus we have

$$g_c - g_J = 1.0117, \quad \langle I_c \rangle \approx 3\hbar/43 = 0.0698\hbar,$$

giving

$$\Delta\mu_c = (g_c - g_J) \langle I_c \rangle = 0.0706 \text{ n.m.}$$

Adding this core correction to the above value of μ, we finally find

$$\mu = -1.8250 \text{ n.m.}$$

This is to be compared with the experimental value [43])

$$\mu_{\text{exp}} = -1.3152(2) \text{ n.m.}$$

Note that, if this had been carried out with Arima and Horie's approximation, i.e. taking only the first-order, off-diagonal corrections, and not bother about the normalization, we would have

$$[0.5+2(-0.001743)]g_S+0.070585 = 1.8292 \text{ n.m.},$$

which is indeed quite close to the exactly-computed value.

Now, the core cannot directly contribute significantly to the magnetic moment, since none of the core states in the highest subshell, i.e. the 1d, 2s shell, can mix with any of the configurations we consider (p, f, and g). Hence μ can only be wrong because our admixtures must be wrong. This, in turn, (assuming we have "the" correct single particle doublet splittings), means that our interaction is incorrect. But we have seen that we do, indeed, need core states to give some of the excited states in Ca 41, 42 and 43. It is quite likely, therefore, that inclusion of core states will influence the interaction, and thus, indirectly, the admixtures. This will not be done here, however; let it suffice to point out that, if we changed the $|\frac{7}{2}^2(2)\frac{5}{2} : \frac{7}{2}\rangle$ and $|\frac{7}{2}^2(4)\frac{5}{2} : \frac{7}{2}\rangle$ amplitudes from 0.053 and −0.011, respectively, to 0.100 and 0.060, the wave function is hardly changed (the overlap is 99.67 %), but μ goes from 0.4954 g_S to 0.4201 g_S, while the correct value is 0.3622 g_S. Clearly another slight change could bring the magnetic moment into exact agreement. Thus, fitting the magnetic moment is no guarantee that we have the correct admixtures, nor a poor fit a guarantee that the admixtures are far from wrong: it is *too* sensitive a test of the admixtures.

6. Electromagnetic Transitions

6.1. GAMMA DECAY TRANSITION PROBABILITIES

If we work to first order only, and make the long-wavelength approximation, i.e. assume that the nuclear radius a is much smaller than λ:

$$\omega a \ll c,$$

the transition probability is

$$T_{\text{if}}^{\sigma LMk} = \frac{8\pi(L+1)}{L([L]!!)^2}\frac{1}{\hbar}\left(\frac{\Delta E}{\hbar c}\right)^{2L+1} B(\sigma L), \tag{32}$$

where σ is E for electric or M for magnetic, $L\hbar$, $M\hbar$ are the angular momentum and z-component of angular momentum of the photon, and $k\hbar$ is its linear momentum. $B(\sigma L)$ is the reduced transition probability:

$$B(\sigma L) = |(\text{f}||\mathscr{M}^{\sigma}_{LM}||\text{i})|^2, \tag{33}$$

where $\mathscr{M}^{\sigma}_{LM}$ are the multipole operators. $\mathscr{M}^{E}_{LM}$ consists of an orbital part, $er^L Y_{LM}$, and a spin part. Their expectation values are denoted Q_{LM} and Q'_{LM}, respectively. For $\sigma = \text{M}$, we have M_{LM} and M'_{LM}.

When there are several particles α involved, we have

$$Q_{LM} = e\sum_{\alpha}\int \psi_{\text{f}}^*(r^L Y_{LM})_{\alpha}{}^*\psi_{\text{i}}\,\text{d}\tau, \text{ etc.}$$

The explicit evaluation of these integrals requires that we have definite nuclear wave functions ψ, i.e. that we have a model. Using shell-model wave functions, summing over the final magnetic substates and averaging over the initial ones, Kennedy and Sharp [44]) find

$$B(\mathrm{E}L) = \frac{a^{2L}}{4\pi} I_L{}^2 e^2 \frac{Z_0{}^2(ljl'j';SL)}{[j]} \left[\varepsilon + \frac{\lambda}{2(L+1)} \frac{\hbar k \mu}{mc}\right]^2,$$

where $\varepsilon = 1$ for proton, 0 for neutron,

$$\lambda \equiv l(l+1) - j(j+1) - l'(l'+1) + j'(j'+1), \quad I_L \equiv \int R_{l'} \left(\frac{r}{a}\right)^L R_l r^2 \mathrm{d}r,$$

and

$$Z_0(ljl'j';SL) \equiv \begin{bmatrix} l & l' & L \\ 0 & 0 & 0 \end{bmatrix} [j]^{\frac{1}{2}} [j']^{\frac{1}{2}} [l]^{\frac{1}{2}} [l']^{\frac{1}{2}} W(ljl'j';SL) = (-1)^{\frac{1}{2}(L+l'-l)} Z(ljl'j';SL),$$

where Z is as defined by Biedenharn [45]). This expression may be simplified somewhat using the identity

$$\begin{bmatrix} j & j' & k \\ \frac{1}{2} & -\frac{1}{2} & 0 \end{bmatrix} = [l]^{\frac{1}{2}} [l']^{\frac{1}{2}} \begin{bmatrix} l & l' & k \\ 0 & 0 & 0 \end{bmatrix} W(ljl'j';\tfrac{1}{2}k)$$

(which is incorrectly given in eq. (A5) of French and Raz.) Thus †

$$B(\mathrm{E}L) = \langle r^L \rangle^2 \frac{[j']}{4\pi} \begin{bmatrix} j & j' & L \\ \frac{1}{2} & -\frac{1}{2} & 0 \end{bmatrix}^2 \left[\varepsilon + \frac{\lambda \hbar k \mu}{2Mc(L+1)}\right]^2.$$

$B(\mathrm{M}L)$ is more complicated, but can be found in Kennedy and Sharp [44]).

It is not quite appropriate to take $\varepsilon = 1$ for proton transitions and $\varepsilon = 0$ for neutron transitions, since a finite core will move about their centre of mass. Thus, a neutron has an effective charge, since it sets the whole core in motion, a "particle" of charge e and mass $A-1$, with velocity $1/(A-1)$ times its own, creating a small current. This effect can be incorporated easily into our calculations by taking effective neutron gyromagnetic ratios; for E2 transitions,

$$g'_L = \frac{Z}{A^2} g_L(\text{proton}) = 0.0108, \text{ rather than } 0,$$

and

$$g'_S = \left(\frac{A-1}{A}\right)^2 g_S(\text{neutron}) = 0.9540\, g_S = -3.6504.$$

For M1 transitions,

---

† A table of the required CG coefficients appears in ref. [31]). Note two errors in that table, however: the $\frac{3}{2}$, $\frac{5}{2}$ term for $J = 3$ should be 12/715 rather than 12/385, and the same term for $J = 4$ should be 81/715 rather than 81/385.

$$g'_L = \frac{Z}{A(A-1)} g_L(\text{proton}) = 0.01107, \quad g'_S = g_S = -3.8263.$$

In general, after performing the sum and the averaging over magnetic substates, the reduced transition probability (33) becomes

$$B(L) = [I']^{-1}|(\Gamma I||\mathscr{M}_L{}^\sigma||\Gamma' I')|^2, \tag{34}$$

where I' is the initial, I the final spin, and Γ, Γ' represent all the other quantum numbers characterizing the states, and

$$\mathscr{M}_L{}^\sigma \equiv \sum_\alpha \mathscr{M}_L{}^\sigma(\alpha),$$

where the sum is over all the relevant particles. For one particle, we find B(E2) and B(M1) to be given by eqs. (19) to (21) of True and Ford [39]).

6.2. CALCIUM 41

Bockelman and Buechner's [8]) stripping curve for the 1.947 MeV level in Ca 41, presumed to be pure $p_{\frac{3}{2}}$, admits, because of the size of the second maximum, the possibility that there is at least some admixture of the (single-particle) $f_{\frac{5}{2}}$ configuration in that state. Therefore we want to calculate the transition probability for M1 decay from the 1.947 MeV level (to ground), to test the hypothesis that a significant fraction of the $f_{\frac{5}{2}}$ level is degenerate with the $p_{\frac{3}{2}}$ level. We are also interested in the E2 decay rate from this level. From (32) we find

$$T(\text{E2}) = \frac{8\pi \times 3}{2 \times 15^2} \frac{1}{\hbar} \left(\frac{\Delta E}{\hbar c}\right)^5 B(\text{E2}),$$

$$B(\text{E2}) = \tfrac{1}{4}|(\tfrac{7}{2}||Q_2||\tfrac{3}{2})|^2,$$

and

$$(\tfrac{7}{2}||Q_2||\tfrac{3}{2}) = \bar{e}\langle r^2\rangle \sqrt{\frac{18}{7\pi}},$$

where $\bar{e}$ = effective charge, and

$$\langle r^2\rangle_{\text{pf}} = -\sqrt{14}\, b^2.$$

(We find $b = 1.97$ *f* on the basis of Hofstadter's electron-scattering density measurements [46]). This gives $b\sqrt{2} = 2.79$ *f*, compared with Kurath's estimate 2.9 *f*). We write

$$\bar{e} \equiv \beta_1 e,$$

and note that according to the Z/A^2 effect for core motion, the smallest value $\beta_1{}^2$ can take on is

$$\beta_{1m}^2 = 20/41^2 = 0.0119. \tag{35}$$

Collecting all these numbers, we find

$$T(\mathrm{E2}) \approx 2.47\, \beta_1{}^2 \times 10^{12}\ \mathrm{sec}^{-1}. \tag{36}$$

Collective modes give rise to large electric quadrupole transitions [47]). Thus even a weak coupling of particle to nuclear surface can enhance the E2 radiation considerably.

By virtue of the fact that the reduced matrix element for the collective transition between neutron states is of a form similar to the quadrupole operator (for protons),

$$Q^{n}_{2m} = \left(\frac{3\ ZeR^2}{4\pi C}\right) \sum_i k(r_i) Y_2{}^m(i),$$

True and Ford show that we can write β as

$$\beta = \left(\frac{3Z}{4\pi C}\right) \frac{\langle k \rangle R^2}{\langle r^2 \rangle}. \tag{37}$$

In general, $\langle r^2 \rangle \approx \frac{3}{5} R^2$ and is fairly constant. Therefore they have

$$\beta \approx \left(\frac{5Z}{4\pi}\right) \frac{\langle k \rangle}{C}.$$

Finally, the expectation value of $k(r)$ is approximately constant, and has the same sign as $\langle r^2 \rangle$. Hence we have $\beta = 0.40\ Z(k/C)$. If we include core effects, then for neutrons,

$$\beta = 0.40\ Z\left(\frac{k}{C}\right) + \frac{\sqrt{Z}}{A}. \tag{38}$$

(For protons, we should have added unity, rather than $Z^{\frac{1}{2}} A^{-1}$.)

Next, we wish to compute $T(\mathrm{M1})$. As before,

$$T(\mathrm{M1}) = \frac{8\pi \times 2}{9\hbar} \kappa^3 B(\mathrm{M1}), \quad B(\mathrm{M1}) = \tfrac{1}{8} |(\tfrac{7}{2}||M_1||\tfrac{5}{2})|^2,$$

and

$$(\tfrac{7}{2}||M_1||\tfrac{5}{2}) = \sqrt{\frac{18}{7\pi}}\, (g_L - g_S)\mu_0.$$

Now, $g_L = 20/41 \times 40 = 0.0122$, and $g_S = 2(\mu_N/\mu_0) = -3.8263$, so that $g_L - g_S = 3.8385$, and therefore

$$T(\mathrm{M1}) = 3.526 \times 10^{13} (\Delta E)^3 = 2.60 \times 10^{14}\ \mathrm{sec}^{-1}, \tag{39}$$

for $\Delta E = 1.947$ MeV.

The experimental gamma-decay transition probability of an isomeric state is given in terms of the experimental half-life τ of this state by means of the equation

$$T_{\mathrm{exp}} = \ln 2/(1+\alpha)\tau,$$

where α is the appropriate internal conversion coefficient.

No direct measurement has yet been made of these transition rates, so that it is not possible to compute an experimental β. However, we may expect that β will not be very much larger than one. For $\beta_1 = 1$, then, the magnetic dipole radiation is expected to be more than 100 times as intense as the electric quadrupole (assuming the same populations for the levels). If there were *no* enhancement, then $\beta^2 \approx 0.01$, and the M1 radiation would be 10 000 times as intense. Therefore, the fact that the 1.947 MeV transition is essentially pure E2 indicates that there is no $f_{\frac{5}{2}}$ component at this energy.

6.3. CALCIUM 42

Following True and Ford [39]), we label the $j-j$ coupling states of the shell model by α and β, and expand the initial and final states:

$$|\Gamma'I'\rangle = \sum_{\alpha} K'_{\alpha}|\alpha I'\rangle, \quad |\Gamma I\rangle = \sum_{\beta} K_{\beta}|\beta I\rangle.$$

The $|\alpha I'\rangle$, etc. are one-, two-, three-, . . . particle wave functions. Then

$$(\Gamma I||M_L||\Gamma' I') = \sum_{\alpha\beta} K_{\beta}^{*} K'_{\alpha} (\beta I||M_L||\alpha I'). \tag{40}$$

The expression for the two-particle reduced matrix elements $(jj'I||M_L||jj''I')$ are given by eq. (18) of ref. [39]).

We are principally interested in the decays from the 2.422, 1.836 and 1.523 MeV levels. First, consider the 2 → 0 transition. There are just ten terms in the sum (40). Taking the admixtures for the 6.3 MeV calculations from Appendix J, we find $(0||Q_2||2) = -5.448\, c_0$, where $c_0 \equiv \bar{e}b^2/\sqrt{\pi}$. This yields

$$T(\mathrm{E2}) = 0.3166\, \frac{e^2 \beta_2{}^2 b^4}{\hbar} \left(\frac{\Delta E}{\hbar c}\right)^5.$$

With $\Delta E = 1.523$ MeV, and $b = 1.97\, f$, this becomes

$$T(\mathrm{E2})_{2\to 0} = 2.86\, \beta_2{}^2 \times 10^{11}\ \mathrm{sec}^{-1}. \tag{41}$$

Next, we go to the 4 → 2 transition. There are only four important terms; these give rise to $(2||Q_2||4) = -6.128\, c_0$. Taking the 2.422 MeV level to be 4+, we have $\Delta E = 2.422 - 1.523 = 0.899$ MeV, and

$$T(\mathrm{E2})_{4\to 2} = 1.72\, b^4 \beta_3{}^2 \times 10^{9}\ \mathrm{sec}^{-1} = 2.60\, \beta_3{}^2 \times 10^{10}\ \mathrm{sec}^{-1} \tag{42}$$

for $b = 1.97\, f$.

Unfortunately, we can say nothing about the 1.836 MeV level, even to compare its expected decay rate with the others, since its shell model configuration is not definitely known.

Now, no direct measurements of the decay rates of Ca 41, 42, 43 have been made. However, Van Patter 48) has made an investigation into the systematics of γ decay rates from the first excited states of even-even nuclei, and estimates 49) the half-life of the 1.523 MeV state as $\tau = 2.5$ nsec. This corresponds to $T(\mathrm{E2}) = (0.693/2.5)\times 10^{12}\ \mathrm{sec}^{-1} = 2.77\times 10^{11}\ \mathrm{sec}^{-1}$. From (41), this would require $\beta_2^{\,2} = 1.03 \rightarrow \beta_2 = 1.02$. Taking the contribution to β_2 from core motion to be $\beta_c = 0.10$, we find the enhancement due to collective surface motion to be

$$\beta_{\mathrm{surf}} = 0.92.$$

6.4. CALCIUM 43

The most interesting radiations here are the E2 and M1 coming from the $\frac{3}{2}$-level at 0.593 MeV. First, consider the E2 radiation. As before,

$$Q_2 = \bar{e}\sum_{i=1}^{3} r_i^{\,2} Y_2^{\,0}(\omega_i).$$

There are only two important terms: $(\frac{7}{2}^3 : \frac{7}{2}||Q_2||\frac{7}{2}^3 : \frac{3}{2})$ and $(\frac{7}{2}^3 : \frac{7}{2}||Q_2||\frac{7}{2}^2(2)\frac{3}{2} : \frac{3}{2})$.

Hence, to a very good approximation,

$$(\tfrac{7}{2}||Q_2||\tfrac{3}{2}) = -4.321\ c_0.$$

Assuming pure $j-j$ coupling (i.e. taking only the first term) gives $-4.066\ c_0$, so that the configuration interaction has enhanced the E2 radiation only a bit. Thus

$$T(\mathrm{E2}) = 9.275\,\beta^2 e^2 b^4 \times 10^7 = 2.02\,\beta^2\times 10^9\ \mathrm{sec}^{-1}. \tag{43}$$

The M1 radiation to the $\frac{5}{2}$-state is strongly inhibited (in pure $j-j$, it would vanish). We must therefore use all of the other configurations. We find the following reduced matrix elements[†]:

$$(j^3 : I||M_1||j^3(J)j' : I') = \sqrt{3}\,F^{I}_{sJ} W(Jj'I1 : I'j)(j||M_1||j')\sqrt{[I][I']},$$

$$\begin{aligned}(j^2(J)j' : I||M_1||j'^2(J')j : I')\\ &= (-1)^{j+j'+1}3(j||M_1||j')\sum_{J_1} F^{I}_{JJ_1}F^{I'}_{J'J_1}W(J_1j'I1 : I'j)\sqrt{[I][I']},\end{aligned}$$

$$\begin{aligned}(j^2(J)j' : I||M_1||j^2(J')j'' : I') = \{&W(Jj''I1 : I'j')(j'||M_1||j'')\delta_{JJ'}\\ &+3(j||M_1||j)\delta_{j'j''}\sum_{J_1}^{e} F^{I}_{JJ_1}F^{I'}_{J'J_1}W(J_1jI1 : I'j)\}\sqrt{[I][I']}.\end{aligned}$$

Next, we have a general class of elements:

$$\begin{aligned}\langle j^2(J)j' : I||M_1||j_1j_2(J')j_3 : I'\rangle = &\sqrt{3}\,F^{I}_{JJ'}\langle jj'(J')j : I||M_1||j_1j_2(J')j_3 : I'\rangle\\ &+ 3\sum_{J_1}^{e} F^{I}_{JJ_1}F^{I'}_{J'J_1}\langle jj'(J_1)j : I||M_1||j_1j_3(J_1)j_2 : I'\rangle\\ &+3\sum_{J_1}^{e} F^{I}_{JJ_1}\hat{F}^{I'}_{J'J_1}\langle jj'(J_1)j : I||M_1||j_3j_2(J_1)j_2 : I'\rangle.\end{aligned}$$

[†] The second equation is precisely eq. (39), FL I, except for their leaving off the phase.

Only one of these terms will be non-vanishing in any particular case. Thus

$$(j^2(J)j':I||M_1||j''j'(J')j:I') = (-1)^{j'+j+1}(j^2(J)j':I||M_1||j''j(J')j':I')$$
$$= 3(j||M_1||j'')\sum_{J_1}^{e} F^{I}_{JJ_1}\hat{F}^{I'}_{J'J_1} W(J_1j''I1:I'j)\sqrt{[I][I']}$$

and

$$(j^2(J)j':I||M_1||jj''(J')j':I') = (j^2(J)j':I||M_1||j'j''(J')j:I')$$
$$= 3(j||M_1||j'')\sum_{J_1}^{e} F^{I}_{JJ_1}F^{I'}_{J'J_1} W(J_1j''I1:I'j)\sqrt{[I][I']}.$$

Finally,

$$(jj'(J)j'':I||M_1||jj'(J')j'':I') = \{(j''||M_1||j'')W(Jj''I1:J'j'')\delta_{JJ'}$$
$$+3(j'||M_1||j')\sum_{J_1}^{e} F^{I}_{JJ_1}F^{I'}_{J'J_1} W(J_1j'I1:I'j')$$
$$+3(j||M_1||j)\sum_{J_1}^{e} \hat{F}^{I}_{JJ_1}\hat{F}^{I'}_{J'J_1} W(J_1jI1:I'j)\}\sqrt{[I][I']}.$$

Again, because of core motion, $g_L = 0.01107$ for the neutron. Adding all the contributions properly weighted by the product of the (unnormalized) mixture amplitudes, we find

$$(\tfrac{5}{2}||M_1||\tfrac{3}{2}) = 0.3095\,\mu_0/\sqrt{\pi}.$$

Therefore

$$T(M_1) = 0.02838\,k^3\mu_0^2/\hbar N_1^2N_2^2,$$

where N_1 and N_2 are the normalizations of the wave functions. Since $\Delta E = 0.593-0.374 = 0.219$ MeV, $k = 0.00111\,f^{-1}$, and

$$T(M_1) = 4.426\times 10^8\ \text{sec}^{-1}. \tag{44}$$

(This may be compared with the LF II estimate of $3\times 10^8\ \text{sec}^{-1}$). Experimentally, we find [50]) that the relative intensities of the 0.593 MeV E2 and 0.220 MeV M1 gamma rays is 23 to < 5, i.e. the crossover dominates the cascade by better than 23/5. Thus, if the internal conversions are small, we can compare the transition probabilities directly, and find that

$$T(\text{E2}) \geqq 5\times 4.426\times 10^8 = 2.213\times 10^9\ \text{sec}^{-1}. \tag{45}$$

Then from (43), we must have $\beta^2 \geqq 1.10 \Rightarrow \beta \geqq 1.05$. As before, β already includes the effect of the core, $\beta_c = 0.10$; hence the surface coupling contribution is

$$\beta_{\text{surf}} \geqq 0.95.$$

This compares very well with the enhancement found for the Ca 42 $2 \rightarrow 0$ decay, just as True and Ford found that the enhancement for Pb 207 was just about the same as for Pb 206. If we were to take the small discrepancy between 0.92 and 0.95 seriously, it is at any rate in the expected direction, as we would expect the core to become more rigid as we go to fewer extra-core particles. Thus at a guess, we take, for Ca^{41},

$$\beta_1^{\mathrm{surface}} = 0.89, \quad \text{giving } \beta_1 = 1.00$$

and therefore we find for the 1.95 MeV gamma-ray in Ca 41, from eq. (36), the decay rate

$$T(\mathrm{E2}) = 2.47 \times 10^{12}\ \mathrm{sec}^{-1}.$$

The only one of these predicted decay times which can be directly measured is the 0.220 MeV M1 radiation from Ca 43. The others might be measurable by Coulomb excitation.

6.5. COLLECTIVE CONTRIBUTION

The particle-surface coupling for Ca 43 was found to contribute $\beta_S \approx 0.95$. Hence we find, from eq. (38), that the coupling strength is $k/C = 0.12$, which is fairly considerable. If we take [47]) $k = 40$ MeV, this gives $C = 340$ MeV for the surface-tensition parameter. The phonon energy is

$$\hbar\omega = \hbar \sqrt{\frac{C}{B}}.$$

The mass parameter $B \equiv B_2$ is given by

$$B_\lambda = \frac{1}{\lambda}\frac{3AMR_0^2}{4\pi},$$

so that for $A = 43$, $R_0 = 1.29\, A^{\frac{1}{3}} = 4.42\, f$, and $\hbar\omega = 11.8$ MeV. These values of C and $\hbar\omega$ are to be compared with the hydrodynamic values $C = 50$ MeV, $\hbar\omega = 4$ MeV (obtained from figs. 1 and 2 of ref. [47])).

7. Conclusions

1) The gamma transition probabilities indicate that the amount of surface to particle coupling is quite considerable and, together with the low energies of the lowest core-excited states in Ca 41, 42, and 43, indicates at least part of the reason why this particular region of the periodic table is not easily amenable to a shell model calculation, except possibly for the ground states (as shown by Talmi, for example), where the core and collective effects are likeliest to be small.

2) It is possible to obtain a "fair" fit to the observed levels (considering the ten calculated levels, $\langle\delta\rangle = 0.224$ MeV) with an unrealistic potential, whose deviation from the reaction matrix presumably compensates in part for ignoring

the core states, the surface-particle interaction, the **L** · **S** interaction, and for using a Gaussian radial dependence, which is a poor approximation to a short-ranged Yukawa plus hard core.

3) The importance of higher configurations in the shell model (particularly for the excited states and for several particles) is made very clear. It seems imperative to take as many configurations into account as possible, rather than trying to guess which ones are likely to be significant. On the other hand, since the number of configurations quickly becomes very large as we increase the number of interacting particles, this argues for the use of fast, large computers for such calculations.

4) The erroneous results obtained by LF resulted principally from underestimating the influence of the p-states, from using perturbation theory in Ca^{42}, rather than performing exact diagonalizations; in Ca^{43}, the p-states were neglected entirely. The approximations made to the Slater parameters also propagated errors in the calculations.

5) The spectra

Calcium 41. The 2.01 MeV level has positive parity, and the probable $l = 2$ assignment makes it reasonable that this is a $d_{\frac{3}{2}}$ level, probably mostly due to the configuration $f_{\frac{7}{2}}^{2}(0)d_{\frac{3}{2}}^{-1}$. There is no pure single-particle $p_{\frac{1}{2}}$ level, the 2.47 and 3.95 MeV levels sharing $p_{\frac{1}{2}}$ character, about 70 % and 30 % respectively. This implies that the 1.95 MeV level is probably not a pure single-particle $p_{\frac{3}{2}}$ level either, but that one of the higher levels also has a large fraction of $p_{\frac{3}{2}}$ single particle character (about 45 %). The $f_{\frac{5}{2}}$ and $g_{\frac{9}{2}}$ levels are probably at 6.3 and 5.3 MeV, respectively.

Calcium 42. The 1.836 MeV level is 0+. The 2.42, 2.75 and 3.25 (or 3.19) MeV levels are probably 4+, 2+, 6+, in that order.

Calcium 43. The third and fourth excited levels are probably core-excited states, $\frac{3}{2}+$ and $\frac{5}{2}+$ in that order, though this analysis could not show this. The next two excited levels are probably $\frac{9}{2}-$ and $\frac{11}{2}-$ in that order. The $\frac{11}{2}-$ level is mostly $f_{\frac{7}{2}}^{3}$, but the $\frac{9}{2}-$ level has very large admixtures of other configurations. Thus Sheline's "paradox" is apparently solved: the $\frac{9}{2}-$ level *is* very high; it is probably the 1.678 MeV level. The fairly low energies of the first core-excited states indicates a considerable particle-surface coupling, which is borne out by the cascade-crossover ratio in Ca 43.

6) There is a weak 2.54(3) MeV gamma ray from Ca 44*, probably from level 4 to ground, so that, assuming the γ to be E2, a 2+ assignment is likely for that level, in agreement with the same tentative assignment made in Ca 42 on the basis of the present work.

7) The ground states of Ca 42 and 43 are quite close to $j-j$ coupling, but the excited states deviate considerably.

8) The magnetic moment calculations indicate that one number may be obtained in many ways — it is so sensitive an indicator of the correct mixture

amplitudes that it can only be useful when the potential is already quite well known, to fix the finer details.

9) Several things need to be done to carry out the above program better:

(a) if the same set of configurations is used, put in the surface coupling found here;

(b) use a "soft-core" Gaussian for the radial part of the internucleon interaction;

(c) introduce the core state $d_{\frac{3}{2}}^{-1}f_{\frac{7}{2}}^{2}$ among the basic single-particle configurations (of course, if this is done, we must *not* include (1), but only any residual amount still called for by further E2 enhancement);

(d) split up the p-states among the appropriate levels (e.g. the $p_{\frac{1}{2}}$ state between the 2.47 and 3.95 MeV levels);

(e) remove possible spurious centre-of-mass motion states [51]);

(f) do not assume any specific values for the particle bonds; rather, let these be calculated;

(g) it may be necessary to include an $\mathbf{L} \cdot \mathbf{S}$ term.

10) From the experimental point of view, the gamma decay rates in Ca 42 and 43 could be measured, to check the theoretical predictions made here, especially T(M1). The search for the $f_{\frac{5}{2}}$ and $g_{\frac{9}{2}}$ single-particle levels in Ca 41 must be extended to 7 MeV or higher, to check the Sc 41 findings. To determine the assignment of levels 3 and 4 more definitely, the pickup reaction Ca 43 (p, d) Ca 42 should be tried. Finally, one must try to understand why the relative reduced widths of the $f_{\frac{5}{2}}$ and $g_{\frac{9}{2}}$ levels are so small.

The author wishes to thank Professor Carl Levinson for his help and encouragement in all phases of this work.

Note added in proof: Recently a preprint has been received from J. D. McCullen and J. J. Kraushaar, who have redetermined the assignments of the low excited states of Ca^{42} and Ca^{44}. They confirm the excited states in Ca^{42} to be 0+, 2+(1+), 4+, and a very tentative (0+, 3+, 4+) for the 1.84, 2.42, 2.75 and 3.25 MeV levels, respectively. Thus the assignments made in this work for the third and fourth excited levels are reversed, and the $T(\mathrm{E2})_{4\to 2}$ transition rate given by eq. (42) is enhanced by the factor 4.75.

Appendix J

RESULTS OF FINAL MACHINE CALCULATION

The calcium 42 matrices for $J = 0, 2, 4, 6$ are shown here.

$$(\Delta f = 6.3\ \mathrm{MeV},\quad E_{g_{\frac{9}{2}}} = 5.3,\quad V = -18.884,\quad V_t = -14.988,$$
$$\rho = 0.760,\quad \alpha = -0.195):$$

$\underline{E(0) = -3.1077}$

$$\begin{pmatrix} -2.48690 & -0.31240 & -\ 1.72012 & -0.33444 & 1.72559 \\ -0.31240 & 2.57364 & -\ 0.38983 & -2.29095 & 0.24318 \\ -1.72012 & -0.38983 & 10.60965 & -0.19172 & 1.56459 \\ -0.33444 & -2.29095 & -\ 0.19172 & 3.99458 & 0.22570 \\ 1.72559 & 0.24318 & 1.56459 & 0.22570 & 8.49188 \end{pmatrix},$$

$\underline{E(2) = -1.5855}$

$$\begin{pmatrix} -1.20059 & -0.21117 & -0.39243 & -1.79368 & 0.75166 & -0.05948 & -0.07426 \\ -0.21117 & -0.21744 & 0.09151 & -0.20214 & 0.11605 & -1.05203 & -0.32126 \\ -0.39243 & 0.09151 & 5.12958 & 1.64969 & -0.66839 & -0.00375 & 0.11330 \\ -1.79368 & -0.20214 & 1.64969 & 11.38578 & 1.10847 & -0.13594 & -0.12223 \\ 0.75166 & 0.11605 & -0.66839 & 1.10847 & 9.24567 & 0.03144 & 0.04572 \\ -0.05948 & -1.05203 & -0.00375 & -0.13594 & 0.03144 & 8.55370 & -0.13115 \\ -0.07426 & -0.32126 & 0.11330 & -0.12223 & 0.04572 & -0.13115 & 3.22867 \end{pmatrix},$$

$\underline{E(4) = -0.9362}$

$$\begin{pmatrix} -0.53074 & -0.10928 & 0.29371 & 0.39186 & -0.13675 & -1.03432 & 0.26652 \\ -0.10928 & 1.70177 & 0.25283 & 1.18547 & -1.36534 & -0.19658 & 0.05300 \\ 0.29371 & 0.25283 & 4.13081 & -0.19328 & 0.24583 & 0.55178 & -0.72779 \\ 0.39186 & 1.18547 & -0.19328 & 1.71724 & 1.63426 & 0.15999 & -0.13137 \\ -0.13675 & -1.36534 & 0.24583 & 1.63426 & 5.99805 & -0.18861 & 0.13166 \\ -1.03432 & -0.19658 & 0.55178 & 0.15999 & -0.18861 & 12.21517 & 0.54250 \\ 0.26652 & 0.05300 & -0.72779 & -0.13137 & 0.13166 & 0.54250 & 10.03731 \end{pmatrix},$$

$\underline{E(6) = -0.1009}$

$$\begin{pmatrix} -0.08706 & -0.18956 & -\ 0.09899 \\ -0.18956 & 2.85949 & -\ 0.53945 \\ -0.09899 & -0.53945 & 10.31560 \end{pmatrix}.$$

The (unnormalized) eigenvectors are respectively

$$\begin{pmatrix} 1.000 \\ 0.108 \\ 0.149 \\ 0.090 \\ -0.173 \end{pmatrix}, \quad \begin{pmatrix} 1.000 \\ 0.212 \\ 0.011 \\ 0.148 \\ -0.086 \\ 0.031 \\ 0.034 \end{pmatrix}, \quad \begin{pmatrix} 1.000 \\ 0.369 \\ -0.121 \\ -0.454 \\ 0.207 \\ 0.100 \\ -0.047 \end{pmatrix}, \quad \begin{pmatrix} 1.000 \\ 0.065 \\ 0.013 \end{pmatrix}.$$

The lowest eigenvalues of the Ca 43 matrices together with the eigenvectors corresponding to them are for

$$E(\tfrac{3}{2}) = -2.9725,\quad E(\tfrac{5}{2}) = 3.1906,\quad E(\tfrac{7}{2}) = -3.5653,\quad E(\tfrac{9}{2}) = -2.4382,\quad E(\tfrac{11}{2}) = -1.9797,$$

$$\begin{pmatrix} 1.000 \\ 0.000 \\ -0.028 \\ -0.075 \\ 0.000 \\ 0.077 \\ -0.615 \\ 0.000 \\ 0.000 \\ -0.439 \\ 0.000 \\ 0.000 \\ 0.000 \\ 0.112 \\ -0.123 \\ 0.072 \\ -0.284 \\ 0.000 \\ 0.059 \\ 0.000 \\ 0.000 \\ -0.064 \\ 0.048 \\ 0.000 \\ -0.000 \end{pmatrix}, \quad \begin{pmatrix} 1.000 \\ -0.079 \\ 0.027 \\ -0.072 \\ 0.000 \\ 0.000 \\ -0.234 \\ -0.265 \\ 0.000 \\ -0.205 \\ 0.000 \\ 0.000 \\ 0.000 \\ 0.188 \\ 0.045 \\ 0.048 \\ 0.113 \\ 0.000 \\ 0.051 \\ 0.000 \\ 0.000 \\ -0.113 \\ -0.019 \\ -0.024 \\ -0.000 \end{pmatrix}, \quad \begin{pmatrix} 1.000 \\ 0.000 \\ 0.053 \\ -0.011 \\ -0.009 \\ 0.000 \\ 0.050 \\ -0.011 \\ 0.000 \\ 0.000 \\ -0.064 \\ 0.000 \\ 0.145 \\ -0.087 \\ -0.049 \\ -0.005 \\ -0.030 \\ 0.098 \\ 0.000 \\ 0.076 \\ -0.157 \\ 0.049 \\ 0.027 \\ -0.019 \\ -0.000 \end{pmatrix}, \quad \begin{pmatrix} 1.000 \\ -0.000 \\ 0.249 \\ 0.066 \\ 0.130 \\ -0.000 \\ -0.000 \\ 0.415 \\ 0.588 \\ -0.000 \\ 0.653 \\ -0.000 \\ -0.000 \\ 0.054 \\ -0.157 \\ -0.098 \\ -0.300 \\ -0.000 \\ -0.043 \\ -0.000 \\ -0.000 \\ -0.028 \\ 0.066 \\ 0.017 \\ 0.001 \end{pmatrix}, \quad \begin{pmatrix} 1.000 \\ 0.000 \\ 0.000 \\ 0.176 \\ -0.076 \\ 0.000 \\ 0.000 \\ 0.071 \\ -0.137 \\ 0.000 \\ 0.000 \\ -0.079 \\ 0.000 \\ 0.174 \\ -0.050 \\ 0.007 \\ -0.068 \\ 0.000 \\ 0.021 \\ 0.000 \\ 0.000 \\ -0.093 \\ 0.027 \\ -0.022 \\ -0.004 \end{pmatrix}.$$

Appendix N

NOTATION

Certain much-used phrases are abbreviated as follows: ci — configuration interaction, ipm — independent particle model, sp — single particle, spm — single particle model, sm — shell model, f — 10^{-13} cm, CG — Clebsch-Gordan, fpc — fractional parentage coefficient.

We use several means for denoting angular momentum coupling; simplest is to juxtapose the two components, and write the resultant in parentheses after them:

$$jj'(J) \leftrightarrow \mathbf{j}+\mathbf{j}' = \mathbf{J}.$$

Similarly,

$$jj'(J) \equiv j\times j'(J) \equiv jj' : J.$$

We use a Dirac-like notation of bras and kets to denote wave functions, as well as the more conventional Greek letters. Thus we have

$$\varphi_\alpha \equiv |\alpha\rangle, \quad (\varphi_\alpha, \varphi_\beta) \equiv \langle\alpha|\beta\rangle.$$

Thus $|jj'(J)j'': J'\times j''': J_0\rangle$ is a wave function for four particles: 1 and 2 vector couple to J: this, in turn, couples with particle 3, with angular momentum j'', to form J'. Finally, J' couples with particle $4(j''')$ to form the total angular momentum J_0.

A wave function will sometimes be denoted by $|lj\rangle$ alone, more often as $|l_j\rangle$ or l_j; e.g. $|\mathrm{f}_{\frac{7}{2}}\rangle$. If several particles are vector coupled, then they will be written in any of the following forms:

$$|l_j l'_{j'}\rangle_J \equiv |l_j l'_{j'}(J)\rangle;$$

for example, $|\mathrm{f}_{\frac{7}{2}}{}^2\rangle_0$ and $|\mathrm{f}_{\frac{7}{2}}{}^2(2)\mathrm{p}_{\frac{3}{2}}\rangle_{\frac{1}{2}}$. Since, for these calculations, each j value corresponds to a unique l value, the latter is redundant, and for the sake of simplicity, is often dropped (in this work), so that the above examples become

$$|\tfrac{7}{2}{}^2\rangle_0 \quad \text{and} \quad |\tfrac{7}{2}{}^2(2)\tfrac{3}{2}\rangle_{\frac{1}{2}}.$$

Moreover, since every j is half an odd integer, we may write, without fear of confusion, $2j$ instead of j. Thus, the examples become $|7^2(0)\rangle$ and $|7^2(2)3:1\rangle$. When there is a possibility of ambiguity, the subscript A will be written after any antisymmetric combination of sp wave functions, and omitted if the product has not been antisymmetrized. Thus the matrix element

$${}_A\langle \mathrm{f}_{\frac{7}{2}}{}^2(J)|V|\mathrm{f}_{\frac{5}{2}}\mathrm{f}_{\frac{7}{2}}(J)\rangle_A \equiv \langle 7^2\colon J|V|57\colon J\rangle.$$

Otherwise, wave functions will be assumed to be properly antisymmetric. Commonly used symbols:

$$n!! \equiv n(n-2)(n-4)\ldots(1 \text{ or } 2), \quad [j] \equiv 2j+1.$$

We use round brackets for matrix elements and reduced matrix elements defined with Racah's phases, etc. We also use angular brackets to denote matrix elements, and the relation between the two is

$$(j||T^k||j') = [j]^{\frac{1}{2}}\langle j||T^k||j'\rangle,$$

where T^k is a spherical tensor of rank k. There are several notations for the CG coefficients for coupling two angular momenta; we write Condon and Shortley's first:

$$\begin{aligned}\langle j_1 j_2 j m|j_1 m_1 j_2 m_2\rangle &\equiv \begin{bmatrix} j_1 & j_2 & j \\ m_1 & m_2 & m \end{bmatrix} \equiv C^{j_1 j_2 j}_{m_1 m_2} \\ &\equiv (-1)^{j_1-j_2+m}[j]^{\frac{1}{2}} \begin{Bmatrix} j_1 & j_2 & j \\ m_1 & m_2 & -m \end{Bmatrix}.\end{aligned}$$

The curly bracket symbol is Wigner's $3j$ symbol. Note that one of the magnetic quantum numbers is redundant, as $m_1+m_2 = m$. This simplifies many summations over the m_i.

When particles are not numbered, they are assumed to be in their "standard" order:

$$1, 2, \ldots, n.$$

$\Delta(abc)$ vanishes unless the triangle inequality is satisfied by a, b and c, in which case it is unity. The triangle inequality is

$$|\mathbf{a}+\mathbf{b}| \geqq c$$

and its permutations, which is equivalent to demanding that a, b and c form the sides of a triangle. Finally,

$$\varepsilon(abc\ldots) = \begin{cases} 1 & \text{if} \quad a+b+c+\ldots = \text{even}, \\ 0 & \text{if} \quad a+b+c+\ldots = \text{odd}. \end{cases}$$

References

1) B. H. Flowers, Progress in Nuclear Physics **2** (1952) 235;
M. Redlich, Ph. D. Thesis, Princeton (1954);
M. G. Mayer and J. H. P. Jensen, Elementary theory of nuclear shell structure (Wiley, New York, 1955);
E. Feenberg, Shell theory of the nucleus (Princeton University Press, 1955);
J. P. Elliott and A. M. Lane, Handbuch der Physik (Springer-Verlag, Berlin, 1957) Vol. **39**, p. 241;
J. P. Elliott and B. H. Flowers, Proc. Roy. Soc. A **229** (1955) 536;
W. W. True and K. W. Ford, Phys. Rev. **109** (1958) 1675
2) T. D. Newton, Can. Journ. Phys. **37** (1959) 944
3) P. F. A. Klinkenberg, Rev. Mod. Phys. **24** (1952) 63
4) C. Levinson and K. W. Ford, Phys. Rev. **99** (1955) 792, **100** (1955) 1, 13;
J. M. Kennedy, private communications to C. Levinson (1955);
S. Goldstein and I. Talmi, Phys. Rev. **102** (1956) 589;
R. Thieberger and I. Talmi, Phys. Rev. **102** (1956) 923;
I. Talmi and R. Thieberger, Phys. Rev. **103** (1956) 718;
R. D. Lawson and J. L. Uretsky, Phys. Rev. **106** (1957) 1369;
S. Goldstein and I. Talmi, Phys. Rev. **105** (1957) 995;
I. Talmi, Phys. Rev. **107** (1957) 326;
B. DuttaRoy, Saha institute of Nuclear Physics (1958), unpublished;
M. K. Banerjee and B. DuttaRoy, Ann. of Phys. **7** (1959) 484
5) R. S. Christian and H. P. Noyes, Phys. Rev. **79** (1950) 85
6) C. M. Braams, Phys. Rev. **103** (1950) 1310
7) J. R. Holt and T. N. Marsham, Proc. Phys. Soc. A **46** (1953) 565
8) C. K. Bockelman and W. W. Buechner, Phys. Rev. **107** (1957) 1366
9) C. M. Class, R. H. Davis and J. H. Johnson, preprint and Phys. Rev. Letters **3** (1959) 41
10) J. P. Schiffer, Phys. Rev. **97** (1955) 428
11) Way, King McGinnis and van Lieshout, USAEC Report TID 5300 (June 1955);
D. T. Stevenon and M. Deutsch, Phys. Rev. **84** (1951) 1071
12) B. H. Flowers, Physica **18** (1952) 1101;
D. Kurath, Phys. Rev. **91** (1953) 1430
13) U. Cappeller and R. Klingelhöfer, Z. für Naturf. **9A** (1954) 1052
14) Way, Kundu, McGinnis and van Lieshout, Ann. Rev. Nuclear Science **7** (1956) 154
15) H. Morinaga, private communication (1959)
16) R. K. Sheline, University of Pittsburgh Conf. on Nuclear Structure (June 1957) 483
17) Lawson and Uretsky, ref. [4]);
M. K. Banerjee and B. DuttaRoy, private communication (1958)
18) R. D. Lawson and J. L. Uretsky, Phys. Rev. **108** (1957) 1300
19) Morinaga, Mutsuro and Sugawara, Phys. Rev. **114** (1959) 1146
20) T. Lindqvist and A. C. G. Mitchell, Phys. Rev. **95** (1954) 1535

21) T. Lindqvist, Arkiv för Fysik **12** (1957) 495
22) Bockelman, Braams, Browne, Buechner, Sharp and Sperduto, Phys. Rev. **107** (1957) 176, **108** (1957) 1647
23) J. B. French and B. J. Raz, Phys. Rev. **104** (1956) 1411
24) S. T. Butler and O. H. Hittmair, Nuclear stripping reactions (Horwitz Publications, Sydney 1957), Ch. VI
25) J. Hughes and K. L. Leconteur, Proc. Phys. Soc. A **63** (1950) 1219;
R. J. Blin-Stoyle, Phil. Mag. **46** (1955) 973;
J. S. Bell and T. H. R. Skyrme, Phil. Mag. **1** (1950) 1055;
R. H. Nussbaum, Rev. Mod. Phys. **28** (1956) 423;
L. S. Kisslinger, Phys. Rev. **104** (1956) 1077;
P. E. Nemirovskii, JETP **6** (1958) 573;
B. P. Nigam and M. K. Sundaresan, Can. J. Phys. **36** (1958) 571; Phys. Rev. **111** (1958) 284;
A. E. S. Green, Proc. Intern. Conf. Nuclear Optical Model (Florida State University, 1959) p. 44;
J. Sawicki, Nuclear Physics **13** (1959) 350
26) P. M. Endt and C. M. Braams, Rev. Mod. Phys. **29** (1957) 683
27) C. M. Braams, Energy levels of calcium isotopes, Thesis (Excelsior, the Hague, the Netherlands, 1956) 71
28) R. S. Christian and E. W. Hart, Phys. Rev. **77** (1950) 441, and ref. 5);
R. Jastrow, Phys. Rev. **81** (1951) 165
29) I. Talmi, Helv. Phys. Acta **25** (1951) 185;
R. Thieberger, Nuclear Physics **2** (1957) 533
30) E. J. Konopinski and K. W. Ford, Nuclear Physics **9** (1958/9) 218
31) A. DeShalit, Phys. Rev. **91** (1953) 1479 (Table 1)
32) R. F. Bacher and S. Goudsmit, Phys. Rev. **46** (1934) 948;
G. Racah, Phys. Rev. **63** (1943) 367: R III;
H. A. Jahn, Proc. Roy. Soc. **205A** (1951) 192;
A. R. Edmonds and B. H. Flowers, Proc. Roy. Soc. A **214** (1952) 515;
N. Rosenweig, Phys. Rev. **88** (1952) 580;
S. Meshkov, Phys. Rev. **91** (1953) 871;
Redlich, ref. 1) p. 38;
Elliott and Lane, ref. 1), p. 24
33) A. Hassitt, Proc. Roy. Soc. **A 229** (1955) 110;
C. Schwartz and A. DeShalit, Phys. Rev. **94** (1954) 1257 (eq. 10)
34) J. P. Elliott, Proc. Roy. Soc. **218A** (1953) 345;
I. Talmi, Phys. Rev. **89** (1953) 1065
35) J. Hope and L. W. Longdon, Phys. Rev. **101** (1956) 710
36) J. Hope, Ph. D. Thesis (London 1951)
37) H. A. Jahn and J. Hope, Phys. Rev. **93** (1954) 318
38) A. Kerman, Phys. Rev. **92** (1953) 1176;
D. C. Choudhoury, Mat. Fys. Medd. Dan. Vid. Selsk. **28**, No. 4 (1954)
39) True and Ford, ref. 1)
40) J. L. Gammel and R. M. Thaler, Phys. Rev. **107** (1957) 291, 1337
41) Ref. 16), p. 486
42) R. J. Blin-Stoyle, Proc. Phys. Soc. **66A** (1953) 1158;
A. Arima and H. Horie, Prog. Theor. Phys. **11** (1954) 509, **12** (1954) 623
43) C. P. Jeffries, Phys. Rev. **90** (1953) 1130
44) J. M. Kennedy and W. T. Sharp, CRT 580 (1954)
45) L. C. Biedenharn, ORNL Report **1098** (1952)
46) R. Hofstadter, Ann. Rev. Nucl. Science **7** (1957) 231
47) A. Bohr and B. R. Mottelson, Mat. Fys. Medd. Dan. Vid. Selsk. **27**, No. 16 (1953)
48) D. M. Van Patter, Jour. Franklin Inst. **266** (1958) 411
49) D. M. Van Patter, private communication (1958)
50) Ref. 36), Table LIX
51) Elliott and Lane, ref. 1), p. 330

7.A

Nuclear Physics **23** (1961) 245—268; ©*North-Holland Publishing Co., Amsterdam*

Not to be reproduced by photoprint or microfilm without written permission from the publisher

CANONICAL AND NON-CANONICAL METHOD OF QUANTISATION IN THE LEE MODEL

KATSUHIKO SEKINE †

Max-Planck-Institut für Physik und Astrophysik, München

Received 13 October 1960

Abstract: The connection between the canonical and the "non-canonical" method of quantisation is studied with the help of the Lee model with indefinite metric. It will be shown that, even when the anticommutator vanishes for equal times, it is still possible to construct a Hamiltonian formalism similar to the conventional one by introducing a small time interval Δt into some basic relations of the theory.

1. Introduction

In a series of papers on the non-linear spinor theory of elementary particles $^{1-8}$), a new method of quantisation has been developed which is characterized especially by the fact that the commutation relations contain no singularities of the δ-type on the light cone. We shall call such a quantisation *non-canonical*.

On the other hand, the conventional quantum theories of fields are characterized by the canonical quantisation. It is well known that the commutation relation

$$\{\psi(x), \psi^*(x')\}_{t=t'} = \delta(\mathbf{x}-\mathbf{x}') \tag{1}$$

is the source of all divergence difficulties, but plays nonetheless an essential role in the formulation of the theory. It is to be noted that in particular the conservation laws in their differential form are usually derived by making use of the canonical commutation relations. Take, for example, a theorem

$$\langle 0|\psi(x_1)\ldots\psi(x_m)\bar{\psi}(y_1)\ldots\bar{\psi}(y_n)|0\rangle = 0 \quad \text{for} \quad m \neq n, \tag{2}$$

which is conventionally called the conservation of charge or of nucleon number. To prove this we utilize

$$[Q, \psi(x)] = -\psi(x), \quad [Q, \bar{\psi}(x)] = \bar{\psi}(x), \tag{3}$$

with

$$Q = \tfrac{1}{2}\int \mathrm{d}^3x[\psi^*(x), \psi(x)]. \tag{4}$$

(This is the general expression for charge, as long as the interaction Lagrangian contains no derivatives of field operators). The eqs. (3) follow, however, only from the canonical commutation relations.

---

† On leave of absence from the Department of Physics, University of Tokyo, Tokyo.

It is thus to be emphasized that with the non-canonical quantisation a completely new concept has been introduced into the traditional framework of quantum field theory. We have so far not yet established how the conservation law can be formulated in the new scheme where we cannot utilize the canonical commutation relations any longer.

In this connection, the question should be raised whether it is nevertheless possible, or not, to establish a relation between the canonical and the non-canonical method of quantisation which is understandable from the correspondence theoretical point of view.

The main purpose of this paper is to answer this question with the help of the Lee model [9-12]), which affords a simple example of the non-canonical quantisation in the limit of infinite cut off, i.e., in the case of point source interaction. As Pauli and Källén have pointed out [10]), one cannot in this model reach the point source keeping a definite metric in Hilbert space. Therefore, the model with which we are concerned must be the Lee model with indefinite metric.

2. Formulation of the Model

The Lee model with indefinite metric is described by the Hamiltonian

$$
\begin{aligned}
H = & -\left|\frac{g}{g_0}\right|^2 m_{\mathrm{V}} \int \psi^*_{\mathrm{Vr}}(\mathbf{p})\psi_{\mathrm{Vr}}(\mathbf{p})\mathrm{d}^3 p + m_{\mathrm{N}} \int \psi_{\mathrm{N}}{}^*(\mathbf{q})\psi_{\mathrm{N}}(\mathbf{q})\,\mathrm{d}^3 q \\
& + \int \omega(\mathbf{k}) a^*(\mathbf{k}) a(\mathbf{k}) \mathrm{d}^3 k \qquad\qquad (5) \\
& - \frac{g}{\sqrt{4\pi}} \int^{\hat{\omega}} \frac{1}{\sqrt{2\omega}} [\psi^*_{\mathrm{Vr}}(\mathbf{p})\psi_{\mathrm{N}}(\mathbf{q}) a(\mathbf{k}) + \mathrm{c.c.}]\,\delta(\mathbf{p}-\mathbf{q}-\mathbf{k})\mathrm{d}^3 p\,\mathrm{d}^3 q\,\mathrm{d}^3 k,
\end{aligned}
$$

together with the commutation relations

$$
\begin{aligned}
\{\psi_{\mathrm{Vr}}(\mathbf{p}), \psi^*_{\mathrm{Vr}}(\mathbf{p}')\} &= -\left|\frac{g_0}{g}\right|^2 \delta(\mathbf{p}-\mathbf{p}'), \\
\{\psi_{\mathrm{N}}(\mathbf{q}), \psi_{\mathrm{N}}{}^*(\mathbf{q}')\} &= \delta(\mathbf{q}-\mathbf{q}'), \qquad\qquad (6) \\
[a(\mathbf{k}), a^*(\mathbf{k}')] &= \delta(\mathbf{k}-\mathbf{k}').
\end{aligned}
$$

The notation is the same as in ref. [11]). If we consider the case where only one heavy particle is present, fixed at the origin, it is convenient to introduce simply ψ_{Vr} and ψ_{N} obeying the commutation relations

$$
\{\psi_{\mathrm{Vr}}, \psi^*_{\mathrm{Vr}}\} = -\left|\frac{g_0}{g}\right|^2, \quad \{\psi_{\mathrm{N}}, \psi_{\mathrm{N}}{}^*\} = 1. \qquad (6a)
$$

In terms of these operators, the Hamiltonian (5) can be brought into the form

$$\begin{aligned} H = -\left|\frac{g}{g_0}\right|^2 m_V \psi^*_{Vr}\psi_{Vr} + m_N \psi_N{}^* \psi_N + \int \omega(\mathbf{k}) a^*(\mathbf{k}) a(\mathbf{k}) \mathrm{d}^3 k \\ - \frac{g}{\sqrt{4\pi}} \int^{\hat{\omega}} \frac{1}{\sqrt{2\omega}} [\psi^*_{Vr}\psi_N a(\mathbf{k}) + \text{c.c.}] \mathrm{d}^3 k. \end{aligned} \tag{5a}$$

As was discussed in ref. 11), m_N can be put equal to zero without loss of generality. $\hat{\omega}$ is a cut-off factor. The limiting case $\hat{\omega} \to \infty$ will be discussed in sect. 4.

The problem is presented at first in the following way:

(I) *The eigenvalue problem*

$$H|\Phi\rangle = E|\Phi\rangle \tag{7}$$

is to be solved under the subsidiary condition

$$\langle\Phi|\Phi\rangle = \varepsilon, \tag{8}$$

where ε *is the constant* 1, −1 *or* 0, *according to the normal, abnormal or dipole ghost state.*

It is here to be noted that the problem can be fixed and uniquely solved if, essentially, three parameters are given. These three may be, for instance, g, $m_V/|g_0|^2$, and $1/|g_0|^2$; the first two define the Hamiltonian, and the third together with the first fixes the commutation relations. It will, however, be shown that these three may be replaced by g,

$$a = \frac{m_V}{|g_0|^2} + \int^{\hat{\omega}} \frac{k^2 \mathrm{d}k}{2\omega^2} \tag{9a}$$

and

$$b = -\frac{1}{|g_0|^2} + \int^{\hat{\omega}} \frac{k^2 \mathrm{d}k}{2\omega^3}. \tag{9b}$$

In Pauli-Källén's method of renormalization, use has been made of the condition

$$\langle 0|\psi_{Vr}|\Phi\rangle = 1, \tag{10}$$

from which one can get an equation connecting the three parameters with each other. Therefore it is necessary to fix only two of them; the rest is to be determined from the condition. This corresponds to the fact that in the unrenormalized theory of the Lee model only two parameters, $m_V{}^0$ and g_0, are at our disposal. On the other hand, we do not wish to take into account the condition (10) explicitly. Thus we have in advance three parameters to fix.

It is well known that the Lee model permits an exact solution. Let us confine ourselves to the lowest non-trivial sector (V, Nθ). Then, a state vector can be written as

$$|\Phi\rangle = O^*|0\rangle,$$

with

$$O^* = -c\left(\frac{g}{g_0}\right)^* \psi^*_{\mathrm{V}_z}+\psi_{\mathrm{N}}{}^* \int \varphi(\mathbf{k})a^*(\mathbf{k})\mathrm{d}^3k. \tag{11}$$

We shall call this the contravariant representation of $|\Phi\rangle$. Substituting (11) into the Schrödinger equation (7), we have

$$\begin{aligned} -m_{\mathrm{V}}c-\frac{1}{\sqrt{4\pi}}\int^{\hat{\omega}}\frac{\mathrm{d}^3k}{\sqrt{2\omega}}g_0{}^*\varphi(\mathbf{k}) &= -Ec,\\ \omega(\mathbf{k})\varphi(\mathbf{k})-\frac{1}{\sqrt{4\pi}}\frac{1}{\sqrt{2\omega}}g_0c &= E\varphi(\mathbf{k}). \end{aligned} \tag{12}$$

3. Application of the Variational Method

Now, we want to formulate the same problem in another way by making use of the variational method. (I) is now replaced by the equivalent problem:

(II) *The quantity*

$$E = \frac{\langle\Phi|H|\Phi\rangle}{\langle\Phi|\Phi\rangle} \tag{13}$$

is to be made stationary as a function of c and $\varphi(\mathbf{k})$.

Substitution of (11) into (13) gives

$$E = \frac{-m_{\mathrm{V}}c^*c+\int\omega(\mathbf{k})\varphi^*(\mathbf{k})\varphi(\mathbf{k})\mathrm{d}^3k-\frac{1}{\sqrt{4\pi}}\int^{\hat{\omega}}\frac{\mathrm{d}^3k}{\sqrt{2\omega}}[g_0{}^*c^*\varphi(\mathbf{k})+\mathrm{c.c.}]}{-c^*c+\int\varphi^*(\mathbf{k})\varphi(\mathbf{k})\mathrm{d}^3k},$$

from which we obtain eqs. (12) as a result of variations with respect to c^* and $\varphi^*(\mathbf{k})$.

The same can also be expressed by means of the so-called Lagrange multiplier method. The new problem equivalent to the one above is:

(III) *The quantity*

$$\Omega = \langle\Phi|H|\Phi\rangle-\lambda(\langle\Phi|\Phi\rangle-\varepsilon) \tag{14}$$

is to be made stationary as a function of c, $\varphi(\mathbf{k})$ *and* λ.

Substitution of (11) gives

$$\begin{aligned}\Omega = -m_{\mathrm{V}}c^*c+\int\omega(\mathbf{k})\varphi^*(\mathbf{k})\varphi(\mathbf{k})\mathrm{d}^3k-\frac{1}{\sqrt{4\pi}}\int^{\hat{\omega}}\frac{\mathrm{d}^3k}{\sqrt{2\omega}}[g_0{}^*c^*\varphi(\mathbf{k})+\mathrm{c.c.}]\\ -\lambda\left(-c^*c+\int\varphi^*(\mathbf{k})\varphi(\mathbf{k})\mathrm{d}^3k-\varepsilon\right)\end{aligned} \tag{15}$$

and the variations with respect to c^* and $\varphi^*(\mathbf{k})$ lead to

$$\begin{aligned} -m_V c - \frac{1}{\sqrt{4\pi}} \int^{\hat{\omega}} \frac{\mathrm{d}^3 k}{\sqrt{2\omega}}\, g_0{}^* \varphi(\mathbf{k}) &= -\lambda c, \\ \omega(\mathbf{k})\varphi(\mathbf{k}) - \frac{1}{\sqrt{4\pi}} \frac{1}{\sqrt{2\omega}}\, g_0 c &= \lambda\varphi(\mathbf{k}). \end{aligned} \tag{16}$$

These equations are also exactly the same as eqs. (12). The Lagrange multiplier λ corresponds to the energy E. Eliminating $\varphi(\mathbf{k})$ we have the equation of the form

$$h(\lambda)c = 0, \tag{17}$$

where

$$h(\lambda) = a + b\lambda + \lambda^2 \int^{\hat{\omega}} \frac{k^2 \mathrm{d}k}{2\omega^3(\omega-\lambda)} \tag{18}$$

with a and b given by (9a, b).

The last integral in $h(\lambda)$ is convergent when $\hat{\omega} \to \infty$.

4. Limiting Case $\hat{\omega} \to \infty$

In this section we want to discuss in some detail what happens when the cut off $\hat{\omega}$ tends to infinity. Keeping a and b finite, then we have

$$m_V \sim -\frac{\hat{\omega}}{\ln \hat{\omega}}, \quad |g_0|^2 \sim \frac{2}{\ln \hat{\omega}}, \tag{19}$$

from which we can immediately see

$$m_V \to -\infty, g_0 \to 0 \quad \text{with} \quad \hat{\omega} \to \infty.$$

Consequently, the eqs. (16) as well as the expression (15) for Ω become meaningless. The contravariant representation (11) of $|\Phi\rangle$ is also not well-defined in this limit, because it contains divergent expressions.

It is, however, to be remarked that one can give the variational function Ω another representation which remains meaningful even when $\hat{\omega} \to \infty$.

Putting

$$c = -\frac{\bar{c}}{g_0}, \tag{20}$$

the variational function can be written as

$$\begin{aligned} \Omega = &-\frac{m_V}{|g_0|^2}\bar{c}^*\bar{c} + \int \omega(\mathbf{k})\varphi^*(\mathbf{k})\varphi(\mathbf{k})\mathrm{d}^3k + \frac{1}{\sqrt{4\pi}} \int^{\hat{\omega}} \frac{\mathrm{d}^3 k}{\sqrt{2\omega}} [\bar{c}^*\varphi(\mathbf{k}) + \text{c.c.}] \\ &-\lambda\left(-\frac{1}{|g_0|^2}\bar{c}^*\bar{c} + \int \omega(\mathbf{k})\varphi^*(\mathbf{k})\varphi(\mathbf{k})\mathrm{d}^3k - \varepsilon\right). \end{aligned} \tag{21}$$

Further, making use of the relations (9a) and (9b), one has

$$\begin{aligned}\Omega &= \left(-a+\int^{\hat{\omega}}\frac{k^2\mathrm{d}k}{2\omega^3}\right)\bar{c}^*\bar{c}+\int^{\infty}\omega(\mathbf{k})\varphi^*(\mathbf{k})\varphi(\mathbf{k})\mathrm{d}^3k \\ &\quad +\frac{1}{\sqrt{4\pi}}\int^{\hat{\omega}}\frac{\mathrm{d}^3k}{\sqrt{2\omega}}[\bar{c}^*\varphi(\mathbf{k})+\text{c.c.}] \qquad (22) \\ &\quad +\lambda\left(-b+\int^{\hat{\omega}}\frac{k^2\mathrm{d}k}{2\omega^3}\right)\bar{c}^*\bar{c}-\lambda\int^{\infty}\varphi^*(k)\varphi(k)\mathrm{d}^3k+\lambda\varepsilon \\ &= -h(\lambda)\bar{c}^*\bar{c}+\int^{\hat{\omega}}\frac{k^2\mathrm{d}k}{2\omega}\,\frac{1}{\omega-\lambda}\bar{c}^*\bar{c}+\frac{1}{\sqrt{4\pi}}\int^{\hat{\omega}}\frac{\mathrm{d}^3k}{\sqrt{2\omega}}[\bar{c}^*\varphi(\mathbf{k})+\text{c.c.}] \qquad (23) \\ &\quad +\int^{\infty}(\omega(\mathbf{k})-\lambda)\varphi^*(\mathbf{k})\varphi(\mathbf{k})\mathrm{d}^3k+\lambda\varepsilon.\end{aligned}$$

Variation with respect to $\varphi^*(\mathbf{k})$ gives

$$\frac{1}{\sqrt{4\pi}}\,\frac{1}{\sqrt{2\omega}}\,\bar{c}+(\omega(\mathbf{k})-\lambda)\varphi(\mathbf{k}) = 0 \quad \text{for} \quad \omega(\mathbf{k}) < \hat{\omega}, \tag{24}$$

$$(\omega(\mathbf{k})-\lambda)\varphi(\mathbf{k}) = 0 \quad \text{for} \quad \omega(\mathbf{k}) \gtrsim \hat{\omega}. \tag{24a}$$

Now, we want to treat this equation as a subsidiary condition. For the discrete spectrum we can solve (24) as

$$\varphi(\mathbf{k}) = \begin{cases} -\dfrac{1}{\sqrt{4\pi}}\,\dfrac{1}{\sqrt{2\omega}}\,\dfrac{1}{\omega-\lambda}\bar{c} & \text{for} \quad \omega(\mathbf{k}) < \hat{\omega}, \qquad (25) \\ 0 & \text{for} \quad \omega(\mathbf{k}) \gtrsim \hat{\omega}. \qquad (25\text{a}) \end{cases}$$

Substituting this into (23) we arrive at a new representation of Ω. Thus, the problem (III) can be replaced by:

(IV) *The quantity*

$$\Omega[\bar{c},\lambda] = -h(\lambda)\bar{c}^*\bar{c}+\lambda\varepsilon \tag{26}$$

is to be made stationary as a function of $\bar{c}$ *and* λ, *where these variables must satisfy the subsidiary condition* (24).

Since $h(\lambda)$ is always well-defined, the new representation (26) for Ω is also well-defined. Therefore the variational problem, if formulated in the form (26), is always meaningful, even in the limit $\hat{\omega} \to \infty$. Variations with respect to $\bar{c}^*$ and λ lead to

$$h(\lambda)\bar{c} = 0 \tag{27}$$

and

$$h'(\lambda)\bar{c}^*\bar{c} = \varepsilon, \tag{28}$$

from which we find

$$h(E) = 0 \tag{29}$$

and

$$|\bar{c}|^2 = \frac{\langle \Phi | \Phi \rangle}{h'(\lambda)}\bigg|_{\lambda=E}. \tag{30}$$

As is seen, the energy eigenvalue can be obtained as a zero point of the function $h(\lambda)$, and eq. (30) together with the subsidiary condition (24) fixes $\bar{c}$ and $\varphi(\mathbf{k})$ which determine the eigenvector.

For the continuous spectrum, on the other hand, the eq. (24) must be solved under the outgoing wave condition

$$\varphi(\mathbf{k}) = \frac{1}{\sqrt{4\pi}k}\delta(k-k_0) + \frac{\bar{c}}{\sqrt{4\pi}\sqrt{2\omega}(E-\omega+i\gamma)} \quad (\gamma \to 0). \tag{31}$$

Accordingly, some alteration is needed in the expression (26), i.e.,

$$\Omega_{\text{cont.}} = -h^+(\lambda)\bar{c}^*\bar{c} - \frac{k_0}{\sqrt{2E}}\bar{c}^* + \lambda\varepsilon, \tag{26a}$$

from which we have, instead of (27),

$$h^+(E)\bar{c} = \frac{k_0}{\sqrt{2E}}. \tag{32}$$

In this way, the problem can be solved completely without any trouble of divergences. Needless to say, we must in the limiting case $\hat{\omega} \to \infty$ use g, a and b in order to define the function $h(\lambda)$, instead of using the divergent constants $m_V/|g_0|^2$ and $1/|g_0|^2$.

As is well known, $-\bar{c}/g$ and $\varphi(\mathbf{k})$ give the covariant representation of the eigenvector, i.e.,

$$\langle 0 | \psi_{V_r} | \Phi \rangle = -\frac{\bar{c}}{g}, \tag{33a}$$

$$\langle 0 | \psi_N a(\mathbf{k}) | \Phi \rangle = \varphi(\mathbf{k}). \tag{33b}$$

It is to be remarked that these quantities are always well-defined, containing no divergence in the limiting case. Divergence occurs only in the contravariant representation.

Further, it can be immediately seen that in the limit $\hat{\omega} \to \infty$ the commutation relation of the V field for equal times is no longer canonical, but vanishes as

$$\{\psi_{V_r}, \psi_{V_r}^*\} = 0, \tag{34}$$

according to $g_0 \to 0$. The relation (34) can be established also by explicit calculations:

$$\langle 0 | \psi_{V_r} \psi_{V_r}^* | 0 \rangle = \frac{1}{g^2}\left[\sum_E \frac{\varepsilon}{h'(E)} + \int_0^\infty \frac{k^2 \mathrm{d}k}{2\omega} \frac{1}{h^+(\omega)h^-(\omega)}\right] = 0. \tag{34a}$$

5. New Formalism

One has thus only to reformulate the contravariant representation of $|\Phi\rangle$ in a suitable way such that no divergence occurs any longer in the essential part of the theory.

It would be very satisfactory if the deviation from the conventional formalism could be restricted to regions of extremely high energy; in other words, the new formalism should be equivalent to the conventional one as far as processes containing relatively low energy are concerned. Therefore, if we take as a new representation of the same vector

$$|\Phi\rangle = O'^{*}|0\rangle \tag{35}$$

instead of (11), then the operator O' would have to satisfy the following requirements:

1) Since $O^{*}|0\rangle$ and $O'^{*}|0\rangle$ are two different contravariant representations of one and the same vector $|\Phi\rangle$, they should lead to the same covariant components as before, i.e.,

$$\langle 0|\psi_{\mathrm{Vr}}O'^{*}|0\rangle = \langle 0|\psi_{\mathrm{Vr}}O^{*}|0\rangle = -\frac{\bar{c}}{g}, \tag{36a}$$

$$\langle 0|\psi_{\mathrm{N}}a(\mathbf{k})O'^{*}|0\rangle = \langle 0|\psi_{\mathrm{N}}a(\mathbf{k})O^{*}|0\rangle = \varphi(\mathbf{k}). \tag{36b}$$

2) We would have to replace, if necessary, the Hamiltonian H by a new expression H', but in such a way that we have again the same variational problem as before; that is,

$$\Omega' \equiv \langle\Phi|H'|\Phi\rangle - \lambda\langle\Phi|\Phi\rangle + \lambda\varepsilon \tag{37}$$

should lead to the same $\Omega[\bar{c}, \lambda]$ and hence the same eigenvalues, but only as far as solutions with not too high energy are concerned.

At first sight the requirement (2) seems to be related only to diagonal elements of the Hamiltonian. But it should be noted that in the expression (37) the bra and the ket vector, $\langle\Phi|$ and $|\Phi\rangle$, are to be varied independently. Therefore, the requirement (2) will imply the following:

3) The nondiagonal matrix element of H' between any two states of energy E_{a} and E_{b} are equal to those of the original Hamiltonian H,

$$\langle\Phi_{\mathrm{a}}|H'|\Phi_{\mathrm{b}}\rangle = \langle\Phi_{\mathrm{a}}|H|\Phi_{\mathrm{b}}\rangle, \tag{38}$$

if E_{a} and E_{b} are small compared with $1/\Delta t$.

As we have shown in the previous section, the contravariant representation of the vector $|\Phi\rangle$ diverges in the limit $g_0 \to 0$, as long as constructed only in terms of the field operators at the fixed time, say, $t=0$. It is possible, however, to represent $|\Phi\rangle$ by means of the time dependent operator $\psi^{*}_{\mathrm{Vr}}(t)$, trying the expression

$$O'^{*} = \bar{c}\int_{-\Delta t}^{\Delta t} F(t)\psi^{*}_{\mathrm{Vr}}(t)\mathrm{d}t + \psi_{\mathrm{N}}{}^{*}(0)\int \sigma(\mathbf{k})a^{*}(\mathbf{k}, 0)\mathrm{d}^{3}k, \tag{39}$$

which contains an integration over a small time interval $\Delta t \ll 1/E$, where E denotes any *discrete* eigenvalue of the system. $\psi_N^*(0)$ and $a^*(\mathbf{k}, 0)$ shall refer to the time $t = 0$.

Then we have from (36a)

$$-\frac{1}{g} = \langle 0|\psi_{\mathrm{V_r}}(0) \int_{-\Delta t}^{\Delta t} F(t)\psi^*_{\mathrm{V_r}}(t)\mathrm{d}t|0\rangle. \tag{40}$$

This equation will determine the constant factor in $F(t)$. By inserting a complete system we have

$$-\frac{1}{g} = \frac{1}{g^2}\int \mathrm{d}t F(t) \left[\sum_E \frac{\varepsilon \mathrm{e}^{iEt}}{h'(E)} + \int_0^\infty \frac{k^2 \mathrm{d}k}{2\omega} \frac{\mathrm{e}^{i\omega t}}{h^+(\omega)h^-(\omega)}\right]. \tag{41}$$

For orientational purpose we assume for instance

$$F(t) = \begin{cases} F & \text{for} \quad -\Delta t \leqq t \leqq \Delta t, \\ 0 & \text{otherwise}. \end{cases} \tag{42}$$

Then we obtain from (41), using eq. (34a),

$$-\frac{1}{g} = \frac{2\Delta t F}{g^2}\left[\sum_E \frac{\varepsilon}{h'(E)}\left(\frac{\sin E\Delta t}{E\Delta t} - 1\right) + \int_{m_\theta}^\infty \frac{k \mathrm{d}\omega}{2h^+(\omega)h^-(\omega)}\left(\frac{\sin \omega\Delta t}{\omega\Delta t} - 1\right)\right]. \tag{43}$$

The first term in the bracket is found to be much smaller than the second under the assumption $\Delta t \ll 1/E$; the main contribution comes from the region $\omega \gtrsim 1/\Delta t$ of the integral. Therefore we can use the asymptotic expression

$$\begin{aligned} h^\pm(\omega) &\approx b\omega - \tfrac{1}{2}\omega\left(\ln\frac{2\omega}{m_\theta} - 1\right) \\ &= -\tfrac{1}{2}\omega \ln\frac{\omega C}{m_\theta}, \quad \text{for} \quad \omega \gg m_\theta, \end{aligned} \tag{44}$$

with

$$C = 2\mathrm{e}^{-2b-1}. \tag{45}$$

Thus, we have from (43), in the first approximation,

$$\frac{1}{g} \approx \frac{4\Delta t F}{g^2}\int_{1/\Delta t}^\infty \frac{\mathrm{d}\omega}{\omega\left(\ln\dfrac{\omega C}{m_\theta}\right)^2}.$$

Hence we have

$$F = \frac{g}{4\Delta t}\ln\frac{C}{\Delta t m_\theta}. \tag{46}$$

In this way $F(t)$ has been determined essentially by the contribution from high energy parts of the integral. The low-lying discrete levels play no essential role;

in particular, it is not important at all whether we have one normal and one abnormal solution (Pauli-Källén's case) or the dipole ghost case.

In terms of (46), the eq. (40) becomes

$$\langle 0|\psi_{\mathrm{Vr}}(0)\int_{-\Delta t}^{\Delta t}\psi^*_{\mathrm{Vr}}(t)\mathrm{d}t|0\rangle = -\frac{1}{g^2}\frac{2\Delta t}{\frac{1}{2}\ln\dfrac{C}{\Delta t\, m_\theta}} \tag{47}$$

and further it can be shown that the corresponding non-diagonal elements are equal to zero,

$$\begin{aligned}&\langle 0|\psi_{\mathrm{Vr}}(0)\int_{-\Delta t}^{\Delta t}\psi^*_{\mathrm{Vr}}(t)\mathrm{d}t|\Phi\rangle\\ &\qquad = \sum\langle 0|\psi_{\mathrm{Vr}}(0)|\Phi_E\rangle\int_{-\Delta t}^{\Delta t}\mathrm{e}^{i(E-E_\phi)t}\mathrm{d}t\langle\Phi^E|\psi^*_{\mathrm{Vr}}(0)|\Phi\rangle = 0\end{aligned} \tag{47a}$$

because of

$$\langle\Phi^E|\psi^*_{\mathrm{Vr}}(0)|\Phi\rangle = 0.$$

Quite similarly we have

$$\langle\Phi|\psi_{\mathrm{Vr}}(0)\int_{-\Delta t}^{\Delta t}\psi^*_{\mathrm{Vr}}(t)\mathrm{d}t|0\rangle = 0. \tag{47b}$$

Next, the function $\sigma(\mathbf{k})$ can be determined by the condition (36b), which leads to

$$\sigma(\mathbf{k}) = \varphi(\mathbf{k})-\bar{\varepsilon}\langle 0|\psi_{\mathrm{N}}a(\mathbf{k})\int F(t)\psi^*_{\mathrm{Vr}}(t)\mathrm{d}t|0\rangle. \tag{48}$$

Notice that the second term in (48) does not vanish; this term can be calculated as follows 12):

$$\begin{aligned}&\langle 0|\psi_{\mathrm{N}}a(\mathbf{k})\int F(t)\psi^*_{\mathrm{Vr}}(t)\mathrm{d}t|0\rangle\\ &\quad = \sum\int\mathrm{d}tF(t)\langle 0|\psi_{\mathrm{N}}a(\mathbf{k})|\Phi_E\rangle\mathrm{e}^{iEt}\langle\Phi^E|\psi^*_{\mathrm{Vr}}(0)|0\rangle\\ &\quad = \int\mathrm{d}tF(t)\Bigg[\sum_E\frac{\varepsilon}{h'(E)}\,\frac{\mathrm{e}^{iEt}}{g\sqrt{4\pi}\sqrt{2\omega}(\omega-E)}-\frac{k\mathrm{e}^{i\omega t}}{g\sqrt{4\pi}\sqrt{2\omega}h^-(\omega)}\\ &\quad -\int\mathrm{d}k'\,k'^2\frac{\mathrm{e}^{i\omega' t}}{g\sqrt{4\pi}\sqrt{2\omega}2\omega' h^+(\omega')h^-(\omega')(\omega'-\omega+i\gamma)}\Bigg].\end{aligned}$$

Assuming (42) we obtain

$$\begin{aligned}&\langle 0|\psi_{\mathrm{N}}a(\mathbf{k})\int F(t)\psi^*_{\mathrm{Vr}}(t)\mathrm{d}t|0\rangle\\ &\quad = \frac{2\Delta tF}{g}\,\frac{1}{\sqrt{4\pi}\sqrt{2\omega}}\Bigg[\frac{k}{h^-(\omega)}\left(1-\frac{\sin\omega\Delta t}{\omega\Delta t}\right)\\ &\quad +\int\mathrm{d}k'\,k'^2\frac{1}{2\omega' h^+(\omega')h^-(\omega')(\omega'-\omega+i\gamma)}\left(1-\frac{\sin\omega'\Delta t}{\omega'\Delta t}\right)\Bigg].\end{aligned} \tag{49}$$

The contribution from the discrete spectrum has been neglected in exactly the same way as in the determination of $F(t)$.

Now, we must consider two cases separately

(1) $\omega \ll 1/\Delta t$

The first term in the bracket in (49) can be neglected; the main contribution comes from the region $\omega' \gtrsim 1/\Delta t$ of the integral. After integrating by parts we have

$$\frac{4\Delta tF}{g\sqrt{4\pi}\sqrt{2\omega}}\int_{1/\Delta t}^{\infty}\frac{\mathrm{d}\omega'}{\omega'^2\left(\ln\dfrac{\omega'C}{m_\theta}\right)^2}=\frac{\Delta t}{\sqrt{4\pi}\sqrt{2\omega}}-\frac{1}{\sqrt{4\pi}\sqrt{2\omega}}\int_{1/\Delta t}^{\infty}\frac{\mathrm{d}\omega'}{\omega'^2}\frac{\ln\dfrac{C}{\Delta t m_\theta}}{\ln\dfrac{\omega'C}{m_\theta}}, \tag{50}$$

where the last integral can be estimated as

$$\frac{1}{\sqrt{4\pi}\sqrt{2\omega}}\int_{1/\Delta t}^{\infty}\frac{\mathrm{d}\omega'}{\omega'^2}\frac{\ln\dfrac{C}{\Delta t m_\theta}}{\ln\dfrac{\omega'C}{m_\theta}}\approx\frac{1}{\sqrt{4\pi}\sqrt{2\omega}}O(\Delta t).$$

Therefore the expression (50) as a whole is also of the order of $1/\sqrt{4\pi}\sqrt{2\omega}O(\Delta t)$. Comparing this with

$$\varphi(\mathbf{k})=-\frac{1}{\sqrt{4\pi}\sqrt{2\omega}}\frac{1}{\omega-E}\bar{c},$$

we have

$$\frac{\langle 0|\psi_{\mathrm{N}}a(\mathbf{k})\int F(t)\psi^{*}_{\mathrm{V}_{\mathrm{r}}}(t)\mathrm{d}t|0\rangle\bar{c}}{\varphi(\mathbf{k})}\approx O((\omega-E)\Delta t). \tag{51a}$$

or

$$\sigma(\mathbf{k})\approx\varphi(\mathbf{k}),\quad\text{for}\quad\omega,E\ll 1/\Delta t. \tag{52a}$$

(2) $\omega \gg 1/\Delta t$

The first term in (49) can be neglected now due to

$$\frac{4\Delta tF}{g\ln\dfrac{\omega C}{m_\theta}}=\frac{\ln\dfrac{C}{\Delta t m_\theta}}{\ln\dfrac{\omega C}{m_\theta}}\ll 1.$$

The integral in the second term is separated into two parts,

$$\frac{4\Delta tF}{g\sqrt{4\pi}\sqrt{2\omega}}\frac{1}{\omega}\int_{1/\Delta t}^{\infty}\frac{\mathrm{d}\omega'}{\left(\ln\dfrac{\omega'C}{m_\theta}\right)^2}\left[-\frac{1}{\omega'}+\frac{1}{\omega'-\omega+i\gamma}\right]. \tag{53}$$

The first part of (53) can be integrated and gives

$$-\frac{1}{\sqrt{4\pi}\sqrt{2\omega}}\frac{1}{\omega},$$

which compensates the main part of $\varphi(\mathbf{k})$. The second integral of (53) can be estimated as follows:

$$\frac{4\Delta tF}{g}\frac{1}{\omega}\int_{1/\Delta t}^{\infty}\frac{\mathrm{d}\omega'}{(\omega'-\omega+i\gamma)\left(\ln\dfrac{\omega' C}{m_0}\right)^2}\approx O\left(\frac{\ln\dfrac{C}{\Delta t m_0}}{\ln\dfrac{\omega C}{m_0}}\right).$$

Therefore,

$$\langle 0|\psi_{\mathrm{N}}a(\mathbf{k})\int F(t)\psi^*_{\mathrm{Vr}}(t)\mathrm{d}t|0\rangle\bar{c}\approx\varphi(\mathbf{k}), \tag{51b}$$

or

$$\sigma(\mathbf{k})\approx 0 \quad\text{for}\quad \omega\gg 1/\Delta t. \tag{52b}$$

Quite similarly to the proof of (47a), one can verify that the non-diagonal elements corresponding to (51) are always equal to zero,

$$\langle 0|\psi_{\mathrm{N}}a(\mathbf{k})\int F(t)\psi^*_{\mathrm{Vr}}(t)\mathrm{d}t|\Phi\rangle=\langle\Phi|\psi_{\mathrm{N}}a(\mathbf{k})\int F(t)\psi^*_{\mathrm{Vr}}(t)\mathrm{d}t|0\rangle=0. \tag{51c}$$

Using $F(t)$ and $\sigma(\mathbf{k})$ determined in the above, we can now evaluate the norm of the vector $|\Phi\rangle$,

$$\begin{aligned}\langle\Phi|\Phi\rangle &=\langle 0|\int F^*(t)\psi_{\mathrm{Vr}}(t)\mathrm{d}t|\Phi\rangle\bar{c}^*+\langle 0|\psi_{\mathrm{N}}\int\sigma^*(\mathbf{k})a(\mathbf{k})\mathrm{d}^3k|\Phi\rangle\\ &=-\int_{-\Delta t}^{\Delta t}\mathrm{d}tF^*(t)\mathrm{e}^{iE_\phi t}\frac{|\bar{c}|^2}{g}+\int\mathrm{d}^3k\sigma^*(\mathbf{k})\varphi(\mathbf{k})\\ &\approx -\tfrac{1}{2}|\bar{c}|^2\ln\frac{C}{\Delta t m_0}+\int^{1/\Delta t}\mathrm{d}^3k|\varphi(\mathbf{k})|^2,\quad\text{for}\quad E_\phi\ll 1/\Delta t.\end{aligned} \tag{54}$$

Notice that in the last integral the cut off $1/\Delta t$ has been introduced automatically as a consequence of the property of $\sigma(\mathbf{k})$, see eqs. (52a) and (52b). In view of (45), it can further be proved

$$\tfrac{1}{2}\ln\frac{C}{\Delta t m_0}=-b+\int_0^{1/\Delta t}\frac{k^2\mathrm{d}k}{2\omega^3}. \tag{55}$$

Hence we have finally

$$\langle\Phi|\Phi\rangle\approx-\left(-b+\int^{1/\Delta t}\frac{k^2\mathrm{d}k}{2\omega^3}\right)|\bar{c}|^2+\int^{1/\Delta t}\mathrm{d}^3k|\varphi(\mathbf{k})|^2 \tag{56}$$

As a Hamiltonian we try

$$\begin{aligned} H' = g^2\left(-a+\int^{\hat{\omega}}\frac{k^2\mathrm{d}k}{2\omega^2}\right)\psi^*_{\mathrm{Vr}}\psi_{\mathrm{Vr}}+\int^{\infty}\omega(\mathbf{k})a^*(\mathbf{k})a(\mathbf{k})\mathrm{d}^3k \\ -\frac{g}{\sqrt{4\pi}}\int^{\hat{\omega}}\frac{\mathrm{d}^3k}{\sqrt{2\omega}}\left[\psi^*_{\mathrm{Vr}}\psi_{\mathrm{N}}a(\mathbf{k})+\text{c.c.}\right], \end{aligned} \tag{57}$$

where it is assumed $\hat{\omega} \geqq 1/\Delta t$. Now, we can calculate the matrix element $\langle\Phi|H'|\Phi\rangle$ in two ways: the one using the old representation $|\Phi\rangle = O^*|0\rangle$, and the other using the new one $|\Phi\rangle = O'^*|0\rangle$. Both of them should lead to the same result.

(i) Using the old representation

We have

$$\begin{aligned} \langle\Phi|H'|\Phi\rangle = g^2\left(-a+\int^{\hat{\omega}}\frac{k^2\mathrm{d}k}{2\omega^2}\right)\sum_{|z\rangle}\langle\Phi|\psi^*_{\mathrm{Vr}}|z\rangle\langle z|\psi_{\mathrm{Vr}}|\Phi\rangle \\ +\int^{\infty}\mathrm{d}^3k\,\omega(\mathbf{k})\langle\Phi|a^*(\mathbf{k})a(\mathbf{k})|\Phi\rangle \\ -\frac{g}{\sqrt{4\pi}}\sum_{|z\rangle}\int^{\hat{\omega}}\frac{\mathrm{d}^3k}{\sqrt{2\omega}}\left[\langle\Phi|\psi^*_{\mathrm{Vr}}|z\rangle\langle z|\psi_{\mathrm{N}}a(\mathbf{k})|\Phi\rangle+\text{c.c.}\right]. \end{aligned}$$

It can be easily seen that in the first and the last term the only nonvanishing contribution comes from $|z> = |0\rangle$. Then, using (36a) and (36b), we get

$$\begin{aligned} \langle\Phi|H'|\Phi\rangle = \left(-a+\int^{\hat{\omega}}\frac{k^2\mathrm{d}k}{2\omega^2}\right)|\bar{c}|^2+\int^{\infty}\mathrm{d}^3k\,\omega(\mathbf{k})|\varphi(\mathbf{k})|^2 \\ -\frac{g}{\sqrt{4\pi}}\int^{\hat{\omega}}\frac{\mathrm{d}^3k}{\sqrt{2\omega}}\left[\bar{c}^*\varphi(\mathbf{k})+\text{c.c.}\right]. \end{aligned} \tag{58}$$

The evaluation of the second term is straightforward, using (11).

(ii) Using the new representation

In the new representation, the same quantity can be calculated as follows:

$$\langle\Phi|H'|\Phi\rangle = \tag{59a}$$

$$\left(a-\int^{\hat{\omega}}\frac{k^2\mathrm{d}k}{2\omega^2}\right)\bar{c}^*\bar{c}\langle 0|\int_{-\Delta t}^{\Delta t}F^*(t)\psi_{\mathrm{Vr}}(t)\mathrm{d}t\,\psi^*_{\mathrm{Vr}}(0)|0\rangle\langle 0|\psi_{\mathrm{Vr}}(0)\int_{-\Delta t}^{\Delta t}F(t)\psi^*_{\mathrm{Vr}}(t)\mathrm{d}t|0\rangle$$

$$\left.\begin{aligned} &+\int^{\infty}\mathrm{d}^3k\,\omega(\mathbf{k})\sigma^*(\mathbf{k})\sigma(\mathbf{k}) \\ &+\left[\int^{\infty}\mathrm{d}^3k\,\omega(\mathbf{k})\langle 0|\int F^*(t)\psi_{\mathrm{Vr}}(t)\mathrm{d}t\,\psi_{\mathrm{N}}{}^*a^*(\mathbf{k})|0\rangle\bar{c}^*\sigma(\mathbf{k})+\text{c.c.}\right] \\ &+\int^{\infty}\mathrm{d}^3k\,\omega(\mathbf{k})\langle 0|\int F^*(t)\psi_{\mathrm{Vr}}(t)\mathrm{d}t\,\psi_{\mathrm{N}}{}^*a^*(\mathbf{k})|0\rangle\bar{c}^*\bar{c}\langle 0|\psi_{\mathrm{N}}a(\mathbf{k})\int F(t)\psi^*_{\mathrm{Vr}}(t)\mathrm{d}t|0\rangle \end{aligned}\right\} \tag{59b}$$

$$\left.\begin{aligned}&-\frac{g}{\sqrt{4\pi}}\int^{\hat{\omega}}\frac{\mathrm{d}^3k}{\sqrt{2\omega}}\left[\langle 0|\int F^*(t)\psi_{\mathrm{Vr}}(t)\mathrm{d}t\psi^*_{\mathrm{Vr}}(0)|0\rangle\bar{c}^*\sigma(\mathbf{k})+\mathrm{c.c.}\right]\\&-\frac{g}{\sqrt{4\pi}}\int^{\hat{\omega}}\frac{\mathrm{d}^3k}{\sqrt{2\omega}}\left[\langle 0|\int F^*(t)\psi_{\mathrm{Vr}}(t)\mathrm{d}t\psi^*_{\mathrm{Vr}}(0)|0\rangle\bar{c}^*\bar{c}\langle 0|\psi_{\mathrm{N}}a(\mathbf{k})\int F(t)\psi^*_{\mathrm{Vr}}(t)\mathrm{d}t|0\rangle+\mathrm{c.c.}\right].\end{aligned}\right\}\quad(59\mathrm{c})$$

The reduction of the sum $\sum_{|a\rangle}$ to the vacuum contribution alone is now justified by means of (47a, b) and (51c). In view of (48), the three terms in (59b) can be brought into the form

$$\int^{\infty}\mathrm{d}^3k\omega(\mathbf{k})|\varphi(\mathbf{k})|^2 \qquad (59\mathrm{b}')$$

and the two terms in (59c) can be written as

$$-\frac{g}{\sqrt{4\pi}}\int^{\hat{\omega}}\frac{\mathrm{d}^3k}{\sqrt{2\omega}}\left[\langle 0|\int_{-\Delta t}^{\Delta t}F^*(t)\psi_{\mathrm{Vr}}(t)\mathrm{d}t\psi^*_{\mathrm{Vr}}(0)|0\rangle\bar{c}^*\varphi(\mathbf{k})+\mathrm{c.c.}\right]. \qquad (59\mathrm{c}')$$

Thus, substituting (40) into (59a) and (59c′), we find again the same result (58). Although in the above no approximation has been needed, it is to be noted that the quantity like $\langle 0|\int F^*(t)\psi_{\mathrm{Vr}}(t)\mathrm{d}t\psi_{\mathrm{N}}{}^*a^*(\mathbf{k})|0\rangle$ is, in fact, negligibly small for values of $|\mathbf{k}|\ll 1/\Delta t$.

From (56) and (58), the variational function is

$$\begin{aligned}\Omega' = &\left(-a+\int^{\hat{\omega}}\frac{k^2\mathrm{d}k}{2\omega^2}\right)|\bar{c}|^2+\int^{\infty}\mathrm{d}^3k\omega(\mathbf{k})|\varphi(\mathbf{k})|^2+\frac{1}{\sqrt{4\pi}}\int^{\hat{\omega}}\frac{\mathrm{d}^3k}{\sqrt{2\omega}}[\bar{c}^*\varphi(\mathbf{k})+\mathrm{c.c.}]\\&+\lambda\left(-b+\int^{1/\Delta t}\frac{k^2\mathrm{d}k}{2\omega^3}\right)|\bar{c}|^2-\lambda\int^{1/\Delta t}\mathrm{d}^3k|\varphi(\mathbf{k})|^2+\lambda\varepsilon.\end{aligned}\qquad(60)$$

It can now be verified that the new variational function Ω' leads to the same expression $\Omega[\bar{c},\lambda]$ as before,

$$\begin{aligned}\Omega' = &-h(\lambda)|\bar{c}|^2+\lambda\varepsilon\\&+\left[\int^{1/\Delta t}\frac{k^2\mathrm{d}k}{2\omega(\omega-\lambda)}+\frac{1}{\sqrt{4\pi}}\int^{1/\Delta t}\frac{\mathrm{d}^3k}{\sqrt{2\omega}}(\bar{c}^*\varphi(\mathbf{k})+\mathrm{c.c.})+\int^{1/\Delta t}\mathrm{d}^3k(\omega(\mathbf{k})-\lambda)|\varphi(\mathbf{k})|^2\right]\\&+\left[\lambda^2\int_{1/\Delta t}^{\hat{\omega}}\frac{k^2\mathrm{d}k}{2\omega^3}\frac{1}{\omega-\lambda}|\bar{c}|^2+\int_{1/\Delta t}^{\hat{\omega}}\frac{k^2\mathrm{d}k}{2\omega^2}|\bar{c}|^2\right.\\&\left.+\frac{1}{\sqrt{4\pi}}\int_{1/\Delta t}^{\hat{\omega}}\frac{\mathrm{d}^3k}{\sqrt{2\omega}}[\bar{c}^*\varphi(\mathbf{k})+\mathrm{c.c.}]+\int_{1/\Delta t}^{\hat{\omega}}\mathrm{d}^3k\omega(\mathbf{k})|\varphi(\mathbf{k})|^2\right]\\&+\int_{\hat{\omega}}^{\infty}\mathrm{d}^3k\omega(\mathbf{k})|\varphi(\mathbf{k})|^2.\end{aligned}\qquad(61)$$

Variation with respect to $\varphi^*(\mathbf{k})$ gives

$$\frac{1}{\sqrt{4\pi}\sqrt{2\omega}}\bar{c}+(\omega(\mathbf{k})-\lambda)\varphi(\mathbf{k}) = 0 \quad \text{for} \quad \omega < 1/\Delta t, \tag{62a}$$

$$\frac{1}{\sqrt{4\pi}\sqrt{2\omega}}\bar{c}+\omega(\mathbf{k})\varphi(\mathbf{k}) = 0 \quad \text{for} \quad 1/\Delta t < \omega < \hat{\omega}, \tag{62b}$$

$$\omega(\mathbf{k})\varphi(\mathbf{k}) = 0 \quad \text{for} \quad \omega > \hat{\omega}. \tag{62c}$$

Substituting these results back into (61), we get the final expression

$$\Omega'[\bar{c}, \lambda] = -h(\lambda)|\bar{c}|^2+\lambda\varepsilon+\lambda^2\int_{1/\Delta t}^{\hat{\omega}} \frac{k^2\mathrm{d}k}{2\omega^3}\,\frac{|\bar{c}|^2}{\omega-\lambda} \tag{63}$$

where the last term can be estimated as

$$\lambda\int_{1/\Delta t}^{\hat{\omega}} \frac{k^2\mathrm{d}k}{2\omega^3}\,\frac{|\bar{c}|^2}{\omega-\lambda} \approx O\left(\lambda\left(\Delta t-\frac{1}{\hat{\omega}}\right)\right),$$

which can be neglected for values of $\lambda \ll 1/\Delta t$. Thus, the new variational function $\Omega'[\bar{c}, \lambda]$ is practically identical with the previous one $\Omega[\bar{c}, \lambda]$, and hence we have exactly the same eigenvalues as before.

To summarize the above, we have the Hamiltonian given by

$$\begin{aligned} H' = g^2\left(-a+\int^{\hat{\omega}} \frac{k^2\mathrm{d}k}{2\omega^2}\right)\psi^*_{\mathrm{V_r}}\psi_{\mathrm{V_r}}+\int^{\infty} \mathrm{d}^3k\,\omega(\mathbf{k})a^*(\mathbf{k})a(\mathbf{k}) \\ -\frac{g}{\sqrt{4\pi}}\int^{\hat{\omega}} \frac{\mathrm{d}^3k}{\sqrt{2\omega}}\,[\psi^*_{\mathrm{V_r}}\psi_{\mathrm{N}}a(\mathbf{k})+\text{c.c.}] \end{aligned} \tag{64}$$

and the commutation relations

$$\langle 0|\left\{\psi_{\mathrm{V_r}}(0), \int_{-\Delta t}^{\Delta t} \psi^*_{\mathrm{V_r}}(t)\mathrm{d}t\right\}|0\rangle = -\frac{1}{g^2}\,\frac{2\Delta t}{-b+\displaystyle\int^{1/\Delta t} \frac{k^2\mathrm{d}k}{2\omega^3}}, \tag{65}$$

$$\langle 0|\left\{\psi_{\mathrm{N}}a(\mathbf{k}), \int_{-\Delta t}^{\Delta t} \psi^*_{\mathrm{V_r}}(t)\mathrm{d}t\right\}|0\rangle\bar{c}$$

$$\approx \begin{cases} 0 & \text{for} \quad \omega \ll 1/\Delta t, \qquad (66\text{a}) \\ \dfrac{1}{g}\,\dfrac{2\Delta t\varphi(\mathbf{k})}{-b+\displaystyle\int^{1/\Delta t} \frac{k^2\mathrm{d}k}{2\omega^3}} & \text{for} \quad \omega \gg 1/\Delta t. \qquad (66\text{b}) \end{cases}$$

Note that, if three constants *a*, *b* and *g* are given, the Hamiltonian as well as the commutation relations are completely fixed.

The upper limit $\hat{\omega}$ of the integrals in H' may be arbitrarily large; in particular, it may be put equal to infinity. In this case we have a causal theory with point source interaction. The Hamiltonians with and without cut off are quite equivalent to each other as far as processes with energy $E \ll 1/\Delta t$ are concerned. In fact, one can prove explicitly the requirement (3), i.e.,

$$\langle \Phi_a | H^{\hat{\omega}} | \Phi_b \rangle \approx \langle \Phi_a | H^{\infty} | \Phi_b \rangle \quad \text{for} \quad E_a, E_b \ll 1/\Delta t. \tag{67}$$

It is now clear that

(III′) *the new variational problem*

$$\delta\Omega' = 0,$$

where

$$\Omega' = \langle \Phi | H' | \Phi \rangle - \lambda(\langle \Phi | \Phi \rangle - \varepsilon),$$

is equivalent to the previous one, as long as $E \ll 1/\Delta t$ *is assumed.*

Correspondingly, one can replace the original eigenvalue problem by

(I′) *the new equivalent one*:

$$H'|\Phi\rangle = E|\Phi\rangle \quad \textit{with} \quad \langle \Phi | \Phi \rangle = \varepsilon,$$

but now under the revised representation of the vector and the new commutation relations.

It is true that our Hamiltonian H' is exactly the same as H in the current cut off theory, as long as $\hat{\omega}$ remains finite. But it should be mentioned that the essential difference between both theories lies in the method of quantisation. In the usual cut off theory, the commutation relation is (i) cut off dependent, and (ii) does not vanish as long as the cut off remains finite. The vanishing anticommutator can be reached only in the asymptotic sense when $\hat{\omega} \to \infty$. In our theory, on the other hand, the anticommutator vanishes *exactly* for equal times, quite independent of the cut off (we call such a quantisation "non-canonical"). Notice that the commutation relation does *not* contain Δt in its original form; such a small time interval appears only through the integration which is necessary for constructing the equivalent Hamiltonian formalism similar to the conventional one.

6. Relation to the Earlier Equation

The purpose of this section is to derive the equation (222-3) in ref. [8]), which contains Δt, but was established in the framework of the conventional canonical theory.

The Lee model with infinite cut off which we have been studying is, however, no longer canonical, and may be characterized by the commutation relations of the form

$$\langle 0|\{\psi_{\mathrm{Vr}}(0),\hat{\psi}^{*}_{\mathrm{Vr}}\}|0\rangle = -\frac{1}{g^{2}}\frac{1}{-b+\displaystyle\int^{1/\Delta t}\frac{k^{2}\mathrm{d}k}{2\omega^{3}}}, \tag{68}$$

$$\langle 0|\{\psi_{\mathrm{N}}(0)a(\mathbf{k},0),\ \hat{\psi}^{*}_{\mathrm{Vr}}\}|0\rangle\tilde{c}$$

$$\approx\begin{cases} 0 & \text{for}\quad \omega \ll 1/\Delta t, \quad (69a)\\ \dfrac{1}{g}\dfrac{\varphi(\mathbf{k})}{-b+\displaystyle\int^{1/\Delta t}\frac{k^{2}\mathrm{d}k}{2\omega^{3}}} & \text{for}\quad \omega \gg 1/\Delta t, \quad (69b)\end{cases}$$

where

$$\hat{\psi}^{*}_{\mathrm{Vr}} = \frac{\displaystyle\int_{-\Delta t}^{\Delta t} F(t)\psi^{*}_{\mathrm{Vr}}(t)\mathrm{d}t}{\displaystyle\int_{-\Delta t}^{\Delta t} F(t)\mathrm{d}t}. \tag{70}$$

The physical meaning of the expression (70) is clear: $\hat{\psi}_{\mathrm{Vr}}$ means the operator "averaged out" over a small time region Δt. In contrast with the commutation relations, the Hamiltonian H' contains only the usual operators, not the averaged ones. From this follows the important fact that one cannot construct the canonical field equation in the conventional form

$$i\frac{\partial}{\partial t}\psi_{\mathrm{Vr}}(t) = [\psi_{\mathrm{Vr}}(t), H']. \tag{71}$$

As is easily seen, the right hand side of (71) vanishes identically because of the commutativity of the operators for equal times, which is manifestly expressed in (34).

Now, we try to write down the canonical equation not for ψ_{Vr} itself, but for the "averaged" operator $\hat{\psi}_{\mathrm{Vr}}$, i.e.,

$$i\frac{\partial}{\partial t}\hat{\psi}_{\mathrm{Vr}}(t) = [\hat{\psi}_{\mathrm{Vr}}(t), H'], \tag{72}$$

or, interpreted in terms of matrix elements,

$$i\frac{\partial}{\partial t}\langle 0|\hat{\psi}_{\mathrm{Vr}}(t)|\Phi\rangle = \langle 0|[\hat{\psi}_{\mathrm{Vr}}(t), H']|\Phi\rangle. \tag{72a}$$

The left hand side of (72a) reduces, under the assumption $E_{\phi}\Delta t \ll 1$, to

$$\begin{aligned} i\frac{\partial}{\partial t}\langle 0|\hat{\psi}_{\mathrm{Vr}}(t)|\Phi\rangle &= i\frac{\partial}{\partial t}\frac{\displaystyle\int_{t-\Delta t}^{t+\Delta t}\mathrm{d}t'\,F(t')\,\mathrm{e}^{iE_{\phi}(t'-t)}\,\langle 0|\psi_{\mathrm{Vr}}(t)\,|\Phi\rangle}{\displaystyle\int_{t-\Delta t}^{t+\Delta t}\mathrm{d}t'\,F(t')}\\ &\approx i\frac{\partial}{\partial t}\langle 0|\psi_{\mathrm{Vr}}(t)|\Phi\rangle. \end{aligned}$$

The right hand side of (72a) can be calculated as follows:

$$
\begin{aligned}
&\langle 0|[\hat{\varphi}_{\mathrm{Vr}}(t), H']|\Phi\rangle \\
&\quad = \sum_{|z\rangle}\Big[g^2\Big(-a+\int^{\hat{\omega}}\frac{k^2\mathrm{d}k}{2\omega^2}\Big)\langle 0|\{\hat{\varphi}_{\mathrm{Vr}}, \psi^*_{\mathrm{Vr}}(0)\}|z\rangle\langle z|\psi_{\mathrm{Vr}}(t)|\Phi\rangle \\
&\quad - \frac{g}{\sqrt{4\pi}}\int^{\hat{\omega}}\frac{\mathrm{d}^3k}{\sqrt{2\omega}}\langle 0|\{\hat{\varphi}_{\mathrm{Vr}}, \psi^*_{\mathrm{Vr}}(0)\}|z\rangle\langle z|\psi_{\mathrm{N}}(t)a(\mathbf{k}, t)|\Phi\rangle \\
&\quad - \frac{g}{\sqrt{4\pi}}\int^{\hat{\omega}}\frac{\mathrm{d}^3k}{\sqrt{2\omega}}\langle 0|\{\hat{\varphi}_{\mathrm{Vr}}, \psi_{\mathrm{N}}{}^*(0)a^*(\mathbf{k}, 0)\}|z\rangle\langle z|\psi_{\mathrm{Vr}}(t)|\Phi\rangle \\
&\quad + \int^{\infty}\mathrm{d}^3k\,\omega(\mathbf{k})\langle 0|\{\hat{\varphi}_{\mathrm{Vr}}, \psi_{\mathrm{N}}{}^*(0)a^*(\mathbf{k}, 0)\}|z\rangle\langle z|\psi_{\mathrm{N}}(t)a(\mathbf{k}, t)|\Phi\rangle\Big].
\end{aligned}
\tag{73}
$$

In evaluating the last term we have utilized the fact that the expression in the original Hamiltonian

$$\int \mathrm{d}^3k\,\omega(\mathbf{k})a^*(\mathbf{k})a(\mathbf{k})$$

can, according to the super selection rules, be substituted by

$$\int \mathrm{d}^3k\,\omega(\mathbf{k})\psi_{\mathrm{N}}{}^*a^*(\mathbf{k})\psi_{\mathrm{N}}a(\mathbf{k})$$

as far as the lowest sector (V, Nθ) is concerned. In view of (47a, b) and (51c), the only non-vanishing contribution in (73) comes from $|z\rangle = |0\rangle$. Then, using the commutation relations (68) and (69a, b), we have

$$
\begin{aligned}
&\langle 0|[\hat{\varphi}_{\mathrm{Vr}}(t), H']|\Phi\rangle \\
&\quad = \Big(a-\int_0^{\hat{\omega}}\frac{k^3\mathrm{d}k}{2\omega^2}\Big)\frac{1}{-b+\int^{1/\Delta t}\frac{k^2\mathrm{d}k}{2\omega^3}}\langle 0|\psi_{\mathrm{Vr}}(t)|\Phi\rangle \\
&\quad + \frac{1}{g}\frac{1}{\sqrt{4\pi}}\int_0^{\hat{\omega}}\frac{\mathrm{d}^3k}{\sqrt{2\omega}}\frac{1}{-b+\int^{1/\Delta t}\frac{k^2\mathrm{d}k}{2\omega^3}}\langle 0|\psi_{\mathrm{N}}(t)a(\mathbf{k}, t)|\Phi\rangle \\
&\quad - \frac{1}{\sqrt{4\pi}}\int_{1/\Delta t}^{\hat{\omega}}\frac{\mathrm{d}^3k}{\sqrt{2\omega}}\frac{1}{-b+\int^{1/\Delta t}\frac{k^3\mathrm{d}k}{2\omega^3}}\frac{\varphi^*(\mathbf{k})}{\bar{c}^*}\langle 0|\psi_{\mathrm{Vr}}(t)|\Phi\rangle \\
&\quad + \frac{1}{g}\int_{1/\Delta t}^{\infty}\mathrm{d}^3k\,\omega(\mathbf{k})\frac{1}{-b+\int^{1/\Delta t}\frac{k^2\mathrm{d}k}{2\omega^3}}\frac{\varphi^*(\mathbf{k})}{\bar{c}^*}\langle 0|\psi_{\mathrm{N}}(t)a(\mathbf{k}, t)|\Phi\rangle
\end{aligned}
$$

$$
\begin{aligned}
&= \left(a - \int_0^{1/\Delta t} \frac{k^2\,\mathrm{d}k}{2\omega^2}\right) \frac{1}{-b + \displaystyle\int^{1/\Delta t} \frac{k^2\,\mathrm{d}k}{2\omega^3}} \langle 0|\psi_{V_r}(t)|\Phi\rangle \\
&+ \frac{1}{g}\frac{1}{\sqrt{4\pi}} \int_0^{1/\Delta t} \frac{\mathrm{d}^3k}{\sqrt{2\omega}} \frac{1}{-b + \displaystyle\int^{1/\Delta t} \frac{k^2\,\mathrm{d}k}{2\omega^3}} \langle 0|\psi_N(t)a(\mathbf{k},t)|\Phi\rangle \\
&- \int_{1/\Delta t}^{\hat{\omega}} \frac{k^2\,\mathrm{d}k}{2\omega^2} \frac{1}{-b + \displaystyle\int^{1/\Delta t} \frac{k^2\,\mathrm{d}k}{2\omega^3}} \langle 0|\psi_{V_r}(t)|\Phi\rangle \\
&+ \frac{1}{g}\frac{1}{\sqrt{4\pi}} \int_{1/\Delta t}^{\hat{\omega}} \frac{\mathrm{d}^3k}{\sqrt{2\omega}} \frac{1}{-b + \displaystyle\int^{1/\Delta t} \frac{k^2\,\mathrm{d}k}{2\omega^3}} \langle 0|\psi_N(t)a(\mathbf{k},t)|\Phi\rangle \\
&- \frac{1}{\sqrt{4\pi}} \int_{1/\Delta t}^{\hat{\omega}} \frac{\mathrm{d}^3k}{\sqrt{2\omega}} \frac{1}{-b + \displaystyle\int^{1/\Delta t} \frac{k^2\,\mathrm{d}k}{2\omega^3}} \frac{\varphi^*(\mathbf{k})}{\bar{c}^*} \langle 0|\psi_{V_r}(t)|\Phi\rangle \\
&+ \frac{1}{g} \int_{1/\Delta t}^{\hat{\omega}} \mathrm{d}^3k\,\omega(\mathbf{k}) \frac{1}{-b + \displaystyle\int^{1/\Delta t} \frac{k^2\,\mathrm{d}k}{2\omega^3}} \frac{\varphi^*(\mathbf{k})}{\bar{c}^*} \langle 0|\psi_N(t)a(\mathbf{k},t)|\Phi\rangle \\
&+ \frac{1}{g} \int_{\hat{\omega}}^{\infty} \mathrm{d}^3k\,\omega(\mathbf{k}) \frac{1}{-b + \displaystyle\int^{1/\Delta t} \frac{k^2\,\mathrm{d}k}{2\omega^3}} \frac{\varphi^*(\mathbf{k})}{\bar{c}^*} \langle 0|\psi_N(t)a(\mathbf{k},t)|\Phi\rangle .
\end{aligned}
$$

Now one can easily see that the last term vanishes due to (62c), and that the four terms before the last compensate each other by virtue of (62b). Thus, the equation (72a) becomes

$$
\begin{aligned}
&\left(a - \int^{1/\Delta t} \frac{k^2\,\mathrm{d}k}{2\omega^2}\right) \langle 0|\psi_{V_r}(t)|\Phi\rangle + i\left(b - \int^{1/\Delta t} \frac{k^2\,\mathrm{d}k}{2\omega^3}\right) \frac{\partial}{\partial t} \langle 0|\psi_{V_r}(t)|\Phi\rangle \\
&\quad = -\frac{1}{g}\frac{1}{\sqrt{4\pi}} \int^{1/\Delta t} \frac{\mathrm{d}^3k}{\sqrt{2\omega}} \langle 0|\psi_N(t)a(\mathbf{k},t)|\Phi\rangle, \quad \text{for} \quad E_\phi \ll 1/\Delta t.
\end{aligned}
\tag{74}
$$

Now, we wish to prove the identity of this equation with the earlier eq. (222-3) in ref. 8), which is given by

$$
\begin{aligned}
&\left(a-\int^{\infty}\frac{k^2\mathrm{d}k}{2\omega^2}\,\mathrm{e}^{-i\omega\Delta t}\right)\psi_{\mathrm{Vr}}(t)+i\left(b-\int^{\infty}\frac{k^2\mathrm{d}k}{2\omega^3}\,\mathrm{e}^{-i\omega\Delta t}\right)\frac{\partial}{\partial t}\psi_{\mathrm{Vr}}(t)\\
&\qquad=-\frac{\pi\sqrt{2}}{g}\,a(t)\psi_{\mathrm{N}}(t-\Delta t)\\
&\qquad-2i\pi^2\int_{t-\Delta t}^{t}\mathrm{d}t'[a(t)a^*(t')-s(t-t')]\psi_{\mathrm{Vr}}(t') \qquad\qquad (75)\\
&\qquad-i\int_{t-\Delta t}^{t}\mathrm{d}t'\left[\psi_{\mathrm{Vr}}(t')-\psi_{\mathrm{Vr}}(t)-(t'-t)\,\frac{\partial\psi_{\mathrm{Vr}}(t)}{\partial t}\right]\int^{\infty}\frac{k^2\mathrm{d}k}{2\omega}\,\mathrm{e}^{i\omega(t'-t)}\\
&\qquad-\Delta t\,\frac{\partial\psi_{\mathrm{Vr}}(t)}{\partial t}\int^{\infty}\frac{k^2\mathrm{d}k}{2\omega^2}\,\mathrm{e}^{-i\omega\Delta t},
\end{aligned}
$$

where the integral of the type $\int^{\infty}\mathrm{d}k\mathrm{e}^{-i\omega\Delta t}\ldots$ is to be understood as Abel's limit. Interpreted in terms of matrix elements, eq. (75) reads

$$
\begin{aligned}
&\left(a-\int^{\infty}\frac{k^2\mathrm{d}k}{2\omega^2}\,\mathrm{e}^{-i\omega\Delta t}\right)\langle 0|\psi_{\mathrm{Vr}}(t)|\Phi\rangle+i\left(b-\int^{\infty}\frac{k^2\mathrm{d}k}{2\omega^3}\,\mathrm{e}^{-i\omega\Delta t}\right)\frac{\partial}{\partial t}\langle 0|\psi_{\mathrm{Vr}}(t)|\Phi\rangle\\
&\qquad=-\frac{\pi\sqrt{2}}{g}\,\langle 0|a(t)\psi_{\mathrm{N}}(t-\Delta t)|\Phi\rangle \qquad\qquad (76a)\\
&\qquad-2i\pi^2\int_{t-\Delta t}^{t}\mathrm{d}t'[\langle 0|a(t)a^*(t')\psi_{\mathrm{Vr}}(t')|\Phi\rangle-s(t-t')\langle 0|\psi_{\mathrm{Vr}}(t')|\Phi\rangle] \qquad (76b)\\
&\qquad-i\int_{t-\Delta t}^{t}\mathrm{d}t'[\langle 0|\psi_{\mathrm{Vr}}(t')|\Phi\rangle-\langle 0|\psi_{\mathrm{Vr}}(t)|\Phi\rangle\\
&\qquad\qquad\qquad-(t'-t)\,\frac{\partial}{\partial t}\langle 0|\psi_{\mathrm{Vr}}(t)|\Phi\rangle]\int^{\infty}\frac{k^2\mathrm{d}k}{2\omega}\,\mathrm{e}^{i\omega(t'-t)} \qquad (76c)\\
&\qquad-\Delta t\frac{\partial}{\partial t}\langle 0|\psi_{\mathrm{Vr}}(t)|\Phi\rangle\int^{\infty}\frac{k^2\mathrm{d}k}{2\omega^2}\,\mathrm{e}^{-i\omega\Delta t}. \qquad\qquad (76d)
\end{aligned}
$$

The first term (76a) is evaluated as

$$
-\frac{\pi\sqrt{2}}{g}\langle 0|a(t)\psi_{\mathrm{N}}(t-\Delta t)|\Phi\rangle=-\frac{\pi\sqrt{2}}{g}\sum_{|z\rangle}\langle 0|a(t)|z\rangle\langle z|\psi_{\mathrm{N}}(t-\Delta t)|\Phi\rangle,
$$

where, as can be seen, the only contribution comes from the one meson states: $|z\rangle=a^*(\mathbf{k})|0\rangle$. Then,

$$
=-\frac{1}{g}\,\frac{1}{\sqrt{4\pi}}\int\mathrm{d}^3k'\int\frac{\mathrm{d}^3k}{\sqrt{2\omega}}\langle 0|a(\mathbf{k},t)a^*(\mathbf{k}',t)|0\rangle\langle 0|a(\mathbf{k}',t)\psi_{\mathrm{N}}(t)|\Phi\rangle\mathrm{e}^{i(E_{\phi}-\omega')\Delta t}
$$

$$
=-\frac{1}{g}\,\frac{1}{\sqrt{4\pi}}\int\frac{\mathrm{d}^3k}{\sqrt{2\omega}}\langle 0|a(\mathbf{k},t)\psi_{\mathrm{N}}(t)|\Phi\rangle\mathrm{e}^{-i\omega\Delta t}\mathrm{e}^{iE_{\phi}\Delta t}.
$$

Neglecting the last exponential factor according to $E_\phi \Delta t \ll 1$, we have

$$-\frac{\pi\sqrt{2}}{g}\langle 0|a(t)\psi_N(t-\Delta t)|\Phi\rangle = -\frac{1}{g}\frac{1}{\sqrt{4\pi}}\int^\infty \frac{d^3k}{\sqrt{2\omega}}\langle 0|a(\mathbf{k},t)\psi_N(t)|\Phi\rangle e^{-i\omega\Delta t}. \qquad (76a')$$

Next, the second term (76b) is found to be zero, because the first term in the bracket

$$\begin{aligned}\langle 0|a(t)a^*(t')\psi_{V_r}(t')|\Phi\rangle &= \sum_{|z\rangle}\langle 0|a(t)a^*(t')|z\rangle\langle z|\psi_{V_r}(t')|\Phi\rangle \\ &= \langle 0|a(t)a^*(t')|0\rangle\langle 0|\psi_{V_r}(t')|\Phi\rangle \\ &= s(t-t')\langle 0|\psi_{V_r}(t')|\Phi\rangle\end{aligned}$$

compensates exactly the rest in the same bracket. Finally, (76c) can be evaluated as being equal to

$$\begin{aligned}&i\langle 0|\psi(0)|\Phi\rangle\int_{t-\Delta t}^{t}dt'[e^{-iE_\phi t'}-e^{-iE_\phi t}-(t'-t)e^{-iE_\phi t}]\int^\infty\frac{k^2dk}{2\omega}e^{i\omega(t'-t)} \\ &\quad=\langle 0|\psi(0)|\Phi\rangle e^{-iE_\phi t}\int\frac{k^2dk}{2\omega}\left[\frac{1-e^{-i(\omega-E_\phi)\Delta t}}{\omega-E_\phi}-\frac{1-e^{-i\omega\Delta t}}{\omega}\right. \\ &\quad\left.-\frac{E_\phi(1-e^{-i\omega\Delta t})}{\omega^2}\right]+\Delta t(-iE_\phi)\langle 0|\psi(0)|\Phi\rangle e^{-iE_\phi t}\int\frac{k^2dk}{2\omega^2}e^{-i\omega\Delta t},\end{aligned}$$

the last term of which compensates (76d). The rest can be brought into a compact form,

$$\langle 0|\psi(t)|\Phi\rangle E_\phi^2\int\frac{k^2dk}{2\omega^3}\frac{1-e^{i\omega\Delta t}}{\omega-E_\phi}, \qquad (77)$$

where, as before, the factor $e^{iE_\phi\Delta t}$ has been neglected. The integral in (77) can be estimated as

$$\begin{aligned}E_\phi\int_0^\infty\frac{k^2dk}{2\omega^3}\frac{1-e^{-i\omega\Delta t}}{\omega-E_\phi} &\approx E_\phi\int_{1/\Delta t}^\infty\frac{k^2dk}{2\omega^3}\frac{1}{\omega-E_\phi} \\ &\approx O(E_\phi\Delta t).\end{aligned}$$

In conclusion, the only contribution comes from (76a'). Thus, the eq. (76) becomes

$$\begin{aligned}&\left(a-\int^\infty\frac{k^2dk}{2\omega^2}e^{-i\omega\Delta t}\right)\langle 0|\psi_{V_r}(t)|\Phi\rangle \\ &\quad+i\left(b-\int^\infty\frac{k^2dk}{2\omega^3}e^{-i\omega\Delta t}\right)\frac{\partial}{\partial t}\langle 0|\psi_{V_r}(t)|\Phi\rangle \qquad (78) \\ &\quad=-\frac{1}{g}\frac{1}{\sqrt{4\pi}}\int^\infty\frac{d^3k}{\sqrt{2\omega}}\langle 0|a(\mathbf{k},t)\psi_N(t)|\Phi\rangle e^{-i\omega\Delta t}\quad\text{for}\quad E_\phi\ll\frac{1}{\Delta t}.\end{aligned}$$

Considering now that

$$\langle 0|a(\mathbf{k},t)\psi_{\mathrm{N}}(t)|\Phi\rangle \approx \varphi(\mathbf{k}) \approx \frac{1}{\omega - E_{\phi}}$$

is a slowly varying function of **k**, one can conclude that this equation is, essentially, identical with the eq. (74), which we had derived from the non-canonical commutation relations. In other words, it turns out that our scheme using the non-canonical quantisation is quite equivalent to the usual canonical theory, as far as matrix elements between the vacuum and the state $|\Phi\rangle$ with $E_{\phi} \ll 1/\Delta t$ are concerned.

It is to be remarked that such a situation is satisfactory from the point of view of the correspondence principle. The deviation of the theory from the conventionally accepted one is thus restricted only to the region of extremely high energy, which is here characterized by $E \gg 1/\Delta t$.

7. Concluding Remarks

It should first be remarked that the matrix element $\langle 0|\psi_{\mathrm{V_r}}(t)|\Phi\rangle$ for $E_{\phi} \gg 1/\Delta t$ has so far not yet been defined. It is quite likely that this quantity becomes singular near $t = 0$. In such a case, eq. (71), which is written as a differential equation for the operator $\psi_{\mathrm{V_r}}$ itself, will fail in the immediate neighbourhood of $t = 0$. If the differential equation is deprived of the analyticity at $t = 0$, then one can *not* conclude that the anticommutator should vanish identically everywhere in $t \geqq 0$ if it certainly vanishes for $t = 0$. It seems that such is the case, in general, for all theories with non-canonical quantisation, because the theory must be not classical, but the anticommutator vanishes for equal times.

In spite of this fact, the new scheme developed in the previous sections can be very reasonably interpreted from the correspondence theoretical point of view. Suppose the case where Δt can practically be considered as infinitely small. Then, the "averaged" operator may be replaced by the usual one, i.e.,

$$\hat{\psi}_{\mathrm{V_r}} = \frac{\int_{-\Delta t}^{\Delta t} F^*(t)\,\psi_{\mathrm{V_r}}(t)\mathrm{d}t}{\int_{-\Delta t}^{\Delta t} F^*(t)\mathrm{d}t} \approx \psi_{\mathrm{V_r}}(0). \tag{75}$$

Correspondingly, the non-canonical commutation relation (68) reduces to the canonical one

$$\langle 0|\{\psi_{\mathrm{V_r}}(0),\, \psi^*_{\mathrm{V_r}}(0)\}|0\rangle \approx -\frac{1}{g^2}\frac{1}{-b+\int\frac{k^2\mathrm{d}k}{2\omega^3}} \approx -\left|\frac{g_0}{g}\right|^2, \tag{76}$$

which is of the form well known in the conventional theory of the Lee model.

Under these circumstances, eq. (72) written in terms of matrix elements can also be identified with the usual operator equation (71).

From the above one can conclude the following: even when the anticommutator vanishes for equal times, it is still possible to construct a formalism which is understandable from the correspondence theoretical point of view, if and only if a small time interval Δt is introduced into the theory. A prescription has been given, at hand of the Lee model, as to how one can get a Hamiltonian formalism for a given theory with *non-canonical* quantisation. Although we have proved it only for a special model of a field theory, it may be expected that the conclusion obtained is of more general validity. One can use, at least practically, the *canonical* commutation relations in case where processes with comparatively large time scale, or with comparatively low energy are concerned.

It is likely that this is also the case in the non-linear spinor theory of Heisenberg [1-8]). Quite similar to the Lee model with infinite cut off, the theory is characterized by the fact that the anticommutator vanishes effectively and the differential equation becomes non-analytic on the light cone.

The author wishes to express his sincere thanks to Prof. W. Heisenberg for his kind guidance, suggestions and discussions, and particularly for inviting him to stay at the Max-Planck-Institute. Thanks are also due to Dr. K. Yamazaki for helpful discussions, and to Dr. S. Gasiorowicz, Dr. H. Mitter and Dr. R. M. Ahrens for their kind reading of the manuscript. He is indebted to Deutscher Akademischer Austauschdienst for financial aid.

Appendix

There is another possibility for constructing a theory with "equivalent" canonical commutation rules. One can introduce the Δt-integration not in the contravariant representation of the state vector, but in the definition of the covariant component of the same vector. In other words, we can define the "averaged" covariant component as

$$\langle 0|\hat{\psi}_{\mathrm{Vr}}|\Phi\rangle = -\frac{\bar{c}}{g}, \quad \langle 0|\psi_{\mathrm{N}} a(\mathbf{k})|\Phi\rangle = \varphi(\mathbf{k}),$$

with

$$\hat{\psi}_{\mathrm{Vr}} = \frac{\int_{-\Delta t}^{\Delta t} F^*(t)\psi_{\mathrm{Vr}}(t)\mathrm{d}t}{\int_{-\Delta t}^{\Delta t} F^*(t)\mathrm{d}t}$$

and

$$|\Phi\rangle = \left[g\bar{c}\left(-b+\int^{1/\Delta t}\frac{k^2\mathrm{d}k}{2\omega^3}\right)\psi_{\mathrm{Vr}}^* + \psi_{\mathrm{N}}{}^*\int \mathrm{d}^3k\sigma(\mathbf{k})a^*(\mathbf{k})\right]|0\rangle.$$

Then, we are led to take

$$\hat{H}' = g^2\left(-a+\int^{\hat{\omega}} \frac{k^2\mathrm{d}k}{2\omega^2}\right)\hat{\psi}^*_{\mathrm{Vr}}\hat{\psi}_{\mathrm{Vr}}+\int^{\infty} \mathrm{d}^3k\omega(\mathbf{k})a^*(\mathbf{k})a(\mathbf{k})$$
$$-\frac{g}{\sqrt{4\pi}}\int^{\hat{\omega}} \frac{\mathrm{d}^3k}{\sqrt{2\omega}}[\hat{\psi}^*_{\mathrm{Vr}}\psi_{\mathrm{N}}a(\mathbf{k})+\mathrm{c.c.}]$$

as the new Hamiltonian, instead of (57). As to the matrix element of the Hamiltonian one can easily verify that

$$\langle\Phi_{\mathrm{a}}|\hat{H}'|\Phi_{\mathrm{b}}\rangle \approx \langle\Phi_{\mathrm{a}}|H'|\Phi_{\mathrm{b}}\rangle \quad \text{for} \quad E_{\mathrm{a}}, E_{\mathrm{b}} \ll 1/\Delta t,$$

because of the revised definitions for the covariant and the contravariant representation of $|\Phi\rangle$.

The canonical field equation of ψ_{Vr} is now, in some sense, equivalent to the eq. (72) in the previous formalism, and the discussion in sect. 6. is still valid as long as the $\hat{\psi}_{\mathrm{Vr}}$ can practically be replaced by ψ_{Vr} under the condition $E \ll 1/\Delta t$. On the other hand, however, the usual form of the covariant representation, i.e.,

$$\langle 0|\psi_{\mathrm{Vr}}(0)|\Phi\rangle$$

vanishes identically due to (34).

The above mentioned version of the theory is thus, in its content, quite equivalent to the one discussed in the text. Both theories are, so to speak, complementary with one another.

References

1) W. Heisenberg, Nachr. Gött. Akad. Wiss. (1953) 111
2) W. Heisenberg, Zs. f. Naturf. **9a** (1954) 282
3) W. Heisenberg, F. Kortel and H. Mitter, Zs. f. Naturf. **10a** (1955) 425
4) W. Heisenberg, Zs. f. Physik **144** (1956) 1
5) W. Heisenberg, Nachr. Gött. Akad. Wiss. (1956) 27
6) R. Ascoli and W. Heisenberg, Zs. f. Naturf. **12a** (1957) 177
7) W. Heisenberg, Rev. Mod. Phys. **29** (1957) 269
8) H. P. Dürr, W. Heisenberg, H. Mitter, S. Schlieder and K. Yamazaki, Zs. f. Naturf. **14a** (1959) 441
9) T. D. Lee, Phys. Rev. **95** (1954) 1329
10) G. Källén and W. Pauli, Mat. Fys. Medd. Dan. Vid. Selsk. **30**, No. 7 (1955)
11) W. Heisenberg, Nuclear Physics **4** (1957) 532
12) W. Heisenberg, Nuclear Physics **5** (1957) 195

2.I

Nuclear Physics **23** (1961) 269—284; ©*North-Holland Publishing Co., Amsterdam*

Not to be reproduced by photoprint or microfilm without written permission from the publisher

THE PHOTODEUTERON YIELD FROM 30 MeV BREMSSTRAHLUNG IRRADIATION

BENGT FORKMAN

Department of Physics, University of Lund, Lund, Sweden

Received 28 November 1960

Abstract: An investigation of the (γ, d) reaction in sulphur, cobalt and copper has been carried out. Bremsstrahlung of 30 MeV maximum energy was used. The emitted charged photo-particles were deflected by a magnetic field and recorded in nuclear emulsions. The range and the orientation of the tracks in the emulsions were measured and the trajectories of the photo-particles were calculated backwards for protons, deuterons and alpha particles. The intersection point of each trajectory with the target plane gave information about the kind of photo-particle which had produced the track. The ratio R_{dp} between the (γ, d) yield and the (γ, p) yield was determined. No strong fluctuation in the ratio between the adjacent elements cobalt and copper was observed. The ratios found were all zero for the three elements sulphur, cobalt and copper, with a standard deviation of respectively 0.009, 0.012 and 0.018. A calculation based on the statistical model of the ratio R_{dp} was made. The ratios obtained are, within the limits of the errors, in agreement with the experimental results. The present results also were compared with the pick-up process theory, with earlier (γ, d) experiments and with the inverse reaction. The obtained ratio between the (γ, α) yield and the (γ, p) yield was in agreement with earlier (γ, α) experiments.

1. Introduction

During a long time the (γ, d) reaction has been a point of question in connection with photonuclear reactions [1]). Both the statistical model and the direct interaction model predict that photodeuterons should be quite rare compared to photoprotons.

However, a number of investigators that have used bremsstrahlung with a maximum energy of about 30 MeV have observed the existence of photodeuterons. The reported yields of photodeuterons vary considerably from element to element. Especially for copper a high yield was obtained, which amounted to about a hundred times the yield predicted from the statistical model [2,3,4]). Photodeuterons have also been observed using sulphur [5]) and zinc [6]).

It is, however, difficult to separate deuterons from protons, especially if they are of low energy. Different techniques have been used to attack the problem. In the case of copper the deuterons and the protons have been recorded in nuclear emulsions, and the separation has been done by grain-counting of the tracks. As the tracks are short a good separation is hard to obtain.

In the case of sulphur and zinc the photodeuteron yield has been determined by measuring the activity of the daughter nuclei in the 2 MeV region above the

(γ, d) threshold. Above this region the (γ, np) reaction will compete and it is therefore difficult to measure the (γ, d) yield only. As the accessible energy region is small this method too gives only crude information about the (γ, d) reaction.

Several investigators, that have used a maximum bremsstrahlung energy of about 80 MeV report, too, the existence of photodeuterons. In copper [7]) and sulphur [8]) the photodeuterons have been separated from the photoprotons by a cloud chamber traversed by a magnetic field. The method shows a good resolution of protons and deuterons. Again a surprisingly high yield of photodeuterons from copper is reported. The irradiated targets were thick and the cloud chamber favoured high-energy particles. Therefore it is difficult to compare the results with those from the 30 MeV irradiation.

The cloud-chamber experiments can, however, be compared with a recently made investigation which thoroughly studied a lot of elements, separating the photodeuterons from the photoprotons by a two-crystal telescope [9, 10]). This method shows, too, a good resolution of protons and deuterons but studies only photodeuterons down to 15 MeV. The yields of photodeuterons are considerably smaller than those obtained with the cloud chamber. No strong fluctuations in the yields are observed. The yield increases continuously with mass number. Even these results are difficult to compare with those from the 30 MeV irradiation as the photodeuterons are of high energy.

An attempt has been made to study the low-energy photodeuterons from gold [11]) by the method of grain-counting but again it is difficult to obtain a good resolution with this method.

The yield of photodeuterons has been investigated also with a maximum bremsstrahlung energy of 300 MeV [12,13,14]). The high-energy deuterons have been studied by a two-crystal telescope. In this energy range too, a continuous increase of the yield with the mass number has been observed. The ratio of the photodeuteron to the photoproton yield was here about 4 times larger than the corresponding ratio obtained with the telescope investigation at the lower irradiation energy.

In order to explain the high yield of photodeuterons it has been assumed that the deuterons are formed in a two-stage process. The incident photon is absorbed by a single nucleon which in its turn picks up another nucleon with the right charge and momentum and forms an outgoing deuteron. Such a pick-up process must occur on the surface of the nucleus. A semi-quantitative calculation of this pick-up process has been made by Sawicki and Czyż [15]).

The aim of this work has been to investigate the photodeuteron yield from some elements with a maximum bremsstrahlung energy of 30 MeV using a new technique worked out in Lund [16]) that is able to separate single deuterons from protons down to 2 MeV. Fluctuations in the yield were looked for. It was also tried to test the proposed theoretical model experimentally. The same technique has recently been used by the Iowa group with a maximum bremsstrahlung energy of 45 MeV [17]).

It is well known that the (γ, α) reaction in medium weight nuclei is satisfactorily explained by the statistical model [18]). This reaction is much easier to study than the (γ, d) reaction, since the alpha particles are easy to separate from singly charged particles and because the stability of the alpha particle ensures the reliability of the activity measurement of the daughter nucleus.

In the present work the (γ, α) reaction has been studied, since the power of the experimental arrangement to separate photo-alpha particles is a proof of its suitability for observing photodeuterons. The observed (γ, α) yields have been compared with earlier measurements.

2. Experimental Arrangement and Measurements

In order to obtain a good separation between protons and deuterons a magnetic field was used to deflect the particles. The photo-particles were recorded in nuclear emulsions. The method is fully described in ref. [16]). The experimental arrangement is shown in fig. 1. As the source of the photons a 30 MeV electron synchrotron was used. The machine was energy stabilized and was run with maximum energy. The γ-beam was collimated by a conic lead collimator and passed then through an evacuated camera. In the camera the photons hit a thin target. The diameter of the γ-beam at the position of the target was 1.5 cm. Three different targets were used. At the first exposure a copper foil rolled out to 10 μm was irradiated. The second exposure was made without target in order to determine the background. Next a sulphur target 34 μm thick, obtained by allowing sulphur to evaporate on a 3 μm thick gold foil, was irradiated. At the fourth exposure a cobalt foil, 10 μm thick, produced by electrolysis on a

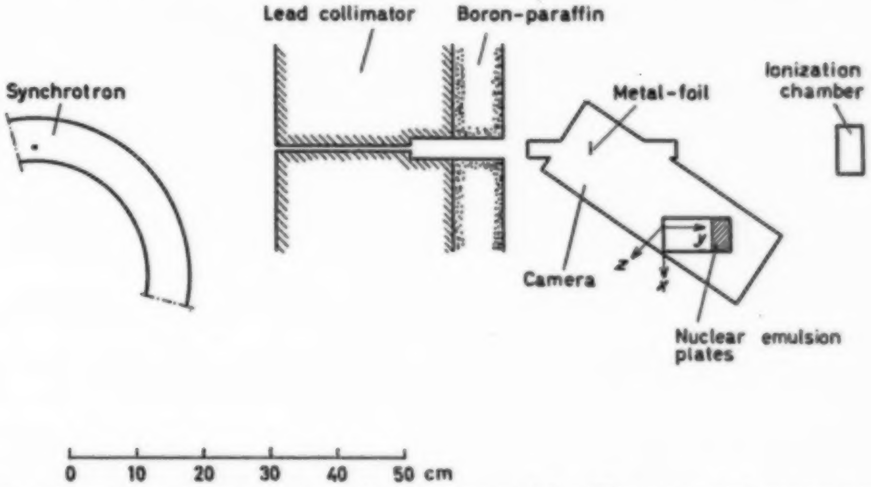

Fig. 1. Experimental arrangement to analyze photo-particles. The evacuated camera was placed in the gap of an electromagnet with the magnetic field parallel with the z-axis. The scanned area in the emulsions is shaded in the figure.

gold foil, also 3 μm thick, was used. The camera was placed in the gap of an electromagnet. The current to the electromagnet was stabilized and gave a constant magnetic field of 1.5 Wb/m^2.

Two Ilford C2 emulsion plates with the size 5.1 cm by 10.2 cm were used to record the photo-particles. The two plates were mounted oblique to each other with an opening angle of 23°. In order to shield the nuclear plates from background radiation the camera was covered with lead and the whole magnet was surrounded with boron-paraffin blocks. Furthermore a lead wall was piled up between the camera and the synchrotron. The camera was watercooled in order to keep the nuclear plates at a safe temperature. The total dose given to the targets at the different exposures amounted to about 3000 r.

In order to test that the experiment was not disturbed by fast neutrons, a phosphorus sample was placed in the beam at the target position. No neutron induced phosphorus activity was observed. As already has been mentioned a background exposure was performed without any target. Unexpectedly many background tracks were obtained in the plates. These originated from the entrance window of the camera which was a 50 μm thick Al-foil. The background from the gold foil in the suphur and cobalt exposures was negligible both through the thinness of the foil and through the high coulomb barrier for proton and deuteron emission.

The nuclear emulsions were developed in the usual way and were scanned and measured by a Leitz microscope. The entrance co-ordinates, the length and the orientation of the tracks were measured. As the position of the nuclear plates in relation to the target was known and also the strength of the magnetic field, it was possible to calculate backwards the trajectories of the photoparticles from the target to the emulsion. Such a calculation was made first assuming that all the recorded particles were protons and then assuming that the particles were deuterons. Finally a calculation was made assuming them to be alpha particles. These calculations were performed using SMIL (the University of Lund digital computer). The co-ordinates of the intersection points between the trajectories of the particles and the plane of the target were calculated.

In the calculations a right-handed system of co-ordinate axes was placed so that the y-axis was parallel with the γ-beam and the z-axis parallel with the direction of the magnetic field. The co-ordinate system is drawn in fig. 1. The length of the target in the x-direction was 2.0 cm and in the z-direction 2.8 cm. In the chosen co-ordinate system the centre of the target had the co-ordinates $x = -10.1$ cm, $y = -10.9$ cm and $z = 0.0$ cm. The errors in the measurements of the dip of the tracks give an uncertainty in the z co-ordinates (z_t) of the intersection points. The distribution of the z_t values of the points in the interval $-8.4 > x_t > -11.6$ is shown in fig. 2. Owing to the broadness of this distribution all measured tracks giving a $|z_t| < 3.0$ have been accepted in the following analysis.

The nuclear plates were scanned in the area shaded in fig. 1. To this area only those photo-particles came that had a small angle Y with the photon direction. Fig. 3 shows the distribution of the angle Y of the particles recorded in the plates. In the nuclear emulsions all tracks having a length more than 30 μm were measured. This corresponds to a proton energy of 1.6 MeV, a deuteron energy of 2.1 MeV and an alpha particle energy of 6.5 MeV. However, in the area measured only protons with an energy above 2.5 MeV will be recorded. Protons with lower energies will cut the camera wall before they reach the plates. The efficiency goes up very steeply and above 3 MeV all protons will be recorded with the same efficiency. The corresponding value for the deuterons is 2 MeV and for alpha particles 3 MeV [16]).

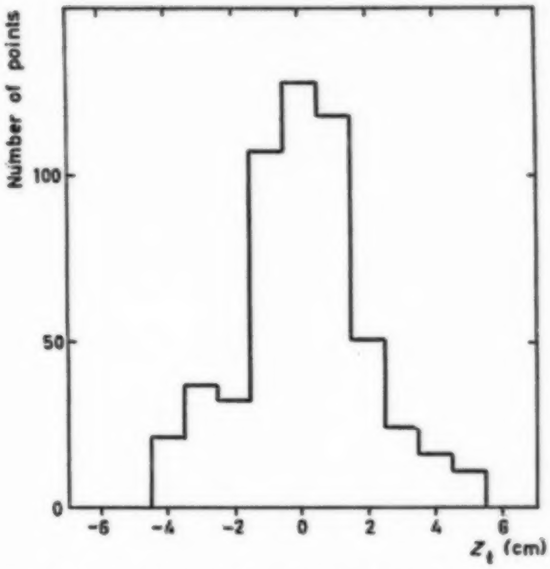

Fig. 2. Experimental distribution from the cobalt exposure of the z co-ordinates z_t of the intersection points of the proton trajectories with the plane of the foil falling in the interval $-8.4 > x_t > -11.6$. The background is subtracted. The centre of the target has the z co-ordinate $z_t = 0.0$.

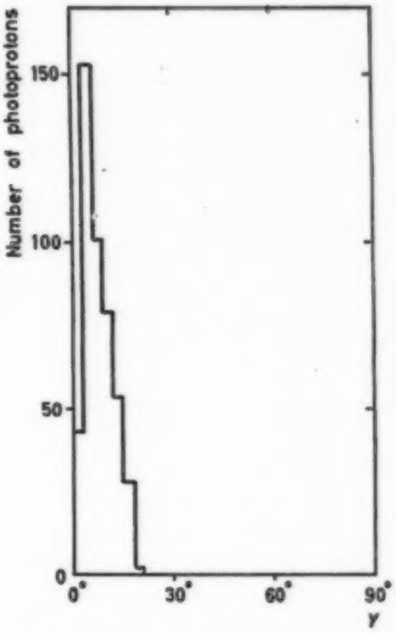

Fig. 3. Experimental distribution from the cobalt exposure of the angles Y of the emitted photoprotons with the y-axis.

3. Results

The value of the x co-ordinate (x_t) of the intersection point between the calculated trajectory and the plane of the target depends on whether the track in the emulsion is assumed to originate from a proton, a deuteron or an alpha particle. In one of these cases x_t may fall in the region of the target and it will be possible to identify the track as that of a proton, a deuteron or an alpha particle. The alpha tracks, however, may also be distinguished directly from singly charged particle tracks as the alpha tracks are denser. Figs. 4, 5 and 6 show the experimental distribution of x_t from the three main exposures after the background has been subtracted. In section A of the figures it is assumed that all the singly charged particle tracks are due to photoprotons, while in section B the assumption is made that the same tracks are due to photodeuterons. There are two reasons, why the number of points in sections A and B is not the same. The first is that the computer rejected trajectories which cut the walls

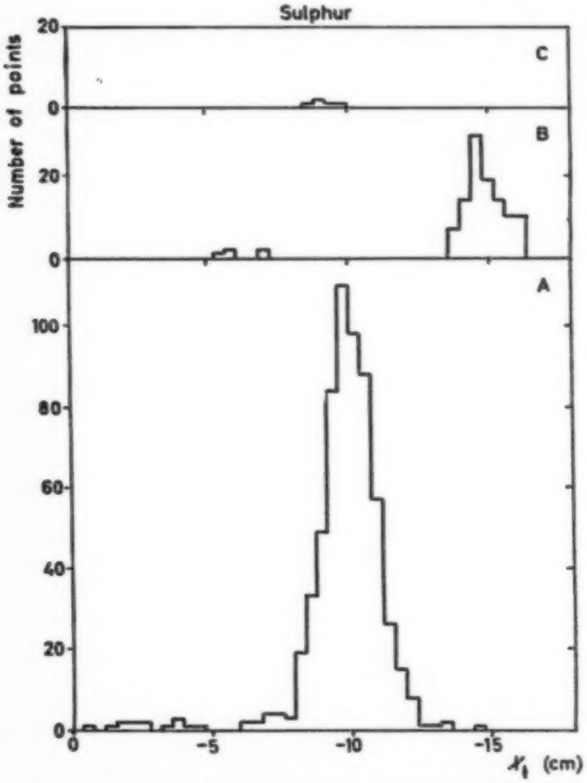

Fig. 4. Experimental distribution from the sulphur exposure of the x co-ordinates of the intersection points of the trajectories with the plane of the target falling in the interval $-3.0 < x_t < 3.0$. The background is subtracted. In section A all the singly charged particle tracks are assumed to originate from protons. In section B they are assumed to originate from deuterons. In section C all the dense tracks are assumed to be alpha particle tracks. The centre of the target has the x co-ordinate $x_t = -10.1$. The area scanned is 13.2 cm^2.

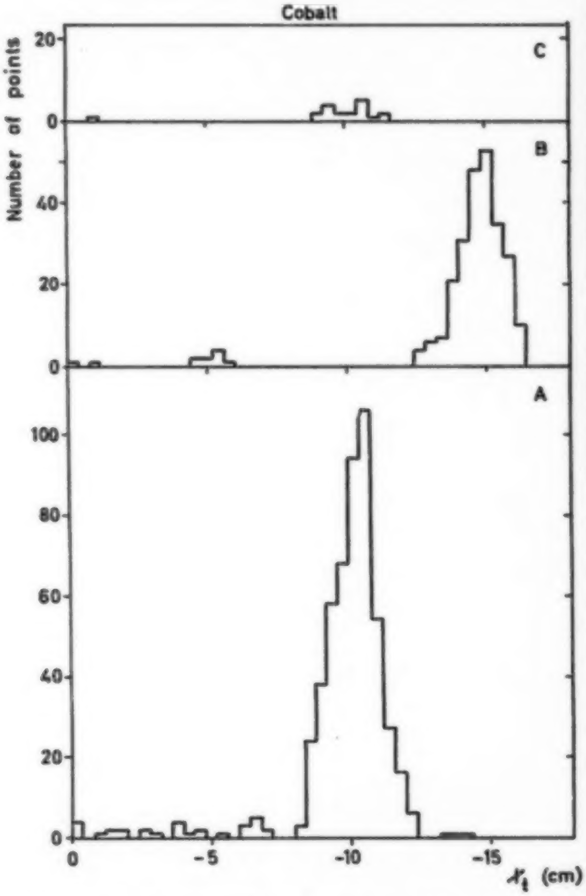

Fig. 5. Experimental distribution from the cobalt exposure of the x co-ordinates of the intersection points of the trajectories with the plane of the target falling in the interval $-3.0 < x_t < 3.0$. The background is subtracted. In section A all the singly charged particle tracks are assumed to originate from protons. In section B they are assumed to originate from deuterons. In section C all the dense tracks are assumed to be alpha particle tracks. The centre of the target has the x co-ordinate $x_t = -10.1$. The area scanned is 18.0 cm^2.

of the camera. The second is that many of the tracks had ranges which corresponded to such high deuteron energies, that they were in conflict with the law of energy conservation. In the deuteron calculations such tracks were rejected. In section C the intersection points of the alpha tracks are shown. Section A of all the figures shows a narrow distribution of the number of intersection points around the centre value $x_t = -10.1$ of the targets. These points therefore are starting points for photoprotons. Such peaks are not observed in the sections B.

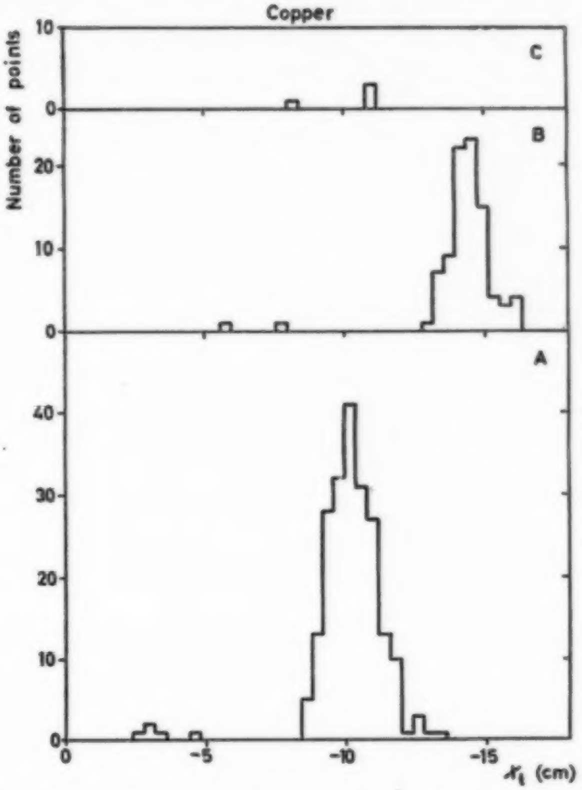

Fig. 6. Experimental distribution from the copper exposure of the x co-ordinates of the intersection points of the trajectories with the plane of the target falling in the interval $-3.0 < z_t < 3.0$. The background is subtracted. In section A all the singly charged particle tracks are assumed to originate from protons. In section B they are assumed to originate from deuterons. In section C all the dense tracks are assumed to be alpha particle tracks. The centre of the target has the x co-ordinate $x_t = -10.1$. The area scanned is 9.8 cm^2.

Only very few tracks give intersection points that fall around $x_t = -10.1$. In sections C again the points originating from alpha particles are concentrated around $x_t = -10.1$.

In fig. 7 the background is shown in the same way. It mainly consists of fast photoprotons originating from the entrance window. The position of the background peak accidentally falls on almost the same place as the peak of the photoprotons from the main exposures. Fig. 7B shows that the background from the entrance window does not disturb the study of photodeuterons. The few background points from $x_t = 0$ down to $x_t = -12$ originated mostly from such recoil protons that are formed in the emulsions and pass through the surface of the emulsions. In most cases they can be sorted out, as they do not have a characteristic track end, but for low-energy protons this separation is hard to perform. No background points originating from alpha particles were obtained.

The energy distributions of the photoprotons from the different exposures that have an x_t value in the interval $-8.4 > x_t > -11.6$ are shown in fig. 8. The distributions are corrected for the background. The photoproton distributions from sulphur, cobalt and copper have been reported earlier with much better statistics[19,20,21]). The dashed histograms drawn in the figure are the expected distributions. It is evident that the distributions here found are in agreement with the expected ones. This agreement shows that the present investigation does not favour any proton energy. The figure gives also the energy distribution of the background tracks.

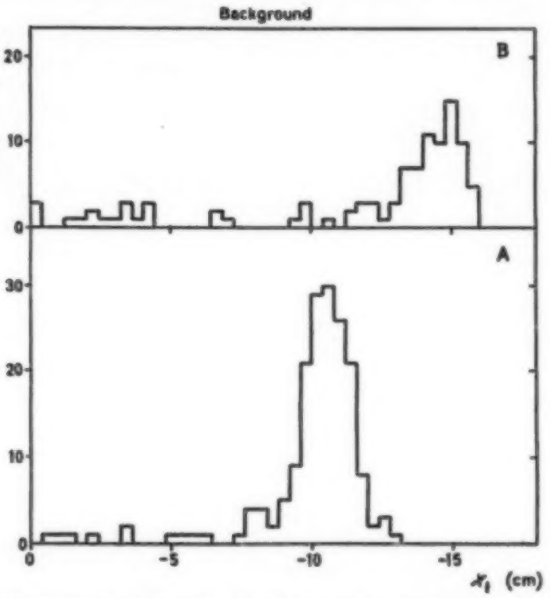

Fig. 7. Experimental distribution from the background exposure of the x co-ordinate of the intersection points of the trajectories with the plane of the target falling in the interval $-3.0 < z_t < 3.0$. In section A all the singly charged particle tracks are assumed to originate from protons. In section B they are assumed to originate from deuterons. No dense tracks gave intersection points in the x region shown in the figure when they were assumed to be alpha particle tracks. The area scanned is 7.1 cm².

The figs. 4, 5 and 6 give the following ratios R_{dp} between the (γ, d) yield and the (γ, p) yield with the corresponding standard deviations s:

S: $R_{dp} = 0.000$, $s = 0.009$;
Co: $R_{dp} = 0.000$, $s = 0.012$;
Cu: $R_{dp} = 0.000$, $s = 0.018$.

The present experiment cannot settle a lower limit of the ratio R_{dp} as no photodeuterons with certainty have been observed in the three exposures. Fig. 9A shows the sum of the three x_t co-ordinate distributions with the assumption that all the singly charged particle tracks were deuteron tracks. This has been done in order to get better statistics. In the figure the background is not subtracted. It is still impossible to observe a peak around $x_t = -10.1$ above

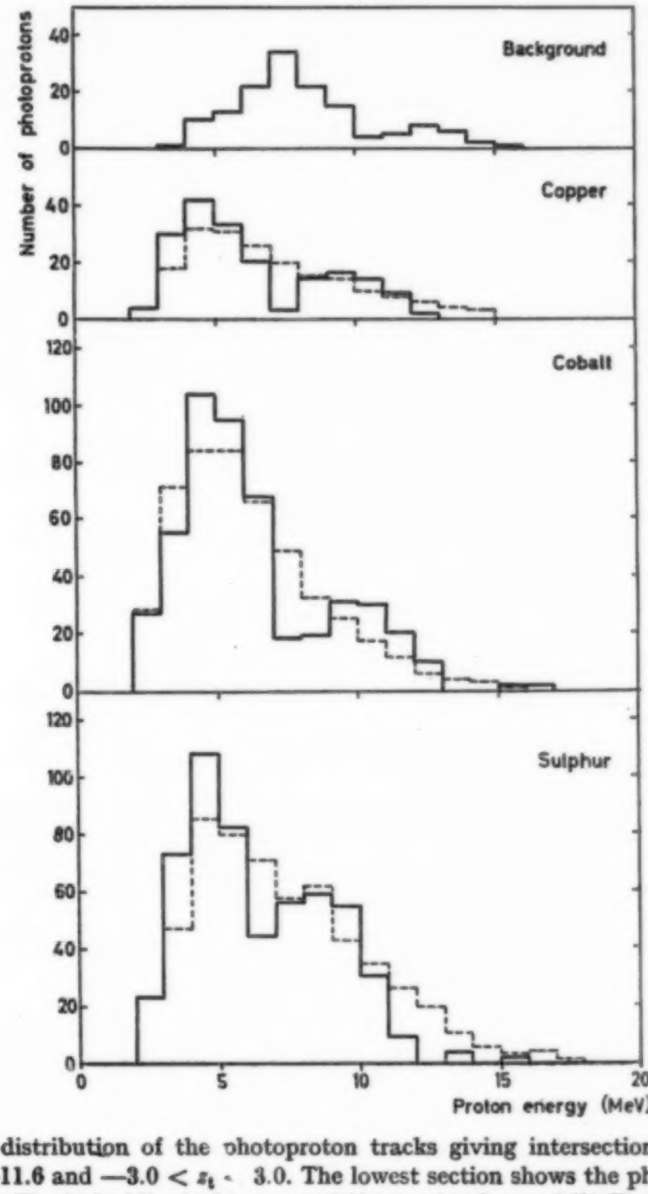

Fig. 8. Energy distribution of the photoproton tracks giving intersection points in the area $-8.4 > x_t > -11.6$ and $-3.0 < x_t < 3.0$. The lowest section shows the photoprotons from the sulphur exposure. The dashed line is the expected distribution from ref. [19]). The second section shows the photoprotons from the cobalt exposure. The dashed line is the expected distribution from ref. [20]). The third section shows the photoprotons from the copper exposure. The dashed line is the expected distribution from ref. [21]). The background is subtracted in these three sections, but shown in the uppermost section. It originates from the entrance window.

the background level. The figure gives for the ratio:

$$\frac{\sum Y(\gamma, \mathrm{d})}{\sum Y(\gamma, \mathrm{p})} = 0.000, \quad \text{with} \quad s = 0.007.$$

Therefore the upper limit is probably not more than 0.007.

In fig. 9B all the tracks originating both from singly and doubly charged particles were assumed to be alpha tracks if they had ranges corresponding to alpha-particle energies between 6.5 and 11.0 MeV. Now a distinct group of points around $x_t = -10.1$ is observed above the background level showing the existence of photo-alpha particles. In fig. 9C trajectories were calculated only for those tracks that during the scanning of the plates were recognized as alpha tracks. In this section no background exists, however the yield of alpha particles determined from figs. 9B and 9C is the same. It is evident that the (γ, d) yield must be less than the (γ, α) yield. Otherwise a group of points at the position of the target similar to that found in fig. 9B should have been observed in fig. 9A.

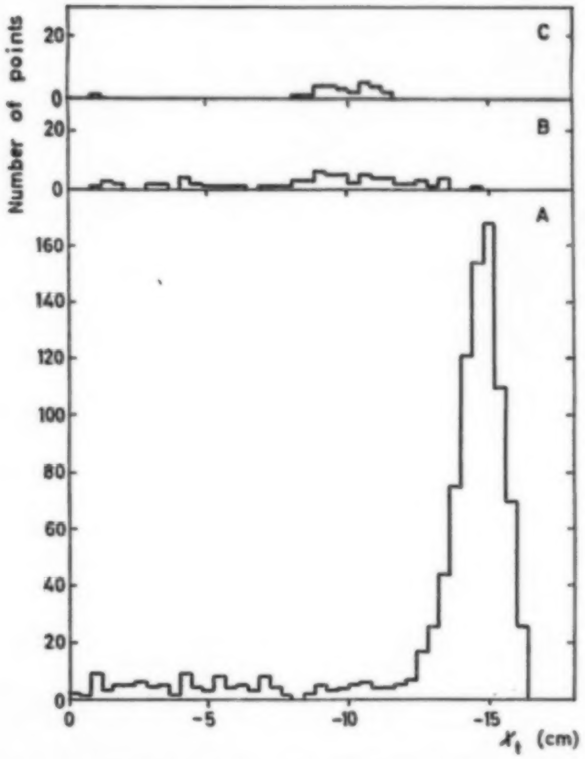

Fig. 9. The sum of the experimental distributions from the three main exposures of the x co-ordinate of the intersection points of the trajectories with the plane of the target falling in the interval $-3.0 < z_t < 3.0$. In section A all the singly charged particle tracks are assumed to originate from deuterons. The background is not subtracted. In section B all the tracks originating both from singly and doubly charged particles are assumed to be alpha particles. The background is not subtracted. In section C only the dense tracks are assumed to be alpha particle tracks. No background exists.

Only alpha tracks with energies more than 6.5 MeV were measured. An 8 MeV alpha particle loses about 1.5 MeV when it passes through half the thickness of the cobalt or copper foil. The energy distribution of the emitted photo-alpha particles from copper using a maximum bremsstrahlung energy of 30.5 MeV is peaked around 8 MeV [22]). It is therefore evident that the lower energy part of the photo-alpha particles are lost in the present experiment. In order to get an estimate of the ratio $R_{\alpha p}$ between the (γ, α) yield and the (γ, p) yield, the number of observed alpha tracks in the case of cobalt and copper has been corrected for this loss. In the case of sulphur too many alpha particles have been lost to get a fair estimate.

The present experiment gives the following ratios:

$$\text{Co: } R_{\alpha p} = 0.09; \quad \text{Cu: } R_{\alpha p} = 0.05.$$

These ratios may be compared with the reported ratios for cobalt at 21.5 MeV bremsstrahlung [20, 23]) $R_{\alpha p} = 0.047$ and for copper at 24 MeV bremsstrahlung [2]) $R_{\alpha p} = 0.040$. The ratio $R_{\alpha p}$ will rise with the irradiation energy. The present ratios therefore are in agreement with earlier (γ, α) experiments.

All the identified alpha particles had energies between 6.5 and 10.5 MeV in agreement with the known energy distribution.

4. Discussion

It is well known [1]) that the statistical model satisfactorily gives an account of the energy distribution of the emitted photoneutrons. This is also the case for photoprotons from light and medium weight nuclei. For these nuclei the statistical model also predicts the yield of photoprotons compared with the yield of photoneutrons. The experimental deviations from the statistical model for heavy nuclei can be explained in terms of the direct photo-effect. The experimental photo-alpha particle yield [18]) and the photo-triton yield [24]) follows also the statistical theory. It will therefore be of interest to compare the present results with this theory. To perform such a calculation it is necessary to know the level density of the daughter nuclei. It has been shown that low-energy nuclear temperatures are independent of the excitation energy [25]). At higher excitation energies, however, the nuclei can be described as a Fermi gas and the excitation energy will be proportional to the temperature squared [26]). The level density will therefore have one of the forms

$$\rho(E) = \text{const} \times \exp \frac{E}{T} \quad \text{(low-energy excitation)}, \tag{1}$$

where T is a constant,
or

$$\rho(E) = \text{const} \times \exp \sqrt{\alpha E} \quad \text{(high-energy excitation)}, \tag{2}$$

where α is a constant.

The ratio R_{dp} is sensitive to which of these formulas is used as the thresholds for the reactions (γ, p) and (γ, d) differ considerably. In the copper region T seems to be constant up to 10 MeV having a value of 1.16 MeV [27]). At excitation energies between 10 and 20 MeV the level density looks more like eq. 2 with a value for α of 5.56 MeV^{-1} [28]). In the sulphur region T has the value 1.6 MeV [25]). As the level density in sulphur is lower than in copper at the same energy, eq. 1 should be expected to be valid for sulphur in the whole energy range of the present experiment. In the calculation of the ratio it has been taken into account that there is a difference in the total number of states for even, odd, and odd mass nuclei at a constant energy. There exists a close connection between the difference and the pairing energy [25]). The calculation is based on the experimental cross-section curves for sulphur [29]) and copper [30]) and Shapiro's penetrability values [31]). Using eq. 1 the following ratios are obtained:

$$\text{S}^{32}\text{: } R_{dp} = 3\times 10^{-3}; \quad \text{Cu}^{63}\text{: } R_{dp} = 6\times 10^{-4}.$$

Using eq. 2 we have

$$\text{Cu}^{63}\text{: } R_{dp} = 7\times 10^{-3}.$$

In the case of copper the estimate from eq. 2 should be more reliable as the level densities in the copper region given by eqs. (1) and (2) with the experimental constants agree fairly well at low excitation energies, and eq. (2) is the best at high energies. Hence the statistical model predicts an R_{dp} of 0.003—0.007 when the maximum bremsstrahlung energy is 30 MeV. This R_{dp} shall be compared with the present experimental result $R_{dp} < 0.007$.

The present results may also be compared with the estimation of the photodeuteron emission by a pick-up process calculated by Sawicki and Czyż [15]). They give for sulphur a ratio of the cross sections $\sigma(\gamma, \text{d})/\sigma(\gamma, \text{p}) = 0.1$ for a photon energy of 25 MeV. The photoproton cross section is that of the direct process only. The ratio $\sigma(\gamma, \text{d})/(\sigma(\gamma, \text{p})_{\text{direct}}+\sigma(\gamma, \text{p})_{\text{compound}})$ must be much lower. The deuteron dissociation within the nucleus may also suppress the deuteron yield.

From a nucleus with $N = Z$ the direct dipole emission of a deuteron is forbidden since the nuclear charge-to-mass ratio is the same as that of the deuteron. Photodeuterons from light and medium weight nuclei must therefore mainly be formed in an evaporation or a pick-up process.

The experimental results from the Iowa group [17]) are in close agreement with the present ones. They report that in copper R_{dp} is less than 1.6 ± 1 %. They have measured the emitted photo-particles in the angle range between 30° and 80° from the incident beam direction and therefore cover a different angular region than the present investigation made in the forward direction.

As the anisotropy in the angular distribution of the direct emitted photoprotons is strong and peaked around 60° [32]) it should be expected that non-statistical photodeuterons will more easily be observed in forward and backward directions. Chizhov [10]) has shown that the emitted photodeuterons of high energy from light elements have an angular distribution which is peaked around 0°, which further argues in favour of measurements at small angles.

The inverse reactions often give valuable information about the photoprocesses. The radiative deuteron capture process $Zn^{64}(d, \gamma)Ga^{66}$ has recently been studied by Carver and Jones [33]) using deuteron energies of about 4 MeV. The magnitude of the cross section was determined by activity measurements of Ga^{66}. As the captured γ-ray spectrum is not known non-statistical processes may contribute to the cross section. However, statistical calculations of the cross section were in good agreement with the experiment showing that in the energy range studied an anomalous yield of photodeuterons is not expected. This supports the present investigation.

Byerly and Stephens [2]) were the first who stated the existence of photodeuterons. They found in the energy distribution of photoprotons from copper an extra peak at 2.5 MeV which they assumed to originate from deuterons. They reported that it is possible to separate single deuterons from protons by grain-counting the last 40 μm of the photo-particle tracks in nuclear emulsions and got in this way a ratio R_{dp} of 0.31 ± 0.09. However, the author [3]) tried to repeat the experiment of Byerly and Stephens and showed that a separation of single deuterons from protons cannot be expected if common nuclear emulsions are used. By a statistical processing of the data R_{dp} for Cu was estimated to $0.16 \pm \pm 0.08$. Grant *et al.* [4]) later used the same technique recording the tracks in fine grain emulsions. Still a separation of single deuterons from protons was not obtained. They report for Cu and R_{dp} of 0.21 ± 0.05. However, they did not succeed in repeating this value but got a considerably lower R_{dp} [34]).

The existence of the extra peak in the energy distribution of the photoprotons from copper have not been observed in a recent investigation by Lin'kova *et al.* [21]). Probably it does not exist but is a background effect. The assumed photodeuterons in the experiment of Byerly and Stephens should have an energy of about 4 MeV and would easily have been detected in the present experiment.

The estimate of the yield of photodeuterons from the present experiment is considerably smaller than that from the grain-counting experiments. The explanation is that the grain-counting method is not well adapted for the present problem. Surface effects in the emulsions cause variations of the grain density in the tracks, which easily disturb the results and make them hard to reproduce. The errors in the measurements are so great that the reported fluctuations in the yield of the photodeuterons from element to element might be statistical deviations and not an effect of the nuclear structure. In the present investigation no difference in the yield of photodeuterons from the adjacent elements cobalt and copper is observed.

The present investigation may also be compared with the activity measurements of the daughter nuclei in the 2 MeV region above the (γ, d) threshold. Katz and Penfold[5]) have with this method reported a cross-section curve for the reaction $S^{32}(\gamma, d)P^{30}$. From this curve and from the total absorption cross-section curve[29]) knowing the (γ, p) and (γ, n) branching ratios from statistical calculations an R_{dp} of 0.02 is obtained which is about 10 times higher than the value predicted from the statistical model. Such a discrepancy may be explained by errors in the measurements of the (γ, d) and the total absorption cross sections and in the estimates of the terms involved in the calculations. Still, however, it is difficult to explain the experimental result, that the photodeuteron emission starts just over the threshold of the reaction. According to the statistical model there will be no photodeuterons with an energy less than 1 MeV because of the coulomb barrier. Even in a pick-up process there must exist a barrier that keeps the photodeuteron emission down in the first MeV region above the threshold.

Ferrero *et al.*[35]) have repeated the experiment of Katz and Penfold. In a first experiment they got some activity below 21 MeV but this was shown to originate from a small oxygen contamination in the sulphur target[36]). O^{15} has a half-life nearly like the half-life of P^{30}. In a second experiment with a fairly pure sulphur target the activation curve from P^{30} started at about 22 MeV well above the (γ, np) threshold. Perhaps this is the explanation of the discrepancy between the Katz-Penfold experiment and the statistical model.

The São Paulo group have in two papers[6, 37]) reported an anomalous yield of photodeuterons. They used the activation technique, too, and studied S^{32}, Zn^{64}, Zn^{66} and Fe^{54}. Their results from sulphur are in agreement with those of Katz and Penfold but presumably the explanation of the discrepancy between these and the statistical model is the same. In the case of zinc the results from the São Paulo group and the Zürich group[38]) are inconsistent. The São Paulo group reports a cross section of the reaction $Zn^{66}(\gamma, {}^{d}_{np})Cu^{64}$ that is about a hundred times higher than the value reported by Hofmann and Stoll. This discrepancy must be explained before an anomalous yield of photodeuterons from zinc is claimed. In the case of iron a much lower yield of the reaction $(\gamma, {}^{d}_{np})$ was found than for zinc.

In Ljubljana[39]) recently a study has been done of the $(\gamma, {}^{d}_{np})$ reaction on K^{39} with the same activation technique. No activity originating from photodeuterons was observed in the energy region between the (γ, d) and the (γ, np) thresholds.

As is seen criticism can be directed against the experiments that report an anomalous yield of photodeuterons using the grain-counting method or the activation technique. It is very difficult to get information about the photodeuteron yield with these methods. Still there may exist an emission of photodeuterons by a pick-up mechanism but at a maximum bremsstrahlung irradiation energy of about 30 MeV the cross section for such a process is of the order of or less than the cross section for the evaporation of a deuteron.

It is difficult to compare the present results with the experiments at much higher irradiation energies as in these only photodeuterons of high energies have been studied. Smith and Laslett [7]) irradiated a thick copper target with 65 MeV maximum bremsstrahlung. They separated deuterons from protons by a magnetic cloud chamber and got an R_{dp} of 0.76 which is surprisingly high and hard to understand. Ring [8]) used the same experimental equipment and irradiated sulphur. He got an R_{dp} of 0.15. Both the results are considerably higher than those obtained by Chizhov [10]) with a telescope arrangement. He studied charged photo-particles in the energy range of 15.5—30 MeV and reports that the ratio R_{dp} increases slowly with the mass number and goes from 0.02 for S to 0.07 for Au. No fluctuations in R_{dp} from element to element is obtained. Only the lightest elements show deviations from this trend and have ratios of the same magnitude as the heaviest. Both the mass-dependence of R_{dp} and the angular distribution of the photodeuterons is shown to be explained by the assumption that the photodeuterons are formed in a pick-up mechanism.

The emission of photodeuterons formed in such a mechanism should increase with the irradiation energy as more combinations will be accessible for the formation of the deuteron. Chizhov has shown experimentally that the cross section for the (γ, d) reaction in Li^6 is strongly dependent on the irradiation energy. The energy dependence of the (γ, d) cross section is confirmed by the telescope measurements at 300 MeV maximum bremsstrahlung irradiation[12, 13, 14]). The ratio R_{dp} still increases continuously with the mass number but is considerably higher than at 90 MeV and now goes from 0.12 for C to 0.24 for Pb.

The yield ratio of photodeuterons to photoprotons with the same energy is experimentally found to increase when the energy of the compared photo-particles decreases [9]), however this ratio must go through a maximum. At photo-particle energies below about 10 MeV the evaporated photoprotons will effect the ratio and press it down. Both this effect depending on evaporated photoprotons and the energy dependence of the (γ, d) cross section cause very low R_{dp} values at irradiation energies around 30 MeV. This is verified in the present experiment. The telescope experiments, the Iowa group results with nuclear emulsions and the present ones together, give knowledge of how the photodeuterons behave.

The author wishes to express his deep gratitude to Dr. S. A. E. Johansson for many helpful discussions and for advice during the course of this experiment. The author also wants to thank Dr. C. E. Fröberg for carrying out the coding of the calculations on SMIL.

References

1) J. S. Levinger, Nuclear Photo-disintegration (Oxford University Press, 1960)
2) P. R. Byerly, Jr., and W. E. Stephens, Phys. Rev. **83** (1951) 54
3) B. Forkman, Ark. f. Fysik **11** (1956) 265
4) J. J. Grant, H. A. Medicus, J. Demers and P. Demers, Photographie Corpusculaire II, ed. by P. Demers (Les Presses Universitaires de Montréal, 1959) p. 255
5) L. Katz and A. S. Penfold, Phys. Rev. **81** (1951) 815; **83** (1951) 169
6) J. Goldemberg and L. Marquez, Nuclear Physics **7** (1958) 202
7) W. H. Smith and L. J. Laslett, Phys. Rev. **86** (1952) 523
8) L. S. Ring, Jr., Phys. Rev. **99** (1955) 137
9) V. P. Chizhov and L. A. Kul'chitskiĭ, JETP **36** (1959) 345
10) V. P. Chizhov, JETP **38** (1960) 809
11) E. D. Makhnovskiĭ, JETP **36** (1959) 739
12) J. F. DeWire, A. Silverman and B. Wolfe, Phys. Rev. **92** (1953) 519
13) D. A. Edwards, B. Wolfe, A. Silverman and J. W. DeWire, Phys. Rev. **95** (1954) 629
14) J. Rosengren and R. Wertheim, M.I.T. Ann. Progr. Rep., May 31 (1954) 128
15) J. Sawicki and W. Czyż, Nuclear Physics **4** (1957) 248, 695
16) B. Forkman and S. A. E. Johansson, Ark. f. Fysik (in press)
17) G. Ho, E. L. Iloff and D. J. Zaffarano, Nuclear Physics (in press)
18) F. Heinrich, H. Wäffler and M. Walter, Helv. Phys. Acta **29** (1956) 3
19) B. Čujec-Dobovišek, Congr. Intern. de Physique Nucléaire (1958) 634
20) M. E. Toms and W. E. Stephens, Phys. Rev. **95** (1954) 1209
21) N. V. Lin'kova, R. M. Osokina, B. S. Ratner, R. Sh. Amirov and V. V. Akindinov, JETP **38** (1960) 780
22) F. Bobard, G. Boulègue and P. Chanson, Comptes Rendus **244** (1957) 1761
23) M. E. Toms and J. McElhinney, Congr. Intern. de Physique Nucléaire (1958) 660
24) F. Heinrich and H. Wäffler, Helv. Phys. Acta **29** (1956) 232
25) T. Ericson, Nuclear Physics **11** (1959) 481
26) J. M. Blatt and V. F. Weisskopf, Theoretical Nuclear Physics (John Wiley and Sons, New York, 1952)
27) H. W. Fulbright, N. O. Lassen and N. O. Roy Poulsen, Mat. Fys. Medd. Dan. Vid. Selsk. **31**, No. 10 (1959)
28) R. M. Eisberg, G. Igo and H. E. Wegner, Phys. Rev. **100** (1955) 1309
29) J. Kockum and N. Starfelt, Nuclear Instruments and Methods **5** (1959) 37
30) A. I. Berman and K. L. Brown, Phys. Rev. **96** (1954) 83
31) M. M. Shapiro, Phys. Rev. **90** (1953) 171
32) S. A. E. Johansson, Phys. Rev. **97** (1955) 434
33) J. H. Carver and G. A. Jones, Nuclear Physics **11** (1959) 400
34) H. A. Medicus (private communication)
35) F. Ferrero, S. Ferroni, R. Malvano, S. Menardi and E. Silva, Nuclear Physics **15** (1960) 436
36) R. Malvano, (private communication)
37) S. S. Villaça and J. Goldemberg, An. Acad. Bras. Ciencias **27** (1955) 427
38) A. Hofmann and P. Stoll, Helv. Phys. Acta **31** (1958) 591
39) P. Horvat, J. Pahor and M. Vakselj, Nuclear Physics **16** (1960) 90

1.D.4

Nuclear Physics **23** (1961) 285—295;©*North-Holland Publishing Co., Amsterdam*

Not to be reproduced by photoprint or microfilm without written permission from the publisher

NOTES ON THE THEORY OF VIBRATIONAL STATES OF SYSTEMS OF FERMIONS (I)

J. SAWICKI

Department of Physics, University of California, Berkeley 4, California †

Received 17 October 1960

Abstract: The system of nonlinear equations for the components of the single particle density matrix operator is discussed, for both infinite and finite systems of fermions interacting through a two-body "residual" interaction. The Hartree-Fock factorization and linearization of that system of equations for the density fluctuations can be performed. Hartree-Fock exchange terms and, particularly, deviations from the random phase approximation, are discussed. The importance of these deviations is illustrated by the example of the quadrupole vibrations of a closed spherical nuclear subshell. An apparent ambiguity in the linearization procedure is discussed and the importance of the nonlinearity of equations is stressed.

1. Introduction

The theory of collective oscillations of the electron gas in the formulation of Sawada and others [1,2]) is essentially based on the idea of the predominant importance of particle-hole pair interactions. Their formulation involves a number of approximations, the most important of which are: linearization of the eigenvalue equations, random phase approximation (further referred to as RPA), and neglect of some exchange terms ††. A linearization of the system of equations for the components of the single particle density matrix as obtained in that theory leads to the equation of Sawada and Brout [2]). The eigenfrequency of the collective oscillation is then found from a simple dispersion relation following from these linearized equations.

This method was applied by Glassgold, Heckrotte, and Watson [3]) to investigate some possible hydrodynamic properties of nuclear matter, such as the existence of compressive waves, spin, isospin, and coupled spin-isospin waves. This method was also applied in more detail to the problem of stability of nuclear matter by Sawada and Rockmore [4]).

Takagi [5]) applied the Sawada method to the finite nuclear system. He introduces operators corresponding to the projection of definite angular momentum states from the particle-hole pair creation and annihilation operators. Otherwise this theory is essentially identical with the usual Sawada theory. This theory

---

† This work was supported in part by the U. S. Atomic Energy Commission and the Office of Naval Research.

†† The exchange terms have been recently treated for the electron gas case by Tai Tsun Wu [18]).

was then applied in some more detail to a two-dimensional model of a quadrupole-quadrupole interaction by Ikeda *et al.* [6]). The three-dimensional quadrupole force model was particularly exploited by Mottelson [7]). Arvieu and Veneroni [8]) applied the same method to the case of the model of the "superconducting nucleus". They take into account the short-range pairing force by using the Bogoliubov transformation, and the long-range residual force which describes the interaction between particle-hole pairs. These authors obtain the correspondence to the result of Belyaev [9]) for the vibrational frequency in the case of one single particle excitation in the nucleus. The same result was also obtained by Kobayasi and Marumori [10]) using a simple quadrupole residual interaction. Most recently, Baranger [11]) presented a discussion of the above theory for a more general interaction potential. Kisslinger and Sorensen [12]) consider the case of a quadrupole force and assume different coupling constants for pairs of different isobaric spin (T_3) states. Marumori [13]) has presented a more extensive treatment of this theory for even spherical nuclei. Brown *et al.* [14]) have discussed the problem of the giant dipole resonance without assuming the pairing force of the "superconducting" type, and Brown *et al.* [15]) have treated the nuclear octupole vibrations.

Most of the above-mentioned authors use procedures essentially corresponding to the RPA form of the Sawada theory which, in turn, is equivalent to the linearized "density approximation" involving neglect of certain Hartree-Fock type exchange [†] and other correlation terms. It is the aim of the present note to point out some of the difficulties and consequences of the nonlinearity of the original density equations as opposed to the usual RPA theory, as well as of the Hartree-Fock exchange terms for infinite and for finite systems of fermions. Particular attention is given to the example of vibrational modes in spherical nuclei. In the following we shall use the "density formalism" as developed by Ehrenreich and Cohen [16]) and used, e.g., by Goldstone and Gottfried [17]).

2. Theory and Discussion

We shall omit the spin indices for the sake of simplicity, and consider a system of particles with identical charge. We shall also consider pairs of two particles and two holes, as well as particle-hole pairs up to the point where we discuss specific examples. We can write the total second-quantized Hamiltonian in the coordinate representation as

$$\hat{H} = \int \psi^+(\mathbf{x}) H_0(\mathbf{x}) \psi(\mathbf{x}) \mathrm{d}\mathbf{x} + \tfrac{1}{2} \int \psi^+(\mathbf{x}) \psi^+(\mathbf{y}) \Delta V(\mathbf{x}, \mathbf{y}) \psi(\mathbf{y}) \psi(\mathbf{x}) \mathrm{d}\mathbf{x}\mathrm{d}\mathbf{y}, \tag{1}$$

where $H_0(\mathbf{x})$ is the zero-order model hamiltonian (e.g., the effective mass-modified kinetic energy operator in the case of an infinite medium), and

---

[†] Not to be confused with what are called "exchange" terms, as e.g. in refs. [14, 15]).

and $\Delta V(\mathbf{x}, \mathbf{y})$ is the "residual" two-body interaction. The destruction (creation) operators can be developed as $\psi(\mathbf{x}) = \Omega^{-\frac{1}{2}} \sum_{\mathbf{k}} a_{\mathbf{k}} e^{i\mathbf{k}\cdot\mathbf{x}}$ for an infinite system, Ω being the volume of the system, or $\psi(\mathbf{x}) = \sum_\nu a_\nu \varphi_\nu(\mathbf{x})$ for a finite system, where $\{\varphi_\nu(\mathbf{x})\}$ is the complete set of the $H_0(\mathbf{x})$ eigenfunctions corresponding to the eigenvalues $\{E_\nu{}^0\}$. We now define

$$\hat{H}(\mathbf{x}) \equiv H_0(\mathbf{x}) + \int \hat{\varrho}(\mathbf{y}, \mathbf{y}) \Delta V(\mathbf{x}, \mathbf{y}) \mathrm{d}\mathbf{y}, \tag{2}$$

where the single particle density operator is

$$\hat{\varrho}(\mathbf{x}, \mathbf{x}') = \psi^+(\mathbf{x}')\psi(\mathbf{x}). \tag{3}$$

For an infinite medium,

$$\hat{\varrho}(\mathbf{x}, \mathbf{x}') = \Omega^{-1} \sum_{\mathbf{k}, \mathbf{k}'} \hat{\varrho}(\mathbf{k}, \mathbf{k}') \exp\left[i(\mathbf{k}\cdot\mathbf{x} - \mathbf{k}'\cdot\mathbf{x}')\right],$$

where $\hat{\varrho}(\mathbf{k}, \mathbf{k}') = a_{\mathbf{k}'}{}^\dagger a_{\mathbf{k}}$; and for a finite system,

$$\hat{\varrho}(\mathbf{x}, \mathbf{x}') = \sum_{\nu\nu'} \hat{\varrho}_{\nu\nu'} \varphi_\nu(\mathbf{x}) \varphi_{\nu'}{}^*(\mathbf{x}'),$$

where $\hat{\varrho}_{\nu\nu'} = a_{\nu'}{}^\dagger a_\nu$. The required density equation can now be obtained from the Liouville-type equation [†]

$$i\hbar \frac{\partial}{\partial t} \hat{\varrho}(\mathbf{x}, \mathbf{x}') = \hat{H}(\mathbf{x})\hat{\varrho}(\mathbf{x}, \mathbf{x}') - \hat{\varrho}(\mathbf{x}, \mathbf{x}')\hat{H}(\mathbf{x}'). \tag{4}$$

For the case of an infinite medium we find the operator equation in the momentum space,

$$\begin{aligned} i\hbar \frac{\partial}{\partial t} \hat{\varrho}(\mathbf{k}, \mathbf{k}+\mathbf{q}) &= (E_{\mathbf{k}}{}^0 - E^0_{\mathbf{k}+\mathbf{q}}) \hat{\varrho}(\mathbf{k}, \mathbf{k}+\mathbf{q}) \\ &+ \frac{(2\pi)^3}{\Omega^2} \sum_{\mathbf{k}', \mathbf{q}', \mathbf{p}} \Delta V(\mathbf{p}, \mathbf{q}') [\hat{\varrho}(\mathbf{k}', \mathbf{k}'+\mathbf{q}') \hat{\varrho}(\mathbf{k}-\mathbf{p}, \mathbf{k}+\mathbf{q}) - \hat{\varrho}(\mathbf{k}, \mathbf{k}+\mathbf{q}+\mathbf{p}) \hat{\varrho}(\mathbf{k}', \mathbf{k}'+\mathbf{q}')]. \end{aligned} \tag{5}$$

This equation is exact. It goes over into eq. (17) of ref. 16) if ΔV is a Coulomb-type potential [of the form $\Delta V(\mathbf{x}-\mathbf{y})$].

Let us denote by $\langle \ldots \rangle_{\mathrm{Av}}$ the ensemble average. The usual procedure applied in most of the references quoted above corresponds essentially to performing the "Hartree factorization", i.e., to the replacement of the expectation value of a product of two density matrices by the product of expectation values, i.e.

$$\langle \hat{\varrho}(\mathbf{y}, \mathbf{y}) \hat{\varrho}(\mathbf{x}, \mathbf{x}') \rangle_{\mathrm{H.Av}} \equiv \langle \hat{\varrho}(\mathbf{y}, \mathbf{y}) \rangle_{\mathrm{Av}} \langle \hat{\varrho}(\mathbf{x}, \mathbf{x}') \rangle_{\mathrm{Av}} \equiv \rho(\mathbf{y}, \mathbf{y}) \rho(\mathbf{x}, \mathbf{x}'). \tag{6}$$

This approximation neglects the Hartree-Fock exchange terms; this may be somewhat justified only for the electron gas in the high density limit. Upon performing the above factorization and neglecting all the terms with $\mathbf{p} \neq -\mathbf{q}$, i.e., assuming the RPA, one arrives at an equation analogous to eq. (25) of ref. [16]). If, in addition, one considers the off-diagonal elements of ρ as perturbations with respect to the diagonal components determined by $H_0(\mathbf{x})$ alone, one obtains a linearized equation, which is the average of the Sawada-Brout equation. One can then work out the usual dispersion-type equation for the energy $\hbar\omega$ of the collective state corresponding to the density fluctuations. Specifically, we can assume a harmonic time evolution of the gas density fluctuation having energy $\hbar\omega$. Following the method of Sawada and others [1, 2]), one then finds the wave function of the collective state corresponding to the excitation $\mathbf{q}$,

---

[†] The following eqs. (5) and (9) can also be obtained by the Sawada method, i.e., calculating the commutators $[\hat{\rho}(\mathbf{k}, \mathbf{k}+\mathbf{q}), \hat{H}]$ and $[\hat{\rho}_{\nu\nu'}, \hat{H}]$, respectively, where $\hat{H}$ is given by eq. (1).

$$|\mathbf{q}\rangle = N_{\mathbf{q}} \sum_{\mathbf{k}} (E^0_{\mathbf{k}+\mathbf{q}} - E_{\mathbf{k}}{}^0 - \hbar\omega)^{-1} \hat{\varrho}(\mathbf{k}, \mathbf{k}+\mathbf{q})|0\rangle,$$

where $N_{\mathbf{q}}$ is the normalization constant, and $|0\rangle$ is the "true" ground state. In the extreme case where ΔV is very small, we could consider the interaction term as a nonhomogeneity, solve for the first-order fluctuation ρ', and employ a successive approximation procedure.

Let us now consider the Hartree-Fock factorization defined by

$$\langle \hat{\varrho}(\mathbf{y}, \mathbf{y})\hat{\varrho}(\mathbf{x}, \mathbf{x}')\rangle_{\text{H.-F.Av}} \equiv \varrho(\mathbf{y}, \mathbf{y})\varrho(\mathbf{x}, \mathbf{x}') - \varrho(\mathbf{x}, \mathbf{y})\varrho(\mathbf{y}, \mathbf{x}'). \tag{7}$$

After carrying out the corresponding calculation in the momentum space for the Fermi gas case, the case where ΔV is a pure Wigner force, we obtain

$$\begin{aligned}\left(E^0_{\mathbf{k}+\mathbf{q}} - E_{\mathbf{k}}{}^0 + i\hbar\frac{\partial}{\partial t}\right)\varrho(\mathbf{k}, \mathbf{k}+\mathbf{q})& \\ = \frac{(2\pi)^3}{\Omega^2} \sum_{\mathbf{k}', \mathbf{q}', \mathbf{p}} \{&\Delta V(\mathbf{p}, \mathbf{q}')[\varrho(\mathbf{k}-\mathbf{p}, \mathbf{k}+\mathbf{q}) - \varrho(\mathbf{k}, \mathbf{k}+\mathbf{q}+\mathbf{p})] \\ &-S[\Delta V(\mathbf{k}-\mathbf{k}', \mathbf{k}'+\mathbf{q}'-\mathbf{p})\varrho(\mathbf{p}, \mathbf{k}+\mathbf{q}) \\ &-\Delta V(\mathbf{k}'+\mathbf{q}'-\mathbf{k}-\mathbf{q}, \mathbf{p})\varrho(\mathbf{k}, \mathbf{k}'+\mathbf{p})]\}\varrho(\mathbf{k}', \mathbf{k}'+\mathbf{q}').\end{aligned} \tag{8}$$

The coefficient of the exchange term is S. If the particles are of identical charge and spin orientation, $S = 1$; in the other cases, S can be equal to $\frac{1}{2}$ or $\frac{1}{4}$. For a zero-range Wigner force $\Delta V(\mathbf{x}, \mathbf{y}) = -g\delta(\mathbf{x}-\mathbf{y})$, the right-hand side of eq. (8) reduces to

$$-g\Omega^{-1}(1-S) \sum_{\mathbf{k}', \mathbf{q}'} [\varrho(\mathbf{k}+\mathbf{q}', \mathbf{k}+\mathbf{q}) - \varrho(\mathbf{k}, \mathbf{k}+\mathbf{q}-\mathbf{q}')]\varrho(\mathbf{k}', \mathbf{k}'+\mathbf{q}').$$

We see that if $S = 1$ there is no collective interaction term.

In the following, we shall concentrate on the problem of finite systems. Similarly to the infinite medium case [eq. (5)], we obtain the equation

$$\Delta_{\nu\nu'}\hat{\varrho}_{\nu\nu'} = \sum_{\kappa\kappa' s} [\Delta V_{s\nu, \kappa\kappa'}\hat{\varrho}_{\kappa\kappa'}\hat{\varrho}_{s\nu'} - \Delta V_{\nu' s, \kappa\kappa'}\hat{\varrho}_{\nu s}\hat{\varrho}_{\kappa\kappa'}], \tag{9}$$

where

$$\varDelta_{\nu\nu'} = E^0_{\nu'} - E_\nu{}^0 + i\hbar \frac{\partial}{\partial t},$$

and

$$\varDelta V_{\alpha\beta,\gamma\delta} = \langle \varphi_\beta{}^*(\mathbf{x})\varphi_\delta{}^*(\mathbf{y}) | \varDelta V(\mathbf{x},\mathbf{y}) | \varphi_\gamma(\mathbf{y})\varphi_\alpha(\mathbf{x}) \rangle.$$

This equation is exact. It is a rather complicated nonlinear equation. The procedure of linearization may appear ambiguous and requires a physical discussion of the terms retained in order for the approximation to be useful. Let us first consider the consequences of a Hartree-Fock factorization in the meaning of eq. (7). We can now linearize systematically the equation so obtained by assuming $\varrho_{\nu\nu'} = \varrho^0_{\nu\nu'} + \varrho'_{\nu\nu'}$, and by retaining only all the first-order terms (linear in the density fluctuations ϱ'). Here $\varrho^0_{\nu\nu'} = n_\nu \delta_{\nu\nu'}$ is the zero-order density corresponding to the absence of $\varDelta V$; n_ν is the occupation number in the Fermi sea. We can write

$$\begin{aligned}\varDelta_{\nu\nu'}\varrho'_{\nu\nu'} = {} & \sum_{\kappa\kappa'} (\varDelta V_{\nu'\nu,\kappa\kappa'} - \varDelta V_{\kappa\nu,\nu'\kappa'})(\varrho^0_{\nu'\nu'} - \varrho^0_{\kappa\kappa})\varrho'_{\kappa\kappa'} \\ & + \sum_{\kappa s} [(\varDelta V_{s\nu,\kappa\kappa} - \varDelta V_{\kappa\nu,s\kappa})\varrho'_{s\nu'} - (\varDelta V_{\nu's,\kappa\kappa} - \varDelta V_{\nu'\kappa,\kappa s})\varrho'_{\nu s}]\varrho^0_{\kappa\kappa'}. \quad (10)\end{aligned}$$

The first sum on the right-hand side corresponds to the usual RPA, the other sum contains deviation terms †. If only the first sum is retained, the right-hand side of eq. (10) vanishes for $\nu' = \nu$, even if the magnetic substates of ν and ν' are different, as in the case of the usual degeneracy. Consequently, the density fluctuation matrix ρ' has only off-diagonal components independently of the detailed properties of $\varDelta V$. This is generally no longer true if the departure from the RPA as in eq. (10) is included. However, for a Wigner force $\varDelta V$, the (diagonal) components of ρ' with $\nu' = \nu$ (also with equal magnetic numbers, i.e., $m_{\nu'} = m_\nu$) vanish. Let us denote the set of quantum numbers $\{n_\nu, l_\nu, j_\nu\}$ by N_ν, and the corresponding j projections by m_ν [we deal with $(2j+1)$-fold initial degeneracy). One can show also that the equations

$$\sum_{m_\nu m_{\nu'}} \varrho'_{N_\nu m_\nu, N_\nu m_{\nu'}} = \sum_{m_\nu m_{\nu'}} \varrho'_{N_{\nu'} m_\nu N_{\nu'} m_{\nu'}} = 0$$

hold for a Wigner force $\varDelta V$.

In the absence of the second sum in eq. (10) (i.e., the RPA) and the Hartree factorization, and for a separable interaction $\varDelta V$, one obtains unambiguously the well-known dispersion relation for $\hbar\omega$ as in the usual Sawada theory. If the potential is not separable one could solve a more complicated secular equation. In the RPA the former well-known dispersion relation can also be easily derived for collective states of a definite angular momentum and its projection. In the calculations the matrix $A^{*}_{LM}(\nu, \nu') = \sum_{m_\nu} (-)^{m_\nu} (j_\nu j_{\nu'};\ -m_\nu m_{\nu'} | LM) \rho'_{\nu\nu'}$ is introduced.

---

† The omission of these terms which is a result of *nonsystematic* linearization can be seen, e.g., in eqs. (5.13)—(5.14) in ref. [13]). That procedure is equivalent to using the "quasiboson" commutation relations in the usual Sawada theory. On the other hand, however, these terms correspond to a "renormalization" of the zero-order potential, i.e., a "renormalization" of $H_0(\mathbf{x})$ due to the presence of $\varDelta V$. They correspond to the "self energy" contributions of $\varDelta V$ in $\varDelta_{\nu\nu'}$; the complete form of these contributions is apparent from eqs. (A-1)—(A-6) of the Appendix. These terms would not occur if we were to solve first the Hartree-Fock self-consistency problem including the self-energy effects.

The situation is not so simple in the most general case of eq. (10). In particular, both Hartree-Fock exchange terms and departures from the RPA provide, in some cases, contributions of the same order of magnitude.

Let us illustrate the situation by the example of the quadrupole vibrational excitations of a closed nuclear subshell described in terms of only one type of single particle level excitations, i.e., in terms of two levels: (1) initially completely occupied level, and (2) the next level completely unoccupied in the absence of ΔV. The example discussed below can be straightforwardly generalized to other multipole vibrations (see Appendix).

For a general Wigner force ΔV we can write its matrix element as

$$\begin{aligned} \Delta V_{\alpha\beta,\gamma\delta} = G \sum_{LM'} [L]^{-1} & \left\{ \frac{[j_\alpha][j_\beta][j_\gamma][j_\delta]}{4\pi[L]} \right\}^{\frac{1}{2}} \\ & \times (j_\alpha j_\beta;\ \tfrac{1}{2} - \tfrac{1}{2} | L0)(j_\gamma j_\delta;\ \tfrac{1}{2} - \tfrac{1}{2} | L0)(-)^{m_\alpha + m_\gamma + M'} \\ & \times (j_\alpha j_\beta;\ m_\alpha - m_\beta | LM')(j_\gamma j_\delta;\ m_\gamma - m_\delta | L - M') v_L(\alpha\beta, \gamma\delta), \end{aligned} \tag{11}$$

where G is the coupling constant, $[j] = 2j+1$, and $v_L(\alpha\beta, \gamma\delta)$ is the radial matrix element of the L^{th} radial coefficient of the expansion of ΔV. In the following example we shall confine ourselves to the component $L = 2$. An example of v_2 used in the Copenhagen work [7]) is

$$v_2(\alpha\beta, \gamma\delta) = v_2(\alpha\beta) v_2(\gamma\delta) = \langle N_\beta | r_1{}^2 | N_\alpha \rangle \langle N_\delta | r_2{}^2 | N_\gamma \rangle .$$

The results obtained below for the case of two levels can easily be generalized to the case of many levels (see Appendix).

Using eq. (10), we assume the Hartree-Fock density

$$\overset{0}{\rho}_{N_1 m N_1 m'} = \delta_{mm'},\ \overset{0}{\varrho}_{N_2 m N_2 m'} = 0 = \overset{0}{\varrho}_{N_1 m N_2 m'} .$$

In this particular example, the symbol "1" corresponds to a hole and the symbol "2" to a particle. We shall project out the collective state with $L = 2$ and the z-projection M via the quantity

$$A^{*}_{2M}(12) = \sum_{m_1} (-)^{m_1} (j_1 j_2;\ -m_1 m_2 | 2M) \varrho'_{1m_1 2m_2} ,$$

and via $A^{*}_{2M}(21)$. It can be shown that, in general, because of the deviation from the RPA (the second sum in eq. (10)), the non-vanishing diagonal components of the density fluctuation also exist. In fact, one finds

$$\Delta_{11} A^{*}_{2M}(11) = -\Delta_{22} A^{*}_{2M}(22) = -\frac{5}{[j_1]} \delta_{j_1 j_2} \delta(j_1{}^2 2) q_{11} q_{12} [A^{*}_{2M}(12) - A^{*}_{2M}(21)]. \tag{12}$$

Here, and in the following, we use the notation

$$q_{\alpha\beta} = \left\{ G \, \frac{1}{5} \sqrt{\frac{[j_\alpha][j_\beta]}{5 \cdot 4\pi}} \right\}^{\frac{1}{2}} (j_\alpha j_\beta; \tfrac{1}{2} - \tfrac{1}{2} | 20) v_2(\alpha\beta);$$

the symbol $\delta(j_1{}^2 2)$ denotes the vectorial condition $2j_1 \geqq 2$. In order to simplify the following equations we shall confine ourselves to the cases of $j_2 \neq j_1$ for which the diagonal components vanish identically. First, let us consider the "pure" RPA case, retaining only the first sum in eq. (10). We can write

$$\begin{aligned} \Delta_{12} \varrho'_{N_1 m_1 N_2 m_2} = & - \sum_{mm'} (\Delta V_{N_2 m_2 N_1 m_1, N_1 m N_2 m'} - \Delta V_{N_1 m N_1 m_1, N_2 m_2 N_2 m'})_{L=2} \varrho'_{N_1 m N_2 m'} \\ & - \sum_{mm'} (\Delta V_{N_2 m_2 N_1 m_1, N_2 m N_1 m'} - \Delta V_{N_2 m N_1 m_1, N_2 m_2 N_1 m'})_{L=2} \varrho'_{N_2 m N_1 m'}, \end{aligned} \quad (13)$$

$$\begin{aligned} \Delta_{21} \varrho'_{N_2 m_2 N_1 m_1} = & \sum_{mm'} (\Delta V_{N_1 m_1 N_2 m_2, N_1 m N_2 m'} - \Delta V_{N_1 m N_2 m_2, N_1 m_1 N_2 m'})_{L=2} \varrho'_{N_1 m N_2 m'} \\ & + \sum_{mm'} (\Delta V_{N_1 m_1 N_2 m_2, N_2 m' N_1 m} - \Delta V_{N_2 m' N_2 m_2, N_1 m_1 N_1 m})_{L=2} \varrho'_{N_2 m' N_1 m}, \end{aligned}$$

where the top equation corresponds to $\nu = 1$, $\nu' = 2$, and the bottom one to the reverse. The final system of equations can be greatly simplified in view of ΔV being a Wigner force and in view of our assumptions. After some Racah algebra we find

$$\Delta_{12} A^*_{2M}(12) = M^{(+)} A^*_{2M}(12) + M^{(-)} A^*_{2M}(21), \quad (14a)$$

$$\Delta_{21} A^*_{2M}(21) = -M^{(+)} A^*_{2M}(21) - M^{(-)} A^*_{2M}(12). \quad (14b)$$

Here

$$\begin{aligned} M^{(+)} &= 5W(j_1 j_1 j_2 j_2; 22) \delta(j_2{}^2 2) q_{11} q_{22} + q^2_{12}, \\ M^{(-)} &= [1 - 5W(j_1 2 2 j_1; j_2 j_2)] q^2_{12}. \end{aligned} \quad (15)$$

The symbol $W(\ldots)$ stands for the usual Racah coefficient. The first term of $M^{(+)}$ is of the "direct" type in the terminology of Brown *et al.* 14)), the other three terms, i.e., the ones proportional to q^2_{12}, are of the "exchange" type in that terminology. We can now define the energy of the collective state $\hbar\omega$ with $\Delta_{ij} = E_j{}^0 - E_i{}^0 - \hbar\omega$ by the coupled system of eq. (14). One obtains the dispersion type equation for $\hbar\omega$ in the form

$$1 = M^{(+)} \left(\frac{1}{\Delta_{12}} - \frac{1}{\Delta_{21}} \right) + \frac{M^{(+)^2} - M^{(-)^2}}{\Delta_{12} \Delta_{21}}, \quad (16)$$

or

$$1 = -\frac{2M^{(+)} \varepsilon_{21} + M^{(-)^2} - M^{(+)^2}}{\varepsilon^2_{21} - (\hbar\omega)^2}, \quad (17)$$

where $\varepsilon_{21} = E_2{}^0 - E_1{}^0 (> 0)$. Correspondence to the familiar equation is obtained if $M^{(+)} = M^{(-)} = M$, e.g., when the direct term vanishes and if the last term involving $W(j_1 2 2 j_1; j_2 j_2)$ is omitted (this term corresponds to the Hartree-Fock exchange term $\Delta V_{\kappa\nu,\nu\kappa'}$ in eq. (10)). From eq. (17) we find

$$\hbar\omega = \varepsilon_{21}\sqrt{1+\frac{2M^{(+)}}{\varepsilon_{21}}+\frac{M^{(+)^2}-M^{(-)^2}}{\varepsilon_{21}^2}}. \tag{18}$$

Let us define $\alpha^+ = M^{(+)}/G$ and $\alpha^- = M^{(-)}/G$. If $\alpha^+ > \alpha^-$, the oscillations are stable provided the coupling constant G satisfies the inequality $G < -\varepsilon_{21}(\alpha^+ + \alpha^-)^{-1} = G_1$ or $G > -\varepsilon_{21}(\alpha^+ - \alpha^-)^{-1} = G_2$; if $\alpha^+ < \alpha^-$, the stability condition is $G_1 < G < G_2$.

If we wanted to renormalize our zero-order energies so that the effect of $M^{(+)}$ would already be contained in the modified Δ_{12} (denoted as $\tilde{\Delta}_{12}$) and the analogous $\tilde{\Delta}_{21}$, we could write

$$\hbar\omega = \tilde{\varepsilon}_{21}\sqrt{1-\frac{M^{(-)^2}}{\tilde{\varepsilon}_{21}^2}},$$

where $\tilde{\varepsilon}_{21} = \varepsilon_{21} + M^{(+)}$.

If the second sum in eq. (10) (deviation from the RPA) is now taken into account, we find that its only non-vanishing contributions to the right-hand side of the first eq. (13) are the terms equal to

$$-\sum_{mm'}[(\Delta V_{N_1 m N_1 m_1, N_1 m' N_1 m})_{L=2}\varrho'_{N_1 m' N_2 m_2} - (\Delta V_{N_2 m_2 N_2 m, N_1 m N_1 m'})_{L=2}\varrho'_{N_1 m_1 N_2 m'}].$$

Since $m' = m_1$ in the first sum, and $m' = m_2$ in the second sum, we see that the above matrix elements are of the diagonal type. Their contribution is found in the form

$$\Delta M^{(+)} A^*_{2M}(12) = 5\{\delta(j_1{}^2 2)[j_1]^{-1}q_{11}^2 - [j_2]^{-1}q_{12}^2\}A^*_{2M}(12). \tag{19}$$

An analogous term $-\Delta M^{(+)}A^*_{2M}(21)$ appears in the modified eq. (14b). As a result the quantity $M^{(+)}$ defined by eq. (15) and occurring in eqs. (14) to (18) has to be replaced by $M^{(+)} + \Delta M^{(+)}$; the quantity $M^{(-)}$ remains unchanged. We see that particularly in view of the extra term $-5[j_2]^{-1}q_{12}^2$ in $\Delta M^{(+)}$, the pairing type contribution discussed here can be quite appreciable. As the contribution $\Delta M^{(+)}$ is of the "diagonal" type we can again renormalize ε_{21}, and use $\bar{\varepsilon}_{21} = \varepsilon_{21} + M^{(+)} + \Delta M^{(+)}$ in the new formula $\hbar\bar{\omega} = \bar{\varepsilon}_{21}\sqrt{1-M^{(-)^2}/\bar{\varepsilon}_{21}^2}$, but the change in ε_{21} may be quite important.

The wave function of the collective state can be written as

$$|\psi_{2M}(\omega)\rangle = \hat{Q}^*_{2M}(\omega)|\psi_0\rangle, \quad \hat{Q}^*_{2M}(\omega) = \sum_{\nu\nu'} C_{2M}(\nu\nu')\hat{A}^*_{2M}(\nu\nu'), \tag{20}$$

where $|\psi_0\rangle$ denotes the ground state, and $\hat{A}^*(\nu\nu')$ is the operator corresponding to $A^*_{2M}(\nu\nu')$ as previously defined. The usual Sawada technique is then applied in order to find the normalized coefficients of the wave function $|\psi_{2M}(\omega)\rangle$. The general case of a 2^L-pole interaction and many single-particle levels included is discussed in the Appendix.

In order to examine the usefulness of the approximation of eq. (10) resulting from factorization and from linearization of the exact eq. (9), let us go back to eq. (9). In fact, the procedure of factorization of eq. (9) leading to eq. (10) may appear not only difficult to justify for the rejection of a number of correlation terms, but also rather ambiguous. In fact, we can commute the ϱ operators as

$$\hat{\varrho}_{\nu s}\hat{\varrho}_{\kappa\kappa'} = a_s{}^\dagger a_\nu a_{\kappa'}{}^\dagger a_\kappa = \delta_{\nu\kappa'}\hat{\varrho}_{\kappa s}-\delta_{\kappa s}\hat{\varrho}_{\nu\kappa'}+\hat{\varrho}_{\kappa\kappa'}\hat{\varrho}_{\nu s}. \tag{21}$$

As a result, we can discuss another exact equation as an alternate to eq. (9)

$$\Delta_{\nu\nu'}\hat{\varrho}_{\nu\nu'}=\sum_{\kappa\kappa'}(\Delta V_{\nu'\kappa,\,\kappa\kappa'}\hat{\varrho}_{\nu\kappa'}-\Delta V_{\nu'\kappa',\,\kappa\nu}\hat{\varrho}_{\kappa\kappa'})+\sum_{\kappa\kappa' s}\hat{\varrho}_{\kappa\kappa'}(\hat{\varrho}_{s\nu'}\Delta V_{s\nu,\,\kappa\kappa'}-\hat{\varrho}_{\nu s}\Delta V_{\nu' s,\,\kappa\kappa'}). \tag{22}$$

Otherwise we can also commute the other parir of $\hat{\varrho}$-operators and obtain a similar expression. Other combinations with the $\hat{\varrho}$-operators lead to final equations redundant with eq. (10), in view of the Hartree-Fock factorization.

We observe, however, that the "vacuum" expectation value of the first sum in eq. (22) vanishes. On the other hand, the fluctuation components in that sum have no direct physical interpretation, and therefore are incompatible with the approximation method and should be rejected.

If one retained these terms, and used eq. (22) literally, one would obtain. instead of eq. (14), a system of equations of the form

$$\begin{aligned}\Delta_{12}A^*_{2M}(12) = {} & [(1-10[j_2]]^{-1}q^2_{12}+5\delta(j_1{}^22)[j_1]^{-1}q^2_{11}-5\delta(j_2{}^22)[j_2]^{-1}q^2_{22}] \\ & \times A^*_{2M}(12)+q^2_{12}A^*_{2M}(21), \\ \Delta_{21}A^*_{2M}(21) = {} & -[(1-5[j_2]^{-1}+5[j_1]^{-1})q^2_{12}+10\delta(j_1{}^22)[j_1]^{-1}q^2_{11}] \\ & \times A^*_{2M}(21)-q^2_{12}A^*_{2M}(12).\end{aligned}$$

The example of eq. (10) discussed above for the quadruple vibrations of a closed subshell indicate that utmost care has to be exercised when linearization procedures are applied to the non-linear density equations.

The very interesting case of the same type of effects in the problem of vibrations due to particle-hole interactions in an unfilled subshell in the presence of the short-range pairing force is under investigation.

Further corrections due to the deviation from linearity are also being investigated.

Note added in proof: If all the multipole terms of eq. (11) are retained then we obtain

$$B_L(\nu\nu'\kappa\kappa') = (n_{\nu'}-n_\nu)[f_L(\nu'\nu,\ \kappa\kappa')\delta(j_\nu j_{\nu'}L)(-)^{j_\nu+j_{\nu'}-j_\kappa-j_{\kappa'}} \\ +\sum_{L'}(-)^{L'}[L']W(j_\nu j_\kappa j_{\nu'}j_{\kappa'};\ L'L)f_{L'}(\kappa\nu,\ \nu'\kappa')],$$

and

$$C_L(\nu\kappa\kappa') = n_\kappa\{\sum_{L'}[L'][j_\nu]^{-1}\delta(j_\nu j_\kappa L')f_{L'}(\kappa\nu,\ \kappa'\kappa)-G(4\pi)^{-\frac{1}{2}}[j_\kappa]v_0(\nu\kappa',\ \kappa\kappa)\}.$$

The author is indebted for several stimulating discussions to Drs. Glassgold, Mottelson, Kisslinger, Baranger, and Brenig. Drs. Brown and Baranger have kindly provided the author with prepublication copies of their work.

Appendix

If we include the contributions from the entire single-particle spectrum in the case of an arbitrary 2^L-pole ($L\neq 0$) component $(\Delta V)_L$ of eq. (11) we obtain the system of equations for the density fluctuation components, following from eq. (10), in the form

$$\Delta_{\nu\nu'}A^*_{LM}(\nu\nu') = -\sum_{\kappa\kappa'}B_L(\nu\nu'\kappa\kappa')A^*_{LM}(\kappa\kappa') \\ +\sum_{\kappa\kappa'}[C_L(\nu\kappa\kappa')\delta_{j_{\kappa'}j_\nu}A^*_{LM}(\kappa'\nu')-C_L(\nu'\kappa\kappa')\delta_{j_{\kappa'}j_{\nu'}}A^*_{LM}(\nu\kappa')], \quad \text{(A.1)}$$

where

$$B_L(\nu\nu'\kappa\kappa') = (n_{\nu'}-n_\nu)[f_L(\nu'\nu,\ \kappa\kappa')\delta(j_\nu j_{\nu'}L)(-)^{j_\nu-j_{\nu'}-j_\kappa-j_{\kappa'}} \\ +(-)^L[L]W(j_\nu j_\kappa j_{\nu'}j_{\kappa'};\ LL)\delta(j_{\nu'}j_{\kappa'}L)f_L(\kappa\nu,\nu'\kappa')], \quad \text{(A.2)}$$

and

$$C_L(\nu\kappa\kappa') = n_\kappa[L][j_\nu]^{-1}\delta(j_\nu j_\kappa L)f_L(\kappa\nu,\ \kappa'\kappa), \quad \text{(A.3)}$$

with

$$f_L(\alpha\beta,\gamma\delta) = G[L]^{-1}\left\{\frac{[j_\alpha][j_\beta][j_\gamma][j_\delta]}{4\pi[L]}\right\}^{\frac{1}{2}}(j_\alpha j_\beta;\ \tfrac{1}{2}-\tfrac{1}{2}|L0)(j_\gamma j_\delta;\ \tfrac{1}{2}-\tfrac{1}{2}|L0)v_L(\alpha\beta,\ \gamma\delta).$$

All the symbols have the meaning explained in the body of the text. Here again the first sum in eq. (A-1) corresponds to the RPA, and the second sum to the deviations from it. The diagonal components are

$$\Delta_{\nu\nu}A^*_{LM}(\nu\nu) = -\sum_{\kappa\kappa'}C_L(\nu\kappa\kappa')\delta_{j_{\kappa'}j_\nu}[A^*_{LM}(\nu\kappa')-A^*_{LM}(\kappa'\nu)]. \quad \text{(A.4)}$$

The secular equation determining the energy of the collective state $\hbar\omega$ is obtained for eq. (A-1) in the form

$$\det\|M^L_{ab}\| \equiv \det\|M^L_{\nu\nu',\kappa\kappa'}\| = 0, \quad \text{(A.5)}$$

where

$$M^L_{\nu\nu',\kappa\kappa'} = \delta_{\nu\kappa}\delta_{\nu'\kappa'} + \Delta^{-1}_{\nu\nu'}\{B_L(\nu\nu'\kappa\kappa') - \sum_s C_L(\nu s\kappa)\delta_{j_\nu j_\kappa}\delta_{\kappa'\nu'} + \sum_s C_L(\nu' s\kappa')\delta_{j_{\kappa'} j_{\nu'}}\delta_{\kappa\nu}\}. \quad \text{(A.6)}$$

References

1) K. Sawada, Phys. Rev. **106** (1957) 372;
G. Wentzel, Phys. Rev. **108** (1957) 1593;
R. A. Ferrell and J. J. Quinn, Phys. Rev. **108** (1957) 570;
R. A. Ferrell, Phys. Rev. **107** (1957) 1631;
see also for nuclear applications S. Fallieros, Thesis, University of Maryland (1959)
2) Sawada, Brueckner, Fukuda and Brout, Phys. Rev. **108** (1957) 507;
R. Brout, Phys. Rev. **108** (1957) 515;
P. W. Anderson, Phys. Rev. **112** (1958) 1900
3) A. E. Glassgold, W. Heckrotte and K. M. Watson, Ann. Phys. **6** (1959) 1
4) K. Sawada and R. M. Rockmore, Phys. Rev. **116** (1959) 1618
5) S. Takagi, Prog. Theor. Phys. **21** (1959) 174
6) K. Ikeda *et al.*, Prog. Theor. Phys. **22** (1959) 663
7) B. R. Mottleson, The many body problem (John Wiley and Sons, New York, 1959); also Proc. Intern. Conf. Nuclear Structure, Kingston (1960)
8) R. Arvieu and M. Veneroni, Comptes Rendus **250** (1960) 992; 2155
9) S. T. Belyaev, Mat. Fys. Medd. Dan. Vid. Selsk. **31**, No. 11 (1959)
10) M. Kobayasi and T. Marumori, Prog. Theor. Phys. **23** (1960) 387
11) M. Baranger, Phys. Rev. **120** (1960) 957
12) L. S. Kisslinger and R. A. Sorensen, private communication from Dr. Kisslinger
13) T. Marumori, Prog. Theor. Phys. **24** (1960) 331
14) G. E. Brown, L. Castillejo and J. A. Evans, to be published
15) G. E. Brown, J. A. Evans and D. J. Thouless, Nuclear Physics (in press)
16) H. Ehrenreich and M. H. Cohen, Phys. Rev. **115** (1959) 786
17) J. Goldstone and K. Gottfried, Nuovo Cim. **13** (1959) 849
18) Tai Tsun Wu, Harvard University, Technical Report No. 321

1.D.1

Nuclear Physics **23** (1961) 296—304; ©*North-Holland Publishing Co., Amsterdam*

Not to be reproduced by photoprint or microfilm without written permission from the publisher

COMPETITION BETWEEN THE PAIRING FORCE AND THE SPIN-ORBIT FORCE IN V^{51}

M. UMEZAWA

Department of Theoretical Physics, The University, Manchester 13, England †

Received 19 September 1960

Abstract: The effect of a pairing force on configuration mixing of spin-orbit partners is estimated. It is found that the effect is comparatively large near closure of the j—j subshells, and detailed results are obtained for the ground state of V^{51}. It is shown that the calculated magnetic moment of V^{51} is considerably improved as compared with the pure j—j pairing result, but the M1 transition from the first excited state to this ground state still remains forbidden.

1. Introduction

It has been pointed out that there was a contradiction between the strongly inhibited M1 transition from the first excited state and the magnetic moment of the ground state of V^{51} (ref. [1a])). In order to explain the considerable deviation of the magnetic moment from the Schmidt line it seems necessary to admix a considerable amount of $f_{\frac{5}{2}}$ component into the proton wave function. This however then leads to a fast M1 transition from the first excited state. One way to avoid this dilemma is that the deviation from the Schmidt line would then have to be interpreted in terms of a modified magnetic moment operator. However, we wish to point out in this note that in fact the deviation of the magnetic moment of V^{51} from the Schmidt line can be accounted for by mixing a $(f_{\frac{7}{2}})^9(f_{\frac{5}{2}})^2$ configuration into the $(f_{\frac{7}{2}})^{11}$ configuration (section 4).

We also wish to show in this note that the above configuration mixing may be expected in view of the fact that the pairing energy in addition to the spin-orbit force, may be important in the ground state of nuclei. In section 4 the amount of mixing of the $(f_{\frac{7}{2}})^9(f_{\frac{5}{2}})^2$ configuration into the $(f_{\frac{7}{2}})^{11}$ configuration is calculated as a function of the depths of the spin-orbit force and of the pairing force.

In section 2 pairing energies are calculated for two extreme cases i.e., j—j pairing scheme and L—S pairing scheme. The definition of those pairing schemes is given in ref. [1]).

In section 3, the pairing energy is calculated for an intermediate coupling which is near to the j—j pairing scheme and also approximate eigenfunctions of the ground state of nuclei are given, for the above intermediate coupling.

---

† Now at Institut de Recherches Nucléaire, Université de Strasbourg.

For the sake of simplicity, we shall deal mainly in this note with only one kind of nucleon.

2. Pairing Energies and Spin-Orbit Energies in *j—j* and *L—S* pairing Scheme

We shall start with defining the following operator † in the $L-S$ coupling scheme:

$$Q = \sum_{i \neq j} q_{ij}, \tag{1}$$

with

$$(l^2LST,|q_{ij},|l^2LST) = (2l+1)\delta(L, 0)(2s+1)\delta(S, 0). \tag{2}$$

By using this operator that part of the nuclear interaction which gives rise pairing energy [2]) can be written in the following form:

$$\begin{aligned}(l^2, L = 0, S = 0|V(i, j)|l^2, L = 0, S = 0)\\ = V^0(l^2, L = 0, S = 0|q_{ij}|l^2, L = 0, S = 0). \end{aligned}\tag{3}$$

We shall compare this pairing energy due to the operator V_0Q with the effect of a spin-orbit force.

Without a spin-orbit interaction, the operator (1) is diagonal in the $L—S$ pairing scheme [1]). Among the quantum numbers defined in ref. [1]), it is only necessary to designate seniority quantum numbers $\mathscr{S}$ and $\mathscr{S}_R$, where $\mathscr{S} = \sum\lambda_{l,S}$ and $\mathscr{S}_R = \sum\lambda_R$; because the Racah operator q_{ij} has strong degeneracy in $Sp^n_{(2l+1)\times 2}$ and $R^n_{(2l+1)}$, so that the value of q_{ij} does not depend upon quantum numbers other than $\mathscr{S}$ and $\mathscr{S}_R$. (Correspondingly we designate $\mathscr{S}$ only in the $j—j$ coupling scheme).

The expectation value of Q for the state with zero seniority in a configuration l^{2n} of a system of one kind of nucleon is [3]),

$$(l^{2n}, \mathscr{S} = 0, \mathscr{S}_R = 0|Q|l^{2n}, \mathscr{S} = 0, \mathscr{S}_R = 0) = [2(2l+1)-2n+2]n. \tag{4}$$

If the spin-orbit force is so strong that a $j—j$ pairing scheme gives a better approximation, we need to calculate the expectation value of Q in the $(j_+)^{2n}$ configuration, where j_+ indicates the orbit with $j = l+\frac{1}{2}$. The expectation value of Q for the ground state of a system of $2n$ nucleons can be shown to be (see appendix)

$$(j_+{}^{2n}, \mathscr{S} = 0|Q|j_+{}^{2n}, \mathscr{S} = 0) = (2j_++1-2n+2)n. \tag{5}$$

For the ground state of the configuration $(j_+)^{2j_++1}(j_-)^{2m}$ the expectation value of Q is

$$\begin{aligned}((j_+)^{2j_++1}(j_-)^{2m}, \mathscr{S} = 0|Q|(j_+)^{2j_++1}(j_-)^{2m}, \mathscr{S} = 0)\\ = (2j_++1)+(2j_-+1-2m+2)m \end{aligned}\tag{6}$$

---

† We shall call this operator the Racah operator (see ref. [1])).

Assuming the usual one-body spin-orbit force

$$\sum_i V_{\sigma l}(\boldsymbol{\sigma}_i \cdot \mathbf{l}_i), \tag{7}$$

the spin-orbit energies of the individual nucleons in the $j-j$ coupling scheme are

$$(j_+|V_{\sigma l}(\boldsymbol{\sigma} \cdot \mathbf{l})|j_+) = \tfrac{1}{2}lV_{\sigma l}, \tag{8}$$

$$(j_-|V_{\sigma l}(\boldsymbol{\sigma} \cdot \mathbf{l})|j_-) = -\tfrac{1}{2}(l+1)V_{\sigma l}. \tag{9}$$

Thus when the spin-orbit force is so small that $(2l+1)V_{\sigma l} \ll (2l+2)V^0$, the evaluated pairing energy and spin-orbit energy of the ground state of the $(l)^{2n}$ configuration in the $L-S$ pairing scheme can be represented by the curve shown in fig. 1.

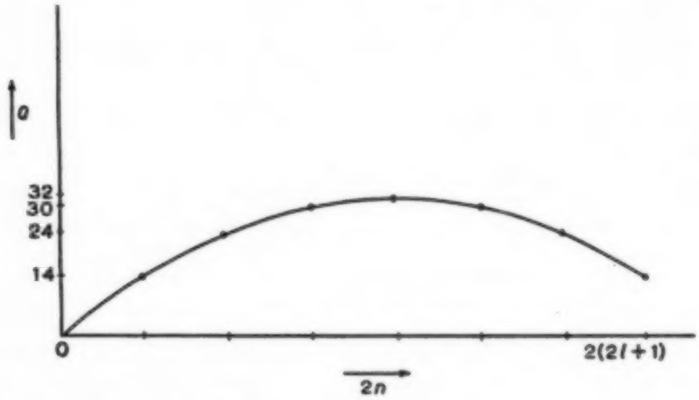

Fig. 1. The pairing energy for the ground state of the $(l)^{2n}$ configuration with $l = 3$.

If the spin-orbit coupling energy is so large that $2lV_{\sigma l} > 2(2l+1)V^0$, then the calculated pairing energy and spin orbit energy in the $j-j$ pairing scheme can be represented by the curve A and the line B shown in fig. 2.

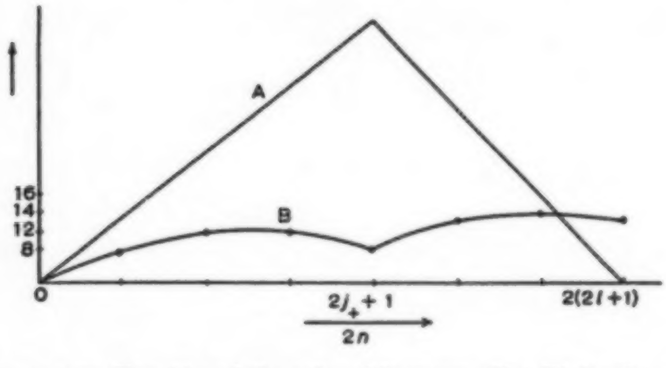

Fig. 2. The pairing energy (line A) and the spin-orbit energy (line B) for the ground state of the $(l)^{2n}$ configuration in the $j-j$ pairing scheme with $l = 3$.

3. The Intermediate Pairing Scheme

In this section we will deal with the case where the spin-orbit force is rather stronger than the pairing force, so that the eigenfunction will be represented by the intermediate pairing scheme which is near to the j—j coupling limit in most cases.

As can be seen clearly from fig. 2, when $2n$ approaches $2j_+ +1$, the pairing energy is so small in j—j coupling, that the configuration $(j_+)^{2n-2}(\ _-)^2$ becomes important since this configuration has a considerable pairing energy. This pairing energy is (see appendix)

$$\begin{aligned}((j_+)^{2n-2}(j_-)^2, \mathscr{S} = 0|Q|(j_+)^{2n-2}(j_-)^2, \mathscr{S} = 0)\\ = (2j_+ +1-2n+4)(n-1)+(2j_- +1). \quad (10)\end{aligned}$$

When $n = 2j_+ +1$ this energy is considerably bigger than the pairing energy (5) for the $(j_+)^{2j_+ +1}$ configuration. Even though the spin-orbit energy of $(j_+)^{2n-2}(j_-)^2$ is less by $(2l+1)V_{\sigma l}$ than that of the $(j_+)^{2n}$ configuration, the $(j_+)^{2n-2}(j_-)^2$ configuration will be mixed into $(j_+)^{2n}$ by a comparable amount if the spin-orbit force is such that the difference of pairing energy between the 2 configurations compensates the difference $2(2l+1)V_{\sigma l}$ in spin-orbit energy. In this case the eigenfunction will be represented by

$$a\psi((j_+)^{2n}, \mathscr{S} = 0)+b\psi((j_-)^{2n-2}(j_-)^2, \mathscr{S} = 0), \quad (11)$$

where $a^2+b^2 = 1$.

Values of a and b are determined by the diagonalization of the interaction $V^0Q+\sum_i V_{\sigma l}(\sigma_i\ , \mathbf{l}_i)$.

The operator Q is not diagonal in the j—j coupling scheme and has matrix elements between the two configurations $(j_+)^2$ and $(j_-)^2$ which for the corresponding ground states is given by (see appendix)

$$(j_+{}^2, \mathscr{S} = 0|Q|j_-{}^2\ \mathscr{S} = 0) = \sqrt{2j_+ +1}\sqrt{2j_- +1} = \sqrt{2l(2l+2)}. \quad (12)$$

In general, for more than 2 particles, the non-diagonal element of Q for the two configurations $(j_+)^{2n}$ and $(j_+)^{2n-2}(j_-)^2$ is given by

$$(j_+{}^2, \mathscr{S} = 0|Q|j_+{}^{2n-2}j_-{}^2, \mathscr{S} = 0) = \sqrt{(2j_+ +1-2n+2)(2j_- +1)n}. \quad (13)$$

Thus a and b can be obtained by diagonalizing the matrix

$$\begin{pmatrix} (2j_- +1-2n+2)nV^0+(2l+1)V_{\sigma l} & \sqrt{(2j_+ +1-2n+2)(2j_- +1)nV_0} \\ \sqrt{(2j_+ +1-2n+2)(2j_- +1)nV_0} & \{(2j_+ +1-2n+4)(n-1)+(2j_- +1)\}V_0 \end{pmatrix}. \quad (14)$$

To illustrate the above procedure we consider the case of eight neutrons in the f shell. The matrix element is then

$$\begin{pmatrix} \frac{7}{2}V_{\sigma l}+4V^0 & \sqrt{12}V^0 \\ \sqrt{12}V^0 & 9V^0 \end{pmatrix}. \quad (14')$$

Thus if $\frac{7}{2}V_{\sigma l} = 5V^0$, the wave function (11) will be a mixture of $(j_+)^{2n}$ and $(j_+)^{2n-2}(j_-)^2$ in equal amounts, i.e., $a = b$.

4. The Ground State of V^{51}

We wish to show in this section that a pairing force of the form (1) together with a spin-orbit force of the form (7) will account for the magnetic moment of V^{51}, if the magnitudes of the two forces satisfies

$$\tfrac{7}{2}V_{\sigma l} \leqq 5V^0.$$

The M1 transition still remains forbidden, as will be shown in section 5.

Since V^{51} has three protons in addition to eight closed shell neutrons, the situation is more complicated than the situation discussed for one type of nucleons in the previous section. However, it will be shown in a following paper that the interaction energy between protons and neutrons due to the pairing force of form (1) is small. Therefore, the calculation (applied only to the neutron configuration in the previous section) is still approximately true even for the case of the ground state of V^{51}. Thus the final wave function of the eleven nucleons in the f shell can be constructed by combining the above wave function of eight nucleons, with $T = 4$, with the wave function of three nucleons with $T = \frac{3}{2}$, in such a way as to produce a wave function with $T = \frac{5}{2}$. To carry out the above procedure we used a method introduced in ref. [4]).

Thus the approximate values of the magnetic moment of V^{51} can be calculated for various relative strengths of the spin-orbit to the pairing forces in the same way as in ref. [4]). Values of the magnetic moment have been calculated for four values of the ratio $V_{\sigma l}/V_0$ and are shown as a function of this ratio in fig. 3.

In fig. 3, the value 5.34 n.m. is the limiting value for $V_0/V_{\sigma l} = \infty$, i.e., in the L—S pairing limit which has previously been obtained in ref. [1]).

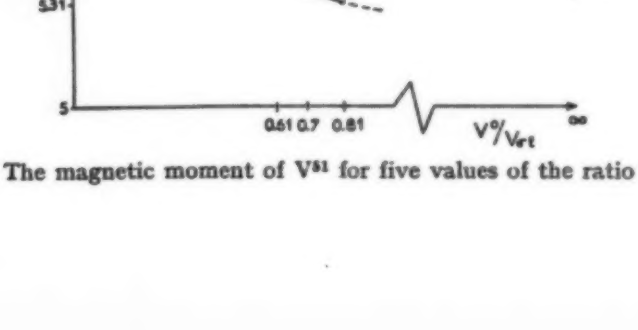

Fig. 3. The magnetic moment of V^{51} for five values of the ratio $V_0/V_{\sigma l}$.

It should be mentioned that the remaining small difference between the measured magnetic moment and the calculated magnetic moment for $V_{\sigma l}/V_0 \approx \approx \frac{10}{7}$ does not necessarily imply al arger spin orbit force than that corresponding to this value of $V_{\sigma l}/V_0$. This small residual difference could be easily accounted for by a more accurate simultaneous treatment of all eleven nucleons and the contribution from further small admixtures of the configurations

$$(j_+)^{2n-2m}(j_-)^{2m} \quad \text{with} \quad m \geqq 2.$$

It should be pointed out that the mixing of the configuration $(f_{\frac{7}{2}})^{2n-2}(p_{\frac{3}{2}})^2$ to the configuration $(f_{\frac{7}{2}})^{2n}$ due to the pairing interaction between the $p_{\frac{3}{2}}$ orbit and the f shell has not yet been estimated, even though we expect admixture to be small.

It should also be mentioned that if the condition $V_{\sigma l}/V_0 \approx \frac{10}{7}$ is satisfied then the ground state wave function for only a few particles in the f shell will be dominantly the *j*—*j* pairing wave function. For example the wave function of two nucleons is

$$0.93\,\psi(j_+)^2 + 0.38\,\psi(j_-)^2 \quad \text{for} \quad V_{\sigma l}/V_0 = \tfrac{5}{14}.$$

5. Selection Rule for the M1 Transition in V^{51}

In this section we wish to show that the M1 transition from the first excited state to the ground state of V^{51} is still strictly forbidden, because the pairing property is still preserved in the wave function of V^{51} obtained in the previous section.

The M1 transition operator can be written as follows:

$$\sqrt{\frac{3}{4\pi}}\,\frac{e\hbar}{2mc}\{\sum \tau_\zeta(a\mathbf{j}+b\boldsymbol{\sigma})+(a'\mathbf{j}+b'\boldsymbol{\sigma})\},$$

with

$$a = -\tfrac{1}{2},\quad b = \mu_n - \mu_p + \tfrac{1}{2},\quad a' = \tfrac{1}{2},\quad b' = \mu_p - \mu_n - \tfrac{1}{2},$$

where the sum is over the relevant nucleons.

Then in a similar way as an M1 transition can be shown to be forbidden in *j*—*j* coupling for one kind of nucleon [5]), it can easily be seen that the second term in (3) does not give rise to a transition. Thus the operator $\tau_\zeta j$ when applied to the following type of product for two nucleons:

$$(\sum(-1)^m \psi_m(i)\psi_m(j))\left[\frac{\alpha\beta+\beta\alpha}{\sqrt{2}} \quad \text{or} \quad \alpha\alpha \quad \text{or} \quad \beta\beta\right], \tag{15}$$

gives zero or some vector product having isobaric spin 0. It therefore increases the seniority quantum number by 2 but conserves the residual isobaric spin.

As we assume the residual isobaric spin and seniority quantum number of $\frac{3}{2}$ and 3 respectively for the first excited state, $\tau_\zeta j$ give rise to no M1 transition from this state. A little more consideration shows that an operator $\tau_\zeta \sigma$, when applied to the scalar product (15) gives either a vector product with isobaric spin 0 or transforms one nucleon in the $\frac{7}{2}$ orbit into the $\frac{5}{2}$ orbit and thus also gives no M1 transition.

6. Concluding Remarks

In section 3 it was pointed out that configuration mixing is most significant near closure of the *j—j* subshells. It is also possible to show that this result seems capable of explaining more closely the experimental nuclear magnetic moments by the following argument.

It has been proved 1) that both the *j—j* and *L—S* pairing schemes treated could explain fairly well the deviations of the nuclear magnetic moments from Schmidt lines, except in certain cases. These cases where *j—j* and *L—S* pairing schemes fail to explain the deviation of magnetic moments occur near closure of the *j—j* subshells.

We expect the configuration mixing to correct those deviations. These cases will be dealt with in a following paper, because it is necessary to deal with the system of proton and neutron simultaneously.

In this note we assume a pairing force and a spin-orbit force only. Therefore our ground states of nuclei correspond to the vacuum state in Bogoliubov's quasi-particle representzation with a nuclear force of the following kind:

$$\sum_{ij} V(x-x')\left(\tfrac{1}{2}-(\sigma_i\cdot\sigma_j)\right)+\sum V_{\sigma l}(\sigma_i\cdot l_i).$$

The relation between present work and Bogoliubov's treatment of the ground states of light nuclei with the above force will be dealt with in a following publication.

Finally the author wishes to express his sincere thanks to Dr. A. R. Bodmer for his constant interest in the present work and for valuable remarks.

Appendix

The expectation value of the Racah operator Q has been given by Racah in ref. 1) as being

$$(l^{2n}, \mathscr{S}=0, \mathscr{S}_R=0|Q|l^{2n}, \mathscr{S}=0, \mathscr{S}_R=0) = (2(2l+1)-2n+2)n. \quad (1.A)$$

To calculate the expectation value of the Racah operator for the wave function of two nucleons $\psi(j_\pm{}^2\ \mathscr{S}=0)$ we decompose this *j—j* coupling wave function into the sum of L—S coupling wave functions,

$$\begin{aligned}
&\sqrt{2(2l+1)}\psi(j_+^2, \mathscr{S}=0) \\
&\qquad = \sqrt{2j_++1}\,\psi(l^2, \mathscr{S}=0, \mathscr{S}_R=0)+\sqrt{2j_-+1}\,\psi(l^2, \mathscr{S}=2, \mathscr{S}_R=2), \\
&\sqrt{2(2l+1)}\psi(j_-^2, \mathscr{S}=0) \\
&\qquad = \sqrt{2j_-+1}\,\psi(l^2, \mathscr{S}=0, \mathscr{S}_R=0)-\sqrt{2j_++1}\,\psi(l^2, \mathscr{S}=2, \mathscr{S}_R=2).
\end{aligned}$$

It is clear from these relations that

$$\begin{aligned}
(j_+^2, \mathscr{S}=0|q_{ij}|j_+^2, \mathscr{S}=0) &= 2j_++1, \\
(j_-^2, \mathscr{S}=0|q_{ij}|j_-^2, \mathscr{S}=0) &= 2j_-+1, \\
(j_+^2, \mathscr{S}=0|q_{ij}|j_-^2, \mathscr{S}=0) &= \sqrt{(2j_++1)(2j_-+1)}.
\end{aligned} \tag{2.A}$$

In order to calculate the expectation value of the Racah operator for the $2n$ nucleon system, we first calculate a fractional percentage coefficient $(j^{2n}, \mathscr{S}=0\,\{|j^{2n-2}, \mathscr{S}=0, j^2, \mathscr{S}=0)$.

By using the well known relations

$$\begin{aligned}
&(j^{2n-1}, \mathscr{S}=1\{|j^{2n-2}, \mathscr{S}=0, j^1\, \mathscr{S}=1, \mathscr{S}=0)^2 \\
&= \frac{(2j+1-2n+2)}{(2n-1)(2j+1)}(j^{2j+1-2n+2}, \mathscr{S}=0\,\{|j^{2j+1-2n+1}, \mathscr{S}=1, j\, \mathscr{S}=1, \mathscr{S}=0)^2
\end{aligned} \tag{3.A}$$

and

$$(j_+^{2n}, \mathscr{S}=0\,\{|j_+^{2n-1}, \mathscr{S}=1, j\, \mathscr{S}=1, \mathscr{S}=0)^2=1,$$

we obtain

$$(j^{2n}, \mathscr{S}=0\,\{|j^{2n-2}, \mathscr{S}=0, j^2, \mathscr{S}=0, \mathscr{S}=0)^2=\frac{2j+1-2n+2}{(2j+1)(2n-1)}\cdot \tag{4.A}$$

Thus we obtain the expectation values of Q as follows:

$$\begin{aligned}
&(j_+^{2n}, \mathscr{S}=0|Q|j_+^{2n}, \mathscr{S}=0) \\
&= n(2n-1)(j_+^{2n}, \mathscr{S}=0\,\{|j_+^{2n-2}, \mathscr{S}=0, j_+^2, \mathscr{S}=0, \mathscr{S}=0)^2(j_+^2|q|j_+^2) \\
&= n(2j_++1-2n+2),
\end{aligned} \tag{5.A}$$

$$\begin{aligned}
&(j_-^{2n}, \mathscr{S}=0|Q|j^{2n}, \mathscr{S}=0) \\
&= n(2n-1)(j_-^{2n}, \mathscr{S}=0\,\{|j_-^{2n-2}, \mathscr{S}=0, j_-^2, \mathscr{S}=0, \mathscr{S}=0)^2(j_-^2|q_{12}|j_-^2) \\
&= n(2j_-+1-2n+2),
\end{aligned} \tag{6.A}$$

$$(j_+^{2n}, \mathscr{S} = 0|Q|j_+^{2n-2}j_-^{2}, \mathscr{S} = 0)$$

$$= n(2n-1)(j_+^{2n}, \mathscr{S} = 0\{|j_+^{2n-2}, \mathscr{S} = 0, j_+^{2}, \mathscr{S} = 0, \mathscr{S} = 0)(j_+^{2}|q_{t2}|j_-^{2})\sqrt{\frac{2}{2(2n-1)n}} \quad (7.A)$$

$$= \sqrt{n(2j_+ +1-2n+2)(2j_- +1)}.$$

The other equations needed in this paper are easily derived by using the same methods.

References

1) M. Umezawa, Proc. Roy. Soc. A **232** (1955) 88
1a) See letter to Nuclear News (June 1960)
2) G. T. Belyaev, Mat. Fys. Dan. Vid. Selsksk. Medd. **31**, No. 11 (1959);
M. Baranger, Phys. Rev. (to be published)
3) G. Racah, Phys. Rev. **63** (1943) 367
4) M. Umezawa, Prog. Theor. Physics. **8** (1952) 509
5) See, e.g., Nuclear News (March 1960)

1.D.1

Nuclear Physics **23** (1961) 305—311; © *North-Holland Publishing Co., Amsterdam*

Not to be reproduced by photoprint or microfilm without written permission from the publisher

SPECTROSCOPIC CALCULATION OF ENERGY LEVELS OF SOME TIN ISOTOPES

J. B. SANDERS
Institute-Lorentz, University of Leyden, Leyden, The Netherlands

Received 24 October 1960

Abstract: Energy-levels of a series of isotopes of tin are calculated. Configuration mixing is taken into account. A reasonable fit with the experimental data is obtained and mixing ratios for wave-functions are also found.

1. Introduction

Recently the modern shell model approach to the calculation of nuclear energy levels has been applied with a great deal of success to heavier nuclei [1]).

In this report an analogous approach is applied to a series of isotopes of tin, which has a magic proton number 50. We take those isotopes into consideration where the wave functions of the neutrons are a mixture of the states $3s_{\frac{1}{2}}{}^{+}$, $2d_{\frac{3}{2}}{}^{+}$, $1h_{\frac{11}{2}}{}^{-}$. This means that we use the ground state of ${}_{50}\mathrm{Sn}_{64}^{114}$ as the zero point of our energy scale and subtract the binding energy of this nucleus from the binding energies or energies of excited levels of those nuclei whose binding energies or excited levels we wish to calculate. We assume, as in the previous work [1]), that the potential energy of the nucleus is due to two-body effective interactions between nucleons. The unknown matrix elements of those interactions, taken to be the same for all nuclei in which the same subshells are being filled, are determined by comparison with the experimental data. We incorporate configuration interaction into this approach by taking non-diagonal matrix elements as unknown quantities which also have the same values throughout the same subshells. These are determined, along with the diagonal elements by comparison with the experimental data. The calculation is considered to be successful if a certain number of such matrix elements reproduce accurately a larger number of experimental energies.

An additional assumption which is made here is that the seniority is taken to be a good quantum number for the neutron shells being filled. This assumption for which there is justification in view of the results, obtained with these calculations in other regions [1]) and which is consistent [2]) with the hypothesis, generally made, that the internucleon forces are of very short range, drastically limits the number of *j—j* coupled states which have to be taken into account when we want to find the actual eigenstates of the nuclei, and this of course implies a great simplification in the mathematics of the problem. We consider only those states of which the wave functions have seniorities either 0 or 1. This means that of the even nuclei we calculate only the levels with spin 0^+ and of the odd ones those with spin $\frac{1}{2}^+$, $\frac{3}{2}^+$ or $\frac{11}{2}^-$. It is impossible to write the wave functions of other levels with seniority 0 or 1.

2. Discussion of Experimental Data and Results

The interaction energies which we want to calculate are the following: A_s (interaction of neutron in state $s_{\frac{1}{2}}{}^+$ with the core), A_d (interaction of neutron in state $d_{\frac{3}{2}}{}^+$ with the core), A_h (interaction of neutron in state $h^-_{\frac{11}{2}}$ with the core). These are single-particle energies.

N. Zeldes 8) demonstrates how for states with *seniority* $v = 0$ or 1 the interaction energy of j^n equivalent nucleons can be represented by the expression $\frac{1}{2}n(n-1)a+[\frac{1}{2}n]b$. Here a and b are linear combinations of the interaction energies $\langle j^2|V|j^2\rangle$ coupled to 0, 2 . . .. So we have for the interactions between equivalent neutrons the following parameters: c (for the interaction between two neutrons in state $s_{\frac{1}{2}}{}^+$), a', b' (for the interaction between two neutrons in state $d_{\frac{3}{2}}{}^+$), a'', b'' (for the interaction between two neutrons in state $h_{\frac{11}{2}}{}^-$). Next we have the interaction between neutrons in different states. w_{sd} is the interaction between one neutron $s_{\frac{1}{2}}{}^+$ and two in the state $d_{\frac{3}{2}}{}^+$ coupled to 0, this being equal to the interaction energy between one neutron in state $d_{\frac{3}{2}}{}^+$ and two in state $s_{\frac{1}{2}}{}^+$ (of course coupled to 0). w_{sh} and w_{dh} are analogous parameters for the interaction between states $s_{\frac{1}{2}}{}^+$ and $h_{\frac{11}{2}}{}^-$ resp. $d_{\frac{3}{2}}{}^+$ and $h_{\frac{11}{2}}{}^-$.

These are the parameters that appear in the expressions for the diagonal elements of the energy matrices.

Then we have the off-diagonal matrix elements $\langle s^2|V|d^2\rangle$, $\langle s^2|V|h^2\rangle$ and $\langle d^2|V|h^2\rangle_0$. Here, V is the operator for the interparticle interaction and as the eigenfunctions of states with pure j—j configurations are not eigenfunctions of this operator, these matrix elements are different from 0 and cause mixing between different j—j configurations in the actual wave functions of the nuclei. Preliminary results of the calculation have shown that it is justified to make the approximation $\langle s^2|V|h^2\rangle = 0$ and $\langle s^2|V|d^2\rangle = \langle d^2|V|h^2\rangle_0$.

The actual numerical calculation has been done by using the WEIZAC electronic computer. We start with certain initial values of the parameters, substitute these in the theoretical expressions for the matrices and diagonalize them. The computer programme gives then also the linearized and normalized equations for the parameters, to be used in a least squares fit on the experimental data. We then diagonalize again with these improved parameters and so on until we get the best possible fit of the calculated eigenvalues with the experimental data. The calculation also yields the ratios in which for each eigenvalue the different j—j coupling eigenfunctions are mixed.

The binding energies we used have been found from a table of atomic masses compiled by Nier [3]) and the excited levels with spins have been taken from the Nuclear Data Sheets [4]). Unfortunately the experimental errors on the measurements of the atomic masses are rather big, which causes great uncertainties in the values we found for the different interaction parameters. (Cf. tables 1 and 2).

TABLE 1

Calculated and experimental energy levels in MeV

Nucleus	J^π	Calculated	Experimental (with error)	Ratios of different *j—j* configurations
Sn^{115}	$\frac{1}{2}^+$	8.472	8.563 ± 0.512	s 100 %
Sn^{116}	0^+	17.562	17.721 ± 0.381	s^2 28 %, d^2 7 %, h^2 65 %
Sn^{117}	$\frac{1}{2}^+$	25.012	24.943 ± 0.363	sd^2 40 %, sh^2 60 %
	$\frac{3}{2}^+$	24.931	24.783 ± 0.363	s^2d 90 %, h^2d 7 %, d^3 3 %
	$\frac{11}{2}^-$	24.765	24.623 ± 0.363	s^2h 20 %, d^2h 7 %, h^3 73 %
Sn^{118}	0^+	34.135	33.990 ± 0.419	s^2d^2 22 %, s^2h^2 4 %, d^4 2 %, d^2h^2 12 %, h^4 60 %
Sn^{119}	$\frac{1}{2}^+$	41.049	41.035 ± 0.381	d^4s 20 %, d^2h^2s 73 %, h^4s 7 %
	$\frac{3}{2}^+$	40.974	41.011 ± 0.381	s^2d^3 35 %, h^2d^3 1 %, s^2h^2d 22 %, h^4d 43 %
	$\frac{11}{2}^-$	40.928	40.946 ± 0.381	s^2d^2h 15 %, s^2h^3 2 %, d^4h 5 %, d^2h^3 72 %, h^5 6 %
Sn^{120}	0^+	49.917	49.997 ± 0.409	s^2d^4 5 %, $s^2d^2h^2$ 5 %, s^2h^4 1 %, d^4h^2 0 %, d^2h^4 33 %, h^6 56 %
Sn^{121}	$\frac{3}{2}^+$	56.304	56.278 ± 0.354	$s^2d^3h^2$ 9 %, s^2d^4 1 %, d^3h^4 47 %, dh^6 42 %
Sn^{122}	0^+	64.964	64.962 ± 0.409	$s^2d^4h^2$ 8 %, $s^2d^2h^4$ 0 %, s^2h^6 0 %, d^2h^6 66 %, h^8 11 %
Sn^{123}	$\frac{11}{2}^-$	71.024	70.941 ± 0.475	$s^2d^4h^3$ 6 %, $s^2d^2h^5$ 9 %, s^2h^7 0 %, d^4h^5 6 %, d^2h^7 79 %, h^9 0 %
	$\frac{3}{2}^+$	71.087	70.941 ± 0.475	$s^2d^3h^4$ 0 %, s^2dh^6 2 %, d^3h^6 80 %, dh^8 18 %
Sn^{124}	0^+	79.291	79.443 ± 0.366	$s^2d^4h^4$ 4 %, $s^2d^2h^6$ 10 %, s^2h^8 0 %, d^4h^6 84 %, d^2h^8 2 %, h^{10} 0 %
Sn^{125}	$\frac{11}{2}^-$	85.139	84.992 ± 0.468	$s^2d^4h^5$ 1 %, $s^2d^2h^7$ 3 %, s^2h^9 0 %, d^4h^7 73 %, d^2h^9 23 %, h^{11} 0 %
	$\frac{3}{2}^+$	84.872	84.962 ± 0.568	$s^2d^3h^6$ 0 %, s^2dh^8 1 %, d^3h^8 93 %, dh^{10} 6 %
Sn^{126}	0^+	92.938	92.660 ± 0.435	$s^2d^4h^6$ 0 %, $s^2d^2h^8$ 2 %, s^2h^{10} 0 %, d^4h^8 81 %, d^2h^{10} 17 %, h^{12} 0 %
Sn^{127}	$\frac{11}{2}^-$	98.431	98.730 ± 0.521	$s^2d^4h^7$ 0 %, $s^2d^2h^9$ 1 %, s^2h^{11} 0 %, d^4h^9 92 %, d^2h^{11} 7 %
Sn^{128}	0^+	105.679	105.534 ± 0.491	$s^2d^4h^8$ 0 %, $s^2d^2h^{10}$ 1 %, s^2h^{12} 0 %, d^4h^{10} 94 %, d^2h^{12} 5 %

Root mean square deviation $\sqrt{\frac{\Sigma \Delta_i^2}{n-k}} = 0.22$, n is the number of data, k the number of parameters

TABLE 2

Values of parameters

A_s	8.472 ± 0.503	b''	1.741 ± 0.218
A_d	6.995 ± 0.308	w_{sd}	1.106 ± 0.698
A_h	7.835 ± 0.258	w_{sh}	-1.382 ± 0.668
c	-0.265 ± 0.500	w_{dh}	0.286 ± 0.229
a'	-0.360 ± 0.167	$\langle s^2 \vert V \vert d^2 \rangle$	1.035 ± 0.311
b'	0.549 ± 0.306	$\langle d^2 \vert V \vert h^2 \rangle$	1.035 ± 0.311
a''	-0.316 ± 0.063		

Due to this fact we can draw about these values only the qualitative conclusion that they are not essentially different from what could be expected on the basis of previous calculations [1, 5, 6]). More interesting is the conclusion we can draw from the mixing ratios we found for the wave functions of the nuclei we considered. We find then that in the ground state wave functions the component with greatest weight is the one with the neutrons in the states $d_{\frac{3}{2}}{}^{+}$ and $h_{\frac{11}{2}}{}^{-}$ and not in the state $s_{\frac{1}{2}}{}^{+}$.

The fit of the calculated with the experimental energy values is rather good in most cases. The deviation is almost everywhere smaller than the error of measurement and furthermore the result is consistent, i.e. in each case the experimental value fits with the lowest eigenvalue of the corresponding matrix, so we do not find any "states below the ground state".

We find that the different possible states we have taken into account are very strongly mixed.

3. Prediction of Levels

The other eigenvalues of the energy matrices, found by diagonalization, should correspond to excited levels of the nuclei which are not yet found. We will therefore in table 3 give a list of these eigenvalues for every nucleus. The lowest calculated level is given the value 0 and the other numbers give the heights of the other levels above the lowest one. Furthermore we have calculated with the parameters listed in table 2 some eigenvalues corresponding to unobserved levels (table 4).

TABLE 3

Predicted excited levels

Nucleus	J^{π}	Energy (MeV)
Sn^{115}	$\frac{1}{2}^{+}$	0
Sn^{116}	0^{+}	0, 0.733, 4.027
Sn^{117}	$\frac{1}{2}^{+}$	0, 2.109
Sn^{117}	$\frac{3}{2}^{+}$	0, 0.486, 4.723
Sn^{118}	0^{+}	0, 0.658, 2.651, 4.076, 7.628
Sn^{119}	$\frac{1}{2}^{+}$	0, 2.923, 4.027
Sn^{119}	$\frac{11}{2}^{-}$	0, 0.776, 2.482, 4.550, 6.143
Sn^{120}	0^{+}	0, 0.784, 2.555, 3.420, 5.232, 6.784
Sn^{121}	$\frac{3}{2}^{+}$	0, 0.449, 2.064, 4.087
Sn^{122}	0^{+}	0, 0.828, 2.954, 4.325, 5.088, 9.690
Sn^{123}	$\frac{3}{2}^{+}$	0, 1.308, 2.681, 6.571
Sn^{123}	$\frac{11}{2}^{-}$	0, 0.826, 2.511, 4.615, 5.481, 11.092
Sn^{124}	0^{+}	0, 1.166, 2.908, 5.845, 6.977, 13.362
Sn^{125}	$\frac{11}{2}^{-}$	0, 1.428, 2.806, 6.721, 7.927, 15.157
Sn^{125}	$\frac{3}{2}^{+}$	0, 2.572, 3.984, 9.532
Sn^{126}	0^{+}	0, 2.021, 3.555, 8.259, 9.657, 17.644
Sn^{127}	$\frac{11}{2}^{-}$	0, 2.526, 3.908, 9.471, 19.733
Sn^{128}	0^{+}	0, 3.224, 4.795, 11.105, 22.292

For the first three of these sets of eigenvalues we have to make the comment that the lowest one of each of them lies slightly lower than the ground state of the corresponding nucleus. Thus we find here a small inconsistency, which however is appreciately smaller than the uncertainties in the experimental data and consequently in the parameters with which we have diagonalized the energy matrices of these states. It may be hoped therefore that when this calculation will be repeated with more accurate experimental data these inconsistencies will disappear.

TABLE 4

Calculated excited levels

Nucleus	J^π	Energy (MeV)
Sn^{121}	$\frac{1}{2}^+$	56.384, 53.692, 51.102
Sn^{121}	$\frac{11}{2}^-$	56.383, 55.643, 54.036, 52.864, 51.986, 48.707
Sn^{123}	$\frac{1}{2}^+$	71,055, 68.094, 63.220
Sn^{125}	$\frac{1}{2}^+$	84.906, 80.854, 74.007
Sn^{127}	$\frac{1}{2}^+$	97.677, 92.981, 92.067
Sn^{127}	$\frac{3}{2}^+$	97.586, 93.618, 92.061, 84.943

This work was financially supported by the Lorentz fund. It forms part of the research programme of the "Stichting voor Fundamenteel Onderzoek der Materie" (F.O.M.) which is financially supported by the Netherlands Organisation for pure scientific research (Z.W.O.). The author wishes to express his gratitude to the Weizmann Institute of Science, Rehovoth, Israel, for its hospitality and to thank Professor I. Talmi, Mr. I. Unna and Dr. A. S. Reiner for many instructive discussions.

Appendix

In this appendix we shall show how the energy matrices are constructed. To illustrate the method, we take as an example the nucleus Sn^{123} with $J = \frac{11}{2}^-$. We have made the hypothesis that the seniority always has the lowest possible value, so in this case $v = 1$. As is well known this means that all particles except one are coupled to pairs with resulting angular momentum 0. In Sn^{123} we have nine neutrons outside the core. For $J = \frac{11}{2}^-$ the following configurations can then be components of the actual wave function of the nucleus: $s^2d^4h^3$, $s^2d^2h^5$, s^2h^7, d^4h^5, d^2h^7, h^9. Between these functions we have to construct the energy-matrix. Let us consider first the diagonal elements of this matrix. These can be written as [1,8]).

$$n_1 A_s + n_2 A_d + n_3 A_h + \delta_{n_1,2} c + \tfrac{1}{2} n_2(n_2-1)a' + [\tfrac{1}{2}n_2]b' + \tfrac{1}{2}n_3(n_3-1)a''$$
$$+[\tfrac{1}{2}n_3]b'' + \tfrac{1}{2}n_1 n_2 w_{sd} + \tfrac{1}{2}n_1 n_3 w_{sh} + \tfrac{1}{2}n_2 n_3 w_{dh}.$$

The meaning of these parameters has been explained above. n_1, n_2 and n_3 are the number of particles in respectively the states $s_{\frac{1}{2}}^+$, $d_{\frac{3}{2}}^+$ and $h_{\frac{11}{2}}^-$ $(n_1+n_2+n_3 = 9)$. We suppose that the configuration mixing is caused by the two-body interaction operator V_{ij} which is the interaction between two neutrons outside the closed shells. So in the j—j representation the matrix is not diagonal in this operator. Now consider for example the non-diagonal element

$$\langle \mathrm{s}^{n_1}\mathrm{d}^{n_2}\mathrm{h}^{n_3}| \sum V_{ij}|\mathrm{s}^{n_1}\mathrm{d}^{n_2+2}\mathrm{h}^{n_3-2}\rangle_{\frac{11}{2}}.$$

The wave functions at both sides of the element are antisymmetric in the equivalent particles. The expression we have written down is actually a sum of matrix elements for 2-body interactions between all particles.Inthis particular case we need only that V_{ij} which acts between the states h^2 and d^2, because in the matrix element of every other term we have an integration over different orthogonal wave functions without an operator between them, so the term is automatically zero. Consider, e.g., in the above element the interaction between the two particles in the state s. If we write this interaction explicitly we get

$$\int \psi^*(\mathrm{s}^2)V\psi(\mathrm{s}^2)\cdot\psi^*(\mathrm{d}^{n_2}\mathrm{h}^{n_3})\psi(\mathrm{d}^{n_2+2}\mathrm{h}^{n_3-2})\mathrm{d}\tau_1\ldots\mathrm{d}\tau_{n_1+n_2+n_3}=0$$

because of the orthogonality between the last pair of wave functions. So we expand the functions on both sides of the element with the help of c.f.p. (coefficients of fractional parentage), on the left for the h, on the right for the d. These expansions, written explicitly are respectively

$$\sum_{J^{\mathrm{I}},\,J^{\mathrm{II}}}(\mathrm{h}^2(J^{\mathrm{I}})\mathrm{h}^{n_3-2}(J^{\mathrm{II}})\tfrac{11}{2}|\}\mathrm{h}^{n_3}\tfrac{11}{2})\psi(\mathrm{s}^{n_1}\mathrm{d}^{n_2}\mathrm{h}^2(J^{\mathrm{I}})\mathrm{h}^{n_3-2}(J^{\mathrm{II}})\tfrac{11}{2})$$

and

$$\sum_{J^{\mathrm{III}},\,J^{\mathrm{IV}}}(\mathrm{d}^2(J^{\mathrm{III}})\mathrm{d}^{n_2}(J^{\mathrm{IV}})0|\}\mathrm{d}^{n_2+2}(0))\psi(\mathrm{s}^{n_1}\mathrm{d}^2(J^{\mathrm{III}})\mathrm{d}^{n_2}(J^{\mathrm{IV}})(0)\mathrm{h}^{n_3-2}(\tfrac{11}{2})).$$

It is evident that n_2 can only have the values 0 or 2. Here we take it to be 2 and J^{III} and J^{IV} can only be 0 or 2. We now form the matrix element of the 2-body interaction between these two expansions.

The wave functions on the left- and right hand side are sums of eigenstates of resp. $\mathrm{h}^2_{\frac{11}{2}}$ and $\mathrm{d}^2_{\frac{3}{2}}$ coupled to all possible values. As of course the J on both sides has to be the same, it can only have the values 0 or 2. But if we separate off on the left- and right hand side of the matrix element d^2, resp. h^2 coupled to 2, we have always in the calculation of the element an integration of the form

$$\int \psi^*(\mathrm{s}^{n_1}_{\frac{1}{2}}\mathrm{d}^2_{\frac{3}{2}}(0)\mathrm{h}^{n_3-2}_{\frac{11}{2}}(\tfrac{11}{2}))\psi(\mathrm{s}^{n_1}_{\frac{1}{2}}\mathrm{d}^2_{\frac{3}{2}}(2)\mathrm{h}^{n_3-2}_{\frac{11}{2}}(\tfrac{11}{2}))\mathrm{d}\tau=0.$$

So the off-diagonal element $\langle \mathrm{d}^2(2)|V|\mathrm{h}^2(2)\rangle$ does not occur in the theoretical expressions of our matrices.

To make the whole expression completely antisymmetric we have now still only to multiply with the factor $\sqrt{\frac{1}{2}n_3(n_3-1)}\cdot\sqrt{\frac{1}{2}n_2(n_2-1)}$ so as to avoid selecting one special pair in state h^2 on one side and d^2 on the other. The final result is

$$\langle s_{\frac{1}{2}}^{n_1} d_{\frac{3}{2}}^{n_2} h_{\frac{11}{2}}^{n_3} | \sum V_{ij} | s_{\frac{1}{2}}^{n_1} d_{\frac{3}{2}}^{n_2+2} h_{\frac{11}{2}}^{n_3-2} \rangle_{\frac{11}{2}}$$
$$= \sqrt{\tfrac{1}{2}n_2(n_2-1)}\sqrt{\tfrac{1}{2}n_3(n_3-1)}\,(d_{\frac{3}{2}}^{2}(0)d_{\frac{3}{2}}^{2}(0)0|\}d_{\frac{3}{2}}^{4}(0))$$
$$(h_{\frac{11}{2}}^{2}(0)h_{\frac{11}{2}}^{n_3-2}(\tfrac{11}{2})\tfrac{11}{2}|\}h_{\frac{11}{2}}^{n_3}\tfrac{11}{2})\langle h^2|V|d^2\rangle_0.$$

All other non-diagonal matrix elements can be found in completely the same way. The c.f.p. have been calculated with the help of the results of Schwartz and de-Shalit [7]).

References

1) I. Unna and I. Talmi, Nuclear Physics **19** (1960) 225
2) B. Mottelson, in The many-body problem (Dunod, Paris, 1958) p. 283
3) A. O. Nier (private communication)
4) Nuclear Data Sheets (National Research Council, Washington, D.C.)
5) I. Unna and I. Talmi, Phys. Rev. **112** (1958) 452
6) I. Talmi and S. Goldstein, Phys. Rev. **105** (1957) 995
7) C. Schwartz and A. de-Shalit, Phys. Rev. **94** (1954) 1257
8) N. Zeldes, Nuclear Physics **7** (1958) 27

Nuclear Physics **23** (1961) 312—318; ©*North-Holland Publishing Co., Amsterdam*

Not to be reproduced by photoprint or microfilm without written permission from the publisher

A NOTE ON PHOTO-MESONS FROM DEUTERONS

V. DEVANATHAN and G. RAMACHANDRAN
A. C. College of Technology, University of Madras, India

Received 26 October 1960

Abstract: The cross-sections for the photo-production of positive pions from deuterons are worked out under impulse approximation using Chew-Low amplitude of photopion production from nucleons. The numerical results obtained are in reasonable agreement with experimental data.

1. Introduction

Chew and Lewis [1]) and later Lax and Feshbach [2]) studied the photo production of pions from deuterons under the impulse approximation using a phenomenological approach, assuming for the amplitude of photo-production of pion from nucleon a general struture $(\boldsymbol{\sigma}\cdot\boldsymbol{\varkappa}+L)$ where the first term represents the spin dependent and the second the non-spin dependent part. Since the complete amplitude for photo-pion production from nucleons [3]) is now available, we use it to derive the cross-sections for photo production of positive pions from deuterons. Numerical evaluation of cross-sections is possible in this case as the expressions involve only the known quantities: the pion-nucleon scattering phase shifts and overlap integrals. The scattering phase-shifts can be obtained either by using the solutions of Salzman and Salzman [4]) or from experimental data. The overlap integrals are evaluated using Hulthen wave function for the deuteron. The energy spectrum of mesons for a given production angle and also the angular distribution of mesons are obtained for the incident photon of energy 320 MeV and the agreement with the experimental results [5,6]) is satisfactory.

2. Evaluation of the Matrix Element

The amplitude for the photo-production of π^+ by a proton can be written as (retaining only the dominant terms) †

$$T=\frac{2\pi}{\sqrt{\mu_0\nu_0}}ef\sqrt{2}\left[\frac{1}{1+\dfrac{\mu_0}{M}}\left\{i\boldsymbol{\sigma}\cdot\boldsymbol{\varepsilon}+\frac{2i\boldsymbol{\sigma}\cdot(\boldsymbol{\nu}-\boldsymbol{\mu})\boldsymbol{\mu}\cdot\boldsymbol{\varepsilon}}{(\boldsymbol{\nu}-\boldsymbol{\mu})^2+1}\right\}\right.$$
$$\left.+i\boldsymbol{\sigma}\cdot(\boldsymbol{\mu}\times(\boldsymbol{\nu}\times\boldsymbol{\varepsilon}))\lambda h^{--}+\boldsymbol{\mu}\cdot(\boldsymbol{\nu}\times\boldsymbol{\varepsilon})\lambda h^{-+}\right], \quad (1)$$

---

† We use natural units in which $\hbar = c = 1$ and the pion mass $= 1$. We follow the same notation as in ref. [1]) and [3]).

where

$$\lambda = \frac{\mu_p - \mu_n}{4Mf^2},$$

$$h^{--} = \tfrac{1}{3}(h_{11} - h_{13} - h_{31} + h_{33}),$$

$$h^{-+} = -\tfrac{1}{3}(h_{11} + 2h_{13} - h_{31} - 2h_{33}),$$

$$h_{11} = \frac{e^{i\delta_{11}} \sin \delta_{11}}{\mu^3}, \quad h_{31} = h_{13} = \frac{e^{i\delta_{13}} \sin \delta_{13}}{\mu^3}, \quad h_{33} = \frac{e^{i\delta_{33}} \sin \delta_{33}}{\mu^3}.$$

The quantities μ_p, μ_n are the magnetic moments of proton and neutron respectively, $\boldsymbol{\nu}$ is the momentum of the photon, ν_0 its energy, $\boldsymbol{\varepsilon}$ its polarisation, $\boldsymbol{\mu}$ is the momentum of the outgoing meson, μ_0 its energy, $\boldsymbol{\sigma}$ is the spin operator for the nucleon and δ_{11}, δ_{13}, δ_{33} are the phase-shifts of meson-nucleon scattering. Since δ_{33} dominates, we shall neglect h_{11}, h_{13} and h_{31} and take into account only h_{33}.

We apply the above amplitude to the case of deuteron and follow essentially the approach of Chew and Lewis. In the impulse approximation, the matrix element for the process can be written as

$$\langle \mathrm{f} | T_1 e^{i(\boldsymbol{\nu}-\boldsymbol{\mu}) \cdot \mathbf{r}_1} \tau_1^{+} + T_2 e^{i(\boldsymbol{\nu}-\boldsymbol{\mu}) \cdot \mathbf{r}_2} \tau_2^{+} | \mathrm{i} \rangle. \tag{2}$$

The subscripts 1 and 2 represent the nucleons in the deuterons and τ^+ is an operator which gives 1 for a proton and 0 for a neutron. $(\boldsymbol{\nu}-\boldsymbol{\mu})$ represents the transfer of momentum to the nucleon and $\mathbf{r}_1$ and $\mathbf{r}_2$ the position coordinates of the nucleons 1 and 2. The initial state of the deuteron can be represented by

$$|\mathrm{i}\rangle = 2^{-\frac{1}{2}}[p(1)n(2) - p(2)n(1)]\,{}^3\chi_m \frac{u(\rho)}{\rho} (2\pi)^{-\frac{3}{2}}. \tag{3}$$

The final state consists of two neutrons which may either be symmetric or antisymmetric in space

$$|\mathrm{f_e}\rangle = (2\pi)^{-\frac{3}{2}} n(1)n(2)\,{}^1\chi_0 u_{t,\mathrm{e}}(\mathbf{k} \cdot \boldsymbol{\varrho}) e^{i(\boldsymbol{\nu}-\boldsymbol{\mu}) \cdot \mathbf{R}}, \tag{4a}$$

$$|\mathrm{f_0}\rangle = (2\pi)^{-\frac{3}{2}} n(1)n(2)\,{}^3\chi_{m'} u_{t,0}(\mathbf{k} \cdot \boldsymbol{\varrho}) e^{i(\boldsymbol{\nu}-\boldsymbol{\mu}) \cdot \mathbf{R}}. \tag{4b}$$

In the above, $\mathbf{k}$ is the relative momentum of the two neutrons $\boldsymbol{\varrho} = \mathbf{r}_1 - \mathbf{r}_2$ and $\mathbf{R} = \frac{1}{2}(\mathbf{r}_1 + \mathbf{r}_2)$.

The matrix elements for the symmetric and antisymmetric cases reduce to

$$Q_\mathrm{e} = 2^{-\frac{1}{2}} \langle {}^1\chi_0 | T_1 - T_2 | {}^3\chi_m \rangle \mathrm{E}, \tag{5a}$$

$$Q_\mathrm{o} = 2^{-\frac{1}{2}} \langle {}^3\chi_{m'} | T_1 + T_2 | {}^3\chi_m \rangle \mathrm{O}, \tag{5b}$$

where

$$\mathrm{E} = \int u^{*}_{\mathbf{f},\mathrm{e}}(\mathbf{k}\cdot\boldsymbol{\varrho}) \cos(\mathbf{k}_0\cdot\boldsymbol{\varrho}) \left[\frac{u(\rho)}{\rho}\right] \mathrm{d}\boldsymbol{\varrho}, \tag{6a}$$

$$\mathrm{O} = \int u^{*}_{\mathbf{f},\mathrm{o}}(\mathbf{k}\cdot\boldsymbol{\varrho}) \sin(\mathbf{k}_0\cdot\boldsymbol{\varrho}) \left[\frac{u(\rho)}{\rho}\right] \mathrm{d}\boldsymbol{\varrho}, \tag{6b}$$

with $\mathbf{k}_0 = \frac{1}{2}(\boldsymbol{\nu}-\boldsymbol{\mu})$.
To evaluate the above matrix elements, we neglect the motion of the nucleons in the deuteron and choose for the operator T the expression (1) which for a particular state of polarisation of the photon, say ε_x, can be conveniently written in the form

$$T = A_x\sigma_+ + B_x\sigma_- + C_x\sigma_z + D_x. \tag{7}$$

We choose for our frame of reference the direction of propagation of the photon as Z-axis and the plane which contains the vectors $\boldsymbol{\nu}$ and $\boldsymbol{\mu}$ as x—z plane. Let θ be the angle between $\boldsymbol{\nu}$ and $\boldsymbol{\mu}$.

Squaring, summing over final states and averaging over initial spin states and photon polarisations, we obtain

$$|\langle {}^1\chi_0|T_1-T_2|{}^3\chi_m\rangle|^2 = \tfrac{2}{3}(|A|^2+|B|^2+2|C|^2), \tag{8a}$$

$$|\langle {}^3\chi_{m'}|T_1+T_2|{}^3\chi_m\rangle|^2 = \tfrac{4}{3}(|A|^2+|B|^2+2|C|^2+3|D|^2), \tag{8b}$$

$$\begin{aligned} |Q|^2 &= |Q_{\mathrm{e}}|^2+|Q_{\mathrm{o}}|^2 \\ &= \tfrac{1}{3}(|A|^2+|B|^2+2|C|^2)|\mathrm{E}|^2+\tfrac{2}{3}(|A|^2+|B|^2+2|C|^2+3|D|^2)|\mathrm{O}|^2, \end{aligned} \tag{9}$$

where

$$|A|^2 = \tfrac{1}{2}\{|A_x|^2+|A_y|^2\}, \quad |B|^2 = \tfrac{1}{2}\{|B_x|^2+|B_y|^2\},$$
$$|C|^2 = \tfrac{1}{2}\{|C_x|^2+|C_y|^2\}, \quad |D|^2 = \tfrac{1}{2}\{|D_x|^2+|D_y|^2\}.$$

Subscripts x and y correspond to photon polarisations ε_x and ε_y

3. Cross-Section

The cross-section is given by

$$\frac{\mathrm{d}\sigma}{\mathrm{d}\boldsymbol{\mu}\mathrm{d}\mathbf{k}} = (2\pi)^{-2}|Q|^2\delta\left(\mu_0+\frac{k^2+k_0^2}{M}+\varepsilon-\nu_0\right), \tag{10a}$$

or

$$\frac{\mathrm{d}\sigma}{\mathrm{d}\Omega\mathrm{d}\mu_0} = (2\pi)^{-2}\mu\mu_0\int |Q|^2\delta\left(\mu_0+\frac{k^2+k_0^2}{M}+\varepsilon-\nu_0\right)\mathrm{d}\mathbf{k}, \tag{10b}$$

where ε is the binding energy of the deuteron (2.226 MeV) and k^2/M is the final relative kinetic energy of the two neutrons in the final state.

$|E|^2$ and $|O|^2$ have been evaluated by Lax and Feshbach choosing the Hulthen function

$$u(\rho) = \left[\frac{\alpha}{2\pi(1-\alpha\rho_1)}\right]^{\frac{1}{2}} (e^{-\alpha\rho} - e^{-\beta\rho})$$

for the initial spacial wave function of the deuteron and

$$u_{f,e}(\mathbf{k}\cdot\boldsymbol{\varrho}) = (2\pi)^{-\frac{3}{2}} \cos(\mathbf{k}\cdot\boldsymbol{\varrho}),$$
$$u_{f,o}(\mathbf{k}\cdot\boldsymbol{\varrho}) = (2\pi)^{-\frac{3}{2}} \sin(\mathbf{k}\cdot\boldsymbol{\varrho})$$

for the final states of the di-neutron. In the above, $\alpha^2 = M\varepsilon$, $\rho_1 = 1.74\times10^{-13}$ cm is the effective triplet scattering range and β is given by

$$\frac{3}{\beta} = \rho_1[1+\tfrac{4}{9}\alpha\rho_1]$$

Using the results of Lax and Feshbach, the cross-section for the meson spectrum can be written in the final form

$$\frac{d\sigma}{d\Omega d\mu_0} = (2\pi)^{-2}\frac{\mu\mu_0}{2}\left[ZI_1 - \frac{Z+4D^2}{3}I_2\right], \tag{11}$$

where

$$Z = |A|^2+|B|^2+2|C|^2+2|D|^2$$
$$= \frac{8\pi^2e^2f^2}{\mu_0\nu_0}\left[\frac{2}{\left(1+\frac{\mu_0}{M}\right)^2}\left(1-\frac{2\mu^2\sin^2\theta}{\{(\nu-\mu)^2+1\}^2}\right)\right.$$
$$+\frac{1}{1+\frac{\mu_0}{M}}\frac{4\nu\lambda}{3\mu}\left(\frac{\nu\sin^2\theta}{(\nu-\mu)^2+1}-\frac{\cos\theta}{\mu}\right)\cos\delta_{33}\sin\delta_{33}$$
$$\left.+\frac{2\nu^2\lambda^2}{9\mu^4}(1+\tfrac{3}{2}\sin^2\theta)\sin^2\delta_{33}\right],$$

$$4|D|^2 = \frac{8\pi^2e^2f^2}{\mu_0\nu_0}\left[\frac{8}{9\mu^4}\nu^2\lambda^2\sin^2\theta\sin^2\delta_{33}\right],$$

$$I_1 = \frac{2M\alpha k_r}{\pi(1-\alpha\rho_1)}\left[\frac{1}{p_\alpha^4-4k_r^2k_0^2}+\frac{1}{p_\beta^4-4k_r^2k_0^2}\right.$$
$$\left.-\frac{1}{2k_rk_0((\beta^2-\alpha^2)}\ln\frac{(p_\beta^2-2k_rk_0)(p_\alpha^2+2k_rk_0)}{(p_\beta^2+2k_rk_0)(p_\alpha^2-2k_rk_0)}\right].$$

$$I_2 = \frac{M\alpha}{2\pi(1-\alpha\rho_1)} \frac{\beta^2-\alpha^2}{k_0(p_\alpha{}^2+p_\beta{}^2)} \left[\frac{1}{p_\alpha{}^2} \ln \frac{p_\alpha{}^2+2k_r k_0}{p_\alpha{}^2-2k_r k_0} - \frac{1}{p_\beta{}^2} \ln \frac{p_\beta{}^2+2k_r k_0}{p_\beta{}^2-2k_r k_0}\right],$$

$$k_r{}^2 = M(\nu_0-\mu_0-\varepsilon)-k_0{}^2,$$

$$p_\alpha{}^2 = M(\nu_0-\mu_0-\varepsilon)+\alpha^2 = M(\nu_0-\mu_0),$$

$$p_\beta{}^2 = M(\nu_0-\mu_0-\varepsilon)+\beta^2 = M(\nu_0-\mu_0)+\beta^2-\alpha^2.$$

4. Numerical Results and Discussions

Expression (11) for the meson spectrum has been evaluated numerically for an incident photon of energy 320 MeV at angles 0°, 45°, 90°, 135° and 180° and the results are given in the form of curves in fig. 1. The angular distribution of mesons is given by curve 1 of fig. 2.

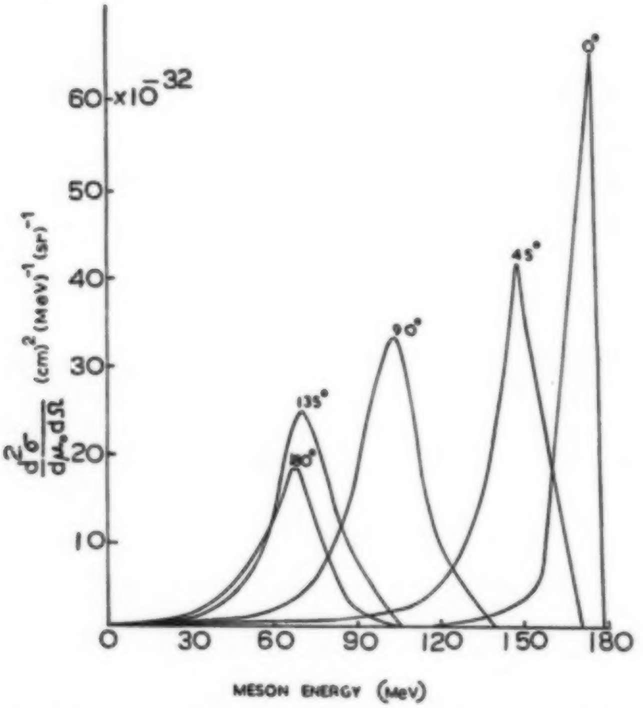

Fig. 1. Energy spectra of π^+ mesons from deuterons at various laboratory angles for incident photon energy 320 MeV.

Although a large number of experiments have been reported on the photo production of charged pions from deuterons, almost all of them deal with the measurement of the π^+/π^- ratio. The available data on the absolute photo production of π^+ mesons from deuterons are meagre, and the only experiments, that we are aware, are those of White, Jacobson and Schulz [5]) and Robert H. Land [6]). The experimental results of White, Jacobson and Schulz are included in fig. 2 for comparison. They have made measurements at three laboratory angles 45°, 90° and 135° using a "spread-out" bremsstrahlung photon beam of 318 ± 10 MeV and hence their results, represented by points in fig. 2, are for an

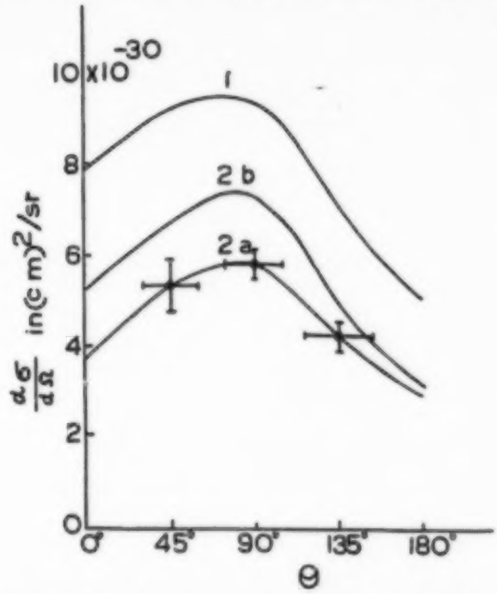

Fig. 2. Differential cross-sections in the laboratory system for the production of π^+ mesons from deuterons: Curve 1 is the theoretical curve for an incident photon of energy 320 MeV. The points on the graph are the experimental points obtained by White, Jacobson and Schulz using a "spread-out" bremsstrahlung photon beam of 318 ± 10 MeV and hence their results are given for an "equivalent quantum". Curve 2(a) is a smooth curve drawn by extrapolation through the experimental points and curve 2(b) is obtained by them after making corrections for nuclear interactions in the absorbers.

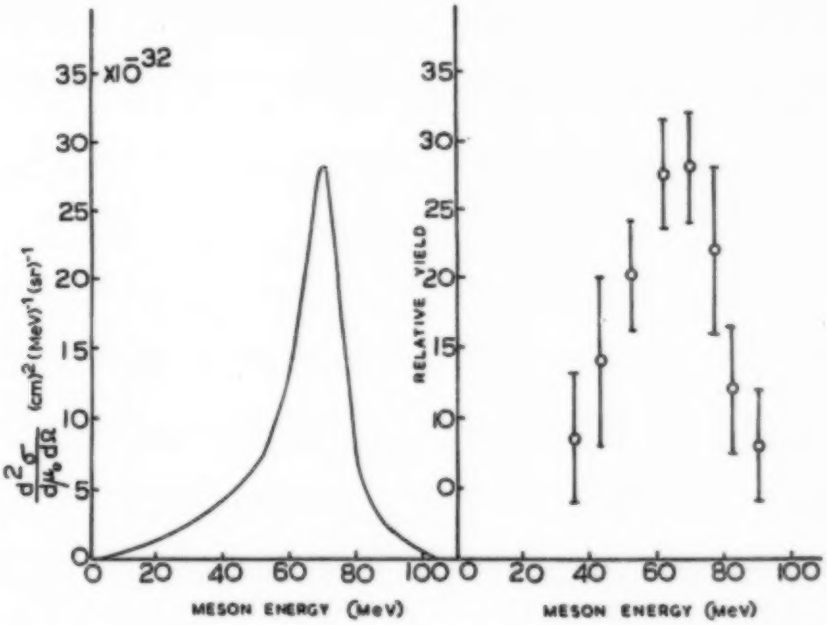

Fig. 3. The meson spectrum at laboratory angle 120° for an incident photon of energy 292 MeV: The smooth curve is the theoretical curve. The experimental points of Robert H. Land given in arbitrary units, are included for comparison.

"equivalent quantum" †. Curve 2 (a) is a smooth curve drawn by them through the experimental points by extrapolation and the curve 2(b) is obtained from the curve 2(a) after making corrections for nuclear interactions. It is to be noted that the curve 2(a) does not include the uncertainties of experimental observations and so also does the curve 2(b).

Robert H. Land [6]) has studied the π^+ meson spectra at 120° using a monochromatic photon beam of 292 MeV and his results are given in arbitrary units. We reproduce in fig. 3 his experimental points along with the theoretical curve that we have obtained for π^+ meson spectrum at 120° for an incident photon of the same energy (292 MeV). The agreement is satisfactory. The curves of White Jacobson and Schulz for meson spectra are, however, broader which may be due to the "spread out" photon beam they have employed.

We are deeply indebted to Professor Alladi Ramakrishnan for encouragement and guidance. We are grateful to Dr. G. E. Brown for his valuable comments and at his suggestion we have made a detailed comparison with the experimental results in section 4. We also acknowledge with thanks many helpful suggestions from Dr. S. K. Srinivasan and Messrs. N. R. Ranganathan and K. Venkatesan.

† The number of equivalent quanta is defined as the total energy in the beam divided by the maximum photon energy.

References

1) G. F. Chew and H. W. Lewis, Phys. Rev. **84** (1951) 779
2) M. Lax and H. Feshbach, Phys. Rev. **88** (1952) 509
3) G. F. Chew *et al.*, Phys. Rev. **106** (1957) 1345
4) G. Salzman and F. Salzman, Phys. Rev. **108** (1957) 1619
5) R. S. White, M. J. Jacobson and A. G. Schulz, Phys. Rev. **88** (1952) 836
6) Robert H. Land, Phys. Rev. **113** (1959) 1141

1.E.1:
3.A

Nuclear Physics **23** (1961) 319—326;©*North-Holland Publishing Co., Amsterdam*
Not to be reproduced by photoprint or microfilm without written permission from the publisher

ANGULAR CORRELATION IN $Be^9(p,\gamma)B^{10}$ AND THE STATES OF B^{10} AT 7.56 AND 5.16 MeV

N. W. TANNER and S. S. HANNA †
The Clarendon Laboratory, Oxford University, Oxford, England

Received 8 November 1960

Abstract: A measurement has been made of the angular correlation of γ-rays from the 7.56 MeV state of B^{10} (the 1.084 MeV resonance of $Be^9(p,\gamma)B^{10}$). An asymmetry of 9 % was found which seems to settle the spin and parity of the 7.56 MeV state as being $J^\pi = 0^+$. The consequence of this definite assignment is that the 5.16 MeV state cannot be the second $T = 1$ state of B^{10}. It is suggested that the state at 4.77 MeV is the $T = 1$ state despite the shift of 0.33 MeV from the expected position. A tentative assignment of $J^\pi = 1^+$, $T = 0$, is made to the 5.16 MeV state.

1. Introduction

There is considerable evidence ¹) that the spins of the levels in B^{10} at 7.56 MeV (the 1.084 MeV resonance of $Be^9(p,\gamma)B^{10}$) and 5.16 MeV are 0 and 2, respectively. However, the radiative transition which takes place ²) between the two levels is of such strength ³) †† that it is almost certainly dipole in nature and therefore inconsistent with a spin change $\Delta J = 2$. Clearly, more evidence is required in order to resolve this difficulty. Additional information on the 7.56-MeV level can be obtained from a study of the dominant radiative decay of the level via the 0.72-MeV level to the ground state of B^{10}. Both gamma rays of the cascade are known ⁴) to be emitted isotropically but this may result from a particular mixture of channel spins in the initial state (Be^9+p) or of multipolarities in the radiation rather than from zero spin for the 7.56-MeV level. However, the separate isotropy of the γ-rays in the cascade does put very severe restrictions on the angular correlation between the two γ-rays in the cascade. Hence, a measurement of the correlation could provide important information on the spin of the state at 7.56 -MeV and so also on the character of the state at 5.16 MeV.

2. Experimental Procedure

A target of evaporated beryllium, 10 keV thick for 1 MeV protons, gave a copious yield of radiation when bombarded with 5 μA of protons from a Van de

---

† Visiting Guggenheim Fellow (1958—59). Permanent address: Argonne National Laboratory, Argonne, Illinois.

†† Recent (unpublished) observations by R. E. Meads and J. E. G. Mc Ildowie have shown unambiguously that the transition is to the 5.16-MeV level and not to the 5.11-MeV level.

Graaff generator. The target thickness was a compromise between the necessity of holding the proton energy on the sharp 1084-keV resonance (natural width, 3.5 keV) and the desire to minimize the background from the broad resonance at 990 keV. In practise the background amounted to about 25 % of the total yield observed from the sharp resonance. However, all but about 10 % of the background was due to γ-decay to the ground state which does not give γ—γ coincidences.

Two NaI crystals, each 10.2 cm in diameter by 10.2 cm long, were used to detect the two γ-radiations. The counters were mounted on two arms free to rotate about a central pillar on which the target chamber was mounted. Considerable care was taken to align the beam, collimated to 0.32 cm, so that it would strike the target on the axis of rotation, but an error of about 0.10 cm, arising from deflection of the central pillar on rotation of one of the counters, had to be tolerated. However, with the detectors 12.7 cm from the target the error was, at most, 0.3 %, and could be easily corrected. Small and reproducible shifts in gain were observed on rotating the 'moving' counter. These shifts were presumably due to the effect of a stray magnetic field on the photomultiplier. They were eliminated by making a small adjustment of the H.T. of the photomultiplier whenever the counter was rotated.

The angular correlation was measured for two separate geometries. In the first case, Geometry I, the fixed counter remained at 90° to the proton beam and the other counter alternated between angles of 90° and 0° to the beam (i.e. 180° and 90° relative to the fixed counter). Observations at only two angles were required, since the intermediate state of the cascade has spin 1 which limits the complexity of the correlation function to $\cos^2\theta$. For Geometry II the fixed counter was at 135° to the beam and the other alternated between angles of 45° on either side of the beam.

Coincidences were observed between pulses from the fixed counter corresponding to $E_\gamma \geqq 4$ MeV and pulses from the moving counter for $E_\gamma \geqq 0.55$ MeV. These coincidences, obtained in a circuit which had a resolving time of 0.2 μsec, were used to gate a 100-channel kicksorter which received pulses from the moving counter. The gated kicksorter, therefore, displayed only the coincident 0.72-MeV radiation as recorded in the *moving* counter. The reaction rate was monitored by observing the intensity of the 0.72-MeV γ-ray as recorded by the *fixed* counter, this particular γ-ray being separated from the spectrum by a single-channel analyzer. A block diagram of the electronic equipment is shown in fig. 1.

Typically, some 5000 counts were recorded in the coincidence spectrum in a 15-minute run so that after a few such observations the statistical errors were of much less importance than possible systematic errors which could arise from variations of the energy and intensity of the proton beam, from electronic drifts, and from geometry effects. The systematic errors were effectively controlled by recording the counts from both coincidence channels separately. A series of runs was accepted only if these 'singles' counts remained constant within about 1 %. In addition, the procedure adopted for recording the data was to make coincidence measurements at both angles (for a particular geometry) and to follow this with *singles* measurements at the same two angles. For these *singles* measurements, the kicksorter was gated by the pulses from the moving counter (i.e. $E_\gamma \geqq 0.55$ MeV), and the proton beam was reduced to 1 μa to avoid serious dead-time losses. The latter measurements were particularly aimed at detecting any geometry effects that had not been eliminated in lining-up apparatus. Very small corrections were applied to the coincidence data for random coincidences, dead-time losses, and room background.

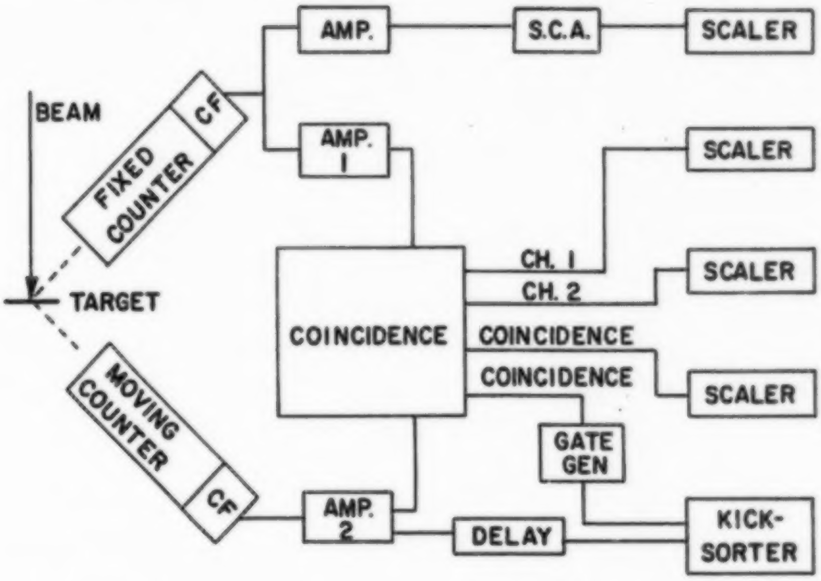

Fig. 1. Block diagram of the apparatus. The abbreviations S.C.A. and C.F. stand for single-channel analyzer and cathode follower, respectively.

As a further test of the experimental arrangement, a measurement was made of the γ—γ correlation in the Co^{60} decay. The result of the measurement, $+(17.0 \pm 1.5)$ %, was in good agreement with the theoretical value 16.6 %.

3. Results and Analysis

The results of the coincidence measurements, normalized to a standard monitor count, are conveniently expressed as the excess of counts at 180° (i.e. at an angle of 180° between the two γ-rays) over the counts at 90°, relative to the counts at 90°. This measure of asymmetry is equivalent to the coefficient A_2 in the expression $1+A_2 \cos^2\theta$. For Geometry I (fixed counter at 90°) an asymmetry of $-(9.5 \pm 1.6)$ % was obtained. For Geometry II (fixed counter at 135°) the asymmetry was $-(8.7 \pm 0.8)$ %. Both of these results have been corrected for the finite geometry used in the experiment. In the measurement in Geometry I limits of 2 % and 5 % were put on the asymmetry, with respect to the proton beam, of the 0.72 MeV γ-ray and 6.84 MeV γ-ray respectively. These limits are in agreement with the work of Paul and Gove [4]) who found the two γ-rays to be isotropic within 5 %.

The analysis of the data was approached from the point of view of determining what restrictions could be placed on the spin and parity of the proton capture state by the angular distributions and correlations of the resulting cascade γ-rays [†]. The only additional data that were used were the spins and parities of the ground state of Be^9, $J^\pi = \frac{3}{2}^-$, of the ground state of B^{10}, $J^\pi = 3^+$, and of the first excited state of B^{10} at 0.72 MeV, $J^\pi = 1^+$, and the radiation width of the state in B^{10} at 7.56 MeV (the proton capture state), $\Gamma_\gamma = 6.0$ eV [2]). This radiation width is quite large for the energy of the transition (6.84 MeV) and implies that the multipole order of the transition is *certainly* not higher than electric quadrupole. With dipole or electric quadrupole radiation, the possible spins and parities of the capture state are $0^\pm$, $1^\pm$, $2^\pm$ and 3^+.

In general, the angular correlation was treated as a triple correlation involving the proton as well as the two γ-rays. Mixtures of channel spin in the initial state and of multipoles (M1 and E2) for the 6.84 MeV γ-ray were introduced into the calculations whenever they were allowed by the selection rules. Interference terms arising from the small non-resonant cross-section ($\sigma \approx 8\ \mu$b) for the 6.84—0.72 MeV γ-ray cascade in the neighbourhood of the 1084 keV resonance ($\sigma_{\text{res.}} = 400\ \mu$b) were also considered using $J^\pi = 0^\pm$, $1^\pm$, $2^\pm$ and 3^+ for the non-resonant process. In principle, these interference terms could produce effects as large as 25 % in the angular distributions and correlations, but in practise the requirement of isotropy for the angular distributions so restricts the magnitude of the interference terms that they produce essentially no effect in the angular correlations. In a good many cases these interference terms were identically zero in at least one of the two geometries employed.

None of the assignments, $J^\pi = 1^-$, 2^- or 3^+, for the resonant capture state could account for the observed angular distributions and correlations under any conditions of mixtures or interference and they are quite definitely eliminated. For example, for completely isotropic angular distributions relative to the proton beam, the asymmetries in the angular correlations for these three cases would be $+5.2$, -1.0 and $+1.5$ %, respectively, in marked disagreement with the experimental result of -9 %. The two cases, $J^\pi = 0^\pm$ are possible assignments since they give isotropic angular distributions and an angular correlation asymmetry of -10.3 % which is independent of the geometry used. Introduction of non-resonant interference could modify the angular correlation asymmetry by no more than 0.3 % if the angular distributions are to be isotropic within 5 %. We shall return to the case $J = 0$ later. The assignments $J^\pi = 1^+$ and 2^+ are more complicated and must be considered in detail.

[†] By an angular distribution we shall mean the directional distribution of a gamma-ray relative to the proton direction; the term angular correlation will be used to denote the directional distribution of one gamma-ray of the cascade relative to the other.

$J^\pi = 1^+$

The computed angular distributions are

$$W(\theta_1) = 1-[(6x-1)(1+6\alpha+\alpha^2)/20(1+\alpha^2)]P_2(\cos\theta_1),$$
$$W(\theta_2) = 1+[(6x-1)(5-\alpha^2)/700(1+\alpha^2)]P_2(\cos\theta_2),$$

where θ_1 and θ_2 are, respectively, the angles defining the directions of propagation of the 6.84 and 0.72 MeV γ-rays with respect to the proton beam, x and $(1-x)$ are, respectively, the weighting factors for the channel spins $s = 1$ and $s = 2$ in the initial state, α is the ratio of the amplitudes of electric quadrupole and magnetic dipole radiation (α is a real but not necessarily positive number), and $P_2(\cos\theta)$ is the Legendre polynomial. We note that the particular mixture of channel spins represented by $x = \frac{1}{6}$ will provide isotropy of both γ-rays.

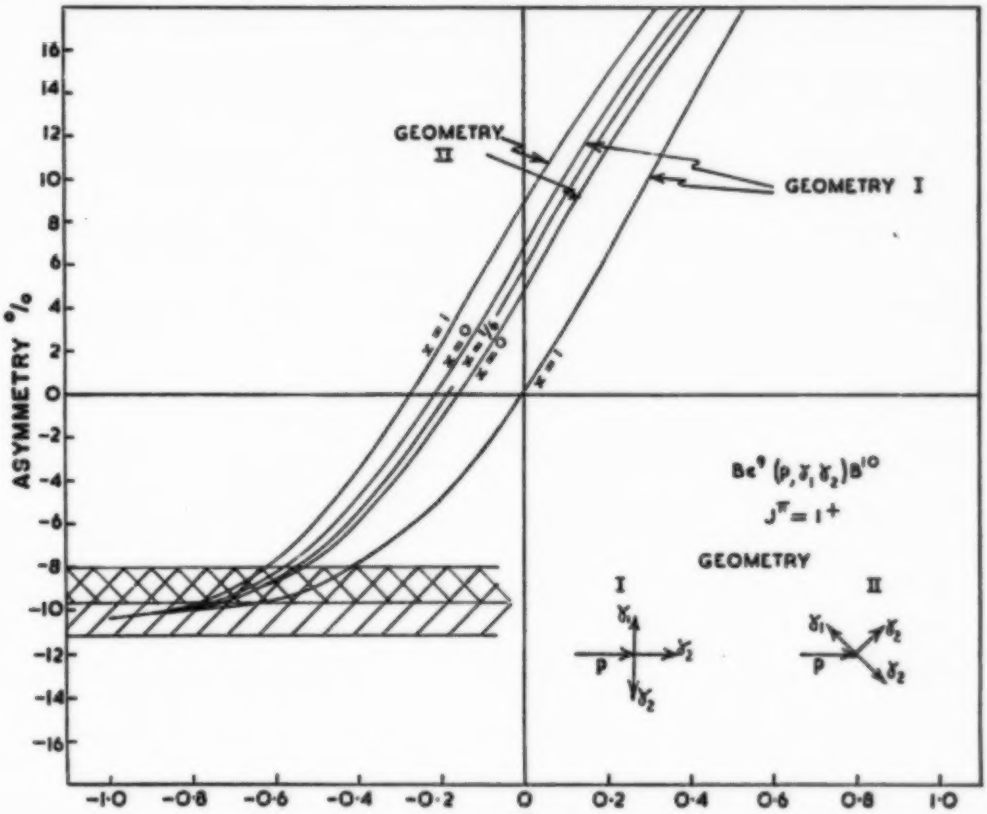

Fig. 2. Calculated values of the asymmetry in the angular correlation of $Be^9(p, \gamma_1, \gamma_2)B^{10}$ as a function of the E2/M1 amplitude ratio α for various values of the channel spin parameter x, assuming a compound state having $J^\pi = 1^+$. The hatched lines indicate the experimental results. The total hatched area gives the result for Geometry I. The upper double hatched area is for Geometry II.

The angular correlationa symmetry is plotted in fig. 2 for the same parameters, x and α, and for the two geometries used in the experiment. Fig. 2 indicates that $\alpha \lesssim -0.5$ will satisfy the experimental angular correlation without any severe restriction on x. The isotropy of the angular distributions can then be obtained by setting $x = \frac{1}{6}$.

$J^\pi = 2^+$

The angular distributions are

$$W(\theta_1) = 1-(2x-1)(7-14\sqrt{5}\alpha-5\alpha^2)/20(1+\alpha^2)]P_2(\cos\theta_1),$$
$$W(\theta_2) = 1+[(2x-1)(1-\alpha^2)/20(1+\alpha^2)]P_2(\cos\theta_2),$$

and the angular correlation asymmetry is plotted in fig. 3. The function $W(\theta_1)$ varies rapidly with α and x, so that isotropy will occur only for $\alpha = +0.217$ or $x = \frac{1}{2}$. However, $\alpha = +0.217$ cannot satisfy the angular correlation in Geometry II so we must put $x = \frac{1}{2}$. Then the requirement obtained from fig. 3 is $\alpha \gtrsim 0.5$.

The non-resonant interference terms in the angular correlation expression for the resonant states $J^\pi = 1^+$ and 2^+ are quite complicated and once the

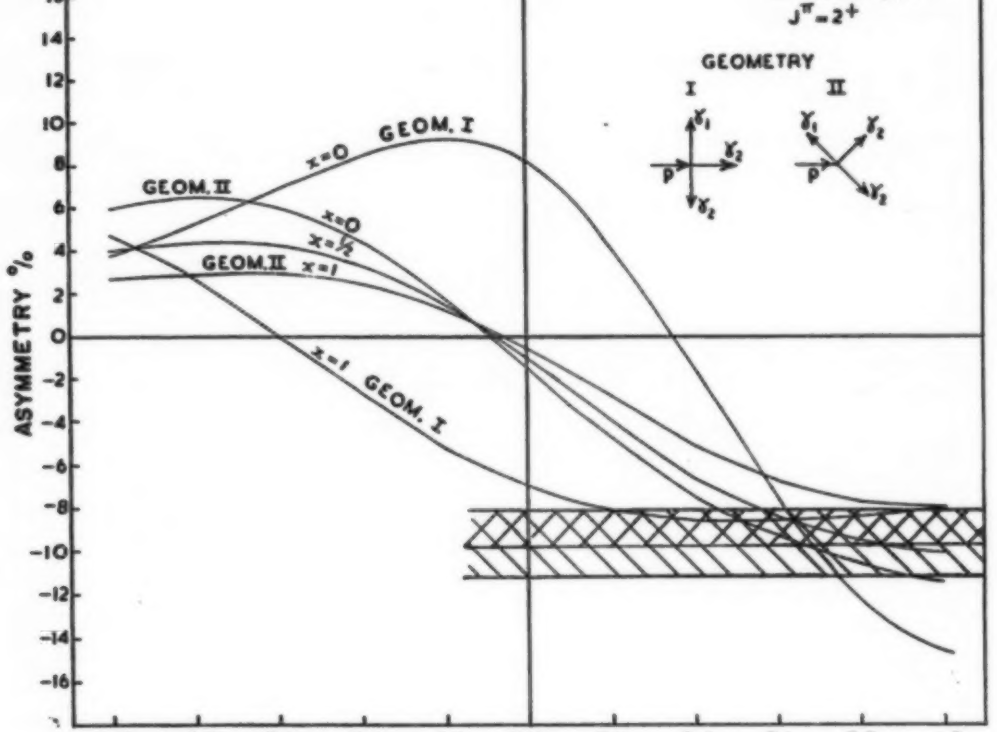

Fig. 3. Calculated values of the asymmtry as in fig. 1, except that the compound state is assumed to have $J^\pi = 2^+$.

requirement for isotropy of the angular distributions has been applied, quite small. As the interference terms have no influence on the conslusions that will be drawn, they will not be discussed further.

In both the cases, $J^\pi = 1^+$ and 2^+, we must have $\alpha^2 \geqq 0.25$ to satisfy the experiments. This condition gives an electric quadrupole radiation width $\gtrsim 1.5$ eV (since the total width is 6.0 eV) which may be compared with the Weisskopf single-particle estimate for an E2 transition of energy 6.84 MeV of 1.5×10^{-2} eV. In the extreme collective sense all five protons of B^{10} could act together and enhance the single particle estimate by a factor of 25 perhaps, but it is impossible to see whence a factor of 100 could come. We conclude that the assignments $J^\pi = 1^+$ or 2^+ cannot satisfy the measurements.

There appears to be no alternative to the assignment of $J = 0$ to the resonant level, which gives an asymmetry of -10.3 % in the angular correlation. It is true that the measured values of $-(8.7 \pm 0.8)$ % and $-(9.5 \pm 1.6)$ % do not quite agree with the theoretical value, but it does not seem improbable that the correlation is slightly attenuated by interaction with local fields in the source, since the lifetime of the intermediate level is $\approx 10^{-9}$ sec [1]). There is, of course, no indication of the parity of the level at 7.56 MeV from these directional distributions. However, the very small α-particle and deuteron partial widths [1]) and the proton scattering data [5]) leave little doubt that the parity is even if the spin is zero.

4. Discussion

The principle consequence of assigning $J^\pi = 0^+$ to the 7.56-MeV state is that the 5.16-MeV state must have $J = 1$ by virtue of the strong radiative transition connecting the two states. In addition, we can then be sure the 5.16-MeV state of B^{10} is not the mirror state of the first excited states of Be^{10} and C^{10} which have $J^\pi = 2^+$. The 5.16-MeV state must then have an isobaric spin $T = 0$.

The 5.16-MeV state has previously been studied through the reaction $Li^6(\alpha, \gamma)B^{10}$. The decay spectrum is consistent with $J^\pi = 1^+$ but not 1^-; in particular, with $J^\pi = 1^-$ the observed transition to the ground state would be an M2 transition with a radiation width ≈ 100 times the single particle estimate. The assignment $J^\pi = 1^+$, $T = 0$, does, however, present a serious difficulty, since the state radiates preferentially to the states at 0.72 and 2.15 MeV, both of which have $J^\pi = 1^+$, $T = 0$, and very weakly, if at all, to the state at 1.74 MeV for which $J^\pi = 0^+$, and $T = 1$. This is a complete contradiction of Morpurgo's isobaric spin rule [6]) that magnetic dipole radiation should be inhibited for $\Delta T = 0$ but not for $\Delta T = 1$. Also unexplained is the very narrow width of the level [3]).

One of the B^{10} states at an excitation of about 5 MeV must be the mirror of the first excited states of B^{10} and C^{10} with the assignment $J^\pi = 2^+$. If the

5.16 MeV state is eliminated, the choice lies between the 4.77- and 5.11-MeV states. The 4.77-MeV state has the smaller reduced α-particle width [7] (Γ_α is zero for a pure $T = 1$ state), has $J^\pi = 2^+$ almost certainly [7,8]), and has a γ-decay spectrum in good agreement with the prediction of the intermediate coupling model [9,10]) †. The 5.11-MeV state is an unsatisfactory choice in all respects except that the angular distribution [8]) from $Li^6(\alpha, \gamma)B^{10}$ allows $J^\pi = 2^+$. However, the first excited states of Be^{10} and C^{10} indicate that the B^{10} $T = 1$ should be near 5.1 MeV. If the 4.77-MeV state is the $T = 1$ state, then it has the largest displacement known for mirror states [11]).

Summarizing, we have a quite definite assignment of $J^\pi = 0^+$ for the 7.56-MeV state and probable assignments of $J^\pi = 1^+$, $T = 0$ for the 5.16-MeV state and $J^\pi = 2^+$, $T = 1$ for the 4.77-MeV state.

The experimental part of this research was carried out using the 3 MeV Van der Graaff at A.W.R.E., Aldermaston. We would like to express our gratitude to K. W. Allen for making available for our use the very excellent facilities at Aldermaston. We are grateful also to D. Akers and his staff for their generous assistance and management during the research at Aldermaston. One of us (S. S. H.) would like to thank Professor D. H. Wilkinson, F.R.S., for his hospitality in extending the facilities of the Clarendon Laboratory for research and study, and also the Guggenheim Memeorial Foundation for the award of a Fellowship. Our thanks are due to R. E. Meads and J. E. G. McIldowie for making available to us their observations on the gamma-ray spectra.

† In the latter ref., Kurath discusses the assignment of $T = 1$ to the 4.77 MeV state.

References

1) F. Ajzenberg-Selove and T. Lauritsen, Nuclear Physics **11** (1959) 1
2) W. F. Hornyak and T. Coor, Phys. Rev., **92** (1953) 675
3) Meyerhof, Tanner and Hudson, Phys. Rev. **115** (1959) 1227
4) E. B. Paul and H. E. Gove, Proc. Roy. Soc. Canada **47** (1953) 145A
5) F. S. Mozer, Phys. Rev. **104** (1956) 1386;
G. Dearnaley, Phil. Mag. (8) **1** (1956) 821
6) G. Morpurgo, Phys. Rev. **110** (1958) 721
7) H. Warhanek, Phil. Mag. **2** (1957) 1085
8) L. Meyer-Schützmeister and S. S. Hanna, Phys. Rev. **108** (1957) 1506
9) D. Kurath, Phys. Rev. **101** (1956) 216
10) D. Kurath, Proc. Rehovoth Conf. on Nuclear Structure, ed. by H. J. Lipkin (North-Holland Publishing Co., Amsterdam, 1958) p. 46
11) D. H. Wilkinson, Phil. Mag. (8) **1** (1956) 1031

2.C

Nuclear Physics **23** (1961) 327—337; ©*North-Holland Publishing Co., Amsterdam*

Not to be reproduced by photoprint or microfilm without written permission from the publisher

CAPTURE AND INELASTIC SCATTERING OF PROTONS BY SILICON-30

A. C. L. BARNARD †, S. BASHKIN ††, C. BROUDE ††† and C. E. HORNBACK ‡

Department of Physics and Astronomy, State University of Iowa, Iowa City, Iowa ‡‡

Received 8 November 1960

Abstract: The reactions $Si^{30}(p, \gamma)P^{31}$ and $Si^{30}(p, p', \gamma)Si^{30}$ have been studied in the range of incident proton energies from 1.0 to 4.25 MeV. Some measurements with Si^{28} were also made. At $E_p = 3.88$ MeV the yield curves suggest that the weak resonance seen with natural silicon targets is caused by Si^{30} and not by Si^{28}. The capture reaction did not give useful information about spins and parities of P^{31} states, but the angular distributions of the gamma-rays following inelastic scattering led to assignments for 10 of these states.

1. Introduction

Some aspects of the level structure of P^{31} have been reported by Litherland *et al.* ¹) and, in a series of papers, by Broude *et al.* ²) In the range of excitation energies up to 5 MeV and between 7.8 and 9.0 MeV, all states with definite assignments have positive parity. If a suggestion ²) of rotational structure ³) of the lower states of P^{31} is valid, at higher excitation energies, negative-parity states (from a $K = \frac{7}{2}$ band) are expected to appear.

This paper reports a study of P^{31} at higher excitation by observation of the gamma-rays following proton capture and proton inelastic scattering.

2. Apparatus

The State University of Iowa electrostatic generator was used as a source of monoenergetic (i.e. less than 4 keV energy spread) protons with energies up to 4.25 MeV. Thin targets of natural silicon and of silicon enriched to about 80 % in Si^{30} were used on 0.25 mm thick gold backings in a conventional target chamber containing an acetone/dry-ice cold trap. The target and backing were insulated from the surrounding chamber and held at +300 volts relative to it, to prevent loss of secondary electrons from the target. The number of protons falling on the target was measured with a current integrator.

---

† Now at Physics Department, The Rice University, Houston, Texas.

†† Presently Fulbright Research Scholar on leave to the Research School of Physical Sciences, Australian National University, Canberra, Australia.

††† Now at Physics Department, Hebrew University, Jerusalem, Israel.

‡ Now at the Boulder, Colorado, Laboratories of the National Bureau of Standards.

‡‡ Supported in part by the U. S. Atomic Energy Commission.

Gamma-rays from the 0.16 cm diameter target spot entered a heavily shieldep 12.7 cm diameter 15.2 cm long NaI(Tl) crystal through a collimator. The front face of the crystal was 14.0 cm from the target spot and the collimator revealed a 5.1 cm diameter circular area at the centre of this face. Thus gamma-rays from the target and within a cone of half-angle 10° were accepted by the detector. Other gamma rays had to penetrate at least 10.2 cm of lead to reach the detector. This detector was mounted on an angular-distribution table so that it could be rotated about a vertical axis through the target centre to make angles between 0° and 90° with the direction of the incoming horizontal beam. The target chamber was cylindrically symmetric about this axis over this angular range and the targets were angled at 45° to the beam. During angular-distribution measurements, a fixed 7.6 cm diameter 7.6 cm long NaI(Tl) crystal was used as a monitor detector. The outputs of the counters were fed through cathode followers to a 256-channel pulse-height analyzer and/or to scaling channels. Each scaling channel consisted of a conventional scaler preceded by a pulse height discriminator. The level of discrimination was set by gating the analyzer with the discriminator output, so that only that part of the spectrum above the discrimination level appeared on the analyzer viewing screen. This part of the spectrum was recorded by the corresponding scaler. In this way the discriminator levels were adjusted so that particular gamma rays could be studied as a function of bombarding energy or angle of emergence.

3. Gamma-Ray Spectra and Yield Curves

Yield curves for various discriminator settings were taken over the incident proton energy range from 1.0 to 4.25 MeV with the detector at 55° to the beam (see figs. 1, 2 and 3). A natural-silicon and a Si^{30}-enriched target were used, both being about 7 keV thick at $E_p = 3$ MeV. Two thinner (about 3 keV) enriched targets were also used, but for $E_p > 2.5$ MeV a large non-resonant background distorted the yield curves from these targets. The curves are *not* corrected for the effects of different multiplicities of gamma-rays at different resonances. In the natural-silicon curves the known inelastic-scattering resonances above $E_p = 3$ MeV [4, 5]) were observed. The enriched-target curves showed a large number of resonances, the thinner targets revealing some of these as closely-spaced pairs of resonances. The data are summarized in table 1. Gamma-ray spectra were taken on many of these resonances, and showed, in addition to many genuine Si^{30} resonances, the presence of some $Na^{23}(p, \alpha\gamma)Ne^{20}$ resonances[6]) in the curve from one of the thinner enriched targets. These, together with the $Si^{28}(p, p'\gamma)Si^{28}$ resonances at 3.11 and 3.35 MeV [4]), the $Si^{30}(p, \gamma)P^{31}$ resonance at 1.697 MeV [1]) and some $Si^{30}(p, \gamma)P^{31}$ resonances at $E_p < 1$ MeV, were used for beam energy calibration. The yield curves shown in figs. 1 and 2 use this calibration and the absolute energies shown are believed good to ±20 keV.

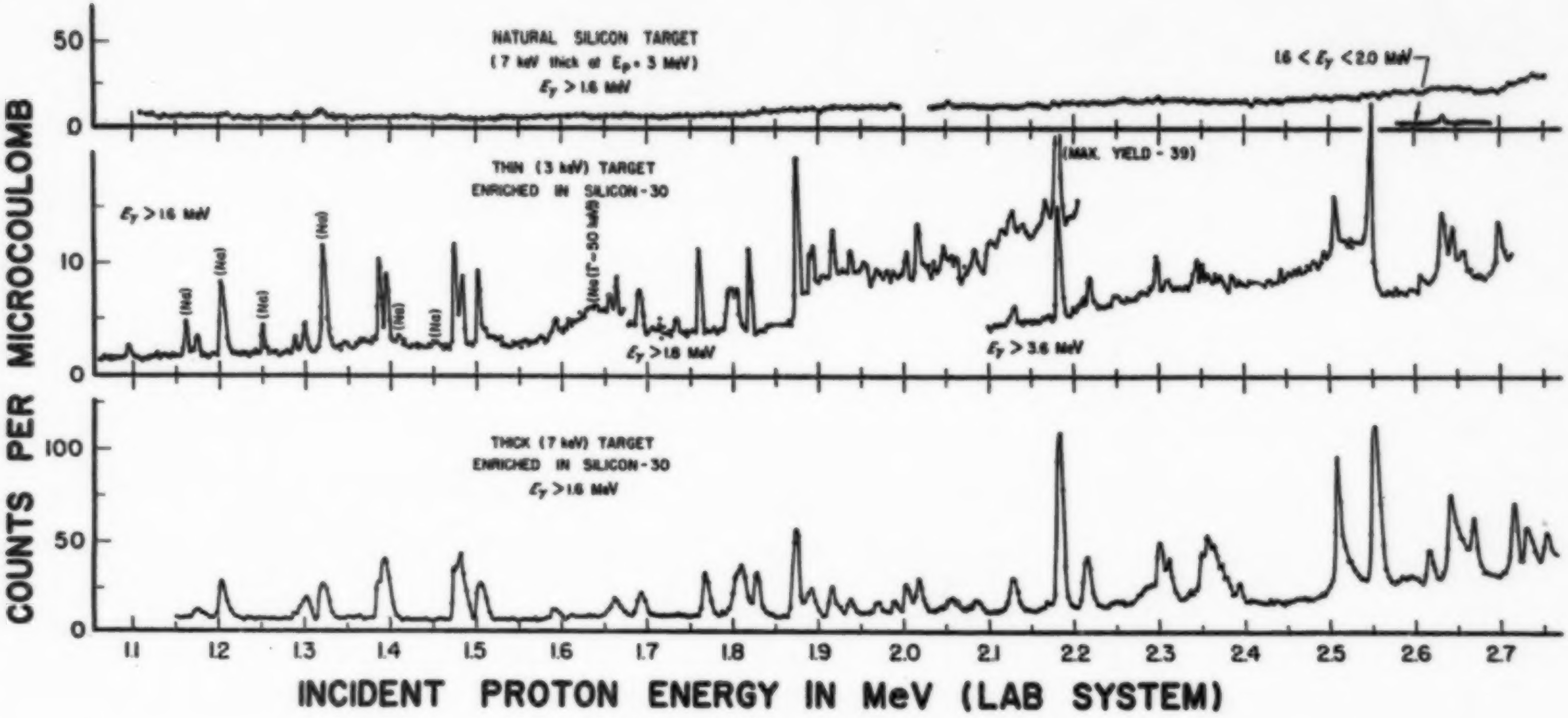

Fig. 1. Gamma-ray yield curves from proton bombardment of silicon $1.1 < E_p < 2.7$ MeV. Detector at 55° to beam.

TABLE 1

Energies of $Si^{30}+p$ resonances and excitation energies of corresponding P^{31} levels

Resonances observed with 7 keV target E_p (MeV)	Extra resonances with thin (3 keV) target	Excitation energy of level (MeV)	Resonances observed with 7 keV target E_p (MeV)	Extra resonances with thin (3 keV) target	Excitation energy of level (MeV)	Resonances observed with 7 keV target E_p (MeV)	Extra resonances with thin (3 keV) target	Excitation energy of level (MeV)
1.177		8.431	2.300		9.518	3.434		10.615
1.204		8.457	2.311		9.528	3.453		10.633
1.302		8.552		5 closely spaced resonances	9.566	3.467		10.647
1.322		8.571			to	3.500		10.679
1.393	1.387	8.634			9.605	3.525		10.703
	1.396	8.643	2.510		9.721	3.558		10.735
1.483	1.476	8.720	2.552		9.762	3.606		10.781
	1.487	8.731	2.616		9.824	3.634		10.809
1.507		8.750	2.643	2.633	9.840	3.667		10.841
1.591		8.832		2.647	9.854	3.677		10.850
1.662	1.657	8.895	2.668		9.874	3.689		10.862
	1.665	8.903	2.716		9.920	3.714		10.886
1.693		8.930	2.730		9.934	3.740		10.911
1.768		9.003	2.753		9.956	3.772		10.942
1.811	1.806	9.040	2.828		10.029	3.820		10.989
	1.815	9.049	2.856		10.056	3.846		11.014
1.828		9.061	2.883		10.082	3.869		11.036
1.874		9.105	2.901		10.099	3.886		11.052
1.890	1.888	9.119	2.910		10.108	3.920		11.085
	1.892	9.123	2.926		10.123	3.980		11.143
1.917		9.147	2.952		10.149	4.012		11.174
1.939		9.168	3.006		10.201	4.055		11.216
1.970		9.198	3.022		10.217			
			3.088		10.280	4.090		11.250
1.990		9.218	3.154		10.344	4.110		11.269
2.004		9.231	3.204		10.393	4.121		11.280
2.019		9.246	3.223		10.411	4.143		11.301
2.057		9.283	3.267		10.453	4.172		11.329
2.087		9.312	3.307		10.492	4.184		11.341
2.129		9.352	3.323		10.508	4.202		11.360
2.183		9.404						
2.215		9.435	3.348		10.532	4.232		11.387

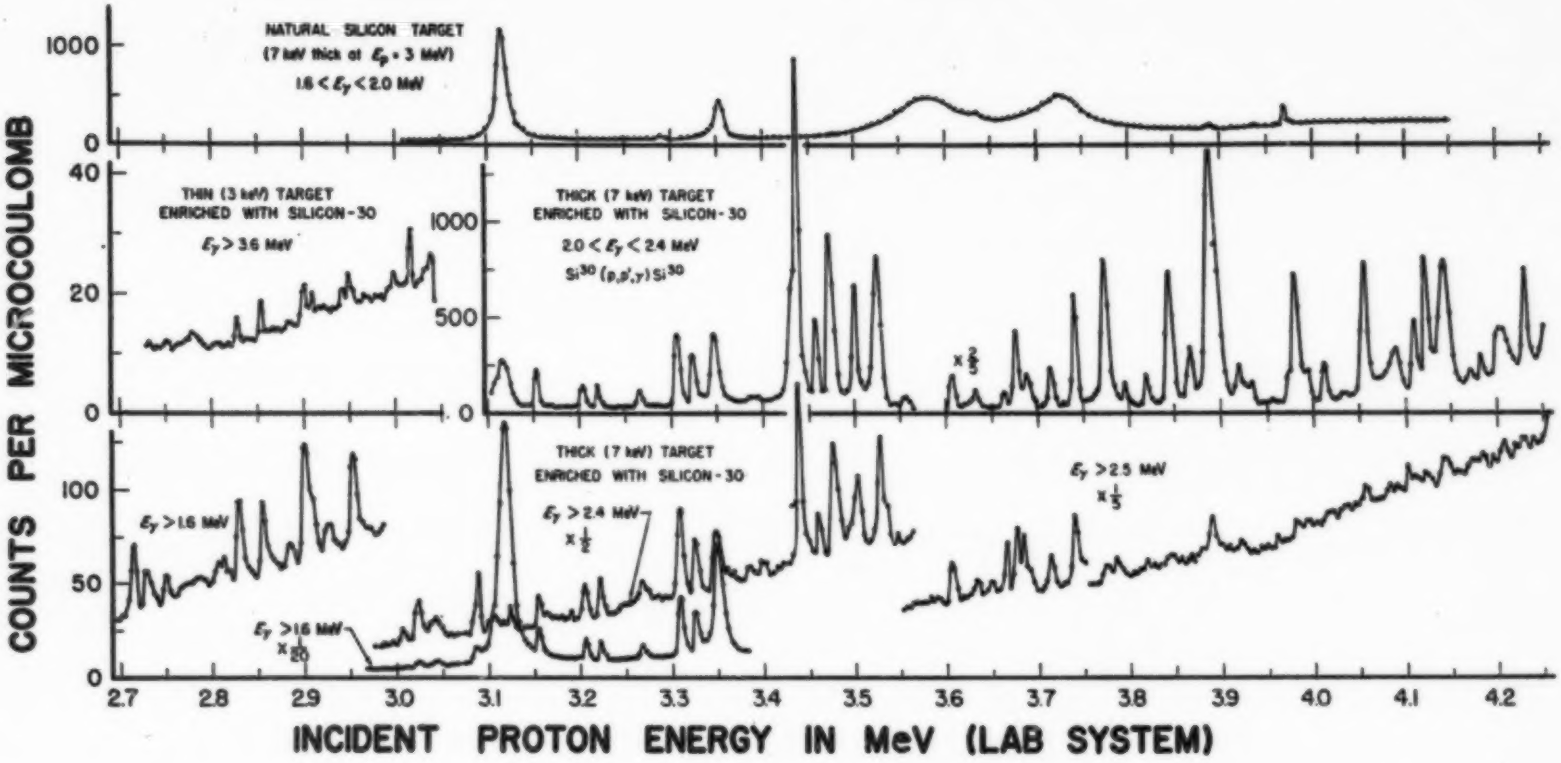

Fig. 2. Gamma-ray yield curves from proton bombardment of silicon 2.7 < E_p < 4.2 MeV. Detector at 55° to beam.

The yield curves taken with different targets were matched and good agreement was generally obtainable. The Si^{30}+p resonance energies are listed in table 1. As the number of Si nuclei per cm^2 of target was not known accurately, only rough absolute cross-sections can be given. The resonance at 3.88 MeV in the enriched-target curve has a peak cross-section of about 30 mb.

From fig. 2 it can be seen that the weak resonance at $E_p = 3.88$ MeV in the natural-silicon yield curve exactly agrees with the largest of all the resonances seen with the enriched targets. The intensities are such that the weak resonance could have come from the 3 % Si^{30} present in natural silicon. This strongly suggests that the resonance corresponds to a level at 11.05 MeV in P^{31} and not to a level at 6.47 MeV in P^{28}, as previously assumed [5]). Fig. 2 also shows that for protons with energies from 3 to 4.3 MeV incident on the enriched targets, the resonances in the yield of gamma-rays with energy between 2.0 and 2.4 MeV are more pronounced than the resonances in the yield of higher-energy gamma-rays. Therefore in this range of incident energies inelastic proton scattering from the 2.24 MeV first excited state of Si^{30} is more important than the competing proton-capture reaction.

Gamma-ray spectra taken on Si^{30} resonances in the range $1.1 < E_p < 2.3$ MeV indicate that proton capture is usually followed by complex cascading rather than by direct transitions to the low states of P^{31}. The energies of gamma-rays appearing in the spectra are listed in table 2. At $E_p = 2.18$ MeV

TABLE 2

Gamma-ray spectra at Si^{30}(p, γ)P^{31} resonances (weak components shown in parentheses, strong components underlined)

P^{31} level energy (MeV)	Energies (MeV) present in gamma spectrum	Remarks
8.43	1.3 1.8 2.2 (5.2) (6.4)	
8.46	1.3 2.1 2.2 5.3 6.4	
8.55	1.3 2.3 (2.9) (5.2) (6.6) 7.5	
8.57	1.3 1.6 2.3 3.1 3.6 4.4 5.2 (6.5) (7.6)	doublet not well resolved
8.63	1.2 1.8 2.2 (3.0) (4.6) 5.5 (6.1) 7.5	
8.64	1.2 2.3 (2.8) 3.2 $\underline{7.5}$	
8.72+8.73	1.3 2.3 3.1 $\underline{8.7}$	doublet not well resolved
8.75	1.3 2.2 5.4 7.7	
8.93	(1.0) 1.3 2.2 6.7 8.9	
9.00	1.3 2.2 3.0 3.5 4.8 5.5 (6.8) (9.0)	
9.04+9.05	1.2 3.2 3.7 4.4 $\underline{9.0}$	doublet not well resolved
9.06	(1.1) 1.3 1.7 2.3 (3.3) (3.5) 4.4 (6.7) 7.8 (9.1)	
9.10	1.1 1.2 2.2 2.9 (3.3) 3.5 4.9 5.6 6.8	
9.12	1.1 1.2 2.2 (3.3) (3.5) 4.4 (5.8) (7.0) 7.9 (9.1)	doublet not well resolved
9.25	1.1 1.3 2.1 2.2 (2.8) 5.8 7.0	
9.40	1.2 1.3 2.0 2.2 5.2	
9.44	1.3 2.2 3.1 3.8 4.6 (5.1) 6.0 8.0	
9.52	1.1 1.3 2.3 3.0 3.8 (5.1) 5.4 (6.1) 7.0	

there is a resonance which is well separated from nearby resonances and which has a spectrum appearing comparatively simple. Measurement of the intensities of the constituent gamma-rays (by decomposing the complex spectrum using experimentally-obtained spectral shapes for monoenergetic gamma-rays) and gamma-gamma coincidence measurements did not, however, reveal a simple decay scheme for the corresponding level. The intensity of the 2.23 MeV gamma-ray was too high to fit into such a scheme and the coincidence measurements were inconclusive, suggesting that the decay scheme is complex. If these capture states had negative parity a comparatively simple decay scheme, involving direct E1 transitions to the low-lying (positive-parity) states of P^{31}, might be expected. However, the inhibition of such transitions could be the result of the Nilsson-band selection rule $\Delta K = 0$ or ± 1 for dipole transitions [7]).

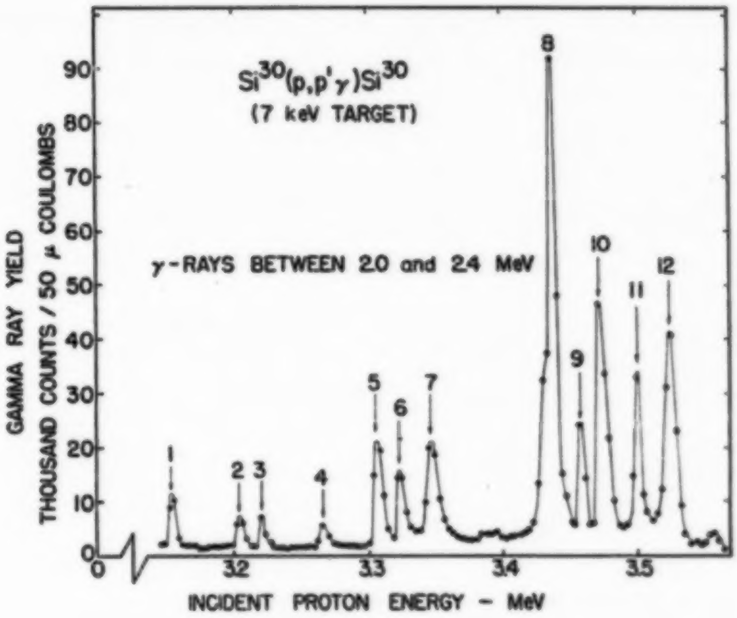

Fig. 3. Yield curve of gamma-rays from the reaction $Si^{30}(p, p', \gamma)Si^{30}$, $3.1 < E_p < 3.6$ MeV.

4. Angular Distributions

Fig. 3 is an enlargement of part of fig. 2. Using the 7 keV enriched target, angular distributions of the 2.24-MeV gamma-rays following proton inelastic scattering by Si^{30} were measured at the resonances marked 1 to 12, with the exception of No. 3. The intensity of the 2.24-MeV gamma-ray was measured by taking the difference between the counts in channels with discriminators set for deposition of more than 2.0 MeV and more than 2.4 MeV in the detector. The counts between 2.4 and 2.8 MeV were also measured and subtracted as a rough correction for small contributions from higher-energy gamma-rays (from the competing proton-capture reaction or from background). Since proton-capture can give a cascade gamma-ray of energy 2.23 MeV (see table 2), corresponding to the energy of the second excited state in P^{31}, it is not possible to make a complete correction for this effect. Using the yield curve for $E_p > 2.4$ MeV (fig. 2) and assuming a capture-gamma spectrum similar to those observed at lower incident energies, the proton-capture contribution to the measured intensities of 2.24 MeV gamma-rays was estimated as less than 10 %.

The apparent widths of the resonances in fig. 3 are of the order of 10 keV and the smallest separation between resolved resonances is about 14 keV. Both interference between neighboring levels and the presence of unresolved pairs of resonances are possible. Inspection of the figure suggests that the levels corresponding to resonances 9 and 11 are particularly liable to interference, as 8 is a

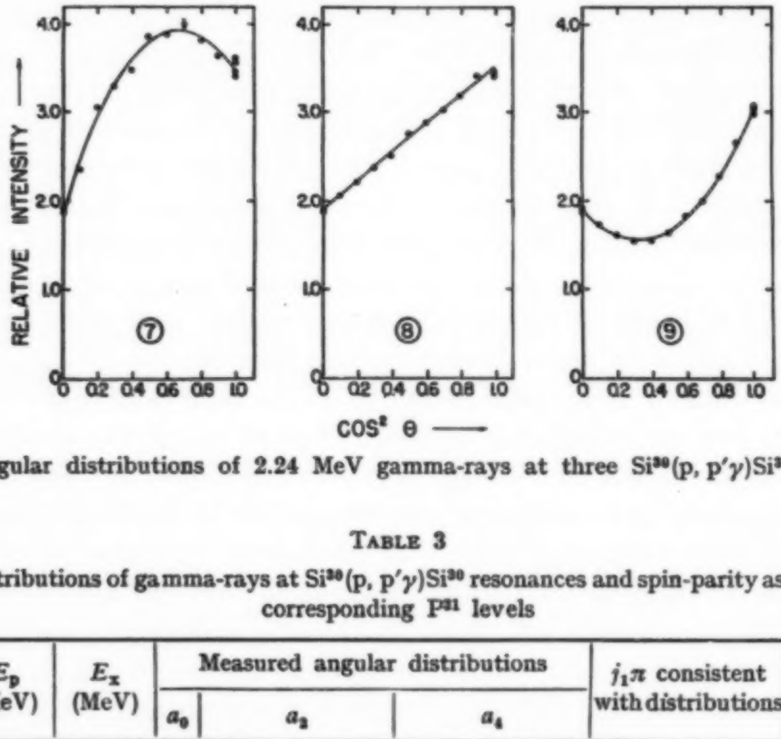

Fig. 4. Angular distributions of 2.24 MeV gamma-rays at three $Si^{30}(p, p'\gamma)Si^{30}$ resonances.

TABLE 3

Angular distributions of gamma-rays at $Si^{30}(p, p'\gamma)Si^{30}$ resonances and spin-parity assignments for corresponding P^{31} levels

Resonance	E_p (MeV)	E_x (MeV)	Measured angular distributions			$j_1\pi$ consistent with distributions	Probable $j_1\pi$
			a_0	a_2	a_4		
1	3.154	10.344	1	0.518 ± 0.025	-0.360 ± 0.030	$\frac{5}{2}-, \frac{7}{2}+$	$\frac{5}{2}-, \frac{7}{2}+$
2	3.204	10.393	1	0.478 ± 0.027	-0.426 ± 0.033		
3	3.223	10.411		Distribution	not measured		
4	3.267	10.453	1	0.496 ± 0.020	-0.319 ± 0.022	$\frac{5}{2}-$ $(\frac{7}{2}+)$	$\frac{5}{2}-$
5	3.307	10.492	1	0.244 ± 0.012		$\frac{3}{2}-$	$\frac{3}{2}-$
6	3.323	10.508	1	0.485 ± 0.010	-0.281 ± 0.011	$\frac{5}{2}-$ $(\frac{7}{2}+, \frac{9}{2}+)$1	$\frac{5}{2}-$
7	3.348	10.532	1	0.498 ± 0.020	-0.368 ± 0.024	$\frac{5}{2}-, \frac{7}{2}-, (\frac{7}{2}+)$	$\frac{5}{2}-, \frac{7}{2}-$
8	3.434	10.615	1	0.447 ± 0.011		$\frac{3}{2}-$	$\frac{3}{2}-$
9	3.453	10.633	1	0.240 ± 0.010	$+0.452 \pm 0.012$		$(\frac{5}{2}-)$
10	3.467	10.647	1	0.067 ± 0.008		$\frac{3}{2}-$	$\frac{3}{2}-$
11	3.500	10.679	1	0.284 ± 0.011	$+0.287 \pm 0.013$		$(\frac{3}{2}-, \frac{5}{2}-)$
12	3.525	10.703	1	0.389 ± 0.008		$\frac{3}{2}-, \frac{5}{2}-$ $(\frac{7}{2}+)$	$\frac{5}{2}-$ $\frac{3}{2}-$

large resonance and 12 a wide one. In this paper the approach will be adopted that interference effects will not be postulated unless it is not possible for the angular distributions to have come from isolated states.

Fig. 4 shows three of the measured angular distributions, the points being experimental and the curves a Legendre-polynomial fit obtained by a least-squares method. Only even-order polynomials were used. The results of analyzing the 11 distributions in this way are given in table 3, where a_K is the coefficient of the polynomial of order K in the distribution and the error is the fitting error. A correction has been made for the finite range of angles accepted by the detector.

5. Spin of First Excited State of Si^{30}

Quantities pertaining to this state will be labeled by the subscript 2. $j_2 = 0$ or 1 is not possible because of the presence of $\cos^4\theta$ terms in some of the distributions and $j_2 = 4$ can be eliminated on the grounds that such a state would have a single-particle lifetime of the order of 10^{-3} seconds, which might be reduced towards 10^{-5} seconds by the enhancement of the transition probability that arises from the cooperative effects of many nucleons [8]). Recent unpublished work by one of the authors (C. Broude) has shown the lifetime to be less than 5×10^{-8} seconds.

The choice between $j_2 = 2$ and 3 is most easily made by putting the usual expressions for the angular distribution of gamma-rays [9]) into the form involving the populations of the magnetic substates of the emitting state,

$$a_k = \sum_{m_2} (-1)^{I_2 - m_2 + L_2 + L_2' + \frac{1}{2}k}\, p(m_2)(j_2 j'_2 m_2 - m_2 \colon k0) Z_1(L_2 j_2 L'_2 j'_2 \colon I_2 k),$$

where Z_1, defined by Sharp *et al.* [10]), involves a Clebsch-Gordon and a Racah coefficient, and $p(m_2)$, which must be a positive number, is the population of the magnetic substate m_2. Other symbols have their usual meaning [10]). For $j_2 = 2$ the populations necessary to give the observed distributions are all positive, whereas for $j_2 = 3$ some are negative. (With $j_2 = 4$ the necessary populations were again all positive, but this spin can be excluded on the lifetime argument given above). It is concluded that $j_2 = 2$. Both the collective and the shell models predict this spin for the first excited state of an even-even nucleus. In accordance with these models, it will be assumed that the parity of the state is positive.

6. Spins and Parities of the Compound States

Quantities pertaining to these states will be labeled by the subscript 1. Under the assumptions of $j_2\pi = 2+$ and isolated compound states, the angular distributions expected for various values of $j_1\pi$ are easily obtained [10, 11]). Column 7 of table 3 lists the values of $j_1\pi$ consistent, within the statistical errors with the measured distributions. For resonances 2, 9 and 11, there were no such values of $j_1\pi$, there being discrepancies of 10–20 % between the measured and calculated coefficients. Some of the listed values can be eliminated by a Wigner-limit argument [12]) as follows. It can be seen from fig. 3 that some resonances are wider than others, for example, that 12 is wider than 11. If this is caused by the intrinsic width of the levels, rather than by the presence of unresolved pairs of resonances, then the levels corresponding to the wider resonances must have intrinsic widths of the order of several kilovolts. Together with the limit on the reduced widths, this is sufficient to rule out an ingoing orbital angular momentum quantum number greater than 3 for these resonances. The values $j_1\pi = \frac{7}{2}+$ and $\frac{9}{2}+$ can therefore be eliminated for the corresponding levels, these being the cases in parentheses in table 3 column 7.

It will now be assumed that the discrepancy in the case of resonances 9 and 11 is caused by interference from neighboring levels. In experiments of the present type, where an intermediate radiation is unobserved, no interference terms arise from overlap of levels of opposite parity and so contributions in this case are proportional to the intensity mixing ratio. Since the resonances are well resolved experimentally, i.e., including the effect of finite target thickness, the intrinsic mixing ratio must be very small, probably too small to account for the discrepancies. This makes it likely that 9 and 11 have the same parity as their neighbors, since only in this case are there interference terms to give angular-distribution contributions proportional to the amplitude mixing ratio. In the case of resonance 9, agreement with the measured distribution was obtained with $j_1\pi = \frac{5}{2}-$ and out-of-phase interference of about 4 % amplitude from the neighbouring $\frac{3}{2}-$ states. Similarly level 11 has either $j_1\pi = \frac{3}{2}-$ or $\frac{5}{2}-$ according as level 12 has $j_1\pi = \frac{5}{2}-$ or $\frac{3}{2}-$. No other reasonable possibilities were found.

Why the distribution for resonance 2 disagrees with the simple predictions is not certain. As resonance 3 was not investigated, the effects of interference terms from it cannot be estimated. Other possibilities which cannot be eliminated are that the observed resonance 2 corresponds to an unresolved pair of resonances, or that the proton-capture gamma spectrum has an unusually large 2.23 MeV component.

In obtaining these results, the possibility of interference from a nonresonant background has been ignored. Such a situation is almost impossible to rule out and, as it tends to give a number of adjustable parameters in the resultant angular distributions, almost any angular distribution could be made to agree with it. For instance, levels 1, 2, 4, 6 and 7 could all have $j_1\pi = \frac{7}{2}-$ with interference from a $\frac{1}{2}-$ background.

7. Conclusions

The first excited state of Si^{30} has been shown to have spin 2, and assumed to have positive parity. Probable spins and parities for several excited states in P^{31} are shown in column 8 of table 3. Almost all parities are negative. In the unlikely event that the Si^{30} state turns out to have negative parity, the parities assigned to the P^{31} levels would be reversed. The levels in the range $8.4 < E_x <$ < 9.5 MeV, investigated inconclusively through the proton-capture reaction, could also have negative parity. The inhibition of E1 transitions from these levels to the low-lying positive-parity states is not regarded as evidence against negative parity for the capture levels, since the inhibition could be caused by the Nilsson-band selection rule.

The authors have had many valuable discussions with Professor James A. Jacobs and have also benefited from informations given by Chalk River personnel. The enriched targets were made by AERE, Harwell, England, whose fast service was appreciated.

References

1) A. E. Litherland, E. B. Paul, G. A. Bartholomew and H. E. Gove, Can. J. Phys. **37** (1959) 53
2) C. Broude, L. L. Green and J. C. Willmott, Proc. Phys. Soc. **72** (1958) 1097
3) S. G. Nilsson, Mat. Fys. Medd. Dan. Vid. Selsk. **29**, No. 16 (1955)
4) H. O. Cohn, J. K. Bair, J. D. Kington and H. B. Willard, Phys. Rev. **99** (1955) 644
5) H. B. Willard, J. K. Bair, H. O. Cohn and J. D. Kington, Bull. Am. Phys. Soc. **1** (1956) 264
6) P. H. Stelson and W. M. Preston, Phys. Rev. **95** (1954) 974
7) A. E. Litherland, H. McManus, E. B. Paul, D. A. Bromley and H. E. Gove, Can. J. Phys. **36** (1958) 378
8) K. Alder, A. Bohr, T. Huus, B. Mottelson and A. Winther, Revs. Mod. Phys. **28** (1956) 432
9) F. Coester and J. M. Jauch, Helv. Phys. Acta **26** (1953) 3;
S. Devons and L. Goldfarb, Handbuch der Physik **42** (Springer-Verlag, Berlin, 1957)
10) W. T. Sharp, J. M. Kennedy, B. J. Sears and M. G. Hoyle, Atomic Energy of Canada Ltd., Report CRT-556 (1954)
11) J. M. Blatt and L. C. Biedenharn, Revs. Mod. Phys. **24** (1952) 258
12) T. Teichman and E. P. Wigner, Phys. Rev. **87** (1952) 123

2.C:3.A

Nuclear Physics **23** (1961) 338—344; ©*North-Holland Publishing Co., Amsterdam*

Not to be reproduced by photoprint or microfilm without written permission from the publisher

STRUCTURE OF THE GIANT RESONANCE IN THE $Al^{27}(p, \gamma)$ REACTION

MOTOHARU KIMURA, KATSUFUSA SHODA, NAOSHI MUTSURO, TSUTOMU TOHEI,
KAZUO SATO, KUNISHIGE KURODA,

Department of Physics, Faculty of Science, Tohoku University, Sendai, Japan

and

KATSUMI KURIYAMA and TOSHIMITSU AKIBA

Department of Physics, Faculty of Science, Tokyo University of Education, Otsuka, Bunkyo-ku, Tokyo, Japan

Received 13 October 1960

Abstract: The variation of the cross section for $Al^{27}(p, \gamma_0+\gamma_1)Si^{28}$ with proton energy from 7.5 to 14.7 MeV, reveals the full structure of the giant resonance. Gamma ray yields for transitions to the ground and first excited states of the product nucleus were measured using a large NaI(Tl) crystal spectrometer. The width of the giant resonance is of the order of 4 MeV, with many resonance peaks and possibly with a splitting due to deformation.

1. Introduction

Radiative capture of protons followed by ground-state gamma ray transitions is of special interest as the inverse process of (γ, p) reaction. Recently, D. S. Gemmel *et al.* [1,2]) have measured the yields of ground-and (sometimes including first-excited-) state gamma rays using the Canberra 76 cm cyclotron. They investigated Li, B, F^{19}, Na^{23}, Al^{27}, P^{31} (p, γ) reactions by changing the proton energy from 7.7 down to 5 MeV in steps of about 70 keV by interposing Al foils in the beam. They found a gross structure which might be interpreted as the giant resonance in the case of Li target. Their results for F, Na, Al and P targets, however, showed rather strong fluctuations of the yield curves and showed no definite feature of giant resonance. Gove *et al.* [3]), using a tandem Van de Graaff, recently installed at Chalk River, also found the giant resonance in the case of $B^{11}(p, \gamma_0)C^{12}$ and probably of $Al^{27}(p, \gamma_0)Si^{28}$. ($\gamma_0$ denotes the gamma rays to the ground state of product nuclei). Gamma rays to the first excited state (γ_1), however, did not show any definite feature of giant resonance. Though the Chalk River tandem machine is a powerful accelerator to investigate the inverse giant resonance, its energy is sometimes somewhat insufficient to cover the full giant resonance region. The variable energy cyclotron of the Institute for Nuclear Study, Tokyo University, provides proton beams of energy of 7.5 to 14.7 MeV. The lower limit can be extended to around 5 MeV if an absorption foil is used. The energy homogeneity and stability are about 50 keV and are sufficient to survey the giant resonance region if the fine structure is not composed of too sharp resonances.

One of the present authors (K. Shoda) is working on the $Si^{28}(\gamma, p)$ reaction using Tohoku University 25-MeV Betatron[4]). It is, therefore, very interesting to know to what extent the detailed balance holds, as pointed out by Bethe[5]), in the inverse reaction.

2. Experimental Procedures and Results

The proton beam extracted from the variable energy cyclotron of the Institute for Nuclear Study, Tokyo University[6]), was led into the target chamber and then to the beam catcher. A scintillation counter of 10.2 cm diam. by 10.2 cm NaI(Tl) sees the Al target at an angle of 90° to the beam with a solid angle of 2.8×10^{-3} sr defined by a Pb slit. The front face of the NaI is situated 60 cm from the Al target with a 5.0 cm thick paraffin sheet in the gamma ray path. Care was taken to shield off unwanted neutrons and gamma rays from the detector as much as possible. For this purpose, the NaI(Tl) crystal with cathode follower was surrounded first by 15 cm thick Pb blocks, then a 0.5 mm thick Cd sheet, 5 cm thick Boron-paraffin blocks and then by 25 cm thick paraffin plates. About 1 m thick concrete walls surrounded the beam duct and the catcher. The response function of our NaI crystal was taken using 17.6 MeV gamma rays from the Li+p reaction produced by te Tokyo University Van de

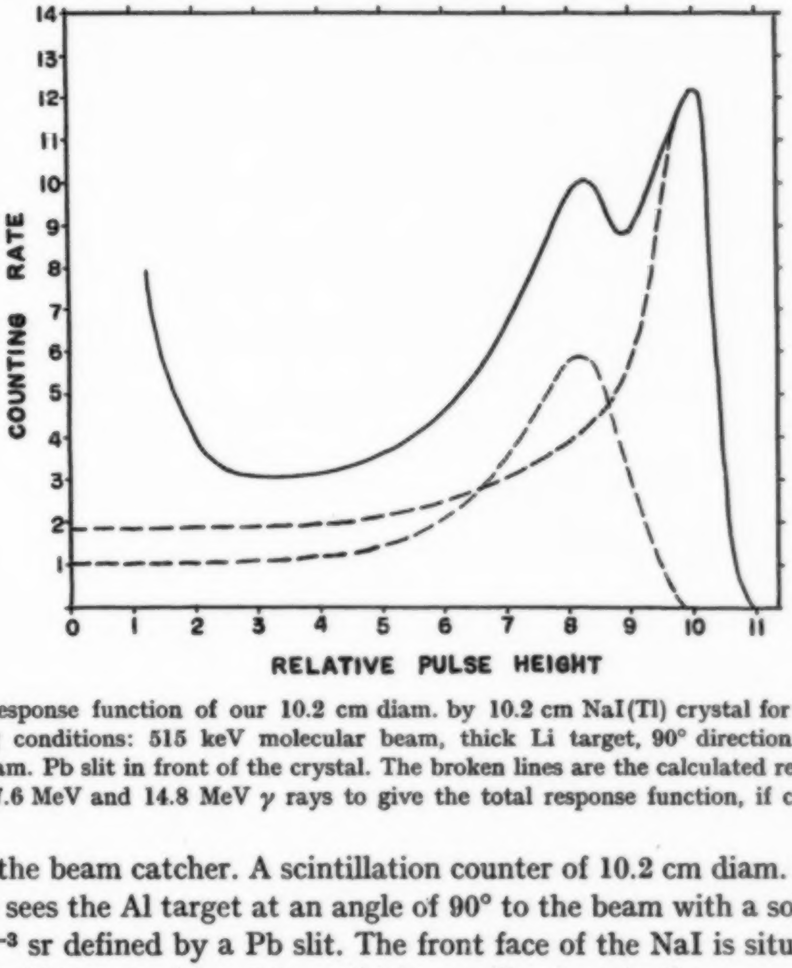

Fig. 1. Response function of our 10.2 cm diam. by 10.2 cm NaI(Tl) crystal for Li+p γ rays. Measuring conditions: 515 keV molecular beam, thick Li target, 90° direction to the beam, 2.5 cm diam. Pb slit in front of the crystal. The broken lines are the calculated response curves for 17.6 MeV and 14.8 MeV γ rays to give the total response function, if combined.

Graaff accelerator, and lower energy gamma rays from conventional radioactive sources. Fig. 1 shows the response functions thus obtained. The Al target was 99.6 % pure and was 9 μm in thickness. The proton beam passed through a quadrupole magnet, a deflecting magnet, an Al target foil with glancing angle of 45° and then was led to the beam catcher which was set at 3 m from the target. A slit system made of carbon defined the beam to 10 mm × 15 mm

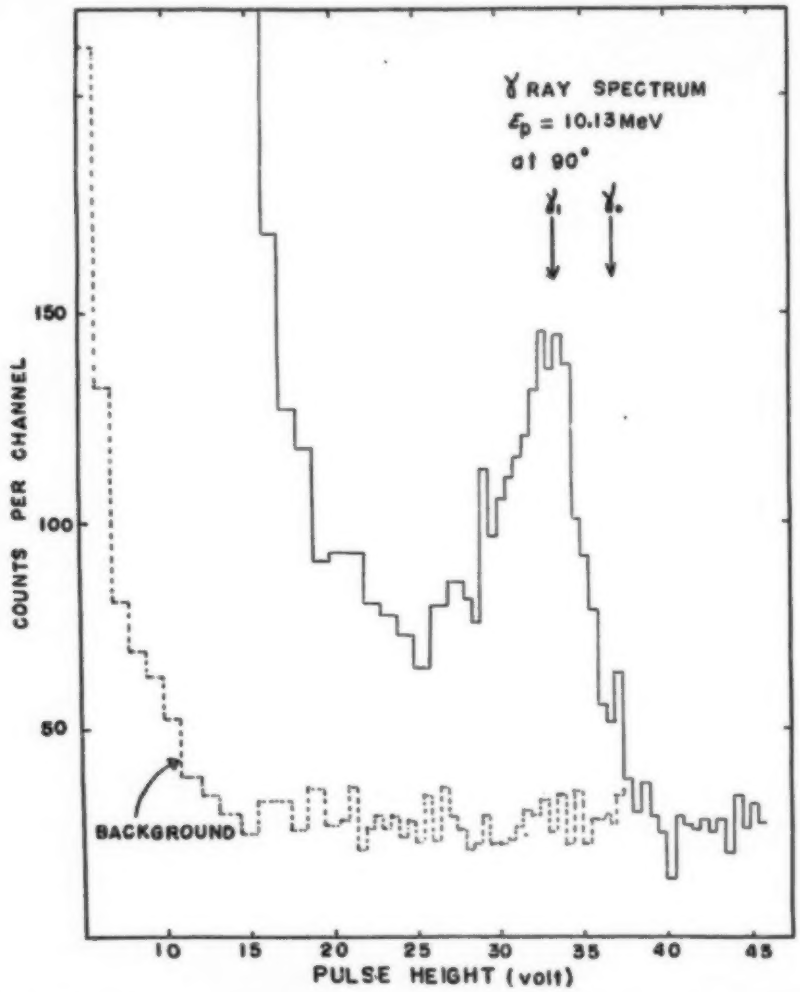

Fig. 2. Gamma ray spectrum for $E = 10.13$ MeV. The broken line is the background spectrum without Al target but with proton beam.

at the target with a beam current of 0.3 to 0.5 μA. The proton beam energy was varied very easily by changing the cyclotron magnetic field and RF frequency simultaneously. It generally takes less than 60 sec to change in fine steps and about 10 min to change in large steps of several MeV. The beam energy was calibrated by range measurements in Al foils and also from the magnetic field and RF frequency. They coincided nicely.

Pileup of the pulses of low-energy gamma rays and neutrons was carefully checked by changing the beam intensity, and it was found that the spectral shape was not influenced by the beam intensity used. Fig. 2 is an example of the gamma ray spectrum which also shows the background spectrum without the target, but with the beam.

It is evident that there exist gamma rays (γ_0) leading to the ground state of Si^{28} ($Q = 11.58$ MeV) and leading to the first excited state (1.78 MeV), γ_1. The two gamma rays were sometimes barely resolved and sometimes not. The yield of $\gamma_0+\gamma_1$ was estimated with reference to the response curve for Li+p gamma rays. It is a somewhat delicate procedure to analyze the spectrum mainly because of the insufficient counting statistics, and also because of the lack of appropriate standard gamma rays. The 17.6 MeV Li+p gamma rays are greatly disturbed by the 14.8 MeV gamma rays to the first excited state of Be^8. The two broken lines in fig. 1 are the expected response functions of the two gamma rays respectively, which give our total response function if added and also the best fit to the data [7]) on the width and the intensity ratio of the two gamma rays. The resolutions of the curves for the two gamma rays, which are 13.1 % and 28.2 % for 17.6 MeV and 14.8 MeV, respectively, as given in fig. 1, are very reasonable figures for our 10.2 cm diam. by 10.2 cm NaI crystal. Assuming the same shape of the response function is applicable to higher gamma rays, we calculated the expected response curve for the 20.4 MeV gamma ray of T^3+p. Our response function agreed well with that of Koch and Wyckoff [8]). We also have taken the 15.1 MeV C$^{12}(\gamma, \gamma)$ peak using the same crystal and Tohoku University 25-MeV Betatron. The shape is as expected, but we have discarded it because of insufficient counting statistics. Again with the same assumption that the response curve is the same for other Al+p$-\gamma_1$ rays, which will become 26 MeV for $E_p = 15$ MeV, we have calculated the cross section σ by

$$\sigma = \frac{n}{NN_p} \frac{4}{\Delta\Omega} \frac{1}{Y} \frac{1}{e^{-\lambda x}}.$$

Here, n is the number of counts under the response curve of γ_1. In practice, however, the counts due to the ground state gamma γ_0 were very small and they were included to γ_1, giving the cross section for (p, $\gamma_0+\gamma_1$). N is the number of Al atoms per cm^2 in the target, taking into account the angle to the beam. N_p is the number of protons corresponding to the current integrator reading, and $\Delta\Omega$ is the solid angle of the Pb slit sees at the target. We neglected the possible anisotropy of gamma emission. The Pb slit is tapered with an entrance diameter of 2.5 cm, an exit diameter of 3.2 cm and 15.2 cm in length. The factor $e^{-\lambda x}$ is the attenuation factor of gamma rays corresponding to the 5 cm boron-paraffin neutron absorber in front of the slit. The total counting efficiency Y of the NaI crystal for the gamma rays was computed by using the table of X-ray attenuation of G. W. Grodstein [9]). The estimation of error in the absolute cross section is rather difficult. The main uncertainty comes from the shape of the NaI response function and also from the poor counting statistics. The overall uncertainty was estimated to be about $\pm 17\,\%$.

Fig. 3 is the result of (p, $\gamma_1+\gamma_0$) cross section as a function of bombarding energy. The figure also includes the Canberra results [2]). In the overlapping region of $E_p = 7.4$—7.7 MeV, the results of the two groups agree very well except for the absolute cross section. It is evident that the full structure of giant resonance is revealed in the region from about 5 MeV to 13 MeV of proton bombarding energy. The half width of giant resonance is of the order of 4 MeV. There are, however, many sharp fluctuations in the cross section. At least three peaks at 7.61 MeV, 8.75 MeV and 10.13 MeV of E_p are clearly seen. Gemmel *et al.* [2]) reported that the 90° cross section at 7.7 MeV was $(190\pm50)\mu$b for $Al^{27}(p, \gamma_0+\gamma_1)$. This is about a factor of two larger than our results. Our maximum cross section lies at $E_p = 10.13$ MeV and is $(170\pm35)\mu$b.

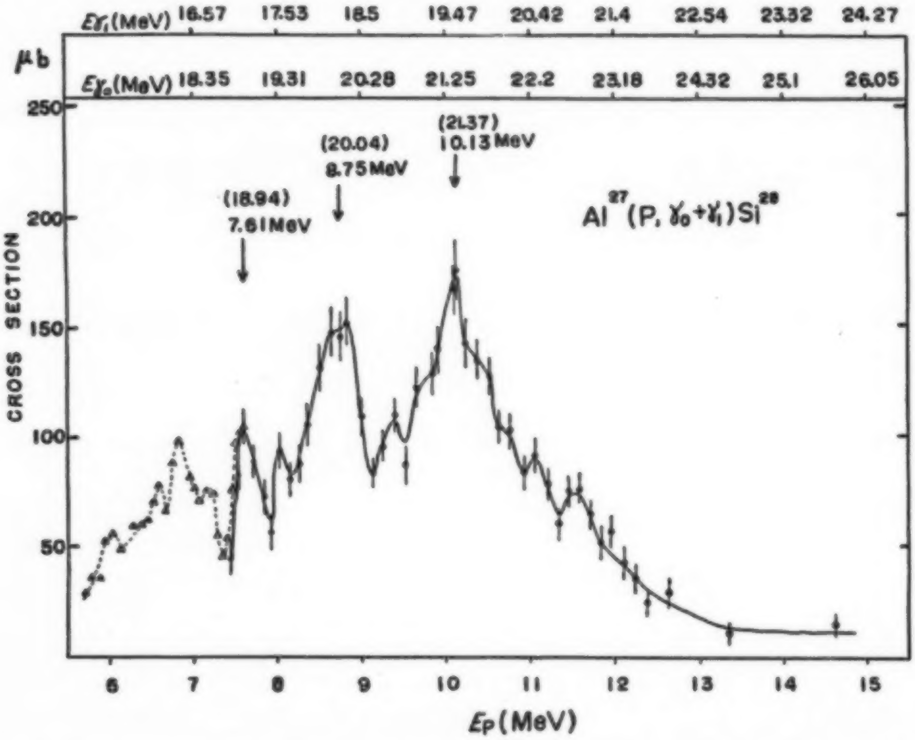

Fig. 3. Relative cross section of the $Al^{27}(p, \gamma_0+\gamma_1)Si^{28}$ reaction. The lower abscissa is the laboratory proton energy, the upper abscissa, the calculated energy of γ_0 and γ_1. The full line gives the present results; the broken line gives the Canberra results continued smoothly to the present results, neglecting the discrepancy in absolute cross sections.

3. Discussion

If we neglect the sharp fluctuations of resonances, it looks very plausible that the main part of giant resonance is split into two peaks. According to the theory of Okamoto and Danos [10]), this means a spheroidal deformation of the compound nucleus. If so, the eccentricity $e \equiv (R_1-R_2)/R_0$ of Si^{28} becomes about 0.05 with possible prolate sign. This is very reasonable if we consider the deformation of Al^{27} and Si^{29} to be $+0.15$ and -0.15 respectively according to Bromley *et al.* [11]) who deduced the above results from their spectroscopic investigation. The (p, γ_0) reaction offers the possibility of finding evidence of triple splitting of the giant resonance †. The sharp fluctuation of the cross section curve may originate from many unresolved resonances. It is very desirable to repeat the experiment with finer resolutions. For this purpose a tandem Van de Graaff would be a powerful tool.

The origin of many sharp resonances may also be interpreted in various ways by other current theories on photonuclear reactions. It may be possible to interprete it by the single particle model as was successful in the case of $N^{15}(p, \gamma)O^{16}$ investigated by Cohen *et al.* [12]). At this time, however, we would like to point out that the yield of $B^{11}(p, \gamma_0)C^{12}$ does not show conspicuous resonances [1,3]), and seems to belong to a different case from that of $N^{15}(p, \gamma)O^{16}$. According to Penfold and Garwin [13]), the gamma ray absorption of C^{12} and that of O^{16} are of very different character. The latter shows sharp resonances at the giant resonance region, whereas the former looks to occur without sharp resonances. The results of Gemmel *et al.* [2]) on F^{19} and $Na^{22}(p, \gamma)$ reactions are the intermediate cases. The fluctuations of Al^{27} we found seem to be similar to the case of O^{16}. However, they may be of different origin, because the level widths of the two cases are entirely different. In relation to this problem we point out the following facts which appear in different fields of nuclear reactions.

Recently, sharp resonances in various reactions at incident particle energies of greater than several MeV for various intermediate nuclei have been found [14,15]). In every case the resonance distances and the widths are of the order of several hundred keV. The phonomena are seen for nuclei with mass numbers between 25 and 60. For nuclei heavier than 60, the same resonances are also expected, though not yet fully investigated. Types of reactions investigated are (p, p'), (p, γ), (n, n'). (n ,p) or (n, γ) is expected to show the same character. Our case also may be the same situation.

Shaw [16]) and H. Izumo [17]) have tried to explain the phenomena by local heating. Tamura and Okai are considering the theory which takes into account the channel coupling. The problem will be clarified if further experiments on (p, γ) as well as on other reactions are carried out.

Application of the principle of detailed balance would be very interesting, but because of the complex situations of both of (γ, p) and (p, γ) reactions, numerical calculations are difficult.

---

† We thank Okamoto for the discussion of this point.

We wish to acknowledge very stimulating and helpful discussions with Dr. K. Okamoto who is now at Tohoku University. We also express sincere thanks to the cyclotron crew of the Institute for the Nuclear Study, University of Tokyo, for their help in cryclotron operation and other arrangements. We are greatly indebted to Prof. Nogami and his Van de Graaff crew for their kind cooperation in taking the response function of the NaI crystal.

References

1) D. S. Gemmel, A. H. Morton and E. W. Titterton, Nuclear Physics **10** (1959) 33
2) D. S. Gemmel, A. H. Morton and W. I. B. Smith, Nuclear Physics **10** (1959) 45
3) H. E. Gove, A. H. Litherland and R. Batchelor, Phys. Rev. Letters **3** (1959) 177
4) K. Shoda ,to be published
5) H. A. Bethe, Rev. Mod. Phys. **9** (1937) sect. 14
6) S. Kikuchi *et al*, J. Phys. Soc. Japan **15** (1960) 41
7) M. B. Stearns and McDaniel, Phys. Rev. **82** (151) 4502
8) R. L. Walker and B. D. McDaniel, Phys. Rev. **74** (1948) 315;
E. K. Inall and A. J. F. Boyle, Phil. Mag. **44** (1953) 1081;
R. S. Foote and H. W. Koch, R. S. I. **25** (1954) 746;
H. W. Koch, J. M. Wyckoff, IRE Transition, NS-5 (1958) 127
9) G. White Grodstein, NBC Circular 518 (1957)
10) K. Okamoto, Prog. Theor. Phys. Japan **15** (1956) 75, Phys. Rev. **110** (1958) 143
11) D. A. Bromley, H. E. Gove, E. B. Paul, A. E. Litherland and E. Almquivist, Can. J. Physics **35** (1957) 1042, 1057
12) S. G. Cohen, P. S. Fisher and E. K. Warburton, Phys. Rev. Letters **3** (1959) 433
13) A. S. Penfold and E. L. Garwin, Phys. Rev. **116** (1959) 120
14) F. D. Seward, Phys. Rev. **114** (1959) 514
15) Y. Oda *et al.*, J. Phys. Soc. Japan **15** (1960) 750
16) Shaw, Annals of Phys. **8** (1959) 509
17) S. Igarashi, K. Izumo and T. Udagawa, Prog. Theor. Phys. **21** (1959) 468

8.B

Nuclear Physics **23** (1961) 345—348; *©North-Holland Publishing Co., Amsterdam*

Not to be reproduced by photoprint or microfilm without written permission from the publisher

ON THE $\pi^-+\mathrm{p}\rightarrow\Lambda^0+\mathrm{K}^0$ AMPLITUDE

R. J. N. PHILLIPS
A.E.R.E., Harwell, England

Received 20 October 1960

Abstract: Two ways to resolve a certain phase-ambiguity, arising in the S+P wave analysis, are pointed out.

1. Introduction

This note points out that two lines of study, previously proposed to elucidate the KΛ and $\Lambda\Sigma$ relative parities, may also resolve a certain ambiguity in the $\pi^-+\mathrm{p}\rightarrow\Lambda^0+\mathrm{K}^0$ amplitude.

For production in final S and P states, the cross section $\sigma_\Lambda(\theta)$ and polarization $P_\Lambda(\theta)$ have the forms [1] †

$$\sigma_\Lambda(\theta) = |a+b\cos\theta|^2+|c\sin\theta|^2, \tag{1}$$

$$P_\Lambda(\theta) = 2\,\mathrm{Im}\,c^*\sin\theta(a+b\cos\theta)/\sigma_\Lambda(\theta). \tag{2}$$

Here θ is the c.m. angle of Λ relative to π, and polarization is in the sense of $\mathbf{n} = \mathbf{p}_\pi\times\mathbf{p}_\Lambda/|\mathbf{p}_\pi\times\mathbf{p}_\Lambda|$, where $\mathbf{p}_\pi$ and $\mathbf{p}_\Lambda$ are the c.m. momenta of the π and Λ. The quantities a, b and c are complex numbers which specify the production amplitude, given the KΛ parity. They are determined to within a fourfold ambiguity and a common phase [2] by σ_Λ and P_Λ, which are inferred from the distribution of π^- from Λ-decay, given the decay asymmetry parameter α [1]. ††

This ambiguity comes partly from a cubic equation for $|c|^2$, which has two positive roots. However, these roots are very close: the corresponding solutions for a, b and c in ref. [2] coincide within the errors. Hence this first ambiguity seems unimportant (though in principle it could be resolved by the energy-dependence of the solution [1]).

There remains an ambiguity of phases: if a, b, c is a solution, so is a^*, b^*, $-c^*$. Production from polarized protons would be needed to resolve this directly; however, the present note points out two indirect methods.

One method uses relations between production phases and π^-—p phase shifts, originally proposed ^{6}) to decide the KΛ parity. The other relies on anomalies in $\Lambda^0+\mathrm{K}^0$ production near the $\Sigma^0+\mathrm{K}^0$ threshold ^{7,8}) of interest in connection with the $\Lambda\Sigma$ parity.

---

† We take the established values 0 and ½ for K⁰ and Λ^0 spins.

†† $|\alpha|$ is near 1. Recent experiments show $|\alpha| \geq 0.95\pm0.08$ (private communication from Dr. F. S. Crawford, Jr.). Experiments [3,4] differ on the sign of α. Provisionally we take $\alpha > 0$, as suggested by theory [5]). Fortunately, a, b and c are not sensitive [2] to small changes in $|\alpha|$, and a sign change simply multiplies c by -1.

2. The Production Amplitude

The production amplitude M is a 2×2 matrix in spin space, characterized by a, b and c. For odd KΛ parity,

$$M = a+b\cos\theta+ic\sin\theta\,\boldsymbol{\sigma}\cdot\mathbf{n}, \tag{3}$$

while for even parity,

$$M = [a+(b+c)\cos\theta]\boldsymbol{\sigma}\cdot\mathbf{p}_\pi/|\mathbf{p}_\pi|-c\boldsymbol{\sigma}\cdot\mathbf{p}_\Lambda/|\mathbf{p}_\Lambda|, \tag{4}$$

where $\boldsymbol{\sigma}$ denotes the Pauli matrices.

We now introduce the partial wave amplitudes, denoted by $(\mathrm{S}_{\frac12}, \mathrm{P}_{\frac12})$ for initial $\mathrm{S}_{\frac12}$ and final $\mathrm{P}_{\frac12}$ states, etc. Then for odd and even parities respectively (see e.g. ref. ^{9})), putting $|\mathbf{p}_\pi| = \hbar k$,

$$\left.\begin{aligned}(\mathrm{S}_{\frac12}, \mathrm{S}_{\frac12})/2k &= a\\ (\mathrm{P}_{\frac12}, \mathrm{P}_{\frac12})/2k &= -\tfrac13(b-2c)\\ (\mathrm{P}_{\frac32}, \mathrm{P}_{\frac32})/2k &= -\tfrac13(b+c)\end{aligned}\right\}\quad\text{(odd)}, \tag{5}$$

$$\left.\begin{aligned}(\mathrm{P}_{\frac12}, \mathrm{S}_{\frac12})/2k &= ia\\ (\mathrm{S}_{\frac12}, \mathrm{P}_{\frac12})/2k &= \tfrac13 i(b-2c)\\ (\mathrm{D}_{\frac32}, \mathrm{P}_{\frac32})/2k &= -\tfrac13 i(b+c)\end{aligned}\right\}\quad\text{(even)}^{\dagger}. \tag{6}$$

We shall denote the phase of each amplitude by $\phi(\mathrm{S}_{\frac12}, \mathrm{P}_{\frac12})$, etc.

3. First Method: Phase Relations

The phases $\phi(\mathrm{S}_{\frac12}, \mathrm{P}_{\frac12})$, etc., are related directly to $\pi-\mathrm{p}$ phase shifts ^{6}), if $\mathrm{K}-\Lambda$ scattering is weak and pion production is ignored. The latter proviso is a serious weakness; however, there is an encouraging example in photopion production ^{10}), where two-channel phase relations hold approximately even though other channels are important.

The phase relations, stated conveniently as differences, are

$$\left.\begin{aligned}\phi(\mathrm{S}_{\frac12}, \mathrm{S}_{\frac12})-\phi(\mathrm{P}_{\frac12}, \mathrm{P}_{\frac12}) &= \delta_1-\delta_{11} &&\text{(within } n\pi),\\ \phi(\mathrm{S}_{\frac12}, \mathrm{S}_{\frac12})-\phi(\mathrm{P}_{\frac32}, \mathrm{P}_{\frac32}) &= \delta_1-\delta_{13} &&\text{(within } n\pi),\end{aligned}\right. \tag{7}$$

$$\left.\begin{aligned}\phi(\mathrm{P}_{\frac12}, \mathrm{S}_{\frac12})-\phi(\mathrm{S}_{\frac12}, \mathrm{P}_{\frac12}) &= \delta_{11}-\delta_1 &&\text{(within } n\pi),\\ \phi(\mathrm{P}_{\frac12}, \mathrm{S}_{\frac12})-\phi(\mathrm{D}_{\frac32}, \mathrm{P}_{\frac32}) &= \delta_{11}-\delta_{13}^{(\mathrm{D})} &&\text{(within } n\pi),\end{aligned}\right. \tag{8}$$

---

† The related formulae of ref. ^{9}) seem to be in error.

for odd (eq. (7)) and even (eq. (8)) KΛ parity, respectively. We use a familiar notation for the pion-nucleon phase shifts (the real parts), distinguishing the D-wave by a superscript.

If eqs. (7) and (8) were precisely true, they would decide both the KΛ parity and the phase ambiguity. Treated hopefully as rough approximations, they might still provide an indication. For the phase ambiguity, this indication would be clearer if the KΛ parity were known.

Pion-nucleon phase shifts are not known in the required energy range; however, Walker *et al.* [11]) have found plausible values at 600 MeV (pion lab. energy), not far below the K+Λ threshold at 760 MeV. The only published S and P wave analysis of production amplitudes is at 990 MeV [2]); however, we do not expect the phases ϕ to vary much near threshold [1]). Therefore, as a preliminary measure, we may compare these results using eqs. (7) and (8). This is done in table 1. The rows labelled "normal" and "alternate" refer to the two solutions allowed by the phase ambiguity, following the notation of ref. [2]).

TABLE 1

Pion-nucleon phase shifts in degrees; comparison of experiment with "theory"

		odd parity		even parity	
		$\delta_1-\delta_{11}$	$\delta_1-\delta_{13}$	$\delta_{11}-\delta_1$	$\delta_{11}-\delta_{13}^{(D)}$
Experiment [11])		49 ± 17	72 ± 9	-49 ± 17	$-7\pm^{15}_{38}$
Theory	normal	95 ± 18	172 ± 25	-85 ± 18	-8 ± 25
	alternate	20 ± 20	118 ± 30	20 ± 20	-62 ± 30

The errors shown in this table prevent any conclusion, for we may expect the two-channel phase relations themselves to be wrong by as much as 20° for each partial wave (judging by the photopion example) [10]). Much greater accuracy is needed before we can apply this method.

However, if table 1 were taken at face value, there would seem to be a preference for the "normal even-parity" and "alternate odd-parity" cases. This again suggests that it would be easier to resolve the phase-ambiguity if the parity were already decided, and vice versa.

Finally we remark that table 1 assumes $\alpha > 0$. Reversing the sign of α amounts to interchanging "normal" and "alternate", and taking conjugate complex production amplitudes (see section 1). This alters the numerical entries, but our conclusions remain the same.

4 Second Method: Threshold Anomalies

The Σ^0+K^0 S-wave production cross section has an infinite slope at threshold, causing anomalies in the coupled processes of $\pi^- - p$ scattering and Λ^0+K^0

production. The nature of the Λ^0+K^0 anomalies determines the $\Lambda\Sigma$ parity [7, 8]; furthermore, quantitative measurements of them can fix the Λ^0+K^0 production amplitude within an overall phase [8]).

However, we shall show that the phase-ambiguity in a, b and c can be decided by qualitative considerations alone, if the $\Lambda\Sigma$ parity is odd. In this case, a quantitative study of the Λ^0+K^0 anomalies would be unpromising; there would remain only the first kind of ambiguity (nearly degenerate), which would be very hard to resolve.

Suppose that measurements of Λ^0+K^0 production around the Σ^0+K^0 threshold are converted into determinations of a, b and c, corresponding for definiteness to the "normal" solution of ref. [2]). Matching angular momentum and parity in the competing Λ^0+K^0 and Σ^0+K^0 channels, and using eqs. (5) and (6), we find the following five possibilities for the presence of anomalies:

(i) Anomaly in a, none in b or c. Then Λ and Σ have the same spin and parity, and the phase-ambiguity is not resolved.

(ii) Anomaly in $b-2c$, none in a or $b+c$. Then Λ and Σ have the same spin but opposite parity, and the "normal" solution is correct.

(iii) Anomaly in $b+2c$, none in a or $b-c$: as (ii) except that the "alternate" solution is correct.

(iv) Anomaly in $b+c$, none in a or $b-2c$. Then Σ has spin $\frac{3}{2}$, Λ and Σ have opposite parity, and the "normal" solution is correct.

(v) Anomaly in $b-c$, none in a or $b+2c$: as (iv) except that the "alternate" solution is correct.

Preliminary measurements [12]) suggest there may be anomalies in certain terms of σ_Λ and $P_\Lambda\sigma_\Lambda$ which depend on b and c alone, and hence that the $\Lambda\Sigma$ parity is indeed odd as we require.

References

1) T. D. Lee, J. Steinberger, G. Feinberg, P. K. Kabir and C. N. Yang, Phys. Rev. **106** (1957) 1367
2) F. S. Crawford, M. Cresti, M. L. Good, K. Gottstein, E. M. Lyman, F. T. Solmitz, M. L. Stevenson and H. K. Ticho, Proc. Conf. High En. Phys. CERN (1958) p. 323
3) E. Boldt, H. S. Bridge, D. O. Caldwell and Y. Pal, Phys. Rev. Letters **1** (1958) 256
4) R. W. Birge and W. B. Fowler, Phys. Rev. Letters **5** (1960) 254
5) S. Okubo, R. E. Marshak and E. C. G. Sudarshan, Phys. Rev. **113** (1959) 944
6) D. Amati and B. Vitale, Nuovo Cim. **9** (1958) 340
7) R. K. Adair, Phys. Rev. **111** (1958) 632
8) A. N. Baz and L. B. Okun, Zh. Eksp. Teor. Fiz. **35** (1958) 757; also: Soviet Physics, JETP **8** (1959) 526
9) R. H. Capps, Phys. Rev. **115** (1959) 736
10) R. H. Capps, Phys. Rev. Letters **2** (1959) 475
11) W. D. Walker, J. Davis and W. D. Shephard, Phys. Rev. **118** (1960) 1612
12) Proc. Conf. High En. Phys. Rochester (1960)

2.E

Nuclear Physics **23** (1961) 349—352; ©*North-Holland Publishing Co., Amsterdam*

Not to be reproduced by photoprint or microfilm without written permission from the publisher

CONVERGENCE OF THE CLUSTER EXPANSION FOR THE OPTICAL MODEL POTENTIAL

P. B. JONES †
Clarendon Laboratory, Oxford

Received 10 November 1960

Abstract: The convergence of the cluster expansion for the optical model potential is examined, at low energies, by comparison of the series with the potential given by a closed form. The problem of antisymmetrization is not considered.

The purpose of this note is to demonstrate a relation between the convergence of the cluster expansion for the optical model operator and the presence of discrete compound states of the whole system. A closed expression for the optical model operator is obtained which contains parts corresponding to both direct interaction and compound nucleus processes. Theories showing how these classes of process can both be understood in terms of the nuclear optical model have been presented by Brown [1]) and by Feshbach [2]) and it is not the purpose of this note to pursue this particular problem further. We are concerned with the relation between the optical model potential and the particle-nucleon potential.

The incident particle is assumed to be different from a nucleon so that the exact cluster expansion for the optical model operator at energy E is

$$\langle \mu_0 \mathbf{k}' | U | \mu_0 \mathbf{k} \rangle = \langle \mu_0 \mathbf{k}' | [\sum_i t_i + \sum_i \sum_{i \neq j} t_i \alpha G(E) t_j + \ldots] | \mu_0 \mathbf{k} \rangle, \tag{1}$$

the summations extending over the A nucleons in the target nucleus. Further definitions are [3])

$$t_i = v_i + v_i \alpha G(E) t_i, \tag{2}$$

$$G(E) = (E - H_0 + i\varepsilon)^{-1}, \quad (\varepsilon > 0), \tag{3}$$

$$\alpha = 1 - \sum_{\mathbf{k}} |\mu_0 \mathbf{k}\rangle\langle \mu_0 \mathbf{k}|, \tag{4}$$

where v_i is the interaction between the incident particle and the nucleon labelled by i and H_0 is the sum of the exact Hamiltonian of the target nucleus and of the kinetic energy operator of the incident particle. $|\mu' \mathbf{k}\rangle$ is an eigenstate of H_0, $\mu' = \mu_0$ denoting the ground state of the target and $\mathbf{k}$ being the momentum of the incident particle. From eq. (2) onwards, use of the appropriate representation, as in eq. (1), is to be understood. The elastic scattering amplitude is given by the series

---

† Central Electricity Generating Board Research Fellow, St. Catherine's College.

$$U + U\beta G(E)U + U\beta G(E)U\beta G(E)U + \ldots,$$

where $\beta = 1-\alpha$ and successive terms represent processes of 1, 2, 3 . . . scatters, the target remaining in the ground state. The convergence of this series will not be considered in this note. If U is represented by a static potential, this is equivalent to the problem of the convergence of the Born series which has recently been solved by H. Davies[4]).

Returning to eq. (1), it is clear that each term in the series leads to a complex potential only when the incident particle is sufficiently fast for the centre of mass energy to be greater than E_1, the energy separation of the ground and first excited states of the target. This is not consistent with the fact that discrete compound states of the whole system can occur at lower energies and lead to an imaginary part in the optical model potential. It will be shown that such states may occur in an energy interval in which the series (1) is not uniformly convergent. Some formalisms are based on a Green's function which contains a single-particle operator, for example $(E-H_0-U+i\varepsilon)^{-1}$, and is equivalent to the partial summation of (1). Since U is a single-particle operator, the physical content of such a function is little different from that of $G(E)$ and the remarks of this note still apply. A more complete theory therefore requires summation of the series. Without the inclusion of some terms of order $1/A$, eq. (1) may be represented by

$$U = \sum_i t_i + \sum_i \sum_{i\neq j} t_i \mathscr{G}' t_j, \tag{5}$$

where $\mathscr{G}'$ is to be determined. $\mathscr{G}'$ is given by

$$\mathscr{G}' = \alpha G(E) + \alpha G(E) V \alpha G(E) + \ldots, \tag{5.1}$$

which may not be summed directly since α has no inverse. The series

$$(\alpha+x)^{-1}\mathscr{G}'(x) = G(E) + G(E)V(\alpha+x)G(E) + \ldots,$$

where x is an operator such that $(\alpha+x)^{-1}$ exists, may be summed and we obtain

$$\mathscr{G}' = \lim_{x\to 0} \mathscr{G}'(x) = \alpha(E-H_0-V\alpha+i\varepsilon)^{-1}, \tag{6}$$

where the total interaction V is the sum of the separate interactions v_i. Spectral decomposition of (6) is not simple as $H_0+V\alpha$ is not hermitian. It is convenient to divide the space $|\mu'\mathbf{k}\rangle$ into two orthogonal subspaces denoted by a and b where a-space consists of the set $|\mu_0\mathbf{k}\rangle$ for all $\mathbf{k}$. The series (5.1) is then just a sum of operators in b-space. Clearly (6) must have the same form. In addition (1) and (5.1) are unchanged when the permutation $\alpha G \to G\alpha$ is made and again (6) must have this property. These two requirements are satisfied if we construct, in b-space, the vectors

$$|\theta\rangle = \alpha G^{\dagger}(E')V|\theta\rangle, \tag{7}$$

and, for $E' > E_1$, the further sets

$$|\theta\rangle = |\mu'\mathbf{k}'\rangle + \alpha G^{\dagger}(E')V|\theta\rangle. \tag{8}$$

Then (5) becomes

$$U = \sum_i t_i + \sum_i \sum_{i \neq j} t_i \sum_\theta |\theta\rangle (E-E'+i\varepsilon)^{-1} \langle\theta|(1-X)^{-1} t_j, \tag{9}$$

where $X = 0$ if the states given by (7) and (8) form a complete set. X is an operator in b-space and is assumed to be independent of E'. Eq. (9) is similar to the result derived by Feshbach [2]). In (9), the first term represents elastic scattering by direct interaction only while the second term includes elastic scattering through the compound nucleus. The separation is clearly not unique. The presence of $G^{\dagger}(E')$ in (7) and (8) is necessary if the sign of the imaginary part of the optical model potential is to be negative. In b-space $H_0 + V\alpha$ is equivalent to $H_0 + V$ so that the states $|\theta\rangle$ are eigenstates of H_0+V orthogonal to $|\mu_0\mathbf{k}'\rangle$ and with an ingoing wave boundary condition. (7) may have solutions for discrete, possibly complex, values of E', while the $|\theta\rangle$ of (8) are continuous functions of E' for $E' > E_1$. The contribution to $\langle\mathbf{k}|U|\mathbf{k}\rangle$ given by a single state $|\theta\rangle$ at $E'' < E_1$ is therefore

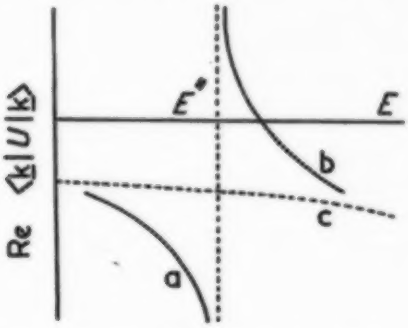

Fig. 1. Sketch of the behaviour of the real part of eq. (9) as a function of energy for $E \approx E''$.

$$\lim_{\varepsilon \to 0} \sum_i \sum_{i \neq j} \langle\mu_0\mathbf{k}|t_i|\theta\rangle \frac{E-E''-i\varepsilon}{(E-E'')^2+\varepsilon^2} \langle\theta|t_j|\mu_0\mathbf{k}\rangle, \tag{10}$$

for E'' real and $X = 0$, which has an imaginary part proportional to $\delta(E-E'')$. In the region near E'', the behaviour of the real part of (9) is sketched in fig. 1, curves (a) and (b).

Returning to (1), we note that U depends on E only through the factors $(E-H_0+i\varepsilon)^{-1}$ and that for $E < E_1$ these are negative-definite. In a model in which all elements of the representation $\langle\mu''\mathbf{k}''|t_i|\mu'\mathbf{k}'\rangle$ are negative, each term in the series (1) will be negative-definite. Further, using the formal result

$$\frac{\partial t_i}{\partial E} = -t_i(E-H_0)^{-2} t_i \leqq 0$$

for $E < E_1$, which may be derived if the perturbation expansion of t_i exists, we see that $\partial U/\partial E$ in the same model is negative-definite. Suppose that E_1 is large. Then for $E \approx 0$ the denominators must always be large and there must certainly exist a v_i for which (1) is uniformaly convergent in this region. If E is now increased, the behaviour of Re $\langle \mathbf{k}|U|\mathbf{k}\rangle$ in the model will correspond to that of curve (a) of fig. 1. Curve (c) shows the contribution to eq. (9) from the single term t_i and from the $|\theta\rangle$ for $E' > E_1$. Both contributions are negative-definite and monotonic functions of E for $E < E_1$. It is therefore possible to conjecture that the energy E'' at which the first discrete state appears is in general a boundary of the region in which (1) is uniformly convergent. Certainly the existence of the imaginary part of $\langle \mathbf{k}|U|\mathbf{k}\rangle$ proportional to $\delta(E-E'')$ is a sufficient condition for (1) not to be convergent at $E = E''$. If there is more than one discrete $|\theta\rangle$ in the interval $0 < E < E_1$, it is not possible to say whether further regions of uniform convergence exist between the discrete values of E'. Another possibility is that the lowest discrete state $|\theta\rangle$ may not be in the region considered but may be at a negative energy. In this case nothing can be said about the convergence of (1).

As a summary, we note that for the model considered the behaviour of (1) and of its derivative $\partial U/\partial E$ as functions of energy near the point where uniform convergence breaks down is similar to the behaviour of the closed form (9) at an energy just below the energy E'' of the first discrete state $|\theta\rangle$. This suggests that in the general case E'' may be a boundary of the region of uniform convergence.

Comparison of (9) and (1) for the scattering of slow neutrons by medium or heavy nuclei shows that (1) is not uniformly convergent in the region near zero neutron energy because there are many compound states (below E_1), which contribute to the imaginary part of the potential. However, as an example in which E_1 is large and for which antisymmetrization is not required we may quote the scattering of slow Λ^0 hyperons by ^{4}He, for which $E_1 = 19.8$ MeV. The ground state of the whole system is at $E = -3.21$ MeV and so it is likely that the lowest $|\theta\rangle$ will be at some $E' > 0$. In this case, if our conjecture is correct, (1) will be uniformly convergent at $E \approx 0$ and may be used to calculate U [5]).

References

1) G. E. Brown, Rev. Mod. Phys. **31** (1959) 893
2) H. Feshbach, Ann. Phys. **5** (1958) 357
3) P. B. Jones, Proc. Roy. Soc. A **255** (1960) 253
4) H. Davies, Nuclear Physics **14** (1960) 465
5) P. B. Jones, Clarendon Laboratory Report No. 24/60.

1.E.8

Nuclear Physics **23** (1961) 353—368; *North-Holland Publishing Co., Amsterdam*

© North-Holland Publishing Co.

Not to be reproduced by photoprint or microfilm without written permission from the publisher

EFFECTS OF THE NUCLEAR BINDING OF NUCLEONS ON PION SPECTRA

H. HELFER, A. S. KUZNETSOV, M. G. MESCHERYAKOV, W. SWIATKOWSKI and V. G. VOVCHENKO

Joint Institute for Nuclear Research, Dubna, USSR

Received 11 July 1960

Abstract: Using a magnetic spectrometer a comparative study was made of the energy spectra of π^+ and π^--mesons produced in free pp-collisions as well as in pp- and pn-collisions in deuterons and in carbon nuclei at 654 MeV. The forms of the spectra of pions from deuterium and carbon are found to differ due to: a) a larger extent of correlation of nucleons in carbon nuclei than in deuterons; b) differences in the momentum distributions of nucleons in these nuclei; c) secondary pion-nucleon interactions in carbon nuclei. At ≈ 90° in the centre-of-mass system of two colliding nucleons the ratio of the differential cross sections for the production of π^+-mesons on free protons and on protons in deuterons and in carbon nuclei was found to be equal to

$$\frac{d\sigma}{d\omega}[p+p\rightarrow\pi^+]_H : \frac{d\sigma}{d\omega}[p+p\rightarrow\pi^+]_D : \frac{d\sigma}{d\omega}[p+p\rightarrow\pi^+]_C = 1 : 0.79 : 0.40,$$

whereas the yields of π^--mesons per neutron for deuterium and carbon were found to be equal.

The measured ratio $(d\sigma^+/d\omega)/(d\sigma^-/d\omega)$ of the differential cross sections for the production of positive and negative pions on deuterium and carbon is equal to 10.3 ± 1.3 and 6.0 ± 0.8, respectively. The decrease of the value of this ratio for carbon is caused by a considerable contribution of the secondary exchange interaction $\pi^0+n\rightarrow\pi^-+p$ to the yield of π^--mesons.

1. Introduction

At present little is known about the difference between the elementary processes of pion production in the collisions of nucleons with free nucleons and nucleons bound in nuclei. This difference, the existence of which is beyond question, may be caused by such obvious factors as the intranuclear motion and mutual "shading" of nucleons, the exclusion principle for recoil nucleons and the reabsorption of pions in the original nuclei as well as by certain specific effects due to the deformation and overlapping of meson shells of nucleons in closely correlated groups.

This paper is concerned with experiments to obtain quantitative information on the effects of nuclear binding of nucleons in deuterons and in carbon nuclei on the process of the production of charged pions. The approach to the problem under consideration is based on comparing the forms of the energy spectra of pions produced in the collisions of protons with free protons and with nucleons bound in deuterons and in carbon nuclei. The procedure employed in the present experiments ensured the measurement of pion spectra in strictly identical conditions and the separation of the effects from pp- and pn-collisions.

Experiments performed at 460, 660 [1, 2]) and 970 [3]) MeV show that pd-collisions without pion production are, mainly, a quasi-elastic scattering of incident protons by single nucleons in deuterons similar, in general, to the scattering of protons by free nucleons. Only in rare cases do the incident protons interact simultaneously with both nucleons inside the deuteron. Such triple collisions also involve the elastic pd-scattering with a differential cross section equal to $\approx 10^{-29}$ cm^2/sr at energies of 460 MeV in the region of large scattering angles.

Owing to a proton-nucleon character of the high energy pd-collisions the following reactions of single pion production are possible:

$$p+p+(n) \rightarrow \pi^+ + p + n + (n), \quad (1)$$

$$p+p+(n) \rightarrow \pi^0 + p + p + (n), \quad (2)$$

$$p+n+(p) \rightarrow \pi^+ + n + n + (p), \quad (3)$$

$$p+n+(p) \rightarrow \pi^0 + p + n + (p), \quad (4)$$

$$p+n+(p) \rightarrow \pi^- + p + p + (p), \quad (5)$$

where (n) and (p) denote nucleons not colliding directly with incident protons and therefore emitted with low energy. According to Batson *et al.* [3]) the probable energy of non-colliding protons in pd-collisions at 970 MeV is about 5 MeV, their angular distribution being weakly correlated with the direction of the incident beam. In pd-collisions the pion production is possible also in reactions in which two or three nucleons in the final state are bound. These reactions can be as follows:

$$p+p+(n) \rightarrow \pi^+ + d + (n), \quad (6)$$

$$p+n+(p) \rightarrow \pi^0 + d + (p), \quad (7)$$

$$p+d \rightarrow \pi^+ + H^3, \quad (8)$$

$$p+d \rightarrow \pi^0 + He^3. \quad (9)$$

The same processes of pion production probably occur in the collisions of protons with single nucleons inside carbon nuclei with the only difference that in this case the nuclear binding effects should be more pronounced than in pd-collisions.

2. Experimental Methods

The present experiments were carried out with the sixmeter synchrocyclotron of the Joint Institute for Nuclear Research. Use was made of the external unpolarized proton beam focused by quadrupole lenses and passed through a deflecting magnet. In measuring the spectra of charged pions from pp- and pd-collisions we used an arrangement designed for prolonged keeping of liquid hydrogen and the liquefaction of deuterium. In these cases the target was a thin-walled cylindrical appendix 4 cm in diameter and 12 cm high filled with liquid hydrogen or liquid deuterium. The appendix was placed into a liquid hydrogen-cooled vacuum chamber whose external casing was cooled by liquid nitrogen. It was assumed that the densities of liquid hydrogen and liquid deuterium at the boiling point of liquid hydrogen should be equal to 0.0708 and 0.169 g/cm^3, respectively [4]). The effect of the empty appendix was smaller than 3 % of the particle emission in the presence of liquid hydrogen or liquid deuterium. A graphite plate $5\times5\times0.3$ cm was used as a target in the experiments with carbon. To reduce the energy losses of pions in the graphite plate the angle between the plane of the target and the proton beam was chosen so that the analysed secondary particles left the target normally to its surface.

The proton energy in the centre of all targets was equal to (654 ± 5) MeV. The mean energy losses of incident protons in hydrogen and deuterium were about 1.4 and 1.7 MeV, respectively; in the carbon target the protons lost $\approx$ 1.9 MeV. Averaged over the irradiated volume of the hydrogen, deuterium and carbon targets, the energy losses of 150 MeV pions were equal to 0.7, 0.8 and 0.5 MeV, respectively. The density of the proton beam of 2×3 cm cross section at the target was $\approx 2\times10^8$ protons/cm^2 sec.

The energy spectra of charged pions were measured by means of a magnetic spectrometer previously described by Azhgirei *et al.* [5]). In our experiments as well as in ref. [5]) two thin scintillation counters placed at the input of the spectrometer determined a particle beam emitted at the angle of 56° to the direction of the primary proton beam. In the case of pion emission from the reaction $p+p\rightarrow\pi^++d$ this angle corresponds to the angle of 90° in the centre-of-mass system (c.m.s.) of the two colliding protons. The analysed beam on the horizontal plane was about $\pm2°$. The particles passed through the spectrometer were detected by a telescope consisting of four scintillation counters. The relative width $\Delta p/p$ of the momentum interval selected by the scintillators was about ±3 % for all measured momenta, the subtended solid angle being about 0.5×10^{-4} sr. The threshold of pion detection was at 35 MeV. The dependence of a mean momentum of particles passing through the spectrometer from the magnet current was determined by current-carrying wire techniques. A small contamination of secondary protons was separated from pions by means of a filter placed between the scintillators of the output telescope. The contamination of μ-mesons and electrons in the particle beam passed through the spectrometer was determined by means of measuring the range curves in copper. The background of accidental coincidences was found by switching on the delay lines shifting the pulses from separate pairs of counters. In choosing the delay value the fine time structure of the synchrocyclotron proton beam was taken into account.

The results of the measurements were corrected to allow for the decay of the pions in flight as well as their slowing down and absorption in the target, scintillators and the filter separating the secondary protons from the mesons. The absolute values of differential cross sections in the spectra, $d^2\sigma/d\omega dE$, were estimated with the accuracy of about 7 % by comparing the yields of pions with that of recoil protons from the elastic pp-scattering, also observed with the spectrometer. For 654 MeV at 56° in the lab. system (120° in c.m.s.), the differential cross section for the elastic pp-scattering was taken equal to $(6.7\pm0.35)\times10^{-27}$ cm^2/sr (in c.m.s. $(3.41\pm0.13)\times10^{-27}$ cm^2/sr [6])). It should be noted that special test measurements showed no difference between the detection efficiency for 150 MeV pions and that for protons with the same energy.

Assuming that pion production occurs in the collisions of protons with single nucleons inside the nuclei and neglecting the intranuclear motion of nucleons in deuterons and in carbon nuclei, it was possible to transform the spectra observed into the c.m.s. of the two colliding nucleons. In this system the angles of emission of a great part of pions lie in the range of 90°—97° for pd-collisions and between 88° and 110° for pC-collisions.

3. Results

3.1. ENERGY SPECTRA OF CHARGED PIONS FROM pp- AND pd-COLLISIONS

The energy spectra of charged pions from pp- and pd-collisions are given in figs. 1 and 2 together with the statistical errors of measurements. All the rest of the errors connected with the determination of absolute values $d^2\sigma/d\omega dE$ and the estimation of corrections introduced were taken into account in calculating the differential cross sections $d\sigma/d\omega$ of the observed reactions. Below 70 MeV the validity of experimental data on the form of specta is not high, due to the considerable difficulties involved in the determination of μ-meson and electron contamination in this energy region.

When double pion production in one nucleon-nucleon interaction is rare, it is sufficient to consider that negative pion production by protons on deuterons occurs only in pn-collisions, while positive pions are produced in both pp- and pn-collisions. Due to charge symmetry, the differential cross sections for the reactions $p+n\rightarrow\pi^++n+n$ and $p+n\rightarrow\pi^-+p+p$ are connected by the relation

$$\frac{d\sigma}{d\omega}[p+n\rightarrow\pi^++n+n]_\vartheta=\frac{d\sigma}{d\omega}[p+n\rightarrow\pi^-+p+p]_{180^\circ-\vartheta},$$

where ϑ is the angle of pion emission in the c.m.s. At $\vartheta = 90°$ the differential cross sections of the above reactions must be equal to each other, and the spectra of positive and negative pions must be of the same form. Taking into account this inference from charge symmetry, one can expect that the result of subtraction of the spectrum of negative pions produced in the reaction (5) from the

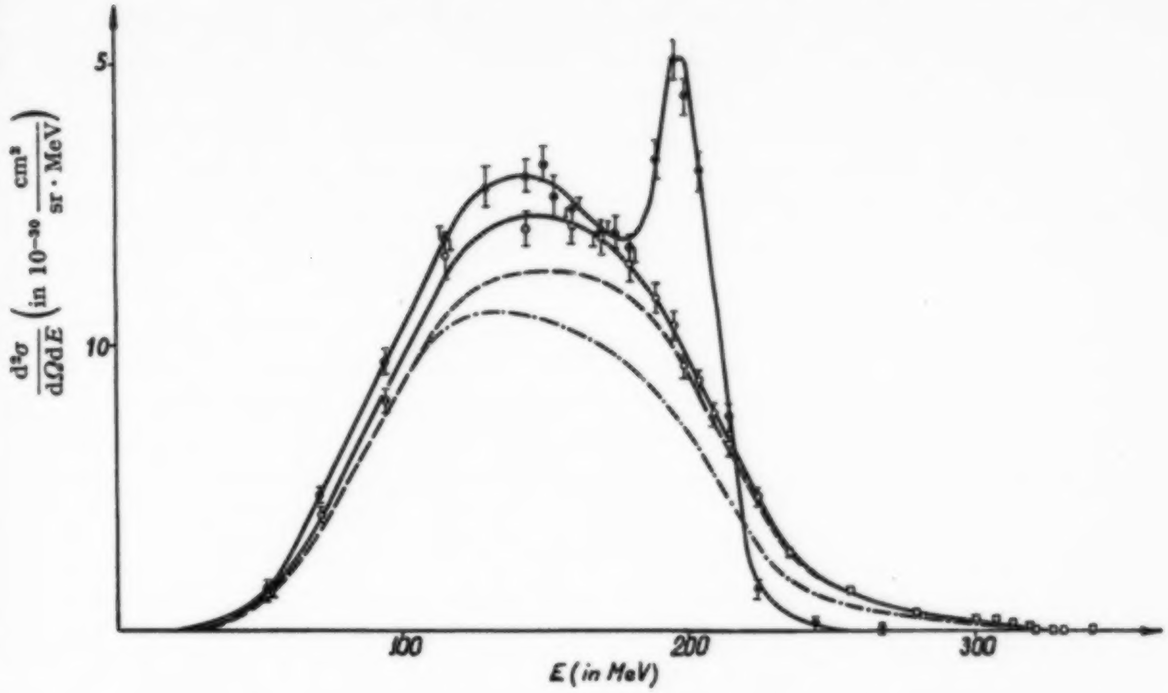

Fig. 1. Positive pion energy spectra measured at an angle of 56° in the laboratory system with respect to the incident 654 MeV proton beam: ● corresponds to free pp-collisions; ○ corresponds to pd-collisions; the curve — — — is the spectrum of π^+-mesons only from $[p+p]_D$-collisions, the curve — · — · — · separates the contribution of the reaction $[p+p]_D \rightarrow \pi^+ + p + n$ from the spectrum of π^+-mesons from $[p+p]_D$ collisions.

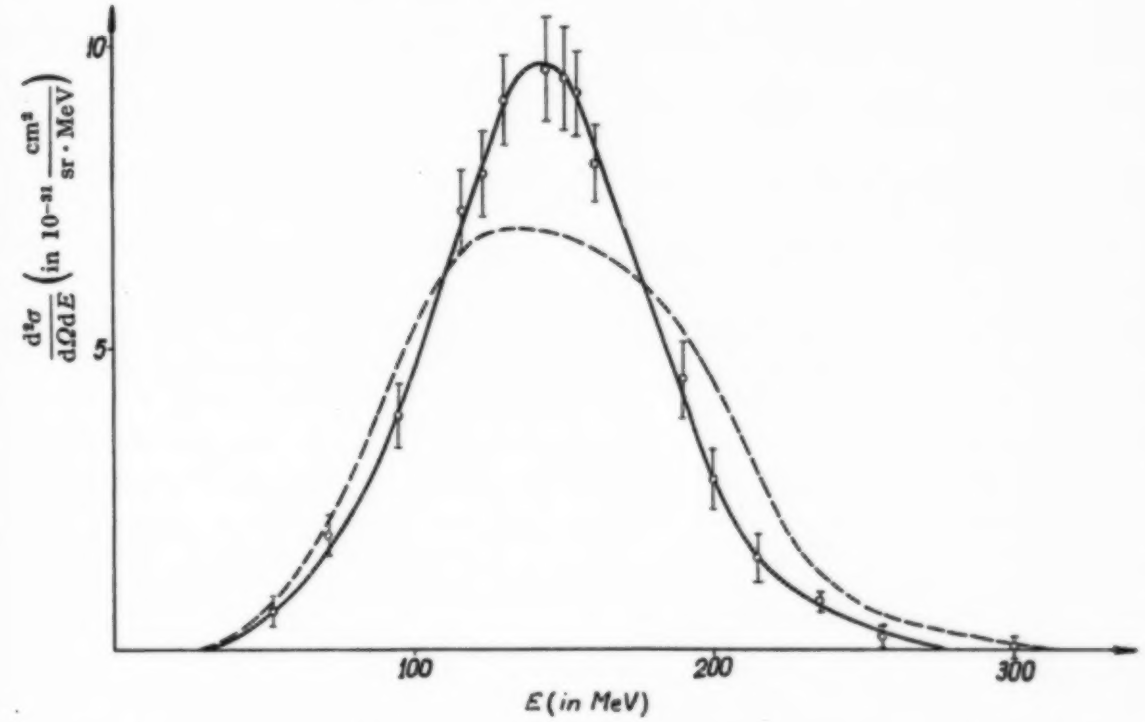

Fig. 2. Energy spectrum of negative pions from $[p+n]_D$-collisions measured at an angle of 56° in the laboratory system with respect to the incident 654 MeV proton beam. The curve — — — is the spectrum of positive pions from the reaction $[p+p]_D \rightarrow \pi^+ + p + n$ normalized to the same area as that of the negative pion spectrum.

observed total spectrum of positive pions of the reactions (1), (3) and (6) is a spectrum of positive pions produced exclusively by pp-collisions in deuterons. The spectrum of positive pions thus obtained and designated in fig. 1 with a dashed line extends towards high energies farther than the spectrum of positive pions from free pp-collisions. This, apparently, is caused by the motion of protons in the deuterons. The same cause can account for there being no peak from the reaction $p+p \rightarrow \pi^+ + d$ in the spectrum of positive pions from pp-collisions in deuterons, distinctly observed at 196 MeV in the case of free pp-collisions. Nevertheless, if one normalizes the spectra of positive pions produced on protons in deuterons and on free protons to equal areas, and then subtracts the contribution of the reaction $p+p \rightarrow \pi^+ + d$ from the spectrum of positive pions produced in free pp-collisions, it appears that in the region of the peak corresponding to the reaction $p+p \rightarrow \pi^+ + d$ the values $d^2\sigma/d\omega dE[p+p \rightarrow \pi^+]_D$ exceed the values $d^2\sigma/d\omega dE[p+p \rightarrow \pi^+ + p+n]_H$. This fact indicates that reaction (6) actually occurs in the collisions of protons with the protons in deuterons.

The smearing-out of the peak of pions from the reaction $p+p \rightarrow \pi^+ + d$ on protons in deuterons as a result of intranuclear motion was evaluated by Prokoshkin [7]) under the assumption that the momentum distribution of the nucleons in deuterons can be approximated by the Salpeter-Goldstein distribution [8]) for the exponential-form potential †. The spectrum of π^+-mesons from reaction (6) he calculated was normalized to the value of the differential cross section $d\sigma/d\omega[p+p \rightarrow \pi^+ + d]$ for $\vartheta = 90°$, equal to $(1.00 \pm 0 \cdot 19).10^{-28}$ cm^2/sr at 660 MeV [9]) and then subtracted from the spectrum of π^+-mesons from pp-collisions in deuterons. The result of this division of the observed spectrum into the contributions of reactions (1) and (6) is also represented in fig. 1.

Comparing the spectra of π^+ and π^-- mesons from reactions (1) and (5), as done in fig. 2, one can see that to the right from the maximum the spectrum of π^--mesons decreases more rapidly with increasing energy than that of π^+-mesons. This difference, exceeding the limits of experimental errors, can be explained by the fact that in the reactions $p+p \rightarrow \pi^+ + p+n$ and $p+n \rightarrow \pi^- + p+p$ the effect of nucleon-nucleon interaction in a final state is not the same. Indeed ††, in the first reaction the transition of $T = 1 \rightarrow T = 0$ of the initial and final isobaric spin states of the two-nucleon system leaves the neutron and the proton in the ^{3}S-state. Due to a strong interaction between nucleons in this state, the nucleons are emitted predominantly with low energies of relative motion and thus the energy carried away by the π^+-meson increases. Now, in the reaction $p+n \rightarrow \pi^- + p+p$ the transition $T = 1 \rightarrow T = 1$ takes a considerable part which leaves the protons in the ^{3}P-state when the interaction between them is weak.

---

† In ref. [7]) it was also shown that the Salpeter-Goldstein momentum distribution for the exponential-form potential makes it possible to predict with a good accuracy the form of the spectrum of π^+-mesons from the reaction $[p+p \rightarrow \pi^+ + p+n]_D$ using the data of the spectrum of π^+-mesons from the same reaction on free protons.

†† At 660 MeV the isobaric cross sections σ_{10}, σ_{11} and σ_{01} are equal to (10.9 ± 0.5), (3.22 ± 0.17) and $(1.7 \pm 1.1) \times 10^{-27}$ cm^2 (ref. [10])), respectively.

The absence of a peak corresponding to the reaction (8) in the spectrum of positive pions from pd-collisions is no surprise as already at 340 MeV [11]) the total cross section of this reaction is about 10^{-29} cm^2. The positive pion yield near the upper limit of the spectrum ($E_\pi = 310$ MeV) where the peak of positive pions from the reaction (8) must be observed warrants the conclusion that if at 660 MeV the reaction (8) does occur, its differential cross section for positive pion emission in the direction of 56° to the proton beam does not exceed $\approx 5 \times 10^{-30}$ cm^2/sr.

The integration of the spectra over energy yields the values, represented in table 1, of the differential cross sections for the production of charged pions in pp- and pd-collisions.

TABLE 1

Differential cross sections for charged pion production in pp-, pd- and pC-collisions at an angle of 56° in the laboratory system with respect to the 654 MeV proton beam (≈ 90° in the c.m.s.)

Differential cross sections 10^{-28} cm^2/sr	$p+p \rightarrow \pi+ \ldots$	$p+d \rightarrow \pi+ \ldots$	$p+C \rightarrow \pi+ \ldots$
$(d\sigma^+/d\omega)_{56^\circ \text{ lab. s.}}$	10.2 ± 1.0	9.1 ± 0.9	30.2 ± 3.0
$(d\sigma^-/d\omega)_{56^\circ \text{ lab. s.}}$		0.88 ± 0.12	5.0 ± 0.8
$(d\sigma^+/d\omega)_{\approx 90^\circ \text{ c.m.s.}}$	6.7 ± 0.7	5.9 ± 0.6	19.5 ± 1.9
$(d\sigma^-/d\omega)_{\approx 90^\circ \text{ c.m.s.}}$		0.57 ± 0.08	3.2 ± 0.5

The differential cross section for positive pion production in free pp-collisions at 660 MeV at 90° in the c.m.s. is close to the value $(6.8 \pm 1.5) \times 10^{-28}$ cm^2/sr obtained by Neganov and Savchenko [12]) but certainly smaller than the value $(9.3 \pm 0.7) \times 10^{-28}$ cm^2/sr reported by Meshkovsky *et al.* [13]).

From the data obtained it follows that at 90° in the c.m.s. the ratio of the integral yield of positive pions to that of negative ones from deuterium is equal to 10.3 ± 1.3. If in nucleon-nucleon collisions, pions were produced only through the resonant state ($J = T = \frac{3}{2}$), the ratio σ^+/σ^- of total cross sections of positive and negative pion production for pd-collisions would be equal to 11 [14]).

The cross section

$$d\sigma[p+p \rightarrow \pi^+ + \ldots]_D/d\omega = d\sigma[p+d \rightarrow \pi^+ + \ldots]/d\omega - d\sigma[p+d \rightarrow \pi^- + \ldots]/d\omega$$
$$= (5.3 \pm 0.7) \times 10^{-28} \text{ cm}^2/\text{sr}$$

corresponds to the integral yield of positive pions from the $[p+p]_D$-collisions. The ratio of probabilities of positive pion production in the collisions of protons with free and bound protons is equal to

$$\frac{d\sigma[p+p \rightarrow \pi^+ + \ldots]_D/d\omega}{d\sigma[p+p \rightarrow \pi^+ + \ldots]_H/d\omega} = 0.79 \pm 0.08.$$

As the spectra of pions from pd- and pp-collisions are measured in strictly identical conditions, the accuracy of determination of the value of this ratio depends solely on the statistical errors of measurements of pion yields and μ-meson and electron contaminations.

3.2. ENERGY SPECTRA OF CHARGED PIONS FROM pC-COLLISIONS

In the present experiments it was found that the spectra of π^+- and π^--mesons from pC-collisions given in ref. 5) were measured with insufficient accuracy at pion energies below 250 MeV. The results of new measurements of the spectra of π^+- and π^--mesons, together with statistical errors, are represented in fig. 3. It will be emphasized that in the energy region of pions above 250 MeV the present experiments yielded the values $d^2\sigma/d\omega dE$ which do not contradict within errors, those obtained in ref. 5), confirming thereby that the spectra of charged pions from pC-collisions extend up to 350 MeV. Therefore the high energy parts of the spectra of π^+- and π^--mesons shown in fig. 3 are those calculated from the results of the present experiments and those of ref. 5) notwithstanding the difference in the energy of the incident protons (654 MeV in the first case and 670 MeV in the second).

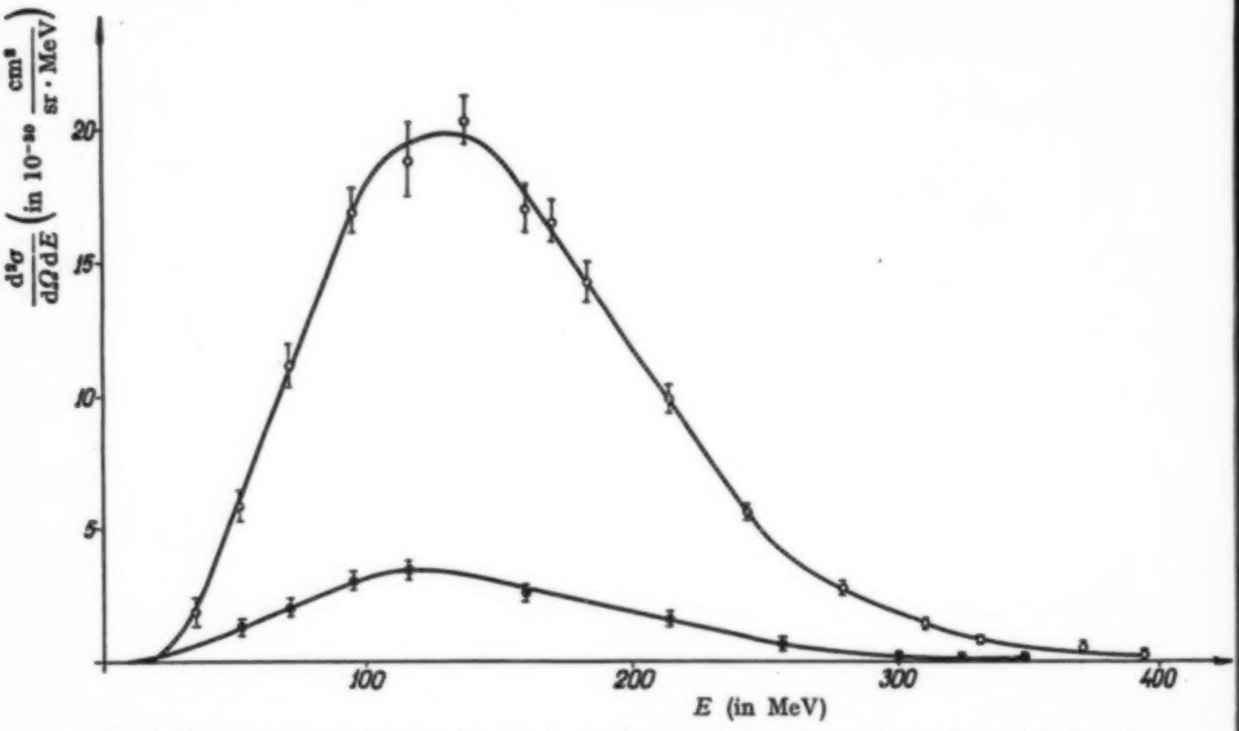

Fig. 3. Energy spectra of charged pions from pC-collisions measured at an angle of 56° in the laboratory system with respect to the 654 MeV proton beam; ○ for π^+-mesons, ● for π^--mesons.

The integration of the spectra over energy yields the values, also represented in table 1, for the differential cross sections of the production of charged pions on carbon nuclei. In this case the ratio of the integral yield of π^+-mesons to that of π^--mesons is equal to 6.0 ± 0.8 for $\approx 90°$ in the c.m.s. The ratio σ^+/σ^- would also be equal to 11 if the production of pions in pC-collisions occurred through the resonant state alone $(J = T = \frac{3}{2})$.

Similarly to the above procedure, the π^--meson spectrum was subtracted from the π^+-meson spectrum to separate the effect from pp-collisions in carbon nuclei. The differential cross sections per one proton (neutron) for the production of π^+ (π^-)-mesons in pC-collisions are found to equal

$$\frac{1}{Z}\left\{\frac{\mathrm{d}\sigma}{\mathrm{d}\omega}[\mathrm{p}+\mathrm{C} \rightarrow \pi^+ + \ldots] - \frac{\mathrm{d}\sigma}{\mathrm{d}\omega}[\mathrm{p}+\mathrm{C} \rightarrow \pi^- + \ldots]\right\} = (2.7 \pm 0.3) \times 10^{-28} \mathrm{cm}^2/\mathrm{sr}$$

and

$$\frac{1}{N}\frac{\mathrm{d}\sigma}{\mathrm{d}\omega}[\mathrm{p}+\mathrm{C} \rightarrow \pi^- + \ldots] = (0.53 \pm 0.08) \times 10^{-28}\ \mathrm{cm}^2/\mathrm{sr}.$$

From the following it will be clear that the difference $(1/Z)\{\mathrm{d}\sigma[\mathrm{p}+\mathrm{C} \rightarrow \pi^+ + \ldots]/\mathrm{d}\omega - \mathrm{d}\sigma[\mathrm{p}+\mathrm{C} \rightarrow \pi^- + \ldots]/\mathrm{d}\omega]\}$ thus obtained can be approximately set equal to $\mathrm{d}\sigma[\mathrm{p}+\mathrm{p} \rightarrow \pi^+ + \ldots]_{\mathrm{C}}/\mathrm{d}\omega$; as regards the value $(1/N)\mathrm{d}\sigma[\mathrm{p}+\mathrm{C} \rightarrow \pi^- + \ldots]/\mathrm{d}\omega$, it cannot be identified with the cross section for π^--meson production per one pn-collision in a carbon nucleus.

4. Comparison of the Pion Spectra Observed

The spectra of charged pions from the collisions under investigation are represented in fig. 4 in the form of smooth curves compatible with the experimental points plotted in the previous graphs. All curves are normalized to the same area. Table 2 gives the mean energies of pions and the energies at the maxima of these spectra. It is evident that the maxima of all the spectra of π^+-mesons and the maximum of the spectrum of π^--mesons from pd-collisions occur in approximately the same energy region. As could be expected, the pion spectra observed differ in form from those corresponding to only the statistical weight of the final states. The position of the maxima of the spectra in the c.m.s. of the two colliding nucleons closely corresponds to the position of the maximum of the curve representing the energy dependence of the total π^+p-scattering cross section. This peculiarity of the spectra of pions produced in nucleon-nucleon collisions is manifest at the given energy also at another angle of observation of pions [15]) as well as at 1000 and 2300 MeV [16]) and indicates that in the processes of pion production the resonance interaction between a pion and a nucleon in the state with $J = T = \frac{3}{2}$ plays an important role [†].

[†] The form of the measured energy spectrum of pions from the reaction $\mathrm{p}+\mathrm{p} \rightarrow \pi^+ + \mathrm{p} + \mathrm{n}$ and the form of the spectrum predicted by the resonance model of pion production in nucleon-nucleon collisions will be compared separately.

The most obvious differences between the spectra under discussion are as follows:

1) The spectrum of π^+-mesons from $[p+p]_C$-collisions extends to higher energies much farther than that of π^+-mesons from $[p+p]_D$-collisions. A similar difference exists between the spectra of π^--mesons; no emission at 300 MeV

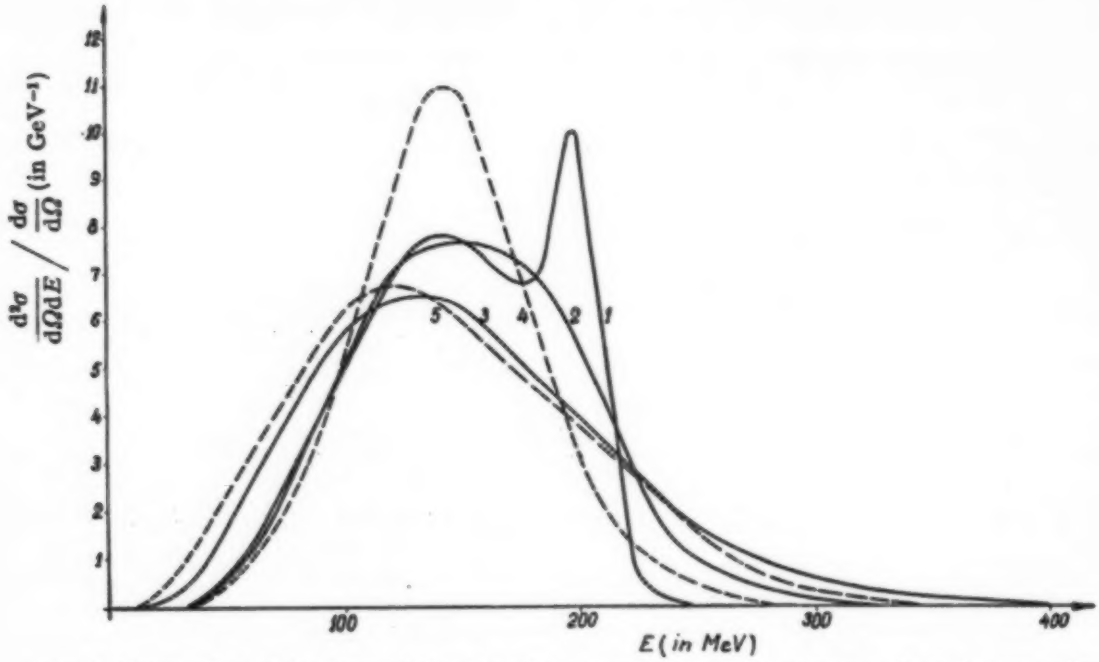

Fig. 4. Comparison of the form of charged pion energy spectra: 1 : π^+-mesons from free pp-collisions. 2 : π^+-mesons from $[p+p]_D$-collisions. 3 : π^+-mesons from $[p+p]_C$-collisions. 4 : π^--mesons from $[p+n]_D$-collisions. 5 : π^--mesons from pC-collisions. All the spectra are normalized to the same area.

TABLE 2

Data on energy spectra of charged pions from pp-, pd- and pC-collisions

Reaction	Energy at the maximum of spectra (lab. s.) (MeV)	Energy at the maximum of spectra (c.m.s.) (MeV)	Mean energy (lab. s.) (MeV)	Mean energy (c.m.s.) (MeV)
$[p+p]_H \to \begin{cases}\pi^+ + p + n\\ \pi^+ + d\end{cases}$	143 ± 5 a)	106 ± 6 a)		
$[p+p]_D \to \begin{cases}\pi^+ + p + n\\ \pi^+ + d\end{cases}$	145 ± 8	109 ± 8	151	116
$[p+n]_D \to \pi^- + p + p$	143 ± 5	107 ± 5	144	108
$[p+p]_C \to \pi^+ + \ldots$	132 ± 8	100 ± 5	148	114
$p+C \to \pi^- + \ldots$	120 ± 12	87 ± 5	141	107

a) These data refer only to the spectrum of π^+-mesons from the reaction $p+p \to \pi^+ + p + n$.

π^--mesons from deuterium was observed at all, whereas the emission of π^--mesons from carbon could be traced up to ≈ 350 MeV. The difference in the relative numbers of high energy pions in the spectra under comparison is caused primarily by the fact that the correlation of nuclear matter is more pronounced in carbon than in deuterium and consequently carbon contains more high momentum nucleons.

2) The spectra of π^+- and π^--mesons from carbon are much broader than the corresponding spectra from deuterium. This is to be expected because the nucleons should have on the average larger momenta in carbon nuclei than in deuterons. Since the excitation curves of pion production in pp- and pn-collisions increase weakly above 650 MeV and decrease rapidly below 650 MeV, the efficiency for the production of pions on the nucleons inside carbon nuclei must be somewhat smaller than in the case of free nucleons or even nucleons bound in deuterium[†]. As is evident from table 2 the intranuclear motion of protons in deuterons and in carbon nuclei has no appreciable effect on the mean pion energy in the spectra.

3) The shift of the maximum of the spectrum of π^--mesons from carbon towards lower energies as compared with that of π^--mesons from deuterium seems to be quite real and amounts to some 20 MeV, which considerably exceeds the difference between the shifts of these spectra due to the Coulomb interaction of pions with the original nuclei. The discrepancy of this kind is more pronounced between the π^--meson spectra under consideration than between the corresponding spectra of π^+-mesons and can hardly be explained by assuming that π^--mesons in carbon nuclei should be produced only due to pn-collisions.

The same difficulty arises when considering the differential cross section per one proton (neutron) of the target nuclei for $\pi^+(\pi^-)$-meson emission in pd- and pC-collisions as well as when considering the fact that the ratio of the yield of π^+-mesons to that of π^--mesons for carbon differs from that for deuterium. The corresponding data are given in table 3. As is evident the differential cross

TABLE 3

Values of the differential cross sections for π^+-meson production in $[p+p]_H$-, $[p+p]_D$- and $[p+p]_C$-collisions, values of the differential cross sections for π^--meson emission in pd- and pC-collisions per one neutron and the ratios between the yield of π^+-mesons to that of π^--mesons for ≈ 90° in c.m.s.

Collisions	$(1/Z)(d\sigma^+/d\omega - d\sigma^-/d\omega)$ 10^{-28} cm^2/sr	$(1/N)(d\sigma^-/d\omega)$ 10^{-28} cm^2/sr	$(d\sigma^+/d\omega)/(d\sigma^-/d\omega)$
pp	6.7 ± 0.7		
pd	5.3 ± 0.7	0.57 ± 0.08	10.3 ± 1.3
pC	2.7 ± 0.3	0.53 ± 0.08	6.0 ± 0.8

[†] According to Prokoshkin's estimate 7), as a result of intranuclear motion, the collisions of protons with nucleons in deuterons of 660 MeV are approximately 4 % less effective as regards pion production than the collisions of protons with free nucleons.

sections per one proton for π^+-meson emission from hydrogen, deuterium and carbon are related by

$$\frac{\mathrm{d}\sigma}{\mathrm{d}\omega}[\mathrm{p}+\mathrm{p}\rightarrow\pi^+]_{\mathrm{H}}:\frac{\mathrm{d}\sigma}{\mathrm{d}\omega}[\mathrm{p}+\mathrm{p}\rightarrow\pi^+]_{\mathrm{D}}:\frac{\mathrm{d}\sigma}{\mathrm{d}\omega}[\mathrm{p}+\mathrm{p}\rightarrow\pi^+]_{\mathrm{C}}=1:0.79:0.40,$$

whereas the differential cross sections per one neutron for π^--meson emission from deuterium and carbon are equal within experimental errors.

The decrease in the efficiency of production of pions on bound nucleons can be caused, together with the intranuclear motion of nucleons, by 1) the exclusion principle for recoil nucleons, 2) the mutual shading of nucleons in deuterons or the absorption of incident protons in nuclear matter in the case of more complex nuclei, and 3) the reabsorption of pions in the original nuclei. The pion production in the collisions of protons with free and bound nucleons must, in general, occur with different efficiencies provided the nuclear binding essentially changes the character of the interference between the amplitudes of possible pion-nucleon states. According to the calculations in ref. [7]), at 660 MeV a) the effect of the exclusion principle on pion production in pd- and pC-collisions is extremely small, and b) the decrease in the cross section for pion production due to the mutual shading of nucleons in deuterons amounts to a mere few per cent.

The decrease in the efficiency of the production of pions on nucleons inside the nuclei due to the absorption of the incident protons and the reabsorption of pions is determined by the factor [17, 18])

$$F=\frac{1}{V}\int \mathrm{e}^{-(k's'+k''s'')}\,\mathrm{d}v, \tag{10}$$

which is a probability averaged over the volume V of the nucleus for the emission of a pion from the nucleons in which the pion was produced. Here, s' is the distance passed by the proton inside the nucleus prior to the production of the pion, s'' the distance passed by the pion inside the nucleus prior to leaving it; k' and k'' are the absorption coefficients for protons and pions in nuclear matter. According to the results of the measurements of the cross section for nucleon-nucleus interactions in a wide energy range [19–23]), the radius R of the nucleus can be assumed to be equal to $1.26\,A^{\frac{1}{3}}\times10^{-13}$ cm and $k'=0.5\times10^{13}$ cm^{-1}. The values k'' were estimated in the quasi-deuteron model approximation of the pion capture in nuclei. According to this, the expression for k'' can be written as follows:

$$k''=\frac{1}{V}\left(\Gamma\sigma[\pi^++\mathrm{d}\rightarrow2\mathrm{p}]\tfrac{1}{2}A\right).$$

The cross sections of the reaction $\pi^++\mathrm{d}\rightarrow2\mathrm{p}$ at energies below 150 MeV were found from the resonance excitation curve of the inverse reaction $\mathrm{p}+\mathrm{p}\rightarrow\pi^++\mathrm{d}$

by means of detailed balance[9]); the data obtained by Neganov and Parfenov[24]) were applied in the case of higher energies. The value of the normalizing factor Γ, showing how much larger is the probability for correlated two-nucleon groups in carbon nuclei than in deuterons, was obtained by comparing the total cross sections for pion absorption in carbon obtained by Lederman *et al.*[25,26]) at 62 and 125 MeV with the total cross sections of the reaction $\pi^+ + d \rightarrow 2p$ at the same energies. The factor Γ was found to be equal to ≈ 3.8.

If there is only absorption of protons or reabsorption of pions, then[17])

$$F(x) = 3\left[\frac{1}{2x} - \frac{1}{x^3} + \frac{1+x}{x^3}\,e^{-x}\right] \tag{11}$$

where $x = 2Rk$. If the absorption of protons alone is taken into account, then for carbon nuclei $F \approx 0.42$. This procedure, undoubtedly, gives smaller values of F since one neglects the process in which, after the first collision some of the nucleons have energies sufficient for pion production. The total effect of proton absorption and reabsorption of pions can be simply evaluated only in the case of backward pion emission when F is also given by expression (11), but with $x = 2R(k'+k'')$, and in the case of forward pion emission[27]), when

$$F = \frac{3}{x'-x''}\left[\frac{1-(1+x'')\exp(-x'')}{x''^2} - \frac{1-(1+x')\exp(-x')}{x'^2}\right], \tag{12}$$

where $x' = 2Rk'$ and $x'' = 2Rk''$; the inequality $x' > x''$ holds even at the energy corresponding to the maximum of the excitation curve of the reaction $\pi^+ + d \rightarrow 2p$. At the emission angle of 56° the factor F can be calculated approximately for different values of pion energies. It was found that in this case the factor F averaged over the energy spectrum of pions equals ≈ 0.30 †. The value of F thus obtained is qualitatively compatible with the observed decrease in the efficiency for π^+-meson production in pp-collisions in carbon as compared with that observed in free pp-collisions. As regards the 20 % decrease in the efficiency for π^+-meson production in $[p+p)_D$- collisions in comparison with that in free pp-collisions, it is probably caused, mainly, by the reabsorption of pions in the final three-nucleon system ††.

The absorption of protons and reabsorption of pions in carbon nuclei must decrease the yields of positive and negative pions equally provided the protons and neutrons are distributed identically over the nuclear volume. In this case, to explain the constancy of $(1/N)(d\sigma^-/d\omega)$, it is necessary again to assume that

---

† It should be noted that the evaluations of this kind are crude. They can be justified only by the difficulties of taking into account the effects caused by the diffuse nuclear surface, the elastic scattering of pions on bound nucleons, the Coulomb interaction, etc.

†† A certain argument in favour of this conclusion is that the probability of the reabsorption of pions in the final two-nucleon system amounts to 10—20 %[28,29]) in the photoproduction of pions on deuterons.

π^--meson production in carbon nuclei is due not only to pn-collisions but also to other additional processes the contribution of which compensates the decrease in the efficiency of pn-collisions owing to the absorption of protons and reabsorption of pions. Two processes can be such additional sources of π^--mesons: pion production in secondary pion-nucleon collisions and the charge-exchange scattering of pions on nucleons. The former process under the conditions of the present experiments caused only a negligibly small weakening of the high-energy parts of the spectra, the secondary pions of this process being entirely unobservable due to the high detection threshold. As to the reactions of exchange scattering $\pi^+ + \mathrm{n} \rightleftarrows \pi^0 + \mathrm{p}$ and $\pi^0 + \mathrm{n} \rightleftarrows \pi^- + \mathrm{p}$, they led, as it can be readily seen, to a relative increase of the π^--meson yield.

An attempt was made to evaluate the effect of the exchange scattering of pions in carbon nuclei by using the usual charge-independent relations: a) between the cross sections for various pion-nucleon scattering processes ($\sigma[\pi^+ + \mathrm{n} \rightarrow \pi^0 + \mathrm{p}] = \sigma[\pi^- + \mathrm{p} \rightarrow \pi^0 + \mathrm{n}] = \frac{2}{9}\sigma[\pi^+ + \mathrm{p} \rightarrow \pi^+ + \mathrm{p}]$), and b) between the cross sections for the processes of π^+-, π^0-, π^--meson production by protons on nuclei with isobaric spin $T = 0(\sigma^+ + \sigma^- = 2\sigma^0)$. Besides, it was assumed that pion production in the nucleon-nucleon collisions inside the nucleus occurs only through the resonant state with $J = T = \frac{3}{2}$ and consequently the cross sections of positive, neutral and negative pion production for carbon should be related as 11 : 6 : 1. The values of the pion charge exchange coefficient in nuclear matter were obtained by using the expression:

$$k = \frac{1}{V}\left(\gamma \tfrac{2}{9}\sigma[\pi^+ + \mathrm{p} \rightarrow \pi^+ + \mathrm{p}]\tfrac{1}{2}A\right),$$

where the factor γ shows how much the known cross sections for pion-nucleon interaction change owing to the nuclear binding. In these estimations it was assumed that $\gamma = 0.5$ †. The probability for charge exchange scattering of a pion with a given energy in the nucleus can be written as follows:

$$W = 1 - \left(\int \mathrm{e}^{-[k's' + (k''+k)s'']}\mathrm{d}v \Big/ \int \mathrm{e}^{-(k's' + k''s'')}\,\mathrm{d}v\right). \tag{13}$$

A very approximate evaluation shows that at the emission angle of 56° the probability, averaged over the energy spectrum, for the charge exchange scattering of pions in the carbon nucleus amounts to approximately 0.12 to 0.16. Assuming this value equal to 0.14 and taking into account the fact that the yield of π^--mesons from the reaction $\pi^0 + \mathrm{n} \rightarrow \pi^- + \mathrm{p}$ is six times as large as their loss due to the inverse reaction $\pi^- + \mathrm{p} \rightarrow \pi^0 + \mathrm{n}$, one can find that owing to the secondary charge exchange interactions, the total π^--meson yield should be increased about 70 % and the total π^+-meson yield should be decreased about 7 %. This, firstly, leads to a certain shift of the spectrum of π^--mesons from pC-collisions towards lower energies and, secondly, entirely compensates the decrease in the efficiency of π^--meson production in pn-collisions due to the absorption of protons and the reabsorption of pions. As a result, the ratio σ^+/σ^- will change from 11 to 6. The fact that a situation like this actually takes place is confirmed by the present experiment as well as by the experiments in which the $(d\sigma^+/d\omega)/(d\sigma^-/d\omega)$ ratio for other emission angles was measured in similar conditions [15, 31]).

---

† According to Kozodaev *et al.* [30]), $\gamma \approx 0.5$ for the scattering of 300 MeV π^+-mesons on nucleons inside helium nuclei. One of the causes of such appreciable decrease in cross sections for the scattering of pions on bound nucleons as compared to that on free nucleons is the prohibition of collisions in which the struck nucleon ends up in momentum states already filled with a similar nucleon.

5. Concluding Remarks

The present experiments have shown how the form of the spectra of pions produced in pp and pn-collisions at 654 MeV in the nuclei investigated changes with the strength of the nuclear binding of nucleons when passing from deuterium to carbon. The nucleon-nucleon character of all primary pion production processes considered is beyond doubt with the exception, perhaps, of those rare events when the incident protons interact inside carbon nuclei with high-momentum nucleons bound into closely correlated groups at the moment of collision.

The results obtained show that even in the case of light nuclei the ratio of the integral yield of π^+-mesons to that of π^--mesons is sensitive to the presence of the secondary reactions of pion charge-exchange interactions in nuclear matter. It is impossible, therefore, to use the ratio observed to draw conclusions on the properties of the nucleon-nucleon system in which the pion production occurs: for example, on the relative contribution to a processs of this kind from the pn-system states with $T = 1$ and $T = 0$. Nevertheless, the difference between the values of the ratio for a deuteron and for a nucleus with an equal number of protons and neutrons can be regarded as a measure showing to what extent the beam originating in the primary pp- and pn-collisions as a beam of strongly isobarically polarized pions depolarizes isobarically owing to the charge exchange interactions in nuclear matter.

References

1) M. G. Mescheryakov, N. P. Bogachev, G. A. Leksin, B. S. Neganov and E. V. Piskarev, Proc. CERN Symposium **2** (1956) 124

2) G. A. Leksin, JETP **32** (1957) 445

3) A. P. Batson, B. B. Culwick, H. B. Klepp and L. Riddiford, Proc. Roy. Soc. A **251** (1959) 233

4) D. B. Chelton and D. B. Mann, Cryogenic Data Book, UCRL-3421 (1956)

5) L. S. Azhgiery, I. K. Vzorov, V. P. Zrelov, M. G. Mescheryakov, V. I. Petrukhin, JETP **34** (1958) 1357

6) N. P. Bogachev and I. K. Vzorov, Dokl. Akad. Nauk USSR **99** (1954) 931
7) Yu. D. Prokoshkin, JETP **38** (1960) 455
8) E. Salpeter and J. Goldstein, Phys. Rev. **90** (1953) 983
9) M. G. Mescheryakov and B. S. Neganov, Dokl. Akad. Nauk USSR **100** (1955) 677
10) A. F. Dunaitzev and Yu. D. Prokoshkin, JETP **38** (1960) 747
11) W. Frank, K. Bandtel, R. Madey and B. Moyer, Phys. Rev. **94** (1954) 1716
12) B. S. Neganov and O. V. Savchenko, JETP **32** (1957) 1265
13) A. G. Meshkovsky, Ya. Ya. Shalamov and V. A. Shebanov, JETP **35** (1958) 64
14) D. Peaslee, Phys. Rev. **94** (1954) 1085; **95** (1954) 1580
15) M. G. Mescheryakov, I. K. Vzorov, V. P. Zrelov, B. S. Neganov and A. F. Shabudin, JETP **31** (1956) 55
16) L. Yuan and S. Lindenbaum, Phys. Rev. **103** (1956) 404
17) K. Brueckner, R. Serber and K. Watson, Phys. Rev. **84** (1951) 258
18) A. A. Anselm and V. M. Shekhter, JETP **33** (1957) 481
19) A. Nedzel, Phys. Rev. **94** (1954) 174
20) H. de Carvalho, Phys. Rev. **96** (1954) 398
21) T. Coor. D. Hill, W. Hornyak, L. Smith and G. Snow, Phys. Rev. **98** (1955) 1369
22) F. Chen, C. Leavitt and A. Shapiro, Phys. Rev. **99** (1955) 857
23) N. Booth, B. Leadley, D. Walker and D. White, Proc. Phys. Soc. A **70** (1957) 209
24) B. S. Neganov and L. B. Parfenov, JETP **34** (1958) 767
25) H. Byfield, J. Kessler and L. Lederman, Phys. Rev. **86** (1952) 17
26) J. Kessler and L. Lederman, Phys. Rev. **94** (1954) 689
27) A. A. Tyapkin, Thesis, Joint Institute for Nuclear Research
28) N. Austern, Phys. Rev. **100** (1955) 1522
29) R. Wilson, Phys. Rev. **104** (1956) 218
30) M. S. Kozodaev, M. M. Kulyukin, R. M. Sulyaev, A. I. Filippov and Yu. A. Scherbakov, JETP **38** (1960) 409
31) V. M. Sidorov, JETP **28** (1955) 727

8.B

Nuclear Physics **23** (1961) 369—385; ©*North-Holland Publishing Co., Amsterdam*

Not to be reproduced by photoprint or microfilm without written permission from the publisher

ANGULAR DISTRIBUTION AND POLARIZATION OF THE NEUTRONS EMITTED IN μ-CAPTURE IN CERTAIN LIGHT NUCLEI

M. K. AKIMOVA, L. D. BLOKHINTSEV and E. I. DOLINSKY

Nuclear Physics Research Institute, Moscow State University, Moscow, USSR

Received 30 July 1960

Abstract: Calculations of the energy spectra, angular distributions and polarization of direct process neutrons formed in μ-capture in the nuclei of C^{12}, Ne^{20}, Si^{28} and S^{32} are performed on the basis of the effective Hamiltonian for μ-capture taking account of relativistic effects of first order with respect to v/c for nucleons, including "weak magnetism" and effective pseudoscalar interaction. The proton states in the nucleus was described by the nuclear shell model with *jj*-coupling; the interaction of the emitted neutrons and the nuclei was taken into account via an optical model. The results obtained are compared with experimental data.

1. Introduction

The investigation of the angular distribution and polarization of the neutrons emitted by the nuclei in μ-capture $\mu^- + P \rightarrow N + \nu$ offers a possibility of establishing the form and magnitude of the coupling constants of weak interaction between μ-mesons and nucleons [1,2]). Refs. [3,4]) present the formulas for the angular distribution and polarization of neutrons calculated in the nonrelativistic approximation for nucleons using Fermi and Gamow-Teller variants and to first order in v_n/c (v_n being the nucleon velocity) for a pseudoscalar variant of four fermion interaction. These formulas were obtained using the nuclear shell model with *jj*-coupling for describing the protons bound in the nucleus, and the optical model for taking account of the interaction between the emitted neutron and the nucleus. Refs. [3,4]) also offer the results of numerical calculations for μ-capture in the nuclei of O^{16} and Ca^{40}.

2. Basic Assumptions and Formulas

In the present paper the discussion is based on the assumption of the universal Fermi interaction theory: interaction of bare fermions is described by V- and A-variants of four-fermion coupling [5,6]). Proceeding from this assumption and taking account of all relativistic terms of the first order in v_n/c we obtain the following expression [7]) for the effective Hamiltonian H_{eff} describing the process of μ-capture ($\hbar = c = 1$):

$$H_{\text{eff}} = \tfrac{1}{2}(1-\boldsymbol{\sigma}\cdot\boldsymbol{\nu})\sum_{i=1}^{A}\tau_i^{(-)}\Big[g_{\text{V}}^{(\mu)}\Big(1+\frac{E_\nu}{2M}\Big)\mathbf{1}\cdot\mathbf{1}_i+\Big(g_{\text{A}}^{(\mu)}-g_{\text{V}}^{(\mu)}\mu\frac{E_\nu}{2M}\Big)\boldsymbol{\sigma}\cdot\boldsymbol{\sigma}_i$$

$$+(g_{\text{P}}^{(\mu)}-g_{\text{A}}^{(\mu)}-g_{\text{V}}^{(\mu)}\mu)\frac{E_\nu}{2M}\boldsymbol{\sigma}_i\cdot\boldsymbol{\nu}+g_{\text{V}}^{(\mu)}\frac{\boldsymbol{\sigma}\cdot\mathbf{p}_i}{M}+g_{\text{A}}^{(\mu)}\frac{\boldsymbol{\sigma}_i\cdot\mathbf{p}_i}{M}\Big]\delta(\mathbf{r}-\mathbf{r}_i). \quad (1)$$

In (1) the following notations are used: the operators which contain the subscript i act on nucleons; those which do not act on leptons; $\tau_i^{(-)}$ is the known isobaric operator, $\boldsymbol{\sigma}$, $\boldsymbol{\sigma}_i$ the Pauli matrices, $\boldsymbol{\nu}$ a unit vector directed as the emission of the neutrino, E_ν the energy of the neutrino, M the mass of the nucleon, and $\mathbf{p}_i = -i\hbar\nabla_i$ is the momentum operator of the ith nucleon.

It is assumed that the neutrino emitted in μ-capture is polarized against its direction of motion. $g_{\text{V}}^{(\mu)}$ and $g_{\text{A}}^{(\mu)}$ are the coupling constants of vector and pseudovector interactions for μ-capture, and $g_{\text{P}}^{(\mu)}$ is the effective coupling constant for the pseudoscalar interaction due to the presence of virtual π-mesons.

In the universal Fermi interaction theory with a conserved vector current[5,6]) the following estimates hold for the quantities $g_{\text{V}}^{(\mu)}$ and μ[7])

$$g_{\text{V}}^{(\mu)} = 0.972\, g_{\text{V}}^{(\beta)}, \quad \mu = 1+\mu_{\text{P}}-\mu_{\text{N}} = 4.71, \quad (2)$$

where $g_{\text{V}}^{(\beta)}$ is the Fermi coupling constant for the β-decay of nucleons, and μ_{P} and μ_{N} are the anomalous magnetic moments of proton and neutron in units of the nuclear magneton. The following relations hold for the quantities $g_{\text{A}}^{(\mu)}$ and $g_{\text{P}}^{(\mu)}$ according to ref. [9]):

$$g_{\text{A}}^{(\mu)} = 0.999\, g_{\text{A}}^{(\beta)}, \quad g_{\text{P}}^{(\mu)} = 8g_{\text{A}}^{(\beta)}, \quad (3)$$

where $g_{\text{A}}^{(\beta)}$ is the Gamow-Teller coupling constant for the β-decay of nucleons.

In the formulas below no account is taken of the contribution made by the two last terms in the effective Hamiltonian which contain the derivatives of nucleon wave functions. Obviously the order of magnitude of the matrix elements of the operators $\mathbf{p}_i/Mc$ is equal to $(\hbar/Mc)/R$, where R is the radius of the nucleus so that the neglected terms for the nuclei considered below ($R \approx 4.10^{-13}$ cm) amount to approximately 5 %. Of the same order of magnitude are other relativistic corrections to the nonrelativistic matrix elements for vector and pseudovector interactions which remain valid in (1) if we put $g_{\text{P}}^{(\mu)} = 0$ and $\mu = 1$. As has been shown by numerical estimates, however, the relativistic corrections of this kind change by no more than 10 % the values of the probability, calculated in non-relativistic approximation, of μ-capture and the asymmetry coefficient in the angular distribution of neutrons and have no practical effect on the magnitude of the longitudinal polarization of neutrons. At the same time, as will be seen from the following, the expected large magnitude of

$g_P^{(\mu)}$ and μ leads to the relativistic terms proportional to $g_P^{(\mu)}E_\nu/2M$ and $\mu E_\nu/2M$ strongly changing the magnitude of the asymmetry coefficient in the angular distribution of neutrons. Therefore, it can be expected that the omission in (1) of the terms containing the derivatives of nucleon wave functions will lead to errors which do not exceed several per cent.

Using the Hamiltonian (1) and eq. (9) from ref. [3]) for the probability of the emission of neutrons from the nucleus with kinetic energy in the interval $(E_N, E_N+\mathrm{d}E_N)$ in an element of the solid angle $\mathrm{d}\Omega_N$ at an angle θ with respect to the polarization of the μ^--meson, we obtain the following expression

$$\mathrm{d}W(E_N, \theta) = \frac{1}{4\pi}(G^{(\mu)})^2 W_0(E_N)[I(E_N)+P_\mu K_1(E_N)\cos\theta]\mathrm{d}E_N\,\mathrm{d}\Omega_N, \tag{4}$$

where

$$I(E_N) = 1+3\lambda^2+2[1+2\lambda\mu-\lambda^2(\kappa-1)]\gamma_1(E_N)+[2\mu^2+\lambda^2(\kappa-1)^2+1]\gamma_2(E_N), \tag{5}$$

$$\begin{aligned} K_1(E_N) &= (1-\lambda^2)\beta_0(E_N)+2[1-2\lambda\mu-\lambda^2(\kappa-1)]\beta_1(E_N)\gamma_1(E_N) \\ &\quad +[-2\mu^2+\lambda^2(\kappa-1)^2+1]\beta_2(E_N)\gamma_2(E_N), \qquad (6) \\ G^{(\mu)} &= g_V^{(\mu)}\times 10^{49}\ \mathrm{erg}^{-1}\,\mathrm{cm}^{-3}, \quad \lambda = -g_A^{(\mu)}/g_V^{(\mu)}, \quad \kappa = g_P^{(\mu)}/g_A^{(\mu)}. \end{aligned}$$

P_μ is the degree of polarization of the μ^--meson in the K-orbit of the mesic atom at the moment of capture. The kinetic energy of the neutron is measured in MeV. The notations which are not indicated here and in the following coincide with those used in ref. [3]).

It will be recalled (for details see ref. [3])) that the formulas discussed in the present paper refer to direct process neutrons emitted from the nucleus immediately after the absorption of the μ^--meson and bypassing thereby the intermediate stage of a compound nucleus. In (4) and the formulas given below for the angular distribution and polarization of neutrons no account is taken of the effect of the hyperfine structure of mesic-atom levels which should be taken into account in considering μ-capture in nuclei with non-zero spin resulting at least partially from the protons of the nucleus (for details see refs. [3, 10, 11])).

Using (4) we can write the angular distribution of the neutrons emitted by the nucleus in the capture of polarized μ^--mesons in the following form

$$q(E_N, \theta) = 1+P_\mu\alpha_1(E_N)\cos\theta, \tag{7}$$

where

$$\alpha_1(E_N) = K_1(E_N)/I(E_N). \tag{8}$$

Taking account of the results of ref. [4]) (eq. (6c)) for the longitudinal polarization of neutrons emitted by the nucleus in the absorption of nonpolarized μ^--mesons, we obtain the following expression

$$P_N^{\,l}(E_N) = L_1(E_N)/I(E_N), \tag{9}$$

where

$$L_1(E_N) = -2\{\lambda(\lambda+1)\beta_0(E_N)+\lambda[2(\mu+1)-\kappa]\beta_1(E_N)\gamma_1(E_N)$$
$$+[\mu^2-\lambda(\kappa-1)]\beta_2(E_N)\gamma_2(E_N)]\}. \quad (10)$$

Eq. (9) also describes the longitudinal polarization of the neutrons emitted at the angle $\theta = \pm\frac{1}{2}\pi$ in the capture of the polarized μ^--mesons.

Eqs. (4), (7) and (9) pertain to neutrons of fixed energy E_N. If we integrate over the energy of the emitted neutron E_N we shall obtain the formulas of a perfectly similar type with the replacement of the functions $W_0(E_N)$, $\beta_k(E_N)$, and $\gamma_k(E_N)$ by the corresponding constants $\tilde{W}_0$, $\tilde{\beta}_k$ and $\tilde{\gamma}_k$.

3. Numerical Calculations

The numerical calculation of the coefficients W_0, β_k, and γ_k in eqs. (4), (7) and (9) was performed on the "Strela" computer at the Moscow State University for the nuclei C^{12}, Ne^{20}, Si^{28} and S^{32} under the following assumptions:

1) The state of protons in the nucleus was described by the shell model with *jj*-coupling; the spin-orbit splitting of proton levels was neglected. The potential of the shell model was taken to be a rectangular well of radius $R = r_0 A^{\frac{1}{3}}$ (where A is the mass number).

2) The interaction between the neutron and the nucleus was taken into account through a complex rectangular well

$$V_N(r) = \begin{cases} -U_N(1+i\zeta) & \text{for } r < R, \\ 0 & \text{for } r > R, \end{cases} \quad (11)$$

with the same radius R as for the protons. The calculations were performed for three values of ζ: $\zeta = 0$ (there being no absorption of neutrons in the nuclei), $\zeta = -0.10$ and $\zeta = -0.15$.

TABLE 1

Potential parameters

Nuclei	$r_0 \times 10^{13}$ (cm)	U_N (MeV)	U_P (MeV)	Nuclear proton energy levels (MeV)[a]				α
				1s	1p	1d	2s	
C^{12}	1.45	42	40.7	28.4	16.0			0.0777
Ne^{20}	1.45	42	49.6	39.9	30.0		12.70	0.154
Si^{28}	1.45	42	36.6	28.9	21.2	11.56		0.240
S^{32}	1.45	42	35.7	28.7	21.4	12.5	8.85	0.287

[a] The binding energies of the outer protons were taken from ref. [12]).

In contrast to refs. [3, 4]) the coordinate dependence of the wave function of the μ^--meson in the K-orbit was taken into account; as ψ_μ the solution of the Schrö-

TABLE 2

Calculated values

1	2	3	4	5	6	7				8				9	10
Nuclei	ζ	$\tilde{W}_0 \times 10^2$ (sec^{-1})	$\tilde{\beta}_0$	$\tilde{\gamma}_1 \times 10$	$\tilde{\gamma}_2 \times 10^2$	Ratio of μ-capture probabilities in different shells				Ratio of specific (per proton) μ-capture probabilities in different shells				Total direct process probability $\tilde{W} \times 10^3$ (sec^{-1})	$\tilde{W}/W_{exp}$ (%)
						1s	1p	1d	2s	1s	1p	1d	2s		
C^{12}	0	4.70	0.174	0.438	0.192	1	20.9			1	10.5			5.40	12.3
	−0.10	2.71	0.416	0.434	0.189	1	32.9			1	16.5			3.10	7.0
	−0.15	2.35	0.500	0.434	0.189	1	34.4			1	17.2			2.69	6.1
Ne^{20}	0	83.9	0.388	0.440	0.195	1	215		1200	1	71.7		1200	96.3	
	−0.10	41.0	0.578	0.441	0.196	1	141		871	1	47.0		871	47.0	
	−0.15	32.1	0.641	0.441	0.196	1	105		673	1	35.0		673	36.8	
Si^{28}	0	187	0.045	0.457	0.209	1	188	1730		1	62.7	577		214	27.5
	−0.10	45.7	0.366	0.451	0.204	1	111	831		1	37.0	277		52.6	6.8
	−0.15	37.4	0.441	0.451	0.204	1	78.2	590		1	26.1	197		43.1	5.5
S^{32}	0	216	0.273	0.463	0.215	1	58.8	890	982	1	19.6	297	982	250	18.0
	−0.10	113	0.515	0.465	0.217	1	58.2	632	961	1	19.4	211	961	130	9.4
	−0.15	93.2	0.590	0.465	0.217	1	50.5	483	752	1	16.8	161	752	108	7.8
Ne^{20}	Born app.	467	0.183	0.355	0.128	1	2.52		0.68	1	0.42		0.34	526	

dinger equation in the Coulomb field of point charge Ze was taken

$$\psi_\mu = \sqrt{\frac{\alpha^3}{\pi}}\, e^{-\alpha r}, \quad \alpha = \frac{Z\mathscr{M}_\mu e^2}{\hbar^2}, \tag{12}$$

where $\mathscr{M}_\mu$ is the mass of the μ-meson.

The parameters describing the proton and neutron potentials as well as the values α are represented in table 1.

The results of the calculations are listed in table 2 and in figs. 1—8. The third column of table 2 represents the quantity $\bar{W}_0$ which is the quantity $W_0(E_N)$ integrated over the energies of the neutrons emitted. $W_0(E_N)$ as a function of the kinetic energy of the neutron E_N is represented in figs. 1—4 from which it is clear that $W_0(E_N)$ reaches a maximum at 5—10 MeV and decreases sharply at $E_N \gtrsim 20$ MeV. The calculations show that with an accuracy of 1—3 %,

$$\gamma_1(E_N) = E_\nu^{\text{out}}/2Mc^2, \quad \gamma_2(E_N) = [\gamma_1(E_N)]^2,$$

where

$$E_\nu^{\text{out}} = \mathscr{M}_\mu c^2 - \mathscr{E}_p^{\text{out}} - E_N$$

is the energy of neutrino emitted together with the neutron of energy E_N in the absorption of the μ^--meson by the proton of the outer nuclear shell with binding energy $\mathscr{E}_p^{\text{out}}$. Since with any reasonable choice of the quantities λ, μ and κ the terms with $\gamma_1(E_N)$ and $\gamma_2(E_N)$ in $I(E_N)$ (eq. (5)) are fairly small compared with the constant term independent of E_N, and besides, the relative change of

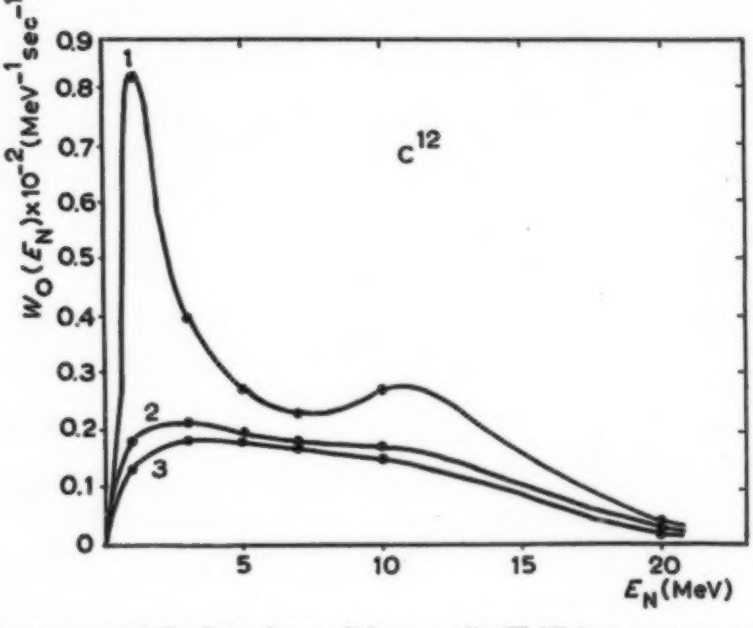

Fig. 1. Figs. 1—4 represent the dependence of the quantity $W_0(E_N)$ on neutron energy E_N for the nuclei of C^{12}, Ne^{20}, Si^{28} and S^{32}. Curves 1, 2 and 3 refer to the cases $\zeta = 0$, -0.10 and -0.15, respectively.

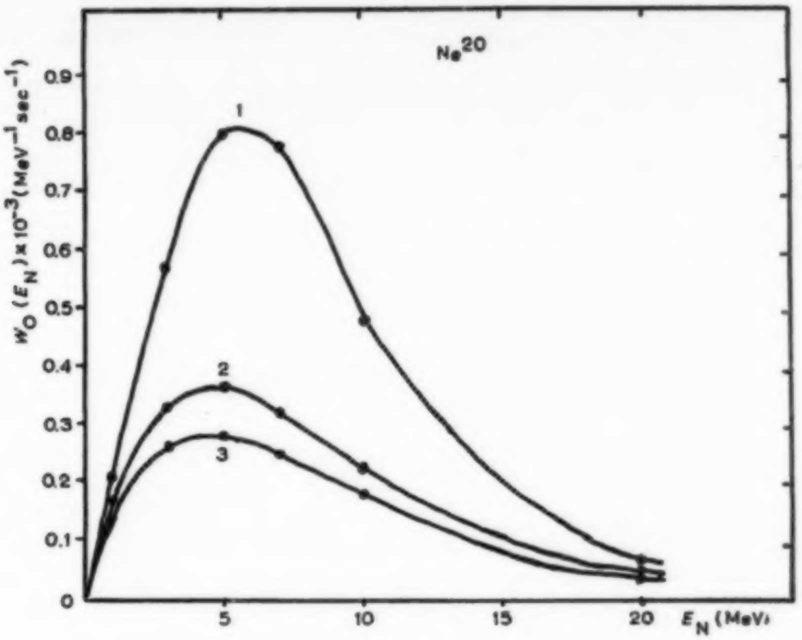
Ne^{20}
$w_0(E_N)\times10^{-3}$(MeV^{-1}sec^{-1})
0.9
0.8
0.7
0.6
0.5
0.4
0.3
0.2
0.1
0
1
2
3
5
10
15
20
E_N (MeV)

Fig. 2.

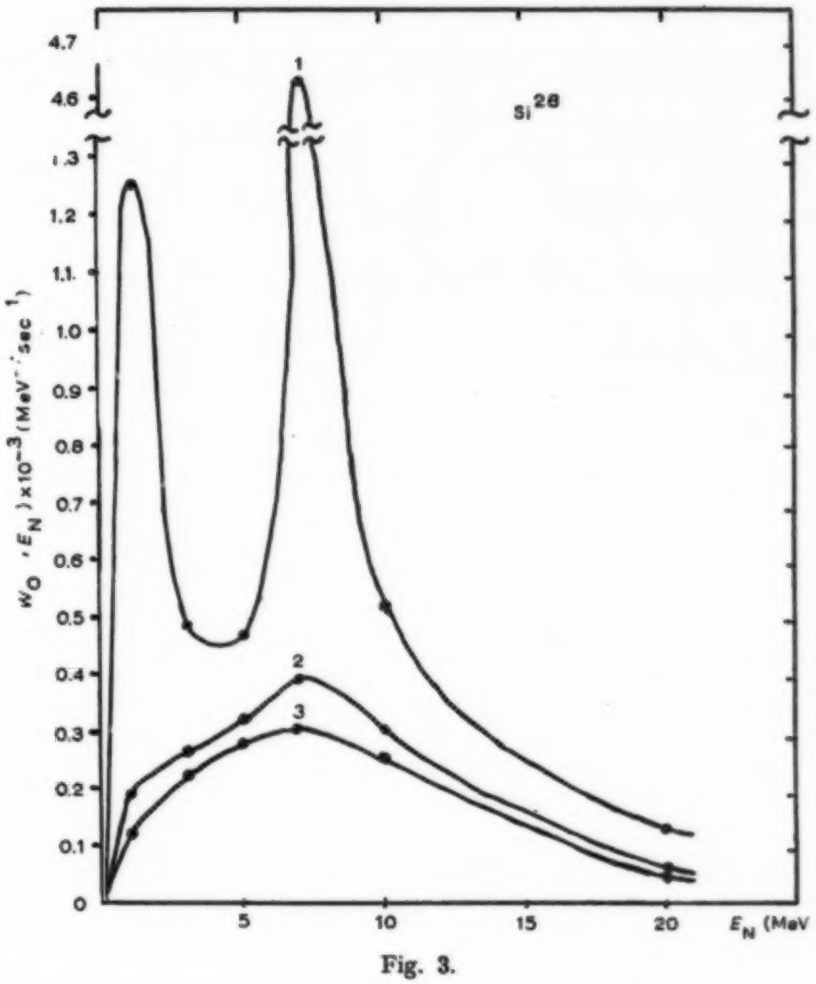
Si^{28}
$w_0(E_N)\times10^{-3}$(MeV^{-1}sec^{-1})
4.7
4.6
1.3
1.2
1.1
1.0
0.9
0.8
0.7
0.6
0.5
0.4
0.3
0.2
0.1
0
1
2
3
5
10
15
20
E_N (MeV

Fig. 3.

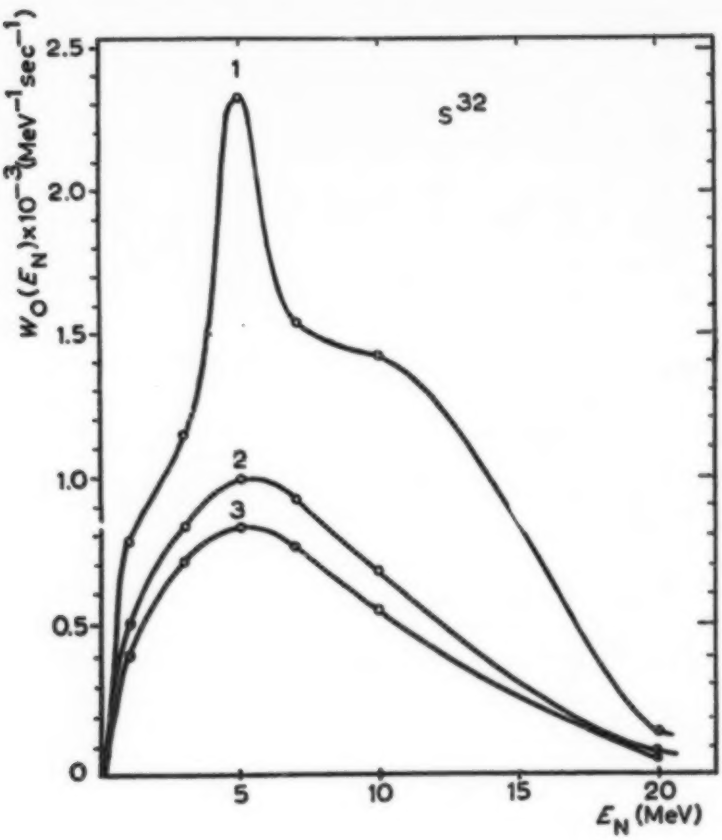

Fig. 4.

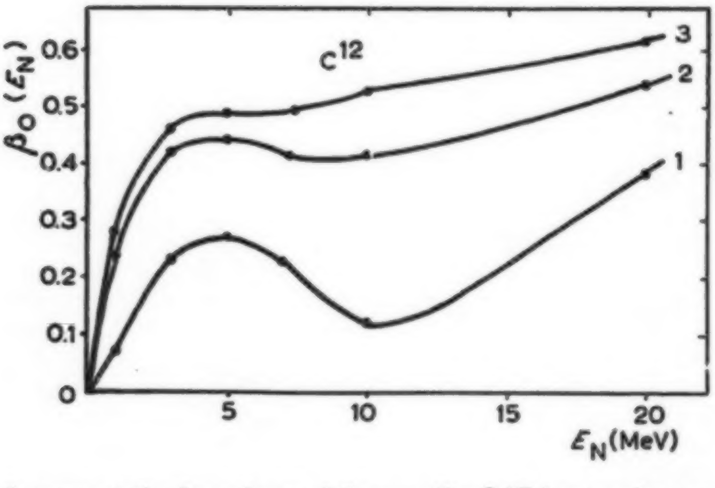

Fig. 5. Figs. 5—8 represent the dependence of the quantity $\beta_0(E_N)$ on neutron energy E_N for the nuclei of C^{12}, Ne^{20}, Si^{28}, and S^{32}. Curves 1, 2 and 3 refer to the cases $\zeta = 0$, -0.10 and -0.15, respectively.

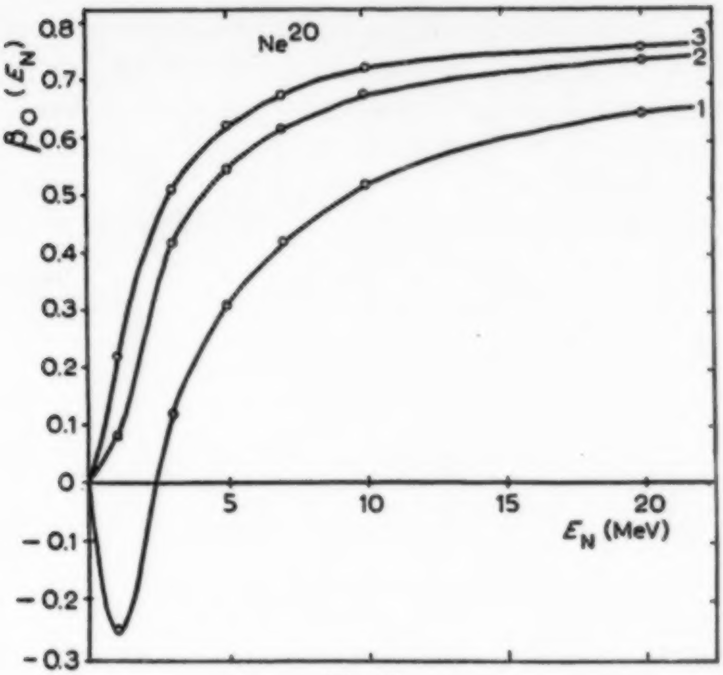

Fig. 6.

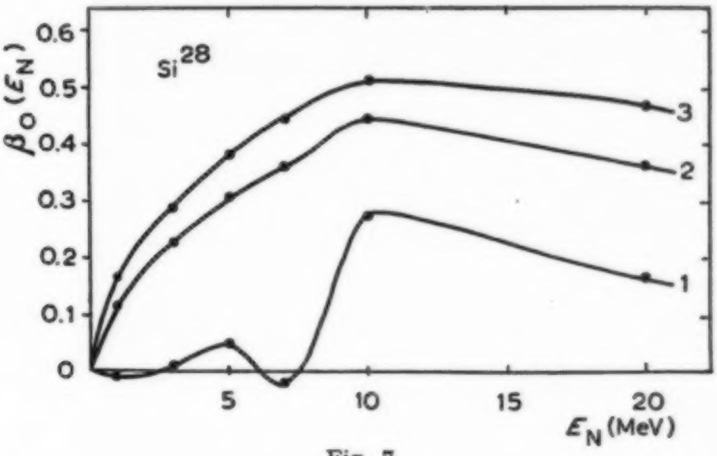

Fig. 7.

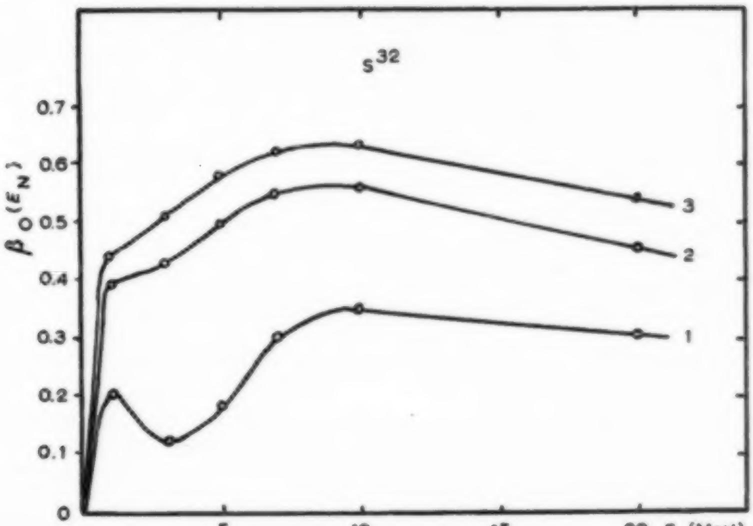

Fig. 8.

$\gamma_1(E_N)$ $(\gamma_2(E_N))$ in the energy region $E_N \lesssim 20$ MeV does not exceed 20 % (40 %), the curves for $W_0(E_N)$ describe the form of the neutron energy spectrum with satisfactory accuracy. From table 2 and figs. 1—4 it follows that taking account of the absorption of neutrons in the nucleus $(\zeta \neq 0)$ considerably decreases the probability of the direct process and flattens out the neutron energy spectrum. As has been shown by the calculations, the quantities β_1 and β_2 differ from the quantity β_0 by no more than one or two per cent. Therefor the functions $K_1(E_N)$ and $L_1(E_N)$ (eqs. (6) and (10)) can be represented with good accuracy in the form

$$K_1(E_N) = \beta_0(E_N)K(E_N), \tag{13}$$

$$L_1(E_N) = \beta_0(E_N)L(E_N), \tag{14}$$

$$\begin{aligned} K(E_N) = -\{&(-1+\lambda^2)+2[-1+2\lambda\mu+\lambda^2(\kappa-1)] \\ &\times\gamma_1(E_N)+[2\mu^2-\lambda^2(\kappa-1)^2-1]\gamma_2(E_N)\}, \end{aligned} \tag{15}$$

$$\begin{aligned} L(E_N) = -2\{&\lambda(\lambda+1)+\lambda[2(\mu+1)-\kappa] \\ &\times\gamma_1(E_N)+[\mu^2-\lambda(\kappa-1)]\gamma_2(E_N)\}. \end{aligned} \tag{16}$$

Thus the formulas for the angular distribution and longitudinal polarization of neutrons assume the form

$$q(E_N, \theta) = 1+P_\mu\beta_0(E_N)\alpha(E_N)\cos\theta, \tag{17}$$

$$P_N^l(E_N) = \beta_0(E_N)P^l(E_N), \tag{18}$$

where

$$\alpha(E_N) = K(E_N)/I(E_N), \quad P^l(E_N) = L(E_N)/I(E_N). \tag{19}$$

Similar formulas hold for the quantities $\tilde{q}(\theta)$ and $\tilde{P}_N^l$ averaged over neutron energy.

It will be noted that with the substitutions $\gamma_1(E_N) \to \gamma_H = 0.053$; $\gamma_2(E_N) \to (\gamma_H)^2 = 0.0028$ $\alpha(E_N)$ and $P^l(E_N)$ pass over into the angular asymmetry coefficient (α_H) calculated without taking into account the hyperfine structure of the mesic atom and the longitudinal polarization (P_H^l) of the neutrons formed in the μ-capture in mesic hydrogen.

The quantities $\alpha(E_N)$ and $P^l(E_N)$ depend weakly on E_N † so that in the neutron energy region $E_N \leqq 20$ MeV they may be replaced, with good accuracy, by the average values $\tilde{\alpha}$ and $\tilde{P}^l$. The energy dependence of the coefficient of angular anisotropy and the longitudinal polarization of neutrons is thus determined by the magnitude of $\beta_0(E_N)$. The quantity $\beta_0(E_N)$, taking into account the effect of the nucleus on the angular distribution and polarization of neutrons, has, as is shown in ref [13]), a simple physical meaning, viz.

---

† For example, at $\lambda = 1.25$, $\mu = 4.71$ and $\kappa = 8$ the difference of $\alpha(E_N)$ from $\tilde{\alpha}$ does not exceed 5 to 10 %, while $P^l(E_N)$ practically coincides with $\tilde{P}^l$.

$$\beta_0(E_N) = -\int f(E_N, \vartheta) \cos \vartheta d\Omega, \int f(E_N, \vartheta) d\Omega = 1, \tag{20}$$

where $f(E_N, \vartheta)$ is a function of neutron-neutrino angular correlation depending on the angle of emission of the neutron and neutrino ϑ and the neutron energy E_N. For μ-capture in mesic hydrogen: $f = \delta(1+\cos\vartheta)/2\pi$ and $\beta_0 = 1$; in the case of a point nucleus, $f = 1/4\pi$ and $\beta_0 = 0$. For an infinite nucleus described by the Fermi gas model $\cos\vartheta < 0$ always, by virtue of momentum conservation and the Pauli principle, and consequently $\beta_0 > 0$. For the real nucleus $0 \leqq |\beta_0| \leqq 1$. The absolute value and sign of β_0 for a specific nucleus is determined by two factors: the character of the momentum distribution of protons in the nucleus and the kind of interaction between the outgoing neutron and the nucleus. Comparison of the calculations performed with neglecting the interaction between the neutron and the nucleus (see below) and calculations with different values of the imaginary part of the optical potential shows that both of the above-mentioned factors are essential; from the analysis of the results of calculation in Born approximation for the neutron it follows that the momentum distribution of the protons, which decreases monotonically with increasing momentum, leads to positive values $\beta_0(E_N)$, while nonmonotonic distributions may lead to $\beta_0(E_N) < 0$. The fourth column of table 2 and figs. 5—8 represent $\tilde{\beta}_0$ and $\beta_0(E_N)$. Comparing the quantities β_0 at different values of the coefficient ζ we can see that taking account of the absorption of neutrons in the nucleus ($\zeta \neq 0$) considerably increases the angular asymmetry and the longitudinal polarization of the neutrons. The latter fact can qualitatively be explained in the following manner. Speaking in quasi-classical terms we can say that the growth of the imaginary part of the complex potential leads to a relative increase of the probability of the emission of the neutrons possessing large "target distances" and to a decrease of the probability of the emision of the neutrons with small "target distances". As a result the contribution of s-neutrons, emitted by the nucleus always isotropically, decreases as compared with the contribution of p—, d—, . . . neutrons, which should naturally cause the growth of asymmetry in the angular distribution. An increase of the longitudinal polarization with the growth of ζ can be interpreted in similar terms.

It will be noted that in the optical model describing neutron scattering the quantity ζ is a function of the energy of the neutron E_N; according to ref. [14]), with the change E_N from 3 to 20 MeV ζ changes approximately from $+0.05$ to $+0.20$. Therefore the values of $\zeta = -(0.10 \text{ to } 0.15)$ are reasonable average values in the energy interval under consideration †. It can be expected that taking account of the energy dependence of ζ will not appreciably change the results obtained in the present paper, all the more so since, as is clear from table 2 and figs. 1—8, the results of calculations at two different non-zero values of ζ prove to be rather close. More detailed calculations using the energy-dependent coefficient ζ are obviously worthwhile only after sufficient experimental data have accumulated.

---

† As was noted in ref. [3]), the sign of ζ must be negative in the case of neutron production.

The seventh and the eighth columns of table 2 represent the ratios of the probabilities of direct emission of neutrons in μ-capture in different nuclear shells. As follows from these results the contribution to the probability of the process under study is made almost completely by the outer shells of nuclei. The last two columns of table 2 contain the total probabilities of the direct process in μ-capture $\tilde{W}$ and the ratios $\tilde{W}/W_{\text{exp}}$, where W_{exp} is the total experimental probability of μ-capture in the nuclei under investigation[†]. The quantity $\tilde{W}$ is determined by the formula[††]

$$\tilde{W} = G^{(\mu)2}\tilde{W}_0 I, \tag{21}$$

where $\tilde{I}$ is obtained from $I(E_{\text{N}})$ by replacing $\gamma_k(E_{\text{N}})$ by $\tilde{\gamma}_k$. Thus we see that the probability of μ-capture leading to the direct emission of neutrons amounts to 5 to 10 % of the total probability of μ-capture at $\zeta \neq 0$. To obtain the share of direct process neutrons in the total number of neutrons emitted in μ-capture, the values of $\tilde{W}/W_{\text{exp}}$ given in table 2 should be divided by the average number of neutrons emitted per μ-capture event.

As was shown by the test calculations for the nucleus of Ne^{20}, taking account of the radial dependence of the wave function of the μ-meson in the K orbit changes the coefficient β_0 by no more than 2 or 3 %; at the same time the probability of direct process decreases by 20 to 25 %. For heavier nuclei a decrease of probability must be even more considerable.

To analyse the influence of the interaction between the neutron and the nucleus on the effects under study, numerical calculations for Ne^{20} were performed in Born approximation for the outgoing neutron, i.e., the wave function of the neutron was taken to be a plane wave. The results of the calculation are shown in the last line of table 2 and in figs. 9 and 10. They differ widely from the data obtained for Ne^{20} taking account of the interaction between the neutron and the nucleus (table 2 and figs. 2 and 6). Taking account of the nuclear interaction of neutrons leads to a decrease of the probability of the process under study by an appreciable factor, a relative increase of the number of neutrons with lower energies, and a considerable increase of the coefficient of asymmetry and the longitudinal polarization of neutrons. Besides, in Born approximation the contribution of different shells to the direct process probability in μ-capture proves to be comparable, and the direct process probability by far exceeds the total experimental probability of absorption of μ^--mesons by the nuclei of Ne^{20}. Thus, in considering the phenomena under study it is necessary to take into account the interaction of the outgoing neutron with the nucleus.

[†] The values of W_{exp} are taken from ref. [15]).

[††] In calculating $\tilde{W}$ the most reasonable of the constants were selected from the viewpoint of the modern concepts on μ-capture: $G^{(\mu)} = 1.37$, $\lambda = 1.25$, $\mu = 4.71$, $\kappa = 8$.

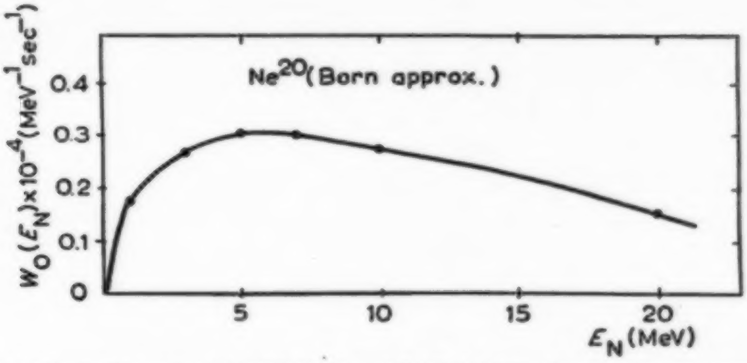

Fig. 9. Figs. 9, 10 show the quantities $W_0(E_N)$ and $\beta_0(E_N)$ depending on the neutron energy E_N for the nucleus of Ne^{20}, calculated in Born approximation.

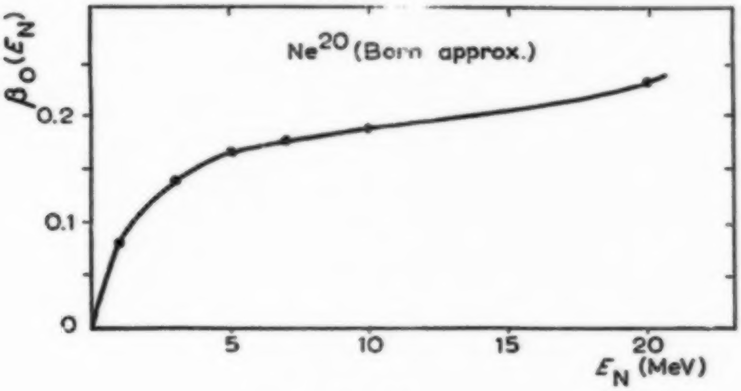

Fig. 10.

4. Comparison of Theory with Experiment

The quantities α and P^l (eqs. (17) and (18)) depend on the constants λ, μ and κ in the μ-meson weak interaction Hamiltonian. Table 3 represents the values of the mesic-hydrogen coefficient of angular asymmetry α_H and polarization P_H^l at $\lambda = 1.25$ and for different combinations of μ and κ. For comparison the values of α_H and P_H^l obtained in the nonrelativistic approximation with respect to nucleons are indicated also. The exact value of λ for the μ-capture is not known, yet from the experiments on μ-capture in C^{12} of ref. 16) it can be concluded that $|\lambda(\mu\text{-capture})/\lambda(\beta\text{-decay})| \approx 1$ and the experiments performed by Telegdi *et al.* 17) indicate that $\lambda > 0$. Therefore for the quantity λ in table 3 its value for β-decay $\lambda = 1.25$ was selected. α_H differs from the asymmetry coefficient $\tilde{\alpha}$ averaged over the energy of the neutron by no more than 10 % for the nuclei under study, while P_{H}^{l} and $\bar{P}^{l}$ coincide with an accuracy up to ≈ 1 %. The values $\tilde{\alpha}$ and $\bar{P}^{l}$ practically do not change from nucleus to nucleus, since $\tilde{\gamma}_k$ for different nuclei are rather close (see table 2). By way of illustration the last but one column of table 3 lists the values of $\tilde{\alpha}$ for the nucleus of S^{32}.

TABLE 3
Calculated values

μ	κ	α_{H}	P_{H}^{l}	$\tilde{\alpha}$	W
4.71	8	−0.45	−0.99	−0.41	1.0
1	8	−0.33	−0.99	−0.30	0.8
4.71	0	−0.23	−0.99	−0.21	1.2
1	0	−0.09	−0.99	−0.09	1.0
nonrelativistic approximation		−0.10	−0.99	−0.10	0.9

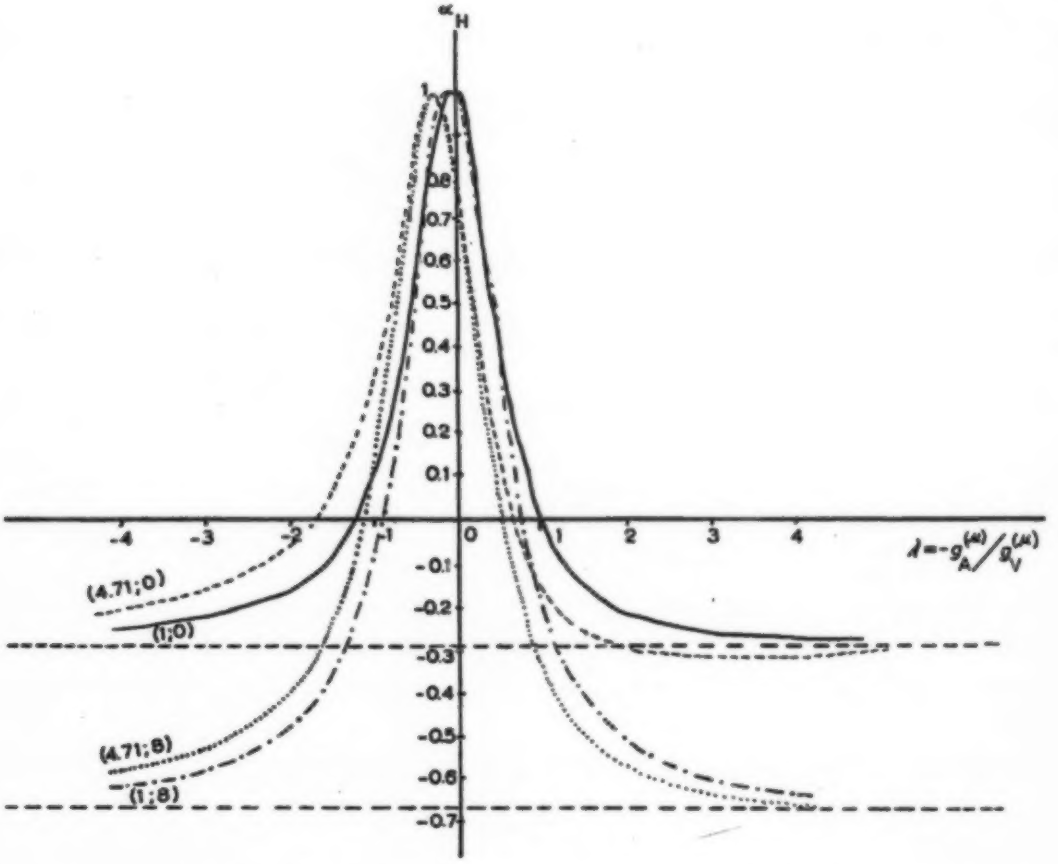

Fig. 11. Figs. 11, 12 show the dependence of the quantities α_{H} and P_{H}^{l} on λ. The first figure in brackets in the figures indicates the value of μ and the second that of κ.

The last column of table 3 indicates in relative units the total probabilities of μ-capture with direct emission of neutrons.

The data given in table 3 shows that at $\lambda = 1.25$ the coefficient of neutron angular asymmetry depends appreciably on whether or not an effective pseudoscalar coupling and the weak magnetism term are present in the μ-meson-nucleon interaction Hamiltonian. At the same time the longitudinal polarization of neutrons in all cases under consideration remains constant and the total probability of the direct process changes by no more than 20 %.

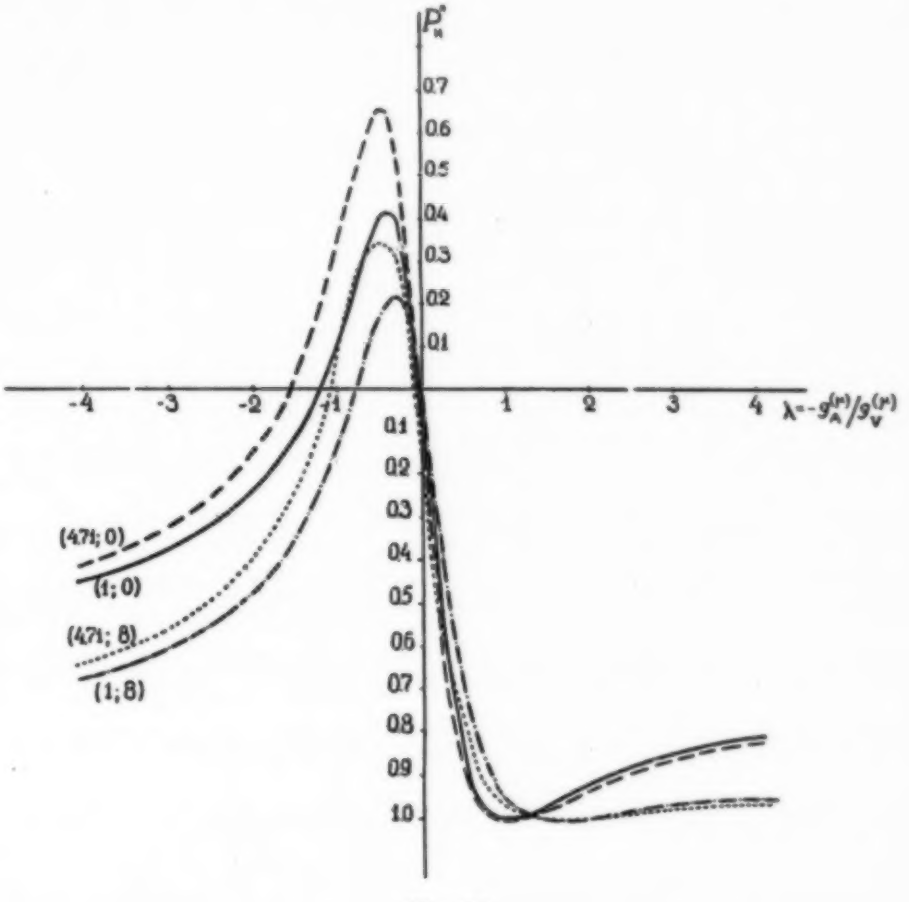

Fig. 12.

Fig. 11 and 12 represent α_H and P_H^1 as functions of λ at $\mu = 1$; 4.71 and $\kappa = 0$; 8. The dependence of α_H and P_H^1 on κ at $\lambda = 1.25$ and $\mu = 1$; 4.71 is represented in fig. 13. As is clear from figs. 12, 14 at $0.75 \lessapprox \lambda \lessapprox 2$, the quantity $P_H^1 \approx 1$ for all reasonable values of μ and κ. This fact makes it possible to obtain the values of $\tilde{\beta}_0$ directly by measuring the longitudinal polarization of the neutron $\tilde{P}_N^1 = \tilde{\beta}_0 \tilde{P}^1$. Comparison of the quantities thus obtained $\tilde{\beta}_0$ with the calculated ones will enable us to estimate the applicability of the accepted models and the correctness of the selection of parameters. If $\tilde{\beta}_0$ is known, it is possible from the experimental value of asymmetry $a = P_\mu \tilde{\beta}_0 \tilde{\alpha}$ to determine $\tilde{\alpha}$ and obtain data on the quantities λ, μ and κ.

With the possibility of the absorption of neutrons in nuclear matter ($\zeta \neq 0$) being taken into account for the nuclei under study in the present paper $\tilde{\beta}_0 \approx$ 0.4—0.6. Therefore it can be expected that the longitudinal polarization of neutrons $\tilde{P}_N^{\parallel} \approx -(0.4—0.6.)$ If we use for P_μ the values obtained by Ignatenko *et al.* [18]) ($P_\mu \approx 0.15—0.20$), in the theoretically most probable case ($\lambda = 1.25$; $\mu = 4.71$; $\kappa = 8$) for the total coefficient of angular anisotropy a we obtain $a \approx -(0.03—0.05)$. At other values of μ and κ (see table 3) the coefficient a will be respectively less.

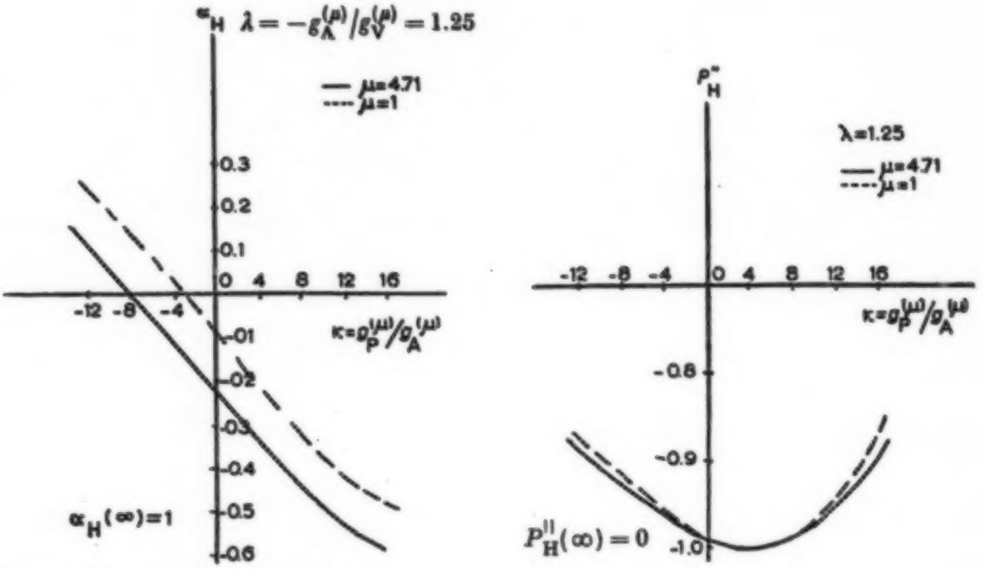

Fig. 13. The dependence of the quantities α_H and $P_H^{\parallel}$ on κ at $\lambda = 1.25$ and $\mu = 1$ and 4.71.

At present two papers have been published on measuring asymmetry in the angular distribution of the neutrons emitted by the nucleus in μ-capture. (Experiments to measure the polarization of neutrons in μ-capture have not yet been performed). Astbury *et al.* [19]) studied the anisotropy of the neutrons emitted in μ-capture in S^{32}. The experimentally observed angular distribution of neutrons is of the form $1 + P_\mu \tilde{\beta}_0 \tilde{\alpha} \phi \cos \theta$, where the factor ϕ takes account of the isotropic background of evaporated neutrons. For the quantity $\tilde{\beta}_0 \tilde{\alpha} \phi$ the authors give the value:

$$\tilde{\beta}_0 \tilde{\alpha} \phi = -0.30 \pm 0.12.$$

Since $\phi \leqq 1$, the above-mentioned number is the upper limit for $\tilde{\beta}_0 \tilde{\alpha}$. According to table 2 for S^{32} at $\zeta \neq 0$ $\tilde{\beta}_0 \approx 0.5—0.6$ so that the upper limit of $\tilde{\alpha}$ in our estimates equals $\tilde{\alpha}_{\max} \approx -(0.5—0.6) \pm 0.2$.

The closest to this upper limit of all represented in table 3 is the variant corresponding to $\mu = 4.71$ and $\kappa = 8$. For all other possibilities considered in table 3 the theoretical values of $\tilde{a}$ differ from the average value of the upper limit by more than one experimental error. A rough estimate of quantity ϕ ($\phi \approx 0.7$) given in ref. [19]) leads the authors to the estimate $\tilde{\beta}_0\tilde{a} \approx -0.4$, which also proves to be the closest to the quantity $\tilde{a}$ predicted by the universal Fermi interaction theory with conserved vector current and with allowance for the effective pseudo-scalar interaction with the coupling constant $g_P^{(\mu)} = 8g_A^{(\mu)}$.

Baker and Rubbia [20]) measured the asymmetry in the angular distribution of neutrons of energy $E_N > 5.5$ MeV emitted in μ-capture in Mg. For $\tilde{\beta}_0\tilde{a}$ the value $+0.15 \pm 0.11$ was obtained, which differs in both magnitude and sign from the results of ref. [19]) and the expected theoretical quantities. It will be noted that though the numerical calculations for μ-capture in Mg have not been performed by the present authors, it ought to be expected that the coefficients β_0 and γ_k for Mg^{24} are close to the respective values for Si^{28} since the structure of these nuclei are rather similar and the outer proton binding energies practically the same. Therefore it is difficult to account for the results obtained by Baker and Rubbia from the viewpoint of the current concepts of μ-capture.

In conclusion we express our deep gratitude to Prof. I. S. Shapiro for discussing the present paper.

References

1) I. S. Shapiro, E. I. Dolinsky and L. D. Blokhintsev, DAN SSSR **116** (1957) 946; Nuclear Physics **4** (1957) 273

2) B. L. Ioffe, JETP **36** (1957) 308;
H. Überall, Nuovo Cim. **6** (1957) 533;
K. Huang, C. N. Yang and T. D. Lee, Phys. Rev. **108** (1957) 1340;
L. Wolfenstein, Nuovo Cim. **7** (1958) 706

3) E. I. Dolinsky and L. D. Blokhintsev, JETP **35** (1958) 1488; Nuclear Physics **10** (1959) 527

4) L. D. Blokhintsev, JETP **36** (1959) 258

5) R. P. Feynman and M. Gell-Mann, Phys. Rev. **109** (1958) 193

6) E. C. G. Sudarshan and R. E. Marshak, Phys. Rev. **109** (1958) 1860

7) A. Fujii and H. Primakoff, Nuovo Cim. **12** (1959) 1329

8) M. Gell-Mann, Phys. Rev. **111** (1958) 362

9) M. L. Goldberger and S. B. Treiman, Phys. Rev. **111** (1958) 354

10) E. I. Dolinsky, JETP **36** (1959) 1179

11) I. M. Shmushkevich, JETP **36** (1959) 953

12) N. Feather, Advances in Physics **2** (1953) 141

13) E. I. Dolinsky, Theses, Joint Institute for Nuclear Research, 1959

14) M. Kawai, M. Nagasaki, M. Soga, T. Terasawa, H. Ui and Y. Wada, Progr. Theor. Phys. **18** (1957) 66

15) J. C. Sens, Phys. Rev. **113** (1959) 679

16) H. V. Argo, F. B. Harrison, H. W. Cruse and A. D. McGuire, Phys. Rev. **114** (1959) 626

17) V. L. Telegdi, Phys. Rev. Lett. **3** (1959) 59

18) A. E. Ignatenko, L. B. Yegorov, B. Khalupa, D. Chultem, JETP **35** (1958) 1131

19) A. Astbury, J. M. Blair, M. Hussain, M. A. R. Kemp, H. Muirhead and R. G. P. Voss, Phys. Rev. Lett. **3** (1959) 476

20) W. F. Baker and C. Rubbia, Phys. Rev. Lett. **3** (1959) 179

2.B

Nuclear Physics **23** (1961) 386—398; © *North-Holland Publishing Co., Amsterdam*

Not to be reproduced by photoprint or microfilm without written permission from the publisher

SOME $Be^9(d, p\gamma)Be^{10}$ ANGULAR CORRELATION MEASUREMENTS OFF THE STRIPPING PEAK

F. H. READ, J. M. CALVERT and G. SCHORK †

The Physical Laboratories, Manchester University

Received 24 November 1960

Abstract: Angular correlations, in the reaction and azimuthal planes, between protons and gamma rays from the first excited state of Be^{10} in the reaction $Be^9(d, p\gamma)Be^{10}$, have been measured for four proton angles between 26° and 86° in the centre-of-mass system. For a pure stripping reaction, with $l = 1$ for the stripped neutron, only $P_2(\cos\theta_{p\gamma})$ terms are allowed in the angular correlation function in the reaction plane. However, P_4 terms have been found, even on the stripping peak, indicating a compound-nucleus contribution to the reaction. Excitation functions for the reaction products of Be^9+d have been measured for incident energies from 3.8 to 6.3 MeV and these show an absence of resonances. Absolute differential cross-sections for the ground state and first excited state proton groups from the $Be^9(d, p)Be^{10}$ reaction have been measured at an incident energy of 5.86 MeV; these have been analysed in terms of the Butler stripping theory to give cut-off radii and reduced neutron widths.

1. Introduction

Measurements of the proton-gamma ray angular correlation functions in $(d, p\gamma)$ reactions provide a sensitive test of the assumptions of deuteron stripping theories. Several workers [1,2,3,4,5]) have measured these correlations for a variety of light target nuclei, and they show that for incident energies greater than about 3 MeV the distorted wave theory of deuteron stripping ((see, for example, Huby *et al.* [6])), or even the simpler plane wave theory (Butler [7])), is a good description of the reaction mechanism. However, all these measurements have been made with the proton detector set on the main stripping peak. It has been suggested by Satchler [8]) that it would be useful to measure these correlations off the stripping peak, as information would then be obtained about the reaction mechanism in this region.

We have selected the $Be^9(d, p)Be^{10}$ reaction leading to the first excited state of Be^{10} at 3.37 MeV for these studies, because the nuclear spins, the l value of the stripped neutron and the gamma ray multipolarity, are all known unambiguously. The only unknown is the incident channel spin mixing ratio. We have also measured excitation functions for some of the reaction products of Be^9+d to see if there are any large resonances, and differential cross-sections for the Be^9 $(d, p)Be^{10}$ reaction to ascertain the positions of the stripping peaks.

---

† Permanent address; Physikalisches Institut, Freiburg University, Germany.

2. Apparatus

The apparatus used for the angular correlation studies is shown in fig. 1. Two detectors (one for detecting gamma radiation, one for charged particles) were mounted inside an evacuated aluminium dome. They could be rotated independently through 360° about the target as centre, in the reaction plane, without breaking the vacuum. For measurements in the azimuthal plane (which we define as the plane at right angles to the recoil axis, see below), the gamma ray detector was suspended beneath the target. The deuteron beam was provided by the Manchester University Physics Department's 6 MV Van de Graaff Generator. The target was a self-supporting beryllium foil, 25 μm thick, supplied by Mallory Metallurgical Products Limited. The energy loss of deuterons in the target at 5.3 MeV was approximately 0.6 MeV.

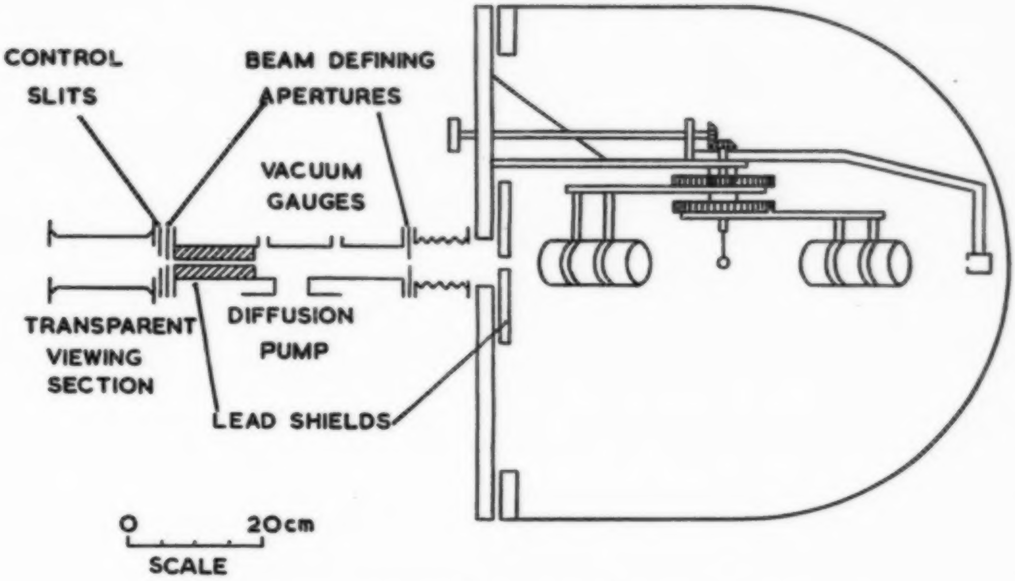

Fig. 1. The apparatus used for the angular correlation studies.

The gamma ray detector was a NaI(Tl) Harshaw crystal (4.5 cm diameter, 5.1 cm long) mounted on an RCA 6810A photomultiplier tube. Two pulses were taken from the photomultiplier tube; one from the 10th dynode for pulse height analysis and one from the 14th dynode for fast coincidence analysis. The differentiating time for the latter, at the dynode, was approximately 10 ns, which effectively changed the slowly rising NaI pulses into ones suitable for fast coincidence analysis. Cathode follower circuits were mounted directly onto the photomultiplier housings, to reduce stray capacities. The gamma ray detector was shielded effectively against background radiation from the Van de Graaff Generator and from the control slits and apertures, by the two lead shields shown in fig. 1, and by a lead cap placed directly over the NaI crystal. The charged particle detector was the same as the gamma ray detector, except that in this case the scintillator was a 2.5 cm diameter by 0.16 cm thick CsI(Tl) crystal, which was covered by a sufficient thickness of aluminium absorber to prevent elastically scattered deuterons from the target reaching the crystal. The gamma ray detector subtended an angle of ±6°, and the proton detector ±1.5° at the target.

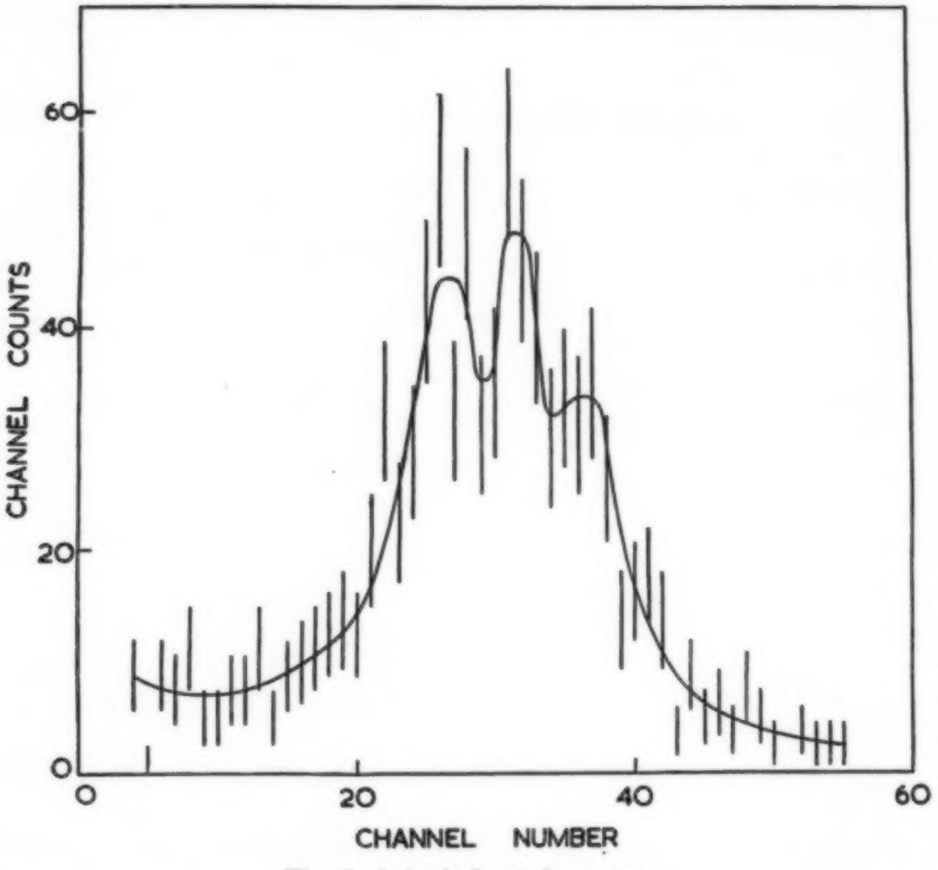

Fig. 2. A typical gated spectrum.

The arrangement of the electronics was as a convential fast-slow coincidence system. The charged particle spectrum (from the 10th dynode) was fed into a single-channel pulse height analyser and the output of this, in coincidence with the output of a fast coincidence unit (fed by pulses from the 14th dynodes) then gated a 100 channel analyser, into which was fed the gamma ray spectrum. A typical gated spectrum is shown in fig. 2; in this the single-channel analyser was set to pass only the proton group (p_1) corresponding to the first excited state of Be^{10} and the triton group (t_0) corresponding to the ground state of Be^8 (these two groups were usually nearly coincident in amplitude). The 3.37 MeV photoelectric peak and escape peaks are clearly seen, while peaks from other excited states of Be^{10} and from the small amounts of target impurities, which are present in ungated spectra, are absent from this gated spectrum.

The details of the fast coincidence unit were as follows. Each train of pulses from the 14th dynodes was fed into a fast trigger unit, very similar to that described by Lewis and Wells [9]) (page 287). The output pulses from the trigger units were shaped by cut-off valves, each with a cable delay line shaper in the anode load. The two trains of shaped pulses were then fed into a conventional 6BN6 coincidence unit. The overall resolving time was $2\tau = 15$ ns. The unit was tested by measuring the angular correlation of the two gamma rays following the β-decay of Co^{60}. The advantage of using this type of coincidence unit is that the input valves trigger at about 0.5 V; it is important to keep this triggering level as low as possible because of the slow decay times of the NaI and CsI scintillators. The effect that these slow decay times had on the time delay in triggering is shown by the absence of the lower part of the gated spectrum in fig. 2.

The apparatus used to measure absolute differential cross-sections and excitation functions for the reaction products of Be^9+d was a conventional scattering chamber, and has been described previously [10]).

3. Measurements and Results

For each value of the incident deuteron energy and the proton detector angle, the experimental procedure in the angular correlation measurements was as follows. The time delay between the fast pulses from the two detectors was varied by inserting lengths of 100 Ω semi air spaced coaxial cable between the detectors and the fast coincidence unit inputs. The single-channel analyser was set to pass only the p_1 group (and the t_0 group, when this was coincident in amplitude), and the ratio of the counts in the photoelectric peak and the escape peaks of the gated coincidence spectrum to the number of pulses passed by the single-channel analyser, was plotted as a function of the time delay. The centre of the flat maximum of this graph then gave the time delay to be used when measuring the "true plus random" coincidence counting rates. The random rates were measured by using a time delay sufficiently long to exclude any true coincidences. The beam current was kept constant, to maintain a constant random coincidence rate; it had previously been shown that the true rate was not a function of the beam current (i.e. counts were not lost at high counting rates). By constantly referring to the ungated gamma ray spectrum, the charged particle spectrum (displayed on a separate multichannel analyser), the beam current, the current integrator, and the four scalers used at various points, conditions could be kept constant and an angular correlation could be measured. The angle of the gamma ray detector was changed in a random way and at each angle both the "true plus random" coincidence counting rate, and the random rate were found. The ratio of true to random coincidence rates was about 10, the true rate being about 40 per minute at the

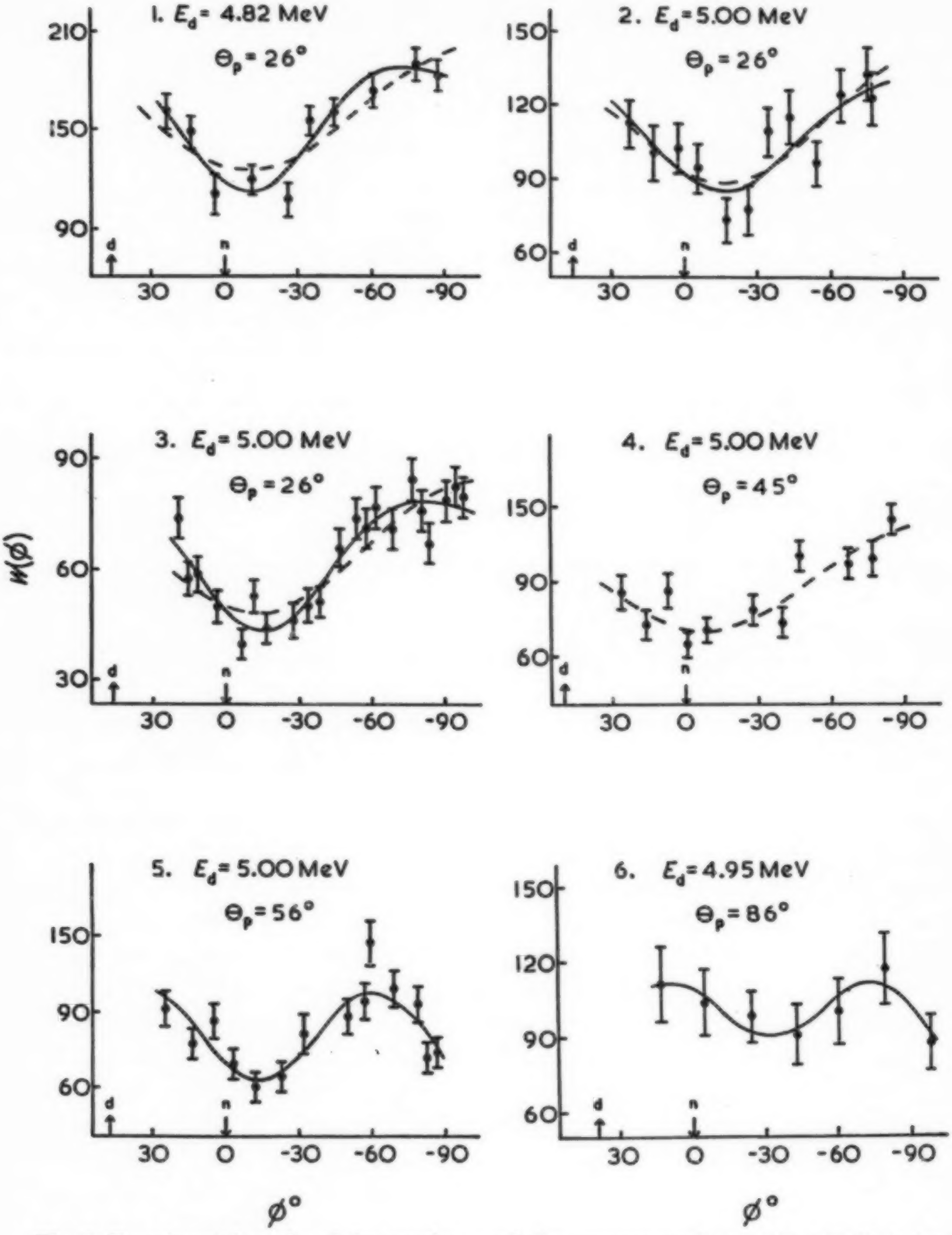

Fig. 3. Experimental results of the angular correlation measurements together with their least square analyses.

smallest proton angle (23°, in the lab. system), and about 10 per minute at the largest (79°).

The azimuthal anisotropies were measured by finding the coincidence counting rate with the gamma ray detector at right angles to the recoil axis, and then suspending the detector below the target (keeping the distance between the target and the detector constant) and again finding the coincidence counting rate. Particular attention was paid here to the constancy of the conditions.

The results of the angular correlation measurements in the reaction plane are shown in fig. 3. The errors are statistical errors only, due to the finite number of counts. The angles θ and ϕ are defined by taking the z axis along $\mathbf{n} = \mathbf{k}_d \times \mathbf{k}_p$ and the x axis along the recoil direction $\mathbf{k} = \mathbf{k}_d - \mathbf{k}_p$ (The recoil axes were at angles of 47°, 46°, 46°, 50°, 48° and 39° to the deuteron beam for correlations 1 to 6 respectively). The full curves are the "least squares" fits of the function

$$W'(\phi) = 1 + \bar{e}_2 P_2(\cos(\phi - \phi'_0)) + \bar{e}_4 P_4(\cos(\phi - \phi'_0)), \tag{1}$$

and the dashed curves are fits of the function

$$W(\phi) = 1 + \bar{e} P_2(\cos(\phi - \phi_0)). \tag{2}$$

The least squares analyses, giving the coefficients and their errors, were done on the Mercury Computer of Manchester University. The coefficients $\bar{e}_2$, $\bar{e}_4$ and $\bar{e}$, when corrected for the finite solid angle of the gamma ray detector [11]), give the coefficients e_2, e_4 and e of the true correlation functions. These coefficients are shown in table 1, which also contains the results of other workers who have measured this angular correlation. The angles ϕ_0, ϕ'_0 are the angles between the recoil axes and the axes of symmetry. The values of χ^2 were also calculated, and the probabilities given in the table are taken to indicate a good fit if they lie between 10 % and 90 %.

The azimuthal correlation was measured by taking two points in the azimuthal plane (the plane at right angles to the recoil axis), namely $\theta = \frac{1}{2}\pi$ (in the reaction plane) and $\theta = 0$ (at right angles to the reaction plane). These measurements give the coefficient f, defined by

$$\frac{W(\theta = 0)}{W(\theta = \frac{1}{2}\pi, \phi = -\frac{1}{2}\pi)} = \frac{1}{f}. \tag{3}$$

Table 1 contains the values found for these coefficients, corrected for the finite solid angle of the gamma ray detector. These measurements were done at mean deuteron energy of 4.95 MeV, but it has been assumed that f varies slowly with E_d. We have also analysed the measurements of Taylor [2]) in the azimuthal plane, and this result is included in the table.

The procedures for measuring absolute differential cross-sections and excitation functions have been described elsewhere [10]). Excitation functions were measured at a laboratory angle of 40° for the proton groups (p_0 and p_1) leading

TABLE 1

Coefficients of the true correlation functions

No.	1	2	3	4	5	6	7[1]	8[2]
E_d (Lab)	4.82	5.00	5.00	5.00	5.00	4.95	3.90	7.78
θ_p(c.m.)	26	26	26	45	56	86	30	23
e	-0.29 ± 0.06	-0.31 ± 0.07	-0.34 ± 0.04	-0.30 ± 0.05	-0.12 ± 0.09	-0.05 ± 0.11	≈-0.4	-0.33 ± 0.04
ϕ_0	$-10\ \pm5$	$-16\ \pm8$	$-13\ \pm4$	$-3\ \pm6$	$-7\ \pm10$	≈-40	≈0	$-6\ \pm8$
χ^2 fit	4 %	25 %	< 1 %	8 %	< 1 %	50 %		
e_2	-0.21 ± 0.04	-0.22 ± 0.16	-0.25 ± 0.04	-0.28 ± 0.07	0.14 ± 0.09	0.29 ± 0.11		
e_4	-0.18 ± 0.06	-0.10 ± 0.13	-0.18 ± 0.05	-0.03 ± 0.09	-0.42 ± 0.09	-0.35 ± 0.10		
ϕ'_0	$-10\ \pm4$	$-15\ \pm6$	$-15\ \pm3$	$-8\ \pm6$	$-14\ \pm4$	$-33\ \pm7$		
χ^2 fit	33 %	23 %	25 %	5 %	15 %	97 %		
f	1.06 ± 0.06	1.06 ± 0.06	1.06 ± 0.06	0.82 ± 0.09	0.85 ± 0.12	1.06 ± 0.09		1.01 ± 0.07

E_d in MeV. Θ_p, ϕ_0 and ϕ'_0 in degrees.

to the ground state and first excited state of Be^{10}) and for the triton group (t_0) leading to the ground state of Be^8. The results are shown in fig. 4. Absolute differential cross-sections were measured for the p_0 and p_1 groups in the reaction Be^9(d, p)Be^{10} at an incident deuteron energy of 5.86 MeV with a thin target. The results are shown in fig. 5. The errors shown in the cross-sections include the error in the absolute normalisation (4.5 %), the errors due to uncertain background subtractions, and statistical errors due to finite numbers of counts. Proton groups corresponding to the ground state and first excited state

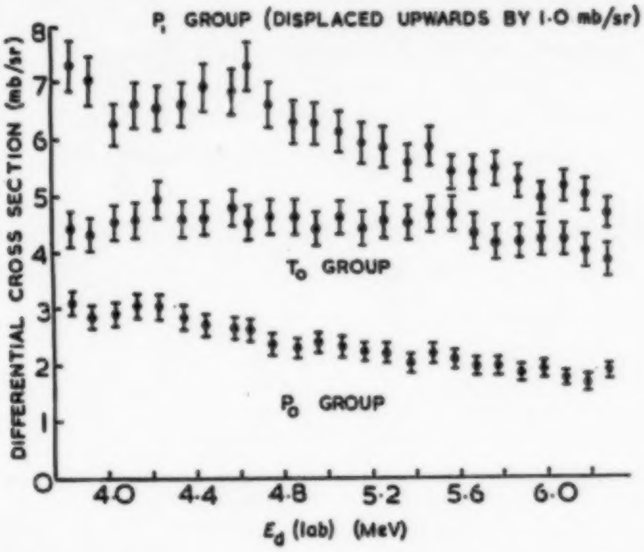

Fig. 4. Excitation functions at 40° for the proton groups p_0 and p_1 and the triton group t_0.

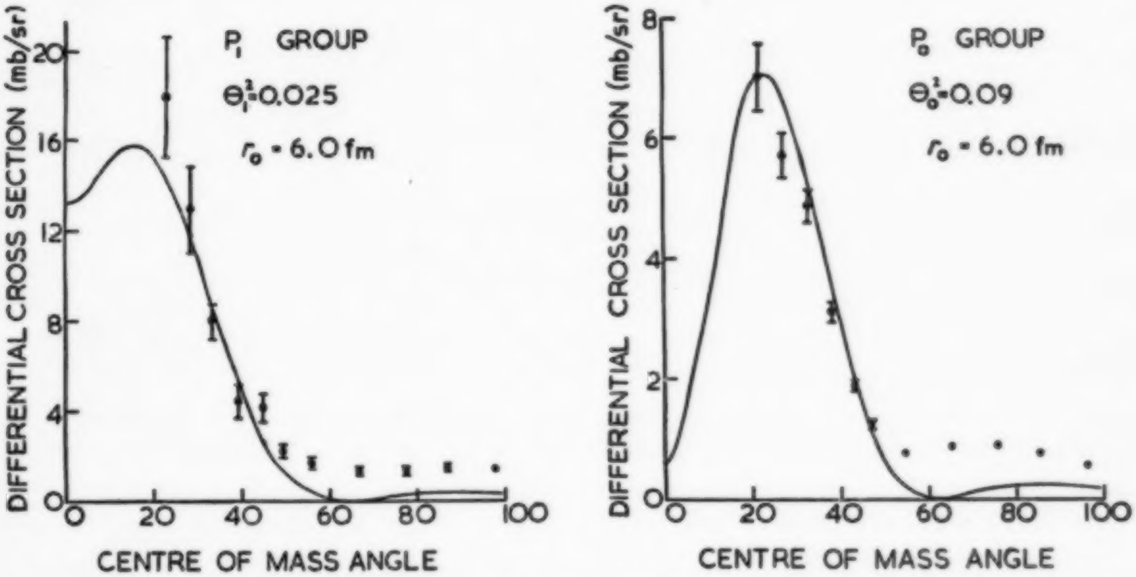

Fig. 5. Absolute differential cross sections for the p_0 and p_1 groups in the reaction Be^9(d, p)Be^{10}.

of O^{17} (due to an O^{16} contaminant in the target) were often coincident in amplitude with the p_1 group from Be^9, and the large errors in the cross-sections for the latter are often a result of the uncertain background subtractions.

4. Analysis of the Cross-Section Measurements

The excitation functions for the deuteron bombardment of Be^9 (fig. 4), do not show any broad resonances; weak narrow resonances might have been missed because of the thickness of the target ($\approx$ 0.07 MeV at 5 MeV). This lack of resonance structure is the result that one might expect since the excitation energy of the compound nucleus B^{11} is high (18.97 to 20.97 MeV). Two other investigations have been made in this region of excitation of B^{11}, and both show a lack of resonance structure; McCrary *et al.* [12]) measured the yield of 3.37 MeV gamma rays from the deuteron bombardment of Be^9, and Becker and Barschall [13]) measured the total neutron cross-sections for the neutron bombardment of B^{10}. The results of these investigations are consistent with the smooth excitation functions found in the present experiments.

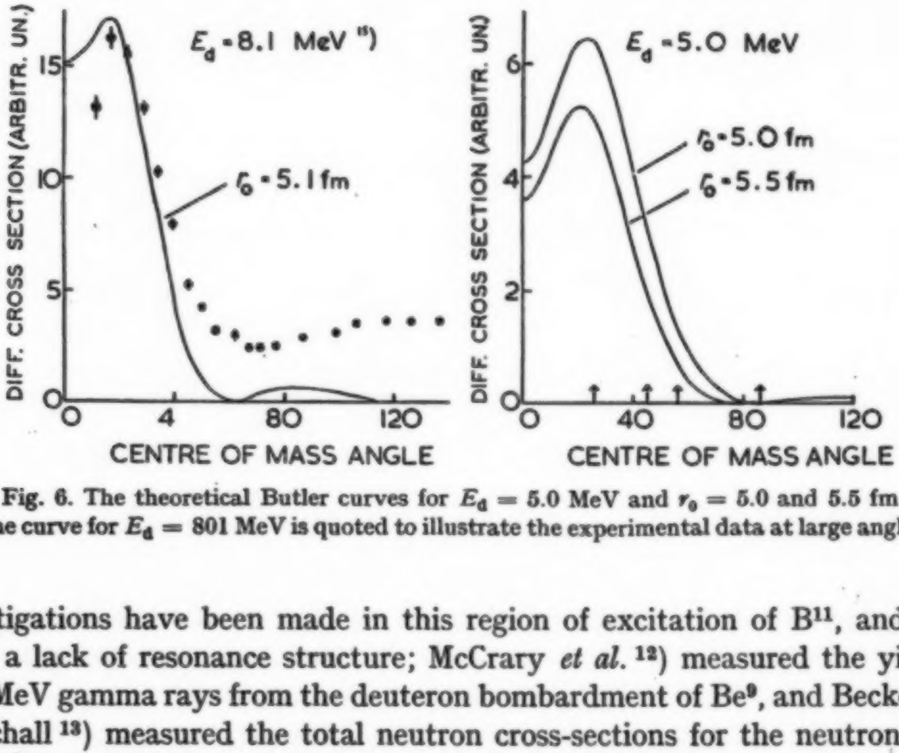

Fig. 6. The theoretical Butler curves for $E_d = 5.0$ MeV and $r_0 = 5.0$ and 5.5 fm. The curve for $E_d = 801$ MeV is quoted to illustrate the experimental data at large angles.

The angular distributions for the p_0 and p_1 groups at $E_d = 5.86$ MeV have been fitted with the Butler formula, see fig. 5. For the p_0 group it is found that a reasonable fit is obtained with $l = 1$ (the orbital angular momentum of the stripped neutron), $r_0 = 6.0 \pm 0.5$ fm (the cut-off radius) and $\theta_0^2 = 0.09$ (the neutron reduced width expressed as a function of the Wigner sum rule limit); for the p_1 group $l = 1$, $r_0 = 6.0 \pm 0.5$ fm, $\theta_1^2 = 0.025$. Previously, (see Ajzenberg-Selove and Lauritsen [14]), values of r_0 from 4.5 fm to 5.7 fm, and values of θ_0^2 of 0.05 and 0.09, have been obtained for the p_0 group in the energy range 3.6 to 14.0

MeV. Our results are not inconsistent with these. For the p_1 group, values of r_0 from 4.2 to 5.1 fm, and values of θ_1^2 of 0.010 and 0.012, have been obtained in the same energy range. The value of r_0 which we obtain is somewhat higher than obtained previously, and this is no doubt due to our large errors caused by an oxygen contaminant in the target. Our main interest in measuring this angular distribution was to see the deviation from theoretical Butler formula in the region of the minimum. The angular distributions were measured at 5.86 MeV, rather than 5.0 MeV, because it was originally intended to make the angular correlation measurements at the higher energy. To give some idea of the positioning of the proton detector in the angular correlation measurements relative to the stripping peak, we show in fig. 6 the theoretical Butler curves for $E_d = 5.0$ MeV and $r_0 = 5.0$ and 5.5 fm. We also show in this figure the more accurate measurements of Zeidman and Fowler [15]) at 8.1 MeV, to illustrate the shape of the angular distribution at large angles.

5. Analysis of the Angular Correlation Measurements

The angular correlation measurements have been analysed to give the quantities e, e_2, e_4, ϕ_0, ϕ'_0 and f, which are the quantities defined by eqs. (1), (2) and (3), corrected for the finite solid angle of the gamma ray detector. The two most careful angular correlation measurements, numbers 3 and 5, show that P_4 terms must be used in the fitting. This angular correlation for θ_p near the stripping peak, has been measured previously at energies between 2.51 and 3.90 MeV by Cox and Williamson [1]), and at 7.78 MeV by Taylor [2]). At 7.78 MeV, $\phi_0 = 6°\pm 8°$, and $e_4 \approx 0$. At 3.90 and 3.50 MeV, $\phi_0 \approx 0°$; a close inspection of these results shows that e_4 is small and negative, as found in the present work (although the original analysis was made in terms of P_2 terms only). At 3.00 and 2.51 MeV, the correlation becomes rather different, which is presumably due to the increasing importance of the Coulomb interaction. Some preliminary measurements have also been reported off the stripping peak ($\theta_p = 50°$) at 5.5 MeV by Gorodetzky *et al.* [16]). These results are very similar to those of the present work at $\theta_p = 56°$ (although again the analysis was in terms of P_2 terms only).

The distorted wave theory for this reaction predicts that the coefficient $e_4 = 0$ (Huby *et al.* [6])), since the l value of the stripped neutron is 1. Although e_4 is not zero, we may make a first analysis of the correlations at the smaller proton angles by the neglecting the P_4 components and assuming that the reaction mechanism is purely stripping. We may then use the distorted wave theory, and writing the correlation function in terms of the incident channel spin, $\mathbf{S} = \mathbf{I}_A + \frac{1}{2}\boldsymbol{\sigma}_n$ (Satchler [17])), we obtain (using the notation and method of Huby *et al.* [6])),

$$\frac{4+2e(2\sin^2\phi_0-\cos^2\phi_0)-f(4+e)}{2+e(2\sin^2\phi_0-\cos^2\phi_0)+f(4+e)} \equiv A_2{}^0$$

$$= \left[1-\frac{3}{l(l+1)}\right]^{-1} \frac{\rho_{20}(l,l)(l0,l0|00)}{\rho_{00}(l,l)(l0,l0|20)} F_2(LLI_B{}'I_B) \tag{4}$$

$$\times[xF_2(llS_1I_B)+(1-x)F_2(llS_2I_B)] \equiv \tfrac{1}{4}-\tfrac{1}{2}x,$$

$$\frac{3ef}{(4+e)f-4-2e(2\sin^2\phi_0-\cos^2\phi_0)} = \lambda = \frac{2}{\left|\dfrac{B_{1,1}}{B_{1,-1}}\right| + \left|\dfrac{B_{1,-1}}{B_{1,1}}\right|}, \tag{5}$$

$$\arg\left(\frac{-B_{1,-1}}{B_{1,1}}\right) = 2\phi_0. \tag{6}$$

These equations are analogous to eqs. 6.4, 6.5 and 6.6 of ref. 6). The quantity x is the fractional contribution of channel spin $S_1 = 1$ and the matrix elements B_{lm} are amplitudes for the absorption of the neutron with quantum numbers (l, m). For the axis of quantisation **n** only $B_{1,1}$ and $B_{1,-1}$ are non-zero.

TABLE 2

Results of the distorted wave analysis

Corr. no.	1	2	3	4	8 2)
λ	1.5 ±0.7	1.7 ±0.8	1.4 ±0.5	0.5 ±0.2	1.1 ±0.4
x	0.31±0.10	0.31±0.10	0.24±0.09	−0.08±0.17	0.19±0.10
x (plane wave limit)	0.21±0.06	0.19±0.07	0.16±0.04	0.20±0.05	0.17±0.04

The results of these analyses are shown in table 2. The results of Taylor 2) at $E_d = 7.78$ MeV, $\theta_p = 23°$ are also included here, the value of f being obtained by a least squares analysis, in terms of $P_2(\cos\theta)$, of the measurements in the azimuthal plane. The number of parameters measured experimentally is equal to the number of free parameters in the distorted wave theory, and there are therefore no equations between the experimental parameters which can test the validity of the theory. However, there is one test in that $\lambda \leqq 1$ must necessarily obtain, the equality sign applying at the plane wave limit. We see that the results do not strongly support the distorted wave theory. The probability that $\lambda \leqq 1$ in correlations 1, 2 and 3 is approximately 20 %, and the probability that $x \geqq 0.2$ in correlation 4 is approximately 5 %. We include in table 2 the values of x obtained by assuming that the plane wave theory applies (i.e. ignoring the facts that $\phi_0 \neq 0, f \neq 1$); Cox and Williamson 1) obtained $x \approx 0.1$ with this assumption.

The mean value of x obtained by using the distorted wave theory is 0.22±

0.05. If one assumes pure L—S coupling and a configuration $^2P_{\frac{3}{2}}$ for Be^9 and either $^3P_2$ or $^1D_2$ for the 3.37 MeV Be^{10} level, one obtains $x = 0.1$ or 1.0 respectively. The values of x obtained therefore seems to show that the excited state configuration is mainly $^3P_2$. Pure j—j coupling, with $j = \frac{1}{2}$ or $\frac{3}{2}$, would give an isotropic correlation function.

If it is assumed that $l=1$ for the stripped neutron, then the P_4 terms cannot be due to the Coulomb interaction (since this is allowed for in the distorted wave theory), or to spin-orbit interactions [18]). Although it is most unlikely that there is any $l = 3$ capture, an attempt was made to fit the angular correlation in the reaction place with a mixture of $l = 1$ and 3, using the plane wave theory. The angular correlation then has the form

$$W(\theta = \tfrac{1}{2}\pi, \phi) \propto \sum_{ll'Sk} F_k(LLI_B'I_B)(-)^S|A(S)|^2 B_{l0}B^*_{l'0} \times (l0, l'0|k0)W(I_BI_Bll'; kS)P_k(\cos\phi), \quad (7)$$

where $|A(S)|^2$ is the proportional contribution of channel spin S, and the other notation is that of Huby *et al.* [6]). The matrix elements B_{lm} are the amplitudes for the absorption of the neutron with quantum numbers (l, m): with the axis of quantisation along the recoil axis, the only non-zero B_{lm} are the B_{l0}. Because the different channel spin contributions add incoherently, the coefficients of P_2 and P_4 (i.e. e_2 and e_4) are linear functions of x (where $|A(1)|^2 = x$, $|A(2)|^2 = 1-x$). Also e_2 and e_4 are quadratic functions of $B = B_{30}/B_{10}$. It is not possible to fit the experimental results by taking a value of x and allowing B to vary with θ_p. For example, at $\theta_p = 56°$, $e_4 = -0.42$ and $e_2 = +0.14$, but using formula (7) it may be shown that the minimum value of e_4 is -0.287, which occurs when $x = 0$, $B = +0.765$, and then $e_2 = -0.569$. Also on the stripping peak, at $\theta_p = 26°$, $e_4 = -0.183$, $e_2 = -0.246$, but this value of e_4 requires $B \geqq 0.29$, $e_2 \leqq -0.60$: this value B is unreasonably large. It is unlikely that the use of a distorted wave theory would improve the fit much, and it therefore seems that the P_4 components cannot be explained by an $l = 3$ component. The proton angular distributions can of course be fitted at these angles with an $l = 1$ and $l = 3$ mixture, since the $l = 3$ distribution has a broad maximum in the region of the $l = 1$ minimum.

It seems clear then that there is a noticeable compound nucleus contribution to the reaction, even on the forward stripping peak. The results (except for those at $\theta_p = 45°$, where the χ^2 fit is poor) seem to indicate that this contribution increases with increasing angle. At the largest angle, 86° the symmetry axis is far from the recoil direction, and is near the direction 90° which may be expected from a purely compound-nucleus reaction.

6. Conclusion

The $Be^9(d, p)Be^{10}$ reaction leading to the first excited state at 3.37 MeV appears to be typical of most stripping reactions, in that the proton angular distribution may be interpreted by straightforward stripping theories in the region of the forward peak, but not in the region of larger angles. Measurements of the p—γ angular correlations, however, show the presence of a compound nucleus contribution.

The authors are grateful for the help given by Miss Lucia Lagatta in the least-squares analysis. One of us (G. S.) wishes to thank Professor S. Devons for the opportunity to work in his laboratory, and one of us (F. H. R.) wishes to thank the Department of Scientific and Industrial Research for a Research Fellowship held during part of this work.

References

1) S. A. Cox and R. M. Williamson, Phys. Rev. **105** (1957) 1799
2) R. T. Taylor, Phys. Rev. **113** (1959) 1293
3) J. A. Kuehner, E. Almquist and D. A. Bromley, Phys. Rev. Letters **4** (1960) 132
4) K. W. Allen, B. Collinge, B. Hird, B. C. Maglic and P. R. Orman, Proc. Phys. Soc. A **69** (1956) 705
5) H. A. Hill and J. M. Blair, Phys. Rev. **111** (1958) 1142
6) R. Huby, M. V. Refai and G. R. Satchler, Nuclear Physics **9** (1958) 94
7) S. T. Butler, Proc. Roy. Soc. A **208** (1951) 559
8) G. R. Satchler, C.R. Congr. Intern. Physique Nucléaire Paris (1958) 101
9) I. A. D. Lewis and F. H. Wells, Millimicrosecond Pulse Techniques (Pergamon Press 1959, 2nd edition)
10) F. H. Read and J. M. Calvert, Proc. Phys. Soc. (to be published)
11) M. E. Rose, Phys. Rev. **91** (1953) 610
12) J. H. McCrary, T. W. Bonner and W. A. Ranken, Phys. Rev. **108** (1957) 392
13) R. L. Becker and H. H. Barschall, Phys. Rev. **102** (1956) 1384
14) F. Ajzenberg-Selove and T. Lauritsen, Nuclear Physics **11** (1959) 1
15) B. Zeidman and J. M. Fowler, Phys. Rev. **112** (1958) 2020
16) S. Gorodetzky, J. Samuel and A. Gallman, J. de Phys. et le Rad. **21** (1960) 349
17) G. R. Satchler, Proc. Phys. Soc. A **66** (1953) 1081
18) L. J. B. Goldfarb and R. C. Johnson, Nuclear Physics (1960) (to be published)

7.A

Nuclear Physics **23** (1961) 399—429; © *North-Holland Publishing Co., Amsterdam*

Not to be reproduced by photoprint or microfilm without written permission from the publisher

EQUIVALENCE THEOREMS AND RENORMALIZATION PROBLEM IN VECTOR FIELD THEORY

(THE YANG-MILLS FIELD WITH NON-VANISHING MASSES)

H. UMEZAWA †
Faculté des Sciences, Université d'Aix-Marseille, France
and
S. KAMEFUCHI ††
Imperial College, University of London, England

Received 27 October 1960

Abstract: Equivalence theorems are derived for the Yang-Mills field with non-vanishing masses and for the electrodynamics of vector fields. A general theory of the Stueckelberg formalism is also presented. On the basis of these theorems the renormalizability problem is discussed for the above cases. It is concluded that quite contrary to the case of a single real vector field, the theory is not renormalizable even when the source current of the field is strictly conserved. The origin of the non-renormalizability can always be traced back to the mass terms. Theorems are further generalized to the case of the intermediate vector particle theory of weak interactions.

1. Introduction

It is well-known that interactions are renormalizable if their coupling constants are dimensionless (interactions of the first kind), while those interactions which are of dimensions of some positive power of length (interactions of the second kind) are in general non-renormalizable [1]). We also know that there are some exceptions to the latter statement, for example, the vector interaction of a neutral vector field, though this is of the second kind, is renormalizable [2]). Thus, it may be interesting to ask under what conditions interactions of the second kind turn out to be renormalizable.

In the case of the neutral vector field the renormalizability is essentially due to the conservation law of the source current: indeed, when applying the Stueckelberg formalism, we can easily see that the interactions of the second kind come only from the so-called B-field, which, however, can completely be eliminated by means of a unitary transformation as a consequence of this conservation law.

However, there has recently been an interesting conjecture that a theory might be renormalizable even when the so-called partial conservation law holds true [3]). Here, the divergence of the current is not zero, but proportional, in most cases, to mass terms, and so it is reduced to the ordinary conservation law when these mass terms are dropped out.

---

† On leave from Department of Physics, University of Tokyo, Japan.

†† I. C. I. Research Fellow of University of London. On leave from Institute of Theoretical Physics, University of Nagoya, Japan.

In view of the importance of this statement, the problem of renormalizability has recently been re-examined by Salam and Kamefuchi [4]) concerning interactions of a single neutral vector field and they have found by using a kind of equivalence theorem that the existence of a conservation law is a necessary and sufficient condition for the renormalization to be possible. The aim of the present paper is to see whether the same statement can still be made also in the case of complex vector fields, by which we mean that two or more real vector fields participate in interactions in such a way that the complex field is not a trivial superposition of real fields.

One simple example of this kind is the interaction $ig\bar{\psi}\gamma_\mu(\boldsymbol{\tau}\cdot\mathbf{u}_\mu)\psi$, where ψ is a dublet spinor field, $\mathbf{u}_\mu$ a triplet vector field and $\boldsymbol{\tau}$ an iso-spin matrix. It is well-known that in contrast with the case of vector coupling of a neutral scalar field with ψ, the vector coupling of a charged scalar field ϕ with ψ, i.e., $ig\bar{\psi}\gamma_\mu(\tau_+\partial_\mu\phi)\psi+\text{c.c.}$ leads to some real physical effects. This means that the field ϕ cannot be eliminated by means of any unitary transformation. This makes us suppose that the B-field part of $\mathbf{u}_\mu$ cannot be eliminated either in the above mentioned interaction. In fact, we can easily check that there exists no gauge-invariance property, nor any conservation law in this case, even when the mass of the vector field is zero. Consequently, the B-field part leads to non-renormalizable divergences.

However, we know a very interesting example of an interaction of vector fields, in which gauge invariance (and so a conservation law) holds true. That is the interaction of the three real fields, first proposed by Yang and Mills [5]). If all the masses are zero, the whole theory is invariant under a group of gauge transformations (with the most general gauge functions) and this leads eventually to the renormalizability of the theory. However, we can further show that even when non-vanishing and equal masses are introduced, the theory still remains invariant under a sub-group of the above mentioned group and accordingly there exists a conservation law. We also know, on the other hand, that in the case of a neutral vector field with partial conservation laws, mass terms are the only agents which give rise to non-renormalizability [4]).

Thus, we may ask ourselves the following questions concerning the Yang-Mills field with non-vanishing masses:

(i) Are the interactions of the second kind of this field renormalizable, if the theory is gauge invariant, or if some conservation laws exist? [†]

(ii) What kind of role do the mass terms play in this case?

Since the interactions of the second kind always arise from the B-field parts only, the question (i) can also be asked as: can the B-field parts be completely eliminated under the above conditions?

[†] This problem has recently been discussed also by Komar and Salam [6]).

For this purpose, it is very convenient to make use of a kind of equivalence theorem, such as given for neutral vector fields [4]). Once such a theorem is established, we can immediately see from it the logical interconnection between gauge-invariance or conservation law, renormalizability and effects of mass terms. Thus, the main part of this paper will be devoted to the derivation of such theorems.

In section 2 we shall first state the various forms of the equivalence theorem for the Yang-Mills field. In this paper we shall take full advantage of the Stueckelberg formalism for vector fields, and so we shall develop in section 3 the most general formalism, which is applicable to any complicated interactions. In section 4, the equivalence theorems stated in section 2 will be proved on the basis of the Stueckelberg formalism and in section 6 these theorems are further generalized to the case of the Yang-Mills field interacting with other source fields. In the final section we shall discuss the renormalizability problem and further implications of our theorems.

2. Equivalence Theorems for the Yang-Mills Fields with Non-Vanishing Masses

We shall first state here the equivalence theorems which will be proved in section 4. Let us consider three real vector fields $u_\mu{}^{(1)}$, $u_\mu{}^{(2)}$ and $u_\mu{}^{(3)}$; $u_\mu{}^{(3)}$ describes a neutral field and $u_\mu{}^{(1)}$ and $u_\mu{}^{(2)}$, when combined, a complex vector field

$$u_\mu = \frac{u_\mu{}^{(1)} - i u_\mu{}^{(2)}}{\sqrt{2}}, \quad u_\mu{}^* = \frac{u_\mu{}^{(1)} + i u_\mu{}^{(2)}}{\sqrt{2}}. \tag{1}$$

We shall denote a set of $(u_\mu{}^{(1)}, u_\mu{}^{(2)}, u_\mu{}^{(3)})$ by a vector symbol $\mathbf{u}_\mu$ and regard it as a vector in "I-space". The symbol $\mathbf{u}_{\mu\nu}$ describes the following I-space vector

$$\mathbf{u}_{\mu\nu} = \partial_\mu \mathbf{u}_\nu - \partial_\nu \mathbf{u}_\mu . \tag{2}$$

Let us consider the system, the Lagrangian of which is given by

$$\begin{aligned}\mathscr{L} = -\tfrac{1}{4}(\mathbf{u}_{\mu\nu} \cdot \mathbf{u}_{\mu\nu}) - \tfrac{1}{2}\kappa^2 \sum_{i=1,2} u_\mu{}^{(i)} u_\mu{}^{(i)} - \tfrac{1}{2}\kappa'^2 u_\mu{}^{(3)} u_\mu{}^{(3)} \\ - \tfrac{1}{2} g(\mathbf{u}_{\mu\nu} \cdot \mathbf{u}_\mu \wedge \mathbf{u}_\nu) - \tfrac{1}{4} g^2 (\mathbf{u}_\mu \wedge \mathbf{u}_\nu \cdot \mathbf{u}_\mu \wedge \mathbf{u}_\nu).\end{aligned} \tag{3}$$

Here, κ and κ' are the masses of the complex and of the neutral field, respectively, and we assume for the moment, $\kappa' \neq 0$. $(\mathbf{A} \cdot \mathbf{B})$ and $(\mathbf{A} \wedge \mathbf{B})$ denote scalar and vector products, respectively. When we put $\kappa = \kappa' = 0$, we obtain the Yang-Mills triplet field [5]).

When the neutral vector field is to describe the photon $(\kappa' = 0,\ g = e)$, the corresponding Lagrangian is

$$\begin{aligned}\mathscr{L} = -\sum_{i=1,2} (\tfrac{1}{4} u_{\mu\nu}^{(i)} u_{\mu\nu}^{(i)} + \tfrac{1}{2}\kappa^2 u_\mu{}^{(i)} u_\mu{}^{(i)}) - \tfrac{1}{2} \partial_\nu A_\mu{}^{(3)} \partial_\nu A_\mu{}^{(3)} \\ - \tfrac{1}{2} e(\mathbf{u}_{\mu\nu} \cdot \mathbf{u}_\mu \wedge \mathbf{u}_\nu) - \tfrac{1}{4} e^2 (\mathbf{u}_\mu \wedge \mathbf{u}_\nu \cdot \mathbf{u}_\mu \wedge \mathbf{u}_\nu),\end{aligned} \tag{4}$$

where $u_\mu^{(3)}$ is put equal to $A_\mu^{(3)}$, the electromagnetic potential:

$$u_\mu^{(3)} = A_\mu^{(3)}, \tag{5}$$

which should satisfy the well-known Lorentz condition. The charged vector particle described by the above Lagrangian (4) has a magnetic moment of two Bohr magnetons [3, 7]).

We are now ready to state our equivalence theorems.

THEOREM (I)

When $\kappa' \neq 0$, the interaction Hamiltonian $\mathscr{H}(x)$ in the interaction representation, which is derived from the Lagrangian (3), is equivalent to the following one:

$$\begin{aligned}\mathscr{H}_1(x) = {} & \tfrac{1}{2}g(\mathbf{u}_{\mu\nu} \cdot \mathbf{A}_\mu \wedge \mathbf{A}_\nu) + \tfrac{1}{4}g^2(\mathbf{A}_\mu \wedge \mathbf{A}_\mu \cdot \mathbf{A}_\nu \wedge \mathbf{A}_\nu) \\ & - \tfrac{1}{2}\kappa^2 \sum_{i=1,2} [U_\mu^{(i)} U_\mu^{(i)} - w_\mu^{(i)} w_\mu^{(i)}] \\ & - \tfrac{1}{2}\kappa'^2 [U_\mu^{(3)} U_\mu^{(3)} - w_\mu^{(3)} w_\mu^{(3)}] + (\text{n.d.}),\end{aligned} \tag{6}$$

with

$$\mathbf{U}_\mu = \mathbf{A}_\mu + \partial_\mu \mathbf{b}, \tag{7}$$

$$\mathbf{w}_\mu = S(g, \mathbf{b})\mathbf{A}_\mu + f(g, \mathbf{b})\partial_\mu \mathbf{b} \tag{8}$$

$$= S(g, \mathbf{b})[\mathbf{A}_\mu + f(-g, \mathbf{b})\partial_\mu \mathbf{b}]. \tag{9}$$

Here, **b** is the I-vector, whose components are $(1/\kappa)B^{(1)}$, $(1/\kappa)B^{(2)}$ and $(1/\kappa')B^{(3)}$. Introducing an operator $\alpha(\mathbf{b})$ which is defined by

$$\alpha(\mathbf{b})\mathbf{a} = \mathbf{a} \wedge \mathbf{b}, \tag{10}$$

we define $S(g, \mathbf{b})$ and $f(g, \mathbf{b})$ as follows:

$$S(g, \mathbf{b}) = 1 + g\alpha(\mathbf{b}) + \frac{g^2}{2!}\alpha^2(\mathbf{b}) + \ldots = \exp[g\alpha(\mathbf{b})], \tag{11}$$

$$\left.\begin{aligned} f(g, \mathbf{b}) &= 1 + \frac{g}{2!}\alpha(\mathbf{b}) + \frac{g^2}{3!}\alpha^2(\mathbf{b}) + \ldots \\ &= \frac{1}{g}\int_0^g \mathrm{d}\rho S(\rho, \mathbf{b}) = \frac{\exp[g\alpha(\mathbf{b})] - 1}{g\alpha(\mathbf{b})}. \end{aligned}\right\} \tag{12}$$

For example,

$$S(g, \mathbf{b})\mathbf{a} = \mathbf{a} + g\mathbf{a} \wedge \mathbf{b} + \frac{g^2}{2!}(\mathbf{a} \wedge \mathbf{b}) \wedge \mathbf{b} + \ldots..$$

In terms of the "spin 1-matrix" **T**, which satisfies the commutation relations $[T^{(i)}, T^{(j)}] = i\varepsilon^{ijk}T^{(k)}$, $\alpha(\mathbf{b})$ can be written as $\alpha(\mathbf{b}) = i(\mathbf{b} \cdot \mathbf{T})$. We can also see that the operators S and f act on an I-vector $\mathbf{a}$ as follows:

$$S(g, \mathbf{b})\mathbf{a} = \frac{g}{x} \sin x(\mathbf{a} \wedge \mathbf{b}) - \frac{g^2}{x^2} (\cos x - 1)(\mathbf{b} \cdot \mathbf{a})\mathbf{b} + \mathbf{a} \cos x,$$

$$f(g, \mathbf{b})\mathbf{a} = -\frac{g}{x^2} (\cos x - 1)(\mathbf{a} \wedge \mathbf{b}) - \frac{g^2}{x^2} \left(\frac{1}{x} \sin x - 1\right) (\mathbf{b} \cdot \mathbf{a})\mathbf{b} + \frac{1}{x} \mathbf{a} \sin x,$$

with $x = g\sqrt{(\mathbf{b} \cdot \mathbf{b})}$.

In deriving (9) from (8), use is made of the relation

$$S(\rho, \mathbf{b})f(-\rho, \mathbf{b}) = f(\rho, \mathbf{b}), \tag{13}$$

which follows directly from (11) and (12).

The A_μ's and B's are vector and scalar fields, which satisfy the following relations:

$$\begin{aligned} &[A_\mu^{(i)}(x), A_\nu^{(j)}(x')] = i\delta_{ij}\delta_{\mu\nu}\Delta(x-x'; \kappa) \quad \text{for} \quad i, j = 1, 2, \\ &[A_\mu^{(3)}(x), A_\nu^{(3)}(x')] = i\delta_{\mu\nu}\Delta(x-x'; \kappa'), \end{aligned} \tag{14}$$

$$\begin{aligned} &[B^{(i)}(x), B^{(j)}(x')] = i\delta_{ij}\Delta(x-x'; \kappa) \quad \text{for} \quad i, j = 1, 2, \\ &[B^{(3)}(x), B^{(3)}(x')] = i\Delta(x-x'; \kappa'), \end{aligned} \tag{15}$$

and

$$\begin{aligned} &(\partial_\mu A_\mu^{(i)}(x) + \kappa\, B^{(i)}(x))\Psi_1[\sigma] = 0 \quad \text{for} \quad i = 1, 2, \\ &(\partial_\mu A_\mu^{(3)}(x) + \kappa' B^{(3)}(x))\Psi_1[\sigma] = 0 \quad \text{for} \quad x/\sigma. \end{aligned} \tag{16}$$

Here, $\Psi_1[\sigma]$ is a state vector in the interaction representation under consideration, and $\Delta(x; \kappa)$ the ordinary delta function for the mass κ. The symbol x/σ means that the point x lies on the space-like surface σ. The notation (n.d.) in (6) denotes the well-known "normal dependent term", which depends on a unit normal vector n_μ of the space-like surface σ. n_μ is normalized by $n_\mu n_\mu = 1$.

It has been well-known that (n.d.) can simply be dropped out when similar terms are also simultaneously dropped out from all internal lines in Feynman diagrams. Since these terms do not give any contributions to observable quantities, say S-matrix, we shall not, in the following, make any explicit calculation of them.

To be more precise, let the propagation function for a field quantity $\varphi_\alpha(x)$ be of the form $d_{\alpha\beta}(\partial)\Delta_F(x-x')$ ($d_{\alpha\beta}(\partial)$ is a differential operator). Then any P-bracket, which corresponds to an internal line of a Feynman diagram, will take the form

$$\begin{aligned} \langle \mathrm{P}[F(\partial)\varphi_\alpha(x), G(\partial')\varphi_\beta(x')]\rangle_0 &= F(\partial)G(\partial')d_{\alpha\beta}(\partial)\Delta^{(1)}(x-x') + i\varepsilon(x-x')F(\partial)G(\partial')d_{\alpha\beta}(\partial)\Delta(x-x') \\ &= \langle \mathrm{P}^*[F(\partial)\varphi_\alpha(x), G(\partial')\varphi_\beta(x')]\rangle_0 - i[F(\partial)G(\partial')d_{\alpha\beta}(\partial), \varepsilon(x-x')]\Delta(x-x'), \end{aligned} \tag{17}$$

with the P*-bracket defined by

$$\langle \mathrm{P}^*[F(\partial)\varphi_\alpha(x), G(\partial')\varphi_\beta(x')]\rangle_0 = F(\partial)G(\partial')d_{\alpha\beta}(\partial)\Delta_F(x-x'). \tag{17'}$$

Here, $F(\partial)$ and $G(\partial')$ are differential operators acting on $\varphi_\alpha(x)$ and $\varphi_\beta(x')$ in the interaction Hamiltonian. The last term in (17) leads to normal dependent terms, for we have, in general, the formula

$$K(x)n_\mu n_\nu = -\tfrac{1}{2}\int d^4x' K(x')[\partial_\mu \partial_\nu, \varepsilon(x-x')]\Delta(x-x'), \tag{18}$$

with $K(x)$ an arbitrary function. Now, it can generally be proved that these normal dependent terms are cancelled out by those terms due to the (n. d.) terms in the interaction Hamiltonian. Therefore we can always drop all (n.d.) terms in the interaction Hamiltonian when we understand that any internal line is replaced not by the P-bracket, but by the P*-bracket as defined above.

In this connection we should add an important remark which is essential in the following argument: When the differential operators (e.g. $F(\partial)$) in the interaction Hamiltonian or $d_{\alpha\beta}(\partial)$ in the propagation function contain the operator $\partial_\mu^2 \equiv \Box$, then (18) gives a normal independent term $K(x)n_\mu n_\nu = -K(x)$. In such a case, we must take special care in carrying through the above procedure: We must drop, in the interaction Hamiltonian, not only those terms which explicitly depend on n_μ, but also part of terms which do not involve n_μ at all. However, this does not take place in the present case (for details see ref. [8])).

The interaction (7) shows that the B-field appears only in the two square brackets and also that only the term $w_\mu^{(i)} w_\mu^{(i)}$ $(i = 1, 2, 3)$ contains non-renormalizable interactions.

To prove the theorem (I) we shall perform a unitary transformation $G[\sigma]$ which transforms the original Schrödinger equation

$$\left(i\frac{\delta}{\delta\sigma(x)} - \mathscr{H}(x)\right)\Psi[\sigma] = 0,$$

with $\mathscr{H}(x)$ derived from the Lagrangian (3), into $(i\delta/\delta\sigma(x) - \mathscr{H}_1(x))\Psi_1[\sigma] = 0$, where the two state vectors are connected by

$$\Psi_1[\sigma] = G^{-1}[\sigma]\Psi[\sigma]. \tag{19}$$

In section 4 we shall further prove the relation

$$w_\mu^{(i)} = G^{-1}[\sigma]U_\mu^{(i)}G[\sigma] + (\text{n.d.}) \quad (i = 1, 2, 3). \tag{20}$$

When using this relation, we can state the above theorem in the following way.

THEOREM (I′)

The interaction Hamiltonian (6) can be written in the form

$$\begin{aligned} \mathscr{H}_1(x) = {} & \tfrac{1}{2}g(\mathbf{u}_{\mu\nu} \cdot \mathbf{A}_\mu \wedge \mathbf{A}_\nu) + \tfrac{1}{4}g^2(\mathbf{A}_\mu \wedge \mathbf{A}_\nu \cdot \mathbf{A}_\mu \wedge \mathbf{A}_\nu) \\ & - \tfrac{1}{2}\kappa^2 \sum_{i=1,2} [U_\mu^{(i)}U_\nu^{(i)} - G^{-1}[\sigma]U_\mu^{(i)}U_\mu^{(i)}G[\sigma]] \\ & - \tfrac{1}{2}\kappa'^2[U_\mu^{(3)}U_\mu^{(3)} - G^{-1}[\sigma]U_\mu^{(3)}U_\mu^{(3)}G[\sigma]] + (\text{n.d.}). \end{aligned} \tag{21}$$

The above theorem clearly indicates that the non-renormalizable terms arise only from the mass terms transformed by $G[\sigma]$.

Next, we shall consider the electromagnetic interaction of a charged vector field (i.e., $\kappa' = 0$, $g = e$). In this case, the third component of $\mathbf{A}_\mu$ describes the photon field and so we have

$$\Box A_\mu^{(3)} = 0, \quad [A_\mu^{(3)}(x), A_\nu^{(3)}(x')] = i\delta_{\mu\nu}D(x-x'), \tag{22}$$

and instead of (16),

$$\partial_\mu A_\mu^{(3)}(x)\Psi_1[\sigma] = 0, \quad \text{for} \quad x/\sigma, \tag{23}$$

where D is the Δ-function for a massless field. No $B^{(3)}$ field appears in this case. The fields $A_\mu^{(i)}$, $B^{(i)}$ $(i = 1, 2)$ satisfy the same relations as (14), (15) and (16). Our theorem in this case reads as follows:

THEOREM (II)

The electromagnetic interaction described by the Lagrangian (4) is equivalent to the following interaction Hamiltonian

$$\begin{aligned}\mathscr{H}_2(x) &= \tfrac{1}{2}e(\mathbf{u}_{\mu\nu}\cdot\mathbf{A}_\mu\wedge\mathbf{A}_\nu)+\tfrac{1}{4}e^2(\mathbf{A}_\mu\wedge\mathbf{A}_\nu\cdot\mathbf{A}_\mu\wedge\mathbf{A}_\nu)\\ &\quad-\tfrac{1}{2}\kappa^2\sum_{i=1,2}[U_\mu^{(i)}U_\mu^{(i)}-w_\mu^{(i)}w_\mu^{(i)}]+(\text{n.d.}),\end{aligned}\tag{24}$$

with $w_\mu^{(i)}$ defined by (8) or (9). Here, the third component of $\mathbf{b}$ is taken to be zero (cf. (7), (8), (9)): $b^{(i)} = (1/\kappa)B^{(i)}$ for $i = 1, 2$, and $b^{(3)} = 0$. In this case, too, the b-field of charged vector particles contributes only to the last square bracket and eventually leads to non-renormalizable interactions.

By using the relation (20), we can give an alternative form of this theorem:

THEOREM (II′)

The interaction Hamiltonian (24) can also be written as

$$\begin{aligned}\mathscr{H}_2(x) &= \tfrac{1}{2}e(\mathbf{u}_{\mu\nu}\cdot\mathbf{A}_\mu\wedge\mathbf{A}_\nu)+\tfrac{1}{4}e^2(\mathbf{A}_\mu\wedge\mathbf{A}_\nu\cdot\mathbf{A}_\mu\wedge\mathbf{A}_\nu)\\ &\quad-\tfrac{1}{2}\kappa^2\sum_{i=1,2}[U_\mu^{(i)}U_\mu^{(i)}-G^{-1}[\sigma]U_\mu^{(i)}U_\mu^{(i)}G[\sigma]]+(\text{n.d.}).\end{aligned}\tag{25}$$

We shall postpone the detailed proofs for these theorems until section 4.

Let us close this section by collecting some formulae for $S(\rho, \mathbf{b})$ and $f(\rho, \mathbf{b})$, which we shall frequently use in the following sections:

$$\begin{aligned}&(S(\rho)\mathbf{a}\cdot\mathbf{c}) = (\mathbf{a}\cdot S(-\rho)\mathbf{c}), \quad (f(\rho)\mathbf{a}\cdot\mathbf{c}) = (\mathbf{a}\cdot f(-\rho)\mathbf{c}), \quad S(\rho)S(-\rho) = 1,\\ &(\rho f(\rho)\mathbf{a})\wedge\mathbf{b} = (S(\rho)-1)\mathbf{a}, \quad (S(\rho)\mathbf{a})\cdot(S(\rho)\mathbf{c}) = (\mathbf{a}\cdot\mathbf{c}),\\ &S(\rho)(\mathbf{a}\wedge\mathbf{c}) = (S(\rho)\mathbf{a})\wedge(S(\rho)\mathbf{c}),\\ &\partial_\mu(S(\rho)\mathbf{a}) = -\rho S(\rho)[(f(-\rho)\partial_\mu\mathbf{b})\wedge\mathbf{a}]+S(\rho)\partial_\mu\mathbf{a},\\ &\partial_\mu(f(\rho)\partial_\nu\mathbf{b})-\partial_\nu(f(\rho)\partial_\mu\mathbf{b}) = -\rho(f(\rho)\partial_\mu\mathbf{b})\wedge(f(\rho)\partial_\nu\mathbf{b}).\end{aligned}\tag{26}$$

Here, $\mathbf{a}$ and $\mathbf{c}$ stand for arbitrary I-vectors commutable with $\mathbf{b}$ and $S(\rho)$ and $f(\rho)$ stand for $S(\rho, \mathbf{b})$ and $f(\rho, \mathbf{b})$, respectively. These formulae can be derived directly from the defining equations (11) and (12). From (26) we see that $S(\rho)$ plays the role of a rotation operator in I-space. For future use, we shall introduce two I-vectors γ_μ defined by

$$(S(\rho)-1)\gamma_\mu(\rho,\mathbf{b}) = (f(\rho)-1)\partial_\mu\mathbf{b}. \tag{27}$$

The solution of this equation is

$$\gamma_\mu(\rho) = \tfrac{1}{2}[\partial_\mu\mathbf{b}\pm\rho\zeta(\mathbf{b})(\partial_\mu\mathbf{b}\wedge\mathbf{b})], \tag{27'}$$

where $\zeta(\mathbf{b})$, a function of $\rho^2(\mathbf{b}\cdot\mathbf{b})$, is defined by[†]

$$\zeta(\mathbf{b}) = -\frac{2}{x^2}-\frac{1}{x}\frac{\sin x}{\cos x-1} = -\tfrac{1}{6}-\frac{\rho^2}{360}(\mathbf{b}\cdot\mathbf{b})-\ldots,$$

with $x\equiv\rho\sqrt{\mathbf{b}\cdot\mathbf{b}}$. It must be noted that ζ, as a function of x, makes sense only when it is regarded as a power series in x^2.

From (27') follows the following relation

$$\partial_\mu\mathbf{b}-\gamma_\mu(\rho,\mathbf{b}) = \gamma_\mu(-\rho,\mathbf{b}). \tag{28}$$

3. The Stueckelberg Formalism

Although the Stueckelberg formalism of vector fields [9]) has sometimes been applied to the simple case of a single neutral vector field, in which the interaction contains the vector variable in linear or quadratic forms, it seems to us that nobody has so far tried to extend this formalism to more general cases, in which some vector variables enter the interaction in a more complicated way (e.g. the electromagnetic interaction). Since for our present purpose it is most convenient to make use of this formalism, we shall first of all develop the general formalism of this theory, thereby making clear its connection with the ordinary vector field formalism.

To start with let us consider a real vector field u_μ with the Lagrangian

$$\mathscr{L} = -\tfrac{1}{4}u_{\mu\nu}u_{\mu\nu}-\tfrac{1}{2}\kappa^2u_\mu u_\mu+\mathscr{L}'(u_\mu,\varphi), \tag{29}$$

where $u_{\mu\nu} = \partial_\mu u_\nu-\partial_\nu u_\mu$ and $\mathscr{L}'$ is the interaction of this field with another field φ. It is almost evident that we cannot connect the Stueckelberg formalism with the above (ordinary) theory by a unitary transformation, because u_μ has only three independent components, whereas the Stueckelberg formalism has five. We shall therefore introduce two auxiliary scalar fields B and C in the following way:

$$\begin{aligned}\mathscr{L}_1 = &-\tfrac{1}{4}u_{\mu\nu}u_{\mu\nu}-\tfrac{1}{2}\kappa^2u_\mu u_\mu-\tfrac{1}{2}\partial_\mu B\partial_\mu B-\tfrac{1}{2}\kappa^2BB\\ &+\tfrac{1}{2}\partial_\mu C\partial_\mu C+\tfrac{1}{2}\kappa^2CC+\mathscr{L}'(U_\mu,\varphi),\end{aligned} \tag{30}$$

[†] We can add to $\gamma_\mu(\rho,\mathbf{b})$ any term of the form $g(\mathbf{b})\mathbf{b}$ with $g(\mathbf{b})$ a function of $(\mathbf{b}\cdot\mathbf{b})$. Here, for simplicity, we have not added such a term.

where U_μ is defined by

$$U_\mu = u_\mu + \frac{1}{\kappa}(\partial_\mu B - \partial_\mu C). \tag{31}$$

(30) shows that the C-field carries negative energies, for C is a real field. Indeed, (30) leads to the following canonical commutation relations:

$$\begin{aligned} [B(\mathbf{x}, t), \dot{B}(\mathbf{x}', t)] &= i\delta^3(\mathbf{x}-\mathbf{x}'), \\ [C(\mathbf{x}, t), \dot{C}(\mathbf{x}', t)] &= -i\delta^3(\mathbf{x}-\mathbf{x}'), \end{aligned} \tag{32}$$

where $\dot{B}$ and $\dot{C}$ means $\partial B/\partial t$ and $\partial C/\partial t$, respectively. The signs of the right hand side are related to those of energies carried by the B and C fields.

Although B and C interact with each other, and also with u_μ, (30) shows that $(B-C)$ is free from interaction,

$$(\Box - \kappa^2)F = 0, \tag{33}$$

where

$$F \equiv B - C. \tag{34}$$

Thus, we can always separate F into its positive and negative frequency parts $F^\pm$. Let us now introduce a subsidiary condition in the Heisenberg representation,

$$F\Psi = 0, \tag{35}$$

which leads to

$$F^\pm\Psi = 0. \tag{35'}$$

By virtue of (33), (35) is always satisfied if (35) and $\partial F/\partial t\Psi = 0$ are satisfied at a given time t_0. In this way we can see that (35) is consistent with the field equations.

It is to be noticed here that B and C play the similar role to longitudinal and scalar photons which appear in connection with the Lorentz condition in quantum electrodynamics. Following Ma's argument 10) for the Lorentz condition, we can show that (35) leads to

$$\Psi = C\Psi' \prod_i \Psi(n_i, n_i), \tag{36}$$

where $\Psi(n_i n_i)$ is a normalised state vector, in which the occupation numbers of B and C particles with momentum $\mathbf{k}^i$ are both n_i and Ψ' is a normalised state vector for particles other than B and C. When putting our system in a box, we have a discrete spectrum of momenta $\mathbf{k}^1, \mathbf{k}^2, \ldots$, and the product in (36) is to be taken over all possible momentum states. Since B and C particles carry positive and negative energies, respectively, their effects cancel out in the state (36) and as a result, no negative energy states appear in observations. This discussion has some defects, however; namely that (36), having infinite norm, does not belong to an ordinary Hilbert space and also that the subsidiary condition contradicts the commutation relations. Such difficulties are exactly of the same nature as those in the Lorentz condition. To settle these difficulties, therefore, we have only to follow the Gupta-Bleuler 11) method. Since there is no danger in applying (35) to practical calculations, we shall make use of (35) throughout the following argument.

As F is a free field, it commutes with the transformation function $S[\sigma]$ connecting the Heisenberg and the interaction representations

$$S^{-1}[\sigma]F(x)S[\sigma] = F(x) \quad \text{for} \quad x/\sigma.$$

This, together with (35) leads, in the interaction representation, to

$$F(x)\Psi[\sigma]=0, \tag{37}$$

where $\Psi[\sigma]=S^{-1}[\sigma]\Psi$. (37) is the subsidiary condition in the interaction representation.

Since the interaction Lagrangian depends on B and C only through the combinations F, so does the interaction Hamiltonian in the interaction representation. In other words, the Schrödinger equation in the interaction representation must have the following form:

$$i\frac{\delta}{\delta\sigma(x)}\Psi[\sigma]=\mathscr{H}\left(u_\mu(x)+\frac{i}{\kappa}\,\partial_\mu F(x),\varphi\right)\Psi[\sigma], \tag{38}$$

where x/σ. Since u_μ and F commute with each other, (37) means that we can simply drop F in (38) and so

$$i\frac{\delta}{\delta\sigma(x)}\Psi[\sigma]=\mathscr{H}(u_\mu(x),\varphi)\Psi[\sigma], \tag{39}$$

which is exactly the Schrödinger equation in the interaction representation for the Lagrangian (29). We thus see that under the condition (35), two Lagrangians (29) and (30) describe the same physical system.

Since the Lagrangian (30) contains five sets of canonical variables, there may be a possibility of deriving the Stueckelberg formalism from (30) by means of a unitary transformation. This can actually be done by writing u_μ as follows:

$$u_\mu=A_\mu+\frac{1}{\kappa}\,\partial_\mu C, \tag{40}$$

thus we have

$$U_\mu=A_\mu+\frac{1}{\kappa}\,\partial_\mu B. \tag{41}$$

Substituting (40) into (30) and making a partial integration, we obtain

$$\int d^4x\mathscr{L}_1(x)=\int d^4x[-\tfrac{1}{2}\partial_\mu A_\nu\partial_\mu A_\nu-\tfrac{1}{2}\kappa^2A_\mu A_\mu-\tfrac{1}{2}\partial_\mu B\partial_\mu B-\tfrac{1}{2}\kappa^2BB$$
$$-\tfrac{1}{2}DD+\mathscr{L}'(U_\mu,\varphi)], \tag{42}$$

with

$$D=\partial_\mu A_\mu+\kappa C. \tag{43}$$

Making a variation of (42) with respect to C, we find that

$$D=0, \tag{44}$$

which enables us to rewrite the subsidiary condition (35) in the Heisenberg representation as follows:

$$(\partial_\mu A_\mu+\kappa B)\Psi=0. \tag{45}$$

In the interaction representation, the subsidiary condition (37) is brought into the form

$$(\partial_\mu A_\mu(x)+\kappa B(x))\Psi[\sigma] = 0 \quad \text{for} \quad x/\sigma. \tag{46}$$

Note here that $\partial_\mu U_\mu = \partial_\mu A_\mu + \kappa B$ in the interaction representation †. We can thus conclude that the Lagrangian (29) for the vector field u_μ is equivalent to the following Lagrangian:

$$\mathscr{L}_{\mathrm{S}} = -\tfrac{1}{2}\partial_\mu A_\nu \partial_\mu A_\nu - \frac{\kappa^2}{2} A_\mu A_\mu - \tfrac{1}{2}\partial_\mu B \partial_\mu B - \frac{\kappa^2}{2} BB + \mathscr{L}'(U_\mu, \varphi) \tag{47}$$

under the condition (45).

Let us now apply this formalism to the Lagrangian (3) for our triplet field $u_\mu^{(i)} (i = 1, 2, 3)$. The Lagrangian $\mathscr{L}_{\mathrm{S}}$ in this case is

$$\mathscr{L}_{\mathrm{S}} = \mathscr{L}_0 + \mathscr{L}' \tag{48}$$

where

$$\mathscr{L}_0 = -\tfrac{1}{2}(\partial_\mu \mathbf{A}_\nu \cdot \partial_\mu \mathbf{A}_\nu) - \tfrac{1}{2}\kappa^2(\mathbf{A}_\mu \cdot \mathbf{A}_\mu) - \tfrac{1}{2}(\partial_\mu \mathbf{B} \cdot \partial_\mu \mathbf{B}) - \tfrac{1}{2}\kappa^2(\mathbf{B} \cdot \mathbf{B}), \tag{49}$$

$$\mathscr{L}' = \tfrac{1}{2}(\kappa^2 - \kappa'^2) U_\mu^{(3)} U_\mu^{(3)} - \tfrac{1}{2} g(\mathbf{u}_{\mu\nu} \cdot \mathbf{U}_\mu \wedge \mathbf{U}_\nu) - \tfrac{1}{4} g^2(\mathbf{U}_\mu \wedge \mathbf{U}_\nu \cdot \mathbf{U}_\mu \wedge \mathbf{U}_\nu), \tag{50}$$

with

$$\mathbf{U}_\mu = \mathbf{A}_\mu + \frac{1}{\kappa}\partial_\mu \mathbf{B}, \quad \mathbf{u}_{\mu\nu} = \partial_\mu \mathbf{A}_\nu - \partial_\nu \mathbf{A}_\mu. \tag{51}$$

It must be noted here that when writing $\kappa'^2 u_\mu^{(3)} u_\mu^{(3)}$ as $\kappa^2 u_\mu^{(3)} u_\mu^{(3)} - (\kappa^2 - \kappa'^2) \times u_\mu^{(3)} u_\mu^{(3)}$, we regard the mass difference term not as a part of the free Lagrangian $\mathscr{L}_0$, but as a part of the interaction Lagrangian $\mathscr{L}'$.

Let us consider a special case $\kappa = \kappa'$. In this case the Lagrangian (3) leads to the conservation law of the current $\mathbf{J}_\mu$,

$$\partial_\mu \mathbf{J}_\mu = 0, \tag{52}$$

where $\mathbf{J}_\mu$ is defined by

$$\partial_\mu \mathbf{u}_{\mu\nu} - \kappa^2 \mathbf{u}_\nu = -\mathbf{J}_\nu. \tag{53}$$

This is due to the rotation symmetry in the I-space. If $\kappa = \kappa' = 0$, then the theory is invariant under the group of the most general gauge transformations with arbitrary gauge functions $\boldsymbol{\Lambda}$ (see section 5 below). However, in the case of non-vanishing mass $\kappa = \kappa' \neq 0$, the Lagrangian (3) is invariant only under a sub-group of transformations with some restricted gauge functions ††. Still, this is enough to lead us to the conservation law (52).

---

† We further note that in the interaction representation we have $[\partial_\mu U_\mu(x), U_\nu(x')] = 0$, where x and x' are not necessarily of space like separation.

†† Under the infinitesimal gauge transformations $\mathbf{u}_\mu \rightarrow \mathbf{u}_\mu + g\mathbf{u}_\mu \wedge \boldsymbol{\Lambda} + \partial\boldsymbol{\Lambda}/\partial x_\mu$ with $\boldsymbol{\Lambda}$ being infinitesimal, the Lagrangian (3) for $\kappa = \kappa' = 0$ is invariant for any function $\boldsymbol{\Lambda}$. However, the Lagrangian for $\kappa = \kappa' \neq 0$ is invariant only for $\boldsymbol{\Lambda}$ which fulfils the condition $\partial\boldsymbol{\Lambda}/\partial x_\mu \cdot \mathbf{u}_\mu = 0$.

In the Stueckelberg formalism, we define the current by

$$(\Box-\kappa^2)\mathbf{A}_\mu = -\mathbf{J}_\mu^{(S)}. \tag{54}$$

From (49) and (50) follows the relation

$$\partial_\mu \mathbf{J}_\mu^{(S)} = g\mathbf{U}_\nu \wedge \partial_\nu(\partial_\mu \mathbf{A}_\mu + \kappa\mathbf{B}). \tag{55}$$

Thus, the conservation law holds true only when (55) operates on a state vector, satisfying (45):

$$\partial_\mu \mathbf{J}_\mu^{(S)} \Psi = 0. \tag{56}$$

When $\kappa' \neq \kappa$, the conservation law is evidently violated by the mass difference term. In the case of $\kappa' = 0$, the Lagrangians (4) and (47) give

$$\left.\begin{aligned} \mathscr{L}_S &= \mathscr{L}_0 + \mathscr{L}'', \\ \mathscr{L}'' &= \tfrac{1}{2}\kappa^2 A_\mu^{(3)} A_\mu^{(3)} - \tfrac{1}{2}e(\mathbf{u}_{\mu\nu} \cdot \mathbf{U}_\mu \wedge \mathbf{U}_\nu) - \tfrac{1}{4}e^2(\mathbf{U}_\mu \wedge \mathbf{U}_\nu \cdot \mathbf{U}_\mu \wedge \mathbf{U}_\nu), \end{aligned}\right\} \tag{57}$$

where $B^{(3)} = 0$, i.e., $U_\mu^{(3)} = A_\mu^{(3)}$ (cf. (5)) and $\mathscr{L}_0$ is given by (49).

4. Derivation of Equivalence Theorems

In this section we shall prove the equivalence theorems given in section 2. To begin with let us consider the simplest case $\kappa = \kappa'$, in which the conservation law (52) holds true. The Lagrangian in the Stueckelberg formalism can be obtained by taking $\kappa = \kappa'$ in (49) and (50). The interaction Hamiltonian density in the interaction representation can be derived in the conventional way as follows:

$$\begin{aligned} \mathscr{H} &= \tfrac{1}{2}g(\mathbf{u}_{\mu\nu} \cdot \mathbf{U}_\mu \wedge \mathbf{U}_\nu) + \tfrac{1}{4}g^2(\mathbf{U}_\mu \wedge \mathbf{U}_\nu \cdot \mathbf{U}_\mu \wedge \mathbf{U}_\nu) \\ &\quad + \tfrac{1}{2}g^2\left[(\mathbf{U}_\mu \wedge \mathbf{U}_\nu \cdot \mathbf{U}_\rho \wedge \mathbf{U}_\nu) + \frac{1}{\kappa^2}(\mathbf{u}_{\nu\rho} \wedge \mathbf{U}_\nu \cdot \mathbf{u}_{\sigma\mu} \wedge \mathbf{U}_\sigma)\right] n_\mu n_\rho, \end{aligned} \tag{58}$$

where the last term is the (n.d.) term and $\mathbf{U}_\mu$ and $\mathbf{u}_{\mu\nu}$ are defined by (51) in terms of $\mathbf{A}_\mu$ and $\mathbf{B}$, which satisfy the relations

$$(\Box-\kappa^2)\mathbf{A}_\mu = 0, \quad (\Box-\kappa^2)\mathbf{B} = 0, \tag{59}$$

$$(\partial_\mu \mathbf{A}_\mu(x) + \kappa\mathbf{B}(x))\Psi[\sigma] = 0 \quad \text{for} \quad x/\sigma, \tag{60}$$

$$\begin{aligned} [A_\mu^{(i)}(x), A_\nu^{(j)}(x')] &= i\delta_{ij}\delta_{\mu\nu}\Delta(x-x';\kappa), \\ [B^{(i)}(x), B^{(j)}(x')] &= i\delta_{ij}\Delta(x-x';\kappa) \qquad (i, j = 1, 2, 3). \end{aligned} \tag{61}$$

Let us now introduce a unitary transformation

$$\Psi[\sigma] \to \Psi_1[\sigma] = G^{-1}[g, \sigma]\Psi[\sigma], \tag{62}$$

with G defined by

$$G[\rho, \sigma] = \exp [\rho N[\sigma]), \tag{63}$$

$$N[\sigma] = \frac{i}{\kappa} \int_{\sigma} \mathrm{d}\sigma_{\mu}(\mathbf{B} \cdot \mathbf{G}_{\mu}). \tag{64}$$

Here ρ is a c-number parameter and taken to be g in the transformation (62). The integration in (64) is taken over a space like surface σ and when σ is a flat surface, $N[\sigma] = 1/\kappa \int \mathrm{d}^3x(\mathbf{B} \cdot \mathbf{G}_4)$. The operator G_{μ} is defined by

$$\mathbf{G}_{\mu} = -(\mathbf{u}_{\nu\mu} \wedge \bar{\mathbf{U}}_{\nu}), \tag{65}$$

with (cf. (28))

$$\bar{\mathbf{U}}_{\mu} = \mathbf{A}_{\mu} + \gamma_{\mu}(g, \mathbf{b}) = \mathbf{U}_{\mu} - \gamma_{\mu}(-g, \mathbf{b}). \tag{66}$$

Throughout this section, unless otherwise stated, **b** is to be understood as an I-vector with the components $(1/\kappa)B^{(1)}$, $(1/\kappa)B^{(2)}$ and $(1/\kappa)B^{(3)}$ (not $1/\kappa' B^{(3)}$), and the notation $S(\rho)$, $f(\rho)$ and $\gamma_{\mu}(\rho)$ will be used for $S(\rho, \mathbf{b})$, $f(\rho, \mathbf{b})$ and $\gamma_{\mu}(\rho, \mathbf{b})$, respectively.

It should be noted that the parameter ρ appears only in front of $N[\sigma]$ in (63) and $N[\sigma]$ itself contains only the coupling constant g (but not ρ).

Thus, we can easily see that

$$\begin{aligned} -iG^{-1}[g, \sigma] \frac{\delta}{\delta\sigma(x)} G[g, \sigma] &= -i \frac{\delta}{\delta\sigma} + \frac{g}{\kappa} \partial_{\mu}(\mathbf{B} \cdot \mathbf{G}_{\mu}) \\ &\qquad + \frac{g^2}{2!\kappa^2} [\partial_{\mu}(\mathbf{B} \cdot \mathbf{G}_{\mu}), N[\sigma]] + \dots \\ &= -i \frac{\delta}{\delta\sigma} + \frac{1}{\kappa} \int_0^g \mathrm{d}\rho G^{-1}[\rho, \sigma] \partial_{\mu}(\mathbf{B} \cdot \mathbf{G}_{\mu}) G[\rho, \sigma]. \end{aligned} \tag{67}$$

In a practical calculation of the above quantity the last expression is more convenient than the middle one. From (65) we get

$$\begin{aligned} \partial_{\mu}(\mathbf{B} \cdot \mathbf{G}_{\mu}) = &-(\partial_{\mu}\mathbf{B} \cdot \mathbf{u}_{\nu\mu} \wedge \bar{\mathbf{U}}_{\nu}) + \kappa^2(\mathbf{B} \cdot \gamma_{\mu}(-g) \wedge \bar{\mathbf{U}}_{\mu}) \\ &+ \tfrac{1}{2}(\mathbf{B} \cdot \mathbf{u}_{\nu\mu} \wedge \mathbf{v}_{\nu\mu}) - (\mathbf{B} \cdot \partial_{\mu}\partial_{\nu}\mathbf{U}_{\nu} \wedge \bar{\mathbf{U}}_{\mu}) \end{aligned}$$

where

$$\mathbf{v}_{\mu\nu} = \partial_{\mu}\gamma_{\nu}(g) - \partial_{\nu}\gamma_{\mu}(g).$$

Among the terms of $G^{-1}[g, \sigma](\mathscr{H} - i\delta/\delta\sigma)G[g, \sigma]$, which is to be a new interaction Hamiltonian $\mathscr{H}_1(x)$ in the Schrödinger equation for $\Psi_1[\sigma]$, we shall first calculate the terms, which bear only space indices $\mu = 1, 2, 3$ †. They are as follows:

---

† The Greek suffices run over 1, 2, 3 and 4, and the Roman over 1, 2 and 3.

$$X(x) = \int_0^g d\rho G^{-1}[\rho, \sigma] \Big[-\frac{1}{\kappa} (\partial_k \mathbf{B} \cdot \mathbf{u}_{lk} \wedge \bar{\mathbf{U}}_l) + \frac{1}{2\kappa} (\mathbf{B} \cdot \mathbf{u}_{kl} \wedge \mathbf{v}_{kl})$$

$$+ \kappa(\mathbf{B} \cdot \gamma_k(-g) \wedge \bar{\mathbf{U}}_k) - \frac{1}{\kappa} (\partial_k \partial_\nu \mathbf{U}_\nu \wedge \bar{\mathbf{U}}_k) \Big] G[\rho, \sigma] \tag{68}$$

$$+ G^{-1}[g, \sigma] \Big[\frac{g}{2} (\mathbf{u}_{kl} \cdot \mathbf{U}_k \wedge \mathbf{U}_l) + \tfrac{1}{4} g^2 (\mathbf{U}_k \wedge \mathbf{U}_l \cdot \mathbf{U}_k \wedge \mathbf{U}_l) \Big] G[g, \sigma].$$

Now, we can easily check that

$$[\bar{\mathbf{U}}_k(x), N[\sigma]] = \frac{1}{\kappa} (\bar{\mathbf{U}}_k \wedge \mathbf{B}(x)) = \alpha(\mathbf{b}) \bar{\mathbf{U}}_k, \quad [\mathbf{B}(x), N[\sigma]] = 0, \tag{69}$$

from which follows

$$G^{-1}[\rho, \sigma] \bar{\mathbf{U}}_k(x) G[\rho, \sigma] = S(\rho) \bar{\mathbf{U}}_k(x) \quad \text{for} \quad x/\sigma. \tag{70}$$

From (70), using (26), (28) and (60), we get

$$G^{-1}[\rho, \sigma] \mathbf{u}_{kl}(x) G[\rho, \sigma] = \partial_k (S(\rho) \bar{\mathbf{U}}_l) - \partial_l (S(\rho) \bar{\mathbf{U}}_k) - \mathbf{v}_{kl}$$

$$= S(\rho) \mathbf{u}_{kl} - \frac{\rho}{\kappa} S(\rho) [(f(-\rho) \partial_k \mathbf{B}) \wedge \bar{\mathbf{U}}_l - (f(-\rho) \partial_l \mathbf{B}) \wedge \bar{\mathbf{U}}_k] + (S(\rho) - 1) \mathbf{v}_{kl}, \tag{71a}$$

and from (70), (66), (27), (28) and (13),

$$\begin{aligned} G^{-1}[\rho, \sigma] \mathbf{U}_k(x) G[\rho, \sigma] &= S(\rho) \bar{\mathbf{U}}_k + \gamma_k(-\rho) \\ &= S(\rho) \mathbf{A}_k + (S(\rho) - 1) \gamma_k(\rho) + \partial_k \mathbf{b} \\ &= S(\rho) (\mathbf{A}_k + f(-\rho) \partial_k \mathbf{b}) \quad \text{for} \quad x/\sigma. \end{aligned} \tag{71b}$$

We also notice that

$$[\mathbf{u}_{k4}(x), N[\sigma]] = \alpha(\mathbf{b}) \mathbf{u}_{k4}(x),$$
$$G^{-1}[\rho, \sigma] \mathbf{u}_{k4}(x) G[\rho, \sigma] = S(\rho) \mathbf{u}_{k4}(x) \quad \text{for} \quad x/\sigma.$$

By making use of (70) and (71), together with the formulae (26) and (29), we can prove the following relation:

$$\begin{aligned} &\int_0^g d\rho G^{-1}[\rho, \sigma] \Big[-\frac{1}{\kappa} (\partial_k \mathbf{B} \cdot \mathbf{u}_{lk} \wedge \bar{\mathbf{U}}_l) + \frac{1}{2\kappa} (\mathbf{B} \cdot \mathbf{u}_{kl} \wedge \mathbf{v}_{kl}) \Big] G[\rho, \sigma] \\ &\quad + G^{-1}[g, \sigma] [\tfrac{1}{2} g (\mathbf{u}_{kl} \cdot \mathbf{U}_k \wedge \mathbf{U}_l) + \tfrac{1}{4} g^2 (\mathbf{U}_k \wedge \mathbf{U}_l \cdot \mathbf{U}_k \wedge \mathbf{U}_l)] G[g, \sigma] \\ &\quad = \tfrac{1}{2} g (\mathbf{u}_{kl} \cdot \mathbf{A}_k \wedge \mathbf{A}_l) + \tfrac{1}{4} g^2 (\mathbf{A}_k \wedge \mathbf{A}_l \cdot \mathbf{A}_k \wedge \mathbf{A}_l). \end{aligned} \tag{72}$$

The proof of this relation proceeds as follows: The calculation of the second line on the left hand side is straightforward when we use (70) and (71). The integrations over ρ in the first line are carried out in the following way: by using (71), the first integral is split into three parts,

$$-\frac{1}{\kappa}\int_0^g \mathrm{d}\rho G^{-1}[\rho](\partial_k\mathbf{B}\cdot\mathbf{u}_{lk}\wedge\bar{\mathbf{U}}_l)G[\rho] = -\frac{1}{\kappa}\int_0^g \mathrm{d}\rho\partial_k\mathbf{B}\cdot[S(\rho)(\mathbf{u}_{lk}\wedge\bar{\mathbf{U}}_l)]$$
$$+\frac{1}{\kappa^2}\int_0^g \rho\mathrm{d}\rho\partial_k\mathbf{B}\cdot S(\rho)[(\boldsymbol{\lambda}_l(\rho)\wedge\bar{\mathbf{U}}_k)\wedge\bar{\mathbf{U}}_l-(\boldsymbol{\lambda}_k(\rho)\wedge\bar{\mathbf{U}}_l)\wedge\bar{\mathbf{U}}_l]$$
$$-\frac{1}{\kappa}\int_0^g \mathrm{d}\rho\partial_k\mathbf{B}\cdot[(S(\rho)-1)\mathbf{v}_{lk}\wedge S(\rho)\bar{\mathbf{U}}_l],$$

where we have put

$$\boldsymbol{\lambda}_k(\rho) = f(-\rho)\partial_k\mathbf{B},$$

each term being calculated as follows:

$$(\text{1st term}) = -\frac{g}{\kappa}\partial_k\mathbf{B}\cdot f(g)(\mathbf{u}_{lk}\wedge\bar{\mathbf{U}}_l) =$$
$$-\frac{g}{\kappa}(\mathbf{u}_{lk}\wedge\bar{\mathbf{U}})\cdot\boldsymbol{\lambda}_{kl}(g),\quad \text{for} \int_0^g S(\rho)\mathrm{d}\rho = gf(g)$$

as is evident from (12):

$$(\text{2nd term}) = \frac{1}{\kappa^2}\int_0^g \rho\mathrm{d}\rho S(-\rho)\partial_k\mathbf{B}\cdot[(\boldsymbol{\lambda}_l(\rho)\wedge\bar{\mathbf{U}}_k)\wedge\bar{\mathbf{U}}_l-(\boldsymbol{\lambda}_k(\rho)\wedge\bar{\mathbf{U}}_l)\wedge\bar{\mathbf{U}}_l]$$
$$= \frac{1}{\kappa^2}\int_0^g \mathrm{d}\rho[(S(-\rho)\partial_k\mathbf{B})\wedge\bar{\mathbf{U}}_l]\cdot[(\rho\boldsymbol{\lambda}_k(\rho)\wedge\bar{\mathbf{U}}_l)-(\rho\boldsymbol{\lambda}_l(\rho)\wedge\bar{\mathbf{U}}_k)]$$
$$= \frac{1}{2\kappa^2}(g\boldsymbol{\lambda}_k(g)\wedge\bar{\mathbf{U}}_l)\cdot[(g\boldsymbol{\lambda}_k(g)\wedge\bar{\mathbf{U}}_l)-(g\boldsymbol{\lambda}_l(g)\wedge\bar{\mathbf{U}}_k)],$$

where we have used $\mathrm{d}(\rho\boldsymbol{\lambda}_k(\rho))/d\rho = S(-\rho)\partial_k\mathbf{B}$, which also follows from (12);

$$(\text{3rd term}) = -\frac{1}{\kappa}\int_0^g \mathrm{d}\rho S(-\rho)\partial_k\mathbf{B}\cdot(\mathbf{v}_{lk}\wedge\bar{\mathbf{U}}_l)+\frac{1}{\kappa}\int_0^g \mathrm{d}\rho\partial_k\mathbf{B}\cdot(\mathbf{v}_{lk}\wedge S(\rho)\bar{\mathbf{U}}_l)$$
$$= -\frac{1}{\kappa}g\boldsymbol{\lambda}_k(g)\cdot(\mathbf{v}_{lk}\wedge\bar{\mathbf{U}}_l)+\frac{g}{\kappa}\partial_k\mathbf{B}\cdot(\mathbf{v}_{lk}\wedge f(g)\bar{\mathbf{U}}_l).$$

Similarly, the second integral can be calculated as

$$\frac{1}{2\kappa}\int_0^g \mathrm{d}\rho G^{-1}[\rho](\mathbf{B}\cdot\mathbf{u}_{kl}\wedge\mathbf{v}_{kl})G[\rho] = \frac{1}{2\kappa}\int_0^g \mathrm{d}\rho\mathbf{B}\cdot[(S(\rho)\mathbf{u}_{kl})\wedge\mathbf{v}_{kl}]$$
$$-\frac{1}{2\kappa^2}\int_0^g \rho\mathrm{d}\rho\mathbf{B}\cdot\{[S(\rho)(\boldsymbol{\lambda}_k(\rho)\wedge\bar{\mathbf{U}}_l)-S(\rho)(\boldsymbol{\lambda}_l(\rho)\wedge\bar{\mathbf{U}}_k)]\wedge\mathbf{v}_{kl}\}$$
$$+\frac{1}{2\kappa}\int_0^g \mathrm{d}\rho\mathbf{B}\cdot[(S(\rho)-1)\mathbf{v}_{kl}\wedge\mathbf{v}_{kl}]$$
$$= -\tfrac{1}{2}\mathbf{v}_{kl}\cdot(S(g)-1)\mathbf{u}_{kl}-\frac{1}{2\kappa^2}\left(\int\quad\right)-\tfrac{1}{2}\mathbf{v}_{kl}\cdot(S(g)-1)\mathbf{v}_{kl}$$

(by use of the 4th relation in (26)), where $(-1/2\kappa^2)(\int\ )$ stands for the second term in the above, which can be calculated (by partial integration) as follows:

$$
\begin{aligned}
-\frac{1}{2\kappa^2}\left(\int\ \right) &= -\frac{1}{2\kappa}\int_0^g \mathrm{d}\rho S(-\rho)(\mathbf{v}_{kl}\wedge\mathbf{b})\cdot[\rho\boldsymbol{\lambda}_k(\rho)\wedge\bar{\mathbf{U}}_l-\rho\boldsymbol{\lambda}_l(\rho)\wedge\bar{\mathbf{U}}_k] \\
&= \frac{1}{2\kappa}\Big\{S(-\rho)\mathbf{v}_{kl}\cdot[\rho\boldsymbol{\lambda}_k(\rho)\wedge\bar{\mathbf{U}}_l-\rho\boldsymbol{\lambda}_l(\rho)\wedge\bar{\mathbf{U}}_k]\Big|_0^g \\
&\quad -\int_0^g \mathrm{d}\rho S(-\rho)\mathbf{v}_{kl}\cdot[(S(-\rho)\partial_k\mathbf{B})\wedge\bar{\mathbf{U}}_l-(S(-\rho)\partial_l\mathbf{B})\wedge\bar{\mathbf{U}}_k]\Big\} \\
&= \frac{1}{2\kappa}\Big\{S(-g)\mathbf{v}_{kl}\cdot[g\boldsymbol{\lambda}_k(g)\wedge\bar{\mathbf{U}}_l-g\boldsymbol{\lambda}_l(g)\wedge\bar{\mathbf{U}}_k] \\
&\quad -g\mathbf{v}_{kl}\cdot[\partial_k\mathbf{B}\wedge f(g)\bar{\mathbf{U}}_l-\partial_l\mathbf{B}\wedge f(g)\bar{\mathbf{U}}_k]\Big\}.
\end{aligned}
$$

The relation (72) can be obtained by collecting al these terms and then by using the following relation:

$$
\begin{aligned}
(1-S(-g))\mathbf{v}_{kl} &= \frac{-g}{\kappa^3}(f(-g)\partial_k\mathbf{B})\wedge(f(-g)\partial_l\mathbf{B}) \\
&\quad +\frac{g}{\kappa}[(f(-g)\partial_k\mathbf{B})\wedge\gamma_l(g)-(f(-g)\partial_l\mathbf{B})\wedge\gamma_k(g)],
\end{aligned} \tag{73}
$$

which can be proved by differentiating (27) and by using (26). On the other hand, we can prove that

$$[\partial_\nu\mathbf{U}_\nu(x), N[\sigma]] = 0 \quad \text{for} \quad x/\sigma,$$

which leads to the relations[†]

$$\partial_\nu\mathbf{U}_\nu(x)\Psi_1[\sigma] = 0 \quad \text{for} \quad x/\sigma, \tag{74}$$

and

$$\partial_k\partial_\nu\mathbf{U}_\nu(x)\Psi_1[\sigma] = 0 \quad \text{for} \quad x/\sigma. \tag{75}$$

Therefore, the 4-th term in $X(x)$ (68) gives no contribution to the Schrödinger equation for $\Psi_1[\sigma]$.

The 3rd term in $X(x)$ can be calculated as follows:

$$
\begin{aligned}
&\int_0^g \mathrm{d}\rho G^{-1}[\rho][\mathbf{B}\cdot(\gamma_k(-g)\wedge\bar{\mathbf{U}}_k)]G[\rho] \\
&\qquad = \int_0^g \mathrm{d}\rho\{\mathbf{B}\cdot[\gamma_k(-g)\wedge(S(\rho)\bar{\mathbf{U}}_k)]\} = g[\gamma_k(-g)\cdot(f(g)\bar{\mathbf{U}}_k\wedge\mathbf{B})].
\end{aligned}
$$

By using the 4-th relation in (26) this becomes

$$\kappa[\gamma_k(-g)\cdot(S(g)-1)\bar{\mathbf{U}}_k],$$

[†] Compare these relations with the one in the footnote following eq. (46). It should be noted that $\partial_4\partial_\nu\mathbf{U}_\nu(x)\Psi_1[\sigma]=0$ is not satisfied even for x/σ.

by using (66) we get herefore

$$\begin{aligned}\kappa[\mathbf{U}_k\cdot(S(-g)-1)\gamma_k(-g)]-\kappa[\gamma_k(-g)\cdot(S(g)-1)\gamma_k(-g)]\\ =\tfrac{1}{2}\kappa(\mathbf{w}_k\cdot\mathbf{w}_k)-\frac{\kappa}{2}(\mathbf{U}_k\cdot\mathbf{U}_k).\end{aligned}\tag{76}$$

Here, at the last stage use is made of the following relations:

$$\mathbf{U}_k+(S(-g)-1)\gamma_k(-g)=S(-g)\mathbf{w}_k,$$

which follows from (9) and (29), and

$$\begin{aligned}[\gamma_k(-g)\cdot(S(-g)-1)\gamma_k(-g)] &= [\gamma_k(-g)\cdot(S(g)-1)\gamma_k(-g)]\\ &=\tfrac{1}{2}[\gamma_k(-g)\cdot(S(g)+S(-g)-2)\gamma_k(-g)]\\ &=-\tfrac{1}{2}[\gamma_k(-g)\cdot(S(g)-1)(S(-g)-1)\gamma_k(-g)]\\ &=-\tfrac{1}{2}(S(-g)-1)\gamma_k(-g)\cdot(S(-g)-1)\gamma_k(-g),\end{aligned}$$

where the first relation in (26) has been used.

The relations (72), (75) and (76) finally lead to

$$\begin{aligned}X(x)\Psi_1[\sigma]=\Big\{\tfrac{1}{2}g(\mathbf{u}_{kl}\cdot\mathbf{A}_k\wedge\mathbf{A}_l)+\frac{g^2}{4}(\mathbf{A}_k\wedge\mathbf{A}_l\cdot\mathbf{A}_k\wedge\mathbf{A}_l)\\ -\tfrac{1}{2}\kappa^2[(\mathbf{U}_k\cdot\mathbf{U}_k)-(\mathbf{w}_k\cdot\mathbf{w}_k)]\Big\}\,\Psi_1[\sigma].\end{aligned}\tag{77}$$

Bearing in mind that the interaction Hamiltonian should be Lorentz invariant, we finally arrive at the following covariant expression:

$$\begin{aligned}\mathscr{H}_1(x)(\kappa=\kappa')=\tfrac{1}{2}g(\mathbf{u}_{\mu\nu}\cdot\mathbf{A}_\mu\wedge\mathbf{A}_\nu)+\frac{g^2}{4}(\mathbf{A}_\mu\wedge\mathbf{A}_\nu\cdot\mathbf{A}_\mu\wedge\mathbf{A}_\nu)\\ -\tfrac{1}{2}\kappa^2[(\mathbf{U}_\mu\cdot\mathbf{U}_\mu)-(\mathbf{w}_\mu\cdot\mathbf{w}_\mu)]+(\text{n.d.}).\end{aligned}\tag{78}$$

This completes the proof of the theorem (I) in the special case of $\kappa=\kappa'$. The last line in (71) indicates hat

$$G^{-1}[g,\sigma]\mathbf{U}_\mu G[g,\sigma]=\mathbf{w}_\mu+(\text{n.d.}).\tag{20}$$

From (78) and (20) we immediately obtain the following expression:

$$\begin{aligned}\mathscr{H}_1(\kappa=\kappa')=\tfrac{1}{2}g(\mathbf{u}_{\mu\nu}\cdot\mathbf{A}_\mu\wedge\mathbf{A}_\nu)+\tfrac{1}{4}g^2(\mathbf{A}_\mu\wedge\mathbf{A}_\nu\cdot\mathbf{A}_\mu\wedge\mathbf{A}_\nu)\\ -\tfrac{1}{2}\kappa^2[(\mathbf{U}_\mu\cdot\mathbf{U}_\mu)-G^{-1}[g,\sigma](\mathbf{U}_\mu\cdot\mathbf{U}_\mu)G[g,\sigma]]+(\text{n.d.}),\end{aligned}\tag{79}$$

which proves the theorem (I′) in the case of $\kappa=\kappa'$.

Let us now turn to the more general case, in which κ' is not necessarily equal to κ. For the moment we shall assume $\kappa'\neq 0$. The Lagrangian (50) gives the following interaction Hamiltonian:

$$\mathscr{H}' = \mathscr{H} + \delta\mathscr{H}, \tag{80}$$

with

$$\delta\mathscr{H} = -\tfrac{1}{2}(\kappa^2 - \kappa'^2)U_\mu^{(3)}U_\mu^{(3)} + (\text{n.d.}), \tag{81}$$

where $\mathscr{H}$ is given by (58). It should be noted that we are concerned with a special interaction representation, in which all the free particles have the same mass κ, and the mass difference is regarded as an interaction term $\delta\mathscr{H}$.

The unitary transformation (62) transforms $\mathscr{H}'$ into $\mathscr{H}'_1$, which is given by

$$\mathscr{H}'_1 = \mathscr{H}_1 + \delta\mathscr{H}_1, \tag{82}$$

with

$$\delta\mathscr{H}_1 = G^{-1}[g, \sigma]\delta\mathscr{H}(x)G[g, \sigma]. \tag{83}$$

Thus, from (79) we have

$$\begin{aligned} \mathscr{H}'_1 = {} & \tfrac{1}{2}g(\mathbf{u}_{\mu\nu} \cdot \mathbf{A}_\mu \wedge \mathbf{A}_\nu) + \tfrac{1}{4}g^2(\mathbf{A}_\mu \wedge \mathbf{A}_\nu \cdot \mathbf{A}_\mu \wedge \mathbf{A}_\nu) - \tfrac{1}{2}(\kappa^2 - \kappa'^2)U_\mu^{(3)}U_\mu^{(3)} \\ & - \tfrac{1}{2}\kappa^2 \sum_{i=1,2} [U_\mu^{(i)}U_\mu^{(i)} - G^{-1}[g, \sigma]U_\mu^{(i)}U_\mu^{(i)}G[g, \sigma]] \\ & - \tfrac{1}{2}\kappa'^2[U_\mu^{(3)}U_\mu^{(3)} - G^{-1}[g, \sigma]U_\mu^{(3)}U_\mu^{(3)}G[g, \sigma]] + (\text{n.d.}). \end{aligned} \tag{84}$$

Let us now introduce another unitary transformation:

$$\Psi_1[\sigma] \to \Psi'_1[\sigma] = F^{-1}[M, \sigma]\Psi_1[\sigma], \tag{85}$$

with

$$F[\rho, \sigma] = \exp\left[i\rho \int_\sigma d\sigma_\mu B^{(3)} A_\mu^{(3)}\right]. \tag{86}$$

The factor M in (85) is of the value

$$M = \frac{\kappa^2 - \kappa'^2}{\kappa}. \tag{87}$$

We can easily see that

$$\begin{aligned} F^{-1}[\rho, \sigma]\mathbf{u}_{\mu\nu}(x)F[\rho, \sigma] &= \mathbf{u}_{\mu\nu}(x), \\ F^{-1}[\rho, \sigma]\mathbf{A}_\mu(x)F[\rho, \sigma] &= \mathbf{A}_\mu(x), \\ F^{-1}[\rho, \sigma]\mathbf{B}(x)\ F[\rho, \sigma] &= \mathbf{B}(x), \\ F^{-1}[\rho, \sigma]\partial_\mu A_\mu^{(3)}(x)F[\rho, \sigma] &= \partial_\mu A_\mu^{(3)}(x) - \rho B^{(3)}(x), \\ F^{-1}[\rho, \sigma]\partial_\mu U_\mu^{(3)}(x)F[\rho, \sigma] &= \partial_\mu U_\mu^{(3)}(x) - \rho B^{(3)}(x). \end{aligned} \tag{88}$$

Because of the above relations the subsidiary condition is now changed into

$$\begin{aligned} &(\partial_\mu A_\mu^{(3)}(x) + \kappa' \left(\frac{\kappa'}{\kappa}\right) B^{(3)}(x))\Psi'_1[\sigma] = 0, \\ &(\partial_\mu A_\mu^{(i)}(x) + \kappa B^{(i)}(x))\Psi'_1[\sigma] = 0 \quad \text{for} \quad x/\sigma \quad \text{and} \quad (i = 1, 2). \end{aligned} \tag{89}$$

By use of (88) we can further show that

$$\begin{aligned}-iF^{-1}[M,\rho]\frac{\delta}{\delta\sigma(x)}F[M,\rho] &= -i\frac{\delta}{\delta\sigma}+\int_0^M d\rho F^{-1}[\rho,\sigma]\partial_\mu(A_\mu^{(3)}B^{(3)})F[\rho,\sigma]\\ &= -i\frac{\delta}{\delta\sigma}+\frac{\kappa^2-\kappa'^2}{\kappa}A_\mu^{(3)}\partial_\mu B^{(3)}-\frac{\kappa^4-\kappa'^4}{2\kappa^3}B^{(3)}B^{(3)} \qquad (90)\\ &\qquad +\frac{\kappa^2-\kappa'^2}{\kappa}B^{(3)}\left(\partial_\mu A_\mu^{(3)}+\kappa'\left(\frac{\kappa'}{\kappa}\right)B^{(3)}\right)+(\text{n.d.}),\end{aligned}$$

where we have used the following relation:

$$\begin{aligned}\int_0^M d\rho F^{-1}[\rho,\sigma]B^{(3)}\partial_\mu A_\mu^{(3)}F[\rho,\sigma] &= \int_0^M d\rho(\partial_\mu A_\mu^{(3)}-\rho B^{(3)})B^{(3)}\\ &= -\frac{(\kappa^2-\kappa'^2)^2}{2\kappa^2}B^{(3)}B^{(3)}+\frac{\kappa^2-\kappa'^2}{\kappa}B^{(3)}\partial_\mu A_\mu^{(3)}.\end{aligned}$$

Then, from (84), (90) and (89) we can get the following Schrödinger equation for $\Psi'_1[\sigma]$:

$$\begin{aligned}i\frac{\delta}{\delta\sigma(x)}\Psi'_1[\sigma] = \Big\{&\tfrac{1}{2}g(\mathbf{u}_{\mu\nu}\cdot\mathbf{A}_\mu\wedge\mathbf{A}_\nu)+\tfrac{1}{4}g^2(\mathbf{A}_\mu\wedge\mathbf{A}_\nu\cdot\mathbf{A}_\mu\wedge\mathbf{A}_\nu)\\ &-\tfrac{1}{2}\kappa^2\sum_{i=1,2}[U_\mu^{(i)}U_\mu^{(i)}-G^{-1}[g,\sigma]U_\mu^{(i)}U_\mu^{(i)}G[g,\sigma]]\\ &-\tfrac{1}{2}\kappa'^2[U_\mu^{(3)}U_\mu^{(3)}-G^{-1}[g,\sigma]U_\mu^{(3)}U_\mu^{(3)}G[g,\sigma]] \qquad (91)\\ &-\tfrac{1}{2}(\kappa^2-\kappa'^2)\left[A_\mu^{(3)}A_\mu^{(3)}+\left(\frac{\kappa'}{\kappa}\right)^2B^{(3)}B^{(3)}\right]\\ &+\left(1-\frac{\kappa'^2}{\kappa^2}\right)\mathscr{L}^0(B^{(3)})+(\text{n.d.})\Big\}\Psi'_1[\sigma],\end{aligned}$$

where

$$\mathscr{L}^0(B^{(3)}) = -\tfrac{1}{2}(\partial_\mu B^{(3)}\partial_\mu B^{(3)}+\kappa^2B^{(3)}B^{(3)}).$$

When deriving (91) we have taken into account the fact that two transformations $G[g,\sigma]$ and $F[M,\sigma]$ are commutable.

Since $\mathscr{L}^0(B^{(3)})$ is just the free Lagrangian for the $B^{(3)}$-field, we can simply drop this term (together with a part of (n.d.)) in (91) if we simultaneously make the following change in the free Lagrangian for this field:

$$\mathscr{L}^0(B^{(3)})\to\left[1-\left(1-\frac{\kappa'^2}{\kappa^2}\right)\right]\mathscr{L}^0(B^{(3)}) = \left(\frac{\kappa'}{\kappa}\right)^2\mathscr{L}^0(B^{(3)})\to\mathscr{L}^0(B^{(3)}), \quad (92)$$

where the last step corresponds to the following transformation:

$$\frac{\kappa'}{\kappa}B^{(3)}\to B^{(3)}. \quad (93)$$

It is easy to see that the overall change (92) is a canonical transformation $C[\sigma]$ with the property

$$\begin{aligned} &\frac{\kappa'}{\kappa} C^{-1}[\sigma] B^{(3)}(x) C[\sigma] = B^{(3)}(x), \\ &\frac{\kappa}{\kappa'} C^{-1}[\sigma] \frac{\partial B^{(3)}(x)}{\partial t} C[\sigma] = \frac{\partial B^{(3)}}{\partial t}, \quad x/\sigma. \end{aligned} \tag{94}$$

We can also argue this point in a different way. In Feynman diagrams the term $\mathscr{L}^0(B^{(3)})$ in (91) gives the following contribution to each internal line of $B^{(3)}$ or to the propagation function $\Delta_F^{(3)}$:

$$\begin{aligned} \Delta_F^{(3)}(x-x') \to \int d^4x_1 \Delta_F^{(3)}(x-x_1) \Big[&\delta^4(x_1-x') + \frac{C}{2i} (\Box_1 - \kappa^2) \Delta_F(x_1-x') \\ &- \tfrac{1}{4} C^2 \int d^4x_2 (\Box_1 - \kappa^2) \Delta_F^{(3)}(x_1-x_2) (\Box_2 - \kappa^2) \Delta_F(x_2-x') + \dots \Big] \\ = \Delta_F^{(3)}(x-x')(1+C+C^2+ \dots) &= \frac{1}{1-C} \Delta_F^{(3)}(x-x') = \left(\frac{\kappa}{\kappa'}\right)^2 \Delta_F^{(3)}(x-x'), \end{aligned}$$

where $C = 1-(\kappa'/\kappa)^2$. Thus, the term $\mathscr{L}^0(B^{(3)})$ plays simply a role of changing normalization of the $B^{(3)}$-field, which is equivalent to (93). We can also prove (94) by using an explicit form for $C[\sigma]$.

After the above transformation (92), the subsidiary conditions (89) are changed into

$$\begin{aligned} &(\partial_\mu A_\mu^{(3)}(x) + \kappa' B^{(3)}(x)) \tilde{\Psi}_1[\sigma] = 0, \\ &(\partial_\mu A_\mu^{(i)}(x) + \kappa B^{(i)}(x)) \tilde{\Psi}_1[\sigma] = 0 \quad (i = 1, 2), x/\sigma, \end{aligned} \tag{95}$$

where $\tilde{\Psi}_1[\sigma]$ is a state vector in the new representation.

The Schrödinger equation (91) is also rewritten as follows:

$$\begin{aligned} i \frac{\delta}{\delta\sigma(x)} \tilde{\Psi}_1[\sigma] = \{ &\tfrac{1}{2} g(\mathbf{u}_{\mu\nu} \cdot \mathbf{A}_\mu \wedge \mathbf{A}_\nu) + \tfrac{1}{4} g^2 (\mathbf{A}_\mu \wedge \mathbf{A}_\nu \cdot \mathbf{A}_\mu \wedge \mathbf{A}_\nu) \\ &- \tfrac{1}{2} \kappa^2 \sum_{i=1,2} [U_\mu^{(i)} U_\mu^{(i)} - \bar{G}^{-1}[g,\sigma] U_\mu^{(i)} U_\mu^{(i)} \bar{G}[g,\sigma]] \\ &- \tfrac{1}{2} \kappa'^2 [\mathring{U}_\mu^{(3)} \mathring{U}_\mu^{(3)} - \bar{G}^{-1}[g,\sigma] \mathring{U}_\mu^{(3)} \mathring{U}_\mu^{(3)} \bar{G}[g,\sigma]] \\ &- \tfrac{1}{2} (\kappa^2 - \kappa'^2)(A_\mu^{(3)} A_\mu^{(3)} + B^{(3)} B^{(3)}) + (\text{n.d.}) \} \tilde{\Psi}_1[\sigma], \end{aligned} \tag{96}$$

where $\bar{G}$ is the same as G, except for the replacement $(1/\kappa)B^{(3)} \to (1/\kappa')B^{(3)}$:

$$\bar{G} = G[(1/\kappa)B^{(3)} \to (1/\kappa')B^{(3)}]$$

and $\mathring{U}_\mu^{(3)}$ is given by $\mathring{U}_\mu^{(3)} = A_\mu^{(3)} + 1/\kappa' \, \partial_\mu B^{(3)}$.

Let us now go over into the ordinary interaction representation, in which free particles of $A_\mu^{(3)}$ and $B^{(3)}$ carry their own mass κ'. This can be done by a well-known unitary transformation $K[\sigma]$ in the following way:

$$\tilde{\Psi}_1[\sigma] \to \Psi_2[\sigma] = K[\sigma]\tilde{\Psi}_1[\sigma], \tag{97}$$

with $K[\sigma]$ defined by

$$\begin{aligned} i\,\frac{\delta K[\sigma]}{\delta\sigma(x)} &= \tfrac{1}{2}(\kappa^2-\kappa'^2)K[\sigma](A_\mu^{(3)}A_\mu^{(3)}+B^{(3)}B^{(3)}) \\ &= \tfrac{1}{2}(\kappa^2-\kappa'^2)(A_\mu^{(3)\prime}A_\mu^{(3)\prime}+B^{(3)\prime}B^{(3)\prime})K[\sigma], \end{aligned} \tag{98}$$

and

$$\begin{aligned} A_\mu^{(3)\prime}(x) &= K[\sigma]A_\mu^{(3)}(x)K^{-1}[\sigma], \\ B^{(3)\prime}(x) &= K[\sigma]B^{(3)}(x)K^{-1}[\sigma], \quad x/\sigma. \end{aligned} \tag{99}$$

We can then prove that

$$(\Box-\kappa'^2)A_\mu^{(3)\prime} = 0, \quad (\Box-\kappa'^2)B^{(3)\prime} = 0, \tag{100}$$

$$\partial_\nu A_\mu^{(3)\prime}(x) = K[\sigma]\partial_\nu A_\mu^{(3)}(x)K^{-1}[\sigma] \quad \text{for} \quad x/\sigma. \tag{101}$$

(100) shows that $A_\mu^{(3)\prime}$ and $B^{(3)\prime}$ describe fields with mass κ', and (101) changes the subsidiary conditions (95) into

$$\begin{aligned} &(\partial_\mu A_\mu^{(3)\prime}(x)+\kappa' B^{(3)\prime}(x))\Psi_2[\sigma] = 0, \\ &(\partial_\mu A_\mu^{(i)}(x)+\kappa B^{(i)}(x))\Psi_2[\sigma] = 0 \quad (i = 1, 2), \quad x/\sigma. \end{aligned} \tag{102}$$

The Schrödinger equation (96) is now transformed into

$$\begin{aligned} i\,\frac{\delta}{\delta\sigma(x)}\,\Psi_2[\sigma] = \{&\tfrac{1}{2}g(\mathbf{u}'_{\mu\nu}\cdot\mathbf{A}'_\mu\wedge\mathbf{A}'_\nu)+\tfrac{1}{4}g^2(\mathbf{A}'_\mu\wedge\mathbf{A}'_\nu\cdot\mathbf{A}'_\mu\wedge\mathbf{A}'_\nu) \\ &-\tfrac{1}{2}\kappa^2\sum_{i=1,2}[U_\mu^{(i)}U_\mu^{(i)}-G'^{-1}[\sigma]U_\mu^{(i)}U_\mu^{(i)}G'[\sigma]] \\ &-\tfrac{1}{2}\kappa'^2[U_\mu^{(3)\prime}U_\mu^{(3)\prime}-G'^{-1}[\sigma]U_\mu^{(3)\prime}U_\mu^{(3)\prime}G'[\sigma]]+(\text{n.d.})\}\Psi_2[\sigma], \end{aligned} \tag{103}$$

with

$$U_\mu^{(3)\prime} = A_\mu^{(3)\prime}+\frac{1}{\kappa'}\partial_\mu B^{(3)\prime}. \tag{104}$$

Here, $\mathbf{A}'_\mu$ denotes the I-vector, whose components are $A_\mu^{(1)}$, $A_\mu^{(2)}$ and $A_\mu^{(3)\prime}$ (not $A_\mu^{(3)}$) and $\mathbf{u}'_{\mu\nu}$ is defined by $\mathbf{u}'_{\mu\nu} = \partial_\mu\mathbf{A}'_\nu-\partial_\nu\mathbf{A}'_\mu$.

The transformation G' is obtained from $G[g, \sigma]$ by replacing $\mathbf{A}_\mu$, $\mathbf{u}_{\mu\nu}$ and $(1/\kappa)B^{(3)}$ by $\mathbf{A}'_\mu$, $\mathbf{u}'_{\mu\nu}$ and $(1/\kappa')B^{(3)\prime}$, respectively:

$$\begin{aligned} G'[\sigma] &= K[\sigma]\bar{G}[g, \sigma]K^{-1}[\sigma] \\ &= G[\mathbf{A}_\mu \to \mathbf{A}'_\mu, \mathbf{u}_{\mu\nu} \to \mathbf{u}'_{\mu\nu}, (1/\kappa)B^{(3)} \to (1/\kappa')B^{(3)\prime}]. \end{aligned} \tag{105}$$

We have thus proved the theorem (I′). The theorem (I) is derived directly from the theorem (I′) by using (20) and (105).

Lastly, we shall consider the case of electromagnetic interaction of the charged vector field ($\kappa' = 0, g = e$). The Lagrangian (57) gives the following interaction Hamiltonian:

$$\mathscr{H}'(x) = \mathscr{H}(x) - \tfrac{1}{2}\kappa^2 A_\mu^{(3)} A_\mu^{(3)}, \tag{106}$$

where $\mathscr{H}(x)$ is given by (58), but with $B^{(3)} = 0$ (i.e., $U_\mu^{(3)} = A_\mu^{(3)}$). It should be noted that we are considering a special representation, in which free photon have mass κ. This mass, however, is cancelled by the mass counter term in (106). In this case, we can proceed almost in the same way as the previous cases, for $\kappa' = 0$ is not a singular point in our formalism. (This is not the case with the ordinary formalism).

The transformation (62) (in which **b** describes $(1/\kappa)B^{(i)}(i = 1, 2, 3))$ gives an interaction Hamiltonian of the form (84) with $\kappa' = 0$, $B^{(3)} = 0$. Performing a further transformation

$$\begin{aligned} &\Psi_1[\sigma] \to \Psi_2[\sigma] = L[\sigma]\Psi_1[\sigma], \\ &i\frac{\delta L[\sigma]}{\delta\sigma} = \tfrac{1}{2}\kappa^2 L[\sigma] A_\mu^{(3)} A_\mu^{(3)} = \tfrac{1}{2}\kappa^2 A_\mu^{(3)\prime} A_\mu^{(3)\prime} L[\sigma], \end{aligned} \tag{107}$$

with

$$A_\mu^{(3)\prime}(x) = L[\sigma] A_\mu^{(3)}(x) L^{-1}[\sigma] \quad \text{for} \quad x/\sigma \tag{108}$$

we arrive at the following relations:

$$\Box A_\mu^{(3)\prime} = 0, \tag{109}$$

$$\begin{aligned} &\partial_\mu A_\mu^{(3)\prime}(x)\Psi_2[\sigma] = 0 \quad \text{for} \quad x/\sigma, \\ &i\frac{\delta}{\delta\sigma(x)}\Psi_2[\sigma] = \mathscr{H}_2(x)\Psi_2[\sigma]. \end{aligned} \tag{110}$$

Here, $\mathscr{H}_2$ is given by

$$\begin{aligned} \mathscr{H}_2 = {} & \tfrac{1}{2}e(\mathbf{u}'_{\mu\nu} \cdot \mathbf{A}'_\mu \wedge \mathbf{A}'_\nu) + \tfrac{1}{4}e^2(\mathbf{A}'_\mu \wedge \mathbf{A}'_\nu \cdot \mathbf{A}'_\mu \wedge \mathbf{A}'_\nu) \\ & - \tfrac{1}{2}\kappa^2 \sum_{i=1,2} [U_\mu^{(i)} U_\mu^{(i)} - G'^{-1}_\mu[\sigma] U_\mu^{(i)} U_\mu^{(i)} G'[\sigma]] + (\text{n.d.}), \end{aligned} \tag{111}$$

where $\mathbf{A}'_\mu$ denotes the I-vector, whose components are $A_\mu^{(1)}$, $A_\mu^{(2)}$ and $A_\mu^{(3)\prime}$, and G' is obtained from G by replacing $\mathbf{A}_\mu$ and $\mathbf{u}_{\mu\nu}$ by $\mathbf{A}'_\mu$ and $\mathbf{u}'_{\mu\nu}$ and by taking $B^{(3)} = 0$. Thus, we have obtained the theorem (II′) which was stated in section 2 in terms of unprimed quantities instead of primed ones. The theorem (II) then follows from the theorem (II′) by using (20).

5. Gauge Invariance of the Yang-Mills Field with Vanishing Mass

In this section let us briefly make a comment on the gauge invariance of the Yang-Mills field with vanishing mass ($\kappa = 0$). The interaction Hamiltonian in this case is given by

$$\mathscr{H} = \tfrac{1}{2}g(\mathbf{u}_{\mu\nu}\cdot\mathbf{A}_\mu\wedge\mathbf{A}_\nu)+\tfrac{1}{4}g^2(\mathbf{A}_\mu\wedge\mathbf{A}_\nu\cdot\mathbf{A}_\mu\wedge\mathbf{A}_\nu)+\tfrac{1}{2}g^2(\mathbf{A}_\mu\wedge\mathbf{A}_\lambda\cdot\mathbf{A}_\nu\wedge\mathbf{A}_\lambda)n_\mu n_\nu. \tag{112}$$

The field $\mathbf{A}_\mu$ satisfies the relations (14) and (16) with $\kappa = 0$.

Now, let us make the following transformation in the Schrödinger equation for $\Psi[\sigma]$:
first, for the operators in the Hamiltonian we make a gauge transformation of the second kind

$$\mathbf{A}_\mu \to \mathbf{U}_\mu = \mathbf{A}_\mu + \partial_\mu \Lambda, \tag{113}$$

where Λ is a c-number I-vector satisfying $\Box\Lambda = 0$ (then, provided that the (n.d.) term is left out of consideration, the transformed Hamiltonian takes the same form as (58), with $\mathbf{U}_\mu$ defined above); next, for the state vector we shall make a gauge transformation of the first kind

$$\Psi[\sigma] \to \Psi_1[\sigma] = G[\sigma, \Lambda]^{-1}\Psi[\sigma], \tag{114}$$

where $G[\sigma, \Lambda]$ is obtained from $G[g, \sigma]$ by replacing $(1/\kappa)\mathbf{B}$ by Λ. Our results in section 4, then, imply that all Λ-dependent terms coming from (113) are completely compensated by the effect of (114); this is because the only term, which led to the **b**-dependence — or the gauge dependence in the present terminology — is the third term in (68), which vanishes, however, if $\kappa = 0$.

Therefore, we can say that our theory is invariant under the combined transformations (113) and (114).

In section 4, we made calculations only for terms with space indices. In the present case, however, we can easily carry out similar calculations also for terms with time index, including the (n.d.) terms †. In this way we can also directly prove the above statement.

6. Theory of the Intermediate Vector Particle

Let us now consider the case in which our vector fields interact with a number of spinor dublets

$$\psi^{(j)} = \begin{pmatrix}\psi_1^{(j)}\\ \psi_2^{(j)}\end{pmatrix} \quad (j = 1, 2, \ldots),$$

and also with a spinless triplet π (e.g. π-meson). We assume that the interactions are of vector and of pseudo-vector type and have a universal coupling constant g 12)). Thus, our Langrangian is

---

† The calculation can be somewhat simplified, concerning the (n.d.) terms, if we make the gauge transformation with $\mathbf{G}_\mu$, defined by $\mathbf{G}_\mu = -g(\mathbf{u}_{\nu\mu}\wedge\overline{\mathbf{U}}_\nu + \partial_\nu\mathbf{A}_\nu\wedge\overline{\mathbf{U}}_\mu)$.

$$\begin{aligned}\bar{\mathscr{L}} = &-\tfrac{1}{4}(\mathbf{u}_{\mu\nu}\cdot\mathbf{u}_{\mu\nu})-\tfrac{1}{2}\kappa^2\sum_{i=1,2}u_\mu{}^{(i)}u_\mu{}^{(i)}-\tfrac{1}{2}\kappa'^2u_\mu{}^{(3)}u_\mu{}^{(3)}\\ &-\sum_j\bar{\psi}^{(j)}[\gamma_\mu\partial_\mu+m_j(1+\alpha_j\tau_3)]\bar{\psi}^{(j)}-\tfrac{1}{2}\partial_\mu\boldsymbol{\pi}\cdot\partial_\mu\boldsymbol{\pi}-\tfrac{1}{2}\mu^2\boldsymbol{\pi}\cdot\boldsymbol{\pi}\\ &-\tfrac{1}{2}g(\mathbf{u}_{\mu\nu}\cdot\mathbf{u}_\mu\wedge\mathbf{u}_\nu)-\tfrac{1}{4}g^2(\mathbf{u}_\mu\wedge\mathbf{u}_\nu\cdot\mathbf{u}_\mu\wedge\mathbf{u}_\nu)\\ &+\sum_j\tfrac{1}{2}ig\bar{\psi}^{(j)}\gamma_\mu\tfrac{1}{2}(1+\varepsilon_j\gamma_5)(\boldsymbol{\tau}\cdot\mathbf{u}_\mu)\psi^{(j)}\\ &+g(\partial_\mu\boldsymbol{\pi}\wedge\boldsymbol{\pi}\cdot\mathbf{u}_\mu)-\tfrac{1}{2}g^2(\boldsymbol{\pi}\wedge\mathbf{u}_\mu\cdot\boldsymbol{\pi}\wedge\mathbf{u}_\mu),\end{aligned}\tag{115}$$

where $\boldsymbol{\tau}$ is the well-known isospin matrix and masses of $\psi_1{}^{(j)}$ and $\psi_2{}^{(j)}$ are not necessarily equal, but $m_j(1+\alpha_j)$ and $m_j(1-\alpha_j)$, respectively. ε_j is not an arbitrary constant, but must be ± 1. That is to say, each spinor particle is supposed to be of a definite handedness. As will be seen later, this is necessary in order that the equivalent theorem be of a simple form. In this connection, we should also notice that the current $\mathbf{J}_\mu$, defined by $\partial_\nu\mathbf{u}_{\nu\mu}-\kappa^2\mathbf{u}_\mu = -\mathbf{J}_\mu$ is conserved if $\kappa=\kappa'$ and $m_j=0$ for all j. Applying the Stueckelberg formalism to the above interaction, we obtain the following Lagrangian:

$$\bar{\mathscr{L}}_{\mathrm{S}} = \mathscr{L}_{\mathrm{S}}+\mathscr{L}_{\mathfrak{f}}+\mathscr{L}_{\mathfrak{b}}+\delta\bar{\mathscr{L}}_{\mathfrak{f}}+\delta\bar{\mathscr{L}}_{\mathfrak{b}},\tag{116}$$

where $\mathscr{L}_{\mathrm{S}}$ is given by (48), $\mathscr{L}_{\mathfrak{f}}$ and $\mathscr{L}_{\mathfrak{b}}$ the free Lagrangians for ψ and $\boldsymbol{\pi}$-fields and

$$\begin{aligned}\delta\bar{\mathscr{L}}_{\mathfrak{f}} &= \sum_j\tfrac{1}{2}ig\bar{\psi}^{(j)}\gamma_\mu\tfrac{1}{2}(1+\varepsilon_j\gamma_5)(\boldsymbol{\tau}\cdot\mathbf{U}_\mu)\psi^{(j)},\\ \delta\bar{\mathscr{L}}_{\mathfrak{b}} &= g(\partial_\mu\boldsymbol{\pi}\wedge\boldsymbol{\pi}\cdot\mathbf{U}_\mu)-\tfrac{1}{2}g^2(\boldsymbol{\pi}\wedge\mathbf{U}_\mu\cdot\boldsymbol{\pi}\wedge\mathbf{U}_\mu),\end{aligned}\tag{117}$$

with $\mathbf{U}_\mu$ as defined by

$$\mathbf{U}_\mu = \mathbf{A}_\mu+\frac{1}{\kappa}\partial_\mu\mathbf{B}.\tag{118}$$

The interaction Hamiltonian is now given by

$$\bar{\mathscr{H}} = \mathscr{H}'+\delta\bar{\mathscr{H}}_{\mathfrak{f}}+\delta\bar{\mathscr{H}}_{\mathfrak{b}},\tag{119}$$

where $\mathscr{H}'$ is given by (80) and

$$\delta\bar{\mathscr{H}}_{\mathfrak{f}} = -\delta\bar{\mathscr{L}}_{\mathfrak{f}}+(\text{n.d.}),\quad \delta\bar{\mathscr{H}}_{\mathfrak{b}} = -\delta\bar{\mathscr{L}}_{\mathfrak{b}}+(\text{n.d.}).\tag{120}$$

The unitary transformation (62) transforms (120) as follows:

$$\begin{aligned}\delta\bar{\mathscr{H}}_{\mathfrak{f},1} &= G^{-1}[g,\sigma]\delta\bar{\mathscr{H}}_{\mathfrak{f}}G[g,\sigma]\\ &= -\sum_j\tfrac{1}{2}ig\bar{\psi}^{(j)}\gamma_\mu\tfrac{1}{2}(1+\varepsilon_j\gamma_5)(\boldsymbol{\tau}\cdot\mathbf{w}_\mu)\psi^{(j)}+(\text{n.d.}),\\ \delta\bar{\mathscr{H}}_{\mathfrak{b},1} &= G^{-1}[g,\sigma]\delta\bar{\mathscr{H}}_{\mathfrak{b}}G[g,\sigma]\\ &= -g(\partial_\mu\boldsymbol{\pi}\wedge\boldsymbol{\pi}\cdot\mathbf{w}_\mu)+\tfrac{1}{2}g^2(\boldsymbol{\pi}\wedge\mathbf{w}_\mu\cdot\boldsymbol{\pi}\wedge\mathbf{w}_\mu)+(\text{n.d.}),\end{aligned}\tag{121}$$

where $\mathbf{w}_\mu$ is given by (9) with $\mathbf{b}$ having components $(1/\kappa)B^{(1)}$, $(1/\kappa)B^{(2)}$ and $(1/\kappa)B^{(3)}$. The transformation (85) does not change $\mathbf{w}_k$ $(k = 1, 2, 3)$, and therefore does not change (121) either, except for (n.d.) terms. The transformations (92) and (97) replace $A_\mu^{(3)}$ and $(1/\kappa)B^{(3)}$ in $\mathbf{w}_\mu$ by $A_\mu^{(3)\prime}$ and $(1/\kappa')B^{(3)\prime}$:

$$\mathbf{w}_\mu \rightarrow \mathbf{w}'_\mu = \mathbf{w}_\mu[\mathbf{A}_\mu \rightarrow \mathbf{A}_\mu^{(3)\prime},\ (1/\kappa)B^{(3)} \rightarrow (1/\kappa')B^{(3)\prime}]. \tag{122}$$

$A_\mu^{(3)\prime}$ and $(1/\kappa')\ B^{(3)\prime}$ satisfy (99)—(101).

In the following we shall denote, for simplicity, $A_\mu^{(3)\prime}$, $B^{(3)\prime}$ and $\mathbf{w}'_\mu$ by $A_\mu^{(3)}$, $B^{(3)}$ and $\mathbf{w}_\mu$, respectively, and the I-vector with the components $(1/\kappa B^{(1)}, 1/\kappa B^{(2)}, 1/\kappa' B^{(3)\prime})$ by $\mathbf{b}$.

Let us now introduce one more transformation:

$$\Psi_2[\sigma] \rightarrow \Psi_3[\sigma] = T^{-1}[g, \sigma]\Psi_2[\sigma], \tag{123}$$

where

$$T[\rho, \sigma] = \exp\Big[-\tfrac{1}{2}\rho \sum_j \int_\sigma \mathrm{d}\sigma_\mu \bar{\psi}^{(j)} \gamma_\mu \tfrac{1}{2}(1+\varepsilon_j\gamma_5)(\boldsymbol{\tau}\cdot\mathbf{b})\psi^{(j)} + i\rho \int \mathrm{d}\sigma_\mu(\partial_\mu \boldsymbol{\pi} \wedge \boldsymbol{\pi}\cdot\mathbf{b})\Big], \tag{124}$$

or for a flat surface σ

$$T[\rho, \sigma] = \exp\Big[\tfrac{1}{2}i\rho \sum_j \int \mathrm{d}^3x \bar{\psi}^{(j)} \gamma_4 \tfrac{1}{2}(1+\varepsilon_j\gamma_5)(\boldsymbol{\tau}\cdot\mathbf{b})\psi^{(j)} + \rho \int \mathrm{d}^3x(\partial_4 \boldsymbol{\pi} \wedge \boldsymbol{\pi}\cdot\mathbf{b})\Big].$$

Since (124) has nothing to do with $\mathbf{A}_\mu$, we have

$$\begin{aligned} T^{-1}[\rho, \sigma]\mathbf{A}_\mu(x)T[\rho, \sigma] &= \mathbf{A}_\mu(x), \\ T^{-1}[\rho, \sigma]\mathbf{u}_{\mu\nu}(x)T[\rho, \sigma] &= \mathbf{u}_{\mu\nu}(x). \end{aligned} \tag{125a}$$

Furthermore,

$$\begin{aligned} T^{-1}[\rho, \sigma]\mathbf{B}(x)T[\rho, \sigma] &= \mathbf{B}(x), \\ T^{-1}[\rho, \sigma]\psi^{(j)}(x)T[\rho, \sigma] &= \{\tfrac{1}{2}(1+\varepsilon_j\gamma_5)\exp[\tfrac{1}{2}i\rho(\boldsymbol{\tau}\cdot\mathbf{b})] + \tfrac{1}{2}(1-\varepsilon_j\gamma_5)\}\psi^{(j)}(x), \\ T^{-1}[\rho, \sigma]\boldsymbol{\pi}(x)T[\rho, \sigma] &= S(\rho)\boldsymbol{\pi}(x), \\ T^{-1}[\rho, \sigma]\partial_\mu\boldsymbol{\pi}(x)T[\rho, \sigma] &= -\rho S(\rho)(f(-\rho)\partial_\mu\mathbf{b} \wedge \boldsymbol{\pi}) \\ &\qquad + S(\rho)\partial_\mu\boldsymbol{\pi} + (\text{n.d.}) \quad \text{for} \quad x/\sigma. \end{aligned} \tag{125b}$$

We also notice the relation

$$\exp[-\tfrac{1}{2}i\rho(\boldsymbol{\tau}\cdot\mathbf{b})](\boldsymbol{\tau}\cdot\mathbf{a})\exp[\tfrac{1}{2}i\rho(\boldsymbol{\tau}\cdot\mathbf{b})] = (S(-\rho)\mathbf{a}\cdot\boldsymbol{\tau}), \tag{126}$$

with $S(\rho)$ defined by (11). In proving (126), use is made of

$$\tfrac{1}{2}[(\boldsymbol{\tau}\cdot\mathbf{a}), (\boldsymbol{\tau}\cdot\mathbf{c})] = i(\boldsymbol{\tau}\cdot\mathbf{a}\wedge\mathbf{c}), \tag{127}$$

where $\mathbf{a}$ and $\mathbf{c}$ represent two commuting I-vectors.

From (125) and (126) we can obtain

$$T^{-1}[\rho, \sigma]\bar{\psi}^{(j)}\gamma_\mu\tfrac{1}{2}(1+\varepsilon_j\gamma_5)(\boldsymbol{\tau}\cdot\mathbf{a})\psi^{(j)}T[\rho, \sigma] = \bar{\psi}^{(j)}\gamma_\mu\tfrac{1}{2}(1+\varepsilon_j\gamma_5)(\boldsymbol{\tau}\cdot S(-\rho)\mathbf{a})\psi^{(j)}, \tag{128}$$

where **a** stands for an I-vector, which commutes with the operator T. Since $\mathbf{w}_k$ and $\partial_k \mathbf{b}$ $(k = 1, 2, 3)$ commute with T for x/σ, we also have

$$\begin{aligned} T^{-1}[\rho, \sigma]\mathbf{w}_\mu(x)T[\rho, \sigma] &= \mathbf{w}_\mu + (\text{n.d.}), \\ T^{-1}[\rho, \sigma]\partial_\mu \mathbf{b}(x)T[\rho, \sigma] &= \partial_\mu \mathbf{b} + (\text{n.d.}). \end{aligned} \tag{129}$$

Now, the calculations proceed as follows:

$$\begin{aligned} T^{-1}[g, \sigma]&\left\{-i\frac{\delta}{\delta\sigma} + \delta\bar{\mathscr{H}}_{\mathrm{t},1} + \delta\bar{\mathscr{H}}_{\mathrm{b},1}\right\} T[g, \sigma] = -i\frac{\delta}{\delta\sigma} \\ &+ \sum_j \tfrac{1}{2} i \int_0^g \mathrm{d}\rho T^{-1}[\rho, \sigma]\partial_\mu(\bar{\psi}^{(j)}\gamma_\mu \tfrac{1}{2}(1+\varepsilon_j\gamma_5)(\boldsymbol{\tau}\cdot\mathbf{b})\psi^{(j)})T[\rho, \sigma] \\ &- \sum_j \tfrac{1}{2} i g T^{-1}[\rho, \sigma]\bar{\psi}^{(j)}\gamma_\mu \tfrac{1}{2}(1+\varepsilon_j\gamma_5)(\boldsymbol{\tau}\cdot\mathbf{w}_\mu)\psi^{(j)} T[g, \sigma] \\ &+ \int_0^g \mathrm{d}\rho T^{-1}[\rho, \sigma](\partial_\mu \boldsymbol{\pi}\wedge\boldsymbol{\pi}\cdot\partial_\mu\mathbf{b})T[\rho, \sigma] - gT^{-1}[g, \sigma](\partial_\mu\boldsymbol{\pi}\wedge\boldsymbol{\pi}\cdot\mathbf{w}_\mu)T[g, \sigma] \\ &+ \tfrac{1}{2}g^2 T^{-1}[g, \sigma](\boldsymbol{\pi}\wedge\mathbf{w}_\mu\cdot\boldsymbol{\pi}\wedge\mathbf{w}_\mu)T[g, \sigma] + (\text{n.d.}). \end{aligned} \tag{130}$$

The 2nd and 3rd lines in (130) become, by use of (128) and (9),

$$\begin{aligned} &\sum_j \tfrac{1}{2} i m_j \int_0^g \mathrm{d}\rho \bar{\psi}^{(j)}\{\tfrac{1}{2}(1+\varepsilon_j\gamma_5)(1+\alpha_j\tau_3)(\boldsymbol{\tau}\cdot\mathbf{b}) \exp[\tfrac{1}{2}i\rho(\boldsymbol{\tau}\cdot\mathbf{b})] \\ &\quad -\tfrac{1}{2}(1-\varepsilon_j\gamma_5)\exp[-\tfrac{1}{2}i\rho(\boldsymbol{\tau}\cdot\mathbf{b})](\boldsymbol{\tau}\cdot\mathbf{b})(1+\alpha_j\tau_3)\}\psi^{(j)} \\ &\quad -\tfrac{1}{2}ig\sum_j \bar{\psi}^{(j)}\gamma_\mu\tfrac{1}{2}(1+\varepsilon_j\gamma_5)(\boldsymbol{\tau}\cdot\mathbf{A}_\mu)\psi^{(j)} + (\text{n.d.}) \\ &\ = -\sum_j m_j\{\bar{\psi}^{(j)}(1+\alpha_j\tau_3)\psi^{(j)} - T^{-1}[g, \sigma]\bar{\psi}^{(j)}(1+\alpha_j\tau_3)\psi^{(j)}T[g, \sigma]\} \\ &\quad -\tfrac{1}{2}ig\sum_j \bar{\psi}^{(j)}\gamma_\mu\tfrac{1}{2}(1+\varepsilon_j\gamma_5)(\boldsymbol{\tau}\cdot\mathbf{A}_\mu)\psi^{(j)} + (\text{n.d.}), \end{aligned} \tag{131}$$

where use is made of the relation

$$\begin{aligned} \frac{\partial}{\partial\rho}&[T^{-1}[\rho, \sigma]\bar{\psi}^{(j)}(1+\alpha_j\tau_3)\psi^{(j)}T[\rho, \sigma]] \\ &= \tfrac{1}{2}i\bar{\psi}^{(j)}\{\tfrac{1}{2}(1+\varepsilon_j\gamma_5)(1+\alpha_j\tau_3)(\boldsymbol{\tau}\cdot\mathbf{b})\exp[\tfrac{1}{2}i\rho(\boldsymbol{\tau}\cdot\mathbf{b})] \\ &\quad -\tfrac{1}{2}(1-\varepsilon_j\gamma_5)\exp[-\tfrac{1}{2}i\rho(\boldsymbol{\tau}\cdot\mathbf{b})](\boldsymbol{\tau}\cdot\mathbf{b})(1+\alpha_j\tau_3)\}\psi^{(j)}. \end{aligned}$$

The last two lines in (130) become, by use of (125) and (12),

$$\begin{aligned} &g(\partial_\mu\boldsymbol{\pi}\wedge\boldsymbol{\pi}\cdot f(-g)\partial_\mu\mathbf{b}) + \tfrac{1}{2}g^2[(f(-g)\partial_\mu\mathbf{b})\wedge\boldsymbol{\pi}]^2 - g(\partial_\mu\boldsymbol{\pi}\wedge\boldsymbol{\pi})\cdot(\mathbf{A}_\mu + f(-g)\partial_\mu\mathbf{b}) \\ &\quad - g^2(\boldsymbol{\pi}\wedge f(-g)\partial_\mu\mathbf{b})\cdot[\boldsymbol{\pi}\wedge(\mathbf{A}_\mu + f(-g)\partial_\mu\mathbf{b})] + \tfrac{1}{2}g^2(\boldsymbol{\pi}\wedge S(-g)\mathbf{w}_\mu)^2 + (\text{n.d.}) \\ &= -g(\partial_\mu\boldsymbol{\pi}\wedge\boldsymbol{\pi}\cdot\mathbf{A}_\mu) + \tfrac{1}{2}g^2(\boldsymbol{\pi}\wedge\mathbf{A}_\mu\cdot\boldsymbol{\pi}\wedge\mathbf{A}_\mu). \end{aligned} \tag{132}$$

Collecting (119), (130), (131) and (132), we arrive at the following theorem:

THEOREM (III)

The theory with the Lagrangian (115) is equivalent to the one with the interaction Hamiltonian

$$\begin{aligned}\mathscr{H}_3 &= \tfrac{1}{2}g(\mathbf{u}_{\mu\nu}\cdot\mathbf{A}_\mu\wedge\mathbf{A}_\nu)+\tfrac{1}{4}g^2(\mathbf{A}_\mu\wedge\mathbf{A}_\nu\cdot\mathbf{A}_\mu\wedge\mathbf{A}_\nu)\\ &-\sum_j\tfrac{1}{2}ig\bar{\psi}^{(j)}\gamma_\mu\tfrac{1}{2}(1+\varepsilon_j\gamma_5)(\boldsymbol{\tau}\cdot\mathbf{A}_\mu)\psi^{(j)}-g(\partial_\mu\boldsymbol{\pi}\wedge\boldsymbol{\pi}\cdot\mathbf{A}_\mu)+\tfrac{1}{2}g^2(\boldsymbol{\pi}\wedge\mathbf{A}_\mu\cdot\boldsymbol{\pi}\wedge\mathbf{A}_\mu)\\ &-\tfrac{1}{2}\kappa^2\sum_{i=1,2}[U_\mu^{(i)}U_\mu^{(i)}-G^{-1}[\sigma]U_\mu^{(i)}U_\mu^{(i)}G[\sigma]]\\ &-\tfrac{1}{2}\kappa'^2[U_\mu^{(3)}U_\mu^{(3)}-G^{-1}[\sigma]U_\mu^{(3)}U_\mu^{(3)}G[\sigma]] \qquad (133)\\ &-\sum_j m_j[\bar{\psi}^{(j)}(1+\alpha_j\tau_3)\psi^{(j)}-T^{-1}[\sigma]\bar{\psi}^{(j)}(1+\alpha_j\tau_3)\psi^{(j)}T[\sigma]]+(\text{n.d.}).\end{aligned}$$

We now see that as in the theorems (I), (I′), (II) and (II′), all $\mathbf{U}_\mu$'s are replaced by $\mathbf{A}_\mu$'s, except in mass terms of the vector and spinor fields, transformed by G and T respectively, where **B**-field parts still survive and give rise to non-renormalizable interactions.

The above result (133) shows that if all the masses are zero (i.e. $\kappa=\kappa'=m_j=$ $=0$), the theory is invariant under a gauge transformation, which consists of three successive transformations (113), (114) and (123) with Λ instead of **b**.

There is another case in which the equivalence theorem takes as simple a form as the theorem (III). That is, the case of pure vector couplings between the vector field and doublet spinor fields. In this case we can also introduce couplings between ψ and $\boldsymbol{\pi}$ fields. Our Lagrangian is then given by

$$\begin{aligned}\tilde{\mathscr{L}} &= -\tfrac{1}{4}(\mathbf{u}_{\mu\nu}\cdot\mathbf{u}_{\mu\nu})-\tfrac{1}{4}\kappa^2\sum_{i=1,2}u_\mu^{(i)}u_\mu^{(i)}-\tfrac{1}{2}\kappa'^2u_\mu^{(3)}u_\mu^{(3)}\\ &-\sum_j\bar{\psi}^{(j)}[\gamma_\mu\partial_\mu+m_j(1+\alpha_j)]\psi^{(j)}-\tfrac{1}{2}\partial_\mu\boldsymbol{\pi}\cdot\partial_\mu\boldsymbol{\pi}-\tfrac{1}{2}\mu^2\boldsymbol{\pi}\cdot\boldsymbol{\pi}\\ &-\tfrac{1}{2}g(\mathbf{u}_{\mu\nu}\cdot\mathbf{u}_\mu\wedge\mathbf{u}_\nu)-\tfrac{1}{4}g^2(\mathbf{u}_\mu\wedge\mathbf{u}_\nu\cdot\mathbf{u}_\mu\wedge\mathbf{u}_\nu) \qquad (134)\\ &+\sum_j\tfrac{1}{2}ig\bar{\psi}^{(j)}\gamma_\mu(\boldsymbol{\tau}\cdot\mathbf{u}_\mu)\psi^{(j)}+g(\partial_\mu\boldsymbol{\pi}\wedge\boldsymbol{\pi}\cdot\mathbf{u}_\mu)-\tfrac{1}{2}g^2(\boldsymbol{\pi}\wedge\mathbf{u}_\mu\cdot\boldsymbol{\pi}\wedge\mathbf{u}_\mu)\\ &+\sum_j f_j\bar{\psi}^{(j)}O^{(j)}(\boldsymbol{\tau}\cdot\boldsymbol{\pi})\psi^{(j)}+\sum_j f'_j\bar{\psi}^{(j)}O_\mu^{(j)}[\boldsymbol{\tau}\cdot(\partial_\mu\boldsymbol{\pi}+g\mathbf{u}_\mu\wedge\boldsymbol{\pi})]\psi^{(j)},\end{aligned}$$

where

$O^{(j)}=(1+C_1^{(j)}\gamma_5)$ and $O_\mu^{(j)}=\gamma_\mu(1+C_2^{(j)}\gamma_5)$, with $C_1^{(j)}$, $C_2^{(j)}$ c-numbers.

THEOREM (IV)

Theory with the above Lagrangian (134) is equivalent to the one with the following interaction Hamiltonian:

$$\begin{aligned}\mathscr{H}_4 = {} & \tfrac{1}{2}g(\mathbf{u}_{\mu\nu}\cdot\mathbf{A}_\mu\wedge\mathbf{A}_\nu)+\tfrac{1}{4}g^2(\mathbf{A}_\mu\wedge\mathbf{A}_\nu\cdot\mathbf{A}_\mu\wedge\mathbf{A}_\nu)\\ & -\sum_j\tfrac{1}{2}ig\bar{\psi}^{(j)}\gamma_\mu(\boldsymbol{\tau}\cdot\mathbf{A}_\mu)\psi^{(j)}-\sum_j f_j\bar{\psi}^{(j)}O^{(j)}(\boldsymbol{\tau}\cdot\boldsymbol{\pi})\psi^{(j)}\\ & -\sum_j f'_j\bar{\psi}^{(j)}O_\mu{}^{(j)}[\boldsymbol{\tau}\cdot(\partial_\mu\boldsymbol{\pi}+g\mathbf{A}_\mu\wedge\boldsymbol{\pi})]\psi^{(j)} \qquad (135)\\ & -\tfrac{1}{2}\kappa^2\sum_{i=1,2}[U_\mu{}^{(i)}U_\mu{}^{(i)}-G^{-1}[\sigma]U_\mu{}^{(i)}U_\mu{}^{(i)}G[\sigma]]\\ & \qquad\qquad -\tfrac{1}{2}\kappa'^2[U_\mu{}^{(3)}U_\mu{}^{(3)}-G^{-1}[\sigma]U_\mu{}^{(3)}U_\mu{}^{(3)}G[\sigma]]\\ & -\sum_j m_j[\bar{\psi}^{(j)}(1+\alpha_j\tau_3)\psi^{(j)}-V^{-1}[\sigma]\bar{\psi}^{(j)}(1+\alpha_j\tau_3)\psi^{(j)}V[\sigma]]+(\text{n.d.}),\end{aligned}$$

where

$$V[g,\sigma]=\exp\Big[-\tfrac{1}{2}g\sum_j\int d\sigma_\mu\bar{\psi}^{(j)}\gamma_\mu(\boldsymbol{\tau}\cdot\mathbf{b})\psi^{(j)}+ig\int d\sigma_\mu(\partial_\mu\boldsymbol{\pi}\wedge\boldsymbol{\pi}\cdot\mathbf{b})\Big]. \qquad (136)$$

The proof of this theorem is similar to that of theorem (III).

It should be noted that in (135), the mass term of the spinor fields disappears if $\alpha_j = 0$. With this last condition, we can also prove that the current, defined as before, is conserved. If $\kappa = \kappa' = \alpha_j = 0$ (for all j), the theory is invariant under the gauge transformation defined by (113), (114) and (136) with $\boldsymbol{\Lambda}$ instead of **b**.

In the case of pure pseudo-vector coupling between our vector field and ψ-field, we cannot get a simple equivalence theorem. For example, the **b**-field part cannot be decoupled even from the spinor fields ψ, and we are finally left with

$$-\tfrac{1}{2}ig\bar{\psi}\gamma_\mu\gamma_5[S(-g\gamma_5)\mathbf{w}_\mu-f(-g\gamma_5)\partial_\mu\mathbf{b}]\cdot\boldsymbol{\tau}\psi,$$

where the functions S and f are defined in the same way as before.

In practical applications of theorem (III) and (IV), the following relations are very useful

$$\begin{aligned}T^{-1}[\sigma]\bar{\psi}^{(j)}(1+\alpha_j\tau_3)\psi^{(j)}T[\sigma] = {} & \cos y\bar{\psi}^{(j)}(1+\alpha_j\tau_3)\psi^{(j)}\\ & +\tfrac{1}{2}g\frac{\sin y}{y}\bar{\psi}^{(j)}\{\alpha_j(\boldsymbol{\tau}\wedge\mathbf{b})^{(3)}+i\varepsilon_j\gamma_5((\boldsymbol{\tau}\cdot\mathbf{b})+\alpha_j b^{(3)})\}\psi^{(j)},\end{aligned}$$

$$V^{-1}[\sigma]\bar{\psi}^{(j)}(1+\alpha_j\tau_3)\psi^{(j)}V[\sigma]=\bar{\psi}^{(j)}\{1+\alpha_j(S(g)\boldsymbol{\tau})^{(3)}\}\psi^{(j)},$$

with $y=\tfrac{1}{2}g\sqrt{(\mathbf{b}\cdot\mathbf{b})}$. (See also the *Note added in proof*)

7. Discussion

We have shown in the preceding sections that after the transformation we are left with a series of the interactions of the second kind, built up mainly with the B-fields. However, this is not enough to conclude non-renormalizability of the theory, for there still remains a possibility that the divergences, arising from these interactions cancel each other out, so that the whole theory becomes renormalizable.

We can show, however, that such cancellations do not take place in all the cases discussed above. Let us consider, for example, the Hamiltonian (6) with $\kappa = \kappa' \neq 0$, where we have a strict conservation law for the currents. The interactions of the second kind are given, in this case, by

$$\tfrac{1}{2}\kappa^2\{2\mathbf{A}_\mu \cdot (f(g, \mathbf{b})-1)\partial_\mu \mathbf{b}+\partial_\mu \mathbf{b} \cdot (f(-g, \mathbf{b})f(g, \mathbf{b})-1)\partial_\mu \mathbf{b}\}.$$

In order to see how non-renormalizable divergences appear, let us consider the process $A^{(1)}+B^{(1)} \rightarrow B^{(2)}+B^{(2)}$. The radiative correction to this process is possible in the fourth order of g and the highest order divergences comes only from a cross term of $g^2\mathbf{A}_\mu \cdot \alpha^2 \partial_\mu \mathbf{b}$ and $g^2 \partial_\mu \mathbf{b} \cdot \alpha^2 \partial_\mu \mathbf{b}$. The calculation shows that the diverging part is of the form

$$g^4 A_\mu{}^{(1)}\{C_1(\partial_\mu B^{(1)} B^{(2)} B^{(2)}-B^{(1)} B^{(2)} \partial_\mu B^{(2)})+C_0(3\partial_\mu B^{(1)} \partial_\nu B^{(2)} \partial_\nu B^{(2)}$$
$$-\Box B^{(1)} B^{(2)} \partial_\mu B^{(2)}+ \ldots)\}$$

where C_1 and C_0 are quadratically and logarithmically diverging constants, respectively. Other possible diagrams give terms like $g^4 A_\mu{}^{(1)}\{C_0(\partial_\mu B^{(1)} B^{(2)} B^{(2)} -B^{(1)} B^{(2)} \partial_\mu B^{(2)})\}$, which do not cancel the above divergences. Another convenient process is $B^{(1)}+B^{(1)}+B^{(1)} \rightarrow B^{(1)}+B^{(1)}+B^{(1)}$. The highest order divergence in the sixth order of g arises from the third order effect of $g^2 \partial_\mu \mathbf{b} \cdot \alpha^2 \partial_\mu \mathbf{b}$ and is of the form $g^6 C_2 B^{(1)} B^{(1)} B^{(1)} B^{(1)} B^{(1)} B^{(1)}$, where C_2 is a quartically diverging constant. Similar results are also obtained for other processes. Thus, in order to renormalize these divergences, new interactions of the second kind are needed. This is a characteristic feature of non-renormalizable theories.

All results obtained above can be summarized by giving answers to two questions which we have asked in the introduction and whose answers are already evident from our theorems.

Question (i): In the case of Yang-Mills field with non-vanishing masses, the existence of conservation law of the current, with which each field is coupled, does not lead to complete elimination of the B-field part and so the theory is non-renormalizable. It should be noted in this connection that in this case the conservation law follows from the invariance of the theory under some restricted group of gauge transformations. In order for the theory to be invariant under the most general gauge transformations, all the masses should be zero, and if so, the theory becomes renormalizable.

Question (ii): Our theorems (I)—(IV) show that the origin of non-renormalizability is always traced back to mass terms transformed by some unitary transformations (such as G, T and V). As in the case of neutral fields, the mass term is the only agent, which gives rise to non-renormalizability of the theory. We might say, therefore, that whenever we are concerned with the problem of renormalizability, we should necessarily come back to a more profound problem about the origin of masses of elementary particles. Our result may also make us conjecture that in a hypothetical world, in which all elementary particles have no masses, interactions might all be renormalizable.

We have seen in section 5 that as far as parity non-conserving interactions are concerned, our equivalence theorem takes the simplest form only when (i) all spinor source fields have definite handedness ($\varepsilon_j = \pm 1$) and (ii) all source fields have a common, universal coupling constant g. This is actually the case for the intermediate vector particle theory of weak interactions. Thus, we may say that our theorems give further support for such theory.

We should like to acknowledge stimulating discussions with Professor A. Salam and Dr. A. Komar of Imperial College and Dr. A. Visconti of Université d'Aix-Marseille. One of us (H. U.) also wishes to thank Université d'Aix-Marseille for hospitality; the other (S. K.) is indebted to Dr. J. Prentki for the hospitality extended to him at CERN, where during the summer, 1960, part of this work was done.

Note added in proof:

1) It can be seen from the method of proof employed that our equivalence theorems are closely connected with the transformation property of the Lagrangians under the gauge transformation

$$\begin{aligned} &\mathbf{u}_\mu \to \mathbf{u}'_\mu = S(g, \Lambda)(\mathbf{u}_\mu + f(-g, \Lambda)\partial_\mu \Lambda), \\ &\psi \to \psi', \quad \text{etc.,} \end{aligned}$$

with Λ an arbitrary, non-infinitesimal function.

In fact, one can prove, in general, that the **B**-field part of the Yang-Mills field can be eliminated from the gauge-invariant part of the Lagrangian, whereas in the non-gauge invariant part the **B**-field remains, generally, in the form of an exponential type function. Examples of gauge invariant and non-gauge invariant parts are the self-interaction terms and the mass term of the Yang-Mills field.

The detailed discussion on this point will be given in a forthcoming paper by A. Salam and S. Kamefuchi.

2) The reason why the equivalence theorems for the interactions $ig\bar{\psi}\gamma_\mu \frac{1}{2}(a+b\gamma_5)(\boldsymbol{\tau}\cdot\mathbf{u}_\mu)\psi$ (cf. Theorems III, IV) take the simplest form only when (a, $b = \pm 1$) or ($a \neq 0$, $b = 0$) is the following:

The generators for the infinitesimal gauge transformation $\psi \to \psi' = [1+ig \frac{1}{2}(a+b\gamma_5)(\boldsymbol{\tau}\cdot\delta\Lambda)]\psi$ constitute a Lie group only when a and b take the above mentioned values. In fact, for the pure pseudo-vector coupling ($a = 0$, $b \neq 0$) one can show that there does not exist any generator for the finite gauge transformation with an arbitrary gauge function Λ.

References

1) S. Sakata, H. Umezawa and S. Kamefuchi, Prog. Theor. Phys. **7** (1952) 377
2) P. T. Matthews, Phys. Rev. **76** (1949) 1254;
R. J. Glauber, Prog. Theor. Phys. **9** (1953) 295;
S. Kamefuchi and H. Umezawa, Prog. Theor. Phys. **8** (1952) 579
3) S. Glashow, Nuclear Physics **10** (1959) 107;
C. G. Bollini, Nuovo Cim. **14** (1959) 560
4) A. Salam, Nuclear Physics **18** (1960) 681;
S. Kamefuchi, Nuclear Physics **18** (1960) 691
5) C. N. Yang and R. L. Mills, Phys. Rev. **96** (1959) 191
6) A. Komar and A. Salam, Nuclear Physics (to be published)
7) A. Salam and J. C. Ward, Nuovo Cim. **11** (1959) 568
8) H. Umezawa, Quantum field theory (North-Holland Publishing Company, Amsterdam 1956) pp. 183, 228, 229
9) E. C. G. Stueckelberg, Helv. Phys. Acta **11** (1938) 299
10) S. T. Ma, Phys. Rev. **75** (1949) 535
11) S. N. Gupta, Proc. Roy. Soc. **63** (1950) 681;
K. Bleuler, Helv. Phys. Acta **23** (1950) 567
12) T. D. Lee and C. N. Yang, Phys. Rev. **119** (1960) 1410

1.D.3

Nuclear Physics **23** (1961) 430—438; © *North-Holland Publishing Co., Amsterdam*

Not to be reproduced by photoprint or microfilm without written permission from the publisher

ALPHA-DEUTERON MODEL OF THE Li^6 NUCLEUS

T. I. KOPALEISHVILI, I. Sh. VASHAKIDZE, V. I. MAMASAKHLISOV
and G. A. CHILASHVILI

Physical Institute ot the Academy of Sciences of the Georgian Republic, Tbilissi GSSR

Received 13 July 1960

Abstract: The stability conditions are investigated for a system of three protons and three neutrons creating subsystems with four or more nucleons in the form of an α-particle and a deuteron respectively. It is shown that the 3.87 MeV level of the nucleus of Li^6 can be obtained via the transition of a deuteron in the nucleus from a triplet into a single state.

1. Introduction

It is commonly known that every nucleon in a nucleus can be regarded in the first approximation as moving in a certain average field of other nucleons. It has recently been found, however, that a better description of the properties of nuclear matter calls for a more strict analysis of the interaction of nucleons. The recent generalized theory of the nucleus takes account of this interaction through analyzing the collective movements of the entire nucleus, while the many-body theory evolved by Bruckner and Bethe for the nuclear system realizes the next-to-average field approximation through correlated pairs. Yet either theory requires that the number of nucleons in a nucleus should be sufficiently great.

In the case of lighter nucleus composed of just a few nucleons, the collectivity factor is unsuitable and it is not impossible that the effect of interaction will lead, with a certain probability, to the formation of separate yet internally bound "clusters" within the nucleus. In other words, in the case of lighter nuclei one of the possibilities of an analysis of the interaction of nucleons, more precise than the introduction of a general average field with one centre of symmetry, can lie in the assumption that the nucleons within this nucleus form separate clusters with a centre of symmetry in each of them. It is likewise known that temporary associations of nucleons arises mostly in the surface layer of the nucleus. Since the relative role of surface effects increases with the nucleus becoming lighter, it may be expected that these associations of nucleons forming subsystems will be comparatively more stable.

The idea of substructures within atomic nuclei, in the form of deuterons, tritons and α-particles, for example, has recently been attracting the attention of many investigators [1-4]).

It stands to reason that the original supposition that in the nucleus there are α-particles in the form of stable and constant structural units is unacceptable. Yet it is quite possible that nucleons in light nuclei mostly group as α-particles, the composition of these particles constantly changing due to nucleon exchange.

Biel [7]) has calculated the binding energy of the nuclei of Be^8 and C^{12} under this assumption and obtained a satisfactory agreement with experiment by a proper selection of the mixture of Serber and symmetrical forces.

It will be noted, however, that all existing works of this kind deal with the light nuclei of the $4n$ type composed of two, three or four α-particles.

The nucleus composed of two or three nucleons, apart from α-particles, remains unexplored. Is it possible to consider the nucleus of Li^6 in a certain approximation as a system of an α-particle and a deuteron with the resulting assumption that two extra nucleons create a bound system in the form of a deuteron?

Before attempting to answer this question it will be recalled that the very fact that there are no nuclei of He^5 and Li^5 implies that one nucleon will not be bound with the first closed shell composed of two protons and two neutrons forming an α-particle. On the other hand, there exists a stable nucleus of Li^6 composed of two nucleons over the closed shell.

Two assumptions consistent with these facts can be made :(1) a proton and a neutron simultaneously joining an α-particle leads to the spacial destruction of the latter and the formation of a complex system of six nucleons with new bonds; (2) an α-particle is not destroyed in forming the nucleus of Li^6 and binds effectively not with each nucleon separately but with a system of a proton and a neutron as a whole.

The second assumption leads naturally to the conclusion that the proton and the nucleon above the closed shell of the nucleus of Li^6 must form a bound system. If, indeed, these nucleons were independent, the fact that either of them is not bound with the closed shell separately would warrant the conclusion that both of them are not bound with the shell simultaneously, which would mean that the formation of the nucleus of Li^6 is impossible. The fact that the nucleus of Li^6 exists implies therefore that the proton and the neutron in this nucleus are not independent but are in a certain bound state.

Further, it will be shown, that if there is a bond between the two nucleons over the closed shell of the nucleus of Li^6, the Schrödinger equation for the entire nucleus has a solution corresponding to the total negative energy. In this connection the present work analyzes the stability conditions of a system of free protons and free neutrons forming clusters with four or two nucleons, or to put it differently, it analyzes the problem of whether the energy of relative motion of these subsystems possesses a minimum in the region of negative values, and if it does, whether the energy in the minimum of the binding energy of the subsystems corresponds to that determined from the data of mass defects of the nucleus of Li^6.

2. Determination of the Hamiltonian

Following Biel, we assume that the forces between two nucleons and their wave functions alike have a Gaussian form, and we use the conditions of the minimum of energy for a system of six nucleons of the Li^6 nucleus; this system disintegrates into two internally bound clusters in the form of an α-particle and a deuteron, these clusters constantly exchanging nucleons. At the same time we determine a number of parameters characterizing the Li^6 nucleus in its ground and excited states.

Each state of the nucleon will be disignated as a vector $\mathbf{i}(i_1, i_2, i_3)$, where i_1 is the usual nucleon spin and can assume two values 1 or 2, i_2 is the isobaric nucleon spin, also assuming two values 1 or 2, and $i_3 = 1$ or 2 indicates whether the given nucleon belongs to an α-particle or a deuteron. Obviously, we shall have 8 states: (111), (121), (211), (221), (112), (122), (212) and (222). We shall designate them 1, 2, 3, . . . 8, respectively. Six nucleons should be distributed among these states. Without violating the generalization, we can assume that the first four nucleons, for instance, fill the states 1, 2, 3 and 4, forming an α-particle. The other two nucleons will then be distributed among the four states 5, 6, 7 and 8. The number of such distributions is obviously equal to 6, and they correspond to different states of the nuclear deuteron. They will also correspond to the states of the entire Li^6 nucleus since under the assumption, with not very large excitations of the nucleus, the α-particle will always be in the ground state with the total and isobaric spins equal to zero.

If the total and isobaric spins of Li^6 nucleus are designated through S and T, their projections through M_S and M_T, then the following states should correspond to the above mentioned six designations:

$$S = 1, \quad T = 0, \quad M_S = 0, \pm 1 \quad \text{and} \quad S = 0, \quad T = 1, \quad M_T = 0, \pm 1.$$

The former three of them correspond to the normal state of the deuteron and determine the ground state of the Li^6 nucleus, whereas the latter three states correspond to the singlet state of a nucleon pair. We suppose that the singlet state of a nucleon pair forming a deuteron ($S = 0$, $T = 1$, $M_T = 0$) determines one of the excited levels of the nucleus of Li^6. As for the other two states ($S = 0$, $T = 1$ and $M_T = \pm 1$) they describe the energy of the isobaric nuclei Be^6 and He^6. Assigning the total moment of the Li^6 nucleus to the deuteron spin, we thereby assume that the orbital moment of the relative motion of the deuteron and the α-particle is equal to 0 both in the ground and excited states considered above.

The antisymmetrized wave functions $\Psi = \Psi^{ST}_{M_S M_T}$ corresponding to the assigned values S, T, M and M_T will be written as

$$\Psi^{10}_{10} = \sum_{\mathrm{P}} \pm \mathrm{P} \alpha^1_{11} \alpha^2_{12} \alpha^3_{21} \alpha^4_{22} \alpha^5_{11} \alpha^6_{12} \Psi(1234; 56) \tag{1}$$

and

$$\Psi_{01}^{01} = \sum_{\mathrm{p}} \pm \mathrm{p}\alpha_{11}^{1}\alpha_{12}^{2}\alpha_{21}^{3}\alpha_{22}^{4}\alpha_{11}^{5}\alpha_{21}^{6}\,\Psi(1234;\,56), \tag{2}$$

where $\alpha_{i_1 i_2}^{f}$ are the products of the spin and isospin wave functions of the nucleon f with the fixed values i_1 and i_2; Ψ (1234; 56) is the spacial part of the Li^6 nucleus wave function in which the first four subscripts correspond to the nucleons in the α-particle and the last two to those forming the deuteron; summation is performed over all permutations p of the superscripts, the sign being determined by the parity of the respective permutation. It will be pointed out that we have not adduced the expression for the other four functions $\Psi_{ST}^{M_S M_T}$ since they are not used for calculating the energy of the system.

Neglecting the Coulomb interactions of protons we obtain for the total Hamiltonian of the system

$$\hat{H} = -\tfrac{1}{4}\hbar^2\left(\frac{1}{M_{\mathrm{n}}} + \frac{1}{M_{\mathrm{p}}}\right)\sum_{i} \nabla_i^2 + \sum_{i>j} V(i,j), \tag{3}$$

where M_{n} and M_{p} are the masses of the neutron and the proton respectively, $V(i,j)$ is given by

$$V(ij) = \mathscr{P}_{ij}F(ij) = (W + BP_{ij}^{\sigma} - \mathscr{H}P_{ij}^{\tau} - MP_{ij}^{\sigma}P_{ij}^{\tau})F(ij), \tag{4}$$

P_{ij}^{σ} and P_{ij}^{τ} being the exchange operators of Bartlett and Heisenberg; W, B, $\mathscr{H}$ and M are the contributions to the energy of interaction made by the forces of Wigner, Bartlett, Heisenberg and Majorana, respectively, and $F(ij)$ is the radial part of nucleon-nucleon interaction.

The problem is to calculate the mean value of energy

$$E = \frac{\int \Psi^* \hat{H} \Psi \mathrm{d}\tau}{\int \Psi^* \Psi \mathrm{d}\tau} \tag{5}$$

through minimizing it with respect to a parameter in Ψ. To obtain the energy in the ground state we must put $\Psi = \Psi_{01}^{01}$, while $\Psi = \Psi_{10}^{10}$ will determine the energy (close to the energy of the isobaric nuclei of He^6 and Be^6) of an excited state of the Li^6 nucleus with the moment 0^+.

As was indicated above, the potential between two nucleons as well as the spacial wave function of the system is taken in the Gaussian form, i.e.,

$$\Psi(1234;\,56) = \exp\{-\tfrac{1}{2}\lambda s_{12}^2 - \tfrac{1}{2}\mu \sum_{i>j}^{4} r_{ij}^2 - \tfrac{1}{2}\nu r_{56}^2\} \tag{6}$$

and

$$F(ij) = V_0 \exp(-\beta r_{ij}^2), \tag{7}$$

where $\mathbf{r}_{ij} = \mathbf{r}_i - \mathbf{r}_j$ is the vector radius between the centres of the α-particle and the deuteron, V_0, β are taken from the data on nucleon —α-particle scattering and are given by [8]) $V_0 = -45$ MeV, $\beta = 0.2657\times 10^{26}$ cm^{-2}; μ is determined from the binding energy of the α-particle and is equal to $\mu = 0.3156\times 10^{26}$ cm^{-2}, whereas λ is a varying parameter determining the equilibrium distance between the centres of the α-particle and the deuteron. The coefficient ν, which is the parameter of the test function of a system of two nucleons 5 and 6, forming a deuteron in a triplet state, is determined from the condition that the energy of this system has a minimum at the fixed values V_0 and β. From this condition it follows that $\nu = 0.1501\times 10^{26}$ cm^{-2}.

It will be noted that the binding energy of the system of nucleons 5 and 6 at this value of ν proves to be negative and numerically equal to 0.41 MeV. Thus, the values of the parameters μ, ν, V_0 and β we have chosen lead to the bound stable states of He^4 and He^2, the binding energy being equal to 27 MeV for the α-particle and 0.41 MeV for the deuteron, instead of the experimental values of 28.1 MeV and 2.2 MeV for free α-particle and deuteron.

We could have obtained a better agreement with experiment with respect to the nucleon-deuteron binding energy with a slight change in the α-particle binding energy but that would have made us take a value for μ different from what we have used in ref. [8]). Yet since we are interested not in the total energy of the Li^6 nucleus, but merely in the difference $\mathscr{E}(Li^6) = \mathscr{E}(\alpha) - \mathscr{E}(H^2)$, which yields a relative energy of the α-particle and the deuteron, the precise magnitude of $\mathscr{E}(H^2)$ is of no essential importance. At the same time it can be shown that a change of the deuteron binding energy within the limits under consideration has no appreciable effect on the position of the energy minimum of the α-particle and deuteron relative motion.

3. Numerical Calculation of the Energy Minimum

Finding the energy minimum analytically does not seem to be possible, since the relevant expressions are too involved. Therefore, we used a numerical method.

Fig. 1 represents the energy curves for the ground state of Li^6. Curve 1 corresponds to the Serber forces and curve 2 to the symmetrical forces, the difference $E(\lambda) - E(0)$ being marked off on the axis of the ordinates (where $E(0)$ is the energy of the system when the α-particle and the deuteron approach infinity).

It can be seen that these curves actually have minima, which shows that the above nucleon configuration in the nucleus of Li^6 is stable, the minimum of energy existing at the same value $\lambda = 0.0316\times 10^{26}$ cm^{-2} in either case. The corresponding values of energy are 1.58 MeV for the Serber forces and 1.42 MeV for the symmetrical forces.

In considering the problem of Be^8 and C^{12} Biel has obtained better agreement with experiment under the assumption that the total nucleon-nucleon interaction consists of a mixture of Serber and symmetric.[1] forces with the weights 0.7 and 0.3 respectively. If we accept the same mixture in our case, the result in energy dependence on the λ parameter assumes the form represented in fig. 2. The energy of the minimum is in this case equal to 1.52 MeV, which is in good agreement with the experimental value of the deuteron binding with the α-particle in the nucleus of Li^6 found from the data on mass defects to be equal to 1.48 MeV. The equilibrium distance equal to 2.52×10^{-13} cm^{-2} between the centres of the α-particle and the deuteron corresponds to $\lambda = 0.0316 \times 10^{26}$ cm^{-2}. Thus it can be seen that the centres of gravity of the clusters in the nucleus of Li^6 are appreciably shifted with respect to each other, the distance between them exceeding their radii.

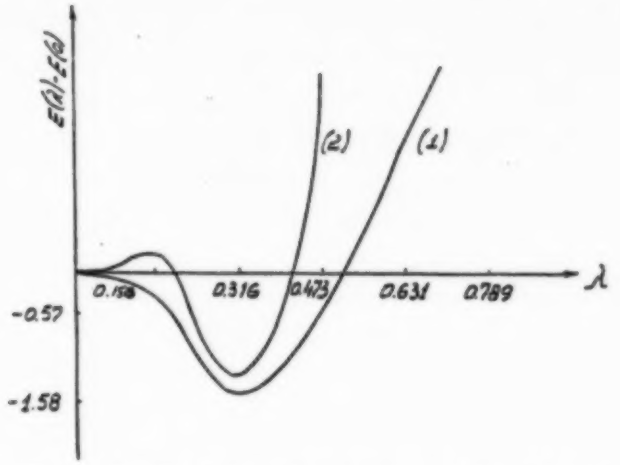

Fig. 1. Energy curves for the ground state of Li^6.

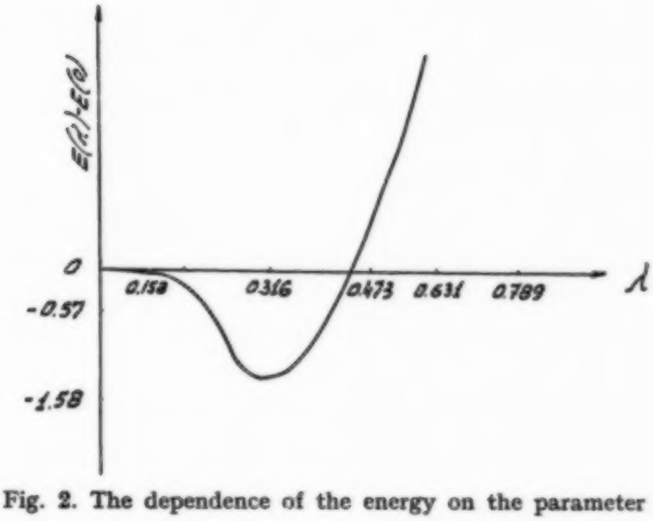

Fig. 2. The dependence of the energy on the parameter λ.

Let us now turn to the excited state of the Li^6 nucleus. According to our model, this state may arise, in general, as a result of the excitation of an α-

particle, a deuteron and their relative motion. Yet it is well known that the α-particle has no bound states with an excitation energy lower than 20 MeV, and therefore the levels of the Li^6 nucleus observed experimentally and lying below 20 MeV cannot be caused by the excitation of the α-particle.

The wave function $\Psi^{01}_{0M_T}$ corresponds to the state of the Li^6 nucleus with $S = 0$ and $T = 1$. In the spectrum of the Li^6 nucleus the level with $T = 1$, a component of the isobaric triplet ($M_T = 0$) has an energy of 3.57 MeV [9]). The other components of the isobaric triplet ($M_T = \pm 1$) correspond to the ground states of the nuclei of He^6 and Be^6. Since the spin 0^+ corresponds to this level, the transition from the ground state with the moment 1^+ into the excited state under consideration can in our model occur only through the transition of the deuteron from a triplet into a singlet state. In this transition account should also be taken of the possibility of some change in the mean energy of relative motion. Therefore the total change of energy will consist of two parts, one of which being conditioned by a change in the binding energy within the deuteron and the other by a change in the relative motion energy.

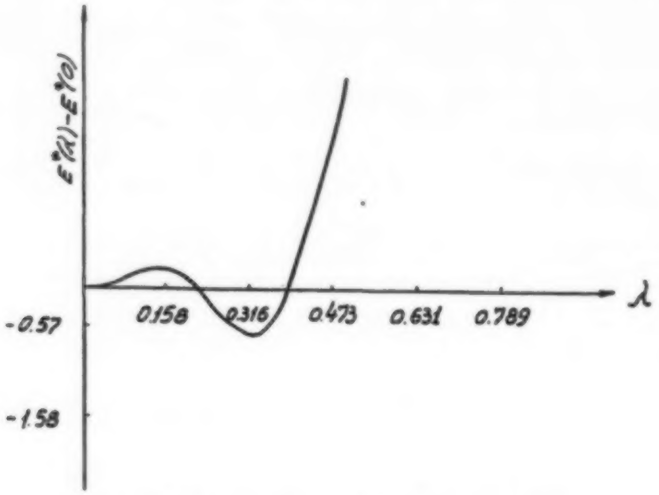

Fig. 3. The dependence of $E^*(\lambda)-E^*(0)$ on λ.

Fig. 3 describes the dependence of the difference of relative motion energy $E^*(\lambda)-E^*(0)$ on the parameter λ for the case of mixed Serber and symmetrical forces. This curve also has a minimum, the energy at the minimum being equal to 0.66 MeV. Since the energy of relative motion at the minimum in the ground state is equal to 1.52 MeV, the change of this energy in the transition under consideration will amount to 0.86 MeV.

As for the energy increase due to the change of the deuteron spin state, it proves to be equal to 3.91 MeV, according to our calculations. Thus, the total energy of the excitation of the Li^6 nucleus in the transition into the state $S = 0$ and $T = 1$ amounts to 4.77 MeV. This quantity differs somewhat from the experimental energy value of the respective level equal to 3.57 MeV.

It will be noted that if we had assumed the experimental value of 2.23 MeV for the increase of the deuteron energy when the spin state alone changes, the total excitation energy would have proved equal to 3.1 MeV, which would warrant the conclusion of more or less satisfactory agreement with experiment. Consequently, the experimental discrepancy is rather insignificant considering the approximate character of our calculations, and reduces to the discrepancy between the increase in the deuteron internal energy and experiment as the deuteron passes into a single state.

This discrepancy can probably be accounted for by the fact that we used the same value β for both ground and excited states, and changed only the depth of nucleon-nucleon interaction for a singlet state by a factor 0.6. Actually the value β for a singlet state differs widely from that for a triplet state. We had to neglect this fact since a consistent registration of the changes of β in passing over from a triplet into a singlet state, is in our calculations due to the potential energy of exchange integrals in the expression. Therefore the coefficient β throughout our calculations was assigned a certain average value obtained from experimental data on nucleon α-particle scattering. As is clear from the present paper, this value of β, together with $V_0 = -45$ MeV, ensures the stability of the He^4 nucleus and yields the correct value for its binding energy.

The mean value of the coefficient used in the present paper differs little from its true value in a deuteron triplet state, and therefore the transition to a mean value should have no appreciable effect on our calculations involving the ground state of the Li^6 nucleus. As for the excited state, this transition can result in an appreciable error since the value of the coefficient β in a singlet state sharply differs from its value in a triplet state. It is this error, in our opinion, that leads to our obtaining the value 4.77 MeV for the excitation energy instead of 3.57 MeV as experimentally observed.

It is possible that a slight rise of the curves in figs. 1 and 3 in the vicinity of the origin of the coordinate is also due to the inaccuracy of the choice of the value of the coefficient β.

The following points should be made concerning the results obtained above.

In refs. [10, 11]) it is pointed out that the wave function of the nucleus of the $4n$ type built up according to the α-particle model is identical, on antisymmetrizing over all nucleons, to the wave function written in the one-particle approximation. It can be seen, however, that this identity arises only if in certain wave functions related to both the internal state of α-particles and their relative motion, the respective parameters of the oscillating functions coincide with and are equal to the parameter in the wave function of one-particle approximation. In the work by Biel quoted above the parameter in the wave function describing the relative motion in the α-particles in the nucleus of Be^8 is regarded as vibrational; it is proved by applying the energy minimum condition, that this parameter is not equal to one describing the internal state of the α-particles. In the case of the Li^6 nucleus too, the parameters in the wave function for the internal states of the α-particle and the deuteron, as well as for their relative motion differ, as can be seen from eq. (6). It can be concluded therefore that our argument p reserves a certain individuality for the α-particle and the deuteron in the nucleus of Li^6 and is not identical to the description of this nucleus in the one-particle approximation.

References

1) V. I. Mamasakhlisov, JETP **24** (1953) 190; Proc. of the Physics Institute of the Academy of Sciences of the Georgian SSR, **3** (1955) 31
2) P. Cuere and G. Combe, C. R. **239** (1954) 351
3) A. Herzenberg, Nuovo Cim. **986** (1955) 1008; Nuclear Physics **3** (1957) 1
4) L. T. Schiff, Phys. Rev. **98** (1955) 1281
5) V. N. Ostroumov and P. A. Filov, JETP **37** (1959) 643
6) I. Sh. Vashakidze and G. A. Chilashvili, JETP **29** (1954) 157
7) S. T. Biel, Proc. Phys. Soc. A **70** (1957) 866
8) S. Hochberg, H. S. W. Massey and L. H. Underhill, Proc. Phys. Soc. A **67** (1954) 957
9) F. Ajzenberg and T. Lauritsen, Rev. Mod. Phys. **27** (1955) 77
10) T. K. Perring and T. H. R. Skyrme, Proc. Phys. Soc. **69** (1956) 69
11) K. Wildermuth and Th. Kanellopoulos, Nuclear Physics **7** (1958) 150; Nuclear Physics **9** (1959) 9

8.C

Nuclear Physics **23** (1961) 439—451; © *North-Holland Publishing Co., Amsterdam*

Not to be reproduced by photoprint or microfilm without written permission from the publisher

ON THE STRUCTURE OF THE FOUR POINT FUNCTIONS IN HEISENBERG'S NON LINEAR SPINOR THEORY

E. MONTALDI †

Max-Planck-Institut für Physik und Astrophysik München, Germany

Received 6 October 1960

Abstract: The vacuum expectation value of a product of four Fermi field operators is investigated within the framework of Heisenberg's non linear spinor theory of elementary particles. It is shown that a spectral representation still enjoying all the symmetry properties of the fundamental equation can be constructed. This representation is characterized by only two independent mass spectra, which satisfy various symmetry requirements. Their connection with the mass spectrum of the two point function is also briefly discussed.

1. Introduction

In recent years, the study of the vacuum expectation values of products of Heisenberg field operators has gained an ever increasing importance. After the pioneer work by Källén, Lehmann and Wightman [1]), many articles have been published, devoted either to the investigation of the analytic properties of these v.e.v., or to the problem of obtaining for them suitable spectral representations, starting from general requirements only (Lorentz-invariance, microcausality, existence of a complete system of "physical" eigenvectors of the energy-momentum operator P_μ in Hilbert space). While, for the scalar case, the situation has been remarkably clarified, comparatively little work has been done concerning the v.e.v. of a product of $n > 2$ Fermi field operators. The presence of spinor indices constitutes, as one easily sees, the greatest source of complications, since they imply a great deal of algebraic work ††. Only by choosing specific cases, characterized by a large number of symmetry properties, one can hope to obtain reasonably simple spectral formulae. In connection with this point, it seems to us useful to undertake an investigation of the problem of the four point functions in Heisenberg's non linear spinor theory of elementary particles, where the fundamental equation shows remarkable invariance properties with respect to various transformation groups. This is the purpose of the present work, which has to be regarded as mainly algebraic in nature. In sect. 2 we show that it is possible to construct, for these functions, a spectral representation still enjoying all the symmetry properties of the fundamental equation †. This representation involves only two independent mass spectra, each of which is a function of six auxiliary masses, and satisfies various symmetry conditions. In sect. 3, the properties of these spectra are investigated in connection with the differential equation for the ψ operator, and with the indefinite metric quantization procedure underlying the whole theory. The problem of their physical interpretation, however, remains — at least for the moment — rather obscure.

---

† On leave of absence from Istituto Nazionale di Fisica Nucleare, Milano, Italy. The financial support of Consiglio Nazionale delle Ricerche, Rome, is gratefully acknowledged.

†† Already in the case of the v.e.v. of a product of two Fermi field operators, one has—assuming only invariance with respect to continuous Lorentz transformations—spectral representations involving four independent mass spectra.

2. Derivation of the Spectral Formula

We first remark that, in our case, the only v.e.v.s. that we need to consider are those containing two ψ and two $\bar{\psi}$ operators; due to gauge invariance, the remaining ones vanish identically. Assuming first a specified order of the operators (we shall later remove this restriction by means of the chronological ordering symbol), we consider

$$\langle \underset{\alpha}{x_1}\underset{\beta}{x_2}\underset{\lambda}{\bar{x}_3}\underset{\mu}{\bar{x}_4}\rangle_0 = \langle \psi_\alpha(x_1)\psi_\beta(x_2)\bar{\psi}_\lambda(x_3)\bar{\psi}_\mu(x_4)\rangle_0 . \tag{1}$$

According to Lehmann's well known procedure, we write

$$\langle \underset{\alpha}{x_1}\underset{\beta}{x_2}\underset{\lambda}{\bar{x}_3}\underset{\mu}{\bar{x}_4}\rangle_0 = \sum_{k_1,k_2,k_3} \langle 0|\psi_\alpha(x_1)|k_1\rangle\langle k_1|\psi_\beta(x_2)|k_2\rangle\langle k_2|\bar{\psi}_\lambda(x_3)|k_3\rangle\langle k_3|\bar{\psi}_\mu(x_4)|0\rangle, \tag{2}$$

where the kets $|k_j\rangle$ constitute a complete set of eigenvectors of the energy-momentum operator P_μ, whose eigenvalues lie in the forward light cone,

$$P_\mu|k_j\rangle = k_{j,\mu}|k_j\rangle, \quad k_j^2 < 0, \quad k_{j,0} \geqq 0 \tag{3}$$

(other variables, which serve to specify completely the state $|k_j\rangle$, are not explicitly indicated). From

$$\begin{aligned} \langle k_1|\psi_\alpha(x)|k_2\rangle &= c^\alpha_{k_1k_2}\mathrm{e}^{i(k_2-k_1)\cdot x}, \\ \langle k_1|\bar{\psi}_\alpha(x)|k_2\rangle &= \langle k_2|\psi_\beta(x)|k_1\rangle^*\gamma_{4,\beta\alpha} = \bar{c}^\alpha_{k_2k_1}\mathrm{e}^{i(k_2-k_1)\cdot x}, \end{aligned} \tag{4}$$

it follows that

$$\langle \underset{\alpha}{x_1}\underset{\beta}{x_2}\underset{\lambda}{\bar{x}_3}\underset{\mu}{\bar{x}_4}\rangle_0 = \sum_{k_1k_2k_3} c^\alpha_{0k_1}c^\beta_{k_1k_2}\bar{c}^\lambda_{k_2k_3}\bar{c}^\mu_{0k_3}\mathrm{e}^{ik_1\cdot(x_1-x_2)+ik_2\cdot(x_2-x_3)+ik_3\cdot(x_3-x_4)}. \tag{5}$$

---

† In a paper by Heisenberg and coworkers [2]) the supposition has been made that, when going from the two point functions to those of a higher order, the total symmetry is gradually lost. Our results, however, show that — at least for the four point functions — this seems not necessarily to be the case.

Now, consider

$$\sum c^{\alpha}_{0k_1} c^{\beta}_{k_1k_2} \bar{c}^{\lambda}_{k_3k_2} \bar{c}^{\mu}_{0k_3}$$

(the sum being extended over all states belonging to fixed values of k_1, k_2 and k_3); by relativistic invariance arguments, we are led to write for this quantity an expression of the form

$$\begin{aligned}\sum c^{\alpha}_{0k_1} c^{\beta}_{k_1k_2} \bar{c}^{\lambda}_{k_3k_2} \bar{c}^{\mu}_{0k_3} = \sum_A \sum_B \{(AC^{-1})_{\alpha\beta}(CB)_{\lambda\mu} f_{AB}(k_1, k_2, k_3)\\ +A_{\alpha\lambda} B_{\beta\mu} g_{AB}(k_1, k_2, k_3)+A_{\alpha\mu} B_{\beta\lambda} h_{AB}(k_1, k_2, k_3)\},\end{aligned} \tag{6}$$

where A and B run independently through the sixteen elements of the Dirac algebra. C (see eq. (25″)) is the charge conjugation matrix †. f, g, h are certain functions of k_1, k_2, k_3, different from zero (compare eq. (3)) only if their arguments all lie in the forward light cone. To express this last fact, we adopt a procedure due to V. N. Gribov [4]), the main lines of which we shall now explain. According to this method, one introduces a suitable factor, depending on k_1, k_2, k_3 as well as a number of auxiliary variables, in such a way that it is different from zero only if k_1, k_2, k_3 all belong to the forward light cone. The quantities f, g and h are then expressed in terms of this factor, multiplied by certain functions of the auxiliary variables and integrated (with respect to these variables) over a certain range. In our case (bearing in mind the structure of the r.h.s. of (6)) a simple extension of the argument given by Gribov (where one considers the v.e.v. of a product of three scalar field operators) leads for the above mentioned factor to the following expression ††:

$$\begin{aligned}&R_{\alpha_1\ldots\alpha_n}(k_1, k_2, k_3; m_1, \ldots, m_6)\\ &= -(2\pi)^{-18}\int d^4k_4 d^4k_5 d^4k_6 \delta((k_1-k_4-k_5)^2+m_1^2)\delta(k_4^2+m_2^2)\delta(k_5^2+m_3^2)\\ &\times\delta(k_6^2+m_4^2)\delta((k_2-k_4-k_5-k_6)^2+m_5^2)\delta((-k_2+k_3+k_4+k_6)^2+m_6^2)\\ &\quad\Theta(k_1-k_4-k_5)\Theta(k_4)\Theta(k_5)\Theta(k_6)\Theta(k_2-k_4-k_5-k_6)\\ &\quad\Theta(-k_2+k_3+k_4+k_6)P_{\alpha_1\ldots\alpha_n}(k_1, \ldots, k_6).\end{aligned} \tag{7}$$

Here, $\alpha_1, \ldots, \alpha_n$ are vector indices, and $P_{\alpha_1\ldots\alpha_n}(k_1, \ldots, k_6)$ is a polynomial (of the n^{th} degree) in the components of $k_1, \ldots, k_6$. For example, if we isolate in (6) the term with $A \equiv B \equiv I$ (I being the 4×4 unity matrix), then the corresponding R factor has no indices, and $P \equiv 1$; if $A \equiv B \equiv \gamma_\mu$, then the corresponding R factor has a vector index, and P depends linearly on the components of $k_1, \ldots, k_6$; and so on. Before we proceed further, we remember now that, for our purposes, we need not consider all the $3 \times 16^2 = 768$ terms contained at r.h.s. of (6); we want, indeed, that the v.e.v. (1) be invariant with respect to certain symmetry operations, and this implies that only a small part of the total number of terms must actually be looked at. In this connection we note that a first, very efficient selection, results from the imposition on the v.e.v. (1) of the invariance with respect to the Touschek transformation ($\psi \to e^{i\eta\gamma_5}\psi$, $\bar{\psi} \to \bar{\psi}\, e^{i\eta\gamma_5}$); that is

---

† The insertion of the matrices C^{-1} and C in the first term at r.h.s. of (6) is necessary in order to secure the correct transformation properties [3]).

† The fact that R is different from zero only if k_1, k_2, k_3 all lie in the forward light cone is, as one can easily see, a simple consequence of the δ and Θ functions appearing in the integrand. Here, the step-function $\Theta(x)$ is defined by $\Theta(x) = 1$ when $x > 0$ and $\Theta(x) = 0$ when $x < 0$. The apparently complicated structure of the R factor choosen above is justified by the very simple expression that follows from it when, by Fourier transformation, one goes from momentum space over to ordinary space-time.

$$\langle \underset{\alpha}{x_1}\underset{\beta}{x_2}\underset{\lambda}{\bar{x}_3}\underset{\mu}{\bar{x}_4}\rangle_0 = (e^{i\eta\gamma_5})_{\alpha\tau}(e^{i\eta\gamma_5})_{\beta\nu}(e^{i\eta\gamma_5})_{\sigma\lambda}(e^{i\eta\gamma_5})_{\rho\mu}\langle \underset{\tau}{x_1}\underset{\nu}{x_2}\underset{\sigma}{\bar{x}_3}\underset{\rho}{\bar{x}_4}\rangle_0 . \tag{8}$$

Indeed, it is easily seen that only the following combinations enjoy the required property:

$$\begin{array}{ll}
(\gamma_{\nu'}C^{-1})_{\alpha\beta}(C\gamma_{\nu''})_{\lambda\mu}R_{\nu'\nu''}, & (\gamma_5\gamma_{\nu'}C^{-1})_{\alpha\beta}(C\gamma_{\nu''}\gamma_5)_{\lambda\mu}R_{\nu'\nu''},\\
(\gamma_{\nu'}C^{-1})_{\alpha\beta}(C\gamma_{\nu''}\gamma_5)_{\lambda\mu}R_{\nu'\nu''}, & (\gamma_5\gamma_{\nu'}C^{-1})_{\alpha\beta}(C\gamma_{\nu''})_{\lambda\mu}R_{\nu'\nu''},\\
(\gamma_{\nu'})_{\alpha\lambda}(\gamma_{\nu''})_{\beta\mu}R_{\nu'\nu''}, & (\gamma_5\gamma_{\nu'})_{\alpha\lambda}(\gamma_5\gamma_{\nu''})_{\beta\mu}R_{\nu'\nu''},\\
(\gamma_{\nu'})_{\alpha\lambda}(\gamma_5\gamma_{\nu''})_{\beta\mu}R_{\nu'\nu''}, & (\gamma_5\gamma_{\nu'})_{\alpha\lambda}(\gamma_{\nu''})_{\alpha\mu}R_{\nu'\nu''},\\
(\gamma_5\gamma_{\nu'})_{\alpha\mu}(\gamma_5\gamma_{\nu''})_{\beta\lambda}R_{\nu'\nu''}, & (\gamma_{\nu'})_{\alpha\mu}(\gamma_5\gamma_{\nu''})_{\beta\lambda}R_{\nu'\nu''},\\
(\gamma_5\gamma_{\nu'})_{\alpha\mu}(\gamma_{\nu''})_{\beta\lambda}R_{\nu'\nu''}, & (\gamma_{\nu'})_{\alpha\mu}(\gamma_{\nu''})_{\beta\lambda}R_{\nu'\nu''}.
\end{array} \tag{9}$$

In each of these, the term $P_{\nu'\nu''}$ is a product of two linear combinations of the components $k_{j,\mu}(j = 1, \ldots, 6;\ \mu = \nu', \nu'')$. If, moreover, we require invariance with respect to the parity operation also ($\psi(\mathbf{x}, t) \to \gamma_4\psi(-\mathbf{x}, t)$), that is (with $\hat{x} = (-\mathbf{x}, t)$)

$$\langle \underset{\alpha}{x_1}\underset{\beta}{x_2}\underset{\lambda}{\bar{x}_3}\underset{\mu}{\bar{x}_4}\rangle_0 = \gamma_{4,\alpha\nu}\gamma_{4,\beta\eta}\gamma_{4,\sigma\lambda}\gamma_{4,\rho\mu}\langle \underset{\nu}{\hat{x}_1}\underset{\eta}{\hat{x}_2}\underset{\sigma}{\hat{\bar{x}}_3}\underset{\rho}{\hat{\bar{x}}_4}\rangle_0 \tag{10}$$

then, of the 12 terms written above, only those containing no γ_5, and those containing two times γ_5, survive, while the remaining six must be ruled out. After these important simplifications, we now come back to the problem of the representation of the spectral functions f, g and h appearing at r.h.s. of (6). According to what we said above, we write these functions in the form

$$f^{(1)}_{AB}(k_1, k_2, k_3) = \int (\mathrm{dm}) R_{AB}(k_1, k_2, k_3; m_1, \cdots, m_6) F^{(1)}_{AB}(m_1^2, \ldots, m_6^2). \tag{11}$$

Here, $\int(\mathrm{d}m)$ is a shorthand notation for $\int_0^\infty \mathrm{d}(m_1^2) \ldots \int_0^\infty \mathrm{d}(m_6^2)$. The upper index (1) means that, in the v.e.v. we are considering, the four field operators have the order $\psi\psi\bar{\psi}\bar{\psi}$; obviously, formulae like (11) hold for g and h also. If we now substitute (6) (taking into account eq. (11), and its analogues for g and h) into (5), convert the sums over k_1, k_2, k_3 into four-dimensional integrals, and perform the following variables transformation:

$$\begin{aligned} p_1 &= k_1 - k_4 - k_5, \quad p_2 = k_4, \quad p_3 = k_5, \quad p_4 = k_6, \\ p_5 &= k_2 - k_4 - k_5 - k_6, \quad p_6 = -k_2 + k_3 + k_4 + k_6, \end{aligned} \tag{12}$$

we find that the result can be expressed in terms of Schwinger's well known invariant functions

$$\Delta^{(\pm)}(x; m) = \mp \frac{i}{(2\pi)^3} \int \mathrm{d}^4 p e^{ip \cdot x} \delta(p^2 + m^2) \Theta(\pm p_0), \tag{13}$$

and of other functions, which we define as follows:

$$K_0{}^{(\pm)}(x) = \gamma \frac{\partial}{\partial x} \Delta^{(\pm)}(x),\ K_{-1}^{(\pm)}(x) = \gamma C^{-1} \frac{\partial}{\partial x} \Delta^{(\pm)}(x),\ K_1{}^{(\pm)}(x) = C\gamma \frac{\partial}{\partial x} \Delta^{(\pm)}(x), \tag{14}$$

$$H_0{}^{(\pm)}(x) = \gamma_5 K_0{}^{(\pm)}(x), \quad H_{-1}^{(\pm)}(x) = \gamma_5 K_{-1}^{(\pm)}(x), \quad H_1{}^{(\pm)}(x) = K_1{}^{(\pm)}(x) \gamma_5. \tag{15}$$

It is convenient to put

$$\begin{gathered} y_{rs} = x_r - x_s, \\ \Delta^{(+)}(y_{12}; m_1) \Delta^{(+)}(y_{13}; m_2) \Delta^{(+)}(y_{14}; m_3) \Delta^{(+)}(y_{23}; m_4) \\ \Delta^{(+)}(y_{24}; m_5) \Delta^{(+)}(y_{34}; m_6) = \prod_{r<s;\, k} \Delta^{(+)}(y_{rs}; m_k), \end{gathered}$$

and introduce the notation $\prod_{r<s;\,k}^{(i,\,j,\,\ldots)} \Delta^{(+)}(y_{rs}; m_k)$ to denote that, in the product of the six $\Delta^{(+)}$ functions, the terms with $k = i, j, \ldots$, must be ruled out. Then, we have:

$$\begin{aligned} \langle \underset{\alpha}{x_1} \underset{\beta}{x_2} \underset{\lambda}{\bar{x}_3} \underset{\mu}{\bar{x}_4} \rangle_0 & \\ = \int (\mathrm{d}m) & K_{-1,\,\alpha\beta}^{(+)}(y_{12}; Km_1)_{1,\,\lambda\mu}^{(+)}(y_{34}; m_6) \prod_{r<s;\,k}^{(1,\,6)} \Delta^{(+)}(y_{rs}; m_k) M_1{}^{(1)}(1 \ldots 6) \\ + \int (\mathrm{d}m) & K_{0,\,\alpha\lambda}^{(+)}(y_{13}; m_2) K_{0,\,\beta\mu}^{(+)}(y_{24}; m_5) \prod_{r<s;\,k}^{(2,5)} \Delta^{(+)}(y_{rs}; m_k) M_2{}^{(1)}(1 \ldots 6) \\ + \int (\mathrm{d}m) & K_{0,\,\alpha\mu}^{(+)}(y_{14}; m_3) K_{0,\,\beta\lambda}^{(+)}(y_{23}; m_4) \prod_{r<s;\,k}^{(3,\,4)} \Delta^{(+)}(y_{rs}; m_k) M_3{}^{(1)}(1 \ldots 6) \\ + \int (\mathrm{d}m) & H_{-1,\,\alpha\beta}^{(+)}(y_{12}; m_1) H_{1,\,\lambda\mu}^{(+)}(y_{34}; m_6) \prod_{r<s;\,k}^{(1,\,6)} \Delta^{(+)}(y_{rs}; m_k) M_4{}^{(1)}(1 \ldots 6) \\ + \int (\mathrm{d}m) & H_{0,\,\alpha\lambda}^{(+)}(y_{13}; m_2) H_{0,\,\beta\mu}^{(+)}(y_{24}; m_5) \prod_{r<s;\,k}^{(2,\,5)} \Delta^{(+)}(y_{rs}; m_k) M_5{}^{(1)}(1 \ldots 6) \\ + \int (\mathrm{d}m) & H_{0,\,\alpha\mu}^{(+)}(y_{14}; m_3) H_{0,\,\beta\lambda}^{(+)}(y_{23}; m_4) \prod_{r<s;\,k}^{(3,\,4)} \Delta^{(+)}(y_{rs}; m_k) M_6{}^{(1)}(1 \ldots 6). \end{aligned} \tag{16}$$

Next we consider a different order of the operators in the v.e.v.; for example,

$$\langle \underset{\alpha}{x_1} \underset{\lambda}{\bar{x}_3} \underset{\beta}{x_2} \underset{\mu}{\bar{x}_4} \rangle_0 .$$

By a straightforward extension of the analysis given above, we are led to an expression quite analogus to (16), the only difference being that the functions K, H and Δ — which, in (16), are all of the positive class † — must be replaced by the corresponding functions of the negative class, when their space-time argument is the y_{23} variable. Furthermore, a priori, one may expect to have, instead of the spectra $M_j^{(1)}(1 \ldots 6)$, some other functions, say $M_j^{(2)}(1 \ldots 6)$. However, it is easy to see that this is not the case. Indeed, when $y_{23}^2 > 0$, we must have

$$\langle \underset{\alpha}{x_1} \underset{\beta}{x_2} \underset{\lambda}{\bar{x}_3} \underset{\mu}{\bar{x}_4} \rangle_0 = -\langle \underset{\alpha}{x_1} \underset{\lambda}{\bar{x}_3} \underset{\beta}{x_2} \underset{\mu}{\bar{x}_4} \rangle_0, \quad y_{23}^2 > 0. \tag{17}$$

But, due to well-known properties of Schwinger's functions, the following relations hold:

$$\Delta^{(+)}(x) = -\Delta^{(-)}(x), \; K_\lambda{}^{(+)}(x) = -K_\lambda{}^{(-)}(x), \; (\lambda = -1, 0, +1) \text{ for } x^2 > 0. \tag{18}$$

Therefore, since (17) must be valid for arbitrary values of $x_1, \ldots, x_4$ (subjected only to the weak restriction $y_{23}^2 > 0$), it follows (compare Gribov 4)) that ††

$$M_j^{(1)}(1 \ldots 6) = M_j^{(2)}(1 \ldots 6), \quad j = 1, \ldots, 6. \tag{19}$$

This argument is quite general: also for the remaining orders of the ψ and $\bar{\psi}$ operators in the v.e.v., the weight functions $M_j^{(i)}(1 \ldots 6)$ are always the same. We can therefore suppress the upper index and then write down our result in a compact way, by introducing the chronological ordering operator T, and the "Feynman functions" †††

$$Z_F(x) = \begin{cases} Z^{(+)}(x) & (x_0 > 0) \\ -Z^{(-)}(x) & (x_0 < 0) \end{cases}; \quad Z \equiv \Delta, K_\lambda \text{ or } H_\lambda, \quad \lambda = -1, 0, +1. \tag{20}$$

---

† For this terminology see W. Pauli 3) (p. 57).

†† It should be noted that eq. (19) is almost certainly, only a particular solution of the condition expressed by eq. (17). However, in view of the formidable mathematical difficulties involved in finding the general solution of the integral equation following from the requirement of local anticommutativity, we prefer to adopt the assumption (19), which leads to a reasonably simple spectral representation, and thus gives a possible solution of the problem investigated in this paper, although not the most general one.

††† The definition (20) differs from the customary one by a factor $2i$.

Thus we have:

$$
\begin{aligned}
&\langle T \underset{\alpha}{x_1} \underset{\beta}{x_2} \underset{\lambda}{\bar{x}_3} \underset{\mu}{\bar{x}_4} \rangle_0 \\
&\quad = \int (\mathrm{d}m) K^{\mathrm{F}}_{-1,\alpha\beta}(y_{12}; m_1) K^{\mathrm{F}}_{1,\lambda\mu}(y_{34}; m_6) \prod_{r<s;k}^{(1,6)} \Delta^{\mathrm{F}}(y_{rs}; m_k) M_1(1\ldots 6) \\
&\quad + \int (\mathrm{d}m) K^{\mathrm{F}}_{0,\alpha\lambda}(y_{13}; m_2) K^{\mathrm{F}}_{0,\beta\mu}(y_{24}; m_5) \prod_{r<s;k}^{(2,5)} \Delta^{\mathrm{F}}(y_{rs}; m_k) M_2(1\ldots 6) \\
&\quad + \int (\mathrm{d}m) K^{\mathrm{F}}_{0,\alpha\mu}(y_{14}; m_3) K^{\mathrm{F}}_{0,\beta\lambda}(y_{23}; m_4) \prod_{r<s;k}^{(3,4)} \Delta^{\mathrm{F}}(y_{rs}; m_k) M_3(1\ldots 6) \\
&\quad + \int (\mathrm{d}m) H^{\mathrm{F}}_{-1,\alpha\beta}(y_{12}; m_1) H^{\mathrm{F}}_{1,\lambda\mu}(y_{34}; m_6) \prod_{r<s;k}^{(1,6)} \Delta^{\mathrm{F}}(y_{rs}; m_k) M_4(1\ldots 6) \\
&\quad + \int (\mathrm{d}m) H^{\mathrm{F}}_{0,\alpha\lambda}(y_{13}; m_2) H^{\mathrm{F}}_{0,\beta\mu}(y_{24}; m_5) \prod_{r<s;k}^{(2,5)} \Delta^{\mathrm{F}}(y_{rs}; m_k) M_5(1\ldots 6) \\
&\quad + \int (\mathrm{d}m) H^{\mathrm{F}}_{0,\alpha\mu}(y_{14}; m_3) H^{\mathrm{F}}_{0,\beta\lambda}(y_{23}; m_4) \prod_{r<s;k}^{(3,4)} \Delta^{\mathrm{F}}(y_{rs}; m_k) M_6(1\ldots 6).
\end{aligned}
\tag{21}
$$

The representation so established, owing to the procedure we have adopted to construct it, is invariant with respect to the Touschek transformation and the parity operation; we must now see how it is possible to account for the causality condition. When $y_{13}^2 > 0$, we must have

$$\langle \underset{\alpha}{x_1} \underset{\beta}{x_2} \underset{\mu}{\bar{x}_3} \underset{\lambda}{\bar{x}_4} \rangle_0 = -\langle \underset{\beta}{x_2} \underset{\alpha}{x_1} \underset{\lambda}{\bar{x}_3} \underset{\mu}{\bar{x}_4} \rangle_0. \tag{22'}$$

Similarly, for $y_{34}^2 > 0$,

$$\langle \underset{\alpha}{x_1} \underset{\beta}{x_2} \underset{\lambda}{\bar{x}_3} \underset{\mu}{\bar{x}_4} \rangle_0 = -\langle \underset{\alpha}{x_1} \underset{\beta}{x_2} \underset{\mu}{\bar{x}_4} \underset{\lambda}{\bar{x}_3} \rangle_0. \tag{22''}$$

Bearing in mind some elementary relations which are satisfied by the Δ_{F}, K_{F} and H_{F} functions, and the symmetry properties of (21) in the spin space, we find — after a trivial calculation — that the eqs. (22) hold true only if the spectral functions M_i satisfy certain symmetry requirements, which we can formulate as follows:

$$
\begin{aligned}
M_1(1\ldots 6) &= M(123456)+M(145236)+M(132546)+M(154326), \\
M_2(1\ldots 6) &= N(123456)+N(154326), \\
M_3(1\ldots 6) &= -N(145236)-N(132546), \\
M_4(1\ldots 6) &= P(123456)-P(145236)-P(132546)+P(154326), \\
M_5(1\ldots 6) &= Q(123456)+Q(154326), \\
M_6(1\ldots 6) &= -Q(145236)-Q(132546).
\end{aligned}
\tag{23}
$$

Further conditions on the spectra M_j follow from the remark that the various v.e.v.s. which we can write (corresponding to the different orders of the ψ and $\bar{\psi}$ operators) are not independent, if — and this is actually our case — we require also charge-conjugation invariance:

$$\langle T\psi_\alpha(x_1)\psi_\beta(x_2)\bar{\psi}_\lambda(x_3)\bar{\psi}_\mu(x_4)\rangle_0 = \langle T\psi'_\alpha(x_1)\psi'_\beta(x_2)\bar{\psi}'_\lambda(x_3)\bar{\psi}'_\mu(x_4)\rangle_0, \tag{24}$$

where

$$\psi'(x) = C^{-1}\bar{\psi}^{\mathrm{T}}(x), \quad \bar{\psi}'(x) = -\psi^{\mathrm{T}}(x)C, \tag{25'}$$

$$C\gamma_\mu C^{-1} = -\gamma_\mu{}^{\mathrm{T}}, \quad C^{\mathrm{T}} = -C, \quad CC^\dagger = 1. \tag{25''}$$

The eq. (24) can be rewritten as

$$\langle T\underset{\alpha}{x_1}\underset{\beta}{x_2}\underset{\lambda}{\bar{x}_3}\underset{\mu}{\bar{x}_4}\rangle_0 = C^{-1}_{\alpha\nu}C^{-1}_{\beta\eta}C_{\sigma\lambda}C_{\rho\mu}\langle T\underset{\nu}{\bar{x}_1}\underset{\eta}{\bar{x}_2}\underset{\sigma}{x_3}\underset{\rho}{x_4}\rangle_0. \tag{24'}$$

Again by elementary calculations, one sees that all conditions embodied in (24′) are satisfied if each function M_j enjoys the additional property of being symmetric with respect to the exchanges $1 \rightleftarrows 6$, and $3 \rightleftarrows 4$. Therefore, due to this new requirement, we complete eqs. (23) by rewriting them in the form:

$$\begin{aligned}
M_1(1\ldots 6) &= M(123456)+M(145236)+M(132546)+M(154326)+(1\rightleftarrows 6, 3\rightleftarrows 4),\\
M_2(1\ldots 6) &= N(123456)+N(154326)+(1\rightleftarrows 6, 3\rightleftarrows 4),\\
M_3(1\ldots 6) &= -\{N(145236)+N(132546)+(1\rightleftarrows 6, 3\rightleftarrows 4)\},\\
M_4(1\ldots 6) &= P(123456)-P(145236)-P(132546)+P(154326)+(1\rightleftarrows 6, 3\rightleftarrows 4),\\
M_5(1\ldots 6) &= Q(123456)+Q(154326)+(1\rightleftarrows 6, 3\rightleftarrows 4),\\
M_6(1\ldots 6) &= -\{Q(145236)+Q(132546)+(1\rightleftarrows 6, 3\rightleftarrows 4)\}.
\end{aligned} \tag{26}$$

Aside from a remarkable reduction of algebraic work, the invariance conditions so far imposed lead to a spectral formula involving only four independent mass spectra. As a final step in this section we shall now show that, if these spectra satisfy further conditions, then (21) enjoys also invariance with respect to the Pauli-Gürsey transformation

$$\psi \to a\psi + b\gamma_5 C^{-1}\bar{\psi}^{\mathrm{T}}, \quad \bar{\psi} \to a^*\bar{\psi} + b^*\psi^{\mathrm{T}}C\gamma_5, \tag{27'}$$

where

$$|a|^2+|b|^2 = 1. \tag{27''}$$

To this end we first remark that — as one sees by a short calculation — the invariance condition on the v.e.v.

$$\langle T\underset{\alpha}{x_1}\underset{\beta}{x_2}\underset{\lambda}{\bar{x}_3}\underset{\mu}{\bar{x}_4}\rangle_0$$

(with respect to (27′)) is given by

$$\begin{aligned}\underset{\alpha\;\beta\;\lambda\;\mu}{\langle x_1x_2\bar{x}_3\bar{x}_4\rangle_0} = {} & |a|^4\underset{\alpha\;\beta\;\lambda\;\mu}{\langle x_1x_2\bar{x}_3\bar{x}_4\rangle_0} \\ & +|b|^4(\gamma_5)_{\alpha\alpha'}(\gamma_5)_{\beta\beta'}(\gamma_5)_{\lambda'\lambda}(\gamma_5)_{\mu'\mu}\underset{\alpha'\;\beta'\;\lambda'\;\mu'}{\langle x_1x_2\bar{x}_3\bar{x}_4\rangle_0} \\ & +|a|^2|b|^2(\gamma_5C^{-1})_{\beta\eta}(C\gamma_5)_{\rho\mu}\underset{\alpha\;\eta\;\lambda\;\rho}{\langle x_1\bar{x}_2\bar{x}_3x_4\rangle_0} \\ & +|a|^2|b|^2(\gamma_5)_{\alpha\alpha'}(\gamma_5)_{\lambda'\lambda}C^{-1}_{\beta\eta'}C_{\rho'\mu}\underset{\alpha'\;\eta'\;\lambda'\;\rho'}{\langle x_1\bar{x}_2\bar{x}_3x_4\rangle_0} \\ & +|a|^2|b|^2(\gamma_5C^{-1})_{\beta\eta}(C\gamma_5)_{\sigma\lambda}\underset{\alpha\;\eta\;\sigma\;\mu}{\langle x_1\bar{x}_2x_3\bar{x}_4\rangle_0} \\ & +|a|^2|b|^2(\gamma_5)_{\alpha\alpha'}(\gamma_5)_{\mu'\mu}C^{-1}_{\beta\eta'}C_{\sigma'\lambda}\underset{\alpha'\;\eta'\;\sigma'\;\mu'}{\langle x_1\bar{x}_2x_3\bar{x}_4\rangle_0}.\end{aligned} \tag{28}$$

Now, by simple transformations, we easily find that †

$$(\gamma_5)_{\alpha\alpha'}(\gamma_5)_{\beta\beta'}(\gamma_5)_{\lambda'\lambda}(\gamma_5)_{\mu'\mu}\underset{\alpha'\;\beta'\;\lambda'\;\mu'}{\langle x_1x_2\bar{x}_3\bar{x}_4\rangle_0} = \underset{\alpha\;\beta\;\lambda\;\mu}{\langle x_1x_2\bar{x}_3\bar{x}_4\rangle_0}, \tag{29′}$$

$$\begin{aligned}(\gamma_5C^{-1})_{\beta\eta}(C\gamma_5)_{\rho\mu}\underset{\alpha\;\eta\;\lambda\;\rho}{\langle x_1\bar{x}_2\bar{x}_3x_4\rangle_0} & = (\gamma_5)_{\alpha\alpha'}(\gamma_5)_{\lambda'\lambda}C^{-1}_{\beta\eta'}C_{\rho'\mu}\underset{\alpha'\;\eta'\;\lambda'\;\rho'}{\langle x_1\bar{x}_2\bar{x}_3x_4\rangle_0} \\ & = \int(\mathrm{d}m)\{(\alpha_1)M_5(312564)-(\alpha_2)M_3(312564)+(\alpha_3)M_4(312564) \\ & \quad +(\alpha_4)M_2(312564)+(\alpha_5)M_6(312564)-(\alpha_6)M_1(312564)\},\end{aligned} \tag{29″}$$

$$\begin{aligned}(\gamma_5C^{-1})_{\beta\eta}(C\gamma_5)_{\sigma\lambda}\underset{\alpha\;\eta\;\sigma\;\mu}{\langle x_1\bar{x}_2x_3\bar{x}_4\rangle_0} & = (\gamma_5)_{\alpha\alpha'}(\gamma_5)_{\mu'\mu}C^{-1}_{\beta\eta'}C_{\sigma'\lambda}\underset{\alpha'\;\eta'\;\sigma'\;\mu'}{\langle x_1\bar{x}_2x_3\bar{x}_4\rangle_0} \\ & = \int(\mathrm{d}m)\{(\alpha_1)M_5(213465)-(\alpha_2)M_4(213465)+(\alpha_3)M_3(213465) \\ & \quad -(\alpha_4)M_2(213465)+(\alpha_5)M_1(213465)-(\alpha_6)M_6(213465)\}.\end{aligned} \tag{29‴}$$

It follows — by virtue of (27′,) — that the required invariance is secured if

$$\begin{aligned}M_5(312564)+M_5(213465) & = M_1(123456), \\ M_6(312564)+M_1(213465) & = M_5(123456), \\ M_1(312564)+M_6(213465) & = -M_6(123456),\end{aligned} \tag{30′}$$

and

$$\begin{aligned}M_3(312564)+M_4(213465) & = -M_2(123456), \\ M_4(312564)+M_3(213465) & = M_3(123456), \\ M_2(312564)-M_2(213465) & = M_4(123456).\end{aligned} \tag{30″}$$

---

† Eqs. (29″) and (29‴) are easily understood if, for simplicity sake, we write the general spectral representation (21) in the shorthand notation: $\langle Tx_1x_2\bar{x}_3\bar{x}_4\rangle_0 = \Sigma_{i=1}^{6}\int(\mathrm{d}m)(\alpha_i)M_i(1\ldots6)$.

These relations are perfectly consistent with the symmetry properties already known fror the spectra M_j, and can in turn be satisfied through a suitable extension of these properties; it would go too far to quote here the very long final expressions. We remark, moreover, that — as a further consequence of (30) — the final representation of our v.e.v. involves only two independent mass spectra.

To conclude, the analysis performed in this section shows that it is possible to construct, in the non linear spinor theory, a spectral representation for the four point functions which is still entirely symmetric; however, the interpretation of the two spectra (each depending on six auxiliary masses) and of their various symmetry properties, appears to be rather obscure. However, in this connection, it is useful to notice the existence of a link between the two mass spectra of the four point function and the usual spectrum $\rho(\kappa^2)$ of the two point function; this link will now be examined, in some detail, in the next section.

3. Connection with the Two Point Functions

In order to get further information about the two spectral functions appearing in the representation previously derived, it is indicated to utilize the differential equation satisfied by the operator $\psi(x)$, which establishes a relation between the space-time derivatives of this operator, and a Wick product of three operators. For this purpose, let us consider the expression of the two point function in the non linear theory,

$$\begin{aligned}&\langle 0|\bar{\psi}_\beta(x')\psi_\alpha(x)|0\rangle\\ &\quad=(2\pi)^{-4}\int\rho(\kappa^2)\mathrm{d}(\kappa^2)\int_{C^-}\mathrm{d}^4p\,\mathrm{e}^{ip\cdot(x-x')}(\gamma\cdot p)_{\alpha\beta}\left\{\frac{1}{p^2+\kappa^2}-\frac{1}{p^2}+\frac{\kappa^2}{(p^2)^2}\right\}.\end{aligned}\tag{31}$$

(C^- being the usual integration contour for the function $\Delta^{(-)}(x)$ in the p_0-complex plane); acting upon this with the differential operator $\gamma\cdot\partial/\partial x$, we get

$$\begin{aligned}\left(\gamma\frac{\partial}{\partial x}\right)_{\nu\alpha}\langle 0|\bar{\psi}_\beta(x')\psi_\alpha(x)|0\rangle&=\frac{i}{(2\pi)^4}\int\rho(\kappa^2)\mathrm{d}(\kappa^2)\int_{C^-}\mathrm{d}^4p\,\mathrm{e}^{ip\cdot(x-x')}\\ \times\delta_{\nu\beta}p^2\left\{\frac{1}{p^2+\kappa^2}-\frac{1}{p^2}+\frac{\kappa^2}{(p^2)^2}\right\}&=i\delta_{\nu\beta}\int\rho(\kappa^2)\kappa^2\mathrm{d}(\kappa^2)\,\frac{1}{(2\pi)^4}\int_{C^-}\mathrm{d}^4p\\ \times\mathrm{e}^{ip\cdot(x-x')}\left\{\frac{1}{p^2}-\frac{1}{p^2+\kappa^2}\right\}&=-i\delta_{\nu\beta}\int\rho(\kappa^2)\kappa^2\mathrm{d}(\kappa^2)\Delta^{(-)}(x-x';\kappa).\end{aligned}\tag{32}$$

Here, use has been made of the relation $\int\rho(\kappa^2)\kappa^2\mathrm{d}(\kappa^2)=0$. By virtue of this same relation, the r.h.s. of (32) does not contain any delta-like singularity. On the other hand, bearing in mind the differential equation satisfied by the ψ

operator, we can rewrite eq. (32) in the following form:

$$l^2(\gamma_5\gamma_\mu)_{\nu\alpha}(\gamma_5\gamma_\mu)_{\rho\sigma}\langle 0|\bar{\psi}_\beta(x')\colon \psi_\alpha(x)\bar{\psi}_\rho(x)\psi_\sigma(x)\colon|0\rangle$$
$$= -i\delta_{\nu\beta}\int \rho(\kappa^2)\kappa^2\mathrm{d}(\kappa^2)\Delta^{(-)}(x-x';\kappa). \qquad (33)$$

To establish the singularities of (33) on the light cone $(x-x')^2 = 0$, we remember that, with $\lambda = -x^2$ (the symbol ψ denotes here the logarithmic derivative of the Γ function),

$$\Delta^{(-)}(x) = \tfrac{1}{2}[\Delta(x)+i\Delta^{(1)}(x)] = -\frac{1}{4\pi}\varepsilon(x_0)\delta(\lambda)+\frac{\kappa^2}{8\pi}\varepsilon(x_0)\Theta(\lambda)\frac{J_1(\kappa\sqrt{\lambda})}{\kappa\sqrt{\lambda}}$$
$$+\tfrac{1}{2}i\frac{\kappa^2}{4\pi^2}\Theta(\lambda)\left\{-\frac{2}{\kappa^2\lambda}+\log(\tfrac{1}{2}\kappa\sqrt{\lambda})-\tfrac{1}{2}\psi(1)-\tfrac{1}{2}\psi(2)+(\ldots)\right\}$$
$$+\tfrac{1}{2}i\frac{\kappa^2}{2\pi^2}\Theta(-\lambda)\left\{-\frac{1}{\kappa^2\lambda}+\tfrac{1}{2}\log(\tfrac{1}{2}\kappa\sqrt{-\lambda})-\tfrac{1}{4}\psi(1)-\tfrac{1}{4}\psi(2)+(\ldots)\right\}$$

(the terms denoted by $(\ldots)$ vanish for $\lambda = 0$). From this it follows that the singularity of (33) on the light cone is a logarithmic one (it would be possible to eliminate this singularity also, by requiring for the spectral function $\rho(\kappa^2)$ the further condition $\int\rho(\kappa^2)\kappa^4\mathrm{d}(\kappa^2) = 0$; this, however, could scarcely be justified from the differential equation. A perfectly similar statement holds for the two point function (31)). After these preliminary remarks, we now come to the consideration of the v.e.v. $\langle 0|\bar{\psi}_\beta(x')\colon \psi_\alpha(x)\bar{\psi}_\rho(x_1)\psi_\sigma(x_2)\colon|0\rangle$ (where all of the points x, x_1, x_2 are at first supposed to be different); by simple manipulations, this can be converted into

$$\langle 0|\bar{\psi}_\beta(x')\colon \psi_\alpha(x)\bar{\psi}_\rho(x_1)\psi_\sigma(x_2)\colon|0\rangle = -\langle 0|T\psi_\alpha(x)\psi_\sigma(x_2)\bar{\psi}_\beta(x')\bar{\psi}_\rho(x_1)|0\rangle$$
$$-\underbrace{\bar{\psi}_\beta(x')\psi_\alpha(x)}\underbrace{\bar{\psi}_\rho(x_1)\psi_\sigma(x_2)}-\underbrace{\bar{\psi}_\beta(x')\psi_\sigma(x_2)}\underbrace{\psi_\alpha(x)\bar{\psi}_\rho(x_1)}. \qquad (34)$$

The first term at r.h.s. is the general four point function, for which we rewrite here the spectral representation previously derived:

$$\langle 0|T\psi_\alpha(x)\psi_\sigma(x_2)\bar{\psi}_\beta(x')\bar{\psi}_\rho(x_1)|0\rangle$$
$$\begin{aligned}
&= \int(\mathrm{d}m)K^{\mathrm{F}}_{-1,\alpha\sigma}(x-x_2;m_1)K^{\mathrm{F}}_{1,\beta\rho}(x'-x_1;m_6)\Delta^{\mathrm{F}}(x-x';m_2)\\
&\times\Delta^{\mathrm{F}}(x-x_1;m_3)\Delta^{\mathrm{F}}(x_2-x';m_4)\Delta^{\mathrm{F}}(x_2-x_1;m_5)M_1(1\ldots 6)\\
&+\int(\mathrm{d}m)K^{\mathrm{F}}_{0,\alpha\beta}(x-x';m_2)K^{\mathrm{F}}_{0,\sigma\rho}(x_2-x_1;m_5)\Delta^{\mathrm{F}}(x-x_2;m_1)\\
&\times\Delta^{\mathrm{F}}(x-x_1;m_3)\Delta^{\mathrm{F}}(x_2-x';m_4)\Delta^{\mathrm{F}}(x'-x_1;m_6)M_2(1\ldots 6)\\
&+\int(\mathrm{d}m)K^{\mathrm{F}}_{0,\alpha\rho}(x-x_1;m_3)K^{\mathrm{F}}_{0,\sigma\beta}(x_2-x';m_4)\Delta^{\mathrm{F}}(x-x_2;m_1)\\
&\times\Delta^{\mathrm{F}}(x-x';m_2)\Delta^{\mathrm{F}}(x_2-x_1;m_5)\Delta^{\mathrm{F}}(x'-x_1;m_6)M_3(1\ldots 6)\\
&+(K\rightarrow H,\ M_j\rightarrow M_{j+3}).
\end{aligned} \qquad (35)$$

When the three points x, x_1 and x_2 coincide, this expression becomes strongly singular; on the other hand, according to (33), we would expect a much more regular behaviour. This apparent contradiction, however, is not at all unexpected. Indeed, in the case of the two point function, the absence of δ and δ'-like singularities on the light cone (which follows from the differential equation) implies, for the spectral function $\rho(\kappa^2)$, the two conditions

$$\int \rho(\kappa^2)\mathrm{d}(\kappa^2) = 0, \quad \int \rho(\kappa^2)\kappa^2\mathrm{d}(\kappa^2) = 0.$$

The calculations above performed show that — always due to the differential equation — quite analogous conditions must hold for the spectra M_j. To be more precise, if we remember that these spectra can be expressed in terms of only two independent functions (which, according to (26), we can identify with $N(1\ldots 6)$ and $Q(1\ldots 6)$), the structure of (35) shows that the above mentioned conditions are of the form ($A \equiv N$, or Q)

$$\int (\mathrm{d}m) A(m_1^2, \ldots, m_6^2) = 0, \tag{36a}$$

$$\int (\mathrm{d}m) m_j^2 A(m_1^2, \ldots, m_6^2) = 0, \quad (j = 1, \ldots, 6) \tag{36b}$$

$$\int (\mathrm{d}m) m_j^2 m_k^2 A(m_1^2, \ldots, m_6^2) = 0, \quad (j \neq k = 1, \ldots, 6) \tag{36c}$$

. . . .

$$\int (\mathrm{d}m) m_1^2 \ldots m_6^2 A(m_1^2, \ldots, m_6^2) = 0. \tag{36g}$$

But, if the eqs. (36) are satisfied, we can replace the various singular functions contained in (35) by the corresponding regularized expressions; in this way, we can give a meaning to eq. (35), when three points coincide. If we further remember that, for $x \equiv x_1 \equiv x_2$, the contractions at r.h.s. of (34) do not give any contribution, we get finally (by substituting into (33)) an integral relation, connecting the two independent mass spectra of the four point function and the spectrum $\rho(\kappa^2)$ of the two point function. One may hope that, in an eventual approximate calculation of these spectra, their various symmetry properties (which follow from the requirement of invariance with respect to certain transformations), together with their integral properties expressed by (33) and (36) — (and due, in turn, to the differential equation for the ψ operator) — turn out to be of some help.

I am deeply indebted to Prof. W. Heisenberg, who suggested this investigation, for numerous discussions and invaluable advice. My thanks are also due to Drs. H. P. Dürr and H. Mitter for their kind interest in this work, and to Dr. T. Ahrens for a critical reading of the manuscript.

References

1) G. Källén, H. P. A. **25** (1952) 417;
H. Lehmann, Nuovo Cim. **11** (1954) 342;
A. S. Wightman, Phys. Rev. **101** (1956) 860;
G. Källén and A. S. Wightman, Mat. Fys. Skr. Dan. Vid. Selsk. **1**, No. 6 (1958);
G. Källén and H. Wilhelmsson, Mat. Fys. Skr. Dan. Vid. Selsk. **1**, No. 9 (1959);
E. Montaldi, Nuovo Cim. **11** (1959) 149; **12** (1959) 571
2) H. P. Dürr, W. Heisenberg, H. Mitter, S. Schlieder and K. Yamazaki, Zs. f. Naturf. **14a** (1959) 441
3) See, e.g., W. Pauli, Continuous groups and reflections in quantum mechanics, 1958(Radiation Laboratory, Berkeley, California) p. 96
4) V. N. Gribov, Soviet Phys. JETP, **7** (1958) 903

3.A

Nuclear Physics **23** (1961) 452—467; © *North-Holland Publishing Co., Amsterdam*

Not to be reproduced by photoprint or microfilm without written permission from the publisher

ON PROCESSES IN THE INTERACTION OF γ-QUANTA WITH UNSTABLE PARTICLES

I. Ya. POMERANCHUK

Theoretical and Experimental Physics Institute of the USSR Academy of Sciences, Moscow, USSR

and

I. M. SHMUSHKEVICH

Physical-Technical Institute of the USSR Academy of Sciences, Leningrad, USSR

Received 25 July 1960

Abstract: This paper deals with various inelastic processes occurring in the collisions of fast particles with the nuclei neither excited nor transformed. At $q^2 = 0$ (q^2 being the invariant square of the momentum transfer to the nucleus) the amplitude of these processes has a pole involving virtual photons. Therefore at sufficiently small q^2 the virtual photon exchange makes a larger contribution to the amplitude than the exchange of strongly interacting particles. This makes it possible to connect at small q^2 the cross section of the process under study and that of the process at work between the γ-quantum and the incident particle. Given q^2 and $E_L \gg m$ (E_L being the energy of incident particle in the laboratory coordinate system and m its mass), the energy w of the particles produced in the reaction in their centre-of-mass system is restricted by the condition $w^2 - m^2 < 2E_L\sqrt{q^2}$.

The relation between the above-mentioned cross sections, equivalent to one following from the Weizsäcker-Williams method, is obtained in the present paper by a covariant method, and the conditions of applicability of this relation are discussed, in particular for strongly interacting particle processes. An appraisal is made of the contribution made by the processes involving the Coulomb nuclear field to the total cross section of interaction between the incident particle and the nucleus. The processes at work in the Coulomb field of the nucleus, such as the bremsstrahlung of π or K-mesons, the conversion of π-mesons into two π-mesons and the transformations of a Λ^0-particle into Σ^0-particle are analyzed in detail.

1. Introduction

Consider a collision of a fast particle a with a nucleus N with the resulting formation of one or several new particles, the nucleus receiving a recoil without excitation or transformation:

$$a + N \rightarrow N + A, \tag{1.1}$$

where A denotes the total set of the particles produced.

Among the graphs corresponding to the amplitude of this process there is a graph represented in fig. 1. Heavy lines in this graph correspond to the nucleus; $\mathbf{P}_1$ and $\mathbf{P}_2$ are the momenta of the nucleus before and after collision, $\mathbf{p}$ is the momentum of the incident particle a and $\mathbf{q} = \mathbf{P}_1 - \mathbf{P}_2$ is the momentum of the virtual photon accounting for the factor $1/q^2$ in the matrix element. Owing to this factor the contribution to the amplitude from the graph in question has a pole at $q^2 = 0$ and consequently is quite large at sufficiently small q^2. The graphs corresponding to the π-meson exchange between the nucleus and the remaining particles involved in the process have no poles at $q^2 = 0$. Therefore at sufficiently small q^2,

$$q^2 \ll m_\pi^2, \tag{1.2}$$

the contributions from all graphs except for the one represented in fig. 1 can be neglected. The condition under which this is possible will be quantitatively formulated below (see (2.4) and (3.6)).

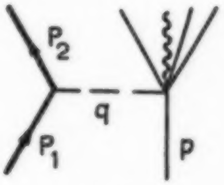

Fig. 1

Designating the energy of the formed particles A in their centre-of-mass system through w and the mass of the particle a through m, we have

$$w^2 = -(p+q)^2 = m^2 - q^2 - 2qp. \tag{1.3}$$

Since we consider the reactions in which $w^2 - m^2$ is not small as compared with m_π^2 we can, in view of (1.2), neglect the term q^2 in the right-hand side of (1.3). Then in the coordinate system in which the particle a is at rest prior to the collision we can obtain from (1.3)

$$q_0 = \frac{w^2 - m^2}{2m}. \tag{1.4}$$

Denoting the velocity and energy of the nucleus before the collision by $\mathbf{V}$ and E_1 respectively, we shall find from the relation $P_2^2 = (P_1 - q)^2$, in the same coordinate system,

$$q_0 = \mathbf{V} \cdot \mathbf{q} - \frac{q^2}{2E_1}. \tag{1.5}$$

Under our conditions the quantity $q^2/2E_1$ in the right-hand side of (1.5) can obviously be neglected, and therefore

$$q_0 = \mathbf{V} \cdot \mathbf{q}. \tag{1.6}$$

Denoting the parallel and perpendicular $\mathbf{V}$ components of the vector $\mathbf{q}$ through $\mathbf{q}_\parallel$ and $\mathbf{q}_\perp$ respectively,

$$\mathbf{q} = \mathbf{q}_\parallel + \mathbf{q}_\perp, \quad \mathbf{q}_\parallel = \frac{1}{V^2}(\mathbf{q} \cdot \mathbf{v})\mathbf{v}, \tag{1.7}$$

we have

$$q^2 = q_\parallel^2+q_\perp^2-q_0^2 = q_\perp^2+q_0^2\left(\frac{1}{V^2}-1\right) = q_\perp^2+\left(\frac{w^2-m^2}{2p_L}\right)^2. \qquad (1.8)$$

Here, p_L is the momentum of the incident particle a in the laboratory coordinate system ($\mathbf{P}_1 = 0$). It will be noted that eq. (1.6) can be written in the invariant form

$$U_\mu q_\mu = 0, \qquad (1.9)$$

where U_μ is the vector of the four-dimensional velocity of the nucleus

$$U_\mu = \frac{1}{M} P_{1\mu}. \qquad (1.10)$$

Consequently, (1.6) holds in an arbitrary coordinate system provided $\mathbf{V}$ denotes the velocity of the nucleus in this system. From (1.8) we find the maximum value of w at the fixed q^2

$$w_{\max}^2-m^2 = 2p_L V q^2. \qquad (1.11)$$

Therefore, even when q^2 is very small and satisfies eq. (1.2) or a more rigid one, w may be quite large if the energy E_L of the incident particle in the laboratory system is sufficiently high.

On the other hand, at a sufficiently small q^2 (at $q^2 = 0$ in the limit) the right-hand section of the graph shown in fig. 1 corresponds to the matrix element for the formation of A particles in the interaction of the photon with the particle a,

$$\gamma+\mathrm{a} \rightarrow \mathrm{A}. \qquad (1.12)$$

Therefore the cross section σ_c for the process (1.1) can, under these conditions, be simply connected with the cross section σ_p of the photoprocesses (1.12).

Thus, the investigation of different processes, accompanied by sufficiently small momentum transfer to the nucleus, in the interaction of a very fast particle a with the nucleus may serve as a means for determining the cross sections of interactions between γ-quanta and unstable particles †.

In sect. 2 of the present paper, the general relation between the cross section of the process (1.1) and that of the corresponding photoprocesses (1.12) is evolved. Both the relation and its deduction are, of course, similar to those of ref. [2]), with two points of difference, however. The amplitude of the processes under consideration has a pole connected with virtual photons at $q^2 = 0$. Though this pole does not lie in the physical region, it can be arbitrarily close to it provided the energy of the incident particle is sufficiently large. Therefore, the residue at this pole determines the amplitude in general at a sufficiently small q^2. Now the amplitude of the processes considered in ref. [2]) has a pole at

---

† Similar ideas are expressed in ref. [1]) received after this paper had been finished.

$q^2 = -m_\pi^2$, at a finite distance from the physical region. The second point of difference involves the vector properties of photons and the gauge invariance of the electromagnetic interaction.

The connection between the cross sections to be established in this paper has to coincide, essentially, with that obtained by the well-known treatment of Weizsäcker-Williams [3]). The covariant method of obtaining this connection † may be of interest, all the more so that it may provide more distinct applicability limits for the formulae, especially for strongly interacting particle reactions.

Sect. 3 offers an evaluation of the contribution made by the processes involving the Coulomb nuclear field to the total cross section of the incident particle interaction with the nucleus, the screening of the nucleus field by the electron shell being also taken into account. Sect. 4 deals with a more detailed analysis of the following reactions:

1. The bremsstrahlung of a π- or K-meson on a nucleus (fig. 2), i.e., the reaction

$$\pi+\mathrm{N} \to \mathrm{N}+\pi+\gamma, \qquad \mathrm{K}+\mathrm{N} \to \mathrm{N}+\mathrm{K}+\gamma. \tag{1.13}$$

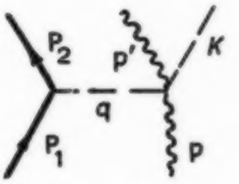

Fig. 2

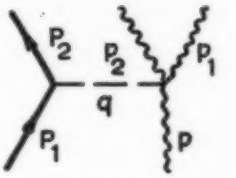

Fig. 3

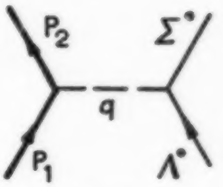

Fig. 4

2. The π-meson transformation in the interaction with the nucleus into two π-mesons (fig. 3), i.e., the reaction

$$\pi+\mathrm{N} \to \mathrm{N}+\pi_1+\pi_2. \tag{1.14}$$

3. The transformation of the Λ^0-particle in the interaction with the nucleus into the Σ^0-particle (fig. 4) i.e., the reaction

$$\Lambda^0+\mathrm{N} \to \mathrm{N}+\Sigma^0. \tag{1.15}$$

2. Derivation of Basic Formula and Discussion of Method

Neglecting the contributions of all graphs except for one in fig. 1 for the matrix element of the S-matrix corresponding to (1.1), we obtain

$$\langle A, P_2|S|p, P_1\rangle = -i(2\pi)^4 \left(\frac{f_a f}{4E_1 E_2}\right)^{\frac{1}{2}} \frac{G_\mu R_\mu}{q^2}\, \delta(P_1+p_1-P_2-Q). \tag{2.1}$$

---

† According to information received from Ya. A. Smorodinsky, this problem was also studied by A. Badolyan.

Here, E_1 and E_2 are the energies of the nucleus before and after the collision, E is the energy of the incident particle a, $f=\prod_{(A)} f_i$ (where $f_i = m_i/E_i$ for the fermion and $f_i = \frac{1}{2}E_i^{-1}$ for the boson whereas the corresponding factors for all created particles A are incorporated under the sign of the product), and f_a is an analogous factor for the incident particle. The total 4-momentum for all particles constituting the set A is denoted by Q.

G_μ and R_μ are electromagnetic vertex functions corresponding to the left- and right-hand parts of the graph.

It follows from the gauge invariance of the theory that

$$q_\mu G_\mu = 0 \tag{2.2}$$

and

$$q_\mu R_\mu = 0. \tag{2.3}$$

In the following, to avoid taking into account the charge distribution inside the nucleus, we shall restrict the possible values q^2 by the condition

$$q^2 \ll m_\pi^2 A^{-\frac{2}{3}}, \tag{2.4}$$

which is more rigid than (1.2). For such values of q^2

$$G_\mu = -iZe(P_{1\mu} + P_{2\mu}). \tag{2.5}$$

Eq. (2.5) is, strictly speaking, valid only for the nucleus with the spin s equal to zero. If $s \neq 0$, the expression for G_μ will contain more terms all of which, however, will have the **q** vector components as factors. These additional terms therefore will be negligibly small, and eq. (2.5) can also be used in the case of $s \neq 0$ †.

According to (2.3), (2.5) and (1.10) we now have

$$G_\mu R_\mu = -2iZeP_{1\mu} R_\mu = -2iZeMU_\mu R_\mu. \tag{2.6}$$

There being no $P_{2\mu}$ in eq. (2.6), U_μ satisfying (1.9) similar to (2.2) if the terms $\approx q^2$ are neglected (see (1.5)), corresponds to the fact that the recoil of the nucleus is, under the conditions, inessential and the Coulomb field of the nucleus can be considered as an external field. Using then (2.3) ,(1.9) and (1.6)

---

† For instance, when $s = \frac{1}{2}$,

$$G_\mu = Ze(\bar{u}_2 \gamma_\mu \bar{u}_1) + \tfrac{1}{2} i \lambda \bar{u}_2 (\not{q} \gamma_\mu - \gamma_\mu \not{q}) u_1,$$

where λ is the anomalous magnetic moment of the nucleus. Obviously

$$G_\mu = -\frac{iZe}{2M}(P_{1\mu} + P_{2\mu})(\bar{u}_2 u_1) + \frac{i}{2}\left(\frac{Ze}{2M} + \lambda\right) \bar{u}_2 (\not{q}\gamma_\mu - \gamma_\mu \not{q}) u_1 \approx -\frac{iZe}{2M}(P_{1\mu} + P_{2\mu}) \bar{u}_2 u_1.$$

The product of the new factor $1/2M$ and the normalizing factors $f_1^{\frac{1}{2}} = (M/E_1)^{\frac{1}{2}}$ and $f_2^{\frac{1}{2}} = (M/E_2)^{2}$ for the nucleus (a fermion in the present case) is equal to $(4E_1 E_2)^{-\frac{1}{2}}$ which exactly coincides with the normalizing factor for a zero-spin nucleus taken into account in (2.1).

and (1.7) we obtain

$$U_\mu R_\mu = \frac{1}{(1-V^2)^{\frac{1}{2}}}(\mathbf{V}\cdot\mathbf{R}-R_0) = \frac{1}{(1-V^2)^{\frac{1}{2}}}\left(\mathbf{V}\cdot\mathbf{R}-\frac{\mathbf{R}\cdot\mathbf{q}}{q_0}\right)$$
$$= \frac{1}{q_0(1-V^2)^{\frac{1}{2}}}\{(\mathbf{V}\cdot\mathbf{q})(\mathbf{V}\cdot R)-\mathbf{q}\cdot\mathbf{R}\} = -\frac{1}{q_0(1-V^2)^{\frac{1}{2}}}\{(1-V^2)\mathbf{q}_\parallel+\mathbf{q}_\perp\}\cdot\mathbf{R}. \tag{2.7}$$

According to (2.3), we have

$$\mathbf{q}_\parallel\cdot\mathbf{R} = \mathbf{q}_\parallel\cdot\mathbf{R}_\parallel = q_0R_0-\mathbf{q}_\perp\cdot\mathbf{R}_\perp, \tag{2.8}$$

where $\mathbf{R}=\mathbf{R}_\parallel+\mathbf{R}_\perp$ and $\mathbf{R}_\parallel = 1/V^2(\mathbf{R}\cdot\mathbf{V})\,\mathbf{V}$, just as in (1.7), and so substituting (2.8) into (2.7) we obtain

$$U_\mu R_\mu = -(1-V^2)^{\frac{1}{2}}R_0-\frac{V^2}{(1-V^2)^{\frac{1}{2}}}\frac{\mathbf{q}_\perp\cdot\mathbf{R}_\perp}{q_0}. \tag{2.9}$$

This formula is valid in any coordinate system (**V** being the velocity of the nucleus in the respective system). Yet dividing the invariant expression $U_\mu R_\mu$ into two terms in (2.9) is not relativistically invariant, i.e., neither of them is invariant. Let us select, therefore, a definite coordinate system, preferably one in which the particle a is at rest before a collision ($\mathbf{p}=0$) as the most convenient. In the following, the corresponding quantities in this system will be understood by V, q_0, R_0. Then $1-V \ll 1$ (since in the laboratory system the particle a is, under the assumption, ultrarelativistic). Yet, according to (1.8) and (2.4) the quantities $q_\perp$ and $q_0(1-V^2)^{\frac{1}{2}}$ are restricted by the same upper limit equal to $m_\pi A^{-\frac{1}{3}}$. If it is assumed that these values are of the same order of smallness, and the components R_μ in the system where the particle a is at rest before the collision are of the same order of magnitude, the first term in (2.9) containing an additional small factor $(1-V^2)^{\frac{1}{2}}$ can be neglected[†].

The latter being certainly permissible when $q_\perp \neq 0$ and V are sufficiently near to unity, we obtain

$$G_\mu R_\mu = \frac{2iZeE_1}{q_0}\mathbf{q}_\perp\cdot\mathbf{R}_\perp. \tag{2.10}$$

As we are interested in the values of the amplitude of process (1.1) when q^2 are small, we can put $q^2=0$ in slowly changing functions. In accordance with (1.8) it can then be assumed that $q_\perp=0$ and $V=1$ in the arguments R_0 and

---

[†] The expression $U_\mu R_\mu$ can be invariantly divided into two parts and put as

$$U_\mu R_\mu = -\frac{pR}{pU}+\left(UR+\frac{pR}{pU}\right).$$

With eqs. (1.9), (2.3) and (1.6) it is easy to show that in the system where $\mathbf{p}=0$,

$$UR+\frac{pR}{pU} = -\frac{V^2}{q_0(1-V^2)^{\frac{1}{2}}}\mathbf{q}_\perp\cdot\mathbf{R}_\perp \text{ and } -\frac{pR}{pU} = -(1-V^2)^{\frac{1}{2}}R_0.$$

$\mathbf{R}_\perp$ in the right-hand side of (2.9) and (2.10). Under these conditions the expression $R_\mu e_\mu$ defines the amplitude of photoprocess (1.12) corresponding to the quantum propagated in the direction $\mathbf{V}$ and having the energy q_0 in the system where $\mathbf{p} = 0$; e is the unit polarization vector of this quantum. The differential cross section of the photoprocess $\mathrm{d}\sigma_\mathrm{p}$ is determined by the formula

$$\mathrm{d}\sigma_\mathrm{p}(w) = \frac{(2\pi)^4}{2q_0 m} g_\mathrm{a} f |e_\mu R_\mu|^2 \delta(q+p-Q)\mathrm{d}\Gamma. \tag{2.11}$$

Here $\mathrm{d}\Gamma = \prod_{(A)} (\mathrm{d}^3 p_i/(2\pi)^3)$, q_0 is the momentum of the photon in the system where $\mathbf{p} = 0$ (see (1.4)), f is the same factor as in (2.1) and g_a is equal to m, if the particle a is a fermion and is equal to $\frac{1}{2}$, if a is a boson ($g_\mathrm{a} = Ef_\mathrm{a}$, see (2.1)).

On the other hand, for the differential cross section of the process (1.1) of interest to us, according to (2.1) we have

$$\mathrm{d}\sigma_\mathrm{c} = \frac{(2\pi)^4}{4P_1{}^0 m} \frac{|G_\mu R_\mu|^2}{(q^2)^2} g_\mathrm{a} \frac{\mathrm{d}^3 P_2}{(2\pi)^3 E_2} f \mathrm{d}\Gamma \delta(q+p-Q), \tag{2.12}$$

where $P_1{}^0$ is the momentum of the nucleus in the system where $\mathbf{p} = 0$. Taking into account (2.10) and (2.11) and noting that

$$\mathrm{d}^3 P_2 = \mathrm{d}^3 q = q_\perp \mathrm{d}q_\perp \mathrm{d}q_\parallel \mathrm{d}\varphi = \tfrac{1}{2}\mathrm{d}q_\perp{}^2 \mathrm{d}q_\parallel \mathrm{d}\varphi \tag{2.13}$$

and that

$$\mathrm{d}q_\parallel = \frac{\mathrm{d}w^2}{2mV} \tag{2.14}$$

in the system where $\mathbf{p} = 0$ (here we have to use this system, since all values in the right-hand side of (2.10) are related to it), we obtain

$$\mathrm{d}\sigma_\mathrm{c} = \frac{Z^2\alpha}{2\pi^2} \frac{q_\perp{}^2 \mathrm{d}q_\perp{}^2 \mathrm{d}\varphi}{(q^2)^2} \frac{\mathrm{d}w^2}{w^2 - m^2} \mathrm{d}\sigma_\mathrm{p}(w, \varphi). \tag{2.15}$$

Now we have neglected the fact that the values E_2/E_1 and V differ from unity; $\mathrm{d}\sigma_\mathrm{p}(w, \varphi)$ is the differential cross section of the process (1.12) corresponding to the quantum polarized in the direction of the azimuth φ, $\alpha = e^2/4\pi$. Passing in (2.15) from the variable $q_\perp{}^2$ to q^2, with the help of (1.8) and no longer making a distinction between p_L and E_L we finally obtain

$$\mathrm{d}\sigma_\mathrm{c} = \frac{Z^2\alpha}{2\pi} \frac{\mathrm{d}w^2}{w^2 - m^2} \frac{q^2 - \left(\dfrac{w^2 - m^2}{2E_\mathrm{L}}\right)^2}{(q^2)^2} \mathrm{d}q^2 \mathrm{d}\varphi \, \mathrm{d}\sigma_\mathrm{p}(w, \varphi). \tag{2.16}$$

Integrating over φ and again denoting the integrated cross section by $\mathrm{d}\sigma_\mathrm{c}$, we find

$$\mathrm{d}\sigma_\mathrm{c} = \frac{Z^2\alpha}{\pi} \frac{\mathrm{d}w^2}{w^2 - m^2} \frac{\mathrm{d}q^2}{(q^2)^2} \left[q^2 - \left(\frac{w^2 - m^2}{2E_\mathrm{L}}\right)^2\right] \mathrm{d}\sigma_\mathrm{p}(w), \tag{2.17}$$

where $\mathrm{d}\sigma_{\mathrm{p}}(w)$ denotes the differential cross section of the photoprocess averaged over polarizations.

Since in R_0 and $\mathbf{R}_\perp$ of (2.9) we have put $q_\perp = 0$, the first term in (2.9) is independent of the azimuth φ, and the second proportional to $\cos\varphi$. Therefore, if the first term is not neglected, in substituting (2.9) into (2.12) we obtain after integrating over φ instead of (2.17)

$$\mathrm{d}\sigma_{\mathrm{c}} = \frac{Z^2\alpha}{\pi}\frac{\mathrm{d}w^2}{w^2-m^2}\frac{\mathrm{d}q^2}{(q^2)^2}\left\{\left[q^2-\left(\frac{w^2-m^2}{2E_{\mathrm{L}}}\right)^2\right]\mathrm{d}\sigma_{\mathrm{p}}+4\pi^4 g_{\mathrm{a}}\frac{m^2(w^2-m^2)}{E_{\mathrm{L}}{}^4}|R_0|^2\mathrm{d}\Omega\right\}, \tag{2.18}$$

where $\mathrm{d}\Omega$ denotes the invariant element of the phase volume

$$\mathrm{d}\Omega = f\mathrm{d}\Gamma\delta(q+p-Q) \tag{2.19}$$

and

$$|R_0|^2 = \frac{1}{m^2}|p_\mu R_\mu|^2. \tag{2.20}$$

Though the multiplier $m^2(w^2-m^2)/E_{\mathrm{L}}{}^4$ is small, we retain the second term within the braces of (2.18). From (2.9) it follows that this term counts only when $q_\perp$ is small and satisfies the condition $q_\perp < q_0(1-V^2)$. In other words, for fixed q^2 the second term in (2.18) should not be taken into account unless w^2-m^2 differs from its maximum value $w^2_{\max}-m^2 = 2E_{\mathrm{L}}\sqrt{q^2}$ by a quantity of the order of $2E_{\mathrm{L}}\sqrt{(q^2)m^2/E_{\mathrm{L}}{}^2}$. Yet it can be seen from (2.9) and (1.8) that even when $q_\perp = 0$ the expression $G_\mu R_\mu/q^2$ contains the factor $(1-V^2)^{-\frac{1}{2}} = E_{\mathrm{L}}/m$. Therefore, at a sufficiently high energy the contribution to the cross section due to the Coulomb field of the nucleus seems to be fundamental even when $q_\perp = 0$.

Another thing is noteworthy. Changing q^2 for zero in the argument of the function R_μ is permissible provided condition (1.2) is satisfied. m_π figures in this inequality since the mass of π-meson is the smallest of all masses of strongly interacting particles. This condition is less rigid than (2.4) and has not, therefore, been taken into account so far. But if we deal with a process occurring in the collision with the nucleus of the particles subject to only electromagnetic and weak interactions, a condition similar to that of (1.2) will be the principal one. Thus, for the processes accompanying the interaction of electrons or μ-mesons with the nuclei (e.g., the bremsstrahlung), the condition

$$q^2 \ll m_{\mathrm{e}}{}^2 \tag{2.21}$$

or respectively

$$q^2 \ll m_\mu{}^2 \tag{2.22}$$

must be satisfied instead of (1.2).

Besides, for the electrons the condition (2.21) is always more rigid than in (2.4). As to the μ-mesons, the condition (2.4) is not very essential, though it may prove more rigid. If inequality (2.22) is satisfied, the relations like (2.16), (2.17) or (2.18) remain valid even if inequality (2.4) has the opposite sign. In this case we only have to replace Z by $Zd(q^2)$, where $d(q^2)$ is the charge form-factor of the nucleus. The data on this form-factor can be taken from experiments on the elastic scattering of electrons by nuclei. For the processes involving strongly interacting particles this procedure is useless. As will be shown in sect. 3, the restriction on q^2 due to taking into account strong interactions, proves, in any case, not less rigid than (2.4).

The formulae derived in this section essentially coincide with those of ref. [3]), the differences being due to the fact that here they are obtained in a differential form, while in ref. [3]) for the cross sections integrated within permissible limits over the spectrum of pseudophotons (over q^2 and w^2 in our designations). It is noteworthy that the restrictions on q^2 in the form of (2.21) are obtained here from the condition of possibility of approximately replacing q^2 in the arguments of the vertex functions $\mathbf{R}_\perp$ and R_0 by the value corresponding to that of a real photon. Now, in the well-known papers cited, inequality (2.21) follows from the uncertainty principle restricting the correctness of the semi-classical manner of consideration used in these papers.

3. Contribution from the Processes Involving the Coulomb Nuclear Field to the Total Cross Section of Interaction of a Relativistic Particle with the Nucleus

Neglecting the second term in the braces (2.18), integrating the latter over all variables except q^2 and w^2, and denoting the result by $\sigma_c(q^2, w^2)\mathrm{d}q^2\mathrm{d}w^2$ we have

$$\sigma_c(q^2w^2)\mathrm{d}q^2\mathrm{d}w^2 = \frac{Z^2\alpha}{\pi}\frac{\mathrm{d}w^2}{w^2-m^2}\frac{\mathrm{d}q^2}{(q^2)^2}\left[q^2-\left(\frac{w^2-m^2}{2E_\mathrm{L}}\right)^2\right]\sigma_\mathrm{p}(w). \qquad (3.1)$$

Let w_0 be the energy threshold of the photoprocess in question (1.12). Then, taking into consideration (1.8) and (1.11), for the limits of integration over w^2 and q^2 we have

$$w^2_{\mathrm{min}} = w_0{}^2, \quad q^2_{\mathrm{min}} = \left(\frac{w_0{}^2-m^2}{2E_\mathrm{L}}\right)^2, \quad w^2_{\mathrm{max}} = 2E_\mathrm{L}\sqrt{q^2+m^2}. \qquad (3.2)$$

Let us sum (3.1) over all inelastic processes (1.1) possible at a given w. Then for the resulting differential cross section $\sigma_c{}^t(q^2, w^2)\mathrm{d}q^2\mathrm{d}w^2$ we obtain an expression differing from the right-hand side of (3.1) only by having $\sigma_\mathrm{p}{}^t(w)$ instead of $\sigma_\mathrm{p}(w)$, i.e., the total cross section of the γ-quantum interaction with the particle

a. Integrating the relation obtained over w^2:

$$\sigma_c{}^t(q^2)\mathrm{d}q^2 = \mathrm{d}q^2 \int_{w_{0,\,\min}^2}^{2E_L\sqrt{q^2}+m^2} \sigma_c{}^t(q^2, w^2)\mathrm{d}w^2$$

$$= \frac{Z^2\alpha}{\pi}\frac{\mathrm{d}q^2}{(q^2)^2}\int_{w_{0,\,\min}^2}^{2E_L\sqrt{q^2}+m^2} \frac{q^2-\left(\dfrac{w^2-m^2}{2E_L}\right)^2}{w^2-m^2}\sigma_p{}^t(w)\mathrm{d}w^2, \tag{3.3}$$

where $w_{0,\,\min}$ is the lowest threshold for inelastic processes. If we took into account in (3.1) the second term in braces (2.18), the contribution from the corresponding term after integrating over w^2 would be negligibly small.

We can make the evaluation $\sigma_c{}^t(q^2)$ assuming that with the increase of w the cross section $\sigma_p{}^t(w)$ becomes constant, starting from some value w equal to ε. Denote this value $\sigma_p{}^t(w)$ simply by $\sigma_p{}^t$. Then, replacing in (3.3) the lower limit by ε, and assuming that $2E_L\sqrt{q^2} \gg \varepsilon^2-m^2$ we obtain

$$\sigma_c{}^t(q^2)\mathrm{d}q^2 = \frac{Z^2\alpha}{\pi}\sigma_p{}^t \ln\frac{2E_L\sqrt{q^2}}{e^{-\frac{1}{2}}(\varepsilon^2-m^2)}\frac{\mathrm{d}q^2}{q^2}. \tag{3.4}$$

It is interesting to compare this cross section with that due to purely nuclear interactions $\sigma_N(q^2)\mathrm{d}q^2$. Let us again consider that at a high energy E_L the total cross section for inelastic processes (1.1) becomes constant and equal to geometric $\pi m_\pi^{-2}A^{\frac{2}{3}}$. Then for $\sigma_N(q^2)$ at small q^2 in order of magnitude, we have

$$\sigma_N(q^2)\mathrm{d}q^2 \approx \frac{\pi A^{\frac{2}{3}}}{m_\pi{}^2}\frac{\mathrm{d}q^2}{\bar{q}^2}, \tag{3.5}$$

where $\bar{q}$ is the mean value of the momentum transfer to the nucleus, for example, in collisions among relativistic π-mesons with the nucleus. Assuming $\sigma_p{}^t \approx \alpha/m_\pi{}^2$, we shall find by comparing (3.4) and (3.5) that the cross sections $\sigma_c{}^t(q^2)$ and $\sigma_N(q^2)$ become equal at

$$\sqrt{q^2} \approx \bar{q}\frac{Z\alpha}{\pi A^{\frac{1}{3}}}. \tag{3.6}$$

Here we consider that $(\ln 2E_L\sqrt{q^2}/e^{\frac{1}{2}}(\varepsilon^2-m^2))^{\frac{1}{2}} \approx 1$, though $2E_L\sqrt{q^2}/(\varepsilon^2-m^2) \gg 1$. Assuming $\bar{q} \approx 2$ to $3m_\pi$ we obtain from (3.6) that even for the heavier nuclei the mechanism involving the Coulomb field of the nucleus begins to predominate at very small momentum transfers to the nucleus $\sqrt{q^2}$ of the order of magnitude of 10 to 15 MeV/c. This leads, of course, to great experimental difficulties in determining the cross sections of the interactions of γ-quanta with the unstable particles from experiments on the interaction of these particles with the nuclei.

Finally, let us estimate the total Coulomb nuclear field contribution to total interaction cross section. For this purpose let us integrate (3.4) over q^2 from

$q^2_{\min} = \{(\varepsilon^2 - m^2)/2E_{\mathrm{L}}\}^2$ (see (3.2)) to $q^2_{\max} = m_\pi^2 A^{\frac{2}{3}}$. This leads to

$$\sigma_{\mathrm{c}} = \frac{Z^2\alpha}{\pi}\,\sigma_{\mathrm{p}}{}^{\mathrm{t}}\left(\ln\frac{2m_\pi E}{e^{\frac{1}{2}}A^{\frac{1}{3}}(\varepsilon^2 - m^2)}\right)^2. \tag{3.7}$$

Yet even if we suppose $\sigma_{\mathrm{p}}{}^{\mathrm{t}}(w)$ to be constant when $\omega > \varepsilon$, σ_{c} increases directly with $(\ln E)^2$ only up to the values of the energy restricted by the condition

$$(\varepsilon^2 - m^2)/2E_{\mathrm{L}} > 1/a_0, \tag{3.8}$$

where

$$a_0 = 1/m_{\mathrm{e}}\alpha Z^{\frac{1}{3}}. \tag{3.9}$$

When

$$(\varepsilon^2 - m^2)/2E_{\mathrm{L}} < 1/a_0, \tag{3.10}$$

the electron screening of the nuclear charge begins to take effect. Replacing the lower limit by $1/a_0{}^2$ as we integrate (3.4) in this case we obtain

$$\sigma_{\mathrm{c}} \approx \frac{2Z^2\alpha}{\pi}\,\sigma_{\mathrm{p}}{}^{\mathrm{t}}\ln\frac{m_\pi}{\alpha m_{\mathrm{e}} Z^{\frac{1}{3}} A^{\frac{1}{3}}}\ln\left[\left(\frac{m_\pi m_{\mathrm{e}}\alpha Z^{\frac{1}{3}}}{eA^{\frac{1}{3}}}\right)^{\frac{1}{2}}\frac{2E_{\mathrm{L}}}{\varepsilon^2 - m^2}\right]. \tag{3.11}$$

If we consider ε to be of the order of several π-meson masses, it follows from (3.10) that screening has effect only at the energies $E_{\mathrm{L}} > 10^{13}$ eV. At $E = 10^{12}$ eV, $Z = 70$ and again considering that $\sigma_{\mathrm{p}}{}^{\mathrm{t}} \approx \alpha/m_\pi{}^2$, with the help of (3.7) we find

$$\sigma_{\mathrm{c}} \approx 40 \text{ mb}. \tag{3.12}$$

4. Application to Some Special Processes

For the bremsstrahlung processes (1.13) we have

$$R_\mu = M_{\mu\nu} e_\nu, \tag{4.1}$$

where e_ν is the polarization vector of the outgoing photon. The momentum of the latter will be denoted by k and the momentum of the meson after the bremsstrahlung by p'. The tensor $M_{\mu\nu}$ corresponds to the vertex part with two meson and two photon lines (see the right-hand part of the graph in fig. 2). In order to write a general expression for $M_{\mu\nu}$, let us construct four orthogonal vectors[4] $n^{(i)}$ out of the vectors p, p', q, k, bearing in mind that $q^2 \neq 0$. First introduce the vectors

$$K = k + q, \quad t = k - q, \quad P = p + p'. \tag{4.2}$$

Then the vectors

$$t' = t - \frac{Kt}{K^2}K, \quad P' = P - \frac{PK}{K^2}K - \frac{Pt'}{t'^2}t', \quad N_\mu = i\varepsilon_{\mu\nu\lambda\rho}P'_\nu K_\lambda t'_\rho \tag{4.3}$$

together with the vector K will constitute the desired system of vectors $n^{(i)}$. Therefore, $M_{\mu\nu}$ can be represented in the following form

$$M_{\mu\nu} = \sum_{i,k} b_{ik}(w^2, t^2, q^2) n_\mu^{(i)} n_\nu^{(k)}. \tag{4.4}$$

The conditions $q_\mu M_{\mu\nu}$ and $M_{\mu\nu} k_\nu = 0$ resulting from the gauge invariance give rise to a number of relations between the quantities b_{ik}. Therefore, for $M_{\mu\nu}$ we finally obtain

$$M_{\mu\nu} = a_1 P'_\mu P'_\nu + a_2 N_\mu N_\nu + c_1 \left(q_\mu - \frac{q^2}{kq} k_\mu\right) P'_\nu + c_2 P'_\mu k_\nu + c_3 \left(q_\mu - \frac{q^2}{kq} k_\mu\right) k_\nu. \tag{4.5}$$

The quantities a_1, a_2, c_1, c_2, c_3, are functions of the same invariants as b_{jk}. Since $k_\nu e_\nu = 0$, then

$$R_\mu = a_1 (P'e) P'_\mu + a_2 (Ne) N_\mu + c_1 (P'e) \left(q_\mu - \frac{q^2}{kq} k_\mu\right). \tag{4.6}$$

Substituting eq. (4.6) into (2.9) and assuming wherever possible that $q^2 = 0$, we shall have

$$\mathrm{d}\sigma_\mathrm{c} = \frac{Z^2\alpha}{\pi} \frac{\mathrm{d}w^2}{w^2 - m^2} \frac{\mathrm{d}q^2}{(q^2)^2} \left\{ \left[q^2 - \left(\frac{w^2 - m^2}{2E_\mathrm{L}} \right)^2 \right] \mathrm{d}\sigma_\mathrm{p} + \frac{(w^2 - m^2)^2 - w^2 t^2}{\pi E_\mathrm{L}{}^4 t^2} \left| a_1 \frac{(w^2 - m^2)^2 - w^2 t^2}{t^2} + c_1 \frac{w^2 - m^2}{4} \right| \mathrm{d}t^2 \right\}, \tag{4.7}$$

where $\mathrm{d}\sigma_\mathrm{p}$ is the Compton differential cross section on π- or K-mesons

$$\mathrm{d}\sigma_\mathrm{p} = \left[\frac{(w^2 - m^2)^2}{t^2} - w^2 \right]^2 (|a_1|^2 + |a_2|^2 t^8) \frac{\mathrm{d}t^2}{2\pi (w^2 - m^2)}. \tag{4.8}$$

Integration over the azimuth of the vector t was performed in (4.7) and (4.8). In the main region of the possible values q^2 and w^2 the second term in (4.7) can be neglected, as mentioned in sect. 2 after eq. (2.20). The measurement of the bremsstrahlung cross section under these conditions would make it possible to determine the Compton cross section on π or K-mesons, and measuring it when $q_\perp \ll m(w^2 - m^2)/2E_\mathrm{L}{}^2$ would make it possible to determine the second term in braces (4.7).

The contribution to $R_0 = -1/m\, p_\mu R_\mu$ from the third term in (4.6) containing the factor $q_\mu - (q^2/kq) k_\mu$ is given only due to the term q_μ, the other term $q^2/kq k_\mu$ being neglected. Since in the initial expression $U_\mu R_\mu$ the terms in R_μ, proportional to q_μ, give no contribution, it might seem that the entire third term in (4.6) ought to be neglected. This would be wrong, however, since (4.6) is substituted into eq. (2.9) already transformed, each of its terms containing, explicitly, the small factors $1 - V^2$ or $q_\perp$. Therefore, in other factors (particularly in $q_\mu - (q^2/kq) k_\mu$) we should put $q^2 = 0$. If right from the outset we take as starting point the expression $U_\mu F_\mu$, where $F_\mu = q_\mu + q^2 f_\mu$, then it follows from $F_\mu q_\mu = 0$ that $q_\mu f_\mu = -1$. Hence it is easy to obtain $U_\mu F_\mu = q^2 U_\mu f_\mu$

$= -(q^2/q_0(1-V^2)^{\frac{1}{2}})\{1+\mathbf{f}_\perp\cdot\mathbf{q}_\perp+\mathbf{f}_\parallel\cdot\mathbf{q}_\parallel(1-V^2)\} \approx -q^2/q_0(1-V^2)^{\frac{1}{2}} = -q_0(1-V^2)^{\frac{1}{2}}-q_\perp^2/q_0(1-V^2)^{\frac{1}{2}}$. Under the conditions when $q_\perp < q_0(1-V^2)$, the second term here can be neglected, and we shall obtain $U_\mu F_\mu = -q_0(1-V^2)^{\frac{1}{2}} = (1-V^2)^{\frac{1}{2}} q_\mu p_\mu/m$ i.e., just the result obtained in substituting in (2.9) q_μ for F_μ.

For the process (1.14) $\pi+\mathrm{N} \to \mathrm{N}+\pi_1+\pi_2$ the vertex part R_μ is a pseudovector. Let p_1 and p_2 be the momenta of the π-mesons produced in the reaction. Then from the vectors q, p, p_1, p_2, satisfying the equation $q+p = p_1+p_2$ one independent pseudovector can only be constructed $N_\mu = i\varepsilon_{\mu\lambda\rho\sigma} p_\lambda p_{1\rho} p_{2\sigma}$. It satisfies the condition $q_\mu N_\mu = 0$.

Therefore, we can assume

$$R_\mu = a(w^2, t^2, q^2)N_\mu, \tag{4.9}$$

where $t = p_1 - p$. For the process under consideration, the formula relating the cross sections of the reactions $\pi+\mathrm{N} \to \mathrm{N}+\pi_1+\pi_2$ and $\gamma+\pi \to \pi_1+\pi_2$ coincides with (2.17). In it there will be no term analogous to the second term in (2.18) or (4.7) since $N_\mu p_\mu = 0$. The differential cross section $\mathrm{d}\sigma_\mathrm{p}$ of the reaction $\gamma+\pi \to \pi_1+\pi_2$ averaged over polarizations and integrated over the vector t azimuth is connected with the form-factor $a(w^2, t^2, 0)$ in the following manner

$$\mathrm{d}\sigma_\mathrm{p} = \frac{|a|^2}{128\pi}\,\frac{w^2 t^2(w^2-3m^2-t^2)}{(w^2-m^2)^2}\,\mathrm{d}t^2. \tag{4.10}$$

Now let us dwell on the process (1.15)

$$\Lambda^0+\mathrm{N} \to \mathrm{N}+\Sigma^0.$$

Putting the given reaction through the same transformations as have led from (2.9) to (2.18) we obtain

$$\mathrm{d}\sigma_\mathrm{e} = \frac{2Z^2\alpha m_\Lambda m_\Sigma}{(m_\Sigma^2-m_\Lambda^2)^2}\left\{\left[q^2-\frac{(m_\Sigma^2-m_\Lambda^2)^2}{4E_\mathrm{L}^2}\right]|\mathbf{R}_\perp|^2+\frac{m_\Lambda^2(m_\Sigma^2-m_\Lambda^2)^2}{2E_\mathrm{L}^4}|R_0|^2\right\}\frac{\mathrm{d}q^2}{(q^2)^2}. \tag{4.11}$$

Averaging this relation over the spins of Λ^0 and summing over the spins of Σ^0-particle, we have

$$\mathrm{d}\sigma_\mathrm{e} = \frac{8\pi Z^2\alpha m_\Sigma^3}{(m_\Sigma^2-m_\Lambda^2)^3}\left\{\left[q^2-\frac{(m_\Sigma^2-m^2{}_\Lambda)^2}{4E_\mathrm{L}^2}\right]\frac{1}{\tau}+\frac{m_\Lambda^3(m_\Sigma^2-m_\Lambda^2)^3}{8\pi m_\Sigma^2 E_\mathrm{L}^4}\overline{|R_0|^2}\right\}\frac{\mathrm{d}q^2}{(q^2)^2}. \tag{4.12}$$

Here we have taken into account the connection between the lifetime τ of Σ^0-particle with respect to the decay $\Sigma^0 \to \Lambda^0+\gamma$ and the value $\overline{|\mathbf{R}_\perp|^2}$

$$\frac{1}{\tau} = \frac{m_\Lambda(m_\Sigma^2-m_\Lambda^2)}{4\pi m_\Sigma^2}\overline{|\mathbf{R}_\perp|^2}. \tag{4.13}$$

Lines above $|R_0|^2$ and $|\mathbf{R}_\perp|^2$ denote averaging and summing over the spins of the initial and final states respectively. To estimate the contribution connected with the Coulomb field, to the total cross section of the transformation of Λ^0 into Σ^0 in collisions of the Λ^0-particle with the nucleus, let us integrate (4.12) over q^2 within the limits from $q^2_{\min} = (m_\Sigma{}^2-m_\Lambda{}^2)/(2E_L)^2$ to $q^2_{\max} = m_\pi{}^2A^{-\frac{2}{3}}$; the second term in braces (4.12) can be neglected. As a result of integrating we obtain

$$\sigma_c = \frac{16\pi Z\alpha^2 m_\Sigma{}^3}{(m_\Sigma{}^2-m_\Lambda{}^2)^3\tau}\ln\frac{2m_\pi E_L}{e^{\frac{1}{2}}(m_\Sigma{}^2-m_\Lambda{}^2)A^{\frac{1}{3}}}. \tag{4.14}$$

The decay $\Sigma^0 \to \Lambda^0+\gamma$ is an M1 or E1 transition (depending upon the relative parity of the Σ^0 and Λ^0 particles). Therefore one can estimate τ, using the formula for the probability of a dipole transition

$$\frac{1}{\tau} = \tfrac{2}{3}(m_\Sigma-m_\Lambda)^3\mu^2$$

and making the natural supposition that the value of the transition dipole momentum μ lies within the range of $\alpha^{\frac{1}{2}}/m_\pi$ and $\alpha^{\frac{1}{2}}/m_N$. When $E_L \approx 10^{10}$ eV and $Z\alpha = \frac{1}{2}$ this leads to the following evaluation:

$$0.4 \text{ mb} < \sigma_c < 20 \text{ mb}.$$

Eq. (4.14) is valid provided

$$E_L < \frac{m_\Sigma{}^2-m_\Lambda{}^2}{2m_e\alpha Z^{\frac{1}{3}}} \approx 10^{13}\text{ eV}, \tag{4.15}$$

when screening the nuclear field by electrons is inessential. Assuming the lower limit of integrating over q^2 to be equal $1/a_0{}^2$ (see (3.9) at higher energies, we find

$$\sigma_c = \frac{16\pi Z^2\alpha m_\Sigma{}^3}{(m_\Sigma{}^2-m_\Lambda{}^2)^3\,\tau}\ln\frac{m_\pi}{m_e\alpha Z^{\frac{1}{3}}A^{\frac{1}{3}}}. \tag{4.16}$$

In the laboratory coordinate system q^2 is connected with the angle θ between the direction of the outgoing Σ^0-particle and that of the Λ^0-particle

$$q^2 = \frac{m_\Sigma{}^2-m_\Lambda{}^2}{2E_L}+E_L{}^2\theta^2. \tag{4.17}$$

Substituting this expression in (4.12) and introducing an element of the solid angle $d\Omega = 2\pi\theta d\theta$ we shall obtain the following formula for the angular distribution of created Σ^0-particles:

$$d\sigma_c = \frac{8Z\alpha^2 m_\Sigma{}^3}{(m_\Sigma{}^2-m_\Lambda{}^2)^3\,\tau}\,\frac{\theta^2+\theta_1{}^2}{(\theta^2+\theta_2{}^2)^2}\,d\Omega, \tag{4.18}$$

where

$$\theta_1{}^2 = \frac{m_\Lambda{}^3(m_\Sigma{}^2-m_\Lambda{}^2)^3}{8\pi m_\Sigma{}^2E_L{}^6}\,|R_0|^2\tau, \qquad \theta_2{}^2 = \left(\frac{m_\Sigma{}^2-m_\Lambda{}^2}{2E_L{}^2}\right)^2. \tag{4.19}$$

The quantities τ and θ_1 can easily be expressed through the form-factors contained in the vertex part R_μ. Having written the latter in the form

$$R_\mu = (\bar{u}_\Sigma | \Gamma_\mu | u_\Lambda), \tag{4.20}$$

we can define the most general expression for Γ_μ satisfying the condition (2.3). The parities P_Λ and P_Σ of the particles Λ^0 and Σ^0 being equal, we have

$$\Gamma_\mu = -i\left\{a(q^2)\left(q_\mu + \frac{iq^2}{m_\Sigma - m_\Lambda}\gamma_\mu\right) + b(q^2)(\gamma_\mu \hat{q} - \hat{q}\gamma_\mu)\right\}. \tag{4.21}$$

If $P_\Lambda = -P_\Sigma$, then

$$\Gamma_\mu = \gamma_5\left\{a(q^2)\left(q_\mu - \frac{iq^2}{m_\Sigma + m_\Lambda}\gamma_\mu\right) + b(q^2)(\gamma_\mu \hat{q} - \hat{q}\gamma_\mu)\right\}. \tag{4.22}$$

The form-factors $a(q^2)$ and $b(q^2)$ in both of these formulae are real values, which follow from the invariance of strong interactions with respect to charge conjugation and from R_μ coinciding, except for trivial factors, with the matrix element $\langle \Sigma^0 | j_\mu(0) | \Lambda^0 \rangle$, where $j_\mu(x)$ is the hermitian current operator.

In both cases $P_\Lambda = P_\Sigma$ and $P_\Lambda = -P_\Sigma$ we have

$$\frac{1}{\tau} = b^2(0)\,\frac{(m_\Sigma{}^2 - m_\Lambda{}^2)^3}{2\pi m_\Sigma{}^3}. \tag{4.23}$$

For θ_1 the following expressions are obtained

$$\theta_1 = \begin{cases} \dfrac{(m_\Sigma{}^2 - m_\Lambda{}^2)(m_\Sigma - m_\Lambda)}{4E_\mathrm{L}{}^3}\left(1 + \dfrac{m_\Sigma + m_\Lambda}{2(m_\Sigma - m_\Lambda)}\,\dfrac{a(0)}{b(0)}\right) & \text{if} \quad P_\Lambda = P_\Sigma, \\[2ex] \dfrac{(m_\Sigma{}^2 - m_\Lambda{}^2)(m_\Sigma + m_\Lambda)}{4E_\mathrm{L}{}^3}\left(1 + \dfrac{m_\Sigma - m_\Lambda}{2(m_\Sigma + m_\Lambda)}\,\dfrac{a(0)}{b(0)}\right) & \text{if} \quad P_\Lambda = -P_\Sigma. \end{cases} \tag{4.24}$$

The applicability condition of the formulae obtained is reduced for the process in question to the following inequality

$$\theta \ll \frac{m_\pi}{E_\mathrm{L} A^{\frac{1}{3}}}. \tag{4.25}$$

Since $\theta_1 \ll \theta_2 \ll m_\pi / E_\mathrm{L} A^{\frac{1}{3}}$, eq. (4.18) contains only one unknown parameter τ, with the exception of the smallest angles $\theta \approx \theta_1$. Therefore, the lifetime of the Σ^0-particle might be determined by measuring the differential cross section of the transformation of the Λ^0-particle into the Σ^0-particle within the range of angles $\theta_1 \ll \theta \ll m_\pi / E_\mathrm{L} A^{\frac{1}{3}}$, or the total cross section of process σ_c (eqs. (4.14) or (4.16)) when a small momentum ($q^2 \ll m_\pi{}^2 A^{-\frac{2}{3}}$) is transferred to the nucleus.

We wish to thank Professor O. Piccioni for his interesting discussions of the problems considered in this paper during the 9th International Conference on the High Energy Physics held in Kiev, in 1959.

We also wish to thank V. B. Berestetsky, V. N. Gribov, I. T. Dyatlov for their discussions, helpful comments and interest in our work.

References

1) M. L. Good and W. D. Walker, preprint
2) G. F. Chew and F. E. Low, Phys. Rev. **113** (1959) 1640
3) G. Weizsäcker, Z. f. Phys. **88** (1934) 612;
E. Williams, Phys. Rev. **45** (1934) 729
4) R. E. Prange, Phys. Rev. **110** (1958) 240

2.1

Nuclear Physics **23** (1961) 468—480; © *North-Holland Publishing Co., Amsterdam*

Not to be reproduced by photoprint or microfilm without written permission from the publisher

CROSS SECTIONS FOR THE (γ, n) REACTION IN Cu^{63}, Cu^{65}, Zn^{64}, Sb^{121} AND Pr^{141}, MEASURED WITH MONOCHROMATIC GAMMA RAYS

G. E. COOTE, W. E. TURCHINETZ † and I. F. WRIGHT ††
Research School of Physical Sciences, Australian National University, Canberra

Received 17 November 1960

Abstract: Cross sections for the (γ, n) reaction in Cu^{63}, Cu^{65}, Zn^{64}, Sb^{121} and Pr^{141} have been measured using gamma rays from the $Li^7(p, \gamma)Be^8$ and $B^{11}(p, \gamma)C^{12}$ reactions. NaI(Tl) crystals were used to monitor the radiation and to measure the residual activity.

The $Cu^{63}(\gamma, n)Cu^{62}$ cross section for the lithium radiation from the 440 keV resonance is 59±6 mb. The cross sections at 12.2, 14.8, 16.7 and 17.6 MeV are then 11±2, 33±4, 63±8 and 73±8 mb, respectively. These results confirm the bremsstrahlung measurement of the shape of the cross section but the absolute cross section values are 25 % lower.

Cross sections for the lithium resonance radiation, measured relative to that of Cu^{63}, are: Cu^{65}, 70±7 mb; Zn^{64}, 40±4 mb; Sb^{121}, 122±13 mb; Pr^{141}, 181±20 mb.

Comparison with previous results suggests that discrepancies are due to inaccuracies in absolute β-counting.

1. Introduction

Most measurements of photonuclear cross sections have been made using the continuous bremsstrahlung spectra from electron accelerators. Because of the low intensities and limited number of energies available few measurements have employed monochromatic gamma rays from nuclear reactions. It is desirable, however, that some measurements be made with such sources, as a more direct method than the unfolding of bremsstrahlung yield curves.

The cross section for the reaction $Cu^{63}(\gamma, n)Cu^{62}$ is often used as a standard for the normalization of new data and has been investigated frequently either with bremsstrahlung or the radiation from the $Li^7(p, \gamma)Be^8$ reaction. Comparison with bremsstrahlung results is made using the experimental intensity ratio of the 17.6 and 14.8 MeV components [1]). Results of work to date are summarized in tables 3 and 4. There are considerable variations between different absolute measurements and although bremsstrahlung values show reasonable agreement with peak cross sections of about 100 mb, most of the lithium radiation measurements yield results about half this value.

For absolute cross section measurements using bremsstrahlung the radiation intensity is usually determined with an ionization chamber, although exceptions to this are Krohn and Shrader [2]) who used a calibrated pair spectrometer, and Berman and Brown [3]) and Scott, Hanson and Kerst [4]) who measured the electron current and calculated the X-ray intensity from this. Difficulties arise in the accurate unfolding of the yield curve, as the thick target bremsstrahlung spectrum is not accurately known and errors in the yield curve become progressively magnified up to the higher energies.

---

† Now at Physics Dept., Massachusetts Institute of Technology, Cambridge, Mass., U.S.A.

†† Now at Dept. of Physics, University of Wisconsin, Madison, Wis., U.S.A.

On the other hand the yields of monochromatic gamma rays are low and entail irradiation in conditions of poor geometry; in most of the experiments the monitoring has been done with geiger counters, which have low efficiency and are difficult to calibrate accurately.

All the activation experiments have used positon detection, for which absolute measurements are difficult due to back-scattering and self-absorption.

In an attempt to resolve the above difficulties, the cross section measurement for lithium gamma rays from the 440 keV resonance has been repeated, using NaI(Tl) crystals to monitor the radiation and to detect the activity produced. As the relative intensity of the two gamma ray lines depends on the excitation energy, by bombarding at higher energies and measuring the ratio accurately it was possible to obtain the cross section at each gamma ray energy separately. The 12 and 16 MeV gamma rays from the $B^{11}(p, \gamma)C^{12}$ reaction were used in a similar way to obtain further points on the cross section curve, enabling a comparison to be made with the curve obtained from bremsstrahlung work.

Using lithium resonance radiation, cross sections relative to that of Cu^{63} were determined for Zn^{64}, Cu^{65}, Sb^{121} and Pr^{141}, for further comparison with bremsstrahlung results.

2. Gamma Rays

Details of the production of the gamma rays are given in table 1. Each lithium target was a spot 0.65 cm in diameter, although for good adherence to the 0.65 cm thick copper target backing the boron targets were 2.5 cm in diameter. Proton beams of 50 to 100 μA from the Canberra 1.2 MeV H.T. set were focused by electrostatic lenses through a 0.48 cm diameter beam-stop on to the target 1.3 cm behind it. The intensity ratios were re-measured during the present work.

The flux was monitored in the line of the beam with a 12.7 cm diameter × 10.3 cm long NaI(Tl) crystal †, mounted with its cylindrical axis vertical and shielded on the sides by 5 cm of steel and 8 cm of lead. The lead collimator was 8 cm thick, with a slightly tapered hole 1.4 cm in diameter at the front face, which was 40 cm from the target. For the absolute cross section measurement the collimator was replaced by another with a 1.4 cm diameter straight hole, to make the geometrical aperture more definite. Pulses from a Dumont 6363 photomultiplier were fed to a 100-channel Hutchinson-Scarrott kicksorter,

---

† One of the „matched window" line of the Harshaw Chemical Co.

TABLE 1

Gamma rays used in experiment

Reaction	Gamma ray energies (MeV)	Target preparation	Target thickness	E_p. (keV)	Intensity ratio at 0° (present work)	Nomenclature	Angular distribution	Approximate relative intensity
$Li^7(p, \gamma)Be^8$	"14.8" $14.35+\frac{7}{8}E_p$. "17.6" $17.25+\frac{7}{8}E_p$.	Vacuum evaporation of natural lithium	Thick	450—550	17.6 : 14.8 1.94± 0.1	Lithium "resonance radiation"	Both isotropic	100
			150—200 keV	800—900	≈0.53	Lithium "non-resonance radiation"	Both anisotropic	6
$B^{11}(p, \gamma)C^{12}$	"12.2" $11.53+\frac{11}{12}E_p$. "16.7" $15.96+\frac{11}{12}E_p$.	Evaporation of slurry of boron in alcohol	1 mg/cm^2	660	12.2 : 16.7 5.62± 0.1		Both anisotropic	5
				900	2.76±0.05		Both anisotropic	8

while two scalers in parallel counted all pulses above the valley of the spectrum at 9.5 MeV. Corrections for drift in gain and variation in flux during a run were usually less than 1 %.

For the measurement of the absolute cross section the effective solid angle subtended by the collimator was needed. This was larger than that subtended by the geometrical aperture, owing to penetration of the edge of the hole by the gamma rays [5, 6]). The magnitude of this effect was measured by moving the collimator and crystal in the 0° position to different distances d from the target, and recording the ratio N of the counts above 9.5 MeV to those in a fixed monitor crystal. To a good approximation the edge effect varies as $1/d^3$, while the number of gamma rays through the geometrical aperture varies as $1/d^2$. A plot of Nd^2 against $1/d$ gave a straight line with a positive slope, which was extrapolated to $1/d = 0$ for which the edge effect is zero. For the straight collimator the total aperture A was related to the geometrical aperture G by

$$A = G\left[1+\frac{1.65}{d}\right],$$

where d is the distance in cm to the rear collimator face.

As the samples were close to the target the angular distribution of the gamma rays was determined immediately after an irradiation by rotating the crystal about the target, with a similar fixed crystal as a monitor. Angular distributions from measurements at 0°, 35° and 55° were used to correct the yields to those for isotropic radiation.

Intercomparison of the cross sections for the lithium and boron radiations and the determination of the relative intensities of the gamma rays required analysis of the spectra. Each spectrum was separated into its constituent peaks, making use of a monochromatic line shape determined using the 20 MeV T(p, γ) line. Comparison with the boron spectra showed that the spectrometer line shape was constant for gamma rays from 16 to 20 MeV, and that at 12 MeV the tail was only slightly lower (see also ref. [7])). In the analysis of the lithium spectra the tritium line (with a suitable energy scale) was normalized to the upper edge of the 17.6 MeV line and subtracted to leave the 14.8 MeV contribution. This had rather a different shape at the high-energy end, owing to the 2 MeV width of the original line. Separation of the boron spectra into components was easier, as the overlap of the lines was much less.

The monitor counts were then corrected so that pulses were counted only above 0.65 of the energy of each peak. This position was below the region where the width of the 14.8 MeV line affected the line shape, but above the low-energy background. The constancy of the line shape then ensured the counting of the same fraction of the pulses in each peak, and comparisons were made directly using these numbers. This method makes no assumption about the low-energy tail, except that it has the same shape in each case. Corrections were made for the slight change of NaI attenuation coefficient with energy.

The results for the 17.6 : 14.8 MeV ratio at 0° to the beam were 1.94 ± 0.1 for the resonant radiation and about 0.53 for the non-resonant, depending somewhat on the target thickness and beam energy. The error quoted is believed to be the maximum error, and arises mainly because the shape of the upper edge of the 14.8 MeV line is not known accurately, making the normalization slightly uncertain. Comparison can be made with the values 2.30 ± 0.04 and 0.54 ± 0.08 obtained by Mainsbridge 8) for thin targets viewed at 90° to the beam. For the boron spectra the 12.2 : 16.7 MeV ratio was 5.62 ± 0.1 at 660 keV and 2.76 ± 0.05 at 900 keV, in reasonable agreement with the data of Gove and Paul 9).

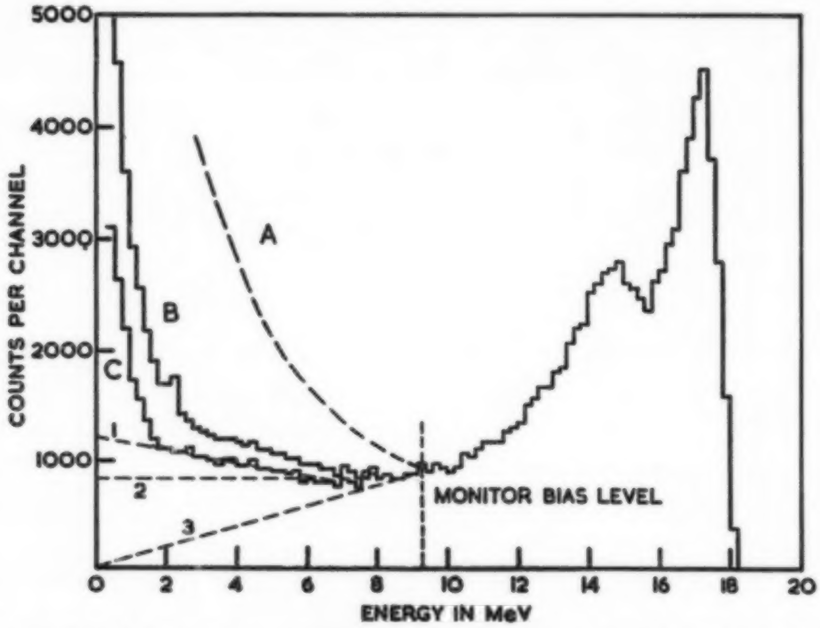

Fig. 1. Spectra from Li^7(p, γ)Be^8 resonance radiation. (A) Normal spectrum taken with 8 cm thick lead collimator. (B) Spectrum taken with 30 cm lead collimator. (C) Spectrum B with background subtracted (see text); three possible low energy extrapolations are shown.

Determination of the Cu^{63}(γ, n) absolute cross section required a knowledge of the fraction of the gamma rays counted by the monitor, hence a knowledge of the line shape in the crystal down to zero energy. As there is discrepancy between previous measurements 7, 10), the shape was studied during the experiment, with the result shown in histogram C of fig. 1. Spectrum B was obtained with the length of the lead collimator increased to 30 cm and the background determined from spectra taken under the following conditions:

i) gamma rays at full intensity, collimator blocked with a 15 cm long lead plug;
ii) lithium target replaced by a blank copper target, with beam conditions unchanged;

iii) H.T. set turned off.

This procedure has not subtracted the contribution from gamma rays scattered by the collimator. Analysis of the change of spectrum shape with collimator distance showed that at the distance used the contribution between 4 and 8 MeV was at most a few percent. The tail was therefore assumed to be horizontal (extrapolation 2).

3. Absolute Cross Section of $Cu^{63}(\gamma, n)Cu^{62}$

3.1. EXPERIMENTAL METHOD

Copper disks 1.9 cm in diameter by 0.32 cm were irradiated with the lithium resonance radiation in a fixed geometry, 1.5 cm from the target.

For measurement of the residual activity a sandwich of the sample between two 0.16 cm thick copper disks was placed between two NaI(Tl) crystals, one 12.7 cm diameter by 10.3 cm and the other 7.6 cm diameter by 7.6 cm. Two independent determinations of the activity were made by measuring the 0.51 MeV photopeak in each crystal. Measurement of the crystal efficiencies was made with a standard Na^{22} source made from a solution calibrated by the National Bureau of Standards, Washington, to a stated accuracy of ±2 %.

3.2. RESULTS

The number of counts in the 0.51 MeV photopeak from the standard Na^{22} source was corrected for (i) counts from the tail of the 1.28 MeV gamma ray, and (ii) counts lost to the sum peak. The corrections were estimated from the relative heights of the 0.51 and 1.28 MeV peaks and the 1.79 MeV sum-peak, and the photofraction for 1.28 MeV obtained from the calculations of Miller *et al.* [11]). The average corrections were −8 % and +14 % respectively for the 7.6 cm crystal and −6 % and +27 % for the larger crystal. Uncertainty in these corrections is the largest source of error in the activity measurement, for which an overall accuracy of 5 % is estimated. The consistency of the results from the two crystals was considerably better than this, as the two measurements of the activity agreed to within 0.4 %. Statistical and geometrical errors in the cross section measurement were much less than the uncertainty in the crystal efficiencies. The half-life of Na^{22} was taken as 2.585±0.006 y [12]), and that of Cu^{62} 9.9±0.1 m.

Corrections were applied for the absorption of the lithium gamma rays in the sample (5.8 %), electron capture in Cu^{62}(1.8 %), and the edge effect in the collimator (3.9 %). The effective flux at the sample in terms of the monitor count was calculated by an integration over the disk, taking the target to be a point source.

Assuming the tail of the gamma ray response function to be horizontal (extrapolation 2 of fig. 1), the cross section for the lithium resonance radiation is 59±3 mb. A tail following extrapolation 1 gives a lower limit to the cross section of 56±3 mb. Although it would appear to be ruled out by the present measurements a tail of the form reported by Koch and Wyckoff, i.e. extrapolation 3, would give a cross section of 68 mb.

Recognizing the uncertainty in the shape of the spectrum we adopt the value 59±6 mb.

4. Shape of $Cu^{63}(\gamma, n)Cu^{62}$ Cross Section

4.1. EXPERIMENTAL METHOD

Copper disks 1.9 cm in diameter by 0.63 cm were irradiated in a recess in the target backing, with the front face of the sample 0.43 cm from the target spot, although for some pairs of lithium irradiations this distance was increased to 1.5 cm. For each target bombardments at the two energies were made in close succession so that conditions remained the same, and an angular distribution was measured after each irradiation. The residual activity was detected with a 7.6 cm × 7.6 cm NaI(Tl) crystal, with a standard sequence of irradiation and counting times. Measurements of the activity induced per monitor count were reproducible to better than 1 %.

4.2. RESULTS

For lithium non-resonance irradiations the corrections for anisotropy were 7 % for the close-up geometry and 2 % for the better geometry. The ratios of resonance- to non-resonance yield at the two positions gave good agreement. Corrections for the boron irradiations were about 4 %. Allowance was made in the calculation for the slight increase of gamma ray energy with proton energy. The correction required a knowledge of the slope of the cross section curve at each of the four energies studied. Figures taken from the curves of Katz and Cameron [13]) and Berman and Brown [3]) were the following:

$$\sigma_{12.3} = 1.1\sigma_{12.1}, \quad \sigma_{15.1} = 1.13\sigma_{14.7}, \quad \sigma_{16.7} = 1.06\sigma_{16.5}, \quad \sigma_{17.6} = \sigma_{17.9}.$$

As a self-consistent shape is obtained it is believed that errors introduced by these corrections are small. A calculation using the shape near 15 MeV found by Berman and Brown showed that the width of the 14.8 MeV line gave it an effective energy about 80 keV higher than its nominal energy, but this makes no significant change in the results. The results obtained for the cross sections, relative to that for the lithium resonance radiation, are:

$$0.18\pm0.03 \ (12.2 \text{ MeV}), \quad 0.56\pm0.04 \ (14.8 \text{ MeV}),$$
$$1.06\pm0.07 \ (16.7 \text{ MeV}), \quad 1.23\pm0.03 \ (17.6 \text{ MeV}).$$

Taking the cross section for the lithium radiation to be 59±6 mb, these become:

$$11\pm2 \text{ mb} \ (12.2 \text{ MeV}), \quad 33\pm4 \text{ mb} \ (14.8 \text{ MeV}),$$
$$63\pm8 \text{ mb} \ (16.7 \text{ MeV}), \quad 73\pm8 \text{ mb} \ (17.6 \text{ MeV}).$$

5. Cross Sections of Zn^{64}, Cu^{65} Sb^{121}, Pr^{141}

5.1. EXPERIMENTAL METHOD

The samples were contained in thin-walled aluminium cans 1.9 cm in diameter and 0.63 cm deep. The copper samples were solid disks, the zinc and antimony Analar-grade powders and the praseodymium was as PrF_3. They were irradiated in the close-up geometry previously described, with irradiation times 6 m for Pr, 4 h for Cu^{65} and about one half-life for the others.

The annihilation radiation was detected with a 3.8 cm×3.8 cm NaI(Tl) crystal, with the disks held in a brass jig sufficiently thick to prevent positons entering the crystal. The spectrum was recorded on the kicksorter and a single-channel analyzer counted the pulses in the photopeak. Frequent checks were made of the background and of the counting efficiency, using a Na^{22} source.

5.2. RESULTS

As annihilation radiation was counted in each case there were no corrections for crystal efficiency. Self-absorption corrections were calculated using the gamma ray attenuation coefficients of Grodstein [14]), allowing for the non-uniform distribution of activity in the disks; this was calculated from the irradiation geometry, assuming the target to be a point source. Corrections were made for absorption of the lithium gamma rays in the disks, the largest being 11 % for Cu. The corrections for absorption do not enter into the comparison of Cu^{63} and Cu^{65} as the same samples were used for each. The mass of PrF_3 was corrected for the presence of 2 % of water. In the estimate of experimental accuracy an allowance of 2 % was made for variations in irradiation and counting geometry from one sample to another and of 1 % for errors in monitor bias setting and variations in irradiation flux. It was assumed that the absorption corrections could be made to within 10 %. Statistical errors derived from the deviations between runs were Cu^{63}, 0.5 % (7 measurements); Cu^{65}, 1.4 % (2); Zn^{64}, 1.4 % (3); Sb^{121}, 1.1 % (3); Pr^{141}, 1 % (4).

The values for the half-life and fraction of positron decay were taken from Strominger *et al.* [15]) or the Nuclear Data Cards [16]). Values used and the resulting cross sections are given in table 2.

TABLE 2

Cross sections measured with the $Li^7(p, \gamma)$ resonance radiation

Isotope	Half-life	Ratio β^+/total decay	Correction for self-absorption (%)	Total cross section relative to Cu^{63}	Total cross section (mb)
Cu^{63}	9.9 m	0.981	25	1	59± 6
Cu^{65}	12.8 h	0.19	25	1.19±0.03	70± 7
Zn^{64}	38.3 m	0.904	10	0.68±0.03	40± 4
Sb^{121}	16.4 m	0.438	11	2.07±0.09	122±13
Pr^{141}	3.4 m	0.54	4	3.07±0.14	181±20

6. Discussion

6.1. $Cu^{63}(\gamma, n)Cu^{62}$ CROSS SECTION

The cross sections in the present section are computed for the same mixture of gamma rays as the lithium radiation. Taking the 17.6 : 14.8 ratio as 1.94, we calculate from the published curves

$$\sigma_{Li} = 0.66\sigma_{17.6}+0.34\sigma_{14.8},$$

to be compared with the present value of 59±6 mb. Figures from experiments using neutron detection are further corrected for the Cu^{65} contribution, using the Cu^{65} : Cu^{63} cross section ratio from the present work. A summary of results from bremsstrahlung measurements is given in table 3 and from lithium radiation measurements in table 4.

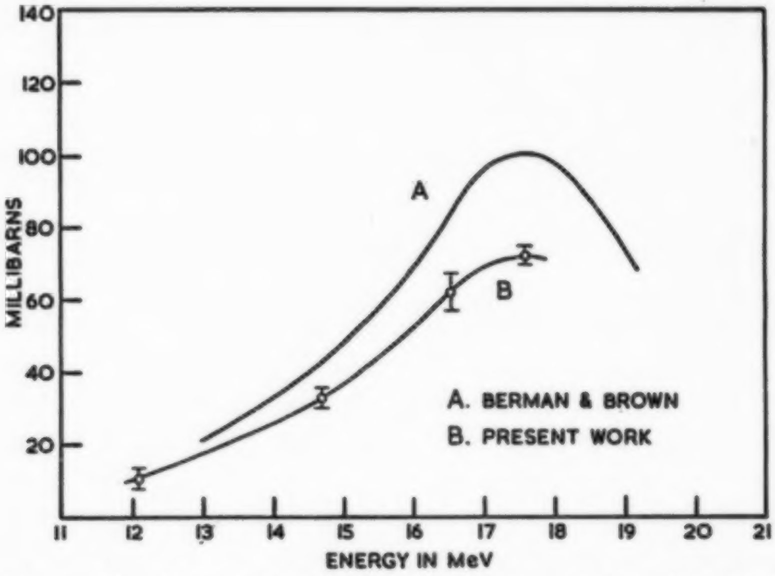

Fig. 2. Comparison of (γ, n) cross section data for Cu^{63}. The errors shown do not include the error in the absolute cross section.

Except for that of Scott, Hanson and Kerst the bremsstrahlung determinations using activation give an average cross section of about 80 mb, while those using neutron detection are higher again.

Of the lithium results, those obtained by McDaniel, Walker and Stearns 17), Hartley, Stephens and Winhold 18) and Yasumi *et al.* 19) are in good agreement with the present results, while that of Carver and Kondaiah 20) is close to the bremsstrahlung value.

Roalsvig *et al.* 21, 22), unfolding their Ni^{58} and Zn^{64} yield curves by both the Penfold-Leiss and the photon difference method, found that the first method gave the same shape as the second, but peak and integrated cross sections about 40 % lower. This surprising result suggests that the discrepancy is related to the

TABLE 3

Bremsstrahlung measurements of $Cu^{63}(\gamma, n)Cu^{62}$ cross section

	Reference	E_{max} (MeV)	σ_{max} (mb)	Half-width (MeV)	$\sigma_{int.}$ (MeV-barn)	σ_{Li} [a]) (mb)	X-ray intensity	Measurement of activity
A. Activation measurements (Cu^{63})	Diven and Almy [23])	17.5	100	5.6	0.6	86	R-meter	β^+ End-window G.M. counter
	Katz and Cameron [13])	18.1	104	6.1	0.66	88	R-meter	β^+ G.M. counter
	Byerly and Stephens [24])	17.5	100	5.3		80	R-meter	β^+ G.M. counter
	Krohn and Shrader [8])	17.0	94	5.1		76	Pair spectrometer	β^+ End-window G.M. counter
	Berman and Brown [3])	17.5	98	4.9	0.55±0.03	80	Electron current	β^+ 4π Scintillation Counter
	Scott, Hanson and Kerst[4])	16.7	80	4.9	0.41	68	Electron current	β^+ 4π Scintillation Counter
	Roalsvig *et al.* [21]) [b])		93			79	R-meter	β^+ Flow proportional counter
B. Neutron detection measurements (natural Cu)	Montalbetti *et al.* [25])	19.5	120	7.1	0.87	94 (Cu) 89 (Cu^{63})	R-meter	BF_3+paraffin
	Gavrilov and Lazareva [26])	17.2	126	4.3	0.93	102 (Cu) 96 (Cu^{63})	Ionization chamber	BF_3+paraffin

[a]) σ_{Li} is the cross section for the same mixture of gamma rays as the lithium resonance radiation.

[b]) Correction to the absolute yield as given by Katz and Cameron.

TABLE 4

$Li^7(p, \gamma)Be^8$ measurements of $Cu^{63}(\gamma, n)Cu^{62}$ cross section

Reference	σ_{Li} (Natural Cu) (mb)	σ_{Li} (Cu^{63}) (mb)	γ-ray monitoring	Activity measurement	Neutron detection
Wäffler and Hirzel [27]		120±30	G.M. counter	G.M. counter	
Shimizu [28]		29 [a]	G.M. counter	G.M. counter	
McDaniel, Walker and Stearns [17]	55±12	52±11	G.M. counter		BF_3+paraffin
Glättli, Seippel and Stoll [29]		48± 8	G.M. counter	G.M. counter	
Hartley, Stephens and Winhold [18]	64±10	60± 9	Small NaI crystal		BF_3+paraffin
Carver and Kondaiah [28]	85±15	80±14	G.M. counter		Szilard-Chalmers
Nakamura *et al.* [30]		38± 6	G.M. counter	G.M. counter	
Yasumi *et al.* [19]		62± 4	NaI crystal	G.M. counter	
Present work		59± 6	NaI crystal	NaI crystal	

[a] As recalculated by Nakamura *et al.*

method of unfolding the yield curve. They found also that careful attention to absolute β-counting gave cross sections for $Ni^{58}(\gamma, n)$ and $Zn^{64}(\gamma, n)$ much lower than previous values.

In fig. 2 the shape obtained in the present work is compared with that found by Berman and Brown. Errors shown are for the relative values only and do not include the error in the absolute cross section.

The curves obtained in the two experiments show good agreement.

6.2. CROSS SECTIONS OF Zn^{64}, Cu^{65}, Sb^{121}, AND Pr^{141}

Comparison with other work is made in table 5 by calculating for each measurement the cross section σ_{β^+} for positon emission and $\sigma_{\beta^+}/\sigma_{Cu^{63}}$, using the decay scheme and Cu^{63} cross section adopted by each author.

TABLE 5

Comparison of relative cross sections for the lithium resonance radiation

Isotope	Reference	σ_{total} (mb)	σ_{β^+} (mb)	$\frac{\sigma_{\beta^+}}{\sigma_{Cu^{63}}\text{(author)}}$	Activity measured
Cu^{65}	Katz and Cameron 13)	127	22.6 a)	0.26	$(\beta^+ + \beta^-)$
	Present work	70	13.3	0.23	γ^+
Zn^{64}	Katz and Cameron 13)	108	101	1.15	β^+
	Roalsvig *et al.* 22)	44	41	0.52	β^+
	Present work	40	36	0.61	γ^+
Sb^{121}	Katz and Cameron 13)	320	140	1.6	β^+
	Present work	122	53	0.9	γ^+
Pr^{141}	Carver and Turchinetz 31)	223	130	1.6	K X-ray
	Ferrero *et al.* 32)	282	152	1.7	γ^+
	Present work	181	98	1.7	γ^+

a) Calculated from authors' value of $\sigma(\beta^+ + \beta^-)$.

Study of the normalized cross sections shows that the present results and those of Katz and Cameron agree well for Cu^{65}, but disagree by almost a factor of 2 for Zn^{64} and Sb^{121}. Roalsvig *et al.* paid special attention to absolute β-counting, and their result for Zn^{64} agrees reasonably well with the present work. The three results for Pr^{141}, each using scintillation counting of the activity, show good agreement.

7. Conclusion

The bremsstrahlung measurement of the shape of the $Cu^{63}(\gamma, n)Cu^{62}$ cross section has been confirmed, but the absolute values obtained are 25 % lower. Measurements of cross sections relative to Cu^{63} and recent results by other workers suggest that the discrepancy is due to inaccuracies in absolute β-counting.

The authors wish to thank Mr. M. J. Vernon for preparation of the PrF_3 sample, and Mr. N. F. Bowkett for maintenance of the H.T. set. These experiments are part of a programme of photonuclear studies under Professor E. W. Titterton.

References

1) M. B. Stearns and B. D. McDaniel, Phys. Rev. **82** (1951) 450
2) V. F. Krohn and E. F. Shrader, Phys. Rev. **87** (1952) 685
3) A. I. Berman and K. L. Brown, Phys. Rev. **96** (1954) 83
4) M. B. Scott, A. O. Hanson and D. W. Kerst, Phys. Rev. **100** (1955) 209
5) R. L. Matter, J. Appl. Phys. **28** (1957) 1200
6) C. S. Cook, Nuclear Instruments and Methods **4** (1959) 103
7) J. Kockum and N. Starfelt, Nuclear Instruments and Methods **4** (1959) 171
8) B. Mainsbridge, Aust. J. Phys. **13** (1960) 204
9) H. E. Gove and E. Paul, Phys. Rev. **97** (1955) 104
10) H. W. Koch and J. M. Wyckoff, I.R.E. Trans. Nucl. Sci. NS-5 (1958) 127
11) W. F. Miller, J. Reynolds and W. J. Snow, U.S.A.E.C. Report ANL-5902 (1958)
12) S. B. Garfinkel, private communication from the National Bureau of Standards, Washington (1960)
13) L. Katz and A. G. W. Cameron, Can. J. Phys. **29** (1951) 518
14) Gladys White Grodstein, N.B.S. Circular 583 (1957)
15) D. Strominger, J. M. Hollander and G. T. Seaborg, Revs. Mod. Phys. **30** (1958) 585
16) Nuclear Data Cards, National Research Council (1959)
17) B. D. McDaniel, R. L. Walker and M. B. Stearns, Phys. Rev. **80** (1950) 807
18) W. H. Hartley, W. E. Stephens and E. J. Winhold, Phys. Rev. **104** (1956) 178
19) S. Yasumi, M. Yata, K. Takamatsu, A. Masaike, and Y. Masuda, J Phys. Soc. Japan **15** (1960) 1913
20) J. H. Carver and E. Kondaiah, Phil. Mag. **45** (1954) 988
21) J. P. Roalsvig, R. N. H. Haslam and D. J. McKenzie, Can. J. Phys. **37** (1959) 607
22) J. P. Roalsvig, R. N. H. Haslam and J. L. Bergsteinsson, Can. J. Phys. **38** (1960) 320
23) B. C. Diven and C. M. Almy, Phys. Rev. **80** (1950) 407
24) P. R. Byerly and W. E. Stephens, Phys. Rev. **83** (1951) 54
25) R. Montalbetti, L. Katz and J. Goldemberg, Phys. Rev. **91** (1953) 659
26) B. I. Gavrilov and L. E. Lazareva, Soviet Physics JETP **3** (1957) 871
27) H. Wäffler and O. Hirzel, Helv. Phys. Acta **21** (1948) 200
28) S. Shimizu, Mem. Coll. Sci. Kyoto **A25** (1949) 193
29) Glättli, Seippel and Stoll, Helv. Phys. Acta **25** (1952) 491
30) Nakamura, Takamatsu, Fukunaga, Yata and Yasumi, J. Phys. Soc. Japan **14** (1959) 693
31) J. H. Carver and W. Turchinetz, Proc. Phys. Soc. A **73** (1959) 110
32) F. Ferrero, R. Malvano, E. Silva, J. Goldemberg and G. Moscati, Nuclear Physics **10** (1959) 423

1.D.2

Nuclear Physics **23** (1961) 481—490; ©*North-Holland Publishing Co., Amsterdam*

Not to be reproduced by photoprint or microfilm without written permission from the publisher

ISOMERIC STATES OF THE SPHERICAL NUCLEI OF Eu^{147}, Eu^{149} AND Eu^{151}

E. Ye. BERLOVICH, V. N. KLEMENTYEV, L. V. KRASNOV, M. K. NIKITIN and I. YURSIK

Physical-Technical Institute of the U.S.S.R. Academy of Sciences, Leningrad, U.S.S.R.

Received 28 July 1960

Abstract: Half-lifes of the $h_{\frac{11}{2}}$ levels of Eu^{147}, Eu^{149} and Eu^{151} are measured and the following respective values obtained: $T_{\frac{1}{2}} = (7.1 \pm 0.4) \times 10^{-7}$ sec, $T_{\frac{1}{2}} = (2.48 \pm 0.05) \times 10^{-6}$ sec and $T_{\frac{1}{2}} = (5.8 \pm 0.3) \times 10^{-5}$ sec. The M2-type transitions from the $h_{\frac{11}{2}}$ levels prove retarded, the degree of retardation increasing with the number of neutrons from 84 to 88. The E3-type transition rates in the nuclei of Eu^{147} and Eu^{149} prove close to one-particle evaluations. The results of the present investigation, together with the data of ref. ²), contradict the analysis performed by Nilsson ¹⁰) and Gottfried ¹¹) on the motion of an odd proton of Eu^{151} in a deformed potential.

1. Introduction

The experimental data so far accumulated on the matrix elements for radiative transitions of various types and multipolarities have only made it possible to obtain a very general pattern of the distribution of these matrix elements as a function of the number of nucleons in the nucleus. The most essential features of this pattern can be reduced to the following points:

1) a higher value as compared with the one-particle estimate of the reduced matrix elements for the E2-type transitions, especially in the region of large deformations;

2) a lower value of the reduced matrix elements for practically all other types of transitions both electric and magnetic;

3) considerable straggling of the values of the reduced matrix elements for the transitions of all types and multipolarities with the exception of the M4-type transitions for which these values differ least of all.

The very high sensitivity of the matrix elements to the details of the nuclear structure and the character of the motion of nucleons has made it possible in certain cases to detect more subtle phenomena, in particular, the evidence of shell effects. Yet work has only begun in this direction, since experimental data are insufficient and their distribution over the transitions of various types are very uneven. Especially scarce are data on the transitions E4, E5, M2 and M3.

We have obtained new data on the dependence of matrix elements on the number of neutrons in the region of the shell $N = 82$ for transitions of the types M2 and E3. The well-known graph by Goldhaber and Sunyar ¹) representing the experimental values of comparative lifetimes for various numbers of neutrons in the nucleus furnishes no data on the M2-type transitions in the region from $N = 82$ to $N = 126$.

The transitions in the spherical nuclei of Eu with odd mass numbers Eu^{147}, Eu^{149} and Eu^{151} have been investigated. These nuclei are of interest in the following aspects:

1) They are located between the neutron shell with $N = 82$ and the region of a jump-like transition from the equilibrium spherical form of the nucleus to the elongated one at $N = 89$.

2) The structure of the low levels of all three nuclei is similar. Investigating the spectra of conversion electrons and photoelectrons, Bashilov and Dzhelepov [2]) established that three lower levels, beginning from the ground one, have the following respective characteristics in all three nuclei: $\mathrm{d}_{\frac{5}{2}}$, $\mathrm{g}_{\frac{7}{2}}$ and $\mathrm{h}_{\frac{11}{2}}$. These levels are in good agreement with the Meyer shell model.

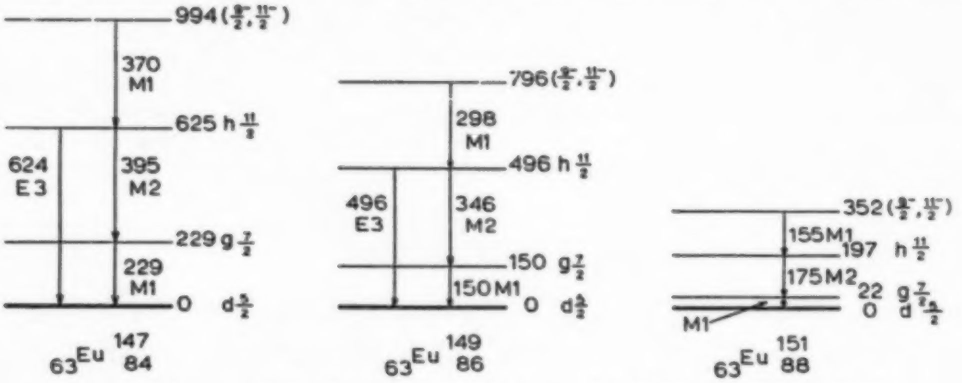
994 ($\frac{9}{2}^-$, $\frac{11}{2}^-$)
370 M1
625 $\mathrm{h}\frac{11}{2}$
624 E3
395 M2
229 $\mathrm{g}\frac{7}{2}$
229 M1
0 $\mathrm{d}\frac{5}{2}$
$_{63}\mathrm{Eu}^{147}_{84}$
796 ($\frac{9}{2}^-$, $\frac{11}{2}^-$)
298 M1
496 $\mathrm{h}\frac{11}{2}$
496 E3
346 M2
150 $\mathrm{g}\frac{7}{2}$
150 M1
0 $\mathrm{d}\frac{5}{2}$
$_{63}\mathrm{Eu}^{149}_{86}$
352 ($\frac{9}{2}^-$, $\frac{11}{2}^-$)
155 M1
197 $\mathrm{h}\frac{11}{2}$
175 M2
22 $\mathrm{g}\frac{7}{2}$
0 $\mathrm{d}\frac{5}{2}$
M1
$_{63}\mathrm{Eu}^{151}_{88}$

Fig. 1. Schemes of the lower levels of the nuclei Eu^{147}, Eu^{149} and Eu^{151}.

3) Regularities in the energies of the respective levels are in evidence as the mass number changes [2]): as we pass from Eu^{147} to Eu^{149} and Eu^{151} the energies of the levels $\mathrm{h}_{\frac{11}{2}}$ and $\mathrm{g}_{\frac{7}{2}}$ diminish.

Fig. 1 represents the schemes of the lower levels of three nuclei proposed by the authors of ref. [2]). The position of the lower transitions agrees with the direct measurements of e—e coincidences in the work by Dzhelepov and Sergiyenko [3]). The position of the M1-type transitions above the isomeric levels ($\mathrm{h}_{\frac{11}{2}}$) in the three nuclei have been established more accurately by the measurements of delayed coincidences in the work of the present authors [4]). It was shown that the levels of the nuclei of Eu^{147}, Eu^{149} and Eu^{151} with energies 625 keV, 496 keV and 197 keV respectively are actually isomeric, and the lifetimes of these levels were measured.

2. Electronic Equipment and Research Method

In investigating the schemes of the levels of the nuclei of Eu^{147}, Eu^{149} and Eu^{151}, the authors of ref. [2]) uniquely assign the relative position of the M1-type

370 keV transition only in the case of the nucleus of Eu^{147}. In the case of the nucleus Eu^{149} the position of the M1 298 keV transition was established by the authors non-uniquely: they propose two variants of the level schemes, in one of which this transition is located above the level $h_{11/2}$, while in the other directly over the ground state. The situation is similar for the nucleus of Eu^{151} for which the M1 150 keV transition is assigned by the authors above the level $h_{11/2}$ in one of the variants and over the ground level in the other.

To determine the lifetime of the levels $h_{11/2}$ by the delayed coincidence method it was above all necessary to abolish the above-mentioned uncertainties in the schemes of the levels.

For this purpose use was made of a double scintillation coincidence spectrometer with NaI crystals and FEU-14 photomultipliers with a jalousie dynod system. Each of the branches of the spectrometer contained a single-channel amplitude analyzer. In investigating the level schemes the window of the amplitude analyzer in one of the branches was fixed for the region on the photopeak selected, while the other branch comprised the entire amplitude spectrum with an adequately selected value of the time delay between the branches. The synchronizing impulse obtained from the coincidence circuit gated a 100-channel amplitude analyzer. The resolving time $(2\tau_0)$ of the coincidence circuit could change from 0.2 to 18 μsec. The variable time delay between the branches covered the range from 0 to 250 μsec.

With the aid of the coincidence spectrometer described it was possible to carry out measurements of delayed or prompt coincidences. In measuring the lifetimes of the levels, the windows of each of two single-channel analyzers were fixed for the regions of the corresponding photopeaks or conversion electrons (a stilbene monocrystal was used for their detection) and the number of coincidences as a function of delay was measured.

3. Sources

Investigations were performed with the aid of sources made from the gadolinium fraction obtained by a chromatographic method from the rare earth elements which appear in a tantalum target under the influence of a 660 MeV beam of protons produced by the synchrocyclotron of the Joint Institute for Nuclear Research.

The nuclei of Gd^{147}, Gd^{149} and Gd^{151} become, through the capture of orbital electrons Eu^{147} ($T_{\frac{1}{2}} = 35$ hours), Eu^{149} (9 days) and Eu^{151} (150 days). The sources of Gd^{147} and Gd^{149} were obtained by short irradiations of the targets (2—4 hours); during the first two or three days the activity of Gd^{147} prevailed, after the decay of which and purification of the accumulated Eu^{147} ($T_{\frac{1}{2}} = 24$ days), the principal share of activity was caused by the nine-day Gd^{149}. The sources of Gd^{151} were obtained by prolonged irradiations of targets (3—6 months). After the decay of the shortlived isotopes of Gd^{147} and Gd^{149} the activity in the source was caused by Gd^{151}, Gd^{153} (230 days), Gd^{146} (55 days) and the 5-day Eu^{146} which was in equilibrium with the latter. After a sufficient period (of the order of one year) the chief activity was due to Gd^{151} and Gd^{153}.

3. Measurements

3.1. THE NUCLEUS Eu^{147}

Both "prompt" coincidences (with resolving time 0.2 μsec) and delayed coincidences between quanta of 370 and 396 keV were shown to exist with the aid of the arrangement described above. This confirms the position of the 370 keV transition above the isomeric level. At the same time only "prompt" coincidences were observed between the quanta 396 keV and 229 keV, but no delayed coincidences. This agrees with the upper limit of the halftime of the 229 keV level established with the double magnetic coincidence spectrometer

$$T_{\frac{1}{2}} \leqq 5\times 10^{-10}\text{ sec.}$$

In measuring the lifetime of the 625 keV level ($h_{\frac{11}{2}}$) of the nucleus Eu^{147}, the windows of single-channel analyzers in both branches of the coincidence

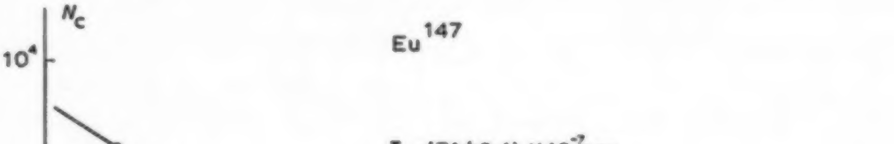

Fig. 2. The decay curve of the 625 keV level of the nucleus Eu^{147}.

circuit were fixed at the region of the photopeaks (unresolved as a consequence of their similar energies) of quanta 370 and 396 keV. Fig. 2 shows (in a semilogarithmic scale) the decay curve of the state under investigation which was traced with the help of the delay introduced throughout approximately seven halftimes. The value of the halftime thus obtained proved to be equal to

$$T_{\frac{1}{2}} = (7.1 \pm 0.4) \times 10^{-7} \text{ sec.}$$

This result was confirmed by test measurements of the coincidences of the X-rays and 396 keV γ-rays which yielded the same value for the halftime.

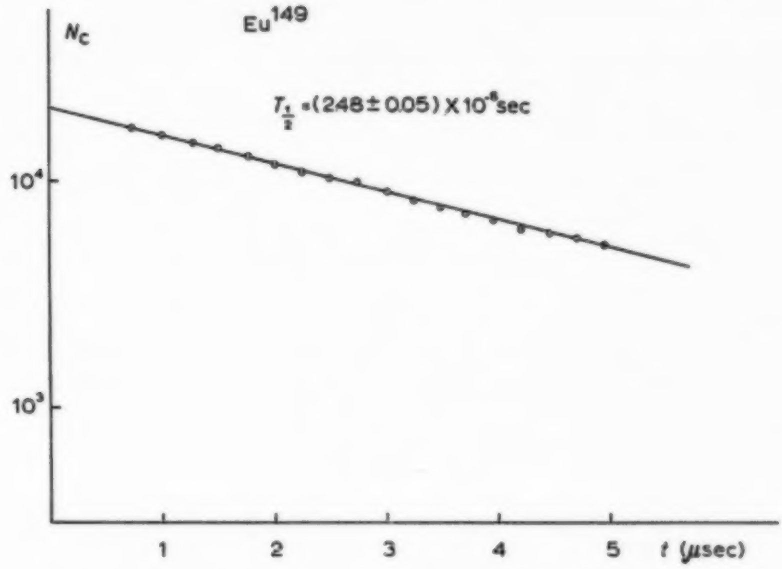

Fig. 3. The decay curve of the 496 keV level of the nucleus Eu^{149}.

From the relations of total intensities of both transitions from this level (according to the estimate of ref. [2]))

$$I_{396} : I_{625} = 10 : 1,$$

we obtain the experimental halftimes for the 396 and 625 keV transitions respectively

$$T_{\frac{1}{2}, 396} = 7.8 \times 10^{-7} \text{ sec}, \quad T_{\frac{1}{2}, 625} = 7.8 \times 10^{-6} \text{ sec.}$$

3.2. THE NUCLEUS Eu^{149}

Direct experiments have established the presence of both "prompt" and delayed coincidences between 298 keV and 346 keV quanta and thereby the position of the 298 keV transition above the 496 keV level ($h_{\frac{11}{2}}$) was confirmed. Besides, it was established that there are "prompt" but no delayed coincidences between 346 keV and 150 keV quanta. Similarly to the nucleus of Eu^{147}, this agrees with the upper limit of the half-life of the first 150 keV excited level of the nucleus Eu^{149} obtained with the double magnetic spectrometer

$$T_{\frac{1}{2}} \leqq 5 \times 10^{-10} \text{ sec.}$$

Fig. 3 gives the results of measurements of the half-life of the 496 keV state of the nucleus of Eu^{149} obtained by investigating the coincidences between 298 keV and 346 keV quanta as a function of time delay. The curve shows that

$$T_{\frac{1}{2}} = (2.48 \pm 0.05) \times 10^{-6} \text{ sec.}$$

According to ref. [2]), the ratio of the total intensities of the two transitions from the 496 level is equal to

$$I_{346} : I_{496} = 0.4 : (0.02),$$

the brackets indicating that the intensity of the direct transition was determined less accurately.

This leads to the following values of experimental half-lives for the 346 keV and 496 keV transitions respectively:

$$T_{\frac{1}{2},346} = 2.62 \times 10^{-6} \text{ sec}, \quad T_{\frac{1}{2},496} = 5.24 \times 10^{-5} \text{ sec.}$$

3.3. THE NUCLEUS Eu^{151}

The principal difficulty of measurement consisted in there being a very intensive γ-radiation accompanying the decay of Gd^{153} ($T_{\frac{1}{2}} = 230$ days) with the energies 98 keV and 103 keV. For both establishing the position of the M1-type 155 keV transition and measuring the lifetime of the 197 keV level, it proved to be convenient to investigate the coincidences between 155 keV γ-quanta and the internal conversion electrons of the 175 keV transition (the internal conversion coefficient of the K-shell being equal to 2.4 for this transition) which were detected with the help of a thin stilbene crystal. The conversion electrons of the 103 keV intense transition in the nucleus of Eu^{153} were absorbed essentially by an aluminium filter of an adequate thickness.

The fact that there are both "prompt" and delayed coincidences for the 155 keV and 175 keV transitions uniquely assigns the position of the 155 keV transition above the isomeric level.

The measurement of the lifetime of the 197 keV level of the nucleus of Eu^{151} represented in fig. 4 leads to the following value of the half-life:

$$T_{\frac{1}{2}} = (5.8 \pm 0.3) \times 10^{-5} \text{ sec},$$

which agrees well with the results obtained by Shirley and Rasmussen [5]),

$$T_{\frac{1}{2}} = (5.8 \pm 1.0) \times 10^{-5} \text{ sec.}$$

The E3-type transition from the 197 keV level to the ground state in this case was not detected experimentally. The intensity of this transition is evidently too small if compared with the M2-type 175 keV transition by virtue of a stronger energy dependence of the probability of the E3-type transition.

Each of the above listed values of half-lives was obtained as a weighted mean for several series of measurements. The graphs in all cases represent the result for only one of the series. Each series was treated by the least squares method.

The indicated errors considerably exceed the statistical errors and take into account the errors due to the calibration of the delay lines and the instability of the set up.

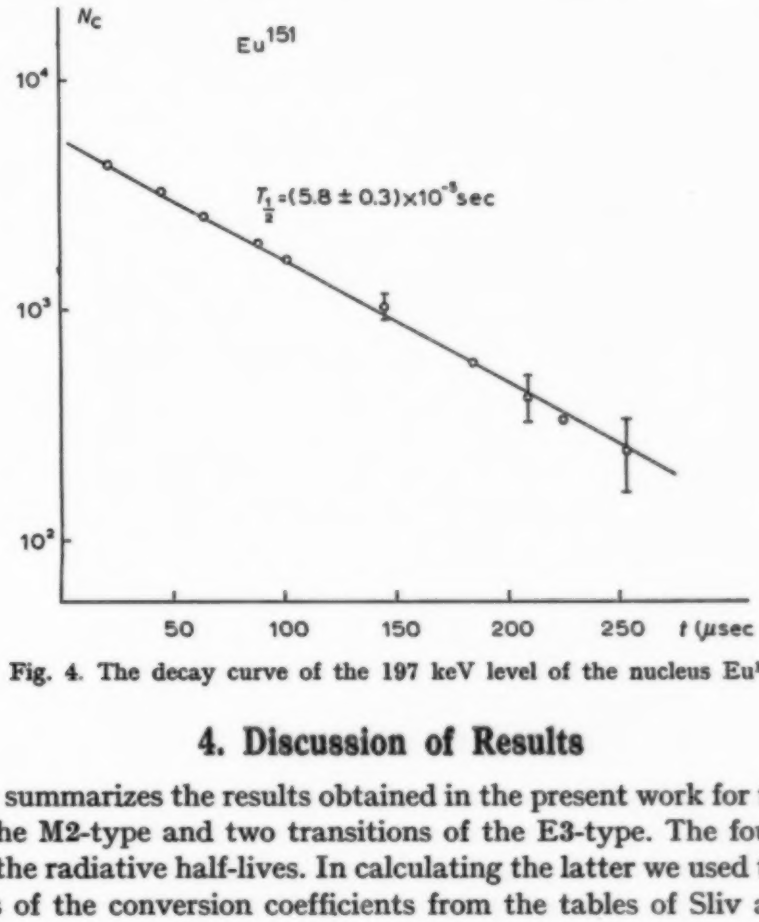

Fig. 4. The decay curve of the 197 keV level of the nucleus Eu^{151}.

4. Discussion of Results

Table 1 summarizes the results obtained in the present work for three transitions of the M2-type and two transitions of the E3-type. The fourth column indicates the radiative half-lives. In calculating the latter we used the theoretical values of the conversion coefficients from the tables of Sliv and Band[6]),

TABLE 1

Experimental results

Nuclei	E_γ (keV)	Type of transition	$T_{\gamma \text{exp.}}$ (sec)	$F = \frac{\lambda_{\text{exp.}}}{\lambda}$	Logarithm of comparative lifetime
${}_{63}Eu^{147}_{84}$	396	M2	9.04×10^{-7}	0.022	$\bar{7}.55$
${}_{63}Eu^{149}_{86}$	346	M2	3.21×10^{-6}	0.012	$\bar{7}.81$
${}_{63}Eu^{151}_{88}$	175	M2	2.4×10^{-4}	0.005	$\bar{6}.21$
${}_{63}Eu^{147}_{84}$	625	E3	7.9×10^{-6}	2.1	$\bar{2}$
${}_{63}Eu^{149}_{86}$	496	E3	5.45×10^{-5}	1.4	$\bar{2}.14$

since the multipolarities of transition are determined reliably enough and the experimental values of the ratio α_K/α_L and α_K are close to the theoretical ones [2]). The conversion coefficient for the other shells was assumed to be equal to $0.3\alpha_L$.

The fifth column gives the enhancement factors which are the ratios between the radiative probabilities obtained from experiment and the one-particle probabilities calculated by the Weisskopf formula [7]). The sixth column contains the logarithms of comparative lifetimes:

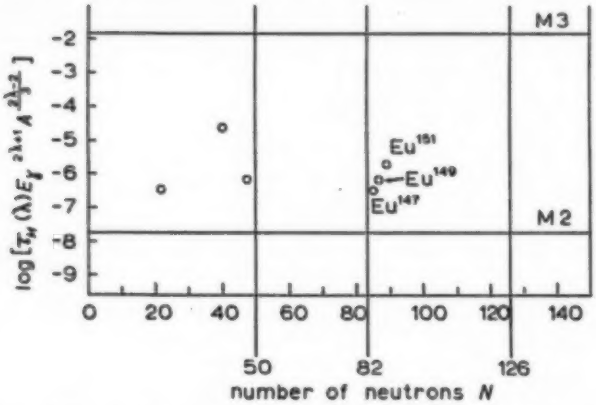

Fig. 5. The logarithms of the comparative lifetimes indicated for several nuclei

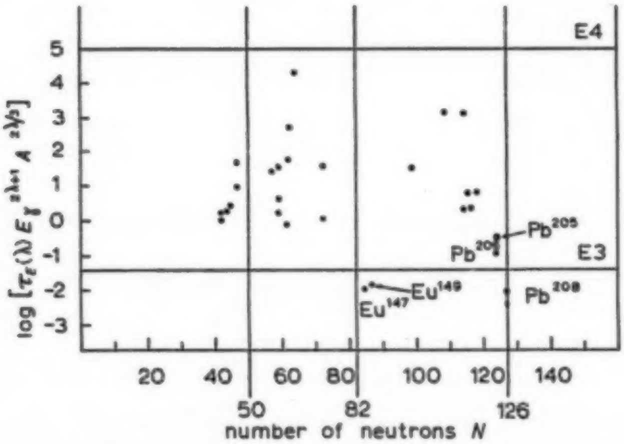

Fig. 6. The logarithms of the comparative lifetimes indicated for several nuclei.

$$\log\,(\tau_\gamma A^{\frac{4}{3}} E_\gamma{}^5) \text{ for the M2 transitions,}$$
$$\log\,(\tau_\gamma A^2 E_\gamma{}^7) \text{ for the E3 transitions.}$$

In fig. 5 and fig. 6 the values obtained for the logarithms of the comparative lifetimes for the M2 and E3 transitions are respectively plotted on the graphs of Goldhaber and Sunyar.

All M2 transitions proved to be delayed on the average by two orders if compared with one-particle estimates, the effect of the shell structure being especially well pronounced: the delay increases monotonically as the number of neutrons increases from 84 in Eu^{147} to 88 in Eu^{151}. An increase in the degree of retardation with the increase of the distance from the shells $N = 82$ probably reflects the worsening of the "purity" of one-particle wave functions as the number of neutrons above the filled shell increases.

The results obtained on the change of comparative lifetimes of the $h_{\frac{11}{2}}$ levels with the change of the number of neutrons alongside the change of the energy of the levels of the nuclei under consideration [2]), are examples of the change of properties of the "corresponding" states [8]), i.e., the states with the assigned odd number of the nucleons of one type (protons) and different even numbers of the nucleons of the other type (neutrons). The properties of such states and in particular the reduced probabilities of transitions from these states change monotonically.

The probabilities of the E3 transitions proved to be rather close to one-particle estimates, in contrast to most of the known transitions of this type which, as a rule, are strongly hindered. The exception like the one we have observed close to the shell $N = 82$ is also known to exist in the region of the twice magic nucleus of Pb^{208} ($N = 126$, $Z = 82$).

The monotonic change of the reduced probability observed for the M2 transitions with increase of mass number is in good agreement with the analogy noted in ref. [2]) in the level schemes of the three nuclei and the monotoni cchange of the energy of the levels: $h_{\frac{11}{2}}$ and $g_{\frac{7}{2}}$.

The sequence $d_{\frac{5}{2}}$, $g_{\frac{7}{2}}$ and $h_{\frac{11}{2}}$ following from ref. [2]) is in good agreement with a simple shell model for spherical nuclei, in contrast to the next odd europium nucleus Eu^{153} with the number of neutrons $N = 90$ revealing rotating structure of levels.

The experimental values of the spins of the nuclei of Eu^{151} and Eu^{153} are equal to $\frac{5}{2}$. Yet the experimentally determined magnetic moment of the nucleus of Eu^{151} is 3.4 nuclear magnetons, whereas for Eu^{153} it amounts to 1.5 nuclear magnetons [9]). It is not surprising that the large difference of magnetic moments observed cannot be explained in terms of the simple shell model, for one of these nuclei is spherical, while the other is elongated. Yet, proceeding from the experimental value of the quadrupole moment of the nucleus of Eu^{151} ($Q = 1.2$ barn [9]), Nilsson [10]) and Gottfried [11]) consider this nucleus, despite the smallness of this value, in terms of the collective model and calculate the deformation parameter $\delta = 0.10$ according to the Bohr-Mottelson scheme. For the ground state of the nucleus of Eu^{151} in ref. [11]) the orbital $h_{\frac{11}{2}, \frac{5}{2}}$ is taken, though the latter corresponds to the deformation ≈ 0.2, whereas for the ground state of the nucleus Eu^{153} the orbital $g_{\frac{7}{2}, \frac{5}{2}}$ is selected. Thus under the assumption that both nuclei are deformed, the large difference in the magnetic moments can be accounted for by ascribing negative parity to the ground state of Eu^{151}.

Since at present much evidence has been accumulated in favour of the fact that the transition from the equilibrium spherical form to the elongated one occurs through a jump with the change of the number of neutrons from 88 to 90 [12]), it appears that the analysis of the nucleus of Eu^{151} in terms of the Nilssen-Gottfried model is not adequate.

It will also be noted that though in the case of the nucleus of Eu^{151} the value of the magnetic moment calculated in ref. [11]). (3.15 nuclear magnetons) is rather close to the experimental one, in the case of the nucleus of Eu^{153} the calculated value (0.69 nuclear magneton) amounts to less than half of the experimental one. As is noted in ref. [11]) the magnetic moments of nuclei are rather sensitive to the structure of the wave function describing the motion of a nucleon in the nucleus, and therefore the residual internucleon interactions are bound to have an essential effect on the magnitude of the magnetic moment. It is possible that taking account of the residual forces will make it possible to explain the difference of the magnetic moments of the nuclei of Eu^{151} and Eu^{153} without the artificial assumption that the odd proton in the nucleus of Eu^{151} moves in a deformed potential.

The authors are indebted to Prof. Dzhelepov, the Director of the Laboratory of Nuclear Problems of the Joint Institute for Nuclear Research and the operating personnel of the synchrocyclotron for the irradiation of the tantalum samples.

References

1) M. Goldhaber and A. W. Sunyar, in Beta- and gamma ray spectroscopy, ed. by K. Siegbahn North-Holland Publishing Co., Amsterdam 1959)
2) N. M. Antonyeva, A. A. Bashilov, B. S. Dzhelepov and B. K. Preobrazhensky, Izv. AN USSR Ser. Fiz. **22** (1958) 895, **22** (1958) 906;
V. K. Adamchuk, A. A. Bashilov and B. K. Preobrazhensky, Izv. Akad. Nauk USSR, Ser. Fiz. **22** (1958) 919;
N. M. Antonyeva, A. A. Bashilov, B. S. Dzhelepov and B. K. Preobrazhensky, Izv. Akad. Nauk USSR Ser. Fiz. **22** (1958) 135
3) B. S. Dzhelepov and V. A. Sergiyenko, Izv. Akad. Nauk USSR Ser. Fiz. **23** (1959) 211;
B. S. Dzhelepov, B. K. Preobrazhensky and V. A. Sergiyenko. Izv. Akad. Nauk USSR, Ser. Fiz. **23** (1959) 219
4) E. E. Berlovich, V. N. Klementyev, L. V. Krasnov, M. K. Nikitin and I. Yursik, DAN USSR (in print)
5) V. S. Shirly and J. O. Rasmussen, Phys. Rev. **109** (1958) 2092
6) L. A. Sliv and N. M. Band, Tables of gamma-radiation internal-conversion coefficients (Izd. Akad. Nauk USSR, Moskva-Leningrad; p. I, 1956; p. II, 1958)
7) D. Blatt and V. Weisskopf, Theoretical nuclear physics (John Wiley and Sons, New York 1952)
8) V. S. Shpinel, Izv. Akad. Nauk USSR, Ser. Fiz. **22** (1958) 995
9) T. Kopfermann, Nuclear moments (Izd. Inostr. Literat., Moscow 1960)
10) S. G. Nilsson, Mat. Fys. Medd. Dan. Vid. Selsk. 29, No. **16** (1955)
11) K. Gottfried, Phys. Rev. **103** (1957) 1017
12) K. Alder, A. Bohr, T. Huns, B. Mottelson and A. Winther, Rev. Mod. Phys. **28** (1956) 432;
B. R. Mottelson and S. G. Nilsson, Mat. Fys. Skr. Dan. Vid. Selsk. **1**, No. **8** (1959);
L. K. Peker, Izv. Akad. Nauk **21** (1957) 1025

2.F:2.L

Nuclear Physics **23** (1961) 491—498; © *North-Holland Publishing Co., Amsterdam*

Not to be reproduced by photoprint or microfilm without written permission from the publisher

BREAKUP OF DEUTERONS ON H, D, He^3 AND He^4

B. V. RYBAKOV, V. A. SIDOROV and N. A. VLASOV

I. V. Kurchatov Atomic Energy Institute, Academy of Sciences, Moscow, USSR

Received 25 September 1960

Abstract: Continuous neutron energy spectra produced by bombardment of H, D, He^3 and He^4 with 18.6 MeV deuterons and D with 8.6 MeV protons and 34.6 MeV alpha particles have been studied by the time-of-flight technique. Peaks in the neutron spectra from the p+d and α+d reactions had been observed which are satisfactorily explained by pair interactions between the reaction products in the final state. No such peaks have been found in the spectra of the d+d and He^3+d reactions. Their shape also differs significantly from that corresponding to the statistical distribution of energy between the three particles in S-states of relative motion, but can be easily explained by the presence of higher angular momenta in the final state.

It has been previously shown that in the interaction between fast deuterons and light nuclei, three-particle reactions occur with a large cross section [1, 2]) and neutrons of continuous energy spectrum are produced. To study the mechanism of such reactions, a multichannel time-of-flight spectrometer [3]) in conjunction with the 1.5 m cyclotron of the AEI, was employed to investigate the energy spectra of neutrons produced in the interaction of deuterons with hydrogen and helium isotopes.

Natural modulation of the cyclotron beam underlies the operation of the spectrometer. The time analyzer works according to the vernier principle. The resolving time of the spectrometer is better than 3 mμsec. The channel width of the time analyzer is about 0.8 mμsec. The memory system consists of 256 channels, each with a capacity of 2^{16} pulses, and has a digital recorder for output of the data.

Thin nickel-window gas targets filled to a pressure of 2—5 atm were employed. The measurements were performed alternatively with a filled and empty target. The difference between the results of these measurements yielded the effect due to the gas. In all cases the neutrons were recorded at an angle of 0° with respect to the bombarding particle beam.

In figs. 1—6 the observed neutron energy spectra in the centre-of-mass system are plotted. The instrumental width, which is equal to three intervals between the points, increases with growth of the energy. The measurements were carried out for two flight distances. The large distance was used to improve the energy resolution in the high energy part of the spectrum. The light points correspond to a distance up to 3 m and the black points to a distance from 5 to 8

m. The statistical accuracy of the measurements is characterized by the observed spread of the points.

Neutron production cross sections (areas under the experimental points) are presented in table 1. E_0 in table 1 is the total kinetic energy in the c.m.s. of the three particles after deuteron breakup.

TABLE 1

Neutron production cross-sections

Reaction	Energy (MeV)	E_0 (MeV)	$\sigma_{\text{lab}}(0)$ (mb/sr)	$\sigma_{\text{c.m.}}(0)$ (mb/sr)
H(d, n)	$E_d = 18.6$	4.0	150±15	20± 2
D(p, n)	$E_p = 8.6$	3.5	47± 5	11± 1
D(d, n)	$E_d = 18.8$	7.2	300±30	78± 8
He^3(d, n)	$E_d = 18.6$	8.9	190±20	66± 7
He^4(d, n)	$E_d = 18.6$	10.2	330±40	154±20
D(α, n)	$E_\alpha = 34.6$	9.3	300±40	54± 8

The simplest of the reactions studied is $d+p \rightarrow 2p+n$ in which only free nucleons are formed. The neutron energy spectrum from this reaction as measured at an angle of 0° with respect to the deuteron beam is shown in fig. 1. The spectrum of neutrons produced at an angle of 0° by bombarding deuterium with protons (180° with respect to the primary deuteron momentum in c.m.s.) is shown in fig. 2. The first results obtained in our laboratory in an investigation of the spectrum at this angle were reported at the Paris conference in 1958.

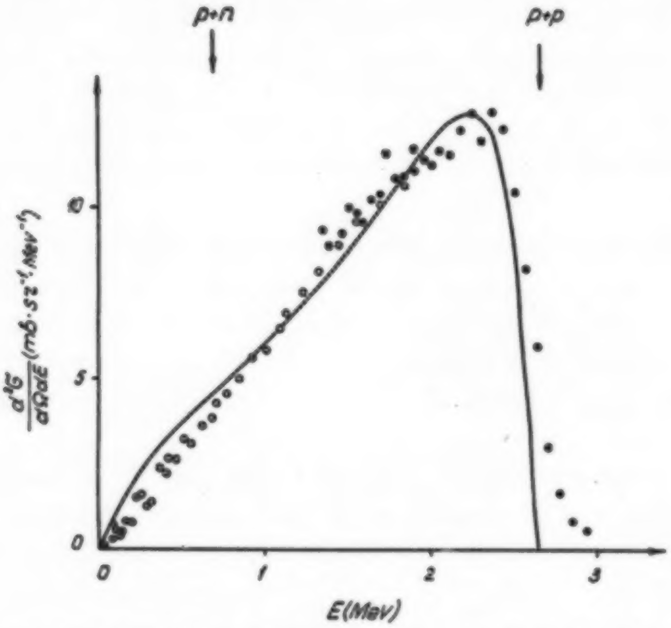

Fig. 1. Neutron spectrum from the p+d reaction in c.m.s. at an angle of 0° with respect to the direction of the deuteron momentum.

Similar results have been obtained by other authors [4–6]). In both energy spectra, peaks near the upper energy limit are observed which correspond to the formation of the protons with small relative energy. Another pronounced peak in the spectra at 180° corresponds to a zero relative energy of the neutron and one of the protons in the final state.

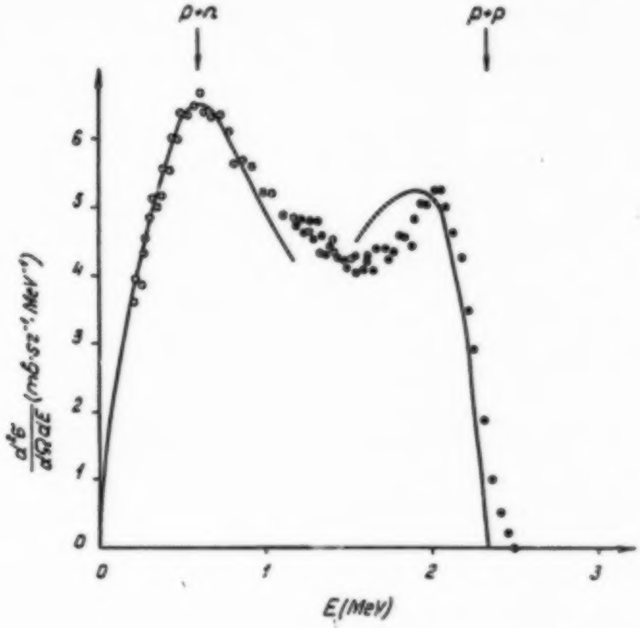

Fig. 2. Neutron spectrum from the p+d reaction in c.m.s. at an angle of 180° with respect to the direction of the deuteron momentum.

The large probability for production of nucleon pairs possessing small relative energies may be explained by their interaction in the final state. The effect of pair interaction in the final state on the slow nucleon spectra was first considered by Migdal [7]). For a proton and neutron the distribution in relative energy E near $E = 0$ has the form

$$d\omega = \text{const.}\ \frac{d\mathbf{q}}{E+\varepsilon}, \tag{1}$$

where $\mathbf{q}$ is the relative momentum of the proton and the neutron, $\varepsilon = 0.07$ MeV for the singlet state and 2.23 MeV for the triplet state. The distribution has a maximum at an energy of the order of ε.

The neutron spectrum calculated near 0.6 MeV based on this formula for $\varepsilon = 0.07$ MeV is plotted in fig. 2. The large apparent width of the peak in the c.m.s. of the three nucleons is due to superposition of the centre-of-mass velocity of two nucleons and the velocity of their relative motion. Curves for ε between 0.03 MeV and 0.15 MeV are consistent with the experimental data within the errors of the measurements. The maximum would be much broader for the (p, n)-interaction in the triplet state.

In the case of two protons the relative energy distribution would be more complicated [7]) due to Coulomb interaction. The corresponding theoretical curves are shown in fig. 1 and fig. 2. The spectra calculated are in satisfactory agreement with the experimental points near the high energy ends of the spectra. A more detailed calculation [8]) yields curves which agree with the experimental spectra throughout the whole neutron energy range.

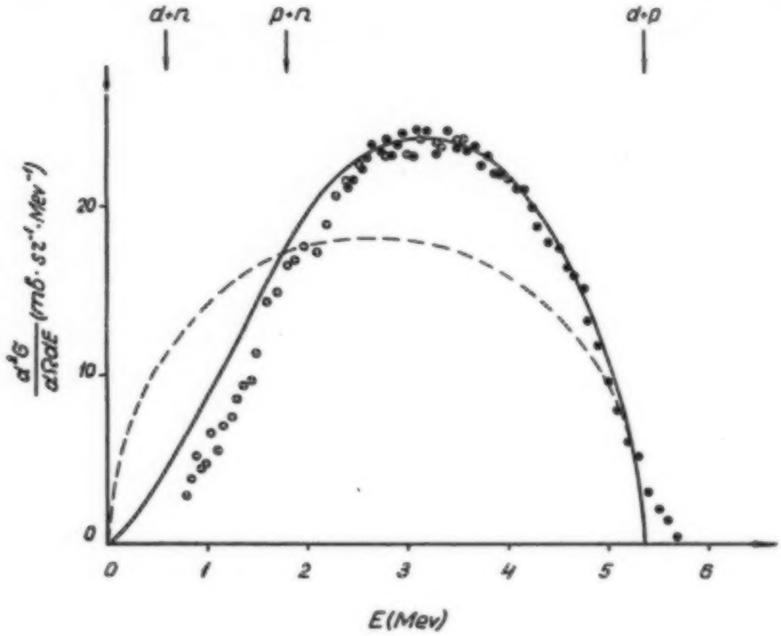

Fig. 3. Neutron spectrum from the d+d reaction in c.m.s. at an angle of 0° with respect to the direction of the deuteron momentum.

Interaction between nucleons in the singlet S state (formation of virtual "binucleons") may also lead to the appearance of peaks in the energy spectra of neutrons produced in the interaction of deuterons with nuclei more complex than the proton. The arrows in the figures denote the neutron energy corresponding to a zero relative energy of various particle pairs. Excluding the p+d reaction, no pronounced peaks due to p, n interaction have been observed. The production of a p+n pair in the singlet S state in the reactions $d+d \rightarrow d+p+n$ and $\alpha+d \rightarrow \alpha+p+n$ is forbidden by the isobaric spin selection rules. It is not forbidden in the case of the $He^3+d \rightarrow He^3+p+n$ reaction, but a spin flip of one of the nucleons of the deuteron is required and this may reduce the probability of the process.

The continuous spectrum for the D(d, n) reaction is shown in fig. 3. The neutron group with an energy of 9.4 MeV in the c.m.s. produced in the reaction D(d, n)He^3 is not shown.

In the d+d reaction the breakup of both deuterons is energetically possible. Yet apparently the neutrons observed come mostly from the d+d → d+p+n reaction, for a considerable part of the experimental energy distribution lies beyond the maximum energy for the four-particle reaction (3.6 MeV).

The semi-circle in fig. 3 (dotted line) represents the phase space factor for the three-particle reaction calculated under the ordinary assumption of zero angular momenta in the final state. The energy spectrum observed differs from this semi-circle considerably. The most prominent peculiarities of the former are a shift to higher neutron energy and lack of neutrons near zero energy. As Dr. Baz pointed out, these peculiarities can readily be understood if the formation of particle pairs with non-zero angular momenta of relative motion is taken into account.

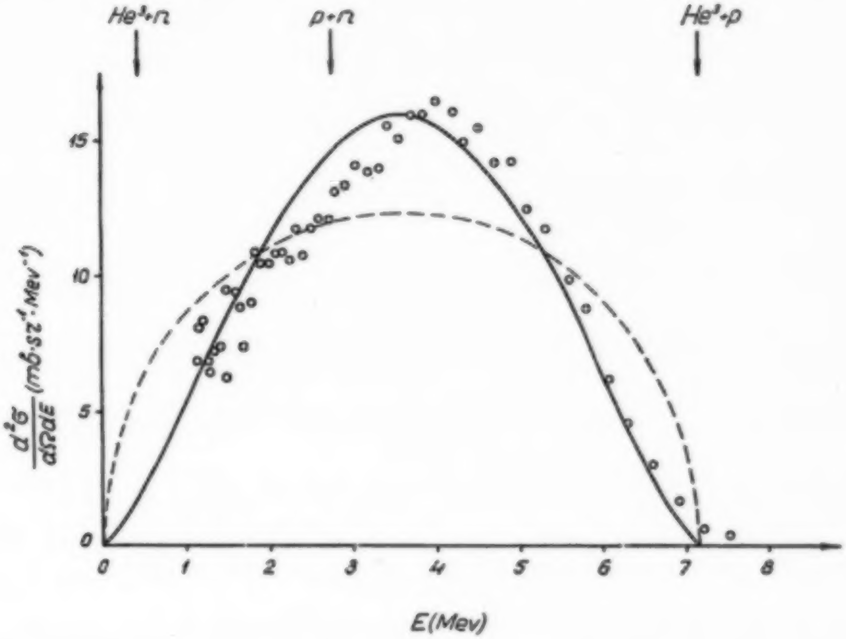

Fig. 4. Neutron spectrum from the He^3+d reaction in c.m.s. at an angle of 0° with respect to the direction of the deuteron momentum.

Let l_1 mean the relative angular momentum of the proton and the target nucleus in the final state and l_2 that of the neutron and the centre-of-mass of the other two particles. Then the above-mentioned semi-circle in fig. 3 will correspond to $l_1 = l_2 = 0$. Taking a suitable mixture of final states with different l_1 and l_2 one can obtain excellent agreement between the calculated curve and the experimental points. The solid line in fig. 3 represents the phase space factor for the simplest mixture of final states fitting the experimental points sufficiently well ($l_1 = 0$; $l_2 = 1$; and $l_1 = l_2 = 1$; in the ratio of 1 : 1).

The neutron energy spectrum for the reaction $He^3 + d \rightarrow He^3 + p + n$ is represented in fig. 4. The dotted line has the same meaning as in fig. 3. The solid line stands for the final state with $l_1 = l_2 = 1$.

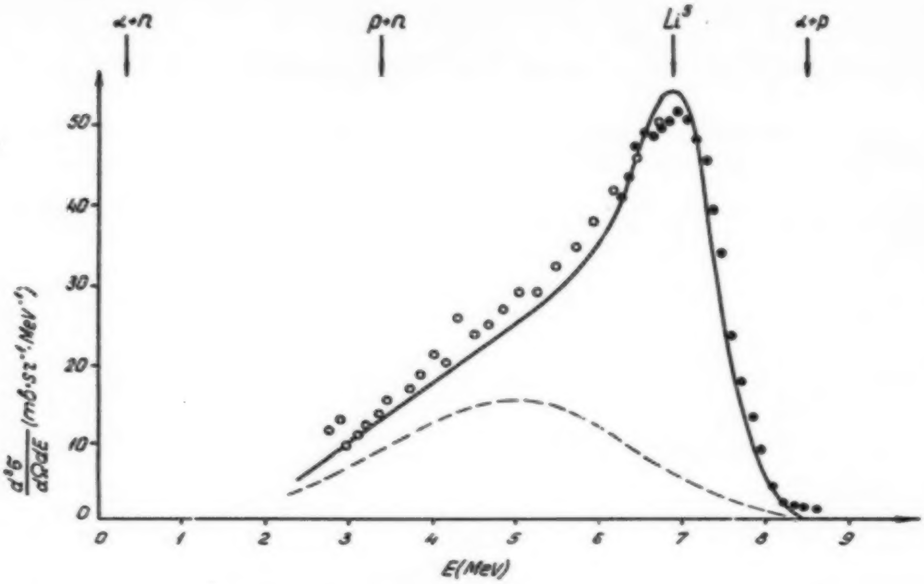

Fig. 5. Neutron spectrum from the α+d reaction in c.m.s. at an angle of 0° with respect to the direction of the deuteron momentum.

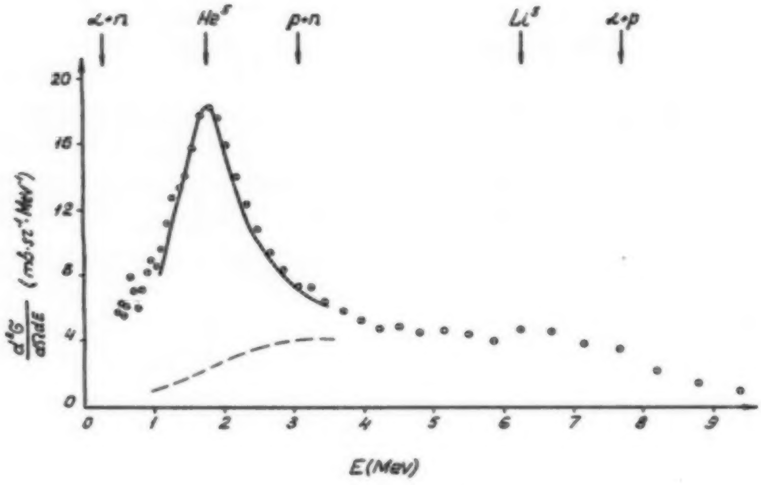

Fig. 6. Neutron spectrum from the α+d reaction in c.m.s. at an angle of 180° with respect to the direction of the deuteron momentum.

Distinct peaks corresponding to resonance interaction of $\alpha+p$ and $\alpha+n$ pairs in the final state $P_{\frac{3}{2}}$ (ground states of Li^5 and He^5) have been observed in the energy spectrum of neutrons emitted in the reactions $\alpha+d \rightarrow \alpha+p+n$ (figs. 5 and 6). Following Watson [9]) we can write for the relative energy distribution of α and p (or α and n)

$$d\omega = \text{const.}\, \frac{\sin^2\delta \mathrm{d}\mathbf{q}}{q^2 p}, \tag{2}$$

where p is the penetration factor [10]), $\delta = \mathrm{arctg}\{\frac{1}{2}\Gamma/(E_{\mathrm{res}}-E)\}$, with $\Gamma = 2\kappa\gamma^2 p$; E and $\kappa = q/\hbar$ are respectively the energy and wave number of the relative motion of the particle pair, γ^2 is the reduced level width.

The curves thus derived are plotted in fig. 5 and 6. The reduced width value $\gamma^2 = 12.10^{-13}$ MeV · cm and the effective radius $R = 2.6\times10^{-13}$ cm for the $Li^5(P_{\frac{3}{2}})$ and $He^5(P_{\frac{3}{2}})$ and also the value $E_{\mathrm{res}} = 2.1$ MeV for $Li^5(P_{\frac{3}{2}})$ are taken from ref. [11]) in which scattering of protons on He^4 was studied. The value $E_{\mathrm{res}} = 1.0$ MeV for $He^5(P_{\frac{3}{2}})$ was determined from the proton energy spectrum of the $He^4(d, p)He^5$ reaction as measured with a magnetic analyzer [12]).

The cross section for neutron production in the $\alpha+d \rightarrow Li^5+n$ reaction is large at an angle of 0° with respect to the direction of the primary deuteron momentum. The calculated curve in this case was obtained directly from (2) and the conservation laws. In the second case (180° with respect to the deuteron momentum in the c.m.s., fig. 6) neutrons are also produced with a high probability as a result of the two-stage process $\alpha+d \rightarrow He^5+p \rightarrow \alpha+n+p$. The spectrum peak occurs at quite a high energy (1.8 MeV) as a result of the fact that the angular distribution of protons from the first reaction is peaked in the forward direction (relative to the deuteron momentum) in the c.m.s. The angular distribution of neutrons produced in the mirror reaction $He^4(d, n)Li^5$ measured by us for the same deuteron energy in the c.m.s. was used in the calculations. The width of the neutron angular distribution in the c.m.s. is about 20° for this reaction.

The curves obtained agree satisfactorily with the experimental data near the peaks. To make them coincide with the experimental points in a broader energy region one is forced to assume the existence of another component in the energy spectrum which we have represented by the dotted line. This component is apparently due to the deuteron breakup without Li^5 or He^5 formation in the final state.

The authors are grateful to Dr. Baz and Dr. Kalinin for interest in this work and valuable discussions.

References

1) G. F. Bogdanov, N. A. Vlasov, S. P. Kalinin, B. V. Rybakov and V. A. Sidorov, JETP **30** (1956) 185
2) G. F. Bogdanov, N. A. Vlasov, S. P. Kalinin, B. V. Rybakov and V. A. Sidorov, JETP **30** (1956) 981
3) A. A. Kurashov, A. F. Linyev, B. V. Rybakov and V. A. Sidorov, Atomnaya Energia **5** (1958) 135
4) M. P. Nakada, J. D. Anderson, C. C. Gardner, J. W. McClure and C. Wong, Phys. Rev. **110** (1958) 594
5) C. Wong, J. D. Anderson, C. C. Gardner, J. W. McClure and M. P. Nakada, Phys. Rev. **116** (1959) 164
6) L. Cranberg and R. K. Smith, Phys. Rev. **113** (1959) 587
7) A. B. Migdal, JETP **28** (1955) 3
8) V. V. Komarov and A. M. Popova, Nuclear Physics **18** (1960) 296
9) K. M. Watson, Phys. Rev. **88** (1952) 1163
10) E. P. Wigner, L. Eisenbud, Phys. Rev. **72** (1947) 29
11) P. D. Miller and G. C. Phillips, Phys. Rev. **112** (1958) 2043
12) E. K. Warburton, and J. N. McGruer, Phys. Rev. **105** (1957) 639

2.E

Nuclear Physics **23** (1961) 499—505; © *North-Holland Publishing Co., Amsterdam*

Not to be reproduced by photoprint or microfilm without written permission from the publisher

AN INVESTIGATION OF NUCLEAR PROBES

P. E. HODGSON

Clarendon Laboratory, Oxford

Received 10 November 1960

Abstract: The optical model is used to study the sensitivity to the outer regions of the nuclear field of the elastic differential cross-sections for the scattering of neutrons, protons, deuterons, tritons, helium-3 and alpha particles by nuclei. It is found that the energy at which the sensitivity is greatest is given approximately by $ZZ'/A^{\frac{1}{3}}$ MeV, where Z and A refer to the target nucleus, and Z' to the probe particle.

1. Introduction

The optical model makes it possible to describe the elastic scattering of nucleons, deuterons 1,2), helium-3 3–5), and alpha-particles 6,7) by nuclei using a two-body potential between the incident particle and the target nucleus of the form

$$V(r) = V_{\mathrm{C}}(r)+(U+iW)f(r)+V_{\mathrm{SO}}(r), \tag{1}$$

where $V_{\mathrm{C}}(r)$ is the Coulomb potential, $V_{\mathrm{SO}}(r)$ the spin-orbit potential, U and W the refracting and absorbing parts of the central potential and $f(r)$ their radial variation. The Saxon-Woods form $f(r) = [1+\exp\{(r-R)/a\}]^{-1}$, with $R = r_0A^{\frac{1}{3}}$ as the nuclear radius and a as the diffuseness of the nuclear surface, has been successfully used for many interactions. Using a potential of this form, the Schrödinger wave equation for the scattering process may be solved to give the observable cross-sections by the methods described elsewhere 8).

The spin-orbit potential affects mainly the polarisation of the scattered particles, and has only a small effect on the differential cross-section. Since extensive polarisation data for a range of incident particles are not yet available, it will not be considered here.

If polarisation effects are neglected, the potential (1) depends on four parameters, U, W, r_0 and a, and comparison with experiment enables them to be determined. This gives information on the strength and radial variation of the nuclear field that may be applied to the study of other processes like stripping reactions. Unfortunately, however, the experimental data do not always determine the parameters uniquely. The calculated cross-sections are frequently insensitive to one or other of the parameters, or to combinations of them that obey a particular relation, for example the $Ur_0^2 = \text{const.}$ ambiguity in nucleon-nucleus scattering. In other cases rapid fluctuations occur, and when minimising the difference between theory and experiment it is difficult to be sure that one has not found a false minimum.

It is therefore important to consider whether by suitable choice of type and energy of incident particle it is possible to minimise these difficulties of interpretation. One possible approach to part of this problem is indicated by recent work on the scattering of 29 MeV helium-3 by several medium-weight nuclei [3]). In these interactions the incident particle has insufficient energy to penetrate far into the nucleus, so strong diffraction effects do not occur and the scattering depends only on the fringe of the nuclear field. The differential cross-section is more sensitive to the nuclear diffuseness than to the other parameters of the model, and so comparison with experiment enables it to be determined with higher accuracy than is possible in other circumstances. For a given nucleus and incident particle this happens for a limited range of energies; if the energy is too low the scattering is pure Coulomb and if it is too high diffraction effects appear and complicate the analysis. The purpose of this work is to define this region more precisely as a function of target nucleus and interacting particle, and hence to indicate the experiments most likely to yield significant and unambiguous information on the fringe of the nuclear field.

2. Helium 3 as a Nuclear Probe

The method of investigation will be described in detail for helium 3 scattered by nickel. To show the sensitivity of the differential cross-section to variations of the optical model parameters we define the quantity

$$S_x(E,\theta) = \frac{\sigma(x_1)-\sigma(1.2\,x_1)}{\sigma(x_1)}, \tag{2}$$

where x is the parameter being varied, the other parameters remaining constant. S_x is thus the fractional change in the differential cross-section σ for a 20 % change in the parameter x. For a given interaction it is a function of the incident energy E of the probe particle in the laboratory system and of the centre-of-mass scattering angle θ. The optical model parameters were chosen from previous work to give approximate agreement with experiment. It is not necessary to find the accurate values as S_x is insensitive to the actual values of the parameters. For the same reason, and also because of the paucity of experimental data, the parameters were taken to be independent of energy.

The sensitivity of the differential cross-section for He^3—Ni elastic scattering at 20 MeV to the optical model parameters U, W, r_0 and a is shown in fig. 1. The scattering is considerably more sensitive to r_0 and a than to U and W. Since r_0 varies by no more than about 5 % from nucleus to nucleus while a can vary by as much as 40 % [3-5]) the nuclear diffuseness a is the most critical parameter.

The variation of S_a with energy for the same interaction is shown in fig. 2. For incident energies less than about 5 MeV, the scattering is almost pure Coulomb, around 20 MeV it is sensitive to the fringe of the nuclear field, and above about 25 MeV it is dominated by bulk diffraction effects.

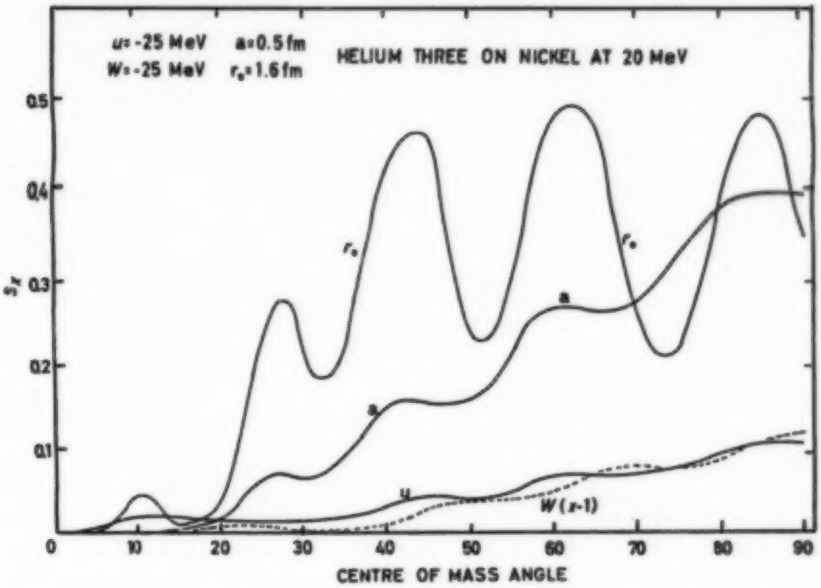

Fig. 1. Sensitivity of the differential cross-section for He^3—Ni scattering at 20 MeV to 20 % variations of the optical model parameters U, W, r_0 and a.

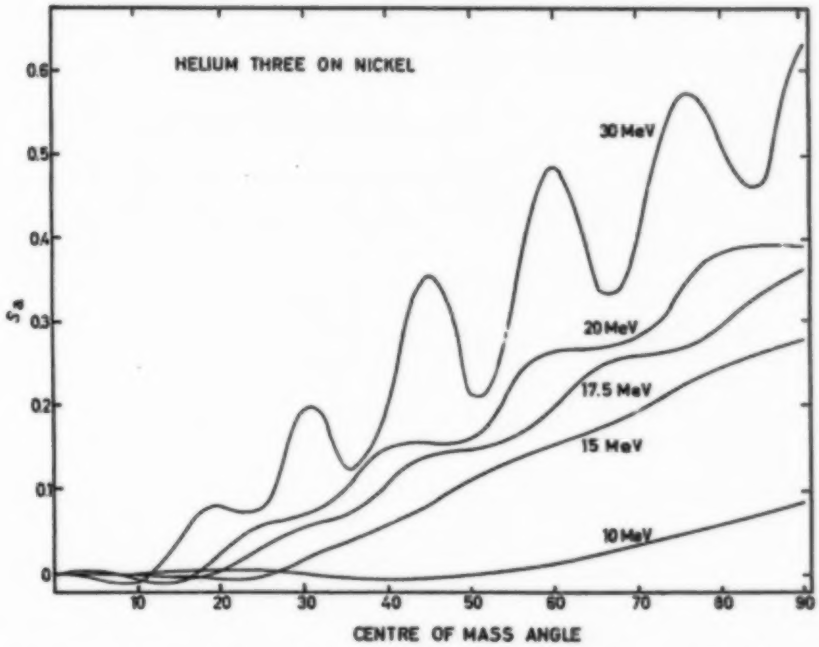

Fig. 2. Variation of the sensitivity of the differential cross-section for He^3—Ni scattering to the nuclear surface diffuseness as a function of energy and angle.

Since S_a varies smoothly with θ for each energy the results may be shown more concisely by plotting S_a as a function of energy for a particular angle, say 90°. This is done in fig. 3. The amplitude of the oscillation of S_a is indicated by the two subsidiary curves. This diagram enables the energy E_a at which the scattering is most smoothly sensitive to the nuclear field to be found. At low energies, $S_a \approx E^3$, so the higher the energy the better, provided the oscillations do not become excessive. If an oscillation of $\pm 10\ \%$ is considered tolerable, reference to fig. 3 enables E_a to be determined.

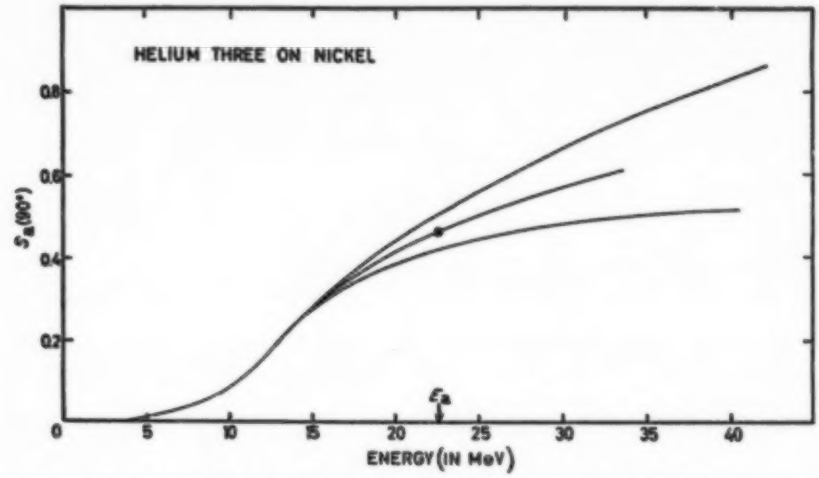

Fig. 3. Variation of the sensitivity of the differential cross-section for He^3—Ni scattering at 90° to the nuclear surface diffuseness as a function of energy.

3. Comparison of Nuclear Probes

The analysis described in the previous section was repeated for the scattering of helium-3 by aluminium, and for the scattering of neutrons, protons, deuterons, tritons and alpha-particles by aluminium and nickel. In each case the

TABLE 1

Parameters of the optical potentials used in the analysis.

Particle	$-U$ (MeV)	$-W$ (MeV)	r_0 (10^{-13} cm)	a (10^{-13} cm)
Neutron	45	10	1.3	0.5
Proton	45	10	1.3	0.5
Deuteron	55	25	1.6	0.5
Triton	50	20	1.6	0.5
Helium-3	25	25	1.6	0.5
Alpha	40	10	1.9	0.5

optical potential parameters were taken to be consistent with those found to fit experimental data on similar nuclei at similar energies; they are given in table 1. The results for neutrons show wild fluctuations of S_a for all energies; this is expected, as there is no Coulomb field to keep the neutrons in the region of the nuclear surface. The results for the other particles are shown in fig. 4. The lines are the same as that in fig. 3, with the envelopes of the oscillations omitted for clarity.

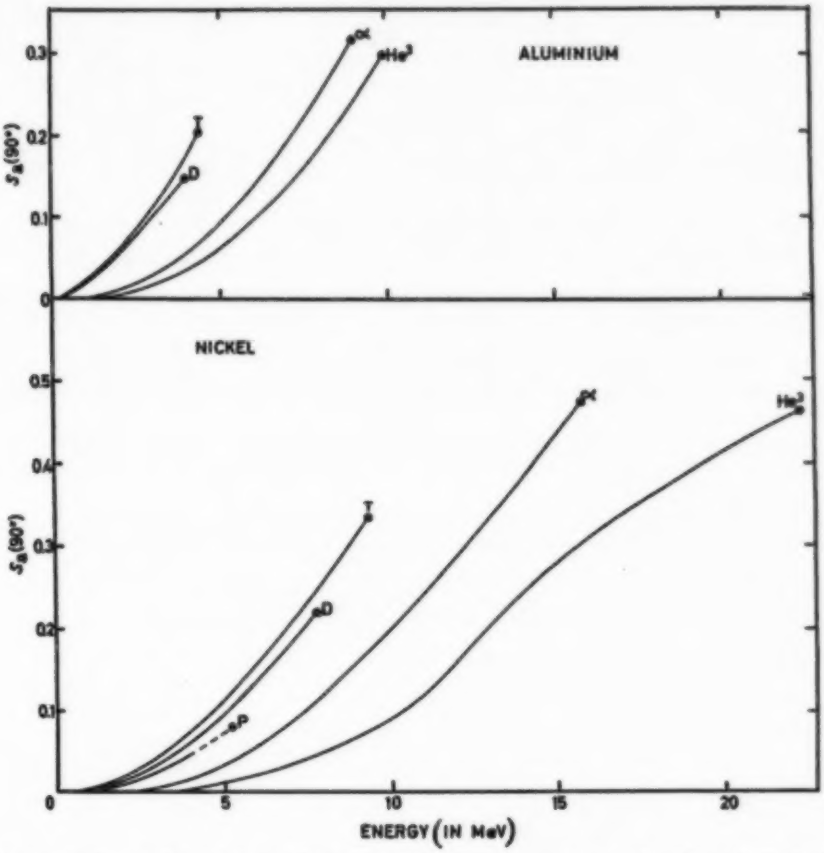

Fig. 4. A comparison of nuclear probes. In each case the curve and value of E_a is found from a diagram similar to fig. 3.

These results may be correlated by assuming that E_a is proportional to the energy corresponding to the distance of nearest approach for a head-on collision in a Coulomb field

$$E_a = K\frac{ZZ'}{A^{\frac{1}{3}}}, \tag{3}$$

where Z and Z' are the target and probe charges, A the atomic weight of the target and K is a constant to be determined. The values found for K for the interactions studied are given in table 2. They are of the same order-of-magnitude, with some small systematic trends. Too much importance should not be attached to these trends in view of the approximations inherent in the analysis.

The results given in fig. 4 show that doubly-charged particles are better probes than singly-charged ones. The "wavelength" of the oscillations of fig. 2 is greater for helium-3 than for alpha-particles, and this makes them slightly better probes.

Table 2

Values of the constant K in eq. (3) for various scattering processes

Target	PROBE				
	Proton	Deuteron	Triton	Helium-3	Alpha- -particle
Aluminium	≈0.6	0.93	0.95	1.15	1.03
Nickel	≈0.6	1.11	1.25	1.56	1.11

The reaction cross-section is also sensitive to the fringe of the nuclear field when the scattering is near-Coulomb. This is shown for the scattering of helium-3 by nickel in fig. 5, where the calculated reaction cross-section is plotted

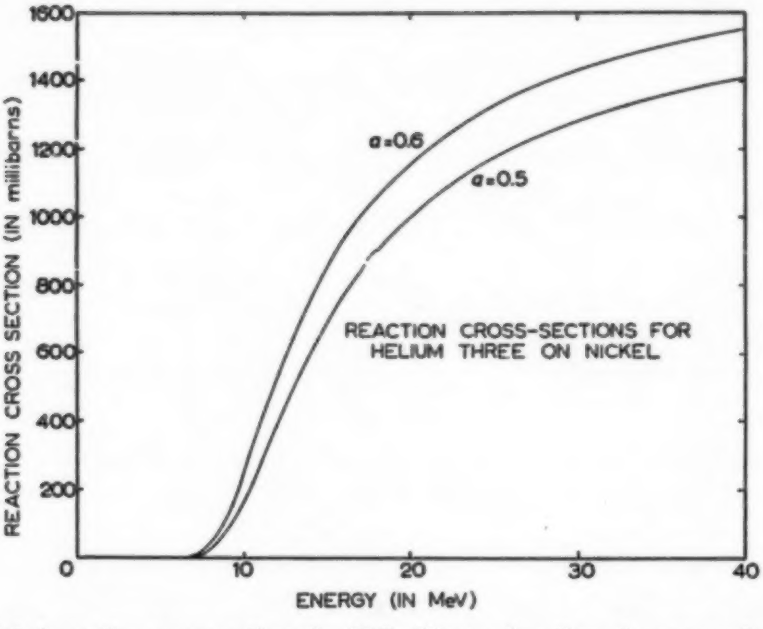

Fig. 5. Calculated reaction cross-sections for He^3—Ni as a function of energy using the optical model parameters of table 1 with two values of the diffuseness of the nuclear surface.

as a function of incident energy for two values of the surface diffuseness, the other parameters being as before. Similar results were obtained for the other scattering processes studied here. The relative difference between the two sets of reaction cross-sections increases as the incident energy decreases, becoming as much as a factor of two for the lowest energy (7.5 MeV) studied. If these small reaction cross-sections at low energies could be measured, perhaps by looking at the gamma rays from the residual nucleus, they would be a sensitive source of information about the fringe of the nuclear field.

Until recently, analyses of scattering processes assumed that the real and imaginary parts of the potential have the same radius and diffuseness. More detailed analyses may well show significant differences, which can be interpreted in terms of competing inelastic processes. The high values of the absorbing potential *W* and the nuclear radius found in the analysis of heavy-particle scattering take account of the stripping and other inelastic processes, and this influences the corresponding value of the diffuseness parameter. It may be found that the values of the surface potentials are similar for different probe particles on the same nucleus. It will then be interesting to look for shell structure effects as a function of nuclear charge. If, however, the surface potentials differ from probe to probe a more complete theory of the interaction process will be required before significant information on nuclear structure can be obtained. When considering the scattering of deuterons and perhaps also tritons and helium-3 from heavy nuclei, account should be taken of the possibility of electric breakup in the strong Coulomb field.

It should be emphasised that the work reported here assumes the applicability of the optical model to all the interactions studied, and uses parameters that are not exactly those giving the best fit to experiment. The sensitivity criteria adopted are also somewhat arbitrary. This is not likely to affect the overall conclusions, but it may well alter matters of detail.

I would like to thank Professor D. H. Wilkinson F.R.S., and Professor W. E. Burcham F.R.S., for valuable discussions; Dr. B. Buck and Mr. R. N. Maddison for their work on the computer programme, the Director of the Oxford University Computing Laboratory for the use of the Ferranti Mercury computer, Miss N. Reynolds, Miss S. Tilley and the staff of the Computing Laboratory for their assistance, and the D.S.I.R. for its support.

References

1) J. B. A. England, R. McKeague and P. E. Hodgson, Nuclear Physics **16** (1960) 52
2) P. E. Hodgson and R. N. Maddison, Proc. Intern. Conf. on Nuclear Structure, Kingston, Ontario (1960)
3) P. E. Hodgson, Nuclear Physics **21** (1960) 28
4) J. Aguilar, W. E. Burcham, J. B. A. England, P. E. Hodgson, P. V. March, J. S. C. McKee, E. M. Monsinger, A. Garcia and W. T. Toner, Proc. Roy. Soc. A **257** (1960) 13
5) G. W. Greenlees, J. S. Lilley, P. C. Rowe and P. E. Hodgson, Nuclear Physics (in the press)
6) G. Igo and R. M. Thaler, Phys. Rev. **106** (1957) 126
7) W. B. Cheston and A. E. Glassgold, Phys. Rev. **106** (1957) 1215
8) B. Buck, R. N. Maddison and P. E. Hodgson, Phil. Mag. **5** (1960) 1181

1.B

Nuclear Physics **23** (1961) 506—512; © *North-Holland Publishing Co., Amsterdam*

Not to be reproduced by photoprint or microfilm without written permission from the publisher

WIGNER CONDITION AND LOW ENERGY SCATTERING

P. MENOTTI and Y. TOMOZAWA [†]

Department of Physics, University College, London

Received 21 November 1960

Abstract: Relations between the interaction range effective range and scattering length for s- and p-waves are derived by using Wigner's inequalities for the momentum derivative of the scattering phase shift. Applications to π—N and n—p scattering are given. In particular it is shown that the obtained value ($R \geqq 0.68\, \hbar/\mu c$) for lower limit of the interaction range for s-wave ($T = \frac{1}{2}$) in π—N scattering might support the existence of π—π interaction.

1. Introduction

Some years ago Wigner derived inequalities for the momentum derivative of the scattering phase shift using his theory of $\mathscr{R}$-matrix [1]. In this note using Wigner inequalities and limiting ourselves to low energy scattering, we want to relate the interaction range R (whose meaning is explained below) with the coefficients of the momentum expansions of the scattering phase shifts. The results will be applied to π—N and n—p scattering.

The basic argument of Wigner in deriving these inequalities is that the momentum derivative of $\mathscr{R}$-matrix is non-negative [2]. The hypothesis for achieving this result is that the total Hamiltonian is an observable, i.e., a Hermitian operator with a complete set of eigenstates and that the interaction essentially vanishes for a separation r greater than a certain radius R in such a way that the particle can be considered free for $r > R$.

Sometimes for a phenomenological treatment of scattering it is convenient to use a momentum dependent potential $V(r, k)$ in the Schrödinger equation. Such an interaction can violate Wigner's condition $\mathrm{d}\mathscr{R}/\mathrm{d}k \geqq 0$, because an interaction of this type is in general non-Hermitian. In the following we restrict ourselves to Hermitian interactions which include of course the spin-orbit interaction. In other words we examine the limitation on R, for a wave mechanical model of π—N and n—p scattering.

2. General Argument

The inequalities for s- and p-waves are respectively [††]

$$\frac{\mathrm{d}\delta_0}{\mathrm{d}k} \geqq -R + \frac{1}{2k} \sin 2(kR + \delta_0), \tag{1a}$$

[†] On leave of absence from the Tokyo University of Education, Tokyo, Japan.

[††] For simplified derivations for potential scattering see refs. [3, 4].

$$\frac{d\delta_1}{dk} \geqq -R + \frac{1}{k^2R}[1-\cos 2(kR+\delta_1)] - \frac{1}{2k}\sin 2(kR+\delta_1). \qquad \text{(1b)}$$

From general arguments 5) we know that the expansions of the phase shifts are

$$\delta_0 = A_0k + B_0k^3 + O(k^5), \qquad \text{(2a) (s-wave)}$$

$$\delta_1 = A_1k^3 + B_1k^5 + O(k^7). \qquad \text{(2b) (p-wave)}$$

Putting (2) into (1) we get:

$$[B_0+\tfrac{1}{3}(A_0+R)^3]k^2+O(k^4) \geqq 0,$$

$$\left[B_1-\frac{A_1^2}{R}+\tfrac{1}{3}R^2A_1+\tfrac{1}{45}R^5\right]k^4+O(k^6) \geqq 0.$$

Thus

$$B_0+\tfrac{1}{3}(A_0+R)^3 \geqq 0, \qquad \text{(3a)}$$

$$B_1-\frac{A_1^2}{R}+\tfrac{1}{3}R^2A_1+\tfrac{1}{45}R^5 \geqq 0. \qquad \text{(3b)}$$

From these we can derive a lower limit for R. Eq. (3a) gives

$$R \geqq -A_0-(3B_0)^{\frac{1}{3}}. \qquad \text{(4)}$$

We put eq. (3b) in the more suitable form (see fig. 1)

$$RB_1 \geqq A_1^2-\tfrac{1}{3}A_1R^3-\tfrac{1}{45}R^6, \qquad \text{(5)}$$

or

$$B_1 \geqq \frac{1}{R}(A_1-\tfrac{1}{6}R^3)^2-\tfrac{1}{20}R^5,$$

from which we obtain independently of A_1

$$B_1 \geqq -\tfrac{1}{20}R^5.$$

It is very simple to relate the coefficients A and B to the scattering length and effective range. Starting from the two formulae

$$k \operatorname{cotg} \delta_0 = -\frac{1}{a_0}+\tfrac{1}{2}r_0k^2, \qquad k^3 \operatorname{cotg} \delta_1 = -\frac{1}{a_1}+\tfrac{1}{2}r_1k^2,$$

where a is the scattering length and r the effective range, and expanding in k we have

$$A_0 = -a_0, \quad B_0 = a_0^2(\tfrac{1}{3}a_0-\tfrac{1}{2}r_0), \quad A_1 = -a_1, \quad B_1 = -\tfrac{1}{2}r_1a_1^2.$$

3. Application to π—N Scattering

We first apply the results of section 2 to π—N scattering. The experimental data for s-waves are 6) †

$$\alpha_1 = 0.178\,k-0.01\,k^3, \quad \alpha_3 = -0.087\,k-0.07\,k^3,$$

† We use the units $\hbar = c = \mu = 1$ throughout this paper (μ being the pion mass).

and from (4) we get

$$R_1 \geqq 0.13 \quad \text{for} \quad T = \tfrac{1}{2}, \qquad R_3 \geqq 0.68 \quad \text{for} \quad T = \tfrac{3}{2}.$$

For p-wave we only consider α_{33} because at present the other p-wave phase shifts are not known with sufficient accuracy. Fitting Orear's data [7]) to 80 MeV we get the low energy behaviour

$$\alpha_{33} = (0.235)k^3 + (0.0057)k^5,$$

and using the plot of fig. 1 we have

$$R_{33} \geqq 0.82.$$

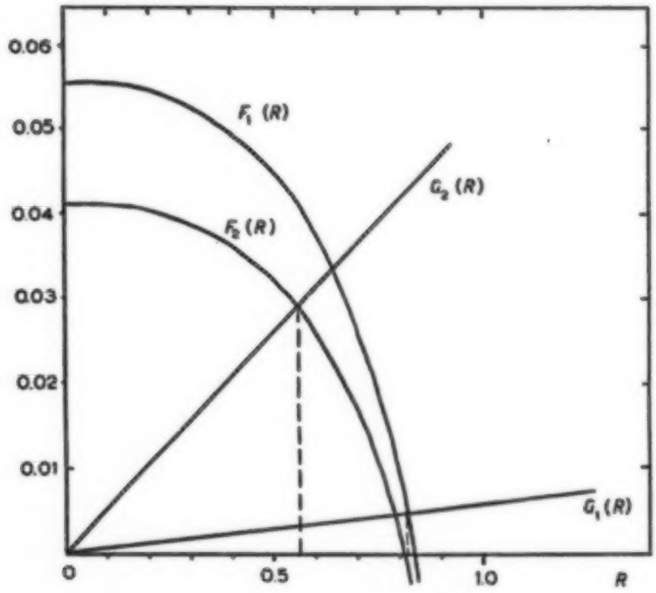

Fig. 1. Evaluation of the lower limit of Wigner radius for p-wave scattering.
$F(R) = A^2 - \frac{1}{3}AR^3 - \frac{1}{45}R^6$.
$G(R) = BR$.
Suffix 1 refers to Orear's data [7]) ($A = 0.235$, $B = 0.0057$).
Suffix 2 refers to Liverpool's data [8]) ($A = 0.203$, $B = 0.0526$).

If we use the low energy data of Liverpool group [8]) we have

$$\alpha_{33} = (0.203)k^3 + (0.0526)k^5,$$

which gives

$$R_{33} \geqq 0.55.$$

We want now to comment briefly on these results. The large interaction range R_3 of s-wave ($T = \frac{3}{2}$) might suggest the existence of π—π interaction. This is due to the fact that if we look at partial wave dispersion relations [9]), the longest range forces are due to the Born term and to the π—π interaction. In s-wave case the Born terms are negligible and thus a long range force can only be due to π—π contribution. On the contrary the p-wave Born terms are very large and this prevents us from drawing the same conclusion in this case [†].

4. Application to n—p Scattering

The experimental data for s-wave neutron-proton scattering give 10, 11) the following values:

	Scattering length	Effective range
Singlet	$-16.7(1\pm0.0024)$	1.68 ± 0.14
Triplet	$3.79(1\pm0.0039)$	$1.20\,(1\pm0.017)$

If we apply the formula (4) to these data we get

$$R_s \geqq 0.80 \quad \text{for the singlet state,} \tag{6a}$$

$$R_t \geqq 0.73 \quad \text{for the triplet state.} \tag{6b}$$

The result for the singlet state is not affected by the existence of tensor forces. Such forces however can modify Wigner's results in the triplet state, because the tensor force mixes s- and d-waves. For the solution in which the s-wave is predominant at low energy (α-wave 12)), which corresponds to the above phase shift), we can show that this modification gives an increase of the lower limit of R_t.

By the calculation of Appendix 2, eqs. (A.9) and (A.10), we get instead of (3a)

$$B+\tfrac{1}{3}(R+A)^3 \geqq 3\frac{\alpha^2}{R^3}A^2 \tag{A.11}$$

for the triplet state, where α is defined in (A.7) and (A.10), and $\alpha\, k^2$ represents the order of mixing of the d-wave for the s-wave predominant solution at low energy. A rough estimate of α is given 12) by

$$\alpha \approx \sqrt{2}Q = 0.192, \tag{7}$$

where Q is quadrupole moment of the deuteron,

$$Q = 2.74\times10^{-27}\ \text{cm}^2 = 0.136 \text{ units.}$$

Eqs. (7), (A.11) and (A.12) give the revised value for (6b)

$$R_t \geqq 0.95. \tag{8}$$

These results (6a) and (8) do not contradict the one-pion exchange force which has a range ≈ 1.

[†] We are indebted to Professor J. Hamilton for pointing out this argument.

For the singlet state, the scattering length is large: $a_s = -16.7$, $|a_s| \gg 1$. If we conjecture the range of force is $R_s \approx 1$ using (3) we can write for the effective range

$$r_s \leqq 2R_s\left[1-\frac{R_s}{a}+\frac{R_s^2}{3a^2}\right] \approx 2R_s \approx 2.$$

This immediately gives an upper limit to r_s without any knowledge of the energy dependence of the scattering cross section [10]).

We are indebted to Professor J. Hamilton, Drs. E. J. Squires, E. Leader and Mr. W. S. Woolcock for helpful discussions. This work was done in part during our staty at Cambridge University (1959—1960), the hospitality of which is gratefully acknowledged. One of us (P. M.) wishes to thank the Istituto Nazionale di Fisica Nucleare, Sezione di Pisa (Italy) for a scholarship and the other (Y. T.) the Department of Scientific and Industrial Research of the United Kingdom for a Research Grant.

Appendix 1. Wigner condition for d-wave

Following Wigner [1,3]) or equivalently from the Schrödinger equation for potential of central force we have

$$\left[\frac{\partial u_l(k,r)}{\partial k}\frac{\partial u_l(k,r)}{\partial r}-u_l(k,r)\frac{\partial^2 u_l(k,r)}{\partial r\partial k}\right]_{r=R} = 2k\int_0^R u_l^2(k,r)\mathrm{d}r \geqq 0, \quad \text{(A.1)}$$

where $u_l(k, r)/r$ is the radial wave function of orbital angular momentum l. Putting external solution for $l = 2$,

$$u_2(k,r) = \sin\,(kr-\pi+\delta_2)+3\,\frac{\cos(kr-\pi+\delta_2)}{kr}-3\,\frac{\sin\,(kr-\pi+\delta_2)}{(kr)^2}, \quad \text{(A.2)}$$

into (A.1) we get

$$\frac{\mathrm{d}\delta_2}{\mathrm{d}k} \geqq -R+\frac{1}{2k}\sin 2(kR+\delta_2)+\frac{6}{k^2R}\left\{\frac{\sin(kR+\delta_2)}{kR}-\cos\,(kR+\delta_2))^2\right\}^2. \quad \text{(A.3)}$$

This result will be used in the derivation of (A.8).

Appendix 2. Wigner condition for triplet n—p scattering

The triplet neutron-proton system in the state of total angular momentum $J = 1$, is a mixture of s and d-wave. We write the wave function as

$$\psi(\mathbf{x}) = \frac{u(r)}{r}\,Y_{101}^M+\frac{w(r)}{r}\,Y_{121}^M, \quad \text{(A.4)}$$

Here Y^M_{JlS} represents spin and angular wave function, corresponding to the state of total angular momentum J, with component M, angular momentum l and total spin S10). The Schrödinger equation is

$$\begin{aligned}
&-\frac{\mathrm{d}^2u}{\mathrm{d}r^2}+V_{\mathrm{C}}(r)u+\sqrt{8}\,V_{\mathrm{T}}(r)w=k^2u,\\
&-\frac{\mathrm{d}^2w}{\mathrm{d}r^2}+\frac{6}{r^2}w+V_{\mathrm{C}}(r)w-2V_{\mathrm{T}}(r)w+\sqrt{8}\,V_{\mathrm{T}}(r)u=k^2w,
\end{aligned}\tag{A.5}$$

where $V_{\mathrm{C}}(r)$ and $V_{\mathrm{T}}(r)$ are the potentials of central and tensor forces. This gives

$$\begin{aligned}
&\frac{\partial}{\partial r}\left[-u(k',r)\frac{\partial}{\partial r}u(k,r)+u(k,r)\frac{\partial}{\partial r}u(k',r)-w(k',r)\frac{\partial}{\partial r}w(k,r)+w(k,r)\frac{\partial}{\partial r}w(k',r)\right]\\
&\quad=(k^2-k'^2)[u(k',r)u(k,r)+w(k',r)w(k,r)].
\end{aligned}$$

Integrating from 0 to R and taking the limit $k'\to k$, we have

$$\begin{aligned}
&\left[\frac{\partial u(k,r)}{\partial k}\frac{\partial u(k,r)}{\partial r}-u(k,r)\frac{\partial^2u(k,r)}{\partial k\partial r}+\frac{\partial w(k,r)}{\partial k}\frac{\partial w(k,r)}{\partial r}-w(k,r)\frac{\partial^2w(k,r)}{\partial k\partial r}\right]_{r=R}\\
&\qquad=2k\int_0^R[u^2(k,r)+w^2(k,r)]\mathrm{d}r.
\end{aligned}\tag{A.6}$$

This has just the form of sum of s- and d-wave parts. Putting the external solution,

$$\begin{aligned}
u(k,r)&=a\sin(kr+\delta),\\
w(k,r)&=b\left[\sin(kr-\pi+\delta)+3\frac{\cos(kr-\pi+\delta)}{kr}-3\frac{\sin(kr-\pi+\delta)}{(kr)^2}\right],
\end{aligned}\tag{A.7}$$

into (A.6) we have

$$\begin{aligned}
&a^2\left[\frac{\mathrm{d}\delta}{\mathrm{d}k}+R-\frac{1}{2k}\sin 2(kR+\delta)\right]\\
&\quad+b^2\left[\frac{\mathrm{d}\delta}{\mathrm{d}k}+R-\frac{1}{2k}\sin 2(kR+\delta)-\frac{6}{k^2R}\left\{\frac{\sin(kR+\delta)}{kR}-\cos(kR+\delta)\right\}^2\right]\\
&\quad=2k\int_0^R[u^2(k,r)+w^2(k,r)]\mathrm{d}r\geqq 0.
\end{aligned}\tag{A.8}$$

Taking the expansion

$$\delta=Ak+Bk^3+\mathrm{O}(k^5),$$

(A.8) becomes

$$\begin{aligned}
&a^2\{[B+\tfrac{1}{3}(R+A)^3]k^2+\mathrm{O}(k^4)\}+b^2\left\{-\frac{3A^2}{k^2R^3}+\mathrm{O}(1)\right\}\\
&\qquad=2\int_0^R(u^2+w^2)\mathrm{d}r\geqq 0.
\end{aligned}\tag{A.9}$$

In order that (A.9) should be valid for low energy b^2/a^2 must start at least from k^4 term, because otherwise the first term of the second bracket predominates and the left-hand side of (A.8) becomes negative. Thus we get

$$b = a(\alpha k^2 + O(k^4)). \tag{A.10}$$

This corresponds to α-wave solution[12]) in which s-wave is predominant at low-energy. From (A.9) and (A.10) we have

$$B + \tfrac{1}{3}(R+A)^3 \geq \frac{3\alpha^2 A^2}{R^3}. \tag{A.11}$$

References

1) E. P. Wigner, Phys. Rev. **98** (1955) 145
2) E. P. Wigner and L. Eisenbud, Phys. Rev. **72** (1947) 29
3) E. Corinaldesi and S. Zienau, Proc. Camb. Phil. Soc. **52** (1956) 599
4) A. Martin, Comptes Rendu **243** (1956) 22
5) E. Fermi, Nuovo Cim. Suppl. **2** (1955) 17
6) J. Hamilton and W. S. Woolcock, Phys. Rev. **118** (1960) 291
7) J. Orear, Phys. Rev. **100** (1955) 288
8) D. N. Edwards *et al.*, private communication to W. S. Woolcock (to be published)
9) S. W. McDowell, Phys. Rev. **116** (1960) 774;
W. R. Frazer and J. R. Fulco, Phys. Rev. **119** (1960) 1420;
J. Hamilton and D. T. Spearman, Annals of Physics (to be published)
10) J. Blatt and V. Weisskopf, Theoretical Nuclear Physics (John Wiley, New York, 1952) Chap. II, section 3
11) E. M. Hafner *et al.*, Phys. Rev. **89** (1953) 204
12) J. Blatt and V. Weisskopf, Theoretical Nuclear Physics (John Wiley, New York 1952) Chap. II, section 5G

2.I

Nuclear Physics **23** (1961) 513—517; *North-Holland Publishing Co., Amsterdam*

©

Not to be reproduced by photoprint or microfilm without written permission from the publisher

ENERGY DEPENDENCE OF THE CROSS SECTION OF THE NUCLEAR REACTION $O^{16}(\gamma, n)O^{15}$

L. KESZTHELYI, I. BERKES, I. DEMETER and I. FODOR
Central Research Institute for Physics, Budapest

Received 21 November 1960

Abstract: The resonances in the $O^{16}(\gamma, n)O^{15}$ reaction at 17.55 MeV and 17.68 MeV were investigated with the γ-radiation of $Li^7(p, \gamma)Be^8$ reaction. It was found that if these levels exist at all their width exceed ≈ 150 keV.

1. Introduction

In the activation curves of (γ, n) reactions resulting from irradiating light nuclei by bremsstrahlung of finely varied peak energy from betatrons, breaks have been observed [1]) which are attributed to resonance-like absorption of the γ-rays into nuclear levels of the target nucleus. These levels lie in general at high excitation energies and their existence is indicated only by the (γ, n) reactions. Therefore, it seems of interest to identify these levels by means of some other methods too. This could be achieved by making use of the γ-radiation of known (p, γ) reactions. One can obtain slight variations in γ-energies either by varying the proton energy [2]) or the angle at which the γ-rays are emitted with respect to the proton beam [3,4]). The nuclear levels in the interval of γ-energy variation can be identified more convincingly than from the breaks in the activation curves.

Cohen and Stephens [2]) attempted to find the levels of C^{12} known from the breaks [1]) by studying them with γ-radiation resulting from the $T(p, \gamma)He^4$ nuclear reaction. As a result of their experiment it is clear that even if these levels exist at all, their integrated cross sections are considerably lower than those computed from the betatron experiments. Bunbury [3]) and Nakamura *et al.* [4]) tried to identify nuclear levels in moderately heavy nuclei (Ca, Zn, Ni, Ag) by irradiating them with the 17.63 MeV γ-radiation resulting from the $Li^7(p, \gamma)Be^8$ reaction. Their results were negative.

Penfold and Spicer [5]) have shown in betatron experiments the existence of resonance levels among others at 17.55 and 17.68 MeV for the $O^{16}(\gamma, n)O^{15}$ reaction. The integrated cross sections for these levels were found to be 0.22 MeV · mb and 0.18 MeV · mb, respectively. These energies lie approximately in the energy range 17.61 MeV±70 keV which is the energy interval obtainable by varying the angle between the γ-rays and the proton beam in the $Li^7(p, \gamma)Be^8$ reaction. We thought it worth while to perform some measurements using the γ-radiation of the $Li^7(p, \gamma)Be^8$ reaction in order to confirm the existence of the above levels. Measurements to identify the 17.68 MeV level were performed also by Campbell [6]).

2. Experiments

The cross section for the above nuclear reaction is very small ($\approx$ 1 mb, thus 40—50 times lower than those for the photonuclear reactions investigated up to now [3,4])), therefore, special methods were required to obtain well-measurable effects.

Lithium metal was used as target and irradiated by a non-analysed proton current of about 6—700 μA, and of 460 keV energy. In this way we obtained an intensity from the 17.6 MeV radiation of about $6 \cdot 10^7$ γ/sec in the total solid angle.

By this γ-radiation a target of $\approx$ 170 cm^3 distilled water was irradiated at different angles. The shape of the water container, however, had to be varied to obtain better energy resolution. After having irradiated the water for 6 min it was introduced into a measuring container to determine its activity.

The resulting O^{15} β^+ activity was measured by using the annihilation radiation detected by means of two scintillation counters in coincidence, each consisting of a 7.6 cm by 7.6 cm NaI(Tl) crystal on a Du Mont 6363 photomultiplier. The scintillation counters were housed in a 10 cm thick Pb shielding. Only the pulses of the photopeaks sorted out by differential discriminators were transmitted to the coincidence circuit of 2 μsec resolving power. In this way the number of background coincidences could be reduced to 1.9 coinc./min. The efficiency of the measuring apparatus as measured on a Na^{22} sample was found to be $\approx 1.4 \times 10^{-2}$ coinc./β^+ disintegration. The measurement started 30 sec after the end of the irradiation and continued for 6 min. The number of counts was read off every $\frac{1}{2}$ min to be sure that no other activity was present. The value of the half-life obtained from our experiment was 121 ± 4 sec, thus consistent with the published value of 123.6 ± 0.45 sec [6]).

For monitoring the γ-radiation we sometimes used a NaI(Tl) scintillation counter, in general, however, a GM-counter surrounded by a 1.5 cm thick Pb shield was used.

As a first step the reaction cross section was measured in the direction of the bombarding protons. The number of the 17.6 MeV energy γ-quanta was determined by considering the calculated efficiency of the scintillation counter. The β^+ activity was obtained from the counting efficiency calibrated against the standard Na^{22} sample as mentioned above. The cross section was found to be 1 mb. The statistical error of this value is 4 %, the error due to inaccurate calibration and to consideration of geometrical factors can be estimated to be 30 %.

After this experiment, we measured the relative cross sections with respect to the value at 0° by varying the γ-energy with the angle between proton beam and γ-rays. The results are plotted in fig. 1. Errors in the values thus obtained are only statistical since systematical errors are of no consequence here. The cross sections were found to be only slightly dependent on energy (about 20 %).

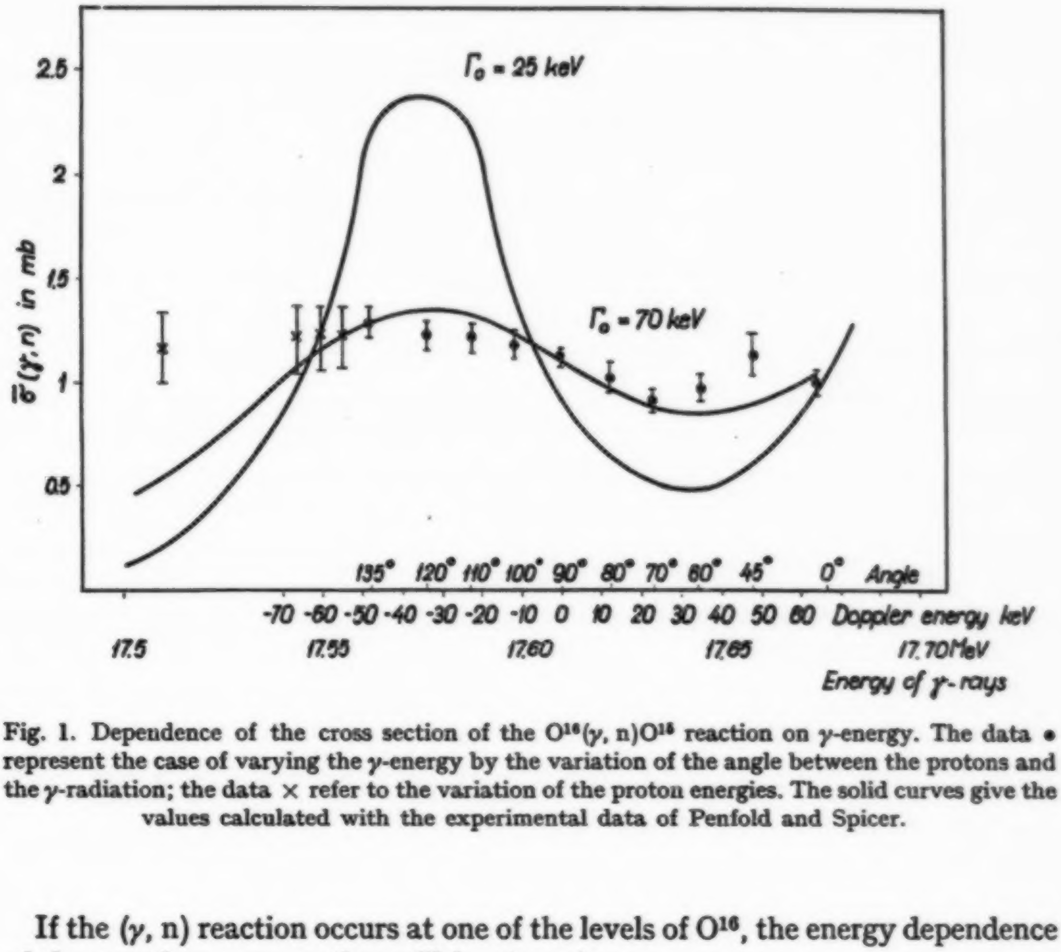

Fig. 1. Dependence of the cross section of the $O^{16}(\gamma, n)O^{15}$ reaction on γ-energy. The data • represent the case of varying the γ-energy by the variation of the angle between the protons and the γ-radiation; the data × refer to the variation of the proton energies. The solid curves give the values calculated with the experimental data of Penfold and Spicer.

If the (γ, n) reaction occurs at one of the levels of O^{16}, the energy dependence of the reaction cross section will be given by

$$\sigma(E) = \frac{\lambda^2}{8\pi} g \frac{\Gamma_n}{\Gamma_0} \frac{\Gamma_0 \Gamma_\gamma}{(E-E_0)+\frac{1}{4}\Gamma_0^2} = \sigma_{\max} \frac{1}{\left(\frac{E-E_0}{\frac{1}{2}\Gamma_0}\right)^2+1}, \qquad (1)$$

where λ is the wavelength of the γ-rays in cm, g the statistical factor, Γ_0 the total width of the O^{16} level, while Γ_γ and Γ_n are partial level widths for the emission of γ-quanta and neutrons, respectively. The γ-spectrum of the

$Li(p, \gamma)Be^8$ reaction normalized to unity at a given angle can be written as

$$f(E-E') = \frac{2}{\Gamma_{Li}\pi} \frac{1}{\left(\frac{E-E'}{\frac{1}{2}\Gamma_{Li}}\right)+1}, \tag{2}$$

where $\Gamma_{Li} = 11$ keV is the width of the 441 keV level and E' is the γ-energy at the corresponding angle.

As a thick-target was used the measured cross sections represent the mean values

$$\bar{\sigma}(E') = \sigma_{max} \int_{-\infty}^{\infty} \frac{dE}{\left[\left(\frac{E-E_0}{\frac{1}{2}\Gamma_0}\right)^2+1\right]\left[\left(\frac{E-E'}{\frac{1}{2}\Gamma_{Li}}\right)^2+1\right]}. \tag{3}$$

Using the integrated cross sections 0.22 MeV · mb and 0.18 MeV · mb and the half width $\Gamma_0 = 25$ keV, given by Penfold and Spicer, the curve ($\Gamma_0 = 25$ keV) shown in fig. 1 is obtained from the integral (3). Our experimental results do not confirm variations of such extent. According to Penfold and Spicer [5]) the maximum width of Γ_0 which can be identified by the "break" technique is about $\Gamma_0 = 70$ keV. The curve computed for this value is approximately consistent with the slight variation in the average cross section found in our experiment. Because of the small variation, however, this agreement cannot be considered as a positive result. If these levels really existed and the half-widths were $\Gamma_0 = 70$ keV, then according to the figure the reaction cross section should strongly decrease for γ-energies 50—60 keV lower than those achieved by varying the angle of the γ-radiation. For this reason measurements were performed with reduced proton energy, thus decreasing the peak energy of the γ-rays. The irradiation was carried out at 135°. By setting the proton energy at the $\frac{1}{2}$, $\frac{1}{4}$ and $\frac{1}{8}$ value of the thick-target yield curve γ-beams with mean energies approximately 6, 12, 18 keV lower than the resonance energy corresponding to 135° were obtained. Reducing the proton energy to 380 keV (this value lies far below the resonance), the maximum γ-energy will be lower by 44 keV than the mean value for 135°. In order to determine the cross section values the strong variation of the ratio of the 17.6 MeV and 14.8 MeV intensities with the proton energy had to be taken into account. This was determined by plotting the spectra in terms of the proton energy, since these values were only known at 90° [7]).

The relative cross sections obtained in this experiment are also shown in fig. 1 (for distinction marked by ×).

3. Conclusion

From our results the conclusion may be drawn that the level widths observed by Penfold and Spicer — if the levels in question exist at all — are very large and certainly exceeding $\approx$ 150 keV. This statement is in agreement with the experimental results of Jones *et al.* [8]) who found in the investigation of the $N^{15}(p, n)O^{15}$ reaction the nucleus O^{16} to have a 250 keV wide level at about 17.5 MeV.

References

1) L. Katz, R. N. H. Haslam, R. J. Horsley, A. S. W. Cameron and R. Montalbetty, Phys. Rev. **95** (1954) 464
2) L. D. Cohen and W. E. Stephens, Phys. Rev. Letters **2** (1959) 236
3) D. St. P. Bunbury, Phil. Mag. **44** (1953) 533
4) T. Nakamura, K. Fukunaga, K. Takamatsu, M. Yata and S. Yasumi, J. Phys. Soc. Japan **14** (1959) 1117
5) A. S. Penfold and B. M. Spicer, Phys. Rev. **100** (1955) 1377
6) J. G. Campbell, Aust. J. Phys. **8** (1955) 449
7) F. Ajzenberg-Selove and T. Lauritsen, Nuclear Physics **11** (1959) 1
8) K. W. Jones, L. J. Lidofsky and J. L. Weil, Phys. Rev. **112** (1958) 1252

2.A

Nuclear Physics **23** (1961) 518—523; © *North-Holland Publishing Co., Amsterdam*

Not to be reproduced by photoprint or microfilm without written permission from the publisher

THE $B^{11}(p, \gamma\alpha)Be^8$ REACTION AND THE 9.63 MeV STATE OF C^{12}

A. G. GREGORY

Research School of Physical Sciences, Australian National University, Canberra

Received 17 November 1960

Abstract: An attempt to measure the cross section for transitions between the 16.11 and 9.63 MeV states of C^{12} is reported and an upper limit of 30 % of that for ground state transitions is given. Theoretical formulae are given for the observable coincidence rate in the $B^{11}(p, \gamma\alpha)Be^8$ reaction at 163 keV bombarding energy as a function of γ detector acceptance angle for two positions of this detector. These formulae are used in conjunction with experimentally determined background rates to assess the possibility of determining the spin of the 9.63 MeV state of C^{12} by means of angular correlation measurements.

1. Introduction

A recent analysis of data from experiments involving the 9.63 MeV state of C^{12} has shown [1]) that this state is probably 3^- rather than 1^- as previously supposed. An apparent means of deciding definitely between these alternatives is through observation of the (γ—α) correlations in the reaction $B^{11}(p, \gamma)C^{12}(\alpha)Be^8$ at 163 keV bombarding energy. The above reference includes an estimate of the radiation width for γ-ray transitions between the 16.11 and 9.63 MeV states together with the theoretical angular correlations associated with each of the possible spin values. In this paper an account is given of experiments to measure the cross section for these γ transitions relative to those through the 4.43 MeV state and an analysis is made of the conditions under which a correlation experiment might be possible.

2. Experimental

Two sets of experiments are to be described here. The first consisted of a straightforward measurement in the 4—12 MeV region of the spectrum of γ rays emitted in the $B^{11}(p, \gamma)C^{12}$ reaction at 163 keV bombarding energy. The second was a measurement of the (γ—α) coincidence rate in the same reaction. In both cases the targets were made by evaporating B_2O_3 on to 1.63 mg/cm^2 Al foils to a thickness of 20—30 keV for 160 keV protons. These targets were set at 45° to the direction of the proton beam.

The γ ray spectrum (fig. 1) was measured at 90° to the proton beam direction with a 10.2 cm by 12.7 cm diameter NaI(Tl) crystal well collimated and used in conjunction with a 7.6 cm Dumont photomultiplier and a 100-channel kicksorter. In order to estimate the maximum possible contribution of 6.5 MeV γ rays to the tail of the 11.7 MeV peak of this spectrum, the area under the peak was found and an equivalent 6.5 MeV peak constructed with 1/30 of this area, thus corresponding to the area of the ground state group peak at 16.1 MeV. The result of subtracting this peak from the appropriate region is shown in fig. 1. Evidently the cross section for transitions through the 9.63 MeV state is less than that for transitions to the ground state.

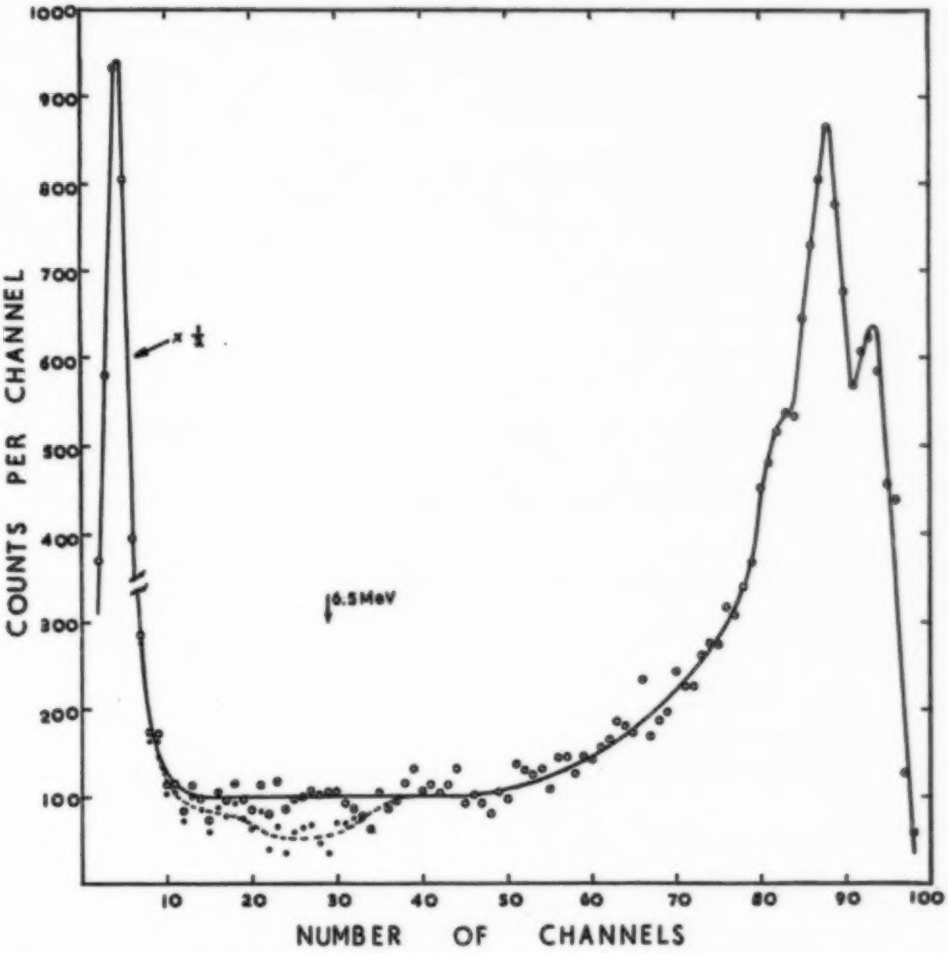

Fig. 1. Spectrum of γ rays from the reaction $B^{11}(p, \gamma)C^{12}$ at 163 keV bombarding energy. Background due to cosmic rays has been subtracted. The dashed line corresponds to subtraction of a 6.5 MeV peak of area equal to 1/30 that of the 11.7 MeV peak.

The coincidence experiments were made with the collimator removed and the face of the NaI crystal set at 6.1 cm from the target axis. The α particle detector was also at 90° to the proton beam direction, being on the opposite side of the target from the γ ray detector. It consisted of a 0.25 mm thick CsI crystal 2.5 cm in diameter cemented to a 5.1 cm Dumont photomultiplier and subtending a $\frac{1}{2}$ angle of 15° at the target axis. A 0.64 μm nickel foil was interposed between the α particle detector and target, in order to absorb light and scattered protons; the 1.5 MeV α particles lost about 0.5 MeV in this foil. The α spectrum was calibrated by means of a ThC+C′ source placed in the target position.

Pulses from the detectors were passed through amplifiers and sorted by single-channel analysers set to accept the appropriate energy range. These settings were made by using the analyser outputs to gate the respective spectra on the 100-channel kicksorter. Owing to possible non-linearity in the low energy response of the α detector and some uncertainty in the energy loss due to the nickel foil a range of α energies estimated to correspond to 0.5 to 1.5 MeV α's entering the detector was accepted. The acceptance range of γ's quoted here was 5—7.5 MeV.

Output pulses from the analysers were each passed into two coincidence units. One of these units was set to accept both true and random coincidences while the other had an extra delay of 1 μs added to one channel to exclude all true coincidences.

The roles of the two units were interchanged in alternate runs to eliminate possible effects due to instrumental differences, e.g. in resolving times. The latter were nominally 0.5 μs, a lower limit set by jitter in the analysers. In addition tests were made: (a) with the γ window moved up over the 12 MeV peak, (b) with the α window moved up above 3 MeV, (c) with both the above adjustments. The results of all runs are given in table 1. Runs 1 and 2 together represent 26 hours counting under normal coincidence conditions.

TABLE 1

Experimental results

Run	T+R	R	(T+R)−R	N_γ
1	477	325	152	137600
2	1058	977	81	318530
3	68	35	33	73190
3a	133	70	63	137600
4	604	556	48	368720
4a	924	851	73	318530

Runs 3 and 4 are results of tests made under comparable conditions to runs 1 and 2 respectively, while 3a and 4a are normalizations of 3 and 4 to the same numbers of disintegrations as 1 and 2. The reason for the quite considerable number of "true" coincidences in the tests is not clear, but allowance is made for these in deducing the cross section for the γ ray transitions. In each set of experiments γ ray spectra were taken simultaneously with the coincidence counts so that the yield could be expressed relative to that of the 11.7 MeV γ rays. The results are thus given in terms of the ratio K of the cross section for 6.5 MeV γ rays to that for 11.7 MeV γ rays. After making the necessary corrections these results become $K = 0.013 \pm 0.009$ and $K = 0.0006 \pm 0.0011$ respectively for run 1 and run 2, giving a final result of $K = 0.007 \pm 0.005$. On the basis of this latter result the upper limit on the cross section is 0.012 times that of γ_1, or 30 % of that of the ground state transition [2]).

3. Analysis of Correlation Experiment

A knowledge of the asymmetry of the (γ, α) correlation in a plane containing the beam direction in the $B^{11}(p, \gamma\alpha)Be^8$ reaction at 163 keV would determine the spin of the intermediate state of C^{12} at 9.63 MeV uniquely. Two convenient points on this correlation are chosen by selecting α particles leaving the target at right angles to the proton beam direction in coincidence with γ rays leaving either at 90° or 180° to the α direction. In practice the yield of this reaction is very low so the acceptance angles required of the detectors are large. It is therefore necessary to obtain equations for yield in terms of solid angles for both positions of the γ detector and both spin possibilities. Such equations, derived assuming zero solid angle for the α detector, are quoted below [3]).

The (γ, α) correlation equation may be written as follows:

$$\frac{d\sigma(\theta, \phi)}{d\Omega} = (A + B\cos^2\theta) + (A' + B'\cos^2\theta)\cos 2\phi, \tag{1}$$

where the constants may be sufficiently determined by using the particular forms for the two spin possibilities:

$$\sigma(\theta, \phi) \propto 80 + 4(1 - 3\cos^2\theta) - 28B - B[5(1 - 3\cos^2\theta) + 27\sin^2\theta\cos 2\phi],$$
$$\sigma(\theta, \phi) \propto 40 + 8(1 - 3\cos^2\theta) - 16B - B[5(1 - 3\cos^2\theta) + 9\sin^2\theta\cos 2\phi],$$

where B is a constant of value 0.41.

In these equations θ and ϕ are the equatorial and azimuthal angles of a point on the γ detector referred to the α direction. The following coincidence yields are then given by integrating eq. (1) over the surface of the γ detector for each position:

$$Y_{180} \propto 2\pi(1 - \cos\theta_0)[A + \tfrac{1}{3}B(1 + \cos\theta_0 + \cos^2\theta_0)] \quad \text{(angle between } \alpha \text{ and } \gamma \text{ is } 180^\circ) \tag{2}$$

$$Y_{90} \propto 2\pi(1 - \cos\theta_0)[A + \tfrac{1}{3}B(1 - \tfrac{1}{2}\cos\theta_0 - \tfrac{1}{2}\cos^2\theta_0) + A'\cos\theta_0 + \tfrac{1}{2}B'\cos\theta_0(1 - \cos\theta_0)], \quad \text{(angle between } \alpha \text{ and } \gamma \text{ is } 90^\circ], \tag{3}$$

where θ_0 is the $\frac{1}{2}$ angle subtended by the γ detector at the target.

The values of the constants are:

$A = 70.47$, $B = -5.85$, $A' = -11.07$, $B' = 11.07$ for spin 1;
$A = 37.37$, $B = -17.85$, $A' = -3.67$, $B' = 3.69$ for spin 3.

The possibility of distinguishing between the two spin assignments depends on the magnitude of the difference of the ratio $R = Y_{180}/Y_{90}$ for the two cases. This difference decreases monotonically from a maximum at θ_0 zero to zero with $\theta_0 = 90°$ (fig. 2). We require the value of θ_0 giving the best compromise and obtain it as follows.

The criterion of sufficient accuracy in the measurement of R is that the error in this measurement be less than the difference in the theoretical values, i.e.

$$\varepsilon(R) < R_3 - R_1 \quad \text{or} \quad \Delta = R_3 - R_1 \fallingdotseq C\sqrt{Y}/Y,$$

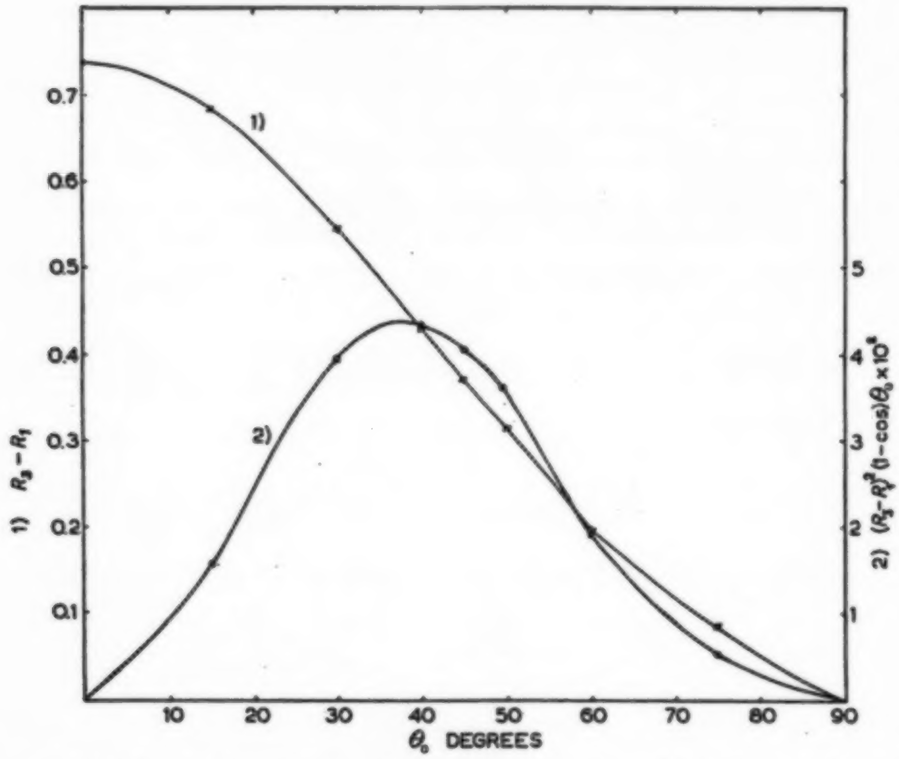

Fig. 2. Data for determining optimum γ counter geometry. Curve 1 is of R_3-R_1 (see text) as a function of γ ray detector $\frac{1}{2}$ angle θ_0. In curve 2 the function $(R_3-R_1)^2(1-\cos\theta_0)$ which is inversely proportional to counting time required is also plotted as a function of θ_0.

where C is an unspecified constant multiplier of the statistical error required to give sufficient accuracy, and Y is a mean value of the yield. The time taken to record this yield is given by

$$T \propto \frac{Y}{1-\cos\theta_0} = \frac{C_1}{\Delta^2(1-\cos\theta_0)}.$$

Fig. 2 includes a plot of $\Delta^2(1-\cos\theta_0)$ as a function of θ_0. This shows 40° to be the optimum $\frac{1}{2}$ angle to use, (R_3-R_1) being about 0.43 here. In the experiments described above the primary object was to ascertain whether the yield from the transition is in fact great enough to make any measurement of it possible. Therefore the greatest available angle (50°) was used, giving $(R_3 - R_1) = 0.318$. The following estimate is based on data obtained with this value of θ_0.

The true coincidence rate (N_c) is obtained as the difference between the total coincidence rate and the random rate (N_r). To reduce the value of N_r, windows may be placed over the two spectra giving individual counting rates of N_α and N_γ. The random rate is then given by the usual formula

$$N_r = 2N_\alpha N_\gamma \tau,$$

and the true rate is given in terms of the α counter efficiency, the ratio (D) of N_c to counts in the 16 MeV peak and the branching ratio K by

$$N_c = \frac{\alpha K N_\gamma}{D}.$$

In these experiments α was 1/60, $D = 0.16$ and typical values for N_α and N_γ using about 3μA of protons were 2.10^3 and 2 per second respectively. Taking the suggested upper limit for $K(0.012)$ and allowing 100 hours running this leads to statistical error of 0.12 in the measurement of R. Under these conditions it should just be possible to distinguish between the two spin values.

4. Conclusions

The results of these experiments suggest that the yield of γ rays from transitions through the 9.63 MeV state of C^{12} is less than one third that of ground state transitions. In principle it should be possible to achieve much better accuracy and the possibility of making a correlation measurement is not entirely ruled out.

It is a great pleasure to acknowledge the helpful suggestions and information supplied by Dr. F. C. Barker and Dr. T. R. Ophel, and the advice and encouragement of Professor E. W. Titterton and Dr. P. B. Treacy.

References

1) F. C. Barker, E. Bradford and L. J. Tassie, Nuclear Physics 19 (1960) 101
2) F. Ajzenberg and T. Lauritsen, Nuclear Physics 11 (1959) 122
3) F. C. Barker (private communication)

3.B

Nuclear Physics **23** (1961) 524—531; © *North-Holland Publishing Co., Amsterdam*

Not to be reproduced by photoprint or microfilm without written permission from the publisher

DIFFERENCES IN NATURAL WIDTHS OF CONVERSION LINES

J. H. DIJKSTRA and C. DE VRIES †

Institute for Nuclear Research, Amsterdam

Received 20 October 1960

Abstract: A folding procedure was applied to K- and L-conversion line pairs due to gamma-ray transitions in Hg- and Bi-isotopes, measured with an ironfree double focussing beta-ray spectrometer. Apart from yielding an accurate determination of the $B\rho$-ratio of corresponding K- and L-lines this procedure indicated the difference of the atomic level widths to be 49±5 eV in Bi and 54±5 eV in Hg, in fair agreement with X-ray data.

1. Introduction

It is already known for a long time that the widths of internal conversion lines measured with a beta-ray spectrometer are partly due to the natural widths of the levels of X-rays which follow the corresponding conversion ¹). These widths are inversely proportional to the life-time of the X-ray level involved; as a result, K-conversion lines are broadened more by this effect than conversion lines of higher atomic shells. Lindström ²) and Slätis ³) were the first to observe this difference in widths; it was later confirmed by several other authors (e.g. by Mladjenovič ⁴), for Auger-lines recently by Ewan *et al.* ⁵))

When calibrating the ironfree double focussing spectrometer newly built at our institute ⁶) the difference in natural widths as mentioned above played an important role. One of the best calibration methods is to measure the momentum ratio of K- and L-conversion lines belonging to one nuclear transition, for which the energy difference of the corresponding electron shells is known accurately ⁸,⁹) (e.g. by X-ray crystal methods). The momentum ratio can be determined most accurately by matching the corresponding K- and L-lines point for point. This can easily be done if their shapes are the same. If the difference in natural widths is important this matching can be carried out only after a folding procedure as applied by Mladjenovič ⁴). This method is again only possible if the instrumental part of the line broadening is independent of the line position in the momentum scale, and if source straggling is unimportant (this effect will broaden the K-line much more than the corresponding L-lines).

One of us ⁶) has shown that when source effects are present, the momentum ratio is not seriously influenced if one takes for the definition of the (relative) line position the intersection of the linearly extrapolated sides of the line. In order to check the influence of the natural width on this definition, we used the folding procedure mentioned above. This procedure then also yields information about the difference in natural widths of the measured lines.

---

† Now at High Energy Physics Department, Stanford University, California, USA.

2. Theoretical Considerations

If $B(p/p_0)$ is the experimental shape of a strictly monoenergetic electron line with momentum p_0, then the shape of a conversion line with electron momentum distribution $f(p)$ becomes

$$F(p) = \int_{-\infty}^{+\infty} f(p-q)\, B\left(\frac{q}{p_0}\right) \mathrm{d}q. \tag{1}$$

Under ideal conditions $B(q/p_0)$ has the same shape for every line. The maximum of $B(q/p_0)$ does not necessarily coincide with p_0 (see e.g. the paper of Wild and Huber [10]). The lower limit $-\infty$ has no physical meaning; for narrow lines this does not matter (in our case halfwidths at most 0.05 %).

If $B(q/p_0)$ is known accurately, e.g. from electron optical considerations, $f(p)$ and thus its halfwidth can be formed by unfolding $F(p)$. Even if no scattering effects, source straggling etc. are present, the instrumental parameters which influence the shape of $B(q/p_0)$ can easily be different from one experiment to another (geometry of source and counter slit; relative position of source and slit; solid angle of accepted beam; magnetic field shape). Therefore we did not try to find $f(p)$ either by experiment or by calculation. Instead we used a modification of the procedure applied by Mladjenovič [4]; keeping in mind that the natural electron momentum distribution $f(p)$ according to quantum mechanics should be a resonance curve (dispersion-, Lorentzian- or Hoyt-function), we shifted the L-line to the K-line position and folded the displaced L-line with a couple of resonance curves (according to (1)) until the best fit with the K-line was obtained (within the statistical error of the measured points).

We shall first see what this means for the folding integral (1). Substituting for $f(p)$ the resonance function (essentially an energy-distribution, which can be expressed in momentum units) we find for the L-line:

$$F_{\mathrm{L}}(p) = \int_{-\infty}^{+\infty} \frac{1}{1+\left(\frac{p-q}{\alpha_{\mathrm{L}}}\right)^2}\, B\left(\frac{q}{p_{\mathrm{L}}}\right) \mathrm{d}q, \tag{2}$$

with

$$\alpha_{\mathrm{L}} = \frac{E_{\mathrm{L}}}{p_{\mathrm{L}}} \Gamma_{\mathrm{L}}.$$

Here $2\Gamma_{\mathrm{L}}$ is the halfwidth of natural energy distribution $f_{\mathrm{L}}(p)$ of L-conversion electrons; for E_L and p_L we can take the values belonging to the maximum of $B(q/p_0)$. This first order approximation is allowed because of the narrow lines we used.

The L-line $F_L(p)$ as a whole can be shifted to the K-line position by replacing p under the integral sign by p/a $(a = p_K/p_L)$. The shifted line $F_L^s(p)$ is then folded with a resonance function having a width 2β. The result $F_L^f(p)$ is then compared with the K-line. We find

$$F_L^f(p) = \int_{-\infty}^{+\infty} \frac{1}{1+\left(\frac{aq-p}{a\alpha_L+\beta}\right)^2} B\left(\frac{aq}{p_K}\right) \mathrm{d}q. \tag{3}$$

We made use of the theorem that folding two resonance curves results in a new resonance curve, with a width equal to the sum of the widths of the original curves.

Now (3) is exactly the shape of a K-line if β is determined by

$$\beta = \alpha_K - a\alpha_L, \tag{4}$$

where

$$\alpha_K = \frac{E_K}{p_K} \Gamma_K.$$

Here we can take for E_K and p_K the values determined by the intersection of the two sides of the K-line; this is again not critical for narrow lines.

3. Discussion of Experiments

With Γ_L-data taken from literature, formula (4) gives us an approximate value for β. The shifted L-line $F_L^s(p)$ was constructed from the measured L-line by reducing the L-line momentum scale with a factor $a = p_K/p_L$, and numerical folding with resonance curves of width β. Variation of the number of summation steps (replacing the integral by a summation) showed that this numerical method did not introduce appreciable errors. We have estimated the error by taking different values of β which resulted in folded lines in agreement with the experimental K-lines within the statistical deviations. (See figs. 1 and 2).

The folding procedure was applied to two cases:

1) ^{212}Bi (Th-B source); 239 keV gamma transition; I- and F-lines used (K- and L_I-conversion lines resp.).

2) ^{199}Hg (Au source); 158 keV gamma transition; K-, L_{II} and L_{III}-lines used.

As the experimental conditions under which the lines are measured have been described in detail by De Vries [6]) (^{212}Bi) and De Vries and Dijkstra [7]) (^{199}Hg) we restricted ourselves here with giving the plots of the experimental line shapes in figs. 1a, 1b and 1c.

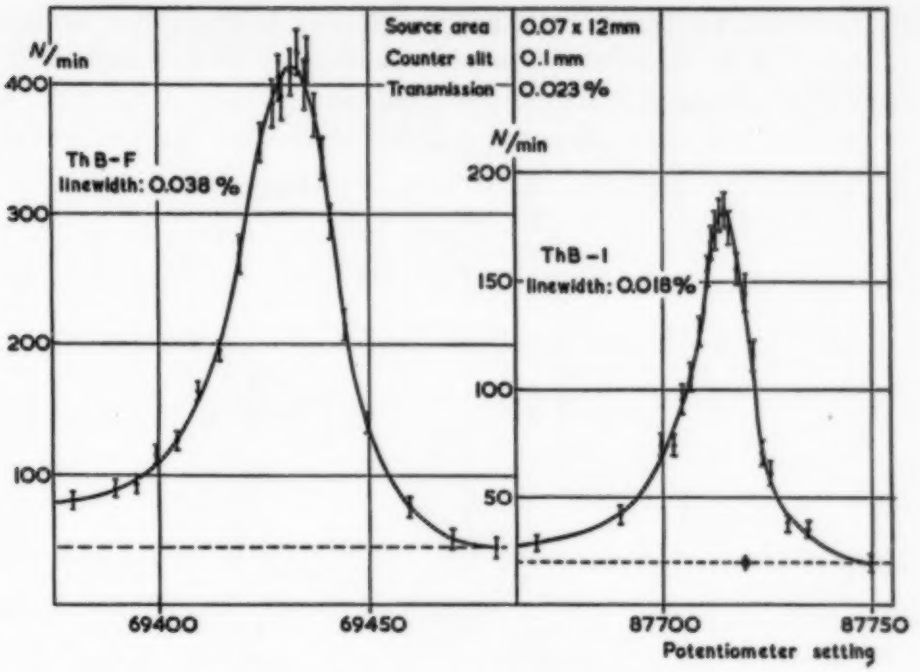

Fig. 1a. Conversion spectra of the 239 keV transition in ^{212}Bi (Th-B source).

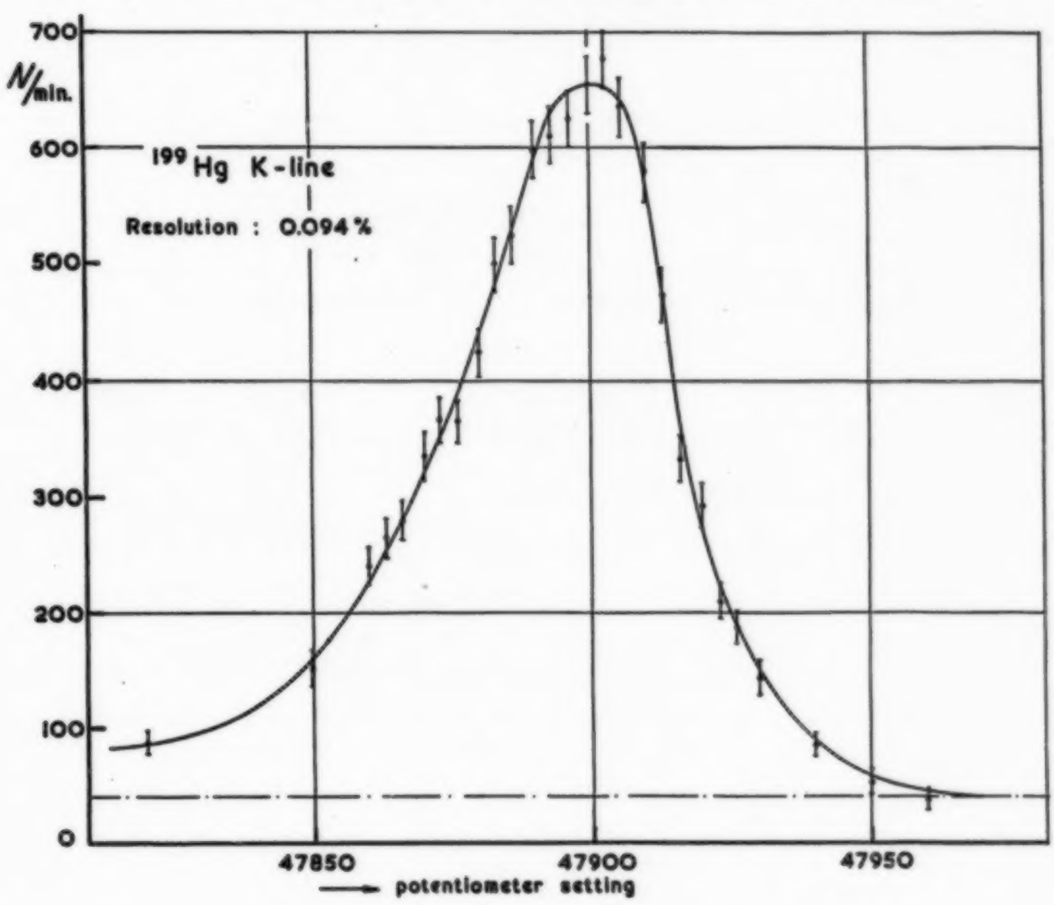

Fig. 1b. Conversion spectrum of the 158 keV transition in ^{199}Hg (K-line).

The difference in relative widths of the K- and L-lines is for Bi: 0.020 %; for Hg: 0.043 % (average of L_{II}- and L_{III}-lines), which corresponds to resp. 52 eV and 60 eV at the K-line positions. With these data we started our folding procedure. The results are shown in figs. 2a, 2b and 2c. The width difference between the K- and L-lines found from the plots is β (eq. 4). Instead of β we give the corrected "true" width difference $\alpha_K - \alpha_L$ (average values):

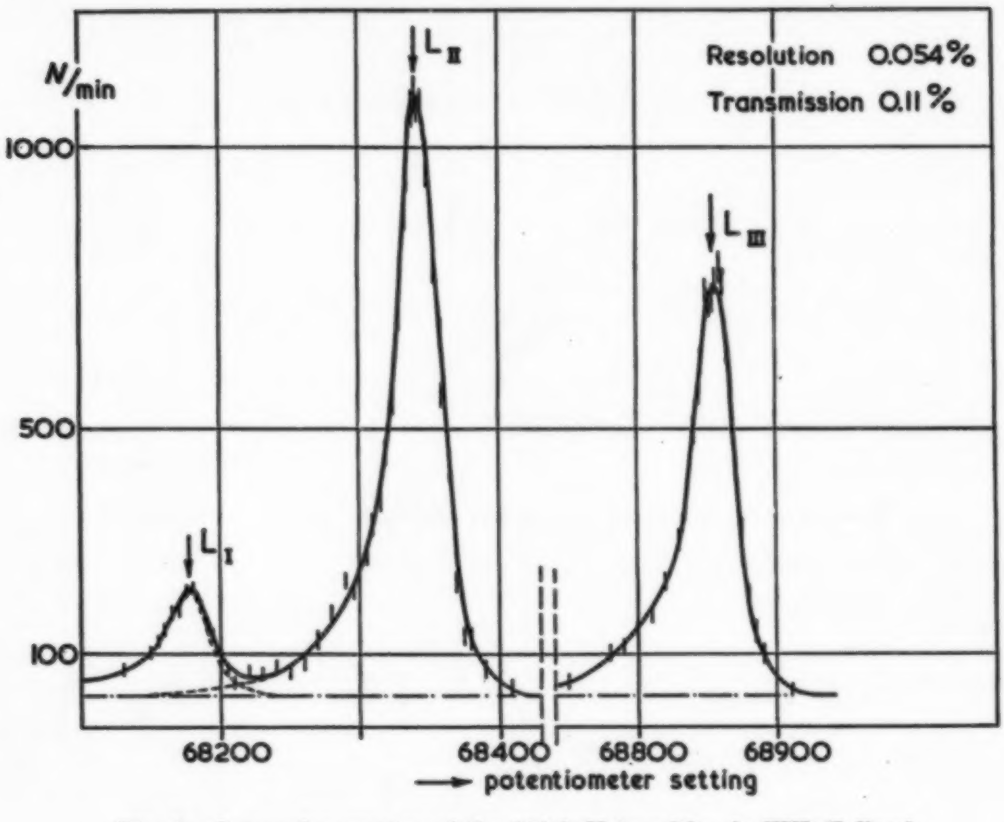

Fig. 1c. Conversion spectra of the 158 keV transition in ^{199}Hg(L-lines).

^{212}Bi : $K-L_I$ difference 49±5 eV;

^{199}Hg: $K-L_{II}$ difference 52±5 eV, $K-L_{III}$ difference 55±5 eV.

For the correction we assumed the natural widths of the L-lines to be: 10 eV for L_I(Bi) and 5 eV for L_{II} and L_{III}(Hg) [4, 12, 14, 16, 17]).

We may compare the width differences in this work with values in the literature. X-ray experiments by Ingelstam [13]) yield differences of 46 eV (Bi) and 45 eV (Hg) †. The data of Compton and Allison [14]) and Gokhale [15]), as treated

---

† We used figs. 31 and 32 of ref. [13]), supposing that eq. (21) of ref. [13]) was valid, i.e. $n = 1$ in eq. (5) of this paper. The average widths of the M_{II} and M_{III} levels were assumed to be 14 eV(Bi) and 11 eV(Hg). For Bi we took the measured value of fig. 31, ref. [13]); for Hg the average of the values of 78 Pt and 81 Tl.

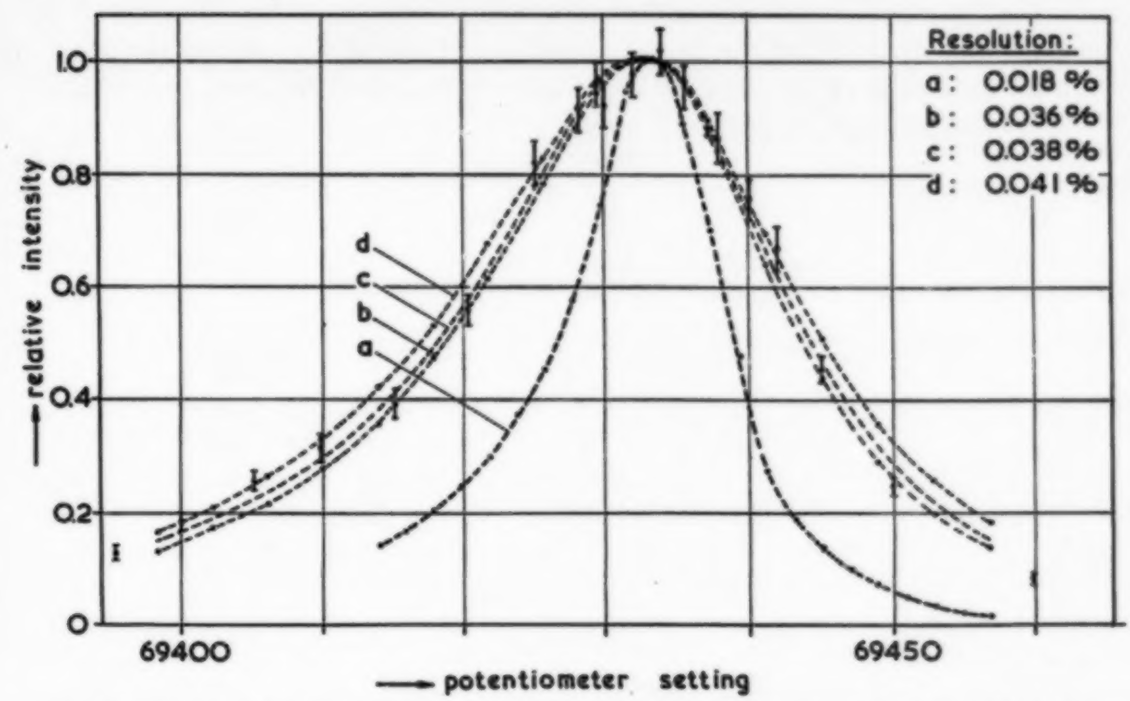

Fig. 2a. Matching of the line profile as measured for the K-line (experimental points) with the line profiles b, c and d, which are obtained after folding the L_I-line (curve a) with resonance curves with halfwidths: 47.5 eV, 52 eV and 60 eV. Curve a has the same shape and relative halfwidth as measured for the L_I-line.

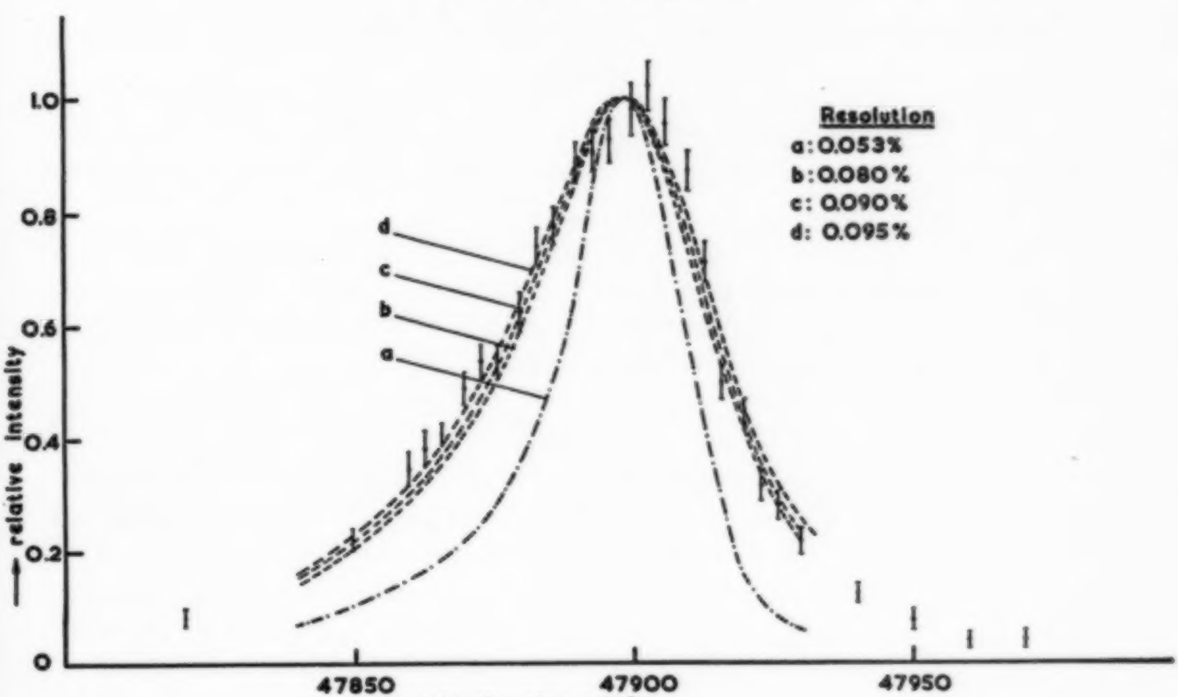

Fig. 2b. Matching (as in fig. 2a) for ^{199}Hg L_{II}-line folded with resonance curves of width 50, 55 and 60 eV.

by Mladjenovič [4]) yield width differences of 47 eV (Bi) and 44 eV (Hg) (the last value extrapolated from the Bi-value with the Z^4 law). If we estimate the uncertainty in the data to be about 10 %, the average width differences become for Bi: 47±5 eV and for Hg: 45±5 eV.

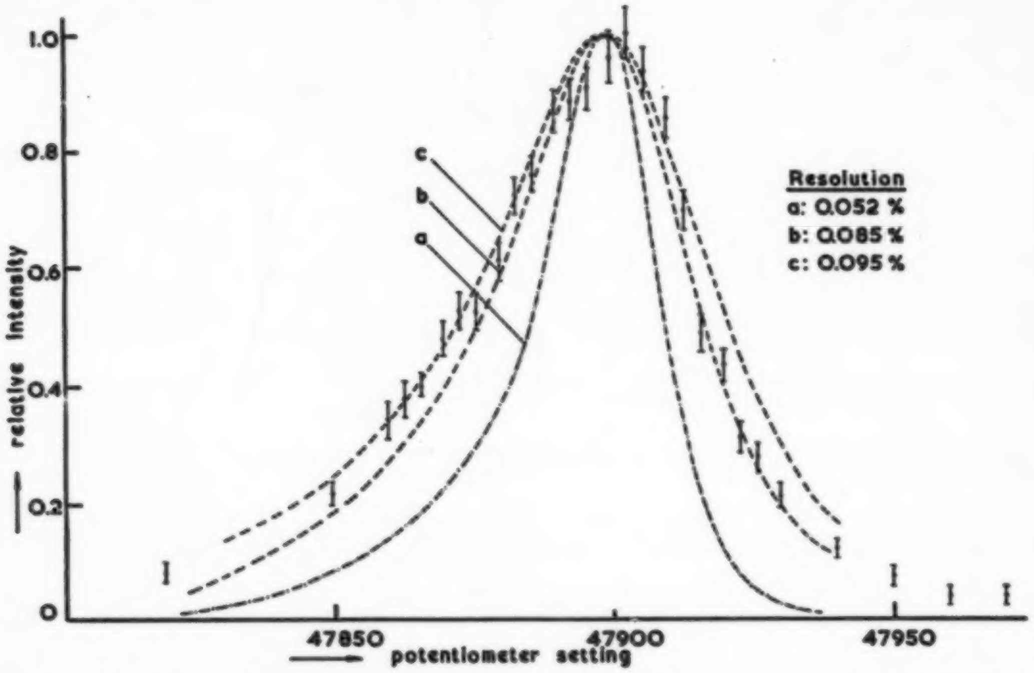

Fig. 2c. Matching (as in fig. 2a) for ^{199}Hg. L_{III}-line folded with resonance curves of width 51 and 61 eV.

Earlier conversion line experiments yielded 80—100 eV for Bi (refs. [2–4])). The better agreement with X-ray data in our case is perhaps due to an advancement in source technique.

Comparison of the X-ray data with the results of this work throws also some light on the question how to combine the halfwidths of the spectrometer window curve and the natural line. According to Nordling *et al.* [11]) the addition formula for the halfwidths can be written as follows:

$$w_{\text{tot}}^n = w_{\text{nat}}^n + w_{\text{sp}}^n, \tag{5}$$

where w_{nat} is the natural halfwidth; w_{sp} is the width of spectrometer window curve. As is well-known, $n = 1$ in combining resonance line shapes, and $n = 2$ for Gaussian curves; for other shapes one would expect a value between these extremes. The above results show that n is about equal to 1 in our case. The electron lines in the experiments of Nordling *et al.* mentioned above (electronic levels of copper) showed a similar behaviour. Mladjenovič [4]) found n about 1.5 with the indication that for better resolving power n tended to become smaller (see also ref. [17]), p. 153).

The matching procedure yields a good check on the determination of the $B\rho$-ratio of the K- and L_I-line positions of Bi by taking the intersection of the extrapolated sides as the line-position 6);

from intersection: 1.26329 ± 0.00003,
from matching : 1.26328 ± 0.00002.

In conclusion our thanks are due to Prof. Dr. P. C. Gugelot for his interest in our work. We are grateful to Prof. Dr. A. H. Wapstra for his criticisms, and profound discussions. We would like to express our appreciation to Mrs N. Salomons-Grobben, Mr. E. J. Bleeker and Mr. P. Goudsmit for executing the calculations of the folding integral. This work constitutes part of the research program of the Institute for Nuclear Research, made possible by financial support from the Foundation for Fundamental Research of Matter (F.O.M.) and the Dutch Organization for Pure Scientific Research (Z.W.O.).

References

1) E. U. Condon and G. H. Shortley, Theory of atomic spectra (Cambridge University Press, Cambridge, 1951) Ch. IV, p. 79;
W. Heitler, Quantum theory of radiation (Oxford University Press, Oxford, 1959) pp. 25, 181;
K. Siegbahn, Beta- and gamma-ray spectroscopy (North-Holland Publishing Company, Amsterdam, 1955) Ch. III, p. 93;
V. F. Weisskopf and E. P. Wigner, Z. f. Physik **63** (1930) 54
2) H. Slätis and G. Lindström, Phys. Rev. **88** (1952) 1429 (L)
3) H. Slätis, Ark. f. Fysik **6** (1953) 415
4) M. Mladjenovič, Ark. f. Fysik **8** (1954) 27
5) G. T. Ewan, J. S. Geiger, R. L. Graham and D. R. MacKenzie, Can. J. Phys. **37** (1957) 174
6) C. de Vries, Nuclear Physics **18** (1960) 428
7) C. de Vries and J. H. Dijkstra, Nuclear Physics **18** (1960) 446
8) K. Siegbahn, Ark. f. Mat. Astr. o. Fys. **28**B (1941) no. 6, **30**A (1944) no. 20
9) D. Lind and A. Hedgran, Ark. f. Fysik **5** (1952) 29
10) H. Wild and O. Huber, Helv. Phys. Acta **30** (1957) 3
11) C. Nordling, E. Sokolowski and K. Siegbahn, Ark. f. Fysik **13** (1958) 483
12) E. G. Ramberg and F. K. Richtmyer, Phys. Rev. **51** (1937) 913;
F. K. Richtmyer and S. W. Barnes, Phys. Rev. **46** (1934) 352;
F. K. Richtmyer, S. W. Barnes and E. G. Ramberg, Phys. Rev. **46** (1934) 843
13) E. Ingelstam, Nova Acta Reg. Soc. Scient. Upsaliensis Ser. IV, **10** (1936) no. 5
14) A. H. Compton and S. K. Allison, X-rays in theory and experiment, pp. 745, 747
15) B. G. Gokhale, Ann. Phys. **7** (1952) 852
16) J. H. Williams, Phys. Rev. **40** (1932) 791; **45** (1934) 71
17) A. E. Sandström, Experimental methods of X-ray spectrometry, in Handbuch der Physik, editor S. Flügge (Springer Verlag, Berlin), Band **30**

2.H

Nuclear Physics **23** (1961) 532—536; © *North-Holland Publishing Co., Amsterdam*

Not to be reproduced by photoprint or microfilm without written permission from the publisher

COULOMB EXCITATION OF Se^{77}

W. R. WISSEMAN † and R. M. WILLIAMSON
Department of Physics, Duke University, Durham, N.C. ††

Received 17 November 1960

Abstract: The 240- and 442-keV levels in Se^{77} were excited with 4.0-MeV protons and 3.5-MeV deuterons, and the scattered particles were observed at angles of 150° and 145°, respectively. They were studied with a magnetic analyzer and detected by photographic plates. The B(E2) values which were obtained were 0.17 ± 0.02 and 0.26 ± 0.03 for the 240- and 442-keV levels, respectively. The ratio of these B(E2) values, 1.5 ± 0.2, is in good agreement with the ratio of 1.5 which is predicted by the unified model for rotational states and spin assignments $(\frac{1}{2}, \frac{3}{2}, \frac{5}{2})$ for the ground, 240- and 442-keV states.

1. Introduction

This experiment was a continuation of a study of inelastically scattered protons and deuterons which result from E2 excitation of levels in medium-weight nuclei. References to earlier Coulomb excitation measurements are given in another paper [1]) and in the review article by Alder *et al.* [2]). The object of the present experiment was a study of the two levels in Se^{77} which can be excited by Coulomb excitation. The energy and the reduced transition probability for excitation, B(E2), were measured for each state. It was found in the previous experiment [1]) that values of B(E2) which were reliable to about $\pm 10\,\%$ could be obtained in the region of medium-weight nuclei by using projectiles with energies not in excess of 4.0 MeV for protons and 3.5 MeV for deuterons. Therefore, these energies were used in this experiment. The energies of excited states can be unambiguously determined by studying the inelastically scattered projectiles. This method is more direct than observation of de-excitation gamma rays when cascade transitions can take place.

Further information about the levels in Se^{77} can be obtained through use of the unified model of Bohr and Mottelson [3, 4]). Se^{77} has a ground state spin of $\frac{1}{2}$, and the states which are excited by E2 excitation are thought to be rotational [5]). The spin sequences $(\frac{1}{2}, \frac{3}{2}, \frac{5}{2})$ and $(\frac{1}{2}, \frac{5}{2}, \frac{3}{2})$ are both possible for rotational states in nuclei with ground state spin $\frac{1}{2}$. Temmer and Heydenburg [5]) have made gamma ray angular distributions for Se^{77}, and they have tentatively assigned spins in the order $(\frac{1}{2}, \frac{3}{2}, \frac{5}{2})$. The unified model gives a result for the ratio of the B(E2) values for the two levels which depends upon the spin sequence that is chosen. Therefore, experimental determination of this ratio can be used to decide upon the correct excited state spins.

---

† Now at Texas Instruments, Inc., Dallas, Texas.

†† This work is supported by the U. S. Atomic Energy Commission.

2. Apparatus and Procedure

The experimental details of this work were covered rather extensively in earlier papers [1, 6]), and only a brief discussion will be given here. The Duke Van de Graaff accelerator provided the 4.0-MeV protons and 3.5-MeV deuterons which were used to bombard Se^{77} targets. The 60° magnetic analyzer was used to study the reaction products after they had left the 25° to 155° pillbox target chamber. The scattered particles were detected with 50 μm Ilford C2 photographic emulsion plates.

The targets were made by evaporating selenium (74.22 % Se^{77}) on formvar in the manner described previously [1]). When the targets were bombarded with the Van de Graaff beam, the selenium either evaporated or was knocked off. It was found that this target deterioration could be reduced and in many cases entirely eliminated by evaporating a thin layer of aluminium onto the formvar prior to the selenium evaporation. Six targets of aluminium and selenium on formvar were made at one time in order that the best one could be used for obtaining the data. The target which was used in taking a plate exposure was examined before and after the run to see if target deterioration had occurred. This was done by observing the selenium elastic group with a scintillation detector at the exit end of the magnetic analyzer.

3. Results and Conclusions

The Coulomb excitation differential cross section is given by

$$\mathrm{d}\sigma_{\mathrm{E2}}/\mathrm{d}\Omega = C_{\mathrm{E2}}(E_{\mathrm{MeV}}-\Delta E'_{\mathrm{MeV}})B(\mathrm{E2})\mathrm{d}f_{\mathrm{E2}}(\theta, \xi, \eta_i)/\mathrm{d}\Omega,$$

where $B(\mathrm{E2})$ has units of $e^2\times 10^{-48}$ cm^4. The above quantities are defined in ref. [2]). The expression was used in the classical limit of $\eta_i \rightarrow \infty$, although η_i ranged from 2.7 to 4.1 in this experiment. Other experimental [1, 7]) and theoretical [8]) studies indicate that the semi-classical calculation of $\mathrm{d}f_{\mathrm{E2}}$ is valid to better than 5 % for the η_i values of this experiment. Table II.8 of ref. [2]) was used to obtain $\mathrm{d}f_{\mathrm{E2}}(\eta_i \rightarrow \infty)$. The above equation was used to get the $B(\mathrm{E2})$ values for the excited states from the experimental cross sections. Since Bang's calculations [8]) show that the quantum mechanical corrections to the back angle differential Coulomb excitation cross section are smaller than the quantum mechanical corrections to the total cross section, the $B(\mathrm{E2})$ values reported here are not corrected using fig. II.6 of ref. [2]) as were the $B(\mathrm{E2})$ values reported in ref. [1]).

Fig. 1 is a momentum spectrum for Se^{77} which was obtained with 4.0-MeV protons at a laboratory scattering angle of 150°. Inelastic groups corresponding to excited states at 240 keV and 442 keV were observed. These groups are labeled (1) and (2), respectively. The elastic group, (0), was reduced in intensity by a factor of 100 by putting a shutter over the high energy end of the photographic plate. The ratio of the Rutherford differential cross section to the Coulomb excitation differential cross section, $d\sigma_R/d\sigma_{E2}$, was obtained by taking the ratio of the areas under the appropriate peaks and by assuming that the elastically scattered group follows the Rutherford scattering law. The standard expression for the differential Rutherford cross section was used to get $d\sigma_{E2}/d\Omega$ from this ratio. The previous experiment with germanium isotopes indicated that this assumption is valid for 4.0-MeV protons and 3.5-MeV deuterons.

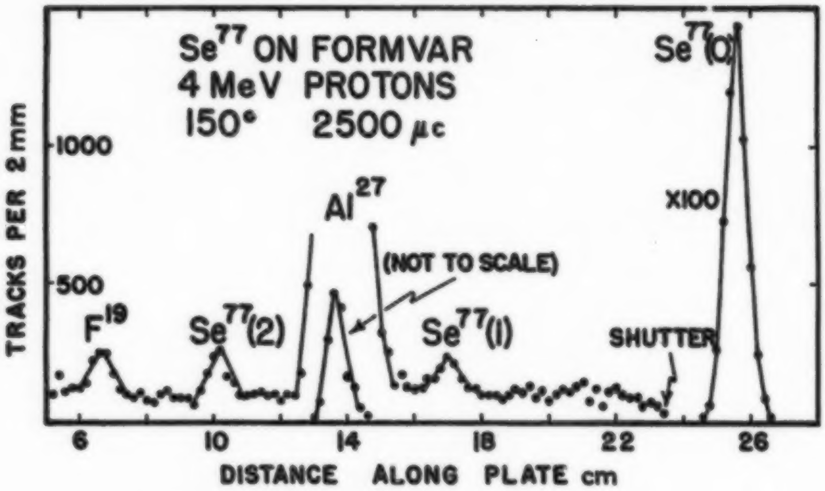

Fig. 1. Momentum spectrum of protons scattered from Se^{77}.

The results obtained in this experiment for $d\sigma_R/d\sigma_{E2}$, $d\sigma_{E2}/d\Omega$, and $B(E2)$ are shown in table 1. The errors which are given are standard deviations, and they include statistical errors along with estimated experimental errors. A discussion of the errors is given in ref. [1]). The values obtained for $B(E2)$ by using protons are in good agreement with those obtained by using deuterons.

Table 1

Results for Se^{77}

ΔE (keV)	E_{MeV} and Projectile	θ_{lab}	$d\sigma_R/d\sigma_{E2}$	$d\sigma_{E2}/d\Omega$ (mb/sr)	$B(E2)$ ($e^2 \times 10^{-48}$ cm^4)
240±3	4.0 p	150°	780	0.14	0.17 ±0.03
	3.5 d	145°	750	0.21	0.175±0.02
442±5	4.0 p	150°	680	0.16	0.255±0.04
	3.5 d	145°	750	0.21	0.27 ±0.03

Some earlier 4.0-MeV deuteron data which is not listed in the table resulted in higher values for B(E2) just as did the 4.0-MeV deuteron data for the germanium isotopes [1]). The reasons for the discrepancy were discussed in ref. [1]), and they will not be repeated here. The combined proton and deuteron values for B(E2) are 0.17±0.02 and 0.26±0.03 for the 240- and 442-keV levels, respectively. Temmer and Heydenburg [5]) determined the level energies and B(E2) values by studying the gamma rays which resulted from excitation of Se^{77} by 7-MeV alpha particles. It was necessary for them to compare excitation curves for the cascade gamma rays in order to get the excited state energies. The experiment done here confirms their results. Our values for B(E2) and the level energies are in agreement with their values for these quantities within the experimental errors with one exception. We disagree slightly on the value of the energy of the higher rotational level. Their result was 457±5 keV as opposed to our value of 442±5 keV.

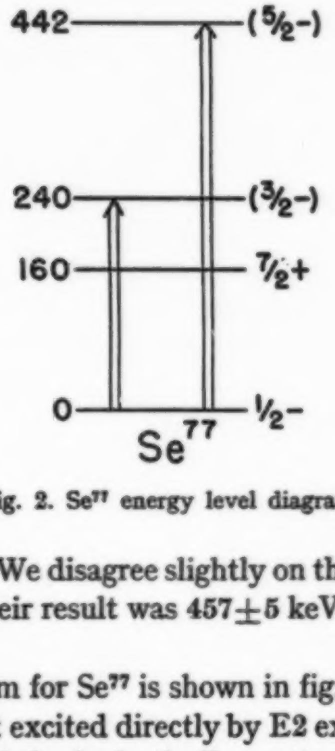

Fig. 2. Se^{77} energy level diagram.

The energy level diagram for Se^{77} is shown in fig. 2. The 160-keV level is an isomeric state which is not excited directly by E2 excitation, and therefore it is not observed in studies of the inelastically scattered projectiles. The excited state spin assignments are the tentative ones made by Temmer and Heydenburg [5]). The energy level spacing for Se^{77} cannot be used to indicate rotational excitations since it has ground state spin $\frac{1}{2}$. If rotational excitations are assumed, the decoupling parameter α and $\hbar^2/2\mathscr{J}$ can be determined from the level spacing (here, $\mathscr{J}$ is the effective nuclear moment of inertia about an axis perpendicular to its symmetry axis). The values for these quantities obtained in this experiment were $\alpha = 0.33$ and $\hbar^2/2\mathscr{J} = 60.2$ keV.

The most interesting application of the unified model to Se^{77} involves the ratio of B(E2) for excitation of the 442-keV level to B(E2) for excitation of the 240-keV level. The predicted ratio for rotational states with the spin sequence shown in fig. 2 is 1.5. The ratio for the spin sequence $(\frac{1}{2}, \frac{5}{2}, \frac{3}{2})$ is $\frac{2}{3}$. Experimentally the ratio was found to be 1.5 ± 0.2. This result supports the tentative spin assignments of Temmer and Heydenburg 5) and indicates that the excited states are rotational.

In conclusion, we feel that observation of the inelastically scattered projectiles is most useful for odd mass nuclei such as Se^{77} where two or more levels are excited by E2 excitation. The energies of these levels are determined quite easily by this technique. The application of the unified model to these nuclei is also very informative.

The authors would like to thank Mr. N. R. Fletcher for his assistance with the experimental work and Dr. M. M. Duncan for his helpful discussions.

References

1) W. R. Wisseman and R. M. Williamson, Nuclear Physics (in press)
2) Alder, Bohr, Huus, Mottelson and Winther, Revs. Mod. Phys. **28** (1956) 432
3) A. Bohr, Mat. Fys. Medd. Dan. Vid. Selsk. **26**, No. 14 (1952)
4) A. Bohr and B. R. Mottelson, Mat. Fys. Medd. Dan. Vid. Selsk. **26**, No. 16 (1953)
5) G. M. Temmer and N. P. Heydenburg, Phys. Rev. **104** (1956) 967
6) Meier, Fletcher, Wisseman and Williamson, Rev. Sci. Instr. **29** (1958) 1004
7) Bernstein and Skurnik, to be published
8) J. Bang, Mat. Fys. Medd. Dan. Vid. Selsk. **32**, No. 5 (1960)

2.D

Nuclear Physics **23** (1961) 537—558; © *North-Holland Publishing Co., Amsterdam*

Not to be reproduced by photoprint or microfilm without written permission from the publisher

VIRTUAL LEVELS IN THE VANADIUM ISOTOPES FROM PROTON BOMBARDMENT OF THE TITANIUM ISOTOPES

J. DUBOIS

Department of Physics, Chalmers University of Technology, Gothenburg

Received 18 July 1960

Abstract: Electromagnetically separated Ti-isotopes were bombarded by protons in the 800–1400 keV interval. From the (p, γ) resonances the virtual levels in the V-isotopes were determined. Levels spacings are discussed.

1. Introduction

Excitation functions for proton induced reactions on light elements have been thoroughly investigated with Van de Graaff generators during the last decade [1, 2]. It is of interest to perform similar measurements on nuclei of intermediate masses ($40 \leqq A \leqq 70$). Here one expects, however, closely spaced levels and low yields owing to the large Coulomb barriers. Accordingly, it is necessary to have good energy resolution, thin targets, comparatively great beam intensity and sensitive detectors with low background. By proton bombardment of the titanium isotopes with proton energy less than 1.4 MeV the only energetically allowed reactions are (p, γ) and (p, p$'\gamma$) reactions [3]. Resonances in the γ-yield from these reactions give information about virtual states in the V-isotopes. No (p, γ)-reactions on the Ti-isotopes seem to have been reported so far.

2. Equipment

The proton beam from the Van de Graaff generator at Chalmers University of Technology was deflected 90° by a magnetic analyzer with 50 cm radius and 2 cm gap width. The field of the analyzer was stabilized by electronical control of the current through the magnet coils, giving a stability of the magnetic field better than $1 : 10^4$. The field strength was measured by magnetic proton resonances. It is shown in fig. 1, how the slits of the analyzer were placed to give the best resolution in the space available [4].

The entire analyzer was movable in a plane perpendicular to the incoming beam so the analyzer could be adjusted to give maximum output beam current after the beam had been focused on the entrance slit. To stabilize the voltage of the generator, the difference signal provided at the exit slit of the analyzer

March 1961

controlled a corona load. Near the target another tantalum slit defined the beam to a rectangular spot, about 1 × 6 mm in size on the target. The proton beam intensity was measured by a current integrator.

Gamma radiations were detected by a NaJ crystal, 12.7 cm in diameter and 10.2 cm deep coupled to a Dumond 6364 photomultiplier tube. A 5 cm thick lead shield around the detector reduced the background from the generator. The detector subtended a useful solid angle of about 30 % of 4π. Output pulses from the photomultiplier tube were amplified by a linear amplifier and fed to a discriminator and a scaler. The gamma spectrum was also studied by a Hutchinson-Scarott multichannel pulse height analyzer.

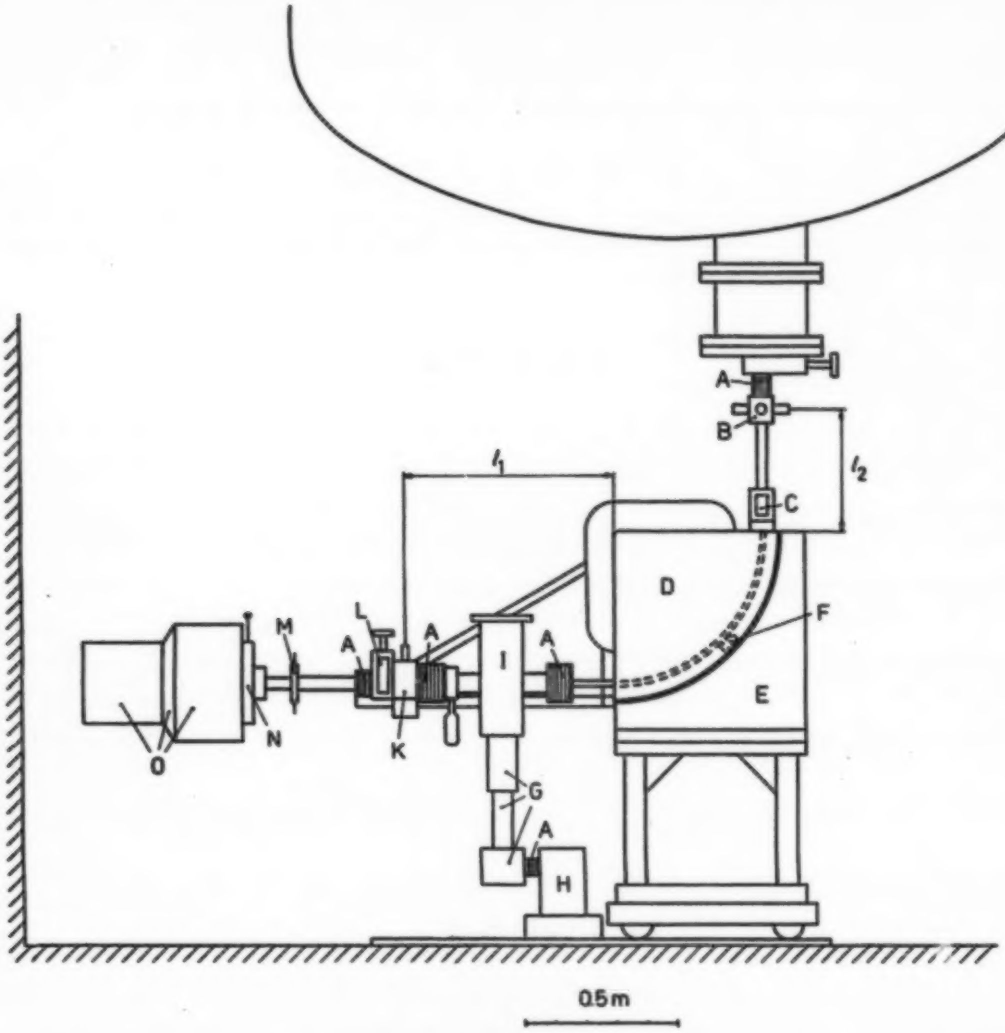

Fig. 1. The experimental set up. A — Metal bellows. B — Entrance slit. C — Beam visualizer. D — Magnet. E — Magnet stand. F — Magnetic resonance probe. G — Oil diffusion pump. H — Rotary pump. I — Liquid air trap. K — Exit slit. L — Beam visualizer. M — Beam defining slit. N — Target holder. O — NaJ-crystal, photomultiplier and lead shield. $l_1 = 65$ cm, $l_2 = 43$ cm.

3. Energy Calibration

The proton energy E_p can be related to the measured frequency f of the magnetic resonance probe by the equation

$$E_p = K(1-\delta)f^2, \tag{1}$$

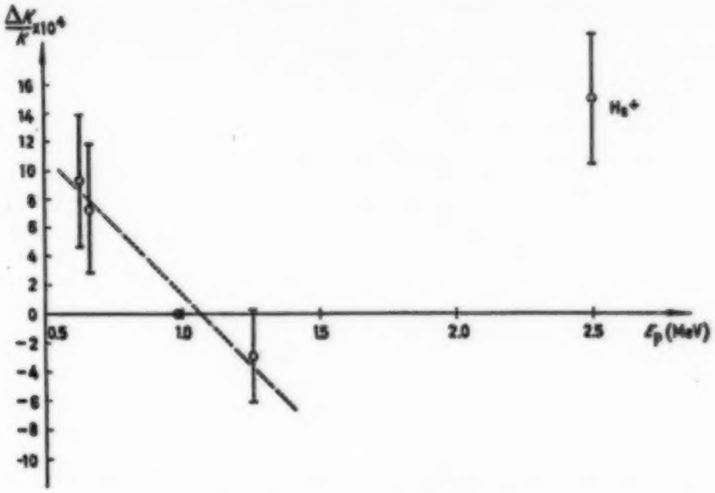

Fig. 2. The energy dependence on the deviations in the K-value of the magnet relative to the K-value determined at the reference energy, 990.8 keV.

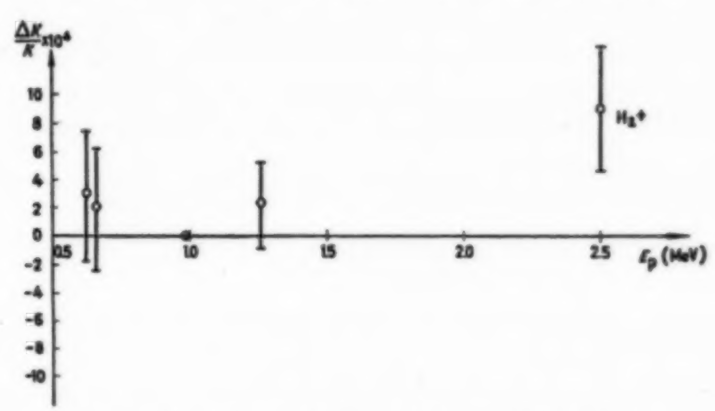

Fig. 3. The energy dependence on the deviations in the K-value of the magnet relative to the K-value determined at the reference energy 990.8 keV when the corrected resonance energies has been used.

where K is a constant depending on the effective radius of the analyzer and certain physical constants [5]) and δ is given by $\delta = \frac{1}{2}E_p/m_0c^2$ with m_0 being the rest mass of the proton and c the velocity of light. For H_2^+-ions the equation for the corresponding proton energy is

$$E_p = \tfrac{1}{4}K(1-\delta)f^2\left(1-\frac{1}{3672}\right), \tag{2}$$

where the last factor corrects for the mass of the electron in the H_2^+-ion.

The *K*-value of the analyzer was determined from the (p, γ) resonance in Al^{27} at 990.8 keV bombarding energy [5]). To check the constancy of the *K*-value with respect to energy, the excitation curve for the same reaction was studied [6]). The aluminium target used was evaporated on a tantalum backing and was thick compared with the natural half-width of the resonances but thin with respect to the spacing between the resonances. In fig. 2 we see that the *K*-value decreases somewhat with increasing energy. If this decrease is due to saturation effects in the magnet analyzer one should expect a still more pronounced decrease for the *K*-value determined by the H_2^+-beam on, for instance, the 632.3 keV resonance, as that requires a magnet field in the analyzer which corresponds to about 2.5 MeV proton energy. However, it turned out that this *K*-value did not differ very much from the *K*-value determined by the proton beam on the same resonance, so the saturation effects should be negligible. On the other hand, the decrease of the *K*-value in fig. 2 can be due to a systematic error in the energy values given in ref. [6]). The authors assume in fact that their values might be 0.08 % too high in the region around 500 keV and 0.06 % too low around 1250 keV. If one corrects for this, the *K*-values are extremely constant (fig. 3). Since the frequency value of a favourable (p, γ) resonance was reproducible within ± 0.01 % it is thought, that energy values given by eq. (1) are correct within ± 0.05 % with the 990.8 keV resonance as an energy standard.

From the results in fig. 3 we see that the value for the H_2^+-beam lies somewhat too high, which indicates that there might be a slight decrease (about 0.06 %) in the energy value of the resonance when one uses the H_2^+-beam instead of the proton beam. It was also apparent that the half-width increased [7]).

4. Energy Spread

The energy spread of the proton beam from the Van de Graaff generator is not completely eliminated by the magnetic analyzer. Due to the finite slit widths and, to a certain extent, to the instability of the magnetic field of the analyzer itself, there remains a small energy spread of the protons, which is assumed to be gaussian. This energy spread can be determined by inspection of the shape of the step in the thick target yield of a (p, γ) resonance, the natural half-width or interquartile range, Γ of which is known. After correcting for the Doppler effect one can assign a half-width Γ_a to the analyzer

$$\Gamma_a^2 = \Gamma_{obs}^2 - \Gamma_D^2 - \Gamma^2, \tag{3}$$

where Γ_{obs} is the observed interquartile range and Γ_D the same quantity attributed to the Doppler effect [6]). The Γ of the 990.8 keV (p, γ) resonance in Al^{27} has been found by several authors to be about 100 eV [8]). From fig. 4 and eq. (3) we get $\Gamma_a = 210$ eV when the entrance and exit slits were 0.3 mm wide.

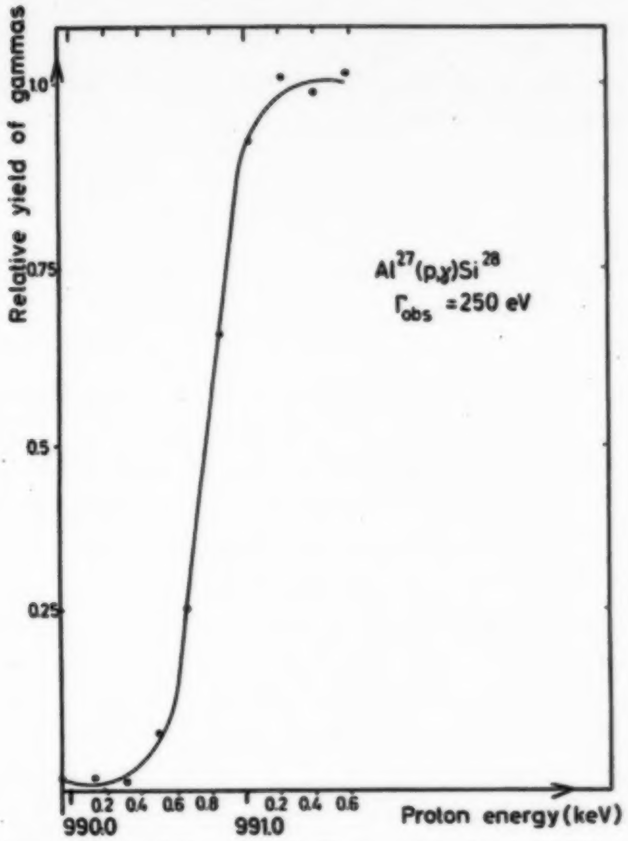

Fig. 4. Thick target yield of the 990.8 keV resonance in the $Al^{27}(p, \gamma)Si^{28}$ reaction.

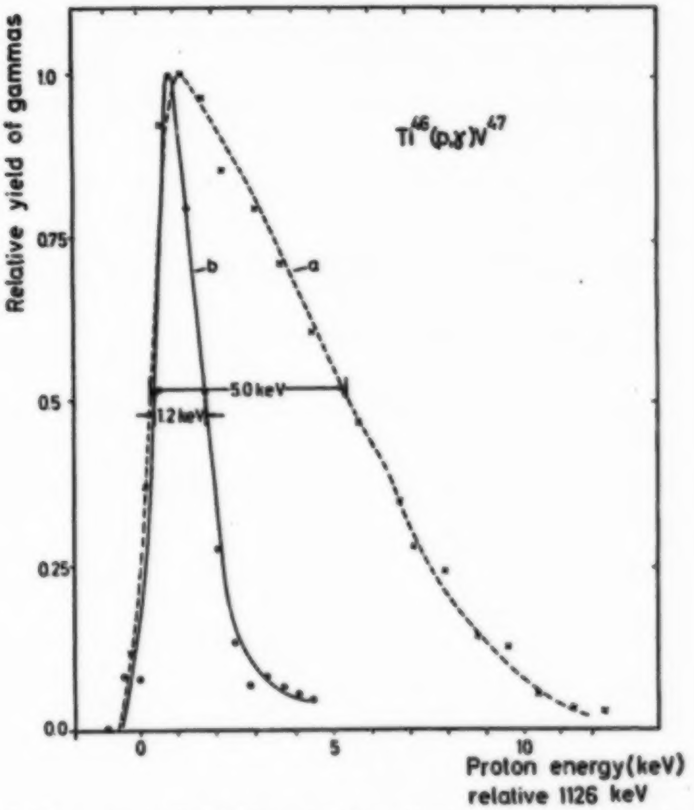

Fig. 5. The 1127 keV resonance in Ti^{46}-targets when the ion beam in the isotope separator was a) unretarded b) retarded to 3 keV.

To increase the ion beam intensity, in most measurements on the Ti-isotopes the slits were opened so that Γ_a was about 400 eV.

5. Targets

The titanium isotopes were separated in the electromagnetic isotope separator at this institute by O. Almén and G. Bruce [9]).

The target thickness was determined from the ratio between the area under the thin target resonance and the step in the thick target yield [6]). Measurements on the 1007 keV resonance in a Ti^{48} target gave 1.2 keV. This value was in good agreement with the target thickness determination from ion beam current and the separation time in the isotope separator, which shows that nearly all Ti-atoms are captured in the tantalum backing.

In fig. 5, curve a shows a (p, γ) resonance at 1127 keV on a 6 μg/cm^2 Ti^{46}-target, when the ion beam energy in the isotope separator had been 45 keV. The long tail at the high energy side of the resonance is due to the distribution of the target nuclei in the backing lattice and to proton straggling.

According to theoretical studies of penetration depths of atomic particles in matter [10, 10a]), the 6 μg/cm^2 Ti^{46}-target would have an effective thickness of about 23 μg/cm^2 in a tantalum backing or 3.5 keV for 1.1 MeV protons. The experimental half-width of the resonance including proton straggling was 5.0 keV, and when corrected for the oblique entrance of the proton beam 3.8 keV.

In most cases these targets were sufficiently thin to resolve the resonances in the excitation curves but, especially when the compound nuclei were of the odd type, the resonances were so close together that there was a need for still thinner targets, which should not, however, give any decrease in the γ-yield. This was accomplished by slowing down the ions in the electromagnetic isotope separator before they hit the tantalum backing, so the penetration depth was only a fraction of the total thickness of the layer of the separated Ti-isotopes. In fig. 5, curve b shows the (p, γ) resonance at 1127 keV on a 6 μg/cm^2 Ti^{46}-target, when the ion beam had been retarded to 3 keV. The half-width of the resonance is only 0.9 keV when corrected for the oblique entrance of the proton beam. Neglecting the energy straggling of the protons in the target and assuming that the natural resonance width is zero, the resonance width of a 6 μg/cm^2 Ti^{46}-target should be about 0.8 keV, which shows that little would have been gained by further decreasing the energy of the Ti-ions in the isotope separator.

The retardation of the Ti-ions increased the defocusing effects of the ion beam, making it necessary to test whether that caused any undue mixing of adjacent isotopes. If this were the case, the most sensitive test would be to see, if the strong resonances at 1007 keV and 1013 keV in Ti^{48}, which is the most abundant isotope of titanium, would be seen on the Ti^{47}- and Ti^{49}-target. The resonances at these two energies, clearly seen on the Ti^{47}-target, were not detectable on the Ti^{49}-target. The γ-spectra gave no definite answer whether the resonances originated from Ti^{48}. Since the resonances were also seen in an unretarded Ti^{47}-target, it was easy to establish the surface distribution of the nuclei giving rise to the resonances by a method, which is clear from fig. 6, where a resonance in a Ti^{46}-target was studied. If the resonance in fig. 6 originated from an adjacent isotope, i.e. Ti^{47}, we should expect an unsymmetrical distribution of the nuclei on the Ti^{46}-target and consequently the resonances at the proton beam positions 1 or 3 should be stronger than at the other positions. Measurements by this method stated that the coincidence of the resonances in Ti^{47}- and Ti^{48}-target at 1007 keV and 1013 keV was only an accidental occurrence.

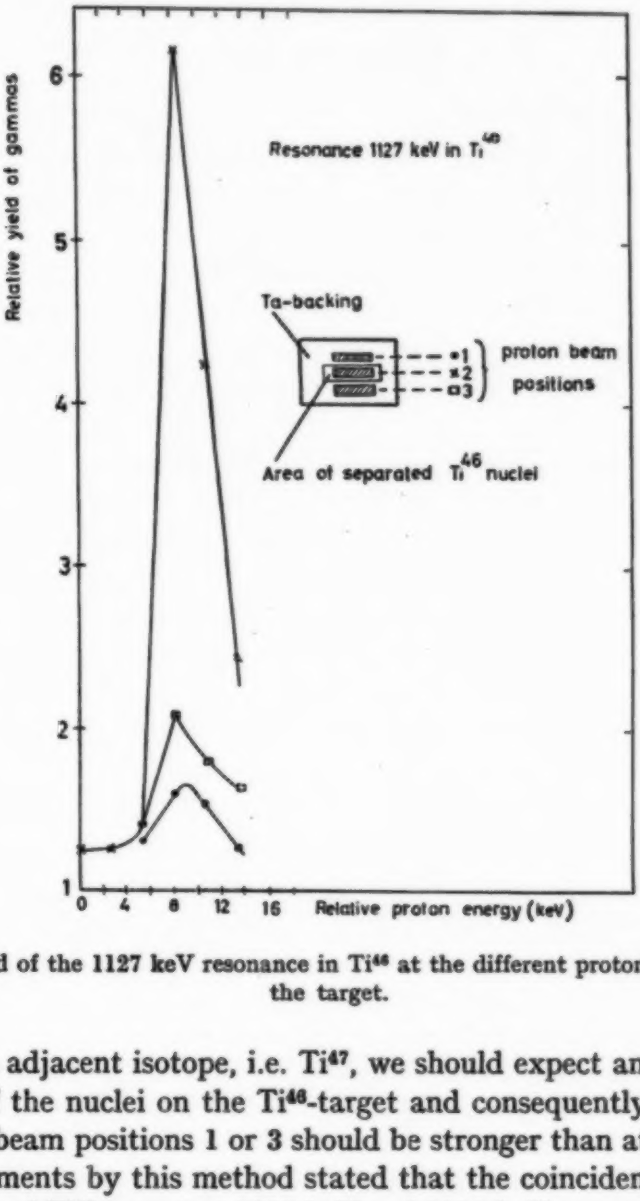

Fig. 6. The γ-yield of the 1127 keV resonance in Ti^{46} at the different proton beam positions on the target.

It is believed that the mixing of adjacent isotopes is too small to influence the certainty of assigning resonances to the different isotopes.

To prevent carbon build up on the target there were heat baffles above the oil diffusion pumps and liquid air traps between target and the pumps. No energy shift of the Ti-resonances due to carbon films could be detected. No contaminations of the targets or of the tantalum backing, other than fluorine, were found.

The targets were extremely stable. They could stand 1 μA/mm^2 proton intensity for several hours, with no detectable changes.

6. Excitation Curves

6.1. THE REACTION $Ti^{46}(p, \gamma)V^{47}$

The target used was 6 μg/cm^2 thick and the energy of the protons was changed in steps of about 0.6 keV. The proton beam was 2–3 μA and at each setting the target was exposed to the same number of protons. To avoid contribution to the γ-yield from the inconveniently long-lived β^+- activity of V^{47}, the discriminator was set at 1.5 MeV to exclude the 0.51 MeV annihilation radiation produced by the β^+-decay. This also decreased the contribution from the proton bremsstrahlung and the γ-energies produced by Coulomb excitation in the tantalum backing.

In fig. 7 a part of the excitation curve is shown. At the high discriminator level it represents only the reaction $Ti^{46}(p, \gamma)V^{47}$ and not the inelastic scattering of protons in Ti^{46} nuclei, $Ti^{46}(p, p'\gamma)Ti^{46}$. No background correction has been made. The standard deviation is indicated to the left in the figure.

The uncertainty of the points is somewhat increased by fluctuations in the beam current and to reduce this effect and to test the ability to reproduce the resonances, the excitation curve was again recorded with another Ti^{46}-target. If any doubt remained regarding certain small resonances, they were studied with an increased number of protons at each energy setting and close-lying resonances were studied with smaller steps in the proton energy. For proton energies lower than 850 keV the yield was too low to indicate any certain resonances. The broad resonance at 871.6 keV was from the reaction $F^{19}(p, \alpha\gamma)O^{16}$, in very good agreement with earlier precision measurements by F. Bumiller *et* al., [5] who found 871.3 keV. The difference is quite acceptable, as the strong 874.4 keV resonance in Ti^{46} somewhat influenced the energy determination. Resonance 26 at 1343.4 keV was overlapped by the fluorine resonance at 1344.5 keV and the broad fluorine resonance at 1373.0 keV was seen [11] at the high energy side of resonance 29.

6.2. THE REACTION $Ti^{47}(p, \gamma)V^{48}$

The target thickness was 6 μg/cm^2. The energy of the protons was changed in steps of about 0.4 keV and the number of protons at each setting was twice as great as in the Ti^{46} case. There was very little fluorine on the target. Otherwise, the conditions were as for Ti^{46} (fig. 8).

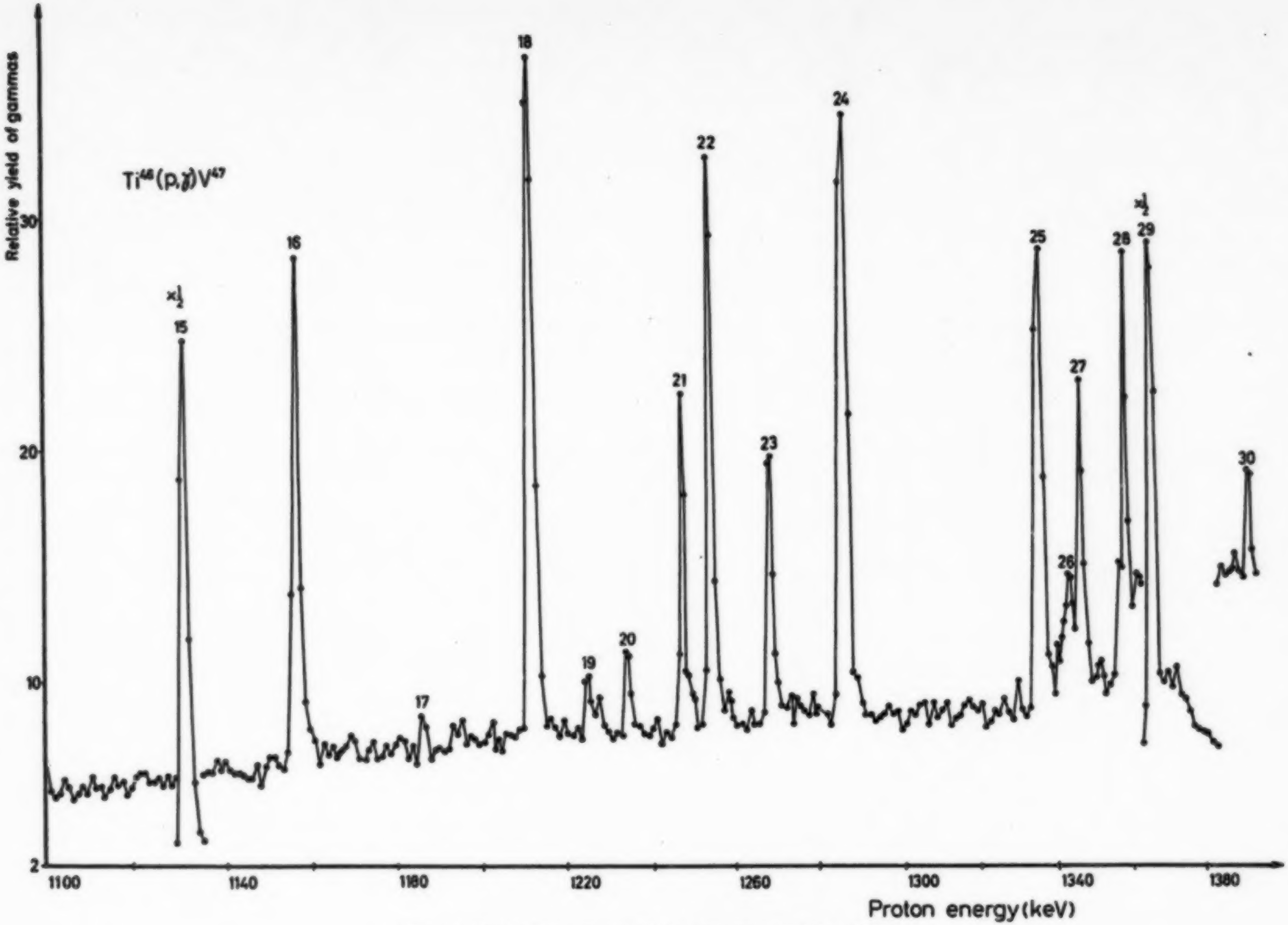

Fig. 7. Excitation curve of the reaction $Ti^{46}(p, \gamma)V^{47}$.

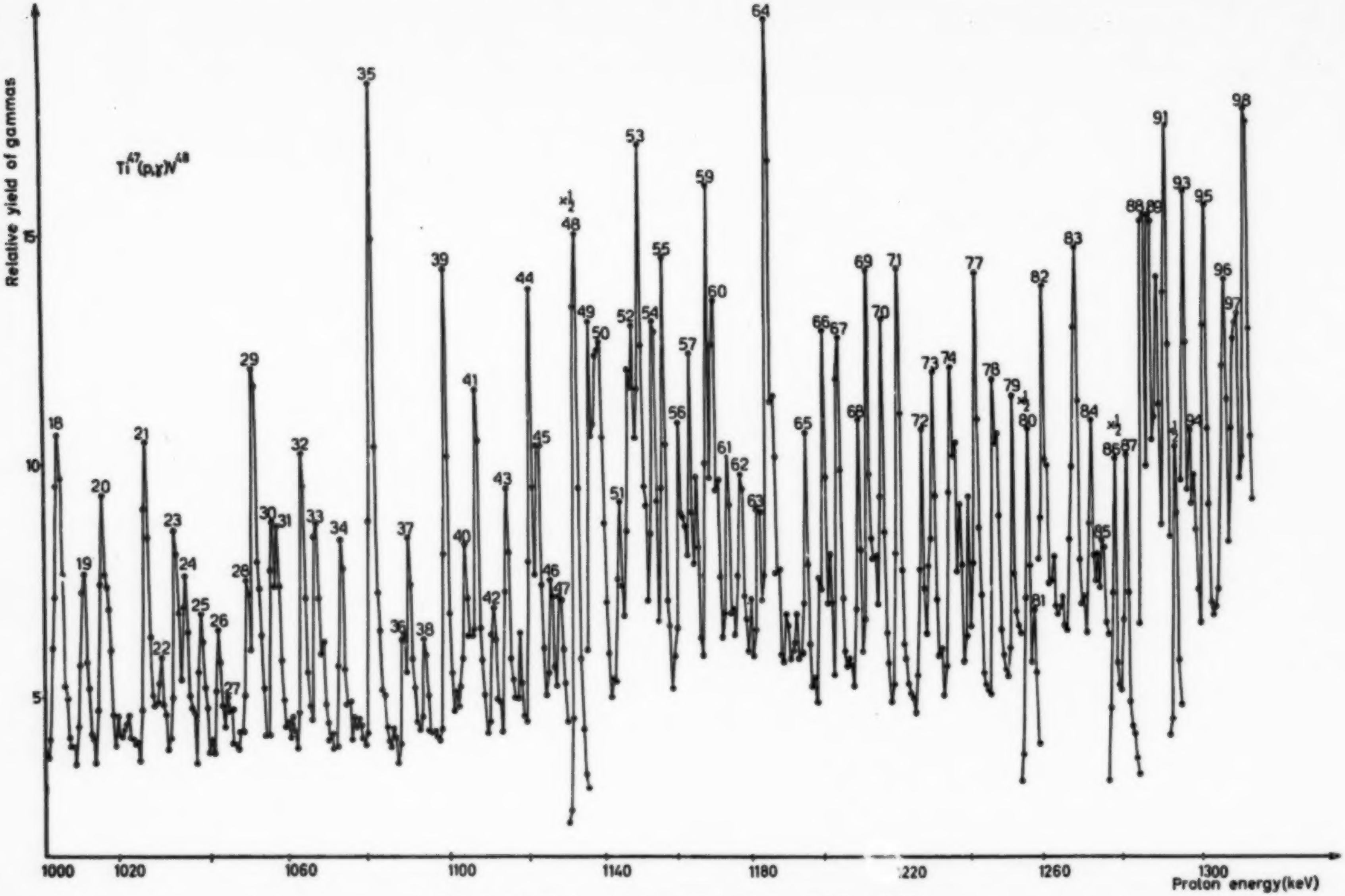

Fig. 8. Excitation curve of the reaction Ti^{47}(p, γ)V^{48}.

6.3. THE REACTION $Ti^{48}(p, \gamma)V^{49}$

The target thickness was 8 μg/cm^2. Otherwise the conditions were as for Ti^{46} except that fluorine was only detected as a thick target yield.

6.4. THE REACTION $Ti^{49}(p, \gamma)V^{50}$

The target thickness was 4 μg/cm^2. In other respects the conditions were as in the Ti^{47} case. The target was, however, somewhat more contaminated by fluorine.

6.5. THE REACTION $Ti^{50}(p, \gamma)V^{51}$

The target thickness was 4 μg/cm^2. Otherwise the conditions were as in the Ti^{47} case.

TABLE 1

Data from $Ti^{46}(p, \gamma)V^{47}$ excitation curve

Res. no. in fig. 7	Proton energy E_p(keV)($\pm$1 keV)	Excitation energy E(MeV)($\pm$0.01 MeV)	Rel. int.	Remarks
	871.6			F [a])
	874.4	6.0467	540	
	898.0			F
	934.3			F
	940.0	6.1109	135	
	951.8	6.1225	70	
	974.8	6.1450	70	
	985.6	6.1555	300	
	1007.2	6.1766	35	
	1010.6	6.1800	50	
	1020.0	6.1892	500	
	1044.9	6.2135	240	
	1084.4	6.2522	270	
	1095.4	6.2629	700	
15	1127.0	6.2939	1350	
16	1152.8	6.3191	750	
17	1182.0	6.3477	670	
18	1208.0	6.3731	1000	
19	1221.9	6.3867	100	
20	1231.6	6.3962	135	
21	1245.5	6.4098	470	
22	1252.2	6.4163	800	
23	1267.3	6.4311	400	
24	1285.7	6.4491	880	
25	1335.4	6.4977	670	
26	1343.4	6.5055	200?	
27	1346.3	6.5083	400	
28	1357.9	6.5197	950	
29	1364.5	6.5262	2100	
30	1390.7	6.5518	250	

[a]) F means fluorine contamination

TABLE 2

Data from $Ti^{47}(p, \gamma)V^{48}$ excitation curve

Res. no. in fig. 8	Proton energy E_p(keV)(±1 keV)	Excitation energy E(MeV)(±0.02 MeV)	Rel. int.	Remarks
	891.7	7.6900	50	
	895.4	7.6936	70	
	898.4	7.6966	70	
	901.6	7.6997	120	
	907.1	7.7051	25	
	913.4	7.7112	25	
	920.2	7.7179	170	
	936.6	7.7339	35	
	941.3	7.7386	100	
	945.8	7.7430	200	D? [a]
	958.4	7.7553	700	
	963.6	7.7604	40	
	968.9	7.7656	145	
	972.4	7.7690	45	
	979.8	7.7763	190	
	982.4	7.7788	80	
	985.5	7.7818	210	
	988.4	7.7847	70	
	995.6	7.7917	55	
	997.4	7.7935	25	
	1001.1	7.7971	15	
18	1007.4	7.8033	230	
19	1013.5	7.8093	130	D
20	1017.5	7.8130	190	
	1023.1	7.8186	25	
21	1026.9	7.8223	230	
22	1030.1	7.8255	70	
23	1032.9	7.8282	160	
24	1035.3	7.8306	130	
25	1038.6	7.8338	100	
26	1042.7	7.8378	90	
27	1044.6	7.8397	40	
28	1049.0	7.8440	130	
29	1050.7	7.8457	280	
30	1055.5	7.8504	170	
31	1056.4	7.8512	170	
32	1062.7	7.8574	220	
33	1066.1	7 8607	170	
	1068.1	7.8627	85	
34	1072.5	7.8670	150	
	1076.9	7.8713	25	
35	1079.8	7.8741	490	
36	1087.3	7.8815	85	
37	1088.9	7.8830	60	
38	1092.7	7.8868	85	
39	1098.1	7.8921	350	
40	1102.8	7.8966	150	
41	1105.9	7.8997	250	
42	1110.6	7.9043	90	
43	1114.2	7.9078	180	
	1118.3	7.9118	75	
44	1120.7	7.9142	330	
45	1122.4	7.9158	210	

[a]) D means double resonance

TABLE 2 (continued)

Res. no. in fig. 8	Proton energy E_p(keV)(±1 keV)	Excitation energy E(MeV)(±0.02 MeV)	Rel. int.	Remarks
46	1125.7	7.9190	120	
47	1128.0	7.9213	100	
48	1132.7	7.9259	880	
49	1136.0	7.9291	270	
50	1138.1	7.9312	260	D?
51	1143.3	7.9363	140	
52	1146.9	7.9398	270	D
53	1148.6	7.9414	400	
54	1152.1	7.9449	270	
55	1155.0	7.9477	320	
56	1159.3	7.9520	200	
57	1162.3	7.9549	250	
58	1164.1	7.9566	160	
59	1167.1	7.9596	370	
60	1168.9	7.9613	290	
61	1172.2	7.9646	180	
62	1176.0	7.9683	160	
63	1180.6	7.9728	130	
64	1183.1	7.9752	490	
65	1193.9	7.9858	200	
66	1198.5	7.9903	280	
67	1202.3	7.9941	280	
68	1207.9	7.9995	220	
69	1210.3	8.0019	330	
70	1214.5	8.0060	290	
71	1218.7	8.0101	330	
72	1225.3	8.0155	310	
73	1228.8	8.0200	250	
74	1233.8	8.0249	250	D?
75	1236.2	8.0272	150	
76	1238.6	8.0296	170	
77	1240.4	8.0313	320	
78	1245.1	8.0359	250	
79	1250.6	8.0413	200	
80	1254.8	8.0454	500	
81	1256.6	8.0472	250	
82	1259.0	8.0495	250	
83	1267.8	8.0581	290	
84	1272.1	8.0624	160	
85	1275.4	8.0656	75	
86	1279.1	8.0692	470	
87	1282.0	8.0720	470	
88	1286.6	8.0765	300	
89	1288.6	8.0785	300	
90	1291.2	8.0810	260	
91	1293.7	8.0835	370	
92	1296.2	8.0860	470	
93	1298.7	8.0884	330	
94	1300.6	8.0903	150	
95	1304.8	8.0944	320	
96	1310.2	8.0996	260	
97	1313.4	8.1028	170	
98	1315.9	8.1052	300	

TABLE 3

Data from $Ti^{48}(p, \gamma)V^{49}$ excitation curve

Proton energy E_p(keV)(±1 keV)	Excitation energy E(MeV)(±0.01 MeV)	Rel. int.	Re-marks	Proton energy E_p(keV)(±1 keV)	Excitation energy E(MeV)(±0.01 MeV)	Rel. int.	Re-marks
876.3	7.6074	170		1157.8	7.8831	50	
882.7	7.6137	35		1163.0	7.8882	370	
895.5	7.6263	70		1170.0	7.8951	50	
911.3	7.6417	135		1175.3	7.9002	270	
925.8	7.6559	100		1176.5	7.9014	400	
930.6	7.6606	70		1180.7	7.9055	50	
933.2	7.6632	135		1187.9	7.9126	440	
942.1	7.6719	170		1195.0	7.9195	135	
959.7	7.6891	470		1204.6	7.9290	300	
969.8	7.6988	340		1209.5	7.9337	570	
975.6	7.7047	340		1226.5	7.9504	70	
979.8	7.7088	45		1241.2	7.9648	100	
991.7	7.7205	45	D?	1250.4	7.9738	270	
996.3	7.7250	35		1253.9	7.9772	750	
1007.0	7.7354	2500		1259.1	7.9823	70	
1013.0	7.7413	2000		1263.1	7.9862	370	
1023.2	7.7513	500		1269.3	7.9923	75	
1032.7	7.7606	370		1280.4	8.0031	570	
1035.5	7.7634	240		1287.9	8.0105	135	
1045.8	7.7734	35		1293.0	8.0155	500	
1048.4	7.7760	100		1302.2	8.0245	75	
1052.4	7.7799	135		1305.8	8.0280	300	
1059.9	7.7868	100		1307.6	8.0298	570	
1070.9	7.7980	100		1308.9	8.0310	135	
1083.1	7.8100	135		1312.8	8.0344	270	
1101.1	7.8276	370		1322.2	8.0441	680	
1103.2	7.8296	200		1326.4	8.0482	135	
1118.1	7.8442	35	D?	1338.5	8.0600	1150	
1123.4	7.8494	70		1341.9	8.0633	340	
1130.6	7.8565	50		1349.7	8.0708	400	
1139.3	7.8650	470		1354.4	8.0756	135	
1148.6	7.8741	135		1361.6	8.0826	3900	
1152.8	7.8782	50		1373.5	8.0943	810	

7. Results

In tables 1—5 the resonance energies E_p are given. They are supposed to be correct within ±1 keV. For strong and well isolated resonances the error is even smaller, or ±0.5 keV. Due to the great uncertainty in the Q-values given in ref. [3]) the two last figures of the excitation energies, E have relative significance only. No precision determination of the cross section has been made. The relative intensities of the yield given in the tables are connected to the thick target yield of the 1007 keV Ti^{48}-resonance, which was set to 10000 units. With the same discriminator setting (1.5 MeV) and otherwise identical conditions the thick target yield of the 990.8 keV resonance in Al was 18000 units.

From inspection of the resonance shape, the natural half-widths of all resonances are certainly less than 0.5 keV. A special investigation of the thick target yield curve of the 1007 keV resonance in Ti^{48} indicated, that the natural half-width is smaller than 0.2 keV.

8. Level Spacings

Since the virtual states in a compound nucleus can be formed by protons with different orbital angular momenta, there are many spin systems, which fact makes it difficult to interpret the distribution of spacings within a single spin system. On the other hand, if we study the combination of all allowed spin systems, we can assume that the levels are distributed nearly at random, i.e. the probability of a level occurring in an interval dS at a distance S from a particular level does not depend on S (refs. [12, 13])). We can then write the number of levels with spacings larger than S as

$$N = N_0 e^{-S/D},$$

where D is the average spacing.

In figs. 9—13 we find that the experimental data follow the proposed distribution very well. Only resonances above 1 MeV proton energy have been considered. The lack of small spacings is mostly due to the finite resolving power of the system and also somewhat to repulsion of levels [12]).

The nuclear level density at an excitation energy E is given by the statistical model to be proportional to $\exp\{[2c(E-\delta)]^{\frac{1}{2}}\}$, where c is nearly constant for the different V-isotopes. δ is a correction for the pairing energy of the two last neutrons in the even neutron isotopes and is given by Cameron [14]). Cameron has also shown that the level spacings are proportional to $(2J+1)^{-1}$, to a good approximation. Since the angular barrier favours protons with low orbital angular momentum, the spin states in the compound nuclei tend to concentrate near the spin of the target nuclei.

From table 6 and the above mentioned rules about level spacings and level

TABLE 4

Data from $Ti^{49}(p, \gamma)V^{50}$ excitation curve

Proton energy E_p(keV) (±1 keV)	Excitation energy E(MeV) (±0.01 MeV)	Rel. int.	Remarks
878.7	8.8016	25	F [a]
880.7	8.8036	20	U [b]
882.9	8.8057	35	
911.4	8.8338	50	
917.0	8.8392	50	
924.0	8.8460	50	
934.0	8.8558	85	
939.6	8.8613	85	
945.6	8.8672	120	
948.8	8.8703	70	
953.3	8.8747	100	
959.9	8.8812	1500	
963.5	8.8847	35	
964.9	8.8861	70	
966.7	8.8879	120	
969.6	8.8907	300	
974.5	8.8955	540	
977.0	8.8979	50	
978.8	8.8997	130	
981.8	8.9027	610	
985.6	8.9064	370	
988.7	8.9094	220	
991.9	8.9125	100	
993.9	8.9145	250	
996.7	8.9172	70	D [c]
999.1	8.9196	240	
1004.8	8.9252	190	
1009.0	8.9294	70	
1013.0	8.9332	25	D?
1021.3	8.9414	120	
1029.3	8.9492	50	
1031.0	8.9509	25	
1035.9	8.9556	35	
1037.8	8.9575	85	
1039.9	8.9596	35	
1044.8	8.9644	35	
1048.2	8.9677	25	
1059.5	8.9788	50	
1062.3	8.9815	50	
1065.0	8.9842	90	
1068.8	8.9879	150	
1076.6	8.9956	100	
1084.3	9.0071	190	
1087.1	9.0058	70	
1089.4	9.0081	50	U
1090.5	9.0091	100	
1094.5	9.0131	50	
1098.0	9.0165	90	
1099.6	9.0181	70	
1102.3	9.0207	130	
1105.0	9.0234	70	

[a] F means fluorine contamination

[b] U means uncertain

[c] D means double resonance

TABLE 4 (continued)

Proton energy E_p(keV)(±1 keV)	Excitation energy E(MeV)(±0.01 MeV)	Rel. int.	Remarks
1107.7	9.0260	100	
1111.1	9.0293	120	
1112.5	9.0307	120	
1115.8	9.0340	70	D
1119.2	9.0373	85	
1124.4	9.0423	250	
1126.6	9.0455	150	
1130.5	9.0483	70	D
1135.6	9.0533	70	
1138.8	9.0565	240	
1143.5	9.0611	220	
1146.5	9.0640	70	
1150.2	9.0676	70	D
1155.4	9.0727	150	
1158.5	9.0758	130	
1161.4	9.0786	85	
1162.8	9.0800	100	
1166.5	9.0836	170	
1171.9	9.0889	240	
1174.9	9.0918	85	
1179.1	9.0960	120	
1181.8	9.0986	100	
1184.5	9.1012	200	
1187.2	9.1039	50	
1190.4	9.1070	300	
1193.7	9.1103	85	
1200.6	9.1170	80	
1202.9	9.1193	340	
1206.5	9.1228	170	
1208.8	9.1250	100	
1216.3	9.1324	200	D
1220.7	9.1367	130	
1223.6	9.1396	170	
1226.3	9.1422	130	
1230.0	9.1458	170	
1233.2	9.1489	290	
1238.1	9.1537	130	
1239.4	9.1550	320	
1241.8	9.1574	100	
1243.7	9.1592	250	
1249.8	9.1652	290	
1251.4	9.1668	70	
1254.5	9.1698	240	
1255.8	9.1711	300	
1258.5	9.1737	220	
1264.6	9.1797	370	
1268.1	9.1831	240	
1273.3	9.1882	300	
1275.1	9.1900	440	
1279.8	9.1946	240	
1283.3	9.1980	130	

TABLE 5

Data from $Ti^{50}(p, \gamma)V^{51}$ excitation curve

Proton energy E_p(keV)(±1 keV)	Excitation energy E(MeV)(±0.01 MeV)	Rel. int.	Remarks
885.5	8.9101	50	
911.1	8.9352	150	
916.3	8.9403	120	
932.9	8.9565		F? [a])
953.4	8.9766	35	D [b])
970.8	8.9937	70	
985.1	9.0077	130	
989.6	9.0121	250	
1007.8	9.0299	80	
1029.3	9.0510	500	
1033.1	9.0547	25	
1038.7	9.0602	250	
1050.7	9.0720	75	
1055.2	9.0764	35	
1061.6	9.0827	230	
1075.3	9.0951	70	
1077.6	9.0984	80	
1079.7	9.1004	230	
1087.5	9.1080	370	
1090.7	9.1112	50	U [c])
1092.2	9.1127	110	
1101.9	9.1222	50	
1106.8	9.1270	25	
1109.0	9.1291	250	
1112.5	9.1326	50	
1121.6	9.1415	370	
1127.5	9.1473	40	
1130.9	9.1506	40	
1132.4	9.1521	20	U
1134.5	9.1541	30	U
1145.9	9.1653	90	
1150.4	9.1697	330	
1153.5	9.1727	25	
1159.5	9.1786	20	U
1162.8	9.1818	50	
1165.1	9.1841	40	
1167.6	9.1865	40	U
1168.8	9.1877	40	
1178.2	9.1970	50	
1179.1	9.1978	40	U
1183.1	9.2017	400	
1186.0	9.2046	400	
1191.0	9.2095	30	U
1193.2	9.2116	70	U
1195.3	9.2137	50	
1198.6	9.2169	25	D?
1201.9	9.2202	35	U
1204.5	9.2227	170	

[a]) F means fluorine contamination

[b]) D means double resonance

[c]) U means uncertain

TABLE 5 (continued)

Proton energy E_p(keV)(±1 keV)	Excitation energy E(MeV)(±0.01 MeV)	Rel. int.	Remarks
1206.9	9.2251	300	
1211.2	9.2293	330	
1214.2	9.2322	400	
1223.5	9.2413	350	
1224.9	9.2427	200?	
1232.3	9.2500	150	
1236.7	9.2543	410	
1237.9	9.2554	200?	
1248.8	9.2661	140	
1255.0	9.2722	650	
1257.1	9.2742	150?	
1262.5	9.2795	330	
1264.8	9.2818	170	
1268.5	9.2854	300	
1276.5	9.2933	380	
1277.9	9.2947	270	
1283.8	9.3004	580	
1287.0	9.3036	810	
1290.3	9.3068	480	
1298.0	9.3143	110	
1301.1	9.3174	50	
1306.1	9.3223	60	U
1309.6	9.3257	40	
1315.8	9.3318	1200	
1322.5	9.3383	1400	

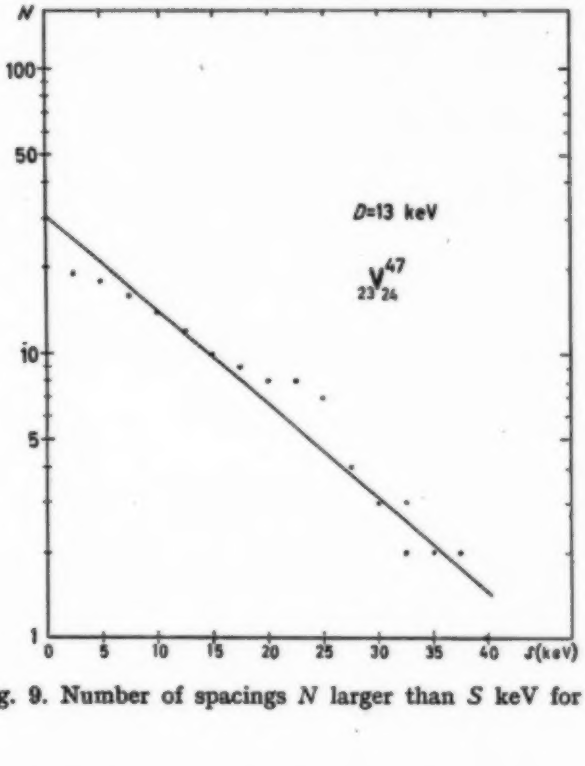

Fig. 9. Number of spacings N larger than S keV for V^{47}.

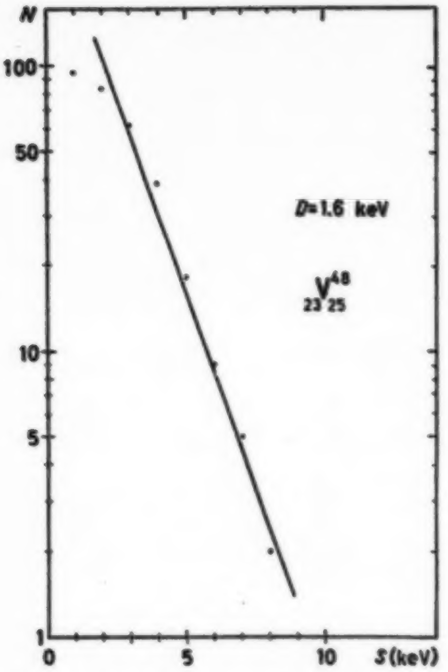

Fig. 10. Number of spacings *N* larger than *S* keV for V^{48}.

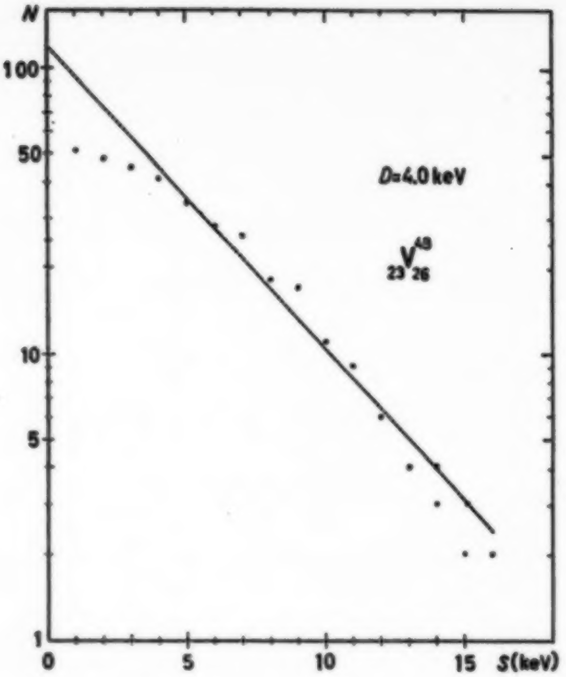

Fig. 11. Number of spacings *N* larger than *S* keV for V^{49}.

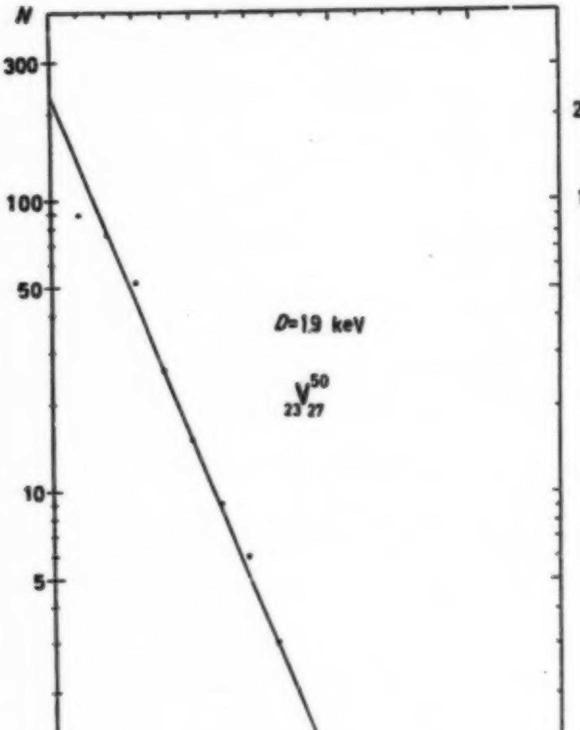

Fig. 12. Number of spacings *N* larger than *S* keV for V^{50}.

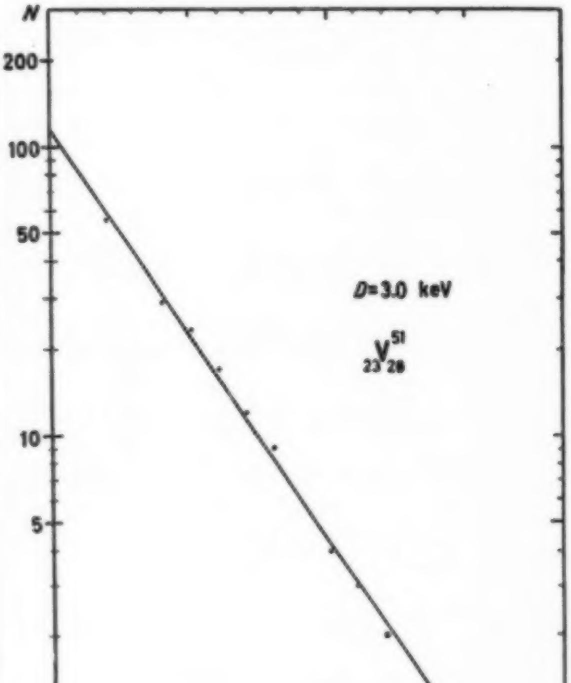

Fig. 13. Number of spacings *N* larger than *S* keV for V^{51}.

densities it turns out that the experimentally found level spacings are related to each other just as one can expect, with the exception that the average spacing of V^{50} should be somewhat smaller than that of V^{48}.

TABLE 6

Values of several quantities

Target nucleus	Ti^{46}	Ti^{47}	Ti^{48}	Ti^{49}	Ti^{50}
Spin of target nucleus	0	$\frac{5}{2}$	0	$\frac{7}{2}$	0
Compound nucleus	V^{47}	V^{48}	V^{49}	V^{50}	V^{51}
δ of the compound nucleus (MeV)	−1.44	0	−1.45	0	−1.37
Average excitation energy of the compound nucleus E (MeV)	6.3	7.9	7.8	9.0	9.1
E–δ (MeV)	4.9	7.9	6.4	9.0	7.7
D (experimental) (keV)	13	1.6	4.0	1.9	3.0
D (calculated with $c = 3.5$)	13	1.4	4.0	0.8	1.6

The excitation curves of V^{48} and V^{50} show, however, that in spite of all efforts to obtain a high resolution system, the resolution is not quite good enough for these nuclei, which fact may explain the discrepancy. Since in the calculation no consideration has been taken to the $(2J+1)^{-1}$ dependence of the level spacings the calculated D-values of V^{48} and V^{50} should be still smaller.

It has been shown by Newton [15]) and others that there should be large shell effects in the average level spacings. The difference between the calculated and the experimental D-values of V^{51}, which nucleus has 28 neutrons, may be attributed to a shell effect, since for this nucleus the resolution seems to be sufficient.

Measurements are going on of the γ-spectras from the resonances of the different V-isotopes, to give information on the low-lying excited levels, which are of special interest from the shell model point of view.

A preliminary account [16]) of a part of the present investigation has been reported at the Conference of the Swedish National Committee for Physics in 1959.

The author wishes to express his sincere gratitude to Professor N. Ryde for his kind interest in this work and to O. Almén and G. Bruce, who separated the targets. My thanks are also due to S. E. Arnell for placing the gamma spectrometer at my disposal. The Swedish Atomic Energy Commission has financially supported the investigation.

References

1) F. Ajzenberg-Selove and T. Lauritsen, Nuclear Physics **11** (1959) 1
2) P. M. Endt and C. M. Braams, Rev. Mod. Phys. **29** (1957) 683
3) V. J. Ashby and H. C. Catron, Lawrence Rad. Lab. UCRL-5419

4) K. T. Bainbridge, in Experimental Nuclear Physics, ed. by Segré (Wiley, New York, 1953) Vol. I

5) F. Bumiller, H. H. Staub and H. E. Weaver, Helv. Ph. Acta, **29** (1956) 83

6) S. L. Andersen, H. Bö, T. Holtebekk, O. Lönsjö and R. Tangen, Nuclear Physics **9** (1958) 509

7) S. L. Andersen, K. Gjötterud, T. Holtebekk and O. Lönsjö, Nuclear Physics **7** (1958) 384

8) R. O. Bondelid and C. A. Kennedy, Phys. Rev. **115** (1959) 1600

9) O. Almén, G. Bruce and A. Lundén, Nuclear Instruments **2** (1958) 249

10) K. O. Nielsen, in Proc. of the 1955 Harwell Isotope Conf., ed. by M. L. Smith (Butterworths scientific publications, London, 1955)

10a) K. O. Nielsen, Thesis, Inst. for theoretical physics, Copenhagen (Munksgaard, Copenhagen, 1958)

11) A. van Lippold, J. W. Müller, H. H. Staub and H. Winkler, Helv. Phys. Acta **32** (1959) 269

12) J. A. Harvey and D. J. Hughes, Phys. Rev. **109** (1958) 471

13) R. L. Clarke, E. Almqvist and E. B. Paul, Nuclear Physics **14** (1960) 472

14) A. G. W. Cameron, Can. Journal of Physics **36** (1958) 1040

15) T. D. Newton, Can. Journal of Physics **34** (1956) 804

16) Report from the Conference of the Swedish National Committee for Physics in 1959, Arkiv for physik **16** (1960) 6

2.A.1 *Nuclear Physics* **23** (1961) 559—561; © *North-Holland Publishing Co., Amsterdam*

Not to be reproduced by photoprint or microfilm without written permission from the publisher

SODIUM-24 EXCITATION FUNCTION FOR LITHIUM-6 IONS ON ALUMINIUM

INGE-MARIA LADENBAUER
Yale University, New Haven, Connecticut

Received 21 November 1960

Abstract: The excitation function for the reaction $Al^{27}(Li^6; 5p, 4n)Na^{24}$ has been measured using the stacked foil technique. The large constant cross section of 43 mb over the energy region from 37 to 63 MeV total beam energy makes this reaction suitable for beam flux monitoring in other nuclear chemical studies.

1. Introduction

With the recent availability of a high energy (63 MeV) Li^6 beam [1]) at the Yale Heavy Ion Accelerator, a series of studies of the reactions produced by Li^6 ions has been undertaken. Since it is desirable to have a monitoring reaction for beams of this type, especially for nuclear chemical studies (where one often has to 'cut-up' a target for different investigations), a search was made to ascertain whether a suitable activity is produced for this purpose. Subsequently a reaction similar to the well known monitoring reactions $Al^{27}(p; 3p, n)Na^{24}$ and $Al^{27}(\alpha; 4p, 3n)Na^{24}$ [2, 3]) for proton and alpha particles beams was found for Li^6 bombardments on aluminium, i.e. $Al^{27}(Li^6; 5p, 4n)Na^{24}$ †.

2. Experimental

Targets consisting of stacks of aluminium foils of approximately 4.65 mg/cm² were bombarded with 63 MeV Li^6 ions. The Li^6 beam was collected in a Faraday cup and integrated with a Cary electrometer. In the energy region considered the Li^6 ion is fully stripped of its electrons. With a mean flux of 3×10^{12} Li^6 ions/min sufficient activities were produced for accurate analysis with bombardment times of 30 to 60 minutes.

The Na^{24} activity was measured with both an end window gas flow beta proportional counter and a 7.6 cm × 7.6 cm sodium iodide (thallium activated) crystal using a 400 channel pulse height analyzer. The characteristic 2.75 MeV and 1.36 MeV gamma rays of Na^{24} were identified and their decay followed. The half life measured by gross beta decay and by gamma ray spectroscopy

---

† The notation 5p, 4n is used only for convenience and is not meant to signify specific reaction products of beam-target break up.

TABLE 1

Experimental cross sections

Li-6 beam energy in MeV	mg Al/cm^2	σ Na−24 in mb
63.3−61.6	0 − 4.67	32.6±4.6
61.6−60.0	4.67− 9.3	43.0±8.0
60.0−58.7	9.3 − 14.0	43.2±7.8
58.7−57.0	14.0 − 18.7	40.3±4.4
57.0−55.6	18.7 − 23.4	40.7±4.0
55.6−54.3	23.4 − 28.1	40.7±4.0
54.3−52.8	28.1 − 32.7	39.5±0.9
52.8−51.0	32.7 − 37.4	41.1±4.6
51.0−49.4	37.4 − 42.1	44.5±3.1
49.4−47.9	42.1 − 46.7	44.0±3.2
47.9−46.2	46.7 − 51.4	45.2±2.4
46.2−44.4	51.4 − 56.1	43.3±1.0
44.4−42.6	56.1 − 60.8	45.5±2.5
42.6−40.5	60.8 − 65.5	43.8±0.9
40.5−38.7	65.5 − 70.2	44.8±1.9
38.7−36.6	70.2 − 74.9	43.3±3.4
36.6−34.7	74.9 − 79.5	34.3±0.7
34.7−32.4	79.5 − 84.2	30.2±0.5
32.4−30.4	84.2 − 88.8	21.2±1.7
30.4−27.9	88.8 − 93.4	14.3±1.2
27.9−25.0	93.4 − 98.1	7.6±0.2
25.0−22.1	98.1 −102.8	3.4±0.6
22.1−18.9	102.8 −107.4	0.9±0.1

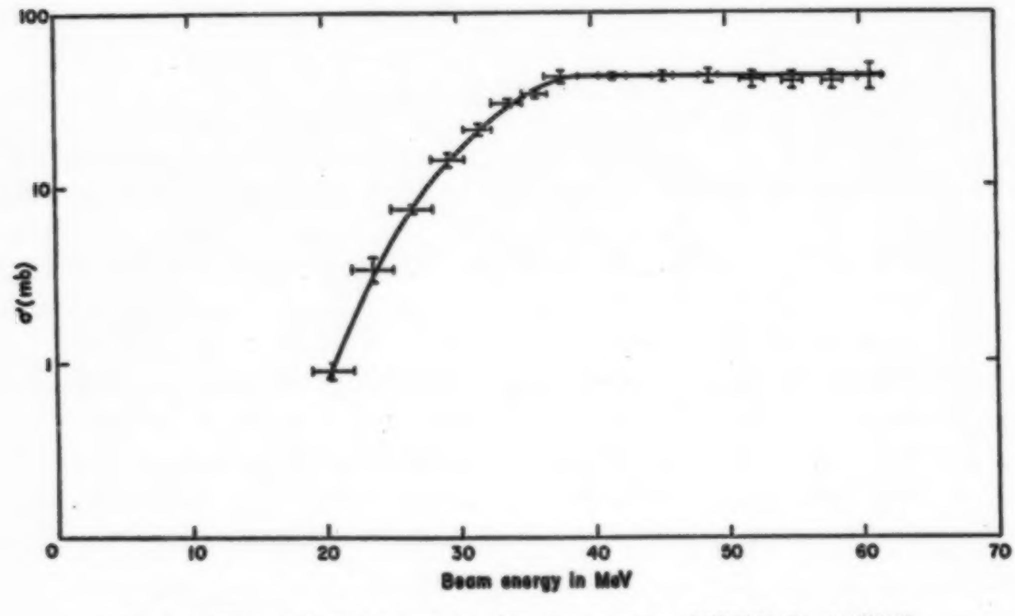

Fig. 1. The excitation function for the reaction $Al^{27}(Li^6; 5p, 4n)Na^{24}$.

agreed within the experimental statistics. Other activities such as Al^{28}, Mg^{27}, Si^{31} and P^{32} were observed and will be reported on at a later time.

The Na^{24} counting rates were converted into disintegration rates by correcting for solid geometry. The correction for the air and window absorption was applied to the data. The counting efficiency of the proportional counter for the beta particles was taken as 100 %. The disintegration rates were calculated to infinite bombardment time and from these saturation disintegration rates the cross sections were calculated using the thin target equation.

The energy scale for Li^6 ions in aluminium was obtained from interpolations of the range-difference curves of L. Northcliffe [4]). The range for 10.55 MeV Li^6 ions in aluminium is 126.5 mg/cm^2.

3. Results and Discussion

The cross sections for Na^{24} versus the total beam energy are shown in table 1 and fig. 1. The nearly constant value for the cross section between 37 and 63 MeV total beam energy allows the use of the $Al^{27}(Li^6; 5p, 4n)Na^{24}$ reaction for monitoring the Li^6 beam in this energy region. The value of 32.6 mb for the Na^{24} cross section in foil 1 indicates that this reaction is a direct interaction with only a small momentum transfer. The "sandwich method" should be used for monitoring the Li^6 ion beam. Three aluminium foils with approximately 4.65 mg/cm^2 in front of the target would decrease the Li^6 ion energy from 10.55 to 9.8 MeV/nucleon. Of these three aluminium foils the second one should be mounted in the same way as the sample and used for calculating the flux.

I wish to thank Dr. C. Anderson and Dr. Ivor Preiss for their interest, advice and help in this work.

References

1) C. E. Anderson, Conf. of Interaction of Complex Nucleii, Gatlinburg, Tenn., May 1960
2) N. M. Hintz and N. F. Ramsay, Phys. Rev. 88 (1952) 19
3) L. Marquez, Phys. Rev. 86 (1952) 405
4) L. Northcliffe, Phys. Rev. 120 (1960) 1744

2.E

Nuclear Physics **23** (1961) 562—593; © *North-Holland Publishing Co., Amsterdam*

Not to be reproduced by photoprint or microfilm without written permission from the publisher

THE SCATTERING OF HIGH ENERGY NUCLEONS BY COMPLEX NUCLEI

C. J. BATTY

National Institute for Research in Nuclear Science, Rutherford High Energy Laboratory †, *Harwell*

Received 18 November 1960

Abstract: An analysis of nucleon-carbon scattering experiments in the energy range 90 to 1000 MeV has been made in terms of the Optical Model using the semi-classical approximation. Values of the differential cross-section and polarization at a number of angles and the absorption and total cross-sections were used in obtaining parameters given a "best-fit" to the experimental data. The analysis was made for protons of energies 95, 135, 155, 220, 310, 420, 635 and 970 MeV and for 155 MeV neutrons. Calculations at various energies were also made using Optical Model potentials obtained by other workers from nucleon-nucleon scattering data.

1. Introduction

Since 1948 several accelerators providing intense beams of protons and neutrons of energy greater than 100 MeV have been in operation and a detailed study of the nucleon-nucleus interaction has been possible. In particular the scattering of protons has been studied extensively and a large amount of experimental results are now available. Early work was confined to measurements of the differential scattering cross-section and total and absorption cross-sections. The analysis of these results was mainly in terms of a phenomenological model, now known as the Optical Model, because a theoretical analysis of these results in terms of nucleon-nucleon forces was not possible. In the Optical Model the interaction between the nucleus and the incident nucleon is represented by a complex potential well. An analysis of this type applied to the scattering of neutrons was first made by Fernbach, Serber and Taylor [1]) who obtained quite good agreement with experimental results using reasonable values for the potentials.

With the discovery of polarization effects by Oxley *et al.* [2]) in 1954 the inclusion of a spin-dependent potential in the Optical Model became necessary. Fermi [3]) proposed the introduction of a potential of the form

$$\gamma \frac{1}{r} \frac{\mathrm{d}V_{\mathrm{n}}}{\mathrm{d}r} \boldsymbol{\sigma} \cdot \mathbf{L},$$

where V_{n} is the central nuclear potential and γ a constant. Later Fernbach

---

† Formerly of the Physics Department, University of Birmingham.

et al. [4]) and Brown [5]) showed that such a form of potential follows from the properties of nucleon-nucleon scattering.

So far we have considered the Optical Model to be purely phenomenological. However, the work of Francis and Watson [6]) and others has shown how the Optical Model Potential can be derived from the individual interactions between the neutrons and protons in the nucleus. This work has been extended by Riesenfeld and Watson [7]) who have demonstrated that the Optical Model Potential can be related in a quantitative manner to the nucleon-nucleon phase-shift data.

This paper is mainly concerned with an analysis of the scattering of high energy neutrons and protons by Carbon using the Optical Model. The potentials (which may be complex) are determined by comparing calculated values of the differential cross-section, polarization, total and absorption cross-sections with experimental observations. In order to see how these potentials vary with the energy of the incident nucleon, the analysis has been made at a series of energies between 90 and 1000 MeV. However, before proceeding with the details of the analysis we shall first consider some general features of this and similar analyses.

In the present analysis we have attempted to fit the available data for the differential cross-section, polarization, absorption and total cross-sections at a particular energy simultaneously with the same set of potentials. Alternatively, if all four sets of data were not available then a fit to three of these has been made. In this way much more definite values for the potentials could be obtained.

In considering the available polarization data the work of Chesnut *et al.* [8]) has shown the importance of obtaining a clear separation between elastic scattering and scattering in which the lowest energy states of the nucleus are excited. We have, therefore, for protons at the lower energies, only considered experiments in which this separation has been obtained. For neutrons and higher energy (> 250 MeV) protons this separation has not been possible with presently available techniques. In these cases we have concentrated our analysis at the smaller angles where effects due to inelastic scattering should be less important.

We have considered data over a wide energy range and in this respect our analysis is similar to that of Bjorklund and Fernbach [9]). However, their analysis has concentrated on the energy region below 100 MeV and they have studied the heavy and medium weight nuclei Lead and Copper. In the present case we have chosen Carbon as the scattering nucleus owing to the large amount of experimental information available for this element. Also for Carbon, scattering leading to excitation of the first few excited states is more clearly resolved than it is for the heavier nuclei.

In the next section we consider the method of analysis used and in the following one the results of this analysis for each of the energies considered. In the last section the results of calculations made with Optical Model potentials obtained from nucleon-nucleon scattering data are given. In particular we shall consider potentials calculated by Ohnuma [10]) from the nucleon-nucleon potential models of Gammel and Thaler [11]) (G.T.) and Signell and Marshak [12]) (S.M.). We shall also consider calculations by Bethe [13]) and Cromer [14]) using the various phase-shift solutions obtained by Stapp *et al.* [15]).

2. Method of Calculation

2.1. THE OPTICAL MODEL POTENTIAL

We write the Optical Model potential in the form

$$V(r) = V_C(r) - V_n\rho(r) + \frac{C|V_n|}{r}\frac{\mathrm{d}}{\mathrm{d}r}\rho(r)\boldsymbol{\sigma}\cdot\mathbf{L}, \tag{2.1}$$

where $\rho(r)$ is a function of the distance from the centre of the nucleus and $V_C(r)$ is the Coulomb potential arising from a charge distribution $\rho'(r)$. $\rho(r)$ and $\rho'(r)$ are normalised to unity at the origin. V_n and C, the central and spin orbit potentials, which may be complex, have to be determined in order to give a good fit to the experimental data. The potential has also been written by some authors as

$$V(r) = V\ (r) - (V_1+iV_2)\rho(r) + (V_3+iV_4)\left(\frac{\hbar}{\mu c}\right)^2\frac{1}{r}\frac{\mathrm{d}}{\mathrm{d}r}\rho(r)\boldsymbol{\sigma}\cdot\mathbf{L}, \tag{2.2}$$

where $(\hbar/\mu c)$ is the pion Compton wavelength and V_1, V_2, V_3 and V_4 are real and related to the real and imaginary parts of V_n and C.

Here we are assuming that V_1 and V_2 have the same density distribution. Bjorklund and Fernbach [9]) in analysing low energy scattering have used a term for V_2 peaked at the nuclear surface. This is to allow for the effect of the Pauli principle since at low energies non-elastic events must take place near the nuclear surface if they are to be allowed. However, at the higher energies inelastic events can take place throughout the nucleus and V_1 and V_2 should have similar shapes.

This is clearly shown by the calculations of Lemmer *et al.* [19]) who have calculated the imaginary part of the Optical Model potential for O^{16}. Their results indicate that the potential is peaked at the nuclear surface for energies below 60 MeV, but above this energy the potential is distributed throughout the nucleus.

A further term should be added to the potential $V(r)$ to allow for spin-dependent effects arising from Coulomb forces. We have made calculations in which this potential was included and the effect was found to be small. We shall later discuss the method used in these calculations and the results obtained but otherwise the effect of such a term will be neglected.

In writing $V(r)$ in the above form and taking $\rho(r)$ to be the nuclear density certain assumptions are involved. Fernbach, Heckrotte and Lepore [4]) and Brown [5]) have shown that such a form of potential can be derived from the nucleon-nucleon potential provided that the range of nuclear forces can be neglected compared to the size of the nucleus and that the nucleon-nucleon scattering amplitudes do not change rapidly with angle and can be replaced by their values at zero angle.

The first approximation will presumably lead to a nuclear potential having a radius somewhat greater than that of the nuclear density, as discussed by Wilson [16]). The angular dependence of the nucleon-nucleon scattering amplitudes has been included in a calculation by Cromer [14]) who finds that the result is to give rise to a potential in which V_1, V_2, V_3, V_4, have the same distribution as the nuclear density but each potential has a different radius. This effect has also been considered by McManus and Thaler [17]) using the impulse approximation who find for the mean square radius of the potentials at 310 MeV that

$$R_1 > R_4 > R_3 > R_2,$$

where the subscripts refer to the potentials V_1, V_2, V_3 and V_4. However, at 156 MeV and 90 MeV they find

$$R_4 > R_1 > R_2 > R_3,$$

indicating that the parameters are energy dependent. Saperstein and Feldman [18]) have also found an increase in the potential radius when the angular dependence of the nucleon-nucleon interaction is taken into account.

However, if we were to allow each potential to have a different radius, then in fitting the experimental data we should have eight parameters, the four potentials and four radii and with the available data it would not be possible to determine these unambiguously. In order to reduce the number of parameters to a reasonable number we have assumed that each potential has the same radius but that this radius need not necessarily be the same as that of the nuclear density distribution. This leaves five parameters to be determined, the radius of the potential and the magnitudes of the real and imaginary parts of the central and spin-orbit potentials.

We shall now show that the use of only one radius for the potentials is reasonable. Using the Optical Model potential in the form given by (2.2) and letting R_i^2 be the mean square radius of the potential V_i $(i = 1, 2, 3, 4)$, then if $R_i^2 = R_c^2+r_i^2$, where R_c^2 is the mean square electron scattering radius, from the results of Cromer [14]) and Kerman *et al.* [18a]) we get the results shown in table 1.

If we are to use the same radius for each potential it is necessary that these quantities should all be similar at a given energy. Neglecting the imaginary spin-orbit potential which we find to be small, then this is true at 90 and 156

MeV. At 310 MeV the imaginary central potential is dominant and the fact that our calculations do not use a large radius for the real potential should not be important. We have checked this using the potentials given by Cromer. Changing the radius of the central real potential by quite large amounts did not markedly alter the calculated polarization or cross-sections. It seems reasonable therefore to take the same radii for all the potentials.

Table 1

Contribution to mean square radius from nucleon-nucleon interaction

	Kerman *et al.* [18a])			Cromer [14])
	310 MeV	156 MeV	90 MeV	310 MeV
r_1^2 (10^{-26} cm^2)	7.5	3.5	3.6	6.9
r_2^2	1.7	3.6	3.5	1.4
r_3^2		1.4	2.0	.9
r_4^2	2.5	5.7	7.4	.8
$\dfrac{R \text{ (central potential)}}{R \text{ (electron scatt.)}}$	1.13	1.27	1.27	1.12

If the range of nucleon-nucleon forces and the angular dependence of the scattering amplitude are neglected then the central nuclear potential may be written [4, 5])

$$V_n(r) = -\frac{2\pi}{E}\sum_i \overline{f_i(0)}\rho(r), \tag{2.3}$$

where $f_i(0)$ is the zero-angle nucleon-nucleon scattering amplitude for the i^{th} nucleon, E the total energy of the incident nucleon and $\rho(r)$ the nucleon density normalised to unit volume. From the Optical Theorem we find

$$\sigma_i = \frac{4\pi}{k}\,\mathrm{Im}\,f_i(0), \tag{2.4}$$

where σ_i is the total nucleon-nucleon cross-section for the i^{th} particle and k the wave number of the incident nucleon.

Hence

$$\mathrm{Im}\,V_n(r) = -\frac{k}{2E}\sum_i \bar{\sigma}_i\rho(r) = -\frac{k}{2E}A\bar{\sigma}\rho(r), \tag{2.5}$$

where $\bar{\sigma}$ is the mean nucleon-nucleon total cross-section and for incident protons

$$\bar{\sigma} = \frac{Z\sigma_{\text{pp}}+(A-Z)\sigma_{\text{pn}}}{A}. \tag{2.6}$$

This derivation neglects effects due to the Pauli principle which tend to reduce $\bar{\sigma}$ [20]) and the antisymmetrization of the nucleus wave function which in general increases $\bar{\sigma}$ [21]). These two effects have been discussed in detail by Beg [22]) for pion-nucleus scattering. At nucleon energies above 300 MeV the two effects are small and as they are of opposite sign the net result is negligible. Hence $\bar{\sigma}$ is the same as for free nucleon-nucleon scattering. However, at energies below 300 MeV the Pauli principle becomes increasingly important and $\bar{\sigma}$ is considerably less than the "free" value.

In the present analysis it was found to be more convenient to vary $\bar{\sigma}$ in fitting the data rather than Im V_n or V_s directly. Hence we shall give values for $\bar{\sigma}$ as it was this parameter which was directly determined but values of Im V_n and V_s calculated from $\bar{\sigma}$ will also be quoted.

2.2. THE SEMI-CLASSICAL APPROXIMATION

The amplitude for the scattering of a nucleon through an angle θ by the potential given in (2.1) is [23])

$$f(\theta) = A(\theta)+B(\theta)\boldsymbol{\sigma}\cdot\mathbf{n}, \tag{2.7}$$

where $\mathbf{n}$ is a unit vector perpendicular to the scattering plane. $A(\theta)$ and $B(\theta)$ can be evaluated exactly in terms of phase-shifts, but the expressions are complicated and at high energies many phase-shifts must be calculated. Much simpler expressions are given by the semi-classical approximation. This has been used by Shapiro [24]) to calculate the differential cross-section for the scattering of 96 MeV protons and neutrons by carbon and the results compared with a phase-shift calculation. The two sets of results agree very well until the first diffraction minimum is reached. As we shall always consider angles less than the first minimum and as the semi-classical method is expected to improve with increasing incident energy, the approximation should give results sufficiently accurate for the present analysis.

In calculating the values of $A(\theta)$ and $B(\theta)$ the Kelin-Gordon equation was used in preference to the Schrödinger equation as the latter is non-relativistic. Similarly all calculations of the kinematics of the scattering were treated relativistically. The final expressions obtained for $A(\theta)$ and $B(\theta)$ are

$$A(\theta) = \frac{k}{i}\int_0^\infty J_0(kb\sin\theta)\{\tfrac{1}{2}(\mathrm{e}^{i\chi^+}+\mathrm{e}^{i\chi^-})-1\}b\mathrm{d}b, \tag{2.8}$$

$$B(\theta) = -\tfrac{1}{2}k\int_0^\infty J_1(kb\sin\theta)\{\mathrm{e}^{i\chi^+}-\mathrm{e}^{i\chi^-}\}b\mathrm{d}b, \tag{2.9}$$

where $\chi^\pm = \chi_1+\chi_C\pm\chi_2$, $r^2 = z^2+b^2$, $\hbar = c = 1$, and

$$\chi_1 = -\frac{E}{k}\int_{-\infty}^\infty V_n(r)\mathrm{d}z,\quad \chi_C = \frac{E}{k}\int_{-\infty}^\infty V_C(r)\mathrm{d}z,\quad \chi_2 = \frac{E}{k}\int_{-\infty}^\infty kbV_s(r)\mathrm{d}z. \tag{2.10}$$

Here b is the "classical" impact parameter of the incident nucleon and J_0 and J_1 are zero and first order Bessel functions.

If now we assume that $\rho(r) = \rho'(r) = 0$ for $r > R$ then for $r > R$

$$\chi_1 = \chi_2 = 0 \quad \text{and} \quad \chi_C = \chi_P = \frac{E}{k}\int_{-\infty}^{\infty} V_P(r)\mathrm{d}z,$$

where $V_P(r)$ is the potential at a distance r due to a point change. The amplitude for the scattering of protons by a point charge is

$$A_P(\theta) = \frac{k}{i}\int_0^{\infty} J_0(kb\sin\theta)\{\mathrm{e}^{i\chi_P}-1\}\, b\mathrm{d}b, \tag{2.11}$$

and hence eqs. (2.8), (2.9) may be written

$$A(\theta) = \frac{k}{i}\int_0^{\infty} J_0(kb\sin\theta)\{\tfrac{1}{2}(\mathrm{e}^{i\chi^+}+\mathrm{e}^{i\chi^-})-\mathrm{e}^{i\chi_P}\}b\mathrm{d}b+A_P, \tag{2.12}$$

$$B(\theta) = -\tfrac{1}{2}k\int_0^{R} J_1(kb\sin\theta)\{\mathrm{e}^{i\chi^+}-\mathrm{e}^{i\chi^-}\}b\mathrm{d}b. \tag{2.13}$$

$A_P(\theta)$ can be calculated directly for a nucleus of known charge [25]) whilst the remaining terms in the above equations can be evaluated by numerical integration once χ_1, χ_2, χ_c and χ_P have been calculated.

χ_P is given by

$$\chi_P = 2\,\frac{Z\alpha E}{k}\ln\frac{kb}{\sqrt{2}}$$

for a nucleus of charge $Z\alpha$ and

$$\chi_c = \frac{2E}{k}\int_0^{\infty} V_C\mathrm{d}z = \frac{2E}{k}\left[\int_0^{\infty} V_P\mathrm{d}z-\int_0^{R} V_P\mathrm{d}z+\int_0^{R} V_C\mathrm{d}z.\right] \tag{2.14}$$

In order to evaluate χ_1, χ_2 and $\int_0^R V_C\mathrm{d}z$ it is necessary to choose suitable distributions for $\rho(r)$ and $\rho'(r)$.

For $\rho'(r)$ the charge distribution

$$\rho'(r) = \frac{1}{\pi^{\frac{3}{2}}a^3}\,\mathrm{e}^{-(r/a)^2} \quad \text{with } a = 1.965\ \mathrm{fm} \tag{2.15}$$

was used. This distribution and radius have been found to give a good fit to the electron scattering data of Fregeau [26]) and has the advantage that the Coulomb potential has the simple form

$$V_C(r) = \frac{Z\alpha}{r}\,\mathrm{erf}\left(\frac{r}{a}\right) \quad \text{where} \quad \mathrm{erf}(x) = \frac{2}{\sqrt{\pi}}\int_0^{x}\mathrm{e}^{-t^2}\mathrm{d}t. \tag{2.16}$$

χ_C can then be calculated using (2.14).

For $\rho(r)$ the distribution

$$\rho(r) = \left(1+\frac{4}{3}\frac{r^2}{a_1^{\,2}}\right)\mathrm{e}^{-r^2/a_1^{\,2}} \tag{2.17}$$

was used. This distribution has been found to give a best fit to electron scattering data (26) with $a_1 = 1.635$ fm. In our analysis, a_1 which determines the radius of the potentials was treated as an adjustable parameter.

χ_1 and χ_2 can then be calculated using (2.10) for given values of the parameters V_n and C (eq. (2.1)) or V_1, V_2, V_3 and V_4 (eq. (2.2)) and hence $A(\theta)$ and $B(\theta)$ determined.

In evaluating (2.12) and (2.13) the value $R = 3a$ was taken. For this value of r both $\rho(r)$ and $\rho'(r)$ are very small and can be replaced by zero to a very good approximation.

The polarization and differential scattering cross-section are then given by

$$\frac{d\sigma}{d\Omega} = |A(\theta)|^2 + |B(\theta)|^2, \tag{2.18}$$

$$P(\theta) = \frac{2\,\mathrm{Re}\,A^*(\theta)B(\theta)}{|A(\theta)|^2 + B(\theta)|^2}. \tag{2.19}$$

The total cross-section is, from the Optical Theorem,

$$\sigma_t = \frac{4\pi}{k} A_1(0) = -4\pi \int_0^R \{\tfrac{1}{2}(e^{i(\chi_1+\chi_2)} + e^{i(\chi_1-\chi_2)}) - 1\} b\,db, \tag{2.20}$$

whilst the absorption cross-section is given by

$$\sigma_a = 2\pi \int_0^R \{1 - \tfrac{1}{2}e^{-2\chi_{1I}}(e^{2\chi_{2I}} + e^{-2\chi_{2I}})\} b\,db, \tag{2.21}$$

where the subscripts R and I are used to denote real and imaginary parts respectively.

2.3. METHOD OF ANALYSIS

As previously discussed it was found preferable to perform the calculations for various values of $\bar{\sigma}$ instead of varying V_{nI} directly. Similarly the parameter $\lambda = V_{nR}/V_{nI}$ was varied rather than V_{nR}.

The remaining parameters used were C_R, C_I (the real and imaginary parts of C) and a_1. From these five parameters values for the differential cross-section and polarization at various angles and the total and absorption cross-sections were calculated using the method outlined in the previous section.

The calculations were performed using a Ferranti Pegasus Digital Computer. The time taken for a computation using one set of parameters depended on the number of angles and to a lesser extent on the values of the parameters but was typically 2—3 minutes.

From a given set of the Optical Model parameters values for $P(\theta)$, $d\sigma/d\Omega$ at the specified angles and σ_a and σ_t were calculated. If the calculations were made at n angles the results were treated as $2n+2$ values W_c which were then compared with the observed results $W_o \pm \Delta W_o$ using the expression

$$M = \sum \left(\frac{W_c - W_o}{\Delta W_o} \right)^2 . \tag{2.22}$$

Here ΔW_o is the experimental error in the measurement of the observed value W_o, the results being weighted according to the inverse of their errors. Clearly for a best-fit, the value of M will be a minimum and the input parameters were therefore varied until a minimum value for M was obtained. In general measurements at about 8 angles were considered giving 18 observables. Occasionally values for $P(\theta)$ or $\mathrm{d}\sigma/\mathrm{d}\Omega$ were not available and so could not be included but values for σ_a and σ_t were always used.

In fitting the calculated values to the observed results for the differential scattering cross-section, the value $\mathrm{d}\sigma/\mathrm{d}\Omega$ was not used directly but rather $N\mathrm{d}\sigma/\mathrm{d}\Omega$, where N is a normalisation constant to allow for possible systematic errors in the normalisation of the experimental results, as in general the relative values of the cross-section are known to a higher accuracy than their absolute value. The value of N was calculated to minimise the value of M_σ where M_σ is the value of M calculated using only values of $N\mathrm{d}\sigma/\mathrm{d}\Omega$. Clearly the value of N should be close to 1.

From the values of M obtained as the result of a calculation a further set of parameters were predicted and the calculation repeated. In this way, starting from a wide range of the Optical Model parameters a minimum value for M was obtained. It would have been preferable for the variation of the parameters to be performed automatically by the computer in order to obtain a best fit as is usually done in making a nucleon-nucleon scattering phase-shift analysis [15]). However, this was not possible with the amount of computer time available and so the above method was used.

The errors on the Optical Model parameters giving a best fit have been estimated from the manner in which M changed when each parameter alone was varied. It would have been preferable to use an error matrix treatment as used by Anderson [27]) in making a phase-shift analysis of π—p scattering but again owing to limitations of computer time this was not possible. An additional error in the results may arise from the size of the increments used in varying the parameters. Allowance for this effect has been included in the estimated errors but occasionally lead to difficulties in finding a good minimum for M.

Widely differing sets of parameters were used in the initial stages of an analysis at a particular energy, so that no possible minima in M should be missed. In no case were two separate minima for M found indicating that the best-fit parameter values may be unique. However, it cannot be said with any certainty that equally good, or possibly better, fits could not be obtained with a slightly differing set of parameters. It is doubtful if sets markedly different from those obtained here would fit the same experimental data equally well.

2.4. ELECTROMAGNETIC SPIN-ORBIT POTENTIAL

As previously discussed the effect of the spin-orbit potential due to electromagnetic effects was normally neglected. In a few calculations, however, this term was included and the method used for these will now be described. Similar calculations using slightly different approximations have also been made by Heckrotte [27a]) and Eriksson [27b]). Including the electromagnetic spin-orbit potential the Optical Model potential may be written

$$V = V_C(r)+(2\mu-T)\,\frac{\hbar^2}{4m^2c^2}\frac{1}{r}\frac{\mathrm{d}V_C}{\mathrm{d}r}\,\sigma\cdot\mathbf{L}-V_n\rho(r)+\frac{C|V_n|}{r}\frac{\mathrm{d}\rho}{\mathrm{d}r}\,\sigma\cdot\mathbf{L}, \tag{2.23}$$

where $T = 1$ for protons, $T = 0$ for neutrons and μ is the magnetic moment of the incident nucleon. The effect of this term is included in eqs. (2.8) and (2.9) by replacing everywhere χ_2 by $\chi_2+\chi_{Cs}$, where

$$\chi_{Cs} = \frac{E}{k}\int_0^\infty kbV_{Cs}(r)\mathrm{d}z, \quad V_{Cs}(r) = (2\mu-T)\,\frac{\hbar^2}{4m^2c^2}\frac{1}{r}\frac{\mathrm{d}V_C}{\mathrm{d}r}. \tag{2.24}$$

For $r > R$, $V_C(r) = V_p(r)$ the point charge potential and so

$$\chi_{ps} = (2\mu-T)\,\frac{\hbar^2}{4m^2c^2}\frac{1}{r}\frac{\mathrm{d}V_p(r)}{\mathrm{d}r}. \tag{2.25}$$

It is easily shown that

$$\chi_{Cs} = \frac{\hbar^2}{4m^2c^2}\,(2\mu-T)k\,\frac{\mathrm{d}\chi_C}{\mathrm{d}b} \tag{2.26}$$

and also using (2.14) and (2.25) that

$$\chi_{ps} = \frac{\hbar^2}{4m^2c^2}\,(2\mu-T)\,\frac{2Z\alpha E}{b}. \tag{2.27}$$

Over the major part of the integration in (2.8) and (2.9) χ_{ps} is small and we can use the approximations $\sin\chi_{ps} = \chi_{ps}$ and $\cos\chi_{ps} = 1$. For very small values of b, where χ_{ps} becomes very large, $\sin\chi_{ps}$ and $\cos\chi_{ps}$ oscillate rapidly so that the total contribution to the integration is zero. We therefore take the integration to be zero for very small b. Also as χ_C is a slowly varying function of b for $r < R$ we take $\chi_{Cs} = 0$. Using these approximations it can be shown that the effect of the extra spin-orbit term on the value of $A(\theta)$ is negligible. $B(\theta)$ can be written

$$\begin{aligned}B(\theta) = &-\tfrac{1}{2}k\int_0^R J_1(kb\sin\theta)[\{\mathrm{e}^{i(\chi_C+\chi_1+\chi_2+\chi_{Cs})}\\ &-\mathrm{e}^{i(\chi_C+\chi_1-\chi_2-\chi_{Cs})}\}-\{\mathrm{e}^{i(\chi_p+\chi_{ps})}-\mathrm{e}^{i(\chi_p-\chi_{ps})}\}]\,b\mathrm{d}b\\ &-\tfrac{1}{2}k\int_0^\infty\{\mathrm{e}^{i(\chi_p+\chi_{ps})}-\mathrm{e}^{i(\chi_p-\chi_{ps})}\}\,J_1(kb\sin\theta)b\mathrm{d}b.\end{aligned} \tag{2.28}$$

Taking $\chi_{\mathrm{Cs}} = 0$ as before, the first term is just that obtained for $B(\theta)$ neglecting electromagnetic spin-orbit forces whilst the second term can be evaluated by numerical integration. The last term, using the above approximation can be shown to equal

$$i\,\frac{\hbar^2(2\mu-T)}{4m^2c^2}\,k^2A_{\mathrm{p}}(\theta)\sin\theta, \tag{2.29}$$

which again can be evaluated.

Calculations were made including the electromagnetic spin-orbit force for both 310 MeV and 960 MeV protons. In both cases including such a term increased the differential scattering cross-section by less than 1 % whilst the polarization was changed only slightly as shown in fig. 9. It was considered that such a small change was negligible for the purposes of this analysis and in all further calculations only the nuclear spin-orbit potential was considered.

3. Analysis of the Experimental Results

In this section we shall consider in detail the various sets of experimental results used in the analysis and the best-fit parameters obtained at each energy. However, first we briefly consider the method used in selecting the experimental results to be analysed.

In considering values of the differential cross-section and polarization, results at small angles were rejected if the cross-section was a steeply rising function of angle, as small angular errors could give rise to considerable errors in the final experimental results. Also corrections for the finite angular resolution of the detecting system must be made resulting in further uncertainties in the data. Values at larger angles were rejected if contamination due to inelastic scattering were possible. Whilst at the lower energies a clean separation between elastic and inelastic scattering is possible, at the higher energies this is not so and here results in the small angle region were used. Further the semi-classical approximation is expected to become inaccurate at angles near the first diffraction minimum again limiting the angular region which may be considered.

It was assumed that the total and absorption cross-sections for nucleon-carbon scattering were the same for both incident protons and neutrons. Certainly the experimental data shows that any difference in the two cases must be extremely small. In obtaining values for σ_{a} and σ_{t} graphical interpolation of results at neighbouring energies was used wherever possible. In this way it was hoped to avoid possible systematic errors due to considering one experimental result only.

The analyses for 95, 135, 310 and 970 MeV protons were the most complete, in that a wide range of parameters were considered in obtaining a best-fit. At the other energies a somewhat smaller range of Optical Model parameters were used.

For convenience we have also included in the next section the predictions of the potentials calculated by Ohnuma [10]) from the G.T. and S.M. nucleon-nucleon potentials. These results will, however, be discussed in a separate section, together with other predictions from nucleon-nucleon scattering data.

3.1. 95 MeV PROTONS

In analysing the scattering of 95 MeV protons the values for the differential cross-sections and polarization were taken from the work of Dickson and Salter [22]) in which fairly clear separation between elastic and inelastic scattering was obtained. The value used for the total cross-section was 503±8 mb. For 93.4 MeV neutrons Culler and Waniak [29]) obtained 518±6 mb and at 97.2 MeV, 494±4 mb. De Juren and Knable [30]) for 95 MeV neutrons found a value 498±3 mb. For the absorption cross-section the value 240±15 mb was obtained by graphical interpolation of the results of Voss and Wilson [31]) for neutrons at 55 MeV (276±24 mb) and 105 MeV (234±7 mb) and of Cassels *et al.* [32]) for 134 MeV protons (220±24 mb).

Using these results a best-fit was obtained with the parameters $a_1 = 2.12 \pm 0.04$ fm, $\bar{\sigma} = 39 \pm 1$ mb, $\lambda = 1.50 \pm 0.05$, $C_R = 2.0 \pm 0.1$ (10^{-27}cm^2) and $C_I = 0^{+0.1}_{-0.3}$(10^{-27} cm^2). The normalisation coefficient $N = 1.066$ for a best-fit to the differential cross-section results and the values for the absorption and total cross-sections were $\sigma_a = 295.9$ mb, $\sigma_t = 510.6$ mb. The latter value is in good agreement with the experimental results but the value for σ_a is much too high. The fit obtained to the differential cross-section and polarization results is shown in figs. 1 and 2.

A second analysis was made using as values for $d\sigma/d\Omega$ those obtained by Gerstein *et al.* [33]), the remaining experimental data being as in the first analysis. In this case a best-fit was obtained with the parameters $a_1 = 1.96 \pm 0.08$, $\bar{\sigma} = 38 \pm 2$, $\lambda = 1.5 \pm 0.05$, $C_R = 1.9 \pm 0.1$, $C_I = 0 \pm 0.2$ the units being as before, whilst $N = 0.83$. Again the value $\sigma_t = 490.7$ mb is in good agreement with experiment whilst $\sigma_a = 274.3$ mb is still too large. A better fit to the experimental value could be obtained by either decreasing $\bar{\sigma}$ or a_1 but in both cases it would be difficult to obtain a good fit to the differential cross-section. The relatively large value for a_1 is required to obtain a good fit to the large angle data and attempts to fit the results using a value for a_1 closer to that obtained in electron scattering experiments were unsuccessful.

We have also plotted in fig. 2 the predicted values using potentials calculated by Ohnuma from the G.T. and S.M. phase-shifts. The predicted total cross-sections are 502.3 mb (G.T.) and 547.3 mb (S.M.) the G.T. phase-shifts giving the best agreement with experiment. However, in both cases the absorption cross-sections, 262.2 mb (G.T.) and 272.7 mb (S.M.), are too high when compared with experimental values.

The fact that at his energy the Optical Model seems consistently to predict too high a value for the absorption cross-section would make a further experimental determination desirable. It could then be shown whether the cause of the discrepancy lay with the present experimental results or with the Optical Model itself.

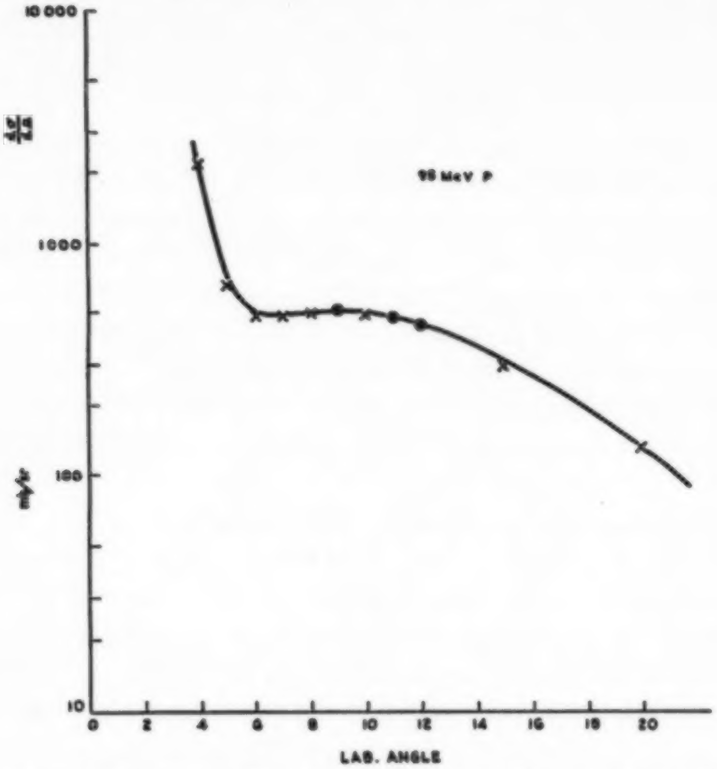

Fig. 1. Differential scattering cross-section for 95 MeV protons. The experimental points have been multiplied by $N = 1.066$. × indicates points used in the analysis.

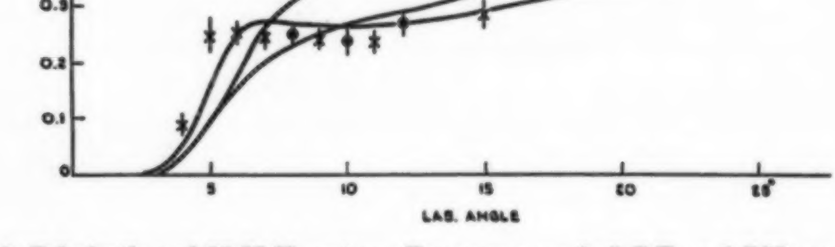

Fig. 2. Polarization of 95 MeV protons. For curves marked G.T. and S.M. see text.

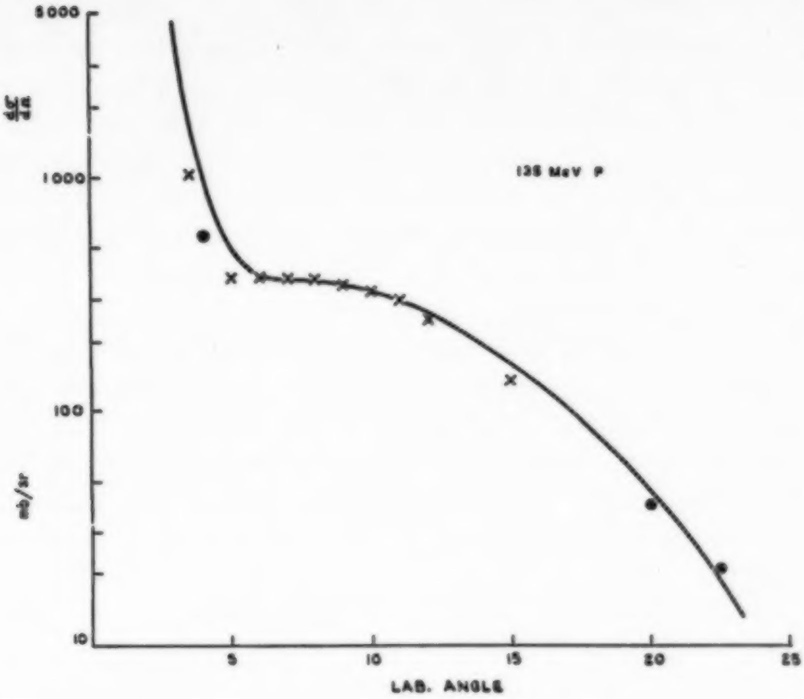

Fig. 3. Differential scattering cross-section for 135 MeV protons. × indicates points used in the analysis.

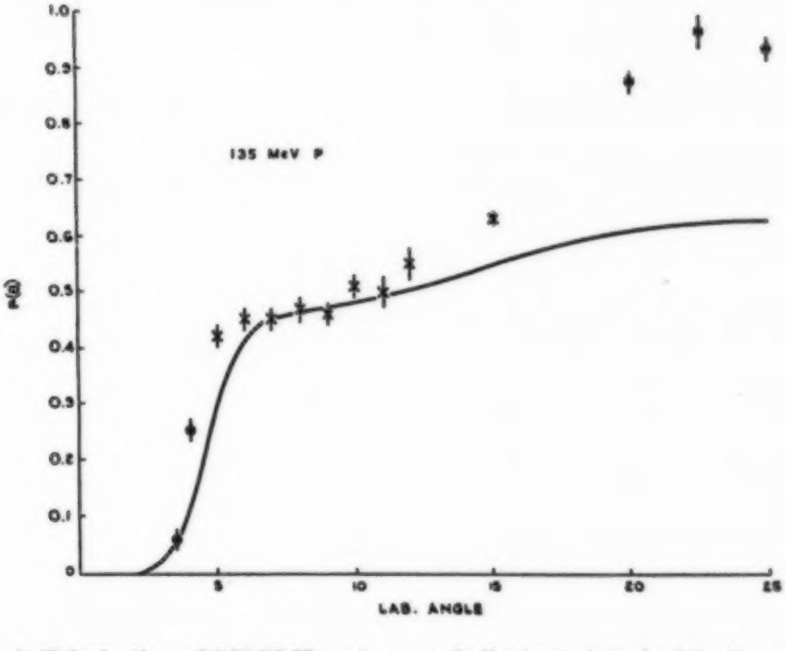

Fig. 4. Polarization of 135 MeV protons. × indicates points used in the analysis.

3.2. 135 MeV PROTONS

For values of the differential cross-section and polarization the data of Dickson and Salter [28]) were used. The absorption cross-section has been measured for 134 MeV protons and 140 MeV neutrons [33]) giving 220±24 mb and 221±9 mb. The value used for this analysis was 221±10 mb. For the total cross-section the value 313±10 mb was used. However, an extrapolation of the results of Taylor and Wood [34]) for 139 and 153 MeV neutrons and of de Juren and Moyer [35]) for 160 and 190 MeV neutrons suggests that this value is too low and that 360±10 mb would be a more reasonable figure.

The best-fit was obtained with parameters $a_1 = 2.04\pm0.04$ fm, $\bar{\sigma} = 30\pm1$ mb, $\lambda = 1.1\pm0.05$, $C_R = 2.5\pm0.1$ (10^{-27} cm^2) and $C_I = 0\pm0.2$ (10^{-27} cm^2) giving $\sigma_a = 243.5$ mb and $\sigma_t = 359.5$ mb. Again as at 95 MeV, the value for σ_a is somewhat too high. The value for $N = 1.06$ was obtained by fitting the data over the full angular range. However, the small angle points are fitted rather better using $N = 1.0$ and this is the value used in fig. 3. The polarization data are ploted in fig. 4.

3.3. 155 MeV NEUTRONS

The asymmetry and differential scattering cross-section for 155 MeV neutrons have been measured by Harding [34]). In converting the measured asymmetry data to values for the polarization we have used the value for the beam polarization given by Harding. It has been suggested by Wilson [16]) that this value may be too low and thus the polarization in scattering from Carbon overestimated. Reducing the polarization would mainly require that the value of C_R be reduced and as we shall see the value obtained by fitting this neutron data is rather larger than that obtained in an analysis of 155 MeV proton scattering data.

For the total cross-section the value of 330±3 mb was obtained by Taylor *et al.* [35]) for 153 MeV neutrons. A graphical fit to experimental values for the absorption cross-section shows little variation with energy in the region considered here and a value $\sigma_a = 221\pm10$ mb was used as at 135 MeV.

A best fit to the experimental data was obtained with the values $a_1 = 2.08\pm 0.05$ fm, $\bar{\sigma} = 28\pm0.5$ mb, $\lambda = 0.8\pm0.05$, $C_R = 3.6\pm0.15$ (10^{-27} cm^2), $C_I = = 0\pm0.4$ (10^{-27} cm^2) requiring $N = 0.62$. This value for N is extremely low indicating that the observed cross-sections are much higher than those calculated using the Optical Model parameters which give a good fit to the polarization data and absorption and total cross-sections.

This difficulty has also been noted by Harding [34]). Wilson [16]) was also unable to fit the neutron differential cross-section results satisfactorily and at the same time fit the experimental results for protons. Cromer (private communication), using an analysis similar to that at 300 MeV [14]) has successfully fitted the neutron and proton data simultaneously. However, he is unable to obtain agreement

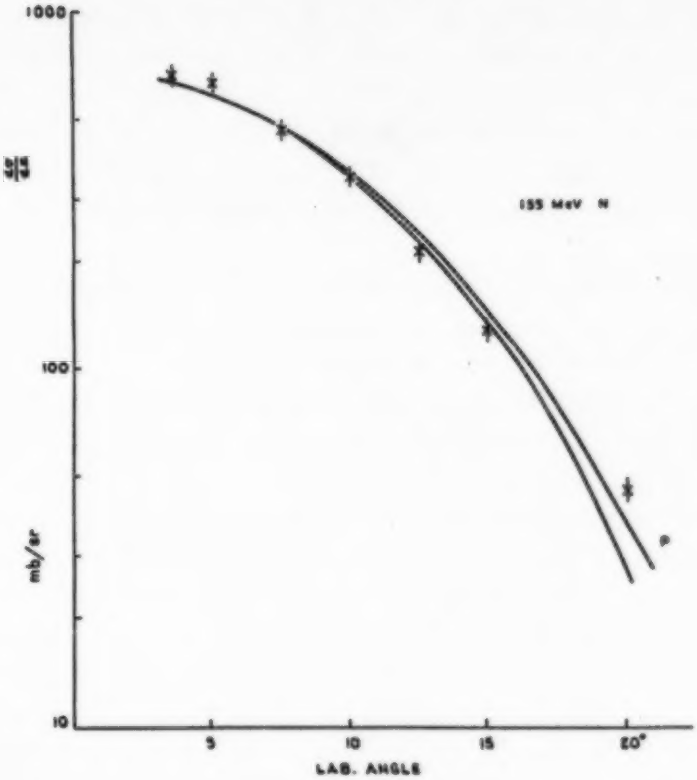

Fig. 5. Differential scattering cross-section for 155 MeV neutrons. The experimental points have been multiplied by $N = 0.62$.
P indicates curve calculated from parameters giving best-fit to proton data.

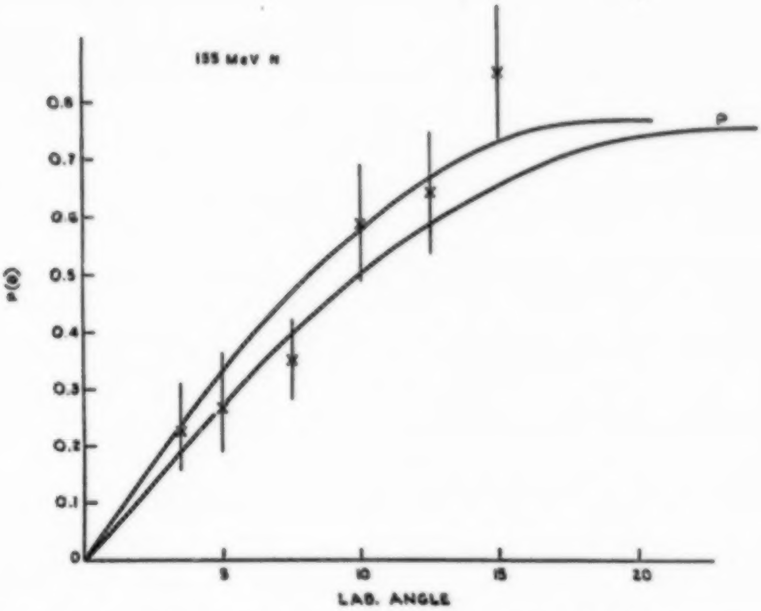

Fig. 6. Polarization of 155 MeV neutrons. P indicates curve calculated from parameters giving best-fit to proton data.

using potentials calculated from nucleon-nucleon scattering potentials 11,12). There is also a large discrepancy between the scattering cross-sections for 155 MeV neutrons 34) and protons 28) at the large angles where effects due to Coulomb scattering should be negligible and hence the cross-sections similar. This is in contradiction to results at 95 and 300 MeV where the agreement is satisfactory within experimental errors. Clearly these points require further investigation.

We also show in figs. 5 and 6 values for the polarization and differential cross-section calculated using the Optical Model parameters which give a good fit to the 155 MeV proton scattering data.

The values for the absorption and total cross-section for the best-fit parameters are $\sigma_a = 235.2$ mb and $\sigma_t = 323.7$ mb in good agreement with experiment.

In fig. 6 we have also plotted values for the polarization calculated with potentials derived from the G.T. and S.M. phase-shifts by Ohnuma 10). The agreement is seen to be best for the S.M. set. The predicted differential cross-section is in both cases in quite good agreement with experiment and requires values of N close to 1. However, whilst the predicted absorption cross-section (238 mb in both cases) is satisfactory the total cross-section for both S.M. and G.T. potentials is far too high. Clearly a set of potentials giving better agreement for σ_t will result in a reduced value for the total elastic cross-section and hence smaller values for N as found here.

3.4. 155 MeV PROTONS

The values of the absorption and total cross-sections were taken to be the same as for 155 MeV neutrons given in the previous section. The polarization data were taken from the work of Alphonce *et al.* 36) who achieved a very clear separation between elastic and inelastic scattering. As no cross-section data are given in their paper, the polarization data together with the absorption and total cross-sections were used to obtain a set of "best-fit" parameters.

These parameters were: $a_1 = 1.96 \pm 0.05$ fm, $\bar{\sigma} = 29 \pm 0.5$ mb, $\lambda = 0.8 \pm 0.1$, $C_R = 2.9 \pm 0.1$ (10^{-27} cm^2), $C_I = 0 \pm 0.4$ (10^{-27} cm^2). The total cross-section given by these values is 325.2 mb and the absorption cross-section 231.9 mb in good agreement with the experimental values.

The fit to the polarization data, however, is not very satisfactory although the trends of the experimental results are qualitatively reproduced. In particular the agreement at the largest angles is most unsatisfactory and whilst probably better agreement could be obtained with the experimental data at small angles, the discrepancy at the larger angles would be worse.

We have also plotted in fig. 7, the predictions from the G.T. and S.M. nucleon-nucleon potentials. The S.M. potential gives quite a good fit to the data but the values from the G.T. potential are clearly too low, in agreement with the neutron data. The absorption and total cross-sections have been discussed in the previous section.

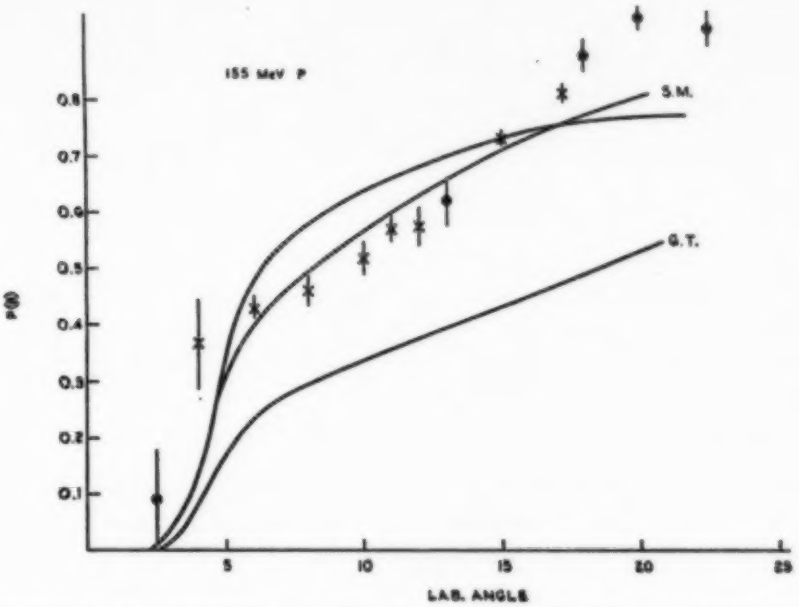

Fig. 7. Polarization of 155 MeV protons. For curves marked G.T. and S.M. see text.

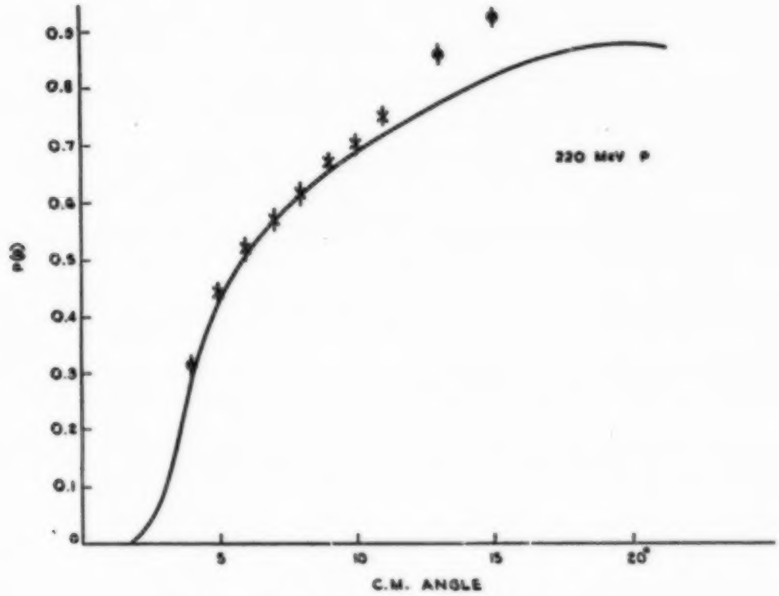

Fig. 8. Polarization of 220 MeV protons.

3.5. 220 MeV PROTONS

As with 155 MeV protons no differential cross-section measurements were available at 220 MeV for determining a set of best-fit parameters. The polarization results (fig. 8) are those of Chesnut *et al.* [37]) who obtained a clean separation between elastic and inelastic scattering. The absorption cross-section seems to be constant over the energy range around 220 MeV, Kirschbaum [38]) obtaining 202±7 mb for 240 MeV protons and 204±12 mb at 180 MeV. A value 203±8 mb was taken. For the total cross-section a value of 291±4 mb was used, this value being obtained by graphical interpolation of the results of de Juren and Moyer [39]) and de Carvalho [40]).

A "best-fit" was obtained using $a_1 = 1.72 \pm 0.1$ fm, $\bar{\sigma} = 28 \pm 0.5$ mb, $\lambda = 0.6 \pm 0.08$, $C_R = 2.1 \pm 0.1$ $(10^{-27}$ $\text{cm}^2)$, $C_I = 0^{+0.1}_{-0.3}(10^{-27}$ $\text{cm}^2)$. These parameters predict $\sigma_a = 206.0$ mb, $\sigma_t = 292.6$ mb in excellent agreement with the experimental value. The fit to the polarization data is good except at the largest angles. Some differential cross-section data which has become available to the author since this work was completed [41]) suggests that the radius should be increased to obtain a good fit to this additional experimental data.

3.6. 310 MeV PROTONS

For values of the differential cross-section and polarization the data of Chamberlain *et al.* [42]) at angles less than 9° was used. The values at angles of 9° and above were part of a separate experiment and a detailed analysis of the

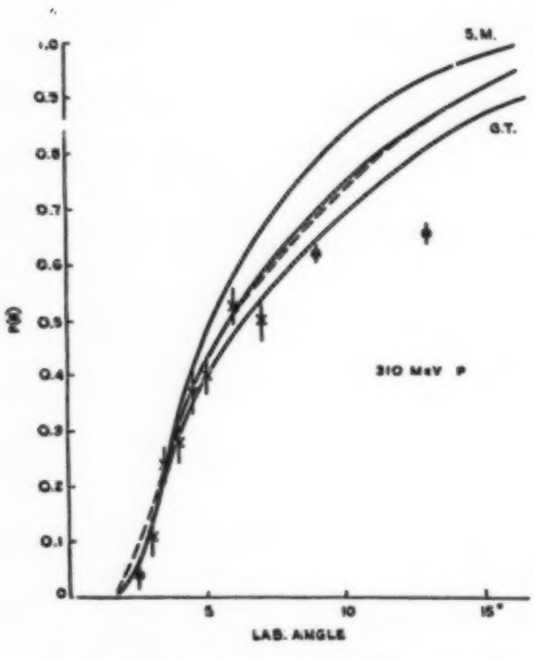

Fig. 9. Polarization of 310 MeV protons. For curves marked G.T. and S.M. see text. × indicates points used in the analysis. – – – shows effect of including electromagnetic spin-orbit term.

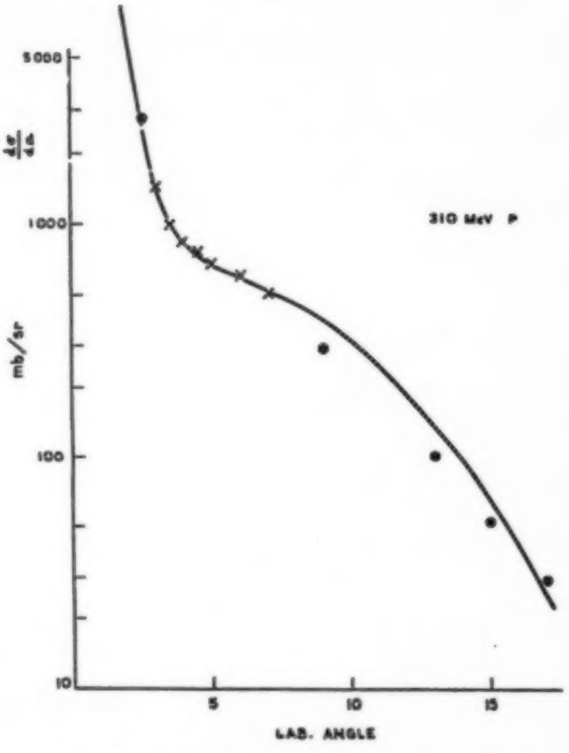

Fig. 10. Differential scattering cross-section for 310 MeV protons. × indicates points used in the analysis. Experimental values have been multiplied by $N = 1.07$.

results shows that the normalization of the large and small angle experiments do not agree. In an analysis which included the point at 9° it was found to be impossible to get a satisfactory fit to the results.

The absorption and total cross-sections are quite well determined at this energy. Graphical interpolation of the results of Kirschbaum [38]) and Millburn *et al.* [42]) gives $\sigma_a = 193 \pm 4.2$ mb. The results of de Juren [43]), Fox *et al.* [44]), Ashmore *et al.* [45]), and de Carvalho [4]) similarly give $\sigma_t = 285 \pm 2$ mb.

A "best-fit" was obtained with the values $a_1 = 1.64^{+0.08}_{-0.07}$ fm, $\bar{\sigma} = 29.5 \pm 0.3$ mb, $\lambda = 0.35 \pm 0.05$, $C_R = 1.7 \pm 0.08 (10^{-27}\ \mathrm{cm}^2)$, $C_I = -0.2 \pm 0.2 (10^{-27} \mathrm{cm}^2)$ and $N = 1.07$. The predicted values for the total and absorption cross-sections are $\sigma_a = 203.1$ mb, $\sigma_t = 282.7$ mb in good agreement with experiment.

The polarization calculations agree well up to 7°, (fig. 9) after which the experimental points fall below the theoretical curve. This may be due to inelastic scattering at these larger angles. For the differential cross-section the theoretical curves lies slightly above the experimental points at the largest angles (fig. 10). If the results do contain inelastic scattering the experimental values should be reduced to give the elastic scattering only, so increasing the discrepancy. In this case using a larger radius would probably improve the fit.

Calculations made with potentials calculated by Ohnuma [10]) for the G. T. and S.M. nucleon-nucleon potentials are shown in fig. 9. The G.T. potential clearly gives a better fit and this is also true for the differential cross-section data. The G.T. potential predicts $\sigma_a = 208.8$ mb, $\sigma_t = 294.5$ mb, the S.M. potential giving $\sigma_a = 208.3$ mb, $\sigma_t = 303.2$ mb, both sets being in good agreement with the experimental data.

3.7. 420 MeV PROTONS

No measurements of the absorption cross-section have been made for Carbon at energies near 420 MeV and the value 210 ± 20 mb used was obtained by graphical interpolation. The total cross-section has been measured for 410 MeV neutrons (46) giving $\sigma_t = 297 \pm 3$ mb. The polarization and differential cross-section data are taken from the paper by Heiberg [47]).

A best-fit to these results was obtained with the parameters $a_1 = 1.64 \pm 0.1$ fm, $\bar{\sigma} = 32 \pm 1$ mb, $\lambda = 0.0 \pm 0.1$, $C_R = 1.4 \pm 0.1$ $(10^{-27}\ \mathrm{cm}^2)$, $C_I = 0 \pm 0.5$ $(10^{-27}\ \mathrm{cm}^2)$ for which $N = 1.44$. The predicted total and absorption cross-sections are 291.0 mb and 212.7 mb respectively, in good agreement with the experimental data.

The shape of the differential cross-section is well reproduced by the above parameters but the large value for $N = 1.44$ indicates a discrepancy in the absolute magnitude. The fact that a good fit has been obtained to the total and absorption cross-sections and hence to the elastic scattering cross-section may indicate that the fault lies with the experimental data. However, this is by no means certain and further data is required to settle this point. Also the fit to the polarization data is most unsatisfactory and this data was neglected in obtaining a final "best-fit". The results of the analysis at this energy must therefore be treated with some caution, but the fact that they lie on reasonably smooth curves through the other parameters found at nearby energies in this paper may show that they are rather more reliable than indicated by the comments above.

3.8. 635 MeV PROTONS

No differential cross-sections for nucleon-complex nuclei scattering have been published at this energy. The polarization in the scattering of 635 MeV protons by beryllium has been measured by Mescheryakov *et al.* [48]). In order to compare this data with calculations made for Carbon the angles at which measurements were made were scaled down by the ratio $9^{\frac{1}{3}}/12^{\frac{1}{3}}$, i.e. (radius Be)/(radius C). For the absorption cross-section the value 220±18 mb was used as obtained by Booth *et al.* [49]) for 765 MeV neutrons. The total cross-section has been measured for 590 MeV neutrons [50]) and 765 MeV neutrons [49]) giving 319±2 mb and 342.1±3.7 mb respectively. The value 320±10 mb was used.

A best fit was obtained using $a_1 = 1.64 \pm 0.1$ fm, $\bar{\sigma} = 39 \pm 2$ mb, $\lambda = -0.2 \pm 0.1$, $C_R = 0.7 \pm 0.1$ (10^{-27} cm^2), $C_1 = 0 \pm 0.5$ (10^{-27} cm^2). The predicted cross-sections are $\sigma_t = 327.3$ mb and $\sigma_a = 235.4$ mb in satisfactory agreement with the experimental data. The fit to the polarization data is also satisfactory

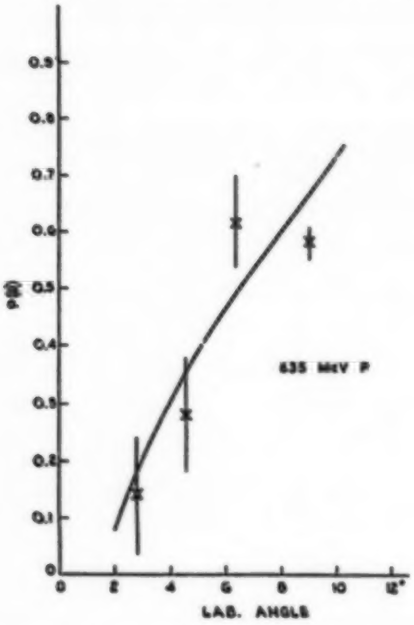

Fig. 11. Polarization of 635 MeV protons.

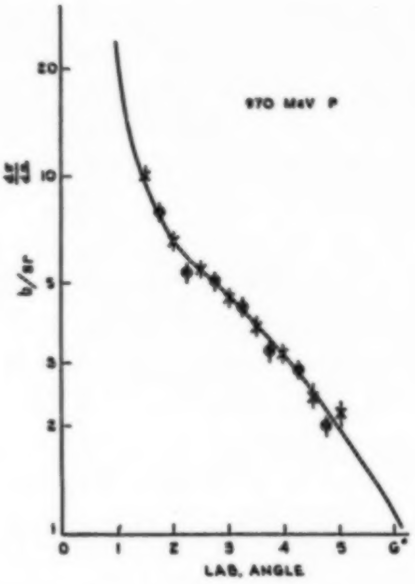

Fig. 12. Differential scattering cross-section for 970 MeV protons. × indicates points used in the analysis. Experimental values have been multiplied by $N = 1.17$.

within the rather large experimental errors (fig. 11). The sign of λ, i.e. the real part of the central nuclear potential is not given by the above analysis. Using $\lambda = 0.2$ would give an identical fit to the total and absorption cross-sections and a similar fit to the polarization data except at the very smallest angles where Coulomb effects are important. Accurate measurements of the differential cross-section at small angles are required to give the sign of λ. In the present analysis the sign has been obtained by interpolation of the parameters at neighbouring energies.

3.9. 970 MeV PROTONS

The differential cross-section for 970 MeV protons has been measured by Batty *et al.* [51]) at small angles (this data has been corrected at the smallest angles for the finite angular resolution used, also for a small error found in the normalization of these results). The total and absorption cross-sections obtained by Law *et al.* [52]) for 910 MeV protons are $\sigma_t = 362.0 \pm 2.4$ mb, $\sigma_a = 241.9 \pm 8.4$ mb and these values were used in this analysis.

The best-fit was given by $a_1 = 1.64^{+0.03}_{-0.05}$, $\bar{\sigma} = 41^{+0.5}_{-1.0}$ mb, $\lambda = -0.4^{+0.06}_{-0.03}$, $C_R = 0.9^{+0.05}_{-0.01}(10^{-27}\ \text{cm}^2)$, $C_I = 0^{+0.2}_{-0.5}(10^{-27}\ \text{cm}^2)$ giving $N = 1.17$ which is rather high when compared with the estimated normalisation error of ±10 %. However, due to the rather complicated method of beam monitoring used, systematic errors may be responsible for the discrepancy. As seen in fig. 12 the shape of the differential scattering cross-section is well reproduced by the above parameters.

The predicted total and absorption cross-sections are 364.7 mb and 241.2 mb in very good agreement with the experimental data.

4. Results of the Analysis

4.1. GENERAL FEATURES

Before discussing some general features of the parameters themselves it seems worthwhile to first comment on the various fits obtained to the experimental results.

The differential cross-section seems to be fitted well at all the energies considered although in one or two cases the normalisation factor deviates considerably from the expected value $N = 1$. These cases have been discussed in detail earlier. The fit to the polarization data seems to be rather better at the higher energies, although the lack of good data at the highest energies considered makes it difficult to say this with certainty. In particular at the lower energies there is great difficulty in fitting the larger angle points where the experimental values for the polarization are very large. The calculated values in general are much smaller than the experimental results. Comparison with results calculated from similar potentials using an exact phase-shift method gives good agreement with the approximate calculations reported here so that the fault is not due to a breakdown in the semi-classical approximation. The use of a large imaginary part to the spin-orbit potential might improve

TABLE 2

Total and absorption cross-sections

Energy (MeV)	Proton or neutron	σ_a calculated (mb)	σ_a experiment (mb)	σ_t calculated (mb)	σ_t experiment (mb)
95	p	295.9	240 ±15	510.6	503 ± 8
95	p	274.3		490.7	
135	p	243.5	221 ±10	359.5	360 ±10
155	n	235.2	221 ±10	323.7	330 ± 3
155	p	231.9		325.2	
220	p	206.0	203 ± 8	292.6	291 ± 4
310	p	203.1	193 ± 4	282.7	285 ± 2
420	p	212.7	210 ±20	291.0	297 ± 3
635	p	235.4	220 ±18	327.3	320 ±10
970	p	241.2	241.9± 8.4	364.7	362.0± 2.4
G.T. potential					
95		262.2	240 ±15	502.3	503 ± 8
155		238.0	221 ±10	411.6	330 ± 3
310		208.8	193 ± 4	294.5	285 ± 2
S.M. potential					
95		272.7	240 ±15	547.3	503 ± 8
155		238.0	221 ±10	444.6	330 ± 3
310		208.3	193 ± 4	303.2	285 ± 2

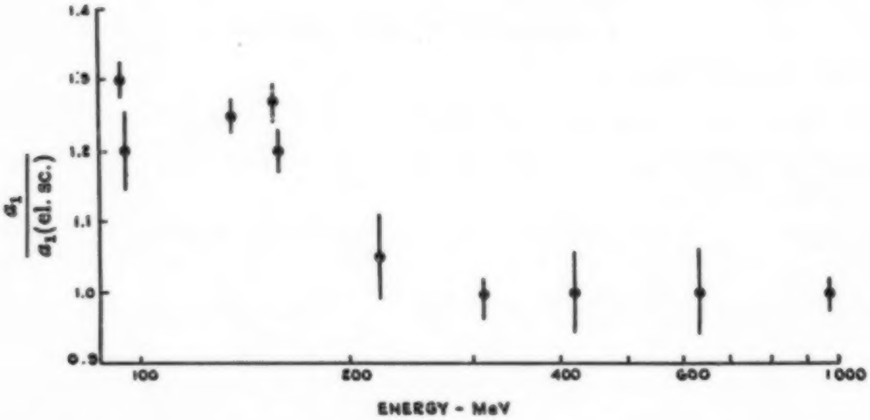

Fig. 13. Ratio of radius to electron-scattering value ($a_1 = 1.635$ fm).

the fit to the polarization results at the larger angles but whether the fits to the differential, total and absorption cross-sections would still be satisfactory is not clear.

In table 2 we show values for the total and absorption cross-sections, calculated using the "best-fit" parameters, compared with the experimental values used. Apart from the calculated absorption cross-section being slightly larger than the measured value at the lowest energies the overall agreement is very good.

In fig. 13 we have plotted the ratio of the best-fit radius parameter to the electron scattering value as a function of energy. The radius is seen to be about 20 % larger than the electron scattering value at 100 MeV but the difference rapidly decreases with increase of energy and between 300 and 400 MeV has disappeared to within the accuracy of the present analysis. However, in connection with the above point it should be remembered that the data suggests that the points at 220 MeV and 310 MeV are low. This variation of the potential radius is also predicted qualitatively by the nucleon-nucleon scattering data and the agreement between the radii found in this work and the calculated values of Kerman *et al.* [18a]) and Cromer [14]) given in table 1 is satisfactory within the limitations mentioned above.

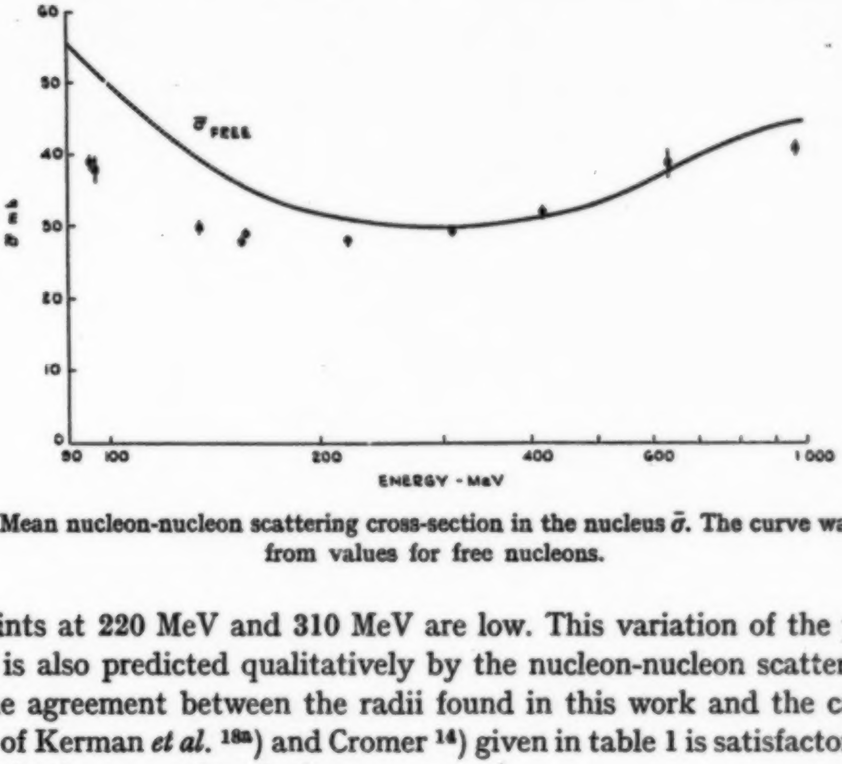

Fig. 14. Mean nucleon-nucleon scattering cross-section in the nucleus $\bar{\sigma}$. The curve was obtained from values for free nucleons.

In fig. 14 we have plotted $\bar{\sigma}$ and also the corresponding free average nucleon-nucleon cross-section as a function of energy. The latter values have been computed from the tables of experimental values given by Hess [52]). $\bar{\sigma}$ is seen to be lower than the free cross-section below 300 MeV but above this energy the two sets of values are very similar. The value of $\bar{\sigma}_{\text{free}}$ for energies above 700 MeV is rather uncertain due to a lack of values for the total n—p cross-section in this energy region. The reduced values for $\bar{\sigma}$ at the lower energies can presumably be explained in terms of the Pauli principle [20]). At the higher energies the effect is much smaller and there are also compensating effects as discussed previously (section 2.1).

TABLE 3

"Best-fit" parameters

Energy (MeV)	Proton or neutron	A_1 (10^{-13} cm)	$\bar{\sigma}$ (mb)	λ	C_R (10^{-27} cm^2)	C_I (10^{-27} cm^2)	V_1 (MeV)	V_2 (MeV)	V_3 (MeV)	V_4 (MeV)
95	p	2.12 ± 0.04	39 ± 1	1.5 ± 0.05	2.0 ± 0.1	$0 \; ^{+0.1}_{-0.3}$	17.0 ± 1.2	11.3 ± 0.7	2.04 ± 0.16	$0 \; ^{+0.1}_{-0.3}$
95	p	1.96 ± 0.08	38 ± 2	1.5 ± 0.05	1.9 ± 0.1	0 ± 0.2	20.9 ± 2.9	14.0 ± 1.9	2.40 ± 0.34	0 ± 0.25
135	p	2.04 ± 0.04	30 ± 1	1.1 ± 0.05	2.5 ± 0.1	0 ± 0.2	12.5 ± 1.0	11.4 ± 0.8	2.12 ± 0.17	0 ± 0.17
155	n	2.08 ± 0.015	28 ± 0.5	0.8 ± 0.05	3.6 ± 0.15	0 ± 0.4	8.5 ± 0.8	10.6 ± 0.8	2.44 ± 0.21	0 ± 0.27
155	p	1.96 ± 0.05	29 ± 0.5	0.8 ± 0.1	2.9 ± 0.1	0 ± 0.4	10.5 ± 0.4	13.1 ± 0.5	2.43 ± 0.13	0 ± 0.34
220	p	1.72 ± 0.10	28 ± 0.5	0.6 ± 0.08	2.3 ± 0.1	$0 \; ^{+0.1}_{-0.3}$	13.0 ± 2.8	21.6 ± 3.8	2.90 ± 0.48	$0 \; ^{+0.12}_{-0.36}$
310	p	$1.64 \; ^{+0.03}_{-0.07}$	29.5 ± 0.3	0.35 ± 0.05	1.7 ± 0.08	-0.2 ± 0.2	$10.5 \; ^{+2.8}_{-2.0}$	$29.9 \; ^{+1.6}_{-3.9}$	$2.68 \; ^{+0.19}_{-0.37}$	-0.32 ± 0.32
420	p	1.64 ± 0.10	32 ± 1	0.0 ± 0.1	1.4 ± 0.1	0 ± 0.5	0.0 ± 3.6	35.7 ± 2.8	2.50 ± 0.26	0 ± 0.9
635	p	1.64 ± 0.10	39 ± 2	-0.2 ± 0.1	0.7 ± 0.1	0 ± 0.5	-9.8 ± 5.2	48.9 ± 9.3	1.75 ± 0.41	0 ± 1.25
970	p	$1.64 \; ^{+0.03}_{-0.05}$	$41 \; ^{+0.5}_{-0.1}$	$-0.4 \; ^{+0.06}_{-0.03}$	$0.9 \; ^{+0.05}_{-0.1}$	$0 \; ^{+0.2}_{-0.5}$	$-22.3 \; ^{+5.9}_{-2.7}$	$55.9 \; ^{+10.0}_{-5.2}$	$2.71 \; ^{+0.49}_{-0.39}$	$0 \; ^{+0.6}_{-1.25}$

4.2. INTEGRATED POTENTIALS

In table 3 we give values for the best-fit parameters a_1, $\bar{\sigma}$, λ, C_R and C_I together also with the potentials V_1, V_2, V_3 and V_4. However, difficulty arises in comparing values obtained over a range of energies in this analysis owing to the varying values used for the potential radius. In comparing this work with that of other authors a further difficulty arises owing to the use of different radial forms for the potential in each analysis.

It has been suggested by Feshbach [53]) and others to overcome this difficulty that it is more appropriate to consider the value of the Optical Model potential integrated over the volume of the nucleus, i.e.

$$I(V) = 4\pi r^2 \int_0^\infty V(r)\mathrm{d}r.$$

This integrated nuclear potential should be rather more independent of the radial form and radius chosen for the potential than V_1, V_2 etc.

In table 4 we show the integrated potential $I(V_1)$, $I(V_2)$ etc. also values found by other workers for comparison. It is easily shown that $I(V_2)$ is proportional to $\bar{\sigma}$ and hence varies in a similar fashion as a function of energy. $I(V_1)$ is seen to decrease with increasing energy becoming negative above about 500 MeV. This is clearly shown in fig. 15 here we have plotted λ, the ratio of the real to the imaginary central nuclear potential i.e. V_1/V_2. The values of λ given in table 4 obtained by other workers are seen to be in reasonable agreement

TABLE 4

Integrated optical model potential

Energy (MeV)	Proton or neutron	$I(V_1)$ (MeV · 10^{-39} cm^3)	$I(V_2)$ (MeV · 10^{-39} cm^3)	$I(V_3)$ (MeV · 10^{-38} cm^3)	$I(V_4)$ (MeV · 10^{-36} cm^3)	Ref.
95	p	2700 ± 110	$1800\pm\ 50$	16.0 ± 1.3	$0\ {}^{+0.8}_{-2.3}$	present work
95	p	2640 ± 160	$1760\pm\ 90$	17.4 ± 2.6	$0\ \pm1.8$	present work
135	p	1780 ± 100	$1620\pm\ 50$	16.0 ± 1.3	$0\ \pm1.3$	present work
155	n	$1280\pm\ 80$	$1590\pm\ 30$	18.8 ± 1.7	$0\ \pm2.1$	present work
155	p	1320 ± 170	$1650\pm\ 30$	17.7 ± 1.0	$0\ \pm2.5$	present work
220	p	1100 ± 145	$1840\pm\ 30$	18.5 ± 3.2	$0\ {}^{+0.9}_{-2.6}$	present work
310	p	770 ± 110	$2200\pm\ 20$	$16.4\ {}^{+1.2}_{-2.4}$	-1.9 ± 1.9	present work
420	p	0 ± 260	$2630\pm\ 80$	15.2 ± 1.8	$0\ \pm5.4$	present work
635	p	$-\ 720\pm360$	3600 ± 180	10.6 ± 2.6	$0\ \pm7.6$	present work
970	p	$-1650\ {}^{+330}_{-130}$	$4110\ {}^{+50}_{-100}$	$16.4\ {}^{+3.0}_{-2.5}$	$0\ {}^{+3.6}_{-9.2}$	present work
310	p	506	2200	19.3		[54])
310	p	605	2310	15.9	-4.9	[12])
310	p	0	2370	7.8	-9.3	[55])
220	p	590	1480	29.8		[37])
155	n	750	1510	25.3		[38])
95	p	2960	2516	21.6	-15.8	[9])
135	p	1924	2960	14.4	-8.6	[9])
310	p	-1332	2368	7.2	-9.3	[9])

with those obtained here. The negative values for the real part at the higher energies have not been found before although several workers have suggested on the basis of nucleon-nucleon data that such an effect would not be unexpected.

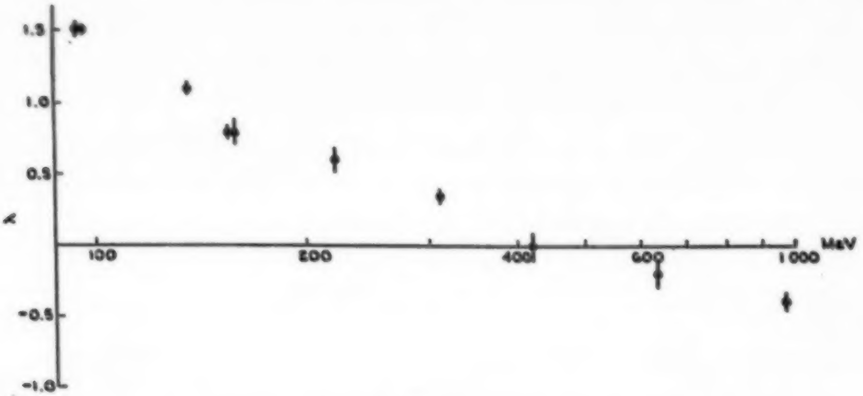

Fig. 15. Ratio of real to imaginary central potential λ.

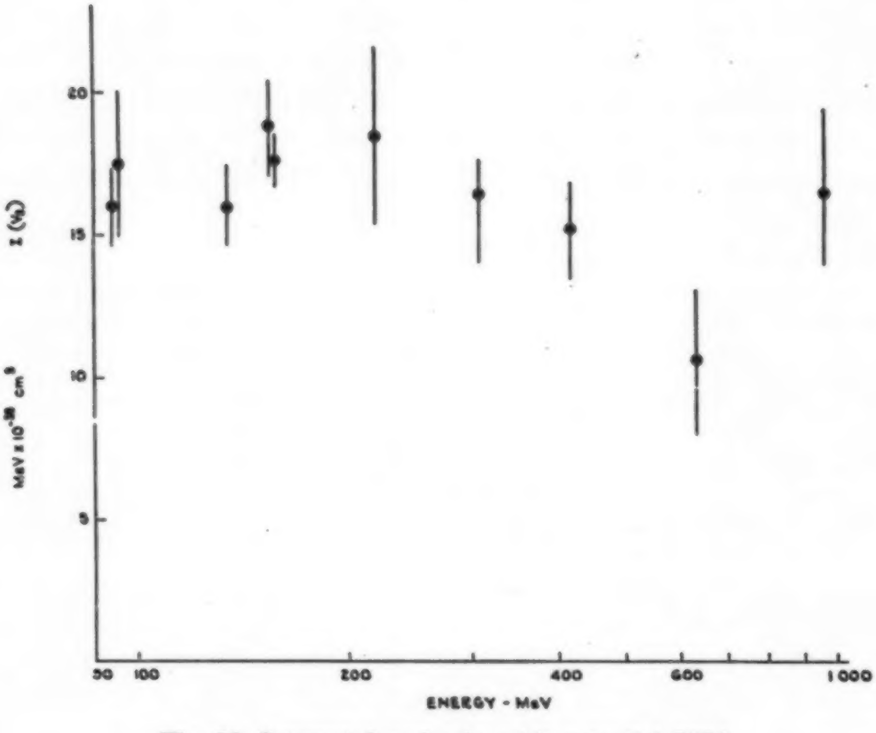

Fig. 16. Integrated real spin orbit potential $I(V_3)$.

From fig. 16 it is seen that $I(V_3)$ is constant over a wide energy range apart from one low point at 635 MeV. However, at this energy the value of C_R could probably be raised, increasing both the polarisation at a given angle and the total cross-section. As neither of these two quantities are well determined the fit to the data would probably not be much worse than the present "best-fit".

$I(V_4)$, as given in table 4 is seen to be small or zero over the whole of the energy range considered. At several energies a small negative value would not give inconsistent results when compared with the experimental data but little further can be said about this parameter.

4.3. COMPARISON WITH OTHER WORK

In table 4 we have also given values for the Integrated Potential calculated from results obtained by several other workers. We have only considered analyses in which a realistic shape for the nuclear potential was used and the nuclear spin-orbit term included. The agreement is seen to be satisfactory particularly when it is considered that in several cases either different methods of analysis of the results for heavier elements have been used. It should also be noted that in some cases the Schrödinger equation has been used and the calculations treated non-relativistically. In general this method gives potentials rather larger than those obtained when relativistic calculations are made.

In some analyses results beyond the first diffraction minimum containing a large inelastic contamination have been used. In general this requires large negative values for the imaginary spin-orbit term to obtain a reasonable fit to the experimental results. This may also be the reason for the negative central potential found by Bjorklund and Fernbach [9]) at high energies.

5. Optical Model Potentials calculated from Nucleon-Nucleon Scattering Data

5.1. G.T. AND S.M. POTENTIALS

In section 3 we have briefly mentioned the fits obtained using the Optical Model potentials calculated by Ohnuma [10]) using the S.M. and G.T. phase-shifts. For the total cross-section the G.T. potential seems to give the best fit to the data at all energies considered although in both cases the total cross-section is too high at 155 MeV. Both the S.M. and G.T. potentials fit the experimental data for the absorption cross-section equally well at all energies although the calculated values are rather high at 95 and 155 MeV (see table 2). For the differential cross-section the best fit at 310 MeV is given by the G.T. potential. At 155 and 95 MeV, however, the predicted cross-sections are much too high. This is due to the very high value of $\bar{\sigma}$ given by the calculations of Ohnuma, at these energies, which do not allow for the effects of the Pauli principle tending to reduce $\bar{\sigma}$. In fact the values for $\bar{\sigma}$ given by Ohnuma are comparable with the free average nucleon-nucleon total cross-section. Reducing the value for $\bar{\sigma}$, and hence V_2 and $I(V_2)$, would decrease the total and absorption cross-sections and give differential cross-section values in better agreement with experimental data. Possibly this would result in the S.M. potential giving the best agreement for σ_s at 95 MeV as it does at present for the polarization data. It should be noted that the change in the polarization is much smaller than changes in the other calculated results when $\bar{\sigma}$ is varied.

It is interesting that the G.T. potential gives consistently the best agreement with the experimental results at 310 MeV. At this energy predictions from the G.T. potential give good agreement with the nucleon-nucleon scattering data. The S.M. potential, which has been mainly used to fit results at lower energies gives rather worse fits to the nucleon-nucleon data at 310 MeV. This suggests that potentials or phase shifts which give a poor fit to nucleon-nucleon data will also give a poor fit to nucleon-nucleus experiments. As the effects of the Pauli principle seem to be small at 310 MeV, as shown in fig. 14, the values of $\bar{\sigma}$ given by Ohnuma's calculations will be more reliable at this energy.

5.2. PHASE-SHIFT ANALYSES AT 310 MeV

The Optical Model potential for the scattering of 310 MeV protons by Carbon has been calculated by Bethe [13]) using the proton-proton phase-shift solutions of Stapp *et al.* [15]) and a special analysis of neutron-proton scattering made by Gammel and Thaler. Using a method in which the experimental data were analysed directly in terms of scattering lengths, Bethe obtained quantitative agreement between the predictions of the nucleon-nucleon and nucleon-nucleus scattering data but was unable to distinguish between the sets of phase-shifts. This analysis has been further extended by Cromer [14]) who has included in the Optical Potential the effect of the angular dependence of the nucleon-nucleon scattering amplitudes. The major effect of including this angular dependence is to give rise to a potential in which the various terms have the same radial shape but different radii.

An examination of the potentials calculated by Bethe shows that solution 6 of Stapp *et al.* gives rise to a potential having a smaller real and much larger imaginary spin orbit potential than that found for the other solutions (1 and 3). It seemed interesting therefore to calculate the differential cross-section, polarization, total and absorption cross-sections and compare these with the

TABLE 5

Value of M for various sets of phase-shifts at 310 MeV

	Solution	M_σ	M_p	M_a	M_t	M	N	σ_a (mb)	σ_t (mb)
Calculations by Bethe	1A	4.57	7.29	12.25	2.89	27.00	1.103	207.7	288.4
	1B	5.21	11.30	6.37	9.92	32.80	1.060	203.6	278.7
	6A	14.35	70.74	1.66	72.25	159.00	1.011	198.4	268.0
	6B	5.34	61.06	2.04	42.25	110.89	0.968	199.0	272.0
Calculations by Cromer	1A	17.57	5.61	87.11	167.70	277.99	1.129	232.2	310.9
	1B	6.16	6.81	62.86	55.50	131.33	1.079	226.3	299.9
	6A	11.12	63.23	66.30	20.25	160.90	1.074	227.2	294.0
	6B	3.85	54.46	62.86	36.60	157.77	1.023	226.3	297.1

experimental data directly. In this way it was hoped to find which set of phase-shifts give an Optical Model potential and hence nucleon-carbon scattering data in best agreement with the experimental results. The calculations were performed using the potentials calculated both by Bethe and by Cromer for solutions 1A, 1C, 6A and 6C. Here we use the same notation for the sets of phase-shift solutions as used by Bethe.

In table 5 we give the values of M (eq. (2.22)) for the various calculations. We also give M_σ, M_p, M_a and M_t where these are the values obtained for M using only the differential cross-section, polarization, absorption and total cross-section respectively. We also give the normalisation parameter and predicted total and absorption cross-sections. The experimental results were those used in section 3.

For the potentials calculated by Bethe, solution 1 is seen to give the best fit to the data. For both solutions 6A and 6B the fit to the polarization and total cross-section is much poorer. Whilst solution 1A gives the lowest value for M, that given by 1B is not much larger and in the latter case the normalisation coefficient is nearer to 1. Hence on the basis of the potentials calculated by Bethe solution 1 of Stapp *et al.* would be preferred.

For the potentials calculated by Cromer solution 1 again gives the best fit to the polarization data and both solutions 1 and 6 give good fits to the differential cross-section data. However, in all cases the calculated total and absorption cross-sections are too large. Calculations in which the radii of the various potentials were varied suggest that an improvement would be obtained if the radius of the imaginary central potential was reduced. However, it is difficult to say more than this without making an extensive analysis of the results using a potential of the type used by Cromer.

It is interesting to note that solution 1 of Stapp *et al.* gives the best fit using the potentials calculated by Bethe. Cziffra *et al.* 56, 57) have made an analysis of proton-proton scattering at 310 MeV in which terms due to the exchange of a single pion have been explicitly included. Using this modified analysis they find that solutions 1 and 2 give the best fit to the nucleon-nucleon data. Solution 6 is found to be extremely unsatisfactory and can be rejected on the basis of their analysis. Solution 6 is also strongly rejected by the experiment of Ashmore *et al.* 58) in which the correlation coefficient C_{Kp} has been measured at 90° c.m. angle. Solution 6 gives a negative value for C_{Kp} whilst the experimental value is positive and in reasonable agreement with the predictions of solutions 1 and 2.

That the set of phase-shifts giving a best fit to the nucleon-nucleon data is that preferred by the above experiments is extremely satisfactory. However, it is rather unsatisfactory that the improved calculations by Cromer do not give such good agreement.

I am indebted to Professor G. E. Brown for many helpful discussions during the course of this work, to Dr. G. H. Stafford and Dr. W. O. Lock for their helpful criticisms during the preparation of the paper and to Dr. K. Parker for the use of his exact phase-shift calculations. I also wish to thank the members of the Applied Mathematics Department of the University of Sheffield for the use of the Ferranti Pegasus Computer and the Department of Scientific and Industrial Research for a Research Fellowship whilst at the University of Birmingham.

References

1) S. Fernbach, R. Serber and T. B. Taylor, Phys. Rev. **75** (1949) 1352
2) C. L. Oxley, W. F. Cartwright and J. Rouvina, Phys. Rev. **93** (1954) 806
3) E. Fermi, Nuovo Cim. **11** (1954) 407
4) S. Fernbach, W. Heckrotte and J. V. Lepore, Phys. Rev. **97** (1955) 1059
5) G. E. Brown, Proc. Phys. Soc. A **70** (1957) 351
6) N. C. Francis, and K. M. Watson, Phys. Rev. **92** (1954) 291
7) W. B. Riesenfeld and K. M. Watson, Phys. Rev. **102** (1956) 1157
8) W. G. Chesnut, E. M. Hafner and A. Roberts, Phys. Rev. **104** (1956) 449
9) F. Bjorklund and S. Fernbach, UCRL Report No. 5028
10) S. Ohnuma, Phys. Rev. **111** (1958) 1173
11) J. L. Gammel and R. M. Thaler, Phys. Rev. **107** (1957) 291, 1337
12) P. S. Signell and R. E. Marshak, Phys. Rev. **106** (1957) 832; Phys. Rev. **109** (1958) 1229
13) H. A. Bethe, Annals of Physics **3** (1958) 190
14) A. Cromer, Phys. Rev. **113** (1959) 1607
15) H. P. Stapp, T. Ypsilantis and N. Metropolis, Phys. Rev. **105** (1957) 302
16) R. Wilson, Phys. Rev. **114** (1959) 260
17) H. McManus and R. M. Thaler, Phys. Rev. **110** (1958) 590
18) A. M. Saperstein and D. Feldman, to be published
18a) A. K. Kerman, H. McManus and R. M. Thaler, Annals of Physics **8** (1959) 551
19) R. H. Lemmer, T. A. J. Maris and Y. C. Tang, Nuclear Physics **12** (1959) 619
20) M. L. Goldberger, Phys. Rev. **74** (1948) 1269
21) R. Glauber, Physica **22** (1956) 1185
22) M. Beg, Phys. Rev. **120** (1960) 1867
23) L. Wolfenstein, Ann. Rev. Nuc. Sci. **6** (1956) 43
24) I. I. Shapiro, Thesis Harvard University (1955)
25) N. F. Mott and H. S. W. Massey, The theory of atomic collisions, 2nd edn. (Clarendon Press, Oxford 1949), p. 48
26) J. H. Fregeau, Phys. Rev. **104** (1956) 225
27) Anderson, Davidson, Glicksman and Kruse, Phys. Rev. **100** (1955) 279
27a) W. Heckrotte, Phys. Rev. **101** (1956) 1406
27b) T. Eriksson, Nuclear Physics **2** (1956) 91
28) J. M. Dickson and D. C. Salter, Nuovo Cim. **6** (1957) 235
29) V. Culler and R. Waniak, Phys. Rev. **99** (1955) 740
30) J. De Juren and N. Knable, Phys. Rev. **77** (1950) 606
31) R. G. P. Voss and R. Wilson, Proc. Roy. Soc. A **236** (1956) 41
32) J. M. Cassels and J. D. Lawson, Proc. Phys. Soc. A **67** (1954) 125
33) G. Gerstein, J. Niederer and K. Strauch, Phys. Rev. **108** (1957) 427
34) R. S. Harding, Phys. Rev. **111** (1958) 1164
35) A. E. Taylor, T. G. Pickavance, J. M. Cassels and T. C. Randle, Phil. Mag. **42** (1950) 751
36) R. Alphonce, A. Johansson and G. Tibell, Nuclear Physics **4** (1957) 672
37) W. G. Chesnut, E. M. Hafner and A. Roberts, Phys. Rev. **104** (1956) 449
38) A. J. Kirschbaum, UCRL Report No. 1967
39) J. De Juren and B. J. Moyer, Phys. Rev. **81** (1951) 919

40) H. G. de Carvalho, Phys. Rev. **96** (1954) 398
41) E. A. Hafner, private communication
42) G. P. Millburn, W. Birnbaum, W. E. Crandall and L. Schechter, Phys. Rev. **95** (1954) 1268
43) J. de Juren, Phys. Rev. **80** (1950) 27
44) R. Fox, C. Leith, L. Wouters and K. R. Mackenzie, Phys. Rev. **80** (1950) 23
45) A. Ashmore, R. G. Jarvis, D. S. Mather and S. K. Sen, Proc. Phys. Soc. A **70** (1957) 745
46) V. A. Nedzel, Phys. Rev. **94** (1954) 174
47) E. Heiberg, Phys. Rev. **106** (1957) 271
48) M. G. Mescheryakov, S. B. Nurushev and G. D. Stoletov, Sov. Phys. JETP **4** (1957) 337
49) N. E. Booth, G. W. Hutchinson and B. Ledley, Proc. Phys. Soc. **71** (1958) 293
50) V. P. Dzhelepov, V. I. Satarov and B. M. Golovin, Sov. Phys. JETP **2** (1956) 349
51) C. J. Batty, W. O. Lock and P. V. March, Proc. Phys. Soc. **73** (1959) 100
52) W. N. Hess, Rev. Mod. Phys. **30** (1958) 368
53) H. Feshbach, Ann. Rev. Nuc. Sci. **8** (1958) 49
54) C. J. Batty, Proc. Phys. Soc. **73** (1959) 185
55) F. Bjorklund, I. Blandford and S. Fernbach, Phys. Rev. **108** (1957) 795
56) P. Cziffra, M. H. MacGregor, M. J. Moravcsik and H. P. Stapp, UCRL Report 8510
57) M. H. MacGregor, M. J. Moravcsik and H. P. Stapp, UCRL Report 5566
58) A. Ashmore, A. N. Diddens and G. B. Huxtable, Proc. Phys. Soc. **73** (1959) 957

1.D.1

Nuclear Physics **23** (1961) 594—611; © *North-Holland Publishing Co., Amsterdam*

Not to be reproduced by photoprint or microfilm without written permission from the publisher

SYMPLECTIC INVARIANTS AND FLOWERS' CLASSIFICATION OF SHELL MODEL STATES

K. HELMERS

II. Institut für Experimentalphysik, Hamburg

Received 8 November 1960

Abstract: Flowers has given a classification of shell model states in *j–j* coupling for a fixed number of nucleons in a shell with respect to a symplectic group. In this paper the relation between these classifications for the various nucleon numbers is studied and is found to be governed by another symplectic group, the transformations of which in general change the nucleon number.

1. Introduction

A classification of shell model states and the group-theoretical definition of "seniority" in *j–j* coupling has been achieved by Flowers [1]) who used the symplectic group † in $2j+1$ dimensions. The states were written as wave functions in configuration space following a general habit in the theory of nuclear spectra. This formalism must necessarily be somewhat clumsy for problems in which states with *different* numbers of particles have to be considered simultaneously. One example for this is the precise definition of the relation between two states $|\alpha\rangle$ and $|\alpha_0\rangle$, where the latter arises from the former by the "omission of all $j^2(J=0)$ nucleon pairs". Such pairs of states occur in the definition of the so-called *pairing property* of nuclear interactions [7–9]). The present author found the relation $|\alpha\rangle \leftrightarrow |\alpha_0\rangle$ and the criteria for pairing property and symplectic invariance [3, 7–9]) much easier to understand in the formalism of second quantization which is especially adapted to changes in the number of particles. Besides this simplification of proofs (which will not be given here as no new results are obtained) the method was found to yield some general theorems on symplectic classification of states that do not seem to have been published previously ††. Flowers, e.g., has studied the reduction of the space of states into irreducible representations of the symplectic group only for $j \leq \frac{7}{2}$, and one would like to know the reduction for general j and by what law the multiplicity is determined with which a given irreducible representation occurs.

The purpose of this paper is to answer these questions by proving the *reduction theorem* of eq. (48). The main difficulties one encounters are a) to identify the type of group generated by the Lie algebra of eq. (45), b) to expand the character χ defined in section 6 in terms of primitive characters.

---

† A more familiar but lengthier nomenclature would be "group of linear homogeneous canonical transformations".

†† See note added in proof at the end of this paper.

For *integer* $j = l$ (L–S coupling) similar results may be expected to hold.

The following section is concerned with notation and definitions in the formalism of field theory. In section 3, we examine the structure of the unit tensor operators u_{kq} with odd k that generate the Flowers group. They are found to be composed of bilinear skew-symmetric forms in $4t+2$ dimensions (t = isospin of the nucleon). Section 4 gives infinitesimal generators of the symplectic group especially suitable for our purposes, together with their commutation relations. The primitive characters of the group are also reproduced. In section 5, the bilinear symplectic invariants are found to constitute the Lie algebra of a new symplectic group which might be called the "commutator group" of Flowers' symplectic group. After these preparations, the reduction theorem is proved (see appendix) and discussed (section 6). Finally, in section 7, we transcribe the seniority operator into our formalism and point out its connection with Flowers' symplectic Casimir operator (eq. (59)). The sum of the latter and of the Casimir operator of the new symplectic group is found to be constant.

2. Notation and Definitions

We essentially adopt the notation of ref. [3]) and consider the $2j+1$ one-particle states

$$\psi_m(\mathbf{r}, \sigma), \quad (m = -j, \ldots, j-1, j), \tag{1}$$

of a nuclear shell with half odd integer angular momentum j. Here, m is the magnetic quantum number, $\mathbf{r}$ is the position, and σ the spin variable (with possible values $\pm\frac{1}{2}$) of the particle. If we restrict ourselves to nucleons of one kind only (say neutrons), we can pass to the formalism of field theory by associating a hermitean conjugate pair $a_m{}^\dagger$, a_m of creation and annihilation operators, respectively, with each state ψ_m. These operators are required to satisfy the usual anticommutation relations and can be used to build up all many-particle states in the shell (allowed by the exclusion principle) from the (normalized) "vacuum" state $|0\rangle$ with no particles. Indeed the allowed states are linear combinations of the following basic ones:

$$|0\rangle, \quad a^\dagger_m|0\rangle, \quad a^\dagger_{m_1}a^\dagger_{m_2}|0\rangle, \quad a^\dagger_{m_1}a^\dagger_{m_2}a^\dagger_{m_3}|0\rangle, \ldots, \tag{2}$$

the number N of particles (which equals the number of $a^\dagger$'s) increasing from left to right from its minimum value $N = 0$ in the vacuum state to its maximum value $N = 2j+1$ in the "filled shell" state

$$a^\dagger_{-j} \ldots a^\dagger_{j-1}a_j{}^\dagger|0\rangle. \tag{3}$$

The space of the allowed states spread out by the basic vectors (2) will be called r_0. It comprises all the configurations j^N from $N = 0$ to $N = [j]$, where we have used the abbreviation

$$[x] \equiv 2x+1. \tag{4}$$

If both neutrons and protons are present in the states (1), we have twice as many operators $a^\dagger$, a which will be written as follows:

$$a^\dagger_{m\tau}, a_{m\tau} \quad (m = -j, \ldots, j-1, j; \quad \tau = \pm\tfrac{1}{2}). \tag{5}$$

The value $\tau = +\frac{1}{2}$ of the charge quantum number τ indicates a neutron, and $\tau = -\frac{1}{2}$ a proton. This case of a fermion with isospin $t = \frac{1}{2}$ is the only one of physical importance in nuclei besides the simpler case discussed above (eq. (2)) which amounts to dealing with fermions with isospin $t = 0$.

The theorems we are going to prove, however, hold good also for fermions with *more* than two charge states, i.e. with isospin $t > \frac{1}{2}$. Thus, from reasons of mathematical completeness it would be a pity if we did not consider those cases (being by no means more complicated) along with the physically important ones. The results for the latter are then easily obtained by putting $t = \frac{1}{2}$ or $t = 0$.

Let therefore be t the integer or half odd integer isospin † of the fermion which has then $[t] = 2t+1$ charge states labelled by a charge quantum number τ. The field operators now are, generalizing eq. (5),

$$a^\dagger_{m\tau}, a_{m\tau} \quad (m = -j, \ldots, j-1, j; \quad \tau = -t, \ldots, t-1, t), \tag{6}$$

satisfying the usual relations

$$a^\dagger_{m\tau} a_{m'\tau'} + a_{m'\tau'} a^\dagger_{m\tau} = \delta_{mm'}\delta_{\tau\tau'}, \quad a_{m\tau}a_{m'\tau'} + a_{m'\tau'}a_{m\tau} = 0. \tag{7}$$

The basic states spanning the space r_t of allowed states are

$$|0\rangle, \quad a^\dagger_{m\tau}|0\rangle, \quad a^\dagger_{m_1\tau_1}a^\dagger_{m_2\tau_2}|0\rangle, \quad a^\dagger_{m_1\tau_1}a^\dagger_{m_2\tau_2}a^\dagger_{m_3\tau_3}|0\rangle, \quad \ldots, \tag{8}$$

where the m's are running from $-j$ to j, and the τ's from $-t$ to t. Some of the vectors will vanish on account of the exclusion principle contained in the relations (7), e.g. if $(m_1, \tau_1) = (m_2, \tau_2)$, and from the same reason only vectors with at most $[j][t]$ operators $a^\dagger$ applied to $|0\rangle$ are non-zero. The "filled shell" state is, in generalization of eq. (3):

$$\left(\prod_{m=-j}^{j} \prod_{\tau=-t}^{t} a^\dagger_{m\tau}\right)|0\rangle, \tag{9}$$

and describes $[j][t]$ particles, which can be seen by applying the particle number operator

$$N = \sum_{m=-j}^{j} \sum_{\tau=-t}^{t} a^\dagger_{m\tau}a_{m\tau} \tag{10}$$

to the state vector (9).

---

† This concept has, although denoted here by the same latter t, nothing to do with Flowers' reduced isospin [1]). The latter will not occur explicitly in this paper, so that confusion will not arise.

Next we shall give Flowers' *unitary symplectic transformation operators* [1]), confining ourselves to those in an infinitesimal neighbourhood of the unit operator. They are of the general form [3])

$$U = 1 + \sum_{m=-j}^{j} \sum_{m'=-j}^{j} \varepsilon_{mm'} \sum_{\tau=-t}^{t} a^\dagger_{m\tau} a_{m'\tau}, \tag{11}$$

with infinitesimal complex parameters $\varepsilon_{mm'}$. We define the transformation of an operator A in r_t by

$$A \to UAU^{-1}, \tag{12}$$

and the transformation of a state vector $|\alpha\rangle$ of r_t by

$$|\alpha\rangle \to U|\alpha\rangle. \tag{13}$$

For $A = a_{m\tau}$ we find, from (12), to first order in the $\varepsilon_{mm'}$,

$$a_{m\tau} \to a_{m\tau} - \sum_{m'} \varepsilon_{mm'} a_{m'\tau}, \tag{14}$$

being a linear transformation of the annihilation operators with the same value of the charge index τ among themselves, the transformation coefficients being independent of τ. Analogously for $A = a^\dagger_{m\tau}$,

$$a^\dagger_{m\tau} \to a^\dagger_{m\tau} + \sum_{m'} \varepsilon_{m'm} a^\dagger_{m'\tau}, \tag{15}$$

and from (13) for $|\alpha\rangle = a^\dagger_{m\tau}|0\rangle$,

$$a^\dagger_{m\tau}|0\rangle \to a^\dagger_{m\tau}|0\rangle + \sum_{m'} \varepsilon_{m'm} a^\dagger_{m'\tau}|0\rangle, \tag{16}$$

being a linear charge-independent transformation (contragredient to that in eq. (14)) of the one-particle states, as it should be. In order that this transformation be unitary, the $\varepsilon_{mm'}$ must form an antihermitean matrix:

$$\varepsilon_{mm'} + \varepsilon_{m'm}^* = 0. \tag{17}$$

In order that the transformation (16) be symplectic, the $\varepsilon_{mm'}$ have to satisfy [3])

$$(-)^{j-m}\varepsilon_{mm'} + (-)^{j-m'}\varepsilon_{-m',-m} = 0. \tag{18}$$

From the infinitesimal transformations (11) with conditions (17) and (18) one can construct Flowers' group of finite unitary symplectic transformations usually denoted by USp $(2j+1) \equiv$ USp $([j])$. If

$$(x_{-j}, \ldots, x_{j-1}, x_j) \quad \text{and} \quad (y_{-j}, \ldots, y_{j-1}, y_j) \tag{19}$$

are two sets of variables that are both transformed under USp $([j])$ as

$$(a^\dagger_{-j,\tau}, \ldots, a^\dagger_{j-1,\tau}, a^\dagger_{j,\tau}) \quad (\tau \text{ fixed}), \tag{20}$$

then the hermitean form

$$H(x, y) \equiv \sum_m x_m^* y_m \tag{21}$$

is invariant under USp ([j]) due to the unitary property (eq. (17)), and the skew-symmetric bilinear form

$$S(x, y) \equiv \sum_m (-)^{j-m} x_m y_{-m} \tag{22}$$

is also invariant under USp ([j]) due to the symplectic property (eq. (18)).

3. The Lie Algebra of the Flowers Group

The general element of the Lie algebra of USp ([j]) is in our space r_t represented by the expression (11) with the unit operator omitted,

$$T = \sum_{mm'} \varepsilon_{mm'} \sum_\tau a_{m\tau}^\dagger a_{m'\tau}, \tag{23}$$

where the $\varepsilon_{mm'}$ are now finite complex parameters *restricted by eqs.* (17) *and* (18). If we take, for example,

$$\varepsilon_{mm'} = (-)^{j-m'} \left(\begin{array}{c|cc} k & j & j \\ q & m & -m' \end{array} \right) \qquad (k = 1, 3, \ldots, 2j;\ q = -k, \ldots, k-1, k), \tag{24}$$

which expression[†] satisfies (18) but not (17), T becomes[††]

$$u_{kq} = \sum_{mm'\tau} (-)^{j-m'} \left(\begin{array}{c|cc} k & j & j \\ q & m & -m' \end{array} \right) a_{m\tau}^\dagger a_{m'\tau} \qquad (k \text{ odd}). \tag{25}$$

(17) can then be fulfilled by forming the antihermitean linear combinations

$$u_{kq} - (-)^q u_{k,-q} \quad \text{and} \quad i[u_{kq} + (-)^q u_{k,-q}] \quad (k \text{ odd}). \tag{26}$$

The $(j+1)(2j+1)$ elements of the Lie algebra constructed in this way are known to constitute a linearly independent basis of the latter.

Let us examine the structure of the expressions (25) more closely. Replacing m' by $-m'$ and using the symmetry of the vector coupling coefficient for odd k and the commutation relations (7) we obtain

$$\begin{aligned} u_{kq} = -\tfrac{1}{2} \sum_{mm'} \left(\begin{array}{c|cc} k & j & j \\ q & m & m' \end{array} \right) \sum_\tau \{ & a_{m\tau}^\dagger (-)^{j-m'} a_{-m'\tau} \\ & - (-)^{j-m} a_{-m\tau} a_{m'\tau}^\dagger + (-)^{j-m} \delta_{m',-m} \}, \quad (k \text{ odd}). \end{aligned} \tag{27}$$

The trivial c-number term in the second line is easily evaluated using the orthogonality relations of the vector coupling coefficients, and is found to vanish for odd k. The remaining terms can be written in a more compact form by putting

---

[†] With a more conventional notation 4) for the vector coupling coefficient, the right-hand side would be $(-)^{j-m'}(jjkq|jmj-m')$.

[††] The operators defined by (25) are $[k]^{\frac{1}{2}}$ times the sums $U_q^{(k)}$ of unit tensor operators in ref. 3).

$$a^\dagger_{m\tau} = b_\tau{}^{(m)}, \quad (-)^{j-m} a_{-m\tau} = \bar{b}_\tau{}^{(m)}. \tag{28}$$

Then (27) goes over into

$$u_{kq} = -\tfrac{1}{2} \sum_{mm'} \left(\begin{matrix} k \\ q \end{matrix} \middle| \begin{matrix} j & j \\ m & m' \end{matrix}\right) \sum_\tau (b_\tau{}^{(m)} \bar{b}_\tau{}^{(m')} - \bar{b}_\tau{}^{(m)} b_\tau{}^{(m')}), \quad (k \text{ odd}). \tag{29}$$

For fixed m, we can regard the $b_\tau{}^{(m)}, \bar{b}_\tau{}^{(m)}$ ($\tau = -t, \ldots t$) as one set of $2[t] = 4t+2$ variables $(x_\tau, \bar{x}_\tau)$ such as occurs in the theory [5]) of the symplectic group Sp $(2[t])$ in $2[t]$ dimensions. The sum over τ in eq. (29) is then of the general type

$$B(x, y) \equiv \sum_\tau (x_\tau \bar{y}_\tau - \bar{x}_\tau y_\tau), \tag{30}$$

i.e. the skew-symmetric bilinear form of two cogredient sets of variables $x = (x_\tau; \bar{x}_\tau)$, $y = (y_\tau; \bar{y}_\tau)$ by the invariance of which one defines the symplectic group of linear transformations Sp $(2[t])$. Therefore we can write

$$u_{kq} = -\tfrac{1}{2} \sum_{mm'} \left(\begin{matrix} k \\ q \end{matrix} \middle| \begin{matrix} j & j \\ m & m' \end{matrix}\right) B(b^{(m)}, b^{(m')}), \quad (k \text{ odd}), \tag{31}$$

with

$$b^{(m)} \equiv (b_\tau{}^{(m)}; \bar{b}_\tau{}^{(m)}) \equiv (a^\dagger_{m,-t} \ldots a^\dagger_{mt}; (-)^{j-m} a_{-m,-t} \ldots (-)^{j-m} a_{-m,t}), \tag{32}$$

and we have the following theorem:

Let U be a linear operator in r_t for which U^{-1} exists, and define transformation by U of an operator A by eq. (12). Let U transform each set $b^{(m)}$ of operators linearly among itself, let that transformation by symplectic with respect to the fundamental form (30), and let it be the same for each m. Then u_{kq} is invariant under the transformation U, i.e.

$$U u_{kq} U^{-1} = u_{kq}, \quad \text{or} \quad [U, u_{kq}] = 0 \quad (k \text{ odd}). \tag{33}$$

Furthermore, any element of the Lie algebra eq. (23) and any finite transformation of the Flowers group USp $([j])$ commutes with U.

Examples of such operators U will be given below in section 5.

4. Some Facts about the Symplectic Group

For the reader's convenience we reproduce here the commutation relations of the infinitesimal generators characteristic for the symplectic group Sp $(2n)$ and the primitive characters of the unitary symplectic group USp $(2n)$.

4.1. INFINITESIMAL GENERATORS AND THEIR COMMUTATION RELATIONS

We consider a vector space of even dimension $2n$, and take the skew-symmetric bilinear form $B(x, y)$ of any two vectors

$$\begin{aligned} x &\equiv (x_{-n} \dots x_{-2} x_{-1}, x_1 x_2 \dots x_n), \\ y &\equiv (y_{-n} \dots y_{-2} y_{-1}, y_1 y_2 \dots y_n), \end{aligned} \tag{34}$$

by the invariance of which the group Sp $(2n)$ is defined, to be

$$B(x, y) = \sum_{\nu=1}^{n} (x_\nu y_{-\nu} - x_{-\nu} y_\nu) \tag{35}$$

(cf. eq. (30)). It is easily verified that any symplectic transformation in an infinitesimal neighbourhood of the unit transformation has a matrix of the following form:

$$S = 1 + \sum_{\rho=1}^{n} \sum_{\sigma=1}^{n} \varepsilon^{(1)}_{\rho\sigma} p_{\rho\sigma} + \sum_{\rho=1}^{n} \sum_{\sigma=\rho}^{n} (\varepsilon^{(2)}_{\rho\sigma} q_{\rho\sigma} + \varepsilon^{(3)}_{\rho\sigma} q^{\dagger}_{\rho\sigma}) \tag{36}$$

where the $\varepsilon^{(k)}_{\rho\sigma}$ are arbitrary complex infinitesimal parameters, and $p_{\rho\sigma}$, $q_{\rho\sigma} = q_{\sigma\rho}$, $q^{\dagger}_{\rho\sigma} = q^{\dagger}_{\sigma\rho}$ are the matrices (with $2n$ rows and columns) of the ***infinitesimal generators of*** Sp$(2n)$ in the representation of the group by itself. These matrices are explicitly given by

$$\begin{aligned} (p_{\rho\sigma})_{\alpha\beta} &= \delta_{\alpha\rho}\delta_{\beta\sigma} - \delta_{\alpha,-\sigma}\delta_{\beta,-\rho}, \\ (q_{\rho\sigma})_{\alpha\beta} &= \delta_{\alpha,-\sigma}\delta_{\beta\rho} + \delta_{\alpha,-\rho}\delta_{\beta,\sigma} = (q_{\sigma\rho})_{\alpha\beta}, \\ (q^{\dagger}_{\rho\sigma})_{\alpha\beta} &= \delta_{\alpha\rho}\delta_{\beta,-\sigma} + \delta_{\alpha\sigma}\delta_{\beta,-\rho} = (q^{\dagger}_{\sigma\rho})_{\alpha\beta}, \end{aligned} \tag{37}$$

with possible values $1, 2, \dots n$ for ρ and σ, and possible values $\pm 1, \pm 2, \dots \pm n$ for α and β. From these definitions one finds the following commutation relations:

$$[q_{\rho\sigma}, q_{\rho'\sigma'}] = [q^{\dagger}_{\rho\sigma}, q^{\dagger}_{\rho'\sigma'}] = 0, \tag{38a}$$

$$[q^{\dagger}_{\rho\sigma}, q_{\rho'\sigma'}] = \delta_{\rho\rho'} p_{\sigma\sigma'} + \delta_{\sigma\sigma'} p_{\rho\rho'} + \delta_{\rho\sigma'} p_{\sigma\rho'} + \delta_{\sigma\rho'} p_{\rho\sigma'}, \tag{38b}$$

$$[q_{\rho\sigma}, p_{\rho'\sigma'}] = \delta_{\rho\rho'} q_{\sigma\sigma'} + \delta_{\sigma\rho'} q_{\rho\sigma'}, \tag{38c}$$

$$[q^{\dagger}_{\rho\sigma}, p_{\rho'\sigma'}] = -\delta_{\rho\sigma'} q^{\dagger}_{\sigma\rho'} - \delta_{\sigma\sigma'} q^{\dagger}_{\rho\rho'}, \tag{38d}$$

$$[p_{\rho\sigma}, p_{\rho'\sigma'}] = \delta_{\sigma\rho'} p_{\rho\sigma'} - \delta_{\rho\sigma'} p_{\rho'\sigma}. \tag{38e}$$

Although derived here only for the *self-representation* of Sp$(2n)$, they are known to be valid in any representation of the group.

If we consider the group USp $(2n)$ of those transformations of Sp$(2n)$ that are also ***unitary***, we have to impose restrictions on the parameters $\varepsilon^{(k)}_{\rho\sigma}$ in eq. (36). The infinitesimal generators (37) are, however, ***the same*** for both groups. The commutation relations (38e) are, by the way, characteristic for a general linear group GL(n) or a unitary group U(n) in n dimensions, and these are, therefore, contained as a ***subgroup*** in Sp$(2n)$ or USp$(2n)$, respectively. Our choice of parameters and infinitesimal generators is especially adapted to the occurrence of such a subgroup.

4.2. PRIMITIVE CHARACTERS [8]

Within USp $(2n)$ each matrix is conjugate to a diagonal matrix with diagonal elements

$$\varepsilon_n^{-1}, \ldots, \varepsilon_2^{-1}, \varepsilon_1^{-1}, \varepsilon_1, \varepsilon_2, \ldots, \varepsilon_n, \tag{39}$$

where $|\varepsilon_\nu| = 1$ $(\nu = 1, 2, \ldots n)$. The character (trace) in a representation of USp $(2n)$ need therefore only be given for the representative matrices of these *diagonal* transformations of USp $(2n)$.

The finite-dimensional *irreducible* representations of USp $(2n)$ can be labelled by a set $(f_1, f_2, \ldots f_n)$ of n integers satisfying

$$f_1 \geqq f_2 \geqq \ldots \geqq f_n \geqq 0. \tag{40}$$

The character of USp $(2n)$ in the irreducible representation $(f_1, f_2, \ldots f_n)$ — it is called a "*primitive*" *character* — is, for the above diagonal transformations,

$$\chi_s^{(f_1 f_2 \ldots f_n)}(\varepsilon_1, \varepsilon_2, \ldots \varepsilon_n) = \frac{|s_{1+f_n}(\varepsilon), s_{2+f_{n-1}}(\varepsilon), \ldots s_{n-1+f_2}(\varepsilon), s_{n+f_1}(\varepsilon)|}{|\ s_1(\varepsilon), \quad s_2(\varepsilon), \ldots \quad s_{n-1}(\varepsilon), \quad s_n(\varepsilon)|}, \tag{41}$$

where the abbreviation

$$s_\nu(x) \equiv x^\nu - x^{-\nu} \tag{42}$$

has been used. The right-hand side of (41) is a quotient of two n-rowed determinants. Only the *general* form of the rows has been given; the αth row is obtained by the replacement $\varepsilon \to \varepsilon_\alpha$.

5. Bilinear Symplectic Invariants

The allowed states that make up the space r_t of section 2 may be classified as usual [1]) with respect to Flowers' group USp $([j])$. For a more complete classification we shall make use of "*symplectic invariants*", i.e. operators wich commute with *all* operators of USp $([j])$. Let us first consider those symplectic invariants that are *bilinear* in the sets $(a_{m\tau})$, $(a^\dagger_{m\tau})$. In the simple case $t = 0$ there are *three* of them [3]):

$$\begin{aligned} q\ &= \sum_m (-)^{j-m} a_{-m} a_m (= [j]^{\frac{1}{2}} Q_{00}), \\ q^\dagger &= \sum_m (-)^{j-m} a^\dagger_m a^\dagger_{-m} (= [j]^{\frac{1}{2}} Q^\dagger_{00}), \\ p\ &= \sum_m a^\dagger_m a_m - \tfrac{1}{2}[j] = N - j - \tfrac{1}{2}. \end{aligned} \tag{43}$$

The constant occurring in the definition of p makes this operator symmetrical with respect to interchange of particles and "holes". q and $q^\dagger$ respectively annihilate and generate nucleon pairs with total angular momentum $J = 0$.

It is now remarkable (and indeed initiated the present investigation) that the three operators q, $q^{\dagger}$, p satisfy the same commutation relations as the angular momentum components $2(J_x-iJ_y)$, $2(J_x+iJ_y)$, $2J_z$, viz.

$$[q^{\dagger}, q] = 4p, \quad [q, p] = 2q, \quad [q^{\dagger}, p] = -2q^{\dagger}. \tag{44}$$

They can therefore be used to construct a 3-dimensional rotation group O⁺(3) that commutes with USp ([j]), and the reduction of r_0 into irreducible representations of O⁺(3) × USp ([j]) can be studied.

For $t=\frac{1}{2}$, one has *ten* bilinear symplectic invariants satisfying commutation relations characteristic for a 5-dimensional rotation group O⁺(5), and thus O⁺(5) × USp ([j]) would have to be studied in this case.

For *general* t, there are $(2t+1)(4t+3) = \binom{2[t]+1}{2}$ bilinear symplectic invariants (see eq. (45) below), thus one would expect, from the number of infinitesimal generators alone, a $(2[t]+1)$-dimensional rotation group $\mathrm{O}^+(2[t]+1)$. Fortunately, however, this is not generally true, the correct answer being much simpler:

The bilinear symplectic invariants are the infinitesimal generators of a unitary group $\overline{\mathrm{USp}}$ (2[t]) † in $2[t] = 4t+2$ *dimensions.*

To prove this, we give the bilinear symplectic invariants for general t:

$$\begin{aligned} q(\tau_1\tau_2) &= \sum_m (-)^{j-m} a_{-m\tau_2} a_{m\tau_1} = q(\tau_2\tau_1), \\ q^{\dagger}(\tau_1\tau_2) &= \sum_m (-)^{j-m} a^{\dagger}_{m\tau_1} a^{\dagger}_{-m\tau_2} = q^{\dagger}(\tau_2\tau_1), \\ p(\tau_1\tau_2) &= \sum_m a^{\dagger}_{m\tau_1} a_{m\tau_2} - \tfrac{1}{2}[j]\delta_{\tau_1\tau_2}, \end{aligned} \tag{45}$$

with possible values $-t, \ldots, t-1, t$ for τ_1 and τ_2. The *invariance* of these operators under USp ([j]) if transformed according to eq. (12) is evident from their structure which is the same as in eq. (22). From (7) one obtains the following commutation relations:

$$[q(\tau_1\tau_2), q(\tau'_1\tau'_2)] = [q^{\dagger}(\tau_1\tau_2), q^{\dagger}(\tau'_1\tau'_2)] = 0, \tag{46a}$$

$$\begin{aligned} [q^{\dagger}(\tau_1\tau_2), q(\tau'_1\tau'_2)] = {} & \delta_{\tau_1\tau'_1} p(\tau_2\tau'_2) + \delta_{\tau_2\tau'_2} p(\tau_1\tau'_1) \\ & + \delta_{\tau_1\tau'_2} p(\tau_2\tau'_1) + \delta_{\tau_2\tau'_1} p(\tau_1\tau'_2), \end{aligned} \tag{46b}$$

$$[q(\tau_1\tau_2), p(\tau'_1\tau'_2)] = \delta_{\tau_1\tau'_1} q(\tau_2\tau'_2) + \delta_{\tau_2\tau'_1} q(\tau_1\tau'_2), \tag{46c}$$

$$[q^{\dagger}(\tau_1\tau_2), p(\tau'_1\tau'_2)] = -\delta_{\tau_1\tau'_2} q^{\dagger}(\tau_2\tau'_1) - \delta_{\tau_2\tau'_2} q^{\dagger}(\tau_1\tau'_1), \tag{46d}$$

$$[p(\tau_1\tau_2), p(\tau'_1\tau'_2)] = \delta_{\tau_2\tau'_1} p(\tau_1\tau'_2) - \delta_{\tau_1\tau'_2} p(\tau'_1\tau_2), \tag{46e}$$

which are obviously the same as those in eqs. (38) *for* $n = [t]$. Our invariants have thus been identified as infinitesimal generators of a unitary symplectic group in 2[t] dimensions, q.e.d.

---

† The bar —— is used to distinguish this group from the Flowers group.

It may be shown that each operator U of this group fulfils the premises of the theorem proved at the end of section 3. This gives us a deeper explanation why it is just a *symplectic* group that commutes with the Flowers group.

By a mere incident, the groups $\overline{\mathrm{USp}}\,(2)$ and $\mathrm{O}^+(3)$ have Lie algebras of identical structure, and so have the groups $\overline{\mathrm{USp}}\,(4)$ and $\mathrm{O}^+(5)$. Thus in the physically important cases $t = 0$ and $t = \frac{1}{2}$ we are justified to deal with the *rotation* groups mentioned which may perhaps be advantageous for parentage problems; but in the present context the simplicity of facts and proofs would then be spoiled. There would, e.g., occur *multiple-valued* ("spin") representations of $\mathrm{O}^+(3)$ and $\mathrm{O}^+(5)$, and numerical factors in the theorem of eq. (61) on the Casimir operators. For this reason we prefer to work here with symplectic groups.

6. Classification of States

As any element of USp $([j])$ commutes with any element of $\overline{\mathrm{USp}}\,(2[t])$, we can form the *direct product group* $g = \overline{\mathrm{USp}}(2[t]) \times \mathrm{USp}\,([j])$. Its irreducible representations are the outer products of the irreducible representations of the factor groups, and its primitive characters are the products of the corresponding primitive characters of the factor groups. The basis vectors of an irreducible representation of g can be arranged into a rectangular block as follows:

$$\left.\underbrace{\begin{matrix} v_{11} v_{12} \cdots v_{1r} \\ v_{21} v_{22} \cdots v_{2r} \\ \cdot \quad \cdot \qquad \cdot \\ \cdot \quad \cdot \qquad \cdot \\ \cdot \quad \cdot \qquad \cdot \\ v_{\bar{r}1} v_{\bar{r}2} \cdots v_{\bar{r}r} \end{matrix}}_{\mathrm{USp}\,(2[j])}\right] \overline{\mathrm{USp}}\,(2[t]) \tag{47}$$

in which USp $([j])$ transforms all *rows* irreducibly in the same way, and $\overline{\mathrm{USp}}\,(2[t])$ transforms all *columns* irreducibly in the same way.

The desired classification of the states of r_t the namounts to finding out which irreducible representations of g occur in r_t, and how often. For this purpose we need merely calculate the character χ of g in r_t and expand it in primitive characters[†] $\chi_{\bar{s}}^{(\bar{f}_1, \bar{f}_2, \cdots \bar{f}_{[t]})} \cdot \chi_{s}^{(f_1, f_2, \cdots f_{j+\frac{1}{2}})}$ of g. This is done in the appendix, the result being

$$\chi = \sum_{[t] \geq f_1 \geq f_2 \geq \cdots \geq f_{j+\frac{1}{2}} \geq 0} \chi_{\bar{s}}^{(\bar{f}_1, \bar{f}_2, \cdots \bar{f}_{[t]})} \cdot \chi_{s}^{(f_1, f_2, \cdots f_{j+\frac{1}{2}})}. \tag{48}$$

[†] Here χ_s is given by eq. (41) and refers to USp $([j])$; $\chi_{\bar{s}}$ is the analogous expression for $\overline{\mathrm{USp}}\,(2[t])$.

The set $(\bar{f}_1, \bar{f}_2, \ldots \bar{f}_{[t]})$ is ***uniquely determined by*** $(f_1, f_2, \ldots f_{j+\frac{1}{2}})$, and is most simply found from the latter in a geometrical way (fig. 1): Let $f_1, f_2, \ldots f_{j+\frac{1}{2}}$ denote the lengths of the rows in a Young tableau (upper left part of fig. 1).

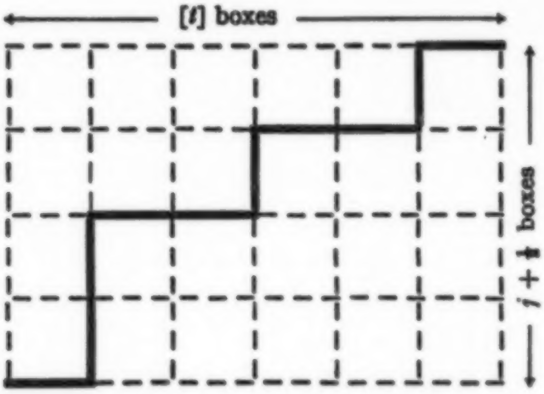

Fig. 1. Definition of the complementary tableau
$t = \frac{5}{2}, j = \frac{7}{2}, (f_1, f_2, f_3, f_4) = (5, 3, 1, 1), (\bar{f}_1, \bar{f}_2, \bar{f}_3, \bar{f}_4, \bar{f}_5, \bar{f}_6) = (4, 3, 3, 2, 2, 0)$.

Draw a rectangular tableau of $j+\frac{1}{2}$ rows and $[t]$ columns as indicated in the figure. Then $\bar{f}_1, \bar{f}_2, \ldots \bar{f}_{[t]}$ are the lengths of the columns (from right to left) in the domain ***complementary*** to the Young tableau, i.e. in the lower right part of fig. 1. This domain becomes an ordinary Young tableau of the representation $(\bar{f}_1, \bar{f}_2, \ldots \bar{f}_{[t]})$ of $\overline{\text{USp}}\,(2[t])$ after a reflection which moves its corner up to the left and interchanges rows and columns. It will then be called the ***complementary tableau*** of the tableau $(f_1, f_2, \ldots f_{j+\frac{1}{2}})$.

We have now to discuss eq. (48). First of all we note that the irreducible representations of g occur in r_t only with multiplicities 0 or 1. The irreducible representations of USp $([j])$ and $\overline{\text{USp}}\,(2[t])$ that are coupled together belong to complementary Young tableaus and are thus in a ***one-to-one correspondence.*** All possible tableaus for USp $([j])$ with at most $[t]$ columns occur, the restriction on the number of columns being of course due to the exclusion principle. Thus for $t = 0$ all possible seniorities occur in r_0, and for $t = \frac{1}{2}$ we have in $r_{\frac{1}{2}}$ all possible combinations of seniority and reduced isobaric spin [1]).

In the case $t = 0$, seniority s corresponds to $(f_1, f_2, \ldots f_{j+\frac{1}{2}}) = (11\ldots10\ldots0)$ with $\sum f_\nu = s$, hence $\bar{f}_1 = j+\frac{1}{2}-s$. The quantum number of the rotation group $\text{O}^+(3)$ isomorphic to $\overline{\text{USp}}\,(2)$ can be shown to be $\frac{1}{2}\bar{f}_1$. The irreducible representation of USp $([j])$ with seniority s thus occurs $2\cdot(\frac{1}{2}\bar{f}_1)+1 = j+\frac{3}{2}-s$ times in r_0, i.e. once for the highest seniority $s = j+\frac{1}{2}$, twice for $s = j-\frac{1}{2}$, etc. For $j \leqq \frac{7}{2}$ this is confirmed by Flowers' tables [1]).

To each term in (48) there corresponds a rectangular block of basis vectors of r_t of type (47). From this it follows: The algebra of symplectic invariants (i.e. operators commuting with USp $([j])$) is (in r_t) the same as the group algebra of $\overline{\mathrm{USp}}\,(2[t])$. More simply expressed, all symplectic invariant operators can be written as polynomials in the *bilinear* invariant operators (45) †. $\overline{\mathrm{USp}}\,(2[t])$ might be called a "commutator group" of $\mathrm{USp}([j])$ in r_t, and vice versa. Well-known examples of such a mutual relationship between two groups are

a) The unitary groups $\mathrm{U}([j])$ (spin-orbit, generators: $\sum_\tau a^\dagger_{m\tau} a_{m'\tau}$) and $\overline{\mathrm{U}}([t])$ (isospin, generators: $p(\tau_1\tau_2)$) in r_t,

b) the corresponding *unimodular* unitary groups $\mathrm{SU}([j])$ and $\mathrm{SU}([t])$ in the subspace $r_t^{(N)}$ of r_t with fixed number N of particles,

c) the unitary group $\mathrm{U}([j])$ (spin-orbit) and the permutation group S_N in the configuration j^N.

In the conventional classification, the states of r_t have not only a definite transformation behaviour ("race") under $\mathrm{USp}\,([j])$, but in addition a definite particle number N and definite isospin and charge quantum numbers T and T_3. Of course we can achieve this in our classification, too, as $\overline{\mathrm{USp}}\,(2[t])$ contains a *subgroup* $\mathrm{O}^+(2)\times\mathrm{O}^+(3)$, with $\mathrm{O}^+(2)$ generated by $\sum_\tau p(\tau\tau) = N - \frac{1}{2}[j][t]$, and $\mathrm{O}^+(3)$ generated by the three operators

$$\sum_{\tau_1\tau_2} \left(\begin{matrix}1\\ \tau\end{matrix}\middle|\begin{matrix}t & t\\ \tau_1 & \tau_2\end{matrix}\right)(-)^{t-\tau_2} p(\tau_1, -\tau_2) \quad (\tau = 0, \pm 1) \tag{49}$$

being essentially the spherical components of the *isospin vector*. The unusual thing with $\overline{\mathrm{USp}}\,(2[t])$ is just that *besides* these, it has generators q, $q^\dagger$ which *change* the number of particles by two units and describe addition or subtraction of $J = 0$ nucleon pairs.

7. The Casimir and Seniority Operators

In the study of "parentage", i.e. the relation between states with different numbers of particles, Racah's *seniority operator* Q plays an important role ††. It is, in our notation,

$$Q = \tfrac{1}{2} \sum_{\tau_1\tau_2} q^\dagger(\tau_1\tau_2)\, q(\tau_1\tau_2). \tag{50}$$

Its expectation value $\langle\alpha|Q|\alpha\rangle$ gives a measure for the number of $J = 0$ pairs in the state $|\alpha\rangle$. For *two-particle* states $|\alpha\rangle$ it can be shown that

$$\langle j^2 JM|Q|j^2 JM\rangle = [j]\delta_{J0} \qquad \text{if} \quad t = 0, \tag{51}$$

$$\langle j^2 JMTT_3|Q|j^2 JMTT_3\rangle = [j]\delta_{J0} \qquad \text{if} \quad t = \tfrac{1}{2}. \tag{52}$$

---

† This result resembles the first main theorem of the theory of invariants 8).

†† See, e.g., Bayman's lectures 6).

The *Casimir operator* of USp ($[j]$) is, in the normalization of Edmonds and Flowers [2, 3]),

$$G(\mathrm{Sp}) = 2 \sum_{k \text{ odd}} \sum_{q} u^{\dagger}_{kq} u_{kq}, \tag{53}$$

where the infinitesimal generators u_{kq} of the group are given by (25). $G(\mathrm{Sp})$ commutes with all of them and hence with the whole group. Its eigenvalue in the irreducible representation $(f_1, f_2, \dots f_{j+\frac{1}{2}})$ of USp($[j]$) is [2, 6])

$$\langle G(\mathrm{Sp})\rangle = \sum_{\nu=1}^{j+\frac{1}{2}} f_\nu (f_\nu + [j] + 2 - 2\nu). \tag{54}$$

The analogously normalized Casimir operator of $\overline{\mathrm{USp}}$ ($2[t]$) can be shown to be

$$G(\overline{\mathrm{Sp}}) = \sum_{\tau_1 \tau_2} \{\tfrac{1}{2} q^{\dagger}(\tau_1\tau_2) q(\tau_1\tau_2) + \tfrac{1}{2} q(\tau_1\tau_2) q^{\dagger}(\tau_1\tau_2) + p^{\dagger}(\tau_1\tau_2) p(\tau_1\tau_2)\}. \tag{55}$$

Its eigenvalues in the irreducible representation $(\bar{f}_1, \bar{f}_2, \dots \bar{f}_{[t]})$ of $\overline{\mathrm{USp}}$ ($2[t]$) are then, from (54):

$$\langle G(\overline{\mathrm{Sp}})\rangle = \sum_{\rho=1}^{[t]} \bar{f}_\rho (\bar{f}_\rho + 2[t] + 2 - 2\rho). \tag{56}$$

Finally, we have for the Casimir operator of the spin-orbit *unitary group* U($[j]$) [1, 3]):

$$G(\mathrm{U}) = \sum_{k=0}^{2j} \sum_{q} u^{\dagger}_{kq} u_{kq}, \tag{57}$$

where the u_{kq} are given by (25), for all k.

There are two interesting relations in r_t between the operators so defined. They will now be given. From the definition (57) and the commutation relations (7) we find

$$G(\mathrm{U}) = \tfrac{1}{4}[j]^2[t] + [t]N - \sum_{\tau_1 \tau_2} p^{\dagger}(\tau_1\tau_2) p(\tau_1\tau_2), \tag{58}$$

and from (53) and (7):

$$G(\mathrm{Sp}) = G(\mathrm{U}) + N - 2Q, \tag{59}$$

which is *the first of the desired relations*. Furthermore, the expression (55) for $G(\overline{\mathrm{Sp}})$ can with the help of (46b) be rewritten as follows:

$$G(\overline{\mathrm{Sp}}) = 2Q + \sum_{\tau_1 \tau_2} p^{\dagger}(\tau_1\tau_2) p(\tau_1\tau_2) + (1 + [t])(-N + \tfrac{1}{2}[j][t]). \tag{60}$$

The *second relation* is then obtained by adding eqs. (59) and (60), taking (58) into account:

$$G(\mathrm{Sp}) + G(\overline{\mathrm{Sp}}) = \tfrac{1}{2}[j][t](1 + \tfrac{1}{2}[j] + [t]), \tag{61}$$

i.e. the sum of the Casimir operators of USp ($[j]$) and its commutator group in

r_t is *a multiple of the unit operator*. The relation is perfectly *symmetrical* in both groups, as $[j]$ and $2[t]$ are the respective dimensionalities. Its correctness may be checked by considering any subspace of r_t defined by a block of basis vectors as in (47), replacing $G(\mathrm{Sp})$ and $\overline{G(}\mathrm{Sp})$ on the left-hand side of (61) by their eigenvalues (54) and (56), with $(\bar{f}_1, \bar{f}_2, \ldots \bar{f}_{[t]})$ determined from $(f_1, f_2, \ldots f_{j+\frac{1}{2}})$ as in fig. 1.

Note added in proof: After finishing the manuscript, the author was kindly informed by Dr. Bayman and Dr. Mang that some of the results of this paper have independently been obtained by Anderson, Kerman and Lipkin. I wish to thank Dr. Bayman and Dr. Lipkin for correspondence on this point.

Appendix

EXPANSION OF THE CHARACTER IN TERMS OF PRIMITIVE CHARACTERS

a) *Calculation of the character*

The one-particle states $a^\dagger_{m\tau}|0\rangle$ for fixed τ, when transformed according to eq. (13), give a *self-representation of Flowers' group* USp $([j])$. The set of diagonal transformations from this group mentioned in section 4.2, eq. (39), may therefore be assumed in the form

$$S(\varepsilon_{\frac{1}{2}}, \varepsilon_{\frac{3}{2}}, \ldots \varepsilon_j) = \prod_{m>0} \varepsilon_m{}^{\sum_\tau (a^\dagger_{m\tau}a_{m\tau} - a^\dagger_{-m\tau}a_{-m\tau})} \tag{A.1}$$

in r_t. Here, $|\varepsilon_m| = 1$ for $m = \frac{1}{2}, \frac{3}{2}, \ldots j$.

Furthermore, it is not difficult to see that, for fixed m, the operator set $b^{(m)}$ of eq. (32) gives a *self-representation of* $\overline{\text{USp}}$ $(2[t])$ when transformed according to the law of eq. (12). The set of diagonal transformations from this group may therefore be assumed in the form

$$\bar{S}(\bar{\varepsilon}_{-t}, \ldots \bar{\varepsilon}_{t-1}, \bar{\varepsilon}_t) = \prod_\tau \bar{\varepsilon}_\tau{}^{p(\tau\tau)} = \prod_\tau \bar{\varepsilon}_\tau{}^{\sum_m a^\dagger_{m\tau}a_{m\tau} - j - \frac{1}{2}} \tag{A.2}$$

in r_t. Here, $|\bar{\varepsilon}_\tau| = 1$ for $\tau = -t, \ldots t-1, t$.

The character χ is then the trace of $\bar{S}S$ in r_t. If with each value of (m, τ) we associate a *two-dimensional* space $r^{(m\tau)}$ in which

$$a^\dagger_{m\tau}a_{m\tau} = \begin{pmatrix} 0 & 0 \\ 0 & 1 \end{pmatrix}, \tag{A.3}$$

then r_t is the *outer product* of all these spaces. From (A.1) and (A.2) we see that $G \equiv \bar{S}S \prod_\tau \bar{\varepsilon}_\tau{}^{j+\frac{1}{2}}$ is a product of commuting factors each of which depends on only *one* occupation number operator $a^\dagger_{m\tau}a_{m\tau}$. Thus, to our factorization of r_t into the $r^{(m\tau)}$, there corresponds a representation of G as an *outer product* of 2×2 matrices

$$\varepsilon_{|m|}{}^{a^\dagger_{m\tau}a_{m\tau} \operatorname{sign} m}\, \bar{\varepsilon}_\tau{}^{a^\dagger_{m\tau}a_{m\tau}}, \tag{A.4}$$

the trace of G being the product of the traces

$$1+\varepsilon_{|m|}{}^{\mathrm{sign}\, m}\,\bar{\varepsilon}_\tau \tag{A.5}$$

of these matrices. Hence the desired expression for the character is

$$\chi = \prod_\tau (\bar{\varepsilon}_\tau)^{-t-\frac{1}{2}} \times \prod_{m\tau} (1+\varepsilon_{|m|}{}^{\mathrm{sign}\, m}\,\bar{\varepsilon}_\tau) \;\; = \prod_{m>0} F(\bar{\varepsilon}_{-t}, \dots \bar{\varepsilon}_t; \varepsilon_m), \tag{A.6}$$

with an auxiliary function

$$F(\bar{\varepsilon}_{-t}, \dots \bar{\varepsilon}_t;\, \varepsilon) \equiv \prod_\tau (\bar{\varepsilon}_\tau)^{-1}(1+\varepsilon\bar{\varepsilon}_\tau)(1+\varepsilon^{-1}\bar{\varepsilon}_\tau). \tag{A.7}$$

The following properties of F (which are easily verified from the definition) will be used:

$$F(\bar{\varepsilon}_{-t}, \dots \bar{\varepsilon}_t; -\bar{\varepsilon}_\tau) = 0 \quad \text{for} \quad \tau = -t, \dots t-1, t, \tag{A.8}$$

$$s_k(\varepsilon)F(\bar{\varepsilon}_{-t}, \dots \bar{\varepsilon}_t; \varepsilon) = s_{[t]+k}(\varepsilon) + \sum_{n=1}^{[t]+k-1} B_n{}^{(k)}(\bar{\varepsilon}_{-t}, \dots \bar{\varepsilon}_t)s_n(\varepsilon)\,^\dagger, \tag{A.9}$$

with certain coefficients $B_n{}^{(k)}$ that depend on the $\bar{\varepsilon}$. As a consequence of these equations we have

$$s_{[t]+k}(-\bar{\varepsilon}_\tau) + \sum_{n=1}^{[t]+k-1} B_n{}^{(k)}(\bar{\varepsilon}_{-t}, \dots \bar{\varepsilon}_t)s_n(-\bar{\varepsilon}_\tau) = 0 \quad (\tau = -t, \dots, t-1, t). \tag{A.10}$$

b) *Proof of the expansion formula, eq.* (48)

The primitive characters of USp ($[j]$) are, from (41),

$$\chi_s^{(f_1, f_2, \dots f_{j+\frac{1}{2}})} = \frac{|s_{1+f_{j+\frac{1}{2}}}(\varepsilon),\, s_{2+f_{j-\frac{1}{2}}}(\varepsilon),\, \dots\, s_{j+\frac{1}{2}+f_1}(\varepsilon)|}{|s_1(\varepsilon) \quad ,\, s_2(\varepsilon) \quad ,\, \dots\, s_{j+\frac{1}{2}}(\varepsilon) \quad |}. \tag{A.11}$$

Similarly, the primitive characters of $\overline{\mathrm{USp}}$ ($2[t]$) are

$$\chi_{\bar{s}}^{(\bar{f}_1, \bar{f}_2) \dots \bar{f}_{[t]}} = \frac{|s_{1+\bar{f}_{[t]}}(\bar{\varepsilon}),\, s_{2+\bar{f}_{[t]-1}}(\bar{\varepsilon}),\, \dots\, s_{[t]+\bar{f}_1}(\bar{\varepsilon})\,|}{|s_1(\bar{\varepsilon}) \quad ,\, s_2(\bar{\varepsilon}) \quad ,\, \dots\, s_{[t]}(\bar{\varepsilon}) \quad |}. \tag{A.12}$$

It is found convenient to multiply the expression (A.6) for χ by the $(j+\frac{1}{2})$-rowed determinant in the numerator of (A.11) and by the $[t]$-rowed determinant in the numerator of (A.12), and to absorb $F(\bar{\varepsilon}_{-t}, \dots \bar{\varepsilon}_t; \varepsilon_m)$ into the $(m+\frac{1}{2})$th row of the former. Furthermore, the identity

$$s_k(\bar{\varepsilon}) = (-)^k s_k(-\bar{\varepsilon}) \tag{A.13}$$

---

† For the definition of $s_k(\varepsilon)$, see eq. (42).

is used. Then

$$
\begin{aligned}
&\chi \cdot |s_1(\bar\varepsilon), \dots s_{[t]}(\bar\varepsilon)| \cdot |s_1(\varepsilon), \dots s_{j+\frac12}(\varepsilon)| = \\
&= (-)^{1+2+\dots+[t]}|s_1(-\bar\varepsilon), \dots s_{[t]}(-\bar\varepsilon)| \cdot |s_1(\varepsilon)F(\dots;\varepsilon), \dots s_{j+\frac12}(\varepsilon)F(\dots;\varepsilon)| \\
&= (-)^{1+2+\dots+[t]}\begin{vmatrix} s_1(-\bar\varepsilon), & \dots s_{[t]}(-\bar\varepsilon), & 0 & \dots & 0 \\ s_1(\varepsilon), & \dots s_{[t]}(\varepsilon), & s_1(\varepsilon)F(\dots;\varepsilon), & \dots & s_{j+\frac12}(\varepsilon)F(\dots;\varepsilon)\end{vmatrix}. \qquad \text{(A.14)}
\end{aligned}
$$

In the last step, we have passed to a "big determinant" with $[t]+j+\frac12$ rows and columns, the first $[t]$ rows of which are represented by the first line, and the last $j+\frac12$ rows by the second line, following the convention of section 4.2.

The "big determinant" will now be given a simpler form by subtraction of columns. For this purpose, we express the $s_k F$ by the right-hand side of (A.9). After this, all the sums $\sum_n B_n^{(k)} s_n$ can successively be eliminated by subtraction of columns, starting with the $([t]+1)$st column, then moving to the right up to the last column. After this, we have $s_{[t]+k}(\varepsilon)$ in the place of $s_k(\varepsilon)F(\dots;\varepsilon)$ for $k=1, 2, \dots j+\frac12$. The *upper* part of the $([t]+k)$th column is then no longer zero, but $s_{[t]+k}(-\bar\varepsilon)$, as can be seen from (A.10). Hence

$$
\text{(A.14)} = (-)^{1+2+\dots+[t]}\begin{vmatrix} s_1(-\bar\varepsilon), & s_2(-\bar\varepsilon), & \dots s_{[t]+j+\frac12}(-\bar\varepsilon) \\ s_1(\varepsilon), & s_2(\varepsilon), & \dots s_{[t]+j+\frac12}(\varepsilon)\end{vmatrix}, \qquad \text{(A.15)}
$$

which becomes after expansion of the determinant with respect to the lowest $j+\frac12$ rows, again using (A.13):

$$
\begin{aligned}
\text{(A.14)} = \sum_{[t]+j+\frac12 \geq l_1 > l_2 > \dots > l_{j+\frac12} \geq 1} &|s_{\bar l_{[t]}}(\bar\varepsilon), \dots s_{\bar l_2}(\bar\varepsilon), s_{\bar l_1}(\bar\varepsilon)| \\
&\cdot |s_{l_{j+\frac12}}(\varepsilon), \dots s_{l_2}(\varepsilon), s_{l_1}(\varepsilon)|. \qquad \text{(A.16)}
\end{aligned}
$$

The summation runs over the $l_1, l_2, \dots l_{j+\frac12}$ with the restrictions indicated; the $\bar l_1, \bar l_2, \dots \bar l_{[t]}$ *are uniquely determined from the* l_ν by the requirements

$$
\bar l_1 > \bar l_2 > \dots > \bar l_{[t]}, \qquad \text{(A.17a)}
$$

and

$$
(l_1, l_2, \dots l_{j+\frac12}, \bar l_1, \bar l_2, \dots \bar l_{[t]}) = \text{permutation of } (1, 2, 3, \dots, [t]+j+\tfrac12). \qquad \text{(A.17b)}
$$

With the new summation indices

$$
f_\nu \equiv l_\nu + \nu - j - \tfrac32 \quad (\nu = 1, 2, \dots j+\tfrac12) \qquad \text{(A.18)}
$$

(A.16) becomes, after division by the two determinants on the left-hand side of (A.14), introducing the primitive characters by (A.11), (A.12):

$$
\chi = \sum_{[t] \geq f_1 \geq f_2 \geq \dots \geq f_{j+\frac12} \geq 0} \chi_{\bar s}^{(\bar f_1 \bar f_2 \dots \bar f_{[t]})} \cdot \chi_s^{(f_1 f_2 \dots f_{j+\frac12})}, \qquad \text{(A.19)}
$$

with

$$
\bar f_\rho \equiv \bar l_\rho + \rho - [t] - 1 \quad (\rho = 1, 2, \dots [t]). \qquad \text{(A.20)}
$$

Eq. (A.19) is already *formally* identical with eq. (48) that we wished to prove. Indeed, the proof will be complete if we can show that the relationship between the f_ν and the $\bar{f}_\rho$, which is here given by eqs. (A.17), (A.18), (A.20), is *the same* as the geometrical relationship described in section 6 with the help of fig. 1.

For this purpose, we consider fig. 1 as part of the "triangular diagram" in fig. 2. The l_ν are then, according to (A.18), the lengths of the parts of the first $j+\frac{1}{2}$ rows on the *left* of the heavy line. Similarly, the $\bar{l}_\rho$ are, by (A.20), the lengths of the parts of the last $[t]$ columns *below* the heavy line. The only thing to be proved is then eq. (A.17b). It is certainly true in the special case $f_1 = f_2 = \ldots = f_{j+\frac{1}{2}} = 0$ when the heavy line coincides with the vertical dotted line. Starting from this case, (A.17b) can be proved by induction. Each inductive step consists in increasing *one* of the f_ν by unity. If eq. (A.17b) is true *before* this change, one sees from fig. 2 that it will hold *afterwards*, too.

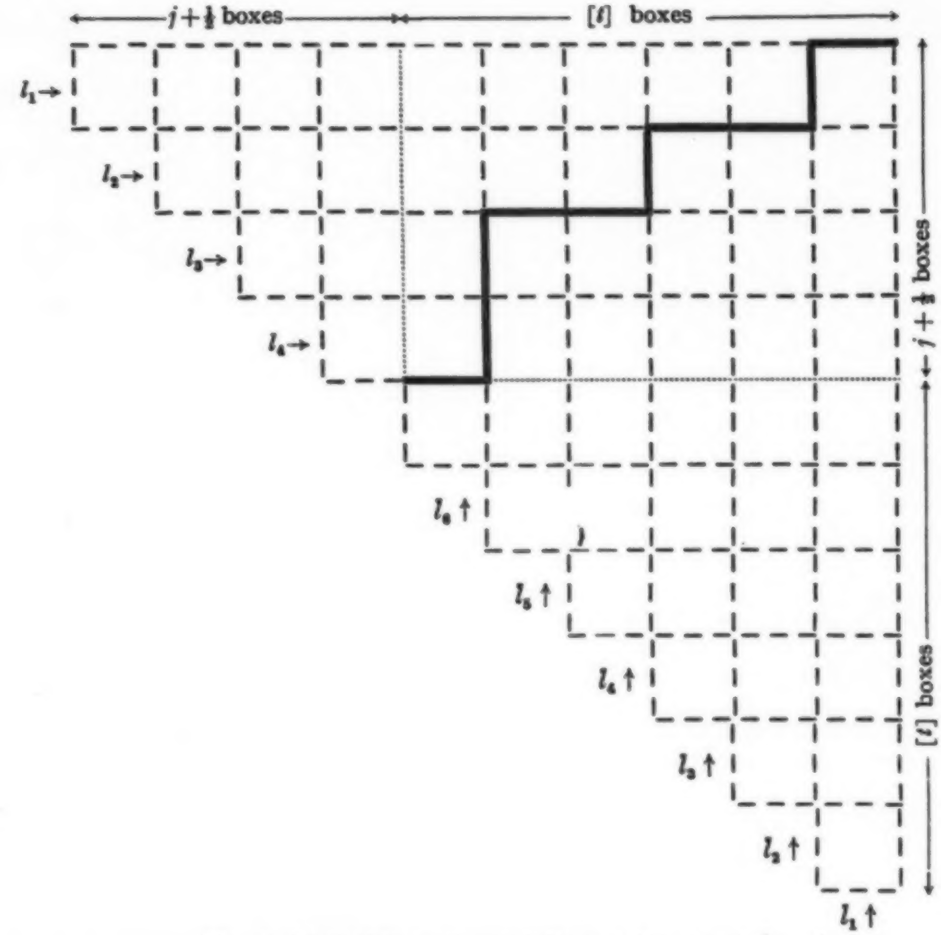
$j+\frac{1}{2}$ boxes
$[t]$ boxes
$l_1 \rightarrow$
$l_2 \rightarrow$
$l_3 \rightarrow$
$l_4 \rightarrow$
$\bar{l}_6 \uparrow$
$\bar{l}_5 \uparrow$
$\bar{l}_4 \uparrow$
$\bar{l}_3 \uparrow$
$\bar{l}_2 \uparrow$
$\bar{l}_1 \uparrow$
$j+\frac{1}{2}$ boxes
$[t]$ boxes

Fig. 2. Geometrical representation of the l_ν and $\bar{l}_\rho$

$t, j, f_\nu, \bar{f}_\rho$ as in fig. 1. $(l_1, l_2, l_3, l_4) = (9, 6, 3, 2)$, $(\bar{l}_1, \bar{l}_2, \bar{l}_3, \bar{l}_4, \bar{l}_5, \bar{l}_6) = (10, 8, 7, 5, 4, 1)$.

References

1) B. H. Flowers, Proc. Roy. Soc. A **212** (1952) 248
2) A. R. Edmonds and B. H. Flowers, Proc. Roy. Soc. A **214** (1952) 515
3) K. Helmers, Nuclear Physics **12** (1959) 647
4) A. R. Edmonds, Angular momentum in quantum mechanics (Princeton University Press, 1957)
5) H. Weyl, The classical groups (Princeton University Press, 1946)
6) B. F. Bayman, Groups and their applications to spectroscopy (Lecture notes, NORDITA, Copenhagen, 1960)
7) G. Racah and I. Talmi, Physica **18** (1952) 1097
8) I. Talmi, Nuclear Physics **16** (1960) 153
9) J. B. French, Nuclear Physics **15** (1960) 393

1.E.6

Nuclear Physics **23** (1961) 612—629; © *North-Holland Publishing Co., Amsterdam*

Not to be reproduced by photoprint or microfilm without written permission from the publisher

THE MOMENT OF INERTIA OF ROTATING NUCLEI

AMNON KATZ
The Weizmann Institute of Science, Rehovoth, Israel †
and
JOHN BLATT
Applied Mathematics Department, University of N.S.W., Sydney, Australia

Received 3 November 1960

Abstract: A method developed for superconductivity and the Meissner effect in refs. 8,9) is applied to the calculation of the rotational moment of inertia of superfluid systems. It is checked that the correct mass is obtained in an analog translational problem. The expressions for the moment of inertia are equivalent to those of A. B. Migdal 7).

1. Introduction

In heavy nuclei far from closed shells, one observes low-lying rotational levels 1), i.e., energies of states J satisfying to a good approximation the formula

$$E_J = \text{constant} + \frac{\hbar^2}{2\mathcal{J}} J(J+1). \tag{1.1}$$

The experimental level spacing determines the "nuclear moment of inertia" $\mathcal{J}$. This quantity may be compared with the "rigid" moment of inertia

$$\mathcal{J}_r = \tfrac{2}{5}MR^2, \tag{1.2}$$

where M is the nuclear mass and R an average nuclear radius. Generally, the experimental moments of inertia are only a fraction of $\mathcal{J}_r$, thereby suggesting that the nuclear system is superfluid.

Belyaev has applied the Bogoliubov 2) methods of the theory of superconductivity to this nuclear problem, with considerable qualitative success. He has deduced a formula for the moment of inertia by applying the Bogoliubov transformation to the Inglis "cranking model" 3,4). The numerical results of Belyaev are in satisfactory agreement with experiment, considering the general qualitative nature of the calculation. Quantitative calculations by Griffin and Rich also yield satisfactory agreement 5).

---

† The research reported in this document has been sponsored in part by the Air Force Office of Scientific Research of the Air Research and Development Command, U. S. Air Force, through its European office.

Nevertheless, there is a difficulty implicit in Belyaev's formula, which has been emphasized recently by Prange [6]). Belyaev's method of derivation can be applied not only to a nucleus in forced rotation, so as to get the moment of inertia $\mathscr{I}$, but also to a nucleus in forced linear translation, so as to get the total *mass* M. In this "pushing model", one transforms to a coordinate system moving with linear velocity V; the Hamiltonian becomes

$$H(V) = H - VP = H - V\sum_{i=1}^{2N} p_i, \tag{1.3}$$

where p_i is the linear momentum of the i^{th} particle, along the direction of the enforced motion, and H is the Hamiltonian in the stationary coordinate system. We use N for the number of pairs, so that the total number of particles is $2N$. Let Ψ be the ground state wave function of H, Ψ' be the ground state of $H(V)$ [†]. Then the total linear momentum of the pushed system is

$$\langle P' \rangle = (\Psi', P\Psi') = MV, \tag{1.4}$$

since $\langle P \rangle = (\Psi, P\Psi) = 0$ if Ψ is the ground state of H. The coefficient M must equal the total mass,

$$M = 2Nm. \tag{1.5}$$

The identity (1.5) is a general consequence of Galilean invariance [4]), not dependent on any specific assumptions about H and Ψ.

However, when Belyaev's method is used to compute the mass M, the result is less than (1.5). This follows from the fact that the Belyaev technique is inconsistent with Galilean invariance, and throws doubt on Belyaev's result for the moment of inertia $\mathscr{I}$.

Migdal [7]) has derived an alternative formula for $\mathscr{I}$, by the use of Green's function techniques. Migdal's technique gives the correct mass M in the pushing model, and his formula for $\mathscr{I}$ differs from Belyaev's formula by correction terms which are numerically small, even though important in principle; thus the agreement with experiment found by Belyaev is maintained in spite of the corrections.

Migdal's derivation is not easy to understand, and he makes a rather restrictive assumption concerning the interaction between particles (δ-function interaction). Thus, although Migdal's results are quite correct, it apperead worth while to construct an alternative and clearer derivation. This is done in the present paper, by the use of methods developed in connection with the theory of superconductity [8, 9]).

[†] There is no need to restrict oneself to the ground state here, but we do so for the sake of simplicity. See ref. [4]) for the pushing and cranking models in statistical mechanics.

The operator for creating a Fermion pair in the quantum state with wave function $\varphi(k, k')$ (k is an arbitrary index here) is

$$b^\dagger = \frac{1}{\sqrt{2}} \sum_{k, k'} \varphi(k, k') a_{k'}^\dagger, a_k^\dagger. \tag{1.6}$$

In the Bogoliubov theory [2]), the pair wave function is restricted to "simple pairs": that is, the one particle states k are paired up, in such a way that to each state k there is assigned a unique "partner" $\tilde{k}$ (usually $\tilde{k}$ is the time-reversed state to k, but this is not necessary). One then assumes the "simple pairing condition":

$$\varphi(k, k') = 0, \quad \text{unless } k' = \tilde{k}. \tag{1.7}$$

Unfortunately, the transformation to a rotating coordinate system destroys the simple pairing; thus, in the rotating coordinate system, it is still possible to write the $2N$-particle wave function Ψ in the form (unnormalized):

$$\Psi = (b^\dagger)^N |0\rangle, \tag{1.8}$$

where N is the number of pairs, and $|0\rangle$ is the vacuum state; but it is *not* possible to insist on the restriction (1.7) on the pair wave function φ.

In ref. [8]), expressions are developed for the expectation values of single-particle and two-particle operators over the wave function (1.8), for an arbitrary pair wave function φ in (1.6). These results are used in ref. [9]) to give a completely gauge-invariant derivation of the Meissner effect, and they are used in this paper to derive an expression for the moment of inertia in the cranking model, consistent with the correct mass in the pushing model[†].

The basic assumptions underlying the calculation are stated in section 2. Section 3 contains the necessary formulas for expectation values, section 4 the verification of the correct mass in the pushing model, section 5 the zero order (no rotation) results, section 6 the change in the pair wave function $\varphi(k, k')$ induced by a small perturbation. The moment of inertia is derived in section 7, and the specialization to Migdal's formula (for a δ-function interaction) is given in an Appendix. Section 8 contains some discussion of the theoretical basis for calculations of this type for nuclei.

2. Basic Assumptions

We assume that the wave function Ψ_N of the ground state of the 2N-particle system of Fermions can be approximated by the (unnormalized) variational trial function

$$\Psi_N = (b^\dagger)^N |0\rangle, \tag{2.1}$$

[†] The pushing model test in moment of inertia calculations is closely related to the gauge-invariance test in superconductivity.

where $b^\dagger$ is given by (1.6), and the pair wave function $\varphi(k, k')$ is antisymmetric and normalized,

$$\varphi(k, k') = -\varphi(k', k), \sum_{k, k'} |\varphi(k, k')|^2 = 1. \tag{2.2}$$

Formula (2.1) means that the system is composed of N pairs, all pairs being in the same quantum state φ, i.e., an extreme Bose-Einstein condensation. The justification for this choice of a trial function is given in earlier work [10]). We propose to determine $\varphi(k, k')$ by minimizing the expectation value

$$\langle H \rangle = \frac{(\Psi, H\Psi)}{(\Psi, \Psi)}, \tag{2.3}$$

where H is the full Hamiltonian. We do *not* assume a "reduced interaction" but retain all matrix elements throughout the calculation. *The "model assumption is an assumption on the trial wave function, not an assumption on the Hamiltonian.*

A slow rotation or translation is a small perturbation which has the form of a sum of single-particle operators. Within the frame-work of our general "model" assumption it is therefore consistent to insist that the new groundstate, in the presence of the perturbation, must still be a Bose-condensed pair state, i.e., the alteration of the Hamiltonian does not lead to breaking up of pairs, but rather leads to a first-order change in the pair wave function $\varphi(kk')$. This is the assumption on which the calculation is based. The transformation to a coordinate system rotating with angular velocity ω about the x-axis replaces the original Hamiltonian H by [4])

$$H(\omega) = H - \omega L_x. \tag{2.4}$$

We determine the new pair wave function

$$\varphi_\omega(k, k') = \varphi(k, k') + \delta\varphi(k, k') \tag{2.5}$$

by minimizing (2.3) for $H(\omega)$; this leads to an integral equation for $\delta\varphi(k, k')$; this integral equation is linear if we restrict ourselves to slow rotations, i.e., keep only terms linear in ω.

The average angular momentum around the axis of rotation is given by

$$L_x(\omega) = \frac{(\Psi(\omega), L_x\Psi(\omega))}{(\Psi(\omega), \Psi(\omega))}, \tag{2.6}$$

and the moment of inertia is defined by

$$\mathscr{J} \equiv \lim_{\omega \to 0} \left[\frac{L_x(\omega)}{\omega}\right]. \tag{2.7}$$

The corresponding formulas for the total mass M in the pushing model are obtained by the replacements in (2.4)—(2.7), of ω by the linear velocity V, and of L_z by the total linear momentum P_z. Unlike the cranking model, however, the integral equations in the pushing model can be solved explicitly and generally.

3. Expressions for Expectation Values

Let Ψ_N be the wave function (2.1), describing N Bose-condensed pairs. Let J be a single-particle operator

$$J = \sum_{k,k'} J_{kk'} a_k{}^\dagger a_{k'}, \tag{3.1}$$

and let K be a two-particle operator

$$K = \sum_{k,l,k'l'} K_{kl,k'l'} a_k{}^\dagger a_l{}^\dagger a_{l'} a_{k'}. \tag{3.2}$$

We define the average values

$$\Omega_N \equiv (\Psi_N, \Psi_N), \tag{3.3}$$

$$J_N \equiv (\Psi_N, J\Psi_N), \tag{3.4}$$

$$K_N \equiv (\Psi_N, K\Psi_N), \tag{3.5}$$

and their generating functions

$$\Omega(v) \equiv \sum_{N=0}^{\infty} \frac{v^N}{(N!)^2} \Omega_N, \tag{3.6}$$

$$J(v) \equiv \sum_{N=0}^{\infty} \frac{v^N}{(N!)^2} J_N, \tag{3.7}$$

$$K(v) \equiv \sum_{N=0}^{\infty} \frac{v^N}{(N!)^2} K_N. \tag{3.8}$$

These definitions differ from the ones of ref. [8]) by an extra factor $N!$ in the denominator. This simplifies the final expressions for (3.6)—(3.8) without loss of generality.

We now quote the necessary results from ref. [8]). We introduce an unnormalized one-particle density matrix ρ by

$$\rho_{kk'} = 2v \sum_{k''} \varphi(k, k'')\varphi^*(k', k''). \tag{3.9}$$

The one-particle matrix $h_{kk'}$ is defined by

$$h_{kk'} = \left(\frac{\rho}{1+\rho}\right)_{kk'} \tag{3.10}$$

and the two-particle operator p by

$$p_{kl,k'l'} = h_{kk'}h_{ll'} - h_{kl'}h_{lk'}. \tag{3.11}$$

We also need the unnormalized wave function $\psi(k, k')$ defined by

$$\psi(k, k') = (2v)^{\frac{1}{2}} \sum_{k''} \left(\frac{1}{1+\rho}\right)_{kk''} \varphi(k'', k'). \tag{3.12}$$

The quantities (3.10)—(3.12) are functions of the parameter v, see (3.9).

Using the techniques of ref. 8) we find the following explicit and exact expressions:

$$\Omega(v) = \exp[\tfrac{1}{2} \operatorname{tr} \ln(1+\rho)], \tag{3.13}$$

$$J(v) = \Omega(v) \operatorname{tr}(hJ), \tag{3.14}$$

$$K(v) = \Omega(v)[\operatorname{tr}_2(pK) + (\psi, K\psi)], \tag{3.15}$$

where tr is a trace over the one-particle space, tr_2 is a trace over the two-particle space, and $(\psi, K\psi)$ is the expectation value of K over the two-particle wave function ψ.

We can recover the values for a given number of pairs N by complex contour integration, e.g.,

$$\Omega_N = \frac{(N!)^2}{2\pi i} \oint \frac{\Omega(v)}{v^{N+1}} \mathrm{d}v, \tag{3.16}$$

where the contour encloses the origin. If N is large, such integrals can be evaluated by the saddle-point method. We then get

$$\langle J \rangle = \frac{J_N}{\Omega_N} = \operatorname{tr}(hJ) + \text{order}\left(\frac{1}{N}\right), \tag{3.17}$$

$$\langle K \rangle = \frac{K_N}{\Omega_N} = \operatorname{tr}_2(pK) + (\psi, K\psi) + \text{order}\left(\frac{1}{N}\right), \tag{3.18}$$

where the parameter v in h, p, and ψ is determined by the condition

$$\operatorname{tr}(h) = 2N. \tag{3.19}$$

We shall use the simplified expressions (3.17)—(3.19) through most of this paper; it is quite possible, however, to find correction terms if N is not very large, by doing the saddle-point evaluation of (3.16) more carefully. For very small N, of course, it is easy to expand (3.13)—(3.15) directly in powers of v.

It should be noted that our $h_{kk'}$ and $\psi(k, k')$ are essentially equal to Migdal's 7) Green's functions G and F, respectively, when the latter are evaluated for equal times.

4. The Total Mass

We shall now check that our procedure gives the correct total mass in the pushing model. The transformation to the moving system changes the Hamiltonian according to eq. (1.3).

We choose the x-space representation for treatment of this problem, and we shall suppress spin indices as being unessential for the present argument. Corresponding to any pair wave function $\varphi(x_1 x_2)$ in the stationary system, we define the pair wave function $\varphi'(x_1 x_2)$ in the moving system by

$$\varphi'(x_1 x_2) \equiv \exp[i\boldsymbol{\varkappa}\cdot(\mathbf{x}_1+\mathbf{x}_2)]\varphi(x_1 x_2), \tag{4.1}$$

where

$$\boldsymbol{\varkappa} = m\mathbf{V}/\hbar. \tag{4.2}$$

It should be noted that (4.1) is a special case of the gauge transformation, eq. (4.2) of reference [9]), provided we select the gauge function $\Lambda(x)$ to be

$$\Lambda(x) = \frac{\hbar c}{e}(\boldsymbol{\varkappa}\cdot\mathbf{x}). \tag{4.3}$$

This shows the close relationship between the pushing model check and the gauge invariance check.

Substitution of (4.1) into the definitions (3.9)—(3.12), and identification of the formal index k with the space coordinate x, yields

$$\langle x|h'|x'\rangle = \exp[i\boldsymbol{\varkappa}\cdot(\mathbf{x}-\mathbf{x}')]\langle x|h|x'\rangle, \tag{4.4}$$

$$\langle x_1 x_2|p'|x'_1 x'_2\rangle = \exp[i\boldsymbol{\varkappa}\cdot(\mathbf{x}_1+\mathbf{x}_2-\mathbf{x}'_1-\mathbf{x}'_2)]\langle x_1 x_2|p|x'_1 x'_2\rangle, \tag{4.5}$$

$$\psi'(x_1 x_2) = \exp[i\boldsymbol{\varkappa}\cdot(\mathbf{x}_1+\mathbf{x}_2)]\psi(x_1 x_2). \tag{4.6}$$

The model Hamiltonian in the stationary system has the form

$$\begin{aligned} H = &\int \psi^\dagger(x)\left[-\frac{\hbar^2}{2m}\nabla_x{}^2+\Phi(x)\right]\psi(x)\mathrm{d}^3x \\ &+\tfrac{1}{2}\iint \psi^\dagger(x_1)\psi^\dagger(x_2)v(x_1x_2)\psi(x_2)\psi(x_1)\mathrm{d}^3x_1\,\mathrm{d}^3x_2, \end{aligned} \tag{4.7}$$

where $\psi(x)$ is the second-quantized wave operator, $\Phi(x)$ is some single-particle potential[†], and $v(x_1, x_2)$ is an arbitrary two-particle interaction. The essential assumptions are:

1) the potentials $\Phi(x)$ and $v(x_1x_2)$ are *local*;
2) the actual mass m appears in the kinetic energy operator.

[†] We include such a term for the sake of generality, since it is often employed in shell model calculations. The exact Hamiltonian in the absence of external fields contains no such term, of course.

We now evaluate the expectation value of H over the wave function of the moving system, by the use of (3.17)—(3.19)[†].
Substitution of (4.5) and (4.6) into (3.18) gives,

$$\begin{aligned}\langle K'\rangle &= \tfrac{1}{2}\iint \mathrm{d}^3x_1\mathrm{d}^3x_2\langle x_1x_2|p'|x_1x_2\rangle v(x_1x_2)\\ &\quad+\tfrac{1}{2}\iint \mathrm{d}^3x_1\mathrm{d}^3x_2|\psi'(x_1x_2)|^2v(x_1x_2)=\langle K\rangle.\end{aligned}\tag{4.8}$$

In the single-particle term (first line of (4.7)), we get

$$\operatorname{tr}(h'\Phi)=\int \mathrm{d}^3x\langle x|h'|x\rangle\Phi(x)=\operatorname{tr}(h\Phi).\tag{4.9}$$

Thus the only term which alters is the kinetic energy. Using (4.4), this can be transformed as follows

$$\begin{aligned}&-\frac{\hbar^2}{2m}\int \mathrm{d}^3x'(\nabla_x{}^2\langle x|h'|x'\rangle)_{x=x'}\\ &=-\frac{\hbar^2}{2m}\int \mathrm{d}^3x'[\nabla_x{}^2\langle x|h|x'\rangle+2i\varkappa\cdot\nabla_x\langle x|h|x'\rangle-\kappa^2\langle x|h|x'\rangle]_{x=x'}.\end{aligned}\tag{4.10}$$

The first term in the square bracket yields the kinetic energy in the stationary system. The second term is proportional to the expectation value of the total linear momentum in the stationary system; this is zero for the ground state. The last term in (4.10) gives an additional kinetic energy equal to

$$\frac{\hbar^2\kappa^2}{2m}\operatorname{tr}(h)=\tfrac{1}{2}mV^2(2N),\tag{4.11}$$

where $2N$ is the number of particles in the system (N is the number of pairs).

We also need the expectation value of the linear momentum P_x over the moving wave function; this is

$$-i\hbar\int \mathrm{d}^3x'(\nabla_x\langle x|h'|x'\rangle)_{x=x'}=-i\hbar\int \mathrm{d}^3x'[i\varkappa\langle x|h|x'\rangle+\nabla_x\langle x|h|x'\rangle]_{x=x'}.\tag{4.12}$$

The second term on the right again vanishes in the ground state, and the first term yields

$$\hbar\varkappa\operatorname{tr}(h)=m\mathbf{V}(2N).\tag{4.13}$$

Combining the results so far, and using (1.3), we get the identity

$$\frac{(\Psi(V),H(V)\Psi(V))}{(\Psi(V),\Psi(V))}=\frac{(\Psi,H\Psi)}{(\Psi,\Psi)}-\tfrac{1}{2}mV^2(2N).\tag{4.14}$$

[†] The exact expressions (3.13)—(3.15) could be used equally well.

Since the additional term, $-NmV^2$, is a constant, independent of the pair wave function $\varphi(x_1 x_2)$ assumed for the stationary system, this term does not affect the minimization of $\langle H\rangle$ or of $\langle H(V)\rangle$. Thus, *if a certain choice of the pair wave function* $\varphi(x_1 x_2)$ *minimizes* $\langle H\rangle$, *then its Galilei transform* $\varphi'(x_1, x_2)$, *equation* (4.1), *minimizes* $\langle H(V)\rangle$; *and the linear momentum in the moving system is given by* (4.13), *i. e., the total mass is correct.*

Since all subsequent equations in this paper are derived from minimization of $\langle H\rangle$, this establishes that our procedure yields the correct linear mass in all cases.

5. Wave Function of the Stationary System

From here on, we employ the methods and results of ref. 9) to carry out the minimization. We shall only quote the necessary equations, referring to ref. 9) for the derivations. We introduce the un-normalized pair wave function $\chi(k, k')$ by

$$\chi(k, k') = (2v)^{\frac{1}{2}}\varphi(k, k') \tag{5.1}$$

and minimize the quantity $\langle H\rangle-\mu\,\mathrm{tr}(h)$ (μ = chemical potential) with respect to the components $\chi(k, k')$, treated as being independently variable. The resulting equation is[†] (M, 5.14) which we repeat here for ready reference. First we define some auxiliary quantities:

$$J_{kk'} = \langle k|-\frac{\hbar^2}{2m}\nabla^2+\Phi|k'\rangle-\mu\delta_{kk'} \tag{5.2}$$

is the single-particle part of the operator $H-\mu N$. Letting $K_{kl,\,k'l'}$ be one half of the matrix element of the interaction between particles, we define

$$L_{kk'} = \sum_{ll'} h_{l'l}(K_{k'l',\,kl}-K_{k'l',\,lk}). \tag{5.3}$$

It should be noted that $L_{kk'}$ involves matrix elements other than those of the "reduced interaction". However, it turns out that the terms involving $L_{kk'}$ are not of qualitative importance. The important terms arise from the quantity

$$\Delta_{kl} = -2\sum_{k'l'} K_{kl,\,k'l'}\varphi(k'l'). \tag{5.4}$$

If the pair wave function obeys the simple pairing condition (1.7), then the matrix elements $K_{kl,\,k'l'} = K_{k\tilde{k},\,k'\tilde{k}'}$ in (5.4) are the ones of the so-called "reduced interaction".

In terms of the quantities defined so far, the minimization equation (M, 5.14) becomes

---

[†] We shall denote ref. 9) by the latter M, for Meissner effect; eq. (M, 5.14) is eq. (5.14) of ref. 9).

$$\sum_{k''} (J_{kk''}+2L_{kk''})\chi(k'', k')-\tfrac{1}{2}\Delta_{kk'}+\tfrac{1}{2}\sum_{l,\, l'} \Delta^*_{ll'}\chi(l, k)\chi(l', k') = 0. \tag{5.5}$$

Following Belyaev [2]) and Migdal [7]), we now *assume* that the stationary system permits simple pairing, i.e., that there exists a set of single-particle states k with a unique pairing $k \leftrightarrow \tilde{k}$ such that the variationally best pair wave function $\varphi(kk')$ has the property

$$\varphi(k, k') = \delta_{k'\tilde{k}}\varphi_k, \quad \varphi_{\tilde{k}} = -\varphi_k. \tag{5.6}$$

This assumption implies

$$\chi(k, k') = \delta_{k'\tilde{k}}\chi_k, \quad \chi_k = (2v)^{\frac{1}{2}}\varphi_k, \tag{5.7}$$

$$\rho_{kk'} = \delta_{kk'}\rho_k, \quad \rho_k = |\chi_k|^2, \tag{5.8}$$

$$h_{kk'} = \delta_{kk'}h_k, \quad h_k = \frac{\rho_k}{1+\rho_k}, \tag{5.9}$$

$$\psi(kk') = \delta_{k'\tilde{k}}\psi_k, \quad \psi_k = -\psi_{\tilde{k}} = \frac{\chi_k}{1+\rho_k}. \tag{5.10}$$

We also *assume* that the quantity

$$J_{kk'}+2L_{kk'} \equiv \left\langle k \left| -\frac{\hbar^2}{2m}\nabla^2+\Phi \right| k' \right\rangle -\mu\delta_{kk'}+2L_{kk'} = \xi_k\delta_{kk'} \tag{5.11}$$

is diagonal in the k-representation; ξ_k is defined by (5.11), and is nearly equal to $\varepsilon_k-\mu$, where ε_k is the eigenvalue of the single-particle part of the Hamiltonian. The correction term $2L_{kk'}$ is ignored by Migdal [7]).

Finally, we *assume* that Δ_{kl} also obeys a simple pairing condition

$$\Delta_{kl} = \delta_{k\tilde{l}}\Delta_k. \tag{5.12}$$

It should be noted that the simple pairing assumptions (5.6), (5.11), (5.12) can be proved rigorously for an infinite uniform system; in that case the pairing $k \leftrightarrow \tilde{k}$ connects opposite momenta and, usually, opposite spins. For finite systems, (5.5), (5.11) and (5.12) are additional assumptions, which may or may not be consistent with the general minimization eq. (5.5).

Using the simple pairing assumptions, (5.5) reduces to the equation

$$\xi_k\chi_k-\tfrac{1}{2}\Delta_k+\tfrac{1}{2}\Delta_k\chi_k^2 = 0, \tag{5.13}$$

with the solution

$$\chi_k = -\frac{\xi_k}{\Delta_k}+\sqrt{1+\left(\frac{\xi_k}{\Delta_k}\right)^2}. \tag{5.14}$$

This is just the usual Bogoliubov [3]) solution; the connection with Bogoliubov's notation is

$$\chi_k = \frac{v_k}{u_k}, \quad \psi_k = u_k v_k = \frac{\Delta_k}{2E_k}, \tag{5.15}$$

where

$$E_k = \sqrt{\xi_k^2 + \Delta_k^2}. \tag{5.16}$$

Also we have, for Bogoliubov's u_k and v_k,

$$u_k^2 = \tfrac{1}{2}\left(1 + \frac{\xi_k}{E_k}\right) = \frac{1}{1+\rho_k}, \quad v_k^2 = \tfrac{1}{2}\left(1 - \frac{\xi_k}{E_k}\right) = \frac{\rho_k}{1+\rho_k} = h_k. \tag{5.17}$$

We shall use the simple pairing solution for the stationary system, and we shall allow for the destruction of the simple pairing by the rotation.

6. A Weak Perturbation

We introduce a weak perturbation of the single-particle type,

$$V = \sum_{kk'} V_{kk'} a_k^\dagger a_{k'}. \tag{6.1}$$

Treating V to first order, we obtain from (5.5), (5.7), (5.11), and (5.12)

$$[V_{k\tilde{l}} + 2(\delta L)_{k\tilde{l}}]\chi_{\tilde{l}} + [\xi_k + \tfrac{1}{2}\Delta_k^*\chi_k + \tfrac{1}{2}\Delta_l^*\chi_l]\delta\chi(k, l) \\ -\tfrac{1}{2}(\delta\Delta)_{kl} + \tfrac{1}{2}(\delta\Delta^*)_{\tilde{k}\tilde{l}}\chi_k\chi_l = 0. \tag{6.2}$$

Here δ denotes the first-order change of a quantity. Using the methods of section 7 of ref. [9]), we get the following expressions for the first-order changes δL and $\delta\Delta$, in terms of $\delta\chi$:

$$(\delta L)_{kk'} = \sum_{ll'} (K_{k'l',kl} - K_{k'l',lk}) \frac{\delta\chi^*(l\bar{l}')\chi_{l'} - \chi_l^*\delta\chi(\bar{l}l')}{(1+\rho_l)(1+\rho_{l'})}, \tag{6.3}$$

$$(\delta\Delta)_{kl} = -2\sum_{k'l'} K_{kl,k'l'}\delta\psi(k'l'), \tag{6.4}$$

$$\delta\psi(kl) = \frac{\delta\chi(k, l) - \chi_k\chi_l\delta\chi^*(kl)}{(1+\rho_k)(1+\rho_l)}. \tag{6.5}$$

Eq. (6.2), with the definitions (6.3)—(6.5), is a linear integral equation for the unknown first-order change $\delta\chi(kl)$ in the variationally best pair wave functions, induced by the change (6.1) in the Hamiltonian. (6.2) must be solved subject to the antisymmetry condition $\delta\chi(k, l) = -\delta\chi(l, k)$.

We can obtain a simple first approximation to $\delta\chi(kl)$ by ignoring, in (6.2), all terms in which $\delta\chi$ appears under an integral (summation) sign, i.e., we ignore the terms involving $(\delta L)_{kl}$, $(\delta \varDelta)_{kl}$, and $(\delta \varDelta^*)_{kl}$, so as to get (with $\chi_{\bar{l}} = -\chi_l$)

$$[\xi_k + \tfrac{1}{2}(\varDelta_k{}^* \chi_k + \varDelta_l{}^* \chi_l)]\delta\chi(k, l) \cong V_{k\tilde{l}}\chi_l. \tag{6.6}$$

In the rotation problem, the perturbation $V = -\omega L$ is odd under time reversal; if the pairing $k \leftrightarrow \tilde{k}$ involves time-reversed states(as we shall assume), we have the identity

$$V_{k\tilde{l}} = -V_{l\tilde{k}}. \tag{6.7}$$

We then get a properly antisymmetric solution of (6.6) by subtracting, from it, the same equation with k and l interchanged, thereby obtaining

$$(\xi_k + \xi_l + \varDelta_k{}^* \chi_k + \varDelta_l{}^* \chi_l)\delta\chi(k, l) \approx V_{k\tilde{l}}\chi_l - V_{l\tilde{k}}\chi_k.$$

Using the identity

$$\xi_k + \varDelta_k \chi_k = E_k \tag{6.8}$$

obeyed by the unperturbed solution (5.14), the approximate expression for $\delta\chi(k, l)$ is

$$\delta\chi(k, l) \approx \frac{V_{k\tilde{l}}\chi_l - V_{l\tilde{k}}\chi_k}{E_k + E_l} \equiv \delta\chi^{(0)}(k, l), \tag{6.9}$$

which is properly antisymmetric according to (6.7). We shall see, later on, that the approximation (6.9) is equivalent to that used by Belyaev [2]).

An improved approximation can be obtained by ignoring only the term $(\delta L)_{k\tilde{l}}$ in (6.2); this is the first-order change in a term which itself is unimportant to start with. Again subtracting from (6.2) the equation with k and l interchanged, we obtain the improved expression

$$\delta\chi(k, l) \approx \frac{V_{k\tilde{l}}\chi_l - V_{lk}\chi_k + (\delta\varDelta)_{kl} - (\delta\varDelta^*)_{\tilde{k}\tilde{l}}\chi_k\chi_l}{E_k + E_l}. \tag{6.10}$$

This expression involves the, so far unknown, change $\delta\varDelta$. Substituting it in (6.5) and using (see (M, 7.5), (M, 7.6))

$$\delta h_{kk'} = \frac{\delta\rho_{kk'}}{(1+\rho_k)(1+\rho_{k'})} = \frac{\delta\chi(k\tilde{k}')\chi_{k'}^* + \chi_k \delta\chi^*(k'k)}{(1+\rho_k)(1+\rho_{k'}),}, \tag{6.11}$$

we arrive at

$$\delta h_{mm'} = \frac{V_{mm'}(\xi_m \xi_{m'} + \varDelta_m \varDelta_{m'} - E_m E_{m'}) - \delta\varDelta_{m\tilde{m}'}\xi_m \varDelta_{m'} + \delta\varDelta^*_{\tilde{m}m'}\xi_{m'}\varDelta_m}{2E_m E_{m'}(E_m + E_{m'})}, \tag{6.12}$$

$$\delta\psi_{m\tilde{m}'} = \frac{-V_{mm'}(\xi_m \varDelta_{m'} - \xi_{m'}\varDelta_m) - \delta\varDelta_{m\tilde{m}'}(E_m E_{m'} + \xi_m \xi_{m'}) - \delta\varDelta^*_{\tilde{m}m'}\varDelta_m \varDelta_{m'}}{2E_m E_{m'}(E_m + E_{m'})}. \tag{6.13}$$

These equations are identical with Migdals eqs. (15), (16). The expression of δh is in terms of $\delta\Delta$ which should in turn be determined from the integral equation

$$\delta\Delta_{mm'} = -2 \sum_{ll'} K_{mm'll'} \delta\psi_{ll'}, \tag{6.14}$$

where the expression for $\delta\psi$ should be taken from (6.13). It is possible to reintroduce the L terms so far neglected into expressions (6.12) (6.13) by the substitution

$$V_{mm'} \to V_{mm'} + 2\delta L_{mm'}. \tag{6.15}$$

If we do this, (6.14) alone is no longer enough to determine both $\delta\Delta$ and δL and we must therefore use it together with (6.3). We then get a coupled pair of integral equations for the unknown quantities $\delta\Delta$ and δL, equivalent to the original integral equation (6.2) for $\delta\chi$.

7. The Moment of Inertia

The operator L_z for the angular momentum is a sum of single-particle operators. Hence its average value is given by the general formula (3.17). In the stationary state, $h_{kk'}$ is diagonal (see (5.9)), and $h_k = h_{\tilde{k}}$. Since L_z is odd under time reversal, its diagonal elements obey

$$(L_z)_{kk} = -(L_z)_{\tilde{k}\tilde{k}}, \tag{7.1}$$

so that (the prime on the sum indicates we are summing over half the states only):

$$\langle L_z \rangle = \mathrm{tr}(hL_z) = \sum_k{}' h_k[(L_z)_{kk} + (L_z)_{\tilde{k}\tilde{k}}] = 0. \tag{7.2}$$

This is the expected result for the stationary system.

As a result of the transformation to the rotating coordinate system, $h_{kk'}$ changes into

$$h_{kk'} = h_k \delta_{kk'} + (\delta h)_{kk'}, \tag{7.3}$$

where, to first order in ω, δh is given by (6.11).

The expectation value of L_z in the rotating system is

$$L_z(\omega) = \mathrm{tr}\,(\delta h L_z) = \sum_{kk'} \frac{\delta\chi(k\tilde{k}')\chi^*_{k'} + \chi_k \delta\chi^*(k'\tilde{k})}{(1+\rho_k)(1+\rho_{k'})} \langle k'|L_z|k\rangle. \tag{7.4}$$

If we use the approximation (6.9) for $\delta\chi$, together with $V = -\omega L_z$, (7.4) reduces considerably. Straightforward substitution of (6.9) into (7.4), use of the Hermiticity and odd time-reversal character of $V = -\omega L_z$, and of the reality of the zero-order function χ_k, leads to

$$\mathscr{I} = \frac{L_z(\omega)}{\omega} \approx \sum_{kk'} \frac{|\langle k|L_z|k'\rangle|^2 (\chi_k - \chi_{k'})^2}{(1+\rho_k)(1+\rho_{k'})(E_k + E_{k'})} \equiv \mathscr{I}_0. \tag{7.5}$$

By the use of (5.14) for χ_k and (5.17a) for $(1+\rho_k)^{-1}$, it is possible to show that (7.5) is identically equal to the Belyaev expression [2])

$$\mathscr{I}_0 = \sum_{kk'} \frac{|\langle k|L_x|k'\rangle|^2 (E_k E_{k'} - \xi_k \xi_{k'} - \Delta_k \Delta_{k'})}{2E_k E_{k'}(E_k + E_{k'})}, \tag{7.6}$$

or,

$$\mathscr{I}_0 = \sum_{kk'} \frac{|\langle k|L_x|k'\rangle|^2 (u_k v_{k'} - v_k u_{k'})^2}{E_k + E_{k'}}. \tag{7.7}$$

An improved approximation can be generated by using (6.10) for $\delta\chi$. Straightforward substitution yields

$$\mathscr{I} = \mathscr{I}_0 + \mathscr{I}_\Delta, \tag{7.8}$$

where $\mathscr{I}_0$ is given by (7.7) and

$$\mathscr{I}_\Delta = \sum_{kk'} \frac{(\delta\Delta)_{k\tilde{k}'} \xi_k \Delta_{k'} - (\delta\Delta^*)_{\tilde{k}k'} \Delta_k \xi_{k'}}{2E_k E_{k'}(E_k + E_{k'})} \langle k'|L_x|k\rangle. \tag{7.9}$$

This is Migdal's result; the correction term (7.9) can be evaluated explicitly only after the integral equation for $\delta\Delta$ has been solved.

Finally, we can solve the full integral equation (6.2) for $\delta\chi$, and substitute the result into (7.4) to obtain the best value for the moment of inertia deducible from this model. It is not expected that the improvement over Migdal's result (7.9) would be significant.

8. Discussion

Since Belyaev [2]) and Migdal [7]) have already given approximate numerical evaluations of eqs. (7.6) and (7.8—9), we need not repeat their comparison with experiment. Rather, we would like to comment briefly on the basis of the theoretical framework used in these calculations.

In an infinite system, e.g., a superconductor, there is a distinction in principle between independent-particle wave functions and the Bose-condensed pair wave functions of the Bogoliubov theory. In the limit $N \to \infty$, the wave function (1.8) is not obtainable from any *finite* superposition of independent-particle configurations. If an infinite number of configurations is superposed so as to yield (1.8), the evaluation of the expectation value of the Hamiltonian over (1.8) requires a non-trivial interchange of the order of summation of infinite series. This shows itself in the non-analytic character of $(\psi, H\psi)$ as a function of the coupling constant.

The situation is completely different in the Belyaev-Migdal theory, which deals with a finite and not very large system (the nucleus), and in which the sums over single-particle states k are usually restricted to the outermost (not completely filled) shell of the nuclear shell model. As a result, all expressions must be analytic in the coupling constant, and can be obtained in principle by a straightforward shell model calculation.

In particular, if the sums over k are restricted even further, to the states arising from only one value of j, then the paired wave function of Belyaev is essentially the same as the shell model function of zero seniority in the Racah [11]) scheme.

The difference between the two descriptions is therefore primarily conceptual, rather than being a strict mathematical distinction. A "simple" wave function in one scheme is "complicated" in the other, and vice versa. To illustrate: if the unfilled shell contains j-values j' j'' j''', say, then a reasonable pair wave function for the ground state of an even nucleus might be

$$\begin{aligned}\varphi(1, 2) = C' &\sum_{m'>0} u_{j'm'}(1)u_{j', -m'}(2) \\ +C'' &\sum_{m''>0} u_{j''m''}(1)u_{j'', -m''}(2) \\ +C''' &\sum_{m'''>0} u_{j'''m'''}(1)u_{j''', -m'''}(2)\end{aligned} \tag{8.1}$$

where the u_{jm} are independent-particle wave functions and C', C'', C''' are constants. A wave function (1.8) for the $2N$-particle (outside closed shells) nucleus, built from (8.1), is "simple" in the Belyaev scheme, but would be considered a very complicated instance of "configuration mixing" in the usual shell model description. Thus the Belyaev scheme is an approximate method of circumventing the need for very elaborate shell model calculations, and a way of describing conceptually, in simple terms, the type of wave function such an elaborate calculation would probably yield if carried out. But, unlike the situation in the theory of superconductivity, the Belyaev scheme is not qualitatively out of the reach of shell model calculations.

This suggests that a direct check can, and should, be carried out so as to test the accuracy of the form (1.8) for the trial wave function of the ground state. By choosing some reasonable interaction between particles, and a value of N within range of present-day electronic computers, the shell-model energy matrix can be diagonalized directly, and the ground state vector compared with the form (1.8). This is a non-trivial check, since the arguments in favour of the extreme Bose-Einstein condensation of pairs (1.8), contained in ref. [10]), apply directly only to the limit $N \rightarrow \infty$, and it is not known how big an error is made by assuming the form (1.8) for finite, and not very large N [†].

On the basis of the ideal Bose gas analogy, we would expect to find the "irrotational" moment of inertia. Migdal [7]) shows that this is indeed the case

---

[†] This question is quite separate from, and much more difficult to answer than, the question of the $1/N$ corrections to the limiting forms (3.17)—(3.19) of expectation values over the function (1.8). This latter question is answered by the exact expressions (3.13)—(3.16).

(his equation (3.7)) provided the size R of the system greatly exceeds the average distance a_0 between the two particles in the pair.

On the other hand, if $R \approx a_0$, the pairs are "squeezed" by the boundaries of the system, and free irrotational flow of the centres of mass of the pairs becomes impossible. Thus the moment of inertia increases, until it reaches the "rigid" value for $R \ll a_0$ (Migdal's eq. (36)) [†].

The actual nuclear size is between these extremes, so that the nuclear moments of inertia lie between the irrotational and rigid values.

We acknowledge with pleasure many interesting discussions with Professors Levinson, Lipkin, and Talmi. One of us (J. M. B.) is grateful to the Weizmann Institute for the hospitality extended to him during the visit in which this work was done.

Appendix A

MIGDAL's FORMULATION

By substitution of the approximate form (6.10) into equations (6.5) and (7.4), we obtain approximations for $\delta\psi(k, l)$ and for $(\delta h)_{kk'}$, respectively. The approximate form for $\delta\psi$ is identical with Migdal's eq. (16), and the approximate form for δh is identical with his eq. (15).

Instead of writing down a general integral equation, as we have done in section 6, Migdal prefers to incorporate certain assumptions into his theory so as to make it more suitable for rough calculations. In this appendix, we shall indicate briefly how Migdal's form of the integral equation for $\delta\Delta$ may be obtained.

Working in a representation where the spin is separated from the other quantum numbers we put $m = \mu, s$. Let us define the x-space pair wave function by

$$\psi(rs, r's') \equiv \sum \psi_{\mu s \mu' s'} \varphi_\mu(r) \varphi_\mu(r'), \tag{A.1}$$

and the x-space representation of $\Delta_{mm'}$ by

$$\Delta(rs, r's') \equiv K(r, r') \psi(rs, r's'), \tag{A.2}$$

where $\varphi_\mu(r)$ is the wave function of the state μ and $K(rr')$ is the interaction. It is easily checked that

$$\begin{aligned} \Delta(rs, r's') &= \sum_{\mu\mu'} \Delta_{\mu s \mu' s'} \varphi_\mu(r) \varphi_{\mu'}(r') \\ &= \sum_{\mu} \Delta_{\mu s} \varphi_\mu(r) \varphi_\mu{}^*(r'). \end{aligned} \tag{A.3}$$

If we assume a δ function interaction

$$K(rr') = -K\delta(r-r'), \tag{A.4}$$

[†] Under these circumstances also the paired wave function (2.1) becomes identical with a simple shell model wave function.

eq. (A.3) reduces to

$$\Delta(rss')\delta(r-r') = \sum_{\mu} \Delta_{\mu s}\varphi_{\mu}(r)\varphi_{\mu}^{*}(r'). \tag{A.5}$$

This implies that $\Delta_{\mu s} = \Delta_s$ and is independent of μ. This further means that $\Delta(rss')$ is independent of r. We thus have

$$\Delta(ss') = \begin{cases} \Delta_s & \text{when} \quad s \neq s', \\ 0 & \text{when} \quad s = s'. \end{cases} \tag{A.6}$$

Using (A.2) we get

$$\Delta_s = K \sum_{\mu} \frac{\Delta_s}{2E_{\mu}} \varphi_{\mu}(r)\varphi_{\mu}^{*}(r), \tag{A.7}$$

or,

$$1 = K \sum_{\mu} \frac{1}{2E_{\mu}} \varphi_{\mu}(r)\varphi_{\mu}^{*}(r). \tag{A.8}$$

Similarly treating $\delta\psi$ and $\delta\Delta$ we get

$$\delta\Delta(rs, r's') = \delta\Delta(rss')\delta(r-r'). \tag{A.9}$$

Consider

$$\begin{aligned} &\sum_{\mu\mu'} \delta\Delta_{\mu s\mu' s'} \frac{1}{2E_{\mu}} \varphi_{\mu}(r)\varphi_{\mu'}^{*}(r') \\ &\qquad = \int \mathrm{d}r_1 \delta\Delta(r_1 ss') \sum_{\mu} \frac{1}{2E_{\mu}} \varphi_{\mu}^{*}(r_1)\varphi_{\mu}(r) \sum_{\mu'} \varphi_{\mu'}^{*}(r_1)\varphi_{\mu}(r) \\ &\qquad = \frac{\delta\Delta(rss')}{K} = -\sum \delta\psi_{\mu s\mu' s'}\varphi_{\mu}(r)\varphi_{\mu'}(r), \end{aligned} \tag{A.10}$$

or

$$\sum_{\mu\mu'} \left\{ \delta\Delta_{\mu\uparrow,\mu'\downarrow} \left[\frac{1}{4E_{\mu}} + \frac{1}{4E_{\mu'}} \right] + \delta\psi_{\mu\uparrow\bar{\mu}'\downarrow} \right\} \varphi_{\mu}(r)\varphi_{\mu'}^{*}(r) = 0. \tag{A.11}$$

It further follows from (A.9) that

$$\delta\Delta_{\mu\uparrow\bar{\mu}'\downarrow} = \delta\Delta^{*}_{\bar{\mu}\downarrow\mu'\uparrow} \equiv if_{\mu\mu'}. \tag{A.12}$$

Substituting (A.12) into (A.11) we get:

$$\sum \frac{V_{\mu\mu'}(\xi_{\mu}-\xi_{\mu'}) - if_{\mu\mu'}\frac{1}{2}(\xi_{\mu}-\xi_{\mu'})^2}{2E_{\mu}E_{\mu'}(E_{\mu}+E_{\mu'})} \varphi_{\mu}(r)\varphi_{\mu}^{*}(r) = 0. \tag{A.13}$$

This is Migdal's equation for $\delta\Delta$. The solution of (A.13) is unique only if we require the additional condition on the form of $\delta\Delta$, namely (A.9). For the case of translation when $V = -vP$ the simple solution

$$f_{\mu\mu'} = -2\Delta i \frac{V_{\mu\mu'}}{\xi_\mu - \xi_{\mu'}} = -2i\Delta v \frac{P_{\mu\mu'}}{\xi_\mu - \xi_{\mu'}}$$

$$= \frac{2\Delta vm}{\hbar} X_{\mu\mu'} \tag{A.14}$$

satisfies this condition. It can be checked that by its use the correct mass is obtained.

Appendix B

PERTURBATIONS EVEN UNDER TIME REVERSAL

For a perturbation which is even under time reversal, the integral equation (6.2) simplifies enormously and allows a very accurate approximate solution. We now *add* to (6.2) the equation obtained by interchanging the indices k and l. The terms in δ drop out identically. The terms in δL are small corrections of little qualitative importance. If we ignore those terms, we arrive at the explicit solution

$$\delta\chi(k, l) = \frac{V_{k\bar{l}}\chi_l + V_{l\tilde{k}}\chi_k}{\xi_k - \xi_l}. \tag{B.1}$$

This is antisymmetric if $V_{k\bar{l}} = V_{l\tilde{k}}$, which is true for a perturbation even under time reversal. The corresponding approximation for δh, eq. (7.4), can be reduced to

$$(\delta h)_{kk'} = \frac{h_k - h_{k'}}{\xi_k - \xi_{k'}} V_{kk'} \tag{B.2}$$

References

1) A. Bohr, Rotational states of atomic nuclei (Ejnar Munksgaard Forlag, Copenhagen, 1954)
2) Belyaev, Mat. Fys. Medd. Dan. Vid. Selsk. **31**, No 11 (1959);
Bogoliubov, Tolmaekev and Shirkov, A new method in the theory of superconductivity (Moscow, 1958)
3) Inglis, Phys. Rev. **96** (1955) 1059, 701
4) Blatt, Butler and Schafroth, Phys. Rev. **100** (1955) 481
5) Griffin and Rich, Phys. Rev. **118** (1960) 850
6) Prange, Lectures at the International Spring School of Physics, Naples 1960
7) Migdal, Nuclear Physics **13** (1959) 655
8) Blatt, Journal of the Australian Math. Soc., in press
9) Blatt, Prog. Theor. Physics (1960), to be published
10) Matsubara and Blatt, Prog. Theor. Phys. **23** (1960) 451
11) Racah, Phys. Rev. **63** (1943) 367

2.E:2.G

Nuclear Physics **23** (1961) 630—647; © *North-Holland Publishing Co., Amsterdam*

Not to be reproduced by photoprint or microfilm without written permission from the publisher

NEUTRON-GAMMA ANGULAR CORRELATION STUDIES OF THE $B^{11}(d, n\gamma)C^{12}$ REACTION

J. B. GARG, N. H. GALE and J. M. CALVERT

The Physical Laboratories, The University, Manchester

Received 28 November 1960

Abstract: Several (n, γ) angular correlations of the neutron group leading to the 4.43 MeV level in C^{12} and the associated γ-rays from the reaction $B^{11}(d, n)C^{12}$ have been measured using time-of-flight techniques. The energies of the incident deuterons were 2.65 MeV and 5.35 MeV, and the angles of the outgoing neutron direction were chosen at intervals of about 20°. The results of these measurements clearly show that the simple theory of Butler stripping is quite inadequate to describe the detailed features of the reaction mechanism but that good qualitative agreement of the results might be obtained with the distorted wave theory. Moreover the (n, γ) angular correlation measurements for backward angles of the neutrons do not show the expected features of the heavy particle stripping mechanism, which has been used by other authors to account for the intensity of neutrons emitted at backward angles.

1. Introduction

Deuteron induced reactions at bombarding energies above a few MeV are well known to proceed by a direct interaction mechanism in which one of the nucleons of the incident deuteron is stripped off and the other is captured by the target nucleus. Simple theories of such reactions have been developed by Butler [1]), Bhatia [2]) and others [3–7]) and these theories have had reasonable success in fitting the observed angular distributions of emitted particles. They have in addition formed a powerful spectroscopic tool in determining the spins and parities of the nuclear levels involved. However, in some cases, for example in the reaction $B^{11}(d, n)C^{12}$, the angular distributions of the outgoing neutrons show a large intensity at backward angles which cannot be explained satisfactorily by such theories. This fact led Madansky and Owen [8]) to propose the idea of heavy particle stripping in which the emergent particle comes from the target nucleus while its remaining core is captured by the incident deuteron. These authors applied their theory to the analysis of the angular distribution of emitted particles from the reactions $B^{11}(d, n)C^{12}$ and $C^{13}(He^3, \alpha)C^{12}$ and obtained very satisfactory agreement with the experimental results [9–10]). Although there are not many known reactions in which the heavy particle stripping features are observed, still their presence in certain cases demands careful investigation of these effects.

It has been suggested by Satchler [11]) and others [12–14]) that studies of the angular distributions of γ-rays in coincidence with the outgoing particle in reactions in which the residual nucleus is left in an excited state, might be more decisive in determining the type of reaction mechanism than the study of the angular distributions of the outgoing particle alone, since these angular correlations are expected to show certain well defined axes of symmetry which depend on the mechanism. If plane waves are used to describe the incoming and outgoing particles in a stripping reaction such as X(d, n)Y the residual nucleus is expected to be formed by capture of a proton incident along the direction defined by the momentum transfer vector $\mathbf{k} = \mathbf{k}_d - \mathbf{k}_n$, where $\mathbf{k}$, $\mathbf{k}_d$ and $\mathbf{k}_n$ are the wave vectors of the captured proton, incident deuteron and the outgoing neutron respectively. Hence if the outgoing neutron direction is kept fixed, the angular distribution of γ-rays in coincidence with neutrons in this chosen direction should be symmetrical about the direction of $\mathbf{k}$, which is also the direction of the recoiling nucleus. The experimental observation of such a symmetry axis in the angular correlations would constitute strong evidence in favour of a direct reaction mechanism as opposed to a compound nucleus process, for which no significance is attached to this particular direction. Moreover, as the direction of the momentum transfer vector is different for ordinary stripping and heavy particle stripping, an experimental determination of these symmetry axes might also show the dominance of a particular type of direct reaction mechanism. Unfortunately there are certain factors which tend to destroy the possibility of such a simple interpretation, e.g.:

1) When different forms of reaction mechanism, such as ordinary and heavy particle stripping and compound nucleus formation are all present, they may interfere with each other and so give quite a different angular correlation from the relatively simple form expected from one of the mechanisms alone. Edwards [15]) has discussed the effects of mixtures of reaction mechanisms on the (n, γ) correlations from the reaction $B^{11}(d, n\gamma)C^{12}$, and has predicted theoretical correlation functions as a function of the outgoing neutron direction for different mode mixtures. These calculations show that the correlation anisotropy varies rapidly as a function of the outgoing neutron direction due to the variation of the relative contributions from the two reaction modes. Moreover, the correlation function is found to be very sensitive to the nucleon coupling schemes used.

2) It has been shown by Horowitz and Messiah [16]), and others [17–18]) that the simple ideas of Butler stripping are not adequate to describe the detailed features of deuteron induced reactions, and effects such as the interaction of the incident deuteron with the target nucleus and of the outgoing particle with the residual nucleus etc., need to be taken into account. Huby *et al.* [19]) have discussed these effects, while Satchler and Tobocman [20]) have recently reported detailed distorted wave calculations for the p—γ correlations from several (d, p) reactions. They have shown

that, for $l = 1$ captures, the γ-ray symmetry axis is rotated away from the recoil direction and azimuthal asymmetry about this axis is introduced, while for captures with higher l, there is usually no longer a symmetry axis.

From the above discussion it is evident that the experimental measurement of (n, γ) or (p, γ) correlations in deuteron induced reactions can be very useful in investigating reaction mechanisms. However, in spite of this, very few correlations [21–26]) have been measured so far, most probably due to the inherent technical difficulties of these measurements.

Previous measurements of the (n, γ) angular correlation in the reaction B^{11}(d, nγ)C^{12} include the work of Rask *et al.* [27]) at an incident deuteron energy of 1 MeV. No detailed theoretical interpretation of their results was given, though the axis of symmetry was found to change as the out-going neutron direction was changed. Similar (n, γ) angular correlations at energies below 2 MeV have been measured by Neilson *et al.* [28]) but they failed to observe any correspondence of the axis of symmetry with any of the predicted recoil directions. Since at these low energies the stripping patterns are rather poorly developed, we undertook to measure the correlations at higher energies, as no (d, nγ) correlation measurements at deuteron energies greater than 2 MeV have been reported before and it is expected that the stripping features would be more pronounced at higher energies.

2. Experimental Method

The experimental arrangement adopted was very similar to the one described previously [29]). Deuterons from the University of Manchester's Van de Graaff generator were analysed by a 90° bending magnet and were re-focussed by means of quadrupole lenses on to a target placed at the centre of a target chamber at a distance of about 10 m from the bending magnet. The energy spread of the analysed beam was stabilised to better than $\frac{1}{2}$ % using the conventional slit arrangement.

The target was of enriched B^{11} (99 % pure) deposited on a gold backing 100 μm thick) †. The estimated thickness of the target was 175 μg/cm^2 which represents an energy loss of about 35 keV for 5 MeV deuterons.

By collimation, the beam spot was limited to 2 mm diameter at the target. The focussing was adjusted for an optimum of target current against current striking the collimator. The centring of the beam on the axis of rotation of the counters was checked as described below.

A neutron time-of-flight spectrometer [30]) using a 5.1 cm by 5.1 cm NaI Harshaw crystal for the γ-ray detector and a liquid scintillator, NE 211

---

† The target was supplied by the Electromagnetic Separator Group, U.K.A.E.A., Harwell, England.

(supplied by Nuclear Enterprises Ltd., Edinburgh, Scotland) 7.6 cm diameter and 5.1 cm long for the neutron detector was employed for these measurements. The two scintillators were mounted on RCA 6810A and Mullard 56 AVP photomultipliers respectively. The energy resolution of the γ-ray detector was found to be 9.5 % for Cs^{137} γ-rays (0.667 MeV) at a counting rate of 5×10^4 pulses per second. Although the use of a NaI scintillator seriously affects the time resolution of the spectrometer, yet its use was imperative in the study of this reaction since some energy resolution was necessary in order to improve the ratio of true to chance counting rates.

The copious yield of neutrons and γ-rays from the stabilising slits, beam defining apertures and target backing material made it necessary to use a single channel analyzer in the slow channel from the γ-ray counter, its bias and window-width being adjusted so that it accepted only pulses corresponding to γ-rays of energy between 3.0 and 4.6 MeV. The bias of the discriminator in the slow channel from the neutron detector was set to accept pulses corresponding to gamma ray energies greater than 1.2 MeV. This bias corresponds to a cut off energy of approximately 3 MeV for neutrons. We have measured the pulse height ratio for γ-rays and neutrons of the same energy incident upon the liquid scintillator NE211 and have found it to have a value of about 2.5 in this energy region. Since the neutrons of interest for the reaction $B^{11}(d, n)C^{12}$ have energies greater than 10 MeV at the bombarding energy employed, a cut off energy of 3 MeV, though it reduced the neutron detection efficiency, was satisfactory and it was found greatly to improve the true to random counting rate over that obtained for a lower bias setting.

The time resolution of the spectrometer was measured using γ—γ coincidences from a Co^{60} source and was found to be less than two nanoseconds for biases in the two detectors corresponding to a γ-ray energy of 1 MeV.

For the correlation measurements the γ-counter subtended a solid angle of 0.196 sr at the target and was rotated round the beam direction at intervals of about 10°. The neutron counter subtended a solid angle of 0.160 sr at the target. The counting rates in the two counters during the course of the measurements were of the order of 10^4 counts per second.

A current integrator collecting the charge on the target was used as a monitor. A separate counter consisting of a NaI crystal mounted on a photomultiplier was also used to monitor the γ-rays in the energy range of 3 to 5.0 MeV. The counting rates in both of these monitors as well as in the fixed neutron counter were consistent within 3 or 4 %, and thus gave a good check on the stability of the electronics used in the experiment.

The experimental geometry of the target and the movable counter was checked by studying the angular distribution of 3.56 MeV γ-rays from the reaction $Be^9(p, \alpha\gamma)Li^6$ at incident proton energy of 2.5 MeV. This distribution was found isotropic in the range of angles used in the correlation measurements.

The angular distribution of 3.56 MeV γ-rays from this reaction has been measured previously [13]) and has been found isotropic.

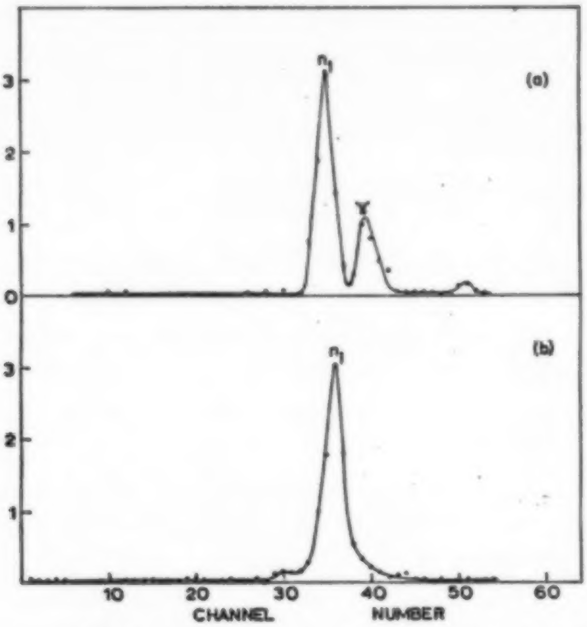

Fig. 1. (a) Neutron time-of-flight spectrum from the reaction $B^{11}(d, n)C^{12}$ observed at 20° in coincidence with γ-rays at an incident deuteron energy of 2.65 MeV; the flight path was 35 cm and the bias of the neutron counter corresponded to a cut off energy of 400 keV for γ-rays. (b) A similar spectrum with a cut off energy of 1.2 MeV γ-rays.

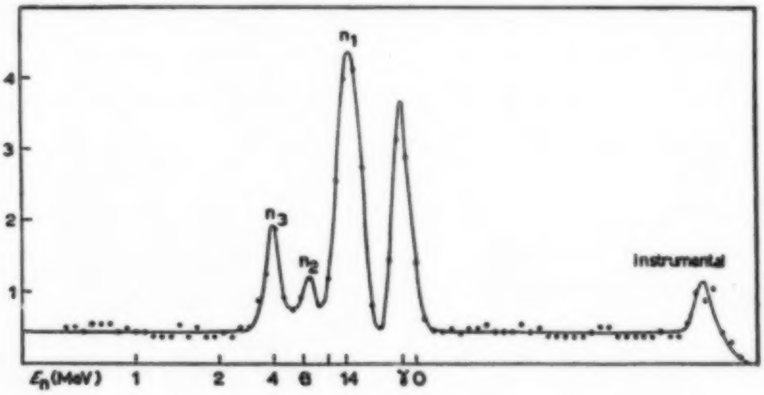

Fig. 2. Neutron time-of-flight spectrum from the reaction $B^{11}(d, n)C^{12}$ at a bombarding deuteron energy of 5.35 MeV and a flight path of 50 cm.

3. Results

3.1. SPECTRA

Fig. 1(a) shows a typical neutron time-of-flight spectrum from the reaction $B^{11}(d, n)C^{12}$ at an incident energy of deuterons of 2.65 MeV. The γ-counter was at a distance of 10 cms from the target and the neutron flight path was 35 cm.

Pulses from the γ-counter were accepted corresponding to γ-ray energies between 3 and 4.5 MeV and the neutron counter bias corresponded to a neutron energy of about 1 MeV. The spectrum shows a single prominent neutron group leading to the 4.43 MeV level of C^{12} and a prompt coincidence peak which arises from some (n, γ) coincidences and possibly $(\gamma—\gamma)$ coincidences of low energy γ-rays. Fig. 1(b) shows the same spectrum with a higher bias in the neutron counter corresponding to a neutron energy of about 3 MeV. The prompt peak is completely suppressed at this high bias. Fig. 2 shows the time-of-flight spectrum at $E_d = 5.35$ MeV and for a flight path of 50 cm, and neutron bias of 1 MeV. This spectrum also shows the predominant neutron group n_1 leading to the 4.43 MeV level in C^{12} and other groups n_2, n_3 which may be due to the 12.7 and 15.1 MeV levels in C^{12} as these levels are known to decay by γ-emission.

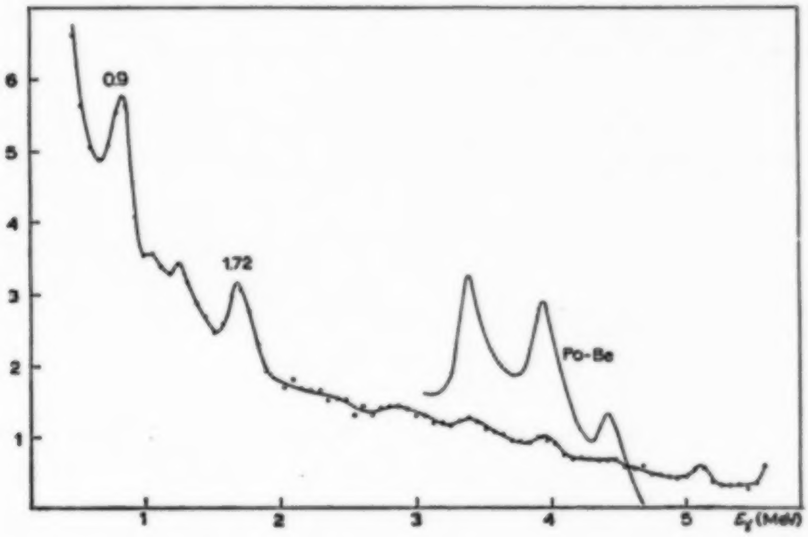

Fig. 3. The γ-ray spectrum from the bombardment of ^{11}B with deuterons of energy 2.65 MeV.

Fig. 3 shows a typical γ-ray spectrum from the bombardment of B^{11} by deuterons. This shows γ-rays of energies of about 0.9, 1.72 and 2.85 MeV and the three peaks due to the 4.43 MeV γ-rays, which are compared with the spectrum from a Po-Be source.

3.2. NEUTRON-GAMMA ANGULAR CORRELATIONS

We have studied the (n, γ) angular correlations from the reaction $B^{11}(d,n)C^{12}$ between the neutron group leading to the 4.43 MeV level in C^{12} and its associated γ-ray at deuteron energies of 2.65 and 5.35 MeV. The excitation function for this reaction has been measured by Burke *et al.* [32]) for energies from 0.8 to 2.0 MeV and no resonance effects were observed. No measurement of excitation curves for this reaction at energies higher than 2 MeV has been reported [33]).

The two energies at which the (n, γ) correlation measurements were made were chosen in order to compare the results at an energy close to the Coulomb barrier (2.13 MeV) and at a somewhat higher energy.

Two sets of (n, γ) angular correlation measurements were made.

In the first set of measurements the γ-counter was kept fixed at 90° to the beam direction for $E_d = 5.35$ MeV and at 140° for $E_d = 2.65$ MeV and the neutron counter was rotated in the plane defined by the incident deuterons and the observed γ-rays.

In the second set of measurements the neutron counter was kept fixed at some angle (θ_{dn}) whose value was chosen from the results of the first set of measurements and the γ-counter was rotated round the beam direction in the plane defined by the deuteron beam and the observed neutron.

As explained previously [29]) the first set of measurements corresponds very nearly to the angular distributions of neutrons. In the limiting case when the (n, γ) correlation is isotropic, they will correspond to the true angular distributions.

The results of the first set of measurements are shown in the figs. 4(a) and 4(b) and the results of the second set of measurements are shown in the figs. 5 to 13. The experimental points in each of the figures are obtained by normalizing the number of counts under the peak in the spectrum to the monitor. The errors shown are statistical errors due to the finite number of counts. The solid curves in the figs. 4(a) and (b) are drawn in an arbitrary manner joining the experimental points, whereas the broken curves represent the expression $[j_l(kR)]^2$, where j_l is the spherical Bessel function of order l and k is the momentum transfer vector defined as $k = k_d - (m_1/m_f)k_n$. R is the radius of interaction and its value was taken as equal to 5.5 fm whilst the value of l was taken as 1.

Solid curves in the figs. 5 to 11 represent the best fitting function $W(\theta) = A_0 + A_2 P_2(\cos(\theta - \theta_0))$ obtained by computing on the Mercury Computer of Manchester University a least squares fit to a series of Legendre polynomials of even order as given by $\sum_0^\nu A_\nu P_\nu \cos(\theta - \theta_0)$, where θ_0 is the angle of symmetry of the correlation function. Since for every correlation there are two axes of symmetry, corresponding to the maxima or minima of the function, the angle (θ_0) was initially chosen by inspection of the experimental points as defining the axis nearest to the classical recoil direction. This value was then substituted in the above expression and the corresponding values of the coefficients A_0, A_2, etc., were determined. The least squares programme was such as to give the values of the coefficients of the fitted function for series terminating in a progressively increasing order of Legendre polynomial and also gave the value of δ^2 — the sum of the squares of the residuals. The angle of symmetry (θ_0) was then varied in intervals of $\pm 5°$ and the least squares fits again computed giving other values of A_0, A_2, A_4 etc., and δ^2. Finally the values of the coeffi-

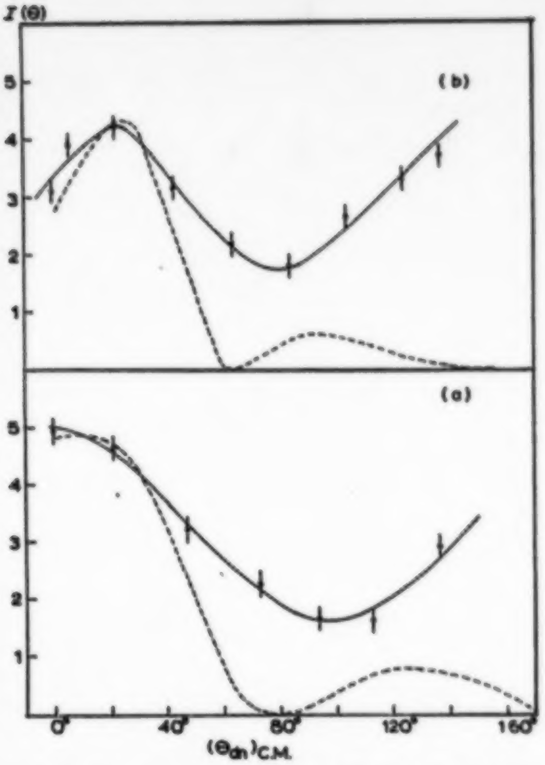

Fig. 4. (a) Angular distribution of neutrons to the (4.43 MeV) state of C^{12} in coincidence with γ-rays detected at a fixed angle of 140° to the direction of the incident deuteron beam of energy of 2.65 MeV; the broken curve represents the expression $[j_1(k_1R_0)]^2$ for $R_0 = 5.5$ fm and $l = 1$. (b) Similar curve for $E_d = 5.35$ MeV.

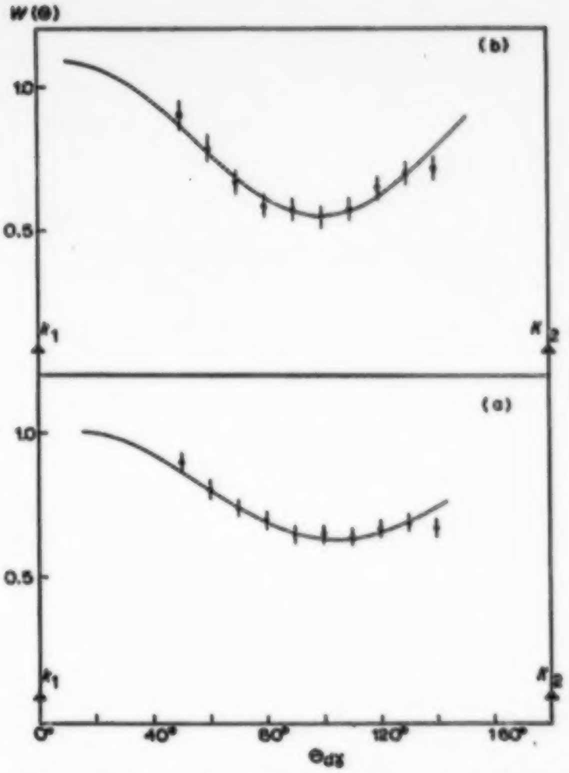

Fig. 5. (a) (n, γ) correlation at $E_d = 2.65$ MeV and $\theta_n = 0°$; solid curve is $W(\theta) = 1 + 0.33\ P_2 \cos(\theta_\gamma - 15°)$; (b) Correlation for $E_d = 5.35$ MeV and $\theta_n = 0°$; solid curve is $W(\theta) = 1 + 0.49\ P_2 \cos(\theta - 10°)$.

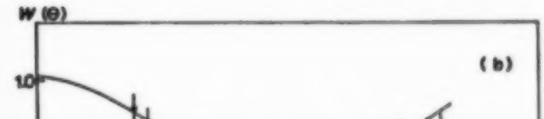

Fig. 6. (a) (n, γ) correlation for $E_d = 2.65$ MeV and $\theta_n = 20°$; solid curve is $W(\theta) = 1 + 0.14\ P_2 \cos(\theta - 170°)$. (b) (n, γ) correlation for $E_d = 5.35$ MeV and $\theta_n = 20°$; solid curve is $W(\theta) = 1 + 0.31\ P_2 \cos(\theta - 180°)$.

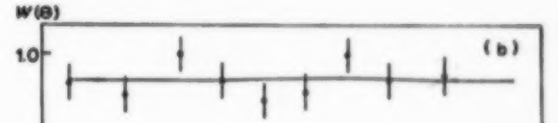

Fig. 7. (a) (n, γ) correlation for $E_d = 2.65$ MeV and $\theta_n = 45°$; solid curve is $W(\theta) = 1 + 0.12\ P_2 \cos(\theta - 35°)$. (b) (n, γ) correlation for $E_d = 5.35$ MeV and $\theta_n = 40°$; solid curve is $W(\theta) = 1 + 0.01\ P_2 \cos(\theta - 105°)$.

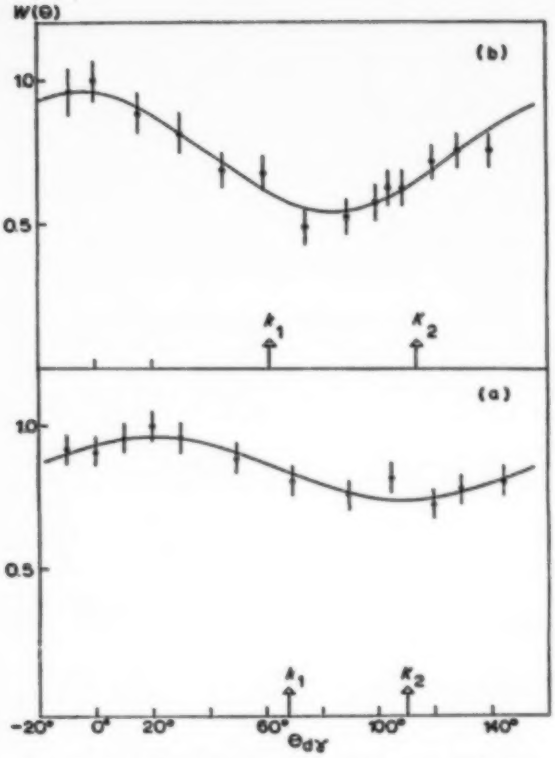

Fig. 8. (a) (n, γ) correlation for $E_d = 2.65$ MeV and $\theta_n = 70°$; solid curve is $W(\theta) = 1+0.18\ P_2 \cos(\theta-20°)$. (b) (n, γ) correlation for $E_d = 5.35$ MeV and $\theta_n = 65°$; solid curve is $W(\theta) = 1+0.40\ P_2 \cos(\theta+5°)$.

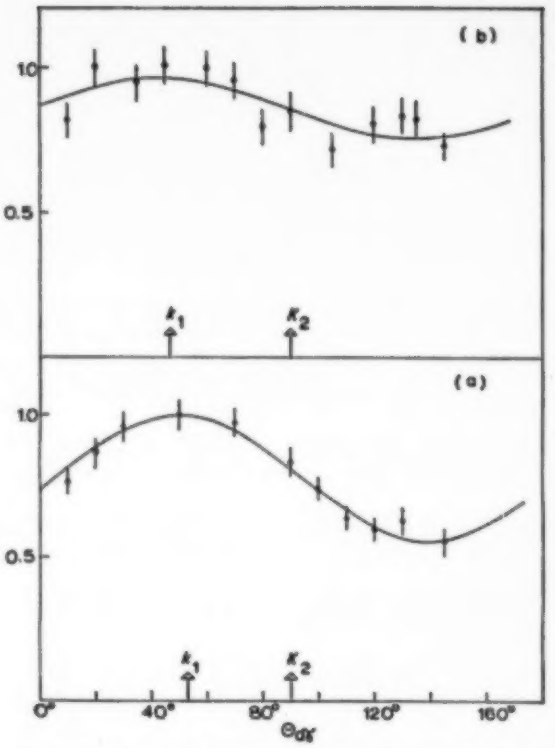

Fig. 9. (a) (n, γ) correlation for $E_d = 2.65$ MeV and $\theta_n = 90°$; solid curve is $W(\theta) = 1+0.41\ P_2 \cos\ (\theta-50°)$. (b) (n, γ) correlation for $E_d = 5.35$ MeV and $\theta_n = 90°$; solid curve is $W(\theta) = 1+0.16\ P_2 \cos(\theta-45°)$.

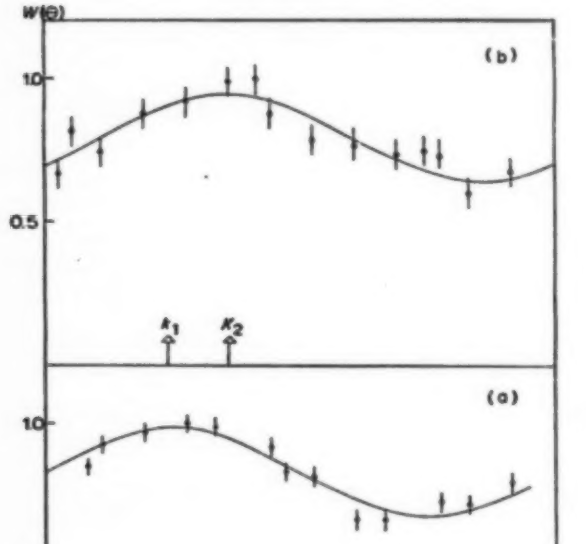

Fig. 10. (a) (n, γ) correlation for $E_d = 2.65$ MeV and $\theta_n = 135°$; solid curve is $W(\theta) = 1+0.26\ P_2 \cos(\theta-25°)$. (b) (n, γ) correlation for $E_d = 5.35$ MeV and $\theta_n = 135°$; solid curve is $W(\theta) = 1+0.27\ P_2 \cos(\theta-45°)$.

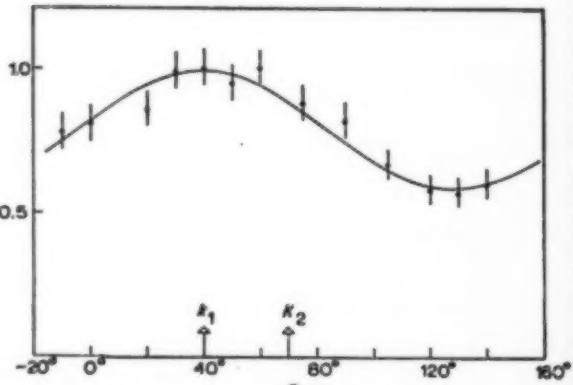

Fig. 11. (n, γ) correlation for $E_d = 2.65$ MeV and $\theta_n = 110°$; solid curve is $W(\theta) = 1+0.38\ P_2 \cos(\theta-40°)$.

cients corresponding to the value of θ_0 which gave the least value of δ^2 for a second order polynomial were accepted as the best fitting values and the corresponding angle of θ_0 as the best angle of symmetry. This procedure was adopted for computing the best functions for all the correlations measured and the results are given in table 1. The corresponding values of the classical recoil direction and the angle of symmetry expected on heavy particle stripping are also given in table 1 for comparison. It might be mentioned here that in some cases, for example, at $E_d = 5.35$ MeV and $(\theta_{dn}) = -40°$, great difficulty was experienced in visualising the angle of symmetry, and in such cases several angles were tried arbitrarily, the one which gave the least value of δ^2 and a positive value for the coefficient A_2 being chosen as the best angle of symmetry. The values of (A_2/A_0) and (A_4/A_0) were calculated from these functions and are given in table 2. It must be pointed out that as most of the correlations were fitted reasonably well by functions containing only P_0 and P_2 terms in

TABLE 1

The best fitting angular correlation functions and the best values of the angles of symmetry

E_d (lab) (MeV)	θ_{dn} (degrees)	$W(\theta) = \sum_{0}^{\nu} A_\nu P_\nu \cos(\theta_\gamma - \theta_0)$	θ_0 (degrees)	$\mathbf{k}_1$ (degrees)	$\mathbf{K}_2$ (degrees)
2.65	0	$1+(0.33\pm0.01)P_2$		180 or	180 or
		$1+(0.36\pm0.01)P_2+(0.06\pm0.01)P_4$	15 ± 5	0	0
2.65	-20	$1+(0.14\pm0.02)P_2$			
		$1+(0.13\pm0.02)P_2-(0.03\pm0.02)P_4$	170 ± 5	128	160
2.65	-45	$1+(0.12\pm0.02)P_2$			
		$1+(0.15\pm0.02)P_2-(0.07\pm0.02)P_4$	35 ± 5	92	135
2.65	-70	$1+(0.18\pm0.01)P_2$			
		$1+(0.16\pm0.01)P_2+(0.04\pm0.01)P_4$	20 ± 5	68	110
2.65	-90	$1+(0.41\pm0.03)P_2$			
		$1+(0.39\pm0.03)P_2+(0.04\pm0.03)P_4$	50 ± 5	53	90
2.65	-110	$1+(0.38\pm0.03)P_2$			
		$1+(0.39\pm0.03)P_2-(0.03\pm0.04)P_4$	40 ± 5	40	70
2.65	-135	$1+(0.26\pm0.03)P_2$			
		$1+(0.26\pm0.03)P_2+(0.03\pm0.03)P_4$	25 ± 5	26	45
5.35	0	$1+(0.49\pm0.03)P_2$			
		$1+(0.56\pm0.03)P_2+(0.09\pm0.05)P_4$	10 ± 5	0	0
5.35	-20	$1+(0.31\pm0.03)P_2$			
		$1+(0.26\pm0.03)P_2-(0.08\pm0.03)P_4$	180 ± 5	105	160
5.35	-40	$1+(0.01\pm0.03)P_2$			
		$1+(0.02\pm0.03)P_2-(0.03\pm0.05)P_4$	105 ± 8	81	140
5.35	-65	$1+(0.40\pm0.03)P_2$			
		$1+(0.40\pm0.03)P_2+(0.00\pm0.03)P_4$	-5 ± 5	62	115
5.35	-90	$1+(0.16\pm0.04)P_2$			
		$1+(0.13\pm0.04)P_2+(0.10\pm0.04)P_4$	45 ± 5	47	90
5.35	-135	$1+(0.27\pm0.04)P_2$			
		$1+(0.25\pm0.04)P_2+(0.03\pm0.06)P_4$	45 ± 5	23	45

agreement with the theoretical expectation and as P_4 terms were found small, it was not felt necessary to find the angle of symmetry which gave a best fit in terms of functions containing polynomials of higher order than two. Hence the correlation functions containing P_4 terms are also calculated for the angle of symmetry which gave the best fit containing terms up to P_2. The experimental values of (A_2/A_0) were finally corrected for the finite solid angle of the γ-ray detector making use of the analysis of Rose [34]) and these values are given in table 2. No correction for the solid angle of the neutron detector was taken into account in this analysis, as it was not considered necessary.

TABLE 2

The values of the different parameters obtained from the best fitting functions

E_d (lab) (MeV)	θ_{dn} (lab) (degrees)	$W(\theta) = A_0+A_2P_2\cos(\theta_\gamma-\theta_0)$ (A_2/A_0)	(A_2/A_0) a)	λ
2.65	0	0.33±0.01	0.35±0.01	0.72
2.65	− 20	0.14±0.02	0.15±0.02	0.30
2.65	− 45	0.12±0.02	0.13±0.02	0.27
2.65	− 70	0.18±0.01	0.19±0.01	0.39
2.65	− 90	0.41±0.03	0.43±0.03	0.88
2.65	−110	0.38±0.03	0.40±0.03	0.81
2.65	−135	0.26±0.03	0.27±0.03	0.56
5.35	0	0.49±0.03	0.51±0.03	1.00
5.35	− 20	0.31±0.03	0.33±0.03	0.70
5.35	− 40	0.01±0.03	0.01±0.03	0.01
5.35	− 65	0.40±0.03	0.42±0.03	0.87
5.35	− 90	0.16±0.04	0.17±0.04	0.37
5.35	−135	0.27±0.04	0.28±0.04	0.56

a) Values which are corrected for the solid angle of the γ-ray detector.

Discussion

4.1. NEUTRON ANGULAR DISTRIBUTIONS

The angular distribution of the ground state neutron group from the reaction $B^{11}(d, n)C^{12}$ has been measured by many investigators [35–41]) in the range of energies from 0.6 MeV to 9 MeV, and the angular distribution of the neutrons leading to the 4.43 MeV level of C^{12} has been measured at energies below 2 MeV by Ames *et al.* [42]) and Neilson *et al.* [43]), and above 9 MeV by Maslin *et al.* [44]) and others [45]). In several cases the distributions were found to be peaked in the forward direction with a large intensity at backward angles. Class *et al.* measured the angular distributions of the ground state neutrons for a number of energies from 2 to 5.0 MeV, and these results were analyzed by Owen and Madansky [9]) in terms of a mixture of ordinary and heavy particle stripping, which gave a good fit to the experimental data. More recently this reaction was studied by Zeidman and Fowler [45]) at an incident energy of 10 MeV and they also observed a strong peak at 20° and a large intensity at backward angles. They also obtained reasonably good agreement with the heavy particle stripping theory of Owen *et al.*, by using a value of 1.4 for the ratio of the amplitudes of heavy particle stripping and ordinary stripping and values of angular momentum of the captured proton of $l_p = 1$ for ordinary stripping and $l_c = 0$ for heavy particle stripping. Neither in the analysis of Zeidman and Fowler [45]) nor in that of Owen and Madansky [9]) was proper account taken of the interference between the two modes; in spite of this, reasonably good fits to the experimental results were obtained, although Hasegave and Ichikawa [46]) have stressed the importance of the interference terms in the analysis of experimental results involving mode mixtures of ordinary and heavy particle stripping.

Since no measurement of the angular distribution of the neutrons leading to the 4.43 MeV level in C^{12} in the energy range of 2 to 9 MeV had been published previously, we measured two angular distributions in the manner described earlier. Our results are similar to those measured in other laboratories at other energies, although as explained before, they are not in principle, angular distributions if the corresponding (n, γ) correlations are not isotropic. These distributions also show a forward peaking, and a large intensity at backward angles. At the higher energy of 5.35 MeV, the peak is shifted to a larger angle and is sharper than at the lower energy. No attempt has been made to fit these distributions with the theory as one can almost always get a good fit by arbitrarily adjusting the different parameters involved in a mixture of Butler and heavy particle stripping, and the most obvious test of this theory would be to look for its effect in the angular correlation measurements. If this type of reaction mechanism is important then the angular correlations would be expected to show the symmetry properties predicted by the theory.

4.2. NEUTRON-GAMMA CORRELATIONS

On the basis of the simple theory of stripping the theoretical expression for the angular correlation function of the γ-rays in coincidence with the outgoing particle for j—j and L—S coupling schemes, has been given by Satchler [14]). The correlation function predicted is independent of the incident deuteron energy and the outgoing neutron direction and has been used in the past[22–24]) for the determination of the type of coupling scheme involved in a reaction, as well as for determining the channel spin mixing ratio. Our measurements of the $(n\gamma)$ correlations in the $B^{11}(d, n)C^{12}$ reaction show that the measured correlation functions vary appreciably both with incident deuteron energy and as a function of the outgoing neutron direction. Hence the value of previous measurements of the type of coupling scheme or the channel spin mixing ratio, analysed by the plane wave theory, must be questioned unless it can be shown that such experiments have been carried out under conditions such that a plane wave description is a good approximation.

4.3. DISTORTED WAVE THEORY

It has been mentioned earlier that distorted wave calculations for (d, pγ) correlations have been made by Satchler and Tobocman [20]) using different forms of potential and it has been shown that on such an analysis one would expect a change in the anisotropy of the correlation function as well as in the angle of symmetry, as a function of the outgoing proton direction.

According to Satchler and Tobocman [20]) the general expression for the angular distribution of γ-rays in coincidence with the outgoing particle is given as

$$W(\phi, \theta) = \sum_{kq} a_{kq} C_{kq}(\phi, \theta),$$

where

$$a_{kq} = g_k d_{kq}.$$

Here ϕ is the angle between the direction of the γ-ray and the axis $\mathbf{k}_d \wedge \mathbf{k}_n$, while θ is the angle between the recoil direction and the projection of the γ-ray direction on the reaction plane. The factor g_k contains the terms dependent on the nuclear spins, and the type of coupling involved in the reaction and is independent of the reaction mechanism whereas d_{kq} contains the terms depending on the type of reaction mechanism as well as on the effects of distorted waves.

In a reaction where the value of k is restricted to 0 or 2, as in the present reaction, the (n, γ) correlation function takes the general form

$$W(\phi, \theta) = 1+A_2^0 P_2(\cos \phi)+A_2^2 P_2^2(\cos \phi)[\cos 2(\theta-\theta_0)],$$

on taking $\phi = \frac{1}{2}\pi$ and $A_2^2/A_2^0 = -\frac{1}{2}\lambda$ the above expression reduces to

$$W(\phi, \theta) = 1+\alpha \cos^2 (\theta-\theta_0),$$

where

$$\alpha = \frac{-6A_2^0\lambda}{2-A_2^0(1-3\lambda)},$$

θ is the angle between γ-rays and the beam direction, and θ_0 is the angle of symmetry of the correlation.

In the plane wave limit, the stripping assumption identifies θ_0 as the angle of the classical recoil direction and makes a definite prediction for the value of α which is independent of the outgoing neutron direction. The parameter λ is called an attenuation coefficient; in the plane wave limit its value is equal to unity and $A_2^0 = -\frac{1}{2}g_2$. However, on distorted wave theory for $l = 1$ capture, λ can vary within the limits $0 \leqq \lambda \leqq 1$ as a function of the outgoing neutron direction, and thus can reduce the anisotropy to λ times its value in the plane wave limit. The value of λ can be calculated theoretically for any reaction using distorted wave analysis and can then be compared with the experimental value.

In order to calculate the value of λ from the experimental results, it is necessary to know the value of g_2 which, in the case of reactions for which all the spins and parities are known, can easily be determined. In the reaction $B^{11}(d, n)C^{12}$ the ground state of B^{11} is known to have spin $\frac{3}{2}$ and odd parity and the first excited state of C^{12} has spin 2 and even parity and decays to the ground state by the emission of pure E2 γ-rays. Hence from the conservation of parity and spin, this state is expected to be formed by capture of protons having $l = 1$ or $l = 3$, the former value being supported by the measured neutron angular distribution. Hence the highest order polynomial in the correlation function should be of order 2. In terms of the channel spin representation, the channel spin can have the values $S = 1$ and $S = 2$, and this is the only unknown parameter in the determination of g_2. If the simple theory of stripping were adequate, it would be quite possible to predict the type of coupling scheme involved as well as to determine the mixing ratio of the two channel spins from the measurement of the (n, γ) correlation function. Since the pure j—j coupling scheme for this reactions predicts an isotropic correlation, the presence of an anisotropy at all angles of the outgoing neutron direction favours the L—S coupling scheme. The maximum value of the coefficient of $P_2(\cos\theta)$ observed at $E_d = 5.35$ MeV and $\theta_n = 0°$ is in agreement with the theoretical value of (+0.5) predicted by simple theory for the L—S coupling scheme and on the assumption that the 4.43 MeV level is a $^1D_2$ state formed by 100 % $S = 1$ capture. This value of anisotropy if accepted, would predict the value of λ as unity in agreement with the expectation of simple theory. However, it should be noted that all our other measured correlations give a lower value of the anisotropy and would predict a different value for the channel spin mixing ratio. Hence it is apparent that the simple theory is not adequate to explain the observed correlations and it appears necessary to resort to a theory taking into account the effect of distorted waves.

4.4. HEAVY PARTICLE STRIPPING

We shall now consider the effects of heavy particle stripping on the (n, γ) angular correlation functions. If it is considered that the B^{11} nucleus consists of a B^{10} core in its ground state plus an odd neutron in the $p_{\frac{3}{2}}$ shell, which is stripped off from its core as the core is being captured by the incident deuteron to form C^{12} in the first excited state, then since B^{10} has spin 3 and even parity, the deuteron has spin 1 and even parity and the 4.43 MeV level of C^{12} has spin 2 and even parity, the selection rules for the conservation of parity and spin allow only even values of the angular momentum of the captured core and these are restricted to 0, 2 and 4. However, it is expected that the cross section for the lowest allowed value of l_c will be dominant. This is partially supported by the analysis of the angular distribution of neutrons by Zeidman and Fowler [45]), who obtained a good fit to their results by using the value $l_c = 0$. In addition, the same value of l_c was used by Owen *et al.* [42]) to analyse their results at 1 MeV and an attempt to fit the experimental data by using $l_c = 2$ was unsuccessful. Hence if heavy particle stripping is considered as the dominant reaction mechanism contributing to the intensity of neutrons at backward angles, the angular distribution of γ-rays in coincidence with neutrons detected at backward angles should be isotropic, because the maximum order of polynomial (ν) in the correlation function is restricted to $\nu \leqq 2l_c$. On the other hand ordinary stripping allows the angular momentum of the captured particle to be $l_p = 1$, and hence the correlation should contain terms up to $P_2(\cos \theta)$. Therefore if either the heavy particle stripping or ordinary stripping is the dominant reaction mechanism (i.e., an order of magnitude greater) the angular correlation measurement on the basis of simple theory should be quite clear cut and should provide evidence in favour of one or other of the reaction mechanisms. However, if the two processes are taking part more or less to the same degree, the correlation functions are expected to be complicated functions of the incident deuteron energy and the outgoing neutron direction [15]).

Our results on the (n, γ) angular correlation measurements show the following features. At the lower deuteron bombarding energy of 2.65 MeV and backward angles of 90°, 110° and 135° of the outgoing neutrons, the correlations are consistent with the simple Butler stripping mechanism as regards the axis of symmetry, for this coincides with the classical recoil direction within the experimental errors (fig. 12). It is significant to note that no correlation is symmetrical about the axis predicted by the heavy particle stripping mechanism, so that this mode appears to be less important than ordinary stripping even at backward angles. The axes of symmetry of the correlations measured for forward angles of 0°, 20°, 40° and 70° of the neutron direction do not coincide with the classical recoil direction as expected on simple theory. Moreover as mentioned before, the simple theory of stripping predicts the value of anisotropy to be independent of the outgoing neutron direction, whereas all the measured correlations show a change in the anisotropy as a function of the angle of the outgoing neutron direction (table 1). It has been mentioned earlier that the presence of heavy particle stripping can produce a change in the anisotropy as a function of the neutron direction depending on the relative contribution from this reaction mechanism to the neutron intensity at the chosen angle. However, since heavy particle stripping is supposed to account for the intensity of neutrons in the backward direction where ordinary stripping contributes very little, it is expected that the correlation anisotropy will be more attenuated in the backward directions due to the expected isotropic correlation from this mechanism. The experimental results show a maximum anisotropy at 90° and a minimum at 45° for $E_d = 2.65$ MeV. This fact is difficult to reconcile with the expectation of heavy particle stripping.

The angular correlations for $E_d = 5.35$ show a similar behaviour except that the anisotropy varies more rapidly as a function of the neutron angle. Apart from the presumably accidental coincidence of the axis of symmetry with the expected direction of K_2 arising from the heavy particle stripping mode for $\theta_n = -135°$, no positive evidence supporting this reaction mechanism is apparent. The anisotropy is found to have a maximum at $\theta_n = 0°$ and a minimum for $\theta_n = 40°$.

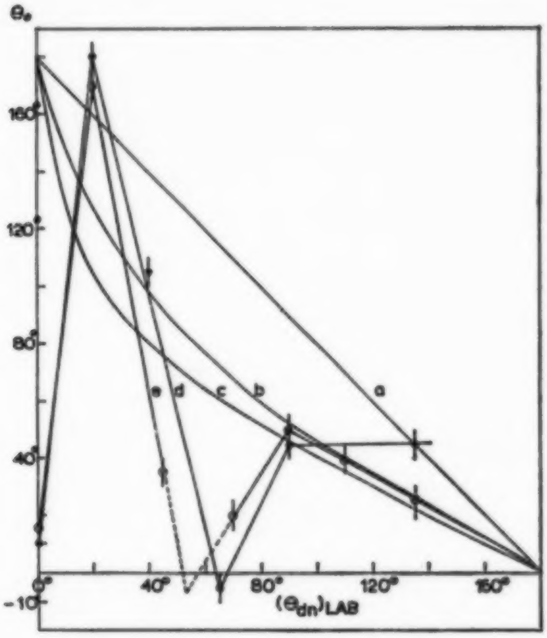

Fig. 12. The angle of the symmetry axis as a function of the outgoing neutron direction (a) the axis $\mathbf{K}_2$ arising from the heavy particle stripping mode at both energies (b) the axis $\mathbf{k}_1$ of Butler stripping for $E_d = 2.65$ MeV, (c) the same for $E_d = 5.35$ MeV, (d) the curve obtained by joining all the experimentally determined values of the angle of symmetry of the (n, γ) correlations for $E_d = 5.35$ MeV, (e) a similar curve for $E_d = 2.65$ MeV.

Referring back to the distorted wave analysis of Satchler *et al.* [20]) we have calculated the value of λ from our experimental angular correlation functions measured at different directions of the outgoing neutrons and for two different energies. These values are shown in fig. 13. The best value of the angle of symmetry of the correlations are shown in fig. 12 and are compared with the classical recoil direction and direction of $\mathbf{K}_2$. (expected angles of symmetry on plane wave theory) for ordinary and heavy particle stripping. Although no distorted wave calculations have been made for the (d, n) reactions, we see that these results show a general behaviour in qualitative agreement with the calculations of Satchler and Tobocman on $B^{10}(d, p\gamma)$ correlations. This suggests that it might be very useful to make similar calculations for the $^{11}B(d, n\gamma)^{12}C$ reaction to compare with the present results.

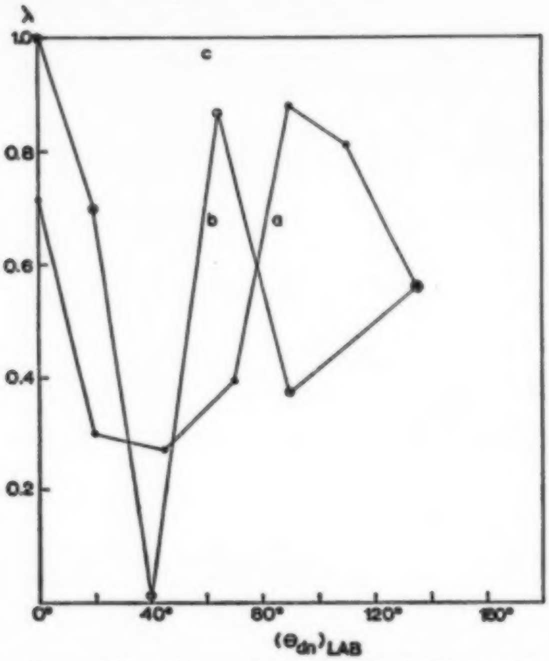

Fig. 13. The observed values of the attenuation coefficient (λ) as a function of the outgoing neutron direction. Curve (a) is for $E_d = 2.65$ MeV, curve (b) is for $E_d = 5.35$ MeV, curve (c) shows the theoretical value for λ expected on plane wave theory.

5. Conclusion

The purpose of this investigation was to examine the extent of validity of the simple Butler theory of stripping as well as to investigate the effects of distortions of the incident and outgoing waves. Particular interest was aroused in this study because of the presence of features usually attributed to heavy particle stripping in the angular distributions of neutrons.

The results of this investigation clearly show that the simple theory is not adequate to explain the detailed features of the reaction mechanism, but that good qualitative agreement might be expected by more sophisticated calculations including distorted wave effects. Our results on the (n, γ) correlation measurements for backward angles of neutrons and those of Hill and Blair for (p, γ) correlation measurements from the $Si^{29}(d, p\gamma)Si^{30}$ reaction [23]) throw doubt on the presence of heavy particle stripping and suggest that it may be possible to explain the backward intensity in the angular distributions purely on the basis of a distorted wave calculation.

As the value of the attenuation coefficient λ in the angular correlations is related to the neutron polarization P by the equation $(2j+1)P = \pm\frac{2}{3}(1-\lambda^2)$ it is suggested that a measurement of neutron polarization from this reaction at the angles of the outgoing neutron direction chosen here, may be very useful as a further test of the distorted wave theory.

We should like to acknowledge our indebtedness to Dr. John O. Newton for his helpful comments.

References

1) S. T. Butler, Phys. Rev. **80** (1950) 1095, Proc. Roy. Soc. A **208** (1951) 559
2) Bhatia, Huang, Huby and Newns, Phil. Mag. **43** (1952) 485
3) E. Gerjuoy, Phys. Rev. **91** (1953) 645
4) P. B. Daitch and J. A. French, Phys. Rev. **87** (1952) 900
5) R. Huby, Proc. Roy. Soc. A **215** (1952) 385
6) N. Austern, Phys. Rev. **89** (1953) 318
7) F. L. Friedman and W. Tobocman, Phys. Rev. **92** (1953) 93
8) L. Madansky and G. E. Owen, Phys. Rev. **99** (1955) 1608
9) G. E. Owen and L. Madansky, Phys. Rev. **105** (1957) 1766
10) Owen, Madansky and Edwards, Phys. Rev. **113** (1959) 1575
11) G. R. Satchler and J. A. Spiers, Proc. Phys. Soc. A **65** (1952) 980
12) Biedenharn, Boyer and Charpie, Phys. Rev. **88** (1952) 517
13) L. J. Gallaher and W. B. Cheston, Phys. Rev. **88** (1952) 684
14) G. R. Satchler, Proc. Phys. Soc. A **66** (1953) 1081
15) S. Edwards, Phys. Rev. **113** (1959) 1277
16) J. Horowitz and A. M. L. Messiah, J. Phys. Rad. **14** (1953) 695, **15** (1954) 142
17) W. Tobocman and M. H. Kalos, Phys. Rev. **97** (1955) 132
18) H. C. Newns and M. Y. Refai, Proc. Phys. Soc. **71** (1958) 627
19) Huby, Refai and Satchler, Nuclear Physics **9** (1958) 94
20) G. R. Satchler and W. Tobocman, Phys. Rev. **118** (1960) 1566
21) Allen, Collinge, Hird, Maglic and Orman, Proc. Phys. Soc. A **69** (1956) 705
22) S. A. Cox and R. M. Williamson, Phys. Rev. **105** (1957) 1799
23) H. A. Hill and J. M. Blair, Phys. Rev. **111** (1958) 1142
24) R. Taylor, Phys. Rev. **113** (1959) 1293
25) Kuehner, Almquist and Bromley, Phys. Rev. letters **4** (1960) 132
26) Gorodetzky, Samuel and Gallman, J. Physique Rad. **21** (1960) 349
27) Rask, Ames and Owen, Bull. Am. Phys. Soc. **2** (1957) 351
28) Neilson, Dawson, Sample and Johnson (private communication)
29) Garg, Calvert and Gale, Nuclear Physics **19** (1960) 264
30) J. B. Garg, Nuclear Instruments and Methods **6** (1960) 72
31) Slotzfus, Frichteruich and Nelson, Bull. Am. Phys. Soc. **1** (1956) 329
32) Burke, Risser and Phillips, Phys. Rev. **93** (1954) 188
33) F. Ajzenberg-Selove and T. Lauritsen, Nuclear Physics **11** (1959) 125
34) M. E. Rose, Phys. Rev. **91** (1953) 610
35) A. Graue, Phil. Mag. **45** (1954) 1205
36) W. M. Gibson, Phil. Mag. **44** (1953) 297
37) Ames, Owen and Swartz, Phys. Rev. **106** (1957) 775
38) A. Ward and P. J. Grant, Proc. Phys. Soc. A **68** (1955) 637
39) M. I. Ihsan, Proc. Phys. Soc. A **68** (1955) 393
40) Bird and Spear, Austr. J. Phys. **10** (1957) 268
41) Bogdanov, Vlasov, Kalinin, Rybakov and Sidorov, Soviet Physics (JETP) **3** (1956) 793
42) O. Ames and G. E. Owen, Phys. Rev. **109** (1958) 1639
43) Neilson, Dawson and Sample, Bull. Am. Phys. Soc. **3** (1958) 323
44) Maslin, Calvert and Jaffe, Proc. Phys. Soc. A **69** (1956) 754
45) B. Zeidman and J. M. Fowler, Phys. Rev. **112** (1958) 2020
46) K. Hasegawa and Y. H. Ichikawa, Prog. Theoret. Phys. **21** (1959) 569

2.B

Nuclear Physics **23** (1961) 648—656; © *North-Holland Publishing Co., Amsterdam*

Not to be reproduced by photoprint or microfilm without written permission from the publisher

THE $C^{12}(d, n)N^{13}$ REACTION UP TO 1.35 MeV

A. N. JAMES
Cavendish Laboratory, Cambridge

Received 2 January 1961

Abstract: Angular distributions and excitation functions were measured for the ground state neutron group in $C^{12}(d, n)N^{13}$ in the energy range $E_d = 0.7$ MeV to 1.35 MeV. The results are interpreted in terms of compound nucleus formation. A comparison with $C^{12}(d, p)C^{13}$ is made.

1. Introduction

Attempts to assess the relative importance of compound nucleus and direct reaction effects in nuclear reactions following deuteron bombardment of C^{12} have led to differing conclusions 1–3)). There are two reasons why difficulty is encountered. Firstly, the effects of interference between these two extreme types of reaction are not understood. Secondly, both Butler type stripping curves with $l = 1$ and sums of Legendre functions $\sum_0^4 a_n P_n(\cos\theta)$, with a_3+a_4 large and negative, predict a peak near 30° in angular distributions from (d, p_0) and (d, n_0) reactions.

Experimental observations of these reactions 1, 2, 4, 5) all show the existence of a peak in the angular distribution near 30° over a range of deuteron energies from 800 keV to 6 MeV (ref. 6)) and higher 7, 8)). In the low energy region (< 2 MeV) the observations always show a large differential cross section for backward angles, often with a peak near 150°. Elwyn *et al.* 1)) have shown that this backward peak cannot be explained in terms of heavy particle stripping-type direct reactions, but point out that it could arise by surface reflections and refractions. (See also Butler, Austern and Pearson 9))). Other aspects of their analysis favour a stripping theory approach. Nevertheless, the success of Sarma *et al.* 4)) in fitting the (d, p_0) angular distributions over the whole range of their measurements by sums of Legendre functions, where the coefficients a_n varied with energy in a way that was entirely consistent with compound nucleus formation, indicates that below 2 MeV compound nucleus formation is the important reaction path for (d, p_0).

It is worth pointing out that the (d, n_0) data below 2 MeV given in the paper of Elwyn *et al.* 1)) can be fitted over the whole angular range of the measurements by a sum of Legendre functions. Also, analysis of (d, p_1) and (d, n_1) data in terms of compound nucleus parameters 2)) is unsound as the angular distributions are very closely fitted by Butler type stripping curves 7, 10)).

The analysis of deuteron elastic scattering and (d, p_0) data by Kashy *et al.* [3]) produced information about the formation and decay of the 11.04, 11.29 and 11.38 MeV levels in N^{14}. This analysis was based on the formulae of Blatt and Biedenharn [11]) derived from single level dispersion theory. It is interesting to consider the differences which might be observed between the mirror reactions (d, p_0) and (d, n_0).

Since the reaction is assumed to pass through the intermediate step of a compound nucleus state, only the break up of this state can give rise to such differences. Apart from the obvious kinetic factor the differences are in the phases of the outgoing nucleon wave functions and in the partial widths for the decay of the states. When the neutron and proton wave functions have different phases the interference terms between different compound states can be entirely different in the two reactions. In this case (C^{12}+d up to 1.4 MeV) odd order interference terms are the only ones which are important and affect a_1 and a_3. Differences in the partial widths affect the total cross section, they can also influence the differential cross section by affecting mixing ratios when more than one decay channel is allowed.

In carrying out some investigations into the performance of a fast neutron time of flight spectrometer the angular distribution of the neutrons in $C^{12}(d, n_0)N^{13}$ and the variation of the differential cross section with energy were found to be different from those reported previously [5, 12]).

2. Experimental Considerations

The Cavendish Laboratory's 1.4 MV Cockcroft-Walton generator has been fitted with a pre-acceleration beam pulsing device of the Brookhaven type [13]). The average target current of 2μA is concentrated in bursts of deuterons from 5 to 6 ns duration separated by 200 ns. These bursts provide a time correlated source of neutrons. Events in a counter (up to 3m from the target) were sorted according to the time delay between the arrival of a beam pulse at the target and the event in the counter. This was accomplished using a time to pulse height converter which developed its output signal by switching on a standard current into a condenser when there was an event in the neutron counter, and stopping it when a delayed signal, from a special scintillation detector [14]) indicating the arrival of the beam pulse at the target, reached the converter.

The neutron counter was a 5.08 cm diameter by 5.08 cm long liquid scintillation cell (Nuclear Enterprise N.E. 213) optically coupled to a photomultiplier. Since good time resolution was not necessary (there being only one neutron group) and low noise current was desirable, an E.M.I. type 6097 photomultiplier was chosen. With this system the time resolution for the neutron burst was 8 ns. Two slow selection conditions determined which events in the neutron counter were registered. A conventional proportional signal, taken from dynode 9, was used to select only those events in the counter which corresponded to proton recoils of energy greater than 330 keV. The final multiplying stage (D_{11}–A) was run as a saturating device [15]) giving neutron discrimination pulses on dynode 11. The fast signal was taken from dynode 10. The extra condition of neutron selection suppressed the gamma-ray peak from the time spectrum (see, for example, fig. 3 of ref. [1])) and reduced the continuous background by a factor of 10 without loss in neutron efficiency. With this reduction in background an open geometry arrangement was possible, a flight path of 1 m being used.

The target used throughout these experiments was an isotopic C^{12} deposit 100 μg/cm^2 thick on a 0.05 cm copper backing. This target thickness corresponds to a loss of deuteron energy in the target of about 25 keV which is less than the width of any of the resonances observed.

In measuring the angular distribution of the neutrons in $C^{12}(d, n_0)N^{13}$ from 0.95 to 1.35 MeV, neutrons of energy not much greater than the counter bias (equivalent to E_b proton recoil energy) have to be recorded. With a phosphor as large as 5.08 cm by 5.08 cm the efficiency will be affected by attenuation of the neutron beam in the phosphor and also by internal multiple scatterings being recorded as a single event. For an ideal small phosphor the efficiency ε_0 for neutrons of energy E_n is

$$\varepsilon_0 = \sigma(E_n)\left(\frac{E_n-E_b}{E_n}\right),$$

where $\sigma(E_n)$ is the neutron-proton elastic section. Rough calculation showed that below 3 MeV the efficiency of the phosphor would be lower than ε_0 by up to 30 %, but that below 1 MeV an approximately linear relationship would exist between $E_n\varepsilon/\sigma$ and E_n, the slope being less than for ε_0. Experimentally, the variation of efficiency with energy was measured by comparing the counting rate (for $C^{12}(d, n)N^{13}$) in the neutron counter with that in a long counter placed in the same relative position to the deuteron beam, the two counters being, therefore, in the same neutron flux. Fig. 1 shows the linear relationship obtained [†]. The counter bias found by this method was the same as that estimated from the proportional spectrum for mono-energetic neutrons.

In the angular distribution measurements possible residual errors, between points at 0° and 150°, in the relative efficiency correction were less than 10 %. (The departure from linearity observed for a long counter of similar design [16]) had a negligible effect on the efficiency function). The effect of such an error on the measured angular distributions was approximately a factor $1+b\cos\theta$, where $b < 0.1$.

[†] Similar efficiency plots measured for the same counter by comparison with the known $T(p, n)He^3$ differential cross section at 3 MeV also verified the conclusions of the rough calculations at higher neutron energies.

Fig. 2 is a typical angular distribution measurement, the smooth curve shown is a sum of Legendre functions where the coefficients a_n were adjusted to give the best fit to the data. Errors in the experimental values of a_n were estimated by finding what changes could be made in a_n before subsequent alteration of $a_i (i \neq n)$ failed to restore an adequate fit to the data. Six angular distributions were measured using the time of flight apparatus.

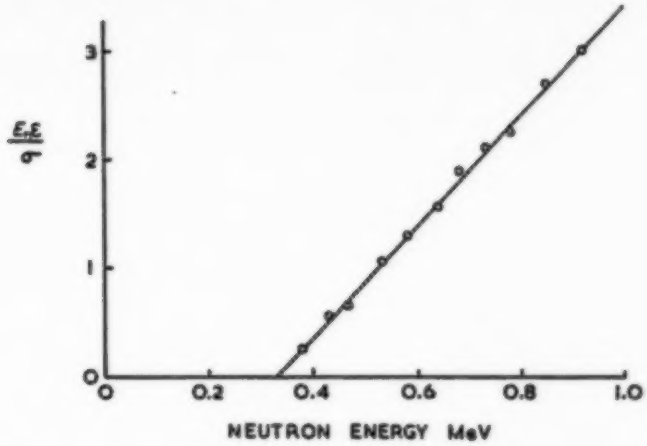

Fig. 1. Variation of the counter efficiency with neutron energy.

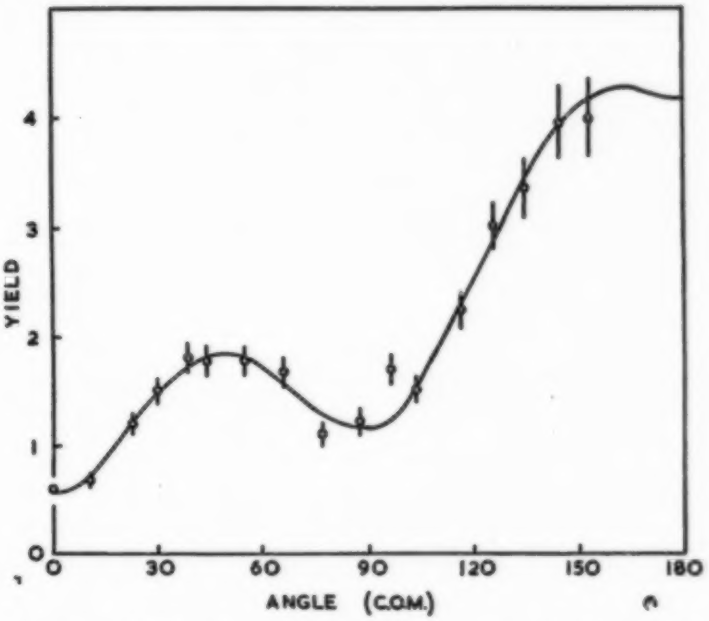

Fig. 2. Angular distribution in the centre-of-mass system for C^{12}(d, n)N^{13} at $E_d = 1.15$ MeV.

In view of the low value for the differential cross section observed at 0° between 1.1 and 1.2 MeV, excitation functions were measured using a long counter twice as far from the target as in the experiment of Bailey *et al.* [12]), thus improving the angular resolution. The energy interval between measurements was 10 keV. Fig. 3 shows the experimental excitation functions after subtraction of background ($\approx 10\%$) measured by bombarding the clean target backing. Included in the excitation function is a further background,

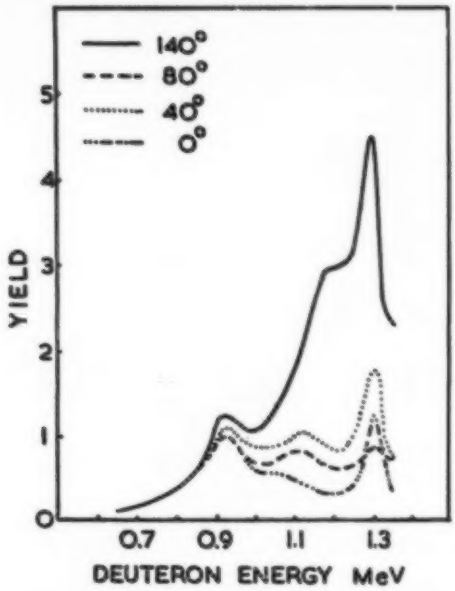

Fig. 3. Long counter excitation functions for C^{12}(d, n)N^{13} in the laboratory system.

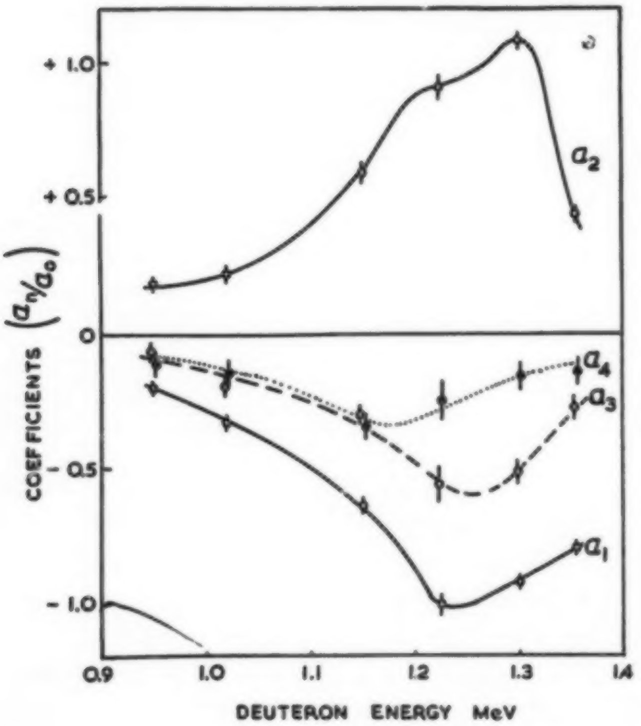

Fig. 4. Variation of the coefficients a_n in the sum $\Sigma_0^4\, a_n P_n(\cos\theta)$ which fits the angular distributions in the centre-of-mass system for C^{12}(d, n)N^{13}.

less than 10 %, which was caused by neutrons from the C^{12} target being scattered into the counter. These excitation functions agreed with the angular distribution measurements and were used to determine the way in which the coefficients a_1 and a_2 changed with energy bewteen the measured points (fig. 4).

In all the measurements maxima and minima were more pronounced than in earlier reports of similar experiments [5, 12]). The coefficient a_4 was much larger than that observed by other experimenters in both the (d, n_0) and (d, p_0) reactions; attempts to find faults in the measurements which would have given spurious a_4 coefficients at all deuteron energies failed. Poor angular resolution and sensitivity to scattered neutrons, features of earlier neutron experiments which might have obscured the observation of a_4, were absent in the time of flight measurements. It is also conceivable that small a_4 coefficients could have been missed in (d, p_0) measurements since the data rarely extends to angles less than 30°. The data of Kashy *et al.* [2]) and Elwyn *et al.* [1]) indicate a similar discrepancy between the (d, n_0) and (d, p_0) reactions near 1.7 MeV.

3. Discussion

Bearing in mind the principles involved in the theoretical expression for the angular distribution of reaction products when two resonances overlap (*e.g.* eq. (2) of ref. [2]), the data of fig. 4 can be used to find the angular distributions which would have been expected from the three resonances, 0.92, 1.19 and 1.30 MeV, had they been totally isolated.

3.1. THE 0.92 MeV RESONANCE (11.04 MeV in N^{14})

There was no evidence to suggest that the angular distribution for this resonance was anything other than isotropic. The assignments $J^\pi = 1^+$, $l_d = 0$, $l_n = 1$ are well substantiated [2]).

3.2. THE 1.19 MeV RESONANCE (11.29 MeV in N^{14})

The angular distribution measured for this resonance was

$$W(\theta) \propto P_0 + (0.83\pm0.10)P_2 - (0.30\pm0.10)P_4.$$

The significance of the P_4 term in the angular distribution is that values of the deuteron angular momentum (l_d) greater than 1 must contribute to the formation of the compound state, and that the compound state must have $J \geqq 2$. The elastic scattering data [2]) restricted the assignments for this state to $J^\pi = 1^-$ or 2^-, 2^- being favoured by the (d, p_0) angular distribution. With the assignment 2^- established the only value allowed for the angular momentum l of the decay of the state is 2. Since the decay is restricted to $l = 2$, with channel spin either 0 or 1, the angular distributions for (d, n_0) and (d, p_0) can only be different by having different fractions of decays by channel spin zero.

The angular distributions expected for formation of a 2^- state by a mixture of $l_d = 1$ and $l_d = 3$ waves were calculated for decay by channel spins 0 and 1 using the tables of Sharpe, Kennedy, Sears and Hoyle [17]) (fig. 5). The amplitude mixing ratio x and the phase difference ξ will have the same value for both decay channel spins since they describe the formation of the compound nuclear state. The range of variables x, ξ and z (the fraction of decays by channel spin 1) which agreed with experiment is large, but as the main contribution to deuteron elastic scattering [2]) is $l_d = 1$ it is probably that z is small. Since this resonance must be partly formed by $l_d = 3$ the behaviour of the coefficients a_1 and a_3, in both (d, n_0) and (d, p_0) near the 1.30 MeV resonance no longer requires that the 1.30 MeV resonance be formed by a mixture of l_d values.

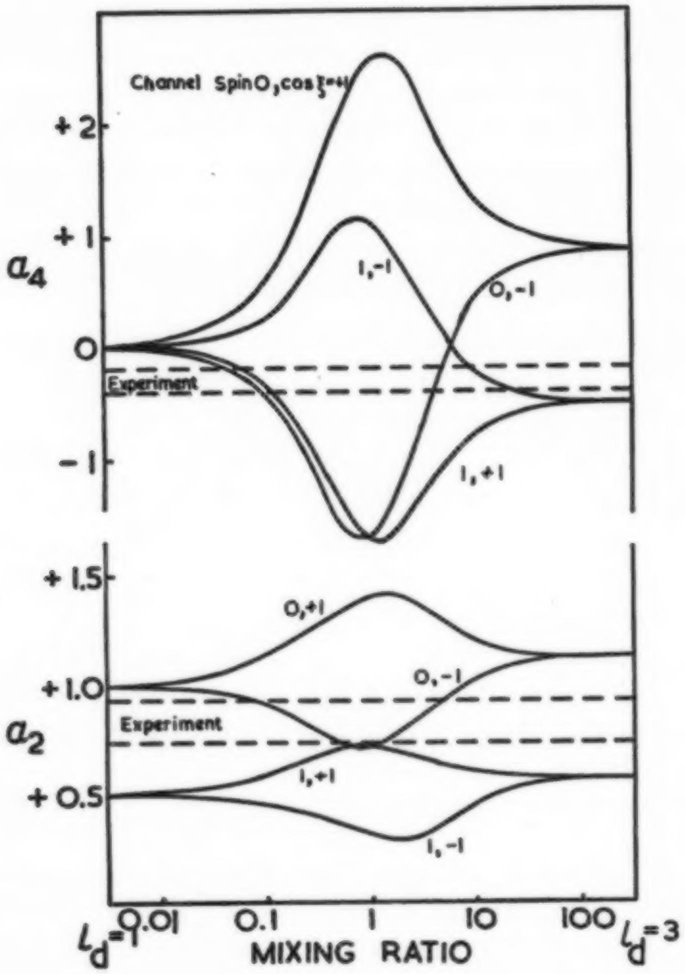

Fig. 5. Theoretical variations of a_n at the 1.19 MeV resonance. The angular distribution is

$$W(\theta) \propto (1-z)\{P_0(\cos\theta)+a_2(x;\ 0,\ \cos\xi)P_2(\cos\theta)+a_4(x;\ 0,\ \cos\xi)P_4(\cos\theta)\}$$
$$+\,z\{P_0(\cos\theta)+a_2(x;\ 1,\ \cos\xi)P_2(\cos\theta)+a_4(x;\ 1,\ \cos\xi)P_4(\cos\theta)\}.$$

3.3. THE 1.30 MeV RESONANCE (11.38 MeV in N^{14})

The neutron angular distribution measured for this resonance was

$$W(\theta) \propto P_0 + (1.00 \pm 0.05) P_2.$$

The only possible spin and angular momentum values forming a positive parity[2]) level where $a_2 \approx 1$ and $a_4 = 0$ are $J = 1$ and $l_d = 0$ and 2, the decay being by $l = 1$. Theoretical values of a_2 calculated for this case show that the values of the mixing ratio x (for $l_d = 0$ and 2) and the phase difference ξ are limited by experiment to the shaded area on fig. 6. The theoretical distributions are such that once values of x and $\cos \xi$ are chosen within this area then only one value of z (the fraction of decays by channel spin 1) is possible for agreement with experiment. A scale of z is shown in fig. 6. With the result $\Gamma_{d0}/\Gamma_{d2} < 0.3$ from elastic scattering [2]), $z < 0.2$.

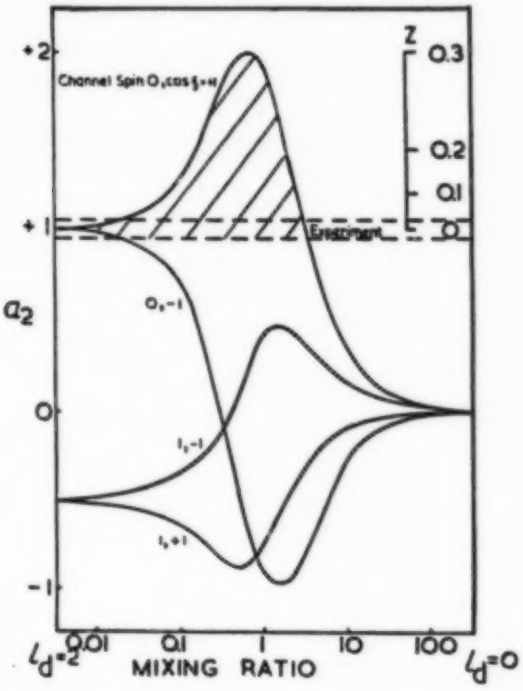

Fig. 6. Theoretical variations of a_n at the 1.30 MeV resonance.

4. Conclusion

The observation of a small a_4 coefficient in the (d, n_0) angular distribution for the 1.19 MeV resonance is consistent with a mixture of l_d values in its formation. Since such a coefficient is not observed in the (d, p_0) angular distribution and the compound state only breaks up by the emission of d wave protons or neutrons, the ratio of the number of decays by channel spin 0 and 1 for neutron emission must be different from that for proton emission indicating a departure from charge symmetry.

The isotopic target was supplied by A.E.R.E. Harwell. The author is indebted to the Department of Scientific and Industrial Research for a Research Fellowship during the course of this work. The author also wishes to acknowledge Mr. D. D. Stewart's invaluable aid in running and maintaining the Cockcroft-Walton generator.

References

1) A. Elwyn, J. V. Kane, S. Ofer and D. H. Wilkinson, Phys. Rev. **116** (1959) 1490
2) E. Kashy, R. R. Perry and J. R. Risser, Phys. Rev. **117** (1960) 1289
3) M. T. McEllistrem, Phys. Rev. **111** (1958) 596
4) N. Sarma, M. Govindjee and H. R. Allan, Proc. Phys. Soc. **A 70** (1957) 68
5) G. C. Phillips, Phys. Rev. (1950) **80** 164
6) T. W. Bonner, J. T. Eisinger, A. A. Kraus and J. B. Marion Phys. Rev. **101** (1956) 200
7) J. M. Calvert, A. A. Jaffe and E. E. Maslin, Proc. Phys. Soc. **A 70** (1957) 78
8) F. Ajzenberg-Selove and T. Lauritsen, Nuclear Physics **11** (1959) 1
9) S. T. Butler, N. Austern and C. Pearson, Phys. Rev. **112** (1958) 1227
10) J. P. F. Sellschop, Phys. Rev. Letters **3** (1959) 346
11) J. M. Blatt and L. C. Biedenharn, Rev. Mod. Phys. **24** (1952) 258
12) C. L. Bailey, G. Freier and J. H. Williams, Phys. Rev. **73** (1948) 274
13) C. M. Turner and S. D. Bloom, Rev. Sci. Instr. **29** (1958) 480
14) A. N. James and C. M. P. Johnson, Nuclear Instruments (to be published)
15) R. B. Owen, Nucleonics **17**, No. 9(1959) 92
16) W. D. Allen and A. T. G. Ferguson, Proc. Phys. Soc. A **70** (1957) 639
17) W. T. Sharpe, J. M. Kennedy, B. J. Sears and M. G. Hoyle, At. En. Canada Lim. Report, AECL-97 (1954)

2.A.1:
4.E

Nuclear Physics **23** (1961) 657—666; ©*North-Holland Publishing Co., Amsterdam*

Not to be reproduced by photoprint or microfilm without written permission from the publisher

'HAMMER' TRACKS EMITTED FROM NUCLEAR DISINTEGRATIONS PRODUCED BY 4.6 GeV/c π^--MESONS

G. C. DEKA [†], D. EVANS,
University of Bristol

D. J. PROWSE,
University of California at Los Angeles
and
M. BALDO-CEOLIN
University of Padua

Received 25 July 1960

Abstract: Results are given concerning the energy and angular distribution of Li^8 fragments produced from interactions of 4.6 GeV/c π^--mesons with the heavy nuclei in emulsions. It is shown that the frequency of Li^9 and Be^8 is low and that the Li^8 production cannot be completely described in terms of evaporation theory. The energy distribution of the α-particles from Li^8 decay is given and its interpretation discussed.

1. Introduction

Since Powell and Occhialini [1]) first observed a T-shaped track (colloquially known as a 'hammer' track) in a photographic emulsion exposed to the cosmic radiation, and interpreted the event as being due to the β decay of Li^8 and subsequent break-up into two α-particles, many further examples have been found. The decay of Li^8 is usually considered to take place in the following two stages:

$$Li^8 \rightarrow Be^8+\beta+\nu, \quad Be^8 \rightarrow \alpha+\alpha.$$

In emulsion the Li^8 is always brought to rest and the decay process is seen as an event consisting of a track of low grain density due to the electron associated with two black tracks of small range ($\approx 5 \mu m$) due to the α-particles. The Be^8 recoils with a very low velocity and the α-particles are thus never expected to be emitted at an angle of more than 6° to one another [2]).

The production features of hammer tracks which have all been assumed to be due to Li^8 decays have been compared with the prediction of evaporation theory by Munir [3]) (who also summarizes earlier work), by Goldsack *et al.* [4]) and by Nakagawa *et al.* [5]). Recently Skjeggestad and Sorensen [6]) have considered the features of fragment production in general, including Li^8 and B^8 fragments, between which they were able to differentiate in their sample of hammer tracks. There remains the possibility that some hammer tracks may be due to the decay of Li^9 and this is considered in some detail in sect. 3. The energy spectrum of the two α-particles in the decay of Li^8 has been extensively studied [7-11], but little success has been attained in interpreting the data.

[†] Now at Cotton College, Gauhati, Assam, India.

In the course of a systematic search for hyperfragments [12] in emulsion stacks exposed to 4.6 GeV/c π^--mesons from the Berkeley Bevatron, a considerable number of hammer tracks have been found. The distributions of their energies and angles of emission have been studied in order to substantially add to the available data, particular attention being given to distinguishing examples of B^8 and Li^9 decays. Further, the interpretation of the α-particle energy spectrum has been critically examined in the light of the present knowledge of the α—α scattering phase shifts.

2. Experimental Method

The hammer tracks were found by following, until they left the plate of origin, every black and dark grey track from large stars ($N_h \geqq 8$) produced by the incident 4.6 GeV/c π^--meson beam. This introduces a certain geometrical bias against observing energetic fragments, but the correction can be rigorously calculated and applied to the energy spectrum of the fragments obtained. The range of each hammer track was recorded and the angle between its direction at the star and that of the incident meson measured.

Track width measurements were made on a sample of flat hammer tracks having a range $\geqq$ 60 μm. Further, the total light obscuration of the last 175 μm of a few flat tracks was measured using a photometer method [13].

The range of each α-particle from the decay point was measured and an attempt was made to ascertain their relative directions of emission. The numerical aperture of the microscope objective used was 1.3 but the resolution in each depth measurement is estimated to have been 0.5 μm at best. The shrinkage factor was obtained on the assumption that the mean unprocessed thickness of the emulsion was 600 μm. It is not known to better than 10 %. The range energy relation of Wilkins [14] was employed. β—α correlation measurements were unfortunately not possible because due to the low β-particle energy and the high background in the stack, the electron track was not always detected.

3. The detection of B^8 and Li^9

B^8, which was first detected by Alvarez [15] undergoes β-decay followed by α-activity in an exactly analogous manner to the decay of Li^8,

$$B^8 \rightarrow {}^*Be^8+\beta+\nu, \quad {}^*Be^8 \rightarrow \alpha+\alpha.$$

The energy spectrum for the decay α-particles has been shown by Gilbert [8]) to be identical with that obtained from Li^8, and therefore the two unstable nuclei cannot be distinguished in emulsion on the basis of their decay characteristics.

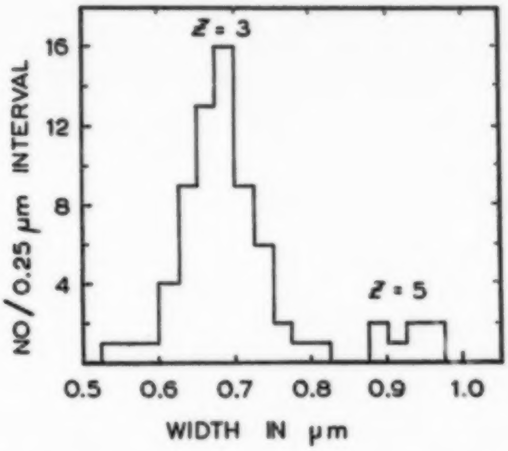

Fig. 1. Distribution of average track width of hammer tracks with range ≧ 60 μm.

The results of the track width measurements are shown in fig. 1. There appear to be a few tracks which display an unusually large average width. Two of these were included in the sample measured on the photometer, and the higher ionisation was again evident. Further, a 2+0 star on one of them has been interpreted as being due to the collision of a B^8 nucleus with that of free hydrogen in the emulsion [16]).

If all the tracks exhibiting a large average width are taken to be due to B^8, the frequency of production from the type of interactions investigated is seen at most to be 7 in a sample of 71 hammer tracks of ≧ 60 μm range. This can be compared with the 4 B^8 found by Skjeggestad and Sorensen [6]) in a sample of 60 hammer tracks of ≧ 100 μm range in emulsion. It would thus seem as though the ratio of Li^8 to B^8 is about 10/1.

Li^9 and Li^8 cannot be distinguished in emulsion from the characteristics of their tracks. The Li^9 decay was first detected by Gardner [17]) and later confirmed by Holt [18]) who obtained a lifetime of 0.17 sec. The decay scheme was given as

$$Li^9 \rightarrow {}^*Be^9 + \beta + \nu, \quad \text{followed by} \quad {}^*Be^9 \rightarrow Be^8(2\alpha) + n \quad \text{or} \quad He^5(\alpha + n) + \alpha.$$

In emulsion the event would have the appearance of a hammer track. However, whereas the angle between the α-particles from the Li^8 decay would not be expected to exceed 6° (see sect. 1), the presence of the neutron in the decay of Li^9 would allow much greater disparity between the momenta taken by the two α-particles and thus give greater angles between their directions of motion. Fry [19]) and Munir [3]) have reported two hammer tracks which were interpreted as being probably due to decays of Li^9 on the basis of angles of

≈ 40° observed between the α-particle tracks. Calculation of the total energy release to conserve momentum indicated that the Be^9 was probably created in the 6.8 MeV excited state, although the measurement errors allowed a large uncertainty on the computed excitation energy.

The distribution in angle between the α-pairs from the hammer tracks found in the present experiment shows the frequent occurrence of large angles ($> 20°$) which might at first be taken as showing a relatively high yield of Li^9. Figs. 2(a) and 2(b) however show respectively the distribution of the components of the angles as measured in the plane of the emulsion and in a plane at right angles to the emulsion surface for a sample of the events. It is clear that the large uncertainties in depth measurements are mainly responsible for the large angles observed. Indeed, the large angle components in the plane of the emulsion seemed to be correlated with large dip angles of the α-particles. It is estimated that the uncertainty in the angle due to undetected multiple Coulomb scattering and the short range of the α-particles would on average be 8°, which must be added to the real spread of up to 6° for Li^8 decays. Further, it must be borne in mind that the projection of a 10° angle on a plane at 45° to one of the vectors defining the angle, can be as much as 14°, and that this magnification increases as the secant of the dip angle.

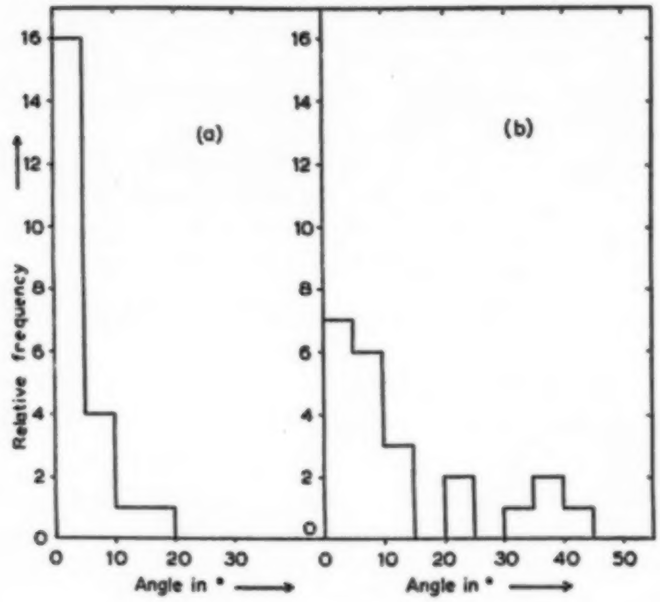

Fig. 2. Distribution of component of angle between α-pairs in Li^8 decay; (a) in emulsion plane, (b) in plane normal to emulsion.

Fig. 3 shows the energy of the neutron required to balance the momentum of the non-collinear α-pairs. The corresponding energy levels of the Be^9 are super-imposed. Some correlation with low lying energy levels of Be^9 could be deduced, but it must be considered that the calculated neutron energy in most cases is practically only a function of the angle between the α-particles, which is seen above to be very uncertain. Clearly only measurements on flat α-particle pairs of appreciable range (each $\geqq 5$ μm), can give definite information as to the presence of Li^9 nuclei in a sample of hammer tracks, and in the present investigation only two examples have been found both of which appeared to involve the 6.9 MeV level in Be^9. It can only be concluded from this that their frequency of production is low, e.g., it would have been surprising if only two examples of Li^9 decay had been found if they had made up 5 % (i.e., ≈ 30 events) of the hammer tracks. No accurate lower limit can, of course, be quoted. In the subsequent sections the Li^9 component is considered negligible.

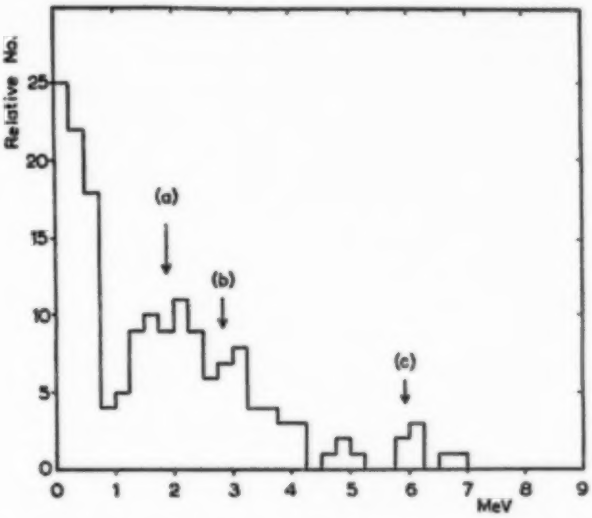

Fig. 3. Energy distribution for neutron assumed to balance momentum between α-pair. (a), (b) and (c) are neutron energies corresponding to the low lying levels in Be^9.

4. Production of Li^8 fragments

In a scan of some 10^5 stars of $N_h \geqq 8$ (average $N_h = 14$), 798 fragments were found, indicating, after correction for geometrical loss, a production frequency of (0.99 ± 0.03) % from such stars. This is in good agreement with the production frequency of 1 % predicted by Le Couteur ^{20}) for such interactions on the basis of evaporation theory.

The work of Skjeggestad and Sorensen ^{6}) on the angular and energy distributions of Li^8 fragments emitted from cosmic ray stars suggests that both may be explained within the framework of evaporation theory, provided one allows for an appreciable forward recoil from the initial meson cascade, and for a possible variation in the values of the parameters defining the evaporation. The angular distribution of the fragments obtained in the present experiment is shown in fig. 4. The variation with fragment energy of the forward/backward ratio of production is shown in table 1. The forward peaking of the angular distribution and the marked increase of the effect with the emission energy of the fragment are in agreement with the work of Skjeggestad and Sorensen and, following these authors, to explain the effects, a value of between 0.01 c and 0.02 c is required for the forward velocity v of the nucleus after impact (c is the velocity of light).

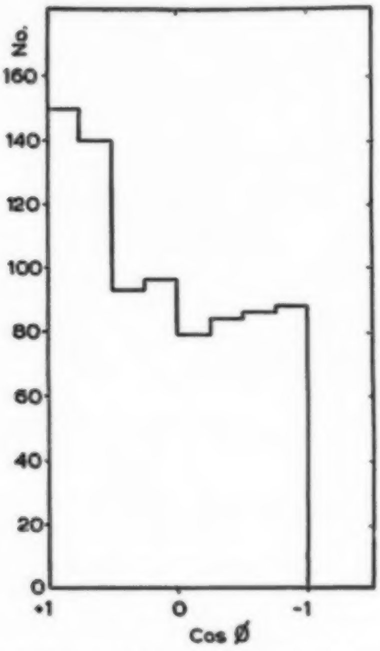

Fig. 4. Distribution of angle between primary and direction of emission of hammer track.

TABLE 1

Forward/backward ratios

All events	0−30 MeV	35 MeV	50 MeV
1.43±0.1	1.03±0.2	1.6±0.2	2.5±0.4

Fig. 5 shows the energy distribution of 884 Li^8 fragments. The observed numbers of high energy fragments have been corrected for geometrical loss. They were all emitted from stars in which $N_h \geq 8$ corresponding to reactions in silver and bromine only. The distribution is not in complete agreement with that obtained by Skjeggestad and Sorensen: more fragments of > 60 MeV and < 20 MeV were found in the present experiment. Using the expression given in ref. [6]), the distribution in fig. 5 has been fitted with a curve calculated with $v = 0.02c$, the nuclear temperature $T = 14$ MeV, and a nuclear barrier height

V of 9 MeV. It is clear that the agreement is not good. Further, the values of the evaporation parameters are not reasonable: a temperature of 14 MeV is impossible to attain when the average binding energy per nucleon is only 8 MeV. The full curve in fig. 5 is calculated with a value of $T = 9$ MeV (i.e., the maximum that seemed feasible) and $v = 0.02c$. The value of *V* is then found to be 13.5 MeV from the experimental position of the peak of the distribution. The curve has been normalized to the observed number of events between 20 and 50 MeV.

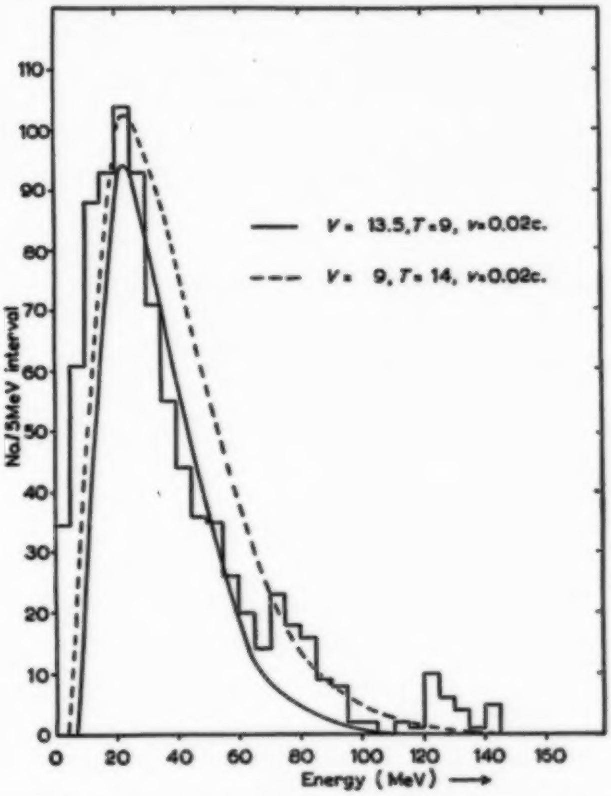

Fig. 5. Distribution of production energy of Li^8.

The slope of the calculated curve in the region 20—60 MeV is in good agreement with that of the distribution found experimentally, but there are far more fragments observed of energies > 60 MeV and < 20 MeV respectively than are predicted by the theory. No superposition of spectra, as was suggested by Skjeggestad and Sorensen, can explain the energetic fragments since the full curve in fig. 5 already gives the highest values of *T* and *V* that seem physically realistic. We are forced to conclude that these fragments are not produced in an evaporation process, but as has been suggested previously (e.g., ref. [3])) are probably directly related to the initial impact of the primary particle with the nucleus. The excesss of fragments having energies of < 20 MeV are more easily reconciled with a description in terms of evaporation since the values of *V* and *T* certainly decrease during the process, e.g., the charge of an evaporating silver nucleus and hence the value of the barrier height, is probably halved (on average) when a star having $N_h = 14$ is produced. Quantitatively, it would seem that at least 10 % of all Li^8 fragments produced by 4.6 GeV π-mesons are not produced by evaporation and have energies > 60 MeV, while up to 15 % of the Li^8 production could occur in later stages of evaporation leading to fragments < 20 MeV. The high energy behaviour is in agreement with that for Li^8 fragments produced by bombarding silver with 2.2 GeV protons [21]). Comparison of the low energy results is difficult because of the stopping power of the silver target expesed to the protons.

5. The energy spectrum of the α-pairs

The energy spectrum obtained in the present experiment is shown in table 2. It is compared with that obtained by Frost and Hanna [10]). The latter results are normalized to the number of events found in the present experiment and are directly comparable. The magnetic spectrometer experiment of Frost and Hanna is based on 7×10^4 events and would be expected to give better resolution than is obtained when the range of the α-particles is measured. The better resolution of the spectrometer is apparent from table 2. Taking the peak at 2.9 MeV, the spectrum drops to half value in an energy interval of 1 MeV compared with the 1.6 MeV necessary in the case of the emulsion results. Above 5 MeV, agreement appears to be exact. The main features are consistent with those of the results of other workers (see sect. 1).

TABLE 2

The energy spectrum

Energy interval (MeV)	2—3	3—4	4—5	5—6	6—7	7—8	8—9	9—10	10—11	>11
No. found in the present experiment	139	273	171	79	53	39	19	13	9	3
Frost and Hanna (normalized)	185	290	146	84	53	36	24	16	7	1

Previous analysis of the α-particle spectrum have been based mainly on the assumption of a single $^*Be^8$ energy level at ≈ 3 MeV and the reaction

$$Li^8 \rightarrow {}^*Be^8+\beta+\nu, \quad {}^*Be^8 \rightarrow \alpha+\alpha.$$

The calculated shape of the energy spectrum [7]) is affected strongly by the resonance denominator term $(E-E_0)^2+\frac{1}{4}\Gamma^2$, and a factor of $(16-2E)^5$ arising from the Gamow-Teller β-decay, where E is the energy of a single α-particle, and E_0, Γ are the energy level parameters. Even modifying with a penetrability factor does not well explain the high energy behaviour of the experimental distribution unless a spin 4 is taken for the level in Be^8 or more than one energy level is assumed (see, e.g. ref. 7)). The position may be compared with the results of experiments on reactions in which Be^8 is a final state product (e.g., $Li^7(d, n)Be^8$, $B^{10}(d, \alpha)Be^8$, $C^{12}(\gamma, \alpha)Be^8$). Levels in Be^8 at 4.1, 4.9, 5.3 and 7.5 MeV have been suggested to explain the spectrum of reaction products on the high excitation energy side of groups corresponding to a 3 MeV excitation of Be^8. (See refs. 9,22) for refs. and discussion). It would be expected that the shape of the spectra obtained in the present experiment and those referred to above could be calculated by using the values experimentally obtained for the (α—α) scattering phase shifts in the relevant energy interval. Nilson *et al.* 23) have calculated from the scattering data that the δ_2 phase shift stays close to 90° from excitation energies between 2.9 MeV to well above 10 MeV. The other phase shifts are small in this energy interval. The behaviour of δ_2 below 2.9 MeV is what would be expected for a level in Be^8 at that energy, but at higher energies the variation is only consistent with a single level if the radius of the interaction is taken to be velocity dependent. The value of δ_2 is not known in the 4 and 5 MeV region and therefore energy levels at those energies cannot be excluded. Assuming, as did Nilson *et al.*, a smooth behaviour of δ_2 with energy, Fowler and Preist have fitted the counter data for reasonable α-particle parameters (see following paper).

6. Conclusions

1 % of stars of $N_h \geqq 8$ produced by 4.6 GeV/*c* π-mesons have been observed to have associated hammer tracks. About one in ten of hammer tracks $\geqq 60$ μm in range are due to B^8 and the fraction of Li^9 nuclei in the remainder is seen to be small (probably < 5 %).

Taking the bulk of hammer tracks to be due to Li^8, evaporation theory with the parameters $T = 9$ MeV, $V = 13.5$ MeV and $v = 0.020$, does not predict ≈ 25 % of the emission energy spectrum of the fragments. At least 10 % are more directly related to the initial impact and ≈ 15% having energies < 20 MeV are probably emitted in the later stages of evaporation.

The energy spectrum of the α-particle pairs from the decay of Li^8 is seen to be consistent with the predictions of a calculation utilizing the value of the phase shifts deduced from the experimental results on (α—α) scattering. The detection of energy level in Be^8 in the 5 MeV region cannot therefore be attempted from experiments of this type and must wait for accurate (α—α) phase shift determinations for the scattering of α-particles having bombarding energies in the region of 8—12 MeV.

We should like to thank Professor C. F. Powell, Professor J. Reginald Richardson and Professor N. Dallaporta for encouragement and for laboratory facilities and Dr. E. J. Lofgren and workers at Berkeley for the Bevatron exposure. We are very grateful to Dr. G. N. Fowler and Mr. T. Preist for many useful discussions.

References

1) C. F. Powell and G. P. S. Occhialini, Nature **159** (1947) 93
2) R. F. Christy, E. R. Cohen, W. . Fowler, C. C. Lauritsen and T. Lauritsen, Phys. Rev. **72** (1947) 698
3) B. A. Munir, Phil. Mag. **1** (1956) 355
4) S. J. Goldsack, W. O. Lock and B. A. Munir, Phil. Mag. **2** (1957) 149
5) S. Nakagawa, Tamai, H. Huzita and K. Okudaira, J. Phys. Soc. Japan **11** (1956) 191; **12** (1957) 747
6) O. Skjeggestad and S. O. Sorensen, Phys. Rev. **113** (1959) 1115
7) T. W. Bonner, J. E. Evans, C. W. Malish and J. R. Risser, Phys. Rev. **73** (1948) 885
8) F. C. Gilbert, Phys. Rev. **93** (1954) 499
9) A. H. Armstrong and G. M. Frye, Fr., Phys. Rev. **103** (1956) 335
10) R. T. Frost and S. S. Hanna, Phys. Rev. **99** (1955) 8
11) M. de Pretis and G. Poiani, Nuovo Cim. Suppl. **15** (1960) 265
12) G. C. Deka, Nuovo Cim. **14** (1959) 1217
13) R. R. Hillier (private communication)
14) J. J. Wilkins, Harwell, A.E.R.E., report G/R 664
15) L. Alvarez, Phys. Rev. **80** (1950) 519
16) G. C. Deka, Thesis, University of Bristol
17) W. L. Gardner, N. Knoble and B. J. Mayer, Phys. Rev. **83** (1951) 1054
18) R. B. Holt, R. N. Thorne and R. W. Watwick, Phys. Rev. **87** (1952) 378
19) W. F. Fry, Phys. Rev. **89** (1953) 325
20) See private communication in ref. [8])
21) S. Katcoff, Phys. Rev. **114** (1959) 905
22) E. W. Titterton, Phys. Rev. **94** (1954) 206
23) R. Nilson, W. K. Jentschke, G. R. Briggs, R. O. Kerman and J. N. Snyder, Phys. Rev. **109** (1958) 850

2.A.1 *Nuclear Physics* **23** (1961) 667—671; ©*North-Holland Publishing Co., Amsterdam*

Not to be reproduced by photoprint or microfilm without written permission from the publisher

NOTE ON THE α PARTICLE ENERGY SPECTRUM IN Li^8 DECAY

G. N. FOWLER and T. W. PREIST

H. H. Wills Physical Laboratory, University of Bristol

Received 25 July 1960

Abstract: An attempt is made to correlate the asymmetry in the energy distribution of α-particles from Li^8 decay with the asymmetry in the behaviour of the phase shift in the $J = 2$ state. A phenomenological potential of the Haefner type is used and the nuclear matrix element is evaluated using the mean value theorem. It is found that the two sets of data can only be correlated if the repulsive core is weakened as the energy increases.

1. Introduction

A considerable amount of experimental evidence has been accumulated in recent times [1,2]) concerning the energy distribution of α-particles emitted after the β-decay of Li^8 and it has been pointed out by Deka *et al.* [2]) and de Pretis and Poiani [5]) that the theoretical predictions available [3,4]) disagree completely with experiment at the high energy end of the spectrum. Briefly, the experimental data show a pronounced high energy tail which is not predicted by the usual Breit Wigner type formula taking account of the well known $J = 2$ virtual level of Be^8 at 2.9 MeV. It has been suggested by Poiani that other levels of Be^8 exist at energies beyond 3 MeV with the same quantum numbers and that these might account for the observed tail in the energy distribution. However, most other workers in this field have failed to find convincing evidence for such levels and the general conclusion appears to be[6,7]) that none such exist. We wish to point out that the observed α—α scattering phase shifts in this state show a similar asymmetry which suggests that an α-particle model for the final nuclear state in the Li^8 β-decay might be a good starting point for an explanation of the observed energy distribution. In the following we try to find an α—α interaction which satisfies both the observed phase shifts in the $J = 2$ state and the α particle energy distribution. We leave out of account the phase shifts in the other angular momentum states because there is some reason to believe that the interaction is velocity dependent [8]).

2. The Decay Probability

The decay probability is given in terms of the usual Gamow Teller matrix element in which the final nuclear state is a state of two particles whose centre of mass is at rest. The matrix element is approximated by using the mean value theorem so that the α-particle energy distribution is simply proportional to the square of the final state wave function describing the relative motion of the two particles evaluated at some average value $\bar{r}$ of the α-particle separation. The final state wave function is a positive energy solution, normalized over unit energy range, of a Schrödinger equation with a suitably chosen interaction. In choosing the interaction, we have followed the work of Haefner 9) by introducing a repulsive core of the form $q^2\hbar^2/Mr^2$ and a square well of depth V_0 and range r_0. The quantities $\bar{r}$, q^2, V_0 and r_0 are then to be chosen to fit both sets of data. The result for the α particle energy distribution is

$$N_\alpha \mathrm{d}E_\alpha \propto \frac{(Q-E_\alpha)^5}{E_\alpha^{\frac{1}{2}}} \left[\frac{J_{L+\frac{1}{2}}(K\bar{r})}{J_{L+\frac{1}{2}}(Kr_0)}\right]^2 [F_2(kr_0)\cos\delta + G_2(kr_0)\sin\delta]^2\, \mathrm{d}E_\alpha. \qquad (1)$$

In this formula $L(L+1) = q^2+6$, $K = \hbar^{-1}\sqrt{M(E_\alpha+V_0)}$, Q is the energy release, M the α-particle mass, F_2 and G_2 are the regular and irregular Coulomb functions respectively and $k = \hbar^{-1}\sqrt{ME_\alpha}$.

3. Results

The method used to fit the data has been to fix r_0 at some reasonable value, 3 to 5×10^{-13} cm, to fit the phase shifts by adjusting q and V_0 and finally to look for a value of $\bar{r}$ which gave a fit to the energy distribution. The result is that although a fit to the phase shifts can be found with $q^2 = 8.2$, $V_0 = 20$ MeV and $r_0 = 3.7\times10^{-13}$ cm no set of parameters could be found which fitted both sets of experimental results.

At this point it seems reasonable to recall that the α model of Be^8 which we have used is in fact a rather crude one and we might expect that at high energies α particle structure effects might be important. This implies that the final state wave function should contain contributions which refer to α particles in excited states. Indeed, effects of this kind have been put forward as a possible cause of the asymmetry in the energy dependence of the $J = 2$ α—α phase shifts by Nilson *et al.* 6, 7). In the present model this effect could be taken into account by weakening the Pauli repulsive core for small values of the relative coordinate. For example, regular Coulomb functions for some suitable value of Z could be used in place of the Bessel functions inside the potential well. However, this would have involved a far larger machine calculation than was necessary for the computation of the fractional order Bessel functions and so we have chosen to modify the interaction rather crudely by allowing q to fall with energy in the high energy region. In this way we have found that a rather good fit is possible to all the data. The appropriate values of the various parameters are $r_0 = 4.0\times10^{-13}$ cm, $V_0 = 20$ MeV, $\bar{r} = 1.7\times10^{-13}$ cm, $q^2 = 11.4$ for $E_\alpha < 5$ MeV falling to 6.7 at 12 MeV; a larger value of r_0 leads to a steeper energy variation in q and a larger value of $\bar{r}$ and a fit is not possible for smaller values of r_0.

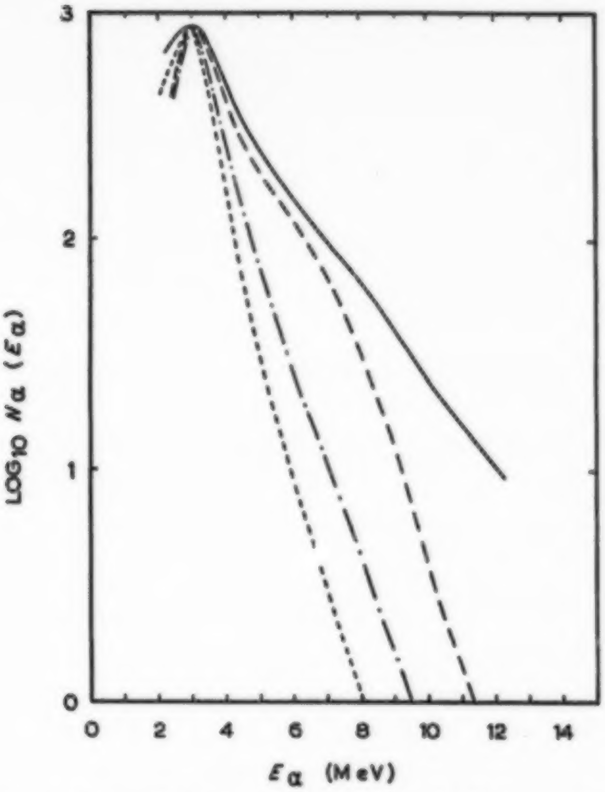

Fig. 1. A comparison between the experimental distribution[1]) (———), the theoretical results of Wheeler[3]) (- - - - -), those of Bonner[4]) (— · — · — · —) and the predictions of eq. (1) with a constant repulsive core (— — —).

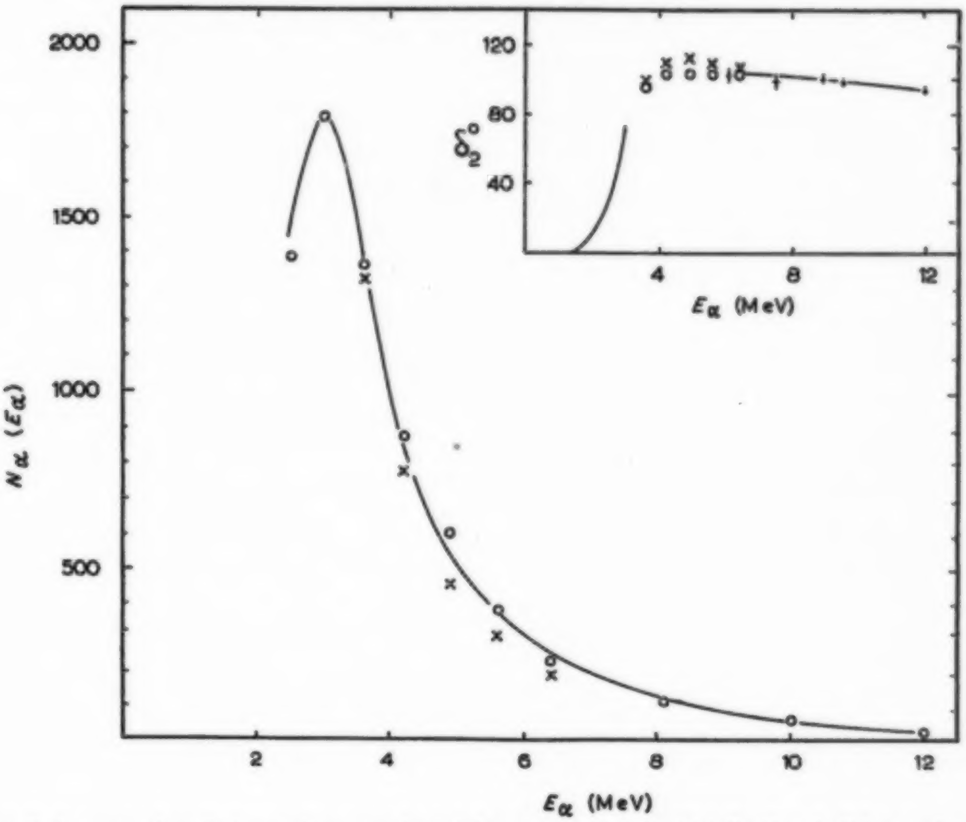

Fig. 2. A comparison between the experimental α-particle energy distribution (solid curve) and the distribution given by eq. (1) with a weakening of the repulsive core in the high energy region. The comparison is given for two choices of the α—α phase shifts (see inset).

Corrections to the mean value result turn out to be small. The fit to the data is shown in figs. 1 and 2, together with the effect produced by slight changes in the phase shifts.

4. Conclusions

By a suitable choice of α-particle interaction parameters we have found a fit to the observed scattering phase shifts in the $J = 2$ state and to the energy distribution of α particles in the Li^8 decay. This has been done by weakening the repulsive core at high energies. This clearly enhances the relative probability of producing two α particles a given short distance apart at high energies and so reproduces the high energy tail in the particle energy distribution. This adds force to the interpretation of the phase shift energy dependence in terms of a weakening of the repulsive core at high energies. It is true that an agreement with experiment obtained in this way is somewhat questionable but, as we have seen, we have at least a rather immediate physical interpretation of our procedure. The alternative explanation in terms of higher states of Be^8 seems even less convincing and our conclusion shows that an explanation can be found without introducing such states.

After this work was completed a paper appeared by Griffy and Biedenharn[10]) in which the connection between the scattering and the energy distribution is also emphasized. However, the conclusion of these authors seems open to question according to the following argument. The expression for the wave functions used depends on assuming that the process may be described in terms of a Breit Wigner one level formula whereas the same assumption is not made for the phase shift (c.f. ref. [11]), formulae (14a) and (14b)) and is in fact not true for the phase shift. Thus it turns out that their result may be derived in a very simple way starting from the Breit Wigner expression given by Wheeler for this process:

$$N_\alpha \mathrm{d}E_\alpha \propto \frac{\Gamma_1\Gamma_2(Q-E_\alpha)^5}{(E_\alpha-E_0)^2+\frac{1}{4}\Gamma^2}\mathrm{d}E_\alpha, \tag{2}$$

where $\Gamma = \Gamma_1+\Gamma_2$. Here, Γ_1 is related to the β-decay probability and Γ_2 is related to the decay probability of the Be^8 excited state to two α particles. If $\Gamma_1 \ll \Gamma_2$ and $E_\alpha \approx E_0$ then the factor $\Gamma_2/\{(E_\alpha-E_0)^2+\frac{1}{4}\Gamma^2\}$ may be replaced by $\sin^2\delta/\Gamma_2$ and we find the result of ref. [10]). However, it is clear that for $E_\alpha \gg E_0$ the quantity $\sin^2\delta/\Gamma$ contains a potential scattering term besides the usual resonance contribution and so no longer has the same physical meaning as the Breit Wigner formula. It would therefore seem that, to be consistent, the potential scattering should be subtracted from the observed phase shifts before comparison with experiment is made. Finally, it must be remarked that although Watson [12]) gives a formula which allows for final state interactions and which is very similar to the result of Griffy and Biedenharn, in fact Watson's result is simply an approximation to eq. (1) of this paper, valid when $kr_0 \ll 1$ which is not true in this case.

We would like to thank Professor M. H. L. Pryce, F.R.S., for extending to us the facilities of his laboratory. We would also like to thank Drs. Deka, Evans and Prowse for drawing our attention to this problem and Messrs. J. M. Hahn and J. B. Bell, of the Mathematical Services Department of the Bristol Aeroplane Company, for computing the Bessel Functions of Fractional Order. One of us (T. W. Preist) is indebted to D.S.I.R. for a research scholarship.

References

1) H. T. Frost and S. S. Hanna, Phys. Rev. **99** (1955) 8
2) G. C. Deka, D. Evans, D. J. Prowse and M. Baldo-Ceolin, Nuclear Physics **23** (1961) 657
3) J. A. Wheeler, Phys. Rev. **59** (1941) 27
4) J. W. Bonner, J. E. Evans, C. W. Malich and J. R. Risser, Phys. Rev. **73** (1948) 884
5) M. de Pretis and G. Poiani, Nuovo Cim. Supp. **15** (1960) 265
6) R. Nilson, W. K. Jentschke, G. R. Briggs and R. O. Kerman, Phys. Rev. **104** (1956) 1673
7) R. Nilson, W. K. Jentschke, G. R. Briggs, R. O. Kerman and J. N. Snyder, Phys. Rev. **109** (1958) 850
8) E. Van der Spuy, Nuclear Physics **11** (1959) 615
9) R. R. Haefner, Rev. Mod. Phys. **23** (1951) 212
10) T. A. Griffy and L. C. Biedenharn, Nuclear Physics **15** (1960) 636
11) L. C. Biedenharn and H. B. Willard, Proc. Phys. Soc. A **72** (1958) 874
12) K. Watson, Phys. Rev. **88** (1952) 1163

2.B

Nuclear Physics **23** (1961) 672—680; ©*North-Holland Publishing Co., Amsterdam*

Not to be reproduced by photoprint or microfilm without written permission from the publisher

SCATTERING OF HIGH ENERGY POLARIZED DEUTERONS BY CARBON

B. A. ROBSON

Australian National University, Canberra

Received 10 October 1960

Abstract: It is shown that the inclusion of a small tensor force in the effective deuteron-carbon potential gives a more satisfactory description of the tensor components of polarization.

1. Introduction

Recently, the scattering of 420 MeV polarized deuterons by carbon has been investigated in considerable detail[1]). Measurements were made by double scattering, of all the parameters required for a complete description of the polarization state of the beam of deuterons. Tensor components of polarization, which may be expected in the scattering of spin-one particles and which were not seen at lower energies[2]) were found to be substantially different from zero. The impulse approximation, which was used[1,2]) to estimate the deuteron polarization on the basis of nucleon scattering gave a poor description of the data. In the notation of Lakin[3]), the quantity $\langle T_{21}\rangle$, especially, was considerably underestimated. It seems reasonable to conclude that the effective deuteron-nucleus potential must contain interactions other than the usual optical model potential and spin-orbit interaction, which have been so successful in describing the scattering of polarized nucleons by nuclei.

As pointed out by Satchler[4]), for spin-one particles it is possible to have interactions which are the scalar products of two tensors, which are of rank two in the separate spin and coordinate spaces. In spin space there is only the spin vector operator, $\boldsymbol{\sigma}$, but in ordinary space there are three vectors, $\mathbf{r}$, $\mathbf{L}$ and $\mathbf{p}$, characterizing the position, orbital momentum and momentum, respectively. The requirements of parity conservation and time reversal invariance do not allow a mixing of vectors from the same space so that the number of possible tensor couplings is considerably restricted. Indeed, there are just three irreducible tensor interactions allowed:

$$f_1(r)T_1 = f_1(r)\{(\boldsymbol{\sigma}\cdot\mathbf{r})^2r^{-2}-\tfrac{2}{3}\}, \tag{1}$$

$$f_2(r)T_2 = f_2(r)\{(\boldsymbol{\sigma}\cdot\mathbf{L})^2+\tfrac{1}{2}(\boldsymbol{\sigma}\cdot\mathbf{L})-\tfrac{2}{3}\mathbf{L}^2\}, \tag{2}$$

$$f_3(r)T_3 = f_3(r)\{(\boldsymbol{\sigma}\cdot\mathbf{p})^2-\tfrac{2}{3}\mathbf{p}^2\}. \tag{3}$$

where the $f_i(r)$ are form factors. It is the aim of the present paper to show that the 420 MeV deuteron-carbon polarization data may be more satisfactorily described if a tensor coupling of the type given by eq. (1) is added to the complex central potential and spin-orbit interaction, which have previously been used, without appreciable success, to describe deuteron scattering [5,6]. This form of tensor interaction may be written [4,7] in the form

$$(\zeta+i\eta)f(r)[3(\boldsymbol{\sigma}_{\rm P}\cdot\mathbf{r})(\boldsymbol{\sigma}_{\rm N}\cdot\mathbf{r})r^{-2}-\boldsymbol{\sigma}_{\rm P}\cdot\boldsymbol{\sigma}_{\rm N}] = (\zeta+i\eta)f(r)S_{12}, \tag{4}$$

where $\boldsymbol{\sigma}_{\rm P}$, $\boldsymbol{\sigma}_{\rm N}$ are the spins of the nucleons in the deuteron, $\mathbf{r}$ is the vector joining the centre of mass of the deuteron to that of the nucleus, ζ and η are constants and $f(r)$ is a form factor. Such a tensor force is analogous to that required to account for the qudruapole moment of the deuteron, although in this case the vector $\mathbf{r}$ has a different meaning. Moreover, this form of the tensor coupling arises in the effective deuteron-nucleus potential, when the D-state of the deuteron is taken into account [8]. However, it will also be shown that the above tensor potential alone is probably not able to describe completely the tensor components of polarization; at least some T_2 interaction is also required. In the following analysis of the experimental data, tensor interactions of the type T_3 are neglected.

2. Theory

For the choice of coordinates axes in which the z-axis is along the incident direction of the deuteron beam and the y-axis is along $-\boldsymbol{\nu}$, $\boldsymbol{\nu} = (\mathbf{k}_1\times\mathbf{k}_f)/k^2\sin\theta$, $\cos\theta = (\mathbf{k}_1\cdot\mathbf{k}_f)k^{-2}$ and $\mathbf{k}_1$, $\mathbf{k}_f$ are $\hbar^{-1}$ times the initial and final momenta of the deuteron, the scattering matrix (for spin zero target nuclei) may be written in the form

$$M(\theta) = A(\theta)+B(\theta)\boldsymbol{\sigma}\cdot\boldsymbol{\nu}-6C(\theta)[(\boldsymbol{\sigma}\cdot\mathbf{K})^2-\tfrac{2}{3}]-6D(\theta)[(\boldsymbol{\sigma}\cdot\boldsymbol{\nu})^2-\tfrac{2}{3}], \tag{5}$$

where $\mathbf{K} = (\mathbf{k}_1-\mathbf{k}_f)/|\mathbf{k}_1-\mathbf{k}_f|$ and $\boldsymbol{\sigma} = \boldsymbol{\sigma}_{\rm P}+\boldsymbol{\sigma}_{\rm N}$. The A and B terms arise from the central and spin-orbit potentials respectively and the C, D terms are a consequence of T_1 and T_2 tensor potentials. This form of $M(\theta)$ is particularly convenient for two reasons:

(i) if T_1 is the only tensor interaction present, then $D = 0$ and T_1 is completely described by the C term;

(ii) if T_1 and T_2 are both present, this is no longer true but $D \neq 0$ is a measure of the T_2 interaction.

If it is assumed that no T_2 interaction is present, the effective deuteron-carbon potential may be written

$$\mathscr{V}(r) = -(V+iW)g(r)+(\gamma+i\delta)r^{-1}({\rm d}g/{\rm d}r)\mathbf{L}\cdot\boldsymbol{\sigma}+(\zeta+i\eta)f(r)S_{12}, \tag{6}$$

where V, W are positive real functions so that the central potential is attractive and absorptive, γ, δ give the strength of the complex spin-orbit force, ζ, η measure the strength of the tensor force, and **L** represents the orbital angular momentum of the deuteron. In the following, $g(r)$ is taken, for convenience, to be of a double trapezoidal form (see fig. 1),

$$\mathrm{g(r)} = \begin{cases} 1, & \text{for } 0 \leqq r \leqq \mathrm{a}, \\ (b-r)/(b-a), & \text{for } a < r \leqq c, \ (b > c), \\ (b-c)(d-r)/(d-c)(b-a), & \text{for } c < r \leqq d, \\ 0, & \text{for } d < r < \infty, \end{cases} \tag{7}$$

where the region $c < r \leqq d$ describes the long-tailed nature of the Watanabe [6]) effective deuteron-nucleus potential arising from the extended structure of the deuteron. In the Watanabe potential, the quantities V, W, γ and δ are related to similar quantities in the nucleon-nucleus potential at an energy one-half that of the incident deuteron. To a fair approximation this relationship is an identity. The S_{12} potential is taken to be concentrated at the nuclear surface, $f(r) = -r(\mathrm{d}h/\mathrm{d}r)$, where, again for convenience, $h(r)$ is of trapezoidal form

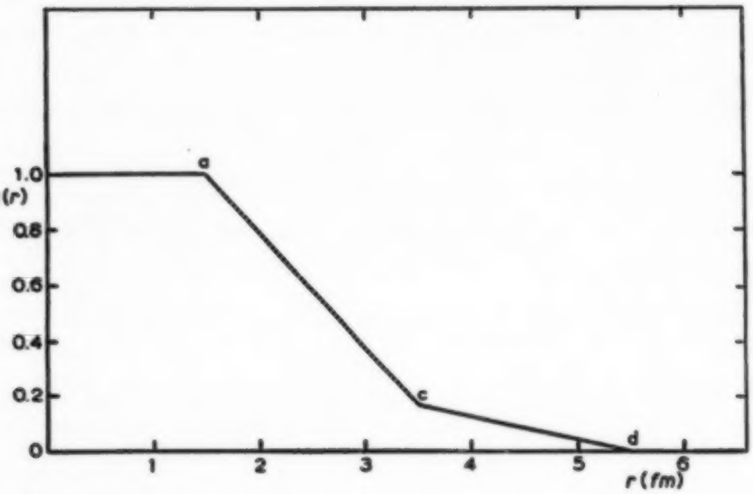

Fig. 1. Simplified form factor $g(r)$ of the effective deuteron-carbon potential.

$$h(r) = \begin{cases} 1 & \text{for } 0 \leqq r \leqq a, \\ (b-r)/(b-a), & \text{for } a < r \leqq b, \\ 0, & \text{for } b < r < \infty. \end{cases} \tag{8}$$

This form of the tensor potential appears likely if such a force arises from the D-state of the deuteron [8]).

Following the approximation developed by the author [9])

$$M(\theta) = -(4\pi)^{-1} \int \exp[-ik\mathbf{n} \cdot \mathbf{r}]U(r)\psi(r)\mathrm{d}\tau, \tag{9}$$

where $U(r) = 2m\hbar^{-2}\mathscr{V}(r)$, m is the reduced mass of the deuteron, **n** is a unit vector in the direction $\mathbf{r}$ and

$$\psi(r) = \begin{cases} p \exp[ik_1\mathbf{n}_0 \cdot \mathbf{r}] + pq \exp[-ik_1\mathbf{n}_0 \cdot \mathbf{r}], & (0 \leqq r \leqq a), \\ \exp[ik\ \mathbf{n}_0 \cdot \mathbf{r}], & (a < r < \infty), \end{cases} \tag{10}$$

where $\mathbf{n}_0$ is a unit vector along the incident direction and

$$p = 2k_1 \exp[ia(k_1 - k)]/(k_1+k)(1-q^2), \tag{11}$$

$$q = (k_1 - k) \exp[2iak_1]/(k_1+k), \tag{12}$$

$$k_1^2 = k^2 - U, \tag{13}$$

$$U = -2m\hbar^{-2}(V+iW). \tag{14}$$

At 420 MeV, $q \approx 0$ and $k_1 - k$ is small so that

$$\psi \approx \begin{cases} p \exp[ik\mathbf{n}_0 \cdot \mathbf{r}], & \text{for} \quad 0 \leqq r \leqq a, \\ \exp[ik\mathbf{n}_0 \cdot \mathbf{r}], & \text{for} \quad a < r < \infty, \end{cases} \tag{15}$$

where

$$p \approx 1 + ia(k_1 - k). \tag{16}$$

At high energies, the phase shift given by eq. (16) is the most important correction to the usual Born approximation and has been discussed by others [10-12]).

One finds

$$A(\theta) = 2m\hbar^{-2}(V+iW)[Z(a)+I(a)], \tag{17}$$

$$B(\theta) = 2im\hbar^{-2}(\gamma+i\delta)[Z'(a)+I(a)] \sin\theta, \tag{18}$$

$$C(\theta) = -2m\hbar^{-2}(\zeta+i\eta)[K \int_a^b j_1(Kr)h(r)r^3\,\mathrm{d}r - pK^{-3}\{(Ka)^2 \sin(Ka) + 3(Ka)\cos(Ka) - 3\sin(Ka)\}], \tag{19}$$

where

$$I(a) = \int_a^d j_0(Kr)g(r)r^2\,\mathrm{d}r, \tag{20}$$

$$Z(a) = a^2 p[j_1(Ka)/K] = pZ'(a), \tag{21}$$

$K = 2k \sin \frac{1}{2}\theta$ and j_n is the spherical Bessel function of order n.

The polarization state of a beam of deuterons is completely specified by the expectation values of a set of irreducible tensor operators [3]) (N.B. the coordinate system used here is different from that used by Lakin), given by

$$\begin{aligned} &T_{00} = 1, \quad T_{10} = \sqrt{\tfrac{3}{2}}\sigma_z, \quad T_{11} = \tfrac{1}{2}\sqrt{3}\,(\sigma_x + i\sigma_y), \\ &T_{20} = \tfrac{1}{2}\sqrt{2}\,(3\sigma_z^2 - 2), \qquad T_{21} = \tfrac{1}{2}\sqrt{3}\,(\sigma_x + i\sigma_y)\sigma_z + \sigma_z(\sigma_x + i\sigma_y), \\ &T_{22} = \tfrac{1}{2}\sqrt{3}\,(\sigma_x + i\sigma_y)^2, \quad T_{A-B} = (-)^B T^+_{AB}, \end{aligned} \tag{22}$$

where σ_i are the usual spin operators

$$\sigma_x = \frac{1}{\sqrt{2}}\begin{pmatrix} 0 & 1 & 0 \\ 1 & 0 & 1 \\ 0 & 1 & 0 \end{pmatrix}, \quad \sigma_y = \frac{1}{\sqrt{2}}\begin{pmatrix} 0 & -i & 0 \\ i & 0 & -i \\ 0 & i & 0 \end{pmatrix}, \quad \sigma_z = \begin{pmatrix} 1 & 0 & 0 \\ 0 & 0 & 0 \\ 0 & 0 & -1 \end{pmatrix}. \tag{23}$$

For our choice of axes, the state of polarization is described by five of these tensor operators, $\langle T_{00}\rangle$ giving the normalization, and the real quantities $\langle iT_{11}\rangle$ and $\langle T_{2B}\rangle$.

Following along the lines indicated by Goldfarb [7]), it may be shown that for the scattering matrix of eq. (5)

$$\langle iT_{11}\rangle = [(A^*B+B^*A)+(B^*C+C^*B)-2(B^*D+D^*B)]/\sqrt{3}I, \tag{24}$$

$$\langle T_{20}\rangle = [-\tfrac{1}{3}|B|^2-(1-3\cos\theta)X+2Z-3Y\sin\theta-2P(1+\cos\theta)]/\sqrt{2}I, \tag{25}$$

$$\langle T_{21}\rangle = [\sqrt{3}Y\cos\theta+\sqrt{3}X\sin\theta-2\sqrt{3}P\sin\theta]/I, \tag{26}$$

$$\langle T_{22}\rangle = [-|B|^2-3X(1+\cos\theta)+6Z+3Y\sin\theta-6P(1-\cos\theta)]/2\sqrt{3}I, \tag{27}$$

where

$$I = |A|^2+\tfrac{2}{3}|B|^2+8|C|^2+8|D|^2-4P, \tag{28}$$

$$X = A^*C+C^*A+2|C|^2, \tag{29}$$

$$Y = i(B^*C-C^*B), \tag{30}$$

$$Z = A^*D+D^*A+2|D|^2, \tag{31}$$

$$P = C^*D+D^*C. \tag{32}$$

3. Analysis of Experimental Data

At angles of about 6°, the vector polarization $\langle iT_{11}\rangle$ depends almost entirely upon the scattering amplitudes A, B of eq. (5). Thus the data at these angles may be used to determine a set of parameters V, W, γ and δ for the optical and spin-orbit interactions. An estimate of these quantities may also be obtained from an analysis of the 220 MeV proton-carbon polarization data [9, 13]). V and W were fixed at 10 MeV and 20 MeV, respectively, and γ and δ allowed to vary. From the nucleon results γ is > 0 and δ is $\leqq 0$. A value of $\delta = 0$ was found to describe the deuteron data most satisfactorily at 6° (lab.), the corresponding value of γ being 2.5 MeV fm^2(1fm $= 10^{-15}$ m). A larger value of γ or a negative value of δ causes $\langle iT_{11}\rangle$ to increase at this angle. The effect of electromagnetic interactions was estimated by including, in strict Born approximation, the amplitudes for scattering by a point charge and a correction for the finite size of the nucleus [14]). It was found that the effect upon $\langle iT_{11}\rangle$ is small for the angles considered. Fig. 2 shows the smaller angle results for $\gamma = 2.5$ MeV fm^2, $\delta = 0$ MeV fm^2, $\zeta = -0.2$ MeV, $\eta = 0.3$ MeV, $a = 1.5$fm, $b = 3.9$fm, $c = 3.5$fm and $d = 5.5$fm with and without electromagnetic interactions. Even at 10° the tensor forces are important. The data at larger angles than 10° almost certainly include inelastic scattering and are therefore of little use in our analysis. Fig. 3 shows the experimental and theoretical results for the differential cross section. The experimental data show no evidence whatsoever of a diffraction minimum. The inclusion of the relatively weak tensor force has little effect upon the differential cross

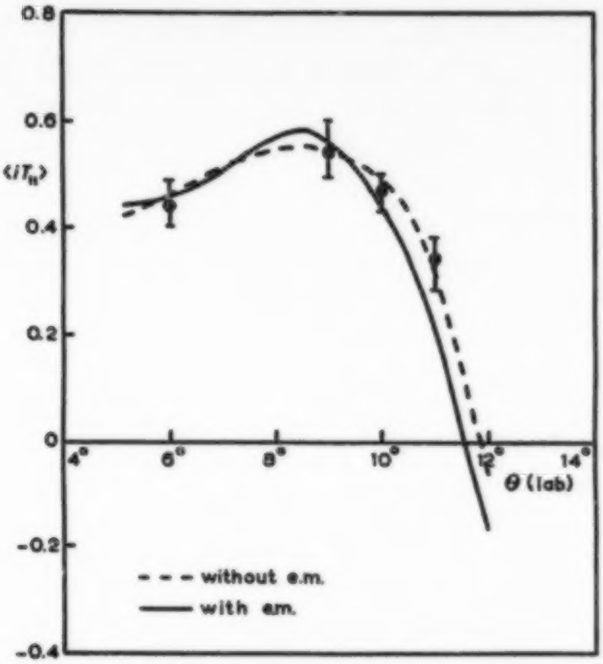

Fig. 2. Vector Polarization, $\langle iT_{11}\rangle$, for 420 MeV deuterons scattered by carbon. The points are the experimental results of Button and Mermod [1]). The two curves are the theoretical predictions for $V=10$ MeV, $W=20$ MeV, $\gamma=2.5$ MeV fm^2, $\delta=0$ MeV fm^3, $\zeta=-0.2$ MeV, $\eta=0.3$ MeV, $a=1.5$fm, $b=3.9$fm, $c=3.5$fm, $d=5.5$fm, with and without the inclusion of electromagnetic interactions.

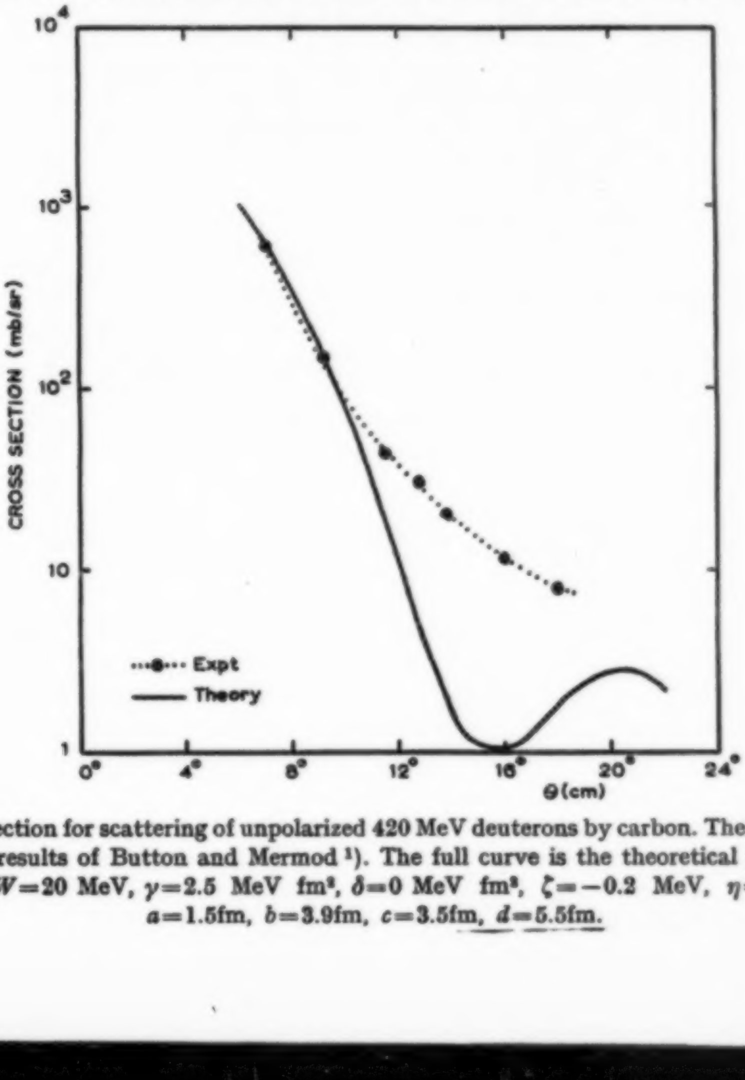

Fig. 3. Cross section for scattering of unpolarized 420 MeV deuterons by carbon. The points are the experimental results of Button and Mermod [1]). The full curve is the theoretical prediction for $V=10$ MeV, $W=20$ MeV, $\gamma=2.5$ MeV fm^2, $\delta=0$ MeV fm^3, $\zeta=-0.2$ MeV, $\eta=+0.3$ MeV, $a=1.5$fm, $b=3.9$fm, $c=3.5$fm, $d=5.5$fm.

section except near the diffraction minimum, where it tends to fill in the trough. Since reasonable changes in the parameters do not fill in the dip, it would seem that the discrepancy between theory and experiment for angles greater than 11° indicates the inclusion of considerable inelastic scattering in the experimental data.

The tensor components of polarization may be conveniently analysed in the following way to determine the tensor force parameters. Firstly, note that

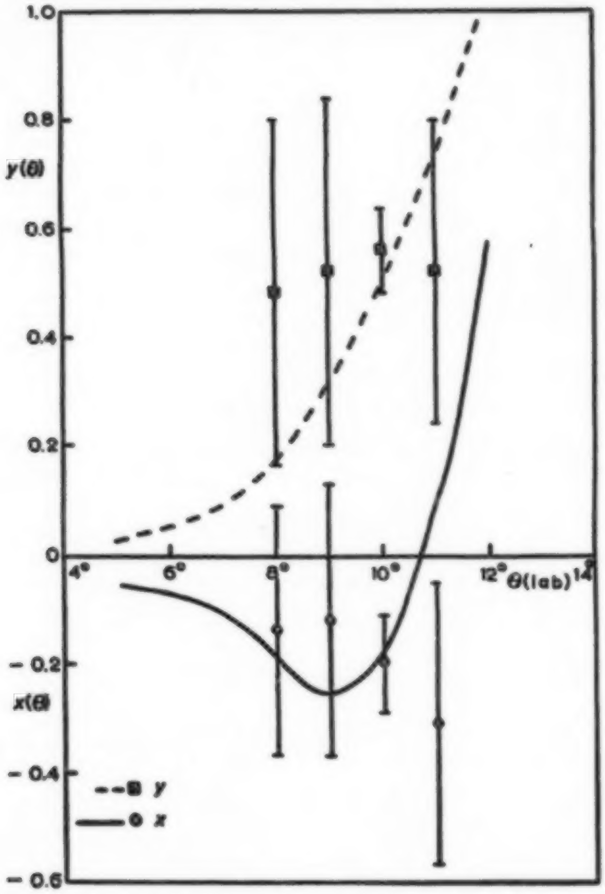

Fig. 4. Plot of $x(\theta)$ and $y(\theta)$. The points are the experimental results of Button and Mermod ¹). The curves are the theoretical predictions for $V=10$ MeV, $W=20$ MeV, $\gamma=2.5$ MeV fm³, $\delta=0$ MeV fm³, $\zeta=-0.2$ MeV, $\eta=+0.3$ MeV, $a=1.5$ fm, $b=3.9$fm, $c=3.5$fm, $d=5.5$fm with the inclusion of electromagnetic interactions.

$$\sqrt{2}\langle T_{20}\rangle+\tfrac{1}{2}\sqrt{3}\langle T_{22}\rangle+\tfrac{2}{3}|B|^2 = [2X(\cos\theta-1)+4Z-2Y\sin\theta-4P(1+\cos\theta)]/I, \qquad (33)$$

and

$$\sqrt{2}\langle T_{20}\rangle-\tfrac{1}{2}\sqrt{3}\langle T_{22}\rangle = [4X\cos\theta-4Y\sin\theta-4P\cos\theta]/I. \qquad (34)$$

If it is assumed that there is no T_2 tensor interaction so that $D=0$, and

$(\cos\theta-1)$ is taken as zero, eqs. (33), (34) become

$$\sqrt{2}\langle T_{20}\rangle+\tfrac{1}{2}\sqrt{3}\langle T_{22}\rangle+\tfrac{2}{3}|B|^2 = [-2Y\sin\theta]/I', \tag{35}$$

$$\sqrt{2}\langle T_{20}\rangle-\tfrac{1}{2}\sqrt{3}\langle T_{22}\rangle = [4X-4Y\sin\theta]/I', \tag{36}$$

and

$$\langle T_{21}\rangle = [\sqrt{3}Y+\sqrt{3}X\sin\theta]/I', \tag{37}$$

where

$$I' = |A|^2+\tfrac{2}{3}|B|^2+8|C|^2. \tag{38}$$

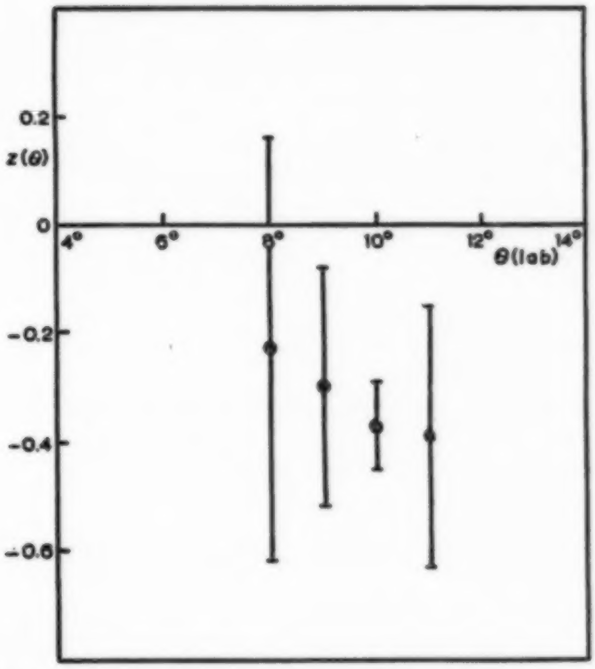

Fig. 5. Plot of $z(\theta)$ determined from the experimental data of Button and Mermod 1) and the analysis of $\langle iT_{11}\rangle$ giving $\gamma=2.5$ MeV fm², $\delta=0$ MeV fm², which measure $|B|^2$.

To a good approximation $y = 4\langle T_{21}\rangle/\sqrt{3} \approx 4Y/I'$ from eq. (37) so that

$$z = \sqrt{2}\langle T_{20}\rangle+\tfrac{1}{2}\sqrt{3}\langle T_{22}\rangle+\tfrac{2}{3}|B|^2+2\langle T_{21}\rangle\sin\theta/\sqrt{3} \approx 0, \tag{39}$$

$$x = \sqrt{2}\langle T_{20}\rangle-\tfrac{1}{2}\sqrt{3}\langle T_{22}\rangle+4\langle T_{21}\rangle\sin\theta/\sqrt{3} \approx 4X/I'. \tag{40}$$

The left-hand-side of both these equations is completely determined by the experimental data and the analysis of $\langle iT_{11}\rangle$ giving γ, δ, which measure $|B|^2$. If the left-hand-side of eq. (39) differs significantly from zero, D cannot be zero and the presence of some T_2 tensor interaction is indicated. Eq. (40) may be used with the relation for y to obtain ζ and η. Fig. 4 shows the fits obtained for x, y for $\zeta = -0.2$ MeV and $\eta = +0.3$ MeV. Provided $|D|$ is small, these values of ζ and η should not be greatly modified when the P terms are included in the expressions for x and y, since these are "second order" tensor effects.

Fig. 5 shows that z is considerably different from zero for angles of about 10°. This means that $|D| \neq 0$ and indicates the existence of interactions of the type T_2.

The author wishes to thank Professor K. J. Le Couteur for his interest in the work and Dr. D. C. Peaslee for many invaluable suggestions and helpful discussions. He is also indebted to Mrs. B. Nerdal for some assistance with the calculations.

References

1) J. Button and R. Mermod, Phys. Rev. **118** (1959) 1333
2) J. Baldwin, O. Chamberlain, E. Segre, R. Tripp, C. Wiegand and T. Ypsilantis, Phys. Rev. **103** (1956) 1502
3) W. Lakin, Phys. Rev. **98** (1955) 139
4) G. R. Satchler, Oak Ridge National Laboratory, Report-2861 (1960)
5) O. D. Cheishvili, JETP (USSR) **32** (1957) 1240
6) S. Watanabe, Nuclear Physics **8** (1958) 484
7) L. J. B. Goldfarb, Nuclear Physics **7** (1958) 622
8) J. L. Gammel, B. J. Hill and R. M. Thaler, Phys. Rev. **119** (1960) 267
9) B. A. Robson, Aust. J. Phys. **12** (1958) 248
10) L. I. Schiff, Phys. Rev. **103** (1956) 443
11) K. Nishimura, Phys. Rev. **110** (1958) 1166
12) K. R. Greider, Phys. Rev. **114** (1959) 786
13) E. M. Hafner, Phys. Rev. **111** (1958) 297
14) W. Heckrotte, Phys. Rev. **101** (1956) 1406

1.E.5

Nuclear Physics **23** (1961) 681—693; © *North-Holland Publishing Co., Amsterdam*

Not to be reproduced by photoprint or microfilm without written permission from the publisher

THE SCATTERING OF NUCLEONS BY NUCLEI AT VERY HIGH ENERGIES

L. R. B. ELTON

Department of Physics, Battersea College of Technology, London

Received 6 December 1960

Abstract: Experimental results on the scattering of neutrons by nuclei in the energy region 0.3–5.0 GeV are analysed in terms of a semi-classical approximation and this is compared with the classical treatment used in an earlier paper. The analysis is used to derive half-way radii of the nuclear density distributions and these are compared with the corresponding quantities obtained from electron scattering. An estimate is given of the magnitude of the depth of the real part of the optical potential in the energy region.

1. Introduction

For some time now the scattering of nucleons by nuclei in the GeV region has been the most promising approach to the problem of the density distribution of nucleons in nuclei. Early experiments were treated by means of a classical theory [1–3]), but more recently [4]) a semi-classical partial wave analysis has been used to interpret experimental data ranging from 0.3 GeV to 5.0 GeV. (For details of these data see ref. [4]).) The purpose of the present paper is to show the relationship between the two methods and to obtain more reliable information about the density distribution of nuclear matter, than has been possible until now.

2. Classical Treatment

In the classical treatment we assume that the distribution of nucleons in the nucleus is given by a spherically symmetric function $\rho(r)$ and that scattering takes place between the incident nucleon and one target nucleon at a time. If the mean two-body cross-section for this process is $\bar{\sigma}$, the reaction cross-section is given by [1])

$$\sigma_{\text{cl}}^{(r)} = \int_0^\infty 2\pi b \left\{1 - \exp\left[-\int_0^\infty \bar{\sigma}\rho(\sqrt{b^2+z^2})\right]\right\} \mathrm{d}b. \tag{2.1}$$

It is not possible to obtain a classical expression for the total scattering since, as is well known, even at the highest energies there is a finite amount of small angle diffraction scattering, the so-called shadow scattering, which cannot be described classically.

3. Partial Wave Analysis

In terms of the amplitudes η_l of the scattered partial waves the reaction and total cross-sections are given by

$$\sigma^{(r)} = \pi\lambda\!\!\!^{-2} \sum_{l=0}^{\infty} (2l+1)(1-|\eta_l|^2), \tag{3.1}$$

$$\sigma^{(t)} = 2\pi\lambda\!\!\!^{-2} \sum_{l=0}^{\infty} (2l+1)(1-\mathrm{Re}\,\eta_l). \tag{3.2}$$

Here $\eta_l = \exp(2i\delta_l)$ and δ_l is the usual phase-shift, which is not necessarily real. These formulae are valid even in the relativistic region, provided spin effects can be neglected. That this is permissible will be shown in the next section.

When a large number of partial waves is involved in a scattering process, it is permissible to replace the sums by integrals. For this purpose we adapt the Euler-Maclaurin formula

$$\sum_{n=0}^{\infty} f(n) = \int_0^{\infty} f(x)\mathrm{d}x + \tfrac{1}{2}f(0) - \tfrac{1}{12}f'(0), \tag{3.3}$$

where we neglect second derivatives and assume that $f(x)$ and $f'(x)$ vanish at infinity. Now we have

$$f(n+\tfrac{1}{2}) = \tfrac{1}{2}[f(n)+f(n+1)] + \tfrac{1}{4}[f'(n)-f'(n+1)] + \tfrac{1}{16}[f''(n)+f''(n+1)],$$

so that

$$\sum_{n=0}^{\infty} f(n+\tfrac{1}{2}) = \sum_{n=0}^{\infty} f(n) - \tfrac{1}{2}f(0) + \tfrac{1}{4}f'(0) + \tfrac{1}{8}\sum_{n=0}^{\infty} f''(n) - \tfrac{1}{16}f''(0).$$

But we have

$$\sum_{n=0}^{\infty} f''(n) = \int_0^{\infty} f''(x)\mathrm{d}x = -f'(0).$$

Hence we get

$$\sum_{n=0}^{\infty} f(n+\tfrac{1}{2}) = \int_0^{\infty} f(x)\mathrm{d}x + \tfrac{1}{24}f'(0). \tag{3.4}$$

This formula is applied to (3.1) and (3.2), where we make the substitutions

$$\delta_l = \lambda_l + i\mu_l, \qquad \zeta_l = \exp(-2\mu_l) \tag{3.5}$$

and

$$b = \lambda\!\!\!^{-}(l+\tfrac{1}{2}). \tag{3.6}$$

Then we get

$$\sigma^{(r)} = 2\pi\left\{\int_0^\infty b[1-\zeta^2(b)]\mathrm{d}b+\frac{\lambda\!\!\!^{-2}}{24}[1-\zeta^2(0)]\right\}, \tag{3.7}$$

$$\sigma^{(t)} = 4\pi\left\{\int_0^\infty b[1-\zeta(b)\cos 2\lambda(b)]\mathrm{d}b+\frac{\lambda\!\!\!^{-2}}{24}[1-\zeta(0)\cos 2\lambda(0)]\right\}. \tag{3.8}$$

We shall sometimes neglect the correction terms, which are very small compared with the integrals. It may be noted that strictly speaking the classical impact parameter b is given by

$$b = \lambda\!\!\!^{-}\sqrt{[l(l+1)]},$$

but the difference between this expression and (3.6) is of an order of magnitude that is systematically neglected in this paper.

Glassgold and Greider [4]) now consider three regions of l:

(a) $0 < l < L-\Delta$: in this region the nucleus is almost completely opaque, i.e., $\zeta \approx 0$;

(b) $L-\Delta < l < L+\Delta$: in this region the opacity gradually decreases to zero;

(c) $L+\Delta < l$: in this region the nucleus is transparent, i.e. $\zeta \approx 1$.

By choosing various arbitrary functional forms for ζ and λ it is then possible to determine L and Δ as functions of the bombarding energy and the mass number of the nucleus in such a manner as to fit the experimental results. Unfortunately the simple functional forms chosen make it difficult to interpret them in terms of the more usual nuclear parameters and it will be shown that more convenient ones can be found which are no more difficult to handle algebraically.

4. The Semi-Classical Expression for the Phase Shift

As is well known, at energies above a few MeV the interaction between an incident nucleon and a nucleus is well represented by a complex potential which contains a central part $V(r)+iW(r)$ and a part that depends on the spin-orbit coupling. This latter is proportional to the gradient of the former. Now at very high energies the change of the real part of the potential over a wavelength of the incident nucleon is small compared to the potential, i.e.

$$\lambda\!\!\!^{-}\frac{\mathrm{d}V}{\mathrm{d}r} \ll V(r). \tag{4.1}$$

Hence terms proportional to $\mathrm{d}V/\mathrm{d}r$ will be neglected, and these include not only the spin-orbit dependent potential, but also certain terms which distinguish the Dirac from the Klein-Gordon equation. The wave equation

$$-i\hbar c\boldsymbol{\alpha}\cdot\nabla\Psi+\beta mc^2\Psi+[V(r)+iW(r)]\Psi = E\Psi \tag{4.2}$$

can therefore be reduced to a Klein-Gordon equation for each of the four components,

$$\hbar^2c^2\nabla^2\Psi_j+\{[E-V(r)-iW(r)]^2-m^2c^4\}\Psi_j = 0, \quad j = 1, 2, 3, 4. \tag{4.3}$$

Making use of the fact that $V(r) \ll E$, $W(r) \ll E$ at high energies, we have

$$\hbar^2c^2\nabla^2\Psi_j+[E^2-2E(V+iW)-m^2c^4]\Psi_j = 0. \tag{4.4}$$

Following Brown and McCauley [5]) we put

$$\Psi_j = \mathrm{e}^{ikz}\psi_j, \quad k^2 = \frac{E^2-m^2c^4}{\hbar^2c^2}.$$

Hence we have

$$\nabla^2\psi_j+2ik\frac{\partial\psi_j}{\partial z}-\frac{2E(V+iW)}{\hbar^2c^2}\psi_j = 0. \tag{4.5}$$

It is now permissible to neglect $\nabla^2\psi_j$, since ψ_j is a slowly varying function of position. The equation can then be integrated at once to yield

$$\psi_j = \exp\left\{-\frac{i}{\hbar v}\int_{-\infty}^{z}(V+iW)\mathrm{d}z\right\}, \tag{4.6}$$

where $v = E/c^2\hbar k$ is the velocity of the incident particle in free space. As $z \to \infty$, the expression in the curly bracket tends to the total phase shift 2δ, the factor 2 arising from the fact that the same phase shift occurs for the incident and the scattered wave. Thus

$$\delta(b) = -\frac{1}{\hbar v}\int_{z}^{\infty}[V(\sqrt{b^2+z^2})+iW(\sqrt{b^2+z^2})]\mathrm{d}z. \tag{4.7}$$

This formula was originally derived non-relativistically by Molière [6]).

5. The Semi-Classical Expressions for the Cross-Sections

We next substitute the expression (4.7) for the phase in the formulae (3.7) and (3.8), where we now neglect the correction terms. Then we have

$$\sigma^{(r)} = 2\pi\int_0^{\infty} b\left\{1-\exp\left[\frac{2}{\hbar v}\int_{-\infty}^{\infty}W(\sqrt{b^2+z^2})\mathrm{d}z\right]\right\}\mathrm{d}b, \tag{5.1}$$

$$\sigma^{(t)} = 4\pi\int_0^{\infty} b\left\{1-\exp\left[\frac{1}{\hbar v}\int_{-\infty}^{\infty}W(\sqrt{b^2+z^2})\mathrm{d}z\right]\right. \\ \left.\times\cos\left[\frac{1}{\hbar v}\int_{-\infty}^{\infty}V(\sqrt{b^2+z^2})\mathrm{d}z\right]\right\}\mathrm{d}b. \tag{5.2}$$

Thus both the total and reaction cross-sections yield information on the imaginary part of the potential, but only the total cross-section yields information on the real part.

It is convenient to write the optical potential in the form

$$V(r)+iW(r) = -V_0 f_R(r) - iW_0 f_I(r), \tag{5.3}$$

where the $f_N(r)$ are given by functions

$$f_N(r) = \left[1+\exp\left(\frac{r^2-c_N^2}{a_N^2}\right)\right]^{-1}, \quad c_N \gg a_N, \quad N = \mathrm{R}, \mathrm{I}, \tag{5.4}$$

or similar functions. Then $-(V_0+iW_0)$ is the potential in infinite nuclear matter.

To investigate (5.1) further, we must go back to the wave equation (4.2). A problem similar to ours, in that there too a wave function decays in time, is that of alpha decay, which has been treated by Gamow[7]) in terms of complex energy levels in a real potential. It will be more convenient here to use real energy levels in a complex potential. The rate of removal of particles from the incident beam of density ρ_i and current $\mathbf{j}$ is

$$P = -\frac{\partial \rho_i}{\partial t} - \nabla \cdot \mathbf{j},$$

where $\rho_i = \Psi^\dagger \Psi$ and $\mathbf{j} = \Psi^\dagger c\alpha \Psi$. Now $\Psi^\dagger \Psi$ is independent of time, so that $\partial \rho_i / \partial t = 0$, and hence, at a point $\mathbf{r}$,

$$P(r) = -\nabla \cdot \mathbf{j} = -\frac{2W(r)}{\hbar} \Psi^\dagger \Psi = -\frac{2W(r)}{\hbar} \rho_i(r), \tag{5.5}$$

with the help of (4.2). Hence the decay constant for the exponential decay of the stream of particles at $\mathbf{r}$ is

$$\Lambda(r) = \frac{P(r)}{\rho_i(r)} = -\frac{2W(r)}{\hbar} \tag{5.6}$$

and the mean free path is

$$L(r) = \frac{v}{\Lambda(r)},$$

where v is the velocity of the nucleons in the incident beam, which for high energies is practically independent of $\mathbf{r}$. Now, classically, we have

$$L(r) = \frac{1}{\rho(r)\bar{\sigma}}, \tag{5.7}$$

and hence

$$\tfrac{1}{2}\rho(r)\bar{\sigma} = -\frac{W(r)}{\hbar v}. \tag{5.8}$$

This result, which we have derived classically, can also be derived from the semi-classical formalism of Brown[5]). He shows that in terms of the average forward scattering amplitude for two-body scattering $\overline{f(0)}$,

$$-EW(r) = 2\pi\hbar^2 c^2 \rho(r)\,\mathrm{Im}\,\overline{f(0)}. \tag{5.9}$$

Using the optical theorem,

$$\bar{\sigma} = -\frac{4\pi}{k}\,\mathrm{Im}\,\overline{f(0)}, \tag{5.10}$$

we at once obtain (5.8)

We therefore see that the relationship (5.8) between the nuclear density and the imaginary part of the optical potential is valid both in the classical and semi-classical approximations. If we now compare the classical expression (2.1) for $\sigma^{(r)}$ with the semi-classical one, given by (5.1) and (5.3), we see at once that they are identical, and that

$$\rho(r) = \rho(0) f_{\mathrm{I}}(r). \tag{5.11}$$

Thus the reaction cross-section determines the density distribution or, alternatively, the imaginary part of the optical potential, with which it is coextensive. In this case the semi-classical analysis does not therefore add anything to the classical one.

The situation is clearly quite different for the total cross-section. It has been pointed out[4]) that this is in fact far more sensitive to small changes in the opacity of the nucleus than the reaction cross-section and it can be interpreted only by means of a semi-classical analysis and not at all classically.

6. The Functional Form of η(b)

In section **3** we expressed the reaction and total cross-sections in terms of the quantity

$$\eta(b) = \zeta(b) \exp\,[2i\lambda(b)]. \tag{6.1}$$

On comparing (3.7) and (3.8) with (5.1) and (5.2) we can relate this to the optical potential and the density distribution through

$$\zeta(b) = \exp\left\{-\int_0^\infty \bar{\sigma}\rho[\sqrt{(b^2+z^2)}]\mathrm{d}z\right\} = \exp\left\{-\frac{W_0}{\hbar v}\int_{-\infty}^{\infty} f_{\mathrm{I}}[\sqrt{(b^2+z^2)}]\mathrm{d}z\right\}, \tag{6.2}$$

$$\lambda(b) = \frac{V_0}{\hbar v}\int_0^\infty f_{\mathrm{R}}[\sqrt{(b^2+z^2)}]\mathrm{d}z. \tag{6.3}$$

If we use the functional form (5.4) for $f_{\mathrm{I}}(r)$, then we get

$$\zeta(b) = \exp\left\{-\frac{a_{\mathrm{I}} W_0}{\hbar v} E(-\tfrac{1}{2}, 1; \kappa_{\mathrm{I}})\right\}, \qquad \kappa_{\mathrm{I}} = \frac{c_{\mathrm{I}}^2 - b^2}{a_{\mathrm{I}}^2}, \tag{6.4}$$

where the integral

$$E(n, m; \kappa) = \int_0^\infty \frac{x^n}{[1+\exp(x-\kappa)]^m} \mathrm{d}x \tag{6.5}$$

is tabulated [8]) for $n = \frac{1}{2}, -\frac{1}{2}, m = 1$. In fig. 1 we have plotted $\zeta(b)$ and $1-\zeta^2(b)$ for two extreme cases in the high energy region, (a) for a heavy nucleus at the

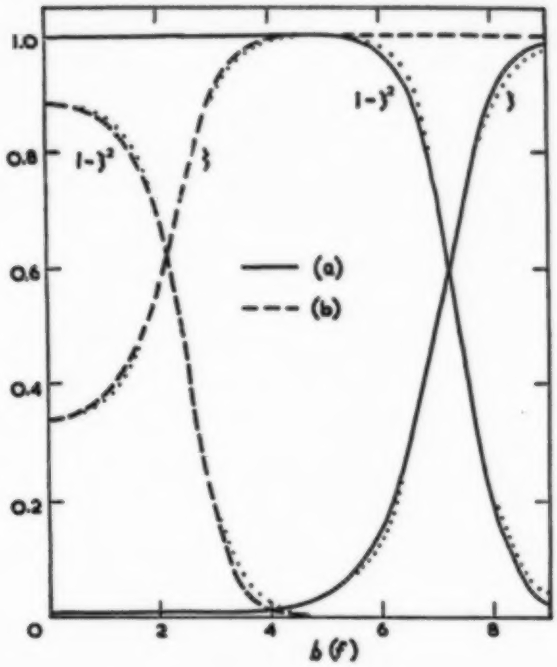

Fig. 1. Plot of $\zeta(b)$, the modulus of the scattering amplitude, and of $1-\zeta^2(b)$ for (a) Pb at 1.4 GeV, (b) C at 0.4 GeV. The full and dashed curves are based on (6.4) and the dotted curves are a best fit of the functional form (6.6).

energy where $\bar{\sigma}$ has a maximum and (b) for a light nucleus at the energy where $\bar{\sigma}$ has a minimum. We assume [3, 4]) that exclusion principle effects are negligible at these energies. This is certainly true at the upper end of the region, and even at the lower end the effect has been estimated [9]) to be only about 5 %. None of our results are sensitive to such small variations in $\bar{\sigma}$.

It is desirable to have simple functional forms for $\zeta(b)$ and $1-\zeta^2(b)$ and it will be observed that both these functions exhibit transition regions which are very nearly symmetrical about a point halfway between the maximum and the minimum for each function. None of the functional forms chosen previously [4]) exhibit this property and we therefore choose the function

$$\zeta(b) = 1 - \frac{B}{1-\exp\dfrac{b-c}{a}}. \tag{6.7}$$

The corresponding best fits are indicated by dotted lines in fig. 1. The agreement is clearly satisfactory.

It is much more difficult to come to any firm conclusions about $\lambda(r)$, since we have no independent information about V_0, c_R and a_R. At lower energies we know [10]) that V_0 decreases monotonically from ≈ 50 MeV to small values, possibly negative, as the energy increases from 0 to 300 MeV, and it seems likely that $|V_0|$ is small at higher energies. Further $f_R(r)$ cannot differ substantially from $f_I(r)$, so that $\lambda(b)$ will be significantly different from zero for small b only. But $\lambda(b)$ only occurs in the combination $\zeta(b) \cos 2\lambda(b)$ in the expression for $\sigma^{(t)}$, and $\zeta(b)$ is small for small b. Hence the experimental results, particularly in the case of heavy absorption, are rather insensitive to $\lambda(b)$. Nevertheless, in disagreement with previous work [4]), it is not possible to put $\lambda(b) = 0$ throughout, and we shall put

$$\zeta(b) \cos 2\lambda(b) = 1 - \frac{B'}{1+\exp\dfrac{b-c}{a}}, \tag{6.7}$$

where $B < B' < 1$. Hence we have

$$\cos 2\lambda(0) = \frac{1-B'}{1-B}. \tag{6.8}$$

7. Explicit Expressions for the Cross-Sections

We now substitute the expressions (6.6) and (6.7) into the cross-section formulae (3.7) and (3.8). Hence, if we neglect terms O[exp($-c/a$)], we get

$$\begin{aligned}\sigma^{(r)} &= 2\pi \int_0^\infty b \left\{ 2B \left(1 - \exp\frac{b-c}{a}\right)^{-1} - B^2 \left(1 - \exp\frac{b-c}{a}\right)^{-2} \right\} \mathrm{d}b + \tfrac{1}{12}\pi\lambdabar^2 B(2-B) \\ &= 2\pi a^2 B \{2E(1, 1; c/a) - BE(1, 2; c/a)\} + \tfrac{1}{12}\pi\lambdabar^2 B(2-B),\end{aligned} \tag{7.1}$$

$$\begin{aligned}\sigma^{(t)} &= 4\pi \int_0^\infty bB' \left(1 - \exp\frac{b-c}{a}\right)^{-1} \mathrm{d}b + \tfrac{1}{6}\pi\lambdabar^2 B' \\ &= 4\pi a^2 B' E(1, 1; c/a) + \tfrac{1}{6}\pi\lambdabar^2 B'.\end{aligned} \tag{7.2}$$

Now, for $n > 0$, we have

$$\begin{aligned}\frac{\mathrm{d}}{\mathrm{d}\kappa} E(n, m; \kappa) &= \int_0^\infty x^n \frac{\partial}{\partial \kappa} (1+\mathrm{e}^{x-\kappa})^{-m} \mathrm{d}x \\ &= -\int_0^\infty x^n \frac{\partial}{\partial x} (1+\mathrm{e}^{x-\kappa})^{-m} \mathrm{d}x = nE(n-1, m; \kappa)\end{aligned} \tag{7.3}$$

and alternatively,

$$\frac{\mathrm{d}}{\mathrm{d}\kappa}E(n, m; \kappa) = m\int_0^\infty x^n \mathrm{e}^{x-\kappa}(1+\mathrm{e}^{x-\kappa})^{-m-1}\mathrm{d}x$$

$$= m\int_0^\infty x^n\{(1+\mathrm{e}^{x-\kappa})^{-m}-(1+\mathrm{e}^{x-\kappa})^{-m-1}\}\mathrm{d}x$$

$$= m\{E(n, m; \kappa)-E(n, m+1; \kappa)\}. \tag{7.4}$$

Hence we have

$$E(n, m+1; \kappa) = E(n, m; \kappa)-\frac{n}{m}E(n-1, m; \kappa). \tag{7.5}$$

Further 11) we have

$$E(1, 1; \kappa) = \tfrac{1}{2}\kappa^2+\tfrac{1}{6}\pi^2+\mathrm{O}(\mathrm{e}^{-\kappa}), \tag{7.6}$$

$$E(0, 1; \kappa) = \kappa+\mathrm{O}(\mathrm{e}^{-\kappa}), \tag{7.7}$$

so that

$$\sigma^{(\mathrm{r})} = \pi(1-\varepsilon^2)(c^2+\tfrac{1}{3}\pi^2a^2+\tfrac{1}{12}\bar{\lambda}^2)+2\pi(1-\varepsilon)^2ac, \tag{7.8}$$

$$\sigma^{(\mathrm{t})} = 2\pi(1-\varepsilon')(c^2+\tfrac{1}{3}\pi^2a^2+\tfrac{1}{12}\bar{\lambda}^2). \tag{7.9}$$

Here we have put $\varepsilon = 1-B$, $\varepsilon' = 1-B'$, which in all cases are small quantities with $0 < \varepsilon' < \varepsilon$.

To compare these expressions with those given previously 4), we introduce the angular momentum quantum number L corresponding to an impact parameter c, and the usual 90–10 % transition region 2Δ for L through

$$c = \bar{\lambda}(L+\tfrac{1}{2}), \qquad 4.4a = 2\bar{\lambda}\Delta. \tag{7.10}$$

Hence we get

$$\sigma^{(\mathrm{r})} = \pi\bar{\lambda}^2\{(1-\varepsilon^2)[(L+\tfrac{1}{2})^2+0.68\Delta^2+\tfrac{1}{12}]+0.90(1-\varepsilon)^2(L+\tfrac{1}{2})\Delta\}, \tag{7.11}$$

$$\sigma^{(\mathrm{t})} = 2\pi\bar{\lambda}^2(1-\varepsilon')[(L+\tfrac{1}{2})^2+0.68\Delta^2+\tfrac{1}{12}]. \tag{7.12}$$

8. Comparison with Experiment

It remains now to compare the theoretical cross-sections (7.8) and (7.9) with experiment. The fact that for each nucleide investigated $\sigma^{(\mathrm{r})}$ is nearly constant over the whole energy range 0.3–5.0 GeV, while $\sigma^{(\mathrm{t})}$ shows substantial energy variation, has led to the suggestion 4) that the whole energy dependence of $\sigma^{(\mathrm{t})}$ must lie in the small quantity ε. Now

$$\varepsilon = \exp\{-\tfrac{1}{2}\rho_0\bar{\sigma}a_1E(-\tfrac{1}{2}, 1; c_1^2/a_1^2)\}, \tag{8.1}$$

and since

$$E(-\tfrac{1}{2}, 1; \kappa) \to 2\kappa^{\frac{1}{2}}, \qquad \text{as } \kappa \to \infty,$$

we have

$$\varepsilon \approx \exp(-\rho_0 \bar{\sigma} c_{\mathrm{I}}), \qquad c_{\mathrm{I}} \gg a_{\mathrm{I}}. \tag{8.2}$$

The quantity $1-\varepsilon$ is quite insensitive to small changes in $\rho_0 \bar{\sigma} c_{\mathrm{I}}$ and it is therefore permissible to use values for ρ_0 and c_{I} derived from electron scattering data. To achieve agreement with experiment it is then necessary to take values of $\bar{\sigma}$ that are up to twice as large as those obtained from free two-body scattering.

An alternative approach is to take $1-\varepsilon$ as given by (8.1) with the experimental values of $\bar{\sigma}$ obtained from two-body scattering. As we have indicated above the value is insensitive to our choice of ρ_0 and c_{I} and we again take electron scattering data. The reason for this insensitivity is of course that $1-\varepsilon$ represents the absorption of the central region of a very opaque nucleus.

It will now be necessary to allow c to vary. In principle it might be necessary to vary a too, but the results are not sensitive to such a variation. Since for the two cases plotted in fig. 1, the values of a are virtually the same as the corresponding quantities obtained from electron scattering [11, 12]), we shall employ these latter quite generally.

The calculation then proceeds in three steps. We first calculate $1-\varepsilon$ and $1-\varepsilon^2$

TABLE 1

Theoretical values for $1-\varepsilon$ and $1-\varepsilon^2$

Energy (GeV)	0.3	0.7	1.4	5.0
$\bar{\sigma}$ (fm²)	3.0	4.0	4.5	3.3
$1-\varepsilon$ for C	0.67	0.77	0.81	0.71
Al	0.79	0.87	0.90	0.82
Cu	0.88	0.94	0.96	0.91
Pb	0.962	0.987	0.993	0.972
$1-\varepsilon^2$ for C	0.89	0.95	0.96	0.92
Al	0.96	0.98	0.99	0.97
Cu	0.99	1.00	1.00	0.99
Pb	1.00	1.00	1.00	1.00

TABLE 2

Values of the half-way radius of the scattering amplitude $\zeta(b)$ and of $\varepsilon' = \zeta(0) \cos 2\lambda(0)$

Energy (GeV)	0.3	0.7	1.4	5.0
c (fm) for C	2.32	2.35	2.44	2.45
Al	2.98	3.14	3.17	3.13
Cu	4.28	4.42	4.54	4.20
Pb	6.76	6.95	7.03	6.53
ε' for C	0.27	0.11	0.10	0.20
Al	0.11	0.06	0.04	0.10
Cu	0.06	0.03	0.02	0.05
Pb	0.02	0.00	0.00	0.02

from (8.1) and obtain the values given in table 1. Those for the opacity $1-\varepsilon^2$ are in good agreement with values calculated previously[4]). As regards the sensitivity of $1-\varepsilon$ and $1-\varepsilon^2$ to variations in the quantity $\rho_0\bar{\sigma}c_{\mathrm{I}}$, it may be noted that an error of 20 % in this quantity leads to corresponding errors in $1-\varepsilon$ and $1-\varepsilon^2$ of only 10 % and 5 % respectively in C, and of 3 % and 0.3 % in Pb.

The next step consists of fitting values of c and ε' to the experimental values of $\sigma^{(r)}$ and $\sigma^{(t)}$. Results are given in table 2 and the kind of agreement obtained with experiment is shown in fig. 2. In general it is not possible to vary values of c by more than 2–3 % without obtaining definite disagreement with experiment, and, while one cannot be equally precise about ε', it is not possible, except in one or two instances, to use values of ε' that are larger than the corresponding value of $\frac{1}{2}\varepsilon$. There is therefore definite evidence here that the real part of the optical potential is non-zero in the energy region investigated.

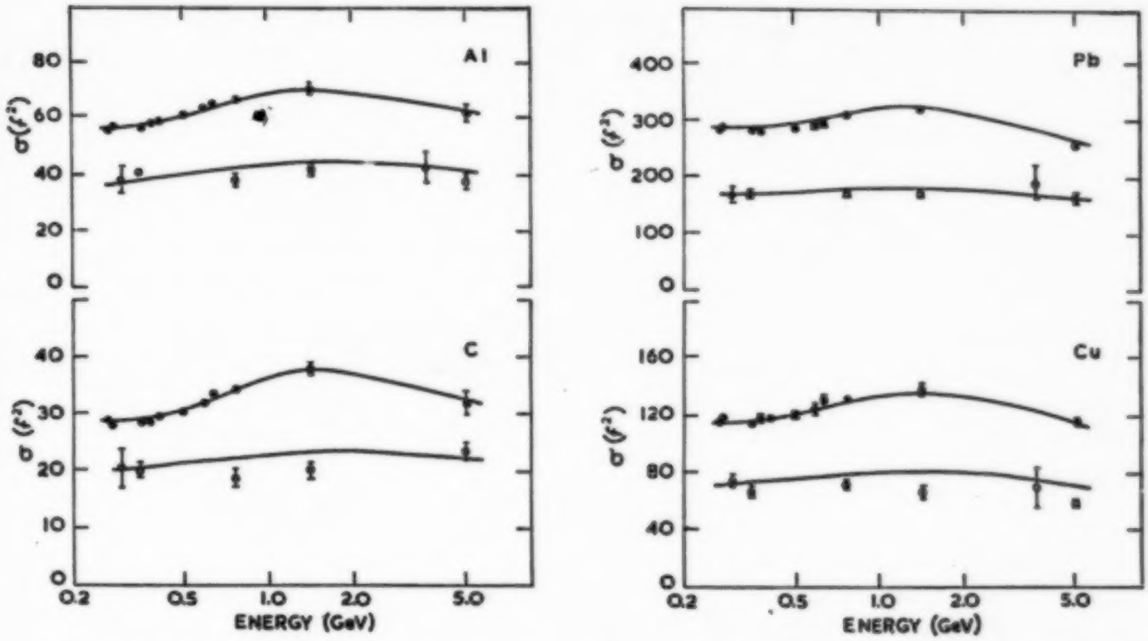

Fig. 2. Total cross-sections (solid circles) and reaction cross-sections (open circles) for the scattering of neutrons by C, Al, Cu and Pb. The curves are theoretical fits, based on the values in tables 1 and 2.

Lastly we deduce values for the half-way density radii c_{I} from the formula

$$\zeta(c) = \tfrac{1}{2}(1+\varepsilon) = \exp\{-\tfrac{1}{2}\rho_0\bar{\sigma}a_{\mathrm{I}}E[-\tfrac{1}{2}, 1; (c_{\mathrm{I}}^2-c^2)/a_{\mathrm{I}}^2]\}. \tag{8.3}$$

The results are given in table 3. With the possible exception of the value for Pb at 5.0 GeV, these exhibit the invariance with respect to energy that was to be expected. The last columns of the table compare the averaged values of c_{I} with half-way radii obtained from electron scattering[11,12]) where those for Al

TABLE 3

Values of the half-way radius c_I of the density distribution in nuclei

Energy (GeV)	c_I (fm)				c_I (fm)	c_I (fm)
	0.3	0.7	1.4	5.0	(average)	(electron scattering)
C	2.27	2.25	2.32	2.40	2.31	2.30
Al	2.95	3.01	3.00	3.09	3.02	3.06
Cu	4.27	4.24	4.31	4.13	4.24	4.26
Pb	6.68	6.61	6.66	6.35	6.57	6.48

and Cu have been interpolated, since experimental values do not exist for them. It will be seen that there is no significant difference for C, Al and Cu, but that c_I is slightly larger than c (electron scattering) for Pb. Since the experimental results are most accurate for Pb, this difference is probably a real one.

It might be thought that by using (8.1) to obtain ε and then (8.3) to obtain c_I, we have gone around in a circle. This is not so, since in (8.3) we consider the absorption in the surface region, and this is very sensitive to variations in c_I, while the absorption in the inner region is not. It is also sensitive to variations in a_I, and if we had taken values of a_I significantly different from the electron scattering values, our values of c_I in table 3 would have been slightly changed. There seems no good reason for doing this.

9. Conclusion

The main conclusion to be drawn from the results is that there is now strong evidence that the neutron distribution does not extend beyond the proton distribution in light and medium nuclei, and that it extends only very slightly, by perhaps 0.1 or 0.2 fm, in heavy nuclei. This confirms previous results based on more slender evidence [3]).

The experiments also throw some light on the depth V_0 of the real part of the optical potential in the GeV region. It is certainly non-zero, and if we take $\varepsilon' = \frac{1}{2}\varepsilon$ for a heavy nucleus then the corresponding absolute value of the depth can be obtained from (6.3) and (6.8), and is

$$|V_0| \approx 14 \text{ MeV}.$$

It is not possible, however, to give any estimate of the accuracy of this figure.

My thanks are due to Dr. A. E. Glassgold for informing me of his work prior to its publication and to The National Institute for Research in Nuclear Science for financial assistance. I am greatly indebted to Mr. L. Castillejo for a most useful discussion.

References

1) R. W. Williams, Phys. Rev. **98** (1955) 1387
2) J. W. Cronin, R. Cool and A. Abashian, Phys. Rev. **107** (1957) 1121
3) L. R. B. Elton, Revs. Mod. Phys. **30** (1958) 557
4) A. E. Glassgold and K. R. Greider, Phys. Rev. Lett. **2** (1959) 169; Ann. Phys. **10** (1960) 100
5) G. E. Brown, Proc. Phys. Soc. A **70** (1957) 361;
G. P. McCauley and G. E. Brown, Proc. Phys. Soc. **71** (1958) 900
6) G. Molière, Z. Naturf. **2a** (1947) 133
7) G. Gamow and C. L. Critchfield, Theory of the Atomic Nucleus and Nuclear Energy Sources (Clarendon Press, Oxford 1949) Ch. VI
8) J. McDougall and E. C. Stoner, Trans. Roy. Soc. A **237** (1939) 67
9) A. K. Kerman, H. McManus and R. M. Thaler, Ann. Phys. **8** (1959) 551
10) F. Bjorklund, Proc. Intern. Conf. on the Optical Model (1959), Florida State University p. 1
11) L. R. B. Elton, Nuclear Physics **5** (1958) 173
12) L. R. B. Elton, Nuclear Sizes (Oxford University Press, 1961)

1.E.4

Nuclear Physics 23 (1961) 694—695; ©*North-Holland Publishing Co., Amsterdam*

Not to be reproduced by photoprint or microfilm without written permission from the publisher

LIFETIME OF THE 3.56 MeV LEVEL OF Li^6

I. Sh. VASHAKIDZE, T. I. KOPALEISHVILI and G. A. CHILASHVILI
Physical Institute of the Academy of Sciences of the Georgian Republic, Tbilissi, GSSR

Received 6 July 1960

Abstract: Using the isobaric invariance the lifetime τ of the excited state of Li^6 with the excitation energy of 3.56 MeV is calculated by means of the matrix elements of the β-decay $He^6 \rightarrow Li^6$. The calculation yields $\tau \approx 0.8 \times 10^{-17}$ sec, which is roughly $^1/_{10}$ of the experimental result.

The lifetime of the excited state of the nucleus of Li^6 with an energy of 3.56 MeV with respect to γ-radiation was determined by Cohen and Tabin 1). It was found to be equal to $\tau = 7.2^{+1.5}_{-1.3} \times 10^{-17}$ sec.

It is known that this excited level belongs to an isobaric triplet $T = 1$ with the moment and parity $J = 0^+$, the ground state of the nucleus of Li^6 being an isobaric singlet $T = 0 (J = 1^+)$. Hence it follows that the radiation transition between these levels is of the M1 type.

If we proceed from the current concept that the first excited levels in the nucleus of Li^6 arise as a result of a change in the state of two excess nucleons over the closed shell, it becomes possible to calculate the life of the abovementioned 3.56 MeV level theoretically. Let us write the wave function for both ground and excited states of the nucleus of Li^6 in the form

$$\Psi = R_J(r_1, r_2)\phi_{JM} V_{TT_z}(\tau_1, \tau_2), \tag{1}$$

where $R_J(r_1, r_2)$ is the radial function of two nucleons in the field of an α-particle, ϕ_{JM} is the spin angular part of the wave function and V_{TT_z} is the isobaric wave function of two nucleons (in the ground state $J = 1$, $T = 0$, $T_z = 0$ and in the excited state $J = 0$, $T = 1$, $T_z = 0$). The contribution of states with non-vanishing orbital moments to the wave function ϕ_{JM} are known to be small. Therefore, purely spin functions of two nucleons can only be meant by ϕ_{JM}. In other words we have good reason to assume that the transition under consideration is caused by a change in the spin states of the nucleons.

The calculations performed for the probability of the transition in question yield

$$W = 4\pi \frac{e^2}{\hbar c} (\mu_n - \mu_p)^2 \frac{(\hbar\omega)^3}{(Mc^2)^2} \left| \int R_0 R_1 \mathrm{d}\tau \right|^2, \tag{2}$$

where μ_n and μ_p are the magnetic moments of a neutron and proton, $\hbar\omega$ the energy of the γ-quantum emitted and M is the nucleon mass.

To find the nucleon matrix element $\int R_0 R_1 \mathrm{d}\tau$ we shall use data on the β-decay of He^6. The nucleus of He^6 is known to be a component of the isobaric triplet He^6, Li^{6*}, Be^6, and therefore its wave function will be represented by eq. (1) in which $J = 0$, $T = 1$ and $T_z = -1$. The β-transition in the nucleus of Li^6 which gives rise to the nucleus of He^6 in the ground state is a purely axial-vector transition. Therefore the probability of the transition of this nucleus will be proportional to the desired nuclear matrix element $\int R_0 R_1 \mathrm{d}\tau$. Using the experimental value of the probability for the β-transition of He^6 we obtain (see ref. [3]))

$$g_{\mathrm{A}}^2 \left| \int R_0 R_1 \mathrm{d}\tau \right|^2 = 2.3, \tag{3}$$

where g_{A} is the constant of the axial-vector β-interactions for the nucleus He^6. Generally speaking the value of the constant g_{A} will differ depending on whether the neutron is in a bound or a free state. For a free neutron, as we know, $g_{\mathrm{A}}{}^{\mathrm{N}} = 1.71 \times 10^{-49}$ unit/hour cm³. Using eq. (3) for lifetime of the 3.56 MeV level of the nucleus of Li^6 we shall finally obtain $\tau = 0.8(g_{\mathrm{A}}/g_{\mathrm{A}}{}^{\mathrm{N}})^2\, 10^{-17}$ sec.

Assuming that $g_{\mathrm{A}} \approx g_{\mathrm{A}}{}^{\mathrm{N}}$, we obtain for the lifetime 0.8×10^{-17} sec, which is an order higher than the experimental value 7.2×10^{-17} sec. This discrepancy could be accounted for by the roughness of our assumptions: first, that only two nucleons over an α-particle take part in the transition, and second, that the contributions to the wave functions from the states of these nucleons with non-vanishing orbital moments are very small. Yet these approximations are successfully used for a number of investigations concerned with the participation of the nucleus in question. For example, ref. [2]) dealing with the μ-capture of the nucleus of Li^6 employs the wave function of the type (1) in which the terms containing the contributions from the states with non-vanishing orbital moments are small. Therefore our rejection of these terms could not lead to such a considerable discrepancy with experiment. This rejection is all the more permissible since the magnetic moment of the nucleus of Li^6, determining the effect under consideration is nearly strictly equal to the sum of the spin magnetic moments of the two excess nucleons.

Of course, we could obtain satisfactory agreement with experiment by assuming that $g_{\mathrm{A}} \approx 3g_{\mathrm{A}}{}^{\mathrm{N}}$, but so large increase in the constant of coupling for the bound neutron seems rather improbable. Therefore before drawing the final conclusions the validity of the experimental value of the lifetime of the 3.56 MeV level of the nucleus of Li^6 should be checked by new measurements.

In conclusion, we express gratitude to Prof. V. I. Mamasakhlisov for stimulating discussions.

References

1) Leslie Cohen and Ralpha Tabin, Nuclear Physics **14** (1959) 243
2) H. Überall, Phys. Rev. **116** (1959) 218
3) B. S. Dzhelepov and L. K. Peker, Decay schemes of radioactive nuclei (Izd. Acad. Nauk SSSR, Moscow-Leningrad, 1958)

10.A *Nuclear Physics* **23** (1961) 696—697; © *North-Holland Publishing Co., Amsterdam*

NEWS ITEMS

THE 18th SESSION OF THE CERN COUNCIL

In its 18th session at Geneva on 8—9 December, 1960, the CERN Council took the following decisions.

Starting from 1 January, 1961, the CERN will comprise 12 Divisions instead of 6; this decision was reached in order to take into account the fact that CERN has passed from the stage of construction to that of actual fundamental research. The 12 Divisions will be respectively in charge of 1) the *proton synchrotron* machine, i.e. the 28 GeV proton accelerator; 2) the *synchrocyclotron* machine, a 600 MeV accelerator in operation since 1957; 3) *nuclear physics* experimentation; 4) *engineering*; 5) *data handling*; 6) *theory*; 7) *track chambers*, such as cloud chambers and hydrogen-filled bubble chambers; 8) *nuclear physics apparatus*, such as propane bubble chamber and beam transport equipment; 9) *accelerator research*, for example designing new types of accelerators; 10) *site and buildings* establishment and maintenance; 11) *finance*; 12) *general administration*.

Furthermore the Director General will be assisted by a *Directorate*, a body consisting of two research members, one administration member and one member in charge of applied physics. The Council appointed Prof. V. Weisskopf as the fourth Director-General of the European Organization for Nuclear Research. Prof. Weisskopf will serve for two years from 1 August 1961. He will succeed Dr. J. B. Adams, the present Director-General of CERN who will, next year, return to the United Kingdom as Director of the Culham Laboratory for Plasma Physics Research. Until 1 August 1961, the two members of the Directorate for research will be Prof. G. Bernardini, who first came to CERN in 1957 and until now has been Director of the Synchro-cyclotron Division, and Prof. V. Weisskopf. The member of the Directorate for administration will be Mr. S. A. ff. Dakin (United Kingdom), who has been associated with CERN since 1954. The member for applied research will be Dr. M. G. N. Hine (United Kingdom), who came to CERN in 1953 to help design and build the 28 GeV proton sychroton.

The budget of CERN for 1961 will amount to 67.7 million Swiss Francs. This sum will cover capital expenditures, such as new experimental apparatus to be used in connection with the two particle accelerators at Meyrin; the very large amount of electric power consumed by the accelerators; the maintenance of the apparatus and buildings on CERN's 100 acres of experimental facilities near the French border; the salaries for the staff of over a thousand, etc.

Thirteen European countries are members of CERN, namely Austria, Belgium, Denmark, France, the German Federal Republic, Greece, Italy, the Netherlands, Norway, Sweden, Switzerland, the United Kingdom and Yugoslavia. Spain has now been accepted by the Council and becomes the 14th Member State of CERN from 1 January 1961.

The CERN Council includes 2 delegates from each of the Member States. The President of the Council and the two Vice-Presidents are elected annually and are not re-eligible more than twice. The Council is assisted by a *Committee of Council*, a *Scientific Policy Committee*, which has the task of advising CERN about its scientific programme, and a *Finance Committee* which is responsible for helping the Council to exercise its functions as far as financial problems are concerned.

The following new officers were elected:

Mr. Jean Willems (Belgium) was elected President of the Council for 1961. He thus succeeds Mr. François de Rose (France) who has been President for 3 years and whose term of office could not be renewed under the terms of the Convention.

Prof. Edoardo Amaldi (Italy) and Mr. Jan Hendrik Bannier (the Netherlands) were appointed Vice-Presidents of the Council.

The Chairman of the Scientific Policy Committee of CERN will be Prof. Cecil Powell (United Kingdom) who succeeds Prof. E. Amaldi.

Dr. W. H. Alexander Hocker (Federal Republic of Germany) will succeed Mr. J. H. Bannier as Chairman of the *Finance Committee*.

New Recommendations on Nomenclature

The General Assembly of IUPAP in Ottawa, on the 5—9 Sept. 1960 has, among other things, approved the following recommendations of interest to nuclear physicists:

1) The Basle convention to define the polarization of particles in nuclear reactions (see this journal **21** (1960) 696),

2) The principle of the ^{12}C scale of atomic masses.

3) A name and symbol for the atomic mass unit: if this unit is regarded as a natural constant (like the Bohr magneton or the Rydberg constant), it should be called the *(unified) atomic constant* and denoted by m_u; if it is regarded as a non-coherent mass unit, it should be called the *unified mass unit* and denoted by the symbol u.

4) Names and symbols for the submultiples 10^{-15} and 10^{-18} of fundamental units:

10^{-15} = femto, symbol f,
10^{-18} = atto, symbol a.

The last recommendation has the consequence that the often needed sub-unit of length 10^{-13} cm = 10^{-15} m will now be called a *femtometer*, with symbol fm. This definitively eliminates the spurious use of names such as "fermi" for this convenient unit of nuclear length.

It may be explained that the origin of the new prefixes is Scandinavian: 15 and 18 are, respectively, *femten* and *atten* in Danish.

10.D

Nuclear Physics **23** (1961) 698; © *North-Holland Publishing Co., Amsterdam*

BOOK REVIEWS

H. Jones, *The theory of Brillouin zones and electronic states in crystals* (North-Holland Publishing Co., Amsterdam, 1960. 268 p. 30 fl.)

Since the original work of Bouckaert, Smoluchowski and Wigner in 1936, methods of group theory have been increasingly applied to the quantum theory of solids. They have been used both to simplify attempted calculations of electronic energy states in crystals and in the interpretation of experimental results. Until now, however, no systematic introduction to these applications has been available to the interested reader. Professor Jones's book therefore fills a real need. In addition, the book is noteworthy for its clarity and simplicity. The emphasis throughout is on examples rather than general theory. This permits subtle points to be put across with the minimum of jargon.

The book begins with a discussion of energy levels in one dimensional periodic potentials. Then the consequences of translational periodicity in three dimensions are treated. The ideas of the Brillouin zone, Fermi surface and density-of-states function are introduced and illustrated with examples. In Chapter 3, the form of the energy spectrum for lattices with simple space groups is discussed. A knowledge of the elementary theorems on the irreducible representations of finite groups is assumed. (This is a pity since, otherwise, the book is an introduction and will appeal to students who have had no previous need for group theory. However, this material is readily available elsewhere and its inclusion might have unnecessarily lengthened the book.) It is shown how these theorems may be used to deduce character tables. These are listed for the principal point groups. The connection between the irreducible representations of the group of the wave vector and the sticking together of energy bands is made. The simple cubic, body centered cubic and face centered cubic lattices are then treated in detail. In Chapter 4, the additional complications that arise when glide planes and screw axes are present in the space group are very clearly discussed, again with reference to examples. Chapter 5 deals with the representations in extended **k**-space and its usefulness in connection with complex structures. (Here the reviewer may mention, as an indication of having earned this copy, that the equi-energy lines promised in the caption to fig. 71 and in the text have been omitted.) The last two chapters deal respectively with calculation al methods in band theory and with spin-orbit effects in terms of the representations of the double groups. At every stage, physical examples are treated and wide use is made of informative figures. One should also mention that sufficient results of practical usefulness (character tables, symmetrized combinations of plane waves, etc.) are listed to make the book additionally valuable as a reference.

Vinay Ambegaskar

Lucien Brunelet, *Les Rayonnements Ionisants* (Gauthier-Villars, Paris 1960, 74 p. 10 NF)

The reviewer could not afford to read more than the first 16 pages of this book, which contains 74 pages of small tables. In the first 16 pages he has noticed at least 25 misprints, inconsistent figures or even faulty figures in the tables and in the headings of the tables. This book must be regarded as worthless.

Jørgen Thomas

AUTHOR INDEX

Akiba, T., *see* Kimura

Akimova, M. K., L. D. Blokhintsev and E. I. Dolinsky, Angular distribution and polarization of the neutrons emitted in μ-capture in certain light nuclei 369

Apalin, V. F., *see* Spivak

Baldo-Ceolin, M., *see* Deka

Bargmann, V. and M. Moshinsky, Group theory of harmonic oscillators (II). The integrals of motion for the quadrupole-quadrupole interaction 177

Barnard, A. C. L., S. Bashkin, C. Broude and C. E. Hornback, Capture and inelastic scattering of protons by silicon-30 327

Bashkin, S., *see* Barnard

Bass, R., T. W. Bonner and H. P. Haenni, Cross section for the $Be^9(n, \alpha)He^6$ reaction 122

Batty, C. J., The scattering of high energy nucleons by complex nuclei . 562

Berkes, I., *see* Keszthelyi

Berlovich, E. Ye., V. N. Klementyev, L. V. Krasnov, M. K. Nikitin and I. Yursik, Isomeric states of the spherical nuclei of Eu^{147}, Eu^{149} and Eu^{151} 481

Blatt, J., *see* Katz

Blokhintsev, L. D., *see* Akimova

Bonner, T. W., Measurements of neutron spectra from fission 116

Bonner, T. W., *see* Bass

Broude, C., *see* Barnard

Calvert, J. M., *see* Garg

Calvert, J. M., *see* Read

Chilashvili, G. A., *see* Kopaleishvili

Chilashvili, G. A., *see* Vashakidze

Chultem, D., *see* Egorov

Cohen, A. V. and J. A. Cookson, Coulomb excitation of Au^{197} and W^{186} by protons of energy up to 12.6 MeV 32

Cookson, J. A., *see* Cohen

Coote, G. E., W. E. Turchinetz and I. F. Wright, Cross sections for the (γ, n) reaction in Cu^{63}, Cu^{65}, Zn^{64}, Sb^{121} and Pr^{141}, measured with monochromatic gamma rays 468

Csongor, E., Investigation of γ-rays from Mg^{24}, Mg^{25}, Mg^{26} isotopes bombarded with Po α-particles 107

Deka, G. C., D. Evans, D. J. Prowse and M. Baldo-ceolin, 'Hammer' tracks emitted from nuclear disintegrations produced by 4.6 GeV/c π^--mesons . . . 657
Demeter, I., *see* Keszthelyi
Devanathan, V. and G. Ramachandran, A note on photo-mesons from deuterons . . . 312
De Vries, C., *see* Dijkstra
Dijkstra, J. H. and C. de Vries, Differences in natural widths of conversion lines . . . 524
Dolinsky, E. I., *see* Akimova
Dubois, J., Virtual levels in the vanadium isotopes from proton bombardment of the titanium isotopes . . . 537
Egorov, L. B., G. V. Zhuravlev, A. E. Ignatenko, Li Syuang-Ming, M. G. Petrashku and D. Chultem, Investigation of the paramagnetism of μ-mesic atoms . . . 62
Eldridge, J. S. and W. S. Lyon, Promethium-148 . . . 131
Elton, L. R. B., The scattering of nucleons by nuclei at very high energies . . . 681
Evans, D., *see* Deka
Fodor, I., *see* Keszthelyi
Forkman, B., The photodeuteron yield from 30 MeV bremsstrahlung irradiation . . . 269
Fowler, G. N. and T. W. Preist, Note on the α particle energy spectrum in Li^8 decay . . . 667
Gale, N. H., *see* Garg
Garg, J. B., N. H. Gale and J. M. Calvert, Neutron-gamma angular correlation studies of the $B^{11}(d, n\gamma)C^{12}$ reaction . . . 630
Goldemberg, J., *see* Tagliabue
Gratot, I., *see* Olkowsky
Gregory, A. G., The $B^{11}(p, \gamma\alpha)Be^8$ reaction and the 9.63 MeV state of C^{12} 518
Haenni, H. P., *see* Bass
Hanna, S. S., *see* Tanner
Helfer, H., A. S. Kuznetsov, M. G. Mescheryakov, W. Swiatkowski and V. G. Vovchenko, Effects of the nuclear binding of nucleons on pion spectra . . . 353
Helmers, K., Symplectic invariants and Flowers' classification of shell model states . . . 594
Hodgson, P. E., An investigation of nuclear probes . . . 499
Hornback, C. E., *see* Barnard
Ignatenko, A. E., Processes of depolarization of negative muons . . . 75
Ignatenko, A. E., *see* Egorov
James, A. N., The $C^{12}(d, n)N^{13}$ reaction up to 1.35 MeV . . . 648

Jones, P. B., Convergence of the cluster expansion for the optical model potential 349

Kamefuchi, S., *see* Umezawa

Katz, A. and J. Blatt, The moment of inertia of rotating nuclei . . . 612

Keszthelyi, L., I. Berkes, I. Demeter and I. Fodor, Energy dependence of the cross section of the $O^{16}(\gamma, n)O^{15}$ nuclear reaction 513

Kimura, M., K. Shoda, N. Mutsuro, T. Tohei, K. Sato, K. Kuroda, K. Kuriyama and T. Akiba, Structure of the giant resonance in the $Al^{27}(p, \gamma)$ reaction 338

Klementyev, V. N., *see* Berlovich

Kopaleishvili, T. I., I. Sh. Vashakidze, V. I. Mamasakhlisov and G. A. Chilashvili, Alpha-deuteron model of the Li^6 nucleus 430

Kopaleishvili, T. I., *see* Vashakidze

Krasnov, L. V., *see* Berlovich

Królikowski, W., Fermions and the intrinsic Pauli principle 53

Kurath, D. and R. D. Lawson, Positive-parity states in mass-13 nuclei 5

Kuriyama, L., *see* Kimura

Kuroda, K., *see* Kimura

Kutikov, I. Ye., *see* Spivak

Kuznetsov, A. S., *see* Helfer

Ladenbauer, I.-M., Sodium-24 excitation function for lithium-6 ions on aluminium 559

Lawson, R. D., *see* Kurath

Le Pape, M., *see* Olkowsky

Li Syuang-Ming, *see* Egorov

Lyon, W. S., *see* Eldridge

Mamasakhlisov, V. I., *see* Kopaleishvili

Marrus, R., W. A. Nierenberg and J. Winocur, Hyperfine structure and nuclear moments of protactinium-233 90

Menotti, P. and Y. Tomozawa, Wigner condition and low energy scattering 506

Mescheryakov, M. G., *see* Helfer

Mikaelyan, L. A., *see* Spivak

Mitler, H. E., Shell-model analysis of calcium isotopes 200

Montaldi, E., On the structure of the four point functions in Heisenberg's non linear spinor theory 439

Moshinsky, M., *see* Bargmann

Mutsuro, N., *see* Kimura

Nierenberg, W. A., *see* Marrus

Nikitin, M. K., *see* Berlovich

Olkowsky, J., M. Le Pape et I. Gratot, Fonction d'excitation de $^{141}Pr(p, n)^{141}Nd$ jusqu'à 11.1 MeV 164

PEIERLS, R. E., Professor H. W. B. Skinner, F. R. S. (1900—1960) . . . 1
PERRING, J. K. and R. J. N. PHILLIPS, On the hard core in nuclear forces 153
PETRASHKU, M. G., *see* EGOROV
PHILLIPS, R. J. N., On the $\pi^- + p \rightarrow \Lambda^0 + K^0$ amplitude 345
PHILLIPS, R. J. N., *see* PERRING
POMERANCHUK, I. Ya. and I. M. SHMUSHKEVICH, On processes in the interaction of γ-quanta with unstable particles 452
PREIST, T. W., *see* FOWLER
PROWSE, D. J., *see* DEKA
RAMACHANDRAN, G., *see* DEVANATHAN
READ, F. H., J. M. CALVERT and G. SCHORK, Some $Be^9(d, p\gamma)Be^{10}$ angular correlation measurements off the stripping peak 386
ROBSON, B. A., Scattering of high energy polarized deuterons by carbon 672
RYBAKOV, B. V., V. A. SIDOROV and N. A. VLASOV, Breakup of deuterons on H, D, He^3 and He^4 491
SANDERS, J. B., Spectroscopic calculation of energy levels of some tin isotopes 305
SATO, K., *see* KIMURA
SAWICKI, J., Notes on the theory of vibrational states of systems of fermions (I) 285
SAXENA, R. P., Two pion annihilation of a $N-\overline{N}$ pair 158
SCHORK, G., *see* READ
SEKINE, K., Canonical and non-canonical method of quantisation in the Lee model 245
SHMUSHKEVICH, I. M., *see* POMERANCHUK
SHODA, K., *see* KIMURA
SIDOROV, V. A., *see* RYBAKOV
SMIRNITSKY, V. A., *see* WAISSENBERG
SPIVAK, P. E., L. A. MIKAELYAN, I. Ye. KUTIKOV and V. F. APALIN, Asymmetry in double Mott scattering and absolute values of beta-electron longitudinal polarization 169
SWIATKOWSKI, W., *see* HELFER
TAGLIABUE, F. and J. GOLDEMBERG, Angular distributions of fast photoneutrons 144
TANNER, N. W. and S. S. HANNA, Angular correlation in $Be^9(p, \gamma)B^{10}$ and the states of B^{10} at 7.56 and 5.16 MeV 319
TOHEI, T., *see* KIMURA
TOMOZAWA, Y., *see* MENOTTI
TURCHINETZ, W. E., *see* COOTE
UMEZAWA, H. and S. KAMEFUCHI, Equivalence theorems and renormalization problem in vector field theory (The Yang-Mills field with non-vanishing masses) 399

UMEZAWA, M., Competition between the pairing force and the spin-orbit force in V^{51} 296
VASHAKIDZE, I. Sh., *see* KOPALEISHVILI
VASHAKIDZE, I. Sh., T. I. KOPALEISHVILI and G. A. CHILASHVILI, Lifetime of the 3.56 MeV level of Li^6 694
VLASOV, N. A., *see* RYBAKOV
VOVCHENKO, V. G., *see* HELFER
WAISSENBERG, A. O. and V. A. SMIRNITSKY, Conservation of μ^+-meson polarization in emulsion with aid of magnetic field 23
WILLIAMSON, R. M., *see* WISSEMAN
WINOCUR, J., *see* MARRUS
WISSEMAN, W. R. and R. M. WILLIAMSON, Coulomb excitation of Se^{77} . 532
WRIGHT, I. F., *see* COOTE
YAMAZAKI, K., On the "new Tamm-Dancoff" approximation treatment of the superconductivity Hamiltonian 139
YOUNG, J. E., The optical model and deuteron stripping 40
YURSIK, I., *see* BERLOVICH
ZHURAVLEV, G. V., *see* EGOROV

SUBJECT INDEX

1. Nuclear Structure

1.B *Two- and three-body problems*

On the hard core in nuclear forces, J. K. Perring and R. J. N. Phillips 153
Wigner condition and low energy scattering, P. Menotti and Y. Tomozawa . . 506

1.C *Many-particle systems*

Group theory of harmonic oscillators (II). The integrals of motion for the quadrupole-quadrupole interaction, V. Bargmann and M. Moshinsky . . . 177

1.D *Nuclear models*

1.D.1 *Shell model*

Shell-model analysis of calcium isotopes H. E. Mitler 200
Competition between the pairing force and the spin-orbit force in V^{51}, M. Umezawa 296
Spectroscopic calculation of energy levels of some tin isotopes, J. B. Sanders 305
Symplectic invariants and Flowers' classification of shell model states, K. Helmers 594

1.D.2 *Collective model*

Isomeric states of the spherical nuclei of Eu^{147}, Eu^{149} and Eu^{151}, E. Ye. Berlovich, V. N. Klementyev, L. V. Krasnov, M. K. Nikitin and I. Yursik 481

1.D.3 *Other models*

Alpha-deuteron model of the Li^6 nucleus, T. I. Kopaleishvili, I. Sh. Vashakidze, V. I. Mamasakhlisov and G. A. Chilashvili 430

1.D.4 *Relationship between different models*

Positive-parity states in mass-13 nuclei, D. Kurath and R. D. Lawson . 5
Notes on the theory of vibrational states of systems of fermions (I), J. Sawicki. 285

1.E *Properties of nuclei*

1.E.1 *Energy levels*

Promethium-148, J. S. Eldridge and W. S. Lyon 131
Angular correlation in $Be^9(p, \gamma)B^{10}$ and the states of B^{10} at 7.56 and 5.16 MeV, N. W. Tanner and S. S. Hanna. 319

1.E.3 *Electric and magnetic moments*

Hyperfine structure and nuclear moments of protactinium-233, R. Marrus, W. A. Nierenberg and J. Winocur 90

1.E.4 *Transition probabilities; Cross sections*

Lifetime of the 3.56 MeV level of Li^6, I. Sh. Vashakidze, T. I. Kopaleishvili and G. A. Chilashvili 694

1.E.5 *Nuclear radii; Matter distributions*

The scattering of nucleons by nuclei at very high energies, L. R. B. Elton 681

1.E.6 *Nuclear moments of inertia*

The moment of inertia of rotating nuclei, A. Katz and J. Blatt 612

1.E.8 *Other properties*

Effects of the nuclear binding of nucleons on pion spectra, H. Helfer, A. S. Kuznetsov, M. G. Mescheryakov, W. Swiatkowski and V. G. Vovchenko 353

2. Nuclear Reactions

2.A *General properties*

The $B^{11}(p, \gamma\alpha)Be^8$ reaction and the 9.63 MeV state of C^{12}, A. G. Gregory . . . 518

2.A.1 *Cross-sections, energy relations*

Cross section for the $Be^9(n, \alpha)He^6$ reaction, R. Bass, T. W. Bonner and H. P. Haenni 122

Fonction d'excitation de $^{141}Pr(p, n)^{141}Nd$ jusqu'à 11.1 MeV, J. Olkowsky, M. Le Pape et I. Gratot 164

Sodium-24 excitation function for lithium-6 ions on aluminium, I. M. Ladenbauer 559

'Hammer' tracks emitted from nuclear disintegrations produced by 4.6 GeV/c π^--mesons, G. C. Deka, D. Evans, D. J. Prowse and M. Baldo-Ceolin 657

Note on the particle energy spectrum in Li^8 decay, G. N. Fowler and T. W. Preist. 667

2.B *Angular distributions, Correlations; Polarization*

A note on photo-mesons from deuterons, V. Devanathan and G. Ramachandran 312

Some $Be^9(d, p\gamma)Be^{10}$ angular correlation measurements off the stripping peak, F. H. Read, J. M. Calvert and G. Schork 386

The $C^{12}(d, n)N^{13}$ reaction up to 1.35 MeV, A. N. James 648

Scattering of high energy polarized deuterons by carbon, B. A. Robson . . . 672

2.C *Resonance reactions; R-matrix theory*

Capture and inelastic scattering of protons by silicon-30, A. C. L. Barnard, S. Bashkin, C. Broude and C. E. Hornback 327

Structure of the giant resonance in the $Al^{27}(p, \gamma)$ reaction, M. Kimura, K. Shoda, N. Mutsuro, T. Tohei, K. Sato, K. Kuroda, K. Kuriyama and T. Akiba . . . 338

2.D *Statistical model*

Virtual levels in the vanadium isotopes from proton bombardment of the titanium isotopes, J. Dubois 537

2.E *Optical model*

The optical model and deuteron stripping, J. E. Young 40

Fonction d'excitation de ^{141}Pr(p, n)^{141}Nd jusqu'à 11.1 MeV, J. Olkowsky, M. Le Pape et I. Gratot . . . 164
Convergence of the cluster expansion for the optical model potential, P. B. Jones 349
An investigation of nuclear probes, P. E. Hodgson . . . 499
The scattering of high energy nucleons by complex nuclei, C. J. Batty . . . 562
Neutron-gamma angular correlation studies of the B^{11}(d, nγ)C^{12} reaction, J. B. Garg, N. H. Gale and J. M. Calvert . . . 630

2.F *Direct interaction (other than stripping)*

Breakup of deuterons on H, D, He^{3} and He^{4}, B. V. Rybakov, V. A. Sidorov and N. A. Vlasov . . . 491

2.G *Stripping and pick-up*

The optical model and deuteron stripping, J. E. Young . . . 40
Measurements of neutron spectra from fission, T. W. Bonner . . . 116
Neutron-gamma angular correlation studies of the B^{11}(d, nγ)C^{12} reaction, J. B. Garg, N. H. Gale and J. M. Calvert . . . 630

2.H *Coulomb excitation*

Coulomb excitation of Au^{197} and W^{186} by protons of energy up to 12.6 MeV, A. V. Cohen and J. A. Cookson . . . 32
Coulomb excitation of Se^{77}, W. R. Wisseman and R. M. Williamson . . . 532

2.I *Photonuclear processes*

Angular distributions of fast photoneutrons, F. Tagliabue and J. Goldemberg . 144
The photodeuteron yield from 30 MeV bremsstrahlung irradiation, B. Forkman 269
Cross sections for the (γ, n) reaction in Cu^{63}, Cu^{65}, Zn^{64}, Sb^{121} and Pr^{141}, measured with monochromatic gamma rays, G. E. Coote, W. E. Turchinetz and I. F. Wright . . . 468
Energy dependence of the cross section of the O^{16}(γ, n)O^{15} nuclear reaction, L. Keszthelyi, I. Berkes, I. Demeter and I. Fodor . . . 513

2.L *Scattering processes (except two-nucleon system and meson scattering)*

Breakup of deuterons on H, D, He^{3} and He^{4}, B. V. Rybakov, V. A. Sidorov and N. A. Vlasov . . . 491

3. Electromagnetic Radiation

3.A *Gamma radiation*

Investigation of γ-rays from Mg^{24}, Mg^{25}, Mg^{26} isotopes bombarded with Po α-particles, E. Csongor . . . 107
Promethium-148, J. S. Eldridge and W. S. Lyon . . . 131
Angular correlation in Be^{9}(p, γ)B^{10} and the states of B^{10} at 7.56 and 5.16 MeV, N. W. Tanner and S. S. Hanna . . . 319
Structure of the giant resonance in the Al^{27}(p, γ) reaction, M. Kimura, K. Shoda, N. Mutsuro, T. Tohei, K. Sato, K. Kuroda, K. Kuriyama and T. Akiba . . 338
On processes in the interaction of γ-quanta with unstable particles, I. Ya. Pomeranchuk and I. M. Shmushkevich . . . 452

3.B *Internal conversion*

Differences in natural widths of conversion lines, J. H. Dijkstra and C. De Vries 524

4. Beta decay; Parity

4.E *Analysis of data*

Promethium-148, J. S. Eldridge and W. S. Lyon . . . 131
Asymmetry in double Mott scattering and absolute values of beta-electron longitudinal polarization, P. E. Spivak, L. A. Mikaelyan, I. Ye. Kutikov and V. F. Apalin . . . 169
'Hammer' tracks emitted from nuclear disintegrations produced by 4.6 GeV/*c* π^--mesons, G. C. Deka, D. Evans, D. J. Prowse and M. Baldo-Ceolin . . . 657

7. Quantum Field Theory

7.A *General*

Canonical and non-canonical method of quantisation in the Lee model, K. Sekine . . . 245
Equivalence theorems and renormalization problem in vector field theory (The Yang-Mills field with non-vanishing masses), H. Umezawa and S. Kamefuchi . . . 399

8. Elementary Particles

8.A *Experimental*

Conservation of μ^+-meson polarization in emulsion with the aid of magnetic field, A. O. Waissenberg and V. A. Smirnitsky . . . 23
Investigation of the paramagnetism of μ-mesic atoms, L. B. Egorov, G. V. Zhuravlev, A. E. Ignatenko, Li Syuang-Ming, M. G. Petrashku and D. Chultem . . . 62

8.B *Theory; interactions, transformations properties*

Processes of depolarization of negative muons, A. E. Ignatenko . . . 75
Two pion annihilation of a $N-\overline{N}$ pair, R. P. Saxena . . . 158
On the $\pi^-+p \to \Lambda^0+K^0$ amplitude, R. J. N. Phillips . . . 345
Angular distribution and polarization of the neutrons emitted in μ-capture in certain light nuclei, M. K. Akimova, L. D. Blokhintsev and E. I. Dolinsky . 369

8.C *Fundamental theory of matter*

Fermions and the intrinsic Pauli principle, W. Królikowski . . . 53
On the "new Tamm-Dancoff" approximation treatment of the superconductivity Hamiltonian, K. Yamazaki . . . 139
On the structure of the four point functions in Heisenberg's non linear spinor theory, E. Montaldi . . . 439

10. News Items

10.A *News Itimes*

The Institute of Physics and the Physical Society awards (16 November 1960) 173
Rutherford Jubilee International Conference at Manchester (4—8 September 1961) . . . 173
Cooperation between IAEA and ENEA . . . 175
Karlsruhe Photonuclear Conference (18—22 August 1960) . . . 186

The 18th Session of the CERN council 696
New recommendations on Nomenclature 697

10.C *Obituaries*

Professor H. W. B. Skinner, F. R. S. (1900—1960), R. E. Peierls 1

10.D *Book Reviews*

H. Jones, the Theory of Brillouin zones and electronic states in crystals (Vinay Ambegaskar) 698
L. Brunelet, Les rayonnements ionisants (Jørgen Thomas) 698